UNIVERSITY OF Southampton

University of Southampton Research Repository
ePrints Soton

http://eprints.soton.ac.uk

UNIVERSITY OF SOUTHAMPTON

FACULTY OF ENGINEERING AND THE ENVIRONMENT

Civil, Maritime and Environment Engineering and Science

Volume 1 of 1

Investigation into Image Technology of Timber for the Assessment of Structural Performance of Fresh-Cut Oak Tree Joints *(Quercus Robur L.)*

by

Eve Alaina Walkden

Thesis for the degree of Doctor of Philosophy

July 14

UNIVERSITY OF SOUTHAMPTON

ABSTRACT

FACULTY OF ENGINEERING AND THE ENVIRONMENT

Civil Engineering

Thesis for the degree of Doctor of Philosophy

INVESTIGATION INTO IMAGE TECHNOLOGY OF TIMBER FOR THE ASSESSMENT OF STRUCTURAL PERFORMANCE OF FRESH-CUT OAK TREE JOINTS *(QUERCUS ROBUR L.)*

By Eve Alaina Walkden

The Institution of Civil Engineers in their first Royal Charter quoted *'Civil Engineering is the art of directing the great sources of power in nature for the use and convenience of mankind'*.

Looking at the fundamental design and stability of the tree branch connection ('Global Joint') response to loading through biomimicry can inspire designs using infrastructure materials. This project develops the process of strain monitoring image technology on timber to analyse the mechanical behaviour of the fibres internal to a Global Joint.

The Particle Image Velocimetry (PIV) is applied to images taken during British Standard structural tension tests of batten samples of timber ('Components') taken from an Oak tree Global Joint. A detailed process is described by which results from the PIV were extrapolated and the interpretation techniques used on the resulting contour plots. The resulting contour plot shows the impending failure of the Component as the tension is applied during the test. The sequential images taken during the test allow the strain values to be evaluated. This means the interaction of the visible timber surface fibres during testing can be analysed without the need for strain gauges or alterations to the Component.

The Components are structurally analysed individually and then reformed back to present the natural structural design of the Global Joint. The PIV strain results from the tension tested Components are combined with the peak stress values to find the structural performance of the interior of the Global Joint. This re-formation enables the analysis of the natural structural design facilitating the review of the internal workings.

Contents

List of tables

List of figures

List of accompanying materials

Appendices 1–8

DECLARATION OF AUTHORSHIP

I, Eve Alaina Walkden

declare that the thesis entitled

Investigation into Image Technology of Timber for the Assessment of Structural Performance of Fresh-Cut Oak Tree Joints *(Quercus Robur L.)*

and the work presented in the thesis are both my own, and have been generated by me as the result of my own original research. I confirm that:

- this work was done wholly or mainly while in candidature for a research degree at this University;

- where any part of this thesis has previously been submitted for a degree or any other qualification at this University or any other institution, this has been clearly stated;

- where I have consulted the published work of others, this is always clearly attributed;

- where I have quoted from the work of others, the source is always given. With the exception of such quotations, this thesis is entirely my own work;

- I have acknowledged all main sources of help;

- where the thesis is based on work done by myself jointly with others, I have made clear exactly what was done by others and what I have contributed myself;

- none of this work has been published before submission, or [delete as appropriate] parts of this work have been published as: [please list references]

Signed: …………………………………………………………………..

Date: …………………………………………………………………..

Acknowledgements

Nomenclature

A   Cross-sectional area

E   Young's Modulus of elasticity

G   Specific gravity

h   Nominal width

I   Moment of inertia

m   Mass

P   Applied load

α PIV conversion ratio

Δ Large change

δ Small change

ϵ Strain

σ Stress

ω Moisture content

1. Introduction – The Wonder of Trees

The places people live and work in are not merely a series of buildings and infrastructures, they influence their well-being. It is important for design to positively influence a person's life; this can be achieved through 'atmospherics'. By creating positive influence in all aspects of design, the well-being of people in their habitat improves.

1.1 Green Infrastructure

Some of the ideas of sustainability and wellbeing have been entangled into a new term *'Green Infrastructure'.* Green Infrastructure is a concept that combines the need for the natural environment with the needs of the built environment and aims to create a balance between the two. Thus the natural environment given through landscapes or technology such as green roofs (shown in Figure 1), creates a positive and sustainable built environment. The landscapes give the positive well-being required for the people who use the built environment, creating a balanced cycle of; sustainability, wellbeing, and habitat.

FIGURE 1: A ROOF GARDEN, AN EXAMPLE OF GREEN INFRASTRUCTURE, IMAGE FROM PUSH (2010)

1.1.1   Sustainability

The sustainable requirements of design are a strong focus to current development legislation but few people have a true knowledge or definition of the meaning. As defined and directed in the United Nations Brundtland Commission (1987) Report, sustainability *'meets the needs of the present without compromising the ability of future generations to meet their own needs'*.

Trees are a sustainable solution to climate change and the different species of trees provide varying carbon intake required to reduce current climate effects. Trees are seen as a sustainable resource as they can be replanted, managed and have a multiuse. An influx of tree planting proves they are recognised as a

positive influence on the urban environment. The cooling property the tree provides creates a natural and economic solution to the urban heat-island effect in big cities. The ability of a tree to transpire allows excess heat and air pollutants to be absorbed. The measurement of the economic benefit of trees has been introduced through i-Tree (1999), a tool which assesses and manages urban forests. An example of the economic value of trees can be seen in Figure 2.

Chicago Urban Forest Summary	
Feature	Measure
Number of trees	3,585,000
Tree cover	17.2%
Most common species	white ash, mulberry, green ash, tree-of-heaven
Percentage of trees < 6-inches diameter	61.2%
Pollution removal	888 tons/year ($6.4 million/year)
Carbon storage	716,000 tons ($14.8 million)
Carbon sequestration	25,200 tons/year ($521,000/year)
Building energy reduction	$360,000/year
Increased carbon emissions	-$25,000/year
Structural value	$2.3 billion
Ton – short ton (U.S.) (2,000 lbs)	

FIGURE 2: EXTRACT FROM I-TREE (1999) OF AN ECONOMIC EVALUATION CASE STUDY OF CHICAGO'S URBAN FOREST BY NOWAK *ET AL* (2009)

The dried product of a tree is timber. Timber in itself is a strong and durable material and has been used for centuries as a material for shelter. When well built and maintained, timber structured buildings can be reliably durable. In comparison to modern materials timber is deemed a weaker material though in some instances found by Greer *et al* (2009), the specific strength of timber is

similar to that of steel. The extent of timber use can only be accepted for the infrastructure feats that it has achieved. For example a 13 storey Sutyagin House in Arkhangelsk, and the planned 16-17 storey building Barents House Kirkenes, Norway or Skellefteå, a four storey municipal building in Sweden with car park, or the oldest wooden building *Hōryū Gakumonji* temple founded in Japan in 607 AD.

1.1.2   Well-being

Gilchrist (2011) found trees are a notable benefit to wellbeing. Trees are good for wellbeing as they naturally reduce temperature. Padgham (1975) found green to be an easy natural colour to the human eye and Dwyer *et al* (1994) found trees to produce feelings of familiarity. Ulrich (1984) considers the tree to increase the recovery time of patients in hospitals and as such this research has encouraged the provision for NHS gardens in the United Kingdom.

1.1.3   Trees/Timber

An interesting similarity about the current vogue discussions about sustainability and wellbeing is how natural material and nature is a common theme. The ideas of trees in landscapes and timber in the built environment, which are in essence the same material, are a universal topic. It is worth noting it is imprudent to say trees/timber are always a sustainable choice. It is often assumed in discussions because the material is timber it automatically makes a project sustainable. This cannot be true. As it is the process by which timber is grown, acquired and the native relationship of the timber to the environment in which it is used that govern its sustainable credentials. If timber/trees are not grown for future use then it cannot be deemed sustainable practice.

Overuse of this 'sustainable' resource will ultimately be of detriment to the recovery of climate change.

Trees have covered a solution to three points raised so far, sustainability, wellbeing, and structural solutions. This natural product seems to be a vital part of life and is humble about its need to be in the natural world. The tree provides numerous resources often overlooked through familiarity and the ambition to make better technologies. However, itself as one organism produces so many benefits. The tree is not perfect, as most organisms, it is susceptible to disease and becoming a hazard through weakness or defective growth. It is surprising these common life issues seem to dominate the minds of tree owners and decision makers, rather than the trees' many benefits.

1.2   Biomimicry

The Biomimicry Institute (2010) describes biomimicry *'studies nature's best ideas and then imitates these designs and processes to solve human problems'*. Fratzl (2007) indicates imitating solutions from 3.8 billion years of development in nature, is becoming popular in finding solutions to problems in the built and technological environment. Using biomimicry means organic design/architecture can influence better designs to suit wellbeing and sustainability.

1.2.1   Concept

One famous example of successful Biomimicry, shown by Ask Nature (2011), was Crystal Palace in London (seen in Figure 3). The design of the large glass panel support mimicked the ribs and struts of the giant water lily. If a tree is akin to a structure, or even a form of air-conditioning, then it is possible by

investigating the tree biology and structure innovative solutions can be developed in new designs and could help in the reinforcement/reinvention of old designs. With trees being vital in the world and their characteristics being similar to that of stationary man-made structure, it is possible this frequently overlooked structure could be used in terms of biomimicry.
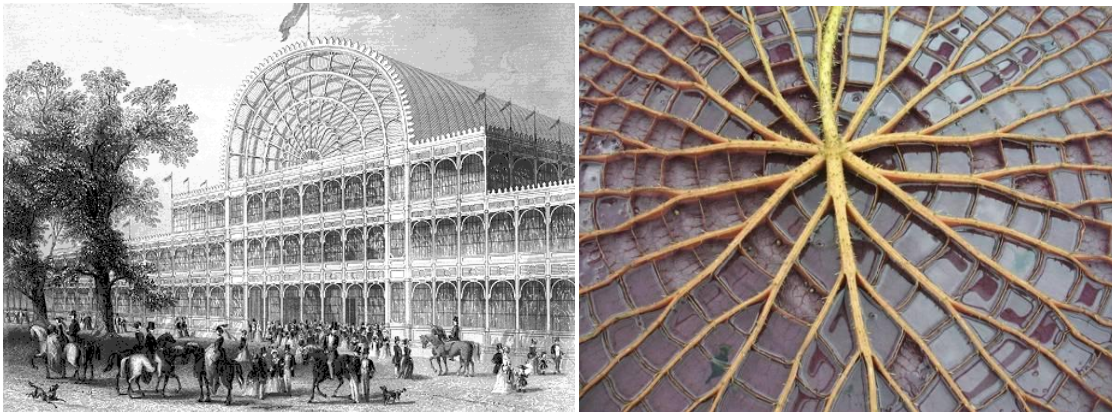
FIGURE 3: EXAMPLE OF BIOMIMICRY USED IN CRYSTAL PALACE – FROM ASKNATURE (2011) CASE STUDY

1.2.2   Mattheck's work

The structural knowledge gained through use of cut timber is not necessarily what is true for trees. For instance, knots in timber lower the grade, reducing the stress it can take. This isn't true in a tree. Mattheck and Burkhardt (1990) finite element analysed von Mises stresses in tree knots and found the 'axiom of uniform stress' is inherent in tree design. The axiom of uniform stress means the localised stresses that might be expected in a material are reduced by natural growth adaptation. The natural ability of nature to prevent weak spots but limit superfluous material leads to optimal growth. Such optimal growth is seen in the base of the tree. This has been adapted to a modelled I-beam (seen in Figure 4). From this research biomimicry principles have led to a computer-aided optimised method which can be run on other structural

elements to enhance their design. Mattheck is known for his work on tree mechanics and computational predictions of tree formations using finite element methods. This has helped in the hazard assessment of trees, particularly important in litigation issues, considering the planting of trees in urban areas to reduce the heat island effect and the need for healthy, strong trees as natural building resources.
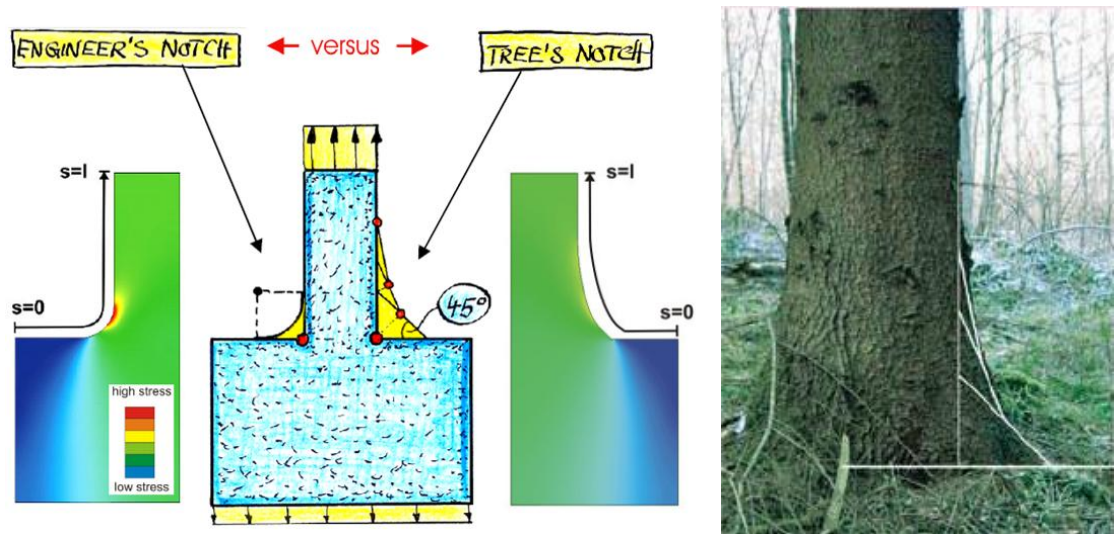
FIGURE 4: MATTHECK (2007)'S BIOMIMICRY EXAMPLE USING TREES OPTIMUM DESIGN TO IMPROVE I-BEAM WELD DESIGN (EXTRACT FROM SECRET DESIGN RULES OF NATURE)

1.3   Aims and Objectives

Trees are needed. They have lots of potential uses and can be learnt from. This research focuses on tree branch 'Global Joints' (intersection between a tree's primary and secondary growths), where there is seen to be a deficit in previous research (later discussed in Chapter 3). This project and thesis aims to explore the potential of trees in Civil Engineering by investigating the fundamental stress-strain behaviour and will indicate the tree's usability within the Civil Engineering world. This research shows structural tests that have been conducted and the development of existing technology.This may lead to

further research of tree structure. There is also the idea of using this research to help influence the building of structure around, on or in trees.

The aims of the proposed research are:

- Supply key information on how the tree joint interacts structurally.

- Expand current technology by conducting analysis of tree joint strength results to stimulate better structural understanding.

- Apply existing strain image measurement technology in timber

- Provide innovative inspiration in tackling construction connections, through biomimicry of the tree joint

The objectives for this research are:

- Develop Particle Image Velocimetry (PIV) methods to measure strain in timber

- Load test components of tree global joints while using PIV techniques

- Combine components from global joints to develop knowledge of the strength characteristics and behaviour.

The project develops a model of a tree global joint that will enable understanding of its strength. This understanding could also be used to inspire further developments in structural material and structural connections.

Therefore the deliverables are:

- Guidance of joint failure mechanisms

- Guidance on the methodologies required to create testing procedures for this research.

- Development of PIV as a resource for testing strain in timber

1.4 Chapter Review

This research covers many industry disciplines. Some of the points touched upon in this introduction will be further developed and explained in this thesis. The structure of the remaining chapters is as follows:

Chapter 2- Tree to Timber - Biology and Structure

An introduction to relevant aspects of tree biology, structure through adaptive growth, and structural behaviour through mechanical properties will be outlined. This basic tree biology covers the growth through tropism balance and the apical dominance that is thought to be the start of branch growth. This includes the generally accepted view of branch growth by Arborists and the process of making trees into timber through drying. From this an overview of basic timber and tree behaviour will be introduced.

Chapter 3 – Review of Previous Research

This chapter will show an overview of previous authors' research and understanding into tree structural performance, global joint structure and fundamental timber tests. It touches on the natural loading on trees by wind, ice and snow and the natural damping response of the tree. It examines the various works conducted in arboricultural and timber research and demonstrates the lack of knowledge and definition in the failure of global joints. The literature review of tree global joint tests found there is limited research. A more specific review of the global joint strength is conducted as it is known the tree is likely to shed branches during stormy conditions, or experience restricted growing due to a changing environment. Changing environments are likely in urban built areas and thereby the failure of the

global joint can impact more on litigation. The review highlights the lack of tests and common understanding of global joint strength.

Chapter 4 – Research Progression and Application

The methods summarise the progression of the thoughts arisen from the literature review. The scope of the outlined research and load test procedure fulfils the understanding of basic global joint structure. The research shows the potential to affect multiple industries and engineering problems.

Chapter 5 – Development of Particle Image Velocimetry (PIV) on Timber

An existing PIV code is developed so it tracks the timber strain through a series of images. The work includes trialling the possible methodologies of achieving quality images and the development of Matlab® code to track the strain during load testing. The various methodologies trialled are improved as the test set-up implications are accounted for. The PIV code develops to successfully run sequential analysis of the multiple images taken during timber tensile testing.

Chapter 6 – Component Tension Testing

Test works are conducted on battens in order to determine the internal structural workings of the global joint. The test includes splitting the joint into battens (components) and tensile loading these samples to British Standard procedures in order to convert timber properties to possible tree strength structural properties. These battens also use a novel technique of Particle Image Velocimetry (PIV) on timber to determine the strain of the tested samples as individual components and as a reformed cross-section through the global joint.

Chapter 7– Conclusion

The overall combination of all test works and modelling have been reviewed. Predictors of failure and an overall interpretation of failures have been analysed for success. The chapter indicates future possibilities of this work and how this research can continue to provide a greater substantial understanding of global joints in trees.

2. Background of Tree to Timber – Biology and Structure

This research is primarily stimulated by the issue of tree joint strength. In the following chapters it will be shown how this need for research has arisen. To obtain an understanding of the tree's structural properties, its growth process and its ability to react to the environment needs to be understood. A thorough and sound understanding of the creation of the tree will be explained so there are no general misconceptions. This background will be a key to further developments and explanations of more complex material that will be encountered later in the thesis. The explanation will outline the general biological growth, environmental compromises and mechanical support structure that develop in the tree and then timber.

2.1 Main Growth

According to Mattheck (1998), there are three growth stimulants in a tree (Figure 5):

- Geotropism encourages outward growth

  o negative geotropism is used by the stem and branches to grow straight

  o positive geotropism encourages root growth in the ground.

- Phototropism makes the branches and stem grow towards the light in order to create maximum photosynthesis opportunities.

- Apical dominance is the encouragement of the branches to grow by encouraging lesser principal growth to move away from the primary dominant growth. The tree uses a favoured growth of the upper side of the branch called 'epinasty,' *i.e.* material grows more on the upper side of the branch to push the lesser growth away from the adjacent growths.

Negative
Geotropism

Phototropism

Apical
Dominance

Positive
Geotropism
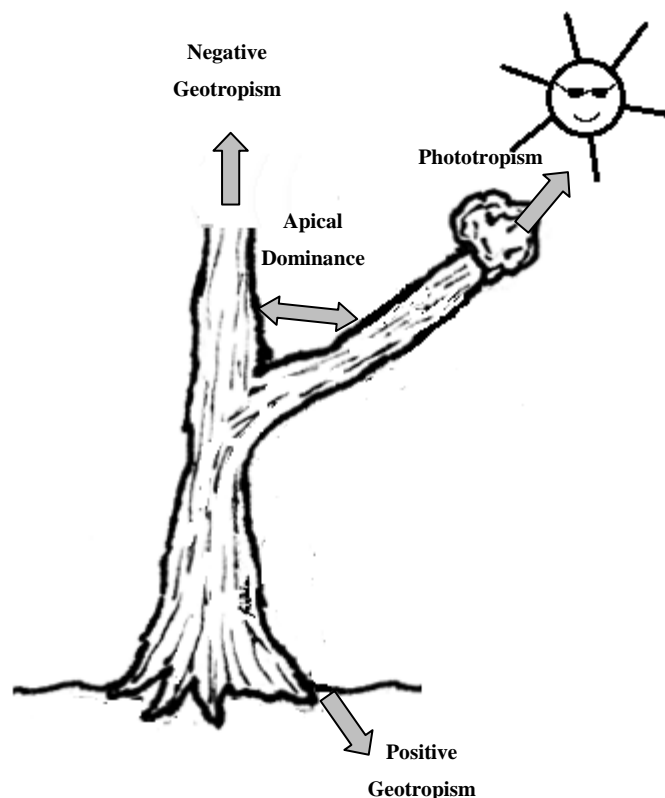
FIGURE 5: GROWTH STIMULANTS WITHIN TREE GROWTH

2.2 Tropism Balance

Trees grow toward the light. The leaves soak up light energy and allow carbon dioxide to 'dissolve' in through microscopic pores called 'stomata'. The energy combines carbon dioxide with the water transported through the 'xylem' vessels (present in the inside cambium layer, the centre core strengthening

14

part of the stem, see Figure 6). This ring development initiates in spring when a new 'xylem' layer is formed to transport the water up the tree to start growth. This is a thick layer which continues into the Summer/Autumn 'phloem' layer which tends to be a thin dark line used for the transport of storage material. To add to the complexity of the structure, medullary rays join the 'xylem' and 'phloem' layers, enabling the storage of food and transport of water and nutrients laterally between the layers should an obstruction occur. As the tree grows outward the bark stretches and develops cracks which give a gnarled appearance.
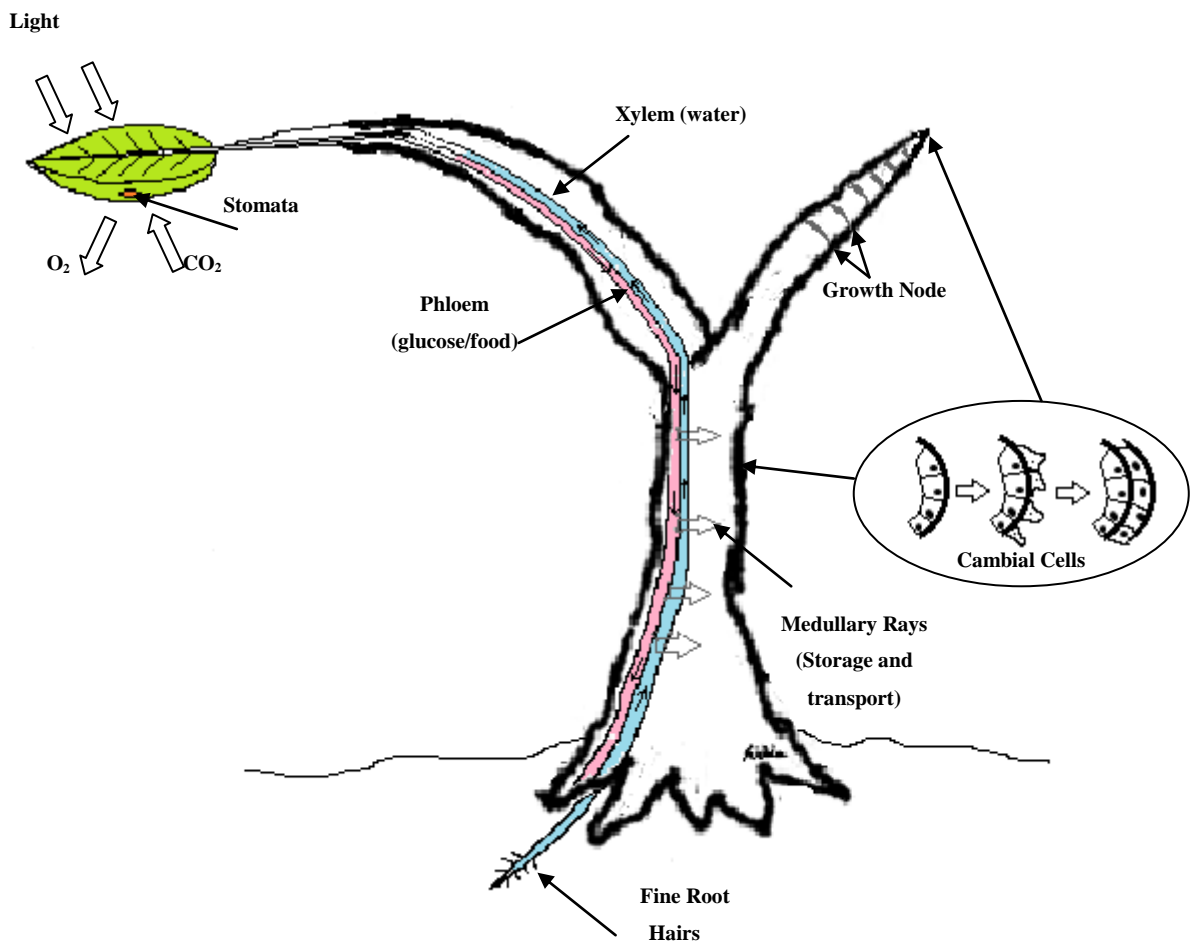
FIGURE 6: GROWTH FUNCTION ANALOGY OF THE TREE

2.3   Apical Dominance

The trees' primary growth is upward towards light. This is done by meristem cells which have no specialized function, but to multiply below the tip of the growing stem or Apical Meristem. After multiplication, the cells adapt into the required cells, such as xylem and phloem. Nodes are created periodically as the Apical Meristem cells divide (similar to cambial cells in Figure 6). Here leaves or flowers propagate. The node contains an axillary meristem at the intersection of the leaf and the stem which can create branches. Generally the axillary meristem is inactive as the Apical Meristem produces a hormone inhibiter that prevents primary growth elsewhere in the plant, giving the growing tip Apical Dominance. This is only stopped when the tip is removed or hindered and the hormone is no longer inhibited when the battle for Apical dominance of the nodes begins.

2.4   Branch Development

A branch can develop for a number of factors. The main need is for food achieved by increasing light capture. These factors determine whether the growth of a branch is necessary on the tree. According to Shigo (1985), the branch develops tissue earlier in the growing season than the stem. The branch tissue is at a direct angle to the stem grain, showing a decisive development action. As the branch develops, the top edge between the branch and stem creates a hole, known as a notch, due to the branch developing from the lower stem. This hole needs packing and the branch needs stabilising so a collar is formed around the notch creating the branch (see 6b and 6c of Figure 7). The collar is the stem tissue wrapping around the fibres of the branch, progressively enveloping the branch structurally every season to secure it in

place. The weakness of the hole at the topside of the branch connection, commonly known as the 'crotch' (formed of packing tissue), can explain the tendency for the branch to shear in this area under load. The collar formed is an important component of the tree's rot and disease prevention system. If the branch is no longer required, the collar thickens restricting the growth of the branch so when the branch does eventually fall, a small hole is sealed quickly by the tree therefore preventing disease, infestation and rot.
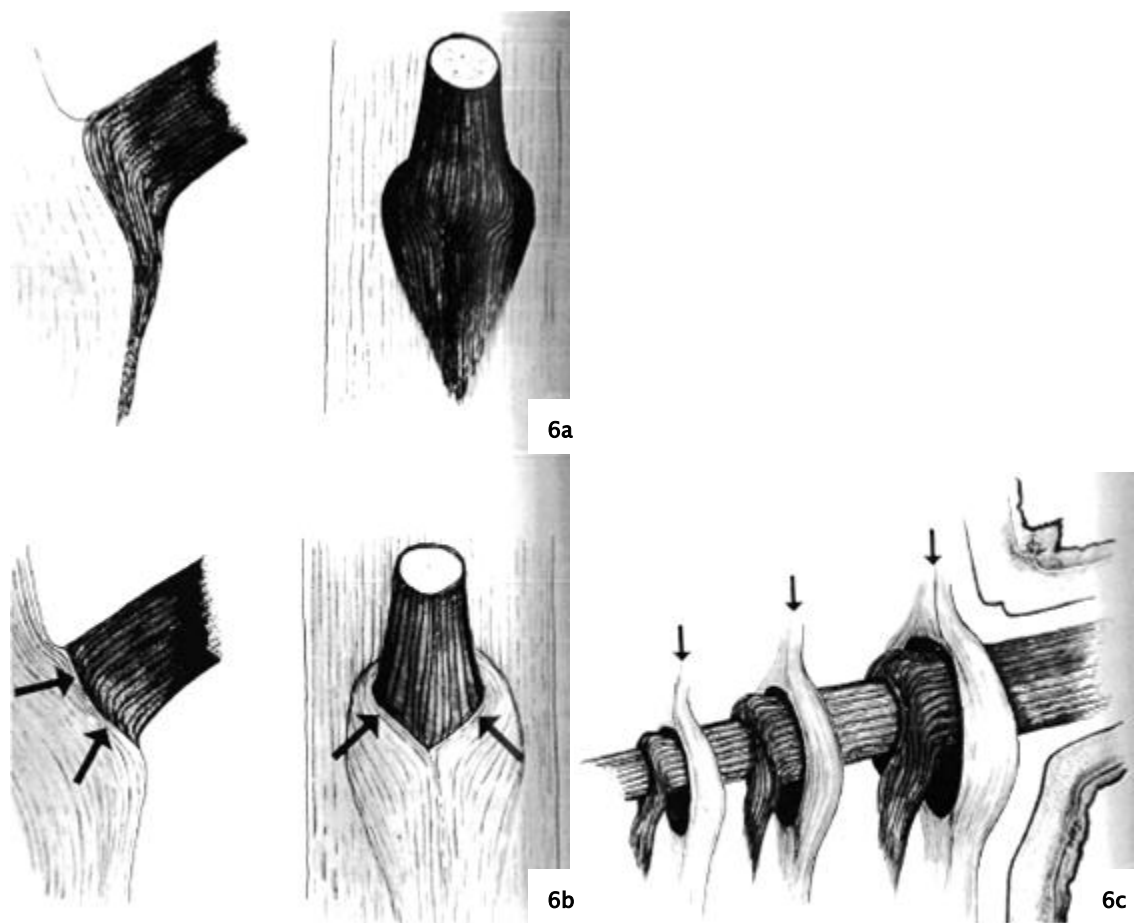
FIGURE 7: EXTRACT FROM SHIGO (1985) SHOWING MODEL OF BRANCH ATTACHMENT

2.5   Loading and Adaptation of Trees

Predominant loading in trees is caused by its self-weight and weather loadings, such as wind and snow. The self-weight (dead load) of a tree is

dependent on additional branches, twigs and leaves. The live loading can affect the tree in different ways depending on its environment. For instance, a tree in an open field will have large branches, whereas a tree in a forest would be slender with top-heavy branches. The branches creates live load settlement areas, however the branches are flexible enough to create aerodynamic forms to reduce surface load when needed.

Tree adaptation has been shown to overcome the most difficult of challenges. Mattheck (1991) has devoted a large proportion of his work to tree adaptation and found trees will bind together (similar to the idea in Figure 8, where the bark encloses around the bullet) in order to find enough light. Not only this, at each challenge, the tree's instinct to survive means it will continue to reduce its notch stresses in order to keep strong.
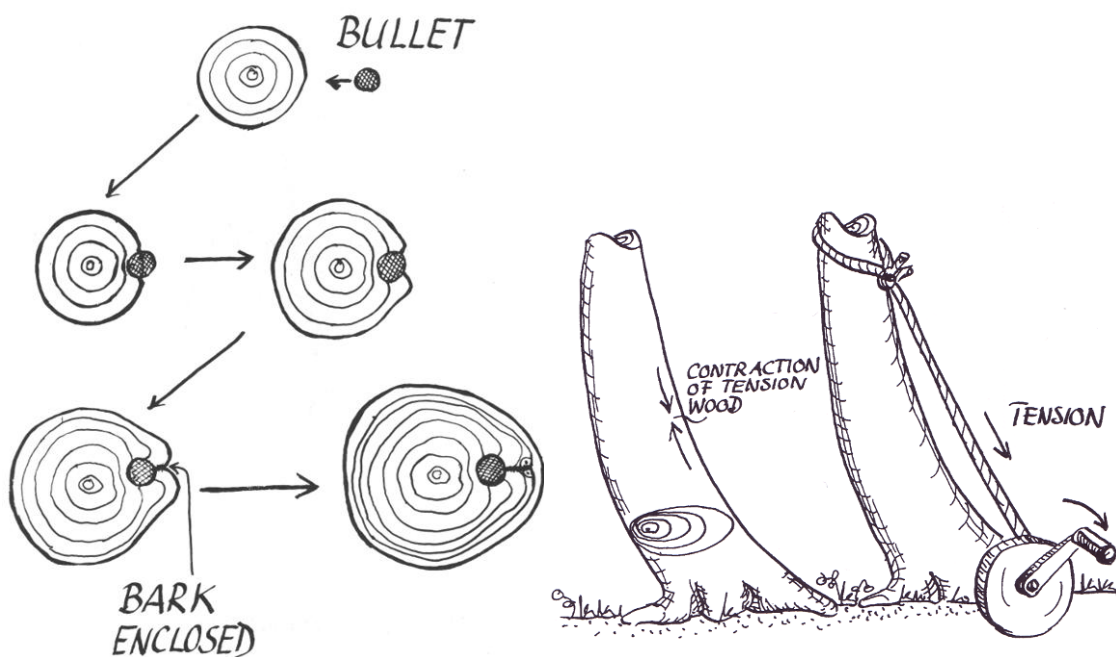
FIGURE 8: ADAPTATION OF TREE DURING GROWTH) EXTRACTS FROM MATTHECK (1991) TREES – THE MECHANICAL DESIGN)

18

The tree creates a structural material 'built for life' and thereby sustainable. Nature in its complexity has already invented the art of finite element analysis through trial and error of its evolutionary adaptation. The irregular cross-section of such trees throughout their structure will enable them to optimise to their environment. Mattheck (1993) found the safety factor of a tree has been predicted through field studies at 4.5 in the stem, yet only 4 in the branches (based on safety factor = failure load/service load). The discrepancy between these values seems to be appropriate, allowing the tree to lose branches in preference to the trunk if necessary, encouraging later growth and reducing further damage to its dominant light absorption position.

2.6   Mechanical Properties of Timber

Different tree species have diverse mechanical properties but generally have high tensile strengths compared to compression. The structure of a tree is pre-stressed due to its adaption to the natural environment. The orientation of the fibres plays a part in the strength of the timber, with perpendicular to the grain being weaker than parallel to the grain when force is applied. Due to this timber is considered as an anisotropic material. Wood samples tend to fail by crack propagation in tension through fibre pull-out mechanism. The cellulose fibres (microfibrils found in the xylem vessels) are strong and wood has a high specific strength due its relatively low density. Timber is a reasonably stiff composite viscoelastic material. It is the microfibrils in the wood stretching/compressing during loading that provide the majority of the mechanical strength of the cell wall. Timber shows some viscoelastic behaviour which prevents excessive deformations on vibration loading, as a result of the lignin matrix, made of elastic (instant response) and viscous (slow response) regions. This combination creates creep and this movement reduces the stress

incurred on the wood. This is shown on loading and unloading of a timber specimen where the load curves do not correspond.

2.7   Moisture Effects on Mechanical Properties

Moisture content will affect the strength of the timber (dried tree sections). Increasing water content lowers the strength and stiffness of timber. The moisture content of a living tree can be up to 200% of the dry mass. Timber used in construction tends to have 20–25% moisture content. The strength and stiffness of timber relies on the extra toughening of the helical winding of the cellulose microfibrils. The moisture within the timber causes the cell walls to expand, this softens the cell wall. Hydrogen bonds in the cellulose can break and form with the water, as this is a stronger more favourable bond. This untangles the fibres allowing them to stretch further. The separation causes fewer cellulose microfibrils per unit area, making the cell wall easier to buckle and reducing the timber's strength.

Vafai and Farshad (1979) showed the modulus of elasticity of the tree varied depending on the moisture content: high moisture would give a low modulus of elasticity. Mencuccini *et al* (1997) discovered there was a significant positive relationship between Young's Modulus and wood specific conductivity of hydraulic content. The growth of the tree accommodated simultaneously mechanical and hydraulic needs. The increase in photosynthetic rate is normally due to more foliage, which requires larger support and nutrient uptake. The variability in Young's Modulus value could be increased by the reduction of inclination angle of the microfibrils. Cannell and Morgan (1987) tested branches to find the Young's Modulus of living sections. Their work involved cutting sections of tree and load testing them. The sections were

found to have lower values of Young's modulus than the trunk dependant on the moisture content. The strength of the tree can only be theorised without further load tests.

As moisture content is a key factor in structural property testing, a brief research project was conducted by the author, which can be seen in Appendix 1. This concluded wrapping a fresh-cut sample in cling film gave the best moisture retainment in cut timber.

2.8   Summary of Biology and Structure

Trees grow and adapt their shape and structural form in order to maintain maximum food production, while adapting to the imposed loads that result from this need. This is a fine balance, as the overproduction of material in the tree can be costly to its dominance within its environment. In general, tests on tree structure are conducted using cut samples, with timber being taken from the main trunk of the tree. By testing only parts or samples of the tree the interaction of the entire tree may not be represented. Taking into account the moisture content within the tree seems to impact the strength of the tree, with lower levels causing greater strength and reduced elasticity. Moisture content retainment during sampling was of concern during any proposed tree tests.

3. Review of Research in Tree Loading and Branch Breakage

Trees, so far, have emerged as a solution to well-being and sustainability due to having interesting shapes, structural forms and behaviours. This chapter will review the work of previous authors who investigated the structural behaviour of trees under loading. The chapter concludes with the current work that is developing in the structural timber industry. The review leads to a conclusion on the need to further investigate branch attachment known as 'global joint'.

3.1   Whole Tree Behaviour

Recently, the application of engineering and biology has combined to improve understanding of the true potential of trees. The research work is progressive and theoretical due to the complex nature of the material, limited technology and combined knowledge in either discipline but has enduring theories from the late 1800's. In this section, an overview of some of the international work in tree stability and structural analysis is shown. In particular, aspects of tree superstructure behaviour in response to load actions will be looked at as this is the main concern to the public's visible perception of trees and tree failures in urban areas and can cause major court case disputes. To reiterate a previous point the main loads, excluding self-weight, that affect the tree structure are the live loads incurred through weather effects such as wind loading. These are the main cause of instability in the tree outside of disease risks. However, this is not to discount the instability caused through tree root failure, which will be touched on.

Trees are natural structures which are maintained and cared for by skilled arboricultural workers. Trees can be seen either as a crop or as an aesthetic feature. This means there is considerable biological research on the health and yield of trees in forests and in open sites. The Bendtsen (1978) literature review looked at the differences in properties of wood in natural and 'man-made' forests, to improve the intensive forestry industry. It notes juvenile wood has lower mechanical property values than mature wood. Wood mechanical properties are not uniform but change as the rings age. In making 'man-made' intensively grown forests, proportions of juvenile wood are higher than a natural forest due to quick growth. This means current practices will need to account for greater juvenile wood proportions.

3.1.1 Internal Canopy Wind Loading

Mattheck and Bethge (2000) created a simple method to estimate the wind load experienced by a tree, which was developed to find the bending moment in a global joint, to help dimension mechanical aids for trees. The research assumes wind load to act mainly in the crown of the tree. When the wind acts on the crown branches, they turn away from the wind to reduce the surface area presented, see Figure 9. As the tree develops branches, different drag coefficients are formed due to the changing cross-sectional area.
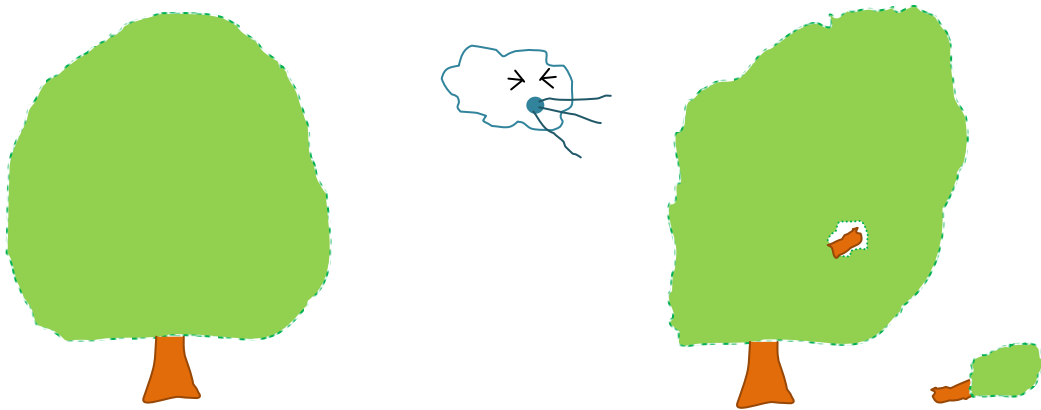
FIGURE 9: SKETCH COMPARISON OF TREE CROWN REDUCING SURFACE AREA AS WIND
LOADING OCCURS RESULTING IN BRANCH BREAKAGE FAILURE (WINDTHROW)

Blackburn *et al* (1988) found windthrow (a result of breakage failure) is too
complex to ever calculate critical windspeeds, though an estimation of dynamic
load factor could be taken. The statement came after displacement controlled
tests were conducted with a winch attached to the trunk at 70% of the tree
height (where the centre of mass was assumed). A Tirfor winch was used to
conduct;

1. a static test to find the deflection curve, weight distribution, and
   maximum turning moments
2. a dynamic test in which the tree was alternately pulled and released
   while being monitored by attached accelerometers.

The research concludes some of the winch methods were inaccurate, such as
measuring the displacement with accelerometers. It concluded the internal
gusts within the canopy made the calculation difficult.

Baker (1997) used a Laser Doppler Interferometer to obtain the power
spectrum of tree velocity under wind loading. Data on natural frequency is
measured using a laser-based technique where a suitable point of reference
was targeted on the tree. The method proved to be useful to find natural

frequency and showed preliminary results in line with previous research. Hassinen *et al* (1998) developed a new prism-based technique to monitor the movement of trees which was found to be successful and portable. This technique was tested in the lab and compared to the common accelerometer measurements. The new technique was developed from marksmanship technology and is based on transmitters and receivers. More recently James *et al* (2013) has developed an inclinometer with GPS technology which can record the movement of the tree during stormy conditons.

3.1.2   Common Tree Stem Failure

Papesch *et al* (1997) established incidence of stem breakage increased where soils are deeper as this allows greater root development. Their experiments winched the trees horizontally and analysed results to determine a relationship exists between maximum resistive bending moment of the tree and measures of size such as height, diameter at breast height (DBH) and stem volume. Uprooting failure was heard in the roots via audible 'popping' as the load increased rapidly with increased stem deflection.

Pong (1956) discovered the breakage point occured at the DBH point on hardwood trees, here the stress was lower than his calculated prediction of maximum stress. The report was commissioned to find the loading for and damage extent on broken and uprooted trees, to give probablistic predictions of future wind damage. The methods conducted were winch tests of 24 trees of which there were 6 species. The test samples selected were straight undefected trees from the Pisgah National Forest, North California in the summer of 1952. Once broken, strategic cuts were made in the stem to investigate the failure characteristics. The data was then used in calculations

which applied Young's Modulus for greenwood. The variabilty of specimens is admitted to give slight changes in calculation answers. During testing, steady drops in force occurred before failure. All specimens tested failed with equal failures of stem breakage and uprooting occurring at similar loads, see Figure 10.
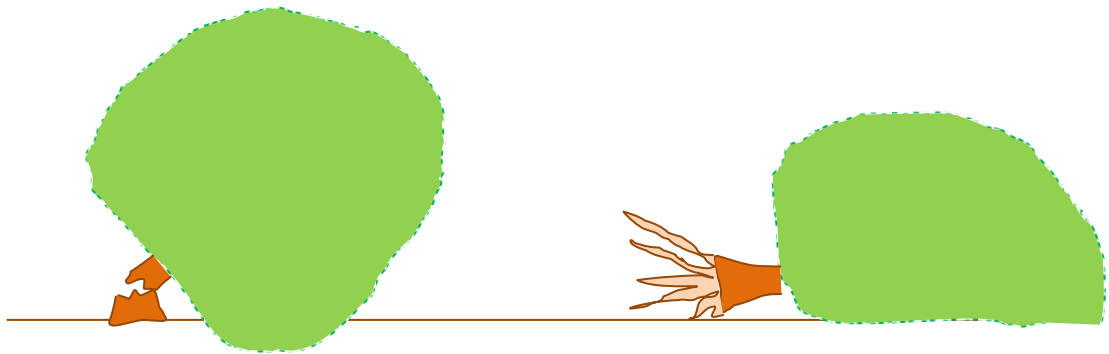
FIGURE 10: TREE FAILURE TYPES: STEM BREAKAGE AND UPROOTING

Fons and Pong (1957) furthered winch tests to prove uprooting tended to occur on poor sites (rocky soil) and stem breakage on good sites. The tests were conducted to predict tree breakage characteristics after nuclear explosions by looking at the energy necessary to cause breakage or uprooting and the extent of damage. The report sets out preliminary measurements required before winching, winching technique and shows the use of the ring dynometer for load measurement. Some failures occurred at knot clusters, although uprooting and breakage happened at the same order of load magnitude.

3.1.3   Live Load in Tree Branches

Cannell and Morgan (1989) showed bending moment failure was found to be linearly related to the cube diameter at midpoint of the branch when the branches were subjected to snow/ice load. Heavy snow load was measured by

removing snow off the lower branches of pine trees and weighing it. Ice was measured by melting the ice off tree samples. Sample lengths of branch or stem sections were cut from trees to find the bending moment at failure by loading them as a simply supported beam. Theoretical bending moments applied at the base of branches, before and after snow/ice, were calculated using a computer program that assumes the branches and laterals (secondary growths, see Figure 11) were horizontal. An increase in diameter increases the bending moment at the base of the branch but the moment is well below the visible failure. Deflections of branches with no laterals exceed 15% of their overall length before failure and with laterals 4% deflection is achieved. The tapering of the branch investigated previously by Morgan and Cannell (1987) showed many small laterals from a branch at a steeper angle to the horizontal are more stable within the tree structure. The centre of mass of these combined laterals is brought more in-line with the base support of the cantilever, allowing the loading direction to be closer to the centre of mass of the stem.

The author conducted similar test work, shown in Appendix 3 where it was found problems with sample stability and cut meant overall behaviour of the tree branch cannot be truly ascertained without a more intensive test set-up and measurement technique. Although the researchers have looked into the structural performance of the tree branch, no tests have yet categorically concluded the global joint structural performance mechanics, a connection of the branch (secondary growth) to the stem/trunk (primary growth).
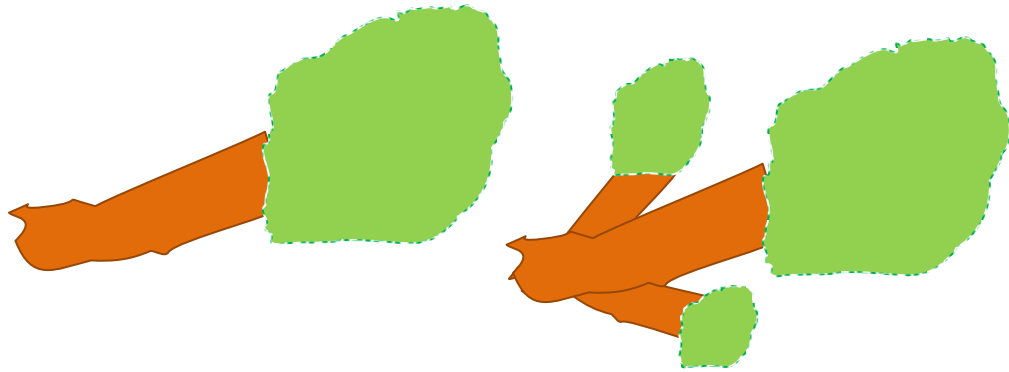
FIGURE 11: TREE BRANCH WITH NO LATERALS ACHIEVES 15% DEFLECTION (LEFT), BRANCH WITH TWO LATERALS ACHIEVES 4% DEFLECTION (RIGHT)

3.2   Whole Tree Internal Structure and Performance

The fibres within the tree provide its structural support. These fibres are small components in a greater structure and any changes within them could change the structural performance of the tree. The following elaborates on research of internal components of the tree previously touched on in Chapter 2.

3.2.1   Medullary Rays Under Load

Burgert *et al* (1999) showed medullary rays orientated their direction to be parallel to the applied load under longterm live testing (Figure 12:) and were proved to provide some structural strength as well as the storage and transport functions previously known about. The investigation applied a radial stress to live trees followed by tangential strength tests on disks cut from the trees, to find the evidence of a strength function of rays.
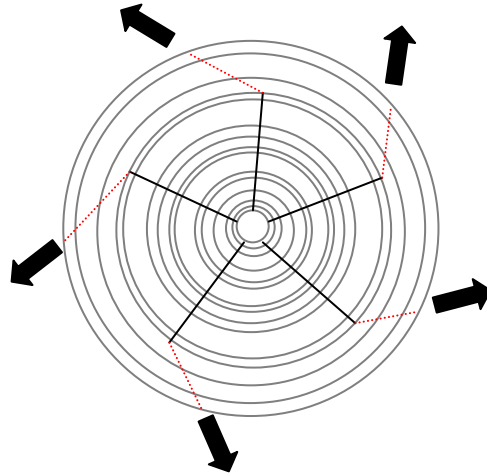
FIGURE 12: INDICATIVE SKETCH OF MEDULLARY RAY CHANGE IN ORIENTATION (SEEN IN RED) DUE TO APPLIED RADIAL LOADING

Reiterer *et al* (2001) investigated influence of nanostructure in the crystalline cellulose molecules (found in the cell wall) on tensile strength. This showed small microfibril angles had smooth surfaces indicating brittle fracture and large microfibril angles torn leaving jagged surfaces. Deformation parallel and perpendicular to tensile load applied parallel to the grain was shown by X-ray scattering techniques.

Burgert and Eckstein (2001) found tensile strengths of rays are larger than the axial tensile strength of non-ray wood. Tensile tests performed on isolated wood rays in Beech showed their contribution to radial strength. Larger numbers of rays were found to give a higher radial modulus of elasticity. Reiterer *et al* (2002) discovered rays were found to be underestimated in the mechanical influence on the tree. An investigation compares transverse behaviour of rays in Oak and Ash. The saturated samples were tensile tested in the transverse direction (radial strength - ray parallel to force). The tests showed the trees had distinctly different properties of radial and tangential strength due to large numbers of radial rays contributing to mechanical strength.

3.2.2   Spiral Grain

Spiral grain is one case of adaption where the tree fibres will rotate forming a helix-type structure that stands strong against the prevailing wind direction (Figure 13). The spiral is caused by the tangential fibres (directioned normal to fibres running up the stem) forming a helix about the stem. Skatter and Kucera (1997) found this uniform spiral grain is produced to increase the tree's torsional strength. The cause of spiral grain according to Kubler (1991) is the root ball having a dry side, hence the spiral supplies a uniform distribution of nutrients from the root to the rest of the tree. In either argument, the spiral grain helps the strength response of the tree allowing it to bend and twist more, therefore offering less wind resistance and reducing the likelihood of overloading which leads to breaking. In asymmetrical cases, torsion applied in the opposite direction to the spiral may cause failure (effectively untwisting the spiral). The shear from torsion is in the same direction as the bending stress which causes critical stress on the tension side in bending and causes the spiral to open as it untwists. Calculations of the maximum shear stress can be made by superimposing bending and torsional stresses.
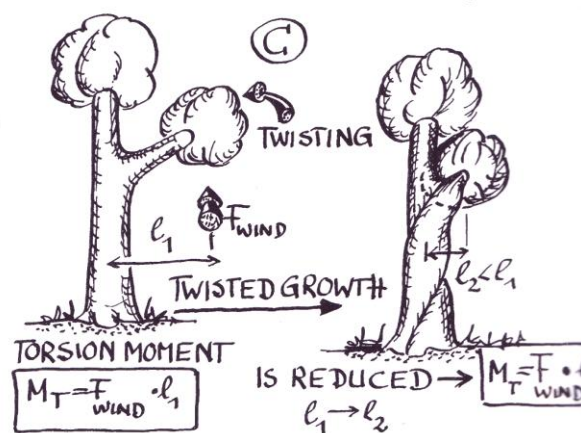

FIGURE 13: TREE SPIRAL GRAIN CAUSED BY PREVAILING WIND (EXTRACT FROM MATTHECK (1994)'S THE BODY LANGUAGE OF TREES)

3.2.3   Optimization

Environmental changes cause optimization seen during the plant's life. This leads to different designs which represents a multiple solution to a complex individual problem. Farnsworth and Niklas (1995) implied plant structure optimization is limited by genetics and environment resources. Genetics uses evolution to adapt to a long term changing environment, and means the adaptive growth (required for optimization) is a balance between genetics and individual environments.

Mattheck and Burkhardt (1990) and Mattheck (1990) found an easy method of predicting the 2D or 3D structural morphology of the tree based on the plausible assumption of self optimised biological structures. This copies the ideals of tree growth in a computer simulation to reduce notch stresses (concentrated stress points) and provide lightweight fatigue resistant construction. This was achieved by showing the load history of the tree to have been recorded in the outermost ring which adapts to external loading. Using this idea, a Finite Element Model (FEM) was utilised to produce a reasonable adaptive design proposal for an existing tree under loading. The FEM reproduces the creation of outer rings with smaller Young's Modulus than the core of the tree. This outer surface layer is simulated as elastic to allow the surface to swell. The surface is converted to a thermal model in order to allow the swelling to occur without inclusion into the existing core. The thermal model equates to the constant von Mises stress based program which runs until notch stress reduces or the design constraints prohibit further dimension changes. The initial parameters of the program are limited to personal judgement as the tree cross section cannot be seen without harming the tree or intensive measured observation. Albrecht *et al* (1995) carried out finite

element models on three trees and calculated internal lateral tensile stresses which were then measured in the actual tree using cored samples. A fractometer was used to measure the strength of lateral core sample wood, finding lateral strength increases where the FEM predicted. This concludes the idea the tree reacts to high stress by a growth reaction.

3.2.4   Predictions of Structural Properties of Trees

The ability of a tree to optimise its design can be shown through some of the morphologies found in tree design. Koizumi and Hirai (2006) evaluated the irregular shape of the tree cross-section by finding the section modulus using binary images. This type of analysis does require the felling of the tree to evaluate the true cross-sectional section modulus. Once analysed, the effect of the section modulus was shown to be critical to the wind response of the tree.

Tests of tree strength have been conducted using harvested samples. Cannell and Morgan (1987) tested branches to estimate the Young's Modulus of living sections. It was proposed the bark does not contribute to the structural strength but cannot be ignored as a characteristic of living trees. Young's Modulus in live trees is smaller than in green sawn timber from mature trees and variation in results could be accounted for by the specific gravity and moisture content in the sample. Young's Modulus decreases with increased moisture content over the previous notional fibre saturation point. Investigations of the Young's Modulus along the grain (parallel) in fresh living sections of tree have limitations such as the wood not being homogenous and therefore only approximately elastic. When testing to timber standards, clear span specimens were difficult to find and therefore shear strains also were accounted for. The samples were assumed to have a uniform taper. The

Modulus of Elasticity was measured by a bending test and the shear deflection was accounted for so that a 'true' Young's Modulus could be derived by assuming $E/G=17$.

Vafai *et al* (1979) showed high moisture content would give a low Modulus of Elasticity. To validate this, five living Chenar trees in Iran were tested on the tension and compression side of the stem and simple beam theory used to analyse the results. An outline method used to find the Modulus of Elasticity in living uncut trees onsite is given and is aimed to correlate the structural properties in trees. The method uses a hydraulic jack to apply a concentrated load to living trees and measures the bending strain with electrical strain gauges. Results were then correlated with linear elastic cantilever beam theory. The stress-strain relationship gives a good positive correlation enabling the modulus of elasticity to be found. The inherent moisture relation results came from live loading on the tree stem showing the tension and compression modulus of elasticity and hence the bimodularity of the tree. The tests were limited in sample size and had discrepancies with the comparative data.

Bruechert *et al* (2000) used observations to verify a prescribed model of mechanical performance. The Flexural stiffness (EI) is mainly altered due to stem dimensions affecting second moment of area, I. Bending strength is based on morphological characteristics. EI varies more than Young's Modulus among stands observed. Self-loading in tested tree stems indicated safety factors were unsafe against buckling. EI of the stem decreases with increasing stem height due to the stem getting younger and more flexible the higher from the base. There is a lower Modulus of Elasticity toward the pith. The research does admit interaction of wood or global behaviour can be lost by creating smaller samples.

3.2.5   Summary of Whole Tree Research

Reames (2005) has shown structures can be cultivated from trees. This idea was expanded on by Terreform (2008), who used the idea to create a theoretical living house. The structural capability of the tree is a relatively diverse and an unusually complex research area. Not only does a tree support its own weight, it copes with live loading imposed by weather conditions. The structural ability of the tree adapts to change with the varying layers of material, moisture content and the environmental effects. Analysis and new technologies have been researched to standardise this complex organism. More recently, Mattheck has been looking into the mechanical design of trees and finding ways to investigate the structural behaviour of the tree. Further understanding of the mechanical response could create more feasible maintenance programs for managed trees.

Computer Tomography (CT) scanning or electron microscopy are the most common methods for analysing fracture failures in timber, exampled by Reiterer *et al* (2001). This can only be achieved in a laboratory. Since progressive failures can really only be analysed at specified points in time during a test, this type of technique, although useful for theoretical confirmation, is impractical and expensive to apply industrially for the maintenance of trees.

Previous research on trees and timber has been conducted and this work has been used to develop British Standards and government reports. This instructs on ways of testing and grading cut timber, seasoning it to suitable standards for use and provides codes of practice for preservation and management. The Lonsdale (1999) report, for instance, looks into the pre-requisite symptoms of tree hazards and advises how to undertake remedial action. The Mattheck

(1998) report on the natural design of trees is so far the only one found by the author to be a known guidance on the structural design of trees. In Mattheck's work a finite element model has been created based on the plausibility of self-optimised biological structures which have the ability to reduce notch stresses and provide a lightweight fatigue resistant structure. Further test work conducted by the author, shown in Appendix 2 and Appendix 3, has given some preliminary ideas as to the complex nature of branch testing. The irregular nature of the tree influences the load response. These lessons in testing persuade the test methodology of future experiments.

3.3   Tree Global Joint Research

Research results and acknowledged methodologies exist for understanding the tree's global response to its environment (as discussed in the previous sections). Wind load causes uprooting of trees or breakage of stems, it is the environment and type of tree that determines its fate. , there is a phenomenon in trees that is limited in structural knowledge which is global joint behaviour. Branches have caused serious injury and economic loss to the urban environment and sometimes they are known just to fall off trees in what is called 'summer branch drop' (Harris (1983)). The attachment of a branch to the primary growth has already been discussed in section 2.4, however the strength of this connection termed a 'global joint', could be deemed a flexible fixed end and is still not truly understood. If the tree is taken as nature's largest cantilever, there must be some merit in understanding how the global joint supports its multitude of cantilever branches.

Any previous work on structural branch connections has been international, diverse and limited. As such, a comprehensive study is required to give a basis

for future research and commercial work. An outline will be given from the currently recognised research and expanded in conjunction with later chapters. Although according to Mattheck and Kubler (1997) a tree adapts to its environment to prevent any hazards, like any other living organism it's susceptible to severe conditions. With branches observed failing close to the junction of the primary growth, investigation into the failure of the global joint is paramount. This review shows work has previously been undertaken and aims to be a concise source of reference for future work on the structural properties of tree branches.

To the author's knowledge there are only a few other scientists who have published in the tree global joint connection area. Shigo (1985) developed a fundamental knowledge on branch attachment that is an accepted model used around the world. Cannell and Morgan (1989) found branches with lots of short secondary branches reduced the need for support material, compared to a branch with fewer but longer secondary branches. Müller (2006) found homogeneity of strain was present in the cut tree joint under loading. Finch (1997) highlights the safety risks of experimenting on tree branches during his investigation of natural pollarding. Kane (2007) and Kane *et al* (2008) tried to estimate the branch strength through test works and have estimated equations for branch strength. Slater (2011) is currently developing understanding of included forks, and has recently disputed some of Shigo's previous works.

Lonsdale (1999) alluded a tree often prefers to shed parts of itself (if possible) in preference to complete failure. This is where the hazard of trees can become problematic. Trees respond to wind by damping the load through their structure (in essence out of phase branch movements) as investigated by James (2010), though it only does this up to a point. At ultimate load, the tree starts

to fail and this can happen in heavy wind conditions, or if the tree is affected by disease. Moore and Maguire (2004) have derived equations to find the effects of natural frequency and damping ratios of trees when loaded. Normally the tree sheds its load to reduce the effect of excessive wind or disease by dropping a branch. This is particularly problematic in urban areas where large branches have the potential to land on people or property.

3.3.1 Branch Attachment

Mattheck (1998) expanded on the work of the biologist, Shigo (1985) who showed the branch development at a decisive angle to the primary growth. As previously explained in Section 2.4, a hole or 'notch' is created at the top edge of the branch join due to the base development providing the link to the tree system. Internationally there is a disjointed collaborative effort to research this area of tree biomechanics and therefore there is no internationally recognised benchmark for testing.

Further investigations into grain orientation in branches have been done by Kramer and Borkowski (2004) indicating the morphological implications of branch creation affect the hydraulic transportation performance through the xylem. Müller *et al* (2006) demonstrated the internal branch/stem interaction showed a homogeneity of strain distribution achieved by natural shape optimisation, material properties and fibre orientation. The strain field was measured using 3D Electronic Speckle Pattern Interferometry (EPSI) during the loading of a loaded half global joint (*i.e.* a global joint cut vertically to provide matching halves) and an identical cast polyester model (Figure 14). Comparisons of the strain fields showed the cast model had localised increased strain intensities compared to a near uniform strain in the harvested

tree joint. The levels of sophistication within the joint system suggests tree material property cannot be treated homogeneuously.
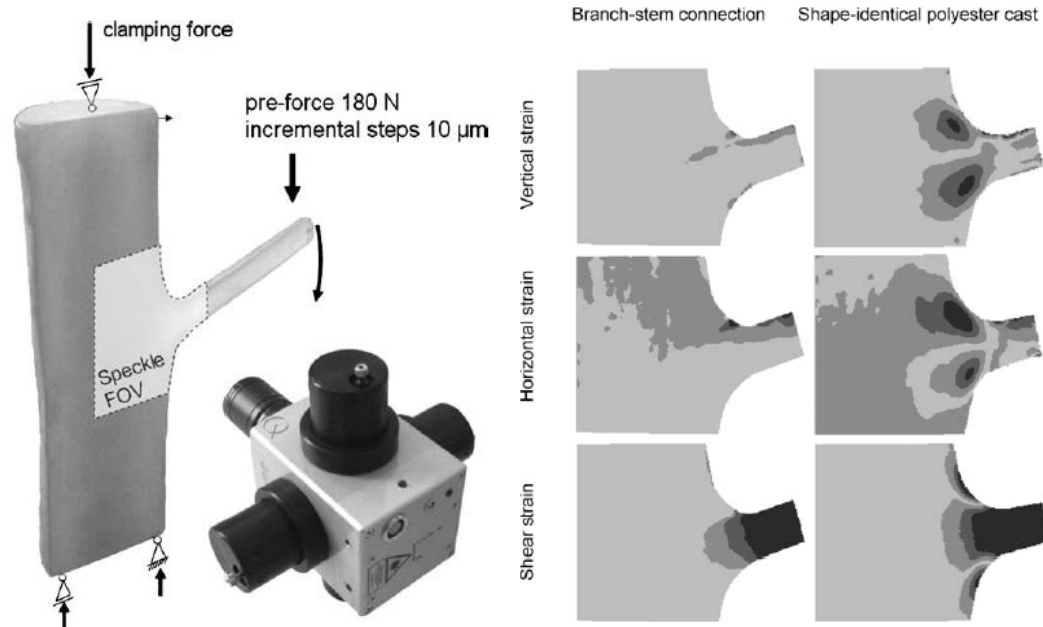
FIGURE 14: HOMOGENEOUS STRAIN DISTRIBUTION IN A LOADED GLOBAL JOINT COMPARED TO UNHOMOGENEOUS STRAIN DISTRIBUTION OF UNIFORM MATERIAL OF SHAPE IDENTICAL CAST POLYESTER MODEL(EXTRACT FROM MÜLLER *ET AL* (2006) INVESTIGATION)

The healthy branch usually breaks in one of two ways either socket tear out at the collar (Figure 15a) or as branch fracture near the connection (Figure 15b). In the author's previous study (shown in Appendix 4) the socket tear out failure appears to be more frequently observed to the laboratory set-up, with the branch failure heading toward the pith of initial growth. In this failure, described by Shigo (1985), the fibres fail in tension on the upper crotch surface and by the compression on the lower surface.
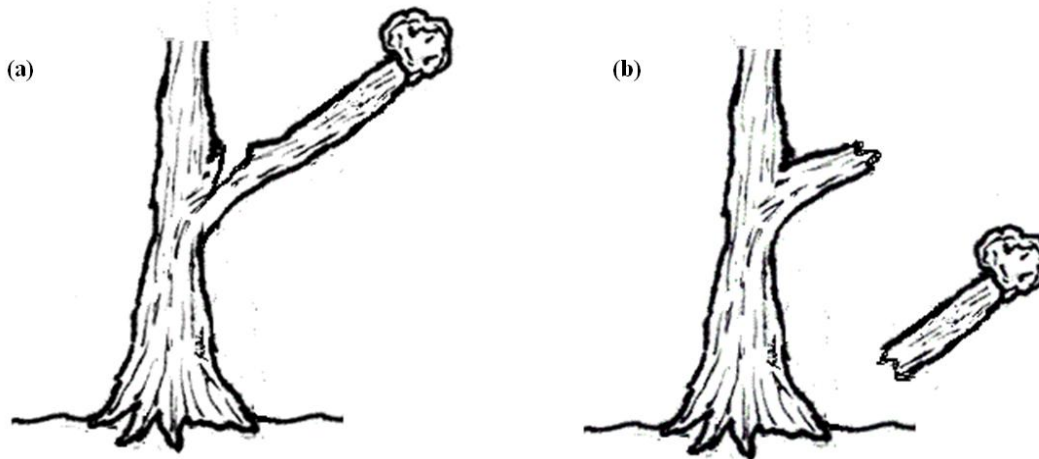
FIGURE 15: BRANCH FAILURE (A) SOCKET TEAR OUT (B) BRANCH FRACTURE

The most accepted argument of branch attachment at present is that of Shigo (1985), whose biological investigation showed how branches attach to stems and the resulting conduction effects. The investigation found the piths of the stem and branch did not meet, proving branches do not initiate from the centre of the stem and the branch's vascular vessels and rays are shown to be at right angles to those of the stem. On loading, the 'crotch' connection broke forming visible cracks in the cambium. This suggested the branch tissue forms the initial collar at the base of the branch/stem connection and the stem tissue then surrounds it in the late season creating a 'ball and socket' shown in Figure 16a.

This work has recently been disputed by Slater and Harbinson (2010) who question the orientation of the vessels. The division of fork and branch they state to be artificial, meaning there is a cross-over of continuum in the flow of vessels. Their hypothesis states a dense xylem zone is created in the upper part of the attachment as a spur on breakage (seen in Figure 16b), not merely as a zone of packing tissue as previously stated by Shigo.
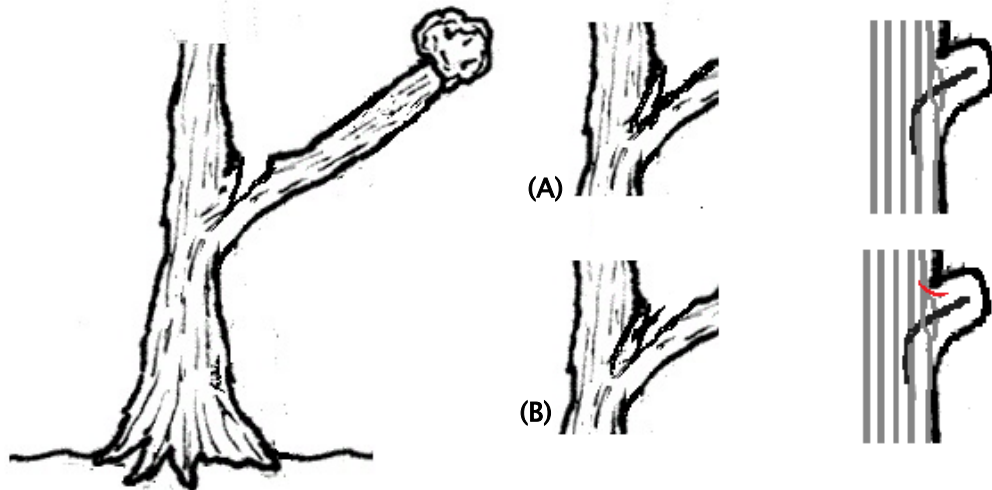
FIGURE 16: BRANCH FAILURES SHOWING ATTACHMENT STYLE; (A) SHIGO'S BALL AND SOCKET FAILURE SHOWING NO CONNECTION OF THE CROTCH, (B) SLATER'S CLEVER CLIP FAILURES SHOWING CONNECTION FIBRES EMANATING INTO UPPER CROTCH (SHOWN IN RED)

Slater (2011) alluded to awareness of lack in research and literature on branch strength and is continuing to work on creating a better model of branch fork attachments. Timber properties are well investigated on clear (no knots *etc.*) specimens, but in global joint investigations the specimens are likely to have changing grain direction and some defects such as knots. These features are currently under investigation by Slater (2011) who is using X-ray Computer Tomography scanning procedures to determine the wood density and grain orientation of the xylem in the forkwood and stemwood. Slater has so far found there are:

"less than half the number of vessels present and approximately 20% more cell wall material within its [the forkwood] volume than the adjacent stemwood".

This research is being further developed through global joint testing to find the effect of internal structure on the strength of the fork and any inclusions at the University of Manchester, UK.

3.3.2   Cantilever Effect of Branches

Morgan and Cannell (1987) modelled the cantilever of the tree branch mathematically by means of smaller divisional elements so the varying tapers and loads on branches can be incorporated into Engineers Bending Theory. The Engineers Bending Theory formulae will only work if the shear force, bending moment, angle, deflection and loading conditions are known and if the cantilever is divided into enough elements so as to have deflection and angle differences between them that are negligible. As previously discussed, Morgan and Cannell (1988) state when the Centre of Mass of a branch is directed towards the bottom of the branch base (toward the joint, see Figure 17), this reduces the material required to support itself. This is achieved when the lateral growth (side shoots on the branch) are closer to the branch base. Lots of short laterals require less support material (implying smaller basal diameter) than a couple of long laterals. In addition, the larger the angle from the horizontal, the less basal support material is required on that lateral. Cannell and Morgan (1988) showed large material investment is made in new shoots and it could be argued branch wood evolves approximately optimally. A computer program based on calculations from the previous Morgan and Cannell (1988) shows this adaptation.

FIGURE 17: TREE JOINT SHOWING THE BRANCH'S CENTRE OF MASS IS DIRECTED TOWARDS THE BASE OF THE CONNECTION

3.3.3   Morphological Branch Design

A popular notion is branch patterns have evolved on trees to optimise photosynthesis. However, an optimal mechanical design model has been researched by McMahon and Kronauer (1976) who investigated the length and mid-diameter of each link (between twigs) of living standalone trees and adapting them to the concept of order numbers used in the Strahler system. The examination of morphological data from several tree species resulted in three doubly-tapered power-law models for branching structures which imply different design principles. The elastically similar model provides the best fit for all species tested. This means what is true for the branch is true for the whole tree (in proportion).

3.3.4   Global Joint Strength Tests

The term 'Global Joint' used in this project refers to the entire cut connection of the branch (secondary growth) and the stem (primary growth), so as to have three cut ends (as seen previously in Figure 17). The investigations by Kane *et*

al (2008) used harvested tree joint samples to determine breaking characteristics. This categorised three failure types:

- flat surface – stem splits longitudinally in half

- embedded branch – wood associated with the branch separated from the stem, leaving groove in the stem

- ball and socket – branch pulls out of stem.

The test involved pulling apart the joint using the upper growths, and found the morphological measurement of branch diameter and branch length attachment at the main stem were predictable measures for breaking strength. The results do not however show conclusive predictability and suggest that other variables are required for better prediction. However the calculations can be used for preliminary investigations.

3.3.5   Live Joint Tests

A 'Live Joint' is similar to a Global Joint, however in this project it is termed differently as it is not cut from the tree but is tested *in situ*. Miller (1959) observed as the crotch angle (see Figure 18) decreased the percentage of branches breaking at the crotch increased, but it did not make them weaker. It was further found there was a greater correlation between branch size than crotch angle and that narrow angles would fail by bark inclusion, which disproved MacDaniels (1923) previously accepted theory.
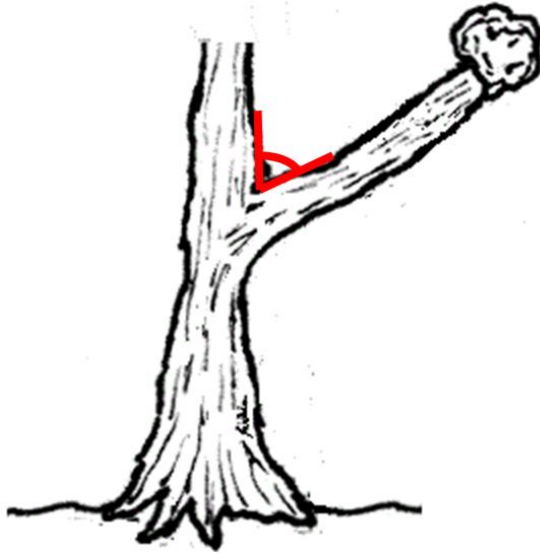
FIGURE 18: CROTCH ANGLE (SHOWN IN RED) OF GLOBAL JOINT

Gilman (2003) highlights previous investigations show the force required to break the branch joint decreased as aspect ratio (ratio between primary and secondary growth sizes) gets closer to one. Gilman investigates the strength and aspect ratio using small diameter branches of red maple (*Acer Rubrum L.*). It was found there was no relationship between angle of branch attachment and strength. Instead the branch attachment correlated with aspect ratio and branch diameter, meaning the larger branches require more force to break provided they are small compared to stem. However the exception was co-dominant stems (forks) that were easier to pull apart. Gilman does conclude these small specimens were like *'pulling a screw from a piece of wood'* and therefore suggests the maturity and limited growth of the branch may have affected the results.

Lilly and Syndor (1995) found no correlation to specific gravity or crotch angle of bending stress during winch tests of live trees. Finch (1997) researched the winching of branches which were in danger of shedding in public areas. This involved the need to weaken the limb by cutting into the stem in order to get

the winch to pull off the branch to produce a natural looking fracture. The experiments gave a mix of results depending on the conditions of the tree and also highlighted awareness for the health and safety implications of these tests.

Kane (2007) investigated branch strength in Bradford Pear, culminating in calculated equations for stress. The investigation on live tree branch winching concluded that neither taper, angle of attachment or wood properties influenced the stress in the joint but the aspect ratio did. Further investigations into the harvested joint morphology and breaking strength by Kane *et al* (2008) categorised three socket tear out failures mentioned earlier.

-

-

-

Again they found breaking stress was best predicted by aspect ratio rather than the ratio of inside-bark branch diameter to width of attachment, *i.e.* the closer the aspect ratio the more similar diameters the lower the stress. Even though these ratios showed correlation they are still not accurate predictors of wood strength.

3.3.6   Summary of Tree Joint Research

The attachment of the tree joint has only recently come under scrutiny but the discrepancies in research results are likely to do with species and the adaptation of the tree joint as development occurs. *In situ* structural testing of the tree joint could help to clear up these discrepancies. However, this type of test is highly hazardous. Onsite live testing has shown uprooting or stem

breakage of the tree could occur and therefore extensive precautions must be taken. Instead tests tend to be conducted on cut joints, but these tend to review theories and have not demonstrated exact ways in which to calculate the failure load of the joint. However, it has been suggested the joint's complex design has a homogeneous strain on a 2D vertical cross–section through its centreline. Reassessment of tree joint strength from a structural prospective could help to clear up the contentions in theoretical and previously tested ideas. The author has already successfully investigated the possibilities of testing the tree joint in a structural laboratory as seen in Appendix 4. This is used as a base for further investigation.

3.4   Fundamental Timber Testing Technology

The research review so far has only looked at the tree as a living structural organism. To understand the research context of this project it is prudent to verify its place within the greater timber/tree industry. A brief overview of standards and current research themes of cut timber will follow and this will help to further guide the testing and technologies involved in timber research.

3.4.1   Current Testing Standards

There are generations of timber research related to the construction industry which have been transferred into standard codes of practice. Mechanical properties obtained have been set within the British Standard convention such as BS5268. BS5820 gives a brief overview of the requirement of testing, with BS EN 408 giving the standards of testing and presentation of results. With these standards there are model sample sizes and grading requirements to determine the type of timber under testing. The grading is a function of the defects in the timber specimen that may otherwise cause structural defects in

cut timber under loading. Standards are updated regularly and some research has been conducted under preceding standards that have similar procedures. Lavers (1967) refers to BS373 when explaining the procedure for timber testing. Timber structures have been extensively investigated under engineering research commissions by such institutes as TRADA technology which has led to timber standards and codes of practice all over the world. However, some old techniques, knowledge and technologies of the timber industry have been lost in time.

3.4.2   Current Research in Timber Technology

It can be seen from the establishment of British Standards the fundamentals of timber in construction are known. This leaves timber research to follow trends such as sustainability and composite design.

Vukotic *et al* (2010) researched the embodied energy of timber compared with steel, with blockwork infill design for a school sports hall and drama studio. This showed for a timber construction option a slightly lower value to that of steel, 2.47GJ/m² and 2.50GJ/m² retrospectively. However, when the total embodied energy and carbon emissions of construction materials were examined, the timber design accounted for 79% and a 178.5kg CO_2/m² compared to steel's 88% and 254.8kg CO_2/m². The work consequently concluded timber structures were a better option for whole building life cycle.

Glulam is a composite material of timber and involves layers of timber being stacked and glued together. This technique and material is not new to structures however, the exploitation of its usability has not been fully achieved. Frese *et al* (2012) demonstrates this when testing the compressive strength of spruce glulam, a fundamental idea that suggests low moisture content glulams

should be considered in current standards for compression values. It is possible to create a composite material that is comprised of only timber. O'Loinsigh *et al* (2012) found a way of using dowels in layers of timber instead of glue like a glulam beam. This type of wood-only construction could improve the fire resistance of composite timber structures while creating greater stiffness than un-joined layers of timber.

Composite construction in timber can be efficacious as presented by Adam and Milner (2012) where three round log stringers were used with a plywood deck. This bridge deck design showed a potential to develop high strength and stiffness due to the composite action under load testing. Multi-material composites such as concrete with timber have been shown by Dias *et al* (2011) to have potential for bridges. The timber and concrete work together combining their strengths in tension and compression to form a timber beam supported concrete deck. The full scale testing of this model demonstrated it to be a viable option of timber bridges due to high stiffness and efficient transverse load distribution.

3.4.3   Image technology in Timber

Timber is used as a component within composite material design. In some cases as described by Godara *et al* (2008), wood fibres are used to mechanically interlock with maleinated polypropylene. This influences the micromechanical behaviour, helping the material to deform further without breaking. Godara *et al* (2009) used Digital Image Correlation (DIC) to find the structural integrity of a composite material reinforced by natural wood fibres. Although the test did not solely use wood, the idea of using a photogrammetric technique to find strain at a micromechanical level is shown

to be successful. The localised strains within the composite material were qualitatively analysed and strain mapped. The results showed the strain of the material was affected by the percentage of the wood fibre reinforcement, the optimum percentage of the composite material being around 75%.

Choi *et al* (1991) proved an early version of image analysis technique would be an ideal method in investigating the dimensional stability of wood and paper. The work showed how digital image correlation could show the strain over two video images of wood/paper under load tests. These images were taken with a microscope with the wood/paper surface painted, a limitation was the overall distribution of strain through a tested sample.

Calculations of stress concentrations in timber using fracture mechanics principles can be problematic depending on the points picked in the sample. Franke *et al* (2007) developed a strain analysis technique using Photogrammetry. Measuring marks were applied to a timber sample under load testing to determine the changed coordinates through a series of images. The measured area of the sample was kept small to give clarity of progressive deformations. The results of the investigation showed values of strain close to that of the theoretical calculation, showing that FEM could successfully evaluate load bearing performance of timber.

Traditional wooden structures need to be maintained for architectural heritage. The techniques needed to analyse the structural integrity must be non-destructive, accurate and minimise manual-labour cost. Cameras or laser-beams can be used to measure the geometry of a structural object avoiding the need for physical contact and access. In order to create a 3D geometric model, Armesto *et al* (2009) photographed an old timber roof from different positions with each position being expressed to a common perspective centre. These

images were then brought together to form a 3D model suitable for FEM and hence give more data point certainties for structural integrity analysis under loading.

3.4.4   Summary of Testing Timber

Timber is considered a sustainable material for use in construction. There are abundant studies into timber that have led to this complex material having its own industry tested standards and codes. This means current timber research tends to embrace new frontiers of research such as the ideas of carbon footprints and composites. It is with composites real material efficiency is shown and timber due to its fibrous nature and tensile strength can be easily combined with other materials to form new material designs. This leads to new possibilities in construction with timber. To add to the techniques of measuring timber image techniques are gathering more momentum within research and it has started to show possibilities of strain measure within composites.

3.5   Overall Review Conclusion

Living trees or cut timbers are a complex fibrous material under which this research is proposed. Current standards show its use with concrete, soil, and steel, using the latest technologies. This research therefore concentrates on the fundamental stress-strain behaviour using new technology but applied to trees and freshly cut timber. As can be seen, there is limited research in the field of tree joint strength and no affirmed predictable way of finding tree joint strength. Filling this gap in knowledge is the target for this research project.

Work into the strength of tree joints is ongoing and growth deviation manifestations such as inclusions are part of this complex investigation. Oak is the most recognised hardwood species within the UK, which the author intends to investigate further as there is an availability and native species near to the University of Southampton. Even though the works of Slater appears to coincide with the author's investigation, and may even overlap in areas, it is important to note that the primary aim of Slater (2011) is to investigate tree forks and not branches. Although these are similar growths, it is more likely a fork will develop an inclusion and the outward growths may both be primary, whereas the author intends to look at branches with definitive primary and secondary growths. The author has conducted work on branch strength before which can be seen in Appendix 4. This has given grounding to the nature of the structure and testing problems that may be encountered in any methodology undertaken in the future.

4. Research Progression and Application

This chapter gives a brief summary of methods considered plausible to analyse the tree joint strength. It also gives an overview of the possible applications of this work. Of particular interest to this project is the orientation and arrangement of fibres in tree design during loading. This could be the answer to creating more effective, economical and sustainable designs in structural materials. By looking at the load response of trees, it may be possible to develop understanding of the mechanics of this natural material which could influence the maintenance programmes of trees.

4.1   Methodology

A joint in a tree is a supporting component of a large cantilever that manages to respond to extreme loads to prevent failure. When considering the extent the branch reaches out with its limited 'fixed' end span, the achievements of the tree structure can really be admired. The design of this area is intriguing to any Engineer. In order to understand the ability of this natural structure, the tree joint will be looked at as cut internal components and further modelled as a whole global joint cut from the tree. Using these divisions will help to find a true understanding of the cut global joint design through strategic testing. Using this method allows for further work to improve the predictive indicators of the global joint failure and better designs in structural materials.

4.1.1   Component Method

By looking at the internal design of the tree joint, it will be possible to assess the interaction of reaction wood within green untreated wood and the

interaction of ring spacing as the branch attaches to the primary growth. Using British Standard engineering tests for timber material, it will be possible to evaluate the components by known and practiced procedures and find an effective comparison between green and standardised structural green wood. In addition with the samples being taken from the cross-section of the branch and stem, an idea of the seasonal ring variants and failure mechanisms can be found, on which a model can be formed. The results from the components will be recombined to form a global joint to show overall interaction. Therefore the model will show an idea of the internal working of a cut green section of global joint based on experimental evidence which followed developed standard experimental practises.

4.1.2   Particle Image Velocimetry Method

To understand the deformation of the timber component during testing it would be better to gain an overall picture of movement in the fibres, as opposed to just singular numeric values of strain or displacement. Investigating strain in timber is difficult due to its multi-fibrous composition, developing stress concentration points and moisture changes that affect its strength and robustness. Electrical strain gauges could be compromised by moisture moving on the surface of fresh cut timber as indicated in Appendix 5 tests and machine measured strain could be compromised by surface fibres tearing under pressure. A fundamental investigation using PIV will be conducted on timber. This should address the issue of trying to measure strain of the timber during testing.

4.2   Potential Applications of Research

The testing stages described allow for development of a previous model that has been adapted and changed to suit new findings. In this development, each stage generates its own model that forms a basis of understanding the tree load response in each test.

Having found test models that emulate the principles of tree design, the findings can be used to adapt international methods of material design and sustainability initiatives and material usage efficiency. These tests are at an early stage of development and are a base for future international test works. However, the works provide possibilities for many areas of sustainable building resources and urban cooling.

4.2.1   Tree Maintenance Development

Tree Houses-Permaculture or Living Architecture

In evaluating the strength of a tree joint it is possible to start assessing the types of structure that could be created in the tree(s) that would allow for both recreation and aesthetics and be safe and stable areas to retreat to in wild environments. Trees used to be the habitat of our ancient human ancestor. They provided shelter and safety from the wild environment and in some under-developed parts of the world this is still true.

Urban planning and maintenance

Better understanding of joint strength and behaviour can aid the use of trees in combating urban cooling by adding load response information to the maintenance toolkit for management of healthy growth and where necessary preventative maintenance reducing potential litigation. Urban cooling is an

issue for many towns and cities all over the world. The heat and emission of the buildings and people in such a confined space add to the lack of sustainability and the cost to the world's climate. A popular solution to this issue is to plant trees in parks and along roadsides of urban areas, using the tree's transpiration process to reduce heat accumulation. However, the culture of urban society means if the tree is to fail in an urban area, there could be a possible economical loss. Consequently, this means investment in maintenance programmes to ensure public and property safety has to be made. It is common the branch will fail in preference to the whole tree, so having an idea of the loading a tree branch could take will help in assessing whether remedial action is required.

Building Resources

Education in tree maintenance and management will be a useful investment for the global future. This will reduce the need for artificial building resources. Sustainability comes at a price between the balance of economic demand and exhaustive resources. Balance is only found through the social view of viability and economic impact. Through better tree management, forests and sustainable cities can start to become a viable concept across the globe.

4.2.2   Further Timber Use

Addition to green timber knowledge

The component testing will provide further data on green timber, giving further knowledge on how ring adaptation and 'imperfection' affects the grading strength. The effect of loading can be assessed and give an idea on

how loading affects the properties of sections of untreated green timber in aerated conditions.

Using joints in structural application

Through the proposed testing of joints, an idea of their strength could lead to finding a structural use for joints and branches which are currently seen as waste zones in the felled tree. This would add to the sustainable credentials of the managed forest and further influence the argument to use as much of the natural resource and reduce wastage. There is a possibility to even use the joints as connection points in structural carpentry.

4.2.3   Future Technology

Biomimicry – Using the knowledge of material design to adapt design

By developing a model of the fibre and structural arrangement of the tree it would be possible to improve structural and material design. The alignment and arrangement of the tree fibres could influence a more economical and sustainable design in new materials. By creating materials that have optimum properties, a sustainable structural enhancement can be achieved. By creating new structural connections and components which apply nature's design, implementation of a lasting and sustainable design can be initiated.

PIV Technology in Timber

Developing existing test techniques to determine the strain effects on timber can only lead to more options and accurate representation of the behaviour of timber under loading. Not only this, if repeatable, it could lead to the development of monitoring techniques of existing timber structures to indicate any future deterioration.

4.3   Summary

Although this research can be seen as a small drop in the vast ocean, it creates possibilities for naturally obtained sustainable builds, this development of tree joint knowledge has the possibility of alleviating some of the world's urban and resource issues. In learning from the natural form of the tree's structure it is conceivable to enhance the design of infrastructure, in order to create a more sustainable and stable solution to built environment design. The three developed experimental tests described should indicate how the internal working of the joint and the overall joint arrangement react to loading in a safe and scientific laboratory environment, with some reference to real application. By creating models from the three progressive experimental tests on tree joints, a deeper understanding of the load response can be developed. Further, the fibre arrangement and the adaptation of the tree can be used to develop more economical, sustainable and stable designs for structural builds. Hence, the developed knowledge derived by looking at what nature has already provided, allows a true sustainable possibility.

5. Development of Particle Image Velocimetry (PIV) on Timber

Particle Image Velocimetry (PIV) is an optical method of measuring movement of particles which initially was used for measuring speed and direction of fluid flow. PIV technology is commonly applied to soil and other materials in order to measure particle positions between images (shown as pixels). So far as the author can find, this image technology has not yet been applied to timber under load, yet Mundell (2009) shows PIV can be used to measure structural movement. White *et al* (2003) measured the deformation in soil using PIV without markers. This trial validated that PIV demonstrated the precision and accuracy comparable to that of localised instrument testing.

5.1   Introduction

This chapter will show the development of a technique and code for strain measurement for timber utilising PIV, derived from existing techniques and code developed by David White of Cambridge University. The process of creating a successful strain measurement technique in timber will be progressively described. It will describe how the physical camera set-up needs to be thoroughly assessed in regard to the context of the loading test through to the process of evolving the coding technique to provide a robust assessment of the strain. This chapter especially highlights the progressions and difficulties encountered during the development of the PIV technique for the analysis of timber strain.

5.1.1   Use of PIV

Franke *et al* (2007) and Choi *et al* (1991) showed timber can be analysed optically using a film of coating whilst measuring specific target points. However, this does not provide an entire picture of the timber fibre interaction under loading. Features on the timber's surface will show a better strain distribution more true to its failure. PIV has already been proven to follow the development of movement through the biomechanical analysis of Hamza *et al* (2006) plant roots and strain measurements can be made of soil as shown by White *et al* (2003).

This PIV technique will be used to reduce the need to attach a separate strain gauge to each fresh cut timber component and give an accurate representation of the movement of grains and surface fibres during the test. The process for PIV experimentation is to take a 'before' and 'after' photo of a sample under load testing. These photos are then compared to show any movement between the images in both the x and y direction.

5.1.2   Existing PIV Code Basic Overview

For the development of the PIV technique with timber a current PIV code (based on White and Take (2002)) was obtained and used to analyse timber samples under load testing experiments. After each experiment, in-focus photos are numerically analysed. The code essentially sets up a grid over the sample photo and each square within the grid is tracked amongst the search zone parameters (a designated perimeter around each grid square for which the search between the two images is conducted). The 'Target Locations' either 'Active Area' and/or 'Fixed Point' are shown in Figure 19. The large blue zone marks the 'Active Area', a section of test sample over which this grid is set up.

The smaller blue zone is a 'Fixed Point' something that remains steady during the test. Having these points and by being able to move 'Active Area' zone accordingly, allows any minor camera movement to be corrected, giving more accurate results.
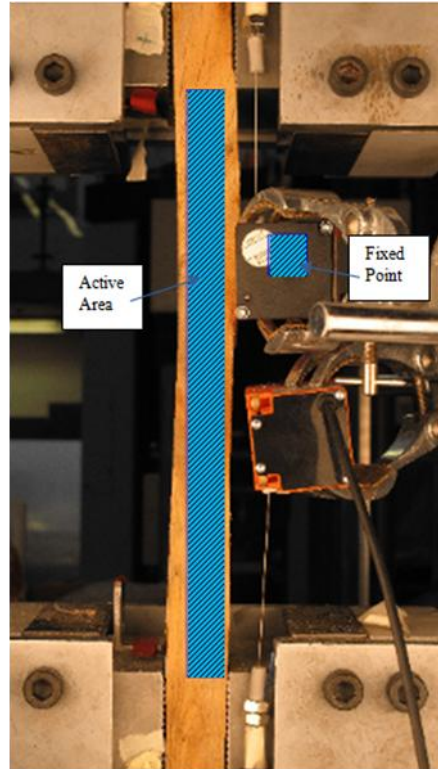
FIGURE 19: PIV MEASUREMENT TARGET LOCATION ("ACTIVE AREA" AND "FIXED POINT")
SETUP ON IMAGE OF TEST

5.2   Physical Test Set-up Methodology Development

Initially to explore the possibilities of using PIV and developing it further, a basic camera (Nikon coolpix 7600, 7.1 Megapixels) was setup parallel to the experiment sample B1's surface (see Figure 20) and an existing PIV Graphical User Interface (GUI) and program is used to analyse the images (Figure 21). The camera was fixed in place and was set to take photos at regular intervals during a tension experiment in order to detect change in movements as the load is increased. The sample was painted to provide a textured surface so that

tracking movements would be easier. The following subsections describe the trial and error development of the test set-up in order to create quality images fit for the PIV technique.

a)

b)
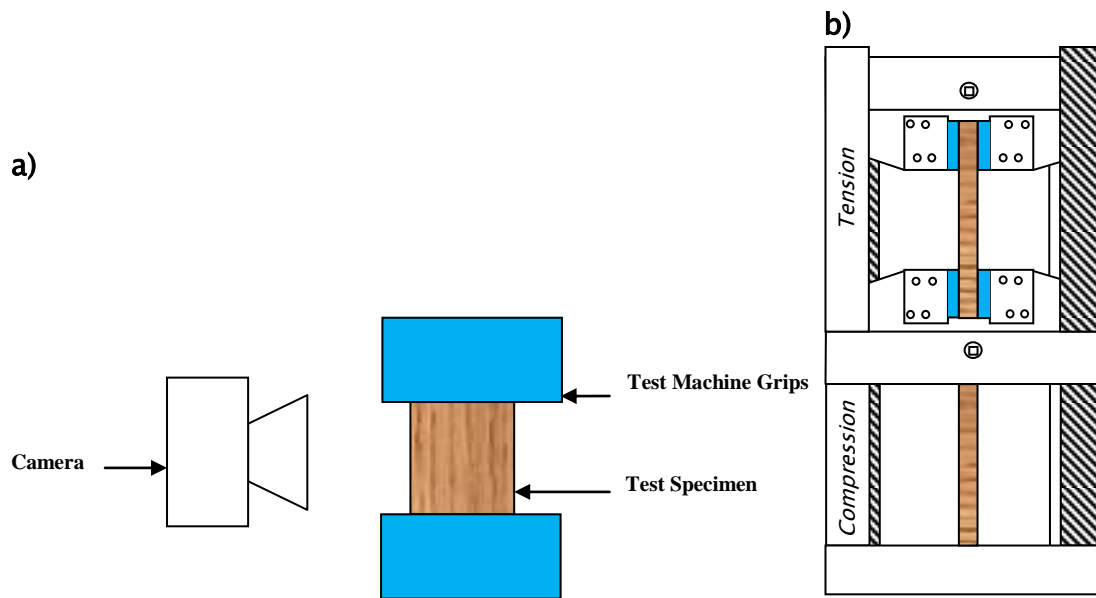
FIGURE 20: SKETCH OF INITIAL PIV TECHNIQUE TEST CAMERA SET-UP (PLAN VIEW (A)) AND RUBICON MACHINE USED FOR COMPONENT LOAD TESTS (B)
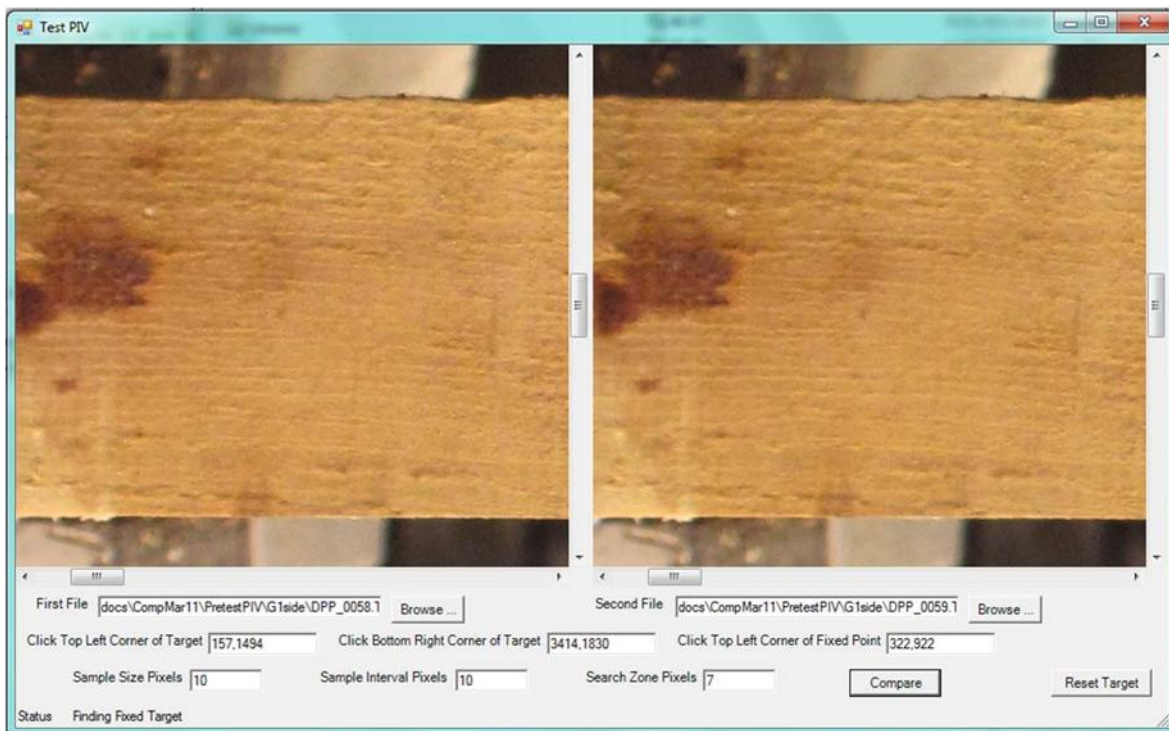
FIGURE 21: EXISTING GUI INPUT FOR PIV PROGRAM FOR COMPARISON OF TWO IMAGES

5.2.1   PIV Basic Overview

After the experiment, the photos are numerically analysed using an existing DJWhite April 1999 program code explained in White and Take (2002). The movements then need to be displayed in a way that can be interpreted easily. For example, a contour plot should show visual contrast of any breakage occurring under strain. Two image methods of analysis were done on B1 to determine the best way forward with the image strain, one looks at first and last image and compares them, the second compares each image in the test sequentially (in total an average of 40 images taken). There are two quantitative comparative strains obtained from the experiment, machine strain and PIV strain. The machine strain is obtained from the final Rubicon machine test measurements of displacement of the machine grips, ΔL, and the PIV strain is a mean of the sum of the individual movement values, δl, of each square. Hence the equations are:

EQUATION 1: $Machine\ Strain, \varepsilon_M = \frac{\Delta L}{L_0}$

EQUATION 2: $Rudimentary\ PIV\ Strain, \varepsilon_{PIV\ Rud} = \overline{\sum \frac{\partial l}{l}}$

From the sequence of images in Figure 22, it can be seen there are some minor issues with the set-up which could cause possible distortion to the results. There is a change in lighting on the sample B1 between images. Another undetectable issue is the image was a jpeg file and therefore may have been too compressed for accurate pixel data analysis.
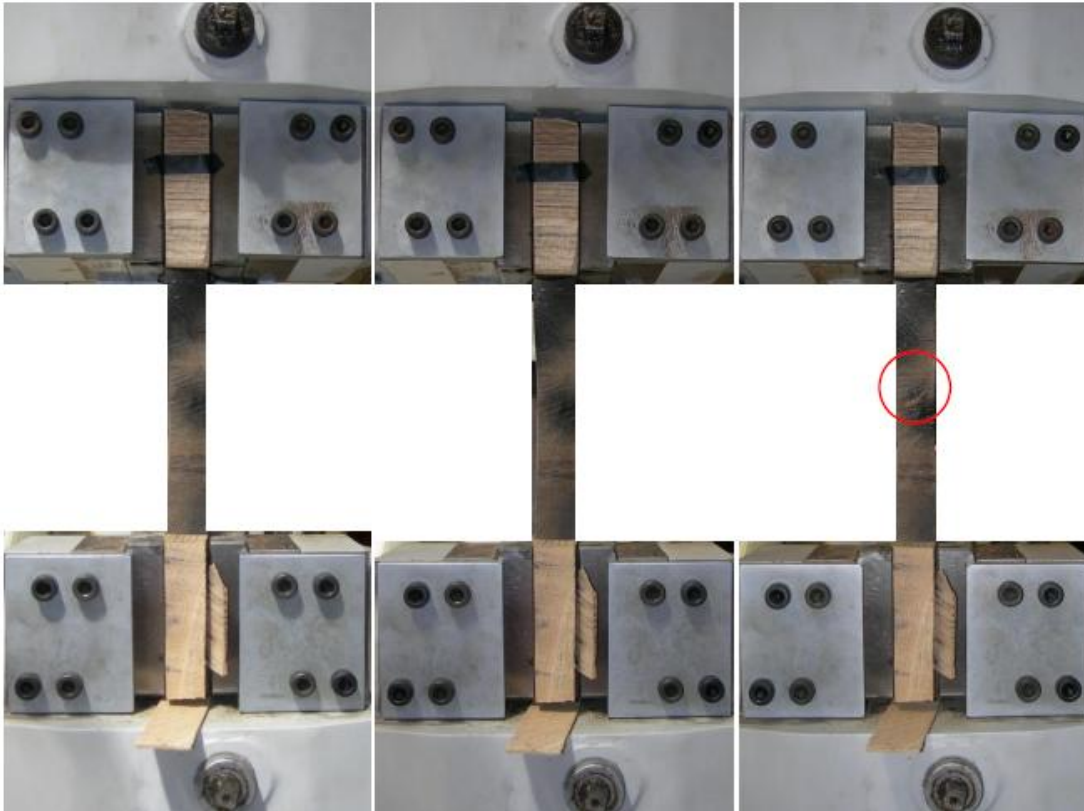
FIGURE 22: IMAGES TAKEN FROM TEST SEQUENCE OF PIV TENSION SAMPLE B1 BEFORE, DURING AND AFTER TEST BREAKAGE SHOWING CHANGE OF LIGHTING BETWEEN IMAGES (RED CIRCLE INDICATES FAILURE LOCATION)

5.2.2   Benefits of Sequential Analysis (Attempt 1)

The results from this test showed signs of strain and breakage from the basic Matlab fundamental code. The code calculated x and y movements which were converted into strain and rudimentary xy-directional shear strain calculated to show a better visual comparison with the sample breakage. From Figure 23, it can be seen the sequential comparison shows better results than the first-last image comparison. The sequential shows a similar pattern of horizontal strain to that of the breakage initially obtained on the sample. However, the precise location is hard to determine due to interference of the image and analysis style needing continuous comparisons. The first-last image comparison shows

the difficulty of predicting the failure using the image technology, as deformation of the sample under testing may go beyond the manually inputted search zone boundaries of the image used in the code. As a result, sequential imagery comparison will be done to show the progressive failure qualitatively. From the rudimentary calculation in Table 1, it appears the First-Last Comparison shows better final quantitative results, compared to the machine measured strain of 0.024 $\mu\epsilon$. Note, at this stage the PIV strain comparisons to the machine measured strain are indicative values (as the existing code determines the calculation)

 but the visualisation should start to have red colour tension concentrations around the failure at the centre of the sample.
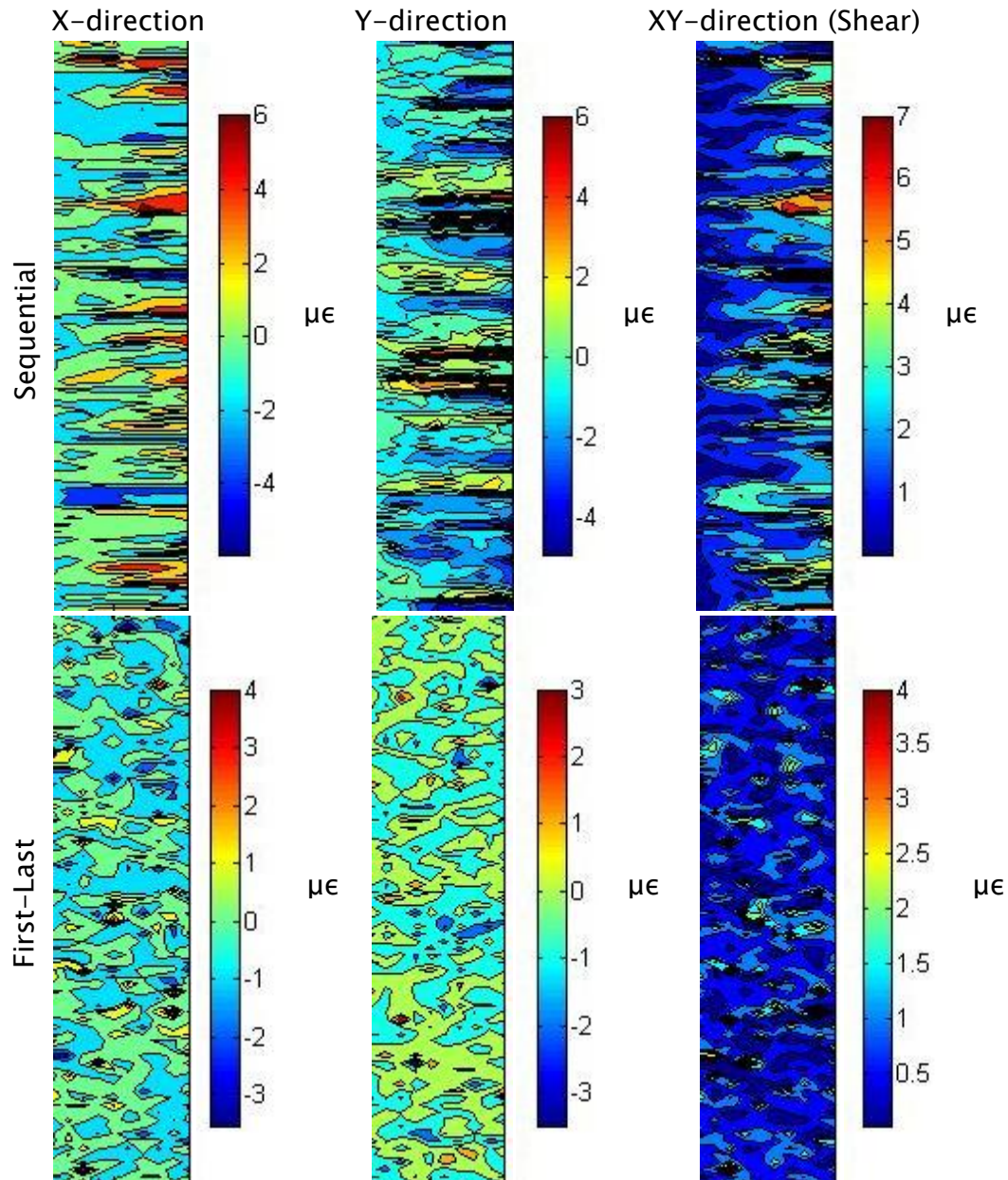
FIGURE 23: PIV RESULTS FOR X-DIRECTION STRAIN; Y-DIRECTION STRAIN; XY-DIRECTION

SHEAR STRAIN (LEFT-RIGHT) CONTOURS PLOTS OF SEQUENTIAL DATA ANALYSIS (TOP) AND

FIRST-LAST IMAGE COMPARISON (BOTTOM) OF TENSION LOADED SAMPLE B1

	Strain Result (µϵ)
PIV Sequential Analysis	0.2785
PIV First-Last Image Comparison	0.0516
Machine Measured Strain	0.0240

TABLE 1: SAMPLE B1 INDICATIVE PIV STRAIN RESULTS SEQUENTIAL AND FIRST-LAST FOR

COMPARISON WITH MACHINE MEASURED STRAIN RESULT

66

5.2.3   Increase in Image Quality (Attempt 2)

To increase image quality, a Canon Powershot G10 (14.6 Megapixel) camera was used and a better strain comparative set-up was carried out to show the accuracy of the data resulting from the PIV code. This set-up gathered jpeg and tiff image files during a compression test of sample B2 and also used a continuous lighting rig to reduce irregularity of colour within the image (Figure 24). The sample was not painted as it was deemed that the fibrous quality of the regular timber would provide the texture required to analyse the image (Figure 25).
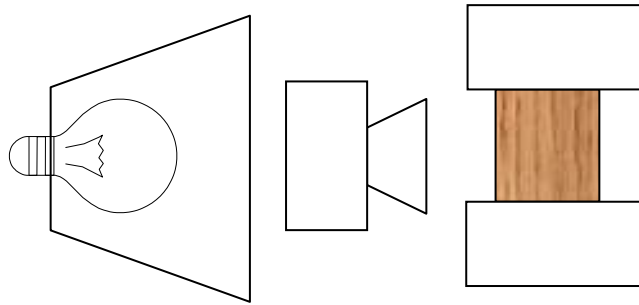
FIGURE 24: PLAN VIEW OF CAMERA SET-UP WITH CONTINUOUS LIGHTING RIG DURING COMPRESSIVE TESTING

FIGURE 25: COMPRESSION TEST SET-UP VIEW FROM CAMERA OF SAMPLE B2 BEFORE AND AFTER TESTING SHOWING COMPRESSION FAILURE AT THE TOP LEFT OF SAMPLE

The data acquisition improved under continuous lighting and the texture of the timber surface was sufficient enough not to need painting further. The failure nature of the compression test (crushing) meant the area of strain measurement for the image was narrow (localised failure at the top), this type of test should be avoided for now. It can be seen from the results in Figure 26 and Figure 27, the jpg and tiff images show slightly different contour results, as the jpg data had been compressed. Hence tiff images should be used to compare more accurately. The contours agree with the test breakage, in that the sample on the right hand side has had to stretch (increase strain shown in red) and the left side compress (blue) in order for the failure to be observed at the top of the sample. From Table 2, it can be seen the tiff showed an improvement in values towards that indicated by the machine measured value of 0.047 µε. However, further work needed to be done in the code.
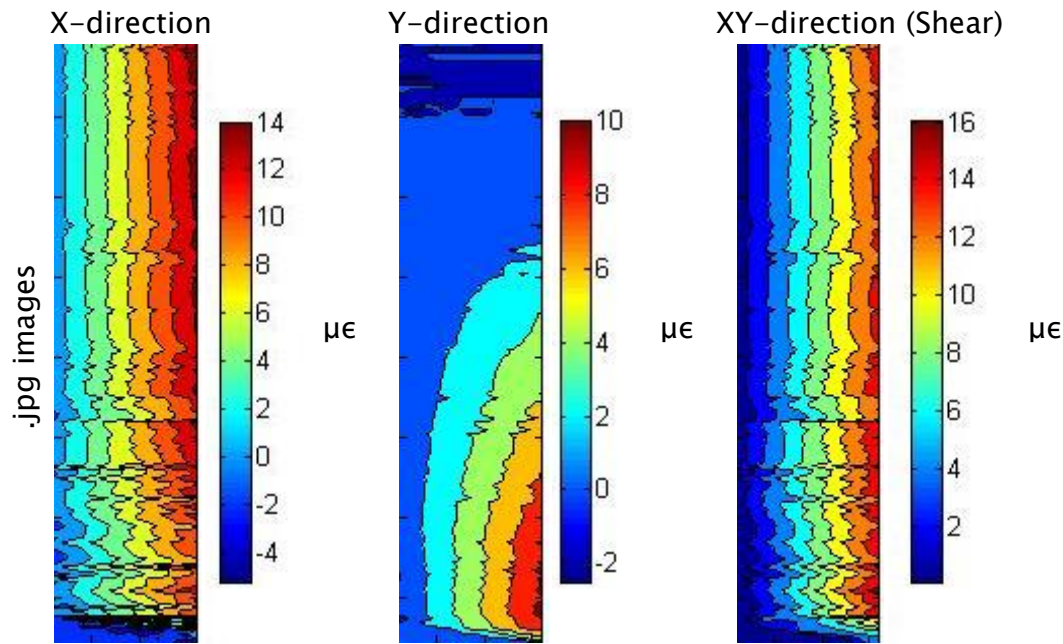
FIGURE 26: X-DIRECTION, Y-DIRECTION, AND XY-DIRECTION STRAIN RESULTS OF B2

SAMPLE OF SEQUENTIAL TEST WITH JPG TYPE IMAGE FILES
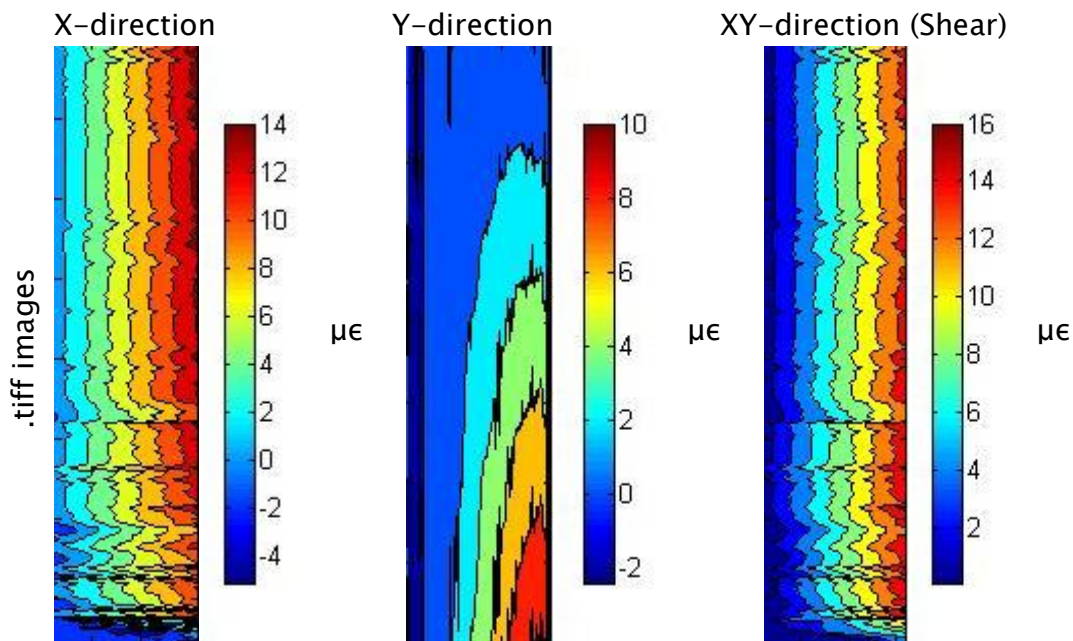
FIGURE 27: X-DIRECTION, Y-DIRECTION, AND XY-DIRECTION STRAIN RESULTS OF B2

SAMPLE OF SEQUENTIAL TEST WITH TIFF TYPE IMAGE FILES

	PIV Sequential Analysis Strain (με)	PIV First-Last Analysis Strain (με)
Sequential Analysis jpg	1.4438	0.0617
Sequential Analysis tiff	1.4387	0.0613

TABLE 2: TIFF VS. JPG STRAIN RESULTS OF SEQUENTIAL AND FIRST-LAST FOR SAMPLE B2

Rationally the sequential analysis should give the most accurate results as it compares the images over time, tracking small movements. Evidently there was a problem with the actual values of strain emerging. No more obvious improvements could be made to the physical experiment set-up so this suggested the current code needed to be reviewed.

5.3   Development of Code for Results

A Matlab® program, built from the base of the basic PIV Matlab code, was developed to automatically find better qualitative and quantitative results for a tension tested sample G1S. The original program from the DJ White code only analysed the subsequent images in turn creating a time consuming step-by-step measure of strain. This produced individual data results that then needed to be added. In addition, the target locations on the image were difficult to obtain accurately between subsequent image comparisons due to the input style of the GUI requiring user manual input selection. The following subsections show how the program was developed by having:

- an initial input screen (see Figure 28) that used the same target locations tracked throughout the image sequences, reduced any GIGO issue. This tracked all target locations using the PIV code in order to ensure the same target locations were being selected with each image.

- all images automatically ran so the individual results were combined efficiently. This meant no image is missed out of the sequence through user error and the final results were shown over time.

The DJ White April 1999 code primarily was used as a base as it is set to compare two images with each other, usually before and after failure. In this case, the idea was to follow the strain during the experiment by using this code to analyse sequential images taken during a sample's load test.
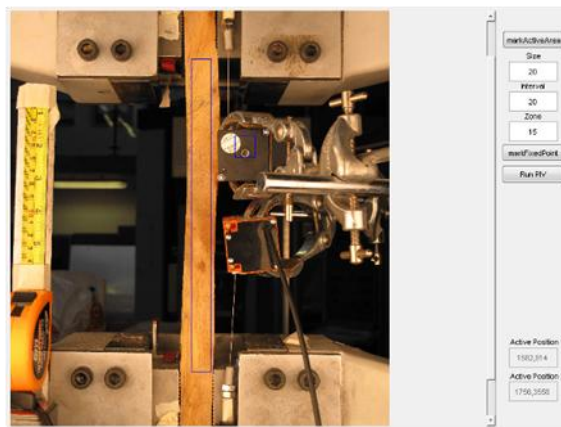
FIGURE 28: NEW GUI FOR INPUT OF PIV ANALYSIS IMAGES

5.3.1 Selecting Points on Image

The program code was developed to select in turn the next image in the sequence. However, any movement of the camera needed to be tracked to ensure that the Active Area is accurately being selected on consequent images. The Fixed Point was tracked using the PIV code in order to increase accuracy of the target selection. However the tracking style of the Fixed Point throughout multiple images needed to be decided. This means first altering the base code to analyse a sequence of photos.

There were two options for tracking the Active Area squares (see Figure 29);

1. Use the first photo as a reference point and track one Active Area from the first photo throughout the subsequent photos.

2. Track the change in position of the Active Area in every consecutive photo with the previous photo, updating it each time.

In the first option, it was likely the fibres tracked are changed in textural consistency as the load was applied thereby the square's colouration eventually changes too much to become accurate. The second option showed subsequent loading effects better but still incurred some minor textural inconsistencies. Both would have given values of change in length during the test in relation to the original length in the first photo. The second option was used to determine the strain, as this reduced the likelihood of strain measurement inconsistency but meant having to create a code that adds up all the movements together.
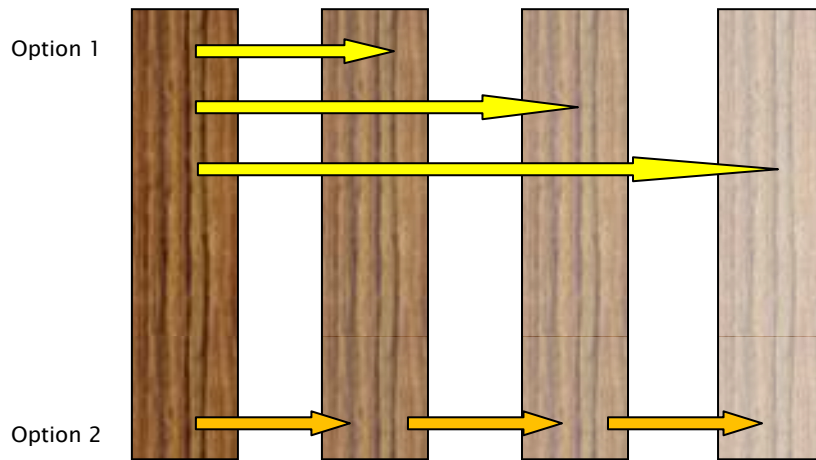
FIGURE 29: OPTIONS FOR TRACKING THE "ACTIVE AREA" STRAIN ELEMENT WITHIN PIV CODE AS THE SAMPLE CHANGES TEXTURAL CONSISTENCY

The same tracking options were then available for correcting any camera movements during analysis. In order for the subsequent images to be compared against the first original image, the Fixed Points of the original image were used against the subsequent images to determine camera

movements, see Option 1of Figure 30. The fixed point was not likely to change in textural consistency so Option 2 would not be required. Option 1's method meant the image in the zone of Fixed Point (along the dotted line in Figure 30) changed (if the camera moves), so the camera movement is only related to the original image (so errors were taken into account in calculations).
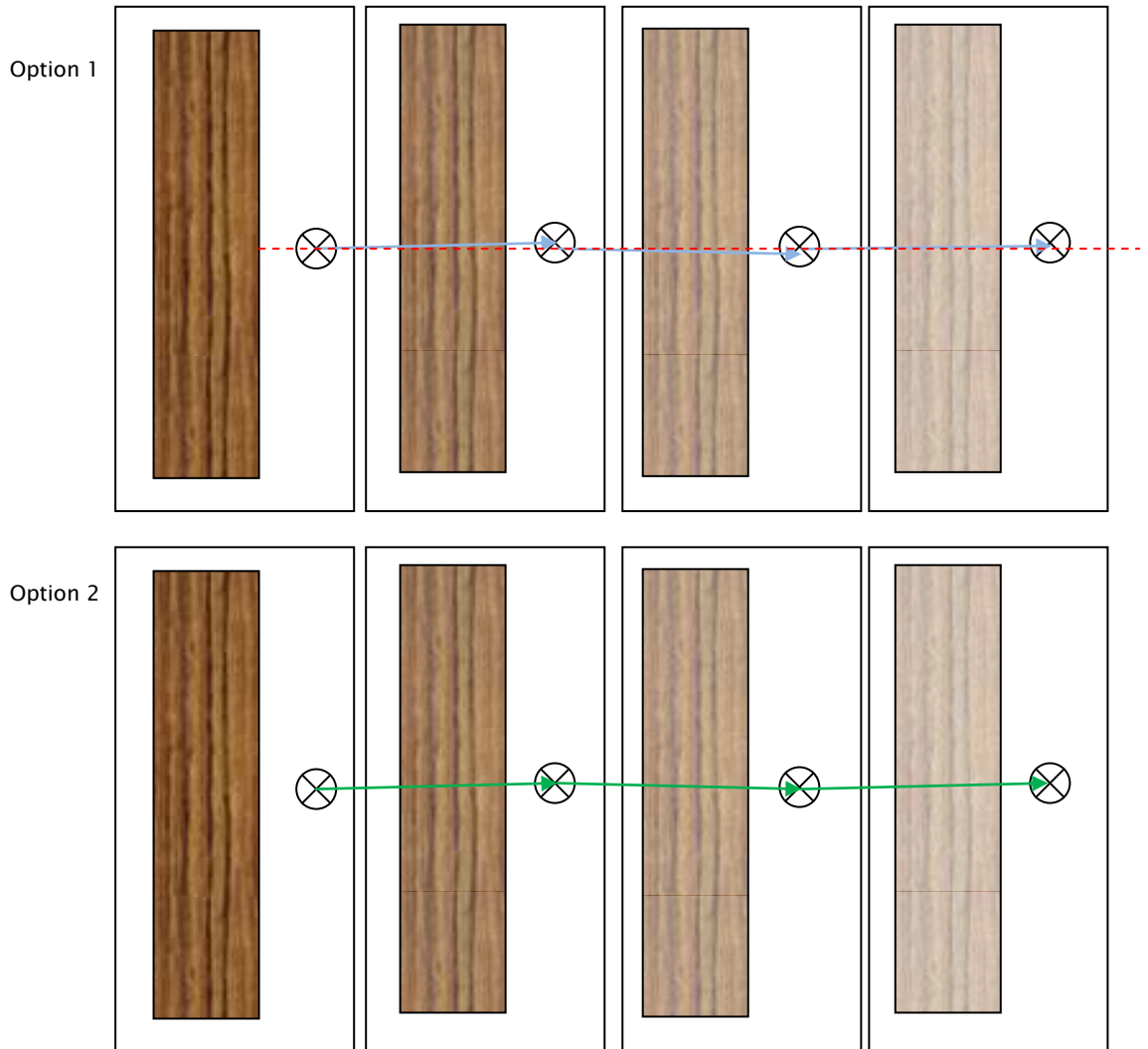
FIGURE 30: OPTIONS FOR TRACKING "FIXED POINT" WITH IMAGE WITHIN PIV CODE

5.3.2   Calculating the Strain

For the PIV strain results two types of strain were obtainable, true strain and engineering strain. True strain shows the change of incremental deformation

within a sample and accounts for the change in cross-sectional area as the sample was loaded. The change of deformation per element of the grid was given as:

Equation 3: $\qquad \varepsilon_T = \ln\frac{\delta L}{L}$

where ϵ_T is true strain, δL is the change of length of the sample and L is the original length. True strain can be expressed as a derivative of the engineering strain in this form:

Equation 4: $\qquad \varepsilon_T = \ln(1 + \varepsilon_E)$

where ϵ_E is engineering strain and ϵ_T is true strain.

Engineering strain is a ratio of the total deformation in the original length of load applied, it is expressed as:

EQUATION 5: $\qquad \varepsilon_E = \frac{\Delta L}{L}$

where ϵ_E is the engineering strain, L is the original length and ΔL is the change in length. Equation 5 was initially used to find the displacement and strain within the PIV software. The strain was evaluated per element in the square grid; thereby the average of summation of the elements within the sample gave the overall strain. Either strains could have been evaluated and displayed but the true strain showed a wider range of values for visualisation. These two versions of strain were accounted for in the calculation of the timber strain to allow for a visual analysis.

There was an order of magnitude, α, to consider between the image and real test specimen. The images 'Active Area' may not take into account the entire length of the sample therefore the pixel 'length' taken must be representative

of the real test sample. The following equation deals with the image-real ratio discrepancy.

Equation 6: $\qquad \dfrac{\varepsilon}{\varepsilon_{pixel}} = \dfrac{L}{L_{pixel}} = \alpha$

5.3.3   Allocating Precision in Pixels (Attempt 3)

There were some initial input parameters to decide upon. One parameter, the grid, is set up over the image and can have grid squares (made up of pixels) of different areas. The smaller the area the more likely it was to be tracked in error, however if the square area is not small enough the accuracy of the data was reduced. Hence the need for a high pixel quality image to be taken.

A brief study of the grid size was done using 10x10 pixel elements, 20x20 pixel elements, and 30x30 pixel elements on a first-last comparison of sample G1S. The results of this are shown in Figure 31 and Table 3. The figure shows a better visual interpretation than the table due to the aforementioned need to develop the code to create strain values. From Figure 31, it can be shown the 20x20 element makes the most comparable contour plot of the breakage shown. In view of this, the 20x20 element was used, although the element sizes were reviewed for each sample when found necessary.
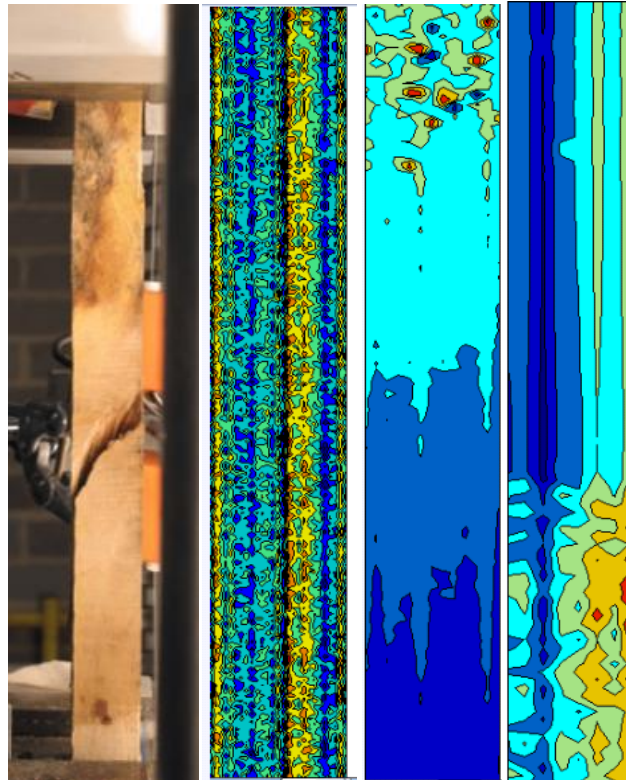
FIGURE 31: VISUALISATION OF GRID ELEMENT SIZE EVALUATION ON PIV XY SHEAR STRAIN QUALITATIVE RESULTS FOR G1S SHOWING: G1S FAILURE, 10X10 ELEMENTS, 20X20 ELEMENTS, 30X30 ELEMENTS FROM (LEFT TO RIGHT)

Machine	10x10	20x20	30x30
0.12 µε	1.12 µε	1.61 µε	3.29 µε

TABLE 3: STRAIN RESULTS FOR G1S UNDER DIFFERENT GRID ELEMENT SIZES

5.3.4 Visualisation of Strain

The strains were plotted as a contour graph which shows the change of the surface deformation in the sample. This produces the strain in each of the x and y directions on the sample and the shear (xy) strain values. There were two types available, one which showed the engineering strain and the other the true strain. These help to locate the position of the break point in the sample qualitatively.

5.3.5   Locating Fixed Point using Initial Code (Attempt 4)

Having decided the calculation, tracking and grid element sizes techniques the code could be run on a tested sample. Initially the user of the PIV program created an Active Area zone over which to pursue the strain record on the sample and any camera movement was corrected for using the rigid Fixed Point location in the image (Figure 32). To develop the code a tension test was undertaken in which images from the same test on sample G1S were compared. Subsequent images were related back to the original image Fixed Point to find any camera movement (shaking), meaning the strain could display true consistent records and need not be adjusted for multiple movements as the number of subsequent images increased (which could only lead to miscalculation errors). The movements that then occurred within the active area zone in the image were developed into contour plots, to show a visual representation of the movements occurring between each image.
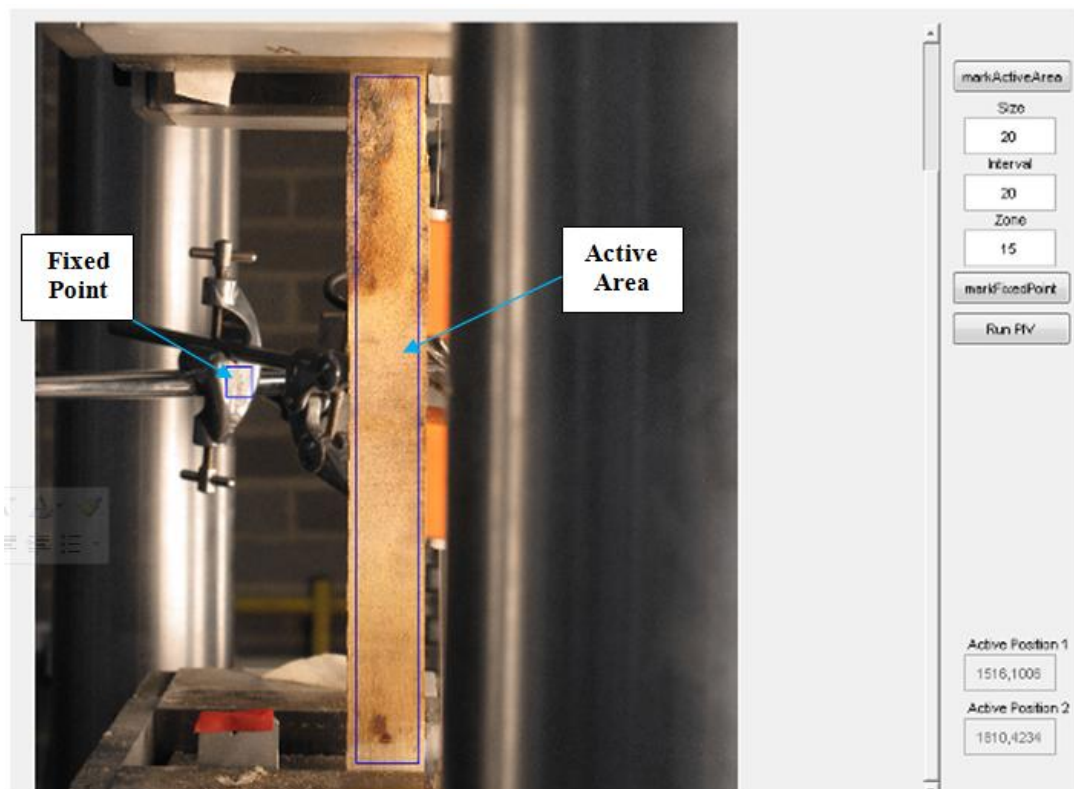
FIGURE 32: SIDE VIEW OF G1, "G1S" USING ADAPTED PIV ANALYSIS SOFTWARE GUI

The results, shown in Figure 33, of this coding sequence applied to G1S show some element of the breakage that occurred but it was not completely clear and therefore inaccurate to follow as a categorical answer. From the PIV contour plots, it was seen the side view of the sample showed some extreme strains in the Y strain direction lower down than the point of breakage. The visualisation at the point of breakage showed as a parting of the higher strains in this zone over time. Hence, a green 'neutral' zone increasing over time within this region. As the Y-direction indicated the upward movement this showed the most extreme strains. The X-strain helped to locate this zone using a similar strategy. This indicated the PIV methodology works, however the delicacies of program and the small movements in the sample suggested that there was still a requirement to refine the contour graphs so these failure areas were easier to visually comprehend.
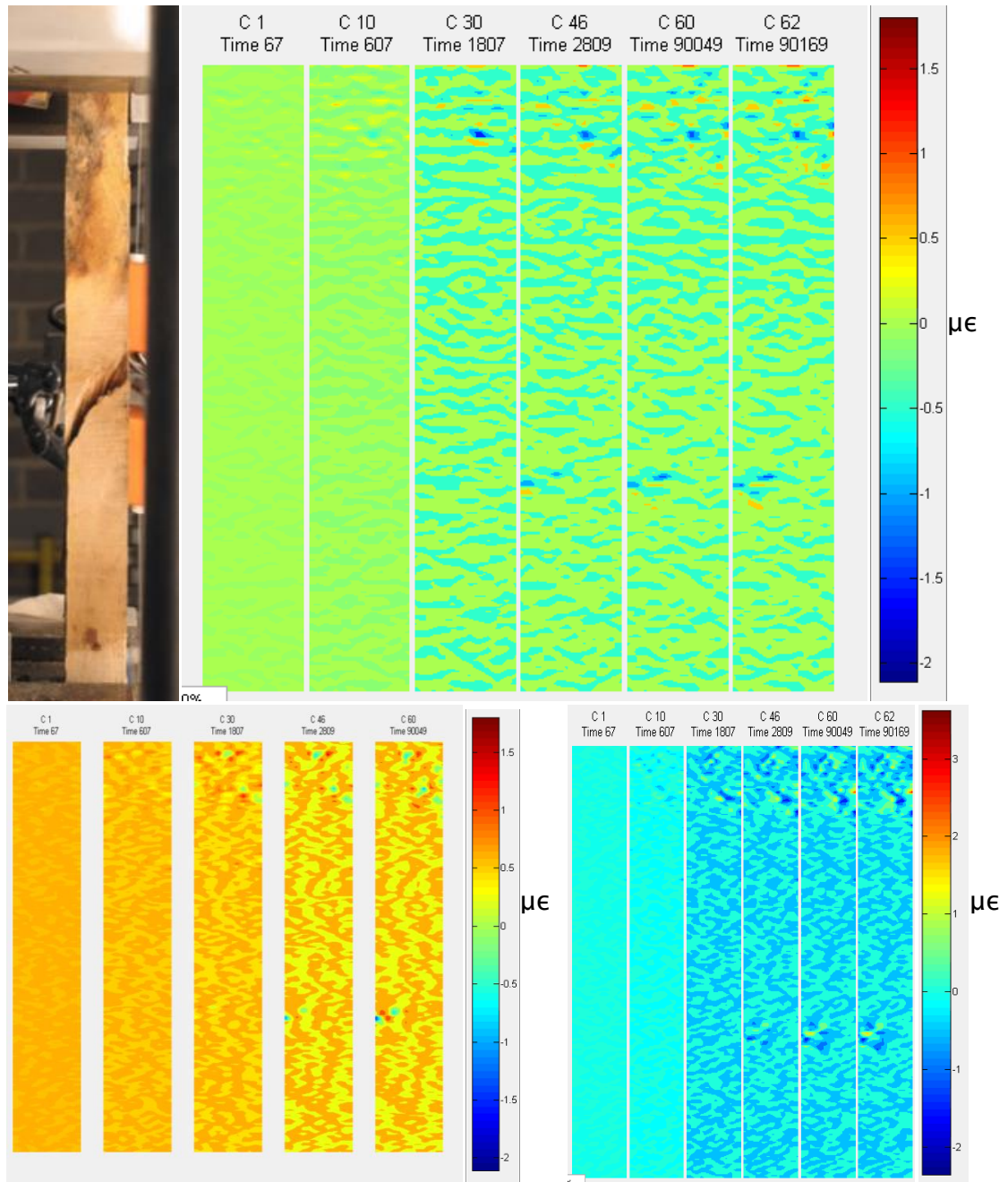
FIGURE 33: SIDE VIEW OF G1S BREAKAGE (TOP LEFT) AND SEQUENTIAL CONTOUR PLOTS (RED INDICATING HIGH TENSION) OF G1S; PIV ANALYSIS: Y-DIRECTION (ABOVE) X-DIRECTION (BOTTOM LEFT) AND XY-DIRECTION (BOTTOM RIGHT) ENGINEERING STRAIN

The extreme strain shown toward the top of all the contour plots suggested there was a greater strain formed from the pulling mechanism of the machine. This could be caused by the localised pinching of the grips against the sample. With greater refinement, strains can be produced for all the samples at all time

intervals of their test. This would show how the force on the sample was distributed through the fibres over time. It could be possible an element in the sample grid could be tracked throughout the time to get a more accurate representation of fibre movement if there was a particular zone of interest.

To prove this PIV method was working, the strain was compared to the machine strain during testing. The results of both PIV final strain and final machine measured movement are compared to determine the validity of this test, Table 4. On comparison to the machine movement the amplitude of the PIV strain seemed to be incompatible (but improved from previous results) but the form of the overall data points over time appeared consistent. The Y movement has been highlighted as this is the most relevant direction to the tensile load direction measured by the machine. It was however likely the strain of the machine would not exactly match the values of the PIV, as the calculation of machine strain did not take into account any sliding of the sample within the grips. Thereby the PIV strain was expected to be slightly lower in value.

Machine Strain	PIV Y –Direction Strain
0.12µє	0.095µє

TABLE 4: G1S ATTEMPT 4 STRAIN RESULTS COMPARISON

5.3.6   Further Fixed Points

The previous section showed a plausible pattern of PIV strain emerging, however further work was required to get better accuracy and understanding. Before and after pictures of the G1S sample are shown in Figure 34 highlighting the Active Area zone to show the problem. The current analysis of

the sample showed it had not only stretched but moved relative to the analysis zone.
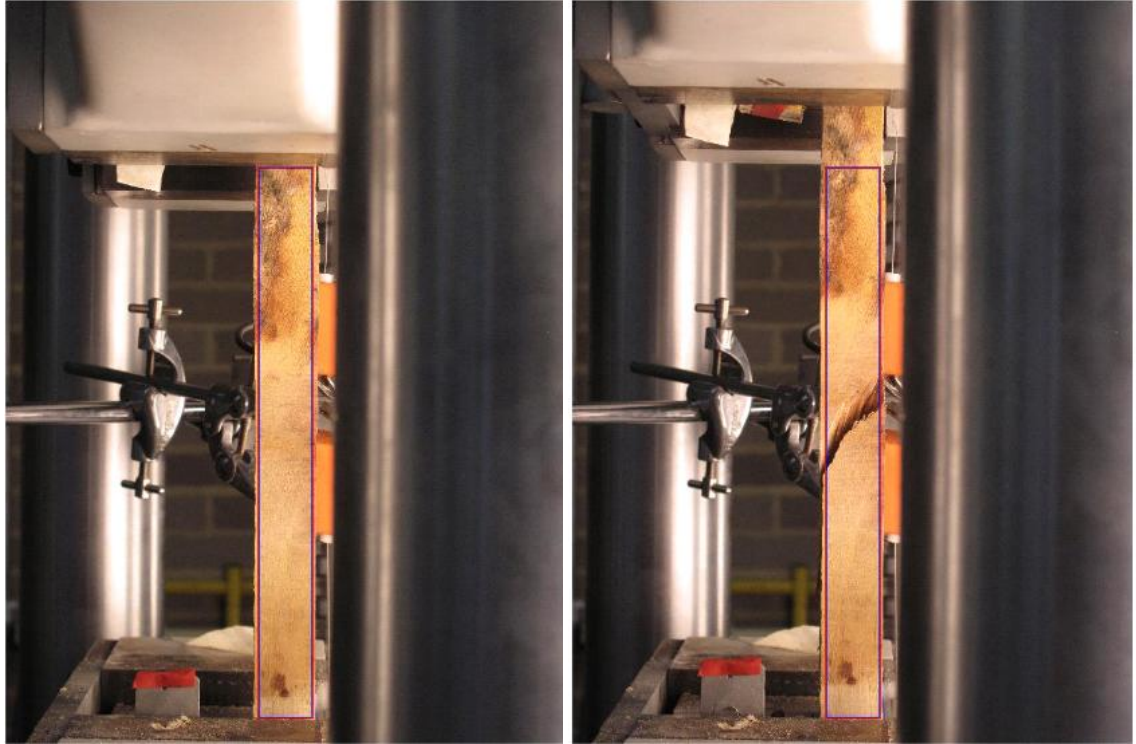
FIGURE 34: BEFORE (LFET) AND AFTER (RIGHT) IMAGES OF G1S VIEW WITH PIV "ACTIVE AREA" ZONE HIGHLIGHTED AS INACCURACY IN CODE

Tracking the sample stretch could be achieved through tracking of a few elements within the sample PIV grid over the time interval pictures. This would lead to better analysis of surface fibre movement during loading. By tracking certain locations on the sample image, it was seen from Figure 35 the sample within the successive images had moved due to the movement of the machine during testing. As the machine pulled the sample, the grips embed onto the sample and slid within the blocks in order to maintain a tight grip. It iwa clear the type of test needed to be taken into account in order for a more accurate account of PIV Strain to be made.
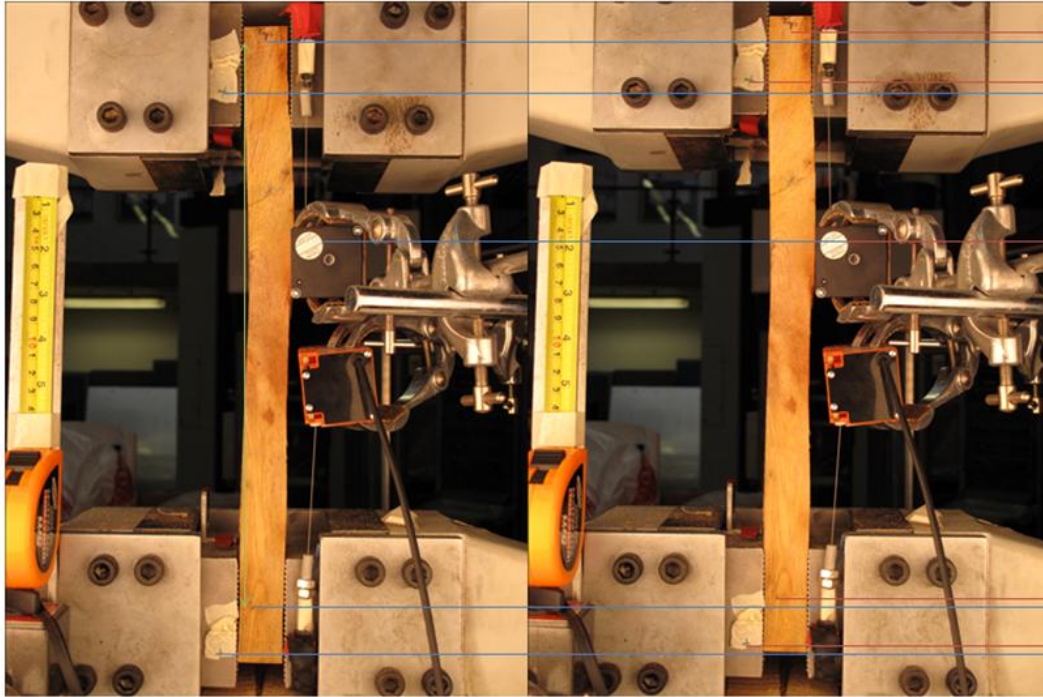
FIGURE 35: FIXED POINT MOVEMENTS ON G1F SAMPLE DURING THE TEST, BLUE LINE SHOWING ORIGINAL FIXED POINT AND RED LINE SHOWING THE MOVEMENT OF THIS POINT IN SUCCESSIVE IMAGE

Due to the stretch issue, the Active Area zone did not follow the sample. The PIV code needed to be modified to take into account not only the movement of the test machine or camera but also any stretching of the sample in order to calculate an accurate strain image and evaluation. This meant tracking the grips of the machine. As the machine pulled the sample from the top, it was the bottom grip that would substitute for the y-direction Fixed Point (the original x-direction Fixed Point movement was still used as the grips tend to move together as they go up). Slipping of the sample within the grips occurred in some instances as there were fibre tears on the gripped zone of tested samples. However this proved hard to track in the image due to textural inconsistency so grips were tracked and used for main calculation. The distance between the grips was calculated so the Active Area zone length could

be changed. The Active Area zone however would only change in length if the stretch between the grips accumulated to a sample size of the PIV grid square in the Active Area (i.e. another row of data could be added), therefore not disturbing the pre-collected data.

To correct for the rigid body movement caused by the machine grips, five Fixed Points were tracked (see Figure 36) throughout the experimental images so an accumulative account of movement could be made. The original Fixed Point (RFP) of a stationery rigid point adjusts x direction movements of the Active Area. The Fixed Point of the bottom grip (BGFP) was used to move the y direction of the Active Area. The Fixed point of the top grip (TGFP) minus the fixed point of the bottom grip would determine the size changes of the Active Area. The tracking on the Rigid Fixed Point (RFP) is done using a fixed zone in subsequent photos (option 1, Figure 29). The tracking of the 'Fixed' points on the moving grips is done in the same way between the current image and next image. However in addition, the tracking of previous images is accumulated using the moved zones of previous figures (option 2, Figure 29). The other two points tracked are in the top (TSFP) and bottom (BSFP) slip zones of the sample. It was thought due to the changes in the texture of the sample this could be inaccurate, so only an indicative result was taken from this tracking. In doing this version of tracking it could be stated there were two versions of strain that are measured, machine measured strain and sample strain. Machine measured strain would show the overall strain measured between two rigid machine points, yet the sample strain should be able to show greater detail within the surface fibres of the sample.
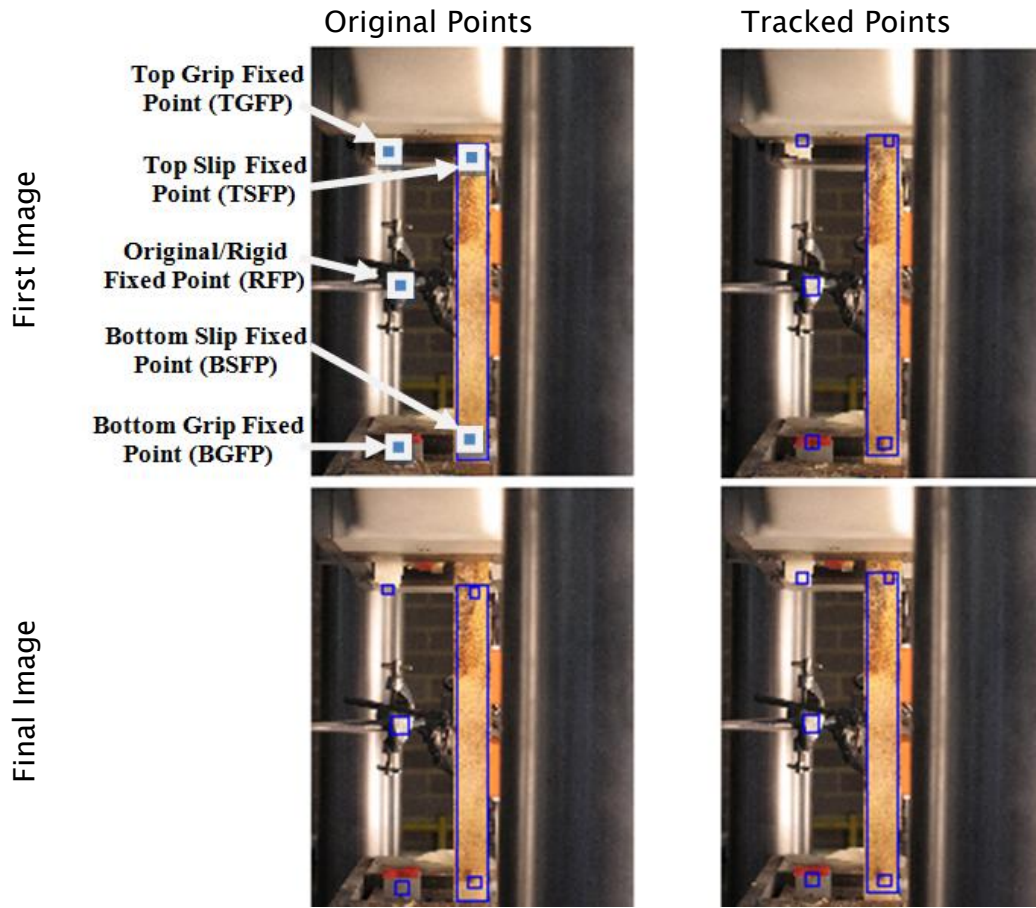
FIGURE 36: PIV ANALYSIS TRACKING OF FIXED POINTS AND ACTIVE AREA OF G1S VIEW BEFORE AND PRE-FAILURE (LEFT COLUMN SHOWS ORIGINAL POINTS HIGHLIGHTED, RIGHT COLUMN HIGHLIGHTS TRACKED POINTS, TOP ROW HAS ORIGINAL IMAGE AND BOTTOM ROW SHOWS FINAL IMAGE)

5.3.7   Tracking extra Fixed Points for better accuracy (Attempt 5)

The main issue with the previous PIV Strain calculation attempt was the analysis did not take into account the machine movement during the test. The machine grips moved within the holders, meaning the sample also moved. This was solved by tracking the BGFP. The Active Area did not account for the sample stretch. This was solved by measuring the distance between the grips to increase the Active Area zone in accordance with the limits of the grid size. Another reason the machine measured strain and PIV strain differed on a

multifibrous sample was the selected Active Area the PIV used was smaller than the machine measurement, therefore it was an expectation the machine measurement strain is larger than the PIV strain obtained.

Firstly, it was important to keep track of the grips so the vertical change in Active Area could be made. Tracking the grips gave an indication of the machine displacement during testing hence an indicative strain of the sample. The code was adjusted to record the movement of various fixed points of the machine and sample so this indication could be calculated.

Secondly, as the grips extend the sample, the Active Area was made larger to account for the sample stretch. The extension of the Active Area however was of magnitude of the grid size elements overlaid on the image, so the strain data recorded could be positioned accurately (see Figure 37). The code was therefore made to measure the difference between the top and bottom grip vertices and at a sufficient magnitude (equal to that of the sample size) the Active Area was expanded.
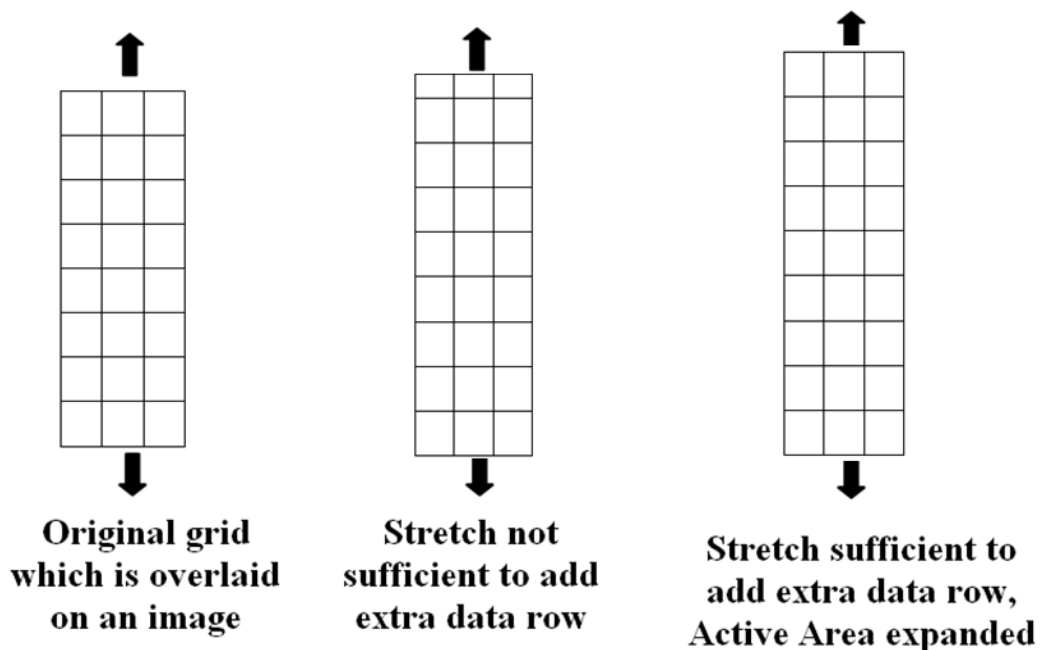
FIGURE 37: ACTIVE AREA GRID EXPANSION UNDER SAMPLE STRETCH

Thirdly, if the Active Area was tracked in this way a final 'last ditch' measure of the sample strain can be obtained. This could compare the first image with the image taken prior to break, as initially attempted in the 'First–Last' comparison with White's original code. This meant monitoring the change of the Active Area made during consecutive analysis and expanding the search zone area accordingly to pick up the changes. This should have given a better final qualitative result.

Figure 38 and Figure 39 show more accurate tracking and the active area change incurred. The top row shows the original image and the bottom row, the final image prior to breakage. The left column shows the original fixed zones and right column the new adjusted fixed points based on the tracking. To validate the results of the PIV tracking in this manner the top left image and fixed points (original image with original fixed points) met the same positions as the bottom right image and fixed points (last image with tracked fixed points). From these images, it can be seen how the grip fixed points (TGFP, BGFP) provided a much more accurate indication of movement where the fixed points on the sample (TSFP, BSFP) showed how tracking could be mistaken through the close texture of the surface. Therefore the track of the grip was used in the coding and could be seen to move the active area zone.

Original Points | Tracked Points

First Image
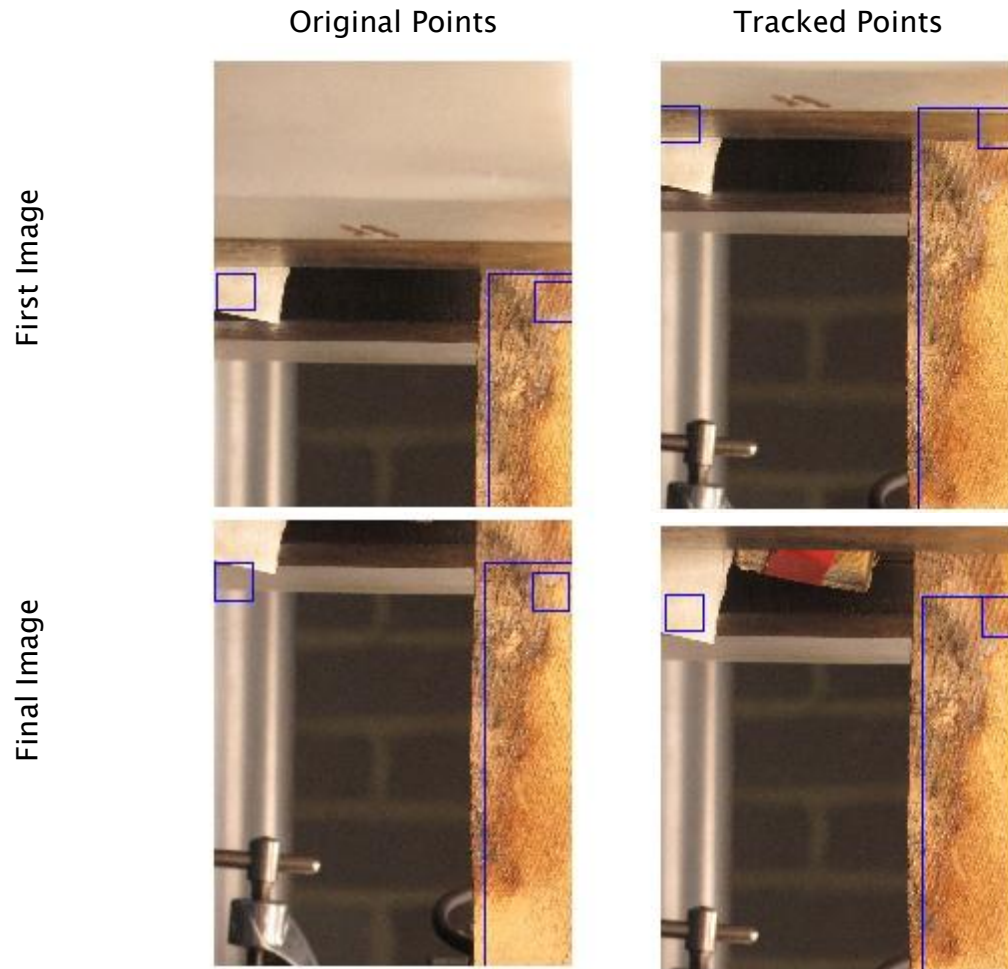
Final Image

FIGURE 38: FIXED POINTS TGFP AND TSFP (BLUE SQUARES FROM LEFT – RIGHT) OF PIV ANALYSED SAMPLE, (ORIGINAL POINTS (LEFT COLUMN), TRACKED POINTS (RIGHT COLUMN), ORIGINAL IMAGE (TOP ROW) AND FINAL IMAGE (BOTTOM ROW))

Original Points   Tracked Points

First Image
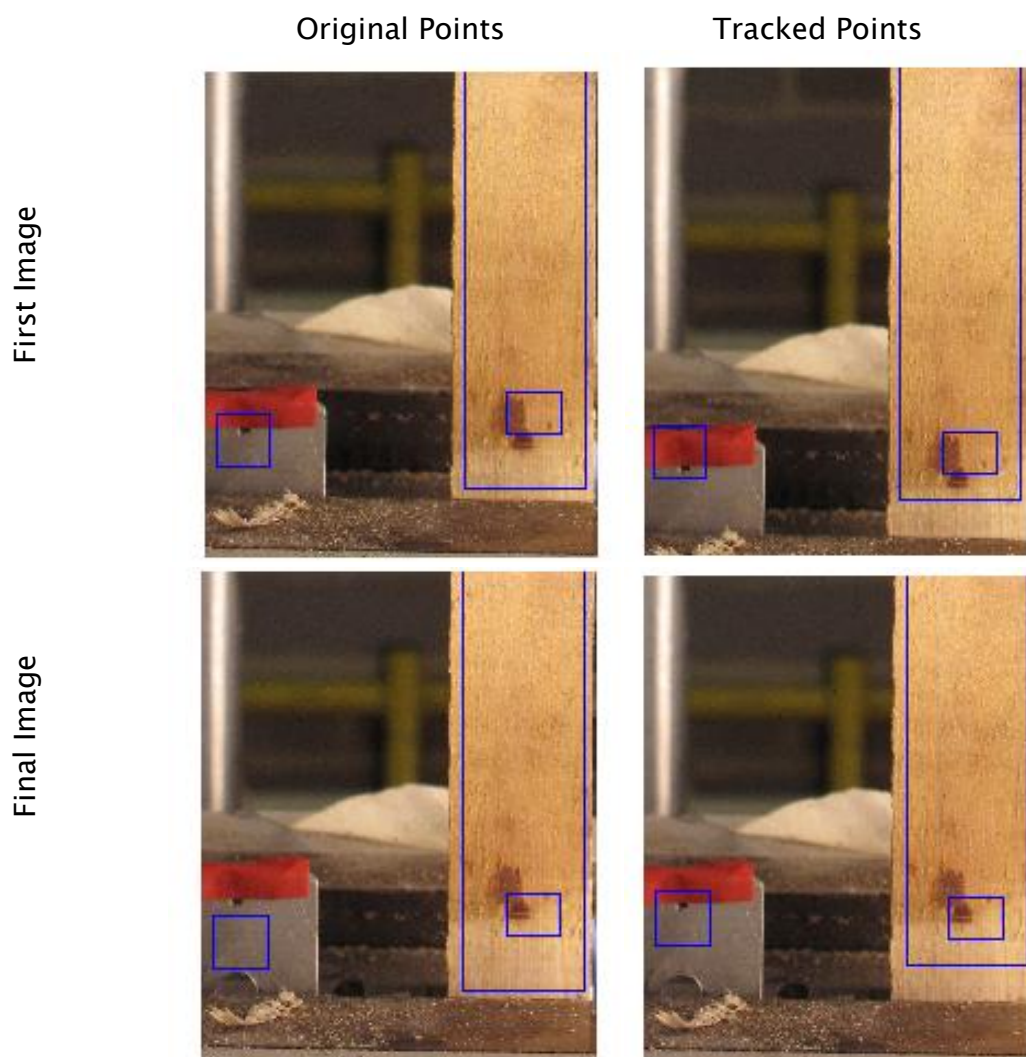
Final Image

FIGURE 39: FIXED POINTS BGFP AND BSFP (BLUE SQUARES FROM LEFT – RIGHT) OF PIV
ANALYSED SAMPLE, (LEFT COLUMN SHOWS ORIGINAL POINTS HIGHLIGHTED, RIGHT COLUMN
HIGHLIGHTS TRACKED POINTS, TOP ROW HAS ORIGINAL IMAGE AND BOTTOM ROW SHOWS FINAL
IMAGE)

When looking closer at the top and bottom of the side view tracked points of
Figure 38 and Figure 39, it could be seen how much the grips and sample were
moving relative to the machine. The top right (original image with tracked
points) and bottom left (last image with original points) image showed how the
movement of the machine had affected the tracked Active Area. This was what
led to the previous inaccuracies and was now accounted for in the PIV code.

In summary, note the Active Area adjustment was made in the vertical axis only as this was the directional alignment of the test machine. An interesting dilemma for the code was not only did the grips move vertically but horizontally due to the grip on the sample being increased as the machine stretched the sample. Hence when looking at the view of the fixed points, the vertical axis would be the crucial changer for the Active Area not the horizontal. The Active Area was also made to follow the bottom of the sample and additions to the Active Area zone made to the top so there was a clear reference zone. By tracking the grips, the Active Area is expanded vertically to account for strains as the sample is stretched and a better match was made between images (see Figure 40). By following the change in the 'Active Area' size, a larger search zone could be given in the First-Last image comparison creating a more logical analysis of the overall strain incurred during testing.
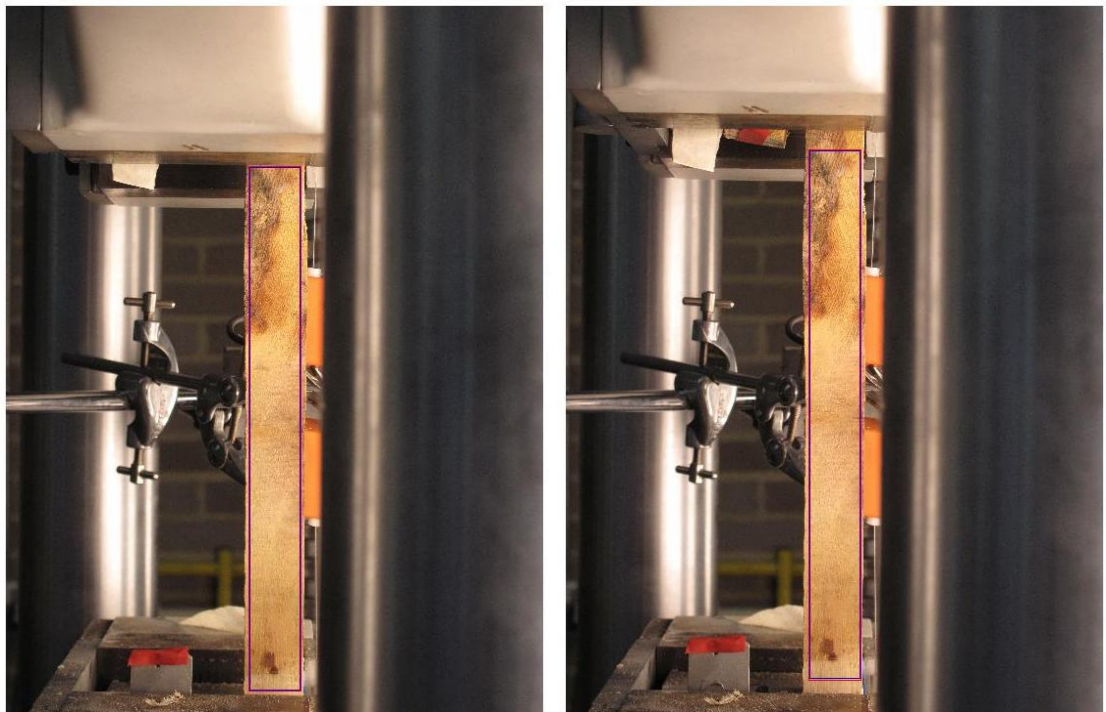
FIGURE 40: G1S VIEW ACTIVE AREA ZONE (LEFT) ORIGINAL IMAGE AND ACTIVE AREA ZONE (RIGHT) LAST IMAGE WITH NEW STRETCHED AS TRACKED ACTIVE AREA ZONE

5.4   Results – Sequential and First-Last Comparison

5.4.1   Attempt 5 – Run Fixed Point Improvements on Code

The PIV strain contour plots are shown in the following section to show directly comparable improvements made to the code by reprocessing the previous images from G1S. There are two types now available, one which shows the progressive strain during the test, 'Sequential' comparison and the second shows first to last image comparison, 'First-Last Ditch.' Here the various forms of strains and sequential/first-last analysis of data show how the contour data is analysed.

Firstly, the analyst looks for common occurrences of colour change and concentration as the Engineering Strain plot progresses through time. In the example shown in Figure 41 this appears as red (tension) and dark blue (compression) at the top and at about a third from the bottom of the sample. This occurs in all the directions shown suggesting a diagonal failure will occur. As the sample is pulled from the top during testing (likely to cause the colour change seen in the contour), the zone a third from the bottom is where the analyst needs to concentrate for breakage.
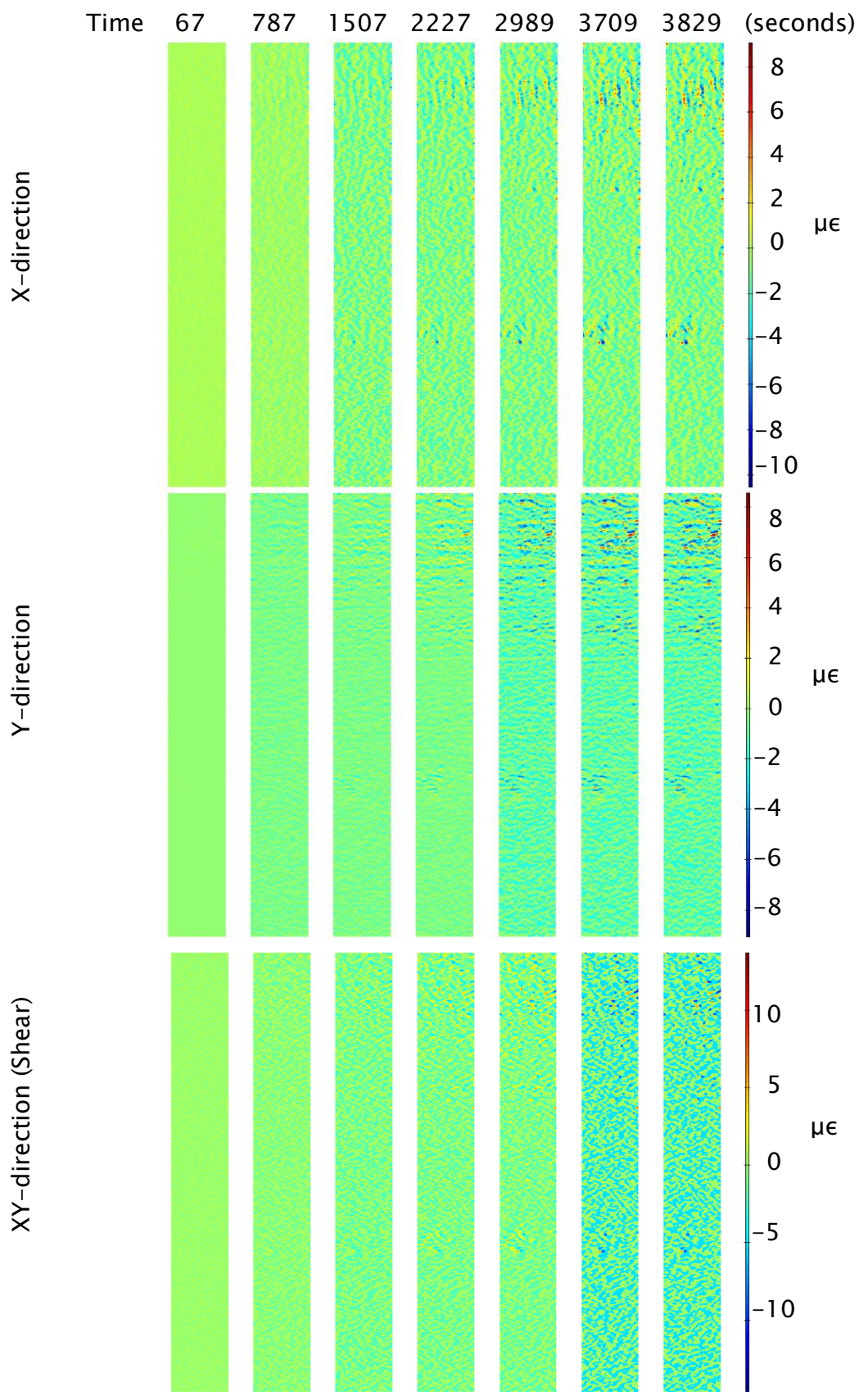
FIGURE 41: G1S TEST DIRECTIONS X, Y, AND XY/SHEAR (TOP TO BOTTOM) SEQUENTIAL

ENGINEERING STRAIN (STRAIN CONCENTRATION A THIRD FROM THE BOTTOM OF THE SAMPLE)

Figure 42 shows true strain as more intense colours in the example of contour plots. When overlaying the final contour plot onto the final image, it was shown the intensity of strain on the contour plot was still misaligned with the breakage point. The intensity found one-third from the bottom however is still along the course of breakage.

On closer inspection of the G1S sample, the zone of concentration shown on the contour plot was not the point of failure but where grain rings were found. The concentration of strain was found where there was a widening of the rings in the sample (Figure 43). If the rings were followed round, the breakage occurred where the space between the grain rings narrow (a point where medullary rays were confined together). Looking at the engineering strain images (Figure 44, Figure 45 and Figure 46) at this location shows the contour plot colours starting to merge to create a rough line. This is the line of breakage.
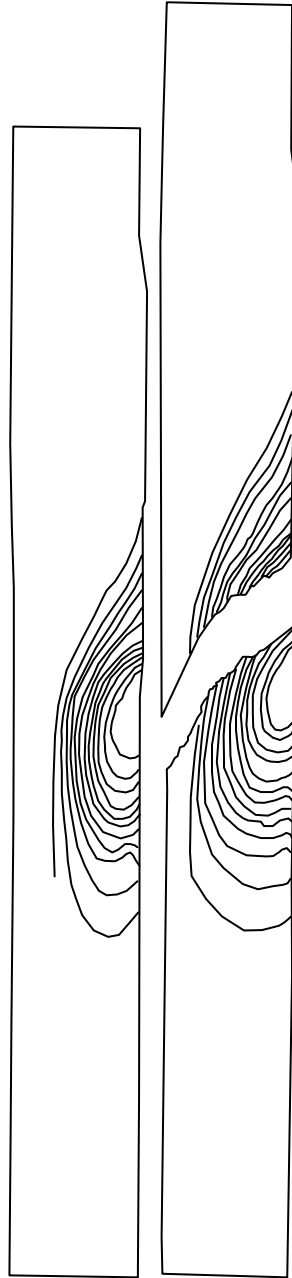
FIGURE 43: GRAIN SKETCH OF THE ORIGINAL AND FAILED SAMPLE G1S
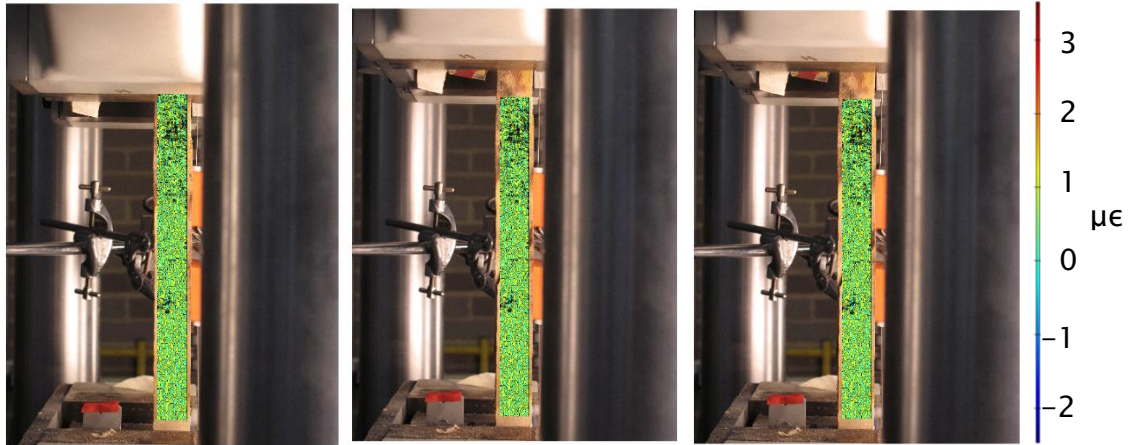
FIGURE 44: PIV X–DIRECTION ENGINEERING SEQUENTIAL STRAIN OVERLAID ON SAMPLE G1S

IMAGE SEQUENCE: FIRST, PRE–FAILURE, FAILURE (LEFT – RIGHT)
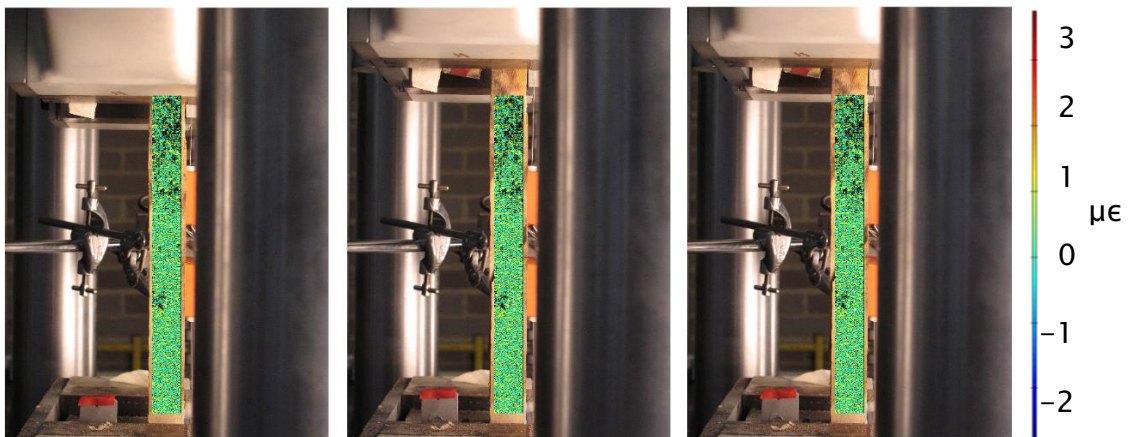
FIGURE 45: PIV Y–DIRECTION ENGINEERING SEQUENTIAL STRAIN OVERLAID ON SAMPLE G1S

IMAGE SEQUENCE: FIRST, PRE–FAILURE, FAILURE (LEFT – RIGHT)
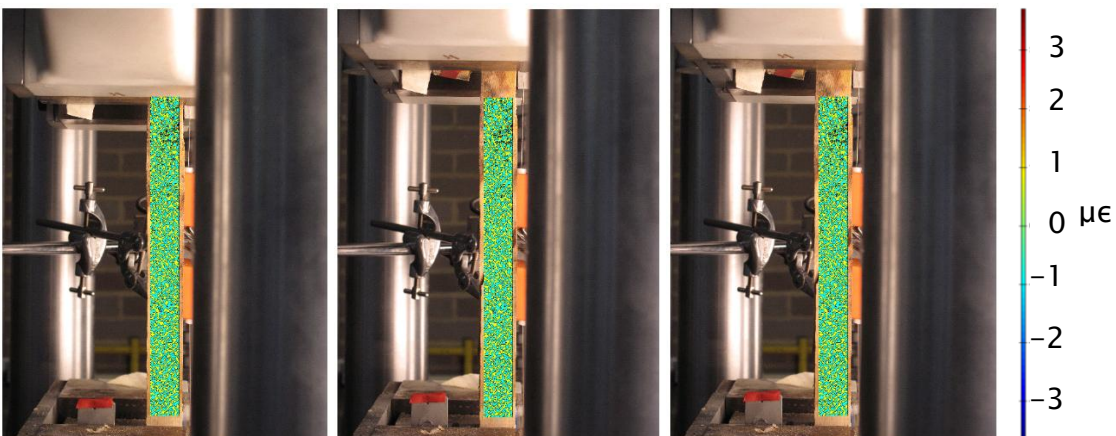
FIGURE 46: PIV XY–DIRECTION ENGINEERING SEQUENTIAL STRAIN OVERLAID ON SAMPLE

G1S IMAGE SEQUENCE: FIRST, PRE–FAILURE, FAILURE (LEFT – RIGHT)

The First-Last Ditch comparison showed the failure of the sample and style of break. These are shown on the following Figure 47 and Figure 48 as dark blue intensities and highlighted for easier comparison by a red dotted line. This was only possible due to the expended effort of sequential analysis where indication of the zone movement could be determined.
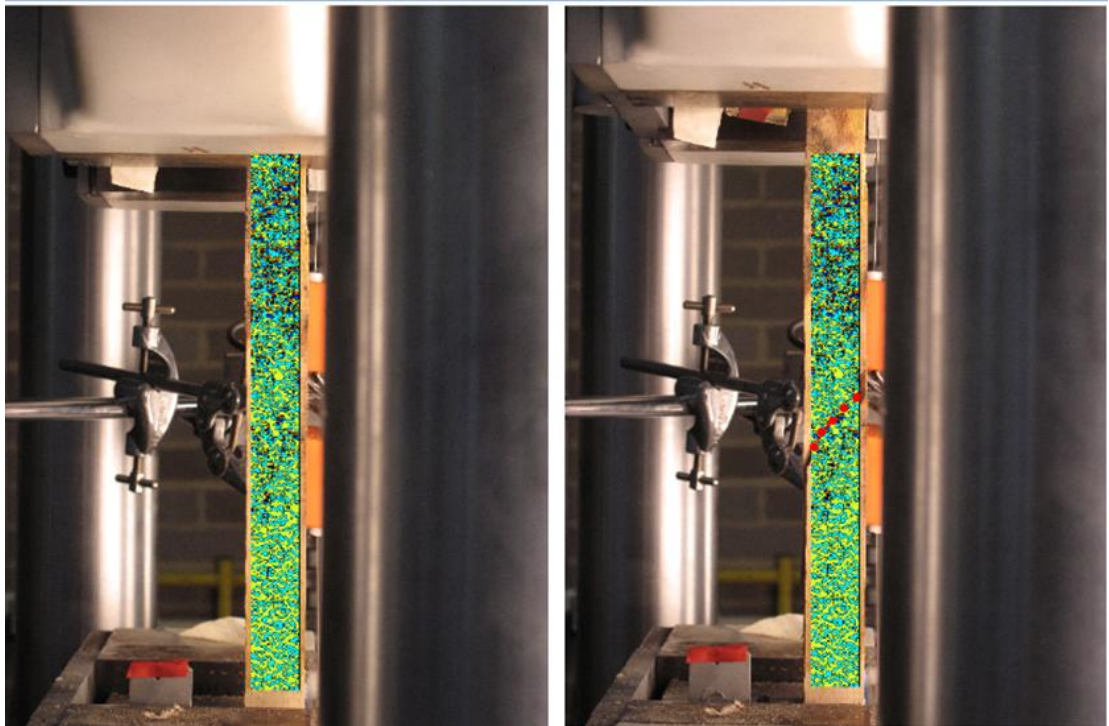
FIGURE 47: PIV Y TRUE STRAIN FIRST-LAST DITCH (OVERLAID ON FIRST AND FAILURE IMAGE) ON SAMPLE G1S, FAILURE IMAGE SHOWING RED DOTTED LINE HIGHLIGHTING CONTOUR PLOT COLOUR INTENSITY
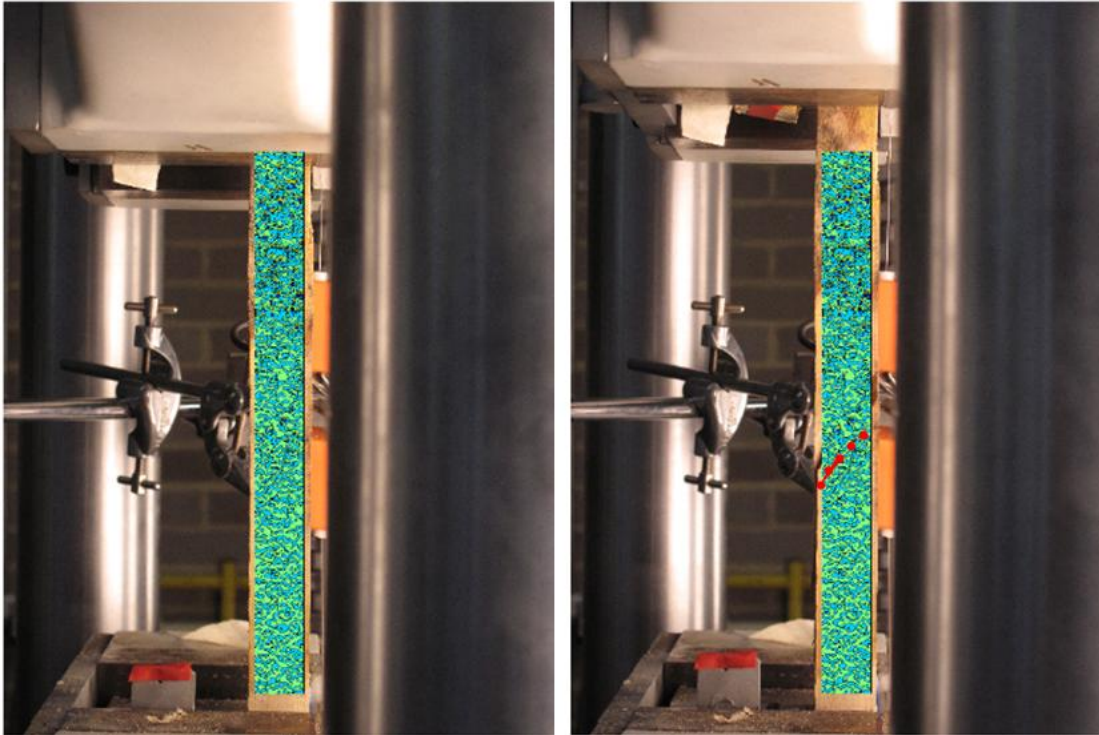
FIGURE 48: PIV Y ENGINEERING STRAIN FIRST LAST DITCH (OVERLAID ON FIRST AND FAILURE IMAGE) ON SAMPLE G1S, FAILURE IMAGE SHOWING RED DOTTED LINE HIGHLIGHTING CONTOUR PLOT COLOUR INTENSITY

The quantitative values of the PIV Strains shown in Table 5 compared to the earlier quoted machine measured strain of 0.12µε are much closer. Remembering the machine was going to have a higher value due to a longer measurement zone, the value obtained for the final 'First-Last' Ditch Engineering showed a close comparison. Note the engineering strain was taken as the quantitative value as Equation 4 and Equation 5 showed true strain was a logarithmic and derived.

Machine Measured	Sequential PIV Engineering	Sequential PIV True	First-Last PIV Engineering	First-Last PIV True
0.120 µε	0.212 µε	0.262 µε	0.105 µε	0.067 µε

TABLE 5: ATTEMPT 5 PIV STRAIN VALUES RESULTS COMPARISON

5.4.2   Attempt 6 – First Sequential Analysis Prototype Test

The sequential analysis has been proven to help to increase the viability of the results presented in the First-Last Ditch Comparison, it is therefore likely that creating a First-Sequential Analysis would increase the viability of the sequential phase of analysis. A coding sequence was created that compares the first image to each subsequent image, expanding the search zone in the same way as the First-Last comparison. From the following Figure 49 and Figure 50 the qualitative results show the accuracy of this technique to be valid.
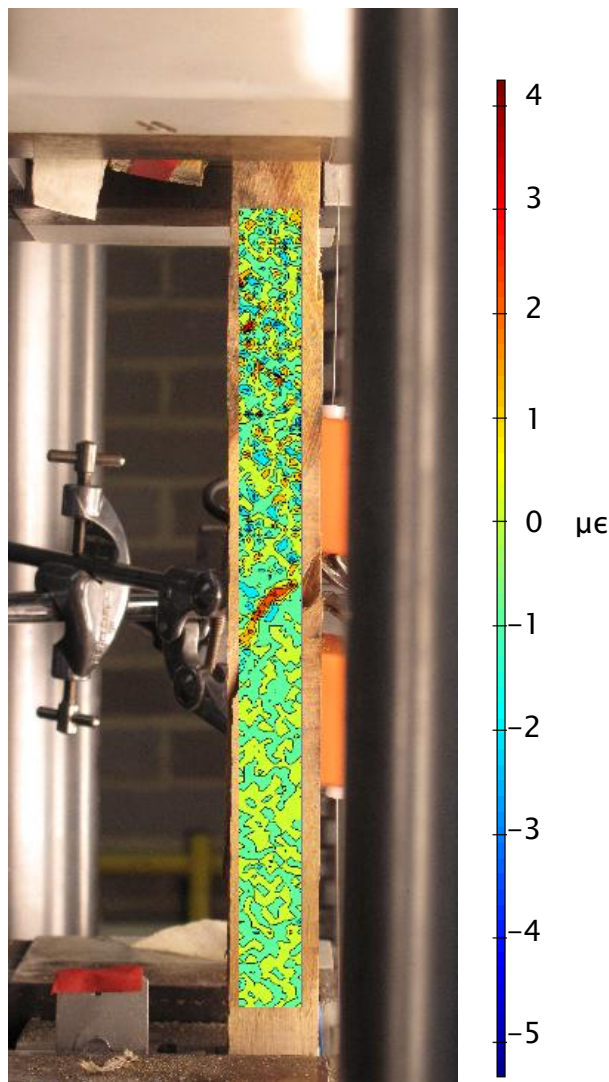
FIGURE 49: PIV FIRST-SEQUENTIAL ANALYSIS FOR XY/SHEAR TRUE STRAIN OVERLAID ON FAILURE IMAGE OF G1S SHOWING INTENSITY AT POINT OF FAILURE
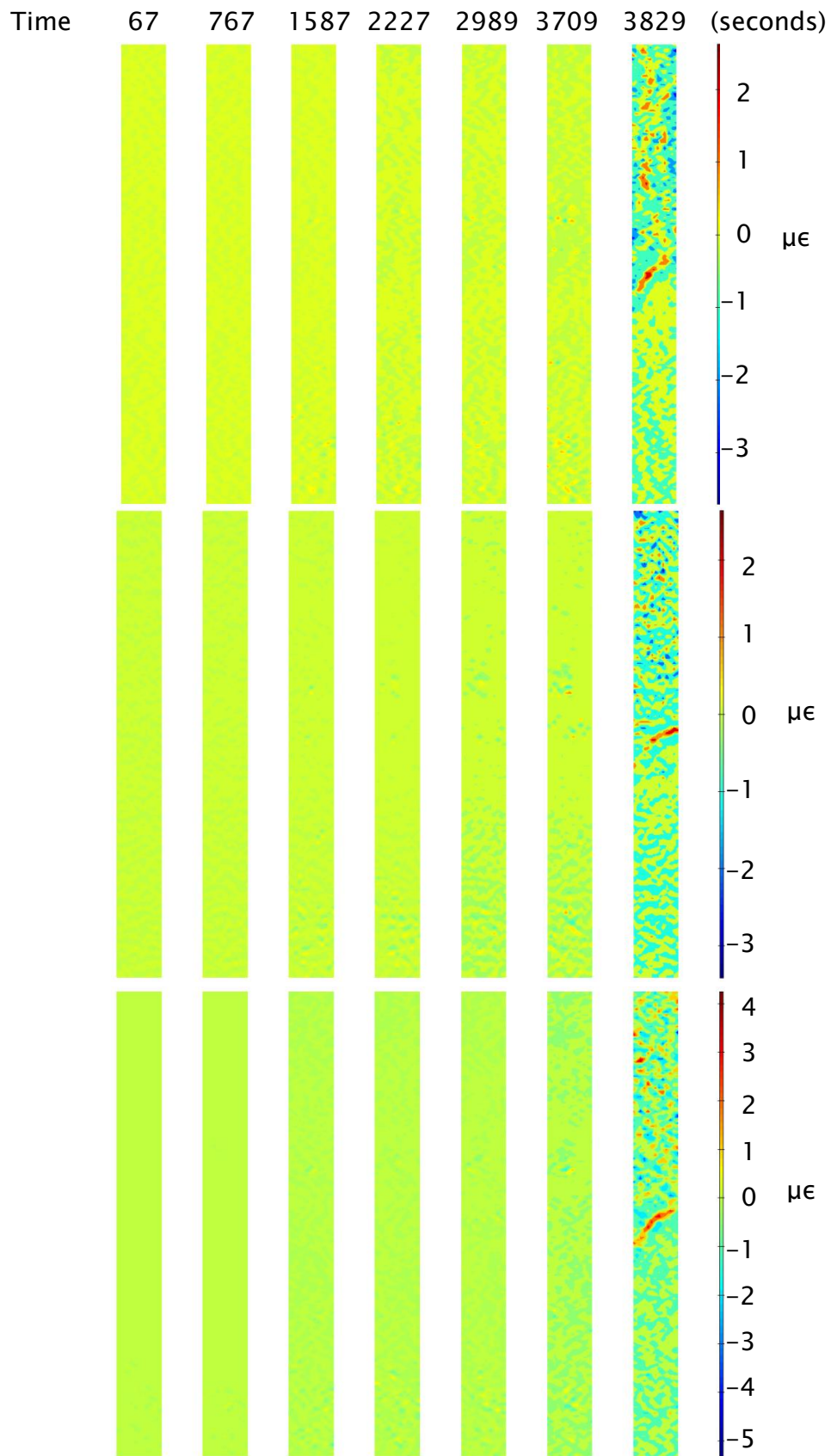
FIGURE 50: FIRST-SEQUENTIAL ANALYSIS FOR DIRECTIONS X, Y, AND XY/SHEAR PIV

ENGINEERING STRAIN OF G1S TEST (TOP TO BOTTOM) SHOWING INTENSITY AT FAILURE

The quantitative results in Table 6 show promise due to being nearer the machine strain of 0.12µϵ and therefore can be used as a progressive strain measure during the test. The real time values of strain compared to that of the machine measurements show a common trend (shown in Figure 51) and an underestimate of the strain as predicted due to the machine grip movements during testing. However again it would seem the First Sequential Analysis produced lower values than the machine measured strain, although the contour plots look to be a success in showing the failure, suggesting again the slippage and machine set-up are affecting the results through producing extra length.

Machine Measured Strain	First– Sequential PIV Engineering Strain	First– Sequential PIV True Strain
0.120 µϵ	0.105 µϵ	0.067 µϵ

TABLE 6: ATTEMPT 6 – FIRST-SEQUENTIAL PIV STRAIN VALUES
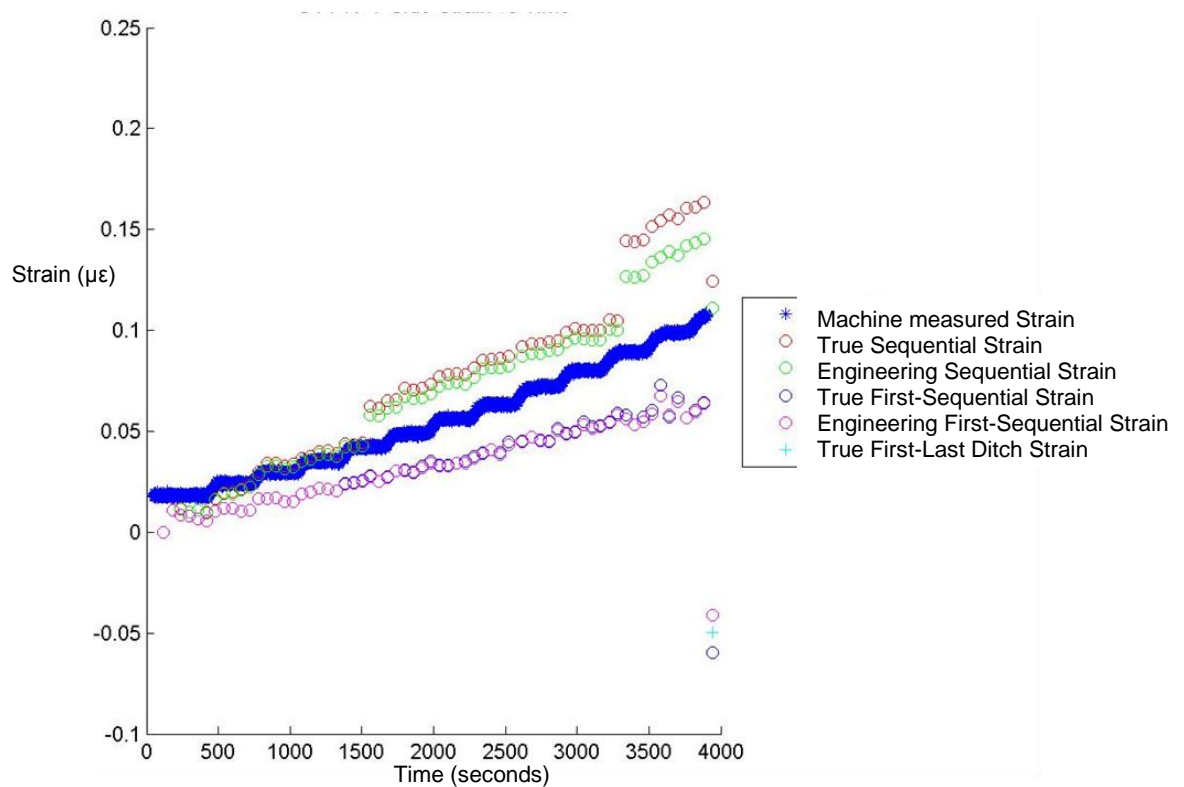
FIGURE 51: COMPARISON OF STRAINS OVER TIME FOR SAMPLE G1S VIEW

Further work on the First-Sequential analysis would suggest a more accurate representation of strain modelling. The example shown has been worked through, with grid element dimension of 10x10 (meaning 8320 instead of 2080 elements per image). This has enabled it to reduce double matching comparisons within search zones but has taken 4 times longer to process. This reduced grid element requires intense time commitment, therefore has not been progressed any further due to time restrictions. In the meantime, a quick solve on the other samples with 20x20 grid elements was to average any double matching comparisons. This allowed for an indication of results but the values would not be taken forward in the strain comparison.

5.5   Discussion of Final Results

Due to the set-up of the experiment with the initial arrangement of just one Fixed Point, the initial results proved to be inaccurate. Tracking this Fixed Point did show some form of failure, the visibility of the failure in the contour plot was vague. This was due to the fact in real time the test machine and sample was moving within the frame of the picture. Hence later, the code included more Fixed Points enabling the Active Area of the picture to track the movement of the machine and stretching sample.

5.5.1   Methodology

The methodology showed the thought required in order to conduct the PIV analysis on tested samples. It is important to create a continuous light over the sample to be analysed in order to prevent shading caused by varying natural light which will cause textural inconsistency. Having a high resolution camera increased the pixel data over which analysis can be done and therefore the accuracy of the results is improved. The timber was deemed to have sufficient

texture as to not need painting in order to undertake image comparisons using PIV. It was important the method used by the machine for the testing was understood so the analysis could be adapted appropriately.

5.5.2   Code Development

The original code was programmed to rely heavily on user inputs such as each image file location, Active and Fixed Zones and hence could realistically only be used for before and after failure analysis (termed First-Last). In this project, the program has been developed to automatically import the next image allowing for an analysis against time to be done. However the code did not allow for the machine's style of test. This led to further adaptations to the code so the Fixed Points and Active Area followed the movement of the machine during testing so the same target locations could be interrogated throughout the sequential images. Also the Active Area was made to expand as the sample stretched. This meant strains and contour plots could be created, however there was still an accumulation of errors arising due to the search zone parameters and conditions assigned to the addition of extra grid elements. This led to a First-Last Ditch attempt to use the movements recorded to re-analyse the first and last images where the search zone was adjusted accordingly. This gave better qualitative and quantitative strain results, even showing the potential breakage occurring as the tension was increased during testing in the first-sequential analysis.

5.5.3   Use of the contour plot
A contour plot of strain has been developed that accumulates the changes of the sample movements detected through the PIV code. The contour plots show a qualitative indication of breakage although they must be used in conjunction with test-type knowledge and sample examination. Identifying failure points

from the sequential contour plots can sometimes seem ominous to the untrained (like a stereogram). It is usually the composition of the plot that makes it difficult to analyse, so it is advisable to change the colours used, or select a smaller zone away from gripping points or localised stress points to analyse.

In summary, the breakage failure analysis of results from the sequential contours are found as follows:

- Higher strain intensity is found in the Engineering Sequential PIV Strain contour plots.
- This intensity needs to be deemed as machine localised or sample localised *i.e.* is the machine or the sample causing the intensity?
- Where the strain intensity is in the sample, the grain of the timber needs to be looked at to determine a new zone to concentrate efforts on.
- This zone under 'First-Last' Comparison should show the line of final breakage by collative colour concentration showing clear high intensity next to neutral intensity.

The first-sequential analysis contour plots show a clearer indication of failure, with the higher strain intensity being located along the breakage point on the sample. Again the contour plots require some knowledge of the machine type and test configuration, as in the example, high intensity is found near the sample ends where the machine pulls it. The use of contour plots can help to indicatively show how the blocks of fibres within the sample are reacting to the loading.

5.5.4   Gaining quantitative results

At each interval of an image being taken, a summation of the element grid movements is calculated giving an overall value for sample movement change and therefore a value of strain at the time each image is taken. This procedure seems to work well and prevents the need to use strain gauges.

The additions to the code has meant, as well as the machine measured strain, the image strain can be calculated giving further reassurance of the strain values obtained during failure. The sequential results show sample movement through time and indicate strain changes. However the results are double that of the machine measured strain. This can only be due to the inaccuracy caused by the code methodology. By only adding an extra row to the grid of the Active Area when the stretch of the sample passes a certain dimension, the stretch occurring on the boundaries or near limits may be unaccounted for. The first-last ditch comparison however uses the stretch data to expand the search zone so each grid square has a larger perimeter to search for a match and creates a more reasonable answer. This means a final strain measurement can be used in calculation of structural property but only an indicative graph of strain against time can be developed at this stage. The First-Last Ditch graph however shows the potential the front and side values of PIV measured strain can be averaged to the machine measured strain. This scenario is likely to happen as the complex fibre arrangement may cause more or less movement depending on the direction the fibres are orientated. It is worth noting the machine measured strain will not accurately represent the strain in the sample due to fibre complexity, slip at the grips and creep.

5.5.5 Assumptions

The results are reasonably accurate, though the methodology of the code needs to be understood to ensure the correct interpretation is made and the right values are used. The calculation of fixed points assumes no slippage in the grips during testing, though slippage was observed in some samples through fibre tearing at the grip location. Values depend on pixel image quality allowing for a grid to be created of the sample to be analysed. Tracking Option 2 of Figure 29, assumes the sample fibres move relative to a constant point as the grid does not move individual squares at each stage to follow the exact course of the sample movement. This means the strain is subjective between each image and not progressive. This is further magnified by the way in which the Active Area is expanded, only doing so when the grips have moved far enough apart, meaning the strains are limited by the boundaries of the search zone until the addition is made. This will mean the PIV code will try to find the best comparison of element within its search zone parameters but this element may have moved beyond the boundaries and over time create a collective error.

5.6 Conclusion

The testing and coding has shown a reasonable success but requires experienced skill to interpret the results. It is important to understand the type of test thoroughly to interpret the data from the contour plot. For example, is there a localised pinch point that might affect the location of failure? When it comes to the quantitative results, the initial first-last comparison did not show enough visual evidence due to its inability to expand as the sample stretches. Therefore, the sequential comparison was deemed a better approach for strain and also gave a time dimension to the strain. Once the stretch of the sample

was ascertained from this sequential analysis, an attempt of first-last ditch comparison was done using an expanded search area to take account of the sample stretch. This shows not only a better quantitative final result but also qualitative output on the comparison of first and last images.

More comprehensive testing and set-up would help to affirm the movement of the timber samples. Further developments of 'First-Last' comparison could help show the progressive failure over time such as the First-Sequential Analysis Prototype Test detailed. The first-sequential analysis showed the best qualitative and quantitative results, though would need the code to have some artificial intelligence written within it that determines which double match comparison to use. This would be achieved by looking at the previous movements of that element and advance to compare the element of the next image, therefore finding the most appropriate match. It may be possible to use Digital Image Correlation (DIC) technology to further analyse the picture for strain comparison. DIC technology uses similar methods to PIV and could be a way of confirming the strains are being accurately mapped across the sample photos.

5.7   Summary of Key Points of Development Progress

The set-up of the physical experiment must allow for continuous lighting of the sample throughout the duration of the test to reduce any shadowing effects over the sample. The type of image file must be high quality with reduced file size compression. The test machine and arrangements must also be accounted for to allow the PIV analysis to have an effective elemental grid set-up.

A contrast of contour colours indicates the location of imminent failure. The failure is highlighted in sequential analyses where the highest strain is adjacent to a clear neutral zone. This area shows a place where the adjacent timber fibres are reacting differently under loading. It is important to review all contour graphs produced to allow a cross reference of the suspected failure point.

The analysis code progression was highlighted through the key stages and the total PIV strain compared to a machine measured strain of 0.12 με (a representative sample value likely to be greater than the actual value experienced by the sample due to machine test style issues such as slipping and stretch of the sample within the grips during the load test):

- First-Last comparison –using original code to compare the first image with the pre-failure image to show the suggestive total movement during a test. The results showed 21% lower strain than the machine strain value.

- Sequential comparison – using original code to compare a series of successive images to build up the progression of failure during loading, however cumulative errors found 77% higher strain than the machine strain value.

- First – Last Ditch comparison – uses the sequential analysis to expand element search parameters and compare the first image and pre-failure image to show a more accurate value of total strain during a test. This indicates a more reasonable test value for strain, 12.5% lower than the machine strain value.

- First-Sequential comparison– uses sequential analysis search parameters to progressively expand the search parameters as the code

runs through a series of images taken during in the test. This gives a

value of progressive strain compared to the results of the First-Last

Ditch comparison.

The improvements through automated PIV Strain analysis has therefore

improved the strain prediction from 21% lower to 12.5% lower than machine

measured strain and has also allowed for the progression of strain to be

analysed over the entire sample through the duration of testing.

6. Component Tension Testing

This chapter explains the test work conducted on battens in order to determine the internal structural workings of the branch joint. The test includes splitting the fresh cut global joint into battens (components) and tensile loading these samples to British Standard procedures, in order to convert timber properties to possible tree strength structural properties. These tests also use the novel technique of Particle Image Velocimetry (PIV) on timber (described in Chapter 5) to determine the strain of the tested samples. The individual components are then reformed to show the strain through layers of the global joint.

6.1   Introduction

The PIV technique is applied to determine the strain of the global joint under load. This technique is applied to the strength testing of the fresh-cut global joint using a component method, discussed later in this chapter. The PIV technique allows for reduced set-up time and reduced the effects of moisture loss compared to strain gauge attachment as well as providing information on the surface fibre movement during testing.

Previous investigations into the internal behaviour of the global joint have been limited. Slater (2011) found through X-Ray CT scanning there were half the number of vessels but more cell wall material within the global joint compared to the adjacent stemwood. This suggests the structural characteristics of the global joint could vary from the standard straight sections of timber. Müller *et al* (2006) showed homogenity of strain using 3D Electronic Speckle Pattern Interferometry (EPSI) on a loaded perfectly symmetrical global joint. This test

however alluded to the difficulties of finding a perfect global joint within the natural tree.

A clear link has not been made between properties of cut timber obtained from known standards and researched knowledge of the investigated strength of the living branch. According to Cannell and Morgan (1989), a living tree has moisture movement within it and the timber tends to have higher moisture content than that of dried/cut timber. This should significantly weaken the branch and this thesis aims to assess the branch joint structural properties. In this chapter, the standard timber tests are applied to components taken from a branch joint. These components are square battens cut through the cross section of the branch joint. The components have been assessed for their material properties under the established British Standards BSEN408 (BSI (2003)), BS373 (BSI (1957)), and BS5820 (BSI (1979)). This will include measuring the moisture content of the fresh cut branch joint components in accordance with BSEN13183 (BSI (2002)). The results will be analysed to give a true representation of the branch internal strength in relation to the standards already set out in, for example BS5820 (BSI (1979)).

6.2   Methodology

The methodology is based on the principle of creating components from the joint to develop knowledge of the joint's internal behaviour under loading, in a testing framework relatable to timber standards. Good representative specimens of branch joints were selected from *Quercus Robur (L.)* oak trees in the New Forest, UK harvested in November 2010. Once the branch joints had been cut from the trees, the angle at which the secondary growth connects to the main stem was brought through into the main stem to provide the

secondary cut (Figure 52). The sample is then further cut into approximately 25mm by 25mm cross sectional linear battens (Figure 52). Once cut, these samples were wrapped to avoid excessive moisture loss. The time from cutting the joint samples into components until testing was minimised as far as practicable and all tests were completed within two weeks of batten cutting. For these tests three joints were acquired, from which a total of twenty battens were cut and load tested.
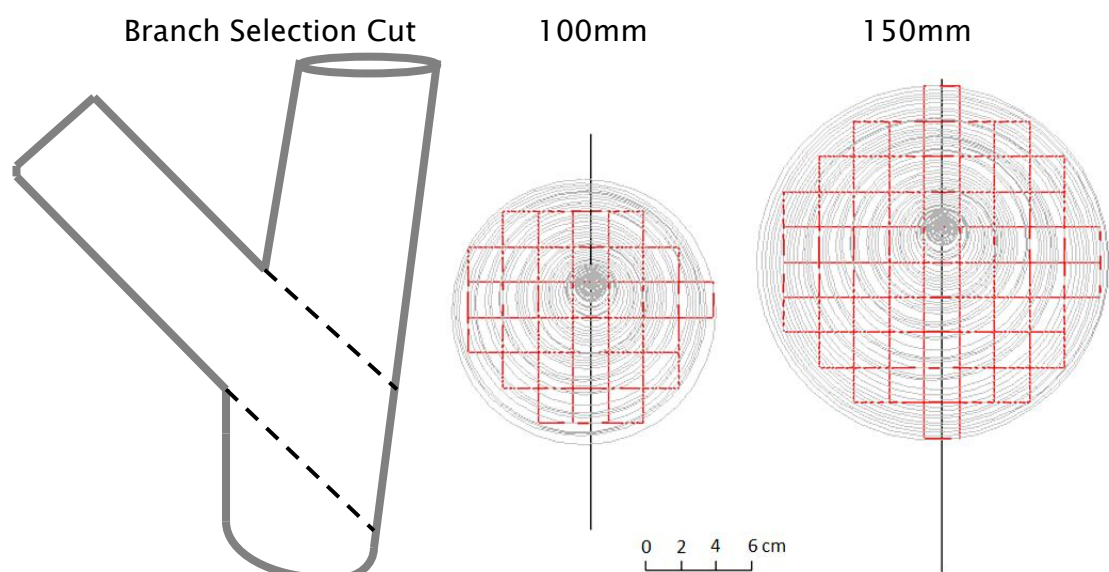
FIGURE 52: FROM LEFT TO RIGHT: BRANCH SELECTION CUT FROM JOINT, 100MM AND 150MM BRANCH CROSS-SECTION BATTEN CUT ARRANGEMENT

The components were tensile tested parallel to the secondary growth consecutively, using the standardised test procedures given within the British Standards. These standards were used as a base for the methodology for this test. The standards (BSEN408 (BSI (2003)), BS373 (BSI (1957)), BS5820 (BSI (1979)) are the closest comparable procedures to achieve the required strength tests. Freshly cut component samples were moisture content tested (as required by the standard test procedure) prior to the tensile test, immediately after the tensile test and after satisfactory oven-drying.

Component dimensions for the tensile test needed to be practical. BS373 (BSI (1957)) requires a 6mm thick dumbbell shaped coupon of timber, in total 300mm long, and 20mm wide, with a 50mm by 3mm clear section in the centre of the coupon. Due to the softness of the freshly cut sample used in this project, this standard shape and size could not be achieved without causing localised weakness through tearing of the wet outer fibres. The dumbbell shape is however required to give a sufficient surface area for the grips of the tensile machine to hold onto during pulling.

BS5820 (BSI (1979)) and BSEN408 (BSI (2003)) shape and size requirements were used. These standards request the size of the sample to be determined by finding the width, h, of the cut sample and multiplying by nine to give the required length of the sample between the grips. The sample length was then extended to give room for the grips to hold the sample in place. The excess zones were then cut off and split into packers and control moisture content off-cuts (shown as P and MC, respectively in Figure 53). The requirement of the dumbbell from BS373 (BSI (1957)) was solved by adding packers in the gaps in the machine grips which reduced the perpendicular embedment of the teeth of the grips into the soft sample.
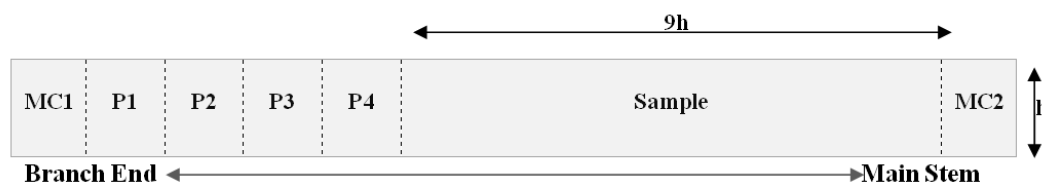
FIGURE 53: BRANCH COMPONENT BATTEN CUTTING ZONES

A Denison Mayes® hydraulic 650kN tension/compression testing machine was used to apply a force under displacement control at a rate of 0.00005h mm/s parallel to the grain in accordance with BSEN408 (BSI (2003)) and BS5820 (BSI

112

(1979)) to stretch the sample to destruction. The displacement increments were paused for 2 minutes at each stage to allow for creep movement in the timber to occur. The strain was measured in two ways, using the displacement of the machine grips pulling the sample and using the photogrammetric technique, Particle Image Velocimetry (PIV). The tensile force applied was recorded by the machine. An incremental force was applied to the sample, with a one minute load time and two minute rest period where no movement took place, in order to show any creep within the sample. The mass of the sample to determine the moisture content was measured at three stages (before the test, after the test and once oven dried) using the oven-drying method in BS13183 (BSI (2002)). The oven drying was done at 70°C, until the mass variation was less than 1% deviation between weighing periods. The moisture content was determined for all tested samples, including any knots or resin which although contrary to the standard, showed the true data representation of the sample's water content.

As the PIV photographic experimental set-up takes images of two perpendicular sides of the sample (seen in Figure 54), for each experiment these zones are selected for later analysis. The strain of the components cut from the branch was analysed under Particle Image Velocimetry (PIV). The PIV technique will remove the need to attach a separate strain gauge to each component and gives an accurate representation of the movement of grains and surface fibres during the test.

FIGURE 54: FRONT (LEFT) AND SIDE (RIGHT) VIEW OF SAMPLE G1 IN PIV ANALYSIS SOFTWARE

The set-up of the PIV equipment is relatively simple, with a camera set-up parallel to each of the observed faces during the experiment (see Figure 55). To ensure the light on the surface of the sample stays consistent, continuous lighting rigs were positioned at approximately 45 degree angles to the setup to allow the sample to have even lighting throughout the experiment. The cameras were set to take photos at (approximately one minute) intervals during the experiment. These in-focus photos are then numerically analysed using a Matlab® program as previously described in Chapter 5.
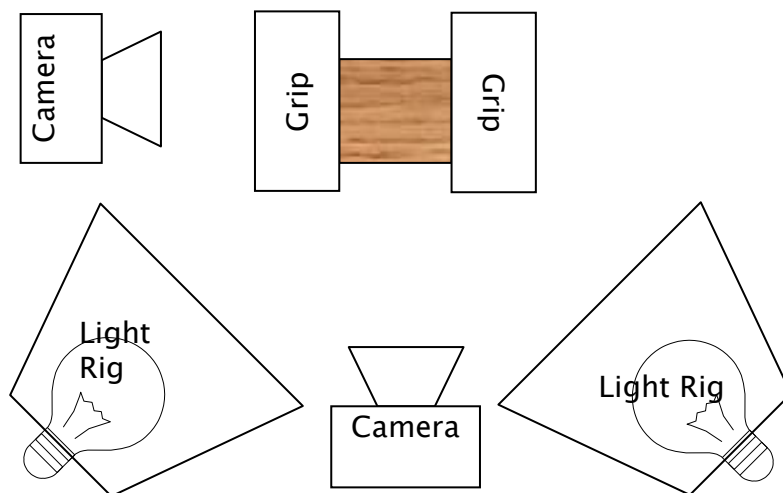
FIGURE 55: PLAN VIEW OF CAMERA SET-UP

6.3 Results and Discussion

Analysis from only one component sample, G1, out of a total twenty will be described fully, with the analysis of further samples shown in Appendix 6. The properties of all the components can then be compiled for further analysis of the entire global joint.

6.3.1 Qualitative Analysis of Samples

Three global joints were taken, from which twenty component samples were obtained. All these samples were tensile tested and the overview of these samples is given in Table 7. The prefix letter to the sample identity, references the global joint the component was taken from. Some samples were deemed 'not obtainable' due to the high moisture content causing problems during cutting.

Joint Image	Sample ID	Nominal Width (mm)	Ultimate Load (N)
	G1	22	8580
	G2	Not obtainable	
	G3	22	3420
	G4	24	2360
	G5	23	6520
	G6	24	4450
	G7	24	1310
	G8	Not obtainable	
	G9	23	6430
	G10	22	3920
	G11	24	4900
	S1	24	7110
	S2	25	4400
	S3	25	4000
	S4	25	3480
	T1	22	3650
	T2	Not obtainable	
	T3	24	6870
	T4	23	6580
	T5	24	5200
	T6	Not obtainable	
	T7	24	7050
	T8	25	1510
	T9	25	6560

TABLE 7: COMPONENT SAMPLES OBTAINED FROM GLOBAL JOINTS (G, S AND T) FOR TENSILE TESTING

It can be seen from the sudden brittle breakage of the majority of the samples the grain and rays play an important factor in the behaviour. The failures can be seen to follow through the lines of medullary rays between grains. The sketches in Figure 56 show the grain orientation of sample G1 before and after

breakage. The failure of the samples tends to occur towards the primary growth (bottom of photo) which tends to be an area of perpendicular grain (further sample sketches are in Appendix 6). It is perhaps not surprising the primary growth attachment is an area of weakness. The samples also showed a tendency to break at knots or weak points close to the crotch and primary growth interface.

Figure 56: G1 Sample Grain Orientations of the Front View (left 4 images) and Side View (right 4 images); with First 2 of 4 Images Before Failure and Last 2 of 4 Images After Failure

6.3.2 Comparison to Structural Timber Standards

A quantitative comparison with British Standards will help to ascertain the structural values of the Oak samples tested. BS5268 (BSI (2002a)) is used for this, data values are shown in Table 8. Service Class 3 (SC3) will be used as the wood samples can be taken as 'external use and fully exposed'. Most other modification factors, 'k-values' will improve the performance values of the timber, thereby just SC3 is used to adjust the values. The standard comparable values are: tensile strength 4.32 N/mm^2, modulus of elasticity 4800 N/mm^2, and average density 680 kg/m^3.

Strength Class	D30	D40	TH1	TH2	THA (> 100mm)	THB (> 100mm)
Bending Parallel to grain (N/mm²) $k_2=0.8$	9	12.5	9.6 Apply to 300mm	7.8 Apply to 300mm	12.6 Apply to 300mm	9.1 Apply to 300mm
Tension parallel to grain (N/mm²) $k_2=0.8$	5.4	7.5	5.8 Apply to 300mm	4.7 Apply to 300mm	7.6 Apply to 300mm	5.5 Apply to 300mm
Compression parallel to grain (N/mm²) $k_2=0.6$	8.1	12.6	9.3	8.4	10.5	9.0
Compression perpendicular to grain (N/mm²) $k_2=0.6$	2.8 2.2	3.9 3	3 Prohibits wane	3 Prohibits wane	3 Prohibits wane	3 Prohibits wane
Shear parallel to grain (N/mm²) $k_2=0.9$	1.4	2	2	2	2	2
Modulus of elasticity mean (N/mm²) $k_2=0.8$	9500	10800	12500	10500	13500	12000
Modulus of elasticity minimum (N/mm²) $k_2=0.8$	6000	7500	8500	7000	10500	7500
Characteristic Density (kg/m³)	530	590	580	580	580	580
Average density (kg/m³)	640	700	690	690	690	690

TABLE 8: BRITISH STANDARD MATERIAL PROPERTY VALUES FOR OAK (BS5268)

6.3.3 Machine Output

The stress and strain results of the tested samples were calculated, from which

graphs were obtained. The stress was calculated using Equation 7 and the

strain calculated from the machine grip displacement and original length using Equation 8.

EQUATION 7: $\quad \sigma_t = \dfrac{P}{A}$

EQUATION 8: $\quad \varepsilon_t = \dfrac{\Delta L}{L}$

where σ_t is the tension stress, P is the load applied, A is the cross-sectional area of the batten, ϵ_t is the tensile strain, L is the original length of sample between the grips and ΔL is the change in length.

The stress and strain were plotted against each other to form a stress–strain graph which shows a curvilinear shape up to the failure point at the peak of the graph (Figure 57). The higher envelope to the graph (indicated by red curve) gives the instantaneous response of the sample and the lower envelope of the graph (indicated by green curve) shows the start of lasting effects on the viscoelastic material, as further explained in the creep analysis section later. The build up in stiffness shown at the start of the plot can be explained through two reasons. Firstly, there is a settling in phase of the test, where the grips may slip against the sample as it is pulled. Secondly, due to the high moisture content, the sample in tension will be more sensitive to creep and hence permanent strain will occur at the start. It is from this graph the Young's Modulus may be determined, however this methodology has been plotted separately later (section 6.3.6).
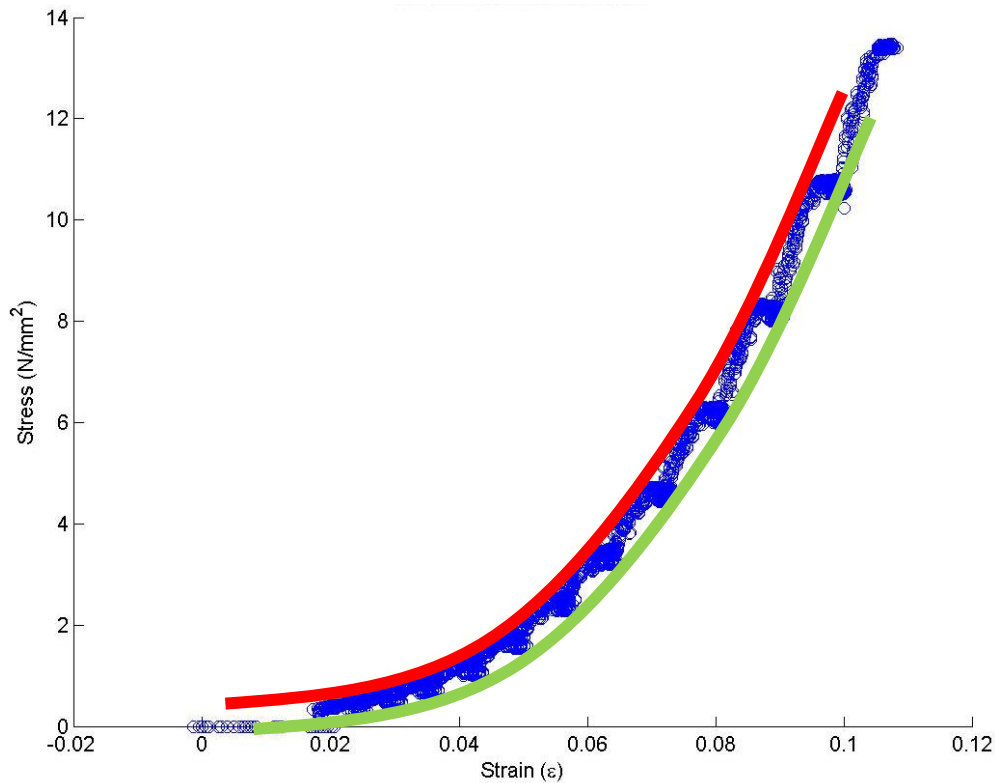
FIGURE 57: G1 STRESS VS. MACHINE MEASURED STRAIN

6.3.4 PIV

From the PIV output results there are two types of strain that can be obtained, true strain and engineering strain. From this testing it will be engineering strain used for analysis. The strain is evaluated per element in the square grid; thereby the summation of the elements within the sample should give the overall strain.

The two views of the sample using the PIV measured strain have similar outputs to the machine measured strain (Figure 58) yet the amplitude of the data points suggest the data point calculation will need to be reviewed. It is clear from this figure the values for strain are either side of the machine measurements, suggesting the overall strain from the PIV can be averaged to that of the machine measured strain. A reasonable explanation for this is the grain pattern and fibres in the views taken for PIV analysis are orientated

differently and hence react differently in flexibility and movement during tension loading. This is further evident in the breakage pattern shown.
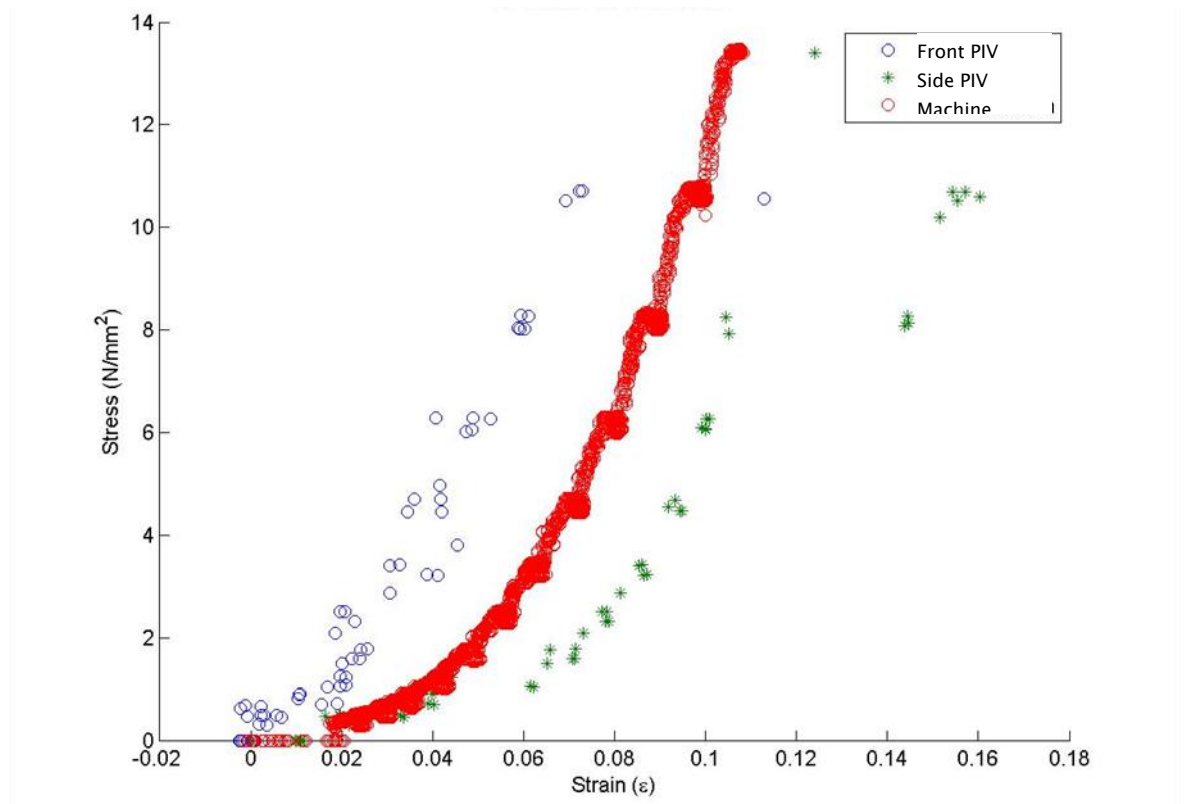
FIGURE 58: SAMPLE G1 TENSILE STRESS VS. COMPARATIVE STRAINS (MACHINE MEASURED AND PIV FRONT AND SIDE VIEW)

The engineering strains from PIV are plotted as contour graphs to show the variation in the surface deformation in the sample. The graphs produced show the strain in their x and y direction on each face of the sample and the shear strain values. The PIV plots show the major movement is in the y-direction of the sample as expected due to the tension pull of the machine. It can be seen a diagonal failure is found (at the lower third – middle of the sample) in both the front (Figure 59) and side (Figure 60) view from the PIV, with a more steeply inclined failure evident in the side view.
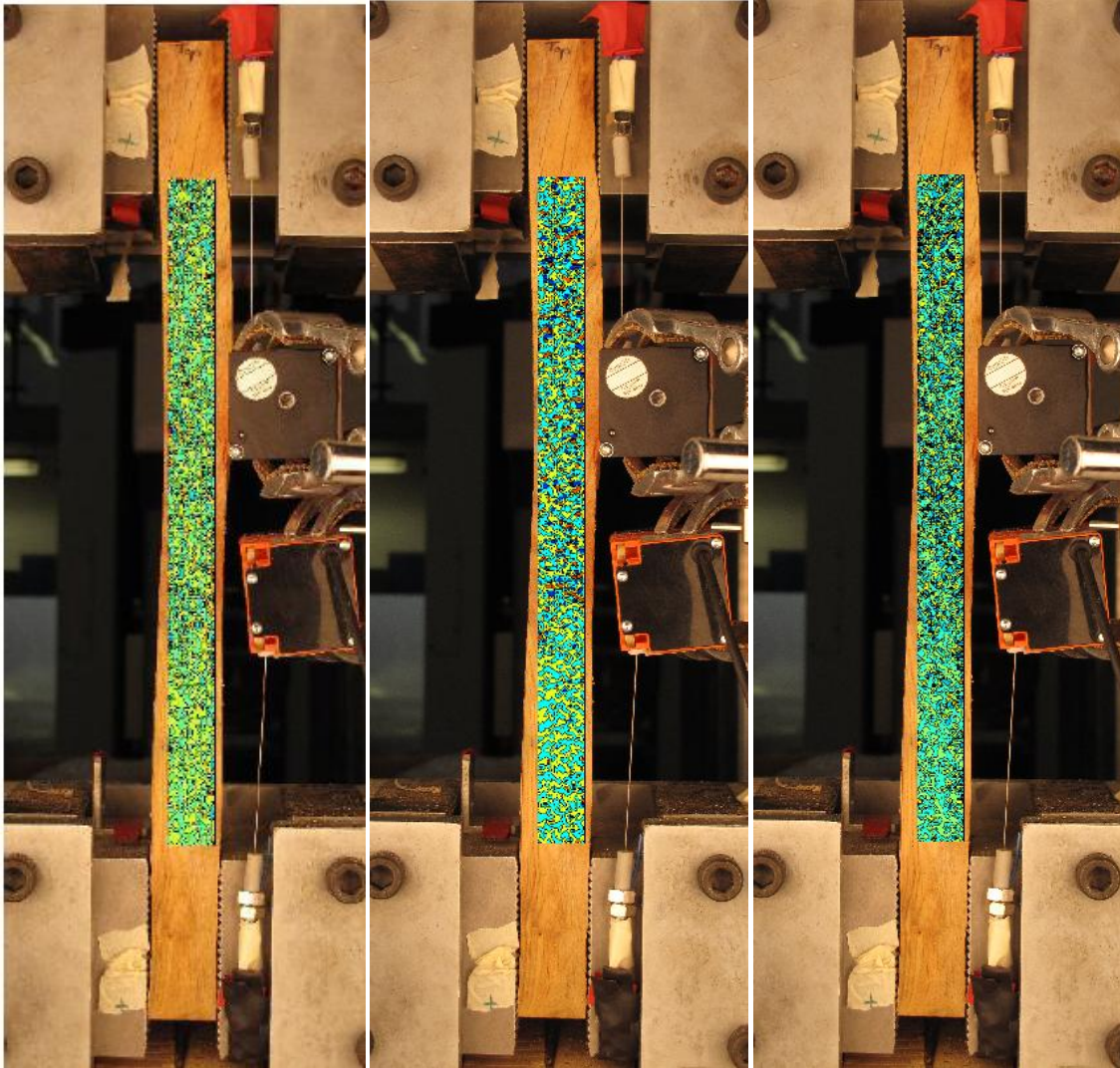
FIGURE 59: PIV ANALYSIS CONTOUR PLOT FOR FRONT VIEW X–DIRECTION, Y–DIRECTION

AND SHEAR STRAIN (FIRST–LAST DITCH ANALYSIS)
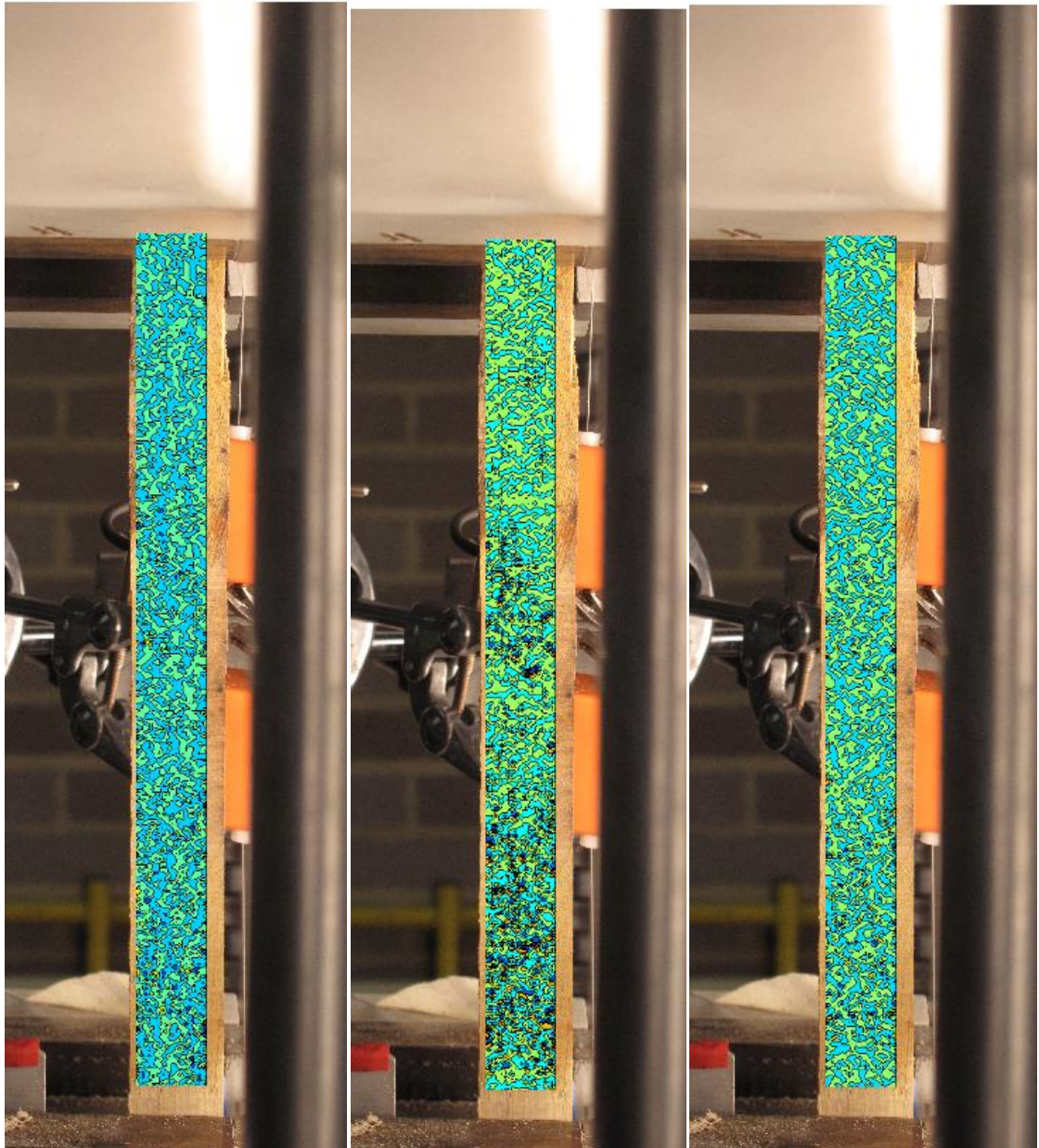
FIGURE 60: PIV ANALYSIS CONTOUR PLOT FOR SIDE VIEW X-DIRECTION, Y-DIRECTION AND
SHEAR STRAIN (FIRST-LAST DITCH ANALYSIS)

6.3.5 Creep

Creep sensitivity has already been shown in the stress-strain graph from the
tension test, due to high moisture causing permanent strain at low stress.
Viscoelastic behaviour of timber is demonstrated in creep occurrences, with
high stress over time creating high strain. This is normally accounted for in
British Standard calculations through a load term modification factor. The load

vs. time graph (Figure 61) and the staging of the loading (Figure 62) allows for the analysis of the creep during the experiment. The steepness of the load increase zone increases and the time for load relaxation as the sample approaches the ultimate load. Carrying these relaxation zones across can also give an idea of the long term response of the timber sample under loading. Figure 62 shows the separation of the loads so the analysis of short term loading (Load increases) and long term loading (Load Decreases) can be extrapolated. By doing this, an estimate of the ultimate service load can be derived that is likely to occur under constant windloading (*i.e.* under initial load (short term) and constant gusting (long term dynamic)).
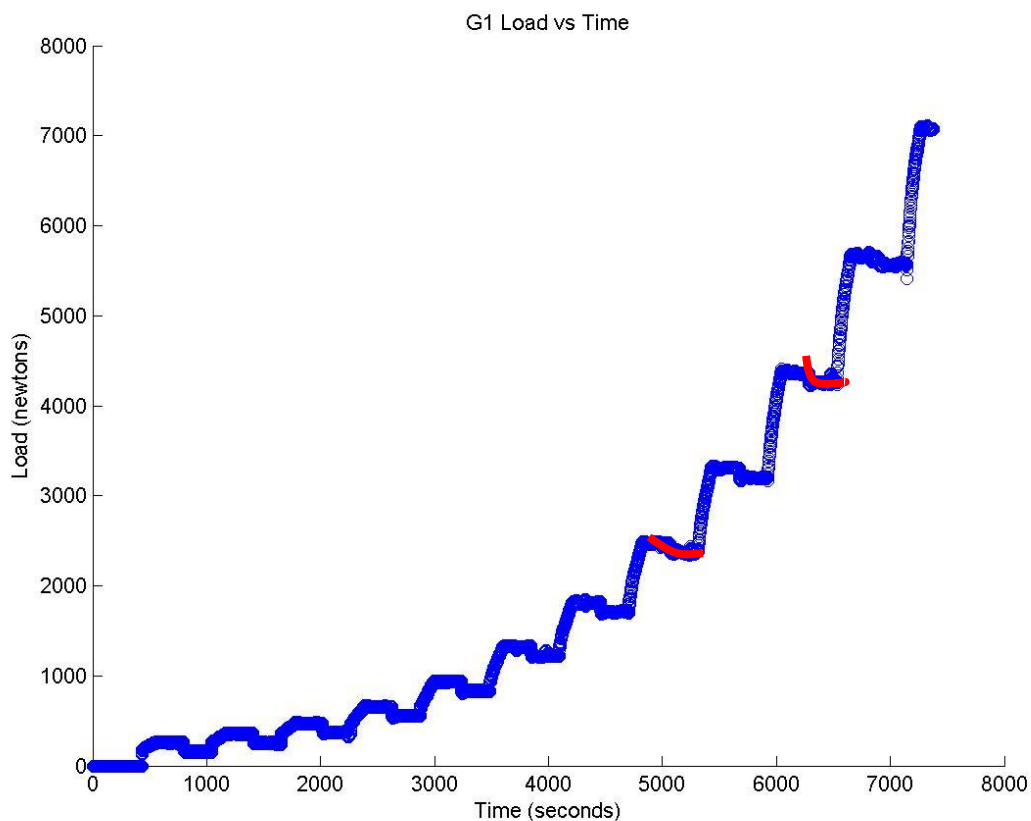
FIGURE 61: LOAD VS. TIME GRAPH USED TO FIND CREEP AND LONGEVITY OF LOADING
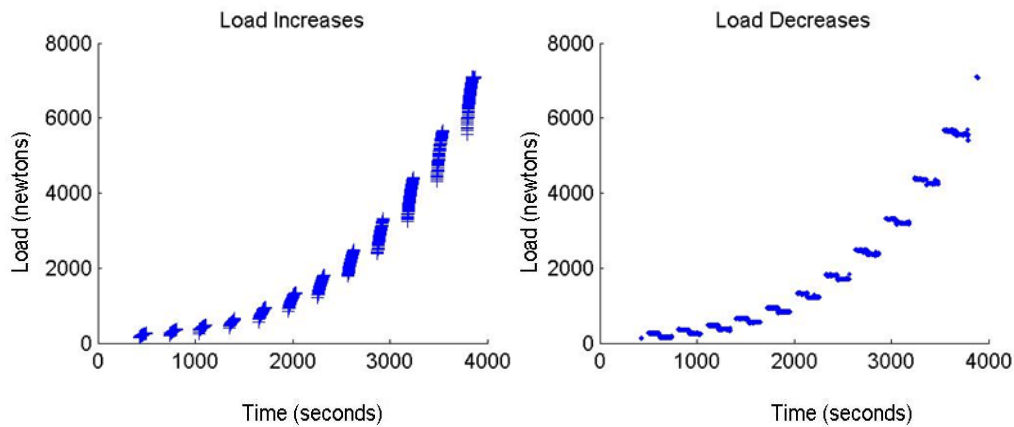
FIGURE 62: CREEP SEPARATION OF LOAD INCREMENTS AND RELAXATION (LOAD VS. TIME)

6.3.6 Modulus of Elasticity

The modulus of elasticity (MoE) is an important property for determining the structural stability in engineering terms. Obtaining the Young's Modulus from the specimens can give an idea of the stiffness of fresh wood components. Having found the strength and strain, the MoE in tension can now be determined. The usual method to obtain this value is based on BSI (1979) and is calculated as follows:

EQUATION 9: $\qquad E_t = \frac{\Delta PL}{A\Delta L}$

where E_t is the tangent MoE in tension, ΔP is the increment of load applied, A is the area of the section, L is the gauge length, and ΔL is the deformation under the load of ΔP. The calculation is taken between creep load increments (highest and lowest data points in each separation) in order to get the tangent between two points. The MoE can be worked out using a simpler formula, known as secant from the stress and strain values calculated in Equation 7 and Equation 8:

EQUATION 10: $\qquad E_s = \frac{\sigma_t}{\varepsilon_t}$

where E_s is the secant MoE in tension, σ_t is the tensile strength of the component and ε_t is the strain. The tangent MoE is adequate for simple

assessments; however the secant can be used for ultimate progression of the MoE up to failure.

Both Young's Moduli are calculated using the machine strain. The secant Modulus of Elasticity increases with time as shown in Figure 63, the peak E_s is 127 N/mm^2. This shows the material becoming more permanently deformed yet having some lasting elasticity as it is loaded. The figure shows how the tangent modulus of elasticity values, E_t, vary considerably through the testing, with large peaks, likely to be at points of fibre failure. The peak value of E_t at load increase was 437 N/mm^2 and the peak value of E_t at relaxation load was – 465 N/mm^2. This negative value is due to the data points going from higher to lower in the calculation, but suggests the sample trying to reverse the failure and rearrange the fibres to compensate. Changes within the Young's Moduli graphs shows the visocelasticity of the material and the varying properties (from different fibres) change to the deemable strength and stiffness properties of the sample.
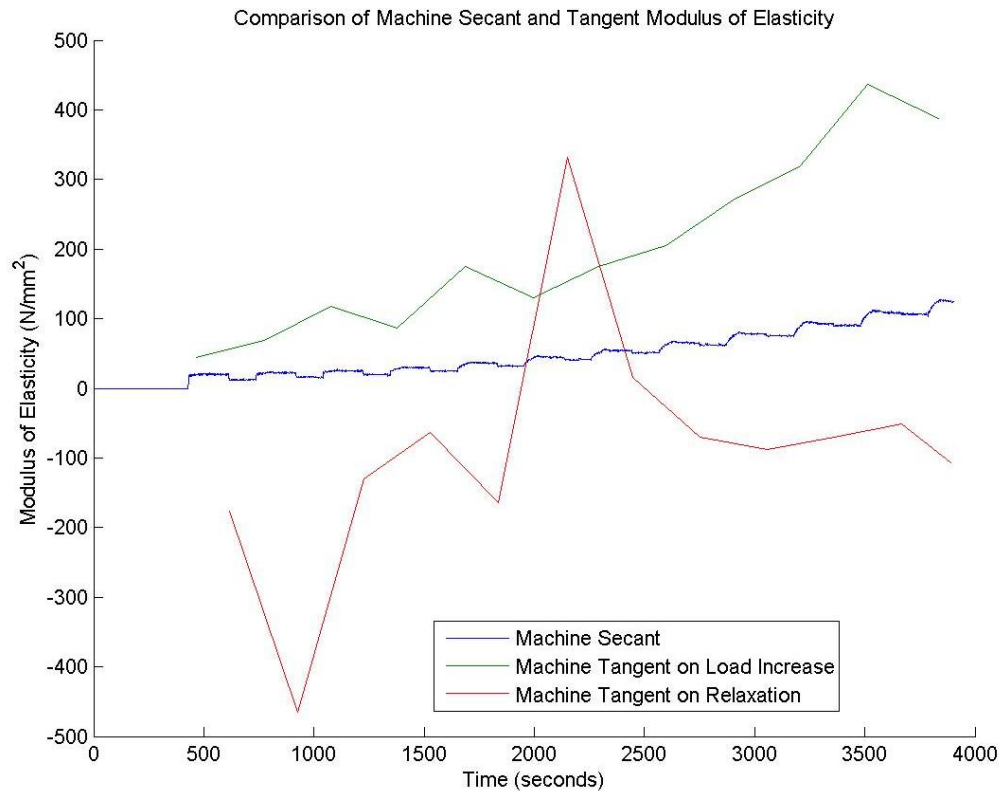
FIGURE 63: G1 YOUNG'S SECANT AND TANGENT MODULI VS. TIME CALCULATED THROUGH MACHINE STRAIN

Figure 64 is a plot of the Secant and Tangent Young's Moduli calculated through PIV strain against time, which shows similar trend of final E values. This is an encouraging result that shows the PIV strains are working and the accumulation of the test results is reasonable. There is some variance within the Front View PIV calculation (shown in the erratic behaviour on the graph). This could have been due to the smaller image area used to calculate the strain, thus giving a likelihood of greater errors. This is not to say the Front View PIV is not accurate but in comparison to the Side View PIV (which has a greater image area to analyse for every sample) there is likely to be a lower accuracy. There could also be a relationship to the failure of the sample too, the front of the sample broke in two places (see Figure 56) suggesting there were probably more radical changes in strain of the monitored images of the front.
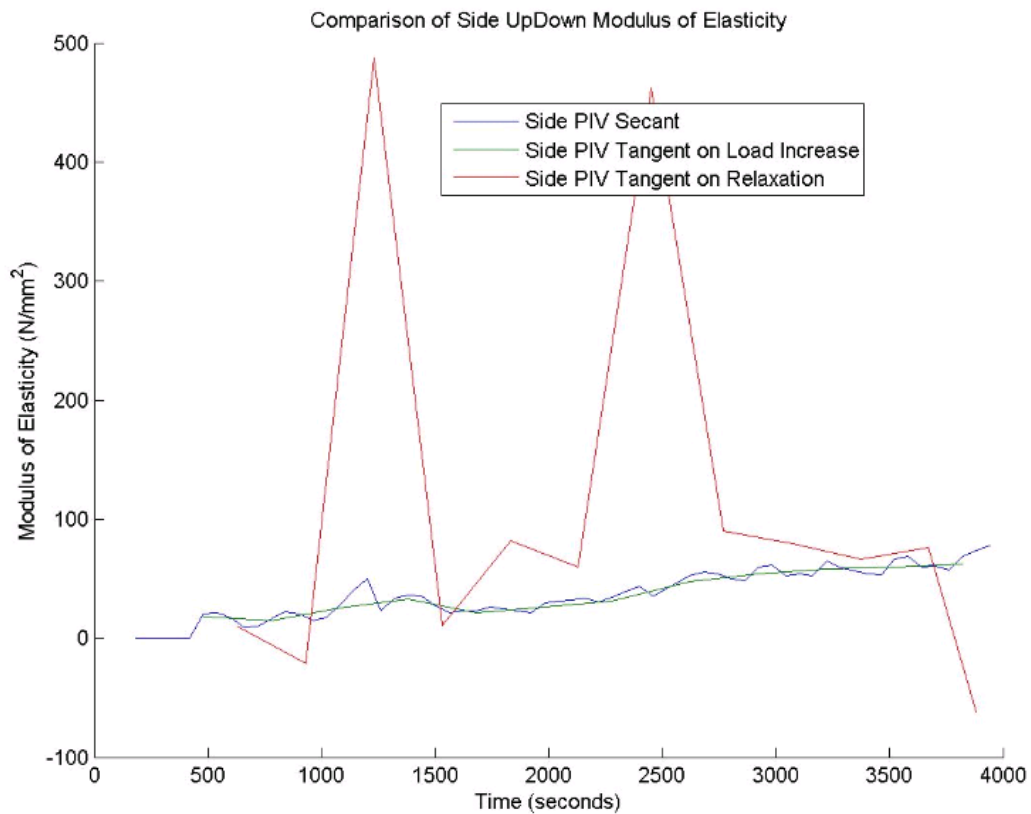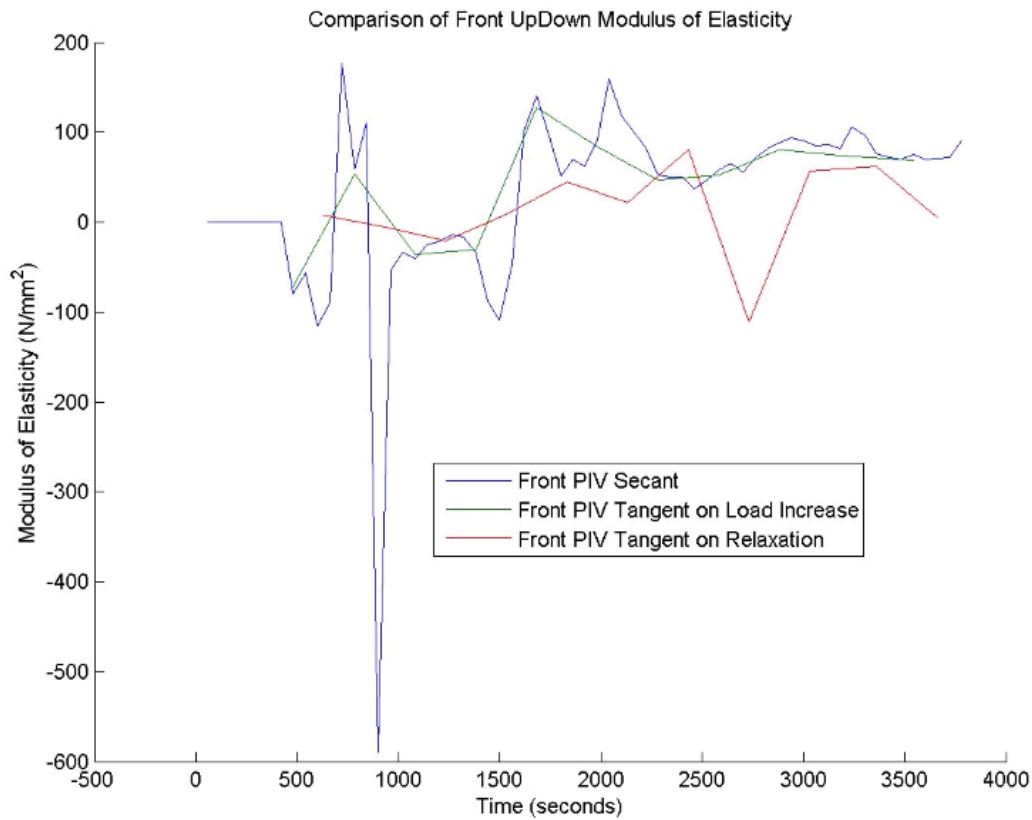
FIGURE 64: PLOT OF YOUNG'S SECANT AND TANGENT MODULI VS. TIME CALCULATED

THROUGH PIV STRAIN (FRONT VIEW (ABOVE), SIDE VIEW (BELOW))

Comparing the machine and PIV moduli values shown in Table 9 and Figure 65 shows the PIV values are less than that given for the machine strain. However this should be expected due to the testing circumstances, such as the machine measuring an overall movement of the sample and grip slippage and not just a sample specific movement. The average of the PIV secant moduli matches that of the machine. However the tangent moduli are not similar due to the number of images taken during the testing not allowing for enough data points.

G1	Secant (N/mm²)	Tangent Increment (N/mm²)	Tangent Relaxation (N/mm²)
Machine	127	437	332(–465)
Front	176	128	80
Side	77.6	62.2	487

TABLE 9: MODULUS OF ELASTICITY CALCULATED FROM DIFFERENT MEASUREMENTS OF STRAIN
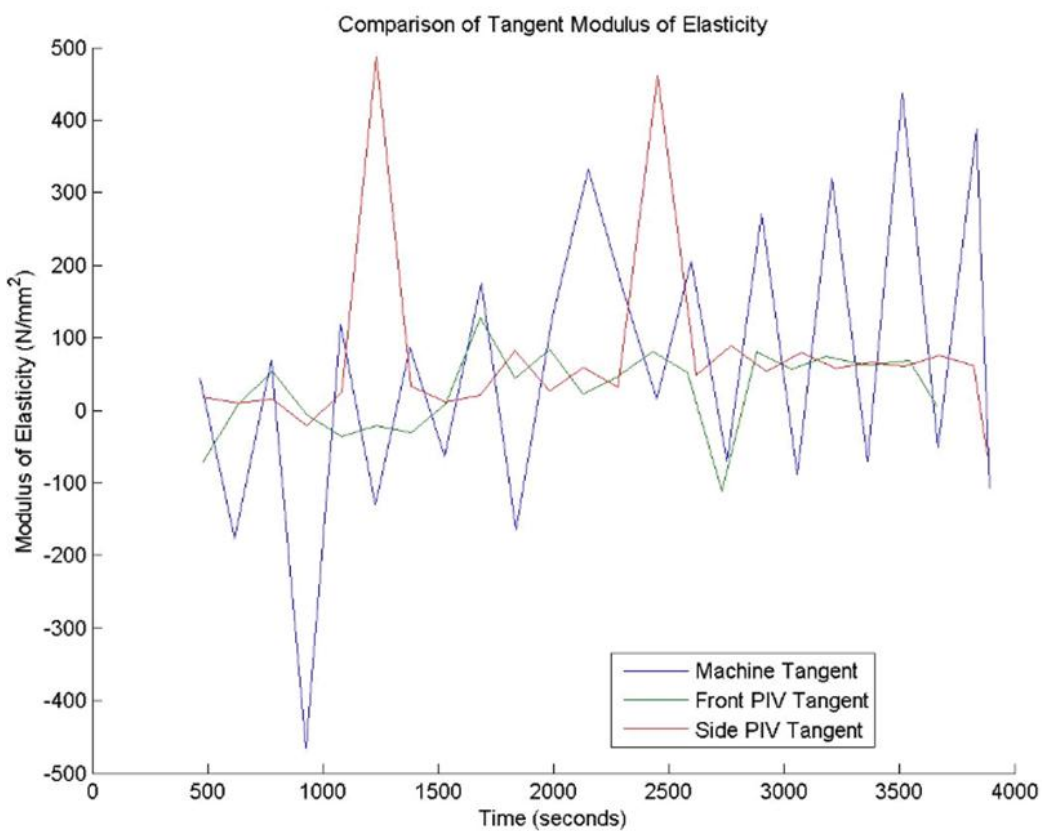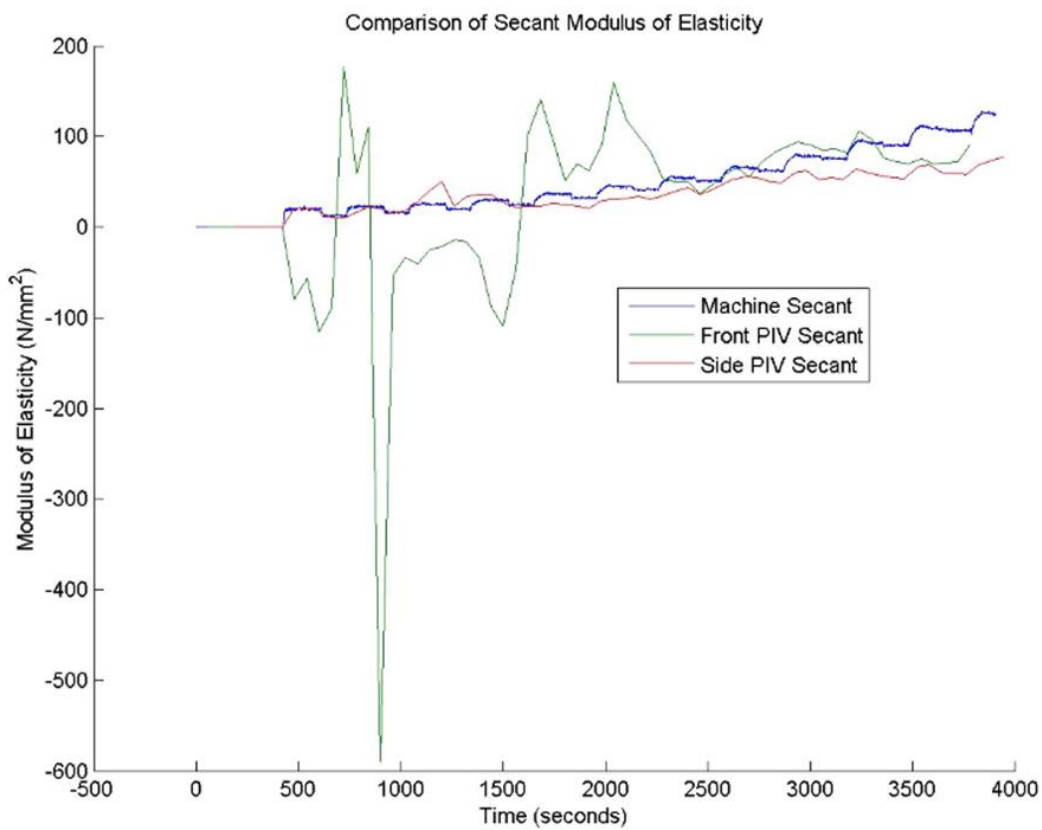
FIGURE 65: SECANT (TOP) AND TANGENT (BOTTOM) MODULUS OF ELASTICITY COMPARISON

OF MACHINE AND PIV RESULTS

6.3.7 Moisture Content

Moisture content of the samples was determined through calculation. The dry mass of the samples was calculated through the standard equation of BSI (2002b):

EQUATION 11: $\omega = \left(\frac{m_1 - m_0}{m_0}\right) \times 100$

where m_1 is the mass in grams of the sample before drying, m_0 is the mass in grams of the sample after drying, and ω is the percentage moisture content.

Table 10 shows the moisture content of the sample of the component during the experiment. The samples appear to have moisture content of 38–44%. However this could be lower than that expected of a fresh cut sample as the joint samples were cut in November 2010 but the batten cutting of the sample and tests were done in March 2011.

Component Element	MC Prior to Test (%)	MC Directly after Test (%)
Sample	41.20	36.29
P1	43.74	39.88
P2	42.90	39.46
P3	40.17	37.45
P4	40.09	36.64
MC1	38.51	35.14
MC2	41.38	35.50

TABLE 10: MOISTURE CONTENT LOST OF G1 DURING TEST

An interesting aspect of the moisture content results is the sample was weighed before testing and directly after the test, at which point the moisture content had changed between 2.7–5.9% (see Table 10). This suggests the energy exerted through the test produces some heat or increases the pressure which causes some moisture loss, as theorised in previous work by the author shown in Appendix 5. However this high level moisture loss could also be attributed to the environment of the testing area, particularly the air from the cooling fan of the hydraulic pump situated near to the testing machine.

6.4   Overview of All Component Samples

6.4.1   Overall Discussion of Methodology

The overall procedure for the test was good. However there were some samples which failed close to the grip areas. This could either be due to the localised stress at the grip point or it could be attributed to the changing grain direction, where the main growth meets the branch growth, which is generally closer to the grips due the batten cut of the samples. The grain directions of the samples have been plotted to further qualitatively analyse this point in Appendix 6. Other failures occurred at weak points such as knots, or central piths. The locations of all failures appear to follow the grain and ray lines within the wood specimen. This suggests once the rays are broken that shear between the laminations of the grain occurred. This could be due to the change in direction of grain near the join of the original joint, seen in the component sample as leading the parallel to the grain load in the branch zone into perpendicular grain failure in the main stem zone.

The image technology of PIV and its strain output compared to machine measured strain shows promise, though the creep staging limited the timings

of images. Therefore more images should be taken in the test time to get more data points and thereby better results. The strength is close to that of the standard values but the modulus of elasticity is not. This may be due to the strain values changing during creep. More test samples would help to gain definitive proof.

6.4.2   Overall Results

The calculations were applied to the other samples within the test series. A summary of results can be seen in Table 11, further details can be found in Appendix 6. According to BS5268 (BSI (2002a)), D30 timber grade, has values: tensile strength, $4.32N/mm^2$, and modulus of elasticity, $4800 N/mm^2$. Note these values are taken for timber with half the moisture content of the tested sample. Therefore variation in results will be expected, especially as moisture content higher than 20% causes an exponential decline in tensile strength and MoE. The tangent MoE is presented as an average of $70.80N/mm^2$ for all components tested. Much lower than the expected value from the BSI (2002a) standard of $4800N/mm^2$. However this fraction should be expected when the sample is so moist. The tensile strength does vary about the standard value of $4.32N/mm^2$, with Joint G averaging $6.35N/mm^2$, Joint S averaging $7.00N/mm^2$, and Joint T averaging $8.17N/mm^2$. If the standards are understood correctly the value of tensile strength is going to be cautionary estimating it as lower than the average to allow for possible timber defects. The average density values do concur with Slater (2010) showing the increased moisture content contributes to an increased density region in the joints.

Sample ID	Nominal Width (mm)	Ultimate Load (N)	Sample Moisture Content (%)	Moisture Content Loss during experiment (%)	Ultimate Tensile Stress (N/mm²)	Ultimate Machine Strain	Ultimate PIV Y Eng Seq Strain Front	Ultimate PIV Y Eng Seq Strain Side	Short-Term MoE (N/mm²) (Tangent)	Long Term MoE (N/mm²) (secant)	Average Density (kg/m³)
D30			20+		4.32					4800	640
G1	22	8580	41.2	4.91	13.47	0.108	0.154	0.184	436	127.4	775
G3	22	3420	39.7	2.50	4.25	0.061	0.101	0.088	1546	74.1	854
G4	24	2360	39.3	2.19	2.69	0.077	0.020	0.076	185	35.2	673
G5	23	6520	44.1	3.88	10.79	0.144	0.182	0.263	1043	77.8	631
G6	24	4450	42.1	3.23	5.33	0.088	0.029	0.151	1499	62.0	732
G7	24	1310	39.8	1.73	1.04	0.055	0.030	0.056	90	20.3	718
G9	23	6430	40.4	1.97	6.65	0.072	0.041	0.035	850	102.9	611
G10	22	3920	42.7	2.85	5.98	0.098	0.111	0.035	468	63.2	899
G11	24	4900	40.1	3.19	6.96	0.130	0.102	0.175	390	52.8	788
S1	24	7110	67.6	3.49	11.90	0.288	0.032	0.939	869	64.0	1109
S2	25	4400	68.7	3.88	7.04	0.282	0.103	0.200	193	179.0	1165

Sample ID	Nominal Width (mm)	Ultimate Load (N)	Sample Moisture Content (%)	Moisture Content Loss during experiment (%)	Ultimate Tensile Stress (N/mm²)	Ultimate Machine Strain	Ultimate PIV Y Eng Seq Strain Front	Ultimate PIV Y Eng Seq Strain Side	Short–Term MoE (N/mm²) (Tangent)	Long Term MoE (N/mm²) (secant)	Average Density (kg/m³)
S3	25	4000	72.4	4.02	6.15	0.262	0.104	0.136	196	33.1	973
S4	25	3480	73.7	4.09	2.90	0.111	0.121	0.026	696	25.8	1048
T1	22	3650	70.4	2.10	5.62	0.110	0.039	0.023	502	52.3	1219
T3	24	6870	72.7	3.53	11.20	0.265	0.071	0.036	1050	88.5	1025
T4	23	6580	72.1	3.53	6.86	0.128	0.023	0.049	579	55.2	1145
T5	24	5200	79.2	3.01	7.49	0.106	0.052	0.040	350	75.1	1111
T7	24	7050	79.1	3.67	11.80	0.202	0.002	0.083	617	94.9	1042
T8	25	1510	71.1	1.75	2.05	0.137	0.043	0.145	222	15.3	1088
T9	25	6560	75.9	2.91	12.2	0.125	0.051	0.034	1180	98.1	1104

Table 11: Overall Results for Component Tensile Tests

6.5 Component Accumulation Model

An investigation of the possible overall properties of the global joint is derived

by using its component parts by accumulating the results of the tested

components of Joint G (seen in Figure 66) to create a 'reassembled joint'. At this stage it is worth noting the cut of the component samples will not always reflect the exact position it held within the joint (due to the precision of cutting), so these results and simulations can only be used as an indication of overall joint behaviour.

FIGURE 66: JOINT G COMPONENTS BATTEN CUT

6.5.1 Quantitative Review

In Figure 67, the stress-strain relationships are analysed for the components in the entire global joint. The stiffness of the components are indicated by the gradients of the curve increased gradients shows a high stiffness under tension, reduced steepness indicates a reduced stiffness in tension. The central

component has a higher stiffness and strength than the surrounding components. The outer component at the top and bottom of the branch also appear to have more substantial structural properties, with the left hand side also having larger values. This suggests the left hand side has experienced tension reaction to loads from presumably the bottom left.
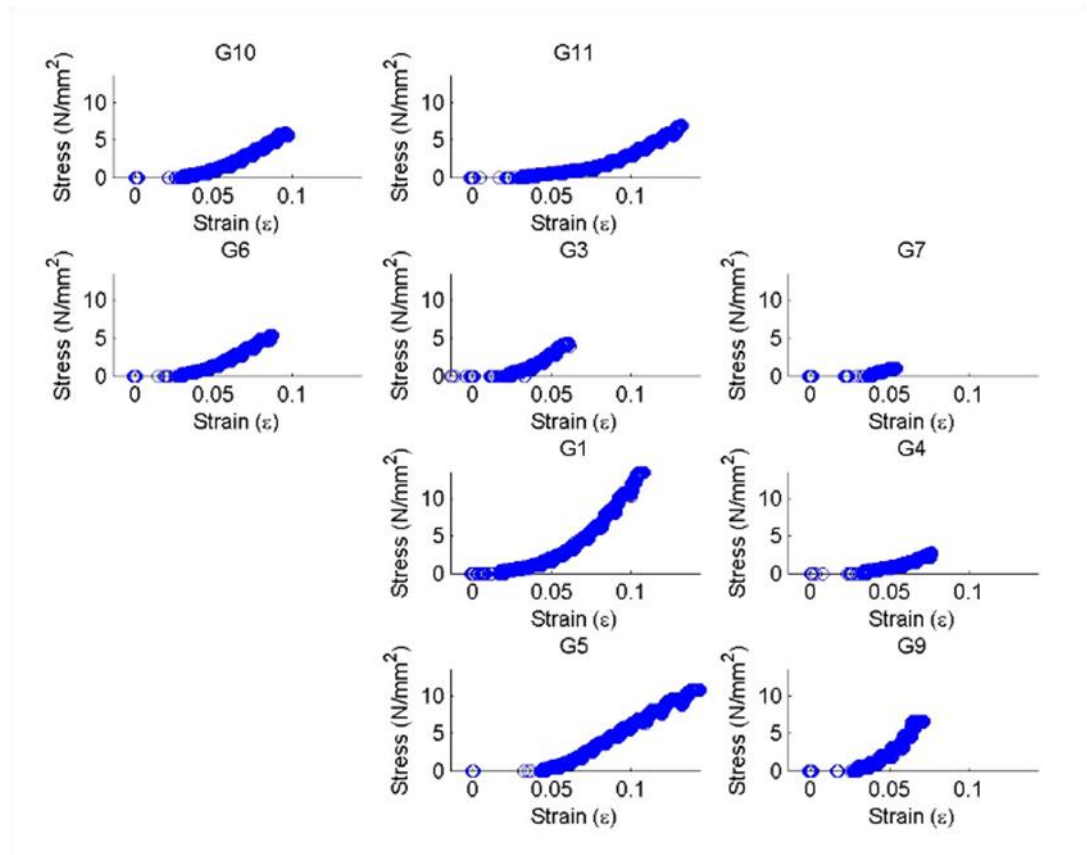
FIGURE 67: GRAPHS OF STRESS VS. STRAIN PLACED AT COMPONENT LOCATIONS WITHIN JOINT G

Analysing the structural property values gained at the locations gives an insight into inherent changes within the global joint (Figure 67). The tensile strength is greater at the centre of the global joint, in conjunction with theories the centre becomes mature and stronger (Bruechert *et al* (2000)). There is a possibility showing through the data values there is some reactive wood for tension at the bottom of the joint suggesting the joint is pushed up when loaded. This follows the theories and observation of James (2010).

Converting the structural values to a contour plot shown in Figure 68, gives a clearer idea of strength distribution within the sample. The following figure shows the ultimate tensile stresses for the component within a joint, with missing sections/components of the joint being reduced to zero (shown in dark blue). The change in properties of the wood as it grows agrees with previous research of Bruechert *et al* (2000). The centre is stronger due to its inactivity in the current growth of the tree. It forms the solid core of support to enable the tree to enhance its optimal food production. The outer layers are weaker allowing for the primary movements of phloem and xylem vessel and hence higher surface moisture content. This reduced strength may also aid in the development of optimal design, allowing fibres to move.
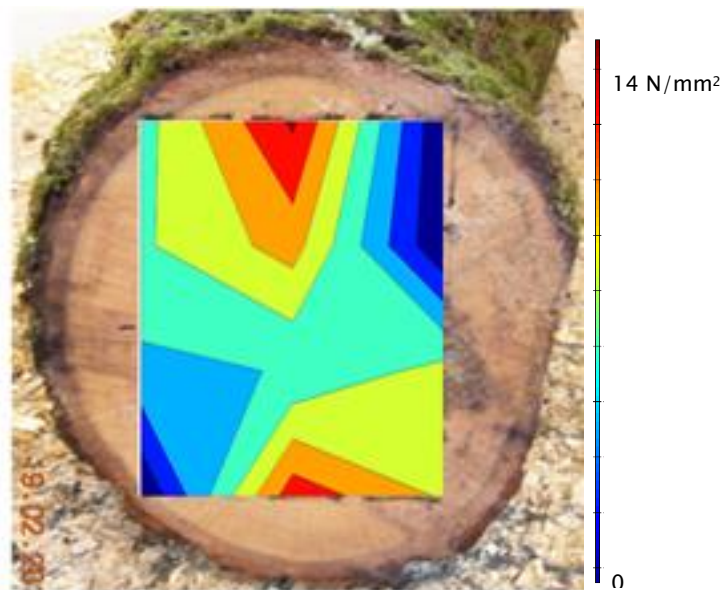
FIGURE 68: JOINT G ULTIMATE TENSION STRESS VALUES AS CONTOUR PLOT SUPERIMPOSED ONTO JOINT IMAGE

Figure 69 shows how the ultimate machine measured strain is distributed through the global joint. The higher stiffness is distributed toward the top and bottom of the contour plot suggesting these zones require more flexibility resistance. Again this adheres to the idea of optimisation suggested by researchers such as Mattheck (1990). The PIV Strains plotted in Figure 70 and

Figure 71 implies how the 3-dimensional strain reacts. However Figure 70 is contrary to the machine measured strains, suggesting the values are still to be improved (as suggested previously in Chapter 5), hence Figure 71 shows better correlation. From this front view First-Sequential it shows there is a tensile stiffness on the top and bottom of the joint, suggesting the joint had moved up and down. The right-side shows high stiffness. This could be due to reaction loads coming from the right-hand side. This is further supported by the side values having a higher stiffness towards the right side and centre.
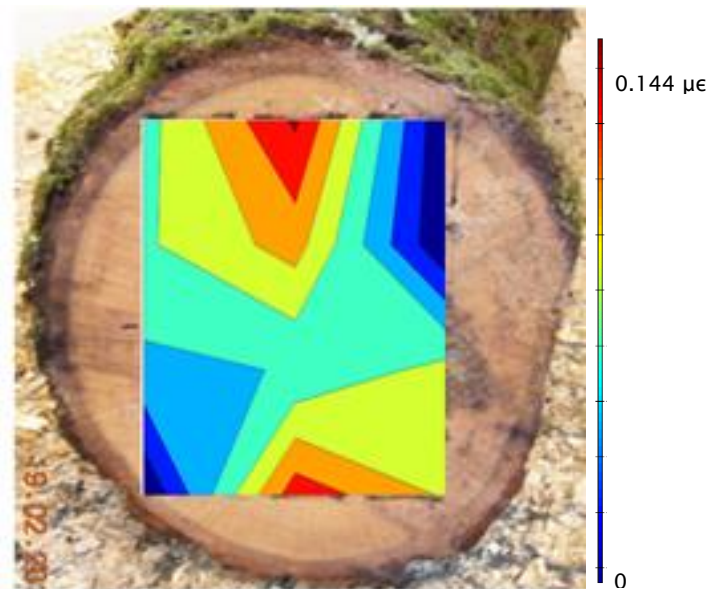
FIGURE 69: JOINT G MACHINE ULTIMATE STRAIN VALUES AS CONTOUR PLOT SUPERIMPOSED ONTO JOINT IMAGE
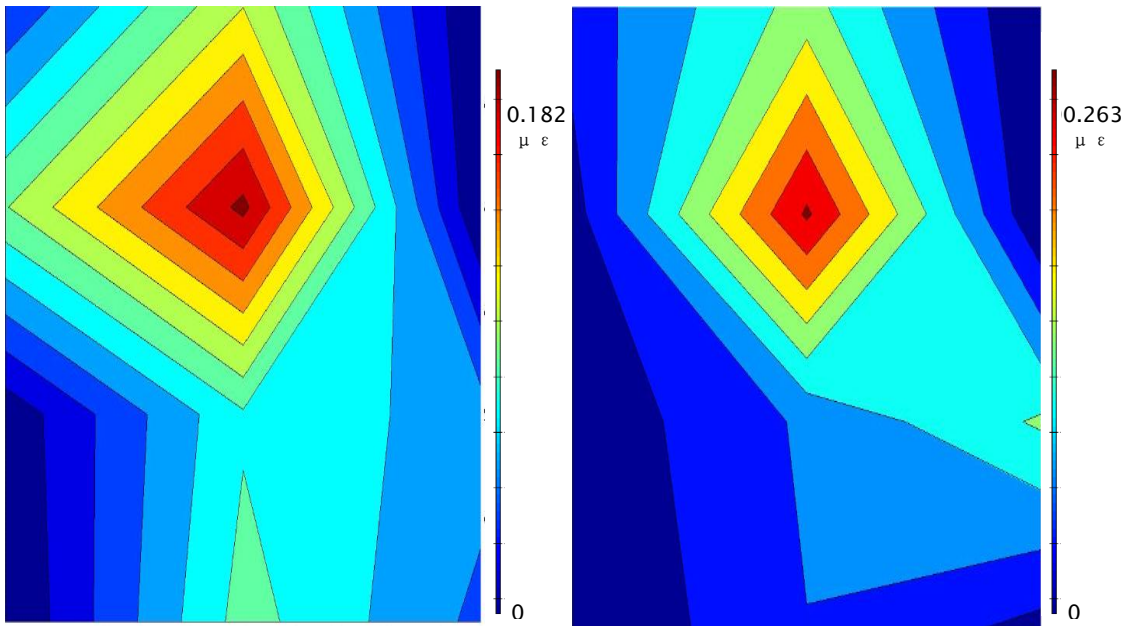
FIGURE 70: FRONT AND SIDE VIEW (LEFT TO RIGHT) PIV SEQUENTIAL ULTIMATE STRAIN
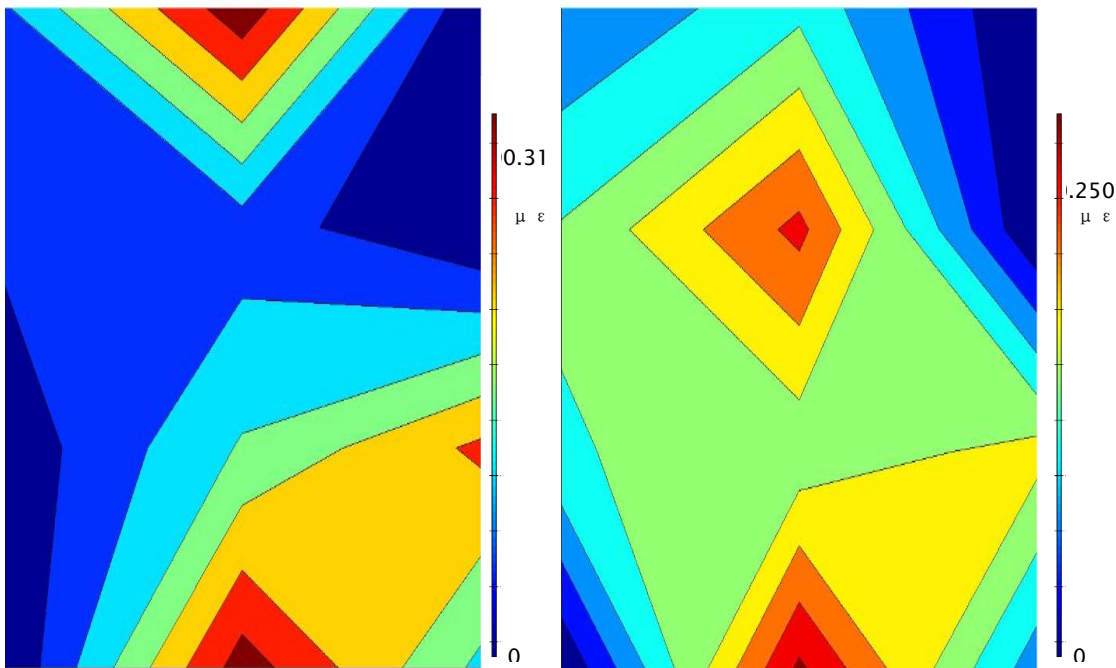
CONTOUR PLOT

FIGURE 71: FRONT AND SIDE VIEW (LEFT TO RIGHT) PIV FIRST-SEQUENTIAL ULTIMATE

STRAIN CONTOUR PLOT

6.5.2 Qualitative Review

It can be seen in Figure 72 and Figure 73, how complex the interior of the

global joint can be. Failures are generally either found through a pith/node or

142

positions of intense grain accumulations (when localised impact of the machine has not contributed). When looking through the global joint, for example Figure 72 (from top to bottom), it can be shown the failure within the layers of components are generally in the same place suggesting the complexity of breakage failure required throughout the global joint. Where the failures are not in a similar zone, attribution to the localised strain of the grip could be assumed. For one example, G1 and G4, the breakages align more with the grain densities.

G10 G11   G6 G3 G7   G1 G4   G5 G9

FIGURE 72: QUALITATIVE FRONT VIEWS OF BROKEN GRAIN (SLICED FROM TOP-DOWN THROUGH GLOBAL JOINT G)

FIGURE 73: QUALITATIVE SIDE VIEWS OF BROKEN GRAIN (SLICED FROM LEFT-RIGHT THROUGH THE GLOBAL JOINT G)

By accumulating the PIV contour plots in order to create a reassembled joint, Figure 74 and Figure 75 and 'slicing' through the original global joint, common trends start to be seen as concentration patterns through previously connected fibres. These regions of strain incurred during testing appear to show some cross-over patterning. However this would need to be investigated further through trials as the exact coordinates of the component within the joint are unknown. Through the grid of the PIV analysis, the idea of how a collection of fibres are behaving in different zones along the sample can also be derived. The central components of the branches take greater strains (showing the material change through maturity of the wood) but generally the strains are homogeneous and only small in movement as the colour bar indicates. In all

144

samples the strains appear to be localised and an indication of failure can be seen prior to it happening, with Figure 75 giving clearer indication.
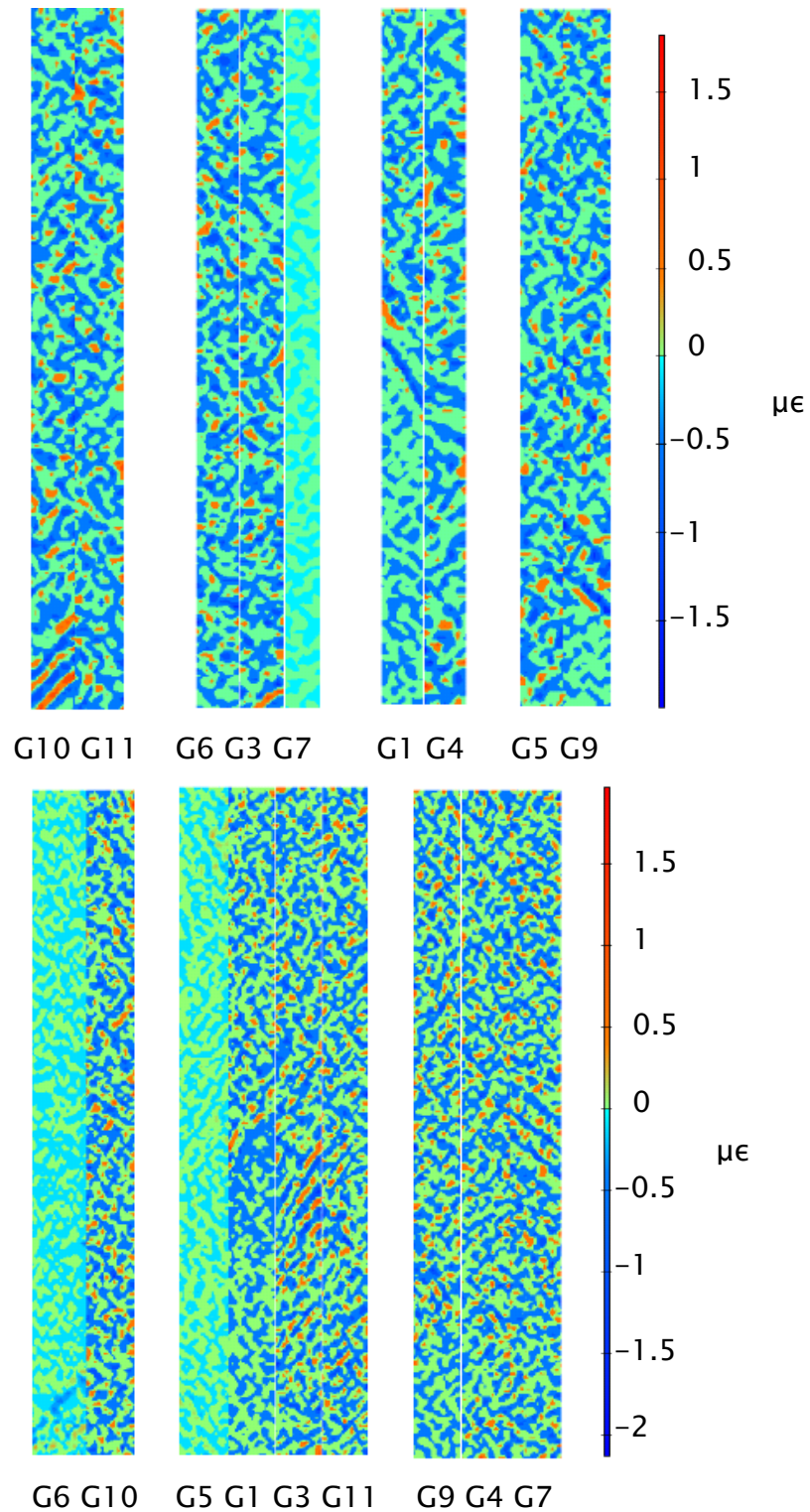
FIGURE 74: SEQUENTIAL PIV CONTOUR GRAPH OF XY-SHEAR STRAIN MEASURE COMPONENT SECTIONS THROUGH THE TOP VIEW OF JOINT (ABOVE) AND SIDE VIEW (BELOW)
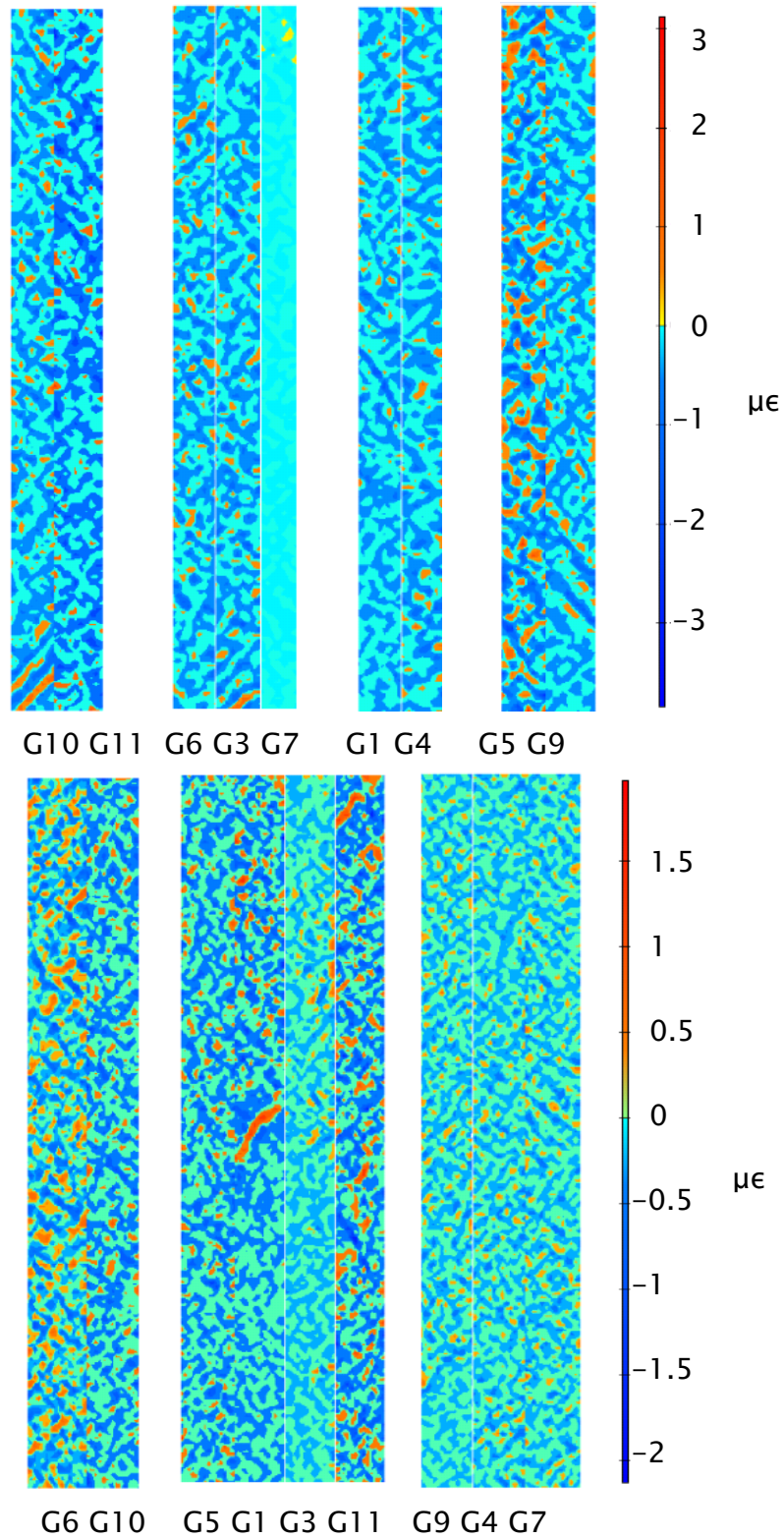
FIGURE 75: FIRST–SEQUENTIAL PIV CONTOUR GRAPH OF XY–SHEAR STRAIN MEASURE

COMPONENT SECTIONS THROUGH THE TOP VIEW OF JOINT (ABOVE) AND SIDE VIEW (BELOW)

6.6 Conclusion

The PIV application to the tensile tests has shown there is a real potential in finding the failure of internal components within the global joint branch as they react with the adjoining fibres. This highlights how the fibres respond as the branch global joint is loaded. Once all the component samples from the one global joint have been compared, a trend of the behaviour is seen where the strain intensity follows a particular path across adjacent components. The separate components can then be analysed as a whole global joint to see how the failures compare to each other. This gives further understanding of the internal behaviour of the global joint. The values of ultimate tensile stress averaging 6.35 N/mm^2, 7.00 N/mm^2 and 8.17 N/mm^2 are close to the British Standard value of 4.32 N/mm^2, though improvements to strain measures (such as increasing the number of images taken during the test) could improve the correlation of the modulus of elasticity values with standards.

The PIV shows promise for strain analysis of timber testing, indicating how the sample reacts to load as the fibres change on the axial surfaces. The resulting calculations need to be comprehensively reviewed, to minimise incurred errors and follow up how the different axial faces of the sample affect the results, but the shape and form of the graphs produced show promise. The contour plots produced give a good indication of the failure zones of the timber sample and potential failure, which could be adapted to monitoring techniques of *in situ* timber structures. By having more images the accuracy of data results can be improved.

The tests conducted are not conclusive and further samples would need to be tested in tension and samples would need to be tested in compression for validation. These further tests could give an indication of the localised internal

147

strengths and whether any reaction wood is being created in stress concentrated regions. This kind of testing would require samples from weather and environment monitored sites in order for environmental growth factors to be taken into account in the structural analysis. In addition the work conducted could be expanded to different species of tree, to ensure any generalisations can be checked. The structural properties of trees differ, so it could be possible the internal strengths of branch global joints vary as well.

6.7   Summary

The components mechanical properties were found to be slightly higher than loading capacity and reduced in stiffness compared to the British Standards. This is to be expected with the increased moisture content of fresh-cut timber allowing the timber to have greater flexibility. The component tensile stress results were reassembled showing the cross-sectional variation of strength of the global. The PIV technique allowed a less time consuming set-up of strain analysis and greater detail of fibre movement during loading than traditional strain gauge measurement techniques. As the PIV results were combined to visualise a cross-section through the global joint, a good correlation of movement patterns between previously adjoining fibres was produced, leading to an ability to analyse adjacent components of the internal global joint under tensile loading. A full code map that creates the technique for PIV global joint analysis is shown in Appendix 7 –

7. Conclusion

This work has shown there is a successful PIV technique to determine the internal structural behaviour of the global joint (tree branch connection). Further analysis and repeated testing can help to establish more conclusive evidence. The work goes some way to being able to adapt the previous timber strength knowledge in tree mechanical analysis. This can help to produce guidelines on the structural performance of trees in different localities, for both management and future timber harvesting. This chapter will look at the success of the assessment techniques developed and their limitations, therefore providing an overall conclusion of the work conducted.

7.1 Testing Components of Global Joints

The application of British Standard tests (with minor adaptations) to high moisture samples with non-aligned grain showed the components (battens cut from the global joint) had similar tensile strength but much lower Moduli of Elasticity when compared to the standard value of seasoned oak. The natural design of the components showed the reduced comparability with British Standard timber structural values (which are based on more linear stemwood samples). Investigating irregular fibre design could prove a key area for progressing structural differences in natural designs.

7.2 Strain Image Technology in Timber

The components had a high moisture content which allowed greater flexibility but sometimes interfered with the grip stability during the test. The machine's basic loading style can sometimes give misleading movement results, such as when the sample slips in the grips. In order to eliminate this slip from the data, PIV was used. PIV was found to be a more precise measure of sample

movement than using machine measured displacement. The movement errors of the machine were eliminated because only the samples within the images were analysed.

A number of processing methods for the PIV data obtained from a series of images have been developed. The success and failure of these has relied on the understanding of the test equipment used. Hence to conduct a PIV analysis of timber, allowances for test style needs to be made to ensure good results. With the machine, it was important to understand any sliding of the grips holding the sample, as this would move within the sequence of images. The analysis area must be taken into account to re-evaluate the stretch of the sample. Once the movements are understood, the fixed point for component movement can be chosen. This will create a movement reference point, where any subsequent movements are due to the sample stretching and not any other movement.

It was noted the chosen face to be viewed by the PIV camera set-up affects the results due to timber fibre anisotropy. The displacements measured by the PIV were converted into strain distribution of the loaded component. The response of the surface fibres under load could be observed on two faces of the component and therefore allowed for indications of failure to be noted.

A limitation found with the PIV technique was the size of images and size of target locations. The file size and type of the image (in this case .tiff instead of .jpg) relates to the total number of pixels. With the front image covering more of the sample, the number of pixels per unit area was lower than the side image which could zoom into part of the sample. This made the side strain contour plots more accurate as they had more calculated data points on the sample to incorporate into the plot.

7.3   Strain Analysis of Timber

For quick analysis of PIV data to obtain displacement and strain, the First-Last attempt can be used. The First-Last technique simply compares the final image prior to failure with the first image. However this technique may give unclear results if the active area is not set correctly i.e. not accounting for the overall movement of the sample during the test. Analysing the strain of a loaded sample over the duration of the test images has been proved to yield better results whilst using the First-Sequential technique. This technique uses a progressive sequential analysis of images to ascertain the movement and stretch of the component. It then uses the movement and stretch values to expand the analysis zones used in the comparison of the first image with the series of later images. By analysing the full sequence of images against the first image a more direct measure of movement throughout a test can be obtained to show a more accurate overall strain picture. However, this technique needs to pay careful attention to the test machine set-up and also requires a longer computational analysis time than the First-Last technique.

7.4 Structural Action of Joint (Tree mechanics)

The PIV technique showed a distribution of the strain within the component samples, providing an insight into the overall reaction of the components under loading. Reforming the component structural test results into a basic model can produce a visual that identifies key structural properties and actions of the global joint. The reforming shows interaction of the components tested within the global joint and begins to show how loading is transmitted through the global joint. As adjacent components are reformed, 'slices' through the joint can be seen. These successfully showed the transmission of loading and movement patterns through the adjacent fibres of the components. This can

help with the analysis of tree mechanics and advance the technologies available to this long standing research. Although the reassembly was successful, it was noted the exact position of the components within the global joint needed to be ascertained to improve the results and the cut of the components would mean a small millimetre (cutting blade thickness) gap would be expected between adjacent components.

Reassembling the results of PIV analyses on individual component samples to analyse the distribution of strain through cross-sectional 'slices' of the global joint, created a further visual technique to investigate the internal mechanical behaviour of a global joint. This allows for the analysis of the reaction of the naturally orientated surface fibres in the sample whilst under loading action. This technique furthers the ability of reviewing the interaction of the wood fibres and grains during loading, showing adjacent components have similar patterns of strain.

The overall component methodology of testing proved successful in providing guidance for the investigation of the internal mechanical behaviour of the global joint. Multi-face set-up allows for a more thorough analysis of timber fibre interaction using the strain image technology. This has an advantage over the machine-measured y-direction strain as more strain directions can be analysed with the PIV and therefore more fibre arrangement reactions can be reviewed. Reassembling the global joint from the split components shows promise to expand the analysis tool available for internal structural action within tree mechanics.

7.5 Tree Management

The results of the test work on components is believed to be season dependant, with harvesting of samples in this project occurring during winter

followed by testing as close to harvest as possible. Testing later season harvesting samples, where greater water absorption in the tree could show differing results. There has been a limited sample size due to the time constraints of the harvesting so further testing would build on the conclusions gained so far.

Additional component tests could be done to further the knowledge of the internal global joint, such as compression and bending tests. Such test values obtained will have some impact on the model development in the future. To relate the component testing to real life, live global joint tests could be done. This style of test has been outlined in Appendix 8. Test data could lead to influence the infrastructure in, on and around trees with manageable techniques to ensure health and stability of the tree.

Although some insights into the tree joint have been made, by continuing this work further an understanding can be developed. This can provide arborists worldwide a tool to determine the tree mechanical safety in which maintained trees can have an appropriate preventative maintenance strategy.

7.6 Biomimicry

Refinement of the modelling of trees and better understanding of tree joint mechanics could show the potential to form biomimetric composite joints appropriate to certain types of loading patterns, for example an unsymmetrical design. To resist the reaction loads within the global joint (shown through the reassembled component contour plot) indicates more thorough site investigation will gain an understanding of loads to a potential structure. The structural materials thought required for the construction of a common symmetrical design may not always be required and therefore potentially save excess materials. In addition greater site investigation creates a possibility for

biomimetric engineering of standard joints of structural elements. Further studies into integral design of natural material reaction to loads, leads towards technology for improved structural designs and futuristic adaptive structures.

Appendices

Appendix 1 – Timber Moisture Retainment for Load Response Testing

When timber is cut it immediately starts drying out and changes the structural strength of the timber. An analysis of the trees strength and structure needs to be investigated to find a way to combat this. This section looks at the moisture changes observed during structural tests as well as some of the pre-test ideas for retaining the moisture within the sample.

Introduction

In order to analyse the strength of a tree in a safe manner, it is necessary to cut some sections and test them in the laboratory. However in cutting a section of tree, the timber starts to dry, changing the structural properties of timber. This means initially finding a way of retaining the moisture after cutting but prior to testing, finding a way of retaining the moisture during testing, or at least finding a way of monitoring the moisture content during testing.

By finding the issues with retaining moisture within the sample, a more intensive test on moisture retainment procedure can be conducted so in future a more realistic idea of tree strength can be gained. This will need to be done by trying moisture retainment procedures for loading tests. An idea of the effects of moisture content will be gained through the load test procedures conducted.

Moisture content tests are a common need in timber testing with the most popular and reliable method being oven-drying. Such institutes such as TRADA, Australian Commonwealth, and BSI having standard protocol for testing, within this work, the oven drying method will be used to ascertain moisture in timber samples.

Methodology

The collection and storage of the samples to be tested needs to be assessed in order for good moisture retention. The issue here is, the samples need to have moisture retainment procedures straight away. However, the safety of the area and operators also needs to be acknowledged in that chainsaws may prevent immediate implication of preservation procedure. For this a series of simple comparative tests were conducted to give some sustenance to the collection of samples. These tests consisted of wrapping up stems in film and foil in various combinations, then leaving for several days. The samples were then compared using standard oven drying methods.

The next stage involves understanding the moisture content change during load testing. The preserved samples were put into various load tests. A control was taken from the sample when it was cut to size, the test was conducted. After testing, portions of the sample were taken at the small end, central and big end regions to assess the final moisture movement. The proportions of the sample were oven dried to assess the moisture content.

Results and Discussion

Moisture Content Retainment

Wrapping the sample in film and/or foil in various ways, gave the following results (Table 12). However the test was limited in sample size and in the wrapping technique possibly creating more than one layer in places. Further to this if the samples are left for too long, the contained moisture begins to degrade the sample. It was also assumed during the tests the samples had the same moisture content distribution as it was taken from the same branch. The

results therefore are indicatively only, to the best practice for moisture retainment preservation.

Sample Number	Description	Oven test after 3 days		Moisture Content After 3 days (%)
		Pre Weight (g)	Post Weight (g)	
1	All wrapped in 1 layer of film and foil	10.26	4.92	108.5
2	All wrapped in 2 alternating layers of film and foil	12.63	6.24	102.4
3	Control	7.32	4.79	53.5
4	Ends wrapped in 1 layer of film and foil	6.66	3.52	89.2
5	Ends wrapped in alternating layers of film and foil	6.91	3.67	88.3
6	Control	6.99	4.22	53.8
7	All wrapped in film only	18.09	8.68	108.4
8	All wrapped in foil only	28.51	12.77	107.3
9	Control	26.01	12.03	65.4

TABLE 12: MOISTURE SAMPLE

The loading showed there were variants in moisture movement during testing. It must be noted however possible variants in lab conditions such as drafts may have affected results. Also the pressure created during loading could also contribute to the loss in moisture during testing.

4 point bending

Moisture content of the 4 point bending tests results can be seen in Figure 76, where small refers to the smallest circumference end, big refers to the biggest circumference end of the sample, middle refers to the middle of the sample

Appendix 1

(normally taken near to breaks)all taken as offcuts of the same sample after mechanical testing. Each moisture content loss is calculated with respect to the pretested and control moisture content samples.
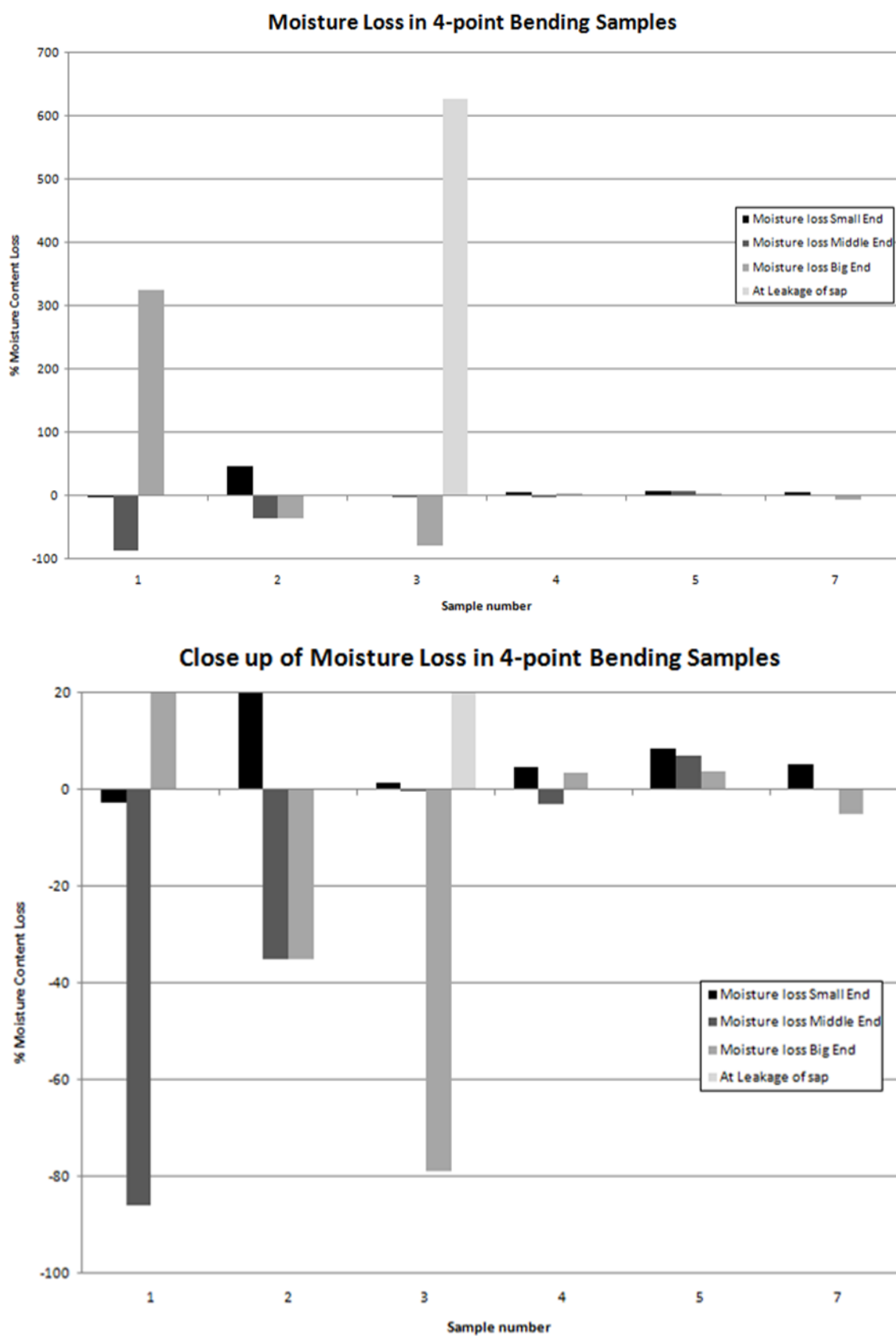
FIGURE 76: MOISTURE CONTENT IN 4–POINT BENDING

Appendix 1

For samples 1-3, moisture content changes can be seen. However in other samples minor changes were seen. The tests suggest the testing increases the movement of moisture. Also the samples 1-3, were larger spans than samples 4-7. Sample 6 is not shown here due to data collection errors on test day.

In sample 1 it can be seen the big circumference end of the sample looses moisture, compared to the middle of the sample which increases in the moisture content. This could mean the moisture has moved from the big circumference end toward the middle of the sample and out to the surroundings.

In sample 2 it can be seen the moisture content increases in the large and middle circumference ends, but the small circumference end is where moisture is lost. This may mean the pretest sample was left too long before being weighed. However as this is relative it suggests the moisture has been lost from the small circumference end under the pressure.

 Sample 3 had an extra test done on a part of the sample that began to leak fluid during testing. As expected moisture was lost from this area. The leaking does however prove the moisture is moving throughout testing. The big circumference end of sample 3 increases in moisture, suggesting again moisture is moving during testing.

Samples 4, 5 and 7 also show moisture movement of lesser extent than the previous samples. This could be due to the shorter span of the samples. It must still be recognised however moisture movement is still evident in these samples.

Compression

Moisture content of the compression tests results can be seen in Figure 77. The compression tests proved there were moisture movements during loading. Again, each moisture content loss is calculated with respect to the pretested and control moisture content samples.

Moisture Loss in Compression Samples
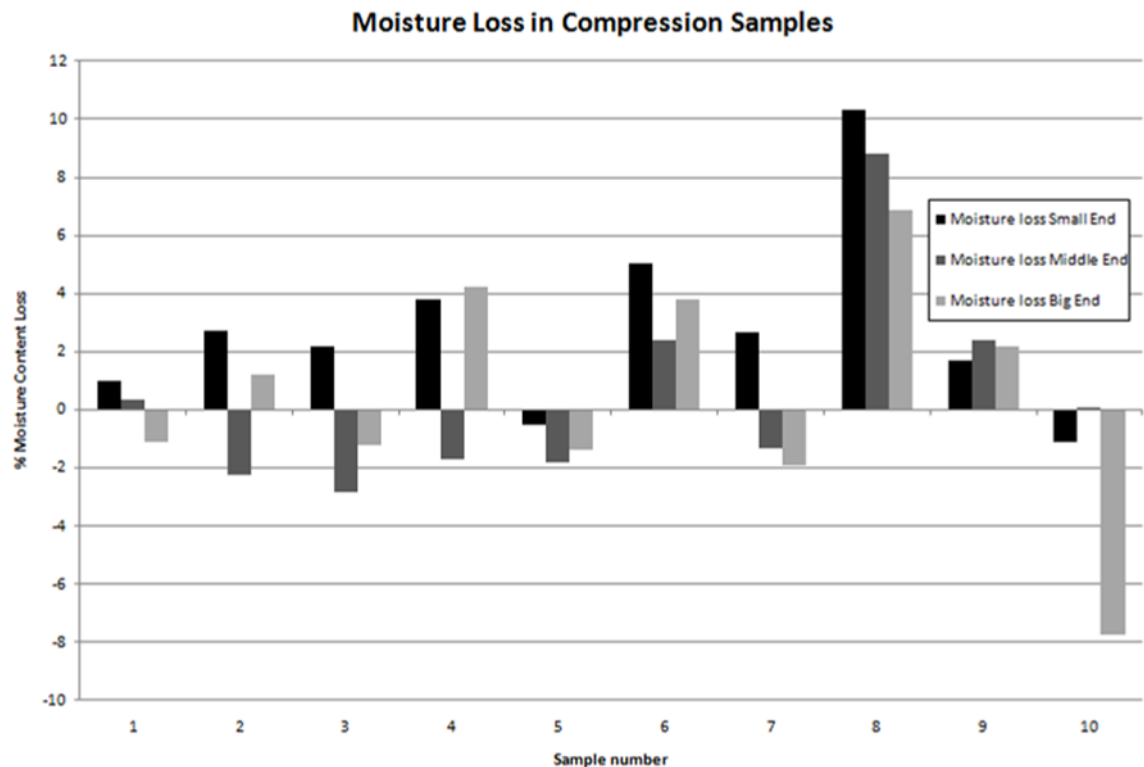
FIGURE 77: MOISTURE CONTENT IN COMPRESSION

Interestingly in these cases of compression testing, the failure mode of the sample seems to correlated with where the moisture is lost. For example, samples 2 and 4 showed signs of longitudinal cracks along the middle of the sample and also some localised end crushing. Samples 3 and 7 already with some bending with the sample, continued to bend and some end failures were noted. Lastly, samples 8 and 9 the middle of the sample had a buckling failure. Although the moisture loss show in the graph does not assume the same proportions, it could be possible the smaller variations in the samples are creating the disproportionate difference.

Conclusion

These tests proved using film for transport and preservation were adequate enough for the retainment of moisture. Though the results show a film and foil layer mixture and film only wrap are around the same moisture content, the added effort to wrap the samples in foil can be deemed irrelevant. However, there is still some inaccuracy in the time taken to wrap up samples in a safe period onsite. Possible improvements to this procedure could be to use polythene bags, however this may mean surrounding air trapped in the bag will dry out the sample.

The load test moisture content proved moisture was still moving within the sample. Further test works are required to give proof to the results ascertained by these moisture tests.   However the moisture change shows the moisture is affecting the structural properties of the timber while green.

The variability in results shows more tests are required to be able to produce final results and theories and a monitoring procedure for moisture movement during testing may need to be set-up. In some samples the moisture content loss may be slight and therefore due to other factors. However when in comparison to the rest of the sample areas, there does seem to be a correlation between loading and moisture movement. This will need to be further investigated in order to give a real insight into the structural capabilities of trees and green wood.

Appendix 2 – 4-Point Bending Preliminary Testing

Introduction

When trees are felled, the stem is seen as the valuable area of the tree, any other elements such as branches are wastage material used for burning or habitat. Although the need for habitat and fuel is necessary, surely with large volumes of branches, there could be a possibility of using larger branches in structural areas. Not only this, but the natural loading of the branch can be assessed to further the tools for hazard assessment of trees. For this the strength of the branch needs to be assessed.

By using current standards as guides for gaining strength properties from branches, an idea of their natural load response and further usage of such branches can be ascertained. By forming a standardised structural test, a basis for further assessment can be created. This will mean variations in site conditions and species can be evaluated more effectively.

Previous works

Timber has an established method of conduct for testing, as shown by the British Standard BSI (2003). Together with government body published reports such as Lavers (1967), the strength properties of timber have been well established showing industry followed standards such as BSI (2002). These standards and reports are an invaluable start to finding the structural properties of any timber and have been developed so computability of varying species and conditions can be conducted.

The strength of a tree is less well known. However, the tree could be considered in itself, a whole cantilever structure with roots as its foundations

and the stem and other branches as the columns and beams. Limited published studies of the branch strength have been conducted in relation to the interest in biomechanical design. Cannell and Morgan (1987) conducted an investigation into the Young's Modulus in along the grain bending of living sections of branch and stem. The samples used were taken from the tree and tested with 3 point bending load within 24 hours. The values of these tests were found to be lower than the known green value properties for the timber and suggested any further researchers to use the lower end distribution of green timber values for Young's Modulus. Cannell and Morgan (1987)'s work will be the basis for these test works.

Further to Cannell and Morgan (1987)'s work, Mattheck (1994) has furthered the understanding of tree mechanical design and developed a theory of axiom of uniform stress. This theory finds there are no notch stresses in the living tree as growth adaptation acts to prevent any localised stress, thereby preventing failure at a point. This theory is in controversy to the timber one which shows knots in the timber section create localised weakness. This means the living tree and the cut timber used for workmanship can have varying properties.

Methodology

Several samples were collected from the Forestry Commission's Alice Holt – Straits site. These samples once collected were wrapped to prevent moisture loss and the tests conducted within a month of collection.

Developing a test procedure

BSI (2003) shows the standard test setup required for determining the local modulus of elasticity in bending for timber. This standard can be used in

developing the test procedure for 4 point bending in branches. Firstly looking at the interaction of the machine with the sample will help to create a more reliable procedure. Following the standard, modifications were made, in order to alleviate any difficulties that may affect the data collection. Timber wedges used for point load application were found to crush under pressure, so metal wedges replaced them. However the metal created localised failure in the timber, this was overcome by placing rubber matting between the metal and sample. Another observation arose in the metal supports where under high pressure the roller plates created a localised failure on the end. However this was only a minor issue found and normally occurred after visible failure and peak loading had happened.

Behaviour During Testing

The standards suggest the length of the section to be tested for 4 point bending should be 18xh, where h is the nominal width. However with such a long piece of timber there were irregular shapes in samples due to their natural orientation. This meant finding the correct orientation to balance the sample so testing could be conducted. It was found to be safer and give better results to make sure the higher points on the arch were being loaded, rather than pushing in the 'bowl' of the sample, as shown in Figure 78.
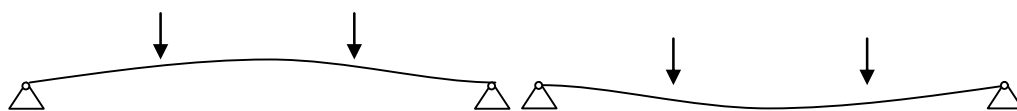
FIGURE 78: 4 POINT BENDING SET-UP: PUSHING THE ARCH OF THE BRANCH, PUSHING THE BOWL (LEFT TO RIGHT RESPECTIVELY)

The tests were conducted with different loading times due to the issues with creep. It was found the 1mm/sec on an Instron® seemed to conduct better results, though this cycle does take time. Also with the length of the samples there were large displacements, which meant the potentiometers needed re-setting frequently in order to measure the creep movement and displacement during loading.

Preliminary Results and Discussion

The main source of failure was longitudinal shear failure on the lower side. However, some crumpling of the top side of the samples was also seen. The failures were predominately near any knots or nodes in the branch. There was great flexibility in the samples under loading meaning the samples were never subject to complete breakage, see Figure 79 and Figure 80.

FIGURE 79: PRE LOAD SET-UP AND SAMPLE AFTER FAILURE (LEFT TO RIGHT)

FIGURE 80: VISIBLE FAILURE ON UNDERSIDE OF BRANCH

There was a large difference in results between the samples load at 1mm/sec (shown as 1 and 2 in the Figure 81 and Figure 82), and the 5mm/sec load rates. Sample 1 was a larger specimen and had higher arch effect within the sample. This suggests the arch creates a structural strength increase. The other defining factor affecting the sample calculation is the diameter used is the nominal diameter of the sample. A more accurate assessment of the stress could be gained through a more defined morphology of the sample.

4-point bending Stress vs Strain
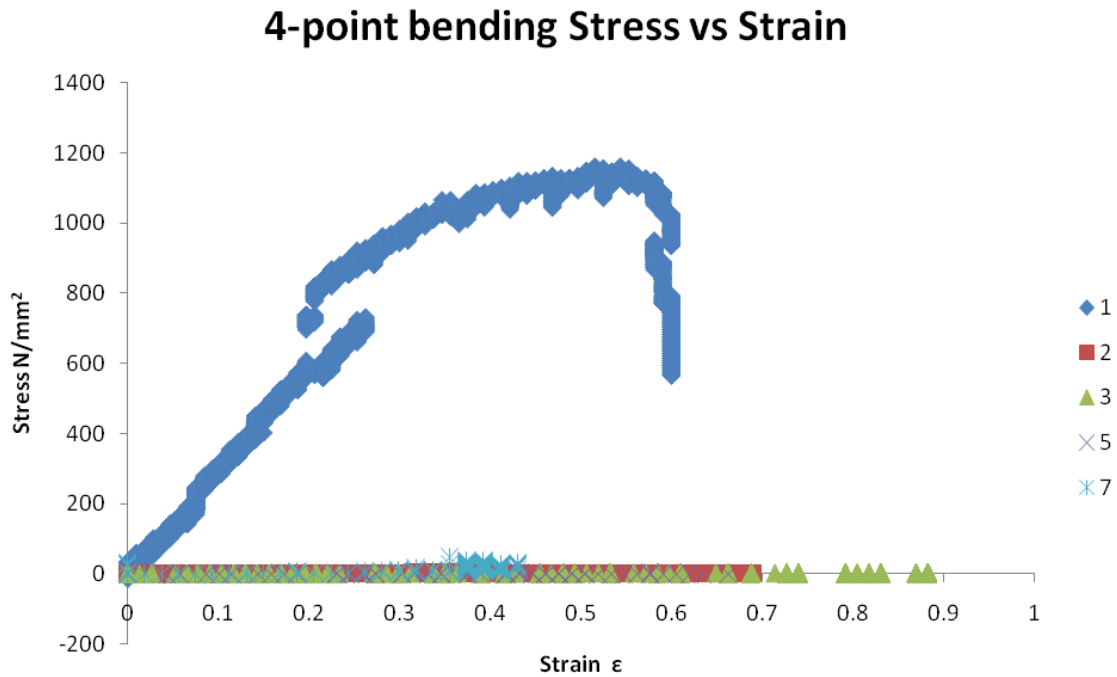
FIGURE 81: 4–POINT BENDING STRESS VS. STRAIN RESULTS

4-point bending Stress vs Strain
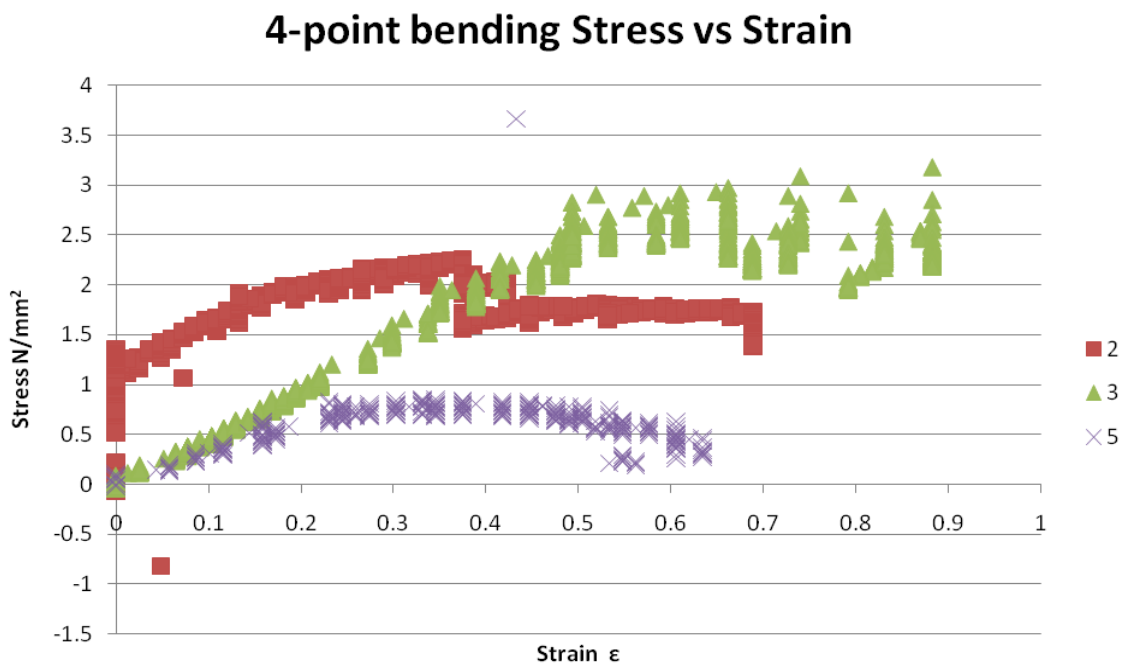
FIGURE 82: PLAUSIBILITY OF YOUNG'S MODULUS

From the stress strain graphs it is plausible to define the secant Young's Modulus of the samples. Some samples are not shown due to experimental variation that made calculation incomparable but a gauge of the Young's

170

Modulus can be made, see Figure 83. The slow load rate however does give an errant result but this could be due to the amount of creep incurred in long length samples and the measurement of the diameter.
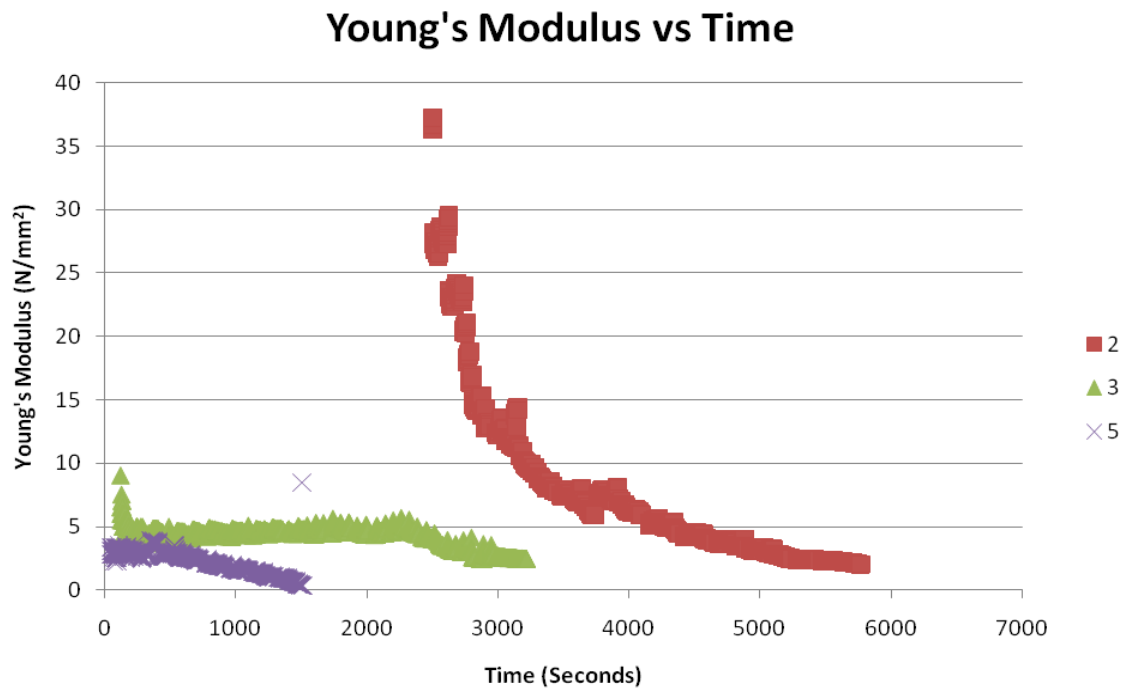
FIGURE 83: 4-POINT BENDING – YOUNG'S MODULUS

Conclusion

The British Standards were a good base for developing a methodology and with some adjustments created a good model for future testing. The repeatability of these tests is possible though the shape and size of the branch needs to be further considered. The variation in the shape of the sample was hard to standardise the evaluation of results, this will need further works. The arching behaviour will also need to be considered in the evaluation of the structural properties, from these tests.

Appendix 3 – Compression Preliminary Testing

Introduction

Further usage of tree branches within the timber industry and a better knowledge within tree hazard assessment can be gained through additional research in strength testing of branches. The compression properties of trees and fresh timber have limited research. There are many standards which exist to show the compressive strength of timber but as with the British Standards, these values show the lower strength tests values due to the discrepancies within this natural material.

When trees are felled, the straight stem is seen as the valuable area of the tree. Other elements such as branches are wastage material used for burning, habitat or creative sculpture. Although the need for habitat and fuel is necessary, surely with large volumes of branches, there is a possibility of using larger branches in structural areas. The natural loading of the branch could also be assessed to further the tools for hazard assessment of trees in urban areas. For this the strength of the branch needs to be intensely assessed. In addition to looking into the compressive strength of fresh timber, an understanding of this composite material can be gained to add to the biomimicry knowledge for other composite materials.

Biomimicry investigation of trees has been recognised in the work of Mattheck (1990). Mattheck (1990) emphasises the development of reaction wood in trees under localised prolonged stresses. This reaction wood develops to reduce stresses occurring through loading, such as wind loading. This development of reaction wood means the wood has ingrown pre-stresses which if known could increase its strength above that of the known standards. If directional loading

can also be acquired axial loading could match the loading required in structures.

Strength investigations by Cannell and Morgan (1987) on living branch breakage show fresh cut tree branches under strength testing. These tests claim to show the effects of Young's Modulus of trees, though only investigate the timber when it is cut away from the rest of the tree meaning the tree organism will not react as a whole. Their investigation thereby shows the fresh cut strength which has not been reviewed to the author's knowledge.

By using current standards as guides for gaining strength properties from branches, an idea of their natural load response and further usage can be ascertained. By forming a standardised structural test, a basis for further assessment can be created. This will mean variations in site conditions and species can be evaluated more effectively. This paper part of a series on structural strength investigation of fresh timber shows the procedural investigation and results of the compression strength tests conducted on Oak samples tested under laboratory conditions.

Methodology

The tests follow an adapted version of the testing standard BSI (2003). The ten samples are taken as linear as possible but the natural variation of the material will give it inherent defects and shape randomisation. These differences in shape will affect results but under controlled testing the effects of compression in the sample can start to be ascertained.

As in BSI (2003), sample lengths of 6h were taken where h was the smallest diameter measured from the approximate smallest circular circumference. This allows for the deviations in shape throughout the sample and enough length

for failure modes to be analysed. The samples were tested with a pin ended support to allow for centralisation of the mass during testing.

The sample under compression testing was measured allowing for creep displacements within the material. This gives an idea of longevity of loading reaction. The samples were loaded to breaking point and the machines loads and displacements taken against time. The load was applied with an Instron® 8500 (see Figure 84) with the load rate being 0.00005h mm/s.

FIGURE 84: COMPRESSION TEST SET-UP

Results

The test procedure showed some promising results. The modes of failure seen during testing vary dependent on the success of the test setup and the quality of the sample. Many samples that already had a curvature in them tended to be restricted by the 2D pin end, this lead to mixed results. If the rotation was in favour of the sample, then the samples tended to buckle in the direction of the major bend. However, if the rotation was not in favour it could result in ends splitting or crushing. The samples would also tend to fail near any nodes, showing these are weak points in the timber.

The ultimate stress of the samples varied between 10-30N/mm², (see Figure 85) again improvement and variations in the sample types could account for this wide spread in values. The results however do show the principles of these tests will give a good repeatable procedure. Further and more vigorous structural testing would need to be conducted in order to get better results in future.
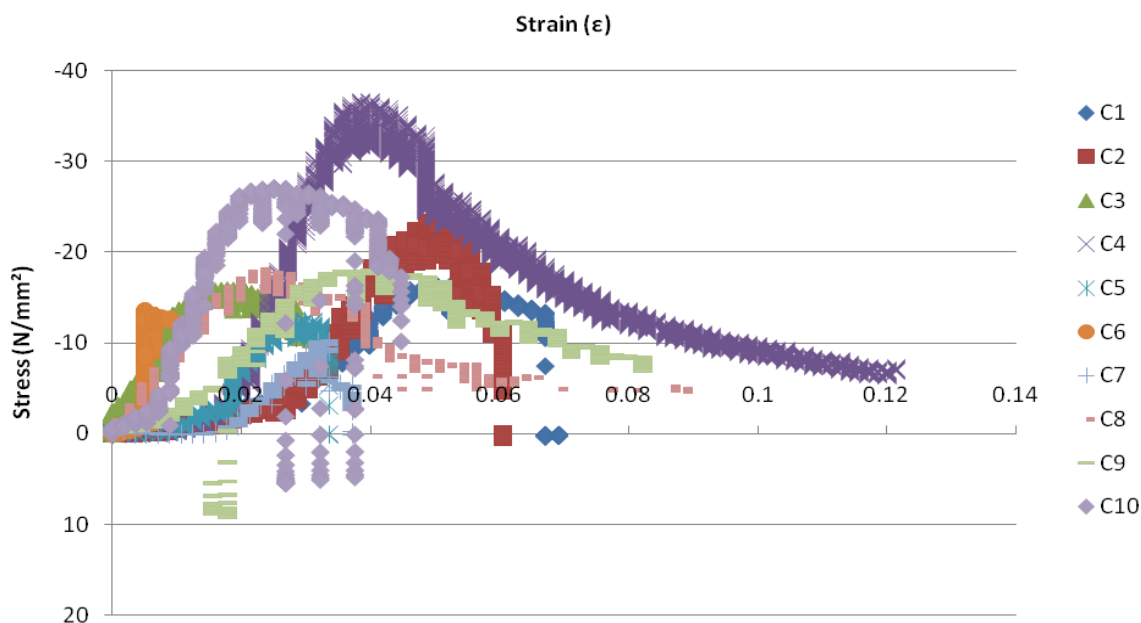
FIGURE 85: COMPRESSION STRESS V STRAIN

Discussion and Conclusion

The set-up procedure and interaction of the machine with the sample of branch will need to be reviewed to ensure good results. Firstly the metal interface between the sample and loading machine creates localised failures, thereby a cushioning material was required to reduce local failure at the load point application. A 2D support point will be used to provide a pin-end support which will allow free rotation. On this support, long sample sections which have bends will need the centre of mass of the sample to be balanced for safe and successful tests.

In transferring the standards to the test setup, a relatively good transfer could be made. However, there were issues with the non-linear samples. This makes the data collection hard to analyse due to the irregular shapes. There is also likely to be some arching behaviour due to end pressures, this could be resolved by the use of a free bearing support that will allow 3D rotation. Also the free bearing support could be the answer to more reliable results by reorientating the centre of mass of the sample allowing a more natural failure.

The results give an insight to the structural strength assessment of fresh cut timber and tree, which will help in the hazard perception assessment. With further data collection of varying species, with varying environmental conditions, really understanding of the strength of these otherwise waste areas of the tree can really start to be known.

Appendix 4 – Branch Joint Preliminary Testing

Introduction

Knots and deformation are seen as a weakness in cut trees and timber; this means that the branch area of harvested timber devalues the wood. However the connection of a branch to the primary growth is of intrinsic interest to biologists and blue thinking engineers. This area which has evolved over millions of years supports what is one of nature's biggest cantilever structures as well as supplying it with the ability to grow and survive. In learning the structural capabilities of the tree joint it could be possible to start to find more uses for it in design. In order to start this process a way of testing the strength of the joint needs to be created.

Previous research on the mechanics of trees has been conducted by Mattheck (1994) though this is generalised information for tree mechanics, and none specific to the species and there is currently no in-depth assessment method for the strength of the branch joint. Knowledge on the creation and attachment of branches to primary growths suggest the branch growth is a decisive action within the tree, and the piths of the branch are not connected to the pith of the primary growth. This investigation by Shigo (1985) also states the flow of nutrients can only come from the negative geotropism incurred within the tree. An investigation currently found by the author done by Müller *et al* (2006) shows the results of a harvest global joint test that suggest a homogeneity of strain through the cross-section of the joint under loading.

Little conclusive research has been conducted on the strength of tree joints, and it is the intention of this paper to develop a test procedure based on the work of Müller. This procedure should further develop the methodology for

assessment of tree branch strength and analysis of natural cantilevers in future.

Methodology

Using Müller *et al* (2006) ideas, as a base for joint load tests, the 'trunk' section must remain static during loading of the 'branch.' To do this, scaffolding was set up to hold the trunk of the sample in place while an Instron® machine loads the branch. In order to ensure breakage of the join the sample was loaded as close to the join of the connection. Displacement of the branch will be monitored and visual observation of failure will be made.

Results and Discussion

The overall test seemed successful, though could be improved. Loading close to the branch ensure that breakage occurred at the join, seen in Figure 86. The scaffolding reduced the movement of the primary growth of the joint, however as the loading of the branch increased the formation of the scaffold structure bent over. This created built up potential energy and was potentially dangerous, especially as the primary growth was not completely clamped in place and itself twisted in the rigging.

FIGURE 86: JOINT SAMPLE AFTER ULTIMATE LOAD FAILURE

It is clear from the set-up that the tearing apart of the joint connection resulted from the increased position of the load actuator. These visible signs of failure were only really apparent after the ultimate load was reached. The initial visible failure was the crack at the crotch opening up, and then later the crumpling of the underside of the branch join. This suggests that the branch fails by shear tension on the upper side, and buckling compression on the underside of the branch. The pith from the branch of the joints was still connected as a clean shear on the wrapping fibres pulled the branch join apart, see Figure 87.

FIGURE 87: FIBRE FAILURE OF THE JOINT

Even though the tests were successful, the health of the joint was critical to the failure; one deadwood sample tested did fail at the base during loading. This unknown failure could be potentially hazardous during testworks. The results of this test are omitted from the following graphs in Figure 88.
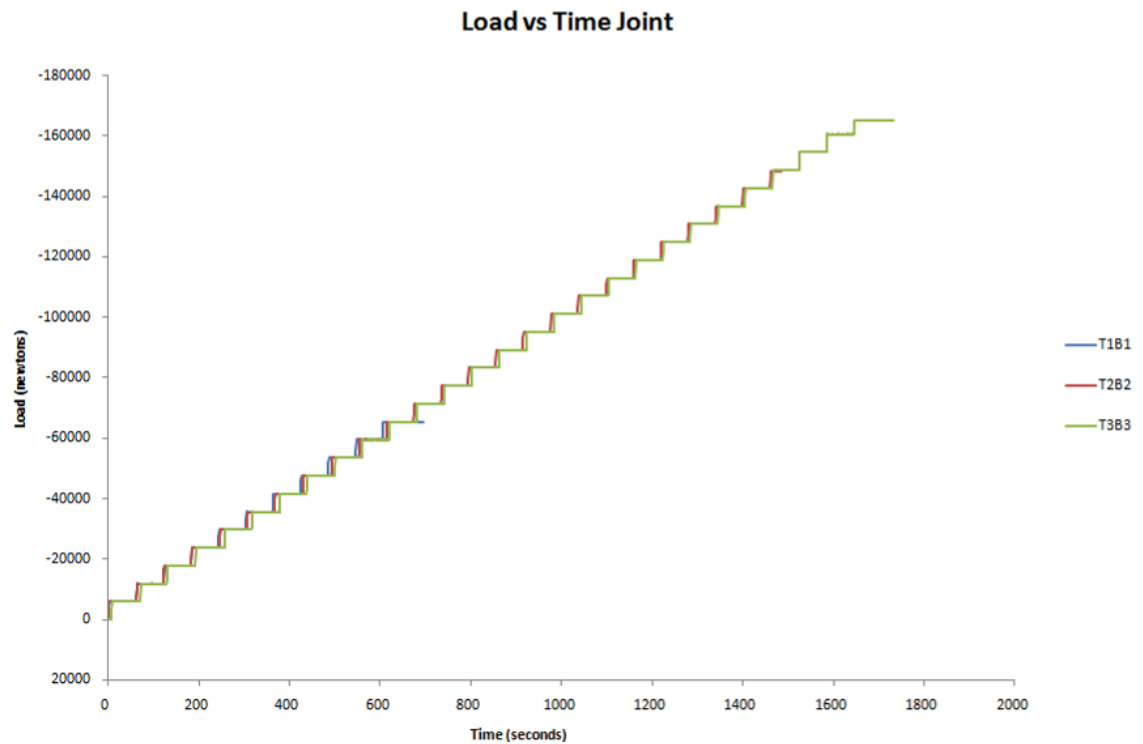
FIGURE 88: LOAD V TIME OF JOINT SAMPLES

From the load vs. time graph, the staging of load can be seen, this was done to assess any creep occurrence in the joint. The graph result implies there was no creep in the samples tested; this could suggest there is limited elasticity in the connection of the joint. However it could be possibly the flexibility seen in the scaffolding rig could have counteracted any elasticity in the joint. On looking at the results and how to calculate stress at the join, it would incur some parameter for joint strength predictability would be in the diameter ratio of the joint. The greater the diameter ratio the greater ultimate force is required to break the sample, (see Figure 89).

Appendix 4

Trunk Stress vs Branch Stress
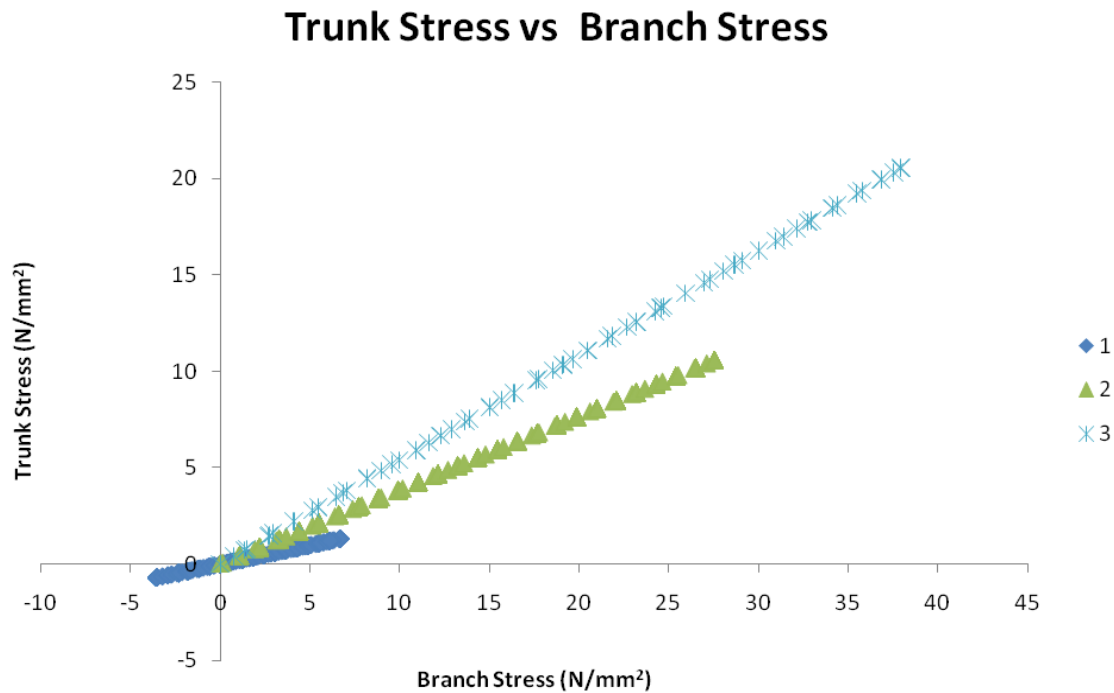
FIGURE 89: TRUNK STRESS V BRANCH STRESS

Conclusion

This test work has shown there is an issue with analysing the data. The hint of a relationship of branch strength shows that it might be due to the diameter ratio; however the amplitude of the graph would be the key of the predictor parameters. The relationship of the joint would need to be further investigated. The methodology set out in this paper needs to be further developed, but shows a promising possibility for future test works, and allows load application adaptability.

Appendix 5 – Electrical Resistivity Preliminary Testing

Introduction

The detection of moisture through timber may help in predicting the load changes within samples. The idea of detecting moisture in timber is common (Commonwealth Scientific and Industrial Research Organisation (1974)) and is used in detecting damp in properties. These methods are well established, showing how moisture content affects the strength of timber, it could be possible there is a relationship between the load of a timber sample and the moisture within it.

Water and electric are not known to be the best combination, however when trying to work out the movement of moisture through a loaded timber sample it could help to understand the properties of a tree. This paper will go through the ideas and preliminary tests started to evaluate the moisture movement of timber and its differences in the recognition of load response.

Methodology

During load tests samples had metal screws drilled into them. These metal screws could then be attached to a wheatstone bridge in order to measure the electrical resistance of the sample under load testing, see Figure 90. The samples would then be put under various load tests to see whether this procedure can be used in any loading tests, and whether the procedure can feasibly provide any additional data.
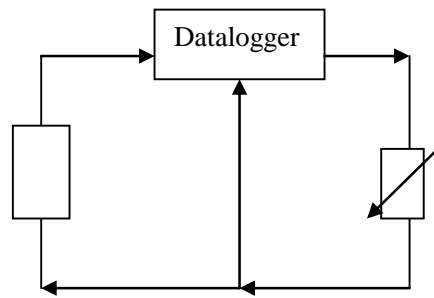
FIGURE 90: RESISTIVITY DIAGRAM WITH WHEATSTONE BRIDGE

Results and Discussion

These tests were very successful even in the limited sampling, there was a correlation between the load and moisture movement, however further testing will need to be done to confirm this. In the 4 point bending test (Figure 91) only detection in the middle of the sample was discovered, this peaked at the point serious deformations of the samples occurred. In compression (Figure 92) the small end electrical detection, did show wavering signs of resistance though this cannot be comprehensively determined.
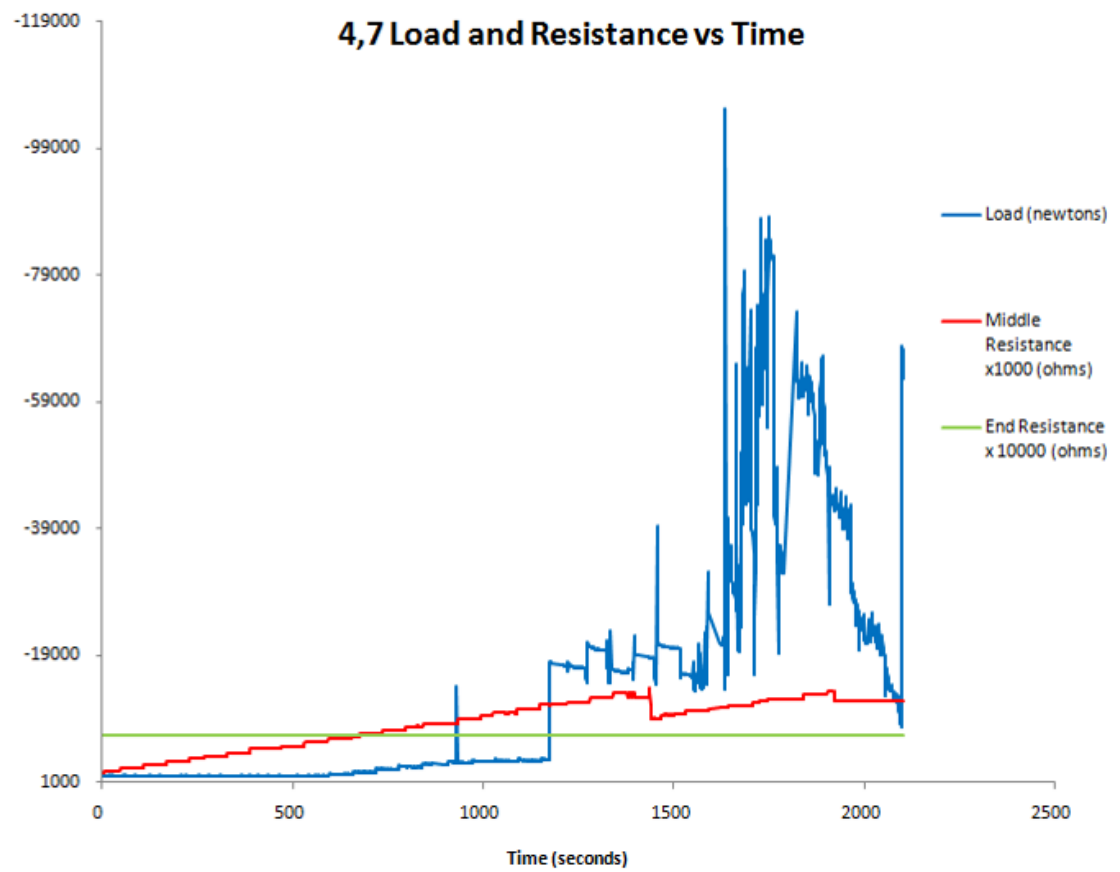
FIGURE 91: 4–POINT BENDING TEST

Appendix 5
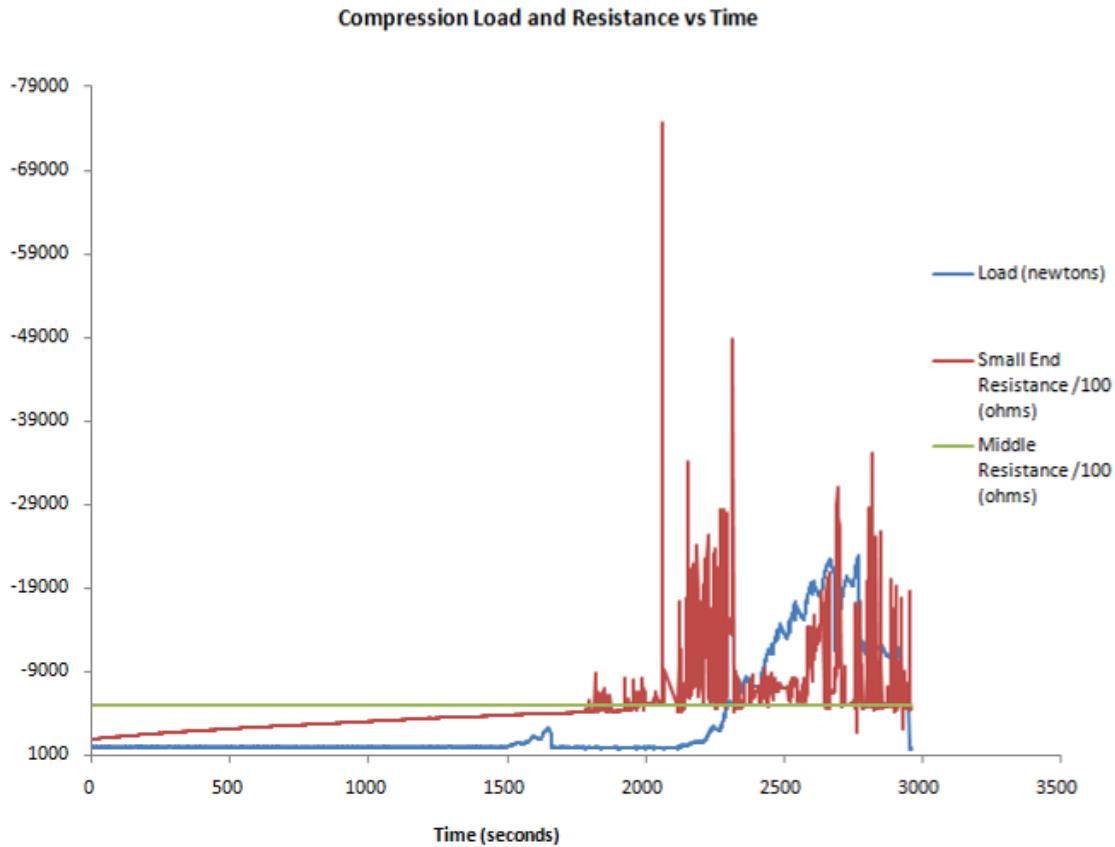
FIGURE 92: COMPRESSION TEST

Of much more interest to the series of tests was the detection of electrical resistance at the visible failure of the branch joint (Figure 93). The peak in the branch resistance of the graph, without which no other graphical indications in the load would detect, shows the failure.
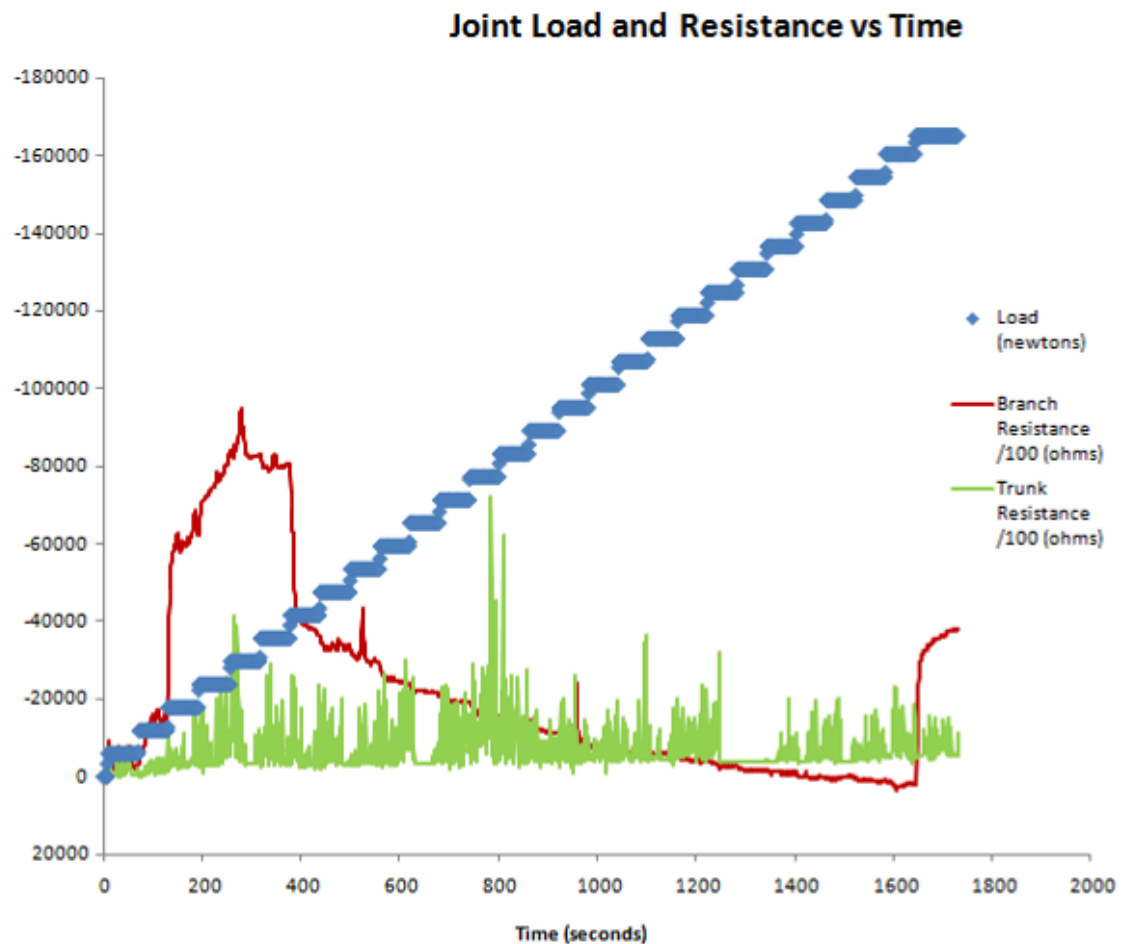
FIGURE 93: BRANCH JOINT TEST

Conclusion

Although these tests were brief there is real potential in developing this procedure to determine the moisture movement in the load test timber. If further work is done there could be a way of monitoring the structural capacity of timber and tree sections in the future with minimum interaction.

Appendix 6 – Component Test Sample Details and Results

Within this section each sample will have: Moisture Contents, Qualitative Images, Stress–Strain Graph, PIV Contour Plots, Creep Plots, and MoE Plots. The final section for each global joint: component accumulation (where dark red value indicates the highest value of the joint from Table 11 to dark blue indicating zero value), located stress–strain graphs, located data values, contour plots, top/side sketches, top/side contour plots. Note all Units for stress and strain are in N/mm^2 and $\mu\epsilon$ respectively.

Joint G
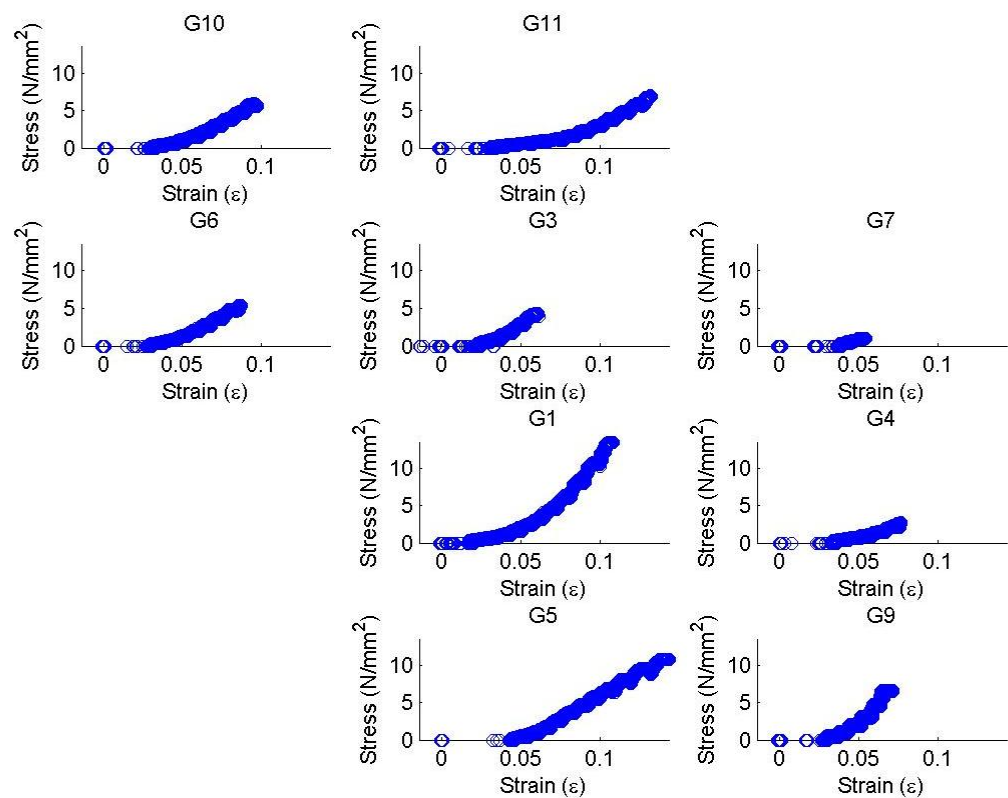
FIGURE 94: G COMPONENTS STRESS VS. MACHINE MEASURED STRAIN AT LOCATION
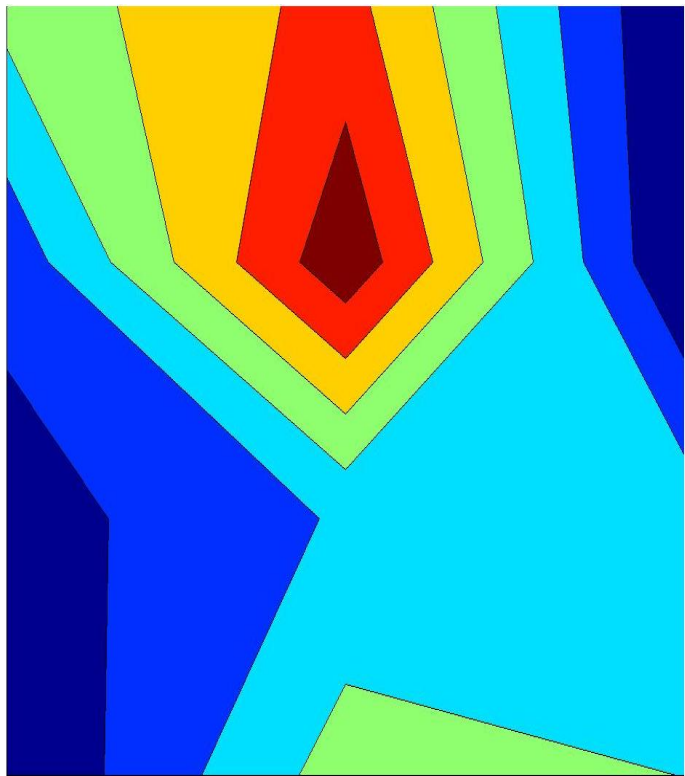
FIGURE 95: G COMPONENTS TENSILE STRESS AT LOCATION AS CONTOUR PLOT
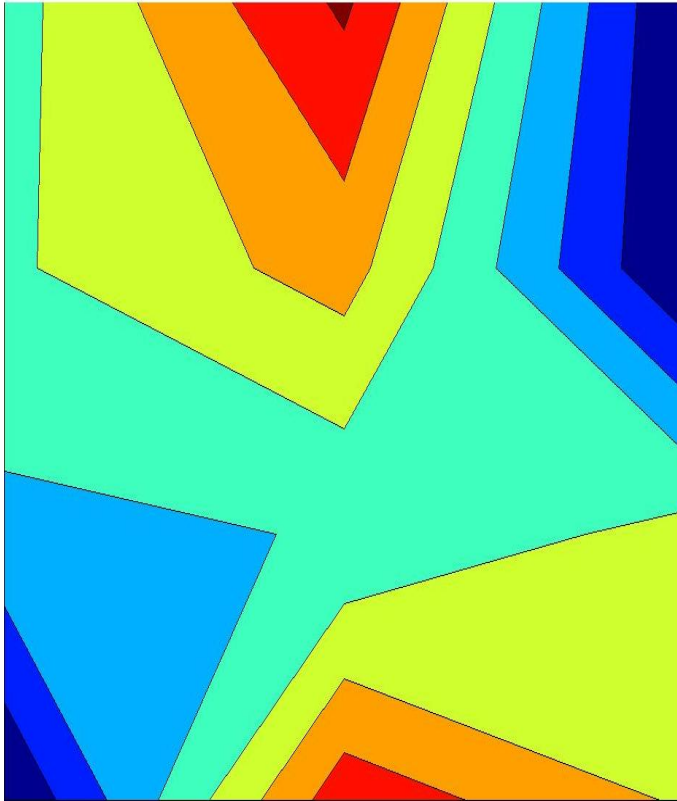
FIGURE 96: G COMPONENTS MACHINE MEASURED STRAIN AT LOCATION AS CONTOUR PLOT
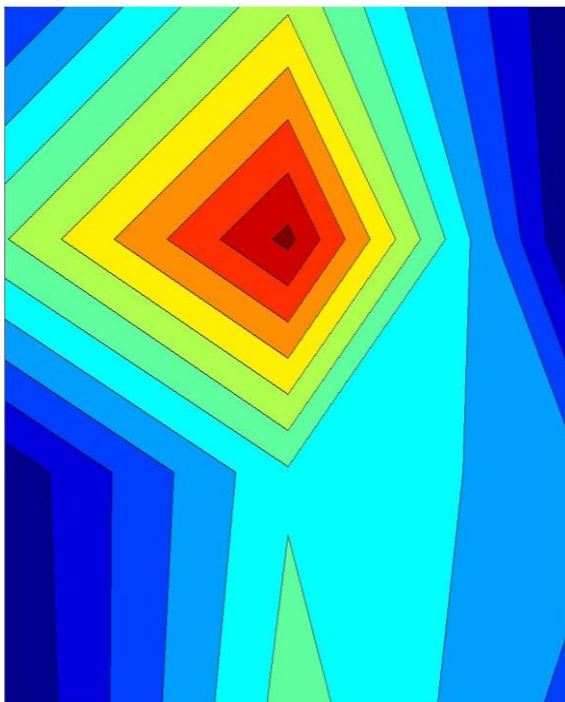
FIGURE 97: G COMPONENTS FRONT SEQUENTIAL STRAIN AT LOCATION AS CONTOUR PLOT

Appendix 6
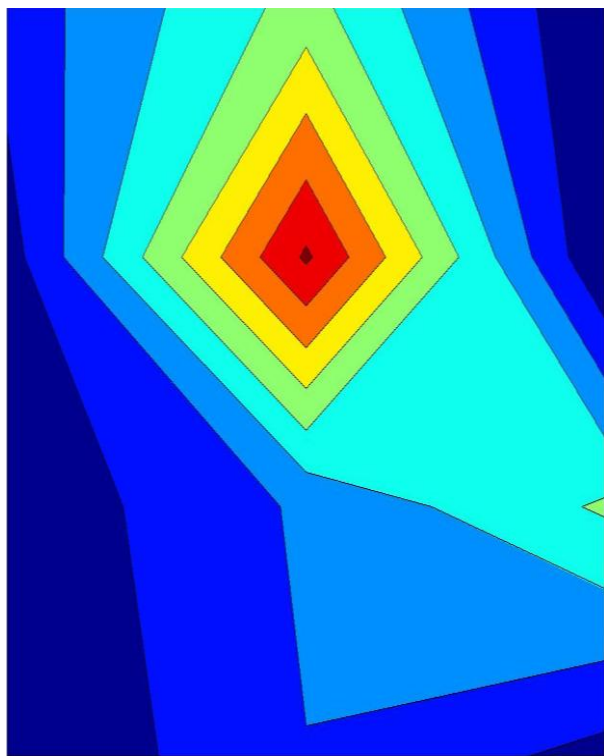
FIGURE 98: G COMPONENTS SIDE SEQUENTIAL STRAIN AT LOCATION AS CONTOUR PLOT
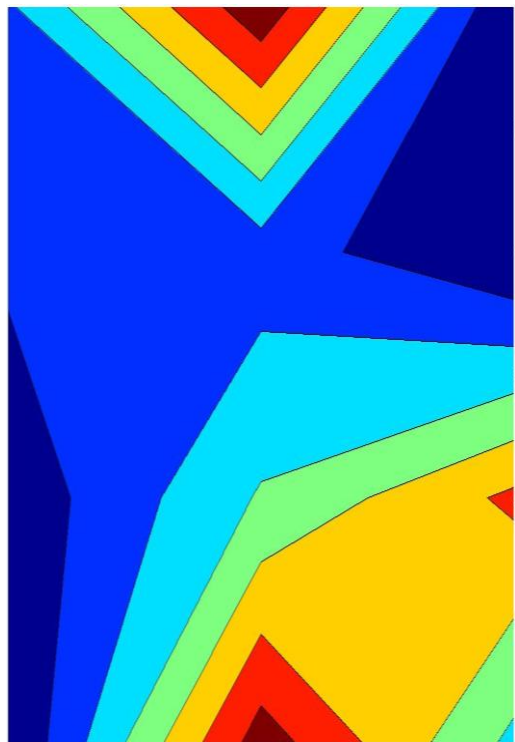
FIGURE 99: G COMPONENTS FRONT FIRST-SEQUENTIAL STRAIN AT LOCATION AS CONTOUR
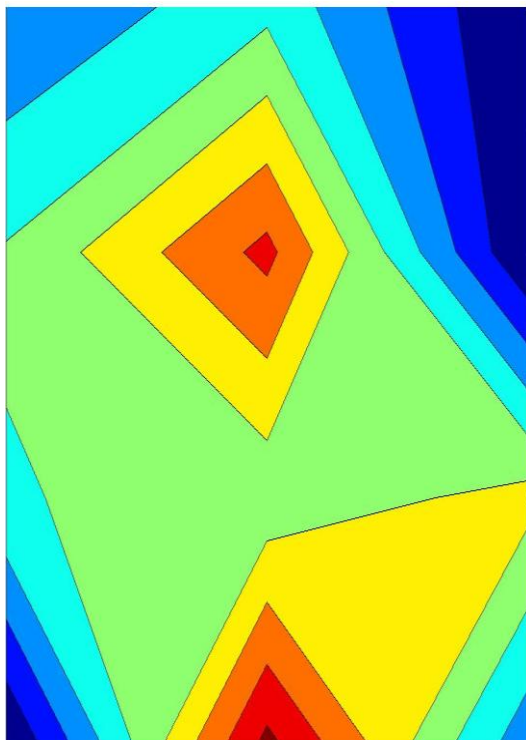
PLOT

FIGURE 100: G COMPONENTS SIDE FIRST–SEQUENTIAL STRAIN AT LOCATION AS CONTOUR

PLOT

G1
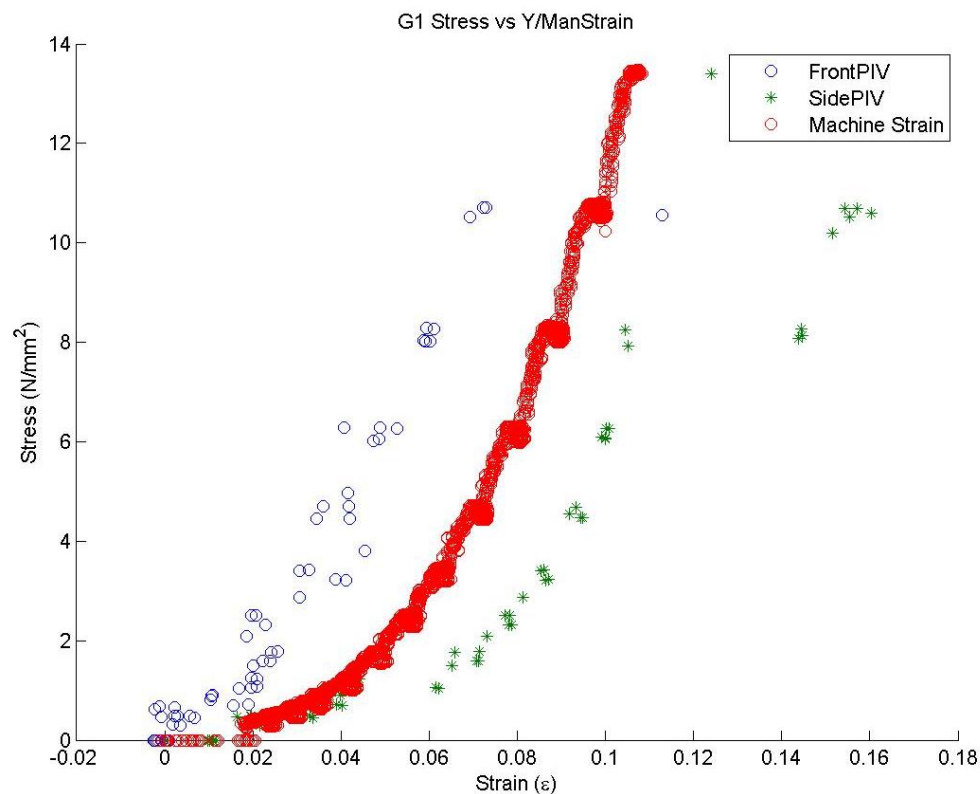
FIGURE 101: G1 TENSILE STRESS VS. MACHINE MEASURED/PIV STRAINS
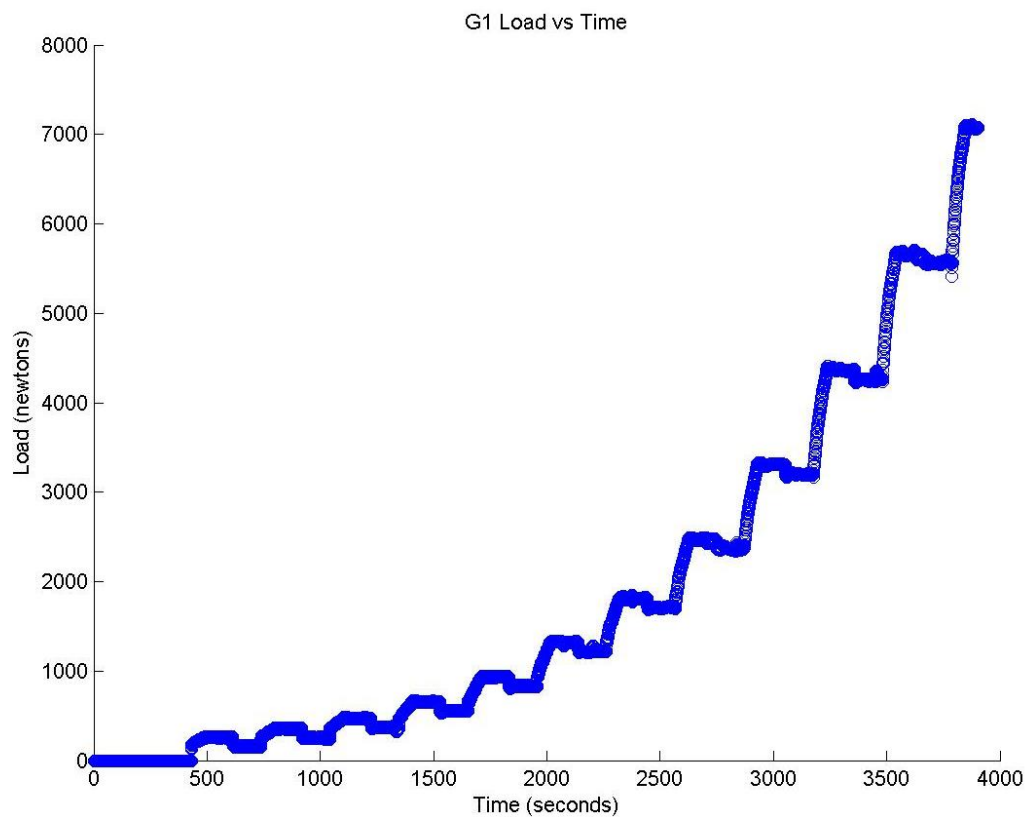
FIGURE 102: G1 TENSILE LOAD VS. TIME
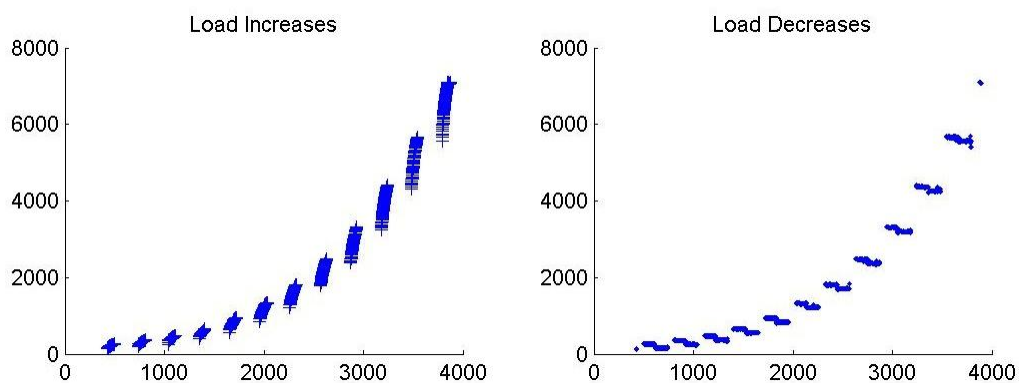
FIGURE 103: G1 CREEP LOADING: INCREMENTS AND RELAXATION
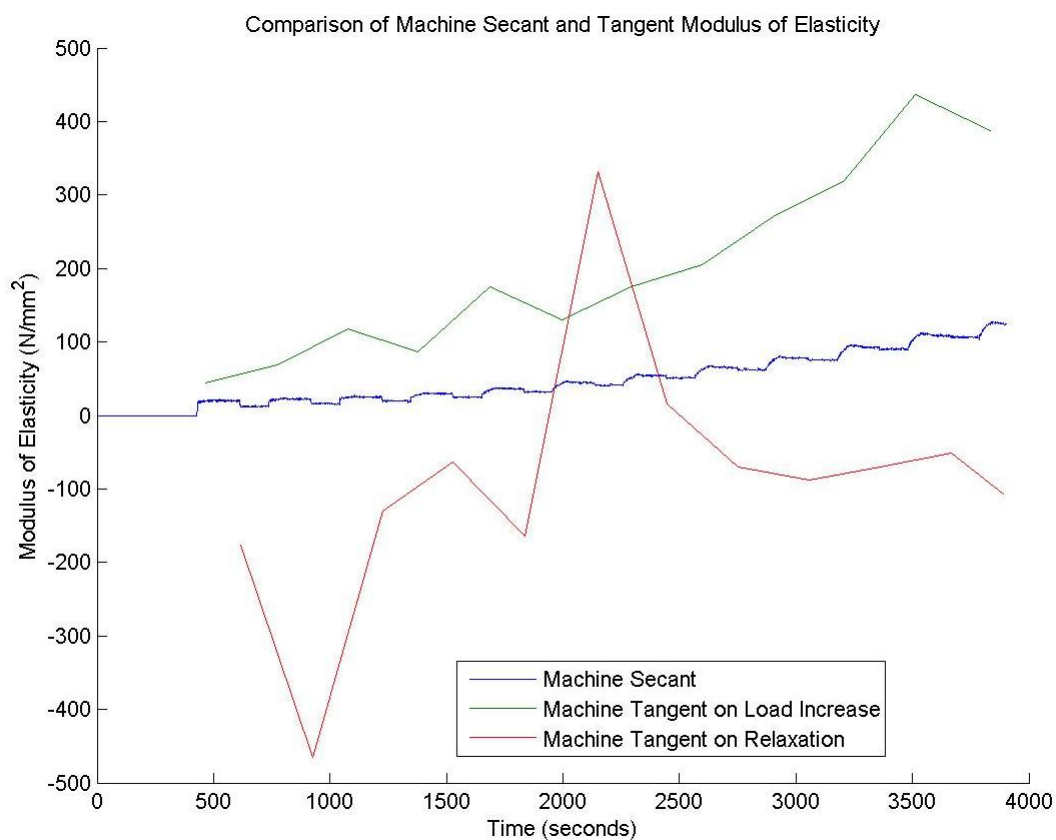
FIGURE 104: G1 MACHINE MEASURED SECANT AND TANGENT MODULUS VS. TIME

Appendix 6
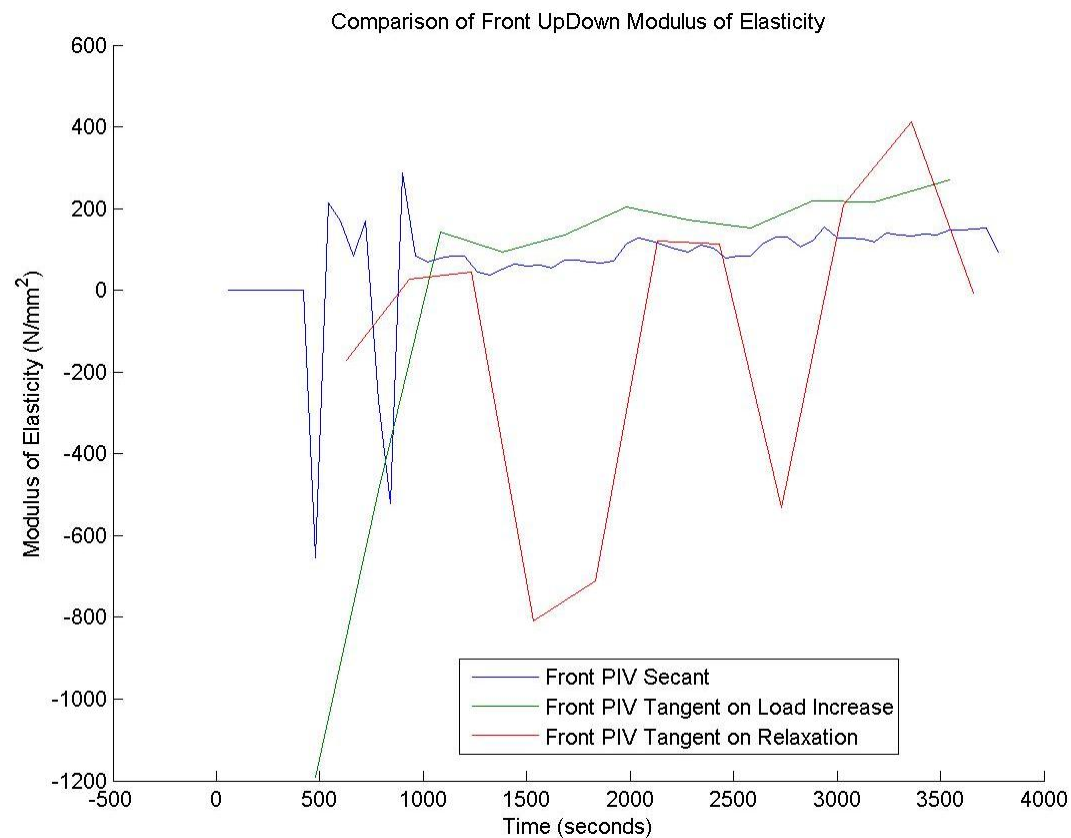
FIGURE 105: G1 FRONT VIEW PIV SECANT AND TANGENT MODULUS VS. TIME
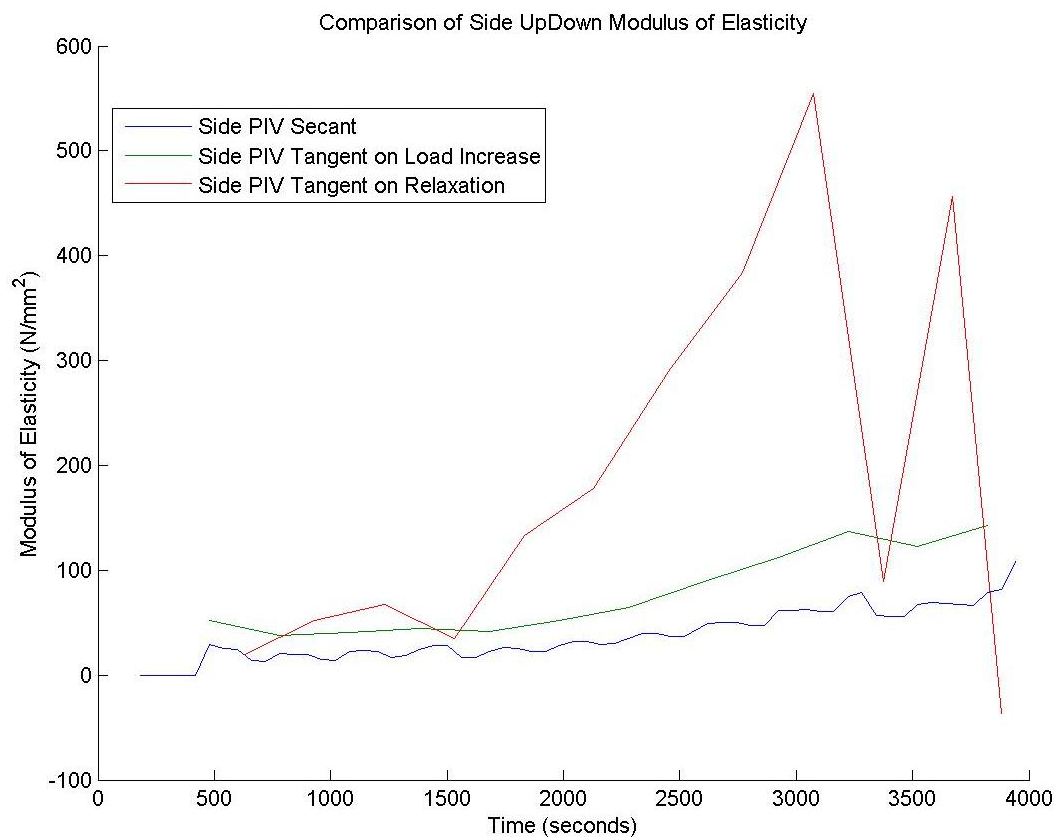
FIGURE 106: G1 SIDE VIEW PIV SECANT AND TANGENT MODULUS VS. TIME
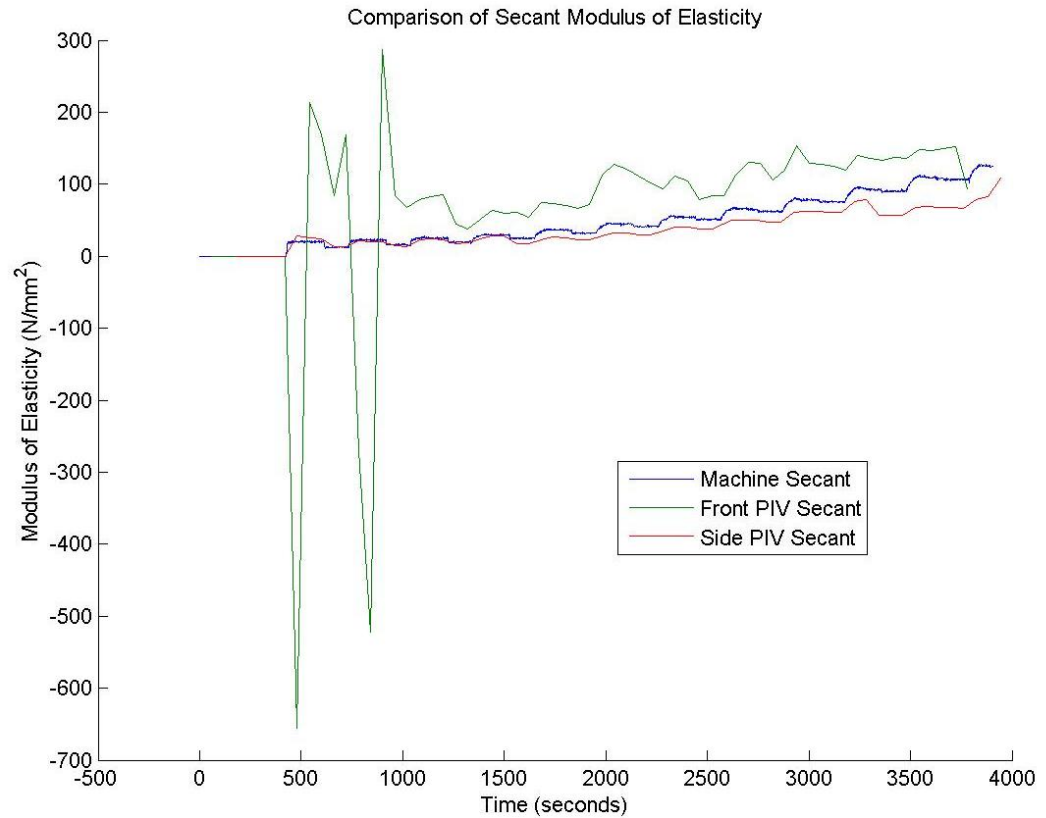
FIGURE 107: G1 COMPARISON OF MACHINE MEASURED AND PIV SECANT MODULUS VS. TIME
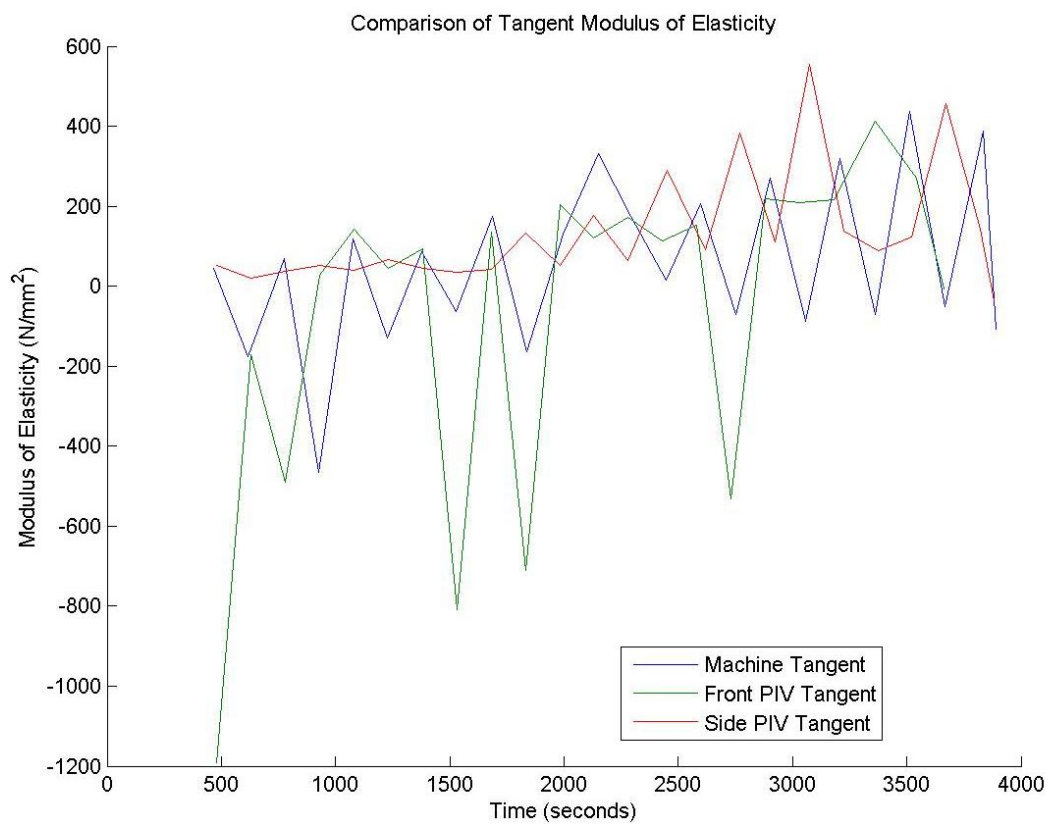
FIGURE 108: G1 COMPARISON OF MACHINE MEASURED AND PIV TANGENT MODULUS VS.

TIME

G1 Sample

FIGURE 109: SAMPLE GRAIN ORIENTATIONS OF THE FRONT (LEFT 4 IMAGES) AND SIDE (RIGHT 4 IMAGES) VIEW BEFORE (FIRST 2 OF 4 IMAGES) AND AFTER (LAST 2 OF 4 IMAGES) BREAKAGE

G1 Front View
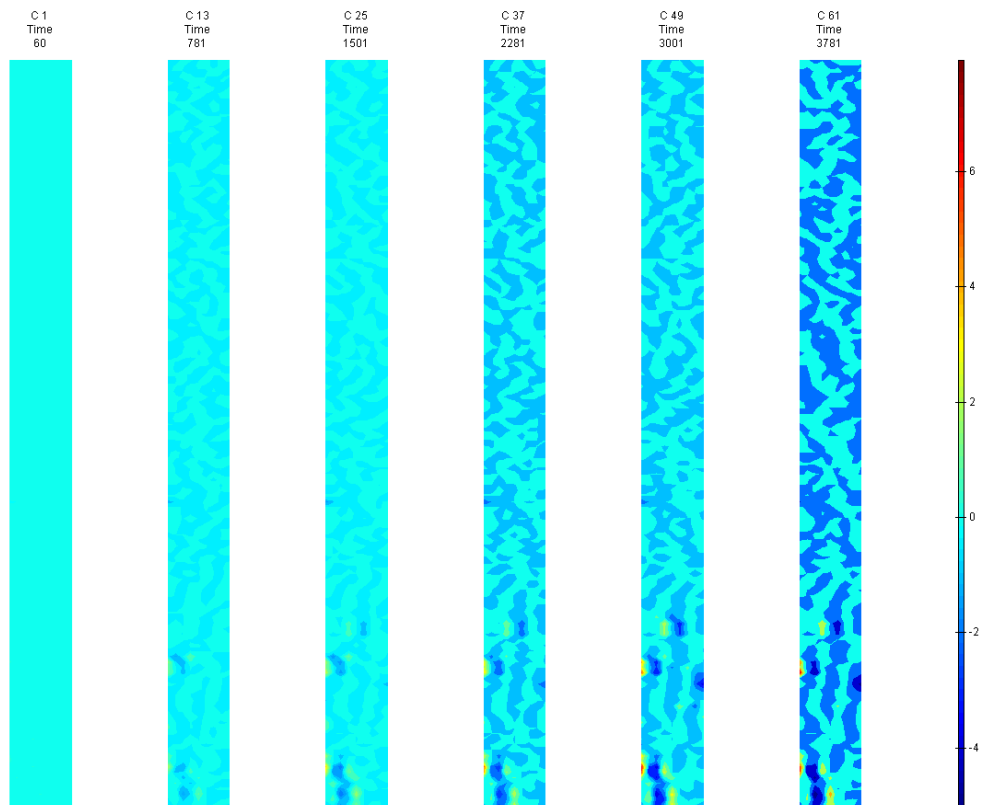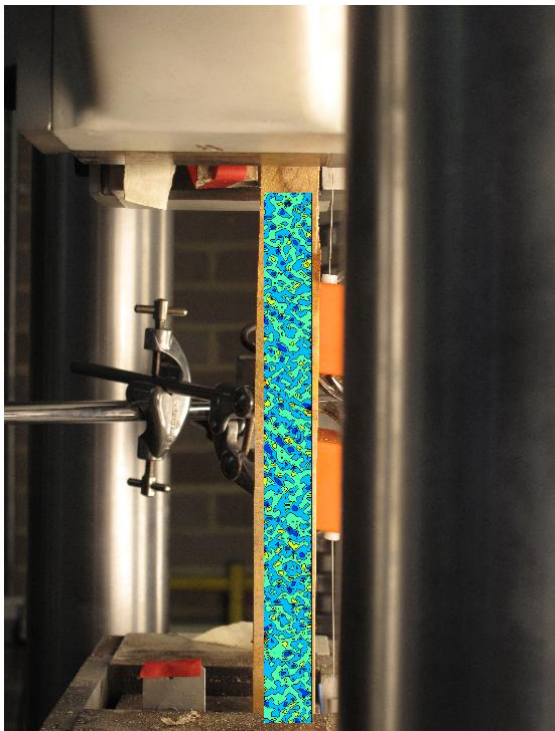

FIGURE 110: X DIRECTION PIV SEQUENTIAL ENGINEERING STRAIN OVER TIME
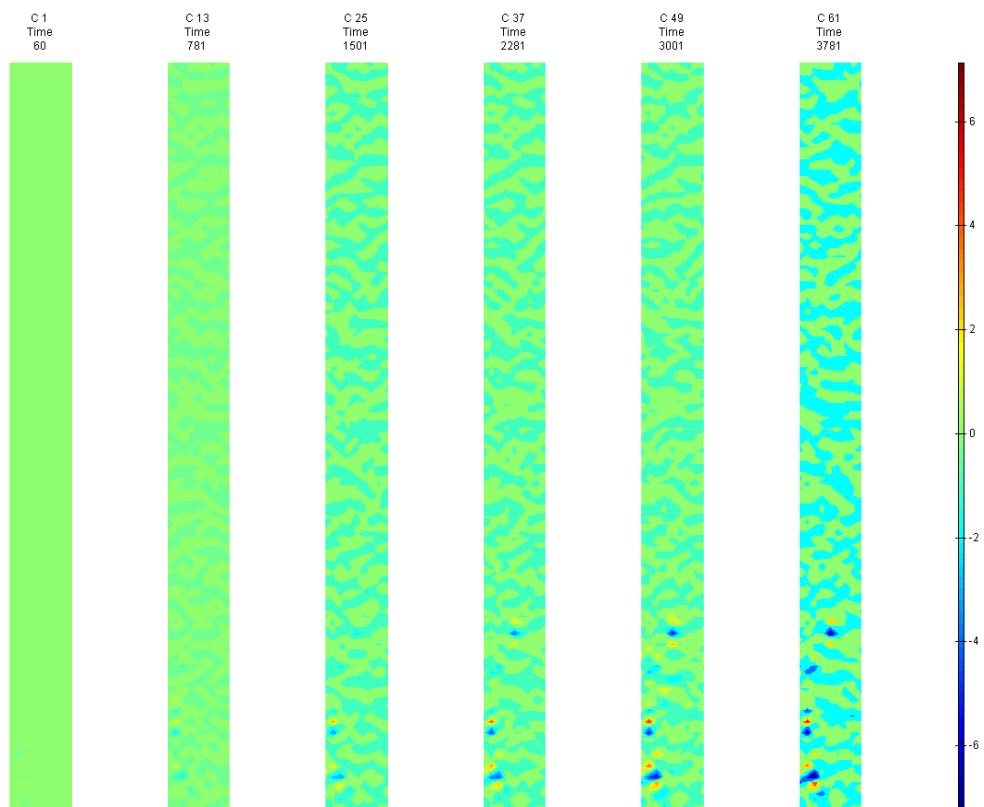
FIGURE 111: Y DIRECTION PIV SEQUENTIAL ENGINEERING STRAIN OVER TIME
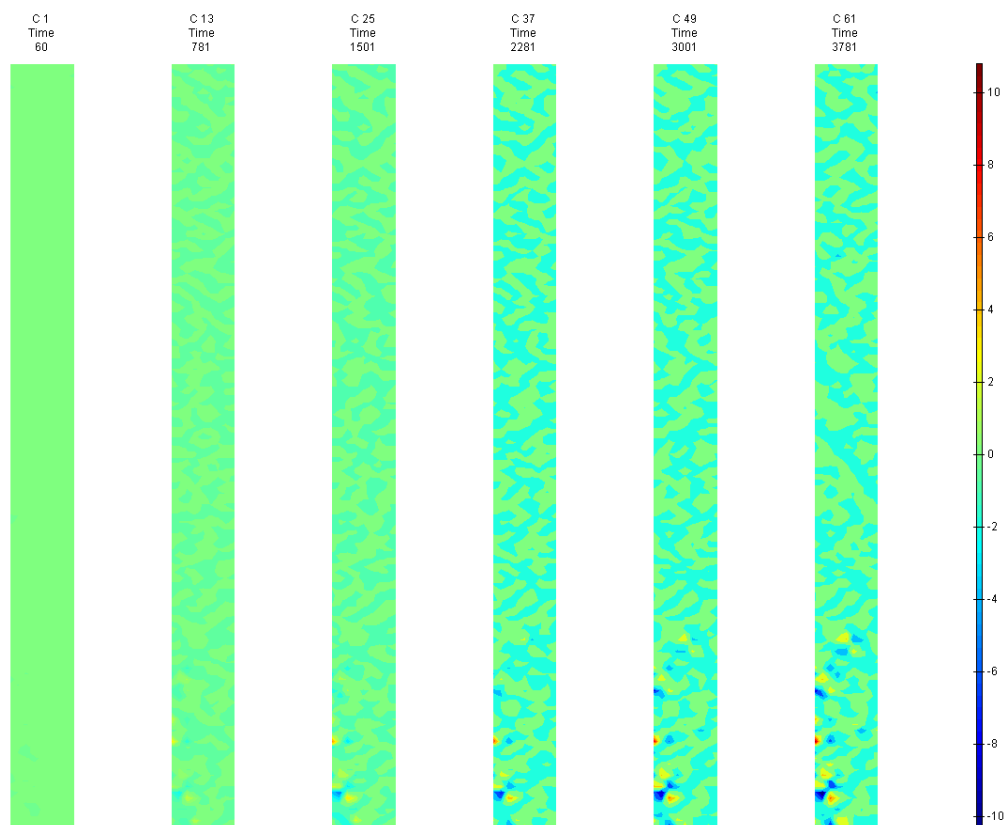
FIGURE 112: XY DIRECTION PIV SEQUENTIAL ENGINEERING SHEAR STRAIN OVER TIME
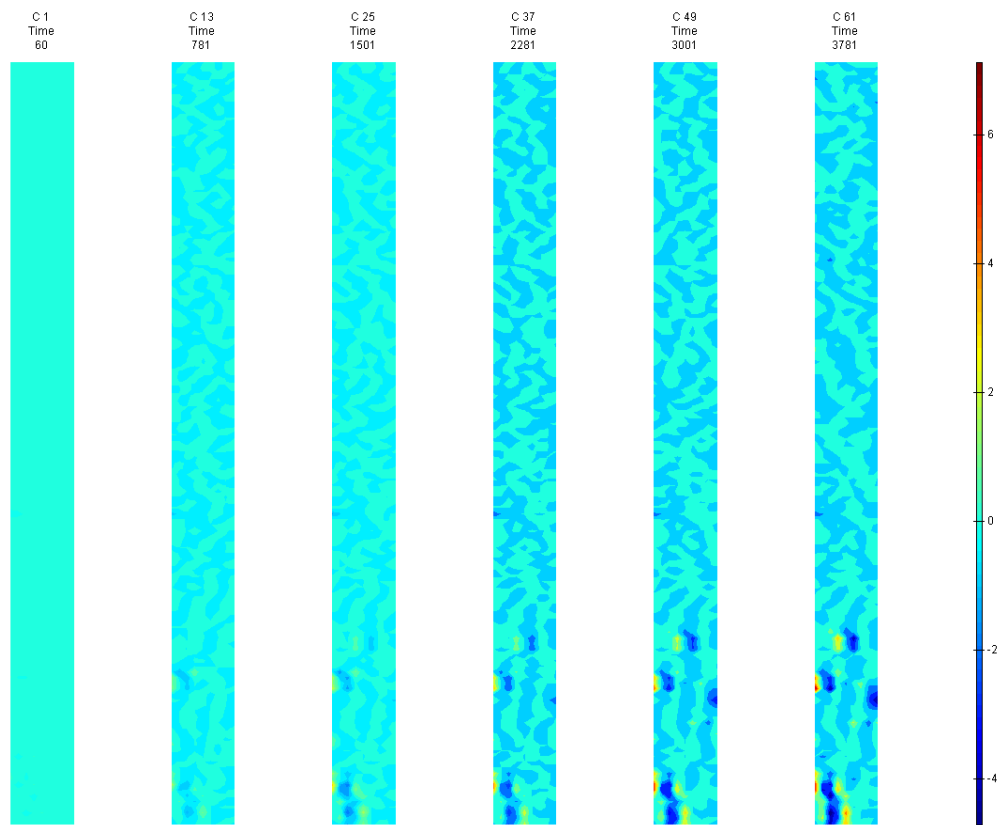
FIGURE 113: X DIRECTION PIV SEQUENTIAL TRUE STRAIN OVER TIME
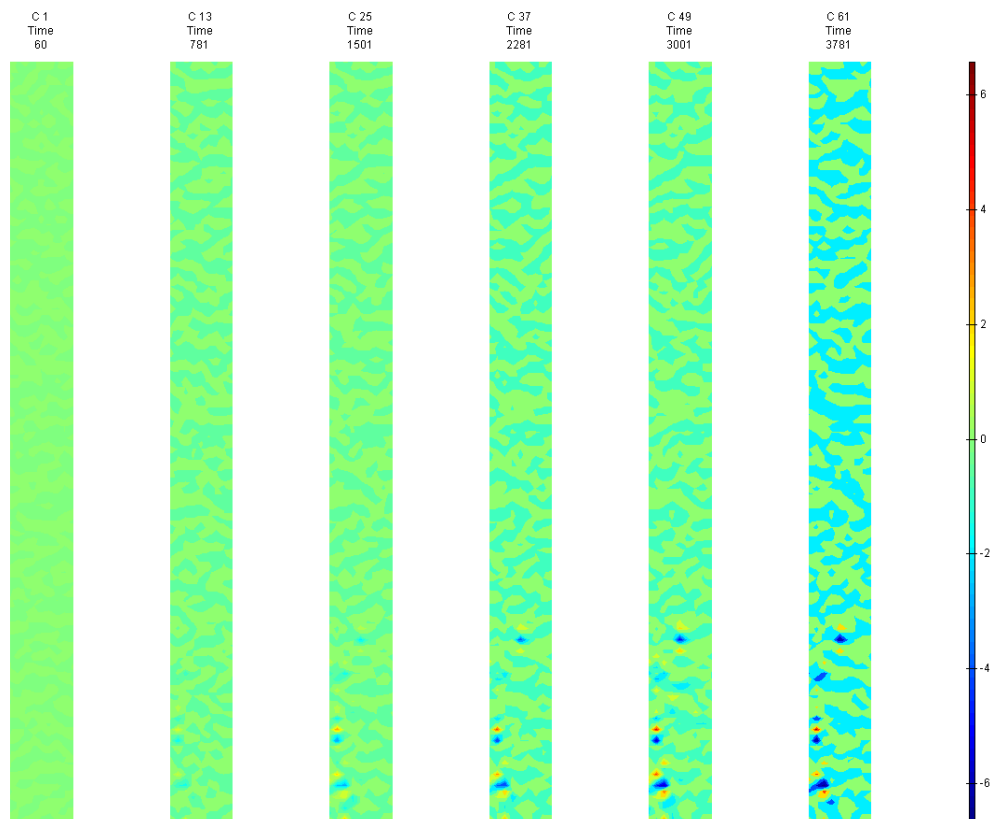
FIGURE 114: Y DIRECTION PIV SEQUENTIAL TRUE STRAIN OVER TIME
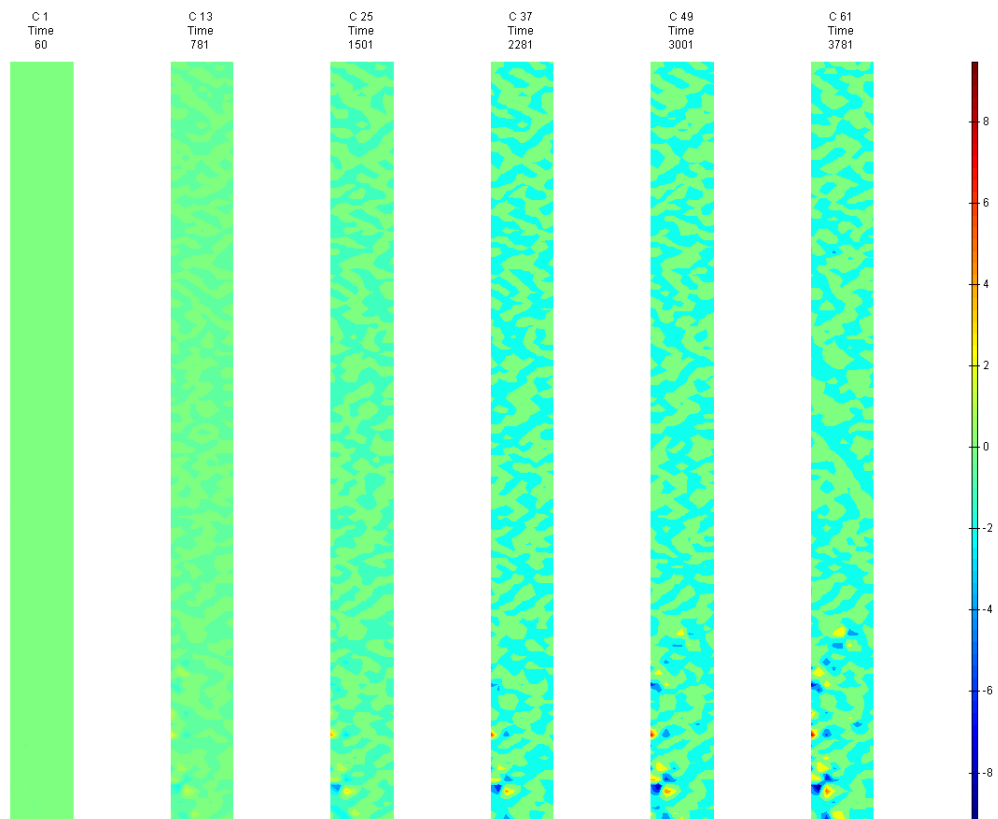
FIGURE 115: XY DIRECTION PIV SEQUENTIAL TRUE SHEAR STRAIN OVER TIME
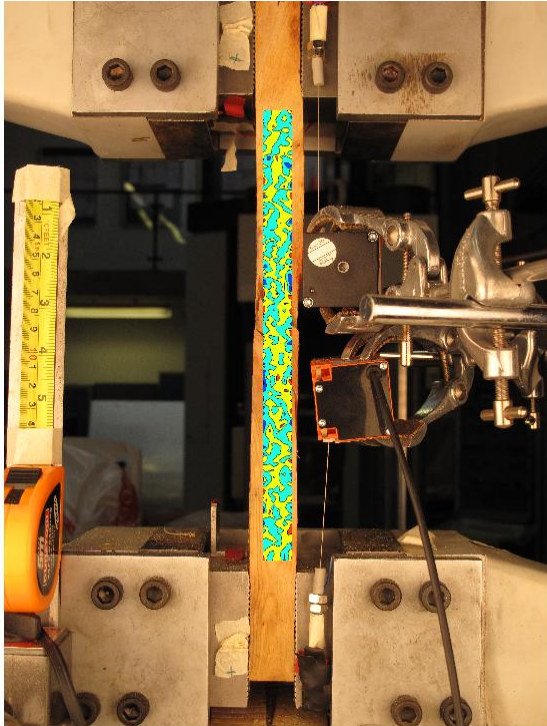
FIGURE 116: X DIRECTION PIV FIRST–LAST DITCH ENGINEERING STRAIN OVER IMAGE
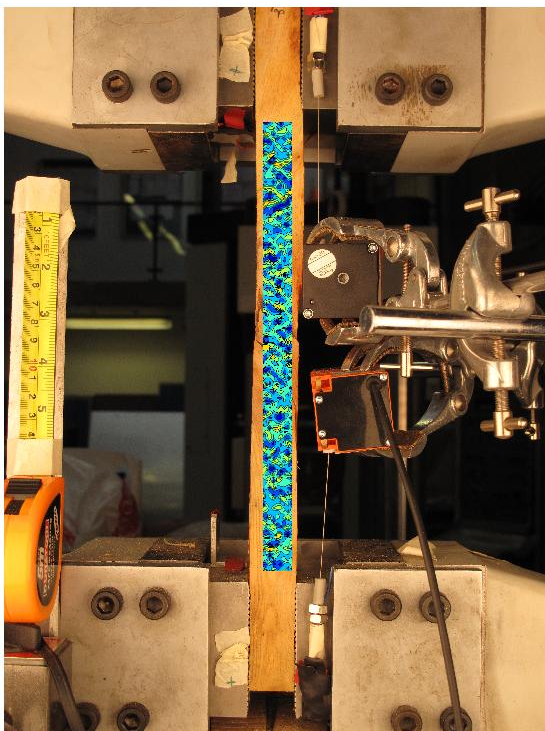
FIGURE 117: Y DIRECTION PIV FIRST–LAST DITCH ENGINEERING STRAIN OVER IMAGE
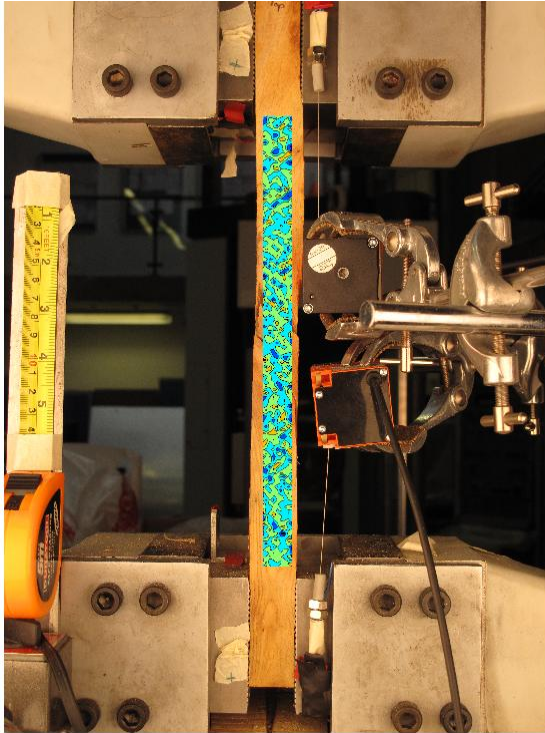
FIGURE 118: XY DIRECTION PIV FIRST–LAST DITCH ENGINEERING SHEAR STRAIN OVER
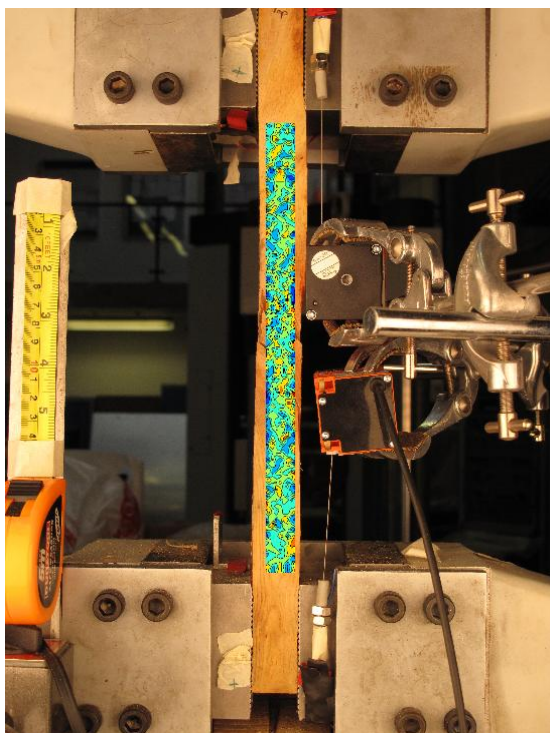
IMAGE

FIGURE 119: X DIRECTION PIV FIRST–LAST DITCH TRUE STRAIN OVER IMAGE

Appendix 6
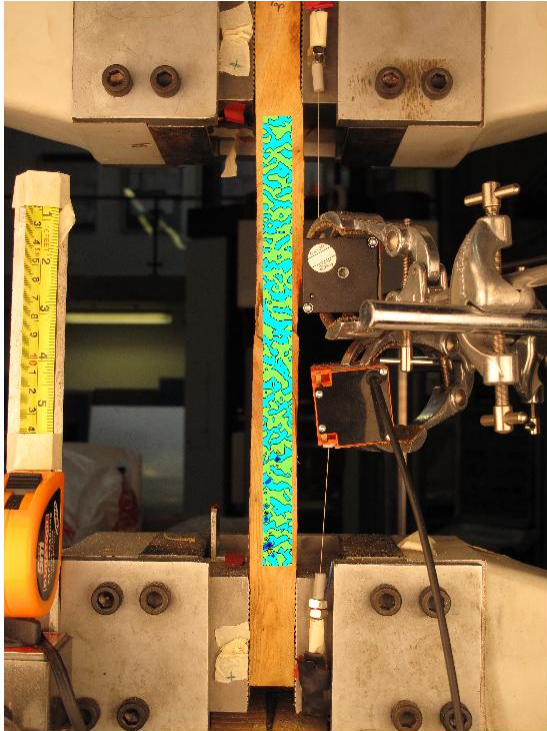
FIGURE 120: Y DIRECTION PIV FIRST–LAST DITCH TRUE STRAIN OVER IMAGE
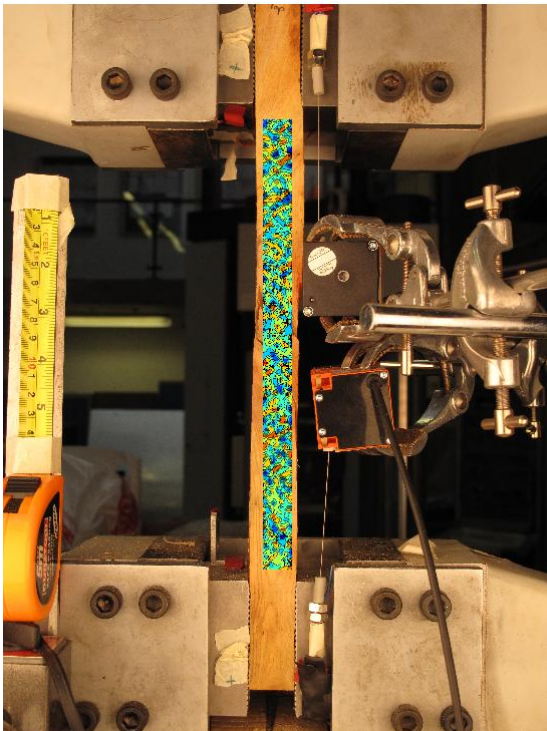
FIGURE 121: XY DIRECTION PIV FIRST–LAST DITCH TRUE SHEAR STRAIN OVER IMAGE
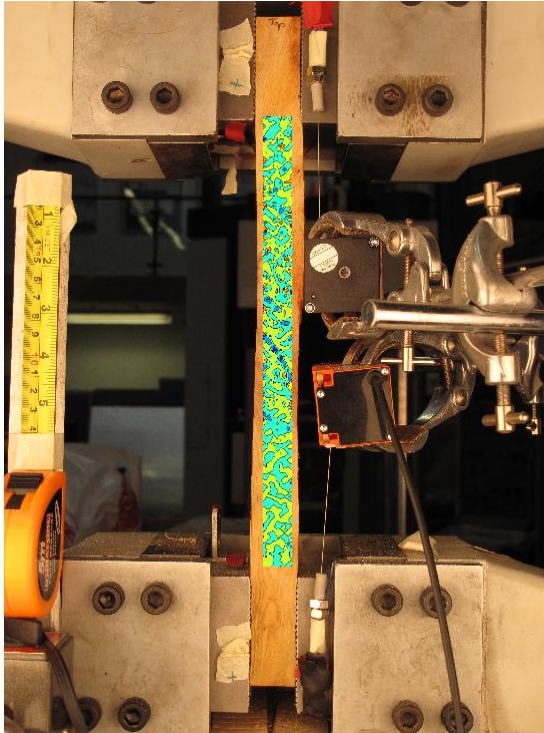
FIGURE 122: XY DIRECTION PIV FIRST–SEQUENTIAL ENGINEERING SHEAR STRAIN OVER

IMAGE
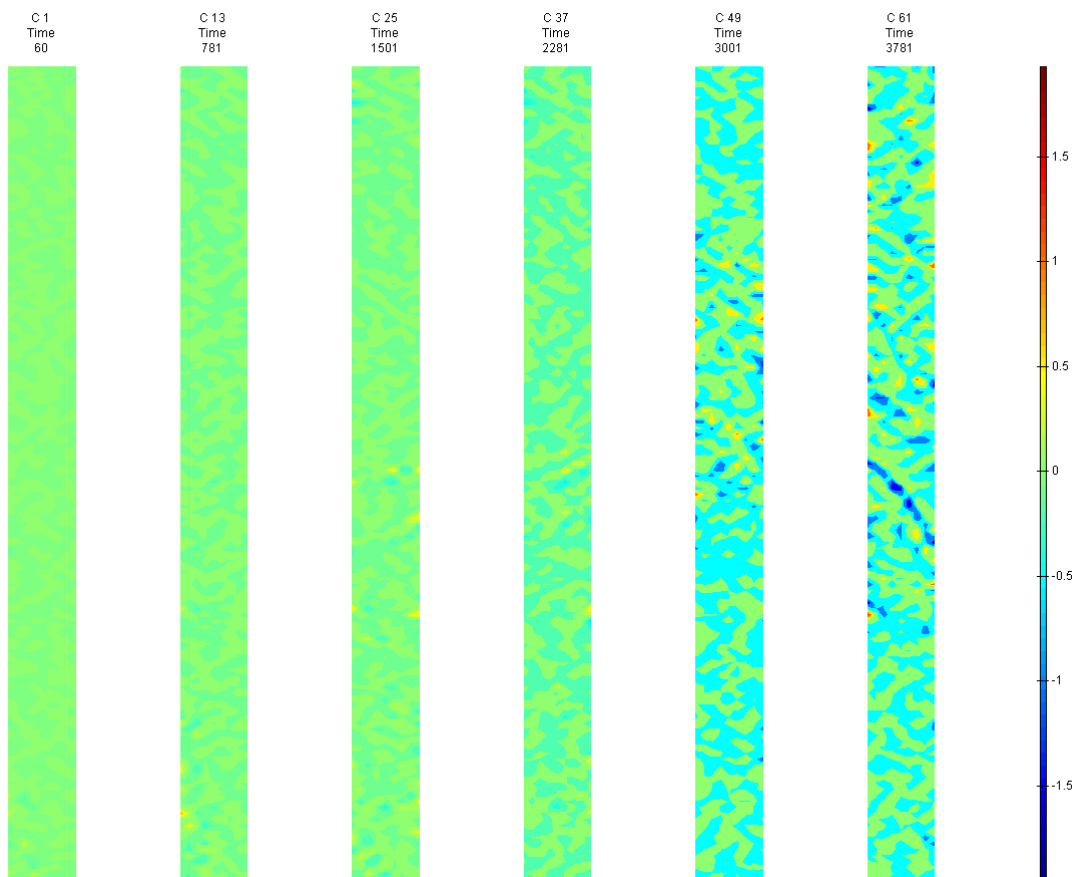
FIGURE 123: XY DIRECTION PIV FIRST–SEQUENTIAL ENGINEERING SHEAR STRAIN OVER TIME

Appendix 6

G1 Side View
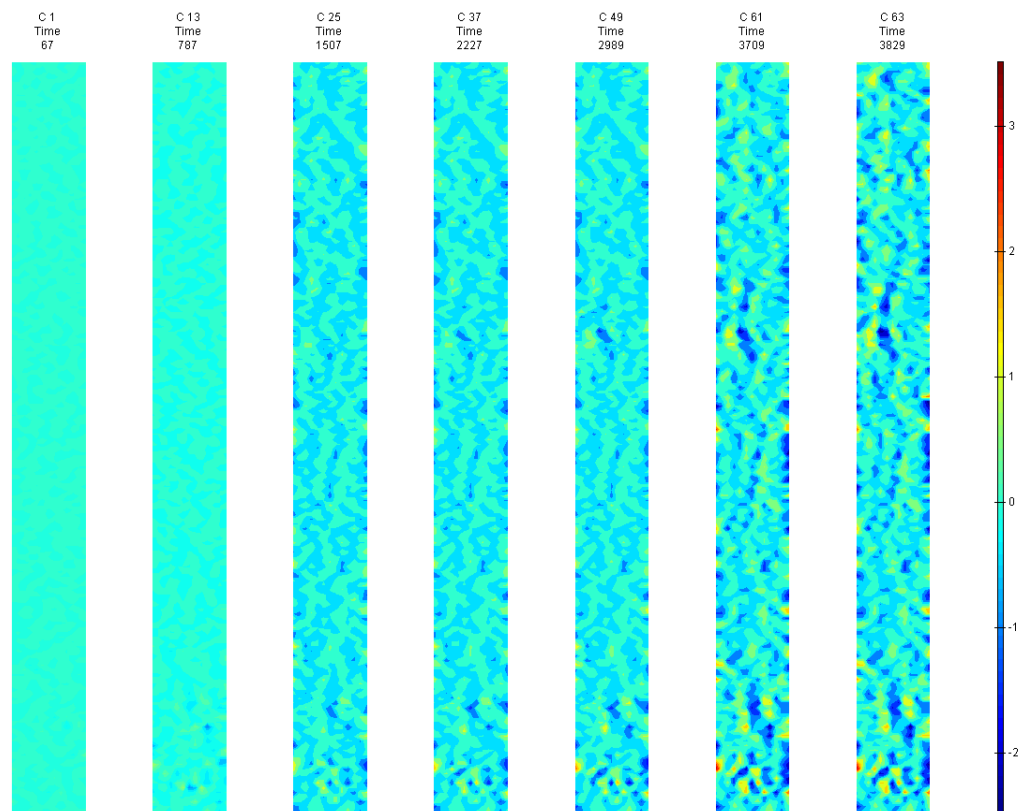
FIGURE 124: X DIRECTION PIV SEQUENTIAL ENGINEERING STRAIN OVER TIME
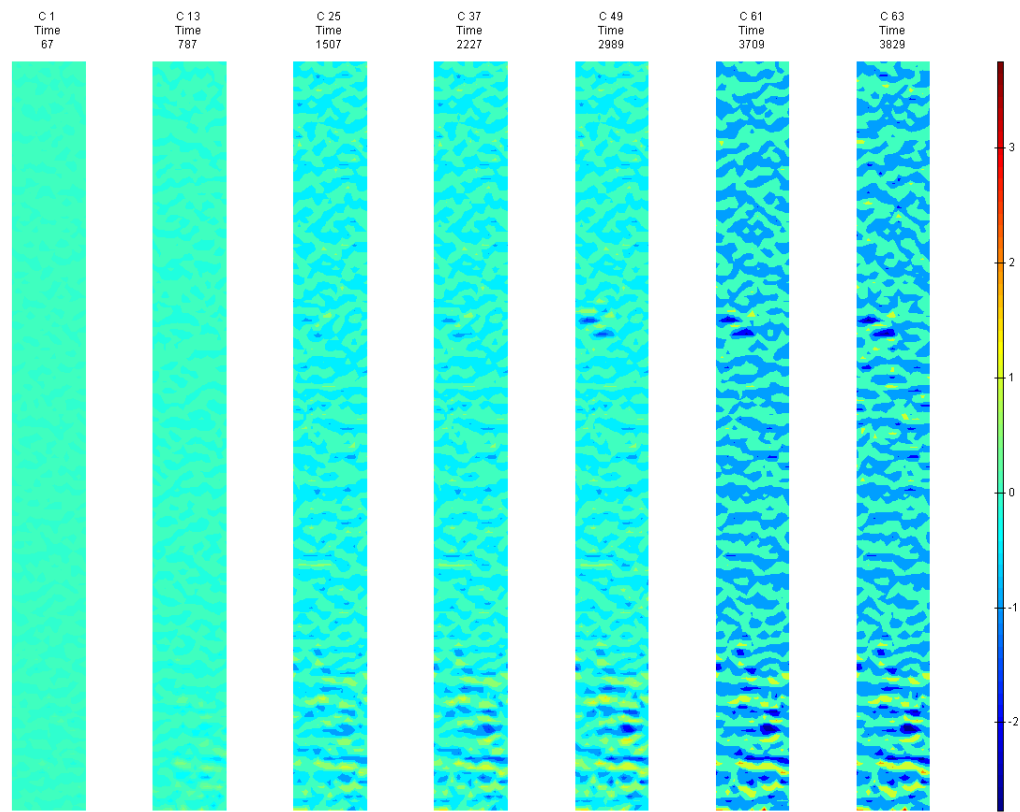
FIGURE 125: Y DIRECTION PIV SEQUENTIAL ENGINEERING STRAIN OVER TIME
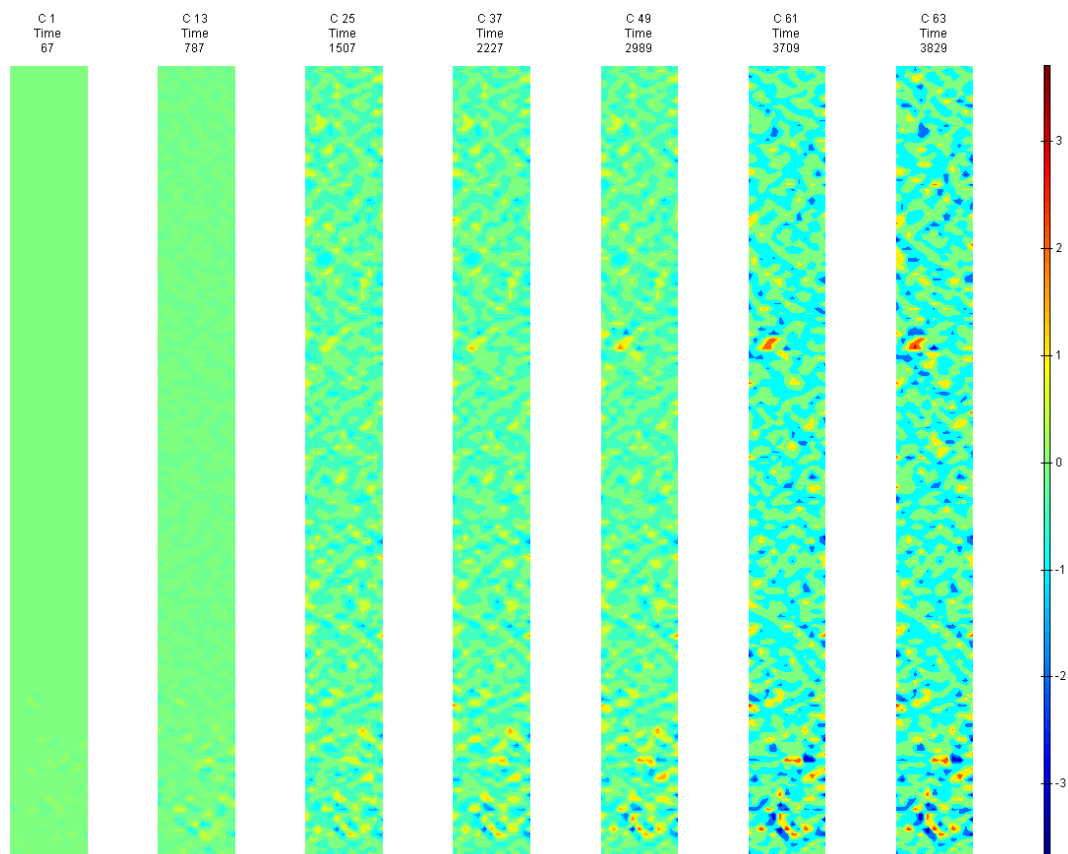
FIGURE 126: XY DIRECTION PIV SEQUENTIAL ENGINEERING SHEAR STRAIN OVER TIME
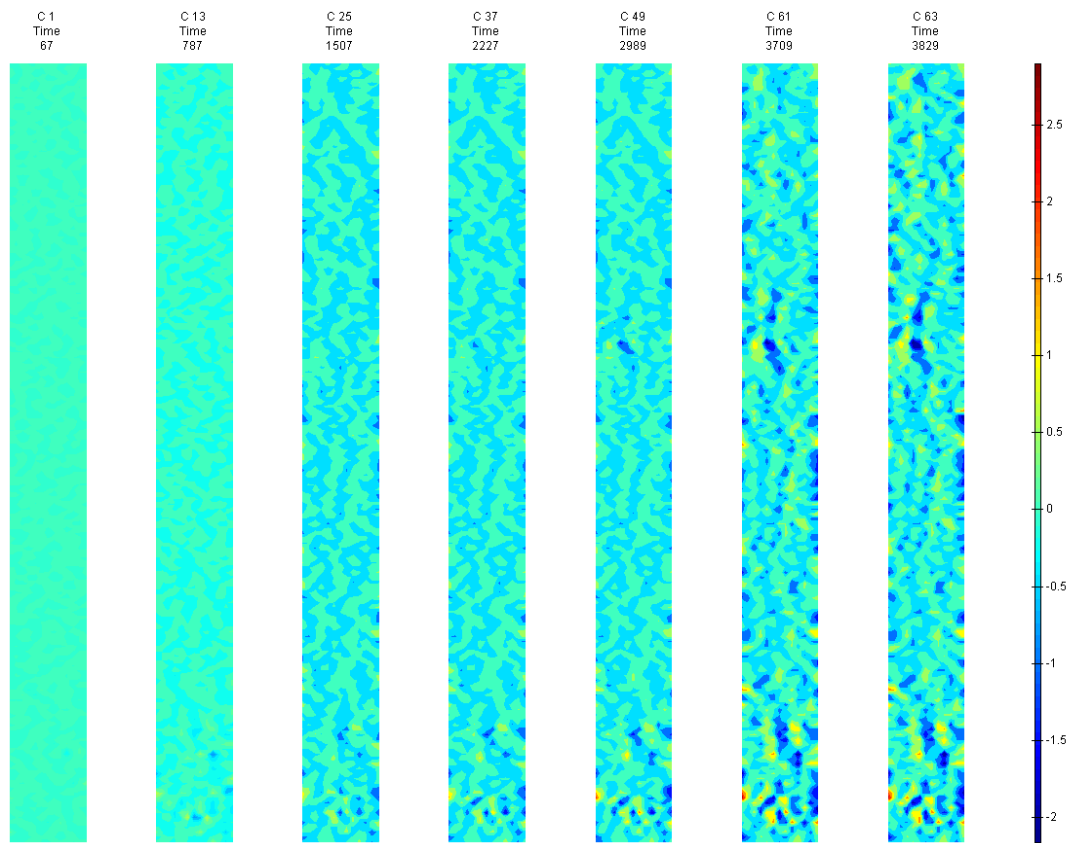
FIGURE 127: X DIRECTION PIV SEQUENTIAL TRUE STRAIN OVER TIME

Appendix 6
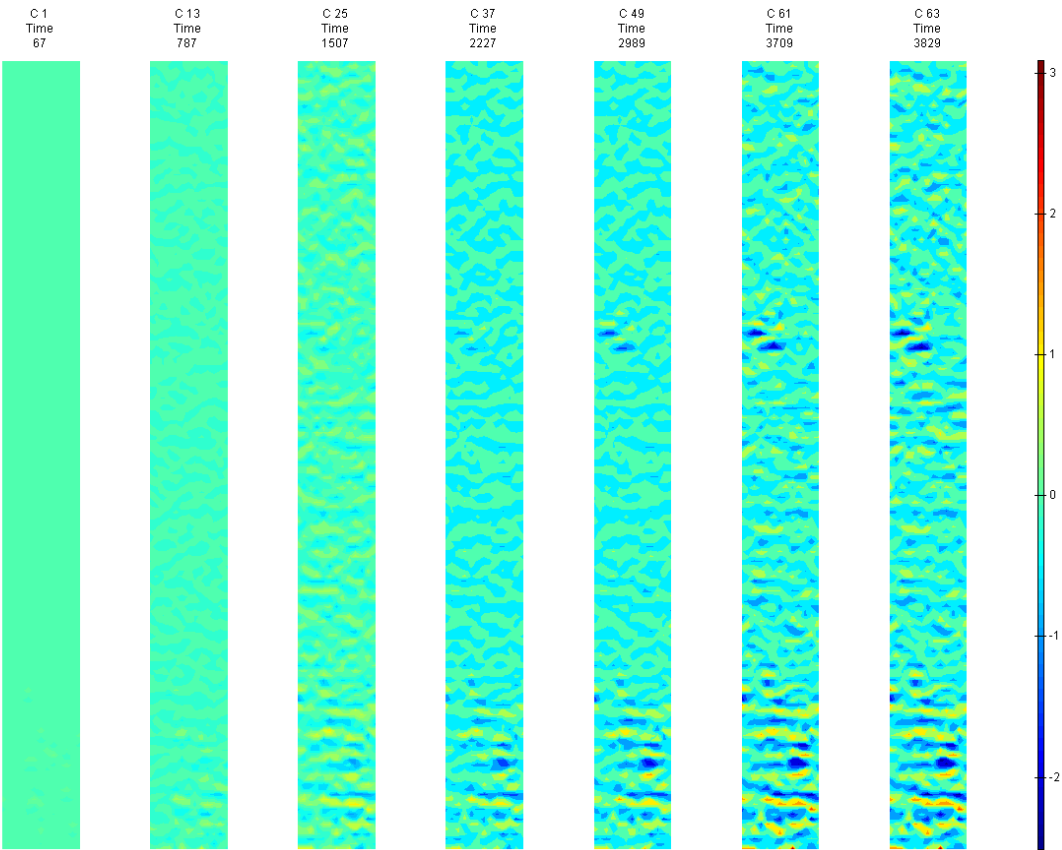
FIGURE 128: Y DIRECTION PIV SEQUENTIAL TRUE STRAIN OVER TIME
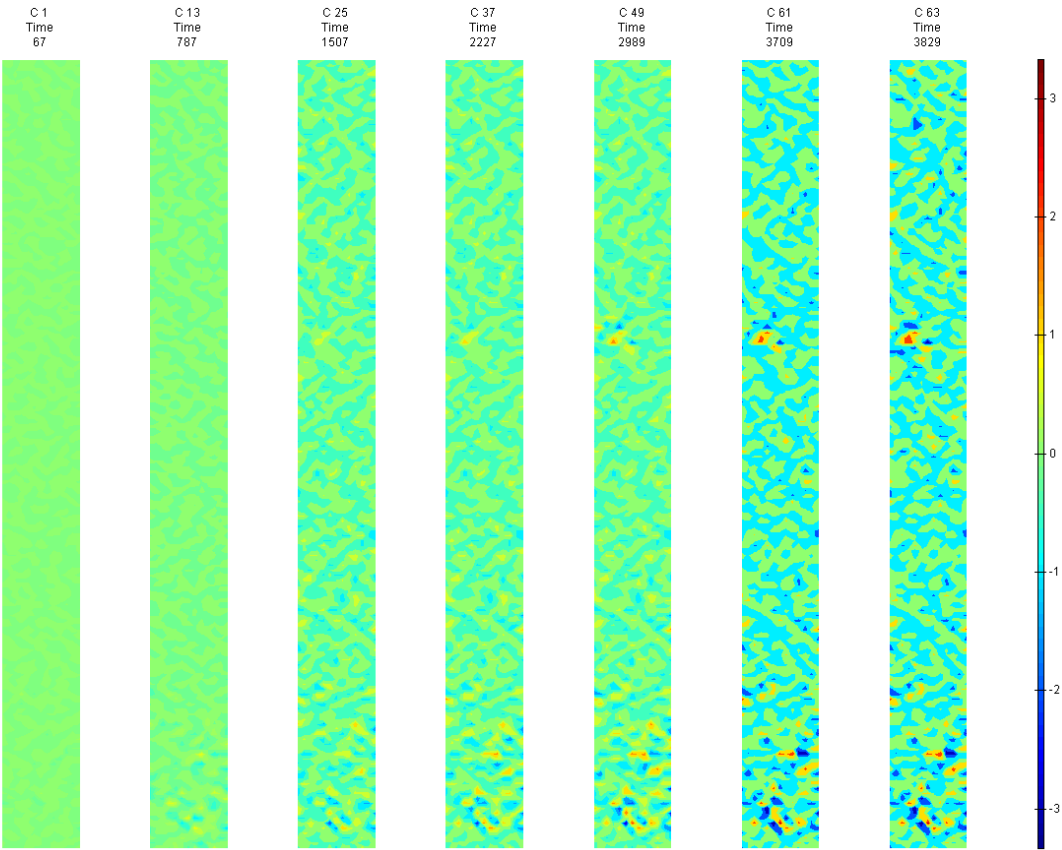
FIGURE 129: XY DIRECTION PIV SEQUENTIAL TRUE SHEAR STRAIN OVER TIME
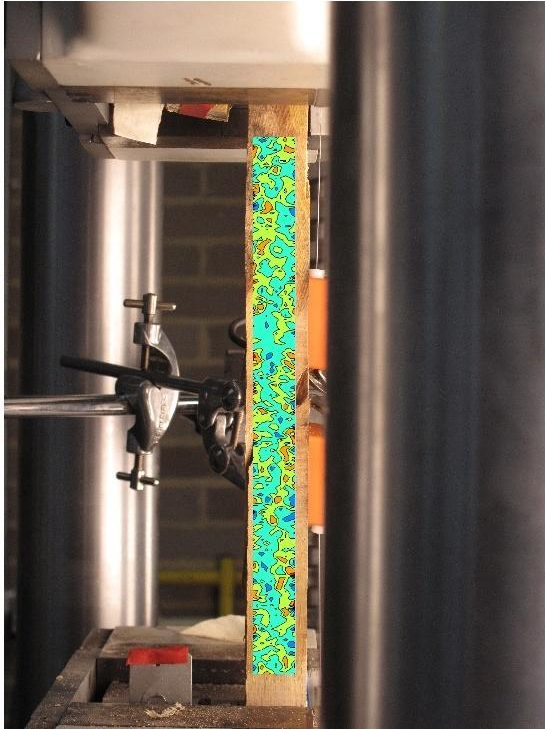
FIGURE 130: X DIRECTION PIV FIRST–LAST DITCH ENGINEERING STRAIN OVER IMAGE
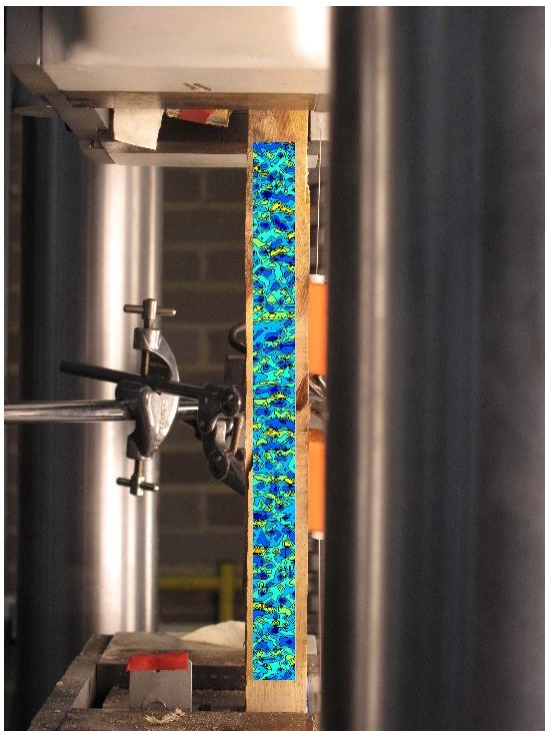
FIGURE 131: Y DIRECTION PIV FIRST–LAST DITCH ENGINEERING STRAIN OVER IMAGE

Appendix 6
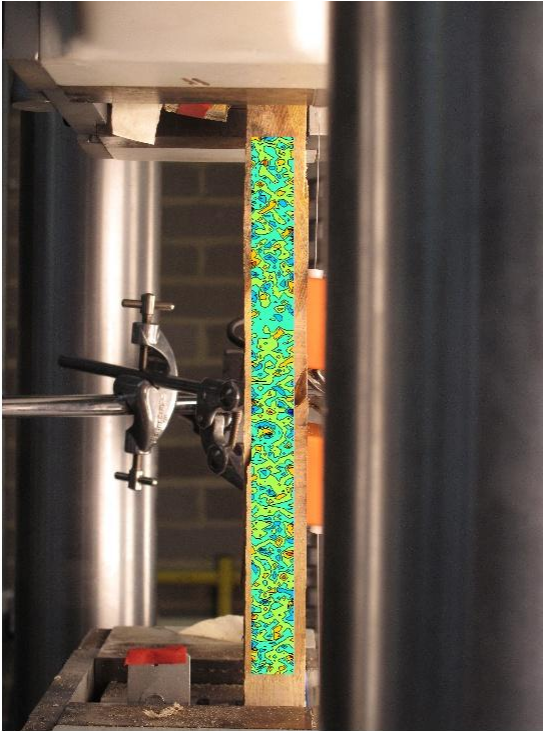
FIGURE 132: XY DIRECTION PIV FIRST-LAST DITCH ENGINEERING SHEAR STRAIN OVER
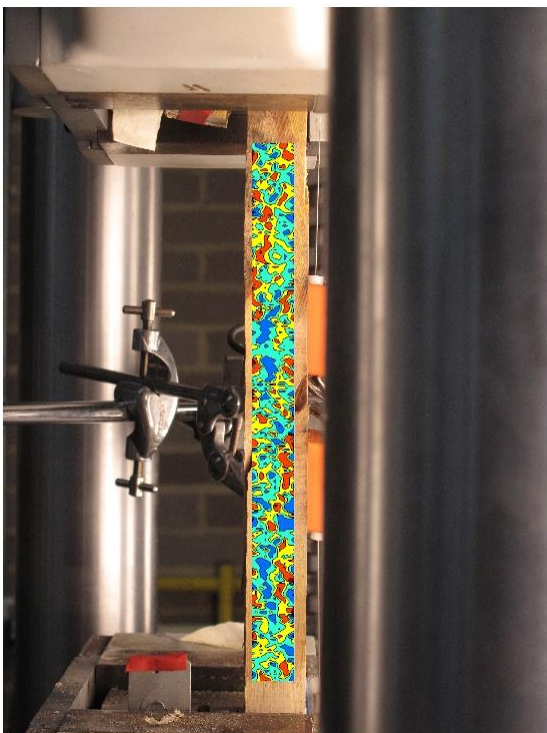
IMAGE

FIGURE 133: X DIRECTION PIV FIRST-LAST DITCH TRUE STRAIN OVER IMAGE
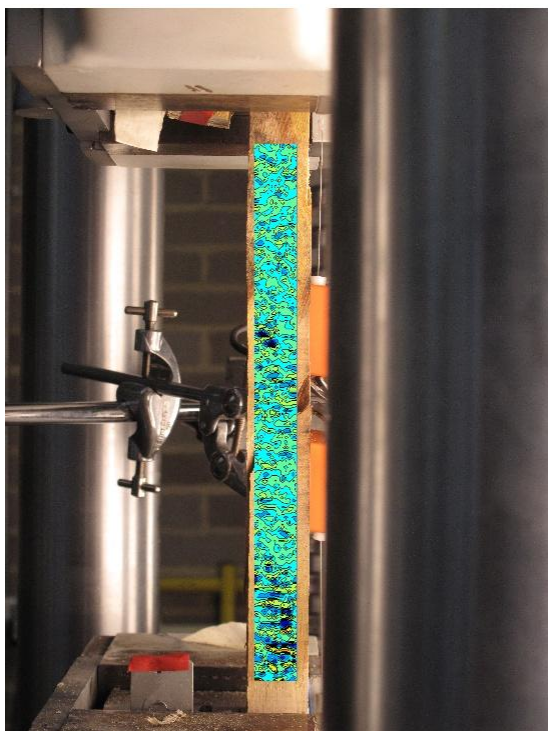
FIGURE 134: Y DIRECTION PIV FIRST–LAST DITCH TRUE STRAIN OVER IMAGE
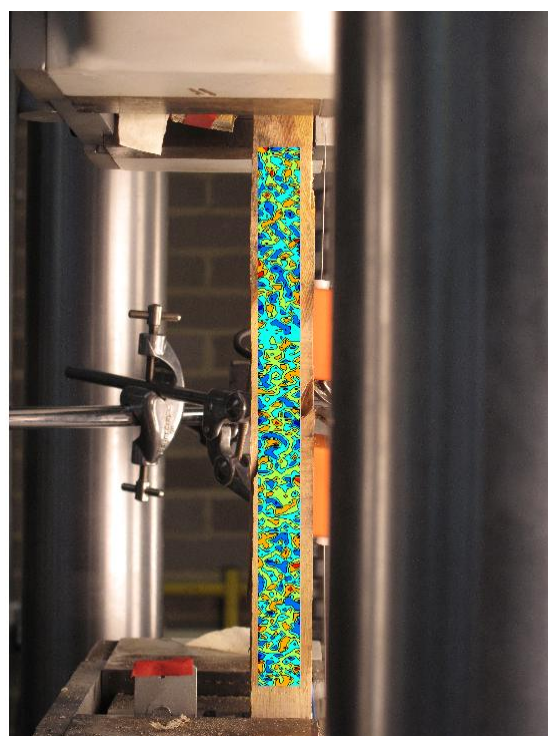
FIGURE 135: XY DIRECTION PIV FIRST–LAST DITCH TRUE SHEAR STRAIN OVER IMAGE

Appendix 6
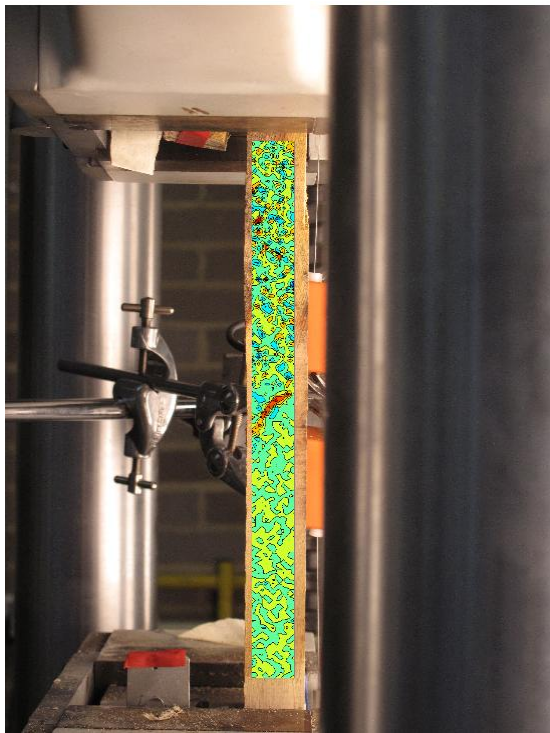
FIGURE 136: XY DIRECTION PIV FIRST–SEQUENTIAL ENGINEERING SHEAR STRAIN OVER

IMAGE
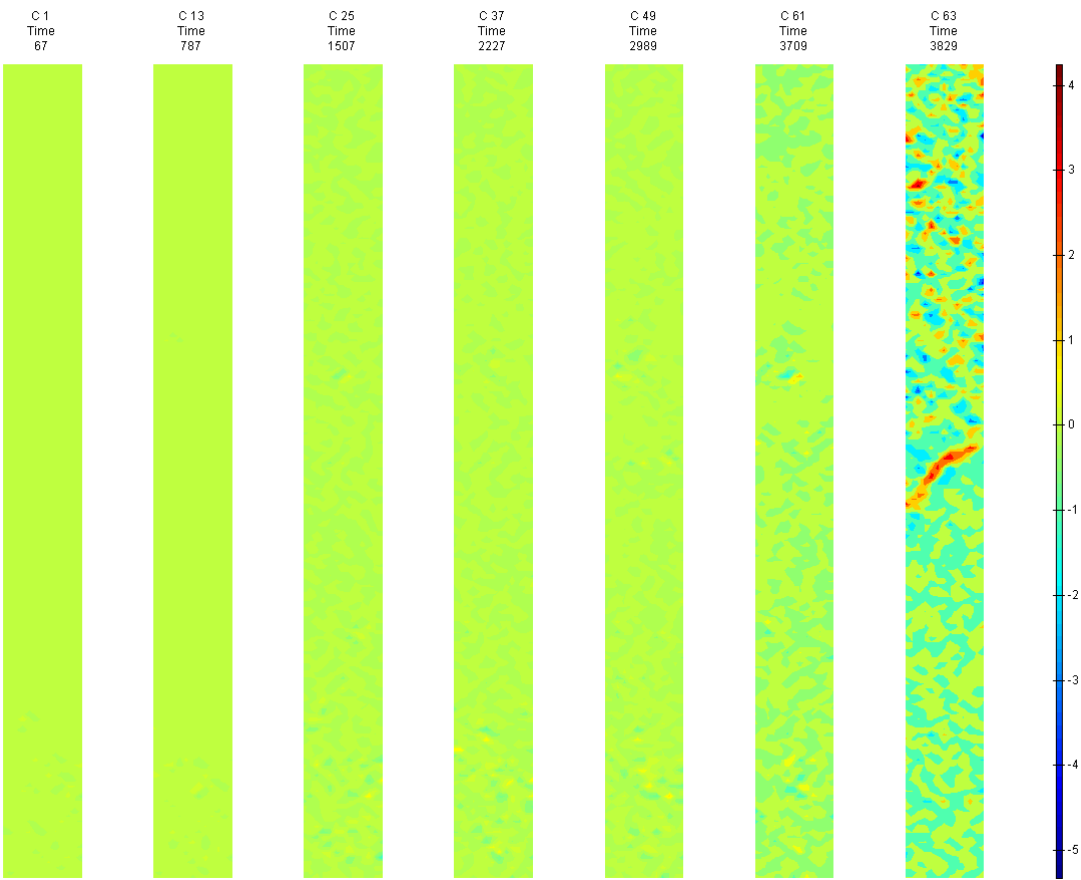
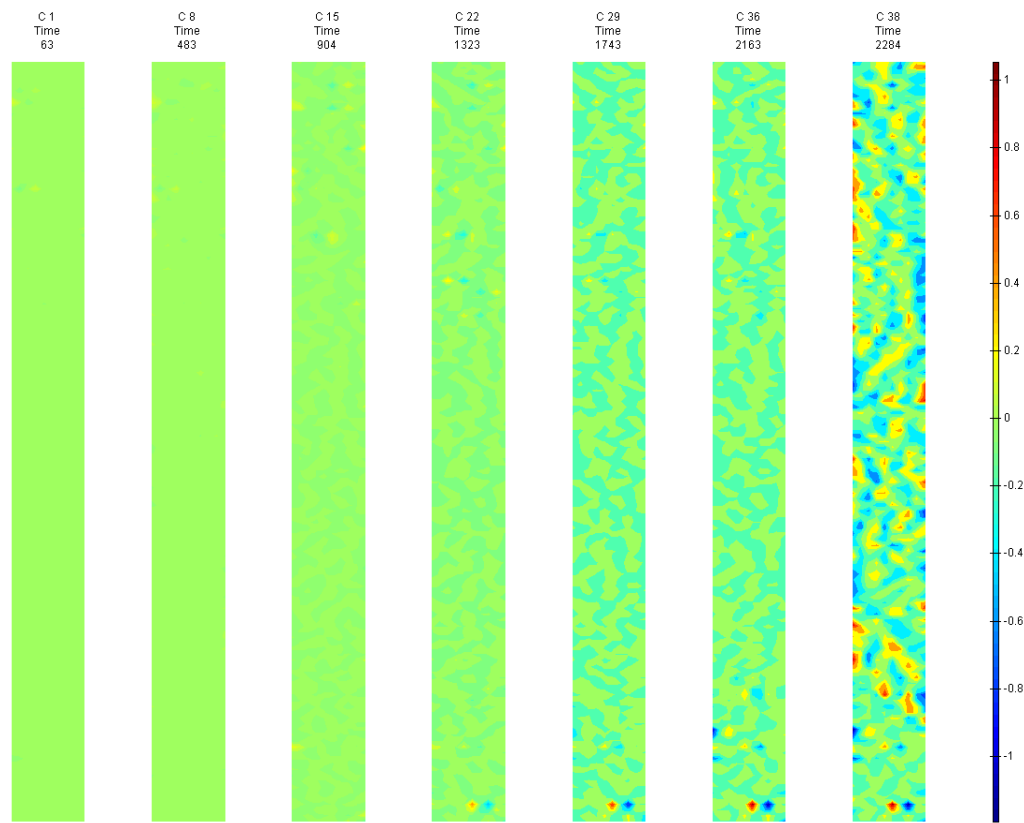FIGURE 137: XY DIRECTION PIV FIRST–SEQUENTIAL ENGINEERING SHEAR STRAIN OVER TIME

G3
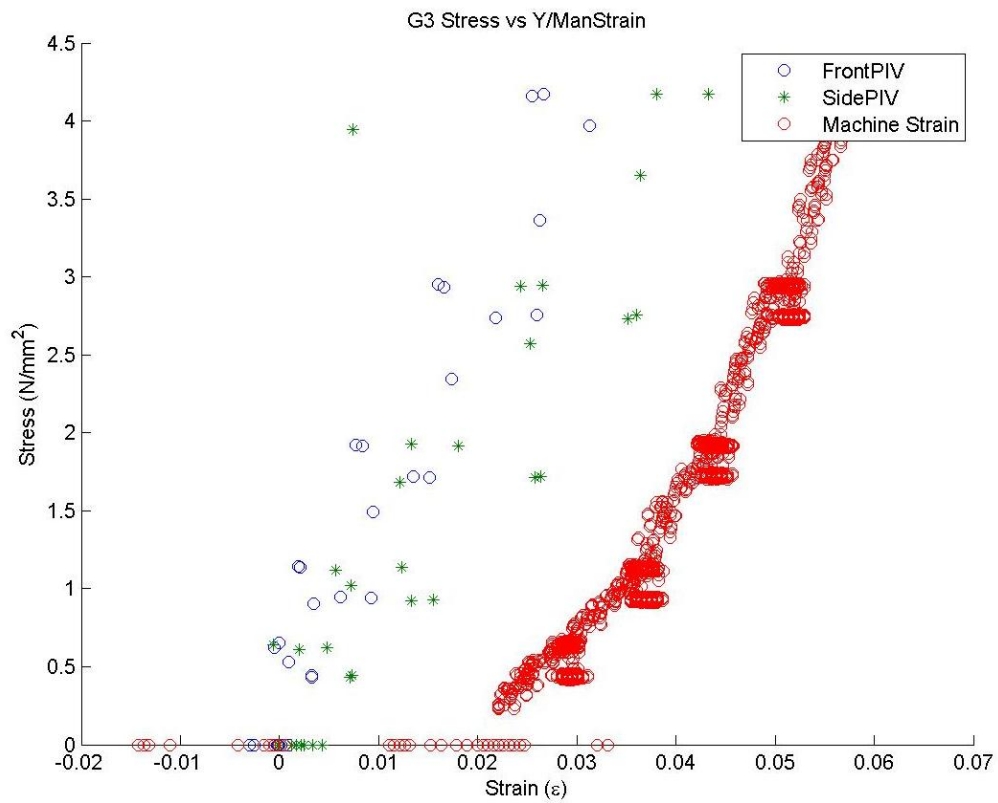
FIGURE 138: G3 TENSILE STRESS VS. MACHINE MEASURED/PIV STRAINS
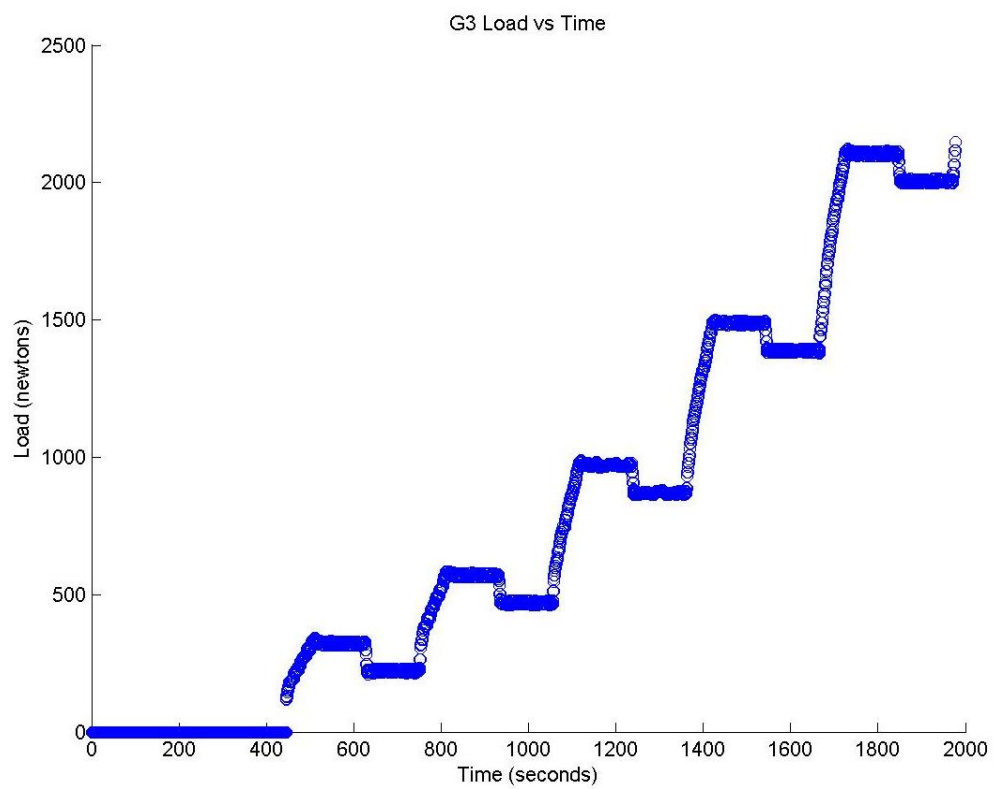
FIGURE 139: G3 TENSILE LOAD VS. TIME
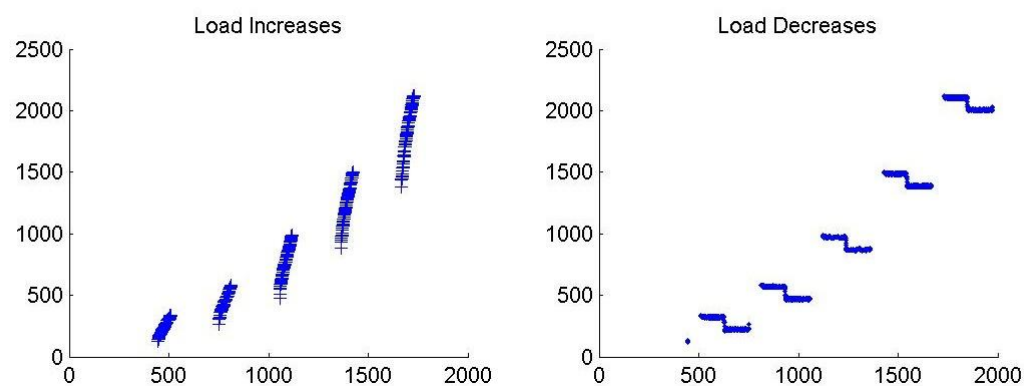
FIGURE 140: G3 CREEP LOADING: INCREMENTS AND RELAXATION
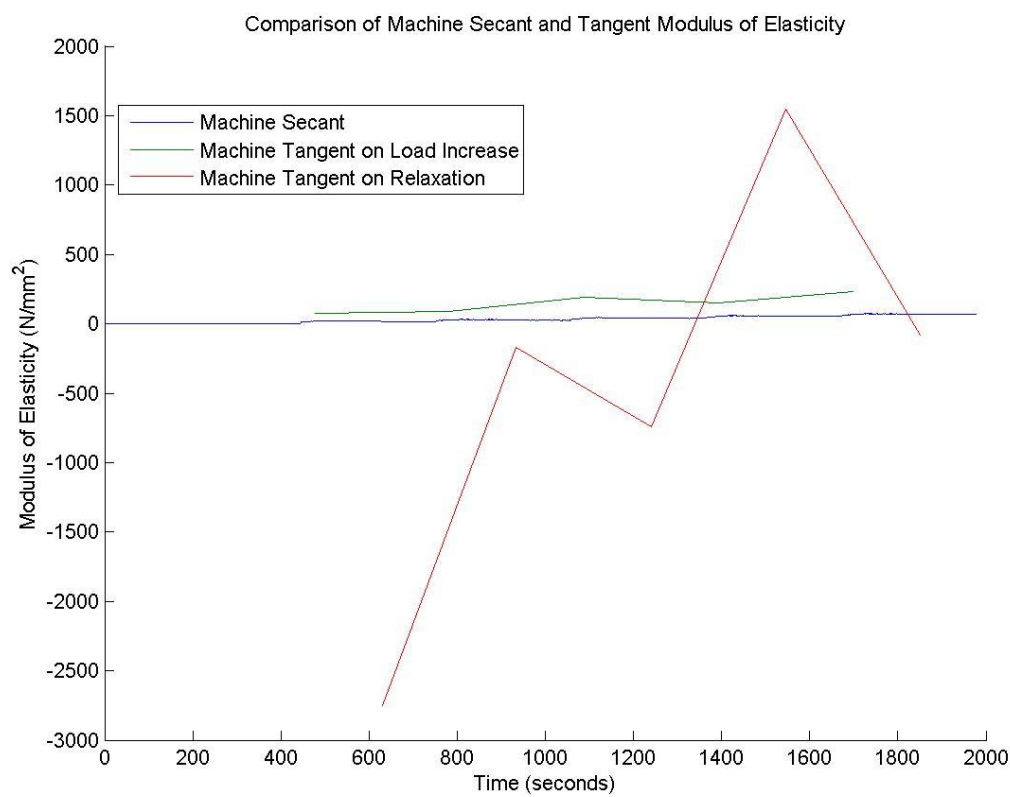
FIGURE 141: G3 MACHINE MEASURED SECANT AND TANGENT MODULUS VS. TIME
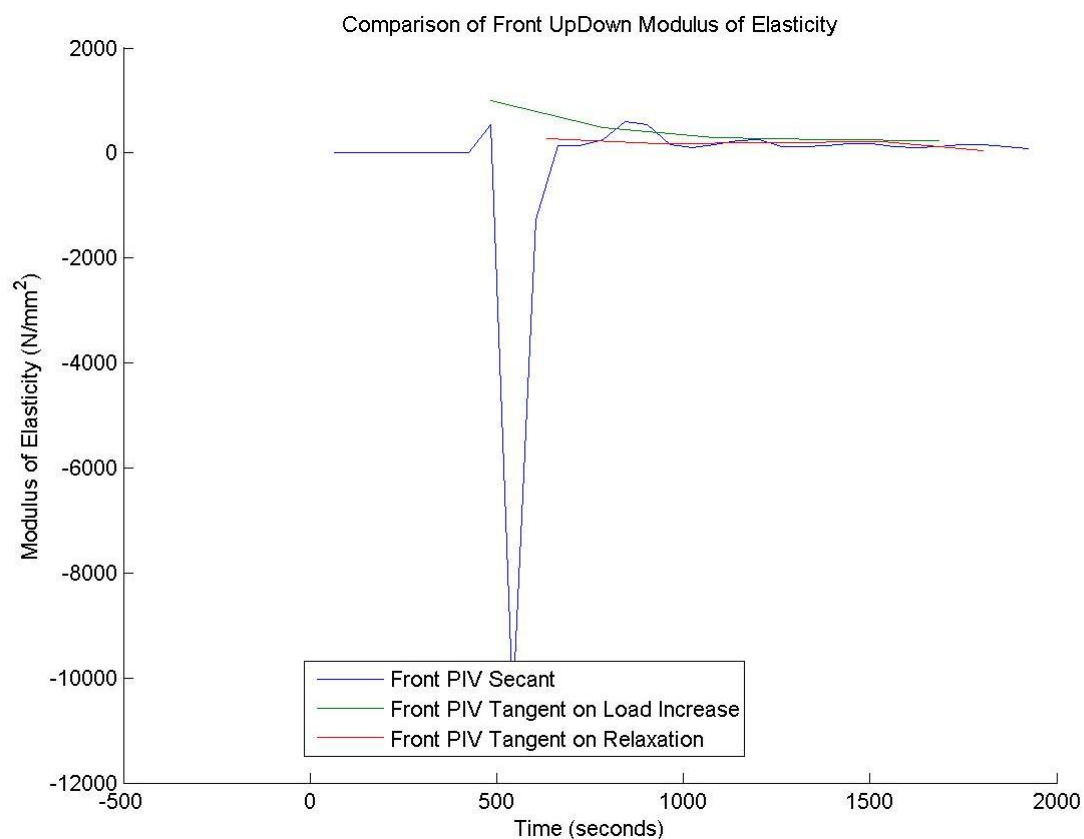
FIGURE 142: G3 FRONT VIEW PIV SECANT AND TANGENT MODULUS VS. TIME
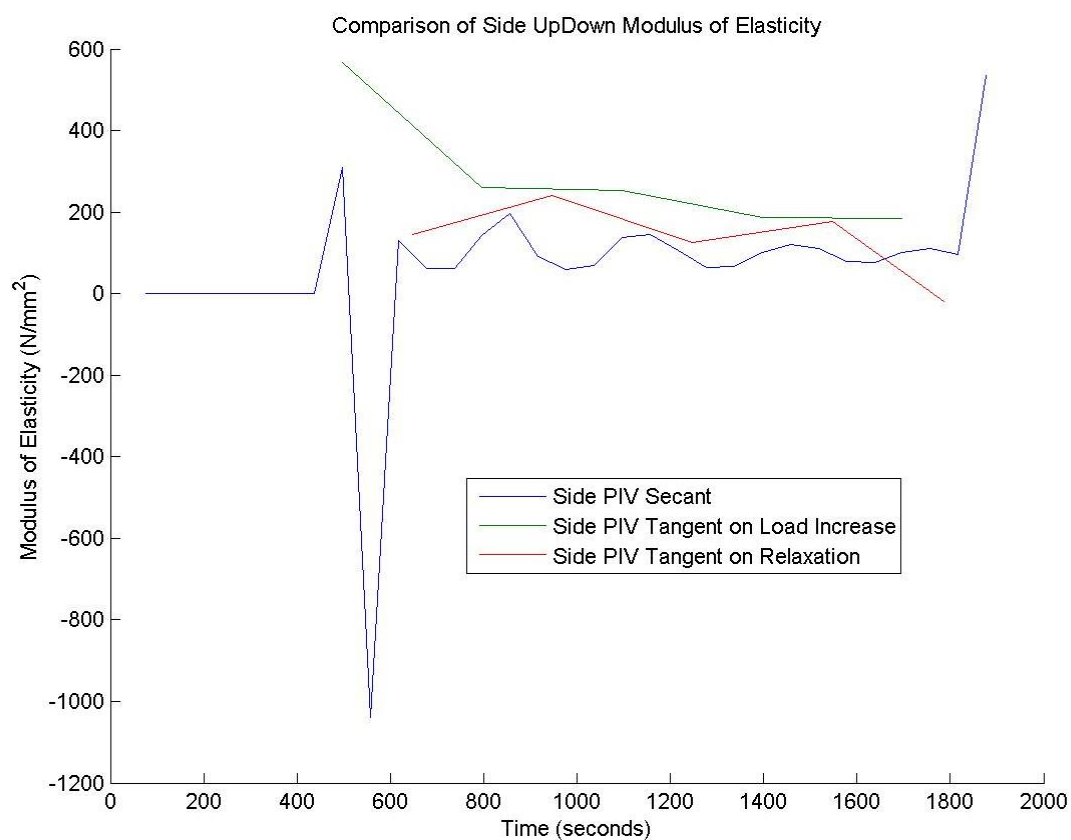
FIGURE 143: G3 SIDE VIEW PIV SECANT AND TANGENT MODULUS VS. TIME

Appendix 6
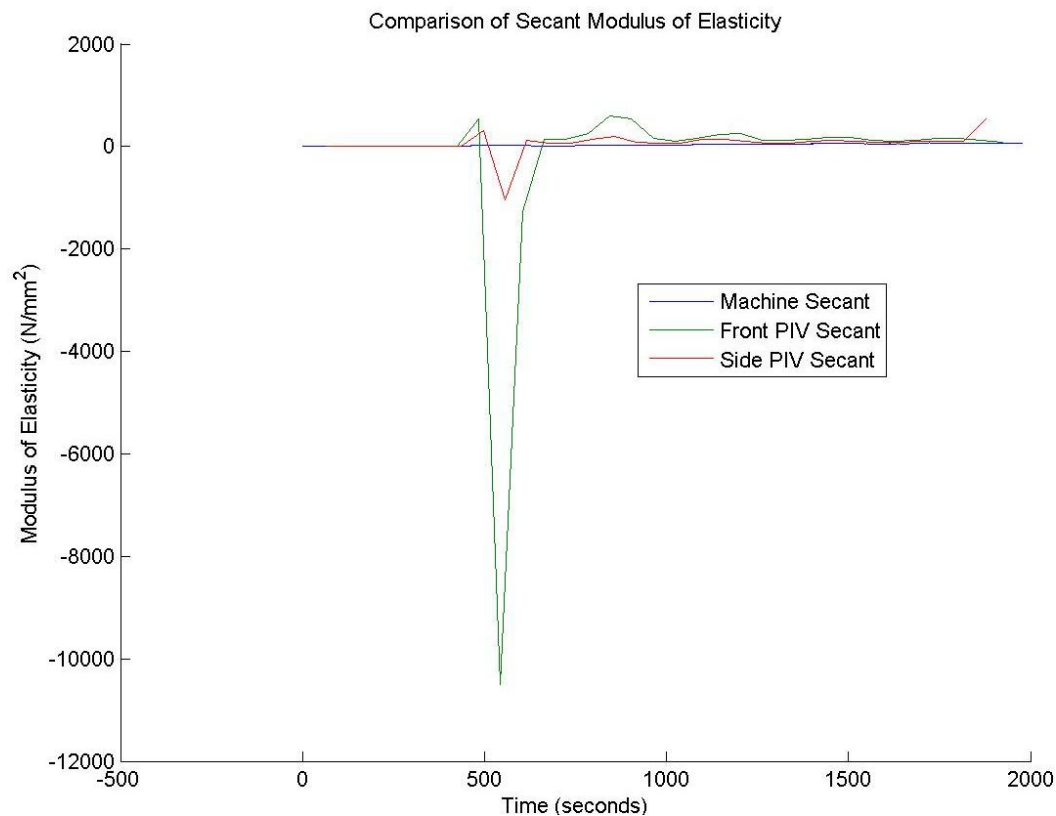
FIGURE 144: G3 COMPARISON OF MACHINE MEASURED AND PIV SECANT MODULUS VS. TIME
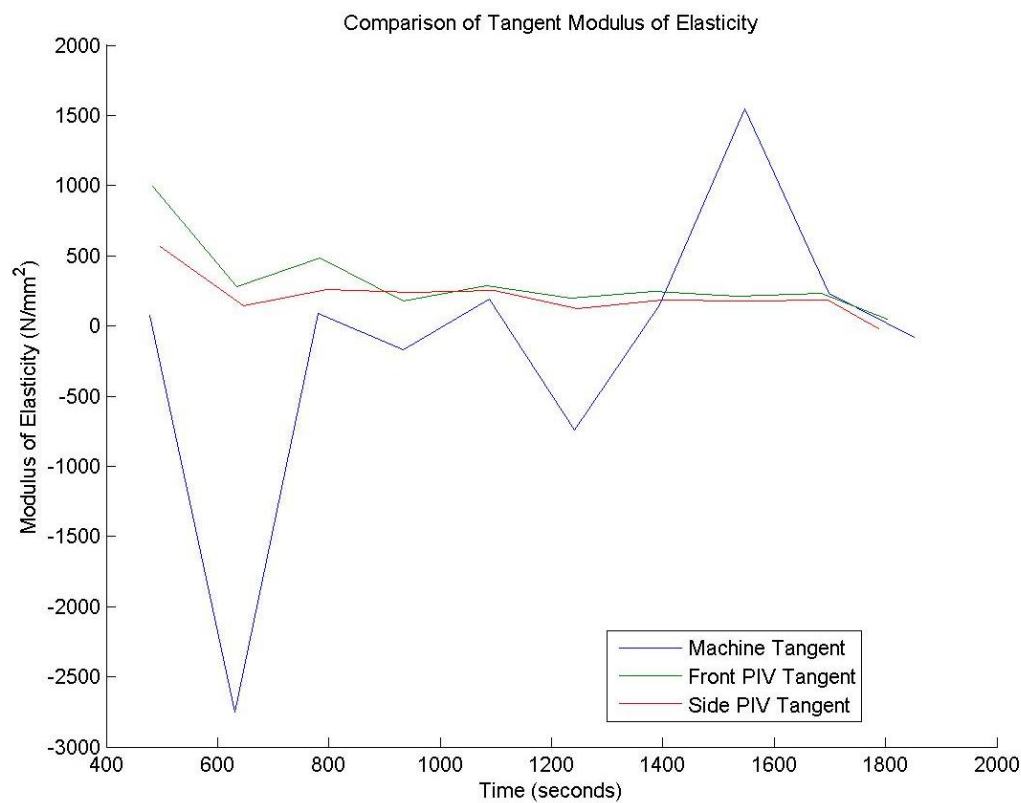
FIGURE 145: G3 COMPARISON OF MACHINE MEASURED AND PIV TANGENT MODULUS VS.

TIME

G3 Sample

F<small>IGURE</small> 146: SAMPLE GRAIN ORIENTATIONS OF THE FRONT (LEFT 4 IMAGES) AND SIDE (RIGHT 4 IMAGES) VIEW BEFORE (FIRST 2 OF 4 IMAGES) AND AFTER (LAST 2 OF 4 IMAGES) BREAKAGE

G3 Front View
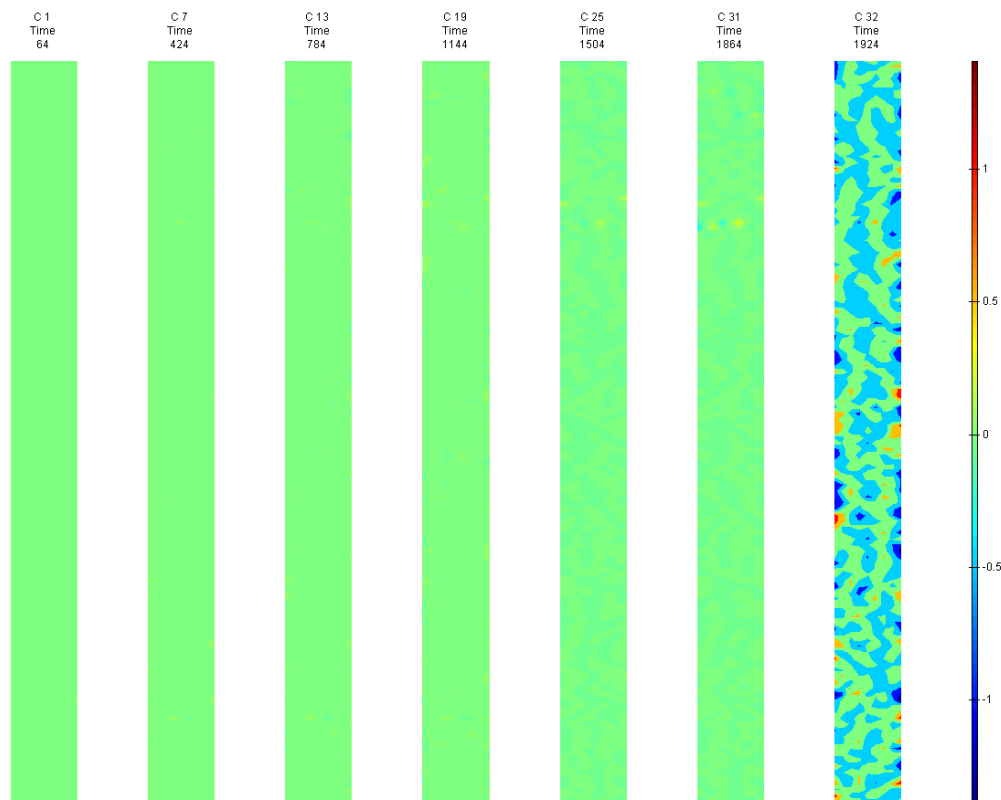
FIGURE 147: X DIRECTION PIV SEQUENTIAL ENGINEERING STRAIN OVER TIME
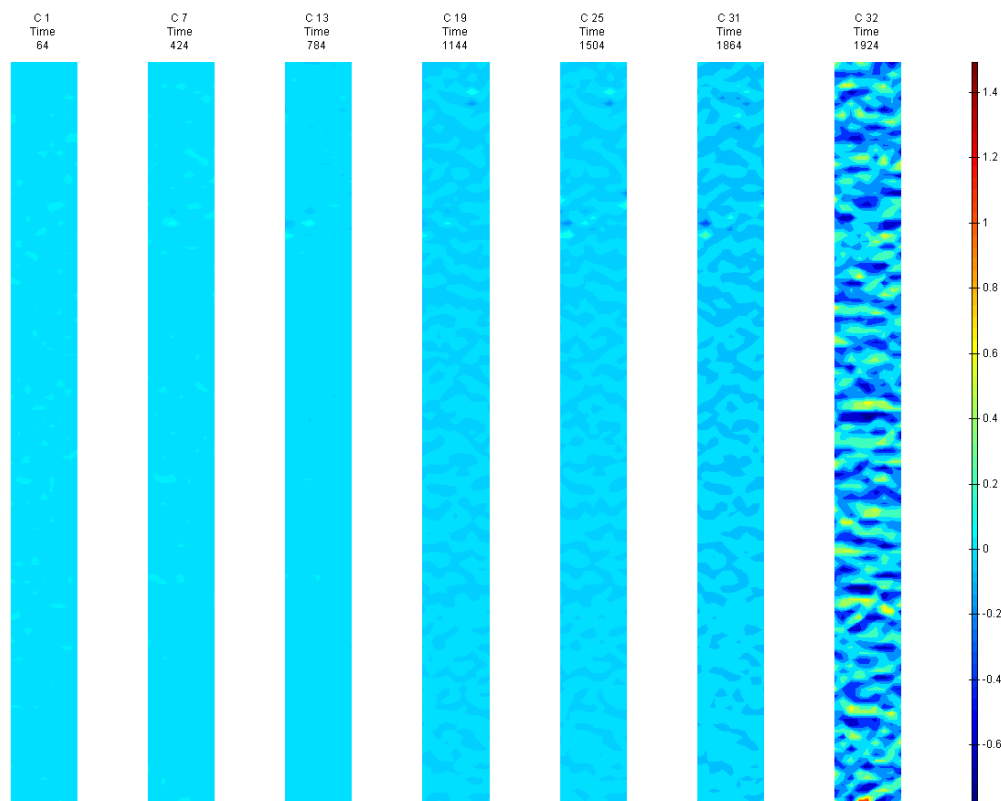
FIGURE 148: Y DIRECTION PIV SEQUENTIAL ENGINEERING STRAIN OVER TIME
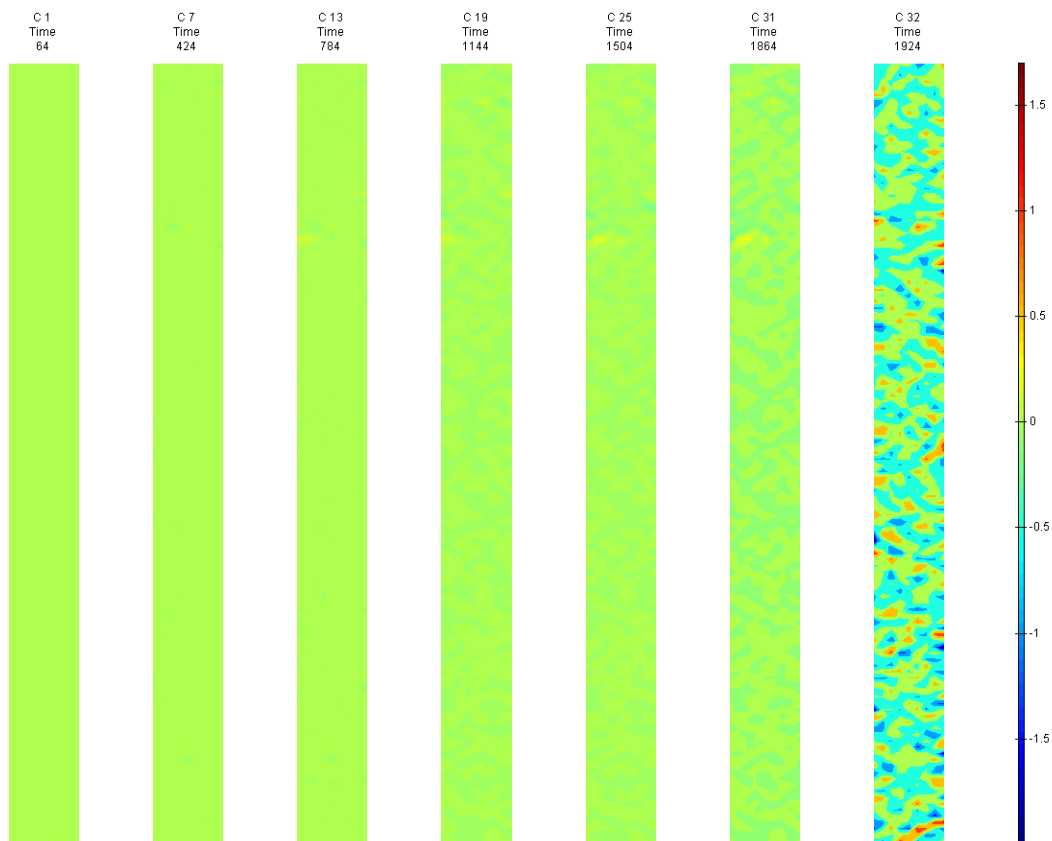
FIGURE 149: XY DIRECTION PIV SEQUENTIAL ENGINEERING SHEAR STRAIN OVER TIME
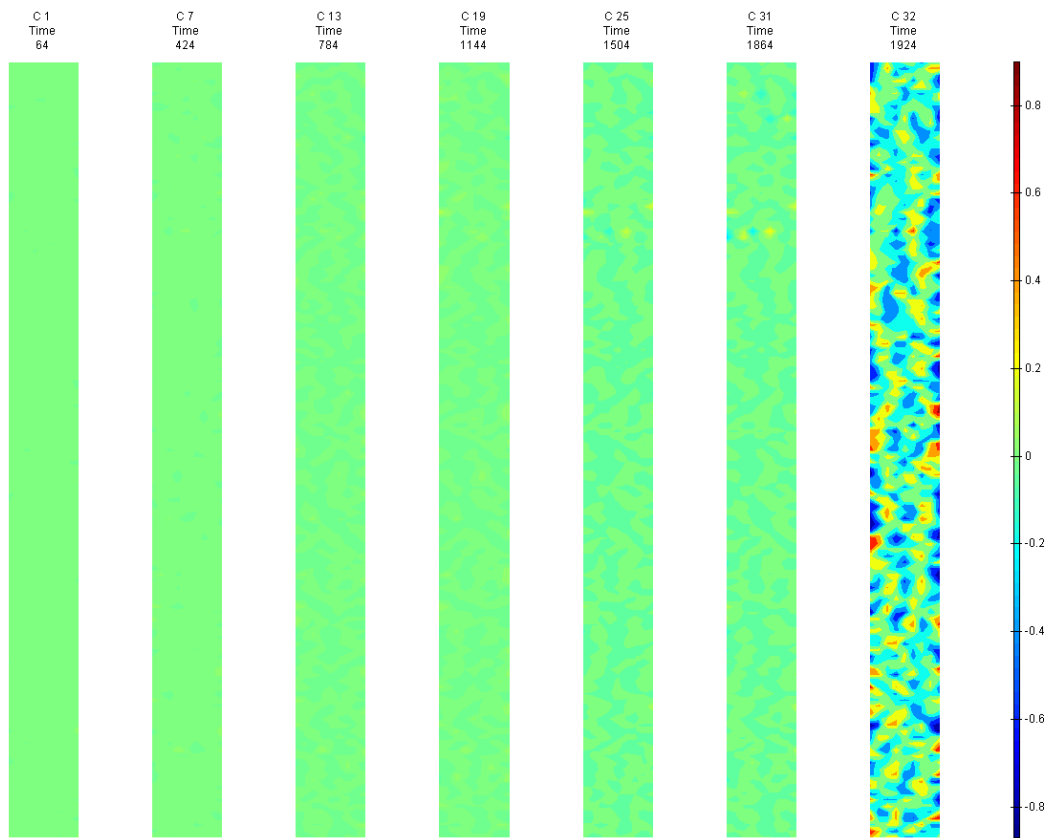
FIGURE 150: X DIRECTION PIV SEQUENTIAL TRUE STRAIN OVER TIME

Appendix 6
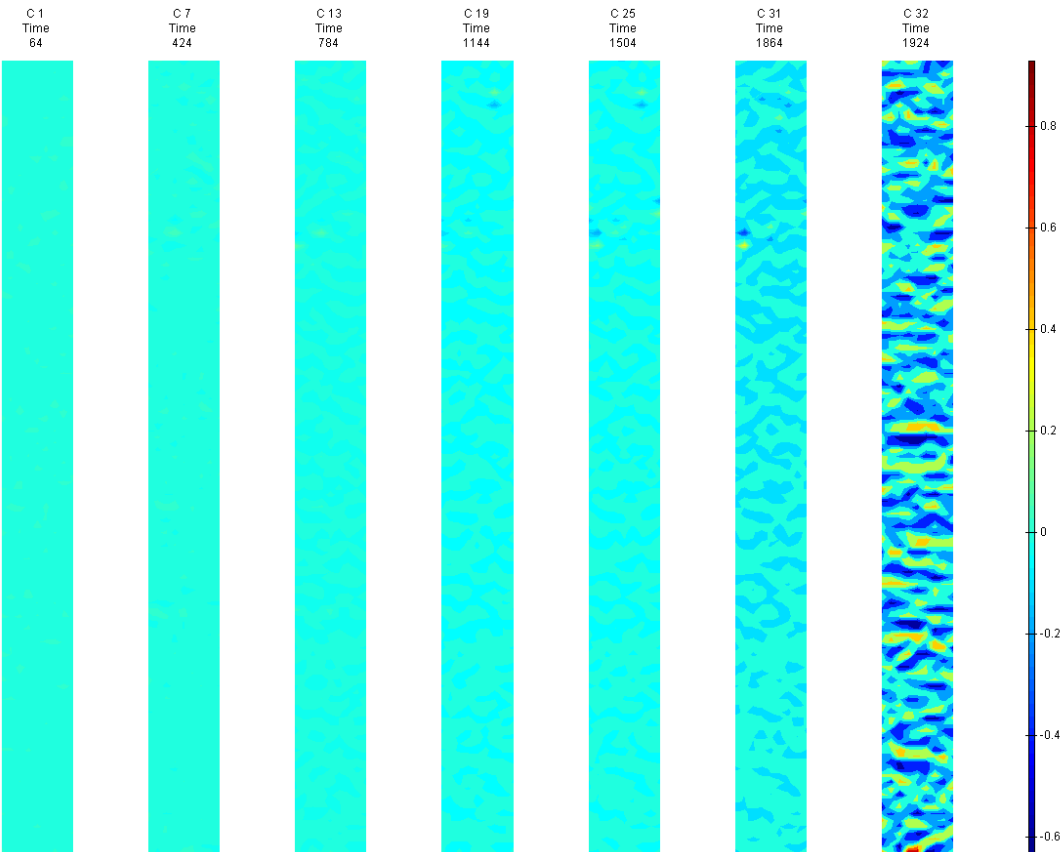
FIGURE 151: Y DIRECTION PIV SEQUENTIAL TRUE STRAIN OVER TIME
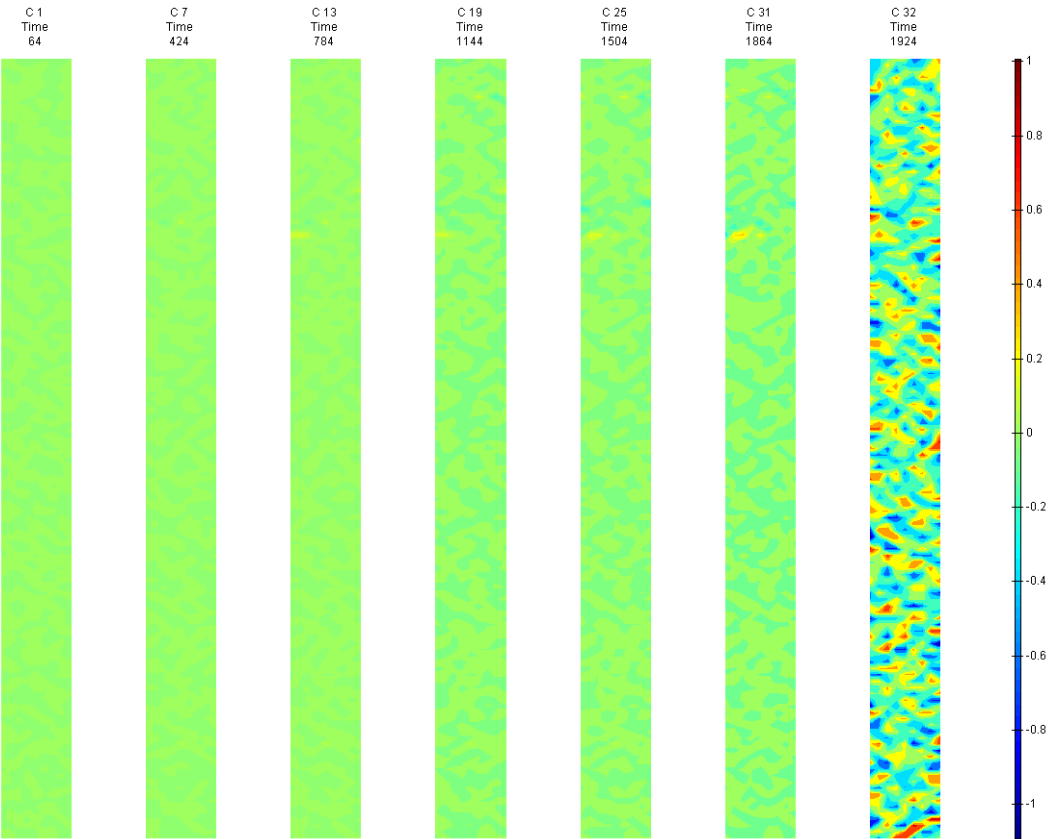
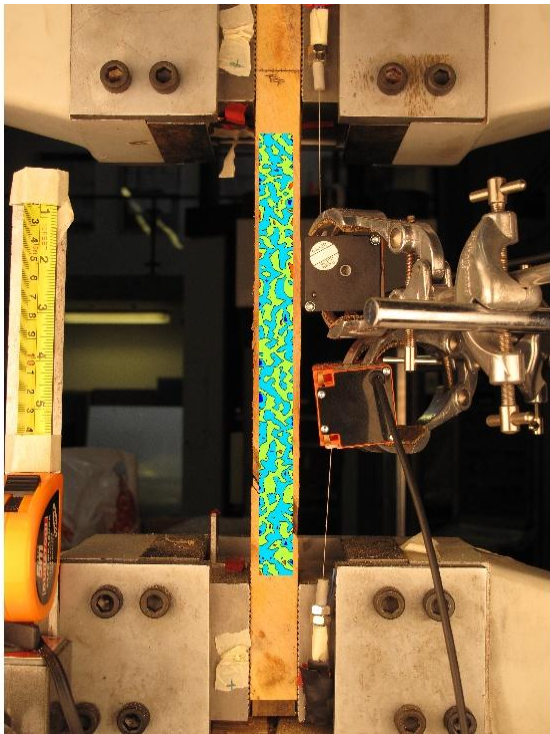FIGURE 152: XY DIRECTION PIV SEQUENTIAL TRUE SHEAR STRAIN OVER TIME
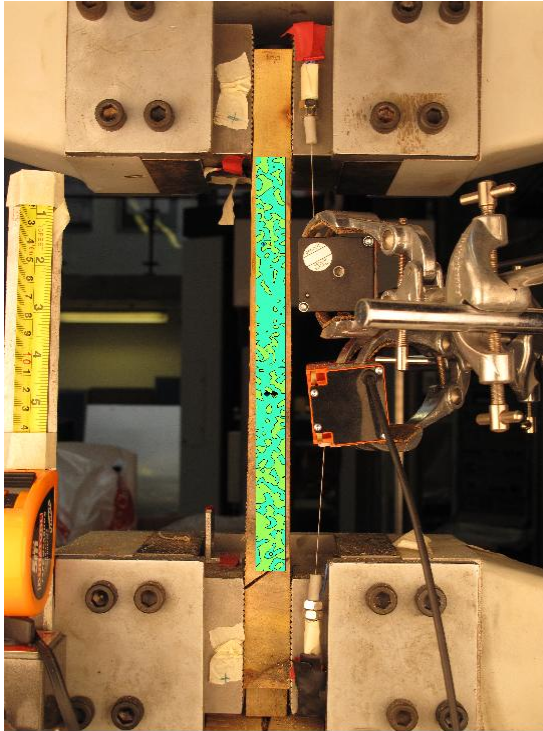
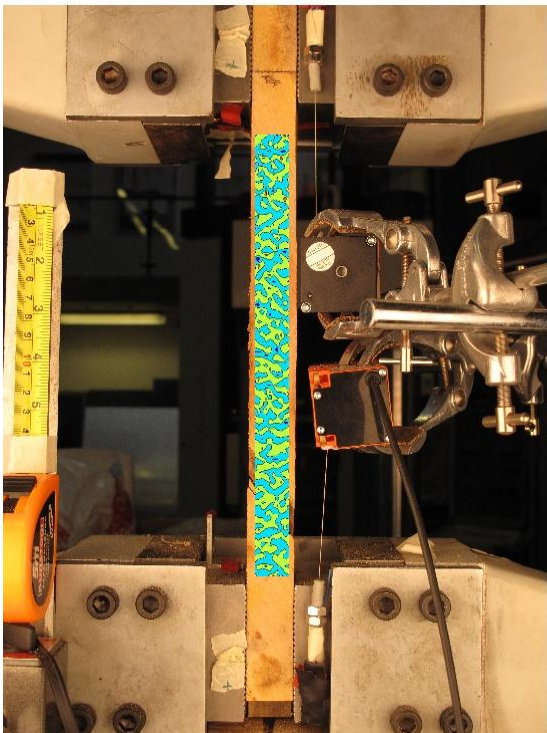FIGURE 153: X DIRECTION PIV FIRST–LAST DITCH ENGINEERING STRAIN OVER IMAGE
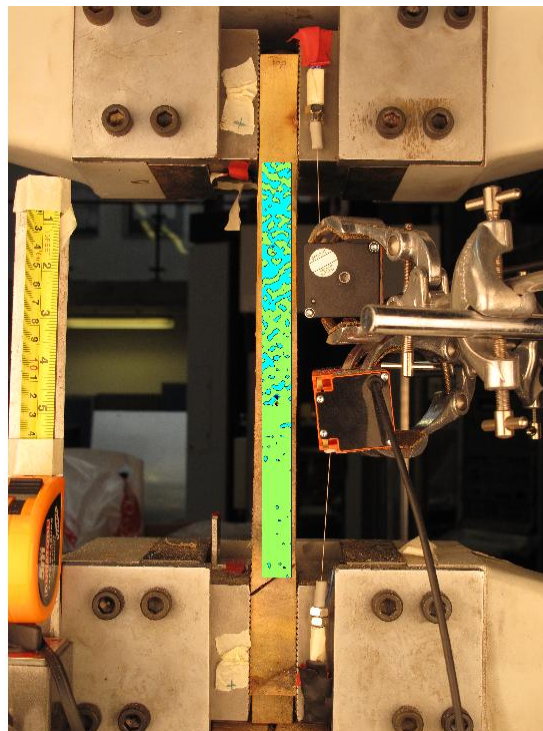
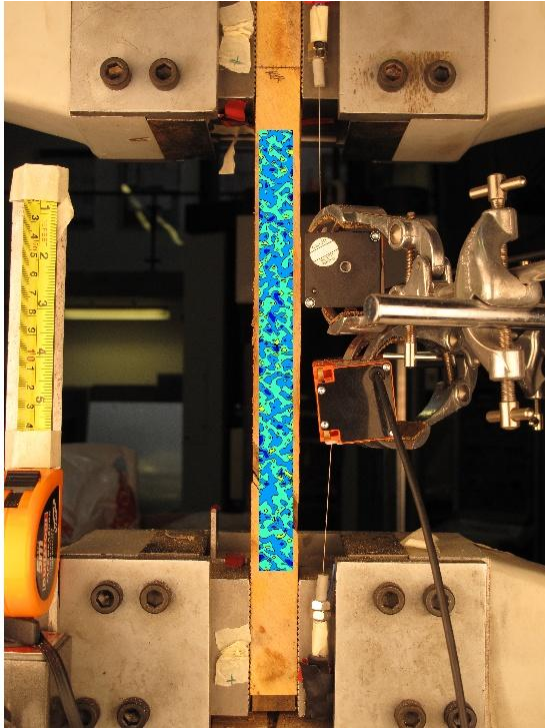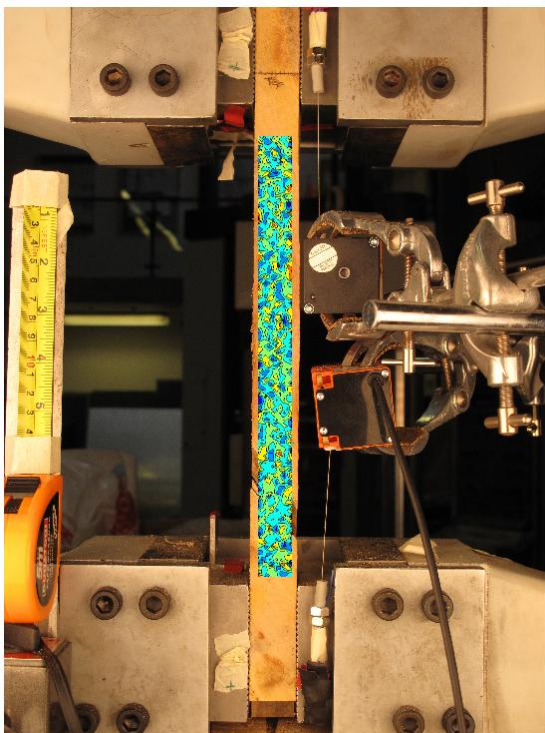FIGURE 154: Y DIRECTION PIV FIRST–LAST DITCH ENGINEERING STRAIN OVER IMAGE

Appendix 6
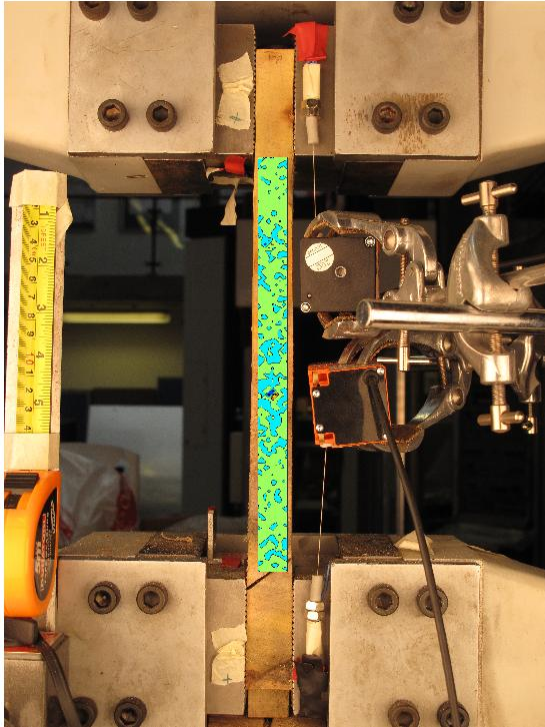
FIGURE 155: XY DIRECTION PIV FIRST–LAST DITCH ENGINEERING SHEAR STRAIN OVER
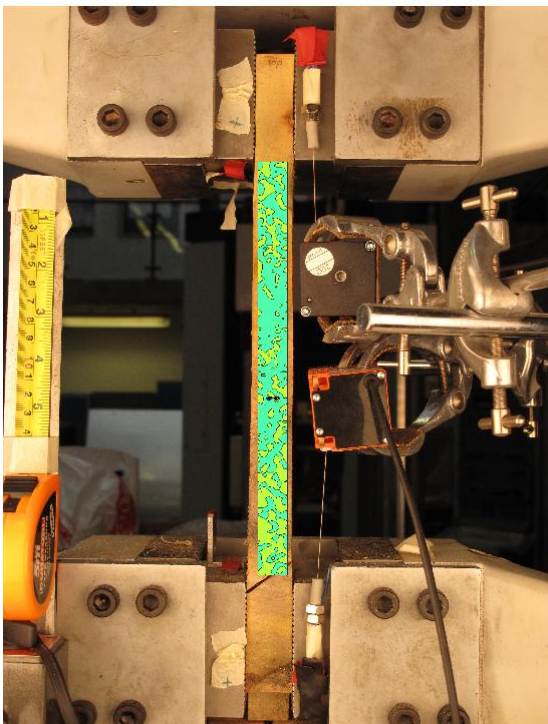
IMAGE

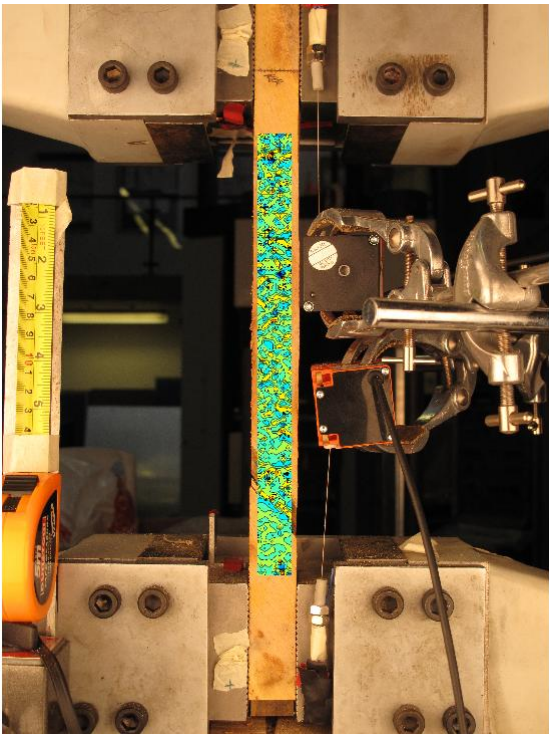FIGURE 156: X DIRECTION PIV FIRST–LAST DITCH TRUE STRAIN OVER IMAGE
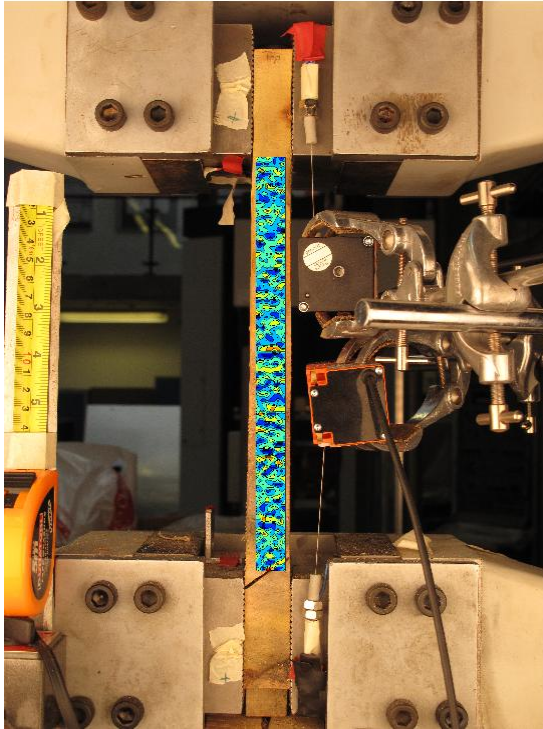
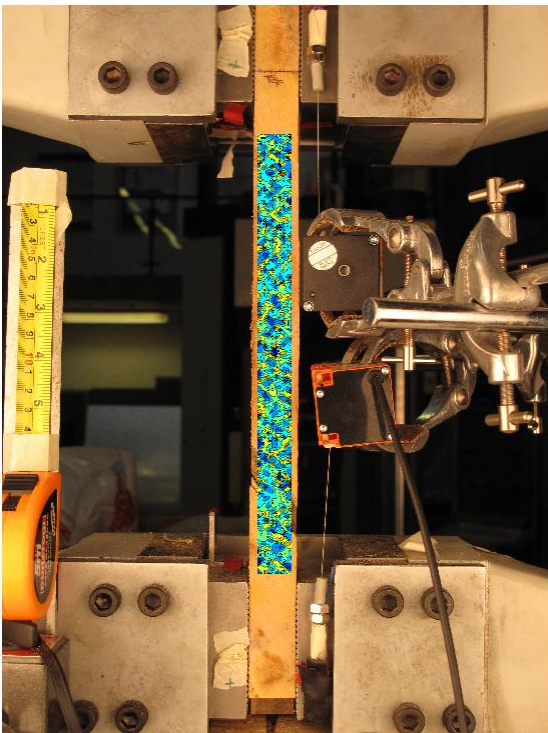FIGURE 157: Y DIRECTION PIV FIRST–LAST DITCH TRUE STRAIN OVER IMAGE
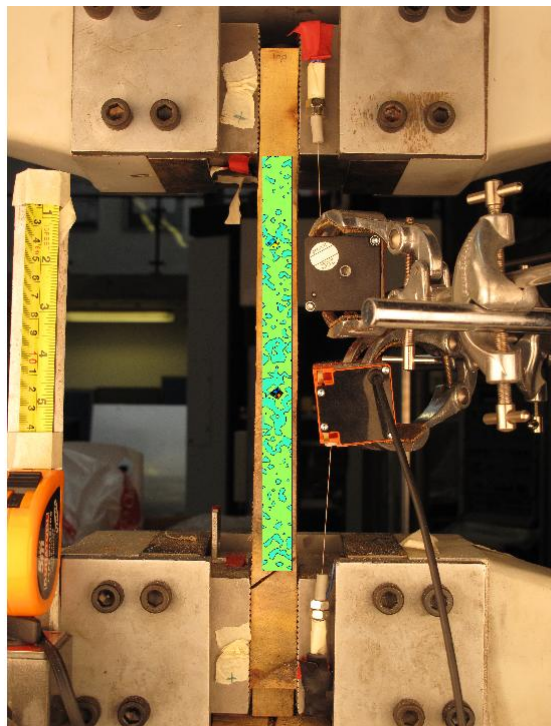
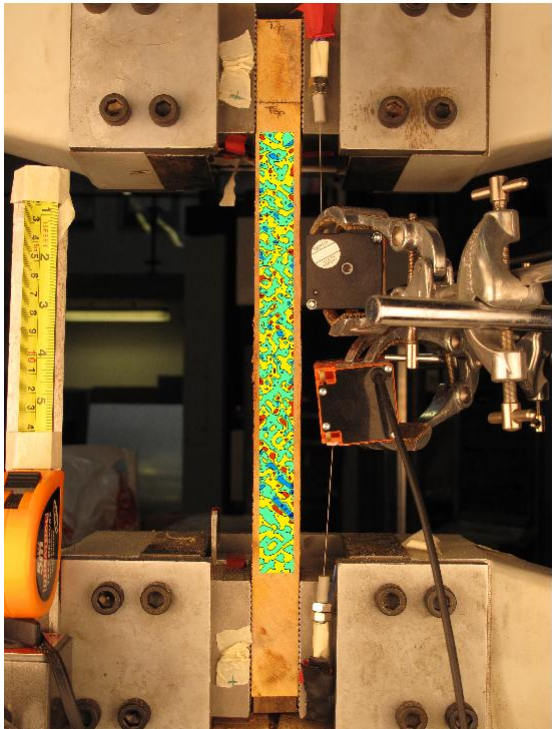FIGURE 158: XY DIRECTION PIV FIRST–LAST DITCH TRUE SHEAR STRAIN OVER IMAGE
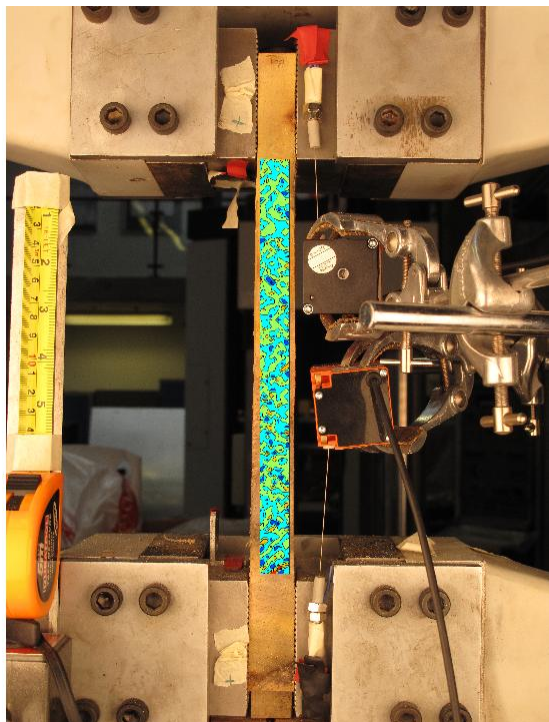
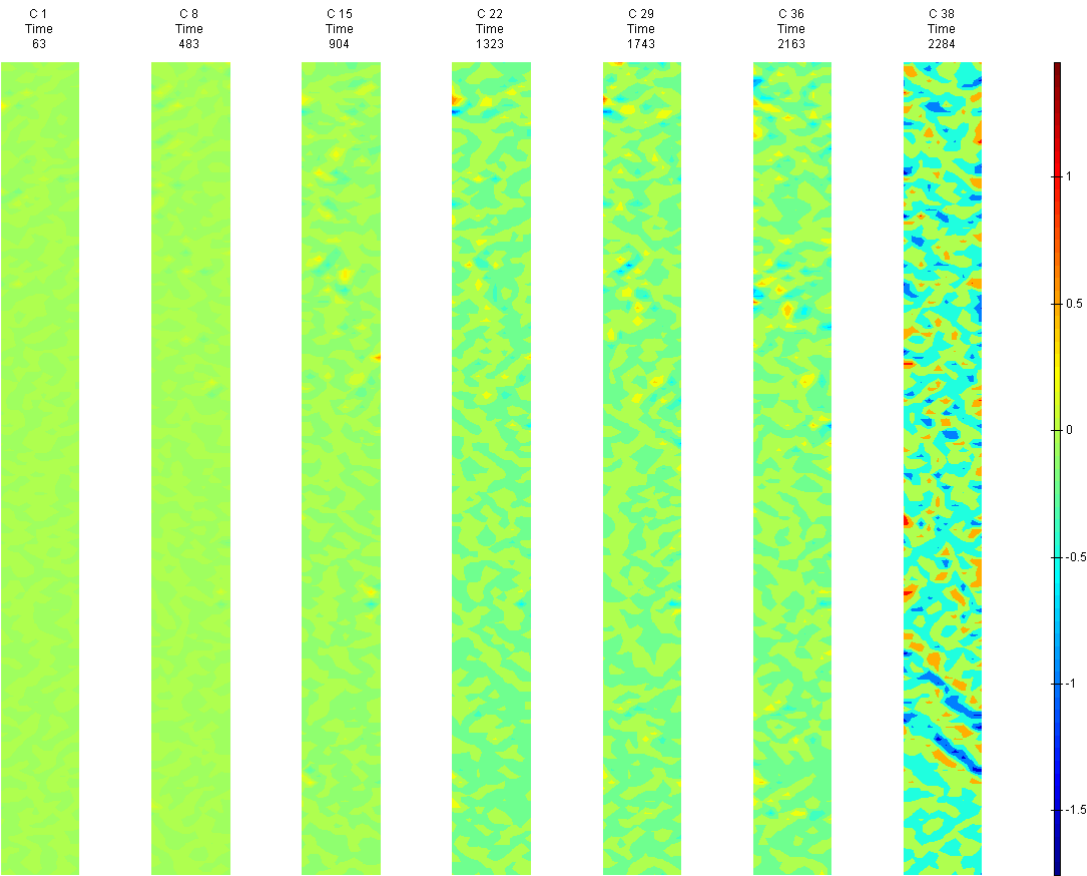FIGURE 159: XY DIRECTION PIV FIRST-SEQUENTIAL ENGINEERING SHEAR STRAIN OVER

IMAGE
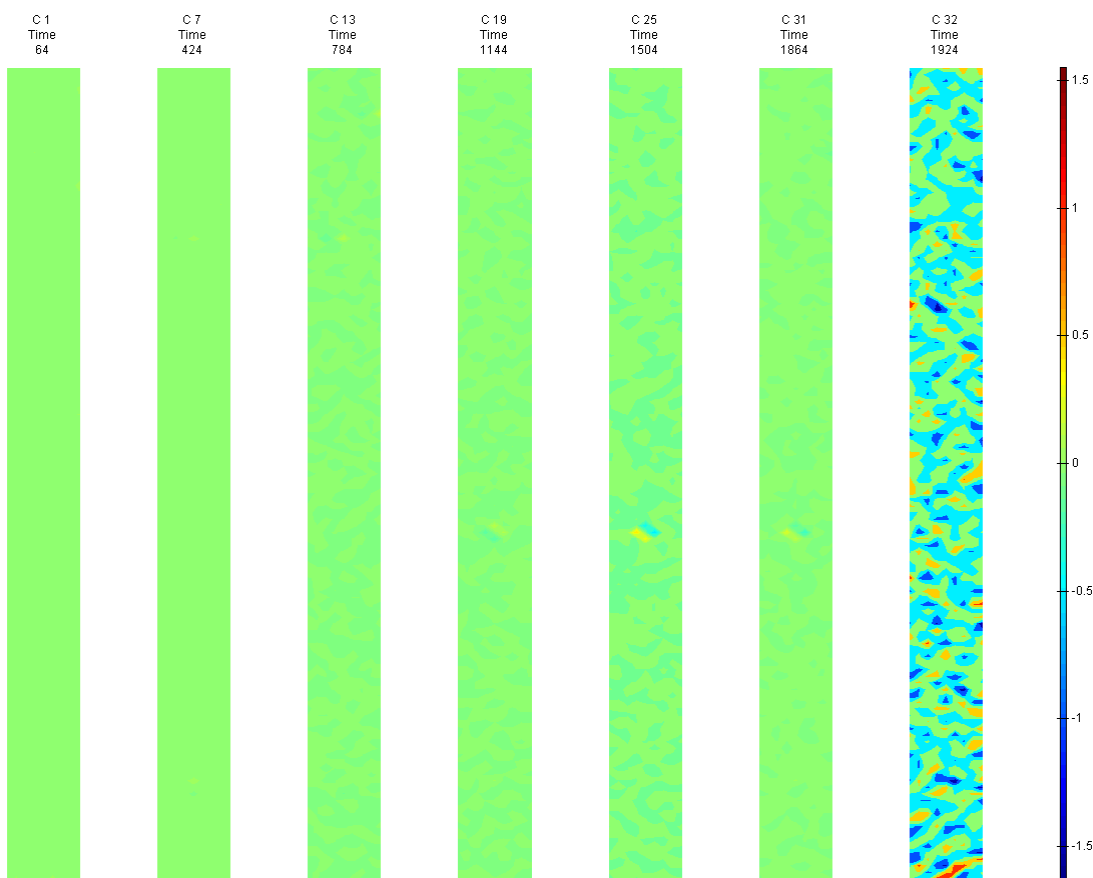
FIGURE 160: XY DIRECTION PIV FIRST-SEQUENTIAL ENGINEERING SHEAR STRAIN OVER TIME
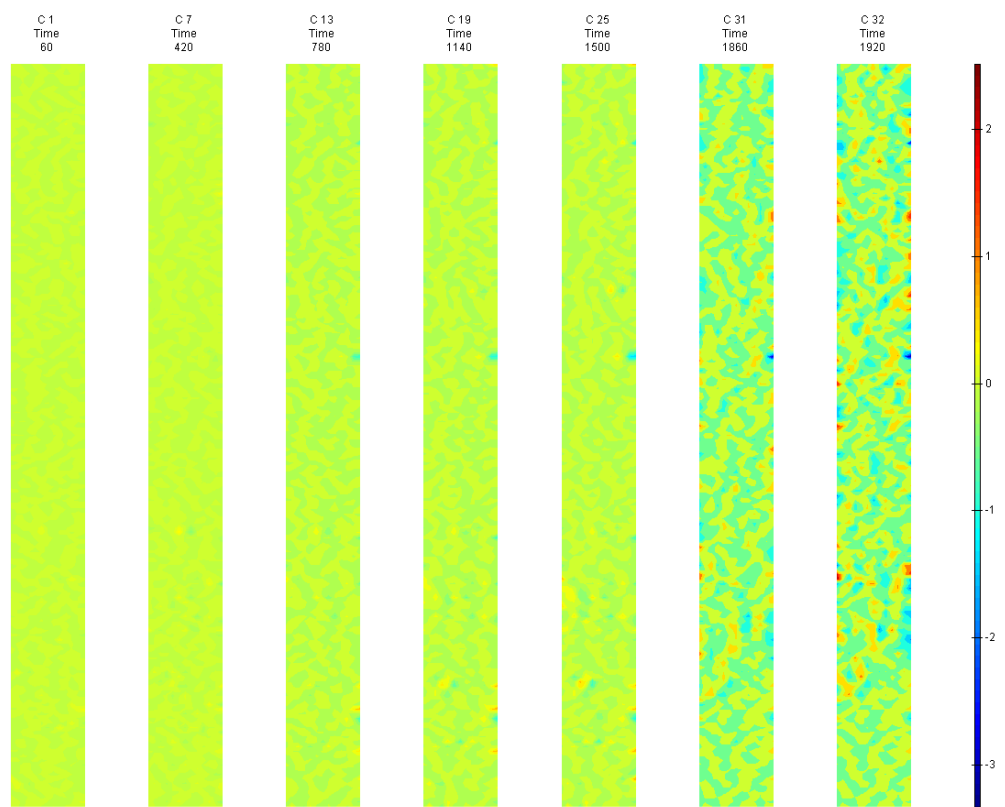
G3 Side View
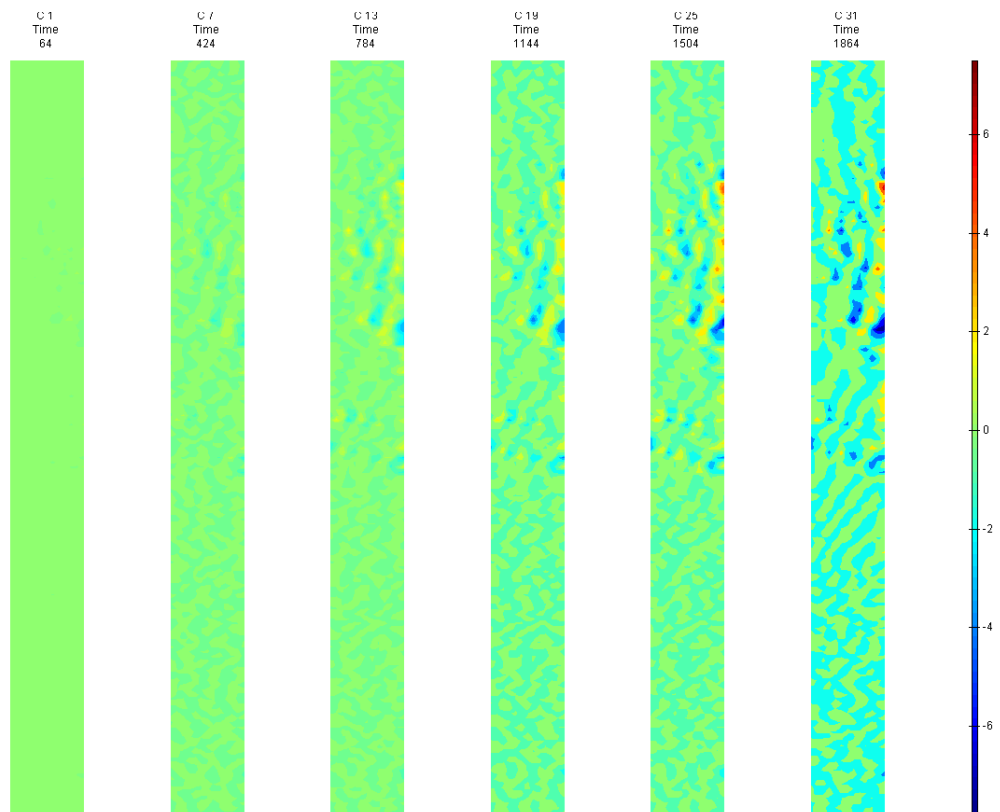
FIGURE 161: X DIRECTION PIV SEQUENTIAL ENGINEERING STRAIN OVER TIME
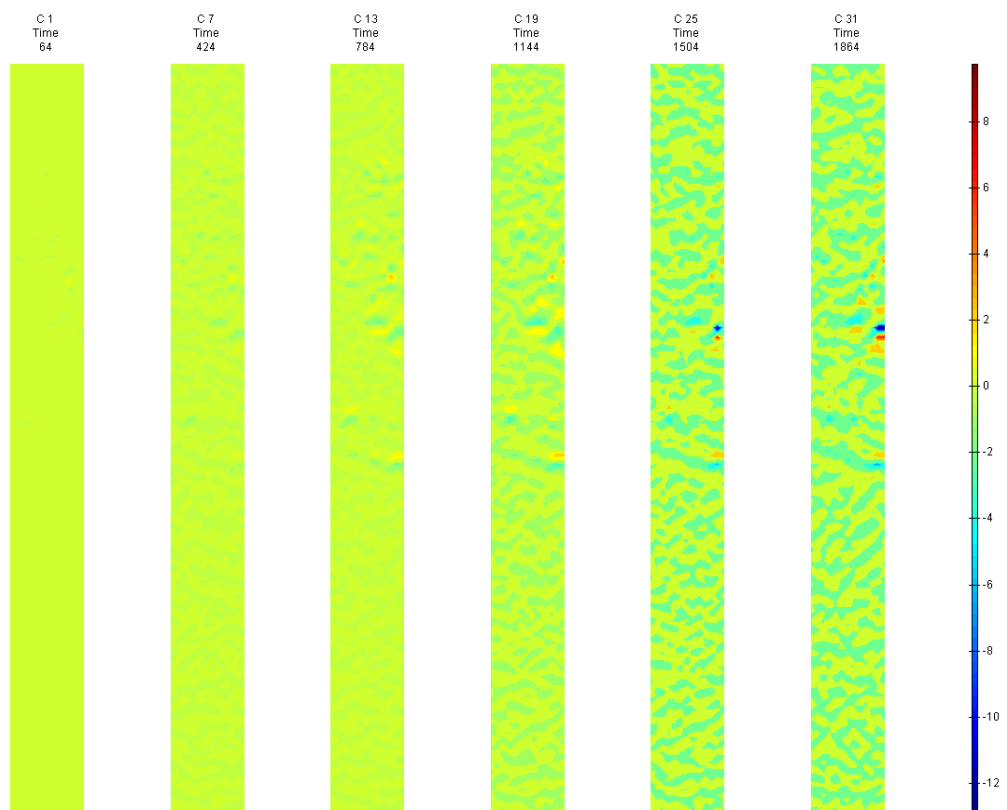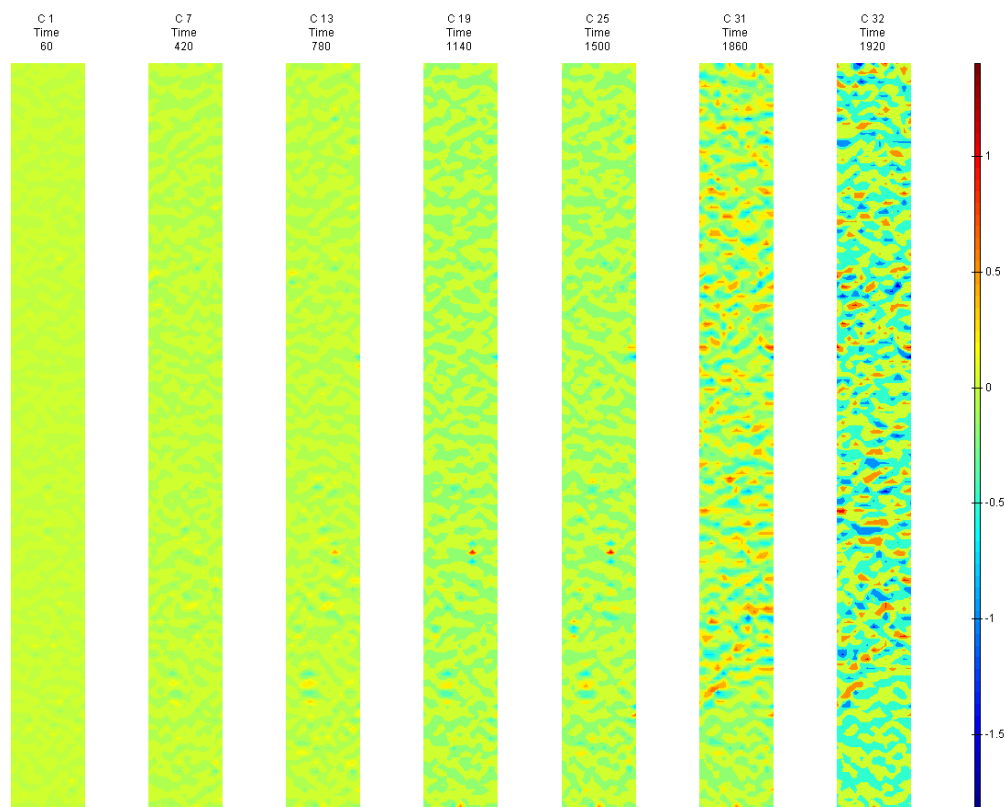

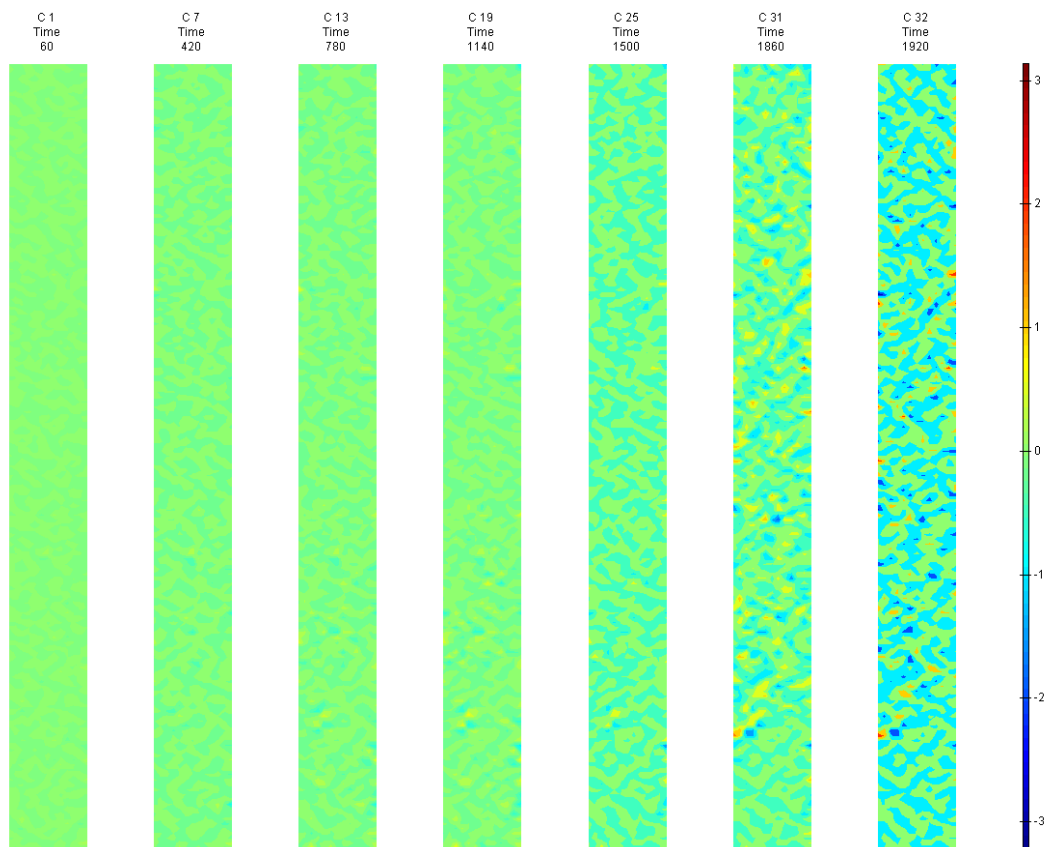FIGURE 162: Y DIRECTION PIV SEQUENTIAL ENGINEERING STRAIN OVER TIME

Appendix 6
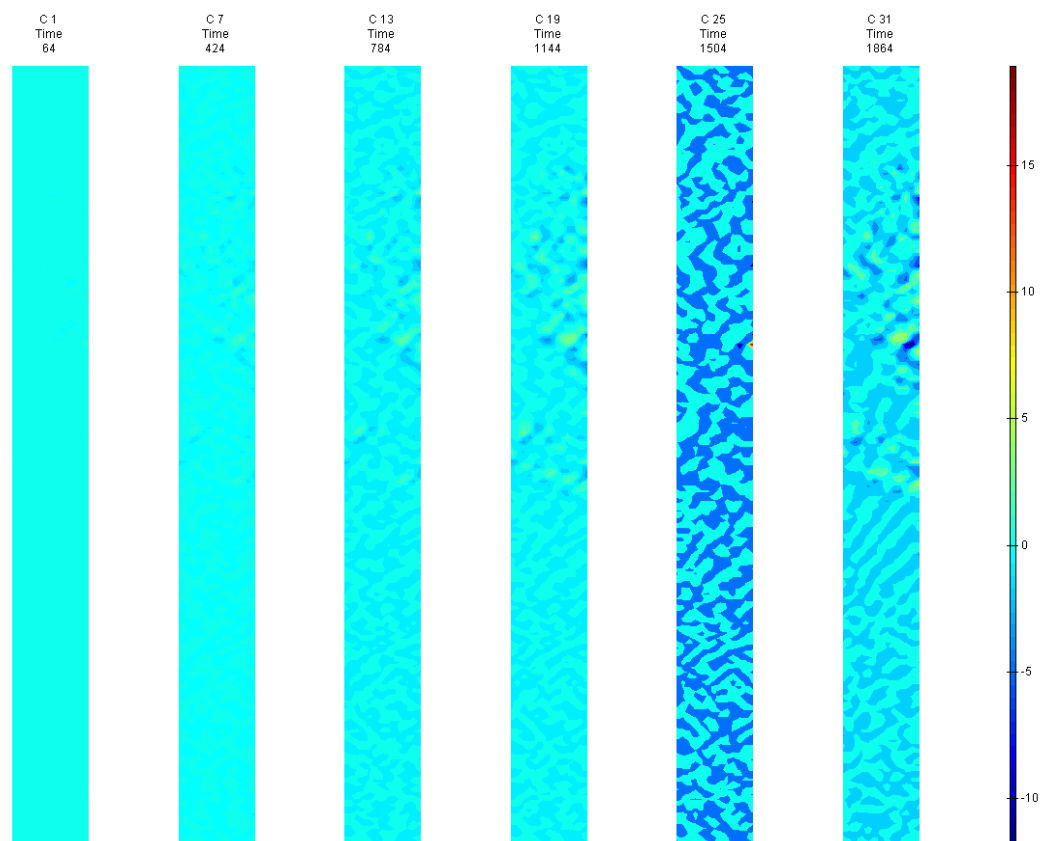
FIGURE 163: XY DIRECTION PIV SEQUENTIAL ENGINEERING SHEAR STRAIN OVER TIME
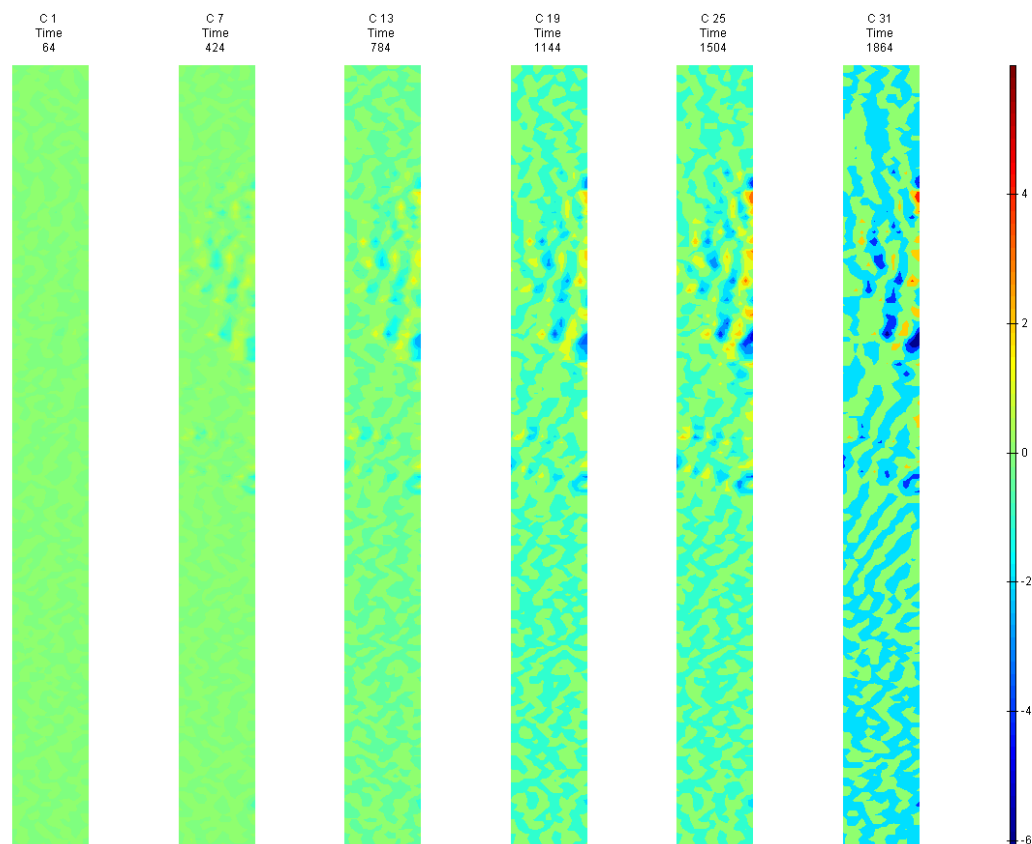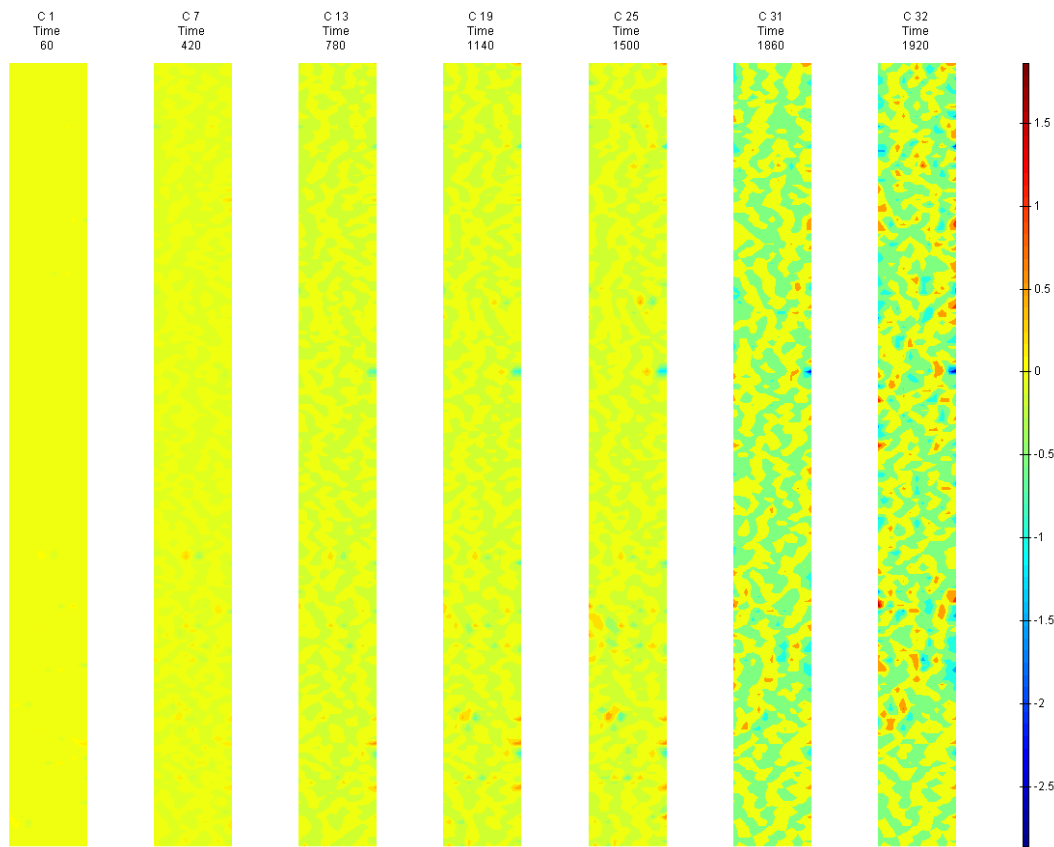

FIGURE 164: X DIRECTION PIV SEQUENTIAL TRUE STRAIN OVER TIME
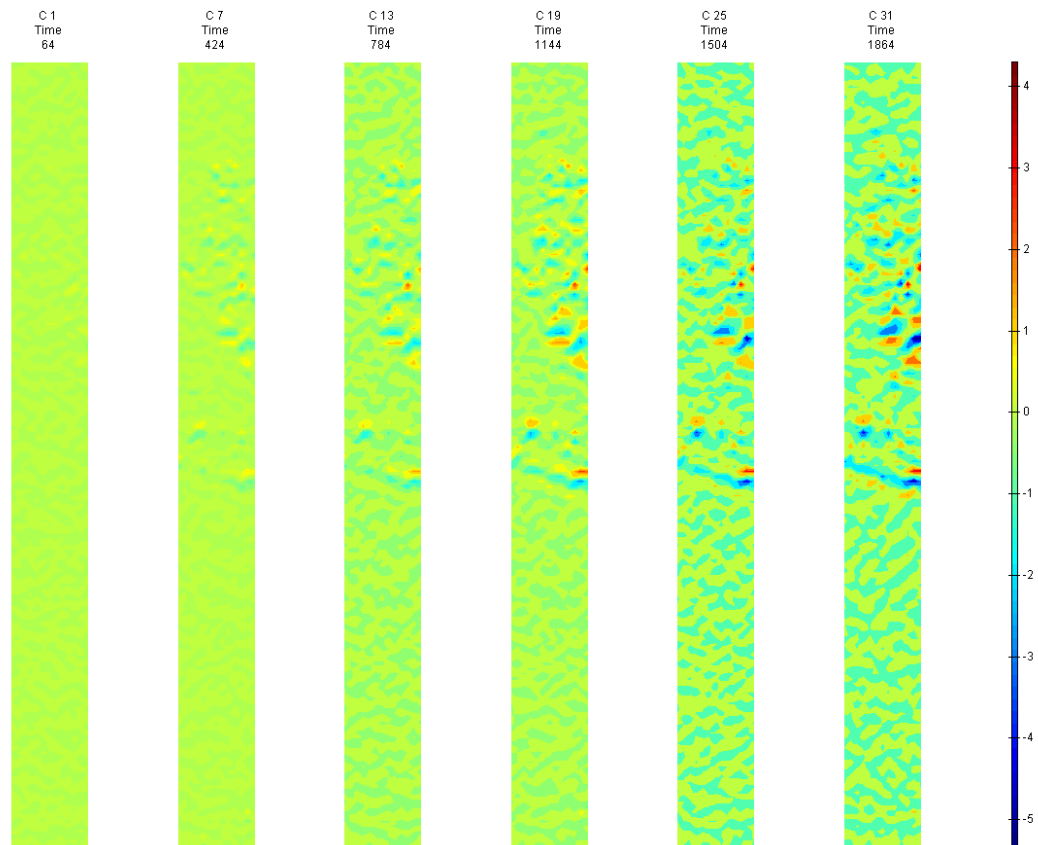
FIGURE 165: Y DIRECTION PIV SEQUENTIAL TRUE STRAIN OVER TIME
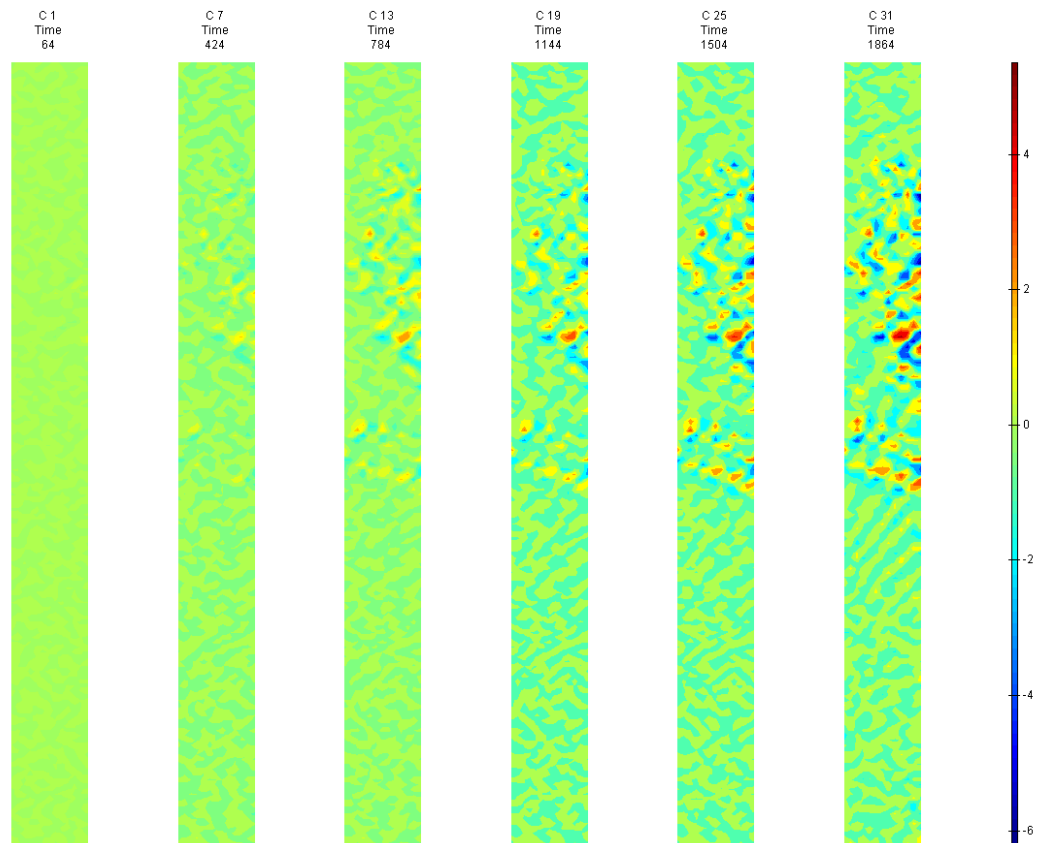
FIGURE 166: XY DIRECTION PIV SEQUENTIAL TRUE SHEAR STRAIN OVER TIME

Appendix 6
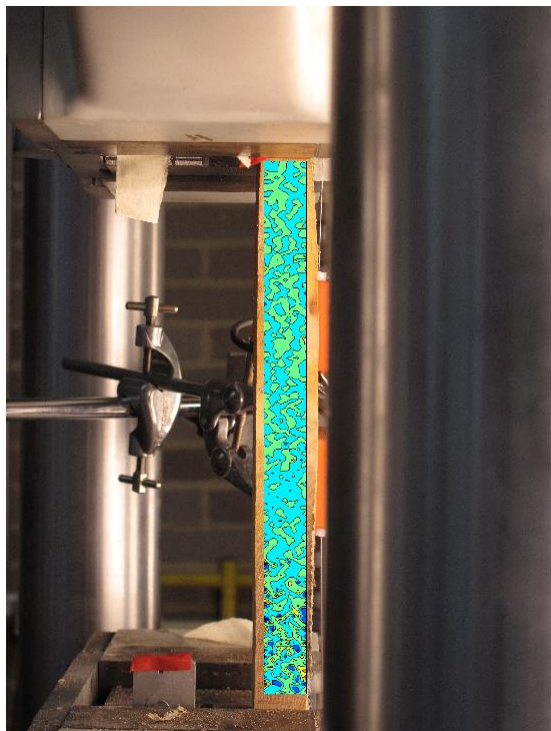
FIGURE 167: X DIRECTION PIV FIRST–LAST DITCH ENGINEERING STRAIN OVER IMAGE
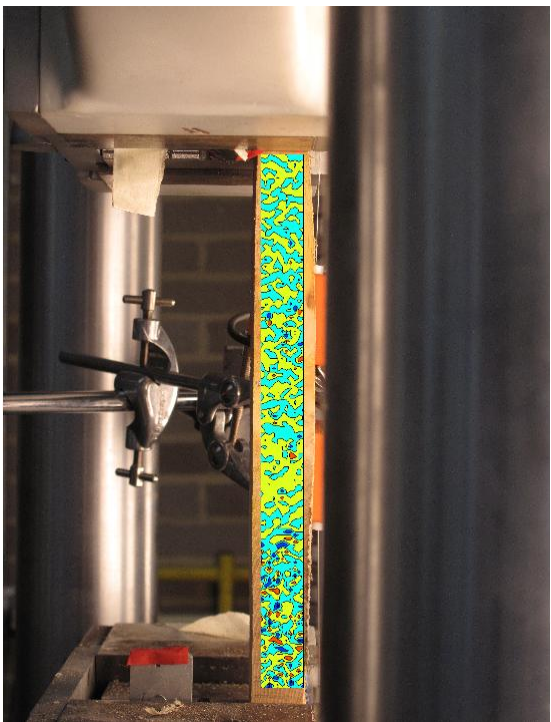
FIGURE 168: Y DIRECTION PIV FIRST–LAST DITCH ENGINEERING STRAIN OVER IMAGE
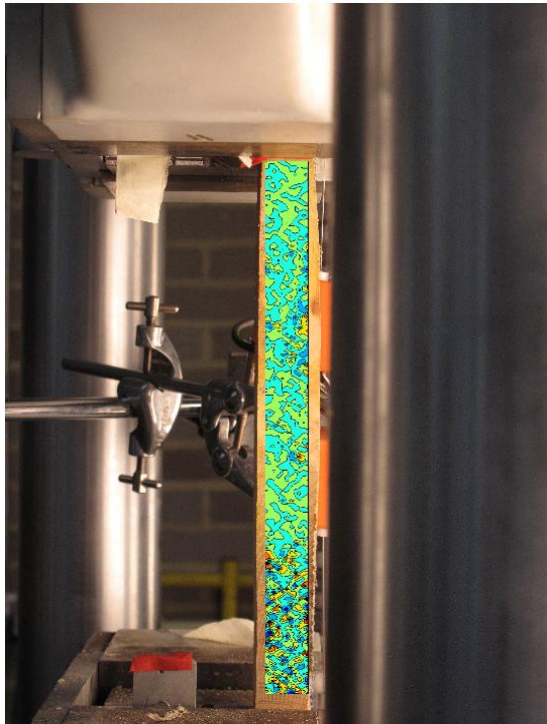
FIGURE 169: XY DIRECTION PIV FIRST–LAST DITCH ENGINEERING SHEAR STRAIN OVER
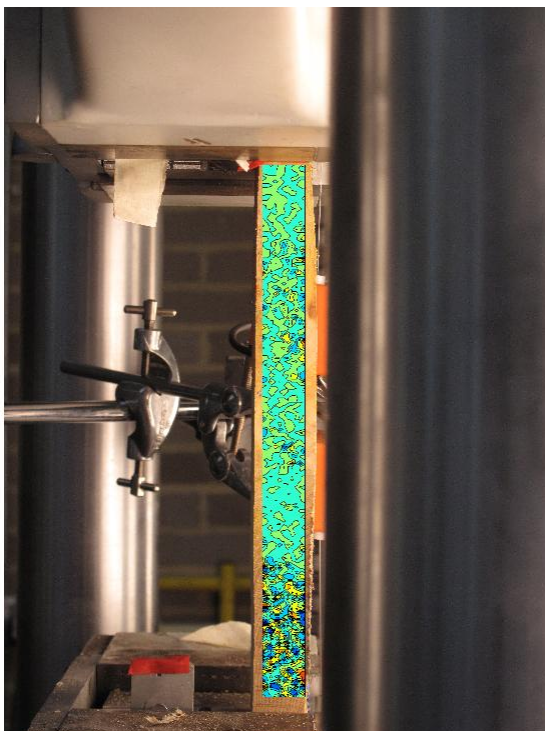
IMAGE

FIGURE 170: X DIRECTION PIV FIRST–LAST DITCH TRUE STRAIN OVER IMAGE

Appendix 6
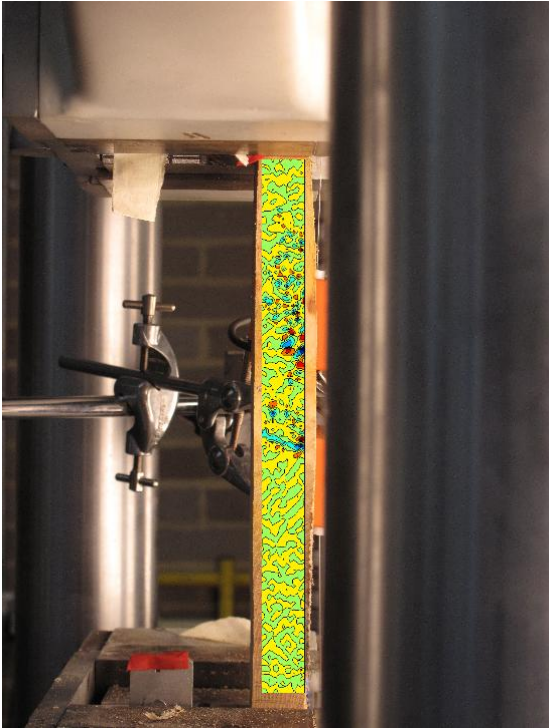
FIGURE 171: Y DIRECTION PIV FIRST–LAST DITCH TRUE STRAIN OVER IMAGE
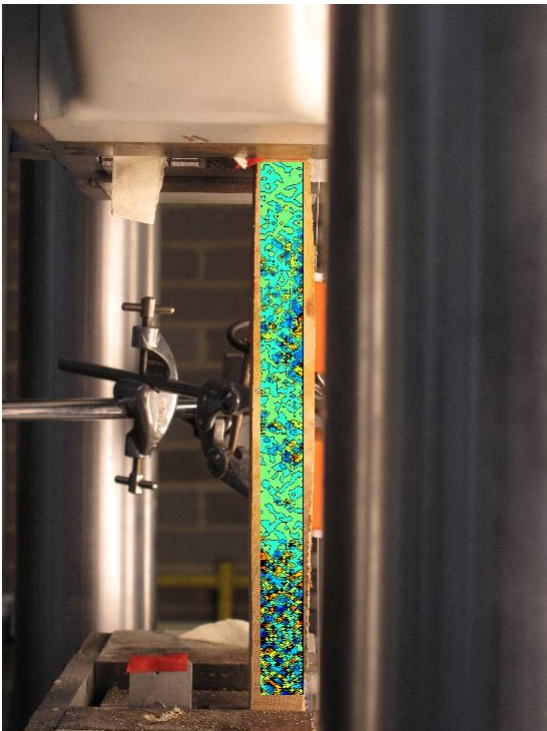
FIGURE 172: XY DIRECTION PIV FIRST–LAST DITCH TRUE SHEAR STRAIN OVER IMAGE
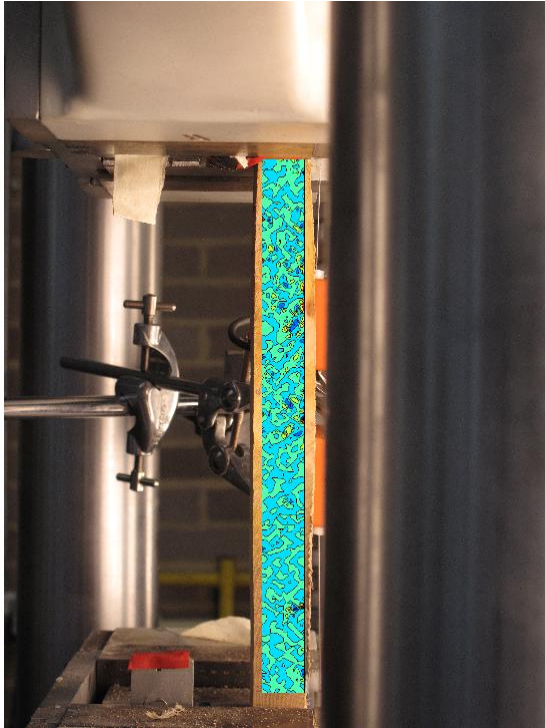
FIGURE 173: XY DIRECTION PIV FIRST–SEQUENTIAL ENGINEERING SHEAR STRAIN OVER

IMAGE
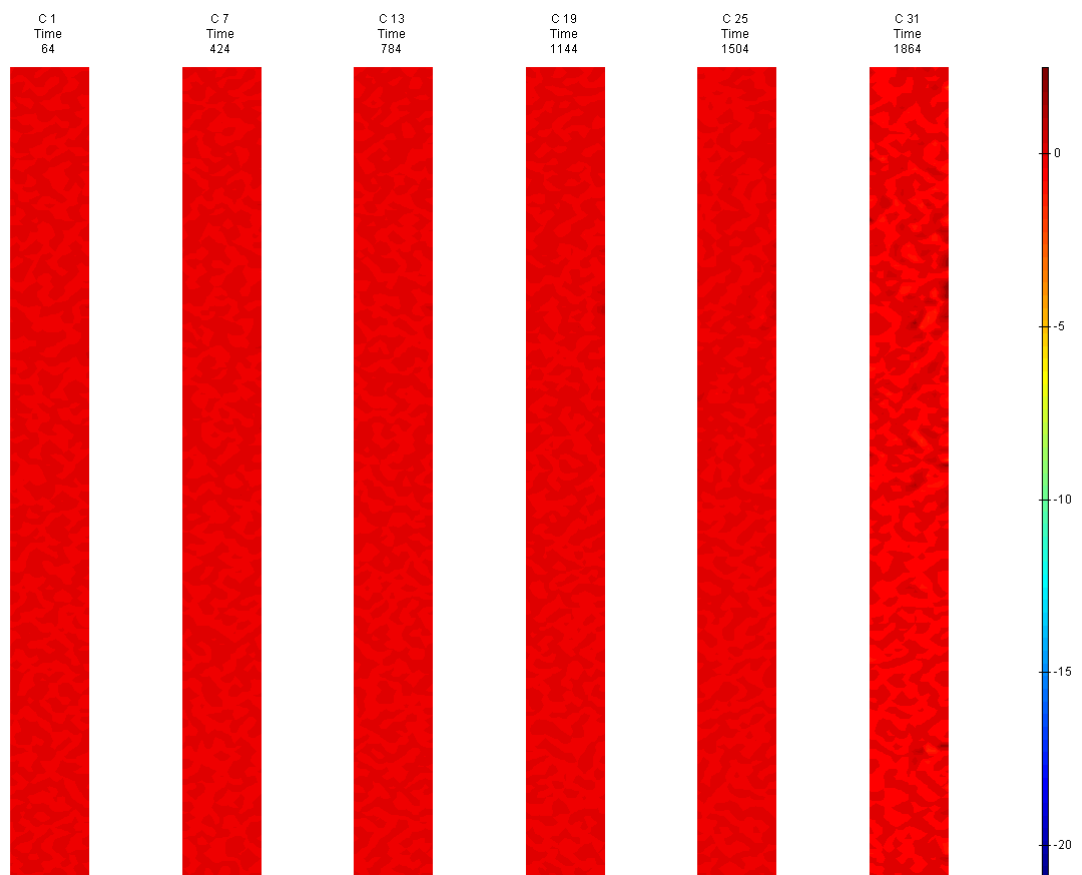
FIGURE 174: XY DIRECTION PIV FIRST–SEQUENTIAL ENGINEERING SHEAR STRAIN OVER TIME

G4
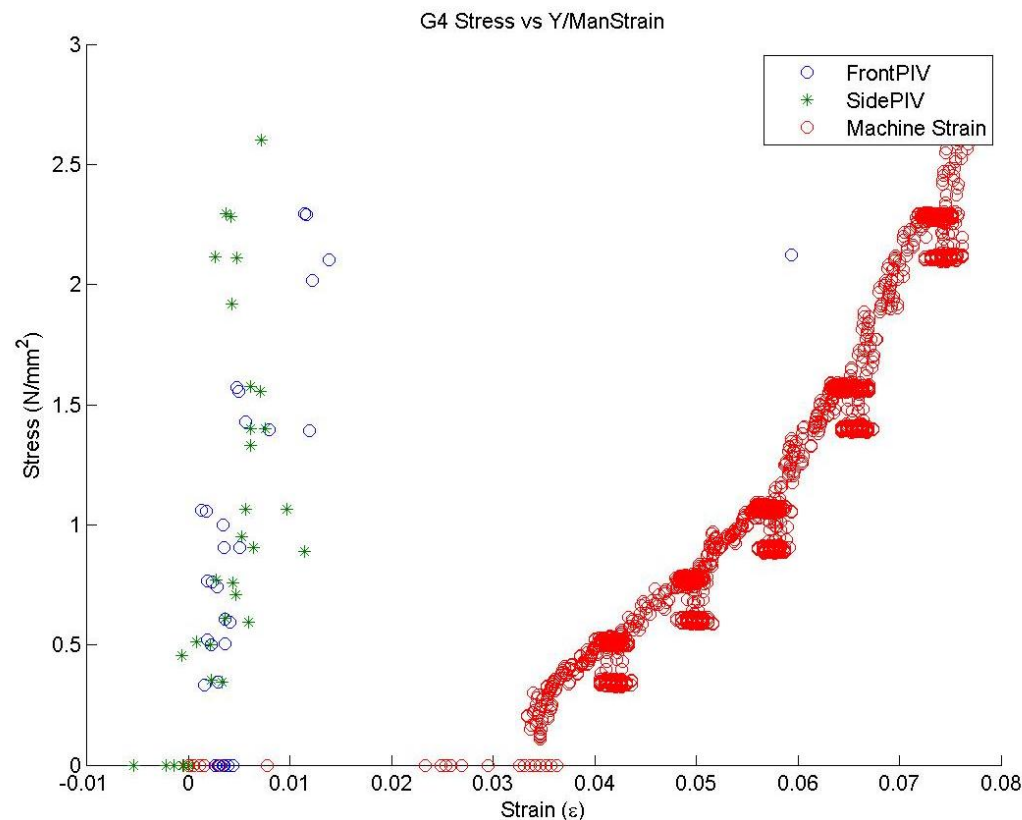
FIGURE 175: G4 TENSILE STRESS VS. MACHINE MEASURED/PIV STRAINS
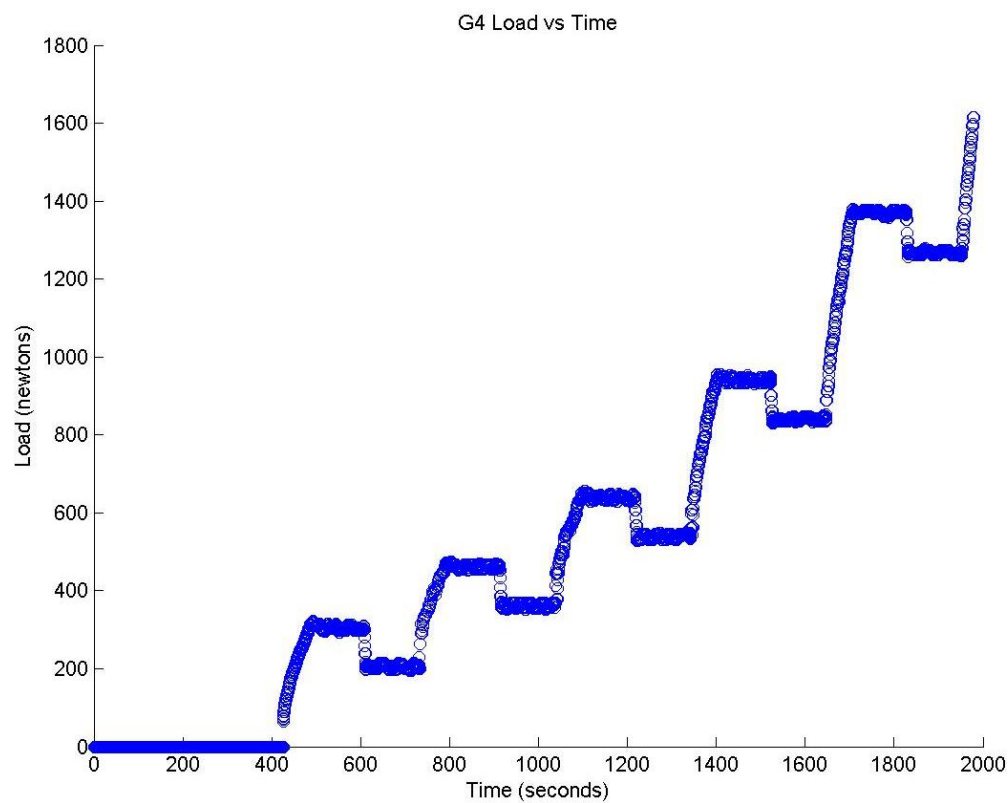
FIGURE 176: G4 TENSILE LOAD VS. TIME
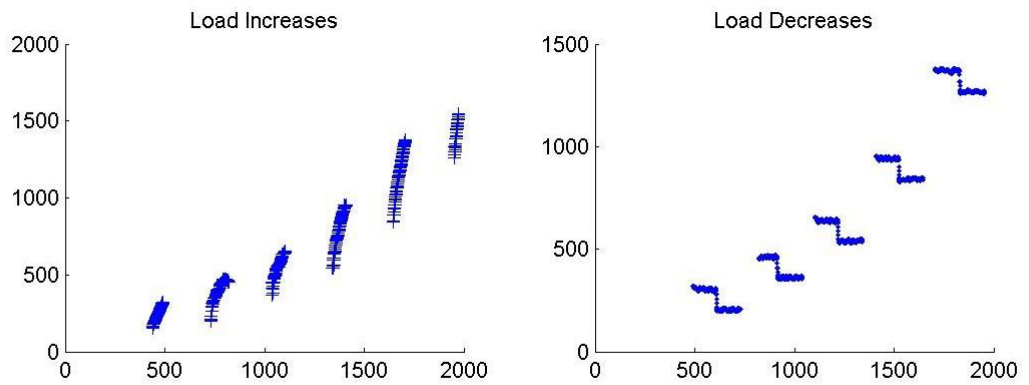
FIGURE 177: G4 CREEP LOADING: INCREMENTS AND RELAXATION
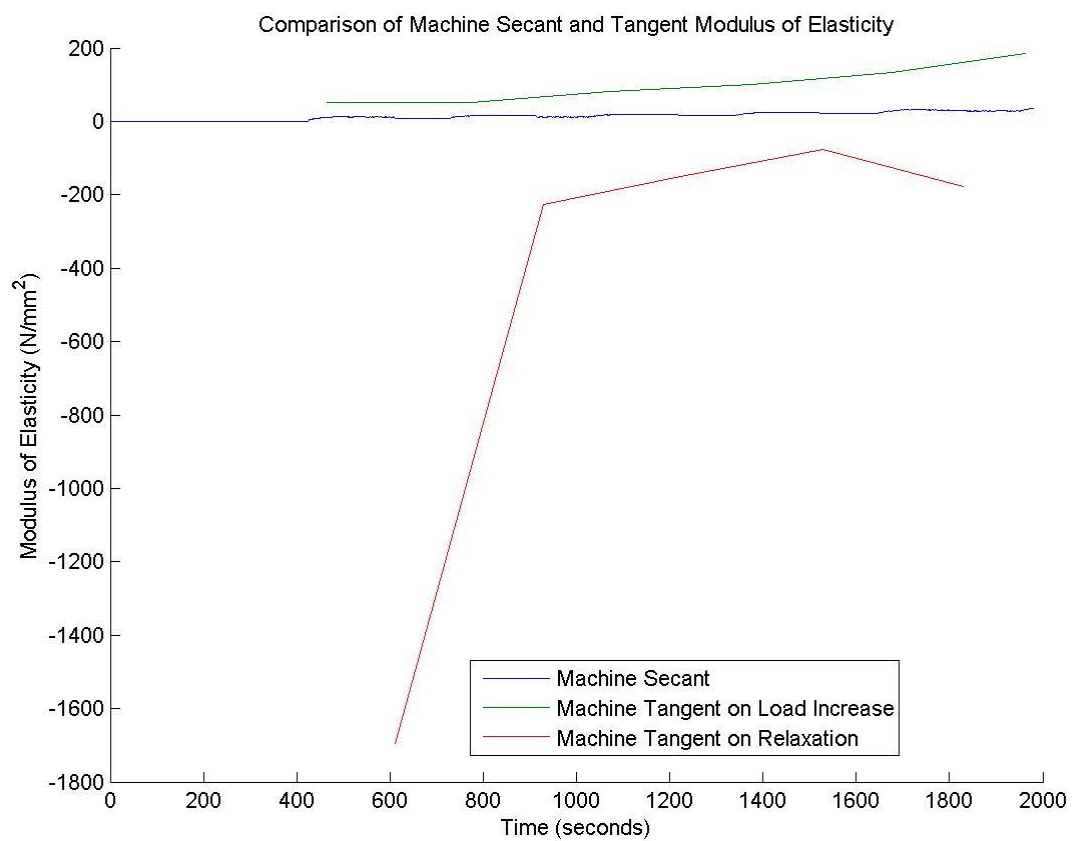
FIGURE 178: G4 MACHINE MEASURED SECANT AND TANGENT MODULUS VS. TIME

Appendix 6
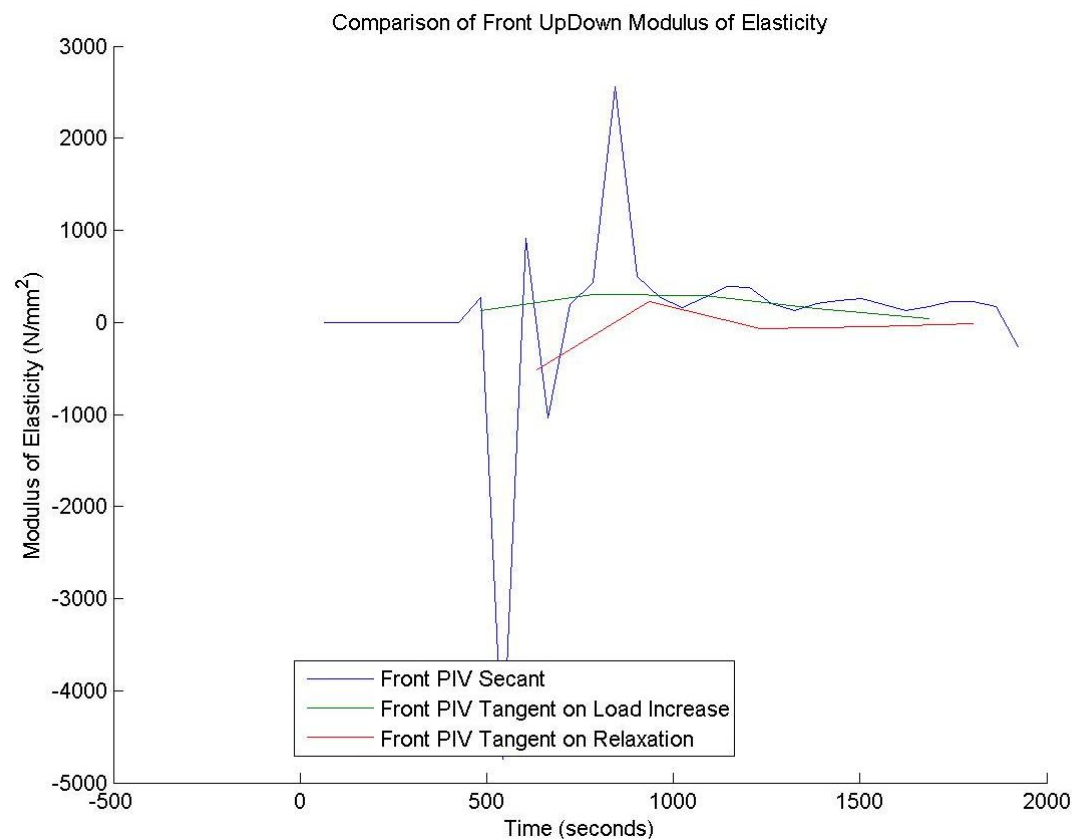
FIGURE 179: G4 FRONT VIEW PIV SECANT AND TANGENT MODULUS VS. TIME
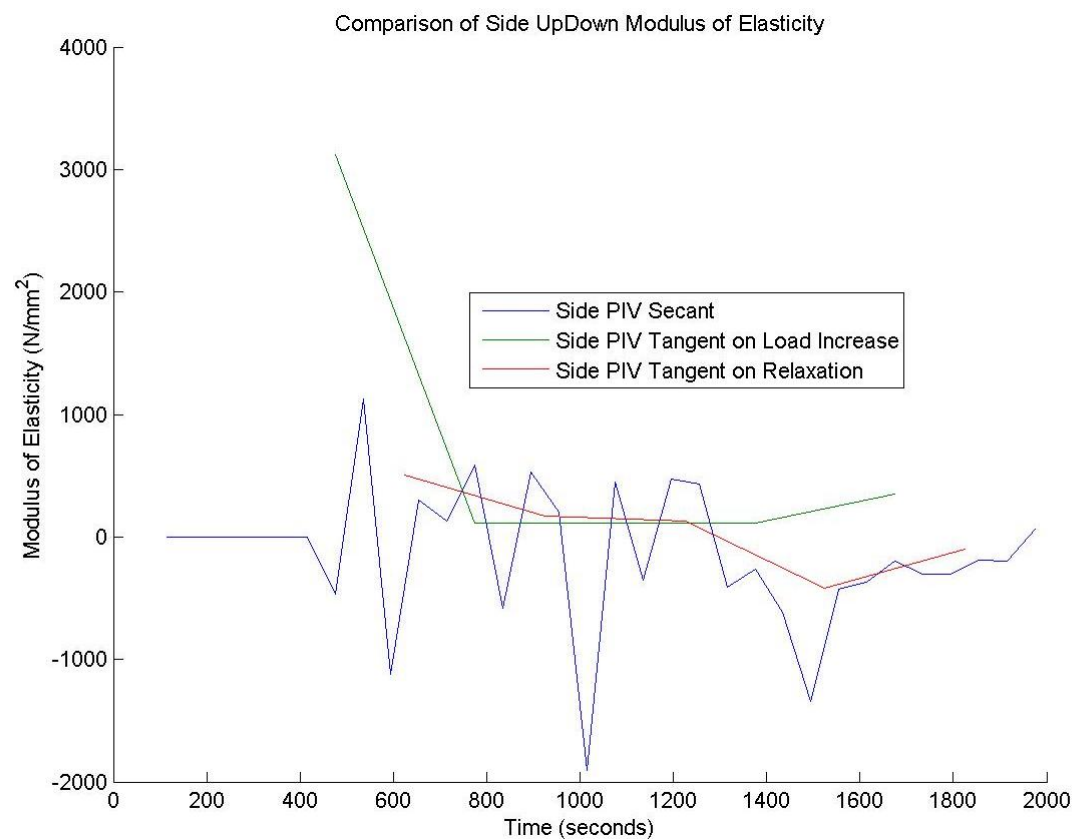
FIGURE 180: G4 SIDE VIEW PIV SECANT AND TANGENT MODULUS VS. TIME
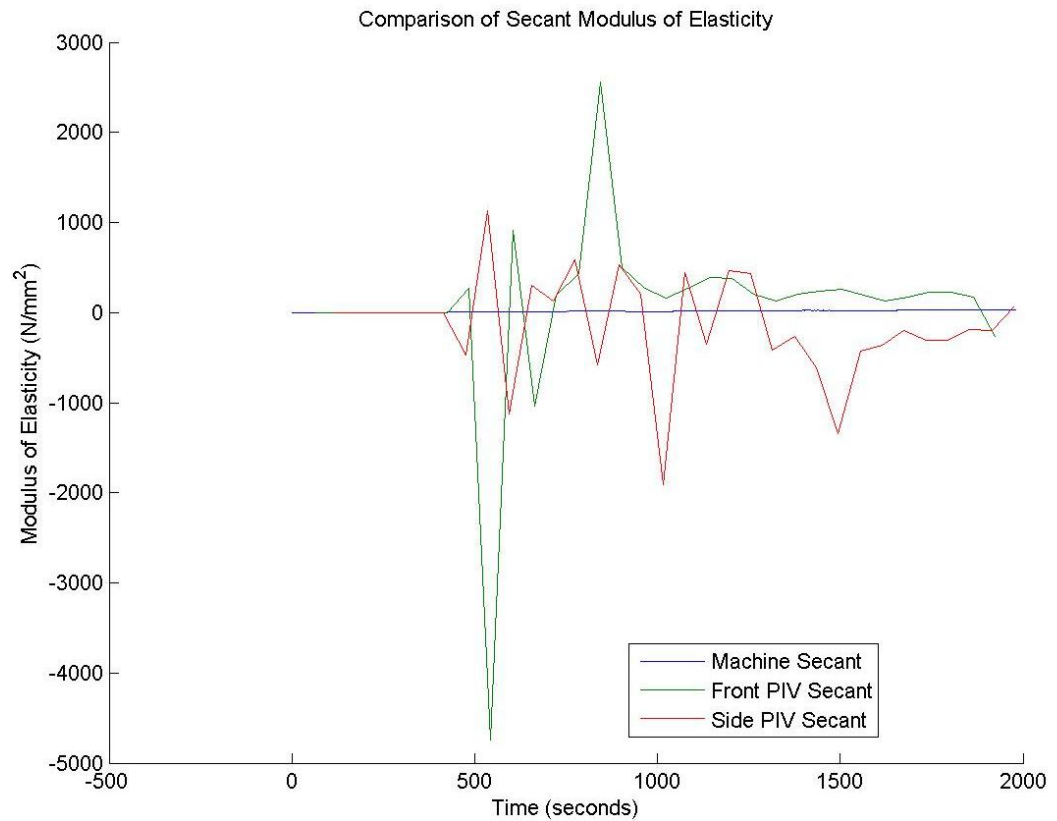
FIGURE 181: G4 COMPARISON OF MACHINE MEASURED AND PIV SECANT MODULUS VS. TIME
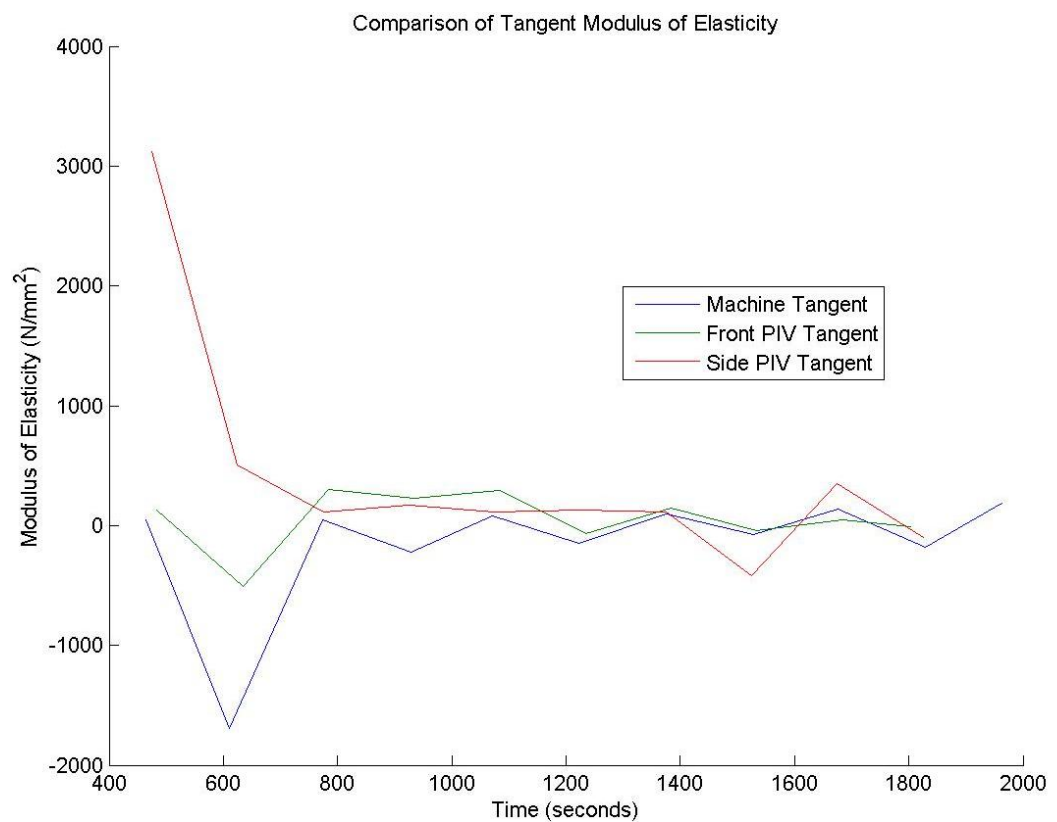
FIGURE 182: G4 COMPARISON OF MACHINE MEASURED AND PIV TANGENT MODULUS VS.

TIME

Appendix 6
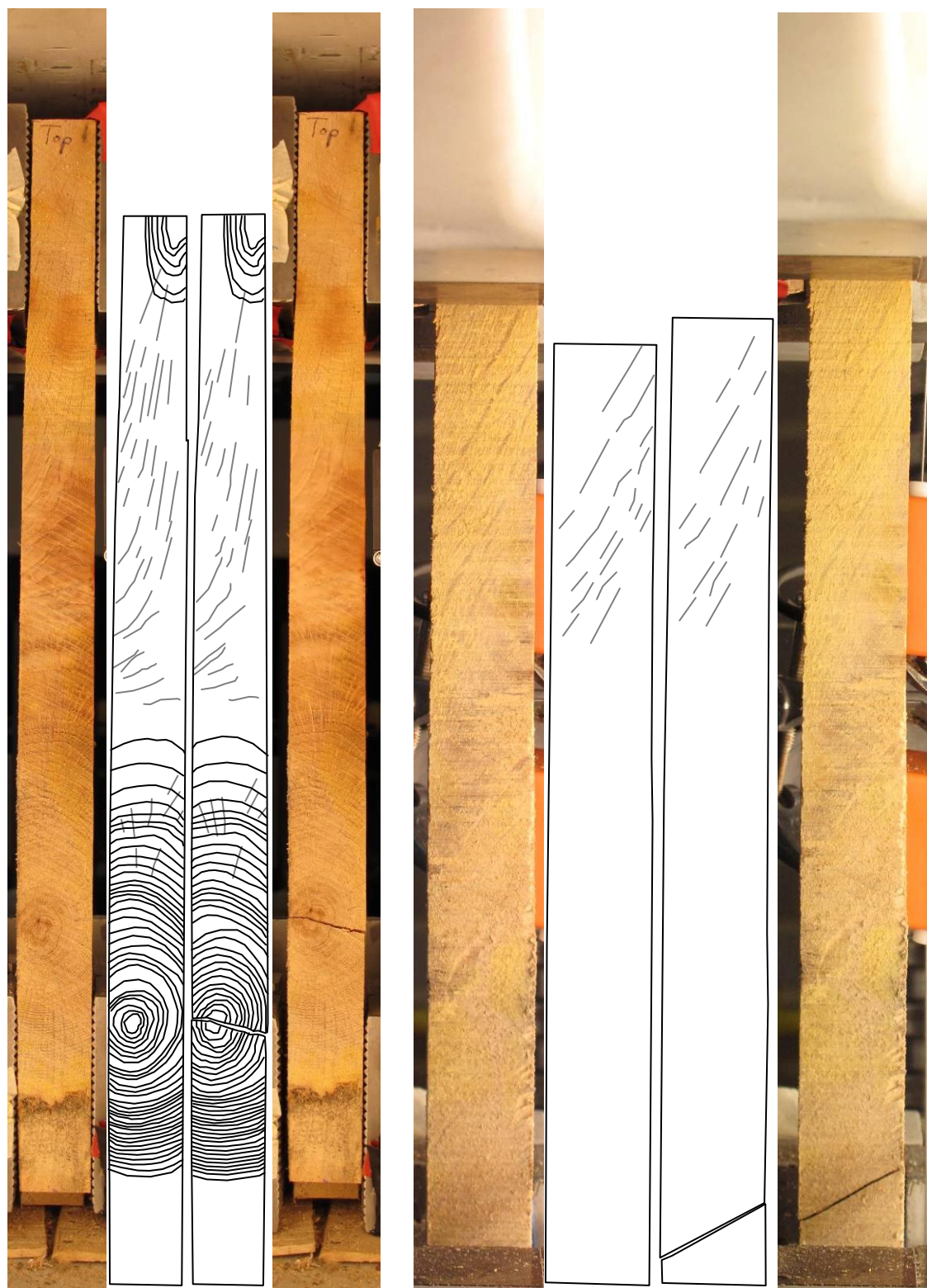
G4 Sample

F<small>IGURE</small> 183: SAMPLE GRAIN ORIENTATIONS OF THE FRONT (LEFT 4 IMAGES) AND SIDE (RIGHT 4 IMAGES) VIEW BEFORE (FIRST 2 OF 4 IMAGES) AND AFTER (LAST 2 OF 4 IMAGES) BREAKAGE

238

G4 Front View
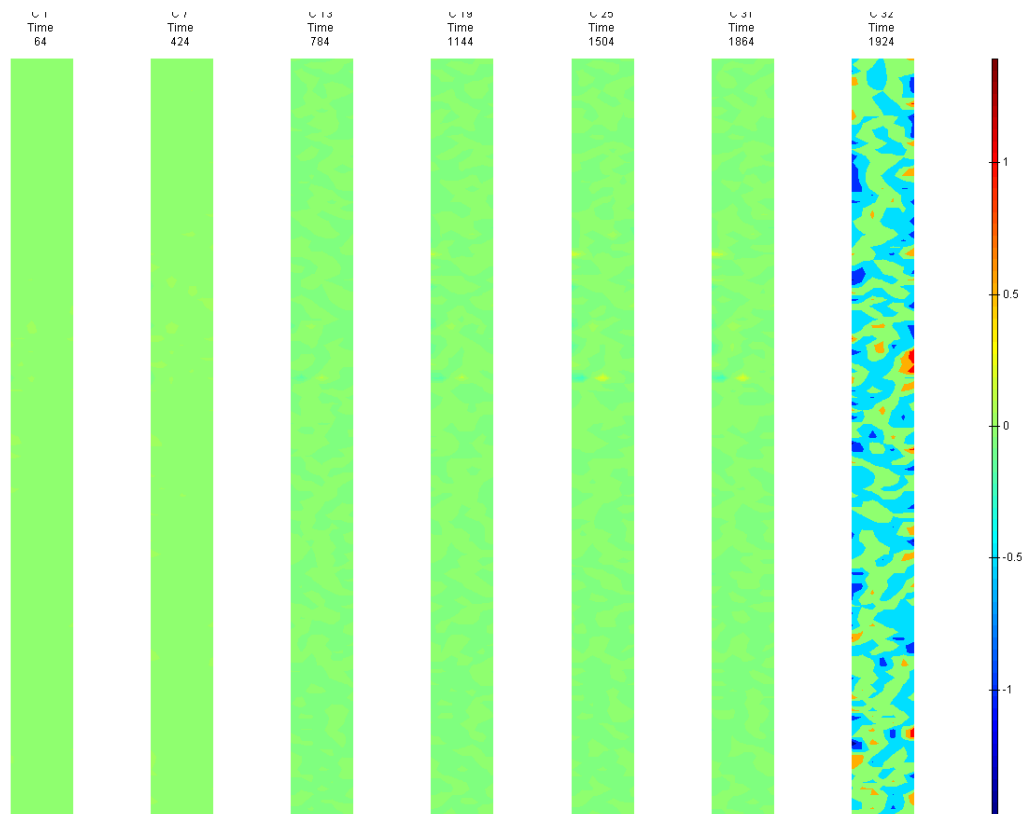
FIGURE 184: X DIRECTION PIV SEQUENTIAL ENGINEERING STRAIN OVER TIME
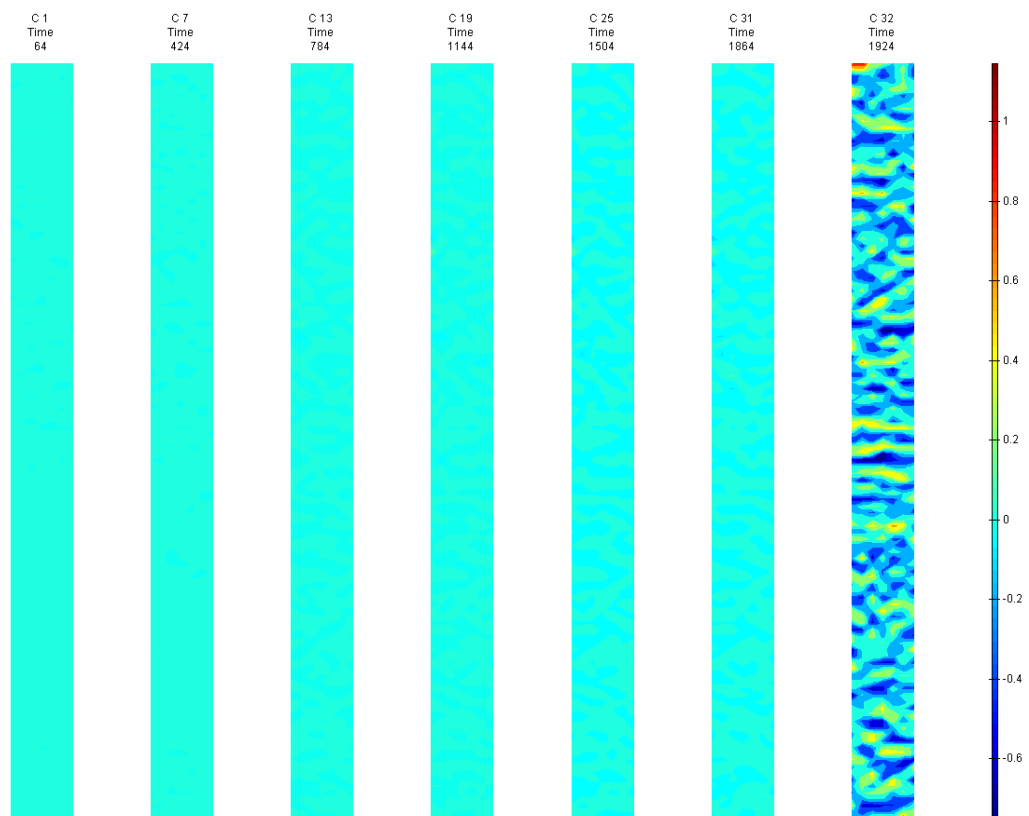
FIGURE 185: Y DIRECTION PIV SEQUENTIAL ENGINEERING STRAIN OVER TIME

Appendix 6
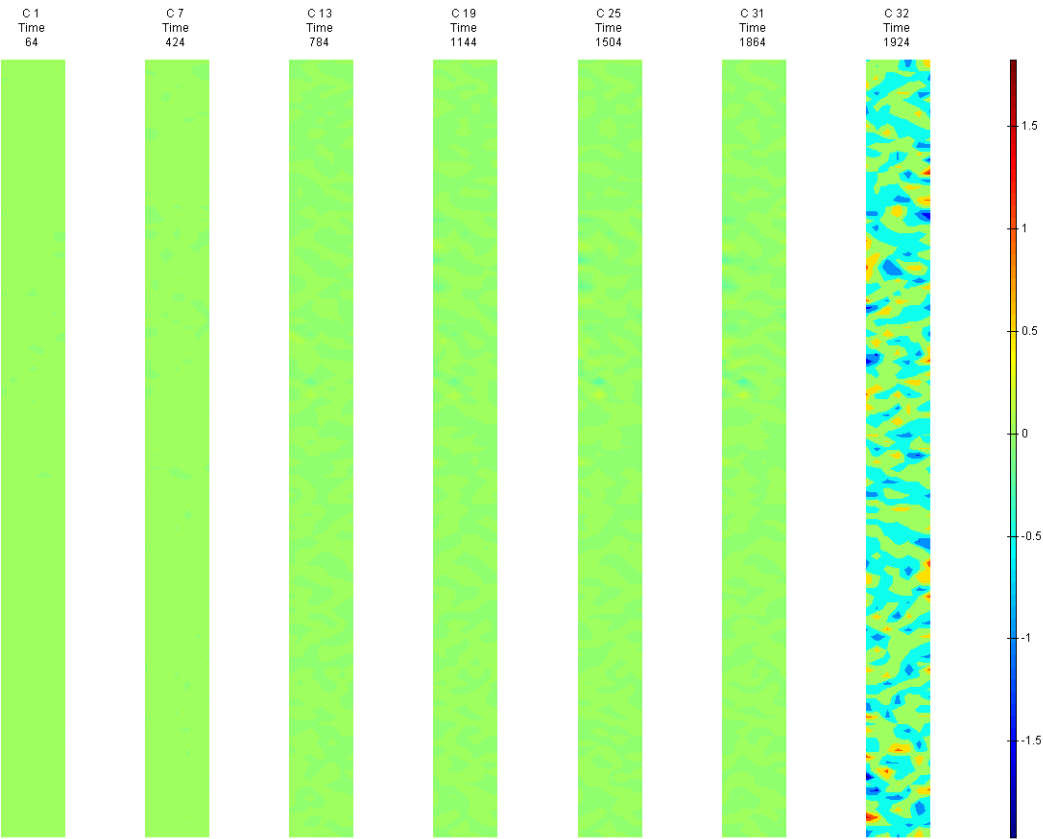
FIGURE 186: XY DIRECTION PIV SEQUENTIAL ENGINEERING SHEAR STRAIN OVER TIME
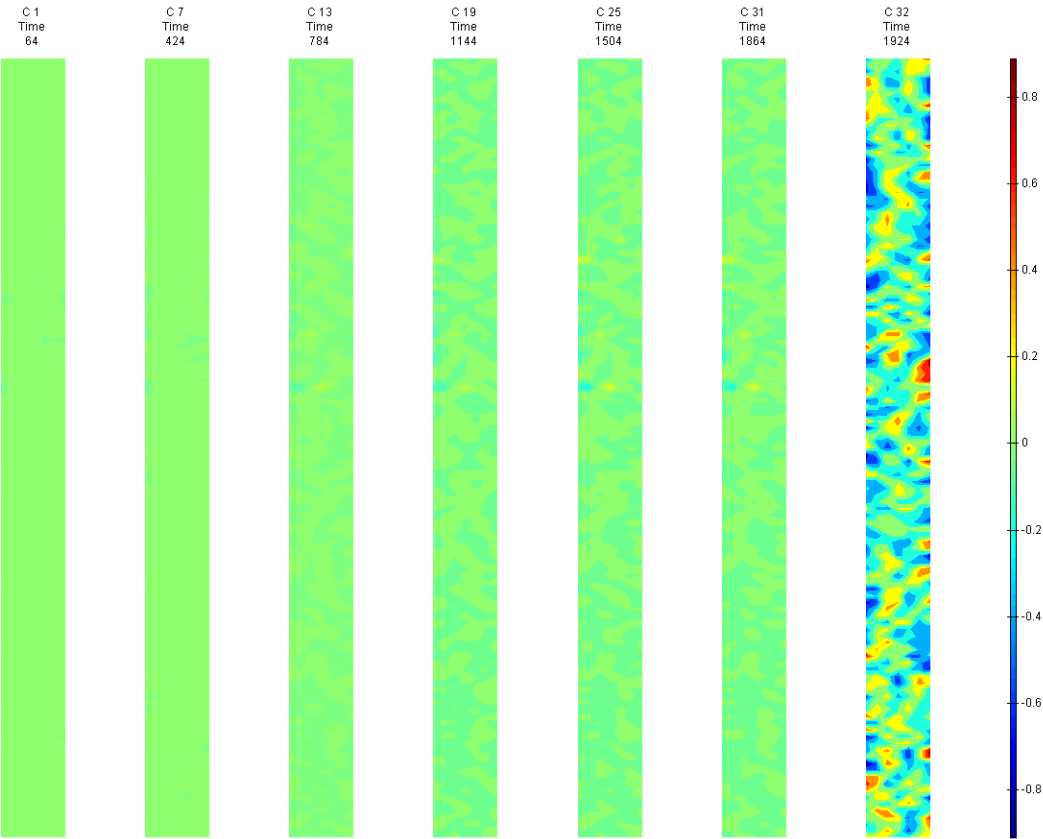
FIGURE 187: X DIRECTION PIV SEQUENTIAL TRUE STRAIN OVER TIME
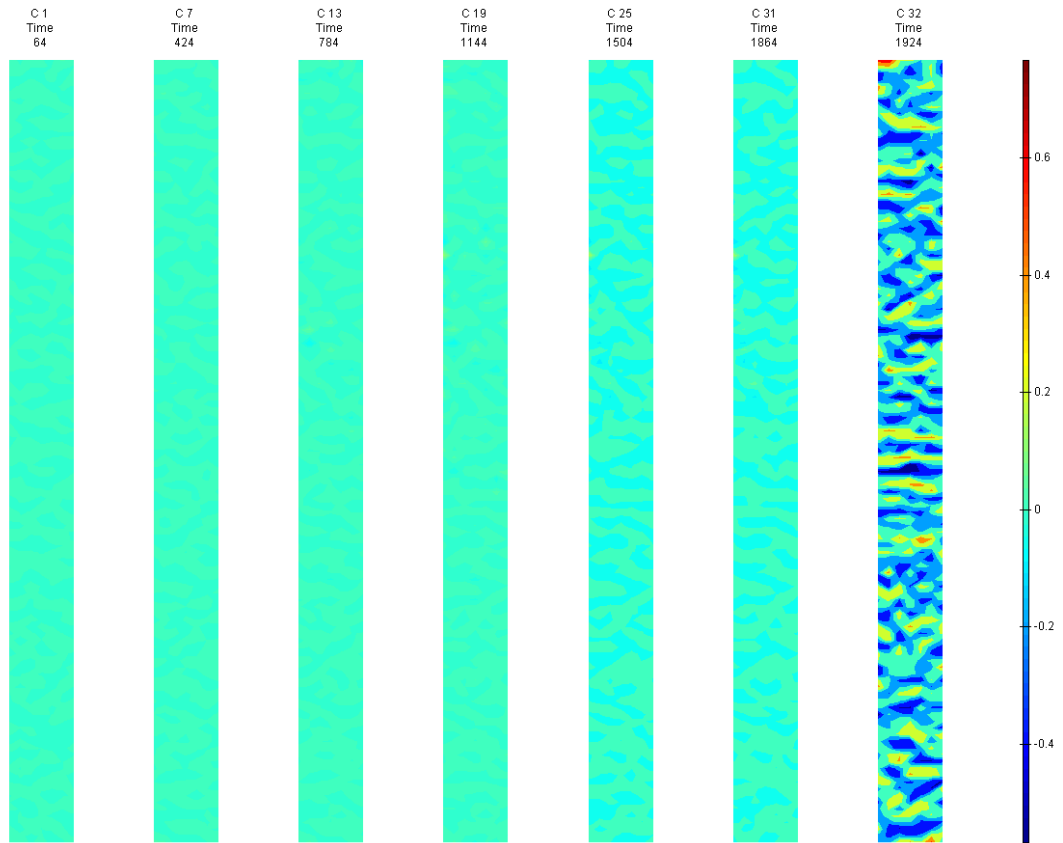
FIGURE 188: Y DIRECTION PIV SEQUENTIAL TRUE STRAIN OVER TIME
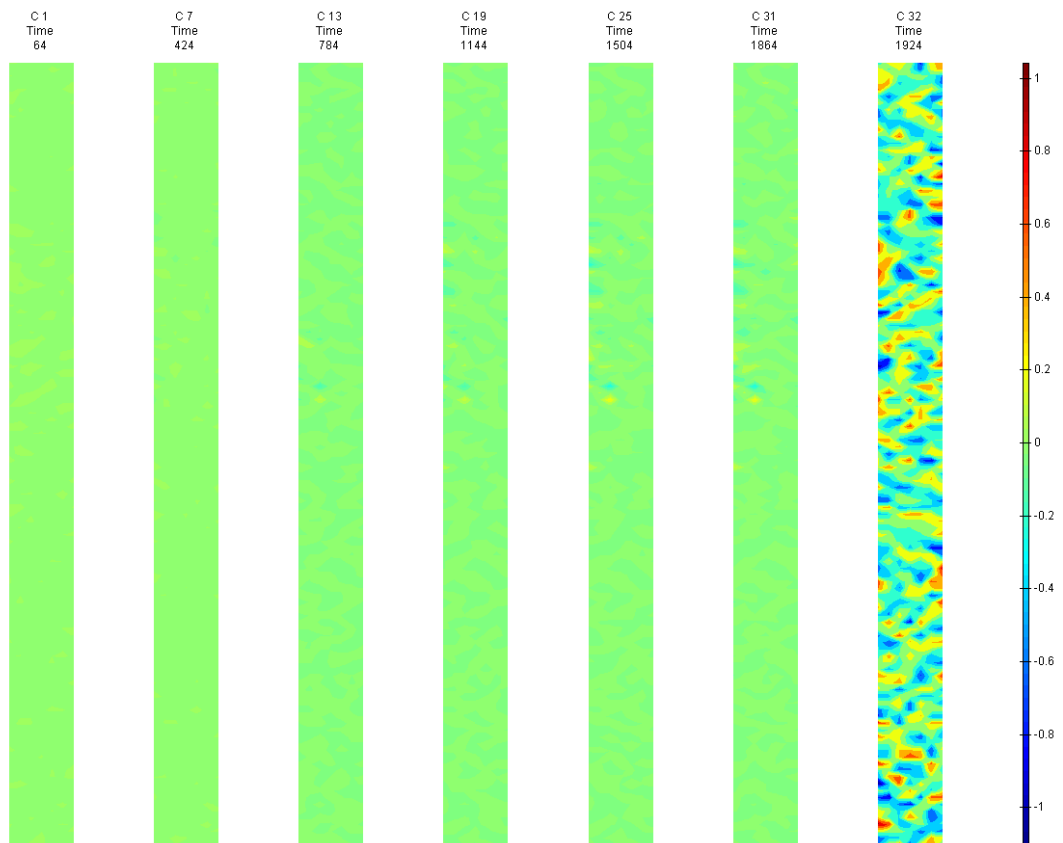
FIGURE 189: XY DIRECTION PIV SEQUENTIAL TRUE SHEAR STRAIN OVER TIME
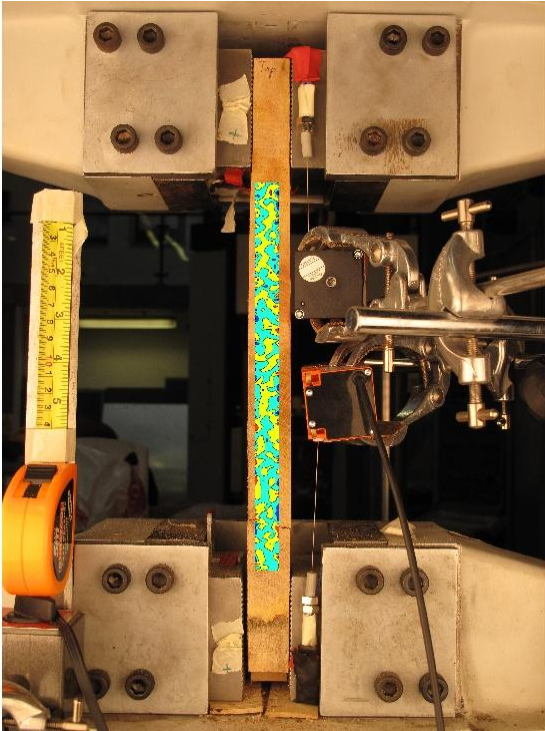
FIGURE 190: X DIRECTION PIV FIRST–LAST DITCH ENGINEERING STRAIN OVER IMAGE
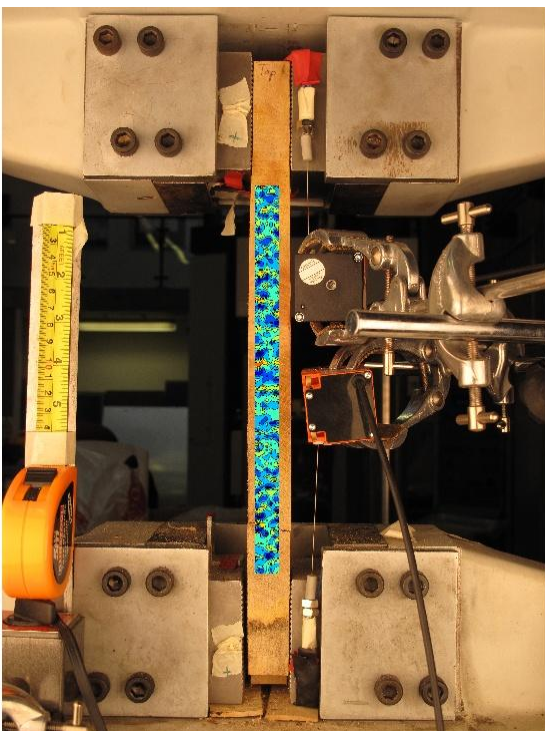
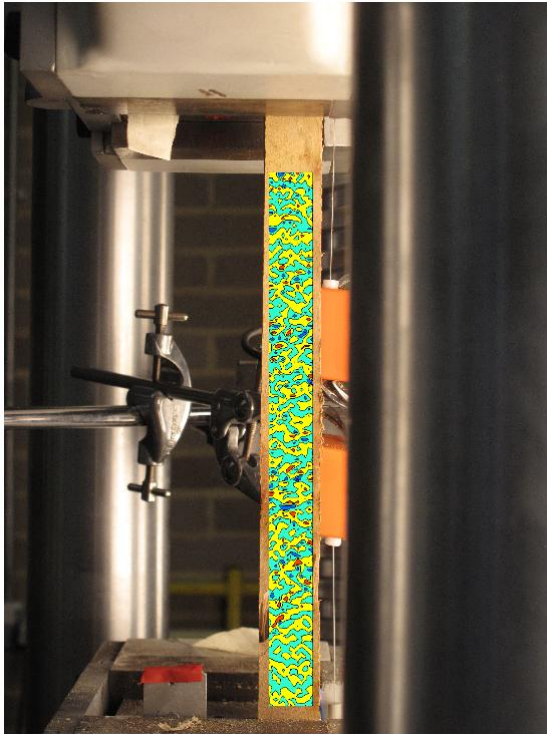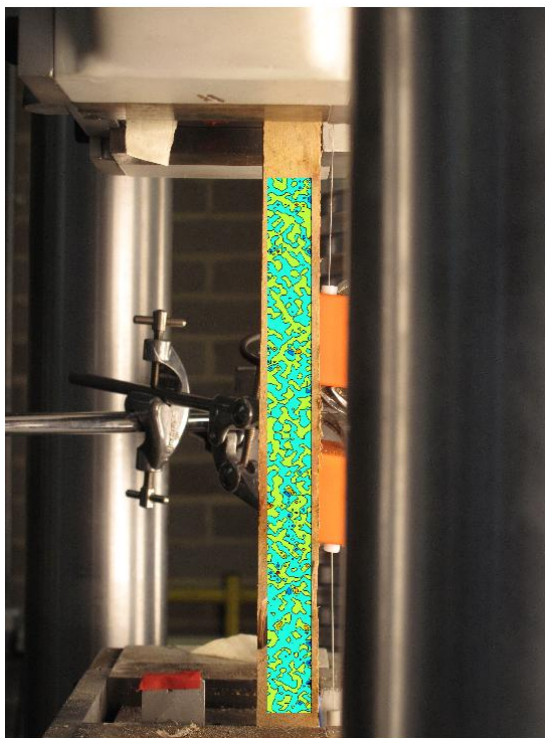FIGURE 191: Y DIRECTION PIV FIRST–LAST DITCH ENGINEERING STRAIN OVER IMAGE
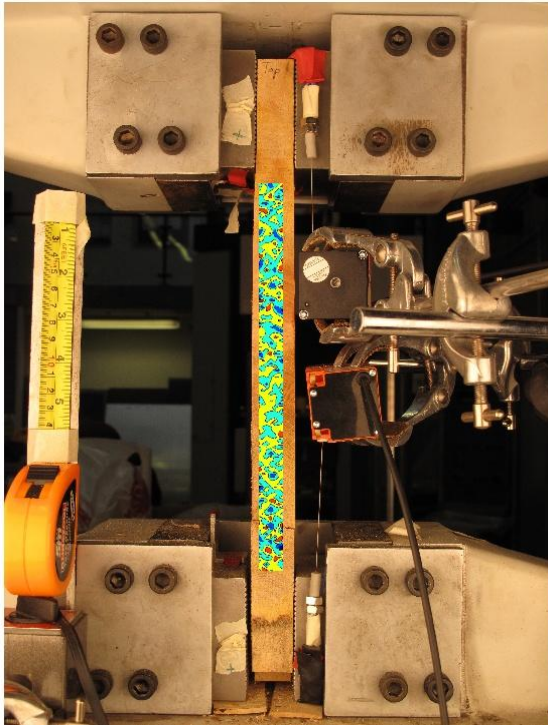
FIGURE 192: XY DIRECTION PIV FIRST-LAST DITCH ENGINEERING SHEAR STRAIN OVER
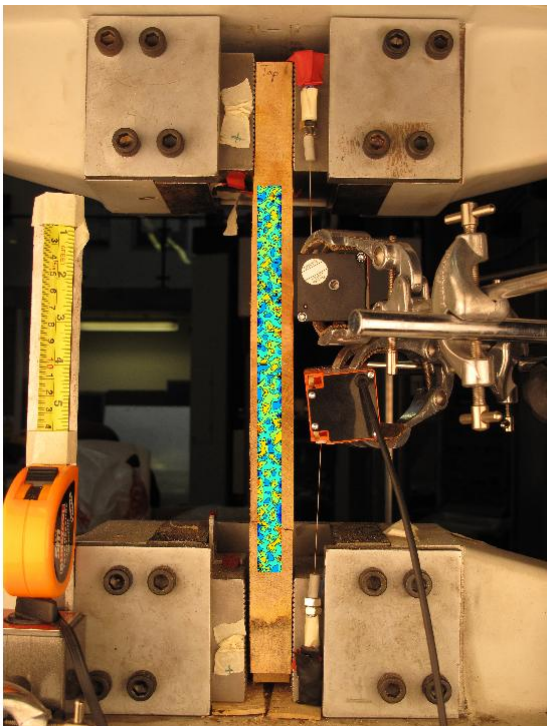
IMAGE

FIGURE 193: X DIRECTION PIV FIRST-LAST DITCH TRUE STRAIN OVER IMAGE
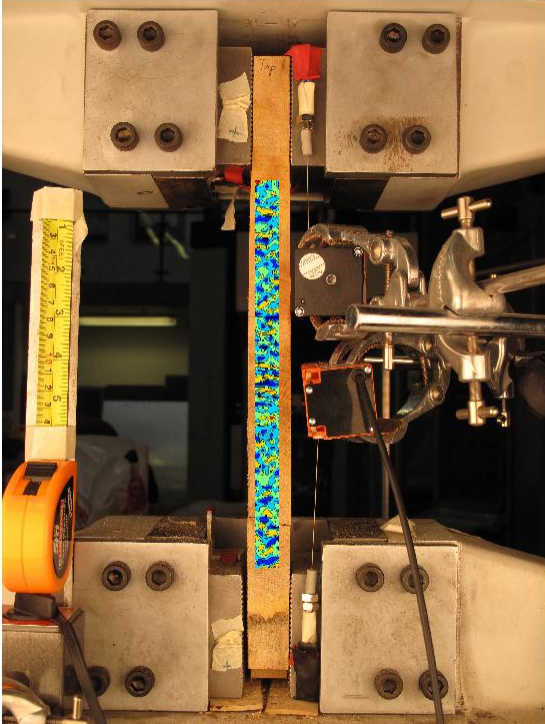
FIGURE 194: Y DIRECTION PIV FIRST–LAST DITCH TRUE STRAIN OVER IMAGE
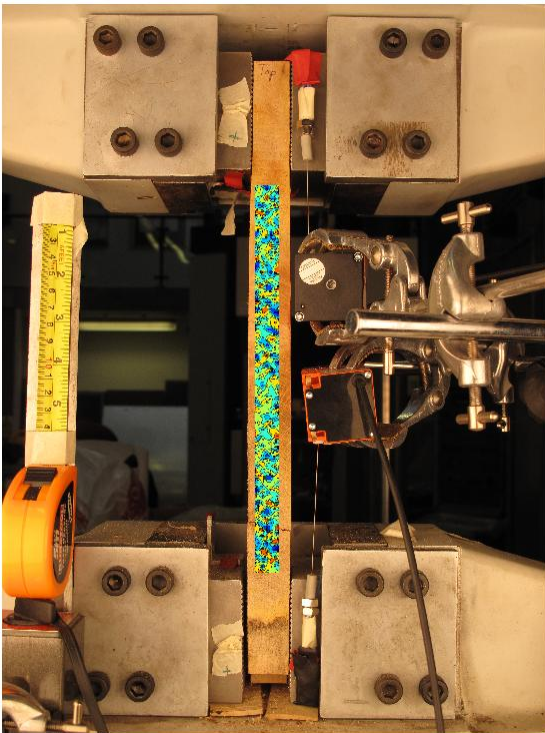
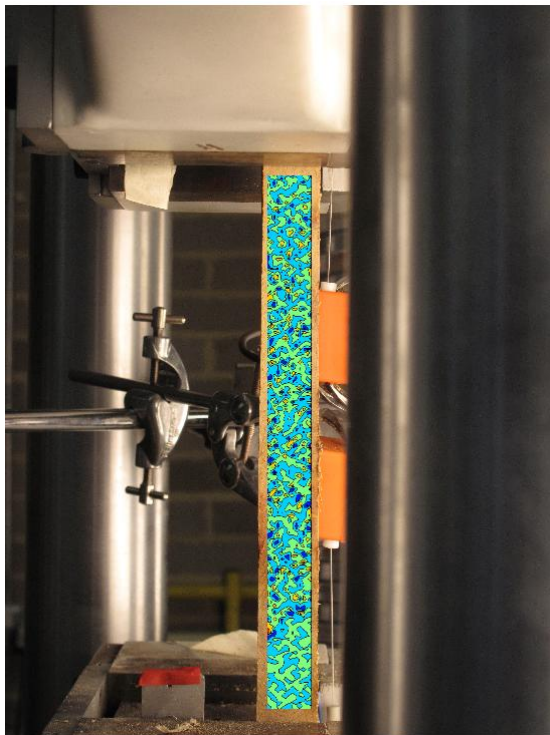FIGURE 195: XY DIRECTION PIV FIRST–LAST DITCH TRUE SHEAR STRAIN OVER IMAGE
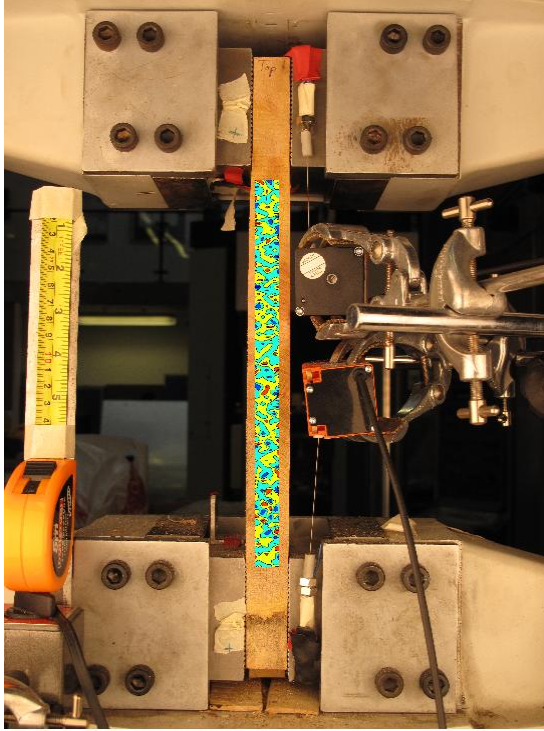
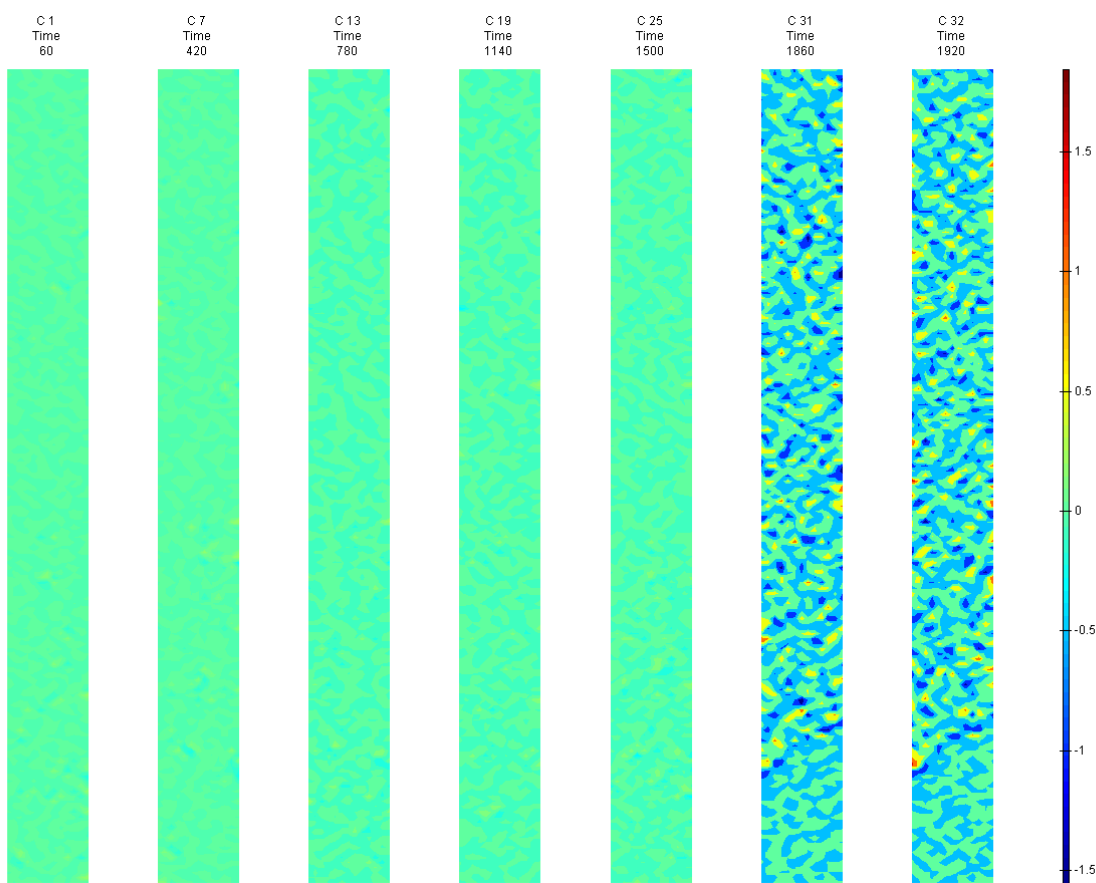FIGURE 196: XY DIRECTION PIV FIRST–SEQUENTIAL ENGINEERING SHEAR STRAIN OVER

IMAGE
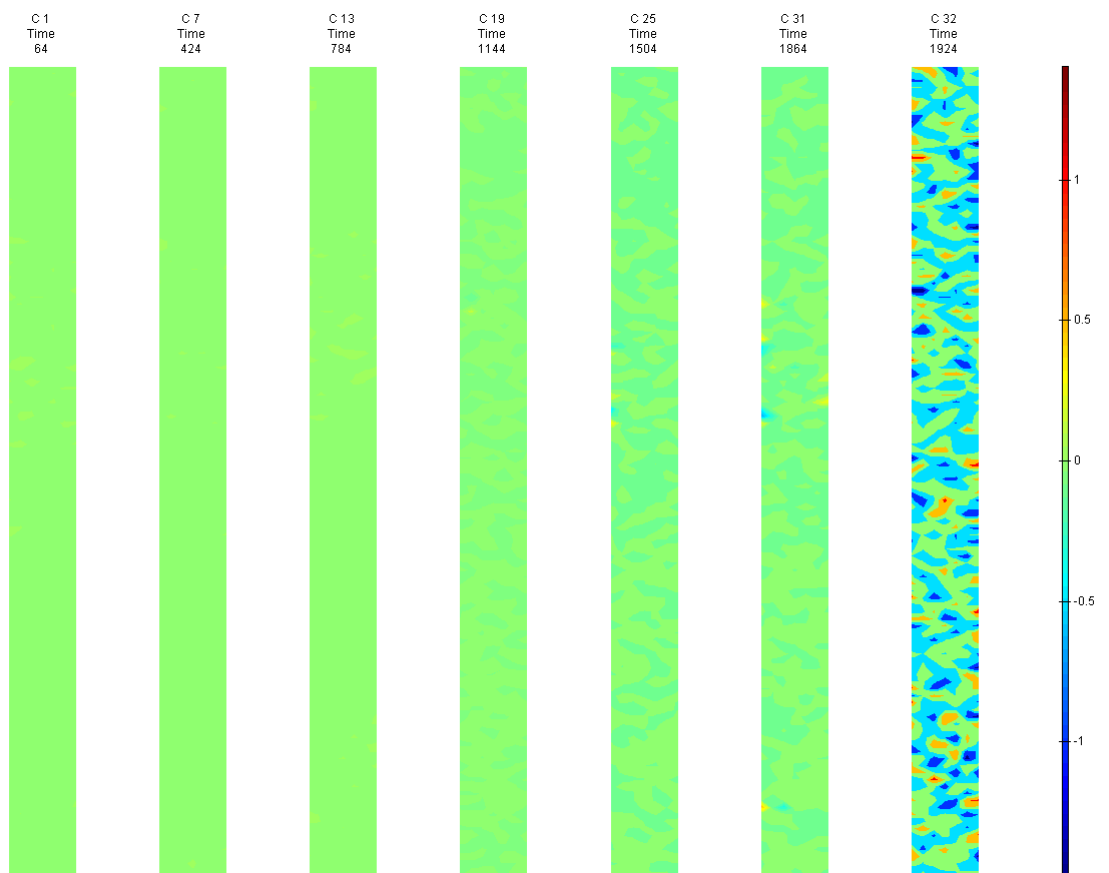
FIGURE 197: XY DIRECTION PIV FIRST–SEQUENTIAL ENGINEERING SHEAR STRAIN OVER TIME

## G4 Side View
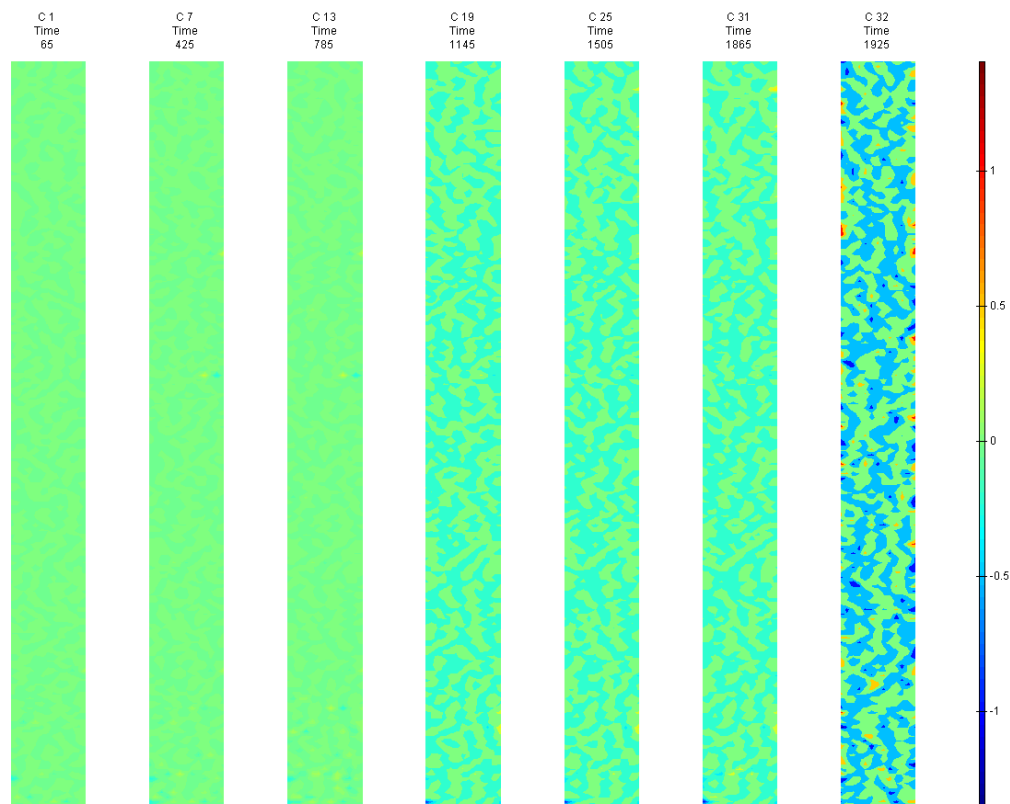
FIGURE 198: X DIRECTION PIV SEQUENTIAL ENGINEERING STRAIN OVER TIME
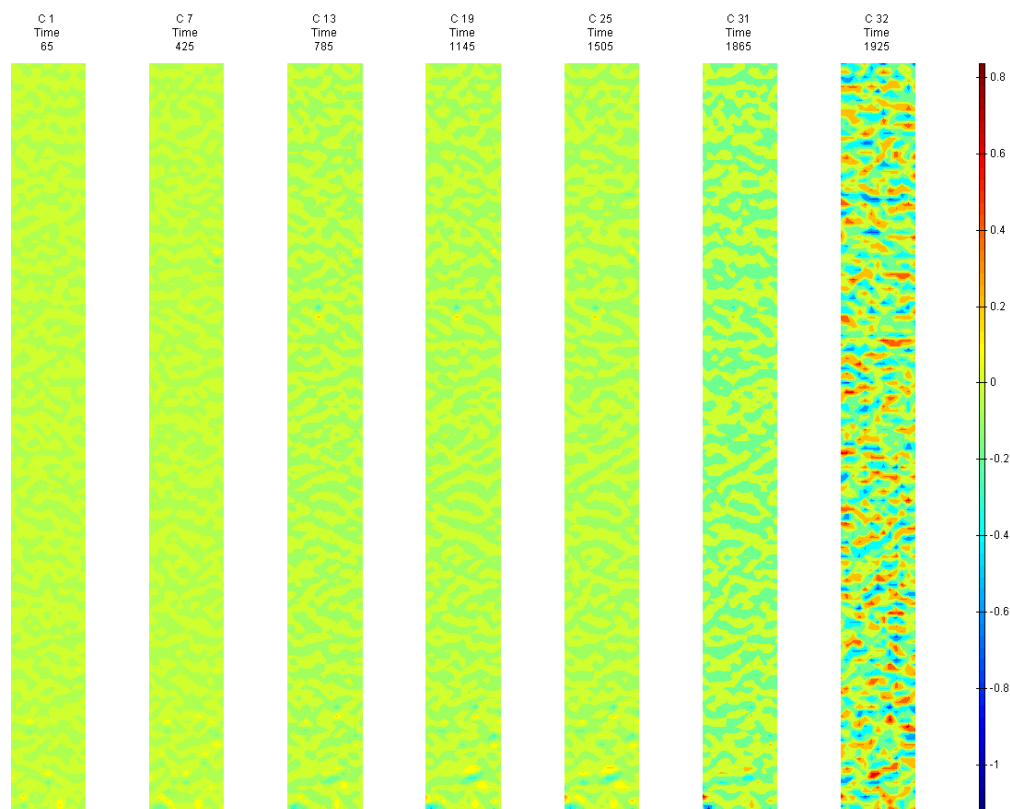
FIGURE 199: Y DIRECTION PIV SEQUENTIAL ENGINEERING STRAIN OVER TIME
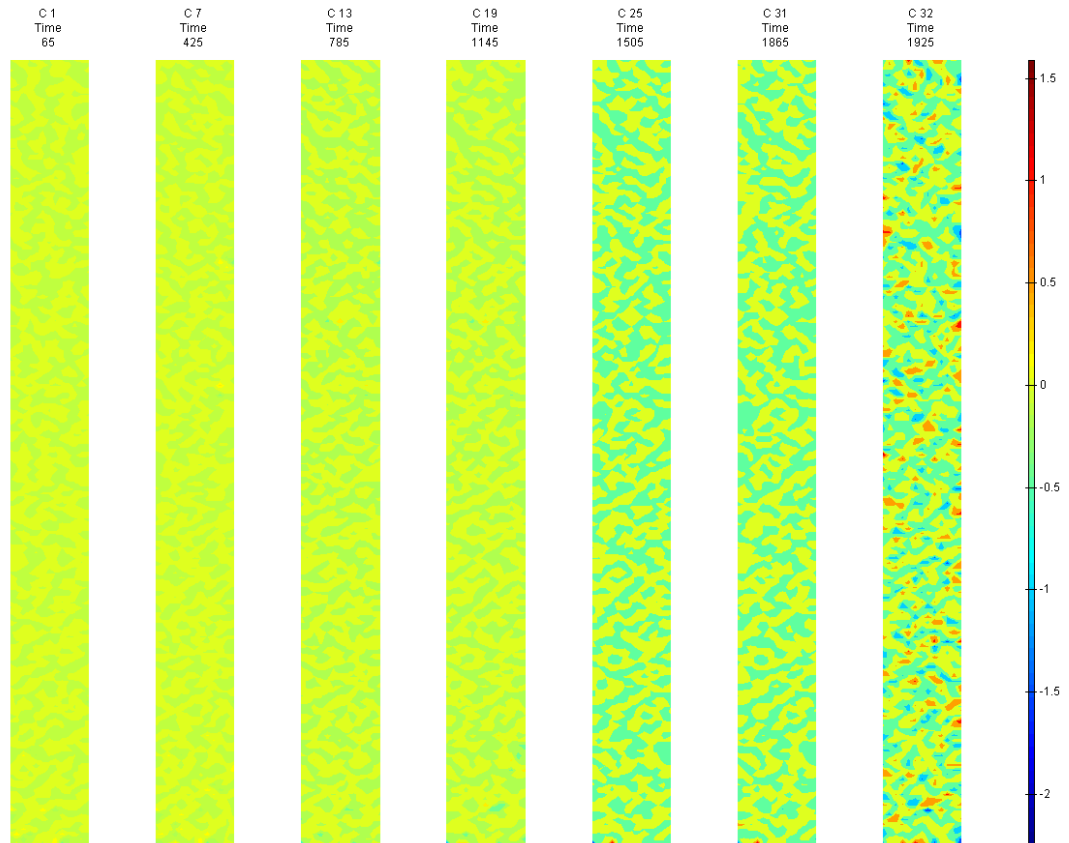
FIGURE 200: XY DIRECTION PIV SEQUENTIAL ENGINEERING SHEAR STRAIN OVER TIME
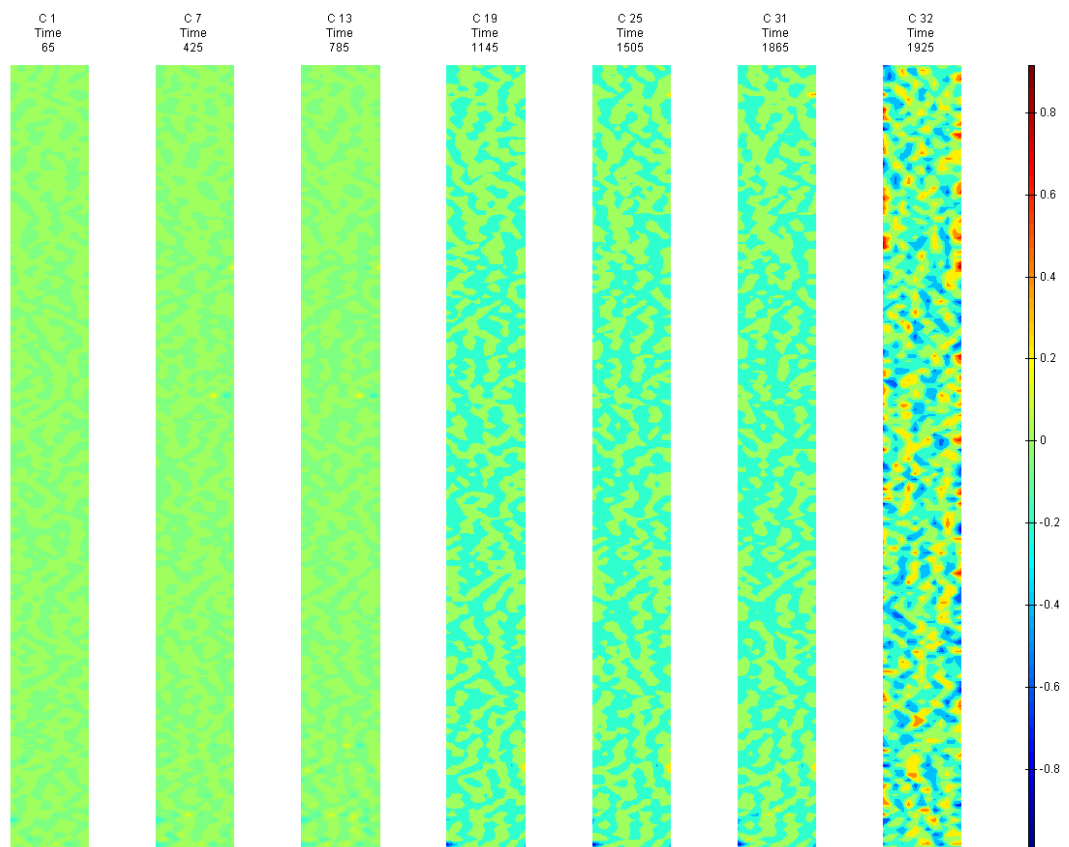
FIGURE 201: X DIRECTION PIV SEQUENTIAL TRUE STRAIN OVER TIME
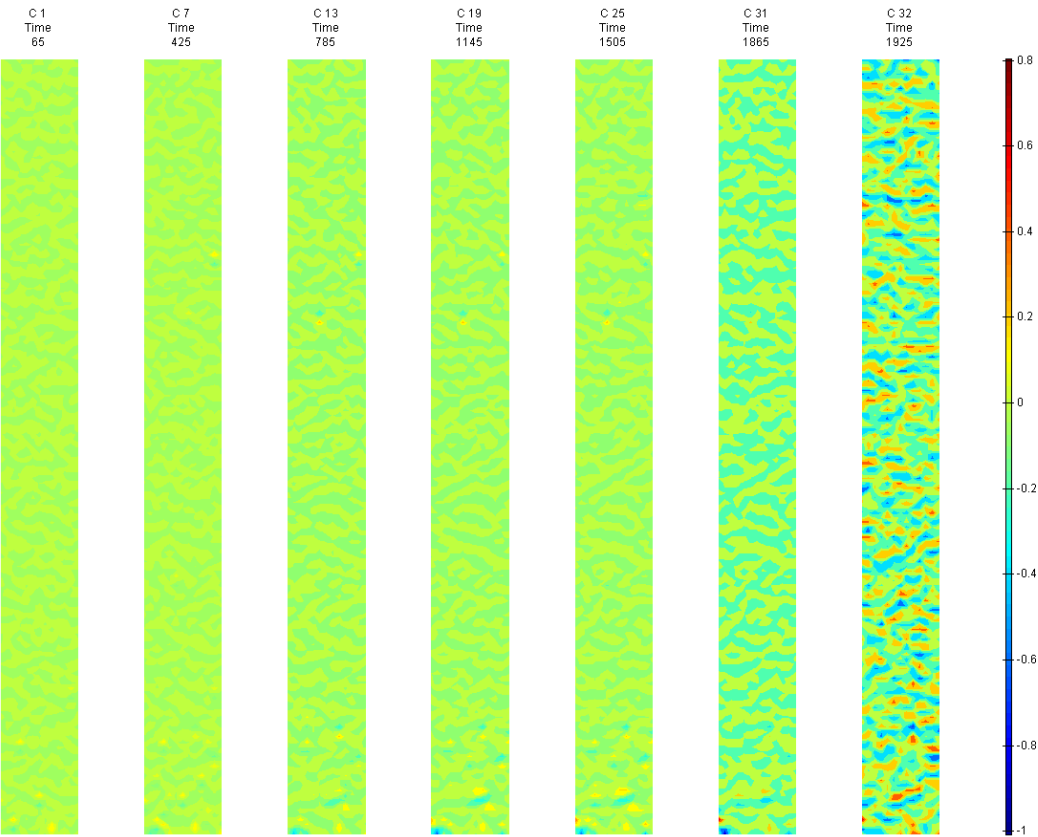
FIGURE 202: Y DIRECTION PIV SEQUENTIAL TRUE STRAIN OVER TIME
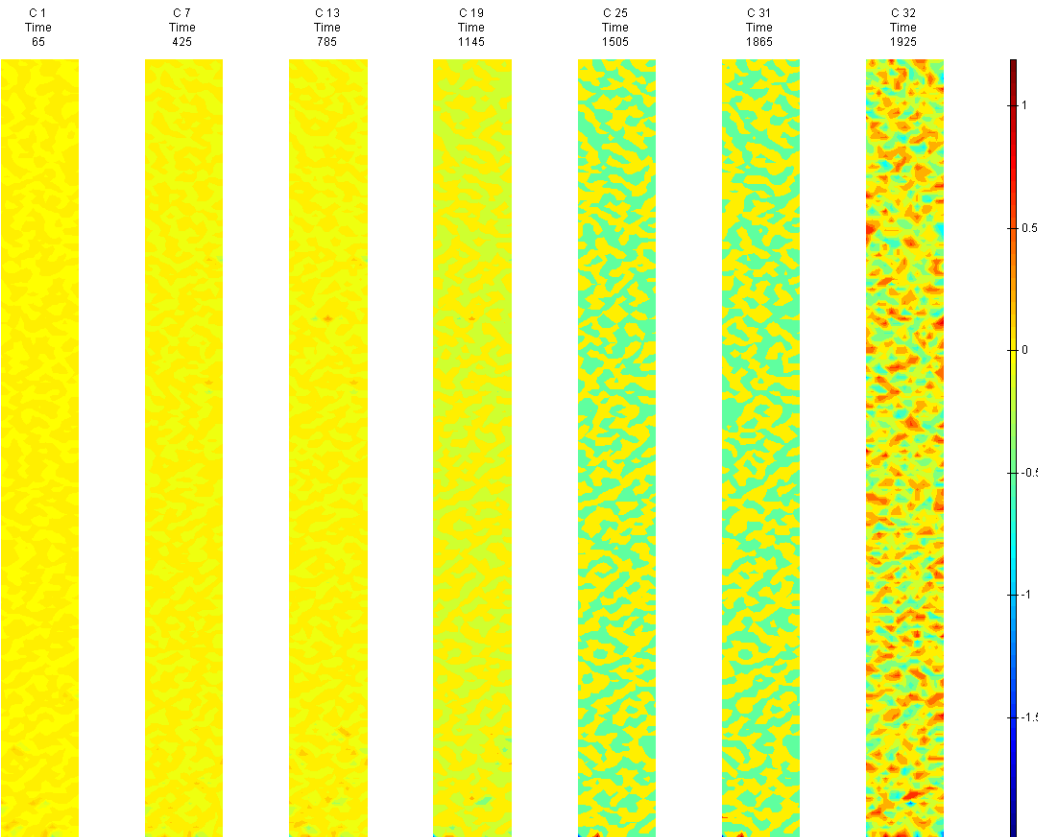
FIGURE 203: XY DIRECTION PIV SEQUENTIAL TRUE SHEAR STRAIN OVER TIME
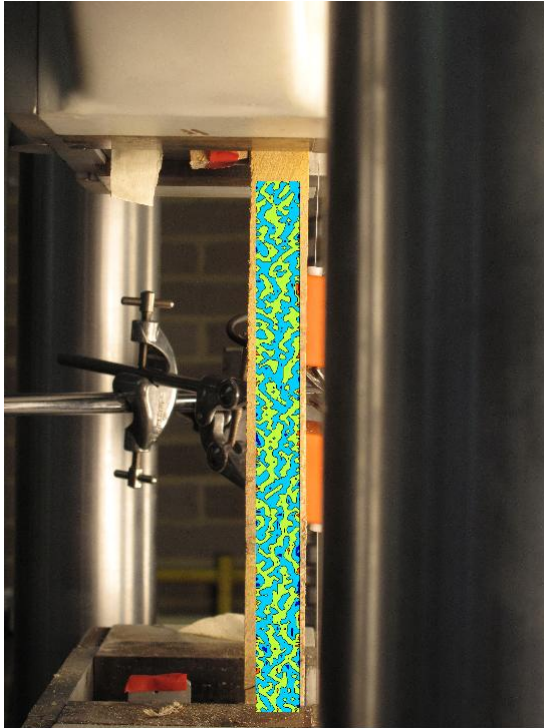
FIGURE 204: X DIRECTION PIV FIRST−LAST DITCH ENGINEERING STRAIN OVER IMAGE
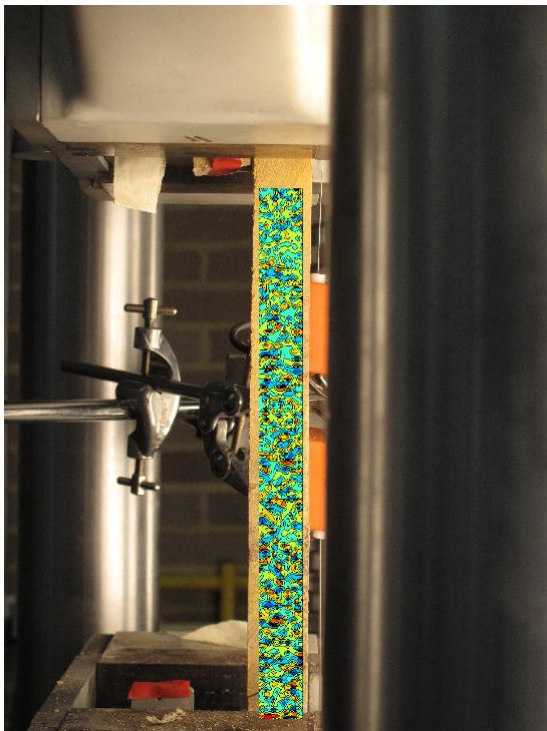
FIGURE 205: Y DIRECTION PIV FIRST−LAST DITCH ENGINEERING STRAIN OVER IMAGE

Appendix 6
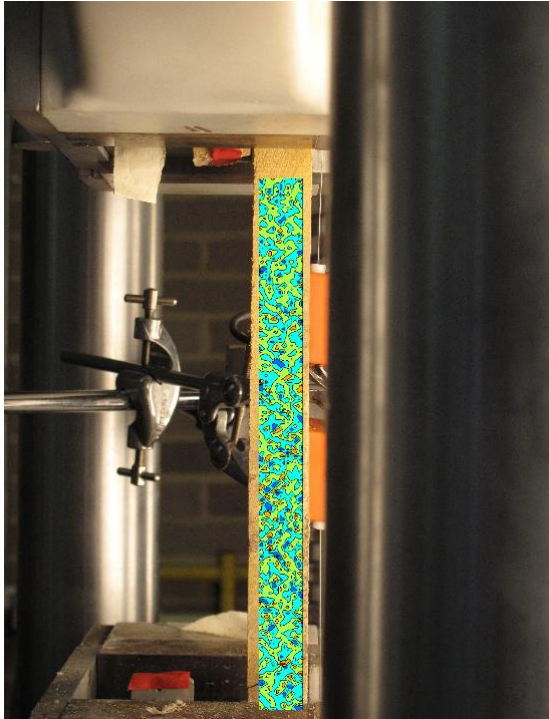
FIGURE 206: XY DIRECTION PIV FIRST-LAST DITCH ENGINEERING SHEAR STRAIN OVER
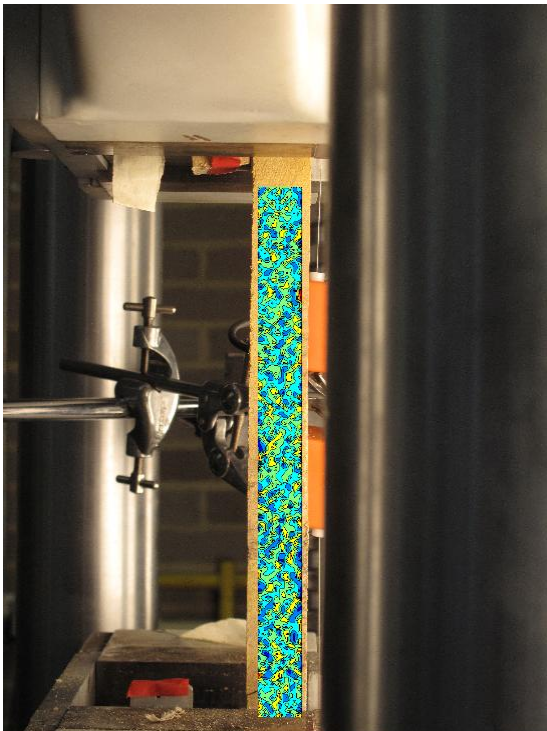
IMAGE

FIGURE 207: X DIRECTION PIV FIRST-LAST DITCH TRUE STRAIN OVER IMAGE
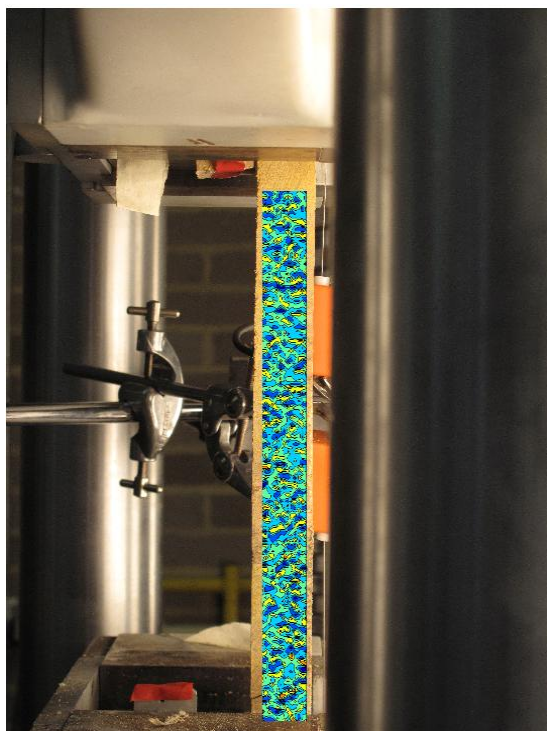
FIGURE 208: Y DIRECTION PIV FIRST–LAST DITCH TRUE STRAIN OVER IMAGE
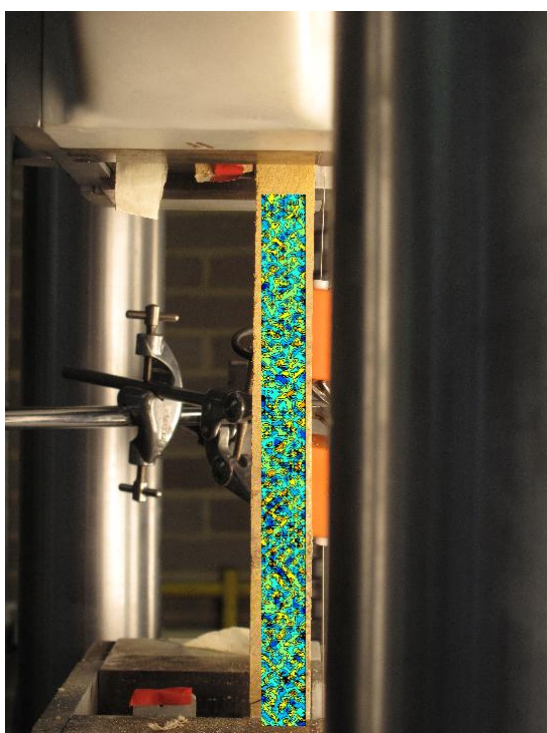
FIGURE 209: XY DIRECTION PIV FIRST–LAST DITCH TRUE SHEAR STRAIN OVER IMAGE

Appendix 6
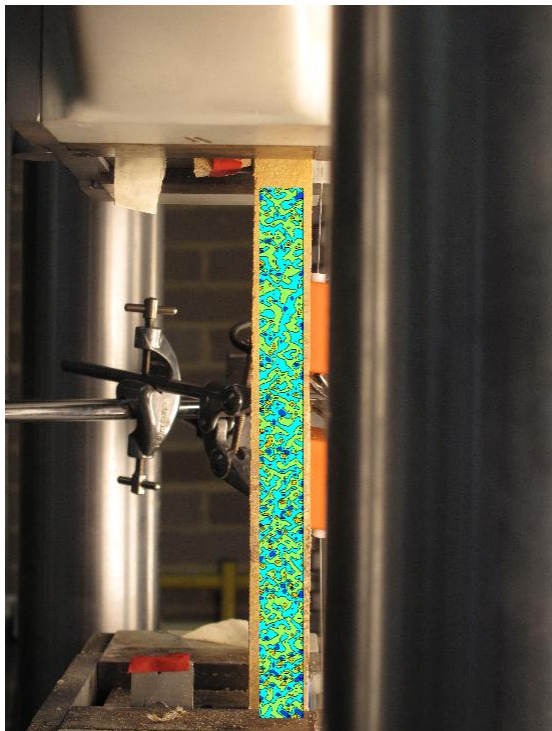
FIGURE 210: XY DIRECTION PIV FIRST−SEQUENTIAL ENGINEERING SHEAR STRAIN OVER

IMAGE
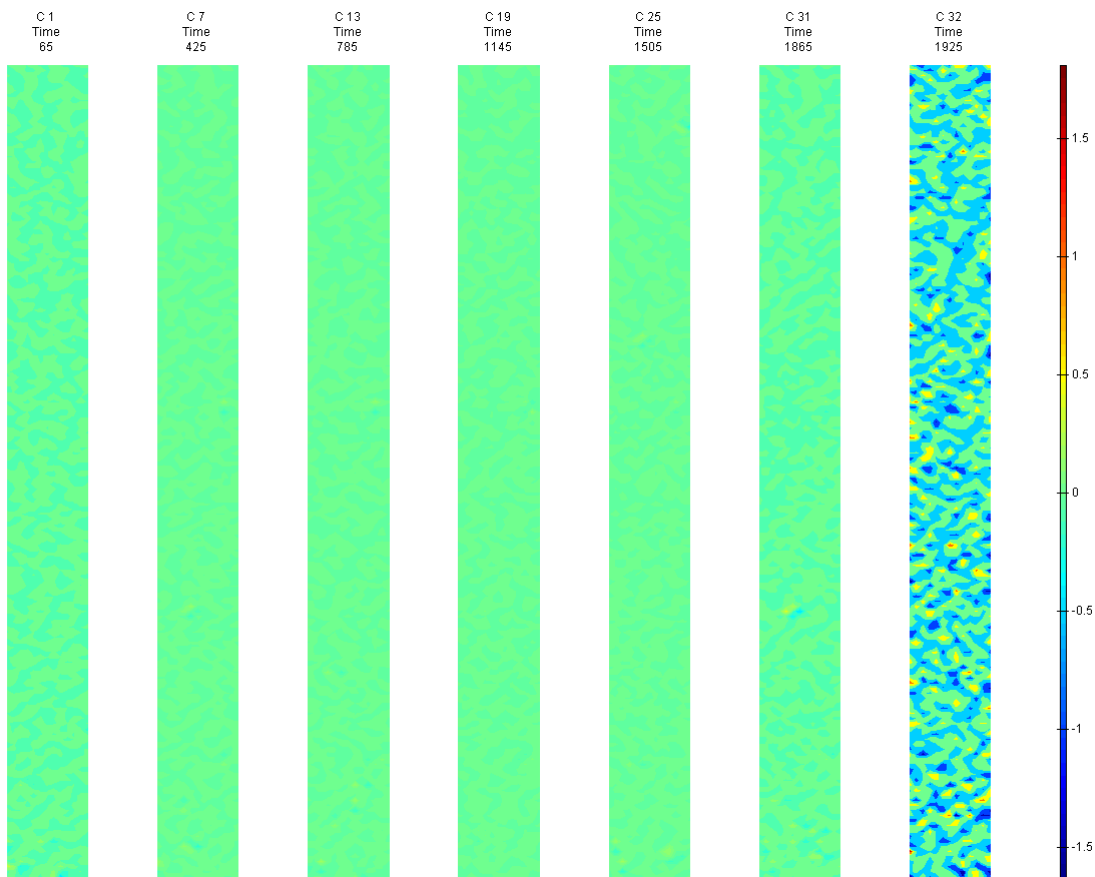
FIGURE 211: XY DIRECTION PIV FIRST−SEQUENTIAL ENGINEERING SHEAR STRAIN OVER TIME

G5
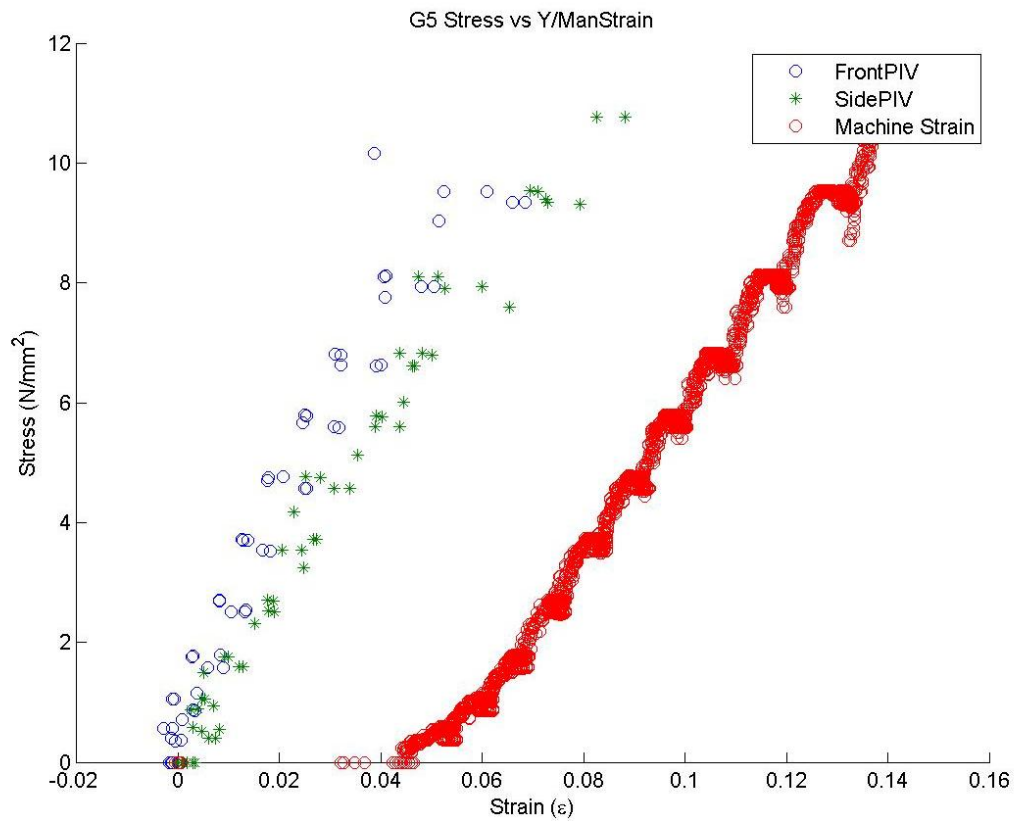
FIGURE 212: G5 TENSILE STRESS VS. MACHINE MEASURED/PIV STRAINS
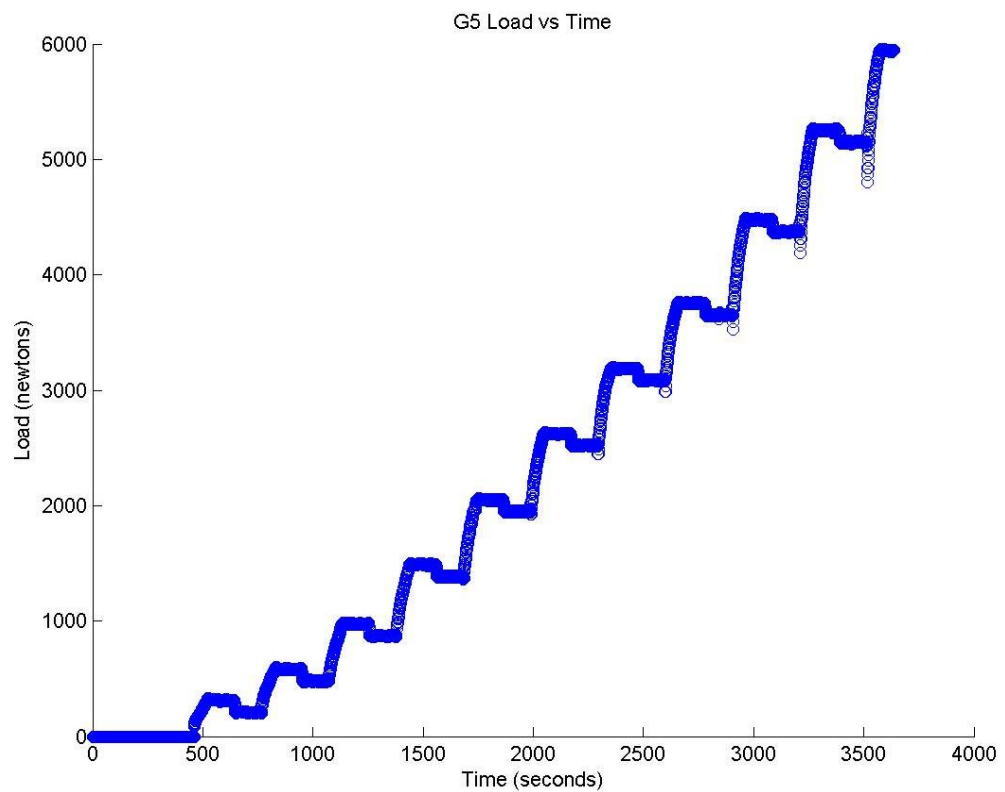
FIGURE 213: G5 TENSILE LOAD VS. TIME

Appendix 6
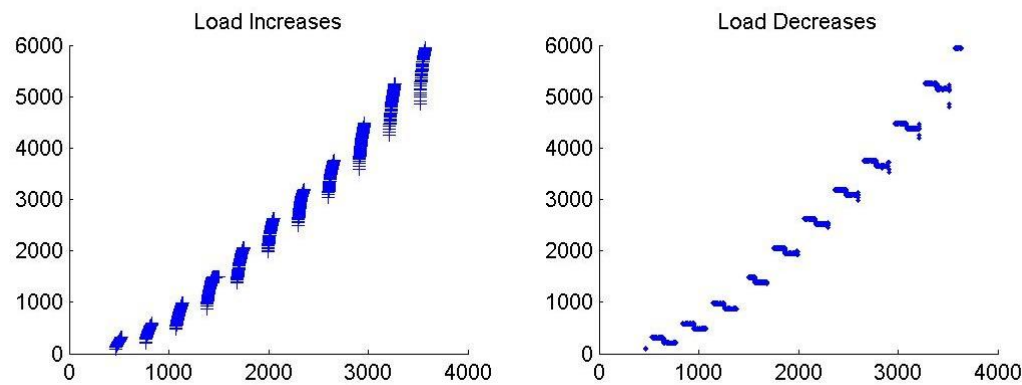
FIGURE 214: G5 CREEP LOADING: INCREMENTS AND RELAXATION
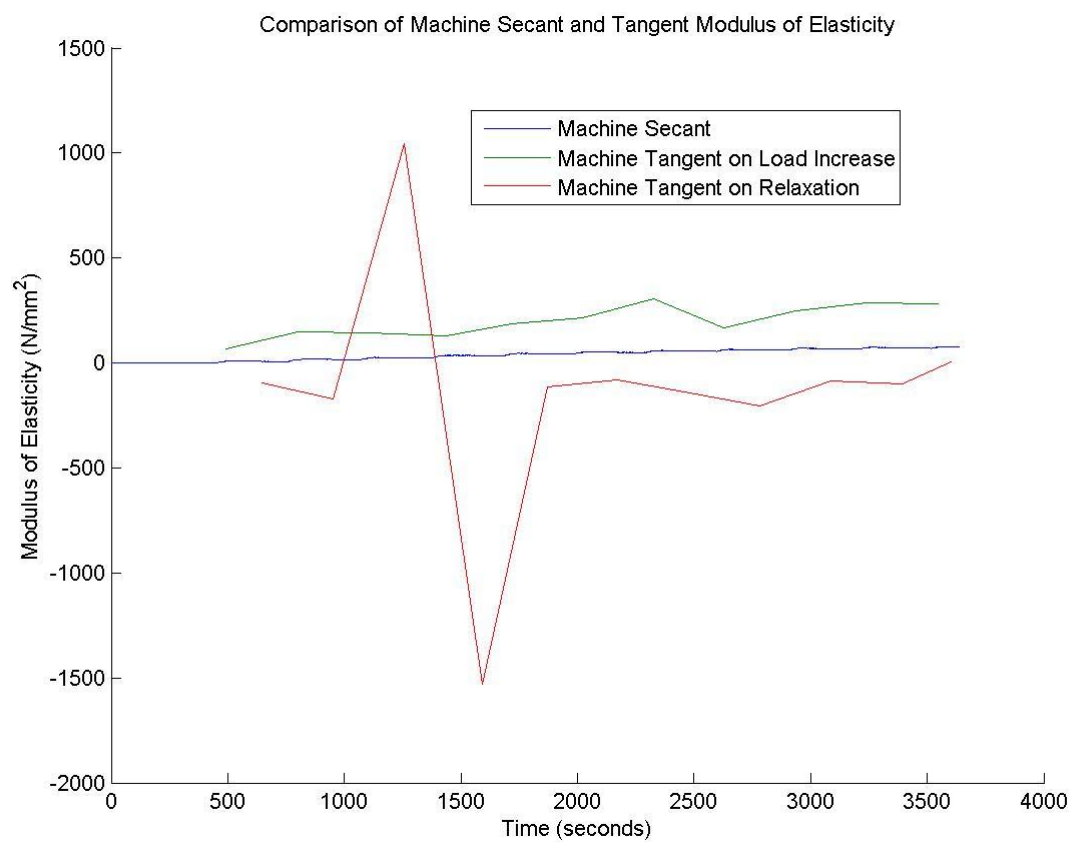
FIGURE 215: G5 MACHINE MEASURED SECANT AND TANGENT MODULUS VS. TIME
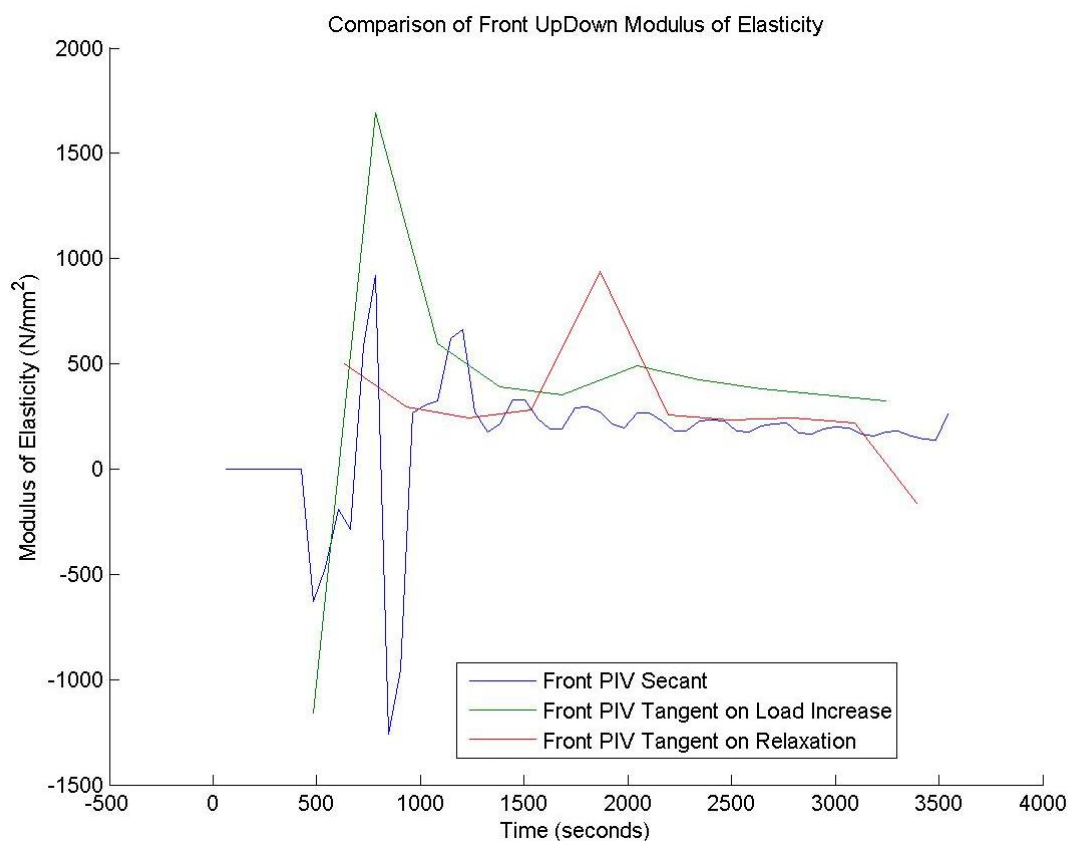
FIGURE 216: G5 FRONT VIEW PIV SECANT AND TANGENT MODULUS VS. TIME
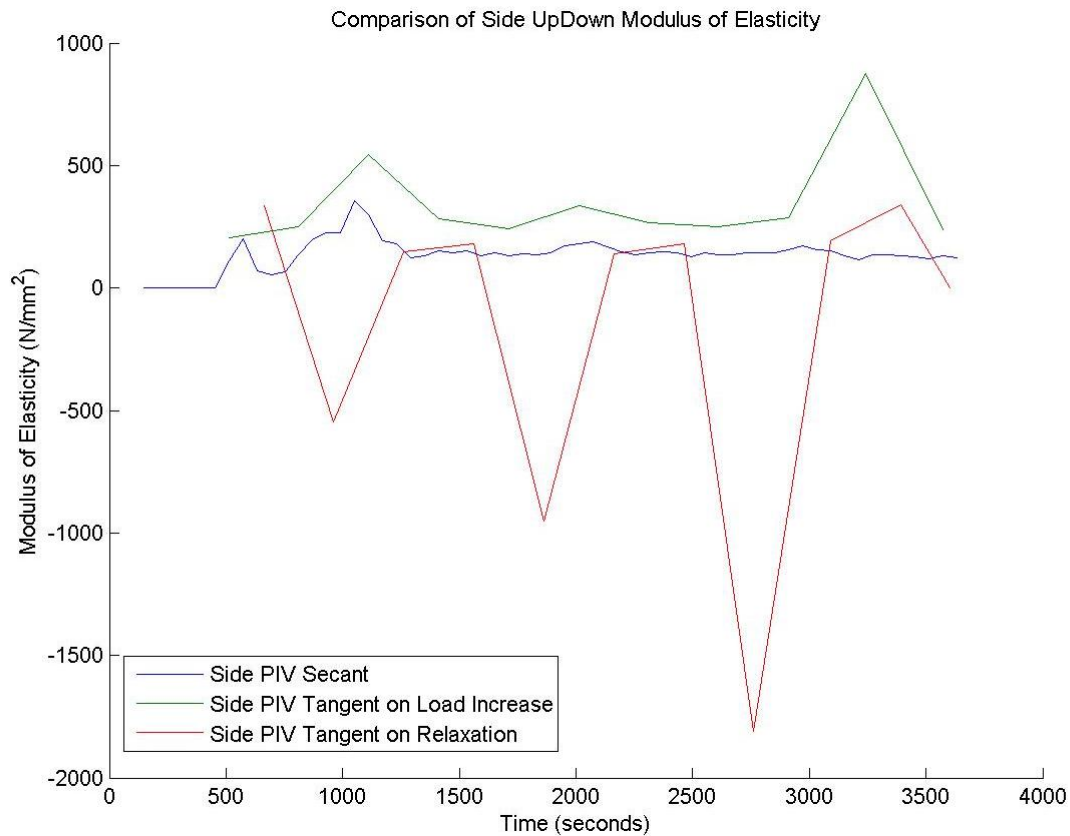
FIGURE 217: G5 SIDE VIEW PIV SECANT AND TANGENT MODULUS VS. TIME

Appendix 6
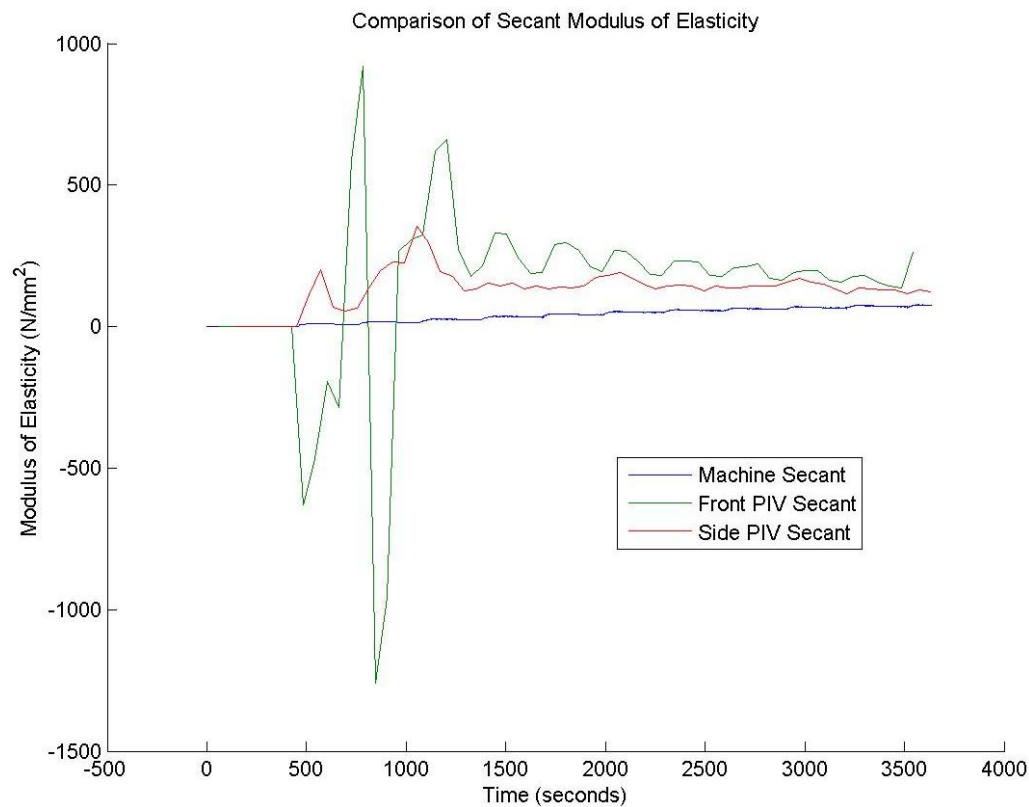
FIGURE 218: G5 COMPARISON OF MACHINE MEASURED AND PIV SECANT MODULUS VS. TIME
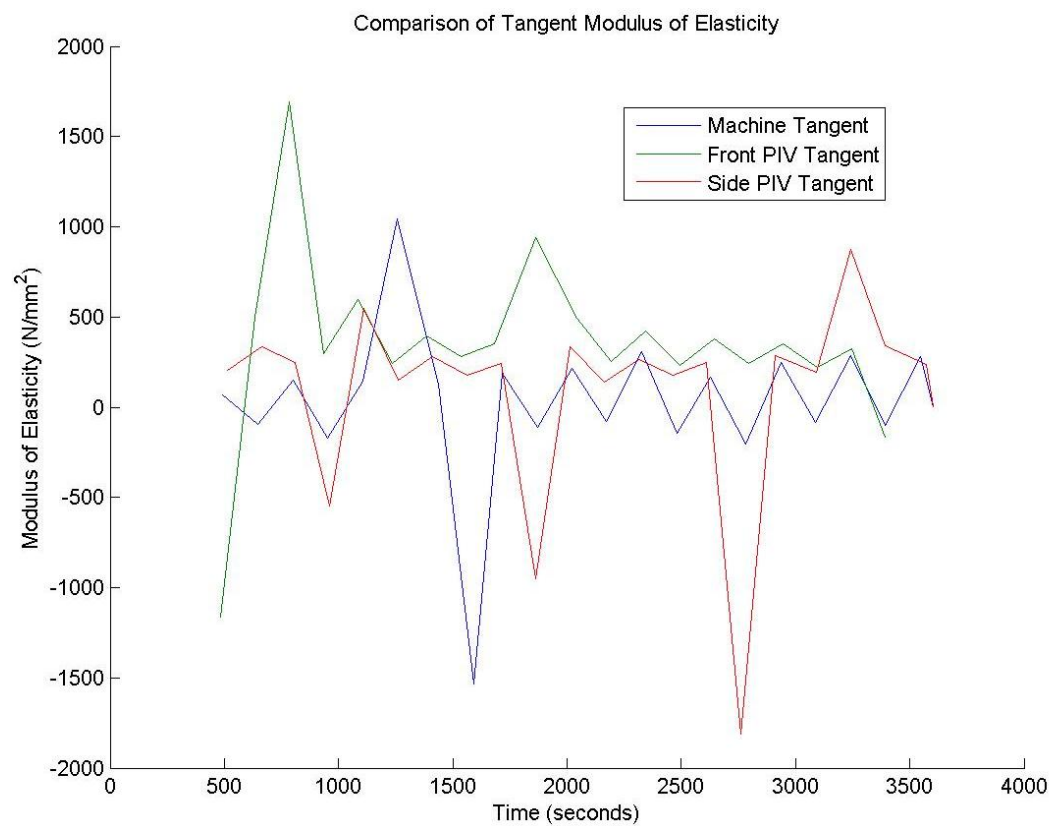
FIGURE 219: G5 COMPARISON OF MACHINE MEASURED AND PIV TANGENT MODULUS VS.

TIME

G5 Sample

FIGURE 220: SAMPLE GRAIN ORIENTATIONS OF THE FRONT (LEFT 4 IMAGES) AND SIDE (RIGHT 4 IMAGES) VIEW BEFORE (FIRST 2 OF 4 IMAGES) AND AFTER (LAST 2 OF 4 IMAGES) BREAKAGE
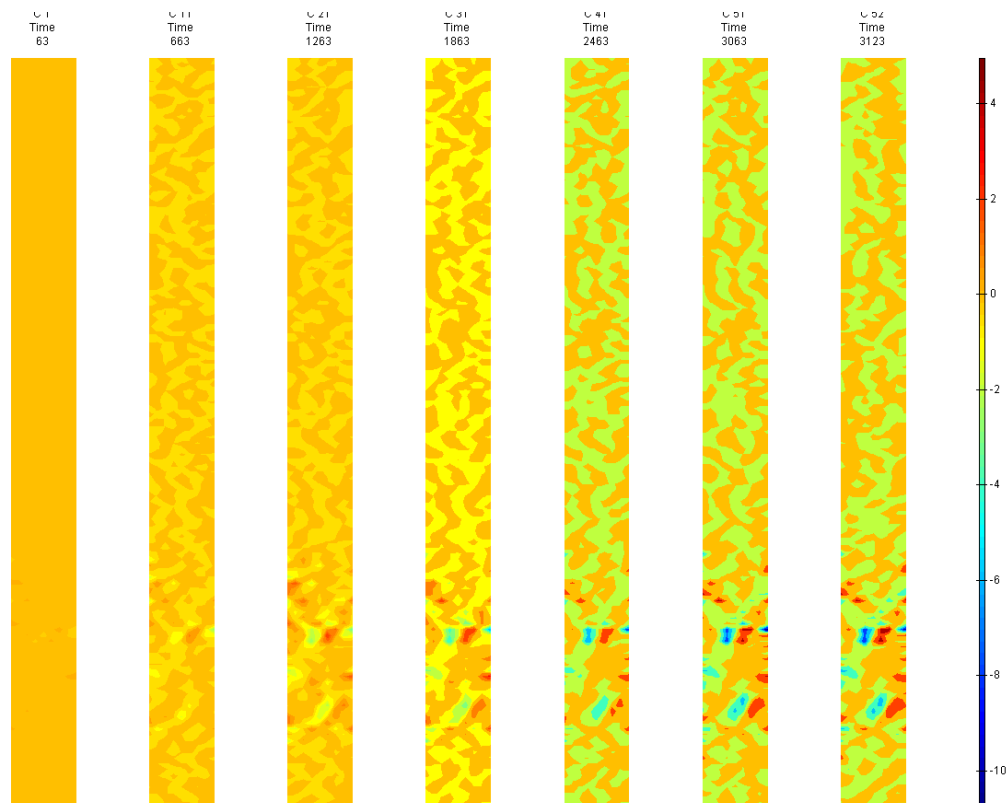
G5 Front View
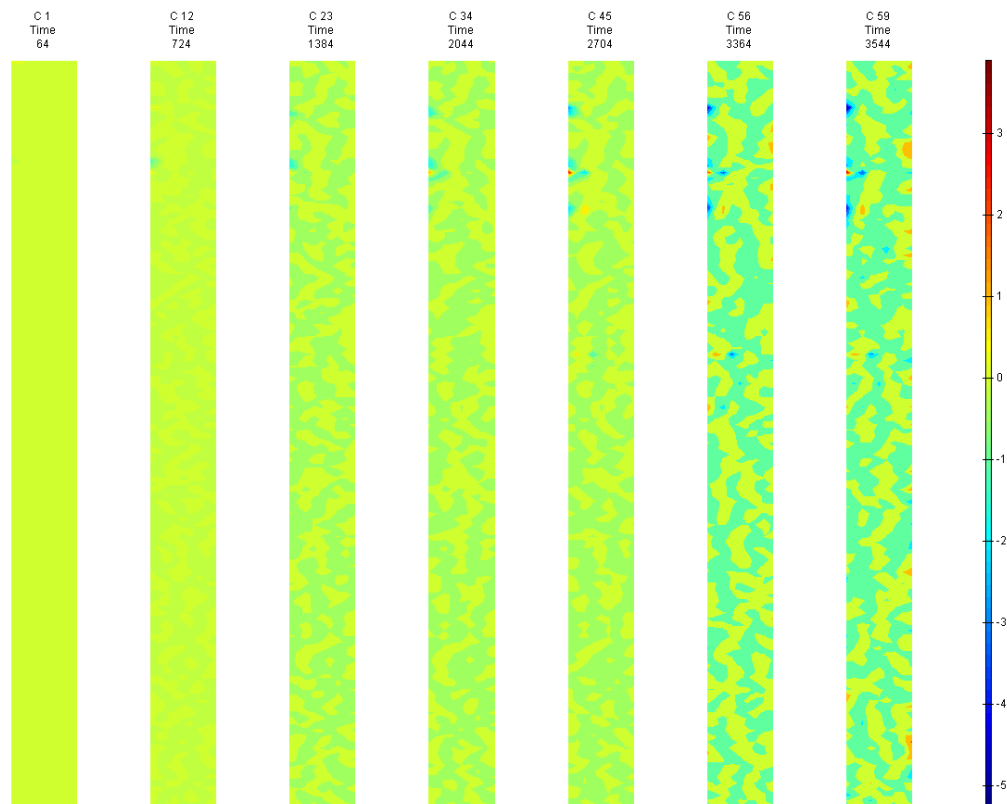
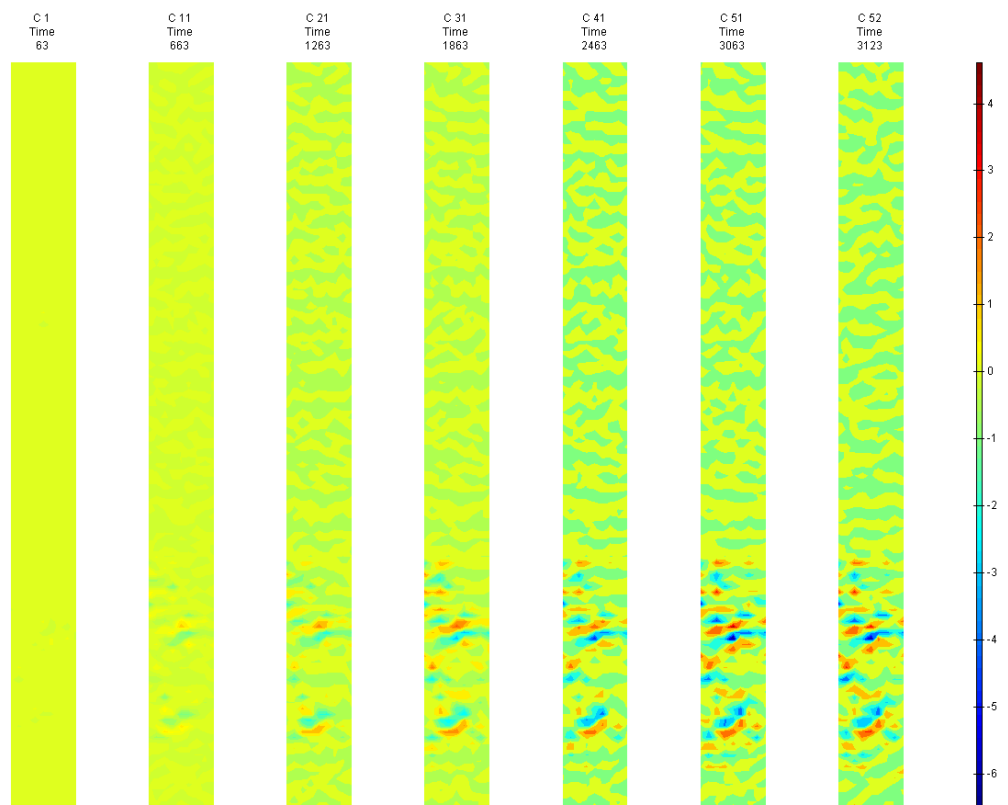FIGURE 221: X DIRECTION PIV SEQUENTIAL ENGINEERING STRAIN OVER TIME
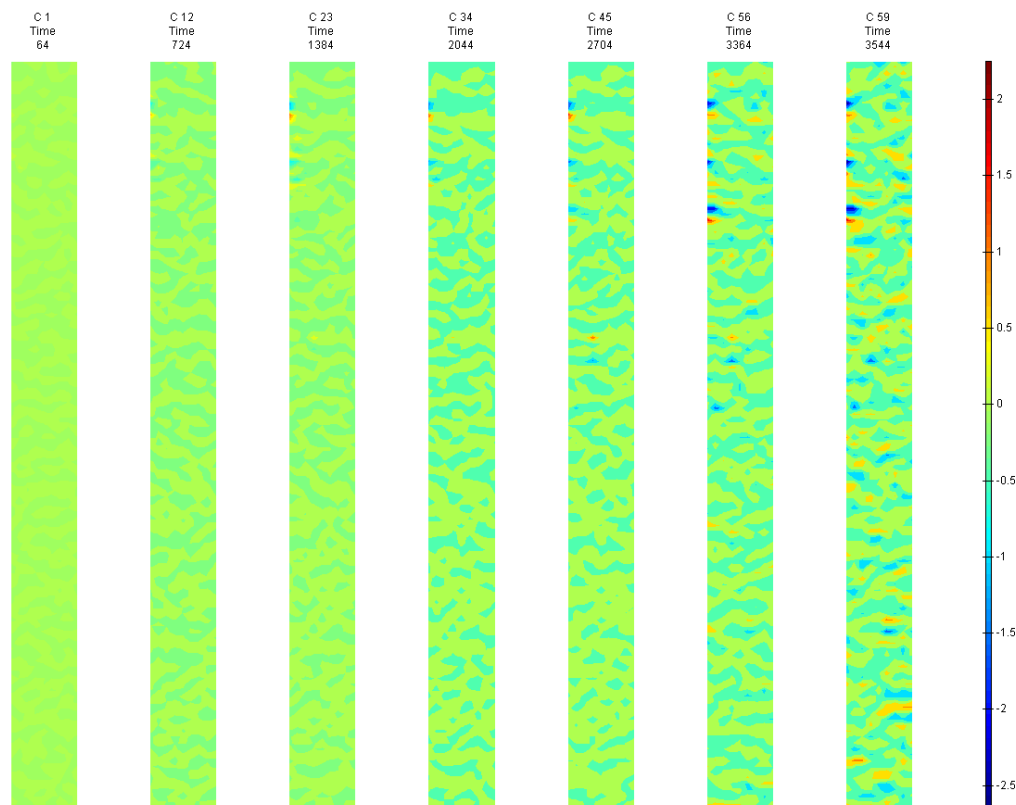
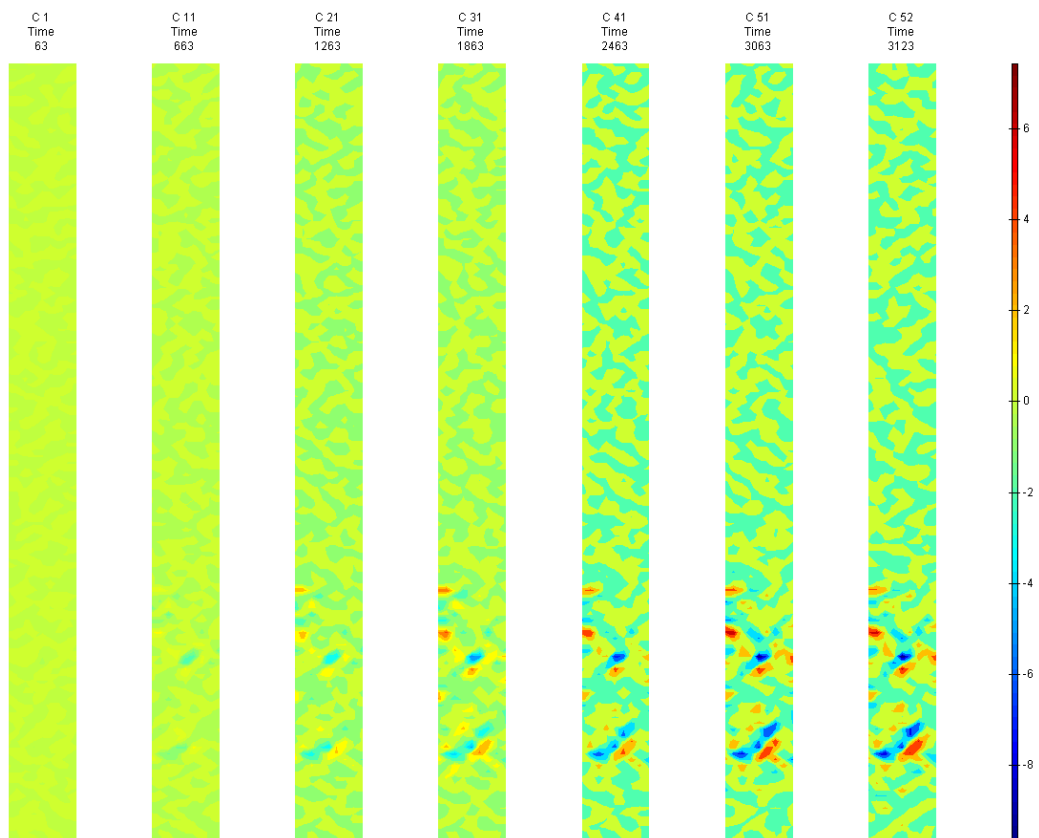FIGURE 222: Y DIRECTION PIV SEQUENTIAL ENGINEERING STRAIN OVER TIME
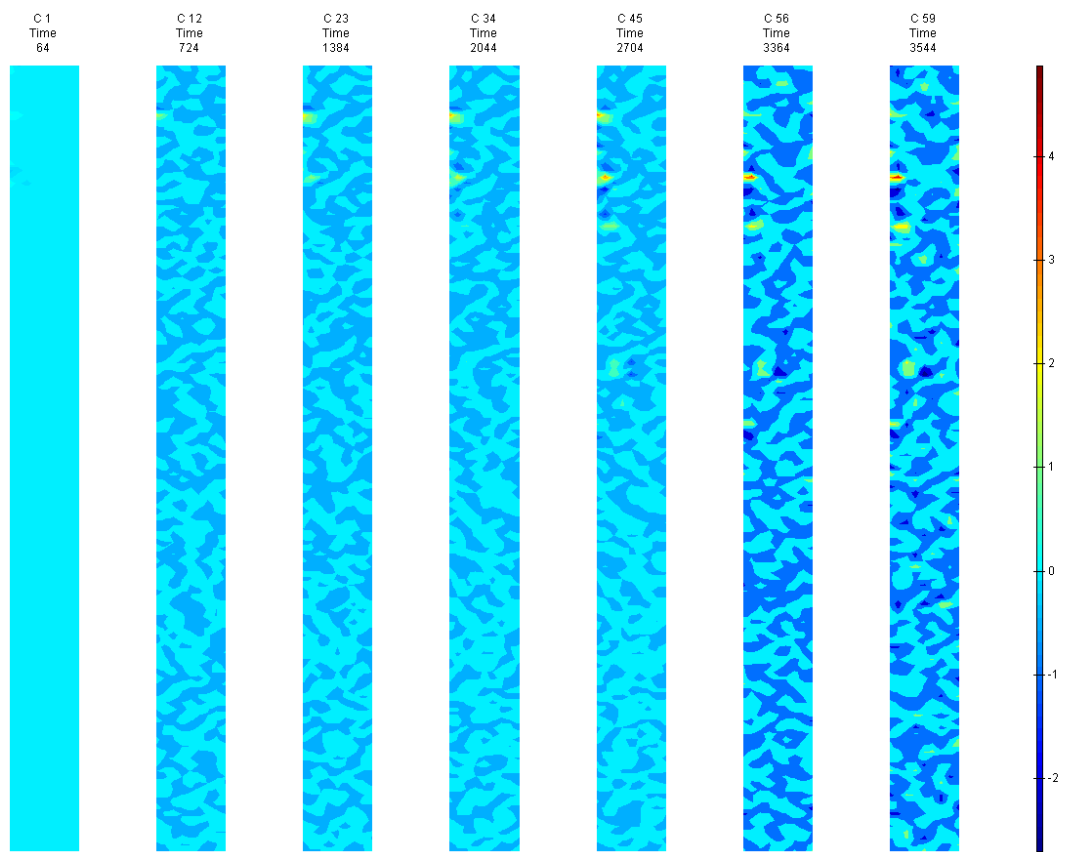
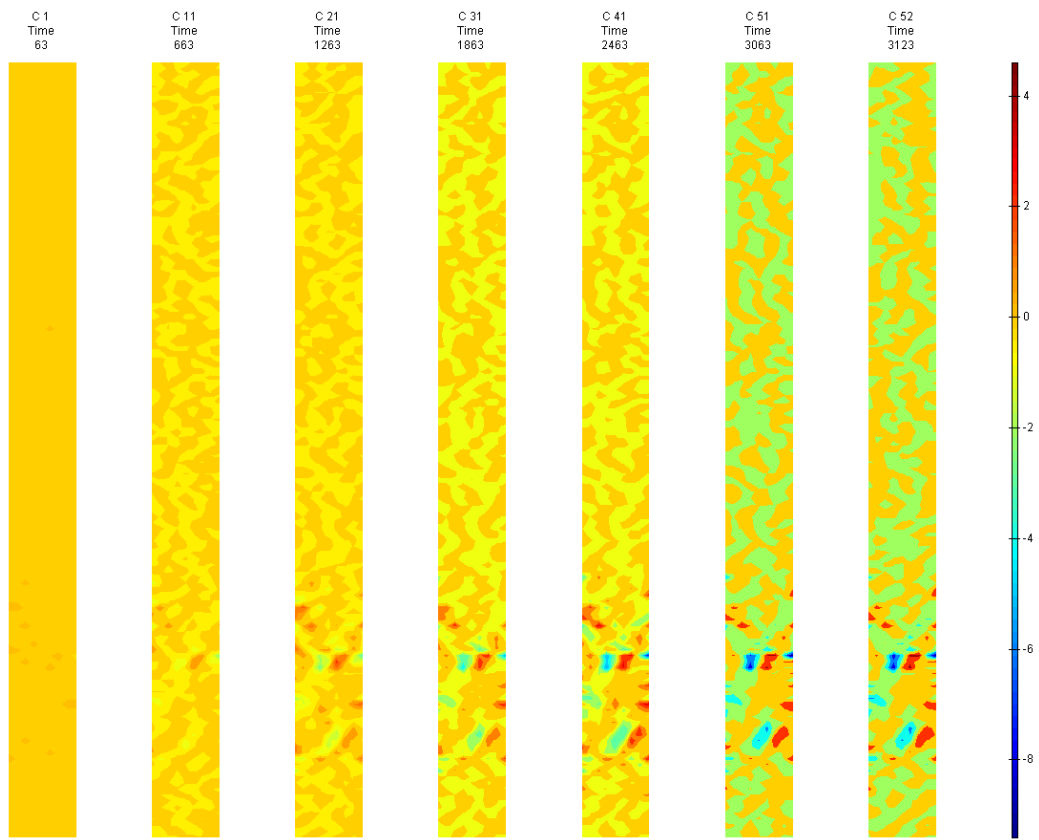FIGURE 223: XY DIRECTION PIV SEQUENTIAL ENGINEERING SHEAR STRAIN OVER TIME
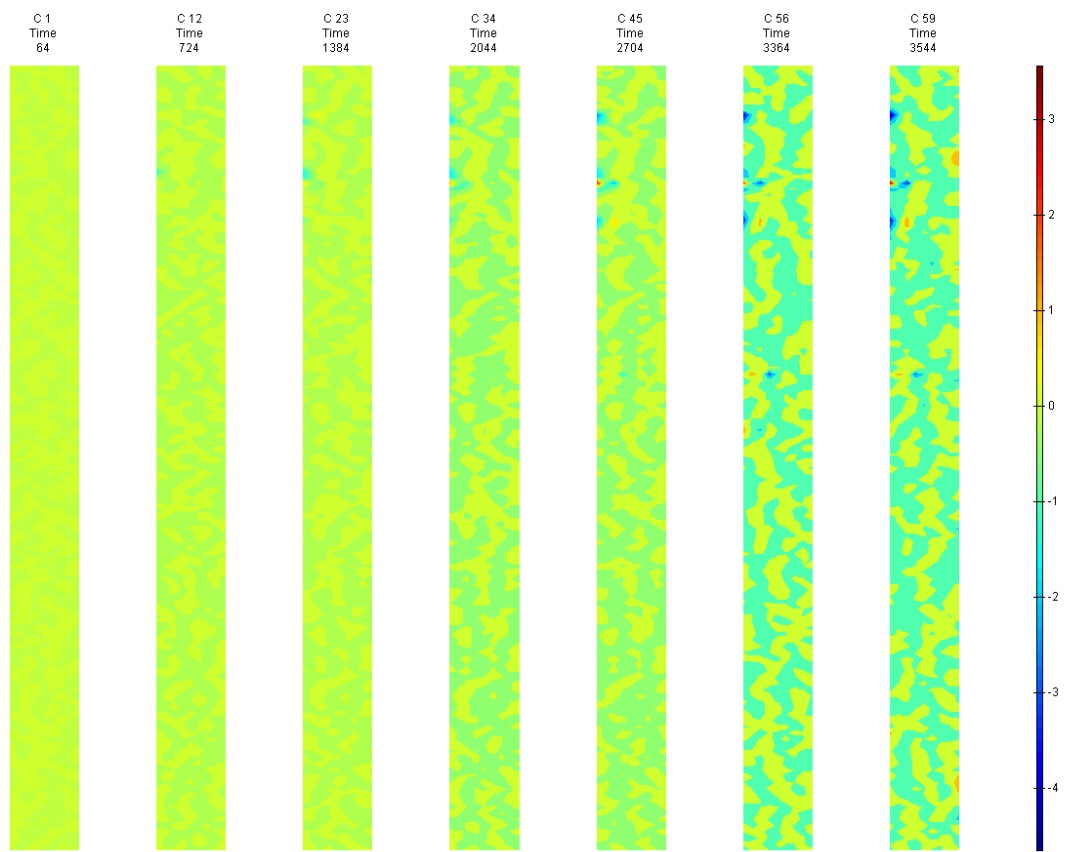
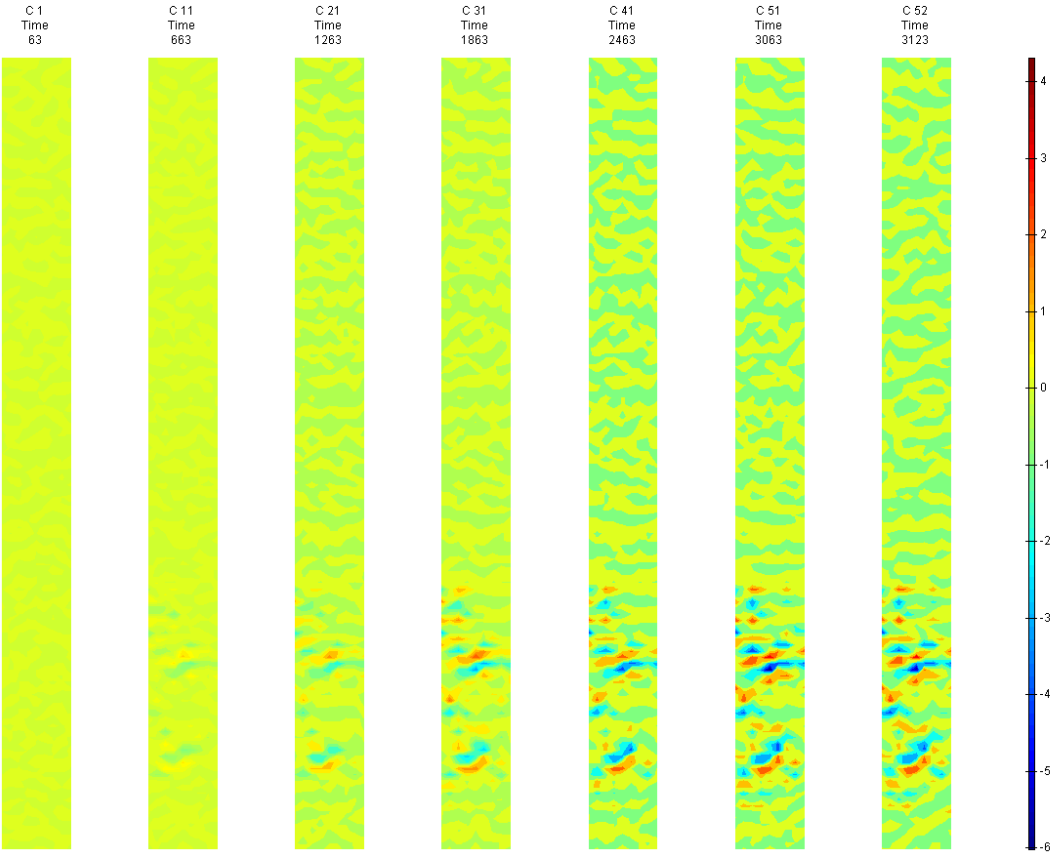FIGURE 224: X DIRECTION PIV SEQUENTIAL TRUE STRAIN OVER TIME
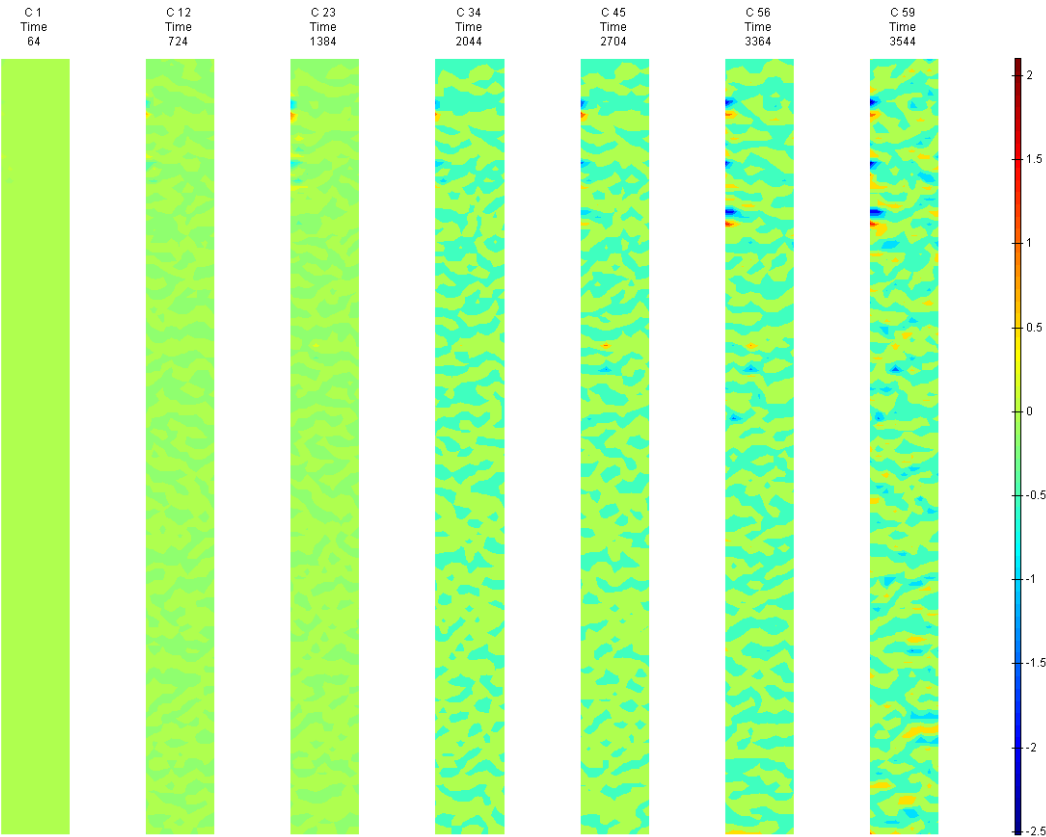
FIGURE 225: Y DIRECTION PIV SEQUENTIAL TRUE STRAIN OVER TIME
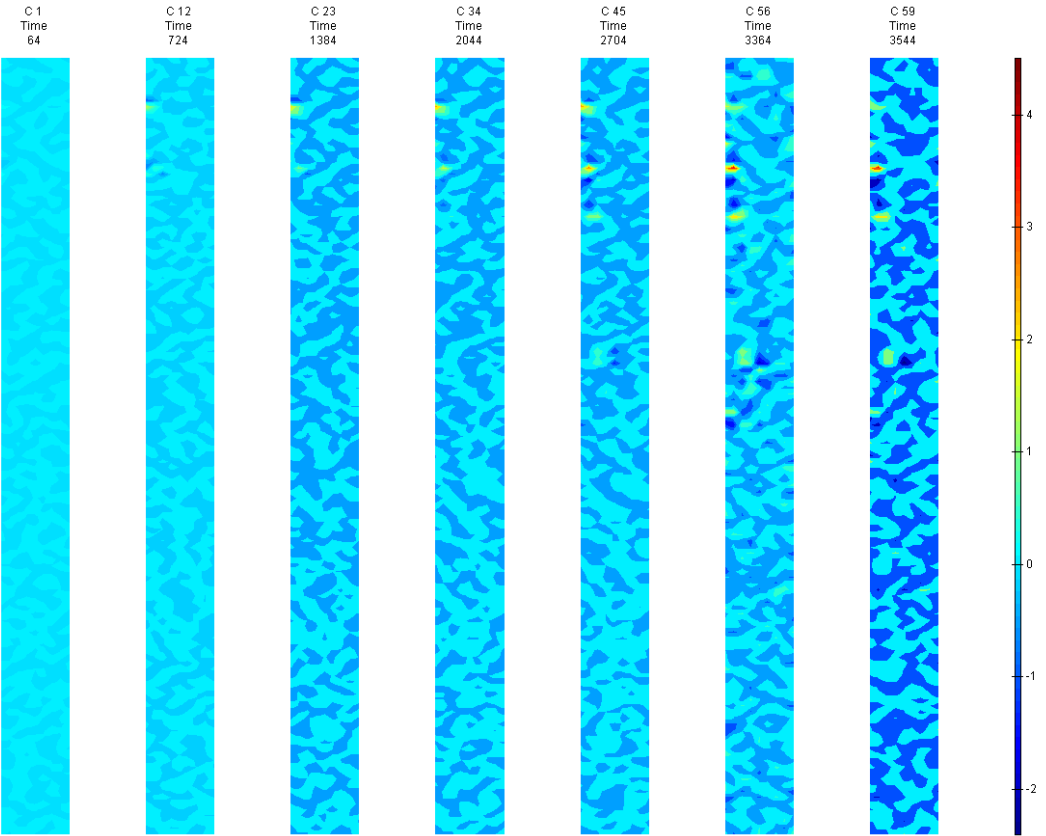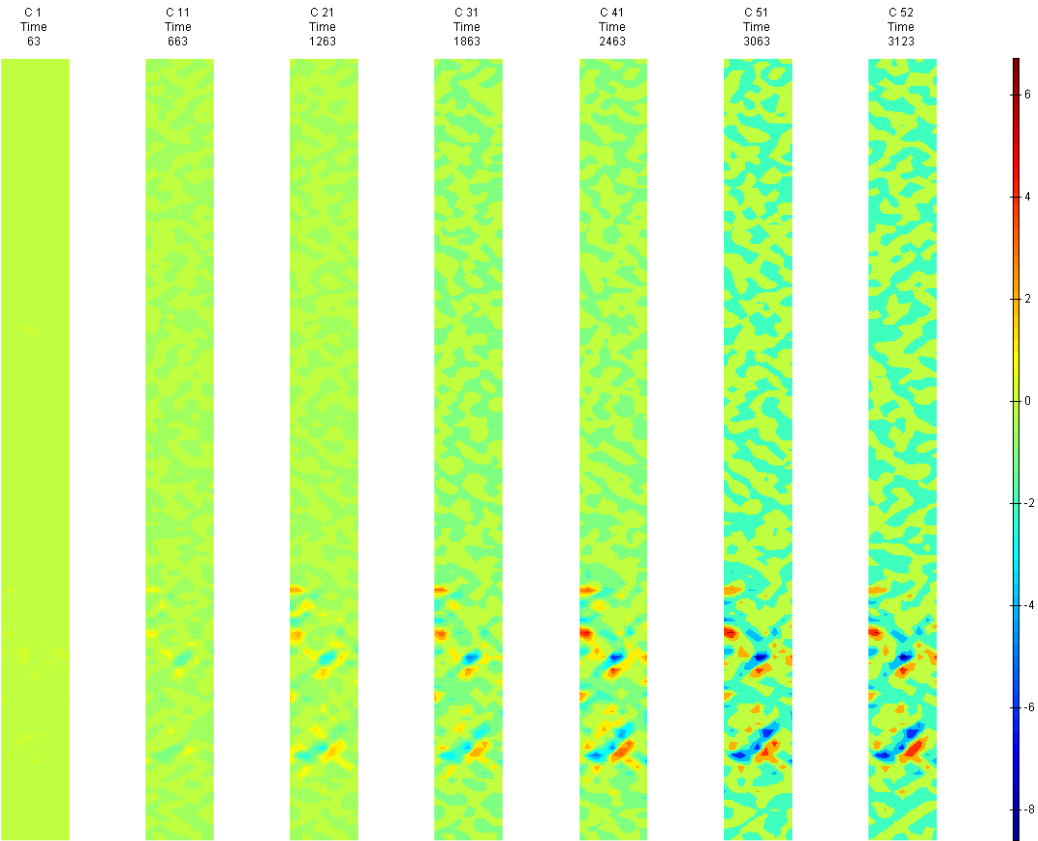

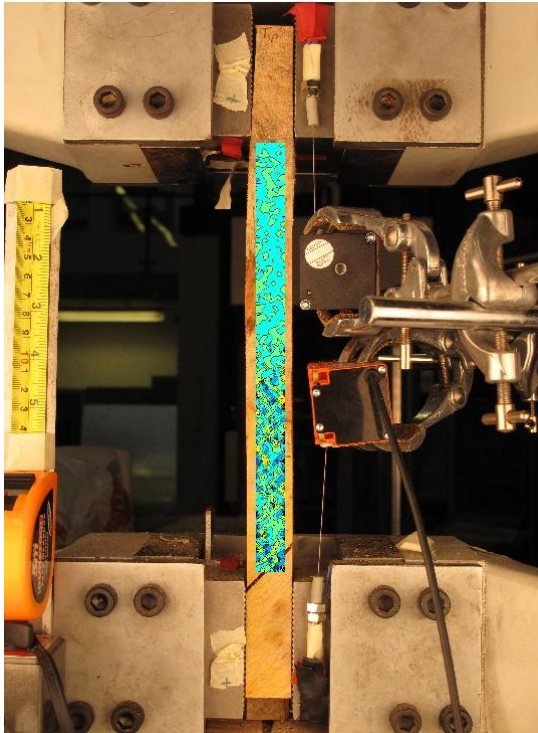FIGURE 226: XY DIRECTION PIV SEQUENTIAL TRUE SHEAR STRAIN OVER TIME
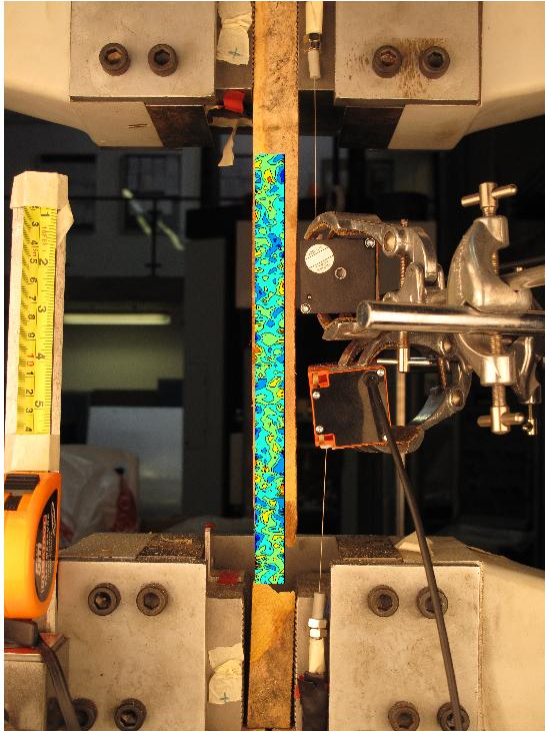
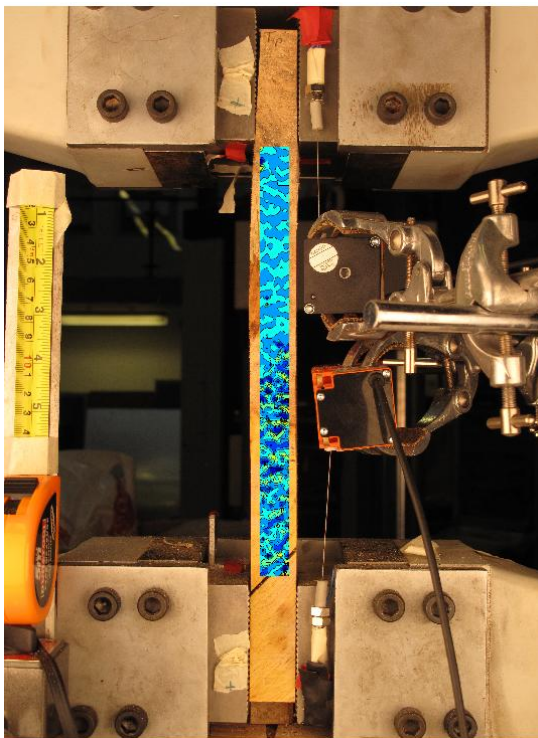FIGURE 227: X DIRECTION PIV FIRST–LAST DITCH ENGINEERING STRAIN OVER IMAGE
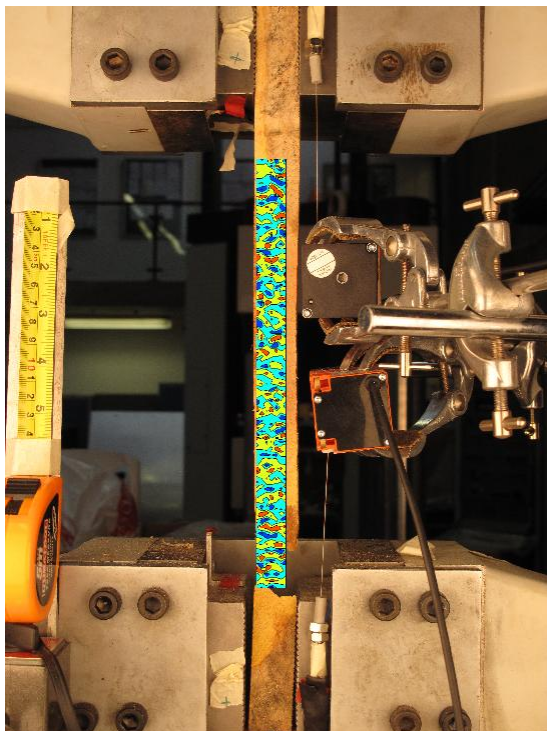
FIGURE 228: Y DIRECTION PIV FIRST–LAST DITCH ENGINEERING STRAIN OVER IMAGE

Appendix 6
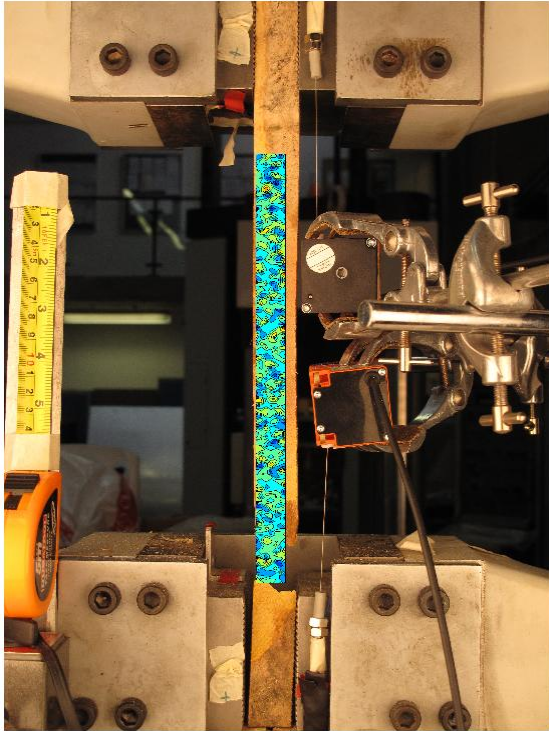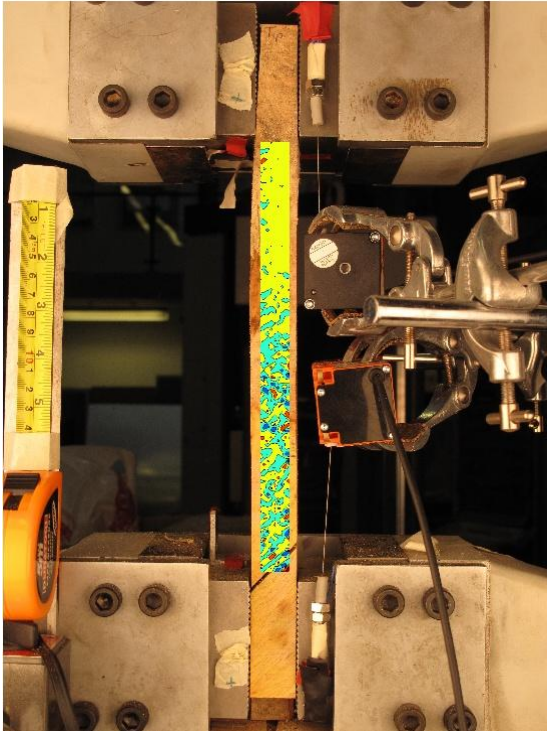

FIGURE 229: XY DIRECTION PIV FIRST–LAST DITCH ENGINEERING SHEAR STRAIN OVER
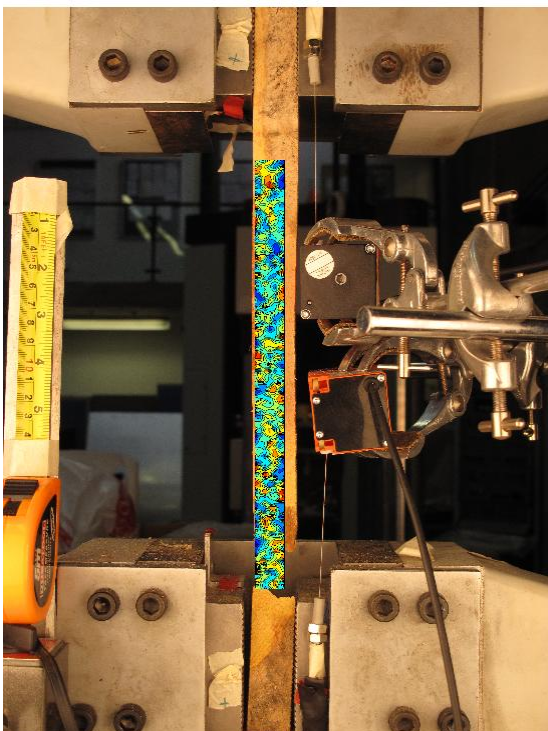
IMAGE
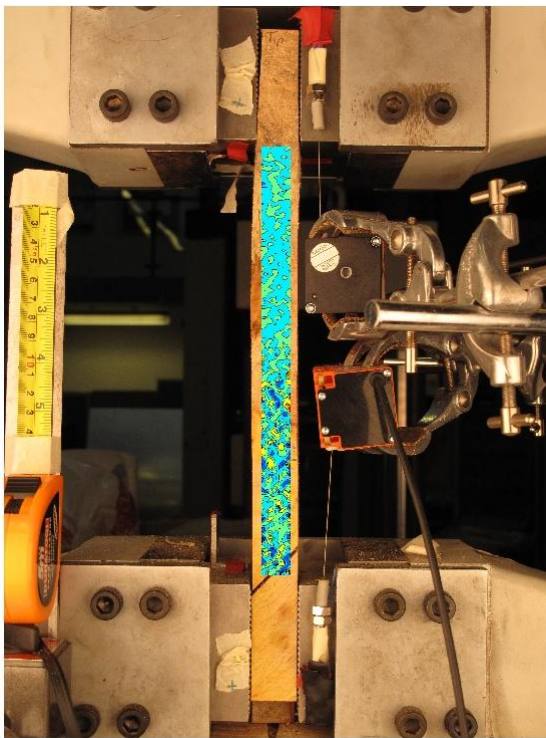

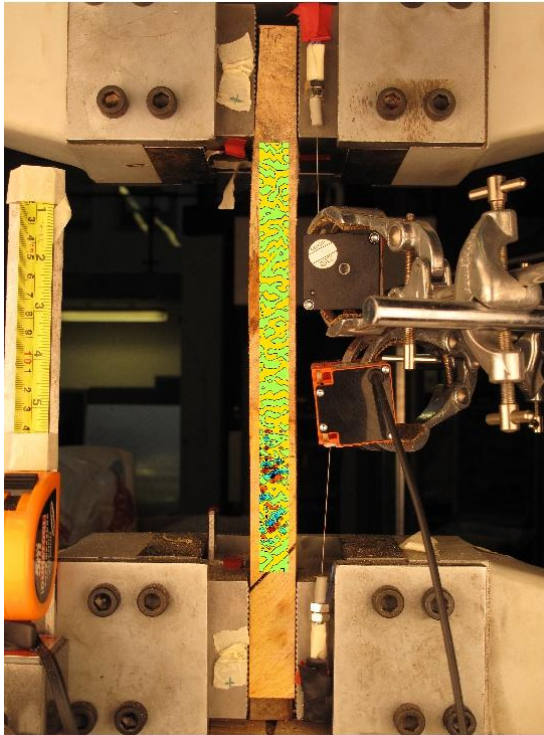FIGURE 230: X DIRECTION PIV FIRST–LAST DITCH TRUE STRAIN OVER IMAGE
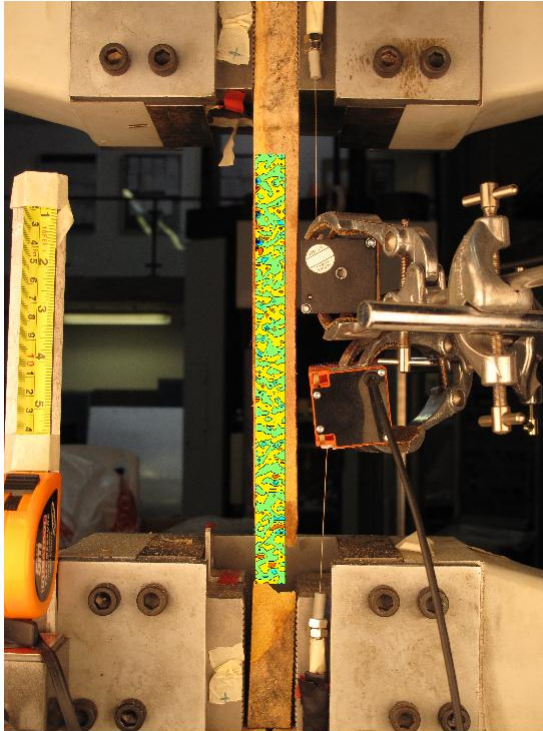
FIGURE 231: Y DIRECTION PIV FIRST–LAST DITCH TRUE STRAIN OVER IMAGE
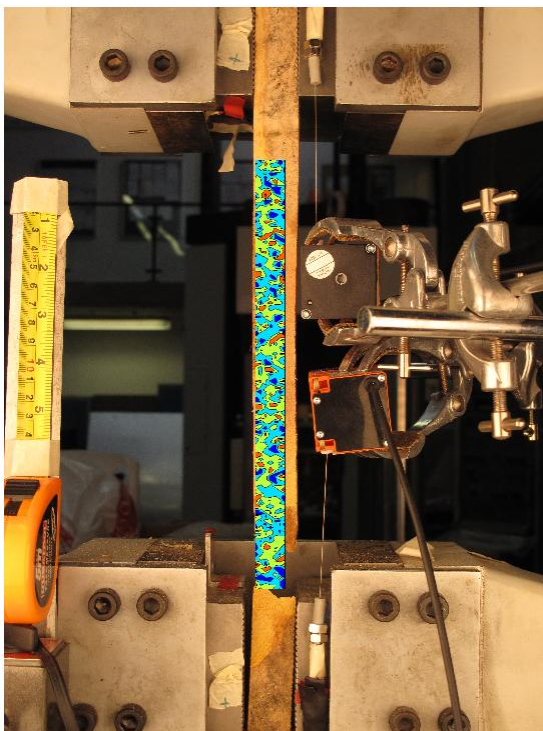
FIGURE 232: XY DIRECTION PIV FIRST–LAST DITCH TRUE SHEAR STRAIN OVER IMAGE

Appendix 6
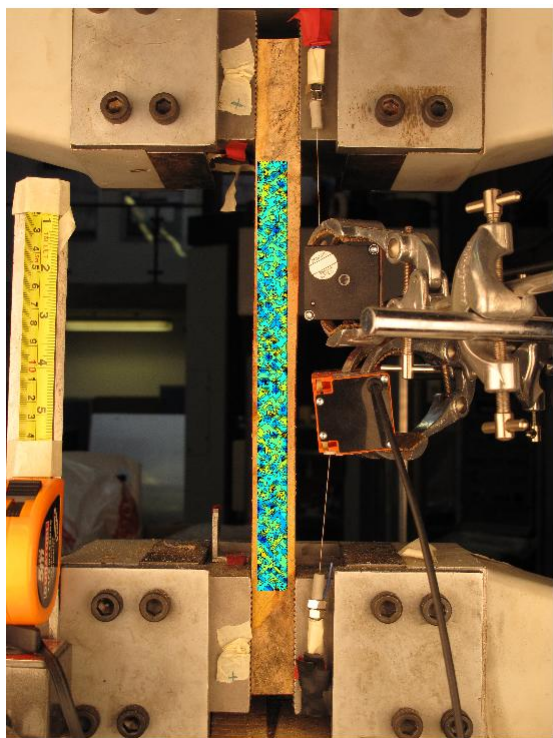
FIGURE 233: XY DIRECTION PIV FIRST-SEQUENTIAL ENGINEERING SHEAR STRAIN OVER

IMAGE
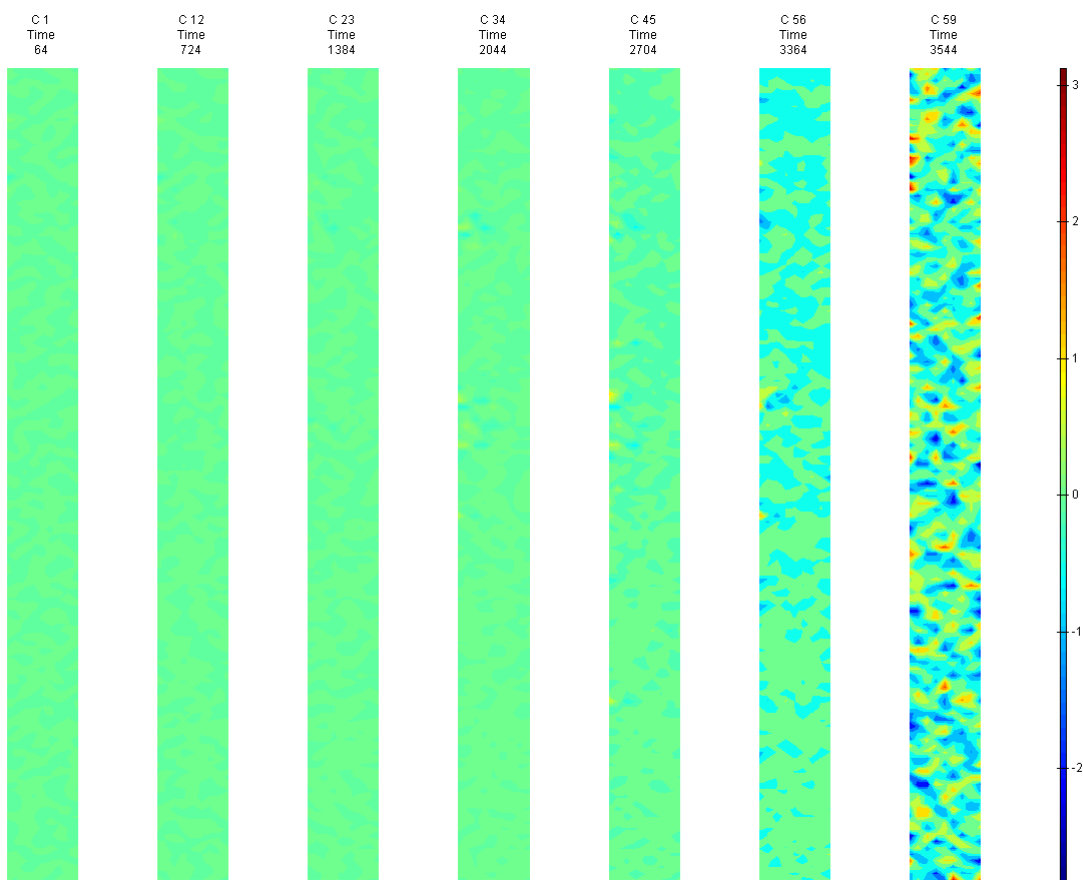
FIGURE 234: XY DIRECTION PIV FIRST-SEQUENTIAL ENGINEERING SHEAR STRAIN OVER TIME

G5 Side View
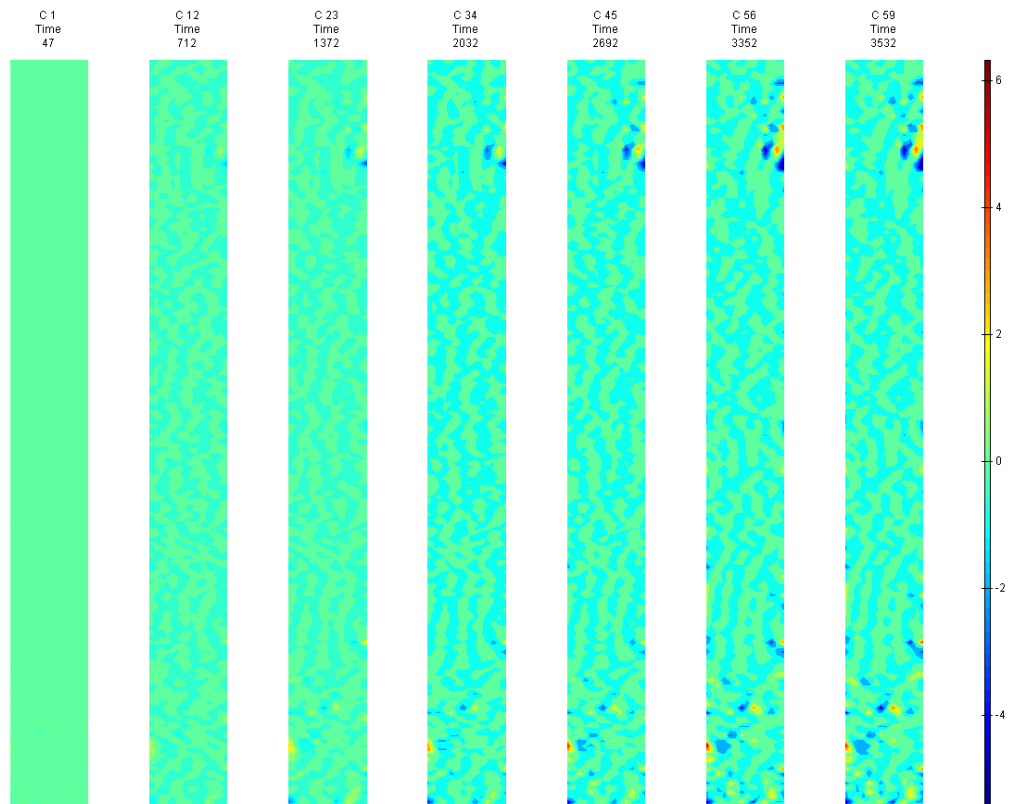
FIGURE 235: X DIRECTION PIV SEQUENTIAL ENGINEERING STRAIN OVER TIME
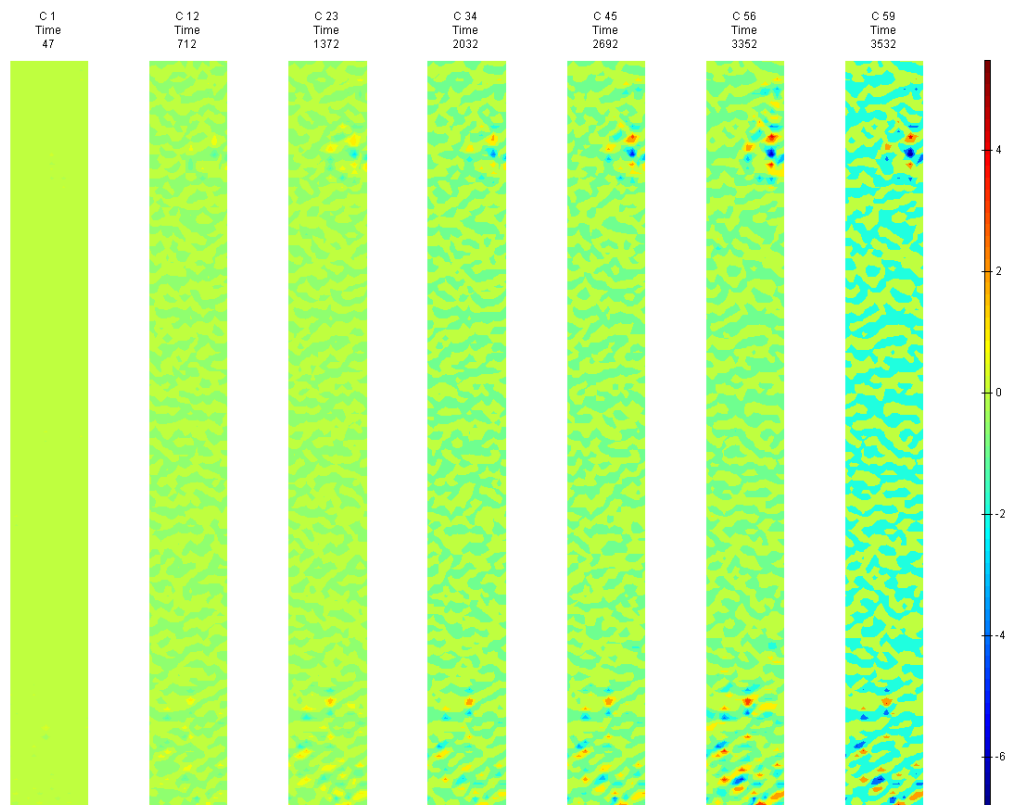
FIGURE 236: Y DIRECTION PIV SEQUENTIAL ENGINEERING STRAIN OVER TIME

Appendix 6
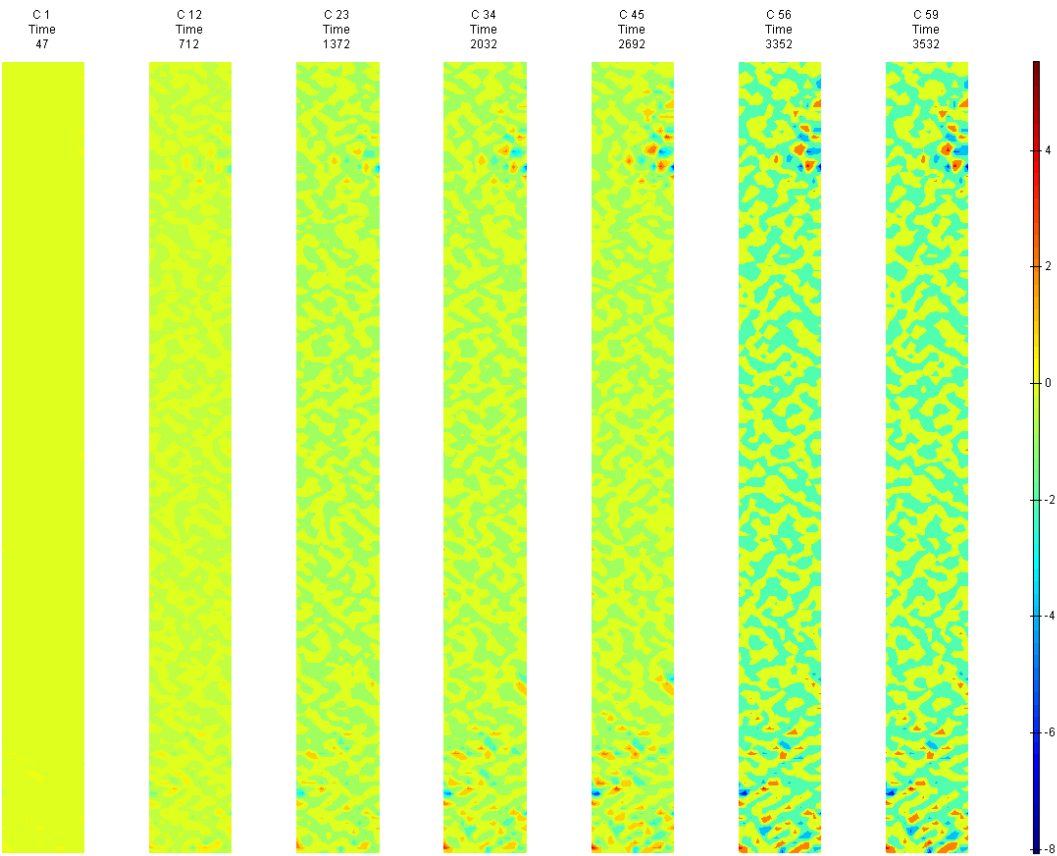
FIGURE 237: XY DIRECTION PIV SEQUENTIAL ENGINEERING SHEAR STRAIN OVER TIME
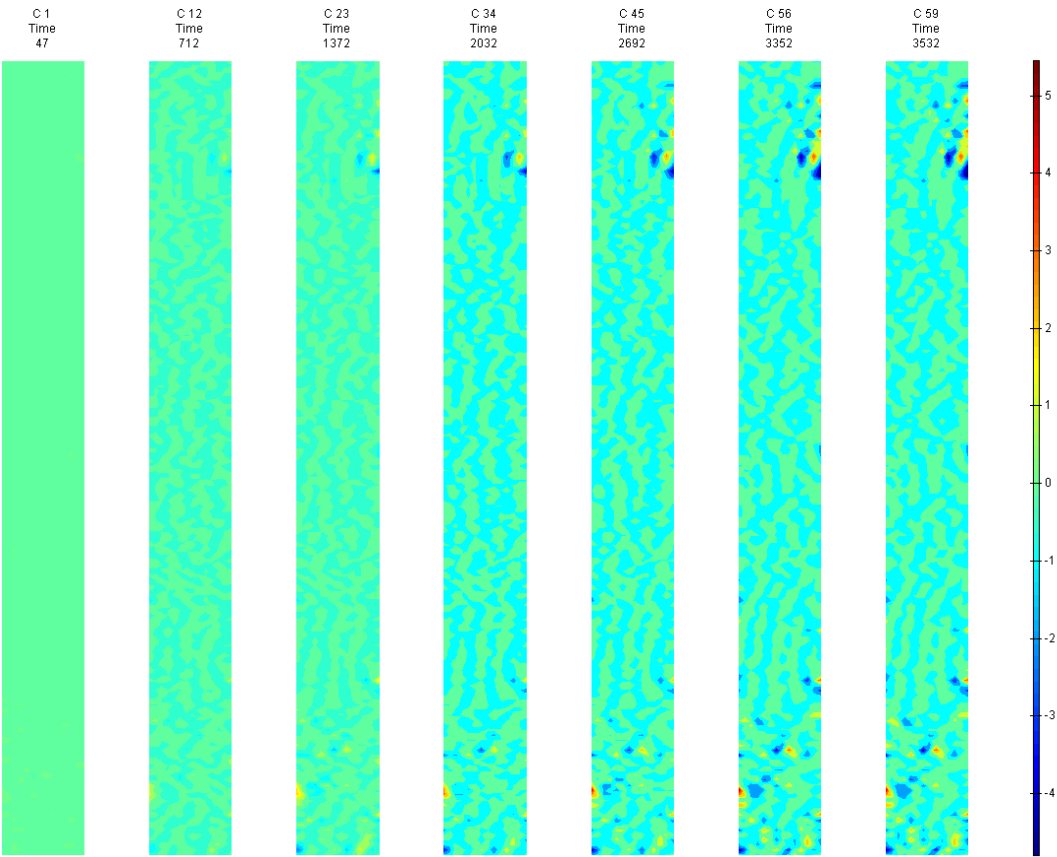
FIGURE 238: X DIRECTION PIV SEQUENTIAL TRUE STRAIN OVER TIME
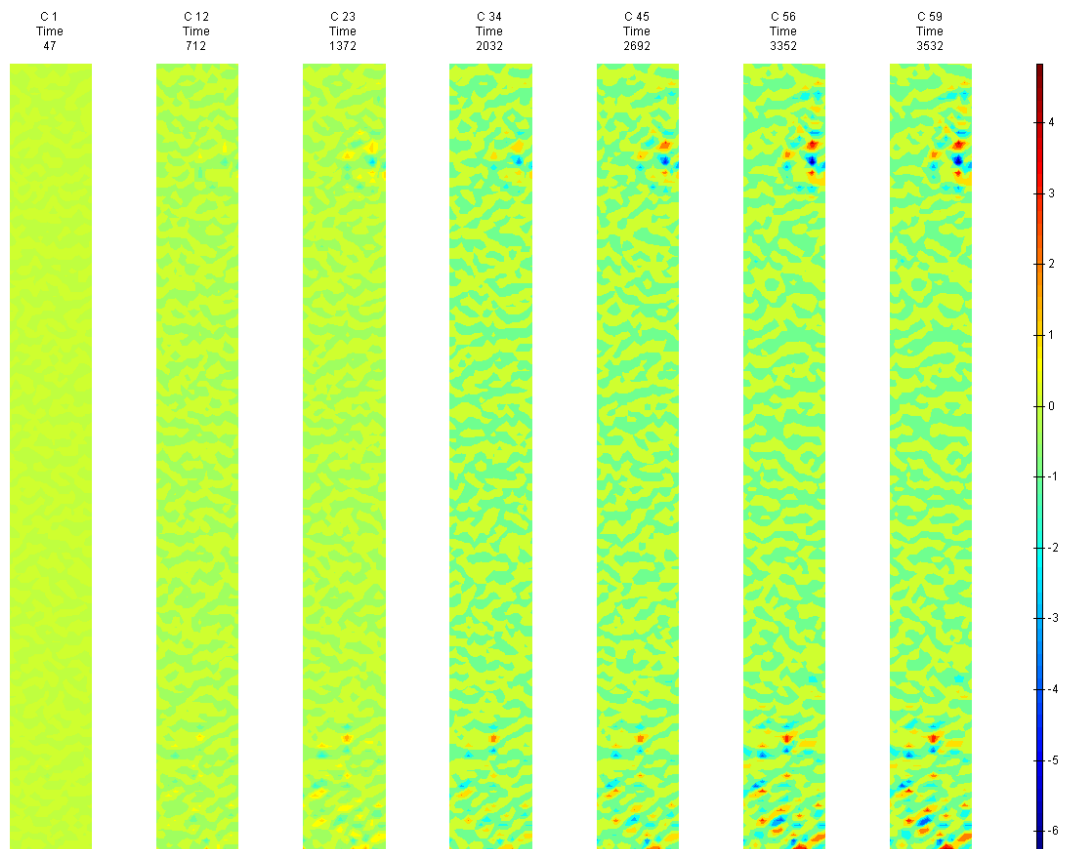
FIGURE 239: Y DIRECTION PIV SEQUENTIAL TRUE STRAIN OVER TIME
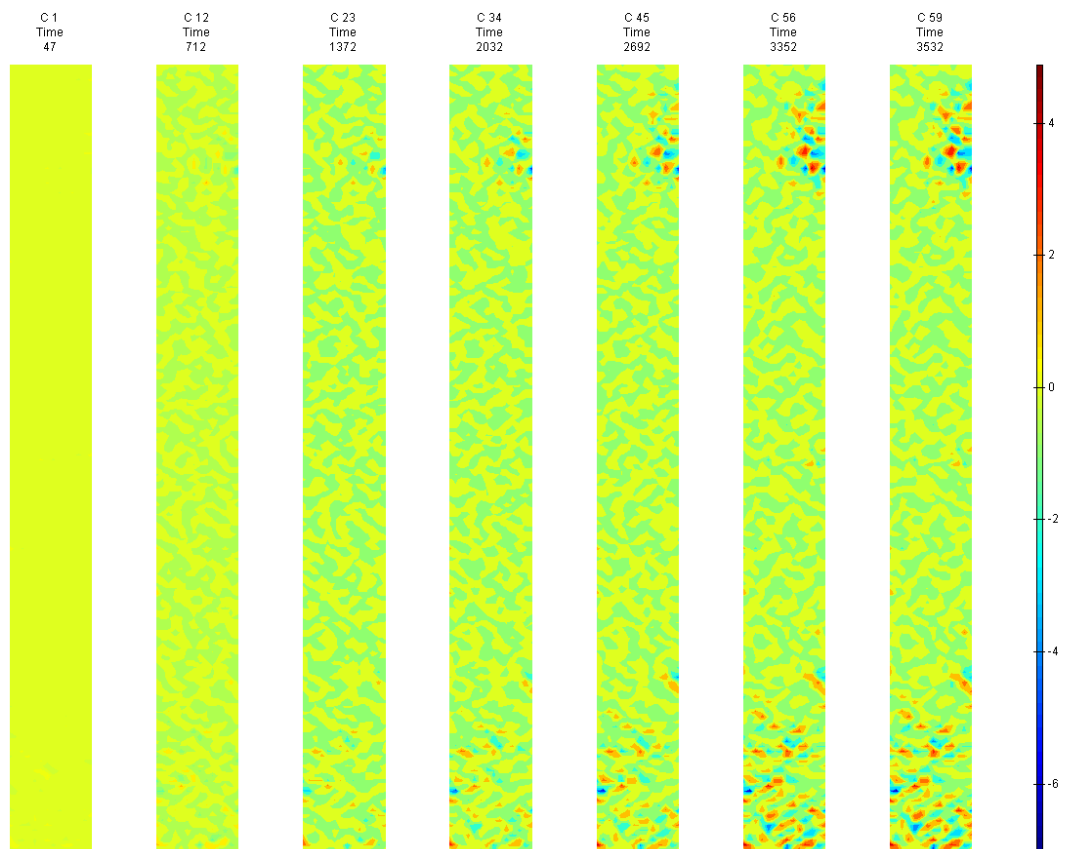
FIGURE 240: XY DIRECTION PIV SEQUENTIAL TRUE SHEAR STRAIN OVER TIME

Appendix 6
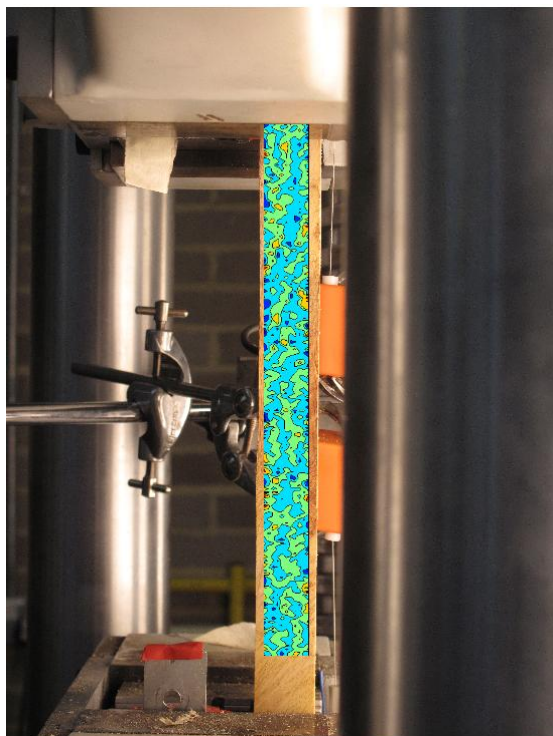
FIGURE 241: X DIRECTION PIV FIRST–LAST DITCH ENGINEERING STRAIN OVER IMAGE
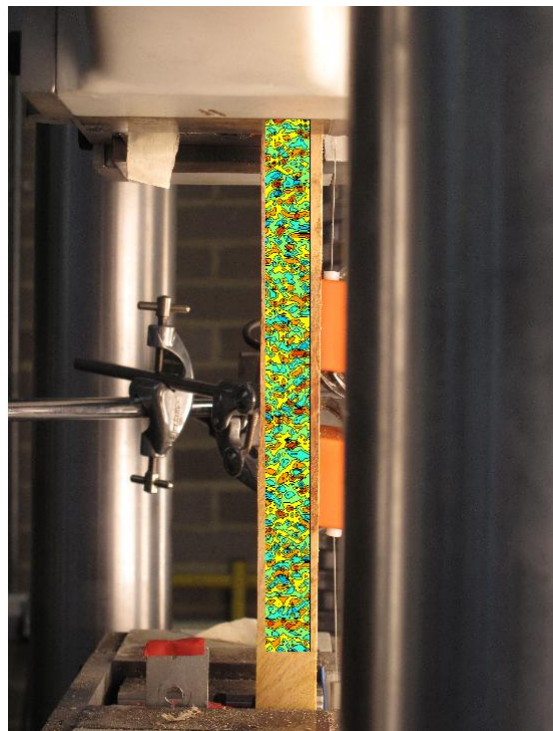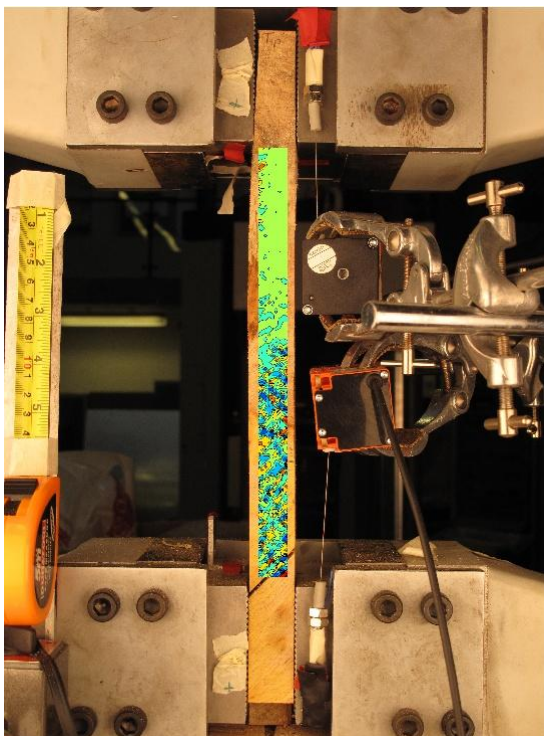

FIGURE 242: Y DIRECTION PIV FIRST–LAST DITCH ENGINEERING STRAIN OVER IMAGE
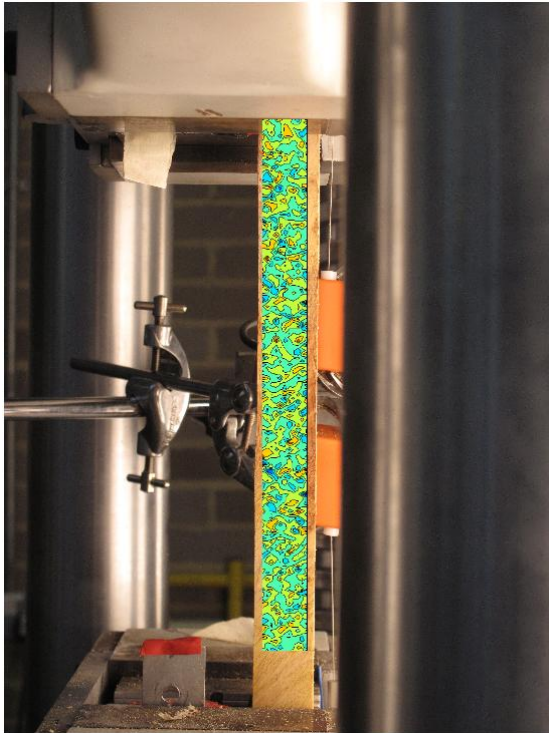
FIGURE 243: XY DIRECTION PIV FIRST–LAST DITCH ENGINEERING SHEAR STRAIN OVER
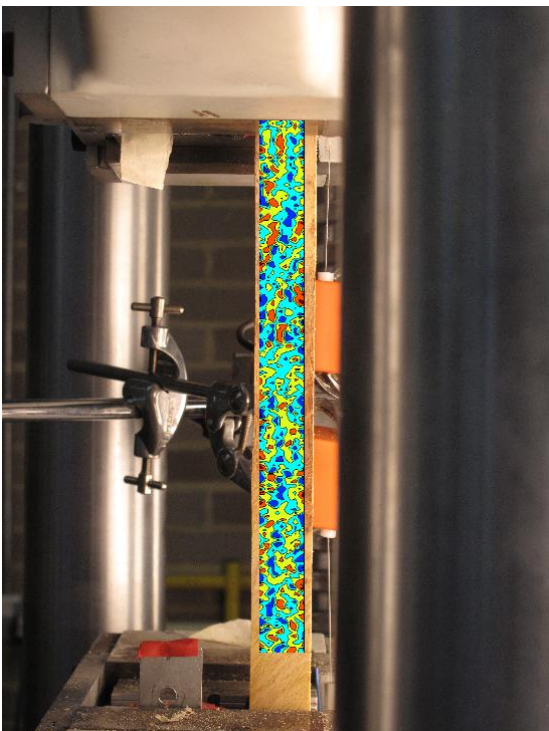
IMAGE

FIGURE 244: X DIRECTION PIV FIRST–LAST DITCH TRUE STRAIN OVER IMAGE

Appendix 6
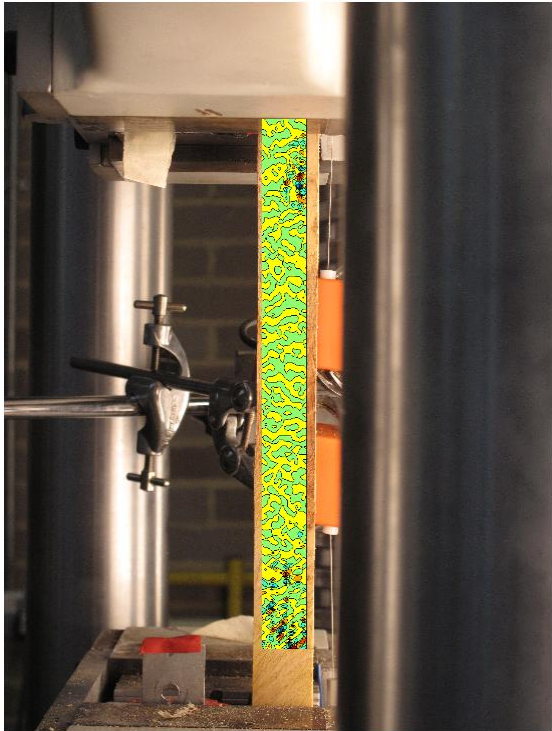
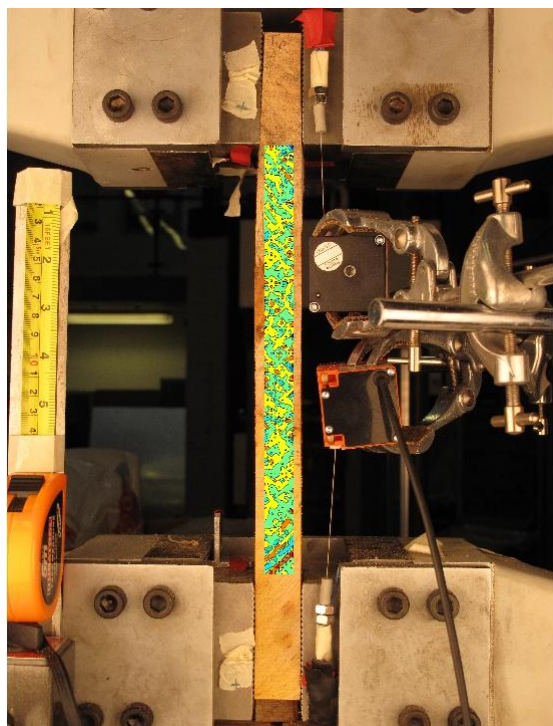FIGURE 245: Y DIRECTION PIV FIRST-LAST DITCH TRUE STRAIN OVER IMAGE
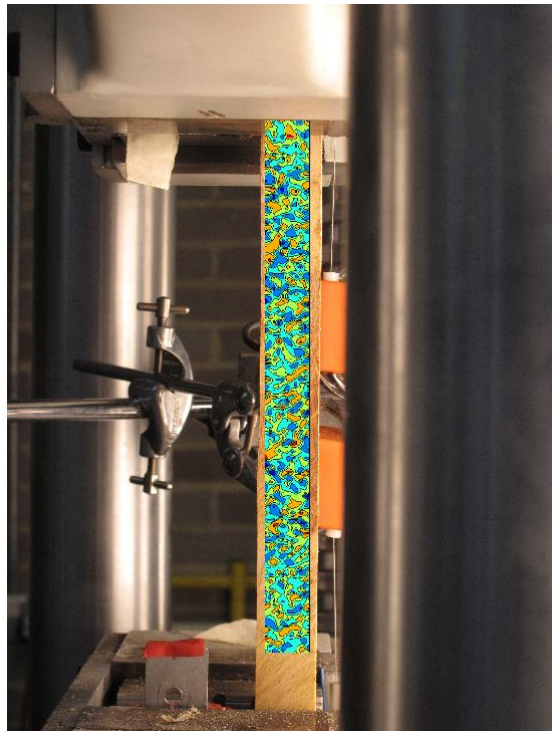
FIGURE 246: XY DIRECTION PIV FIRST-LAST DITCH TRUE SHEAR STRAIN OVER IMAGE
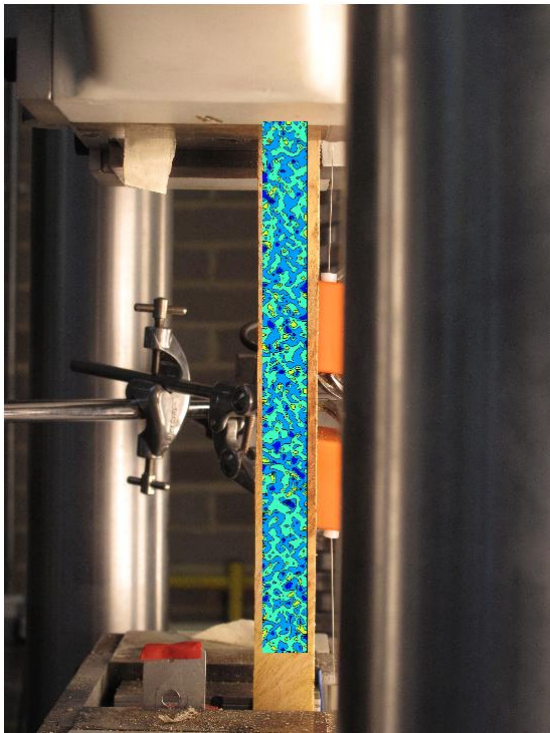
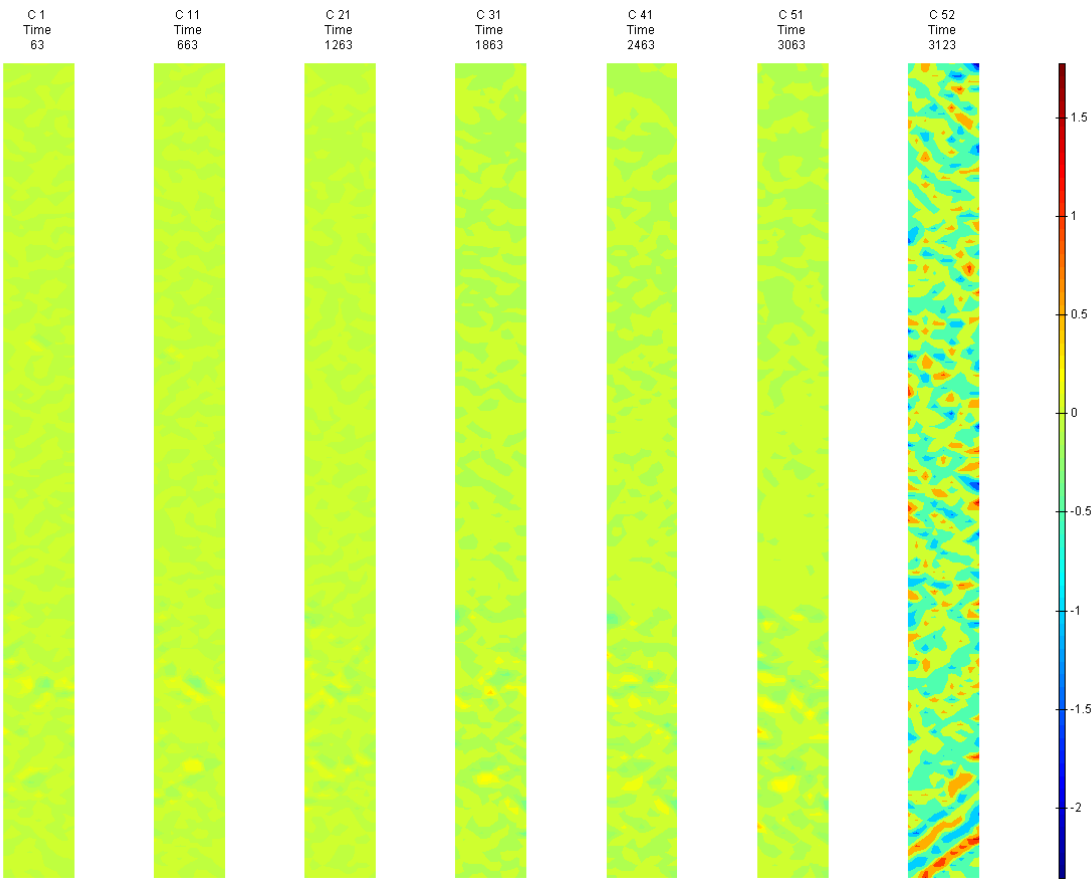FIGURE 247: XY DIRECTION PIV FIRST–SEQUENTIAL ENGINEERING SHEAR STRAIN OVER

IMAGE
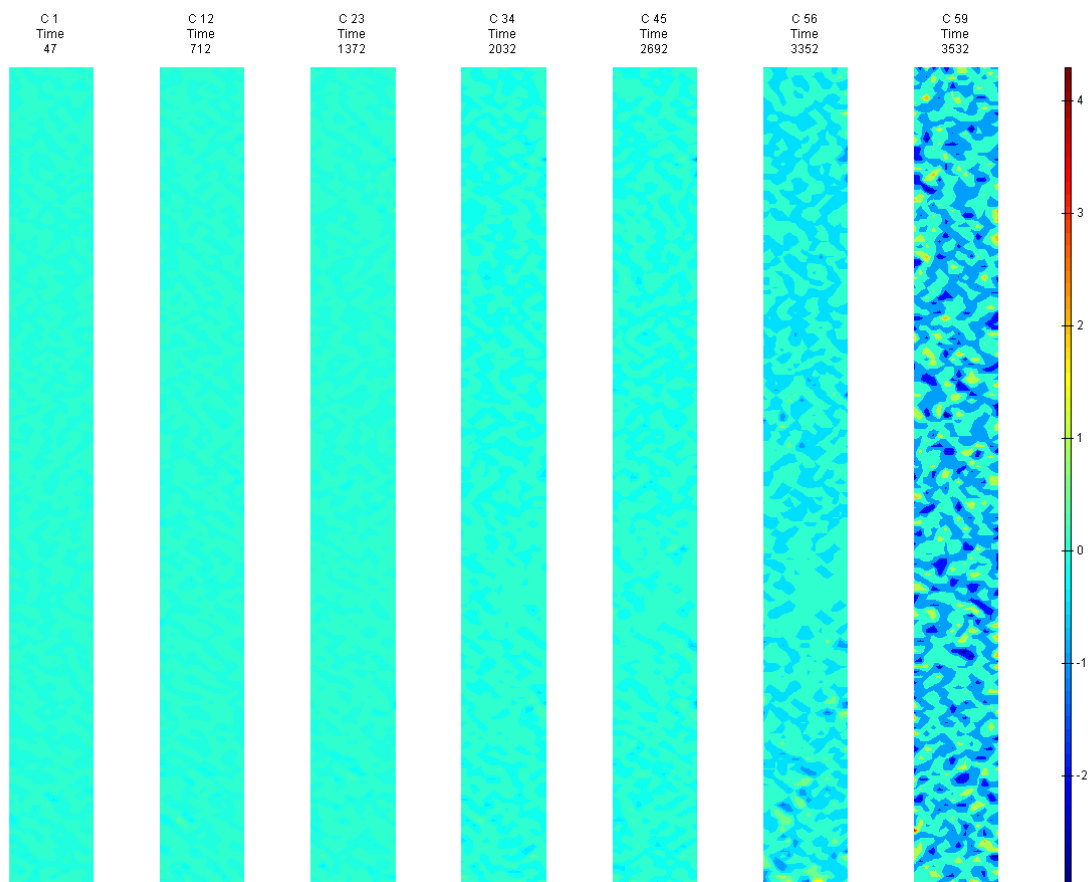
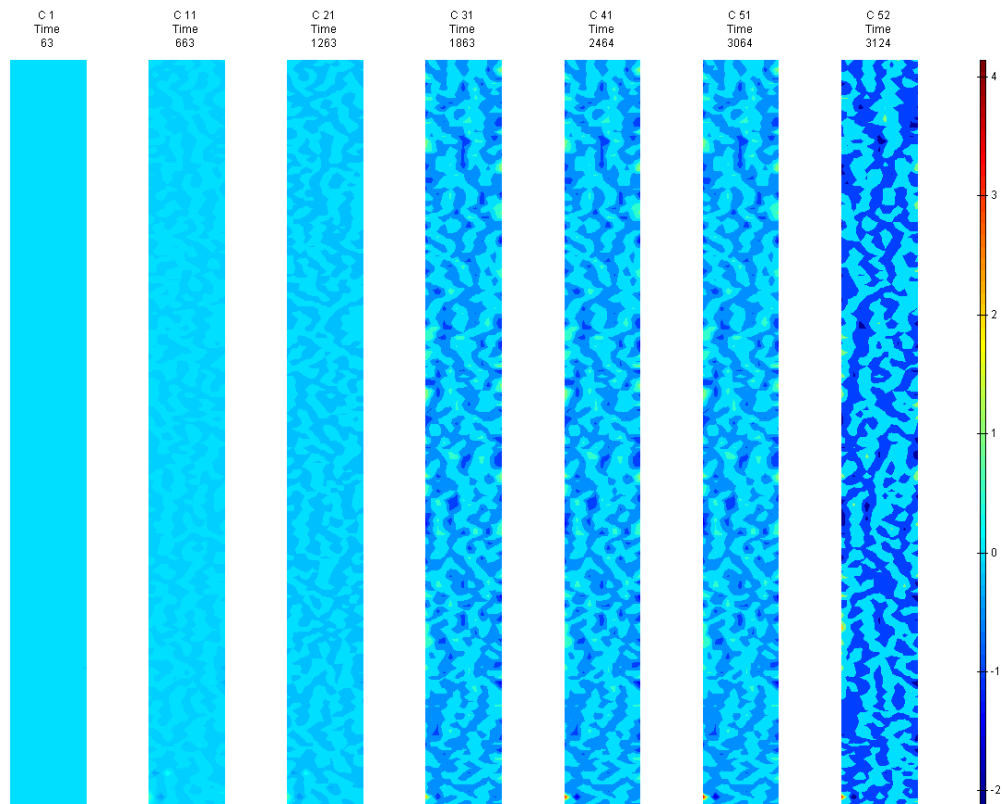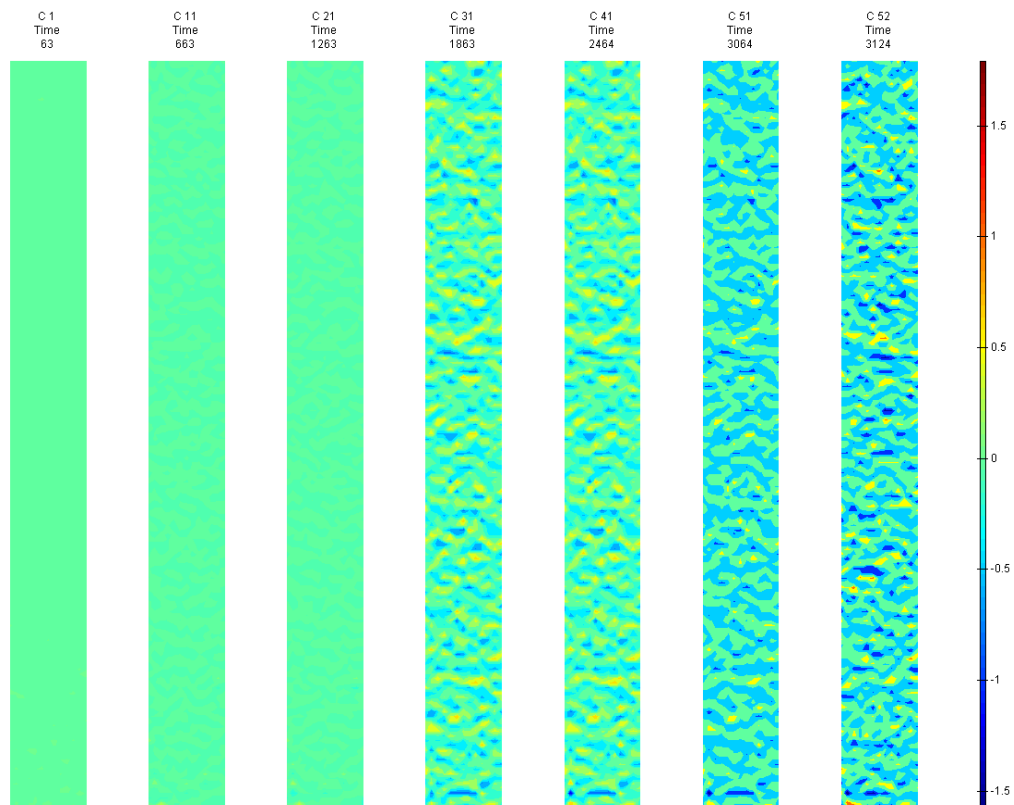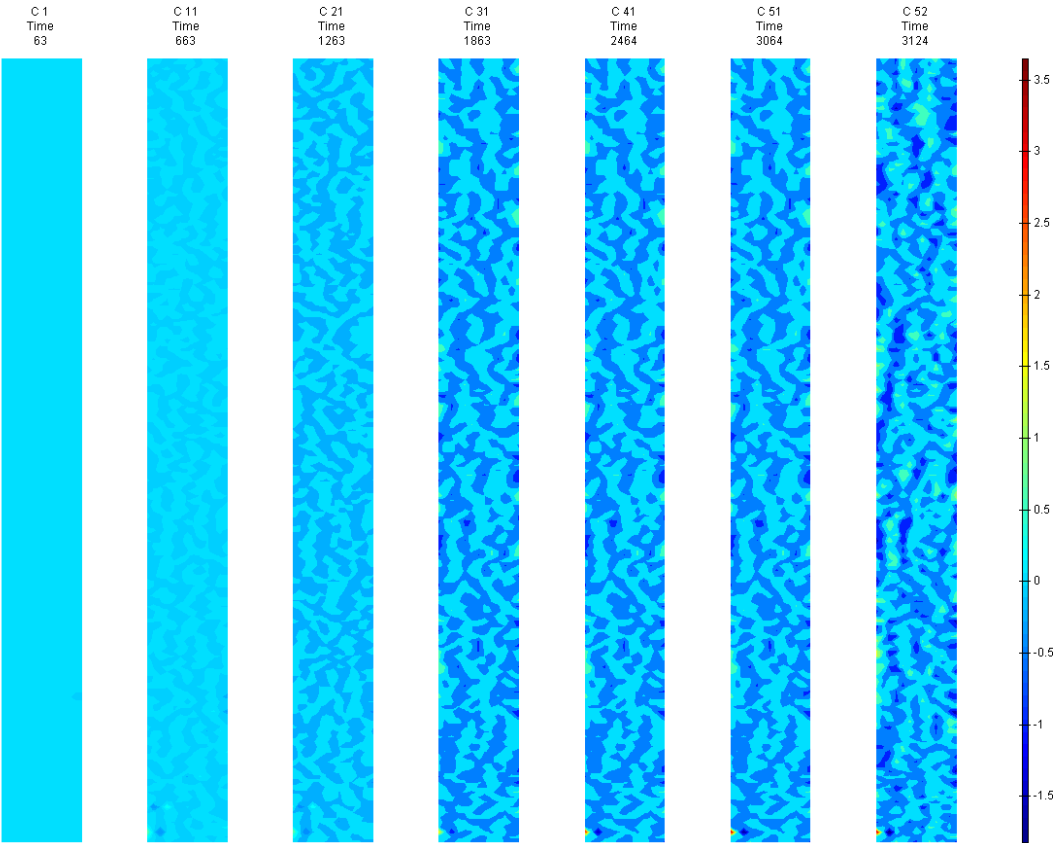FIGURE 248: XY DIRECTION PIV FIRST–SEQUENTIAL ENGINEERING SHEAR STRAIN OVER TIME

G6
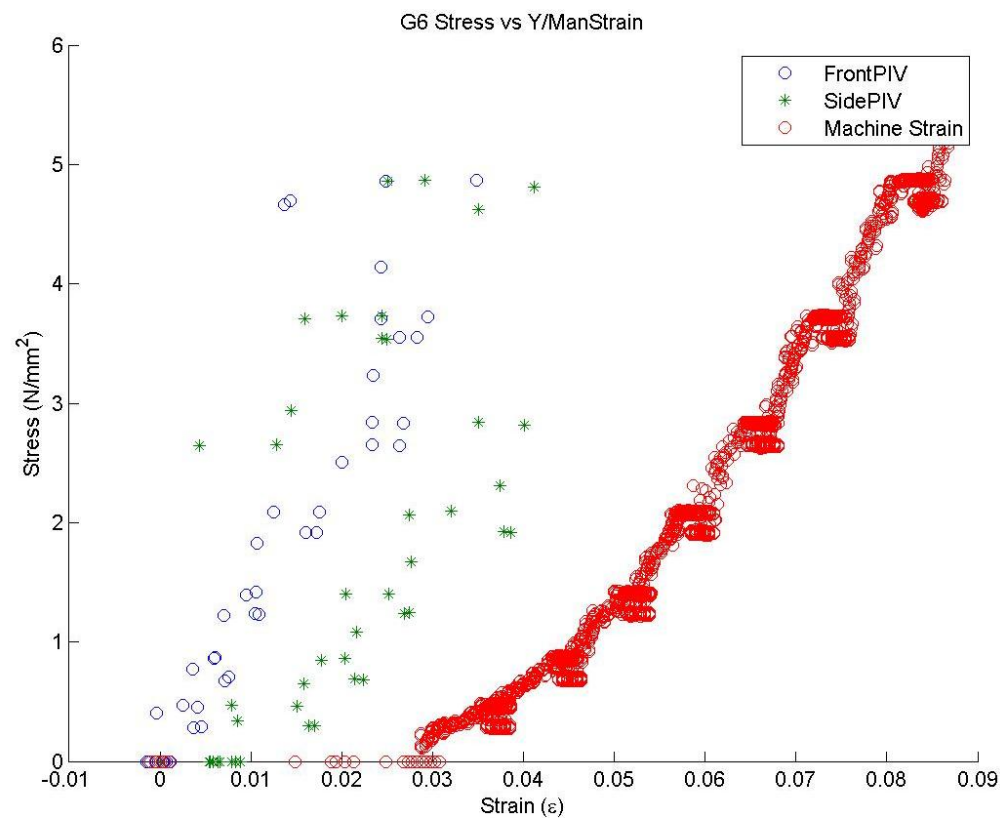
FIGURE 249: G6 TENSILE STRESS VS. MACHINE MEASURED/PIV STRAINS
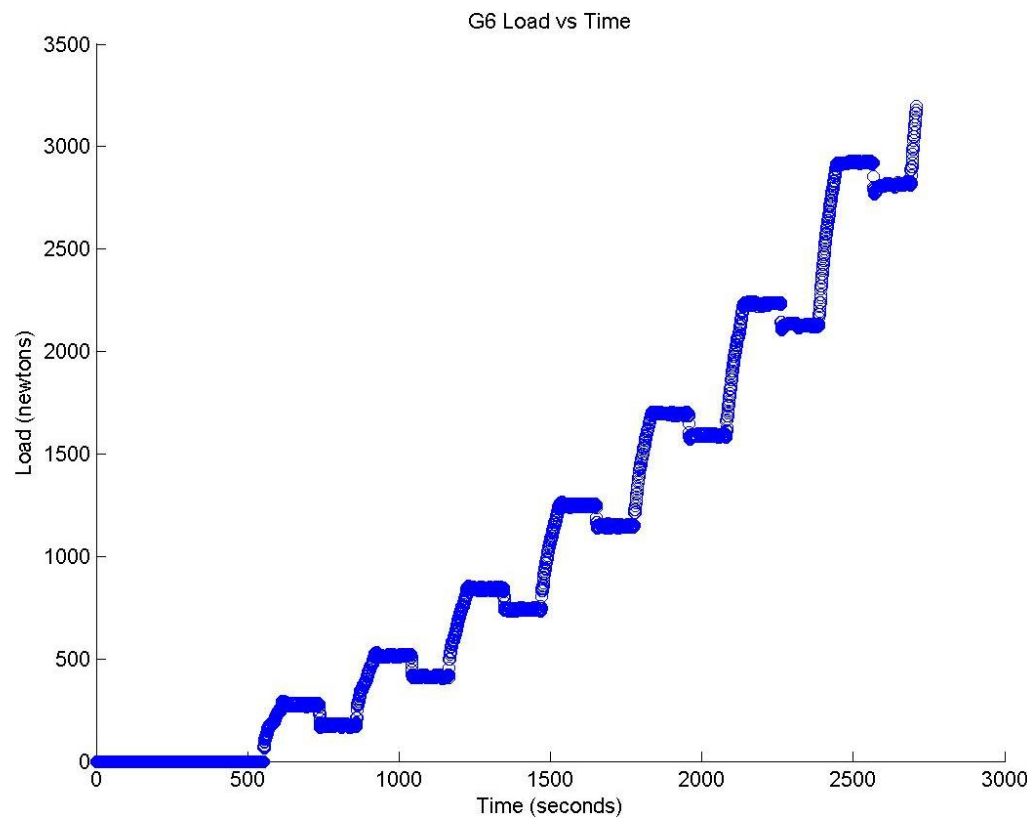
FIGURE 250: G6 TENSILE LOAD VS. TIME
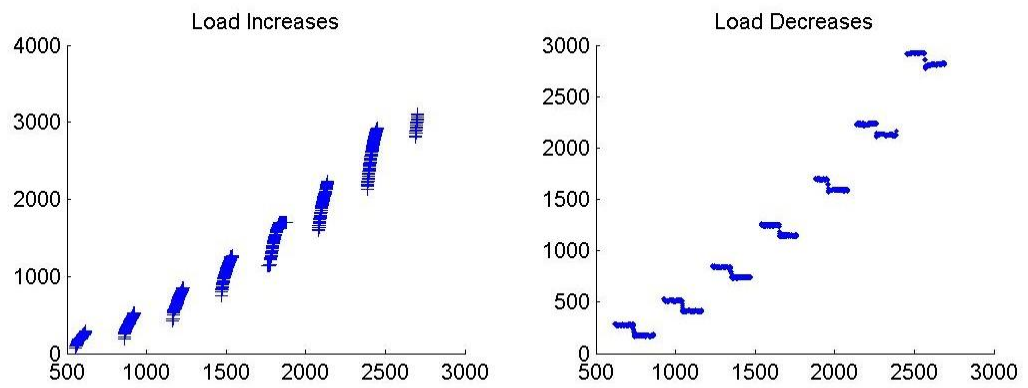
FIGURE 251: G6 CREEP LOADING: INCREMENTS AND RELAXATION
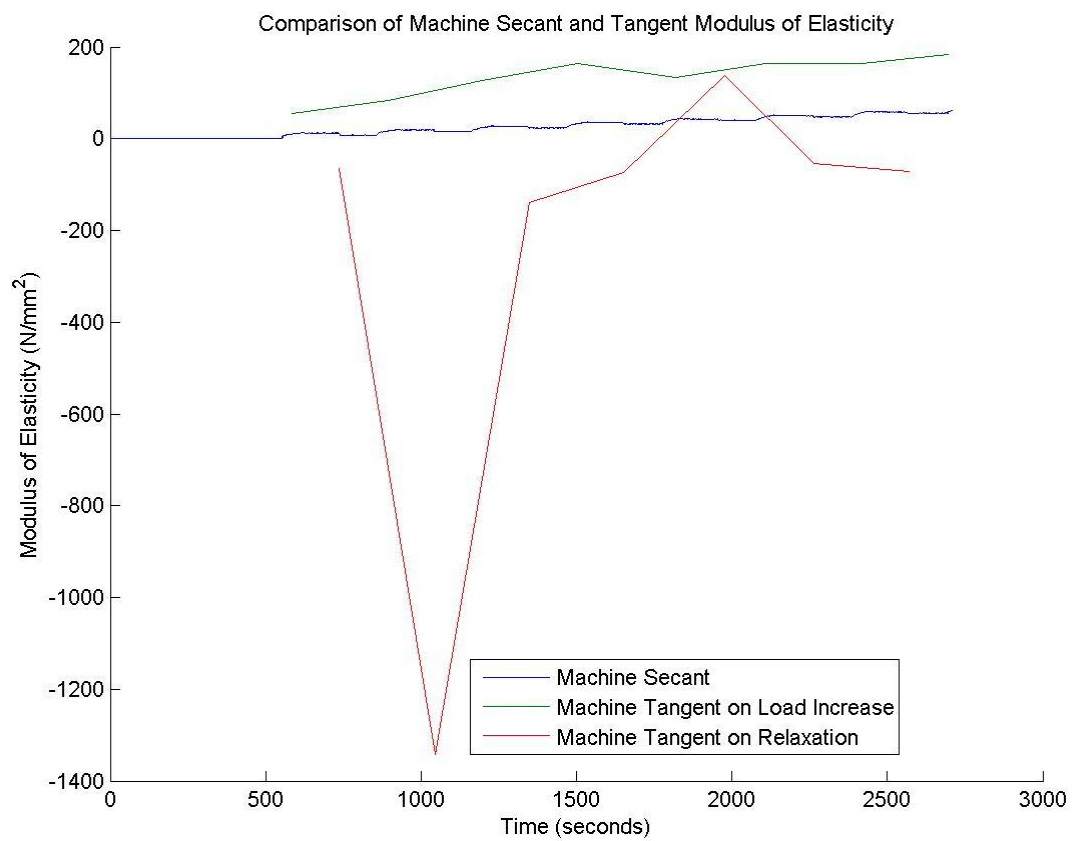
FIGURE 252: G6 MACHINE MEASURED SECANT AND TANGENT MODULUS VS. TIME
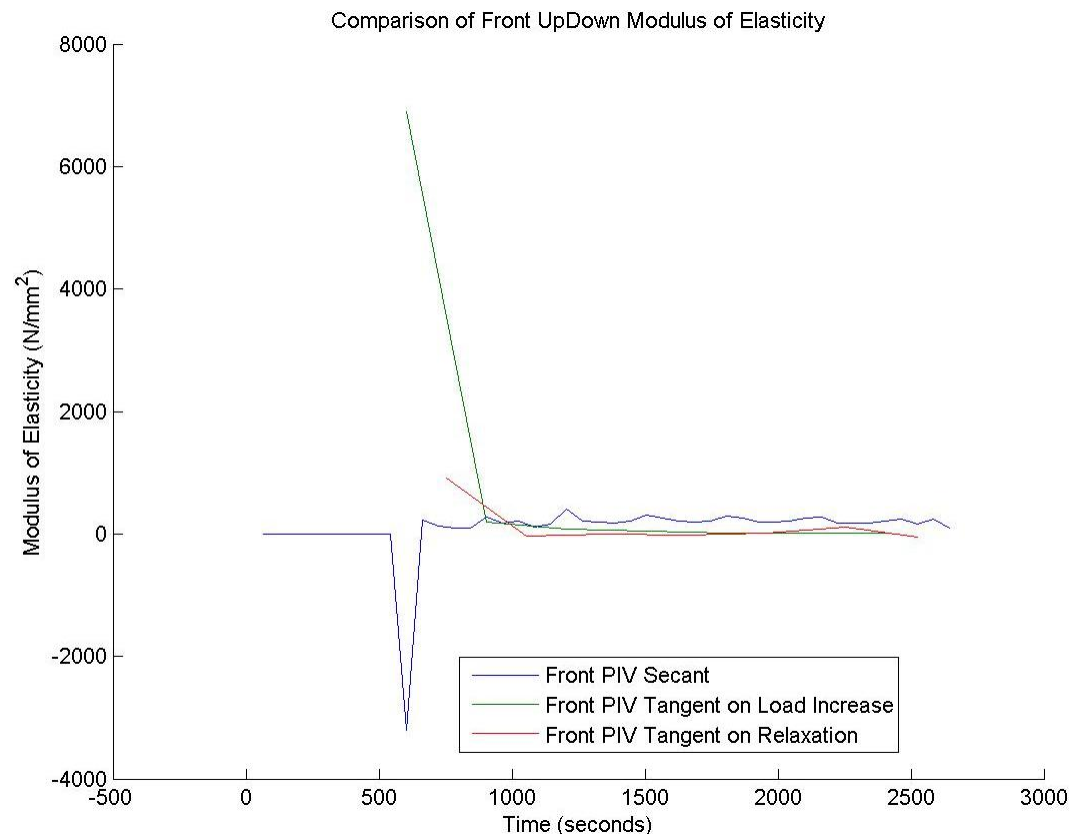
FIGURE 253: G6 FRONT VIEW PIV SECANT AND TANGENT MODULUS VS. TIME
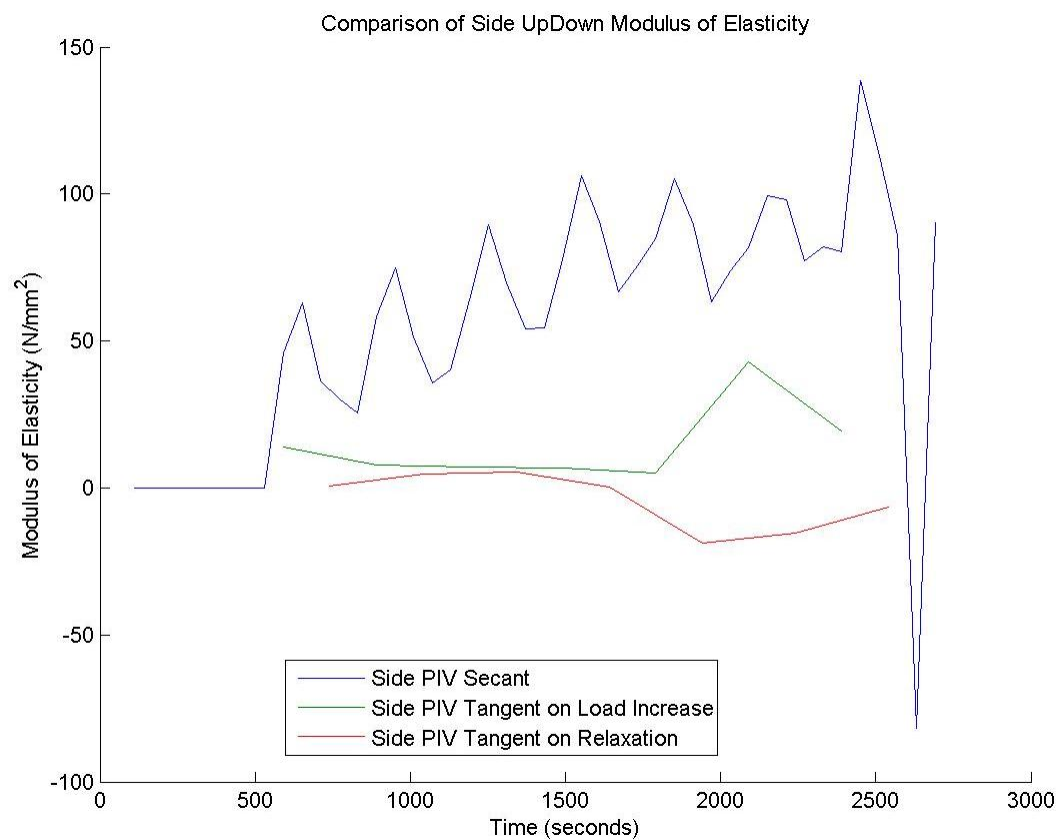
FIGURE 254: G6 SIDE VIEW PIV SECANT AND TANGENT MODULUS VS. TIME
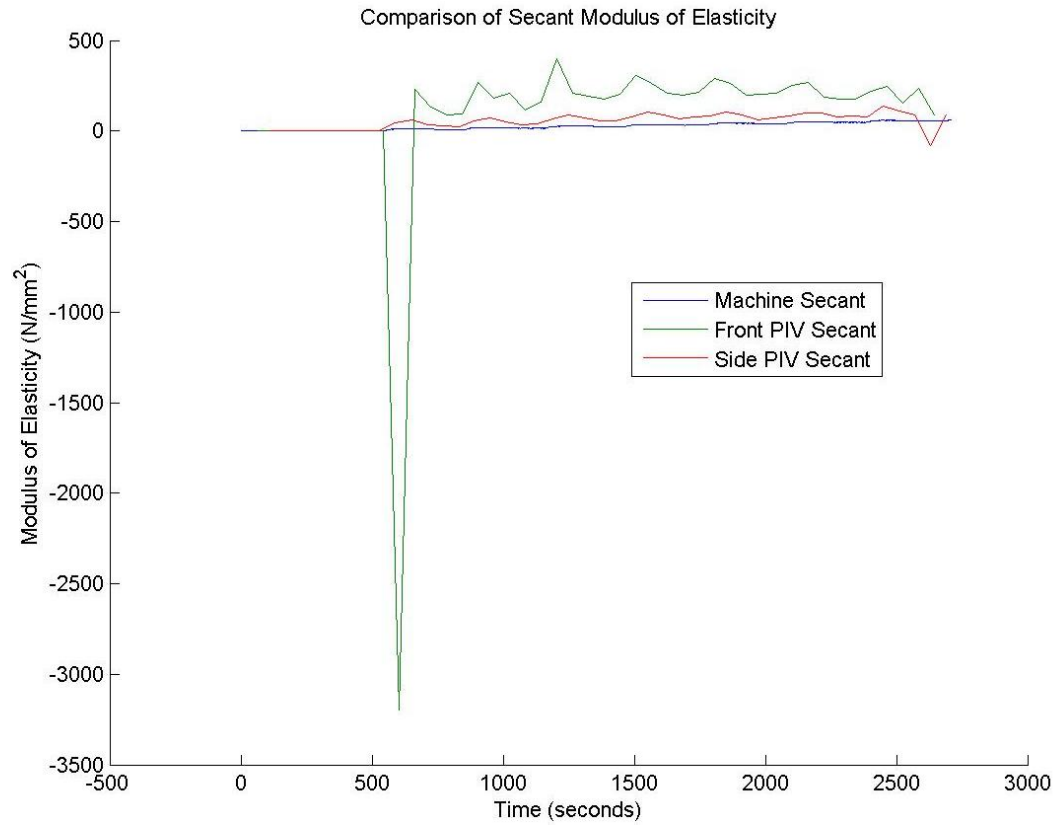
FIGURE 255: G6 COMPARISON OF MACHINE MEASURED AND PIV SECANT MODULUS VS. TIME
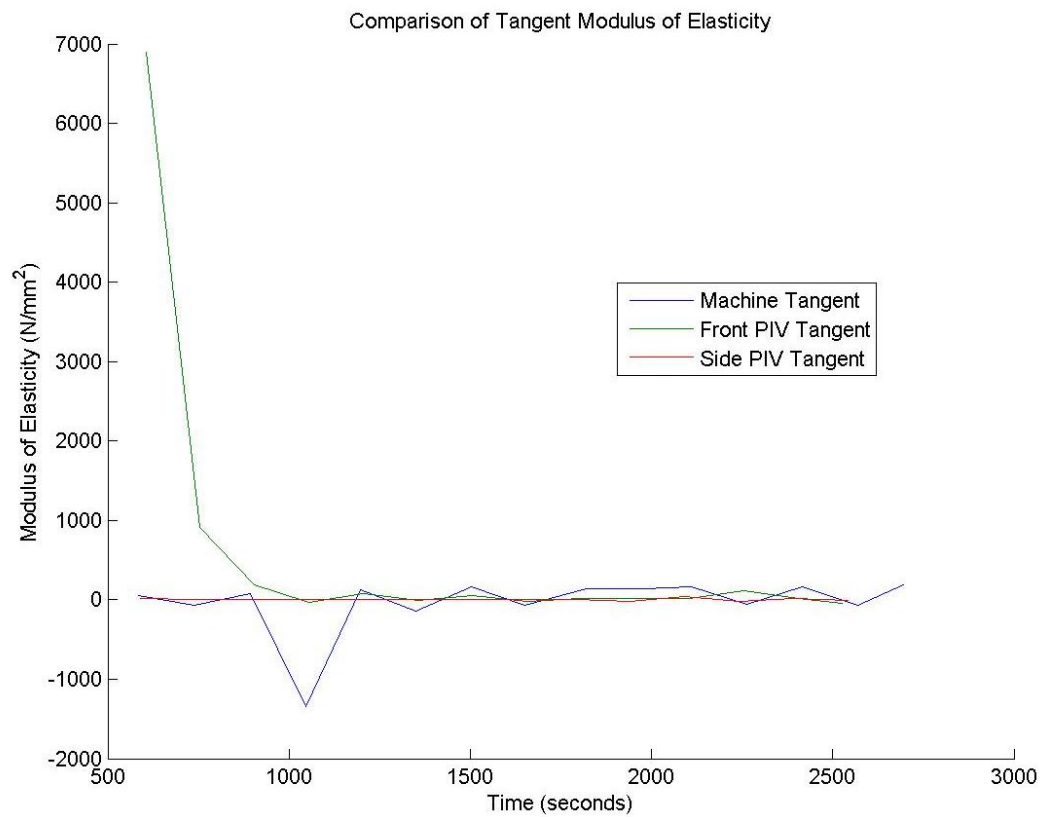
FIGURE 256: G6 COMPARISON OF MACHINE MEASURED AND PIV TANGENT MODULUS VS.

TIME

Appendix 6

G6 Sample

FIGURE 257: SAMPLE GRAIN ORIENTATIONS OF THE FRONT (LEFT 4 IMAGES) AND SIDE (RIGHT

4 IMAGES) VIEW BEFORE (FIRST 2 OF 4 IMAGES) AND AFTER (LAST 2 OF 4 IMAGES) BREAKAGE

G6 Front View
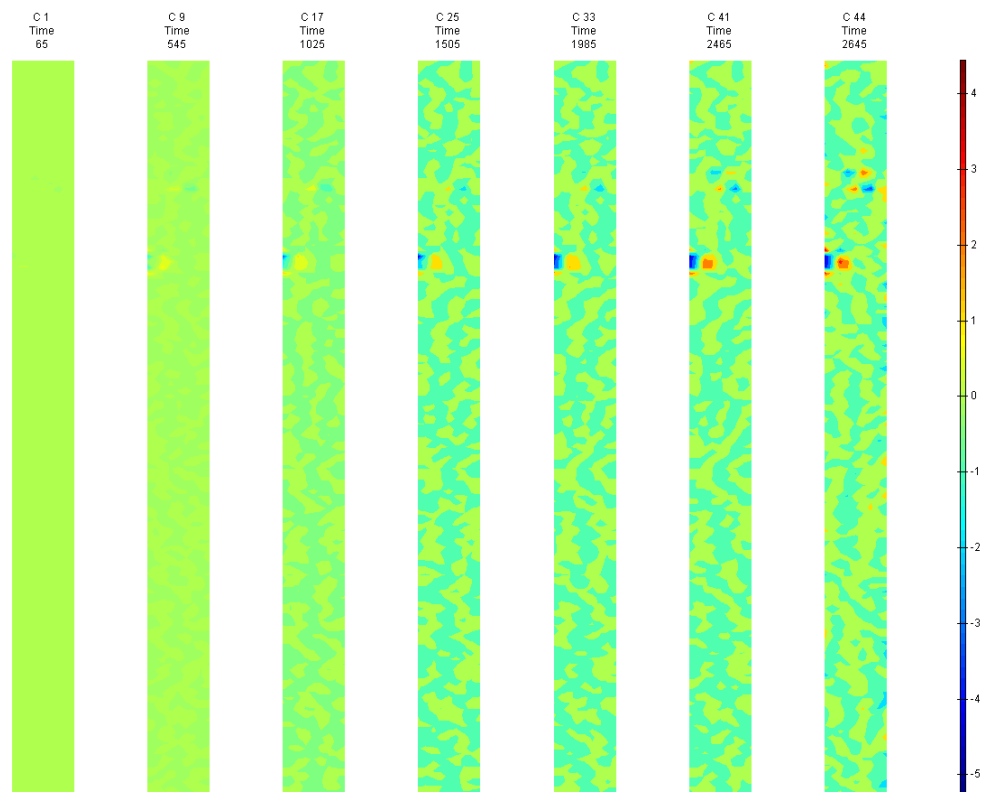
FIGURE 258: X DIRECTION PIV SEQUENTIAL ENGINEERING STRAIN OVER TIME
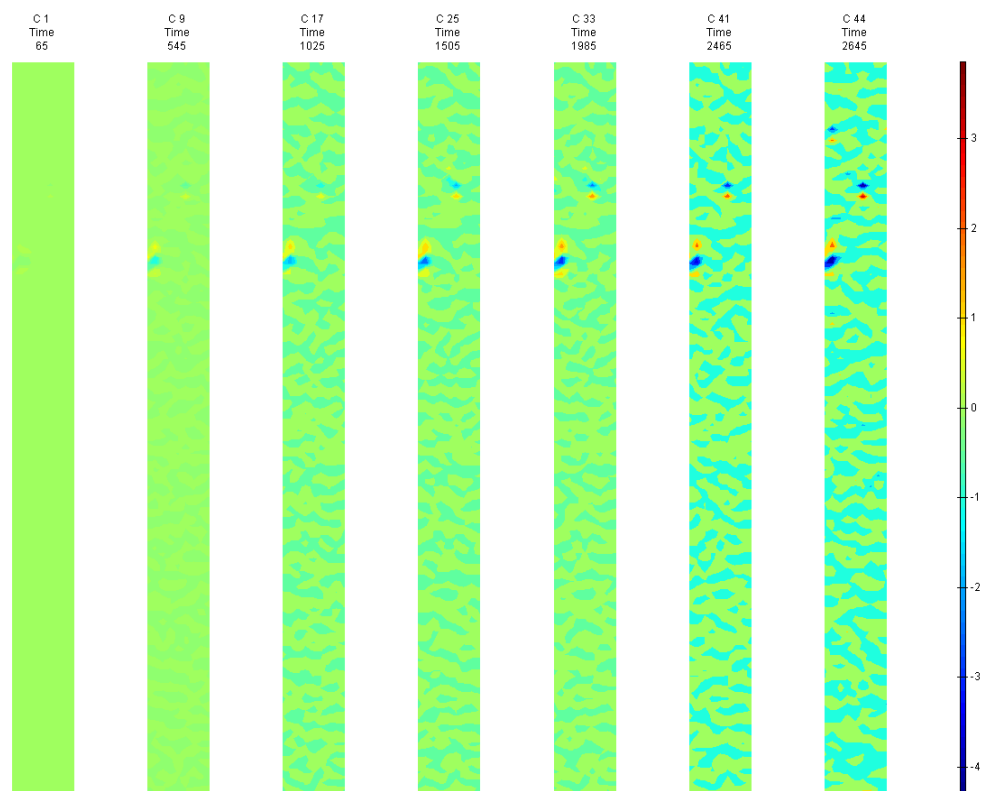
FIGURE 259: Y DIRECTION PIV SEQUENTIAL ENGINEERING STRAIN OVER TIME

Appendix 6
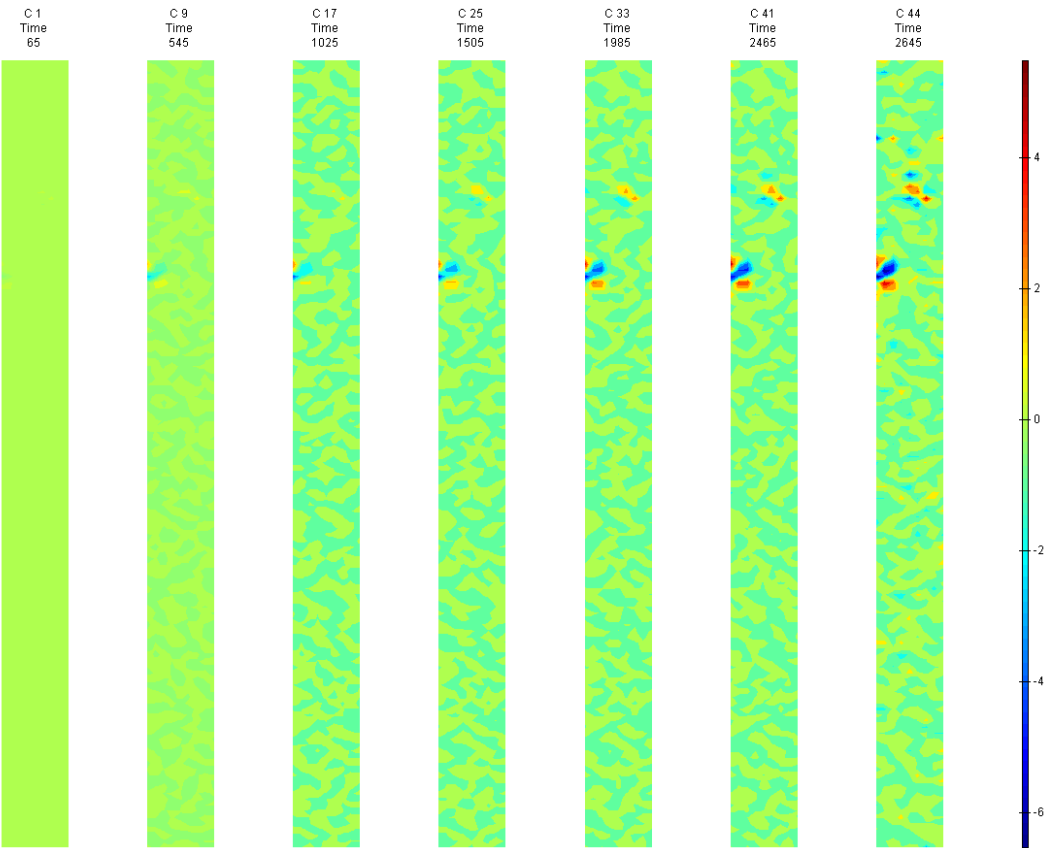
FIGURE 260: XY DIRECTION PIV SEQUENTIAL ENGINEERING SHEAR STRAIN OVER TIME
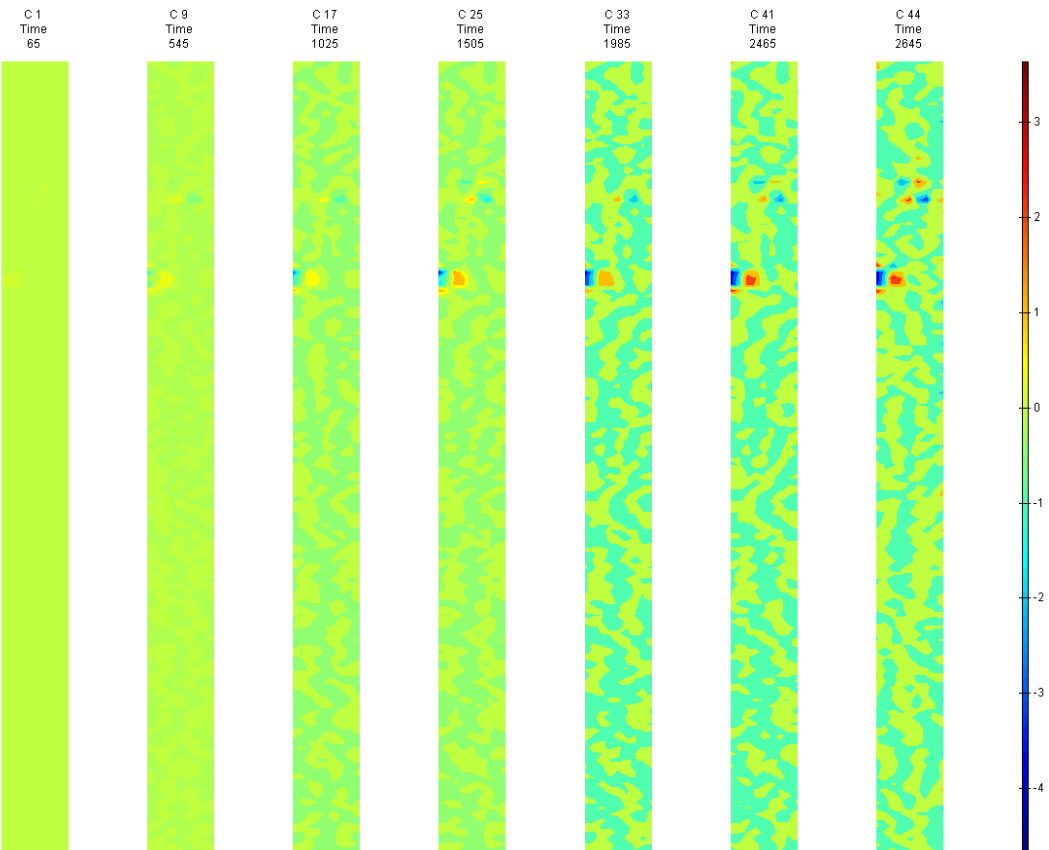
FIGURE 261: X DIRECTION PIV SEQUENTIAL TRUE STRAIN OVER TIME

278
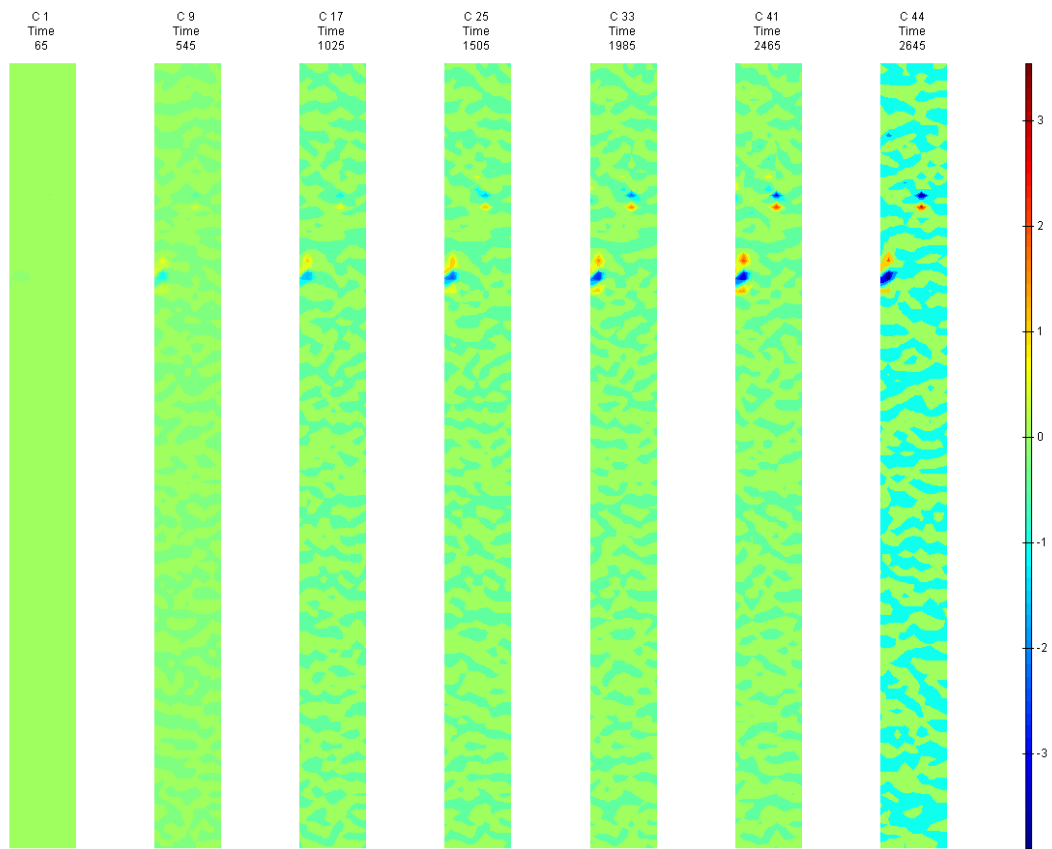
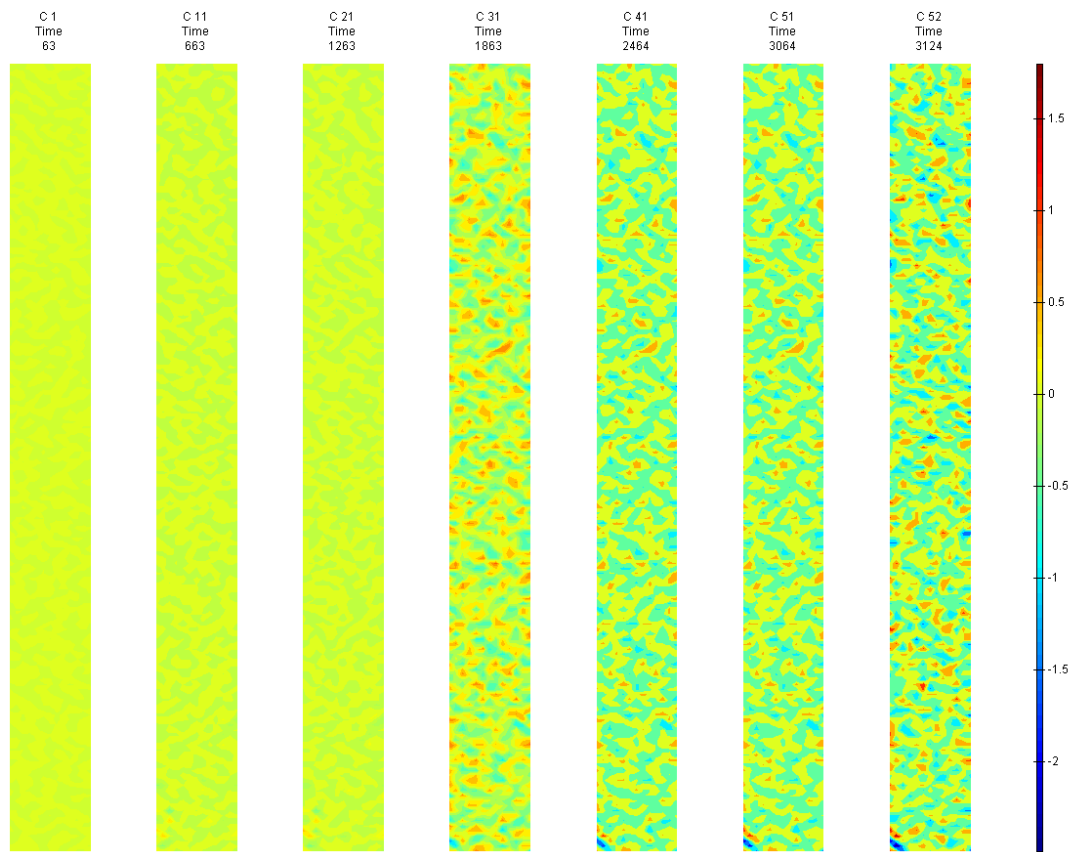FIGURE 262: Y DIRECTION PIV SEQUENTIAL TRUE STRAIN OVER TIME
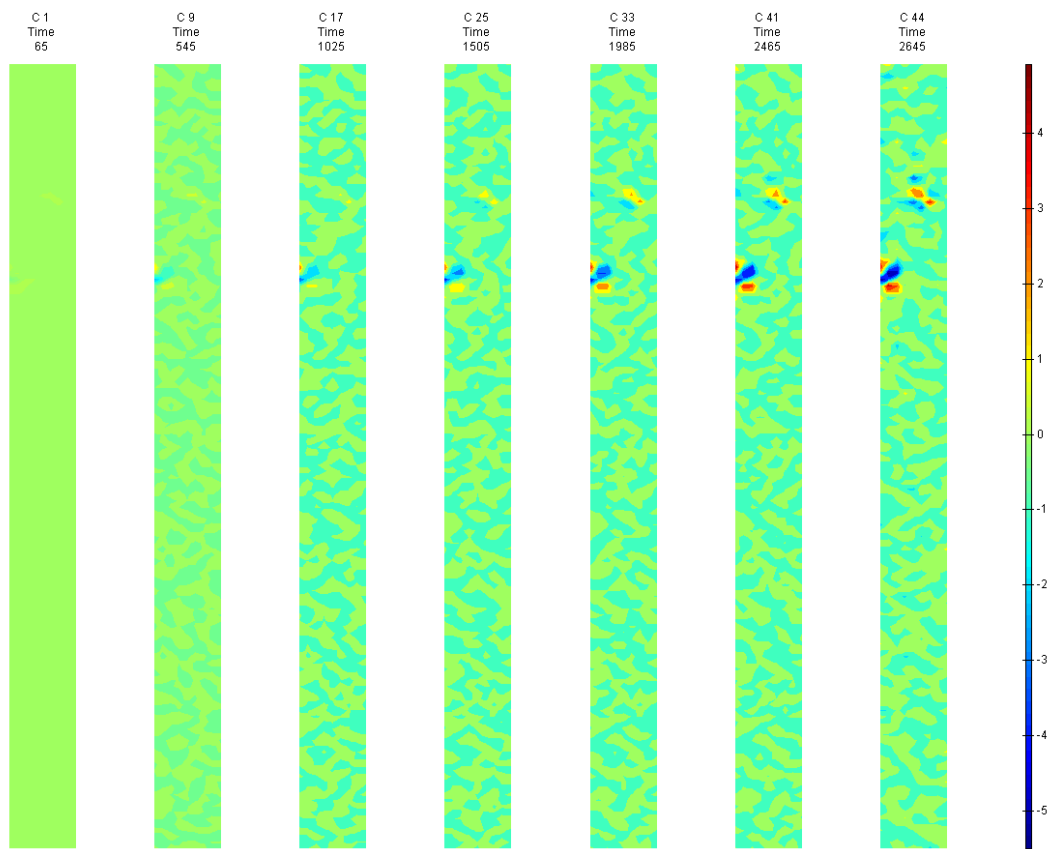
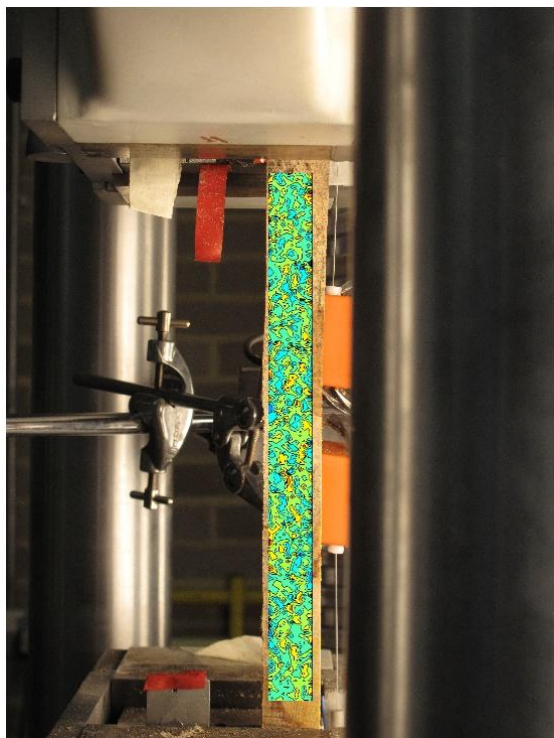FIGURE 263: XY DIRECTION PIV SEQUENTIAL TRUE SHEAR STRAIN OVER TIME
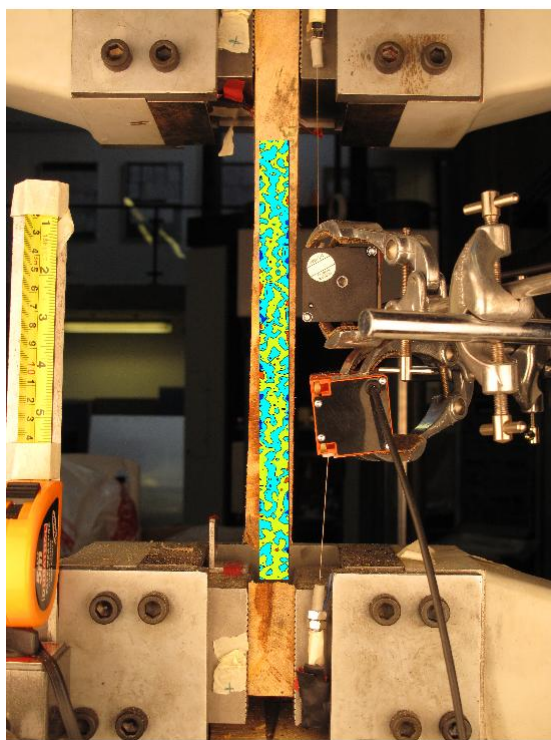
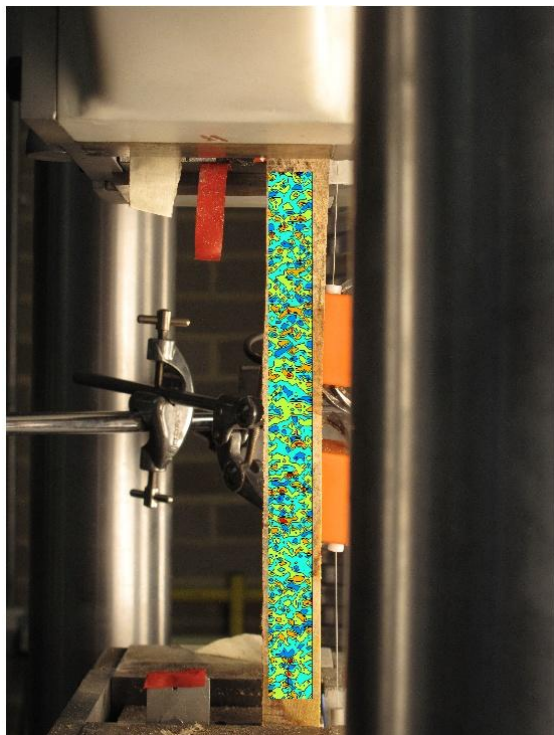FIGURE 264: X DIRECTION PIV FIRST–LAST DITCH ENGINEERING STRAIN OVER IMAGE
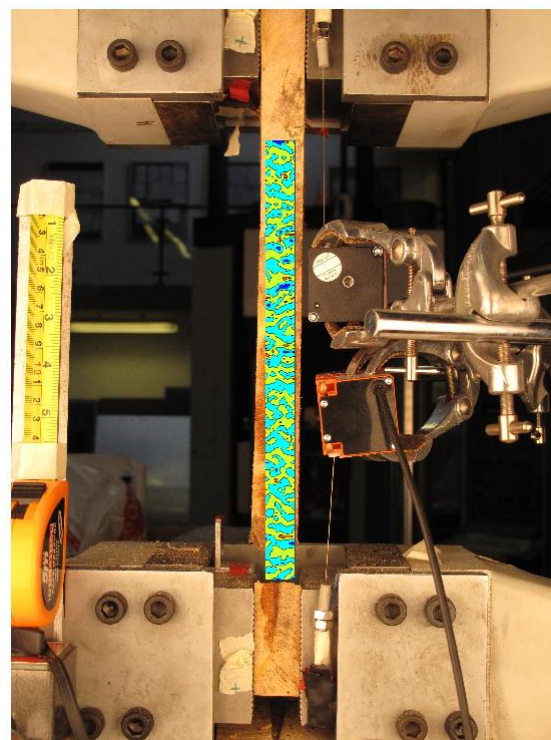
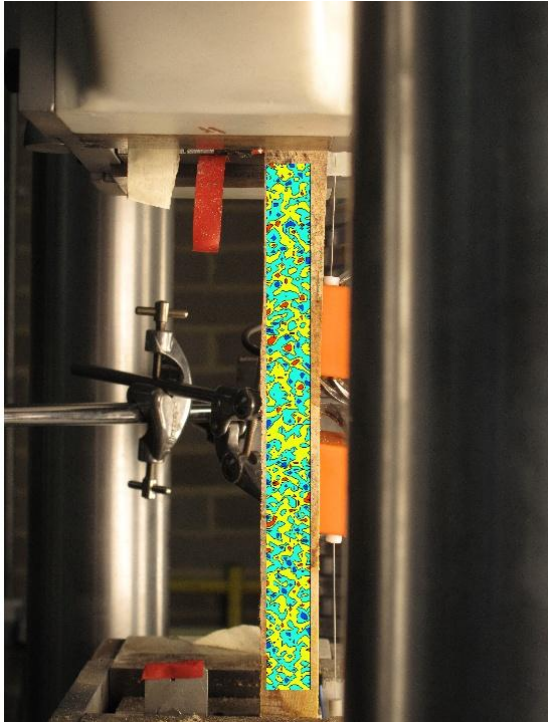FIGURE 265: Y DIRECTION PIV FIRST–LAST DITCH ENGINEERING STRAIN OVER IMAGE
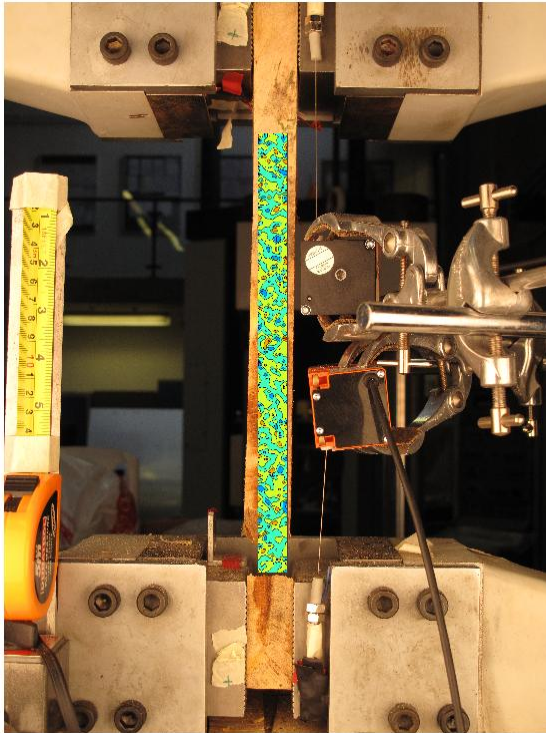
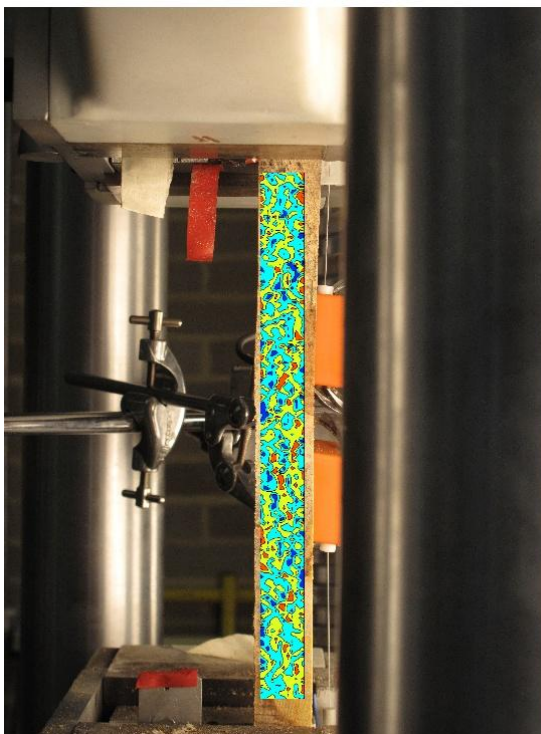FIGURE 266: XY DIRECTION PIV FIRST-LAST DITCH ENGINEERING SHEAR STRAIN OVER
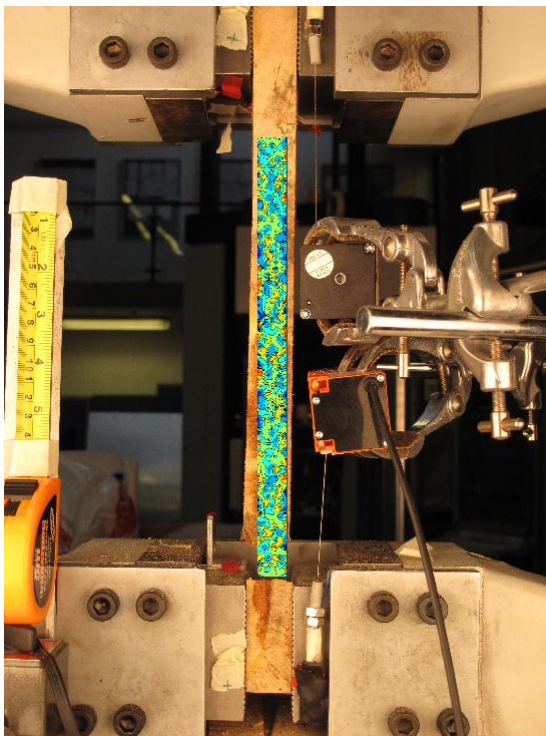
IMAGE

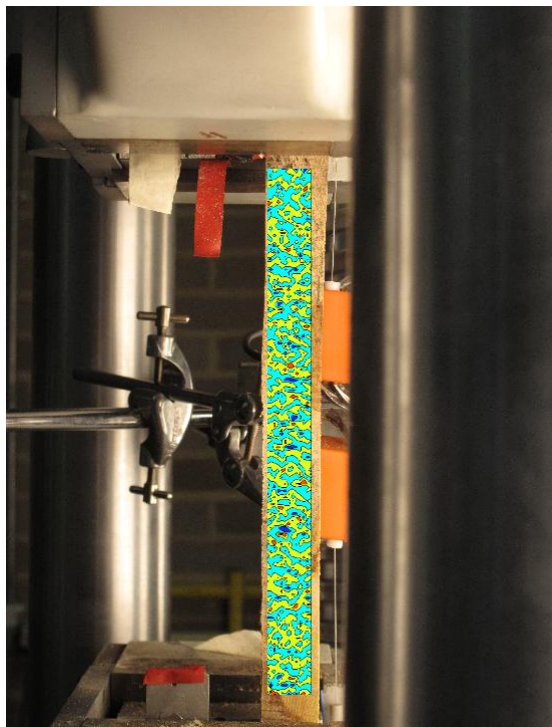FIGURE 267: X DIRECTION PIV FIRST-LAST DITCH TRUE STRAIN OVER IMAGE

Appendix 6
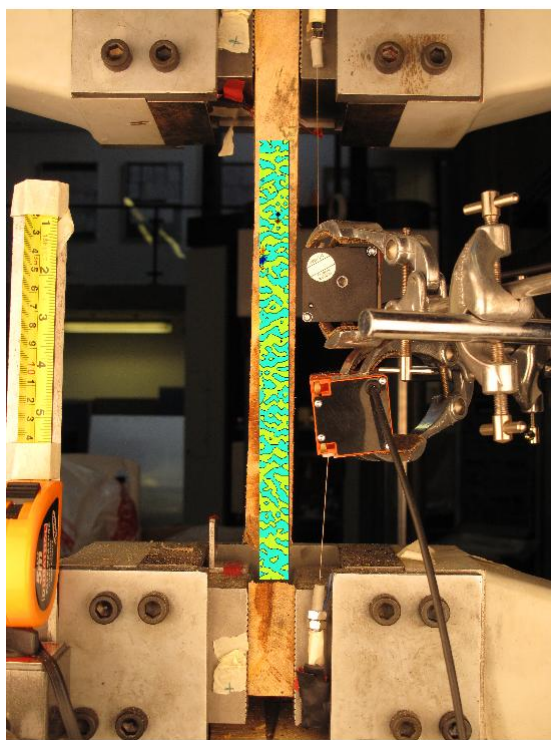
FIGURE 268: Y DIRECTION PIV FIRST–LAST DITCH TRUE STRAIN OVER IMAGE
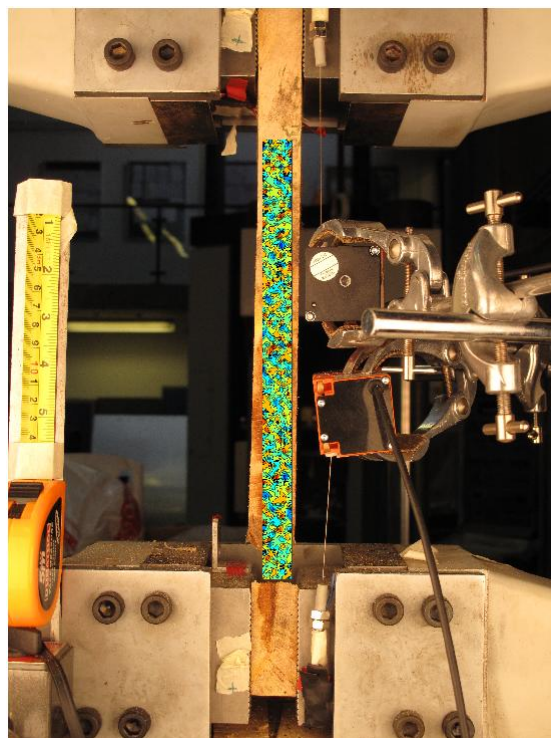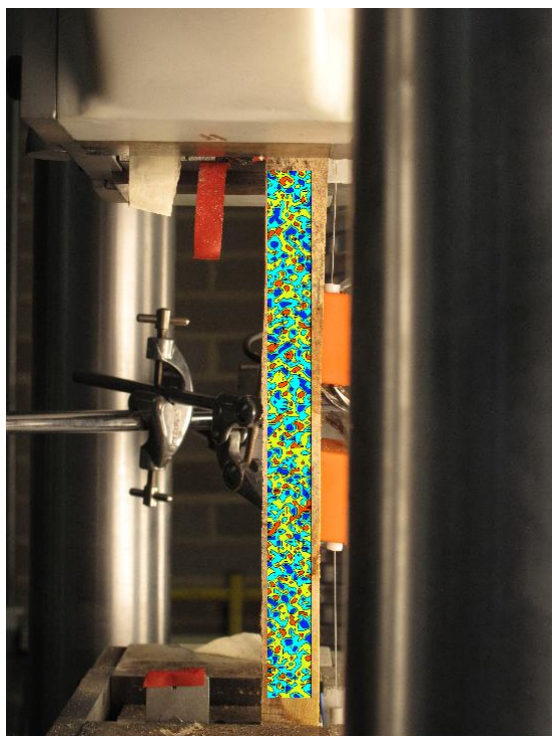

FIGURE 269: XY DIRECTION PIV FIRST–LAST DITCH TRUE SHEAR STRAIN OVER IMAGE
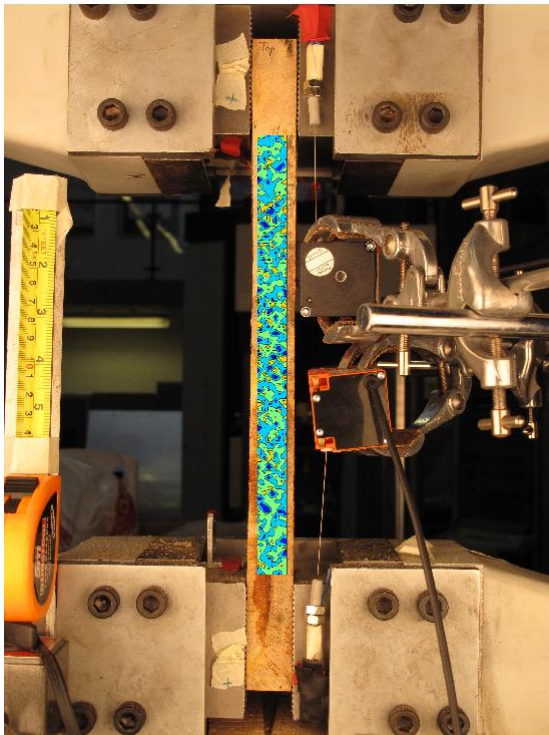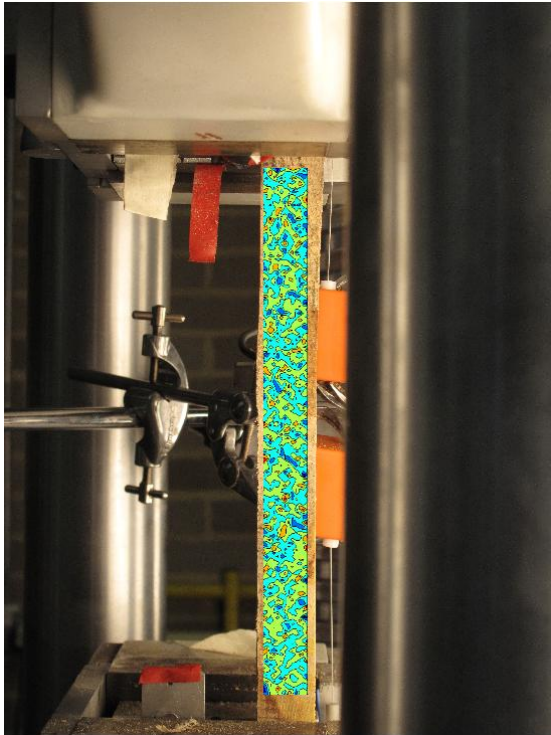
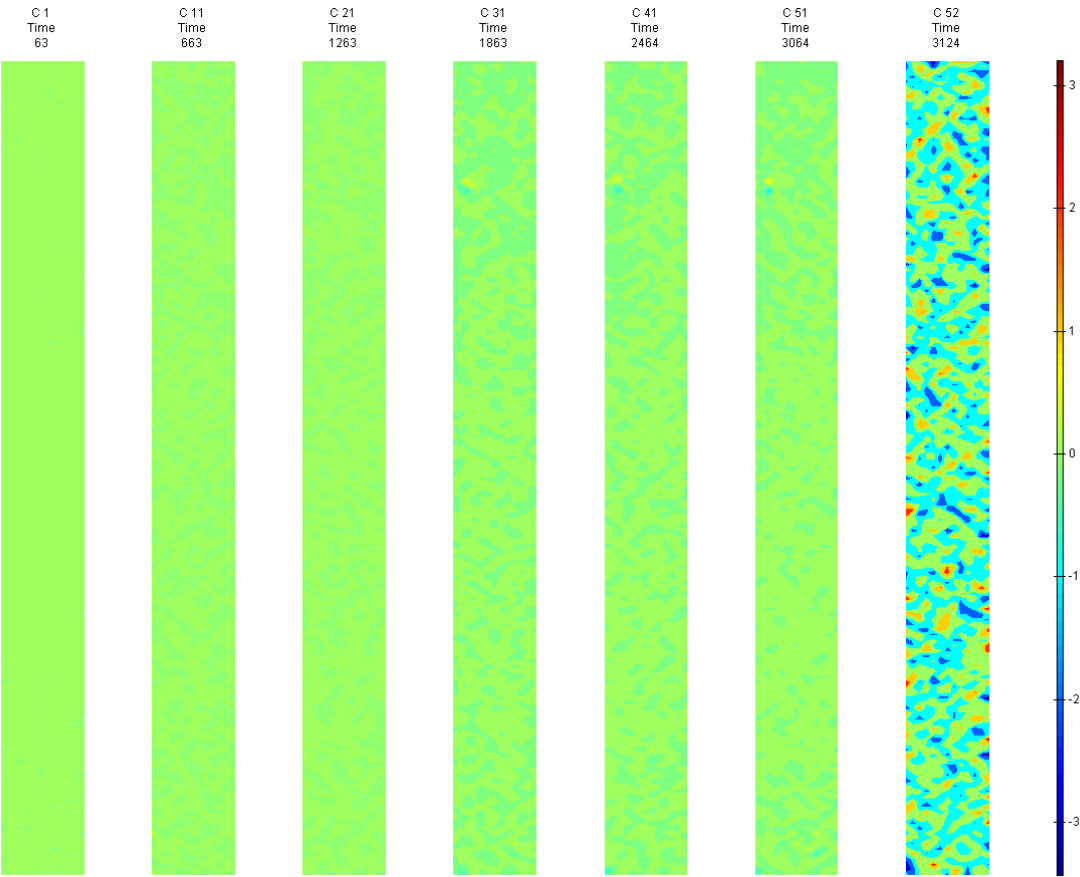FIGURE 270: XY DIRECTION PIV FIRST–SEQUENTIAL ENGINEERING SHEAR STRAIN OVER

IMAGE
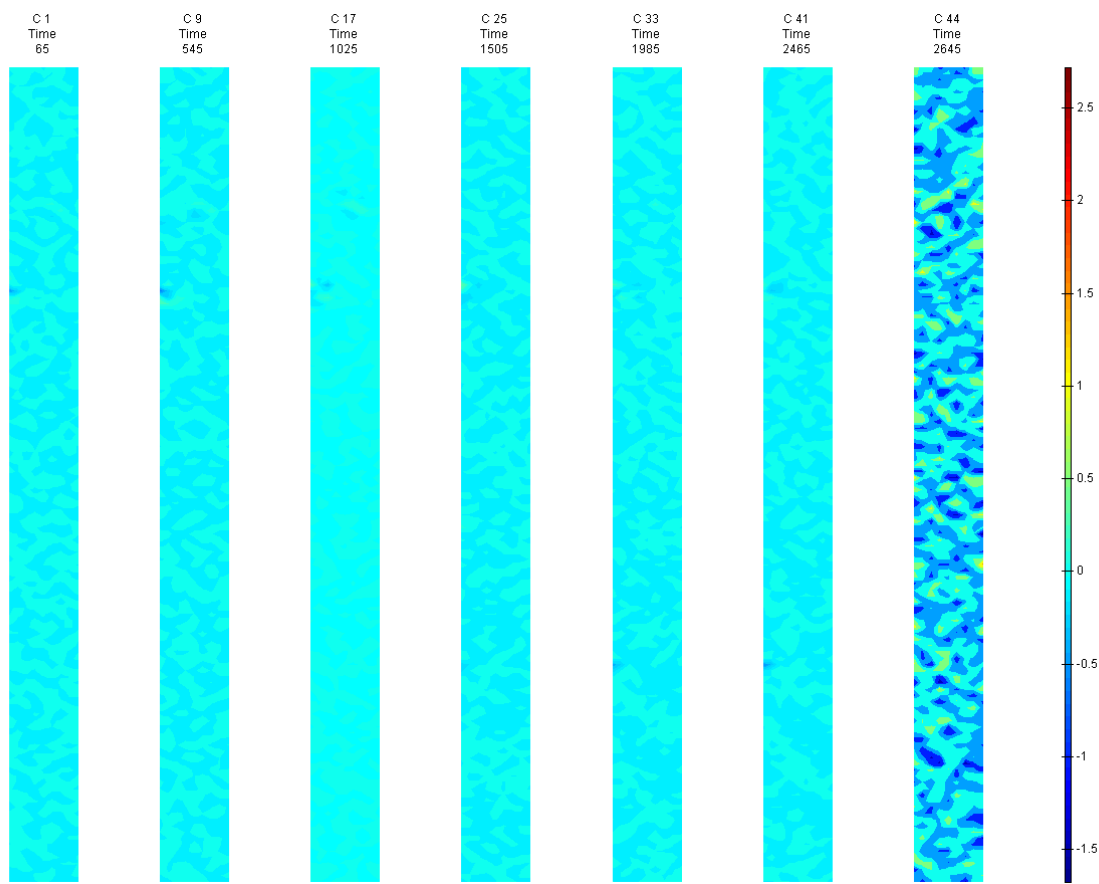
FIGURE 271: XY DIRECTION PIV FIRST–SEQUENTIAL ENGINEERING SHEAR STRAIN OVER TIME

G6 Side View
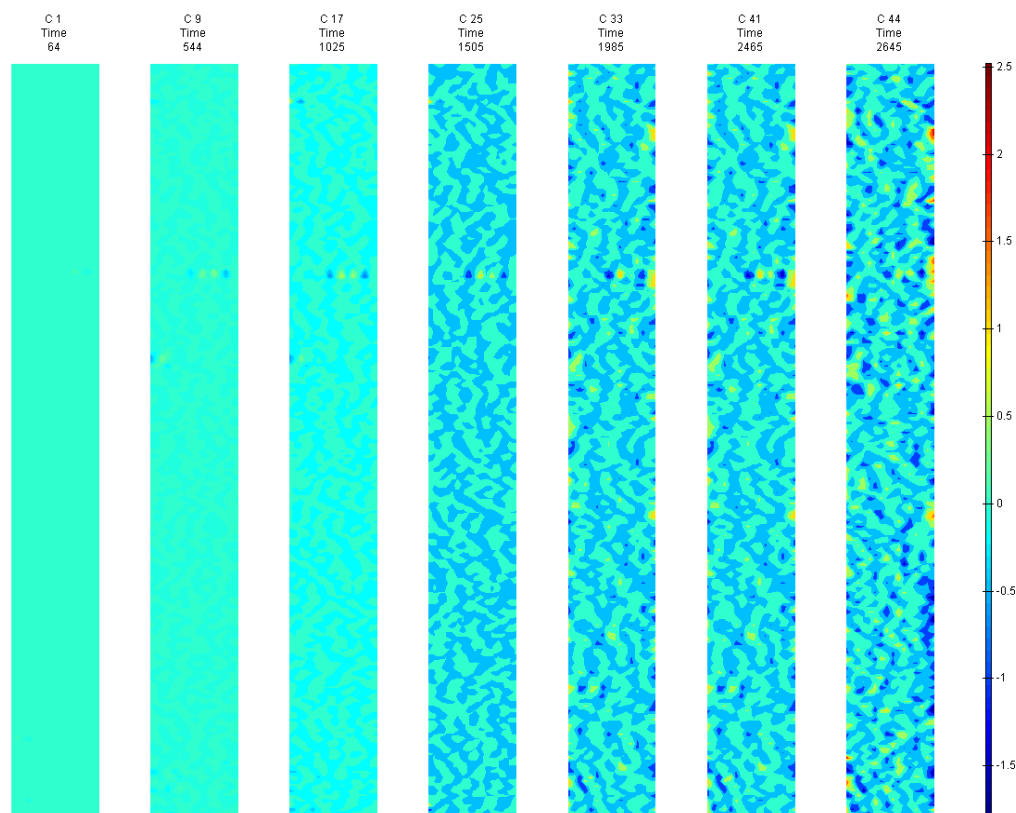
FIGURE 272: X DIRECTION PIV SEQUENTIAL ENGINEERING STRAIN OVER TIME
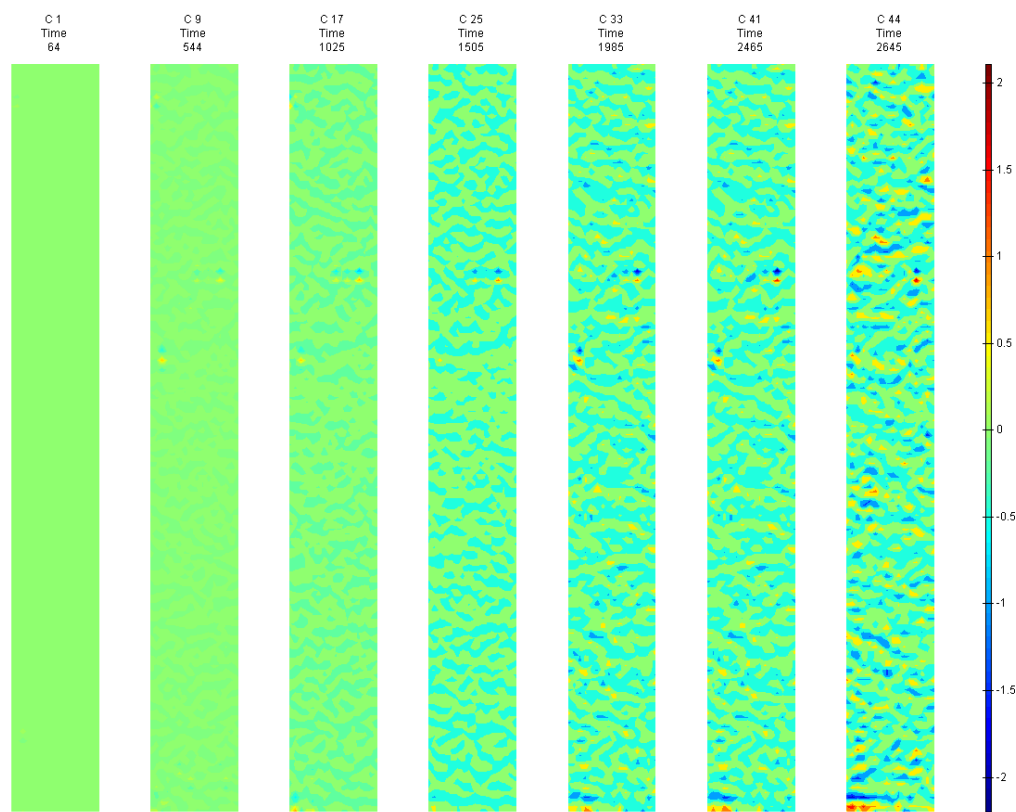
FIGURE 273: Y DIRECTION PIV SEQUENTIAL ENGINEERING STRAIN OVER TIME
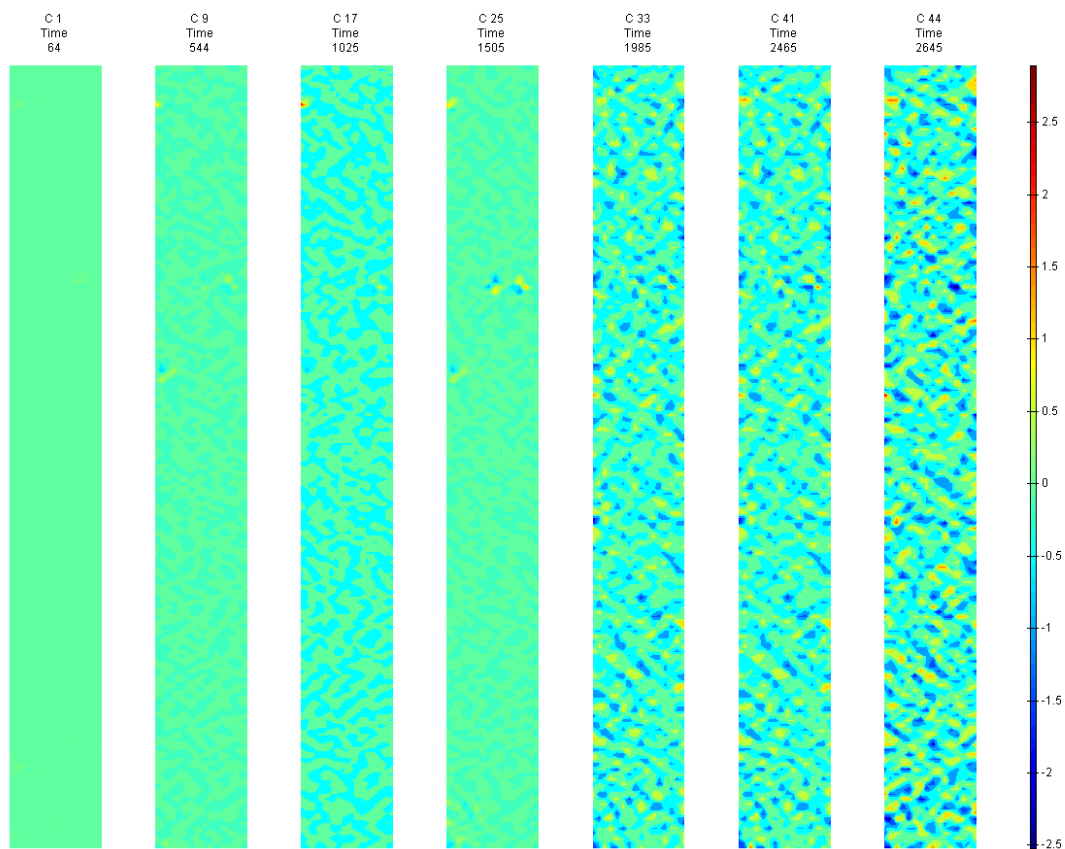
FIGURE 274: XY DIRECTION PIV SEQUENTIAL ENGINEERING SHEAR STRAIN OVER TIME
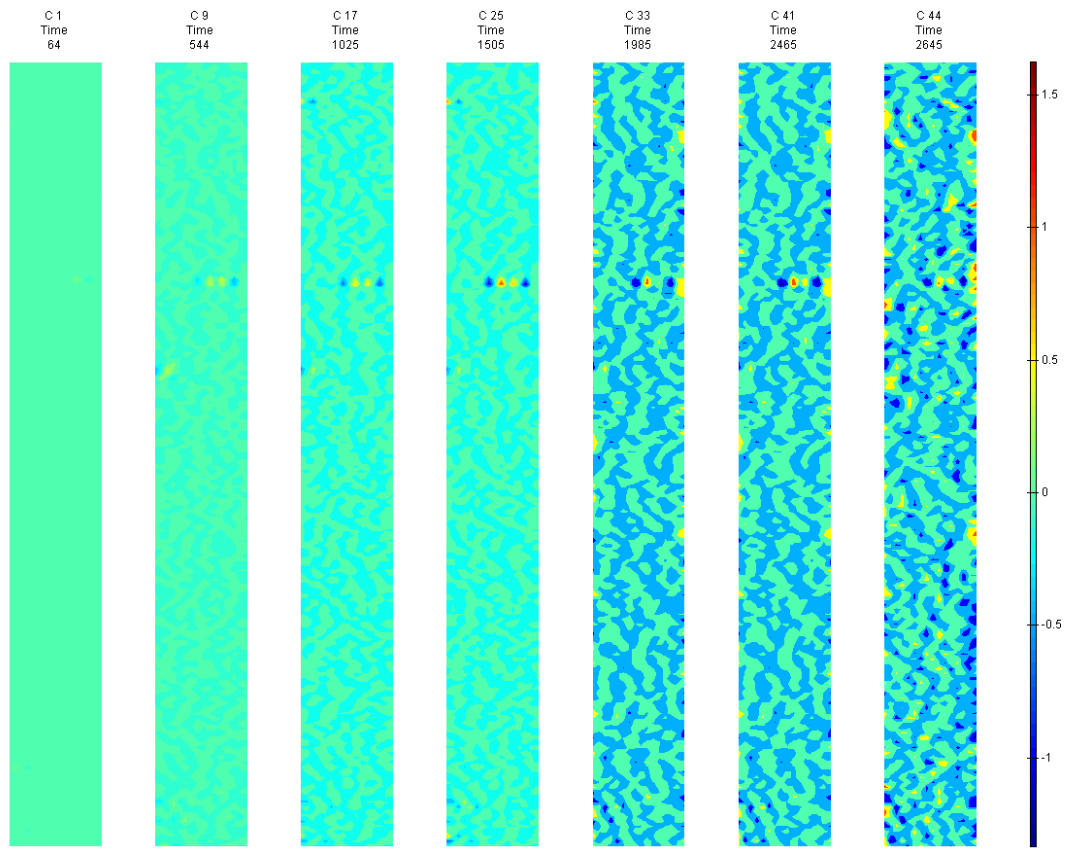
FIGURE 275: X DIRECTION PIV SEQUENTIAL TRUE STRAIN OVER TIME
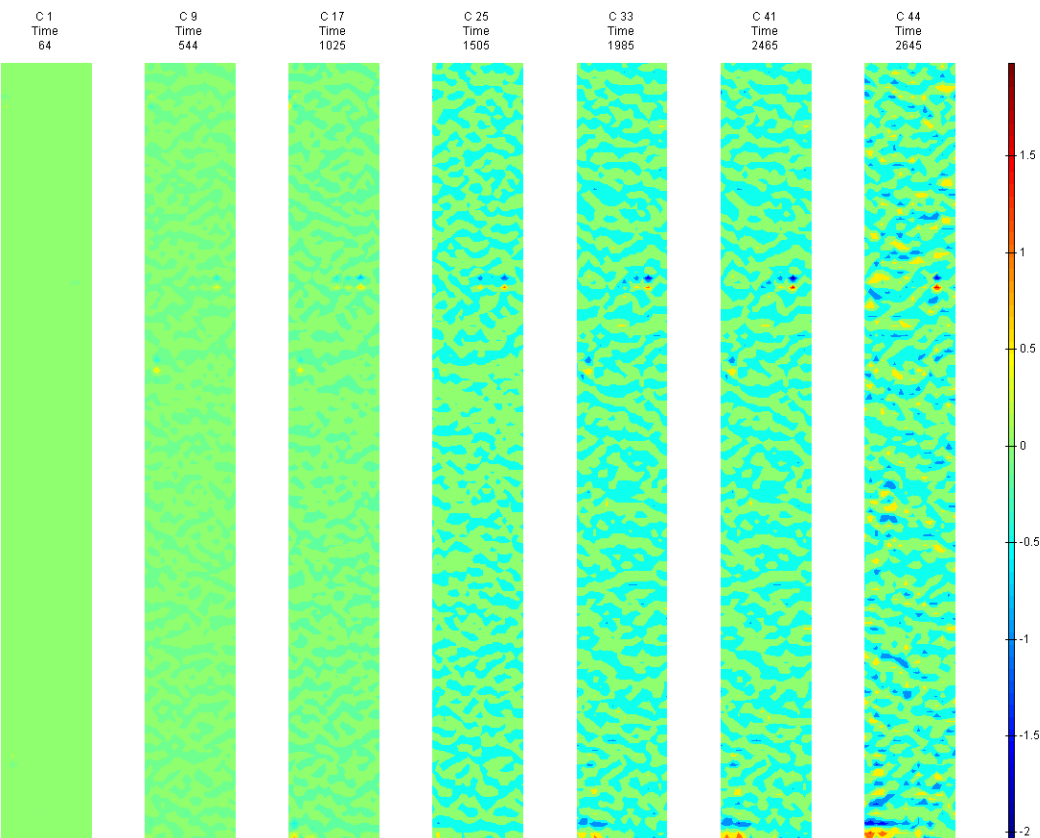
FIGURE 276: Y DIRECTION PIV SEQUENTIAL TRUE STRAIN OVER TIME
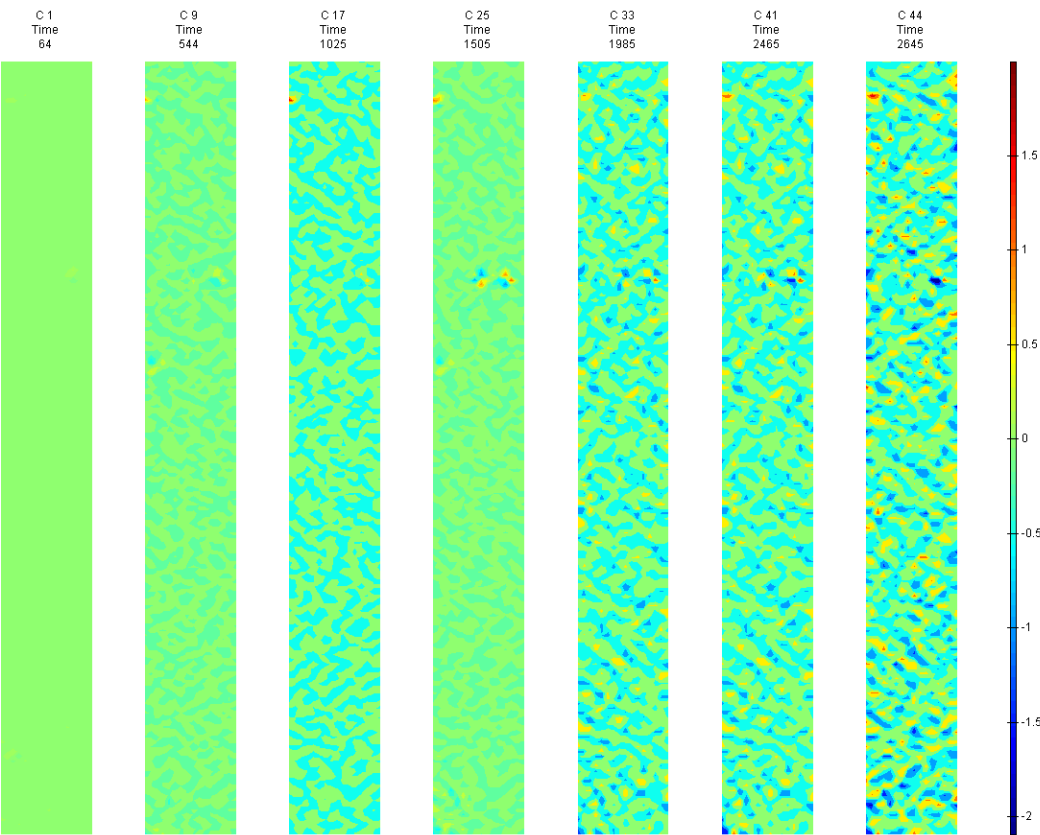
FIGURE 277: XY DIRECTION PIV SEQUENTIAL TRUE SHEAR STRAIN OVER TIME
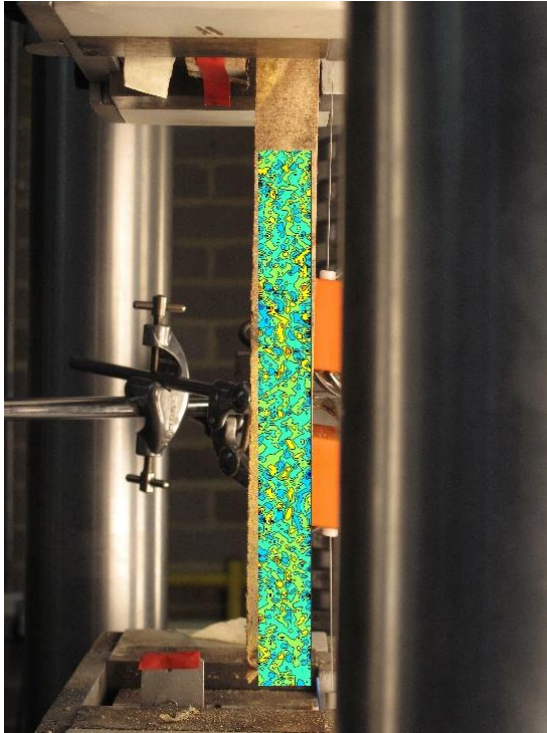
FIGURE 278: X DIRECTION PIV FIRST–LAST DITCH ENGINEERING STRAIN OVER IMAGE
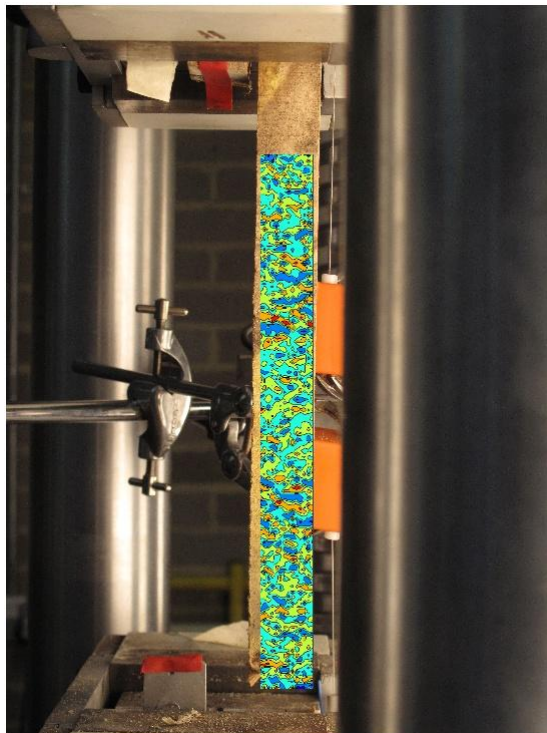
FIGURE 279: Y DIRECTION PIV FIRST–LAST DITCH ENGINEERING STRAIN OVER IMAGE

Appendix 6
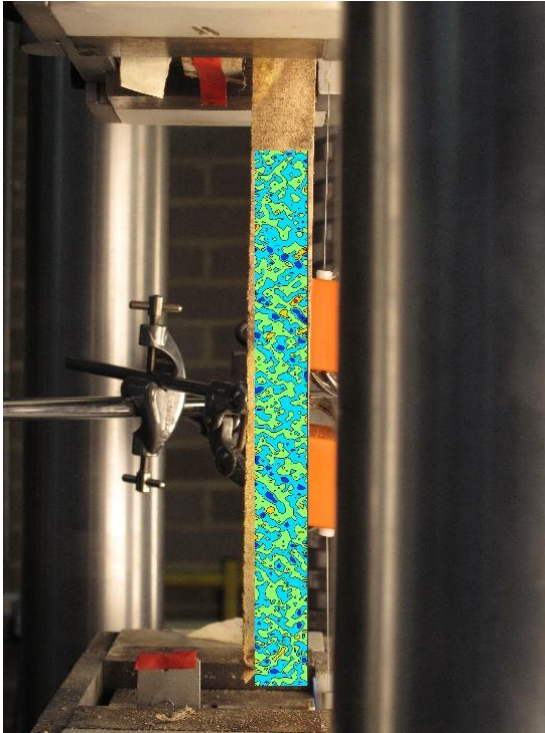
FIGURE 280: XY DIRECTION PIV FIRST–LAST DITCH ENGINEERING SHEAR STRAIN OVER
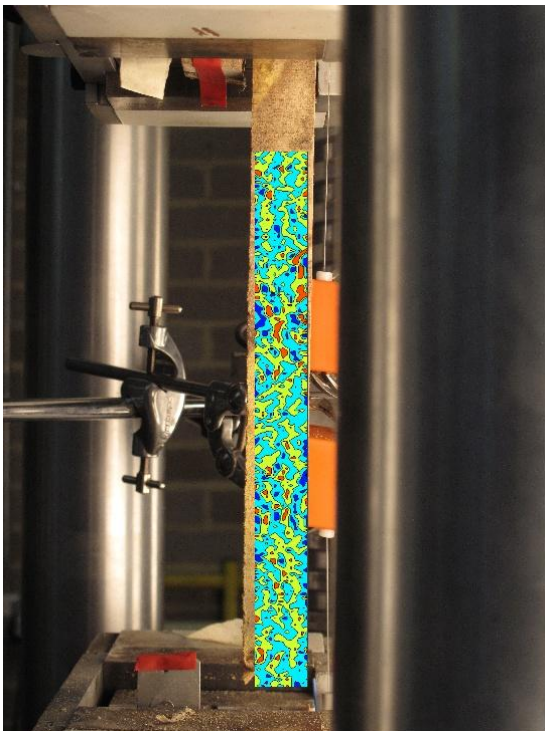
IMAGE

FIGURE 281: X DIRECTION PIV FIRST–LAST DITCH TRUE STRAIN OVER IMAGE
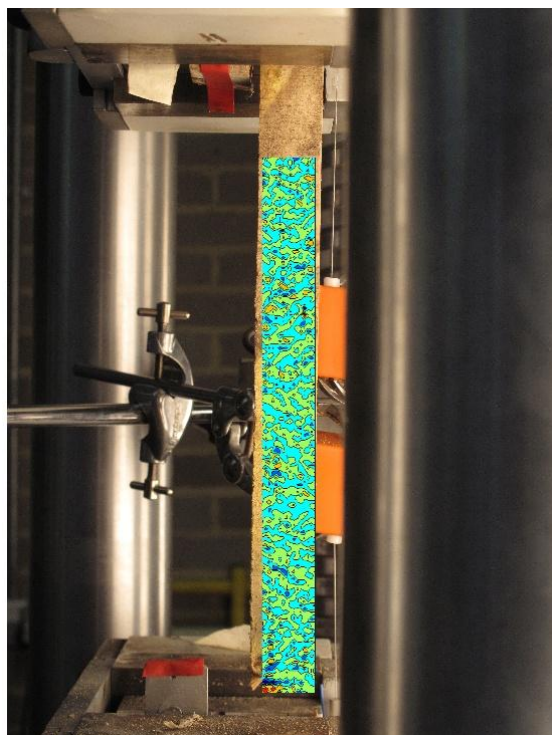
FIGURE 282: Y DIRECTION PIV FIRST–LAST DITCH TRUE STRAIN OVER IMAGE
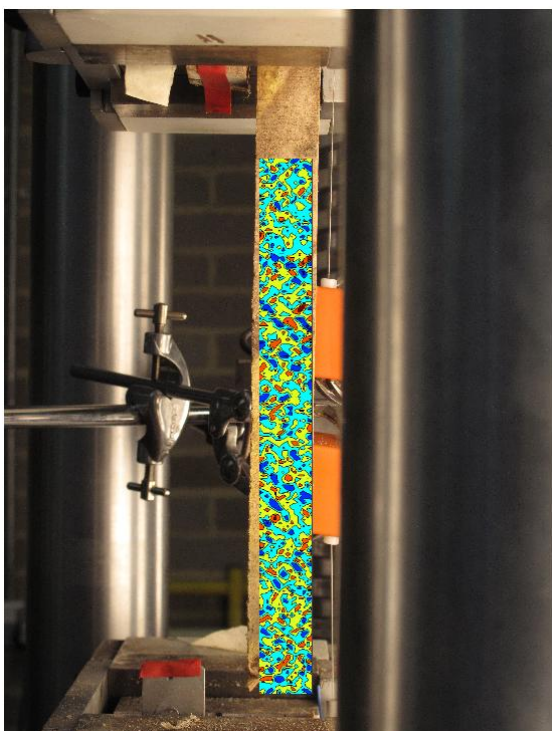
FIGURE 283: XY DIRECTION PIV FIRST–LAST DITCH TRUE SHEAR STRAIN OVER IMAGE

Appendix 6
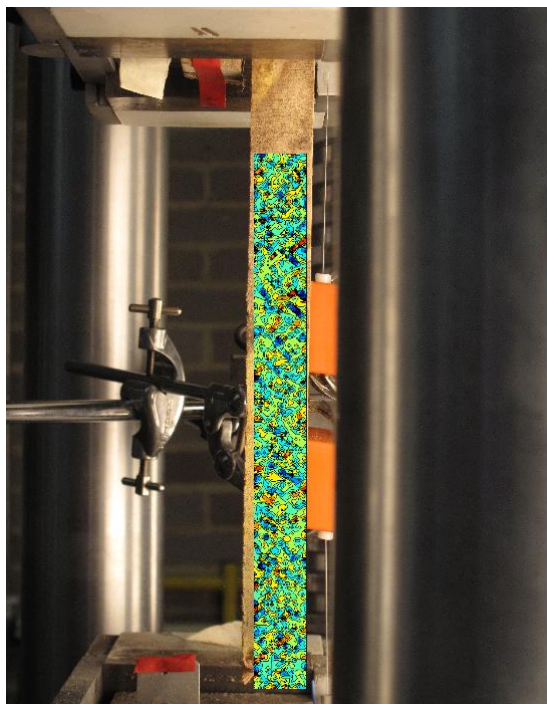
FIGURE 284: XY DIRECTION PIV FIRST–SEQUENTIAL ENGINEERING SHEAR STRAIN OVER

IMAGE
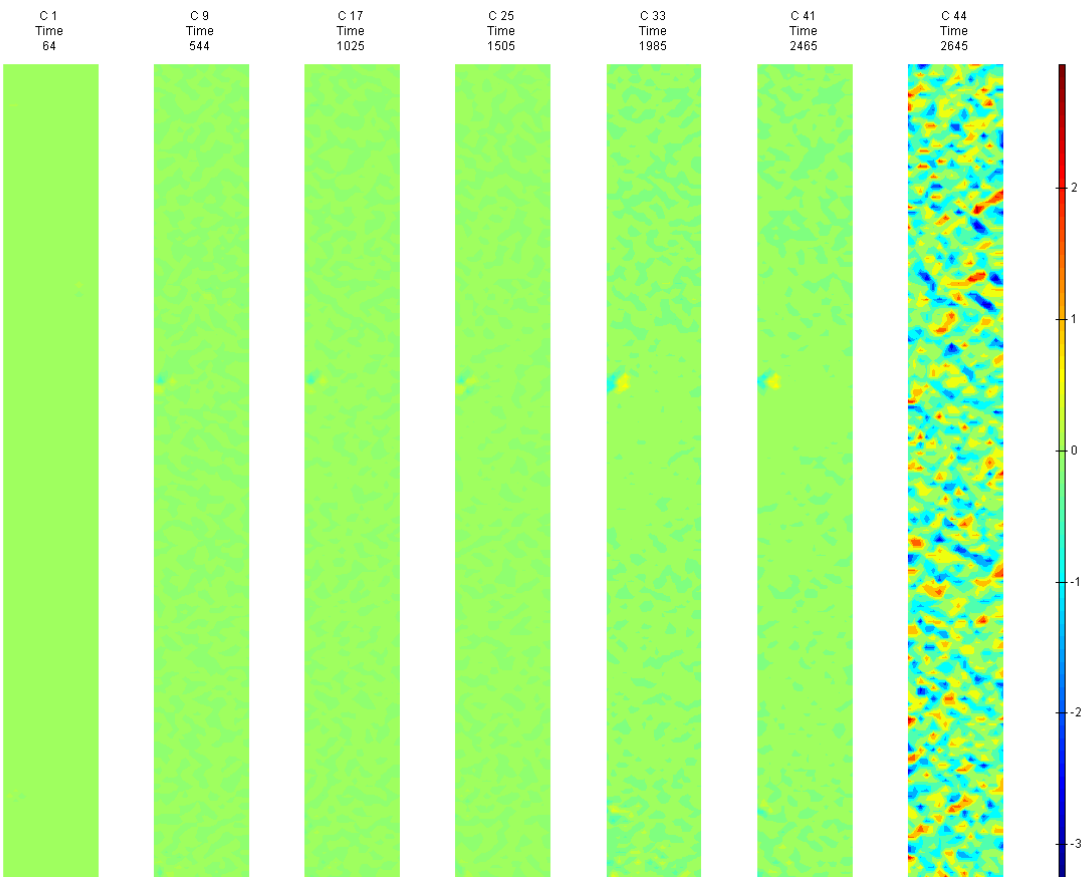
FIGURE 285: XY DIRECTION PIV FIRST–SEQUENTIAL ENGINEERING SHEAR STRAIN OVER TIME

G7
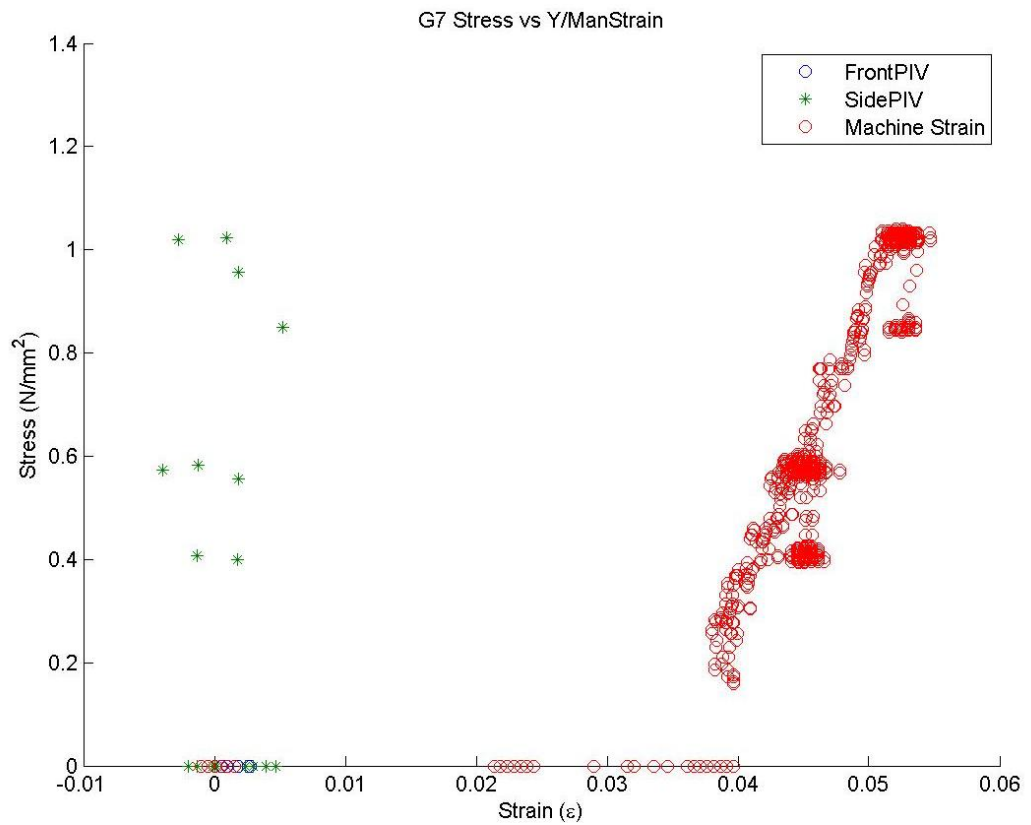
FIGURE 286: G7 TENSILE STRESS VS. MACHINE MEASURED/PIV STRAINS
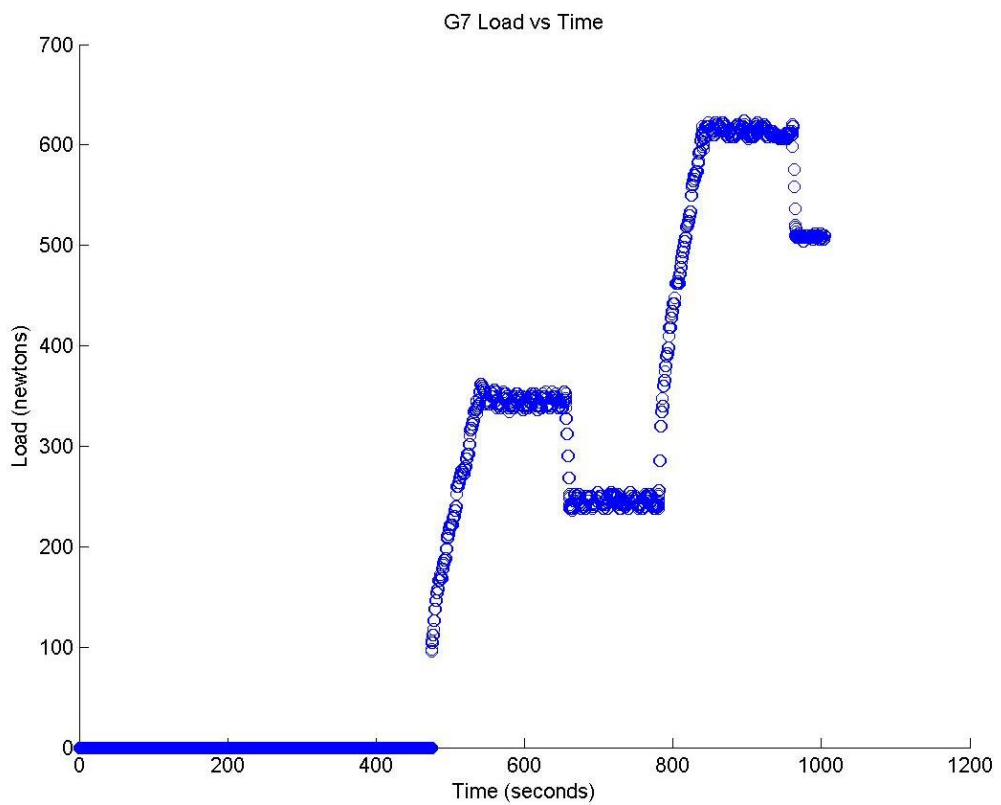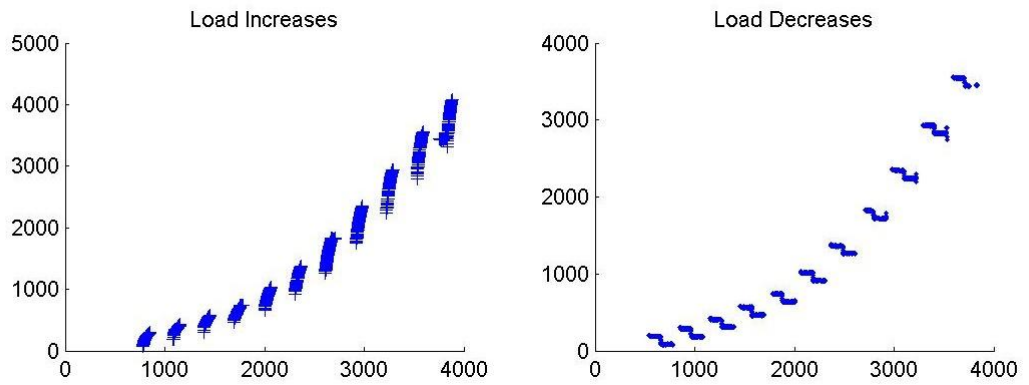

FIGURE 287: G7 TENSILE LOAD VS. TIME
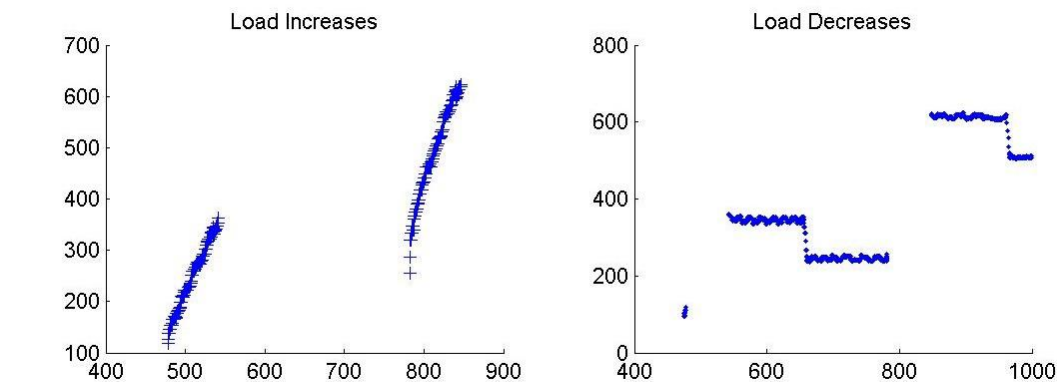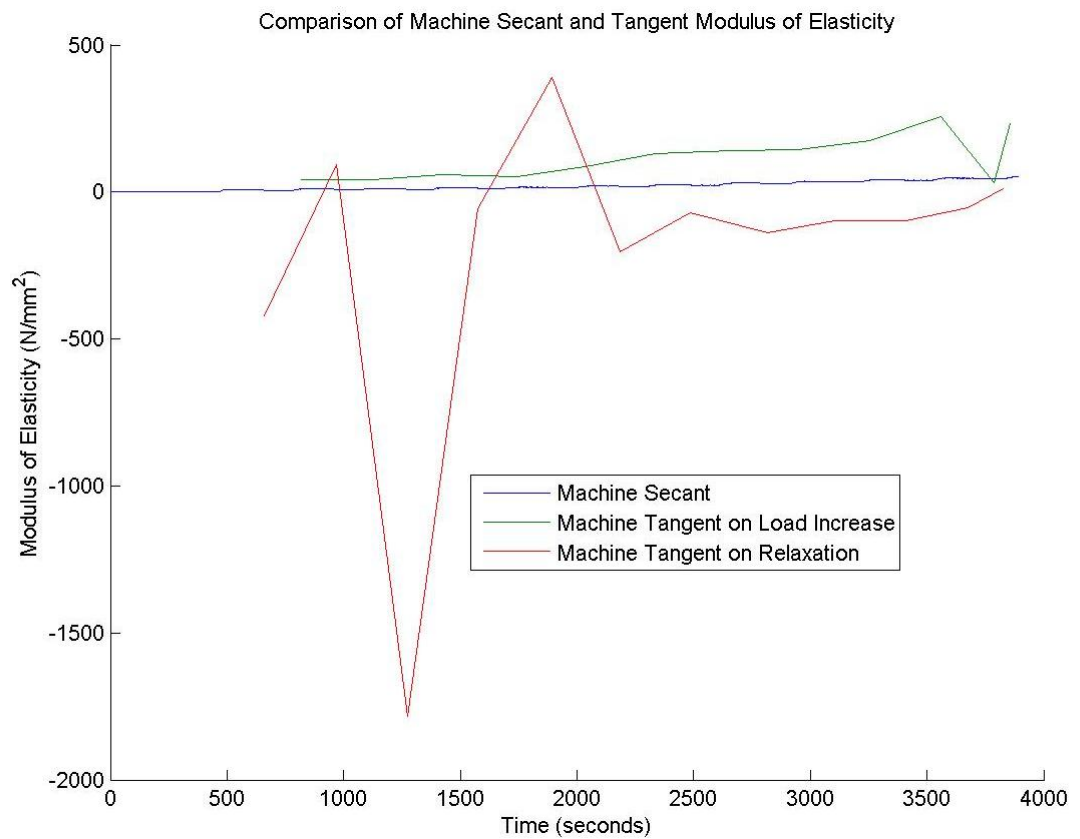
FIGURE 288: G7 CREEP LOADING: INCREMENTS AND RELAXATION
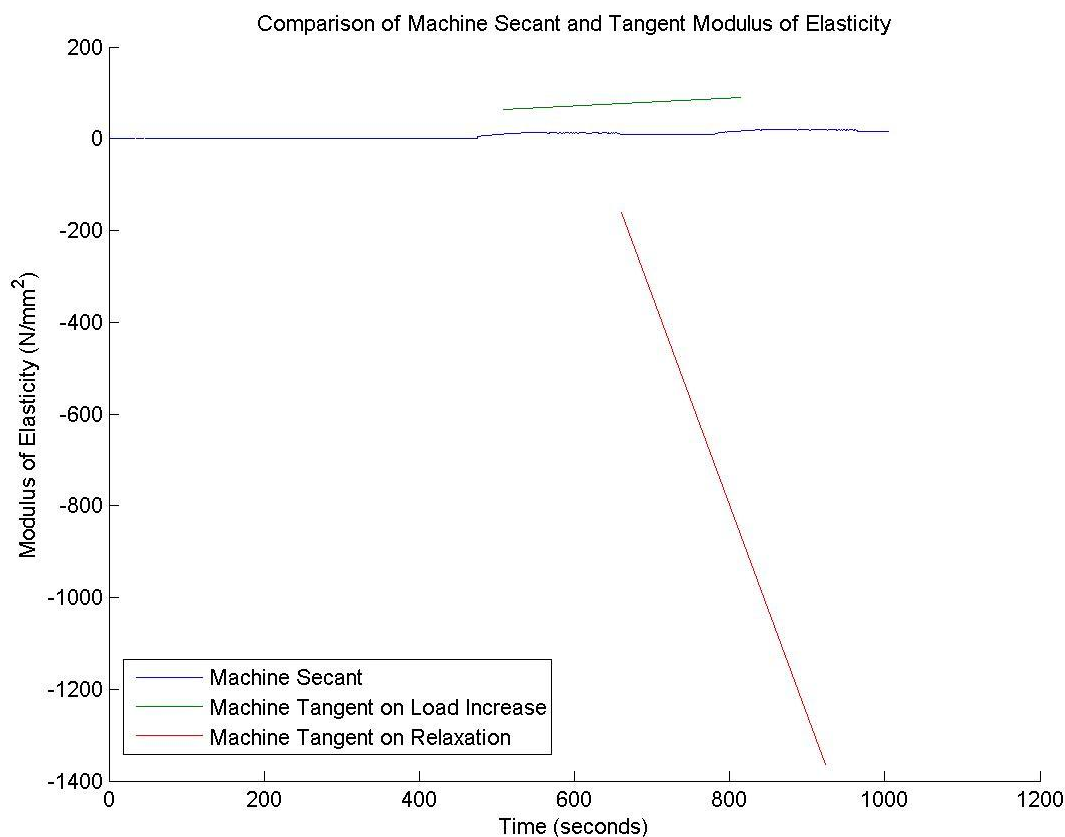
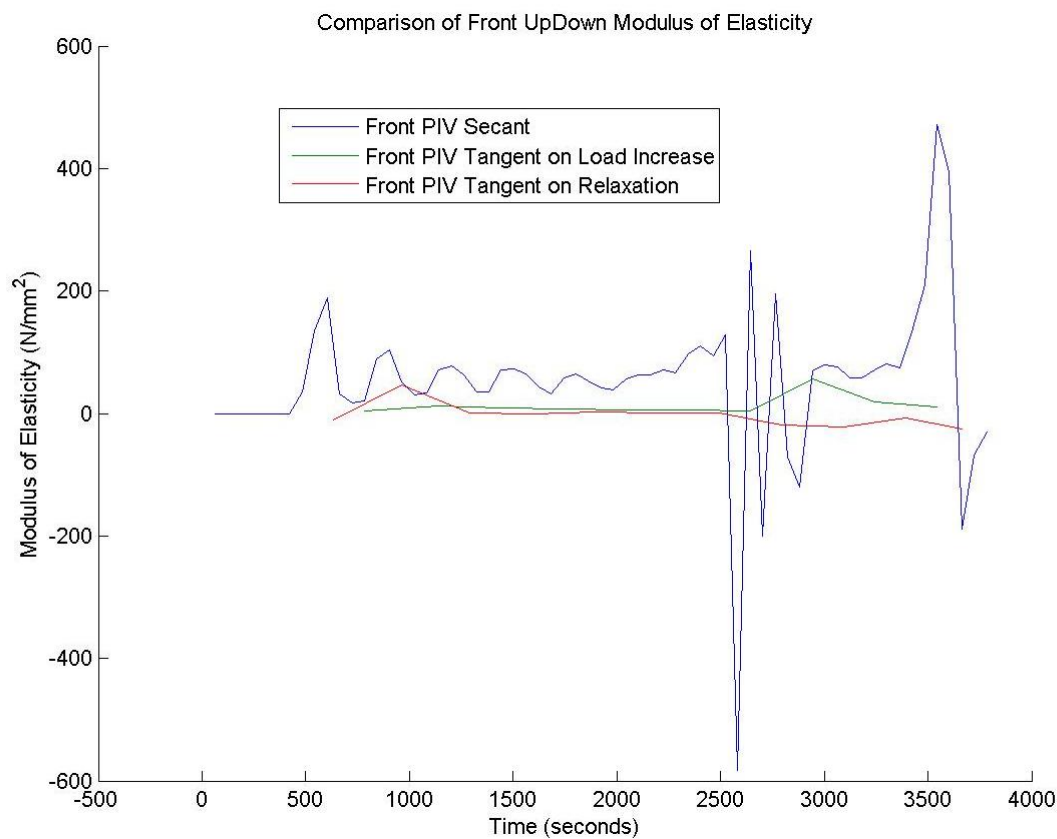FIGURE 289: G7 MACHINE MEASURED SECANT AND TANGENT MODULUS VS. TIME
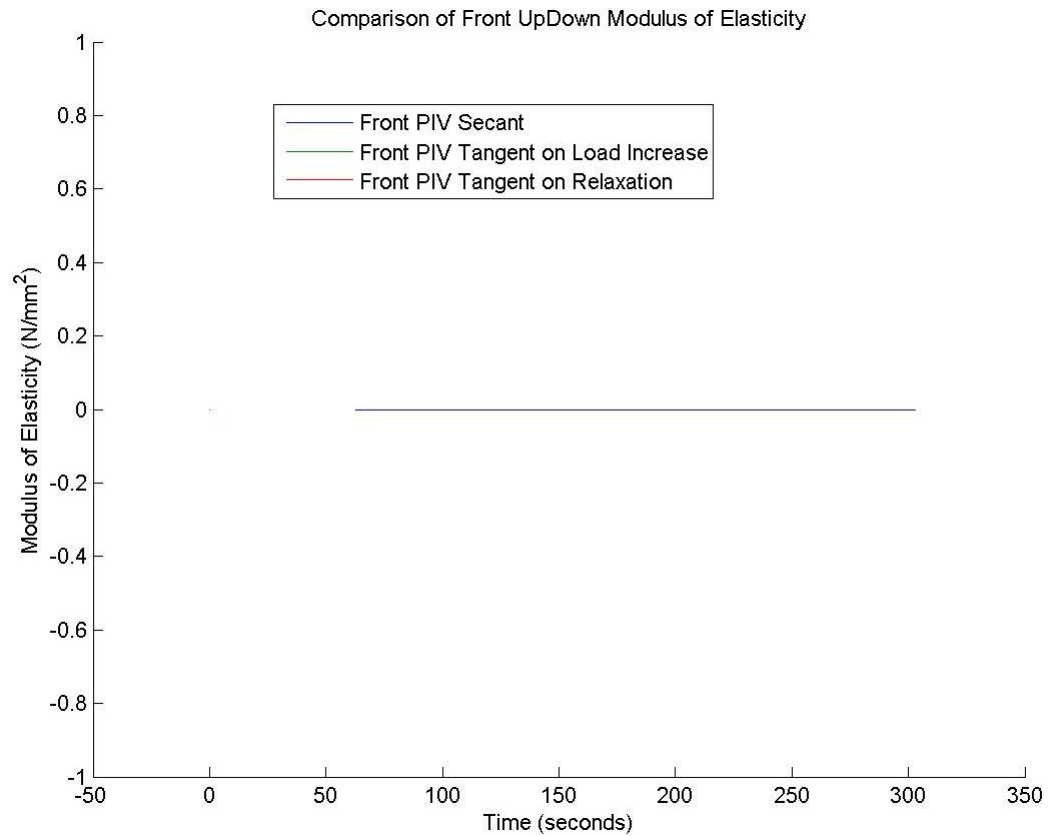
FIGURE 290: G7 FRONT VIEW PIV SECANT AND TANGENT MODULUS VS. TIME
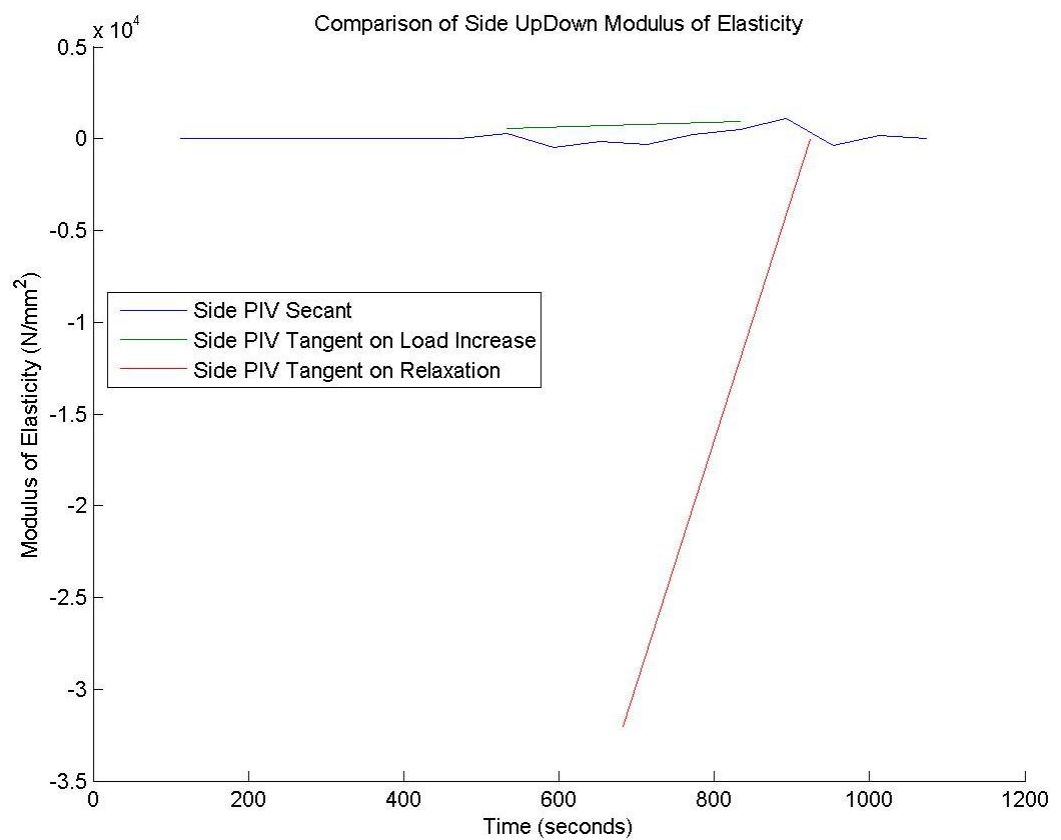
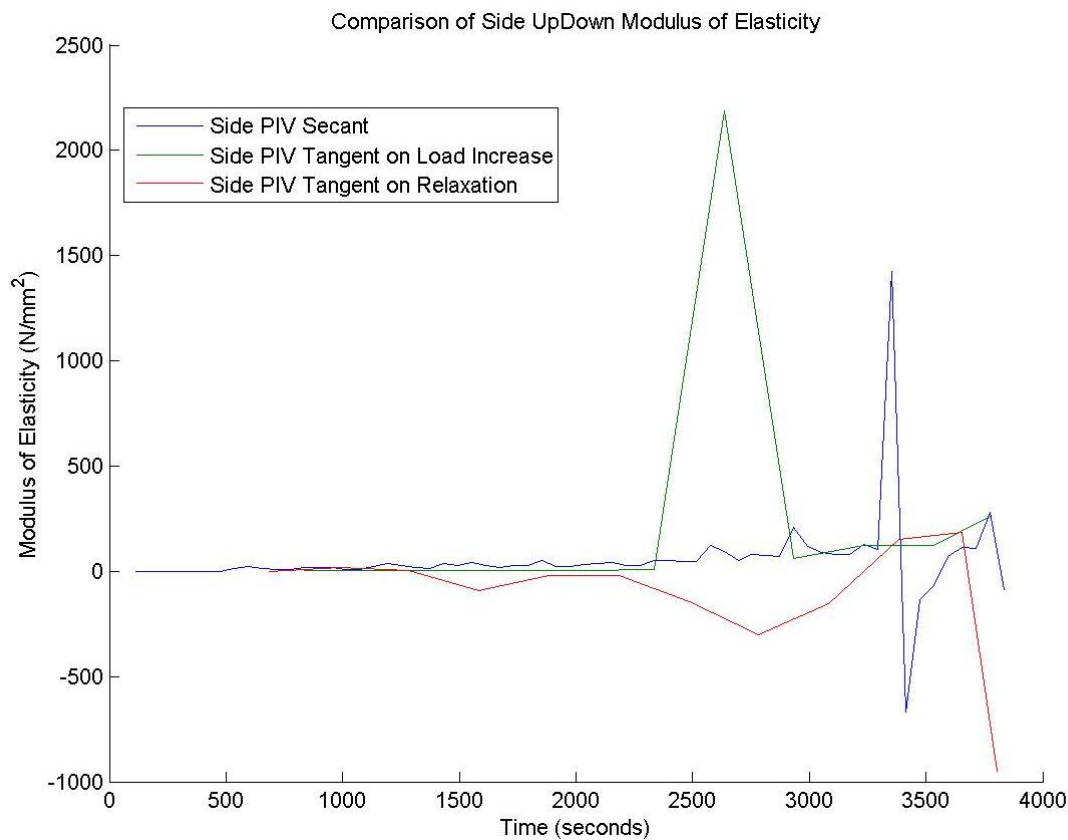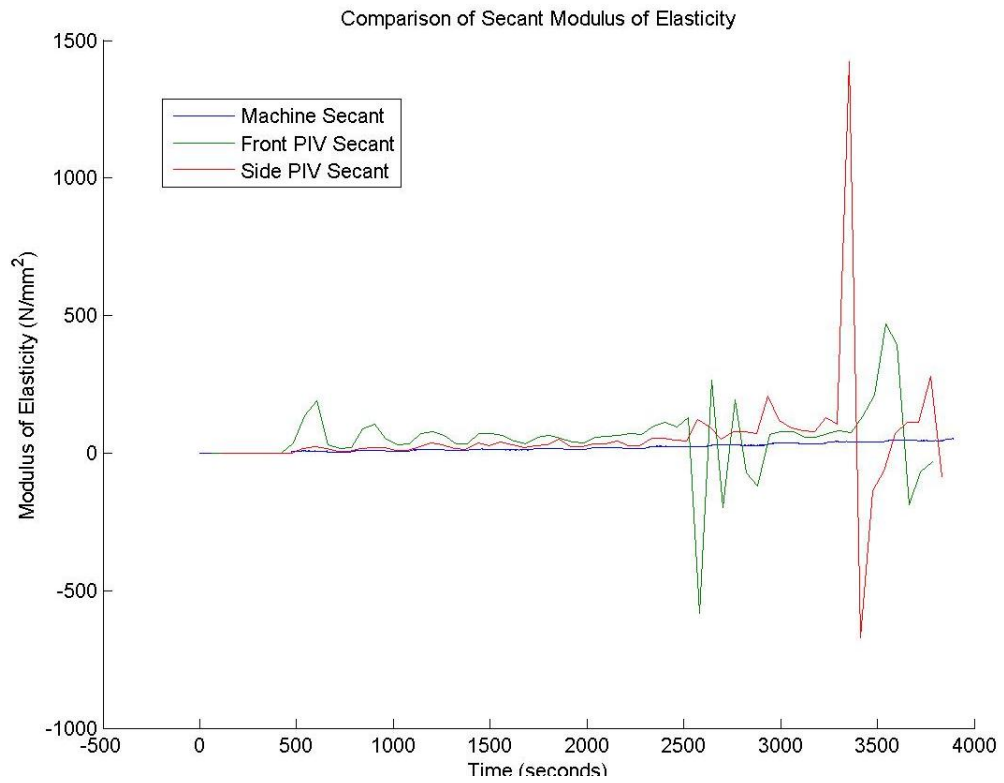FIGURE 291: G7 SIDE VIEW PIV SECANT AND TANGENT MODULUS VS. TIME

Appendix 6
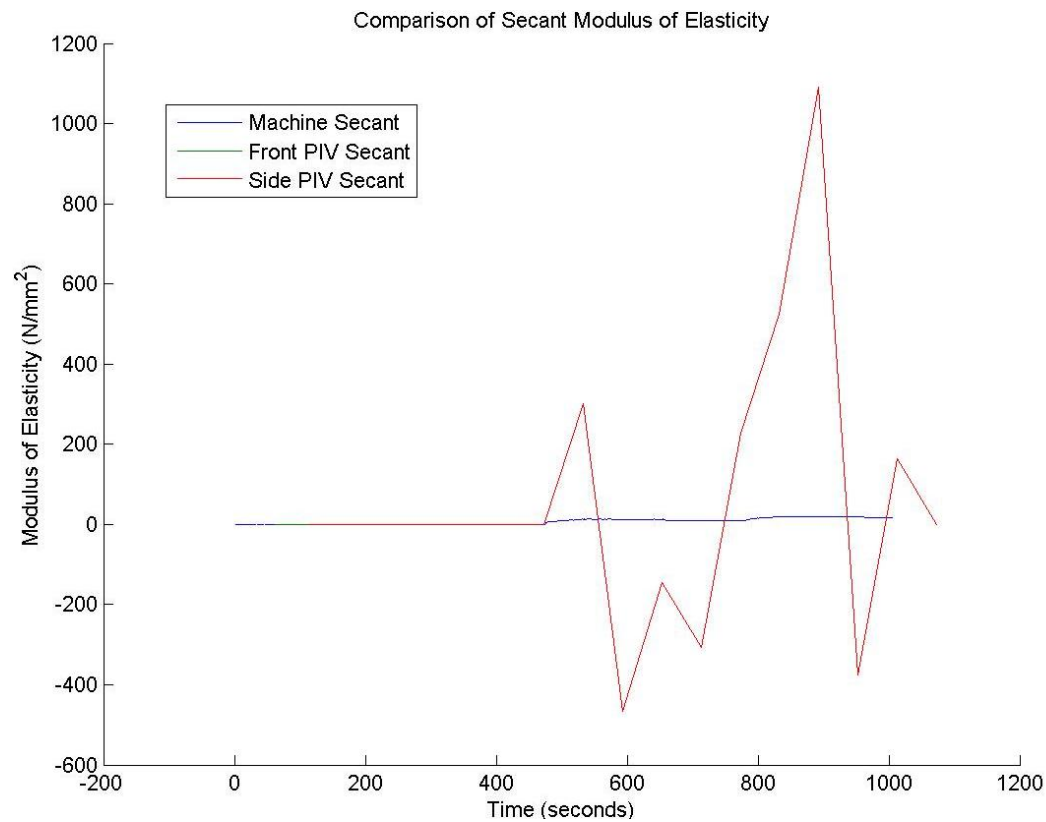
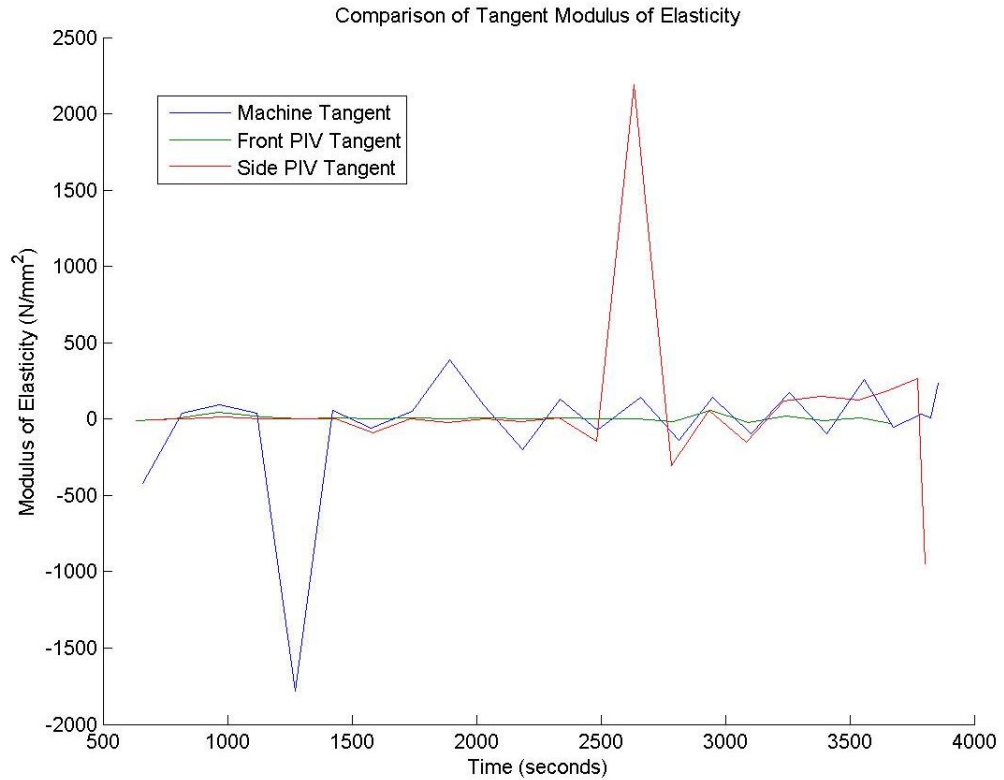FIGURE 292: G7 COMPARISON OF MACHINE MEASURED AND PIV SECANT MODULUS VS. TIME
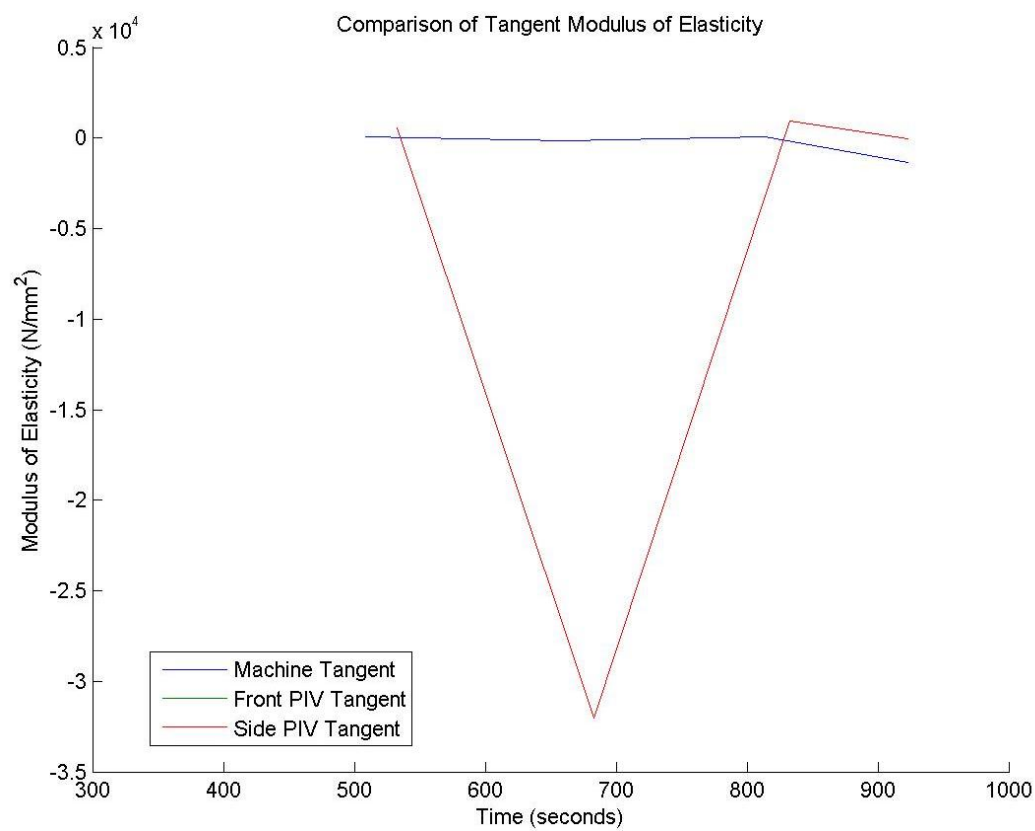
FIGURE 293: G7 COMPARISON OF MACHINE MEASURED AND PIV TANGENT MODULUS VS.

TIME

G7 Sample

FIGURE 294: SAMPLE GRAIN ORIENTATIONS OF THE FRONT (LEFT 4 IMAGES) AND SIDE (RIGHT 4 IMAGES) VIEW BEFORE (FIRST 2 OF 4 IMAGES) AND AFTER (LAST 2 OF 4 IMAGES) BREAKAGE

Appendix 6

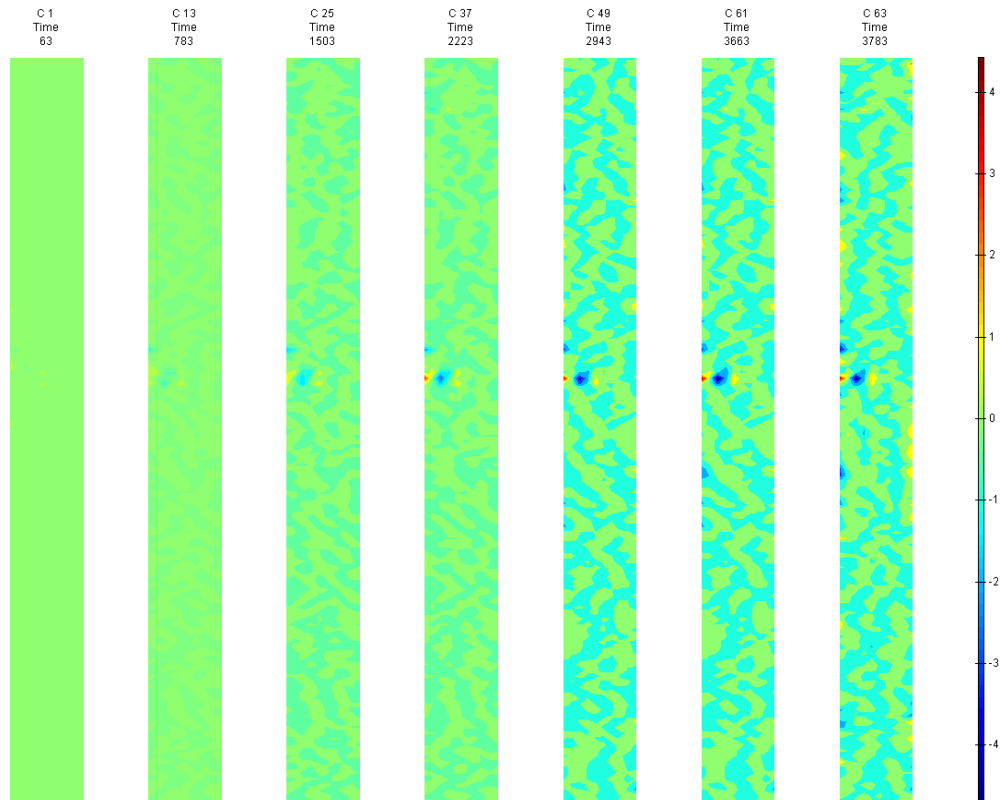## G7 Front View
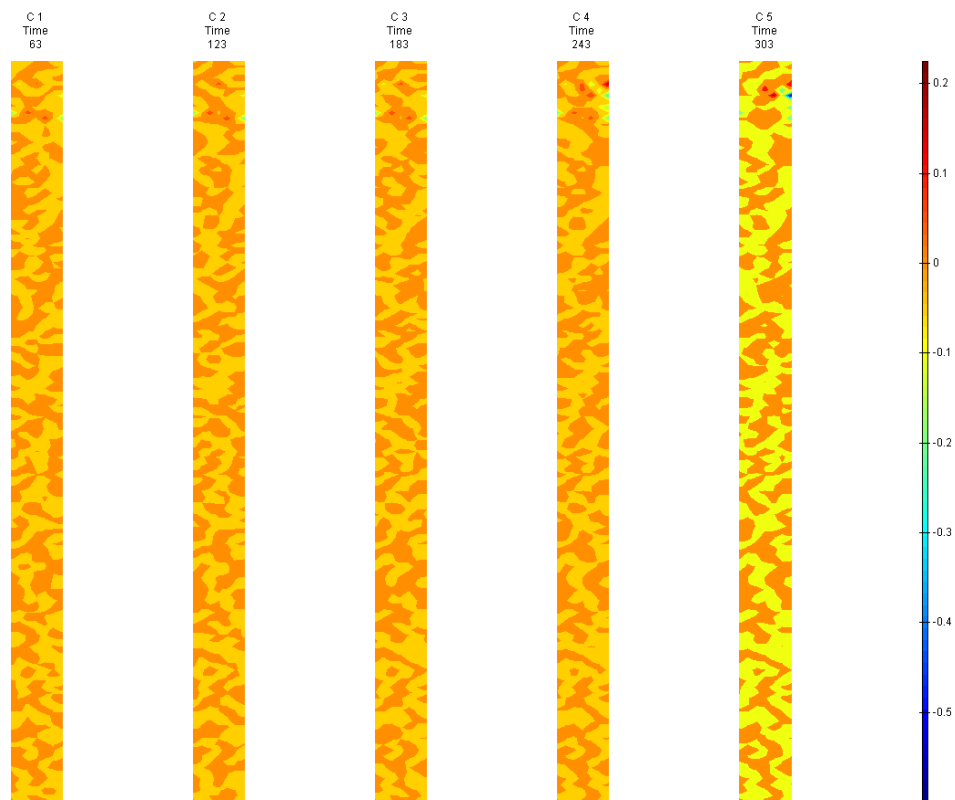
FIGURE 295: X DIRECTION PIV SEQUENTIAL ENGINEERING STRAIN OVER TIME
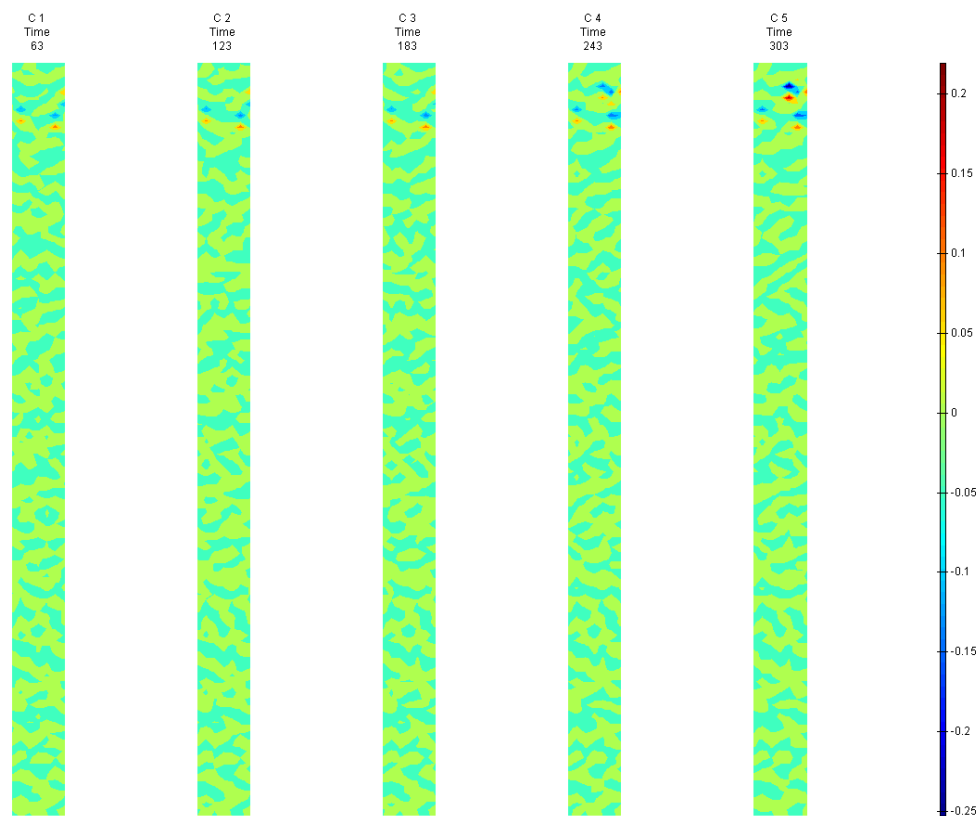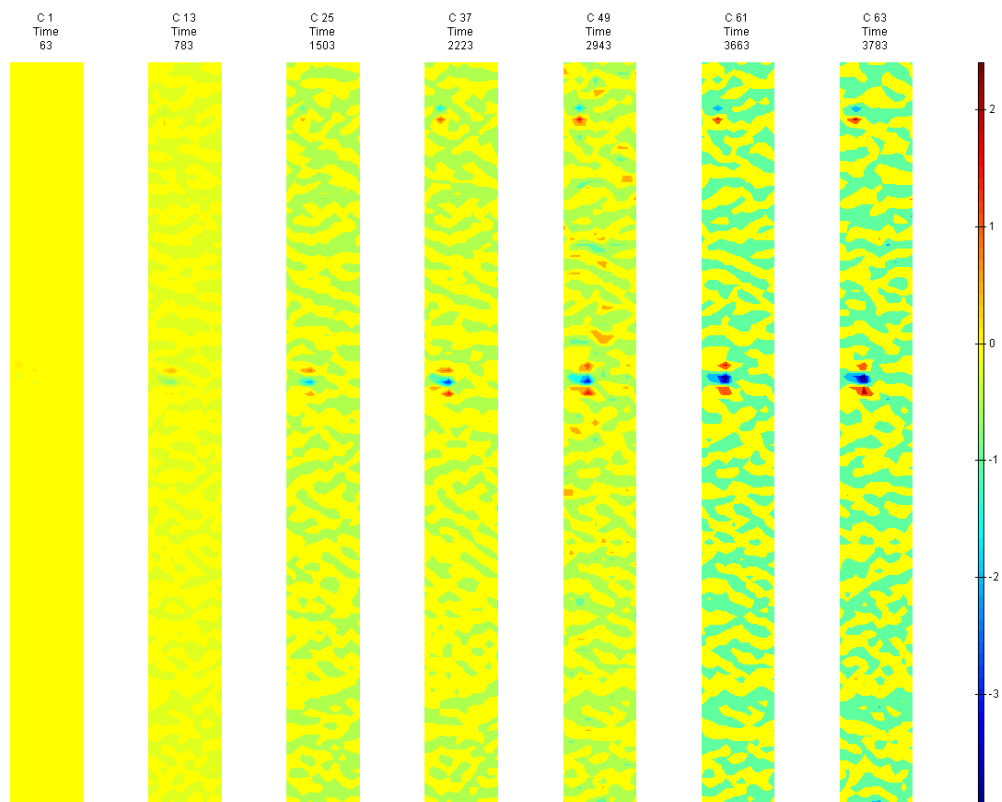

FIGURE 296: Y DIRECTION PIV SEQUENTIAL ENGINEERING STRAIN OVER TIME
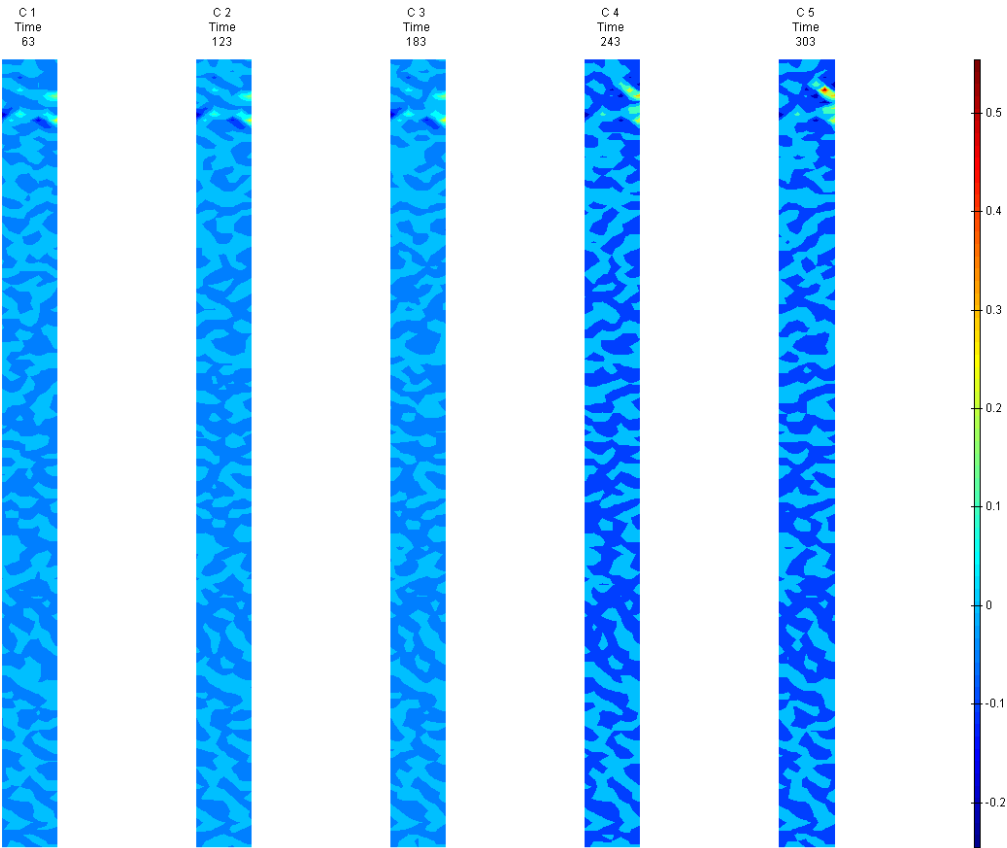
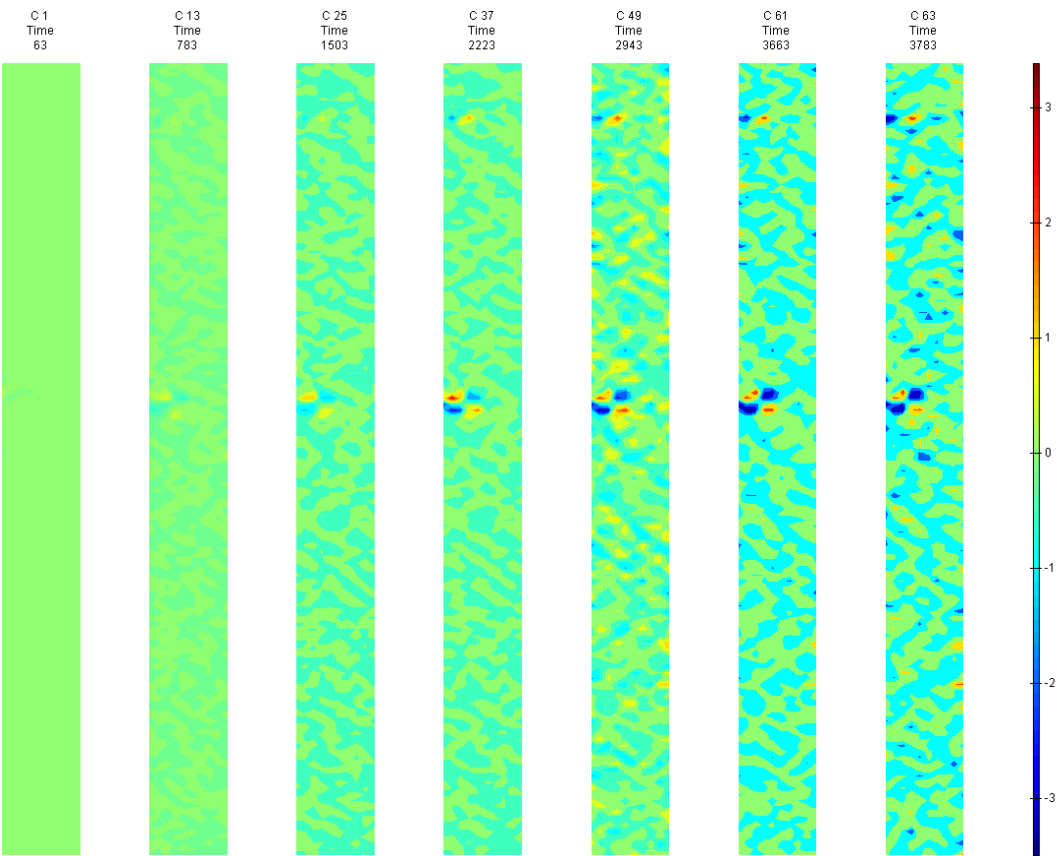FIGURE 297: XY DIRECTION PIV SEQUENTIAL ENGINEERING SHEAR STRAIN OVER TIME
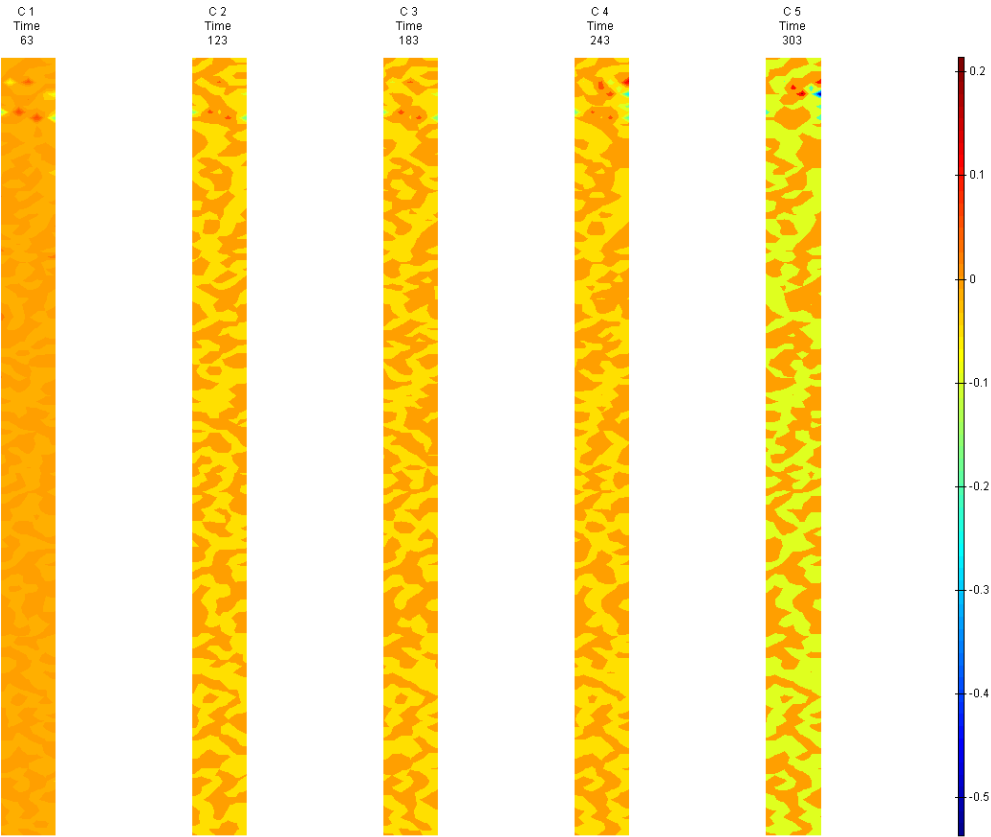
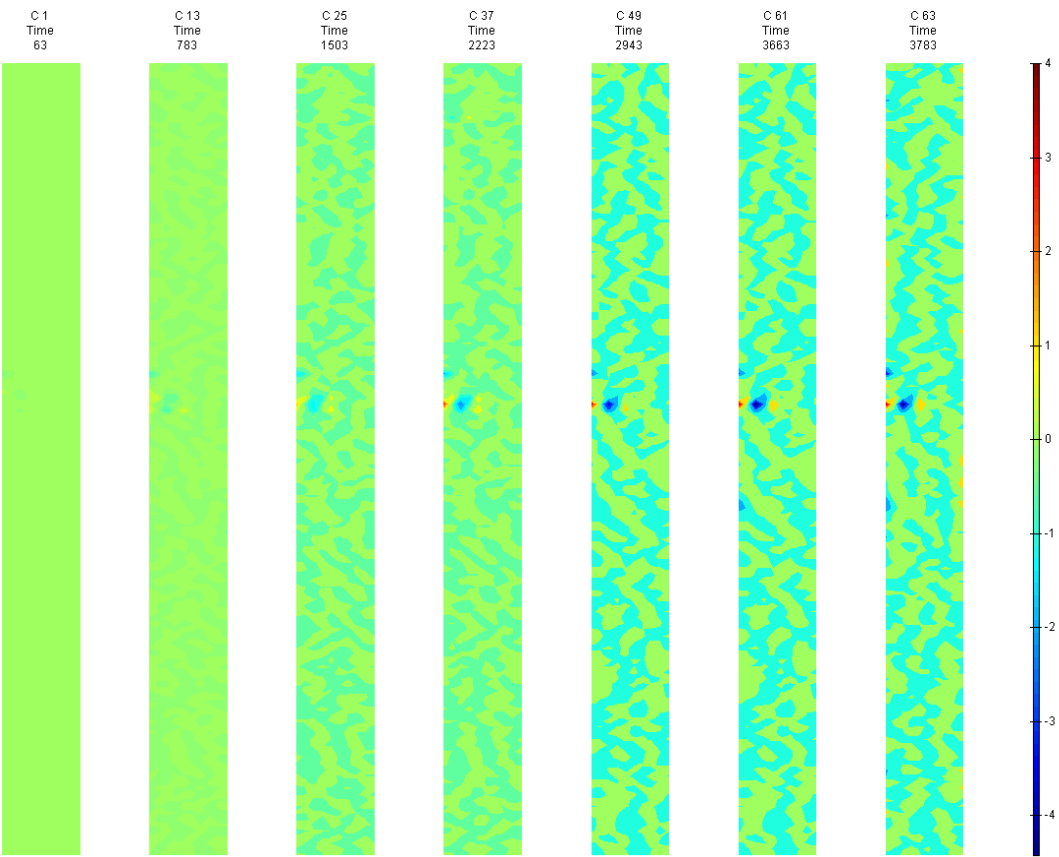FIGURE 298: X DIRECTION PIV SEQUENTIAL TRUE STRAIN OVER TIME

Appendix 6
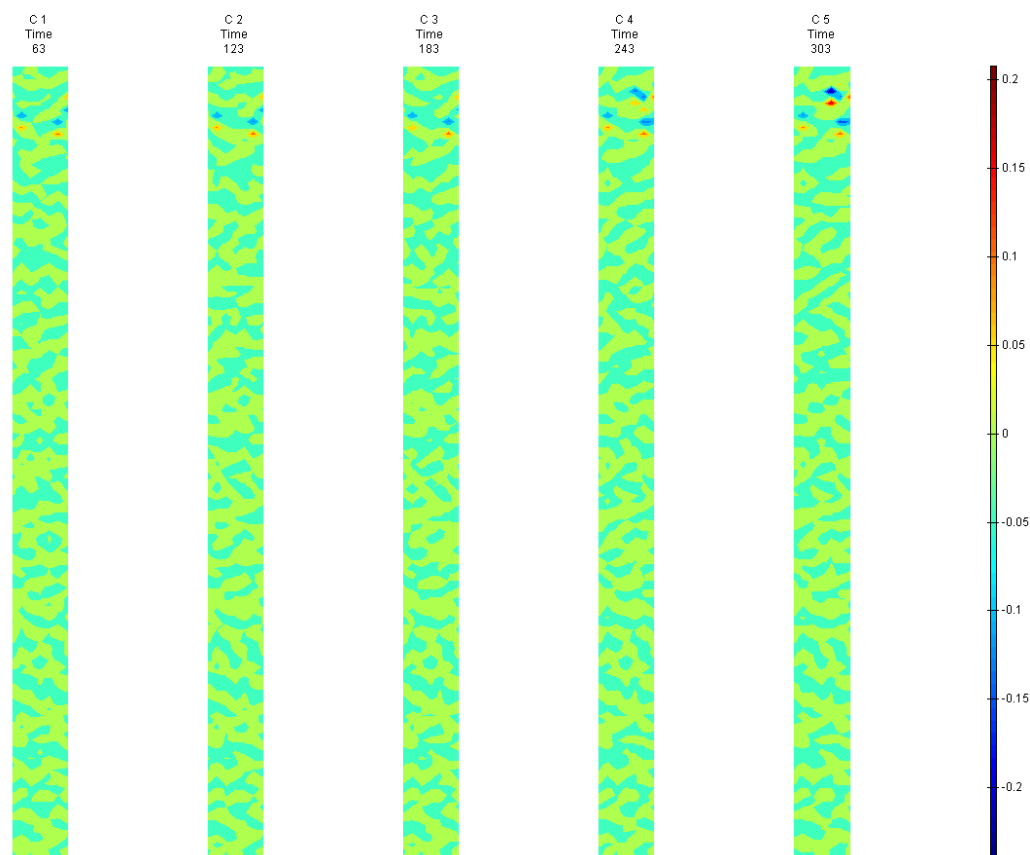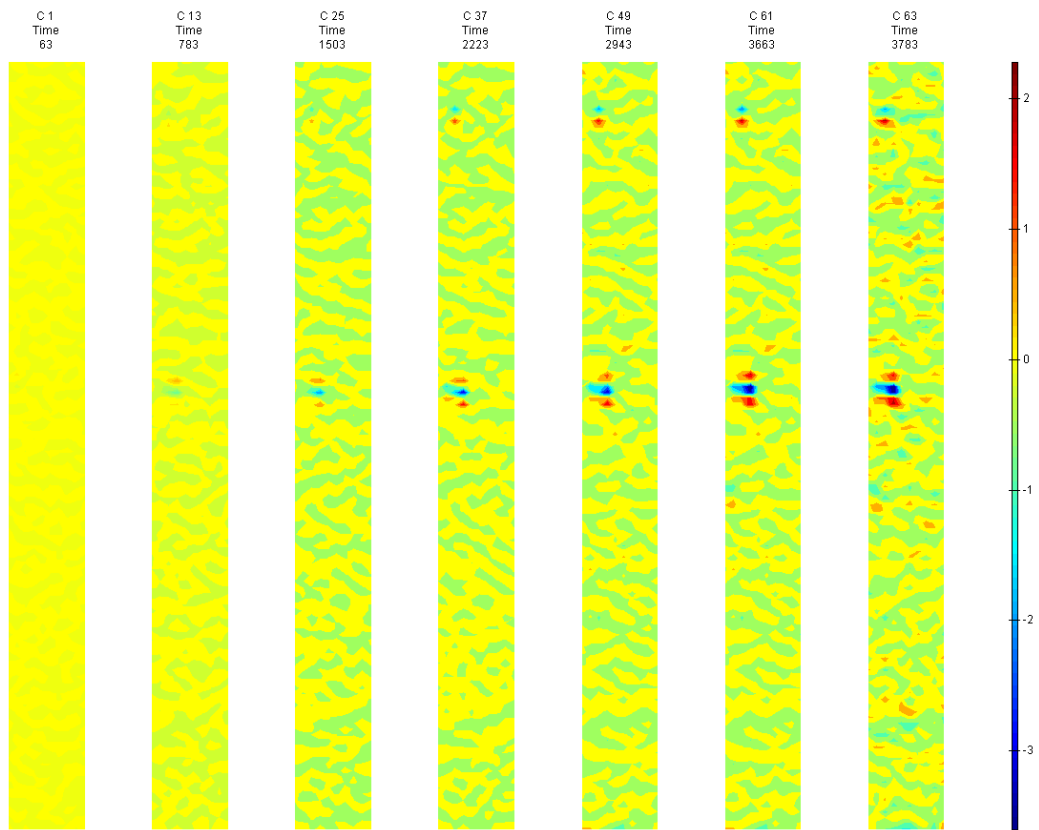

FIGURE 299: Y DIRECTION PIV SEQUENTIAL TRUE STRAIN OVER TIME
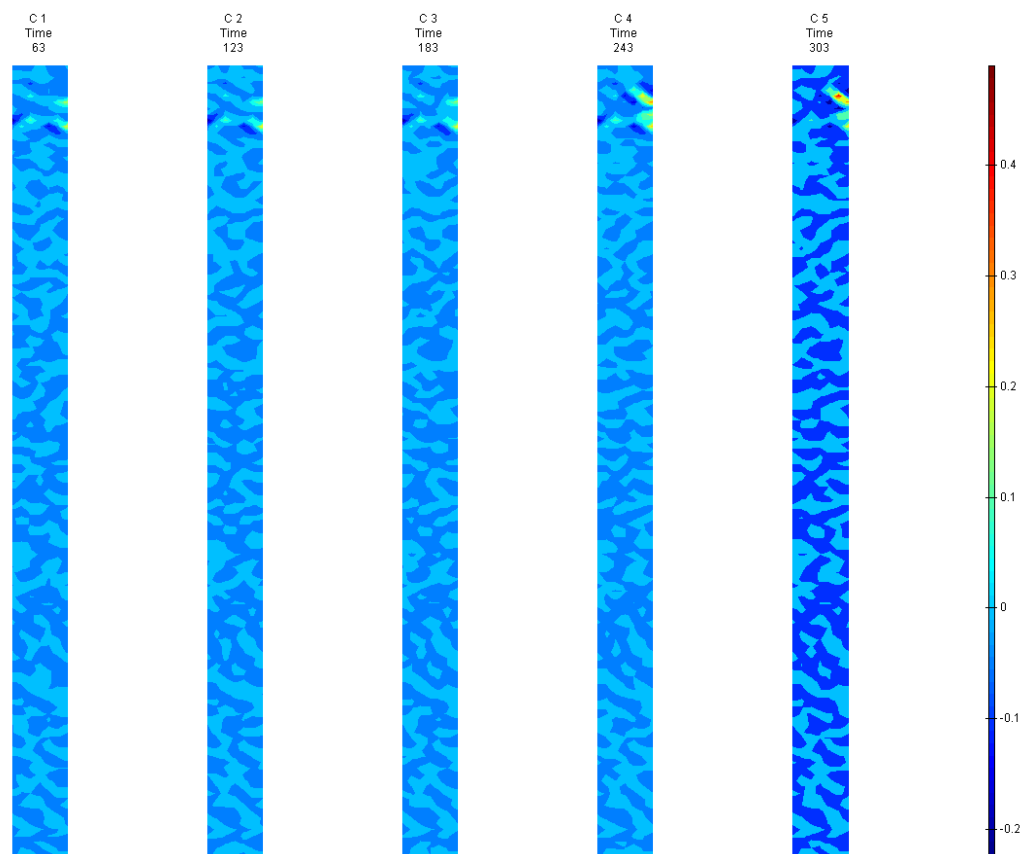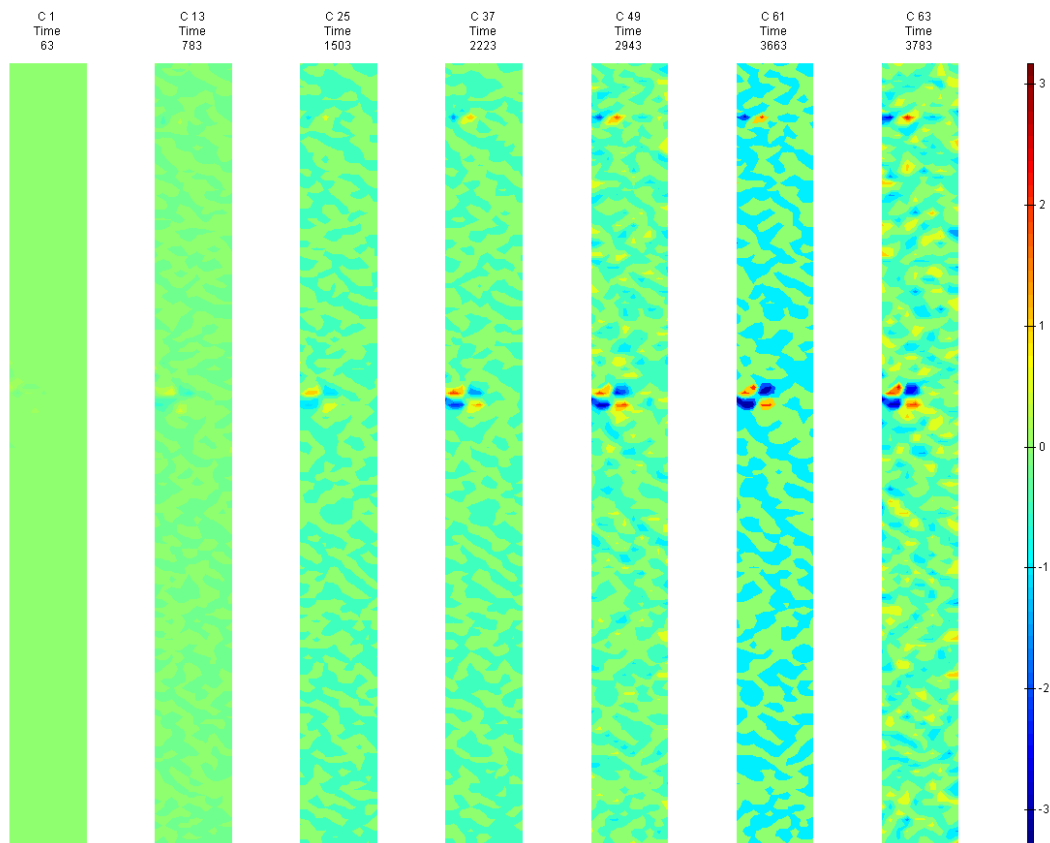

FIGURE 300: XY DIRECTION PIV SEQUENTIAL TRUE SHEAR STRAIN OVER TIME
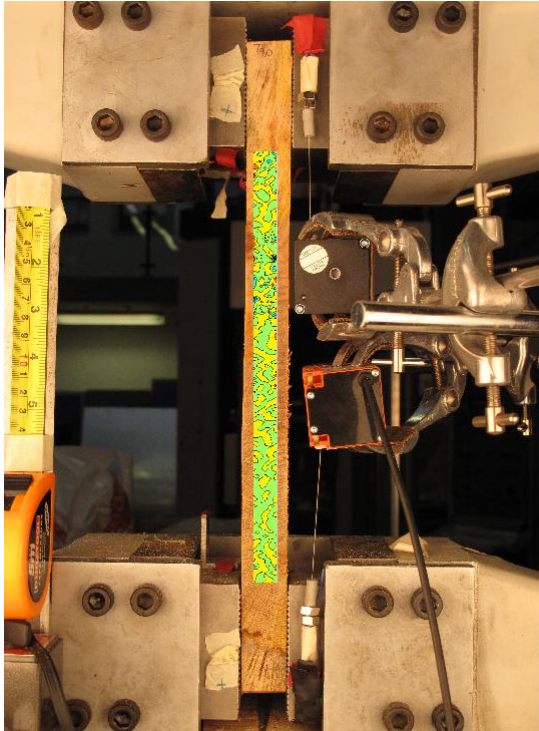
FIGURE 301: X DIRECTION PIV FIRST–LAST DITCH ENGINEERING STRAIN OVER IMAGE
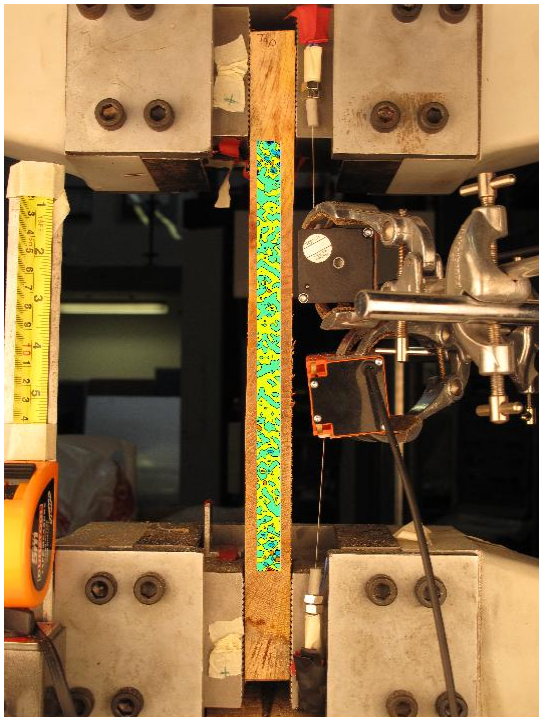
FIGURE 302: Y DIRECTION PIV FIRST–LAST DITCH ENGINEERING STRAIN OVER IMAGE
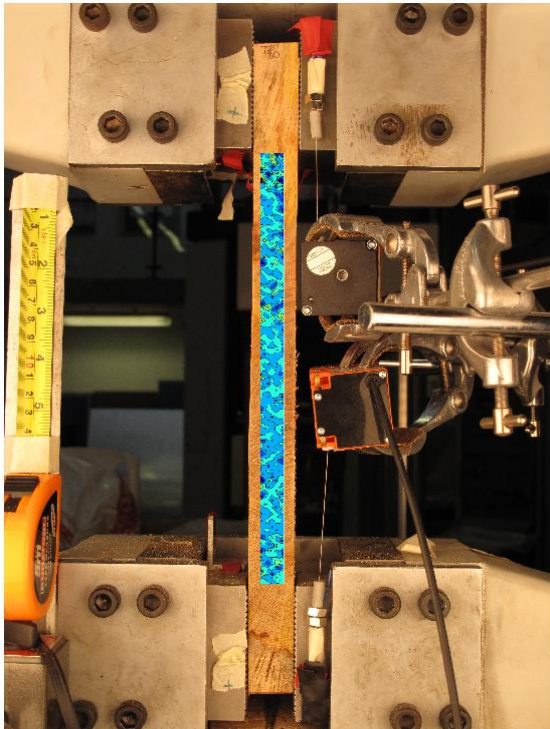
FIGURE 303: XY DIRECTION PIV FIRST–LAST DITCH ENGINEERING SHEAR STRAIN OVER
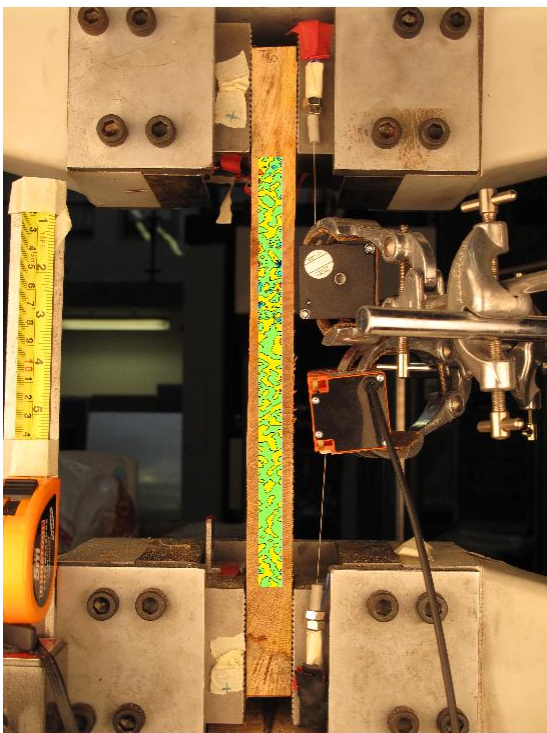
IMAGE

FIGURE 304: X DIRECTION PIV FIRST–LAST DITCH TRUE STRAIN OVER IMAGE
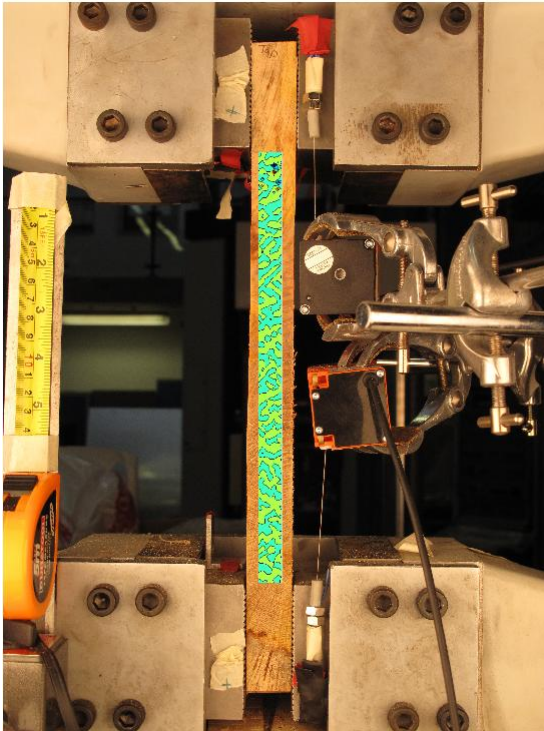
FIGURE 305: Y DIRECTION PIV FIRST–LAST DITCH TRUE STRAIN OVER IMAGE
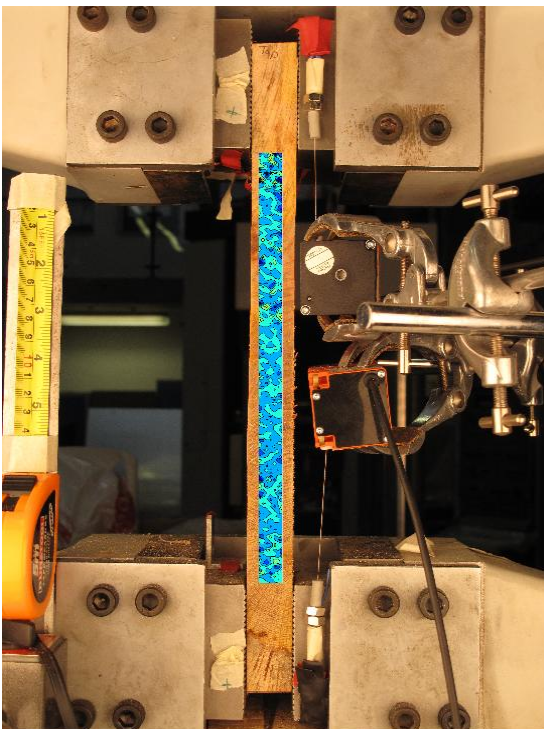
FIGURE 306: XY DIRECTION PIV FIRST–LAST DITCH TRUE SHEAR STRAIN OVER IMAGE

Appendix 6
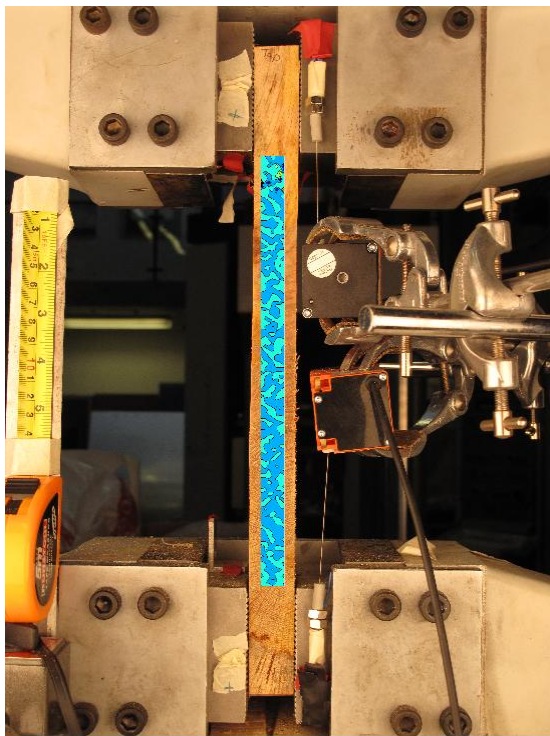
FIGURE 307: XY DIRECTION PIV FIRST–SEQUENTIAL ENGINEERING SHEAR STRAIN OVER

IMAGE
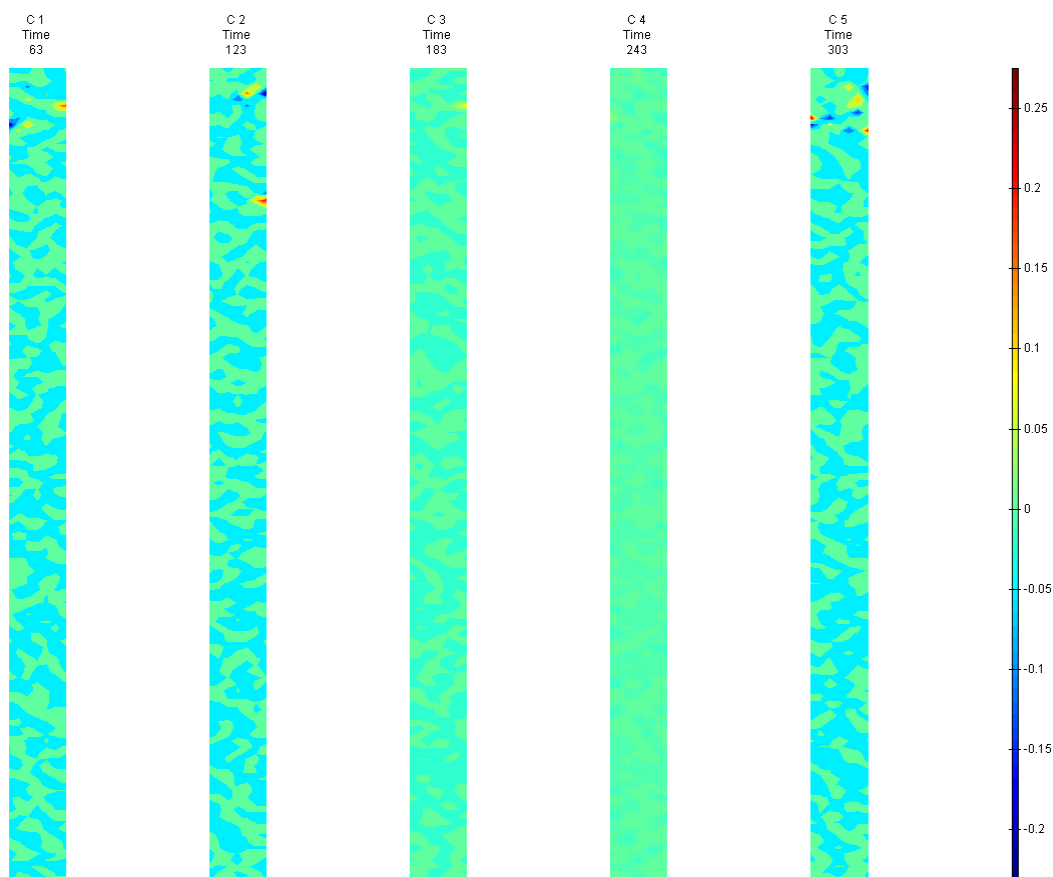
FIGURE 308: XY DIRECTION PIV FIRST–SEQUENTIAL ENGINEERING SHEAR STRAIN OVER TIME

G7 Side View
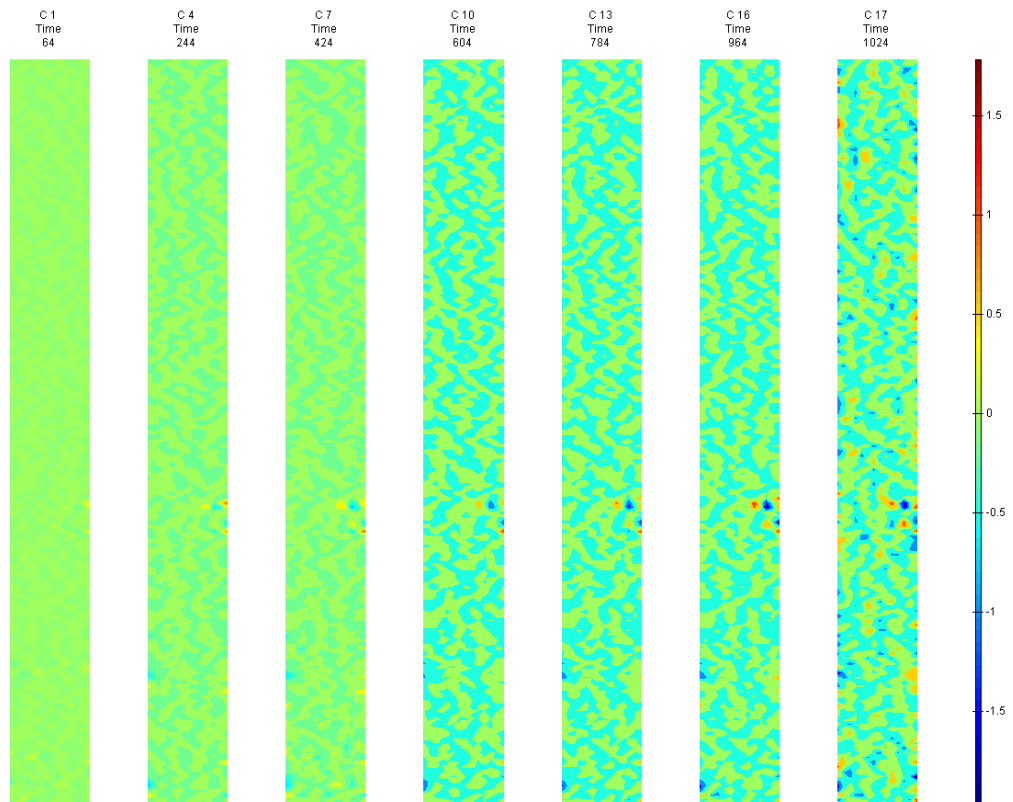
FIGURE 309: X DIRECTION PIV SEQUENTIAL ENGINEERING STRAIN OVER TIME
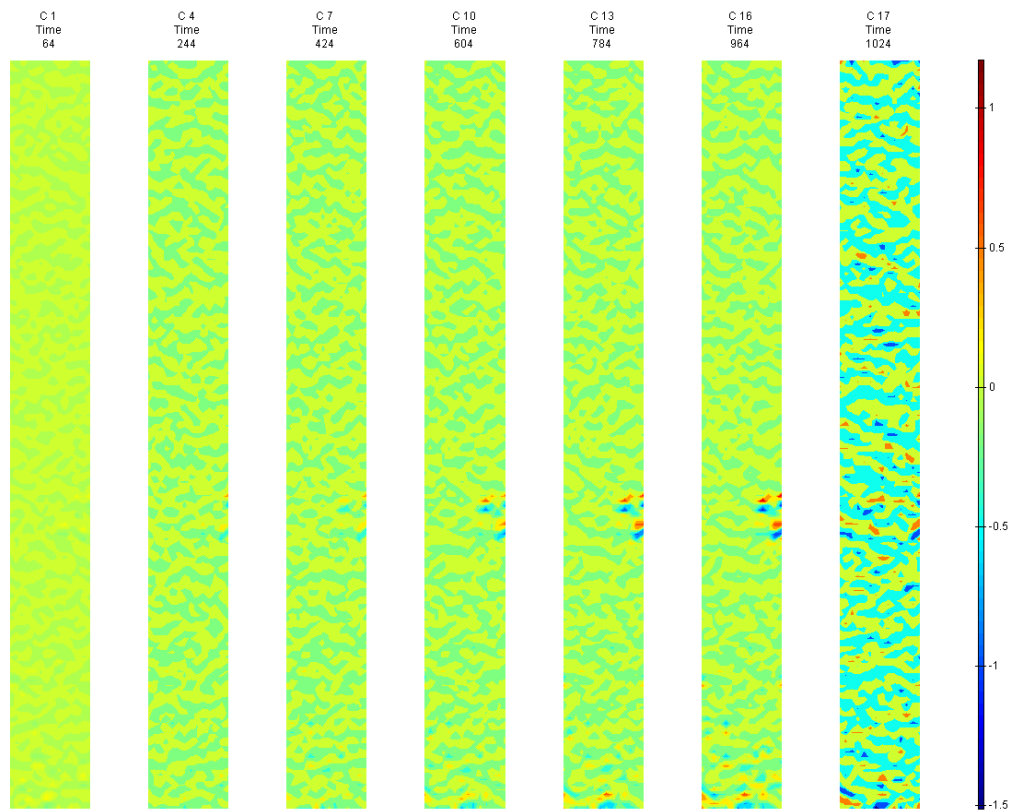
FIGURE 310: Y DIRECTION PIV SEQUENTIAL ENGINEERING STRAIN OVER TIME

Appendix 6
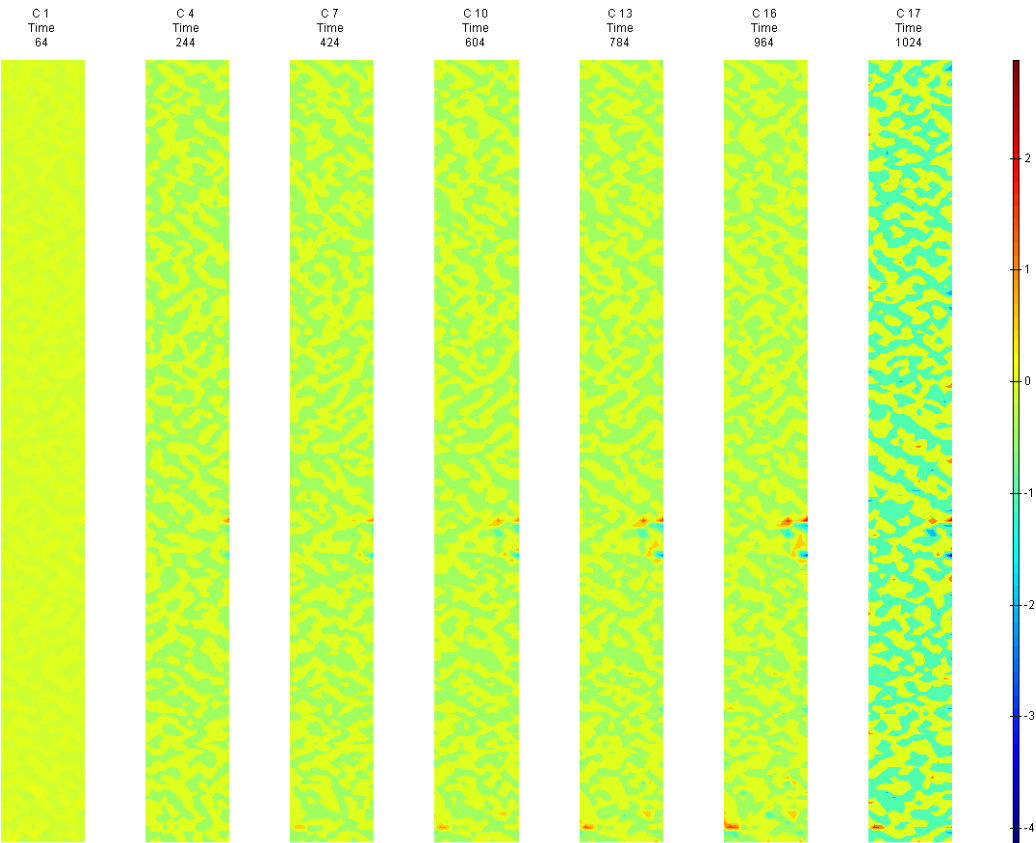
FIGURE 311: XY DIRECTION PIV SEQUENTIAL ENGINEERING SHEAR STRAIN OVER TIME
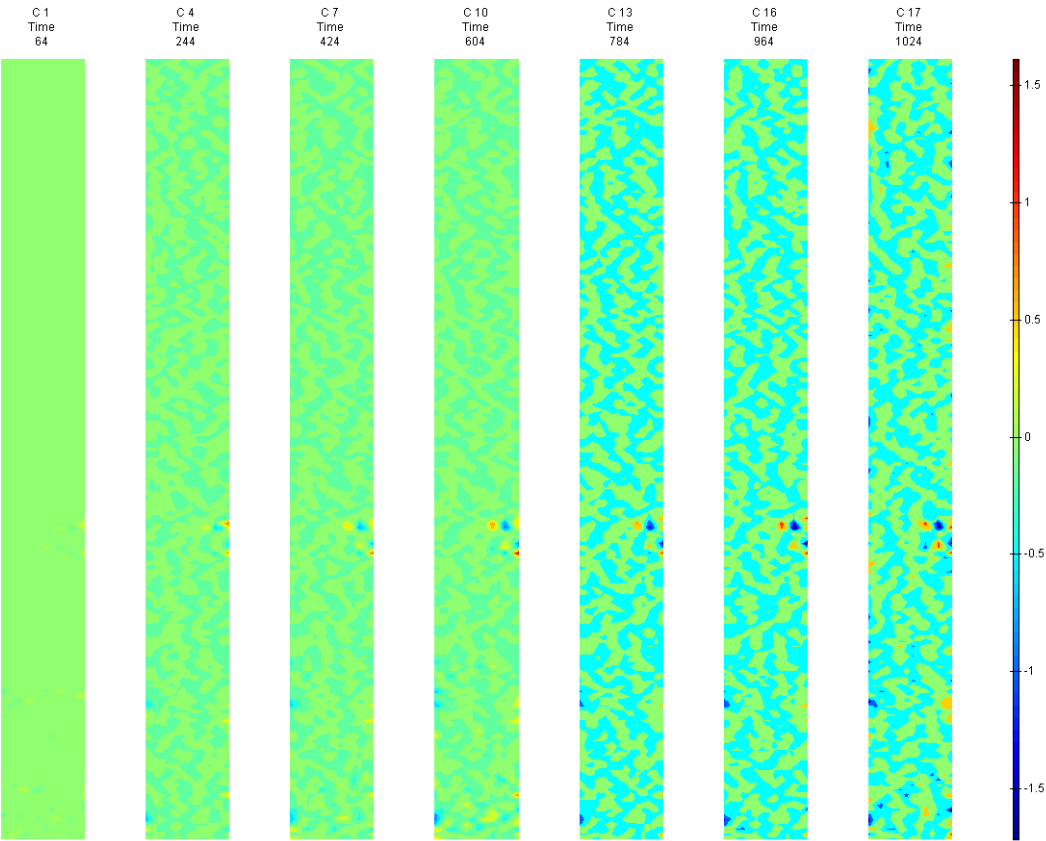
FIGURE 312: X DIRECTION PIV SEQUENTIAL TRUE STRAIN OVER TIME
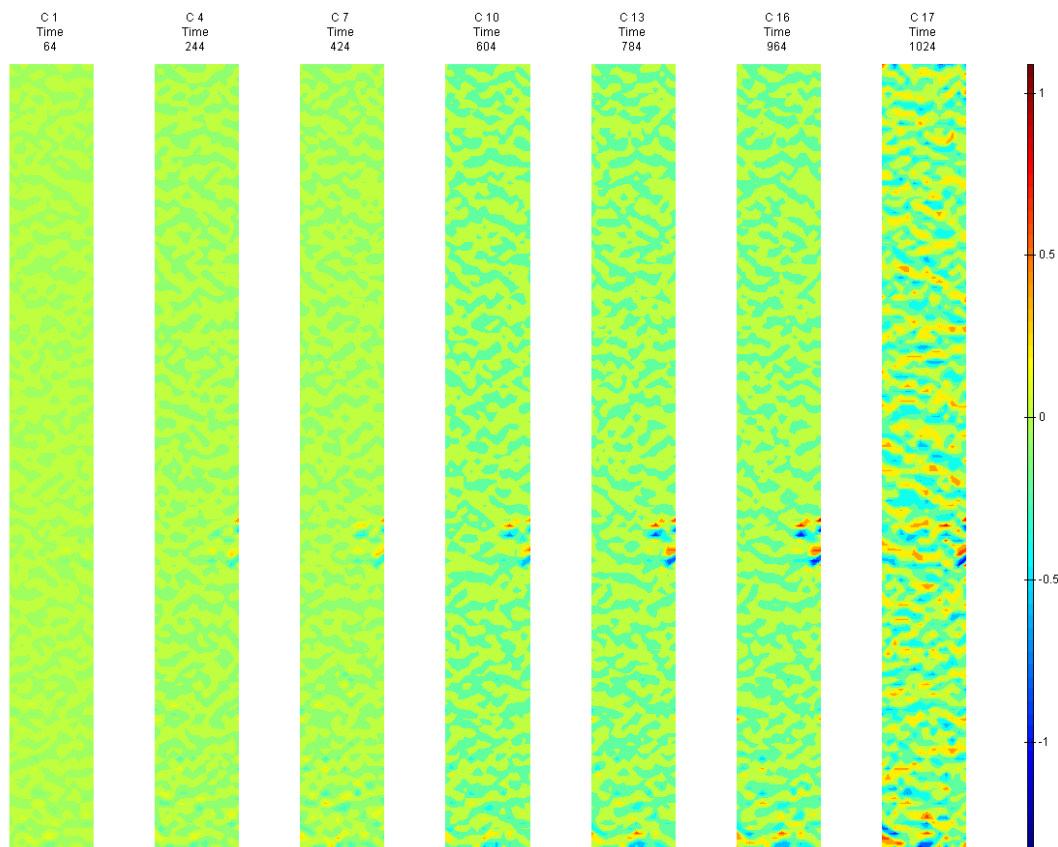
FIGURE 313: Y DIRECTION PIV SEQUENTIAL TRUE STRAIN OVER TIME
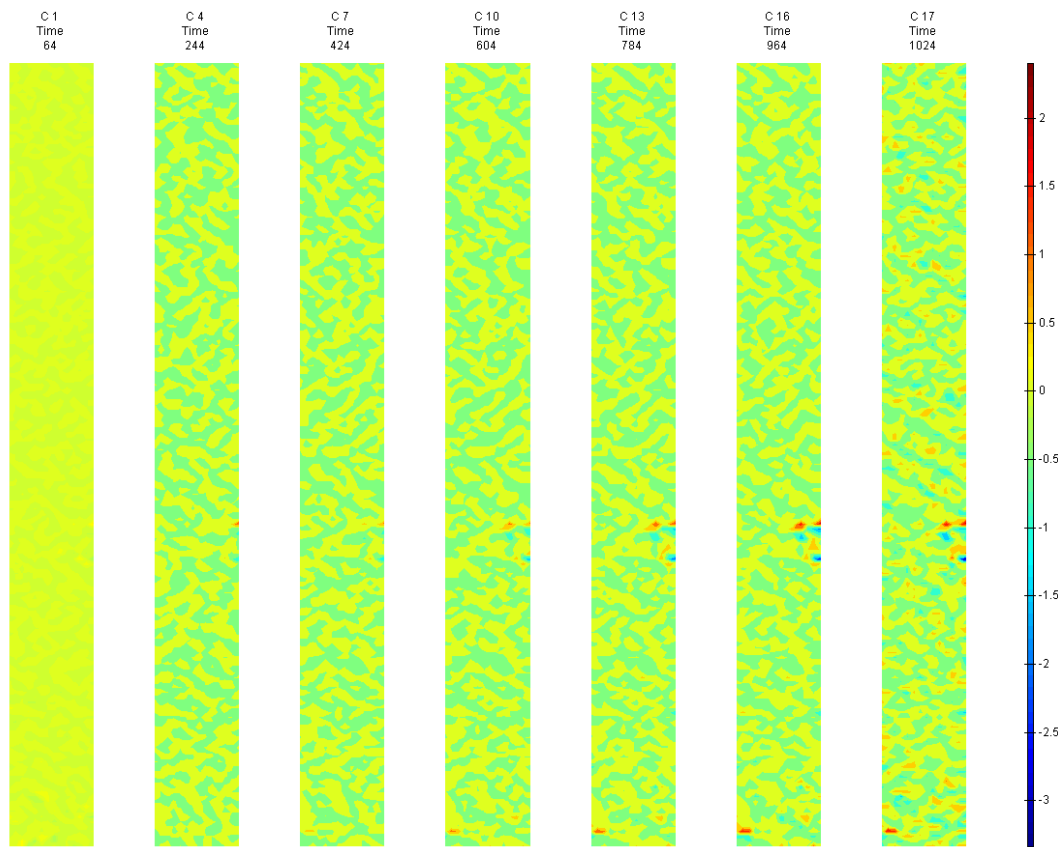
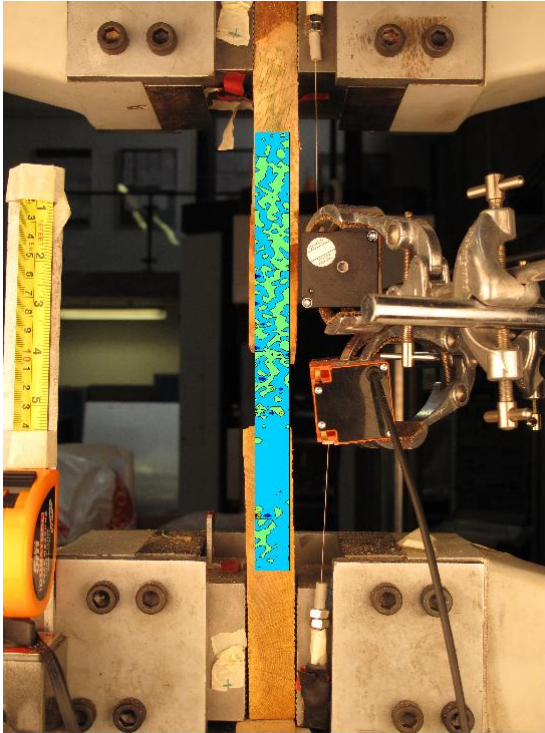FIGURE 314: XY DIRECTION PIV SEQUENTIAL TRUE SHEAR STRAIN OVER TIME
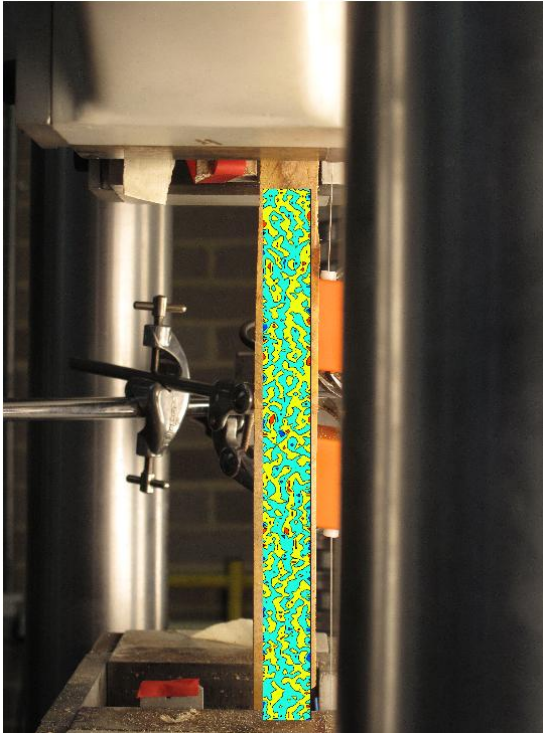
FIGURE 315: X DIRECTION PIV FIRST−LAST DITCH ENGINEERING STRAIN OVER IMAGE
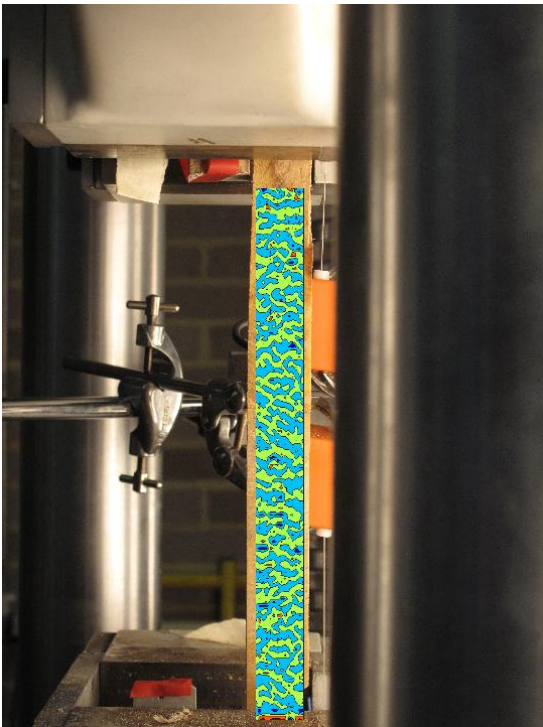
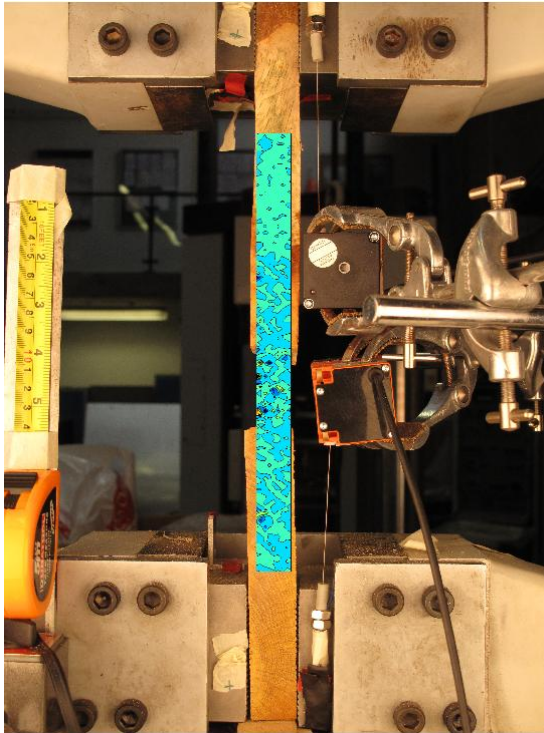FIGURE 316: Y DIRECTION PIV FIRST−LAST DITCH ENGINEERING STRAIN OVER IMAGE
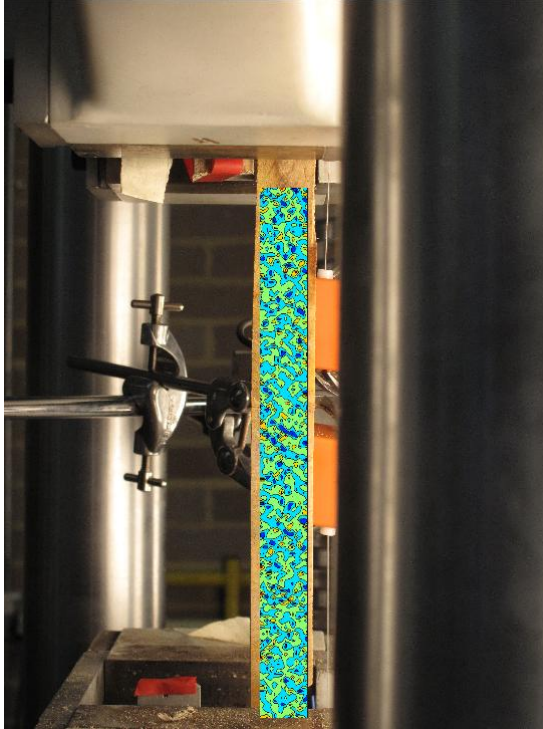
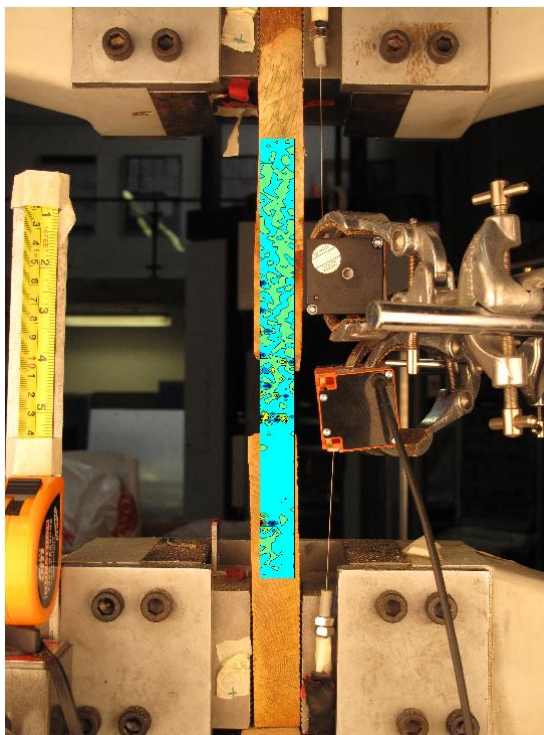FIGURE 317: XY DIRECTION PIV FIRST-LAST DITCH ENGINEERING SHEAR STRAIN OVER
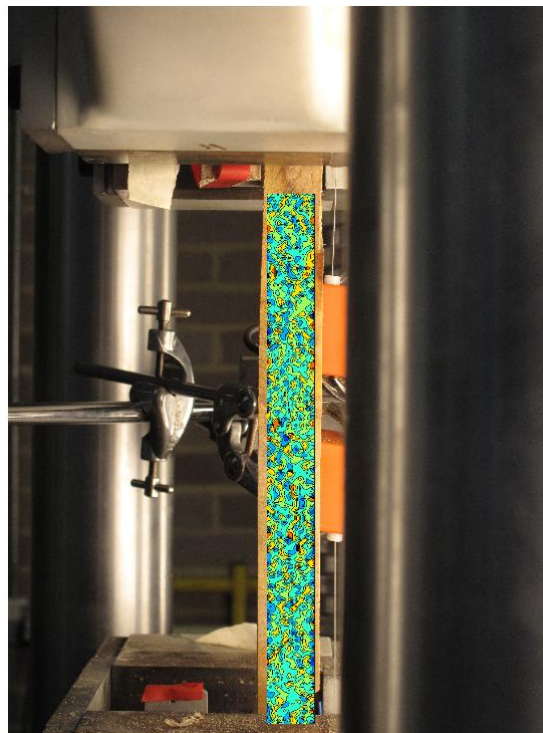
IMAGE

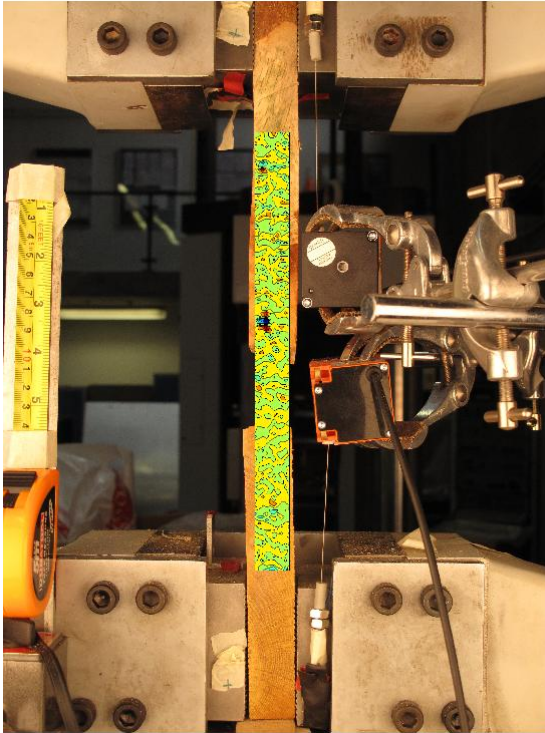FIGURE 318: X DIRECTION PIV FIRST-LAST DITCH TRUE STRAIN OVER IMAGE

Appendix 6
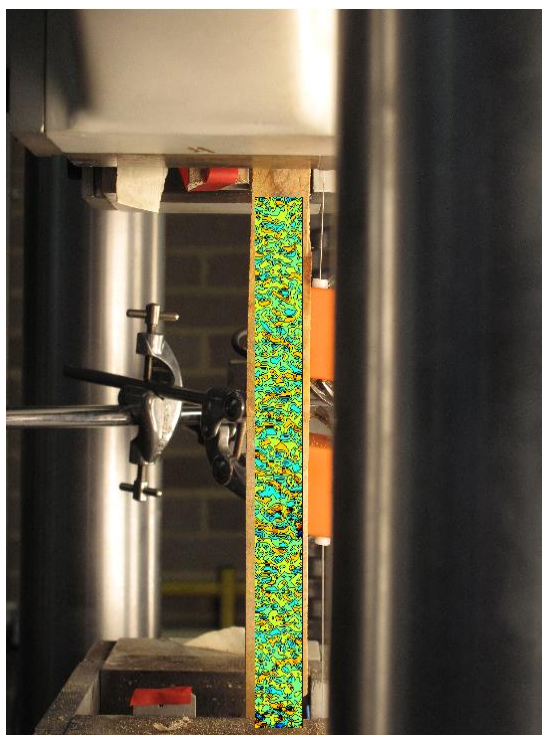
FIGURE 319: Y DIRECTION PIV FIRST−LAST DITCH TRUE STRAIN OVER IMAGE
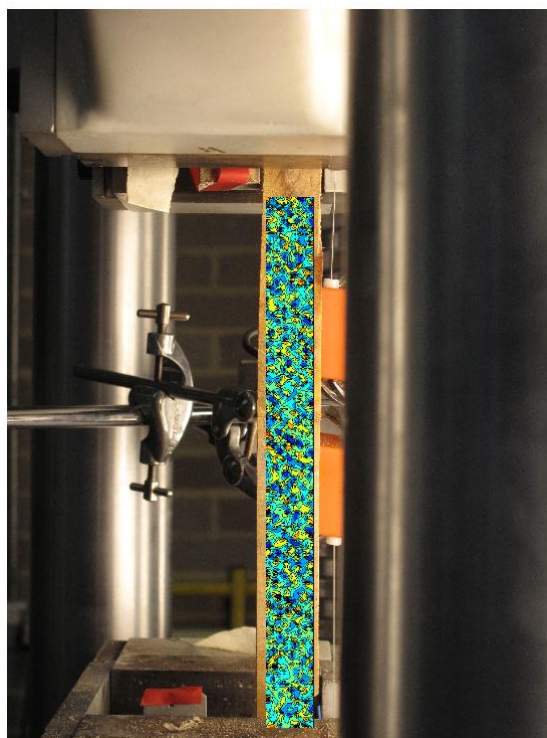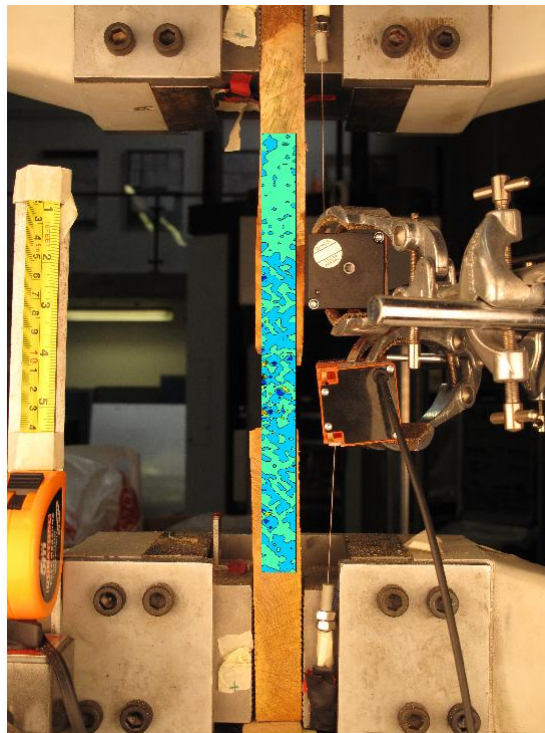

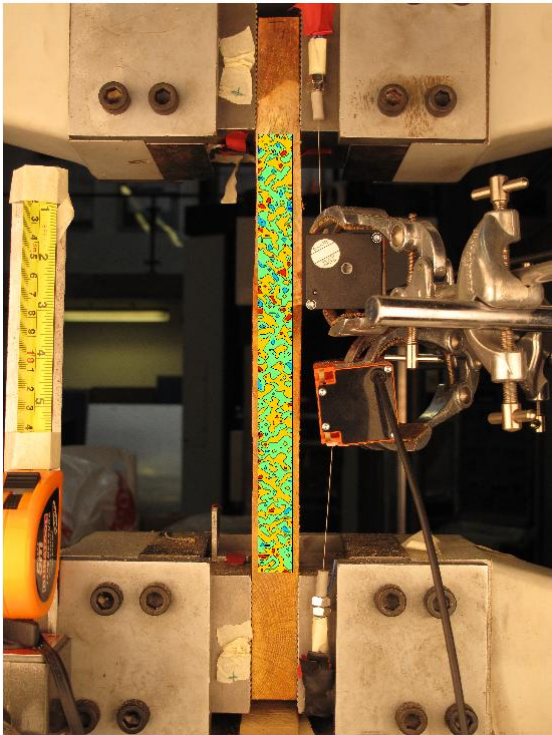FIGURE 320: XY DIRECTION PIV FIRST−LAST DITCH TRUE SHEAR STRAIN OVER IMAGE

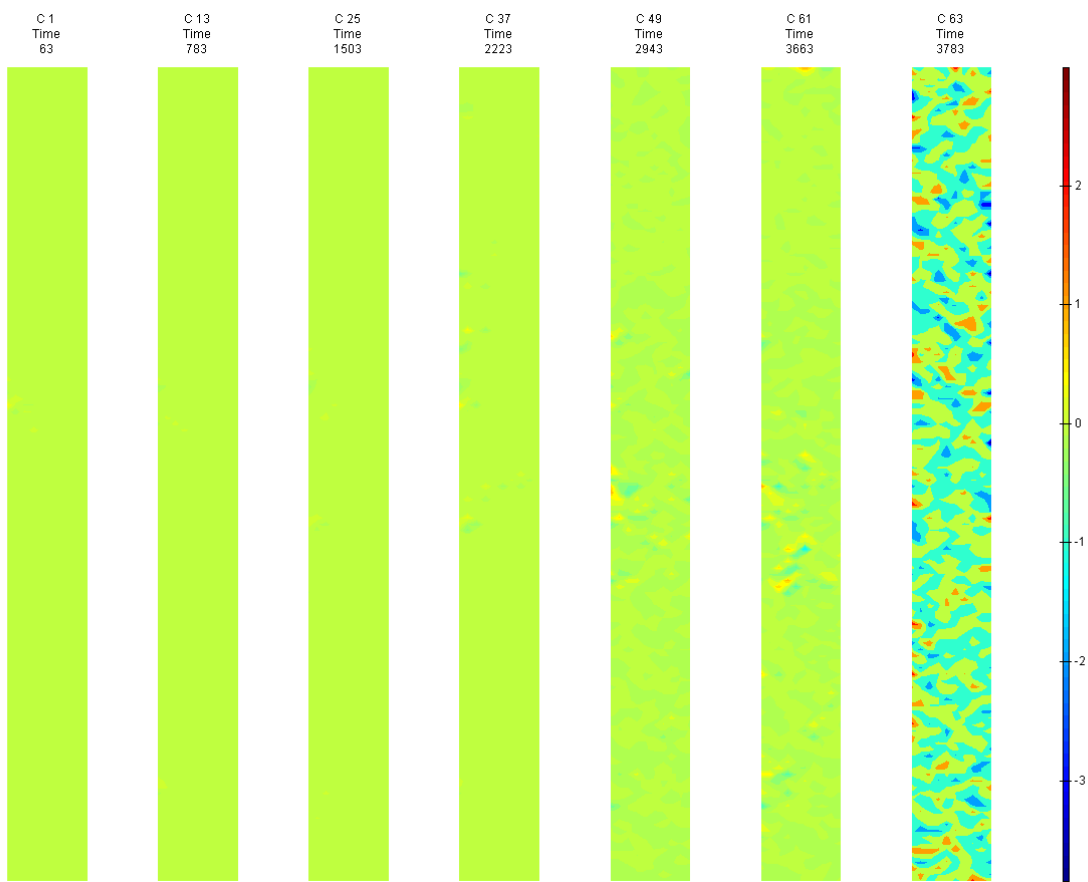FIGURE 321: XY DIRECTION PIV FIRST−SEQUENTIAL ENGINEERING SHEAR STRAIN OVER

IMAGE
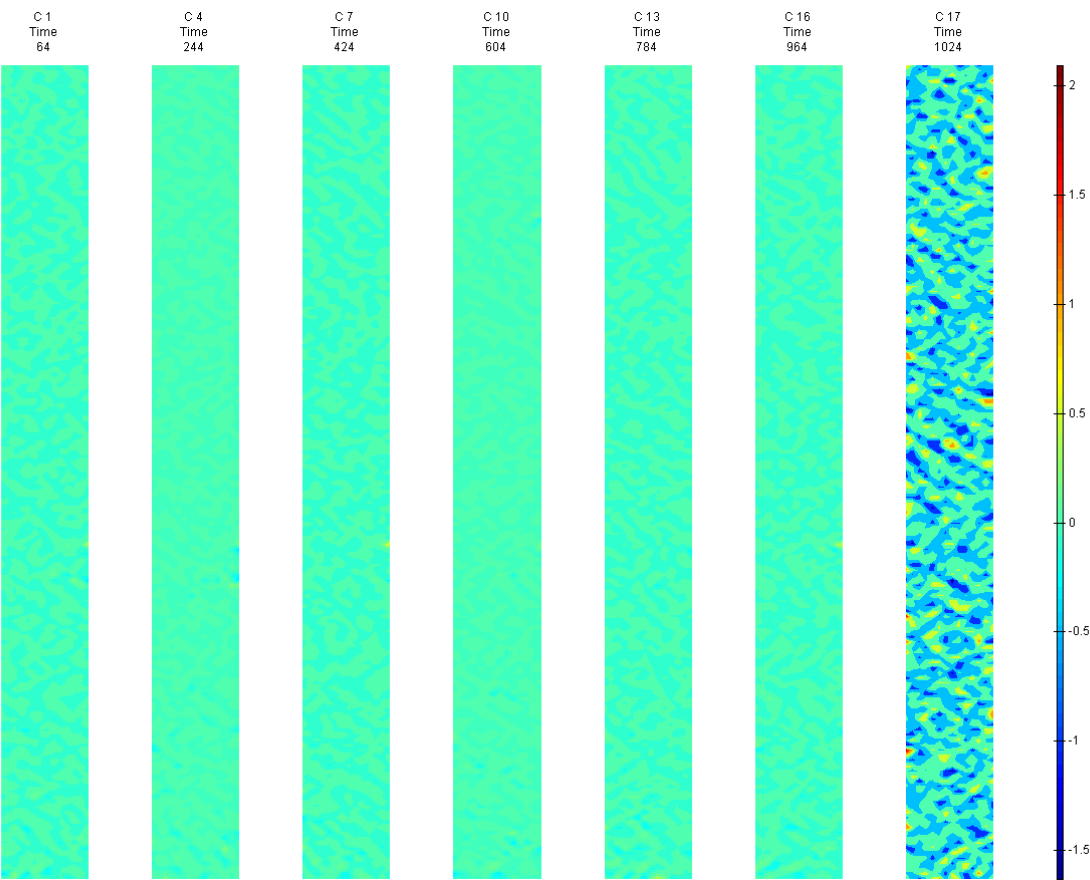
FIGURE 322: XY DIRECTION PIV FIRST−SEQUENTIAL ENGINEERING SHEAR STRAIN OVER TIME

G9
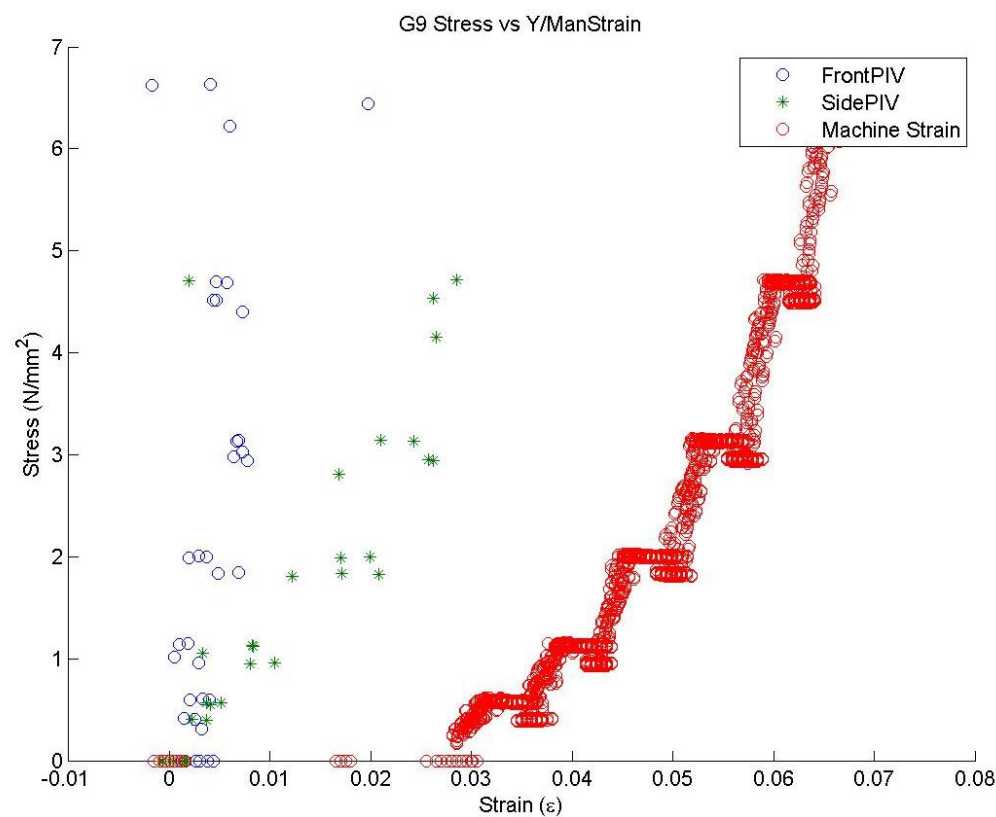
FIGURE 323: G9 TENSILE STRESS VS. MACHINE MEASURED/PIV STRAINS
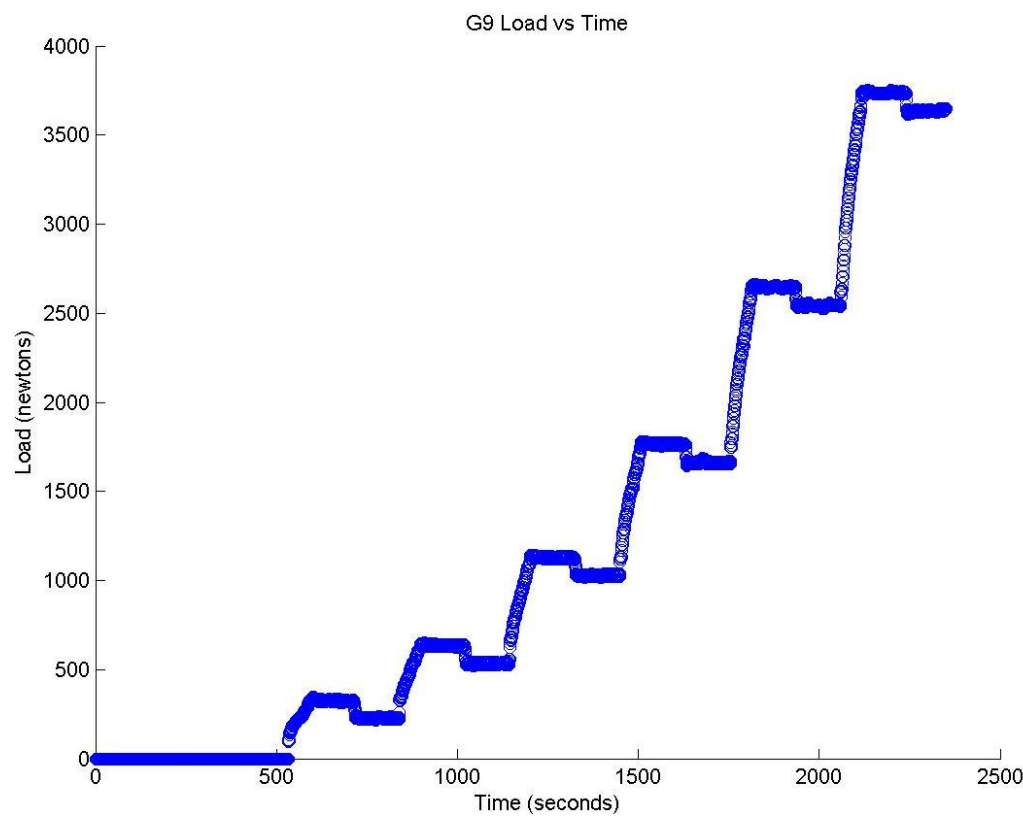
FIGURE 324: G9 TENSILE LOAD VS. TIME
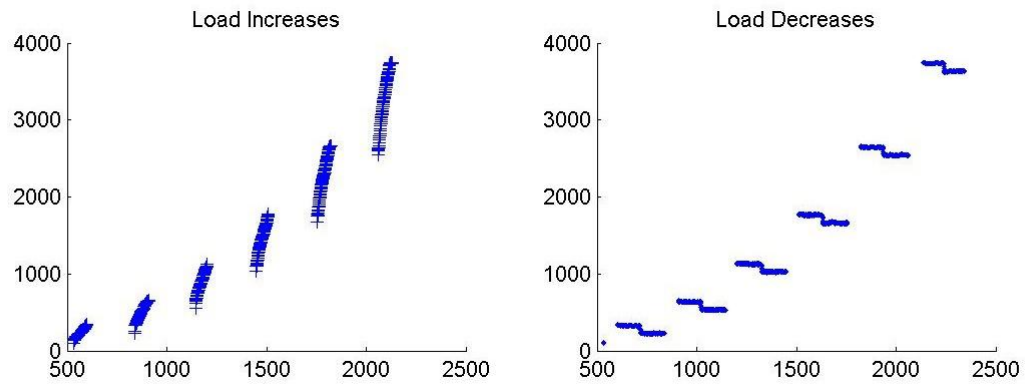
FIGURE 325: G9 CREEP LOADING: INCREMENTS AND RELAXATION
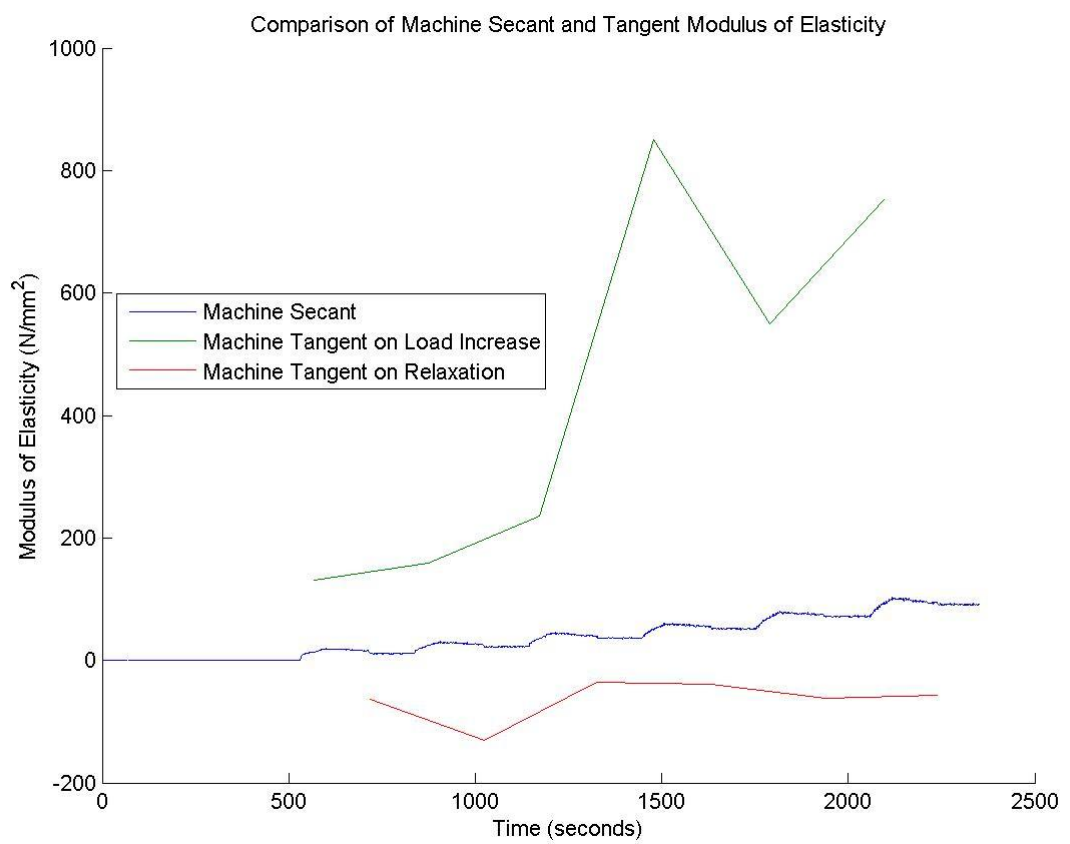
FIGURE 326: G9 MACHINE MEASURED SECANT AND TANGENT MODULUS VS. TIME

Appendix 6
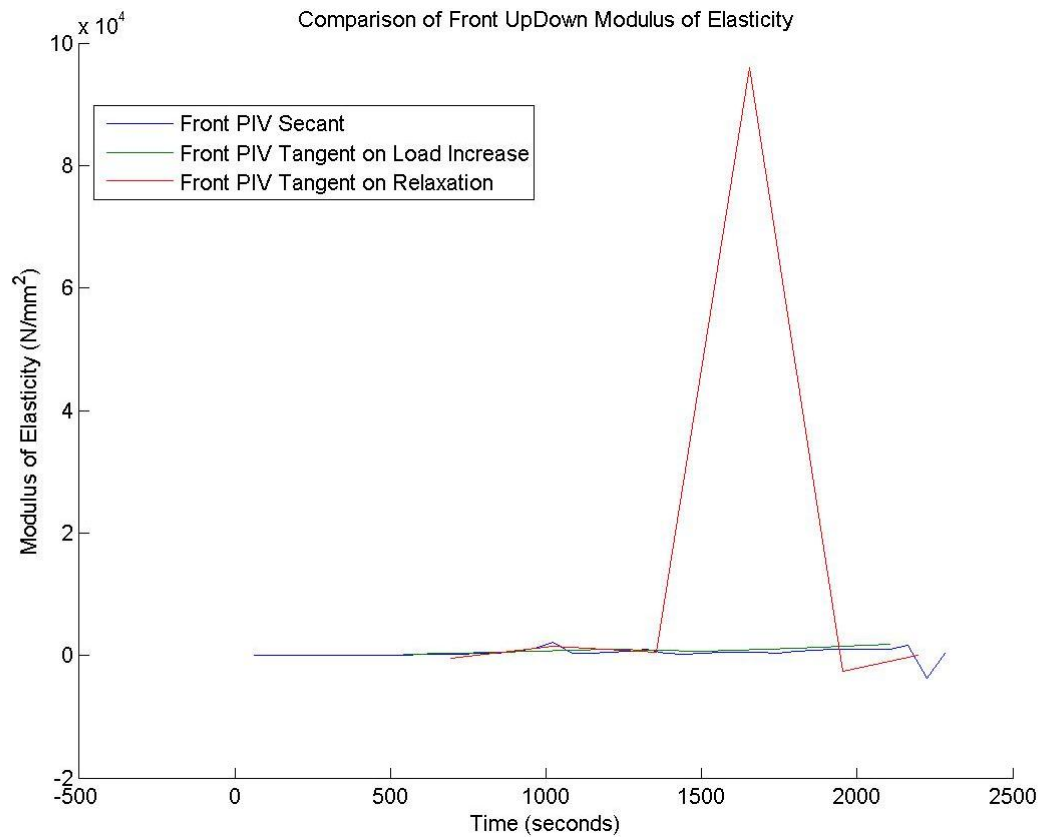
FIGURE 327: G9 FRONT VIEW PIV SECANT AND TANGENT MODULUS VS. TIME
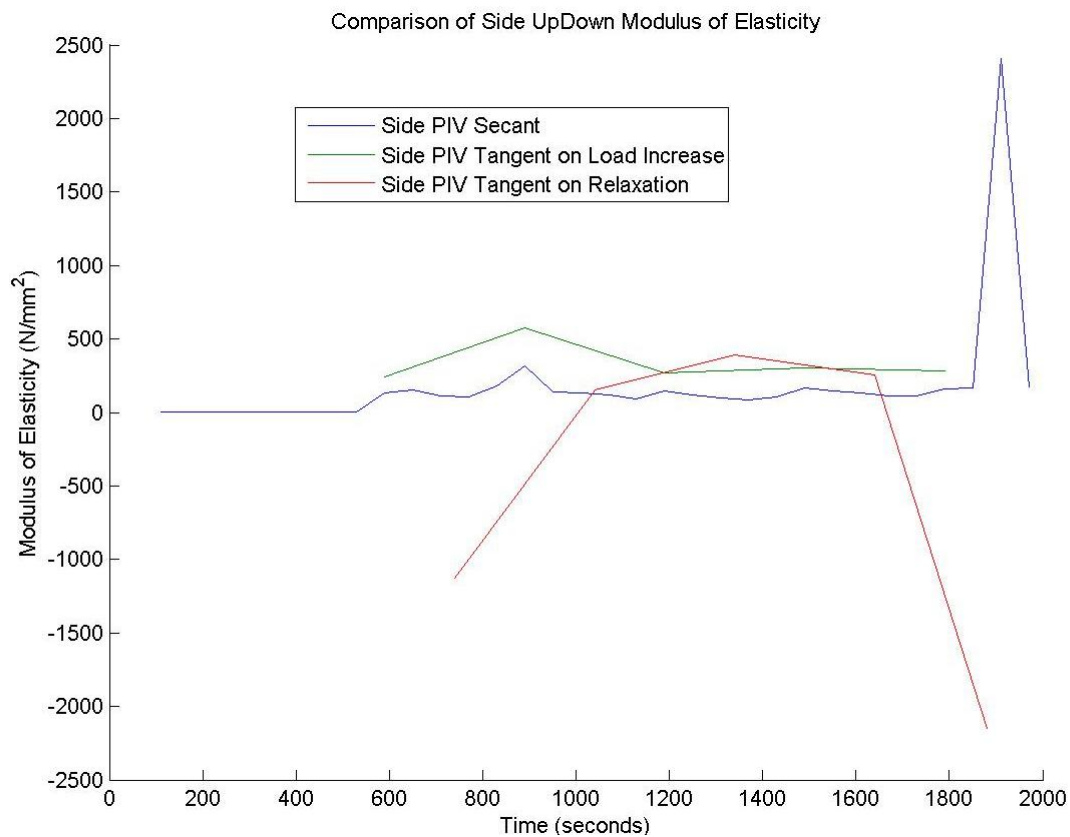
FIGURE 328: G9 SIDE VIEW PIV SECANT AND TANGENT MODULUS VS. TIME
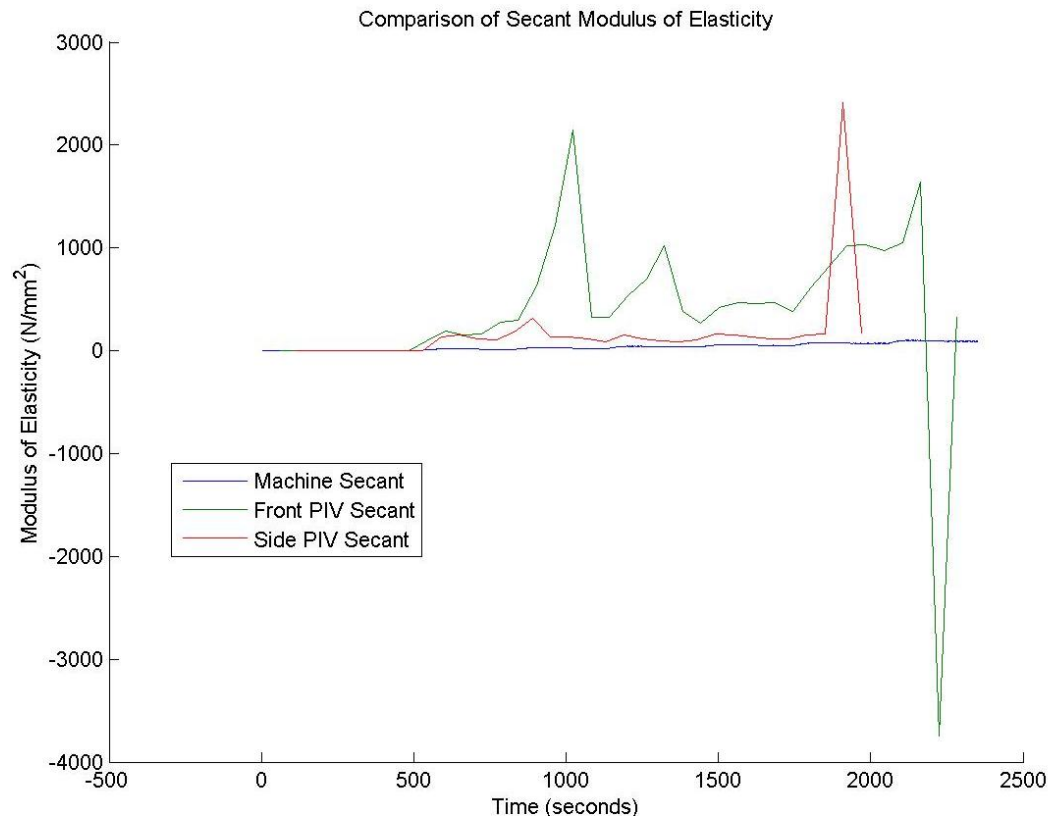
FIGURE 329: G9 COMPARISON OF MACHINE MEASURED AND PIV SECANT MODULUS VS. TIME
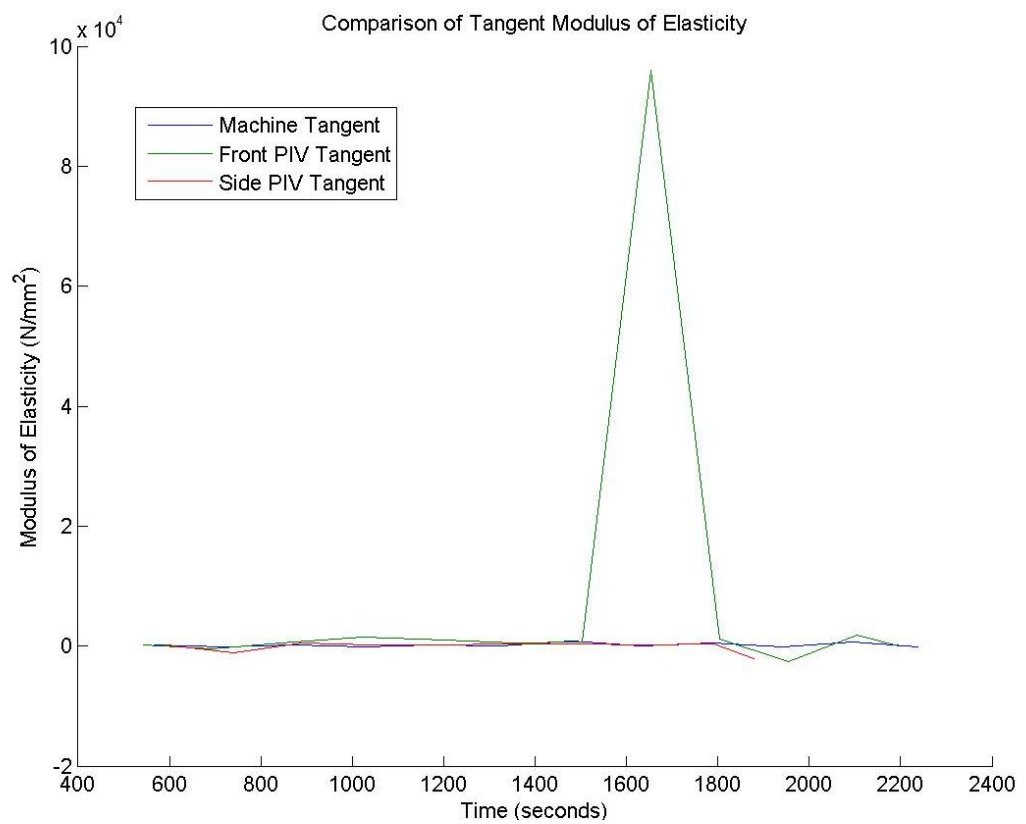
FIGURE 330: G9 COMPARISON OF MACHINE MEASURED AND PIV TANGENT MODULUS VS.

TIME

Appendix 6

G9 Sample

FIGURE 331: SAMPLE GRAIN ORIENTATIONS OF THE FRONT (LEFT 4 IMAGES) AND SIDE (RIGHT 4 IMAGES) VIEW BEFORE (FIRST 2 OF 4 IMAGES) AND AFTER (LAST 2 OF 4 IMAGES) BREAKAGE

G9 Front View
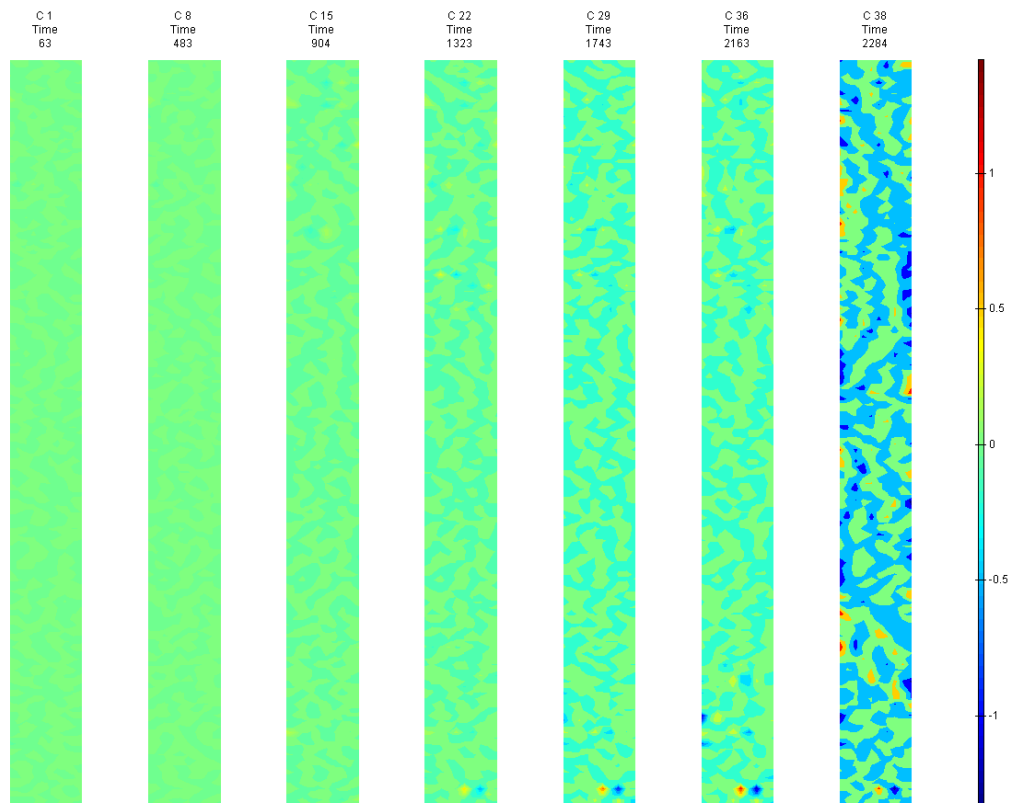
FIGURE 332: X DIRECTION PIV SEQUENTIAL ENGINEERING STRAIN OVER TIME
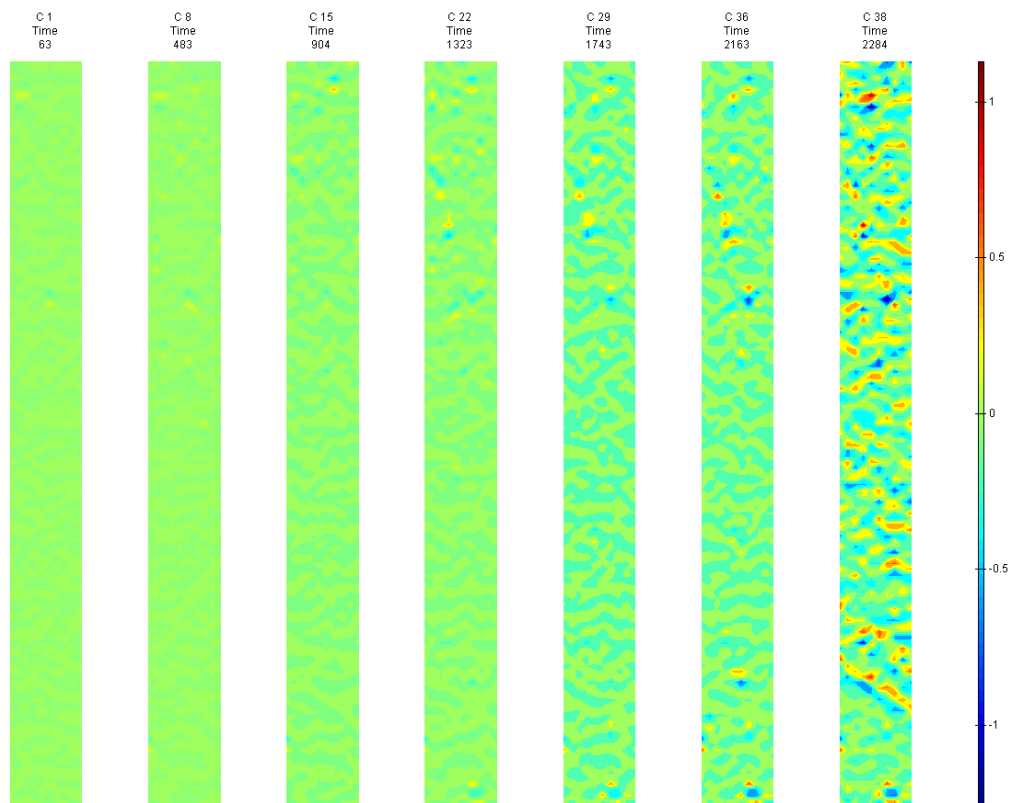
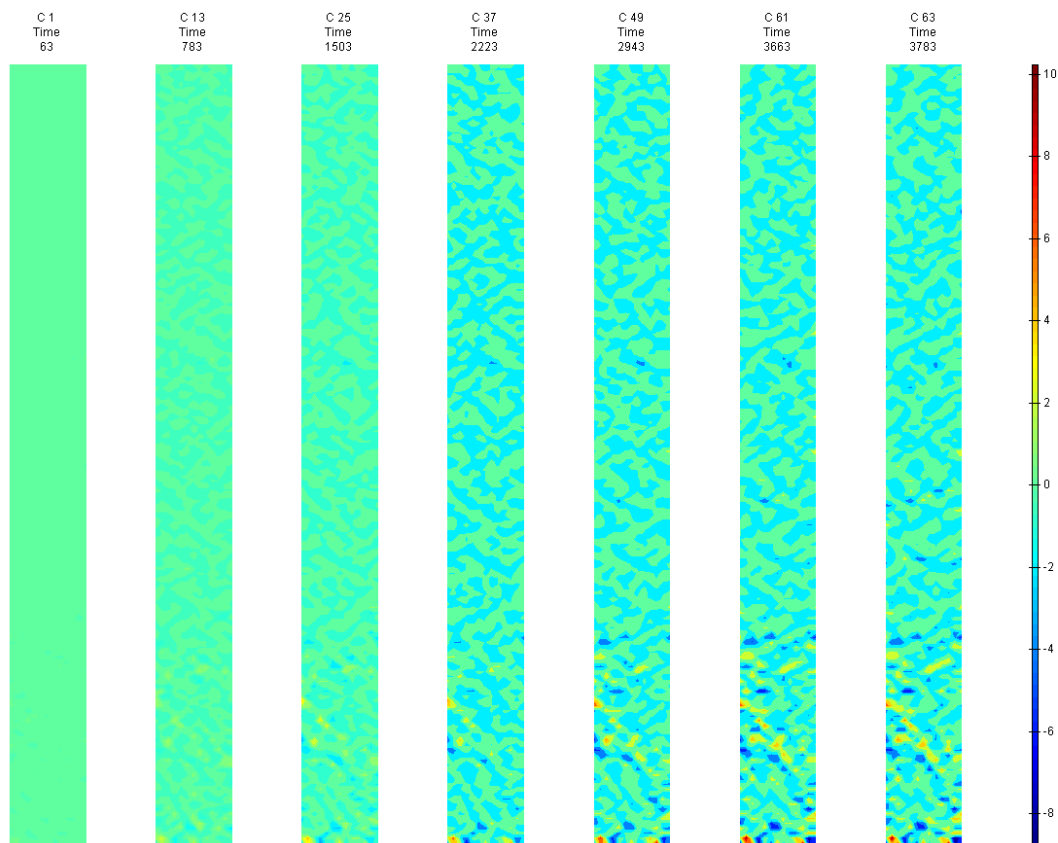FIGURE 333: Y DIRECTION PIV SEQUENTIAL ENGINEERING STRAIN OVER TIME

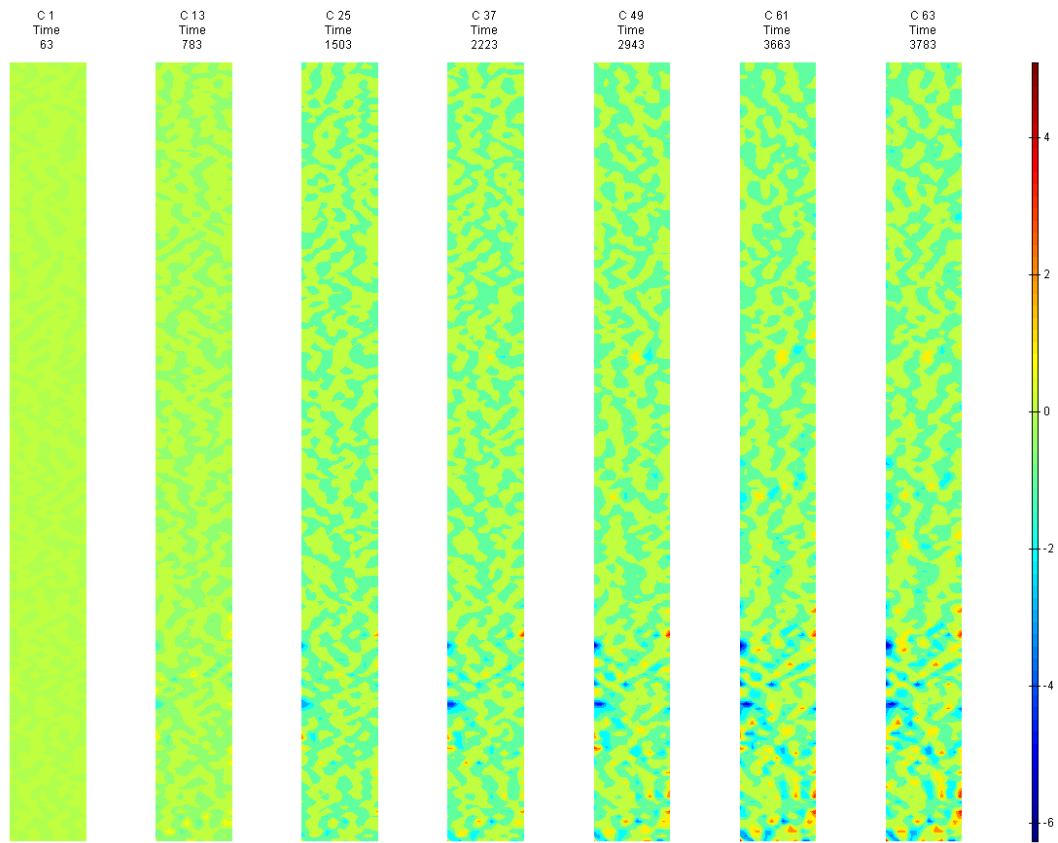Appendix 6
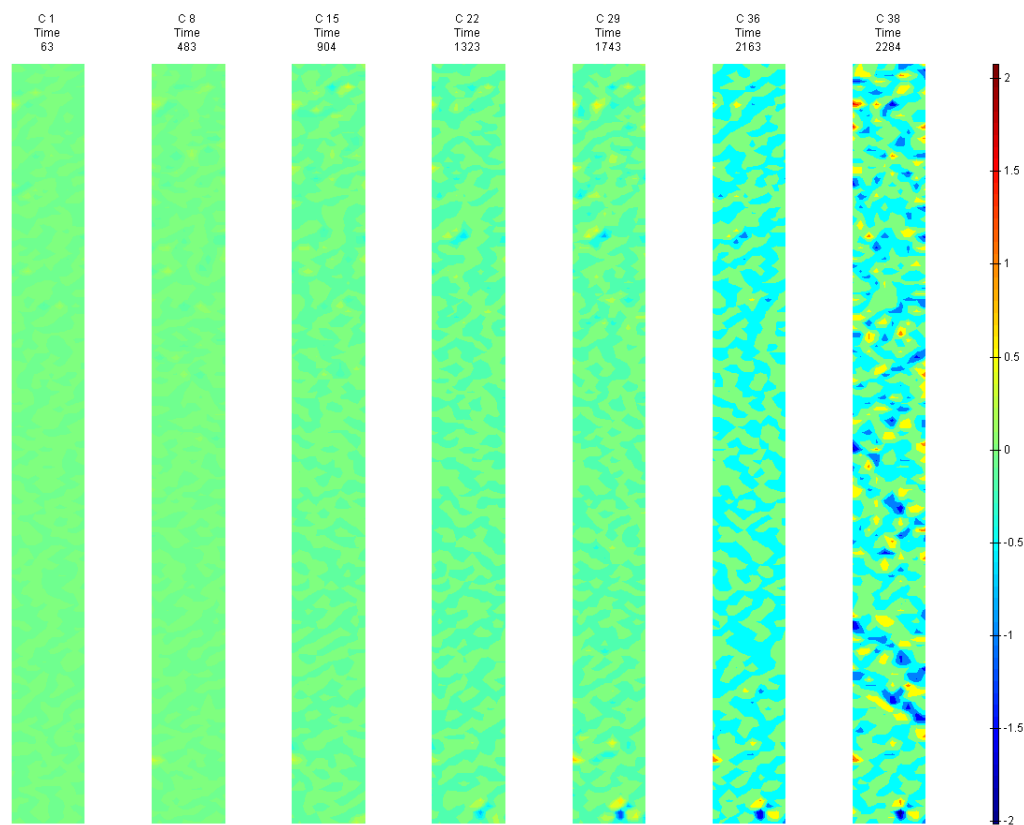
FIGURE 334: XY DIRECTION PIV SEQUENTIAL ENGINEERING SHEAR STRAIN OVER TIME

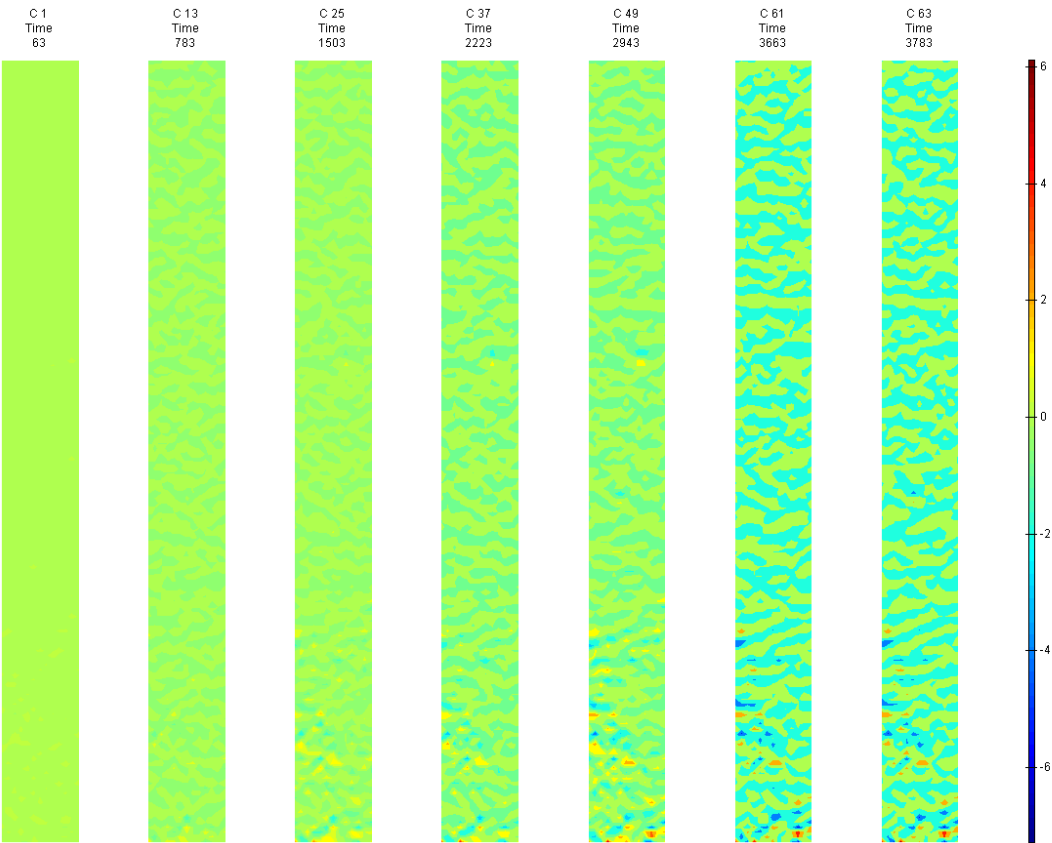FIGURE 335: X DIRECTION PIV SEQUENTIAL TRUE STRAIN OVER TIME
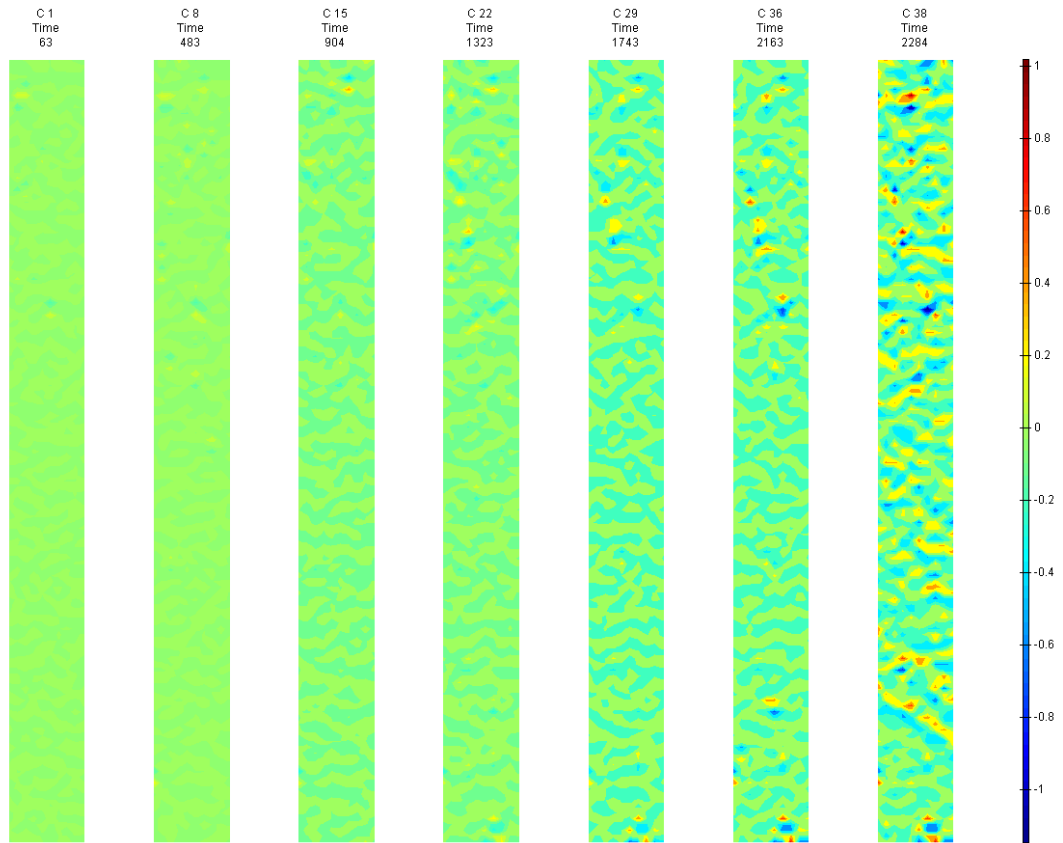
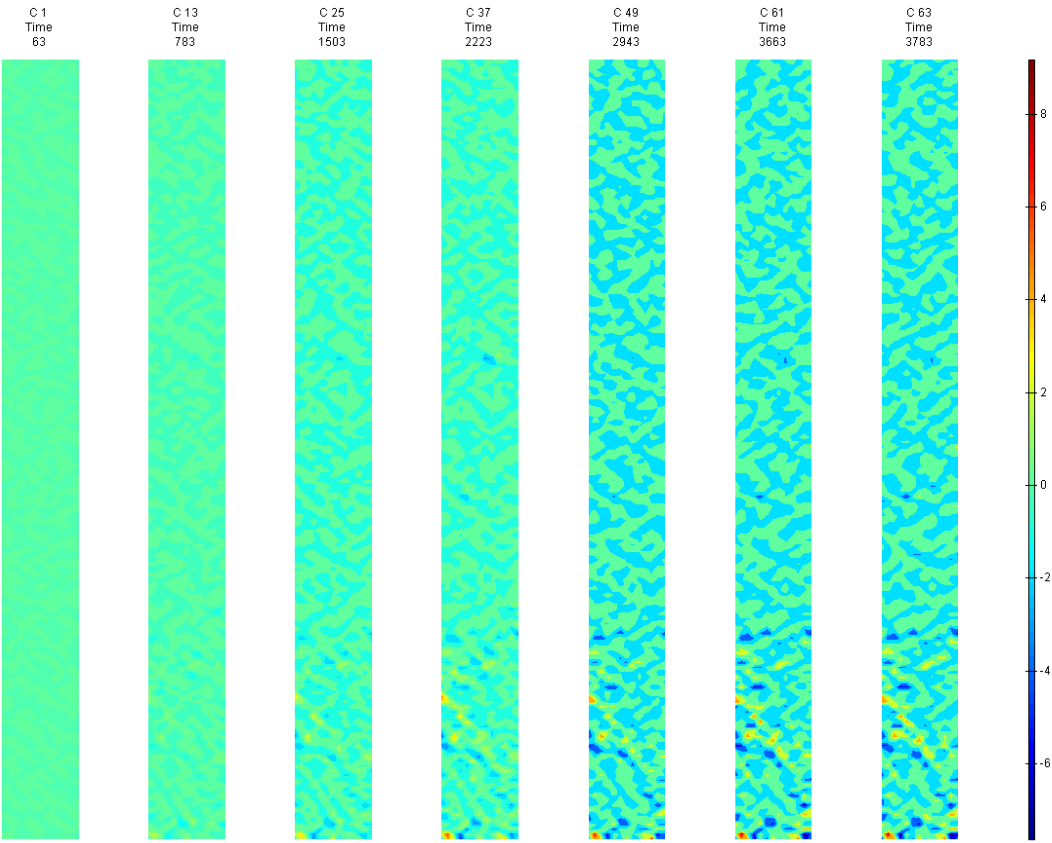FIGURE 336: Y DIRECTION PIV SEQUENTIAL TRUE STRAIN OVER TIME
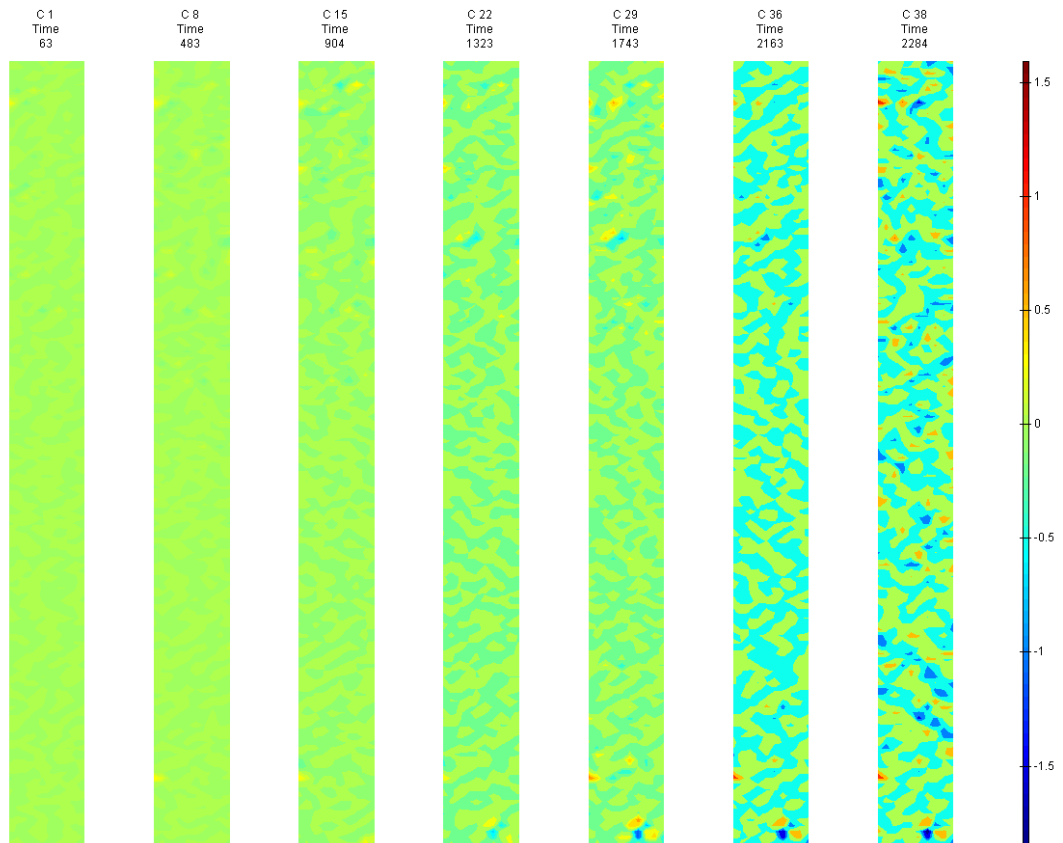
FIGURE 337: XY DIRECTION PIV SEQUENTIAL TRUE SHEAR STRAIN OVER TIME

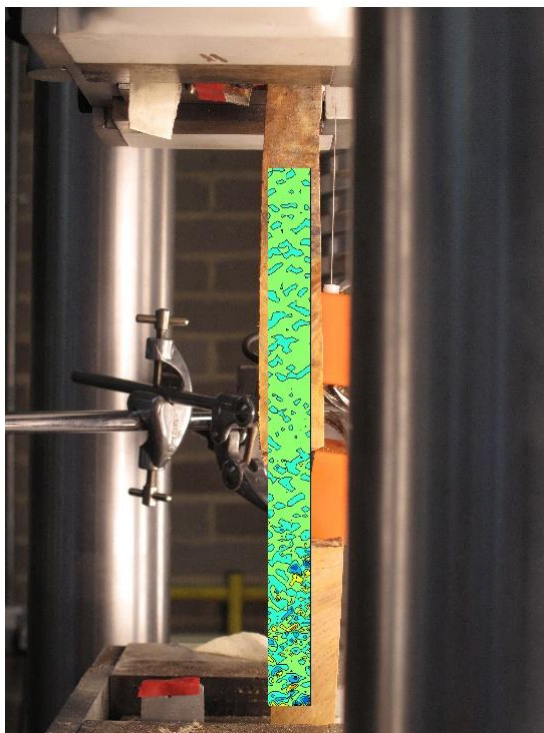FIGURE 338: X DIRECTION PIV FIRST–LAST DITCH ENGINEERING STRAIN OVER IMAGE

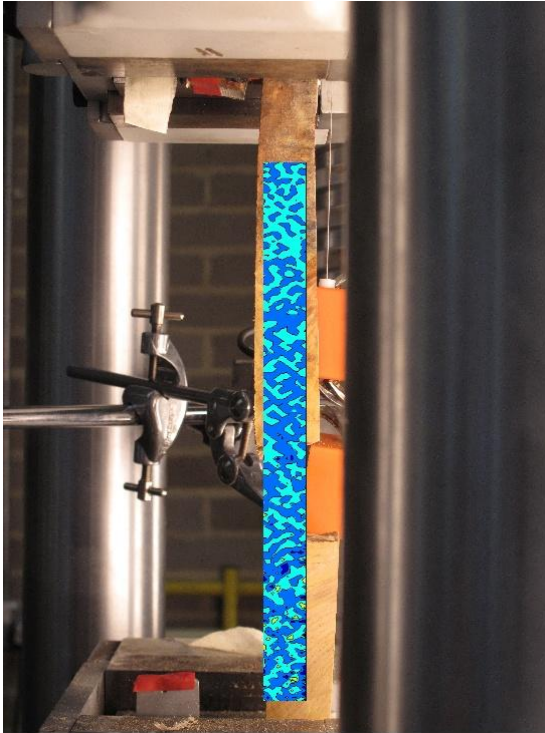FIGURE 339: Y DIRECTION PIV FIRST–LAST DITCH ENGINEERING STRAIN OVER IMAGE

FIGURE 340: XY DIRECTION PIV FIRST–LAST DITCH ENGINEERING SHEAR STRAIN OVER
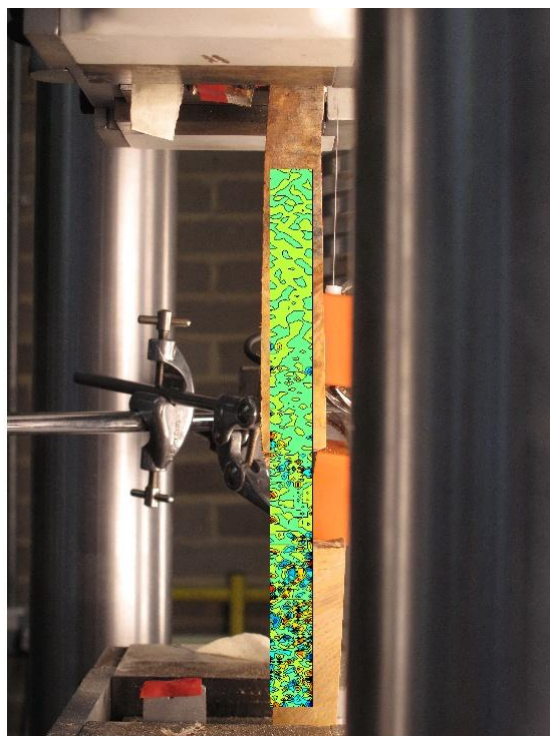
IMAGE

FIGURE 341: X DIRECTION PIV FIRST–LAST DITCH TRUE STRAIN OVER IMAGE

FIGURE 342: Y DIRECTION PIV FIRST–LAST DITCH TRUE STRAIN OVER IMAGE
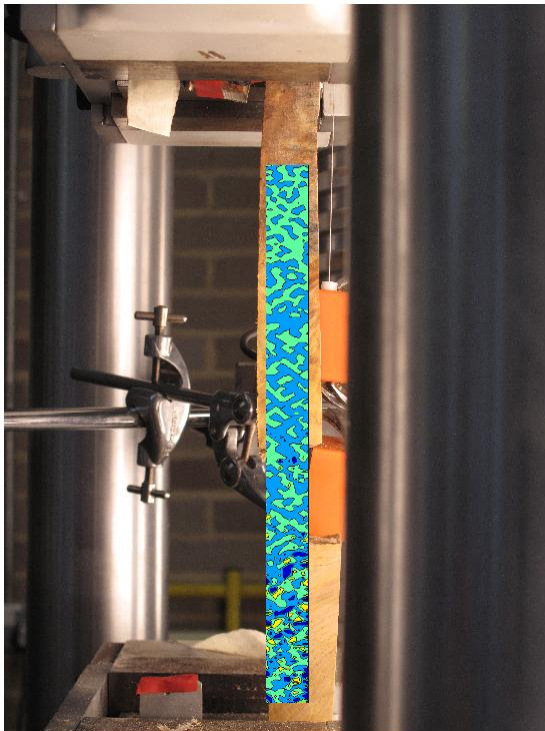

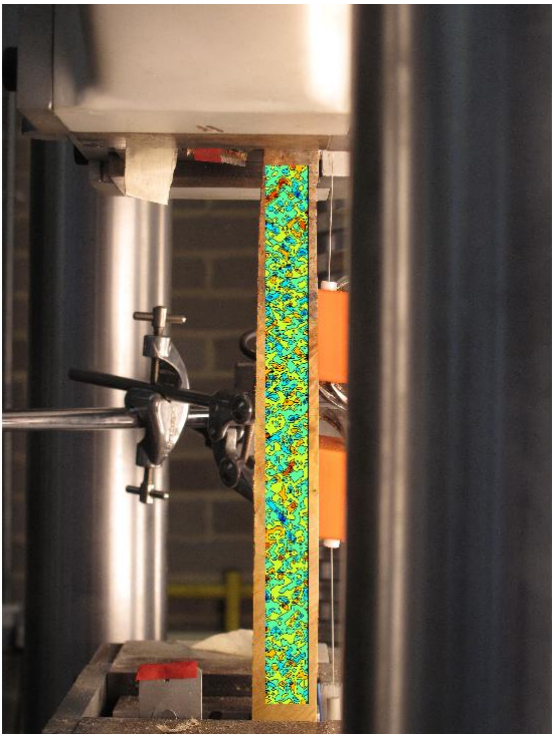FIGURE 343: XY DIRECTION PIV FIRST–LAST DITCH TRUE SHEAR STRAIN OVER IMAGE

FIGURE 344: XY DIRECTION PIV FIRST–SEQUENTIAL ENGINEERING SHEAR STRAIN OVER

IMAGE

FIGURE 345: XY DIRECTION PIV FIRST–SEQUENTIAL ENGINEERING SHEAR STRAIN OVER TIME

G9 Side View

FIGURE 346: X DIRECTION PIV SEQUENTIAL ENGINEERING STRAIN OVER TIME

FIGURE 347: Y DIRECTION PIV SEQUENTIAL ENGINEERING STRAIN OVER TIME

FIGURE 348: XY DIRECTION PIV SEQUENTIAL ENGINEERING SHEAR STRAIN OVER TIME

FIGURE 349: X DIRECTION PIV SEQUENTIAL TRUE STRAIN OVER TIME
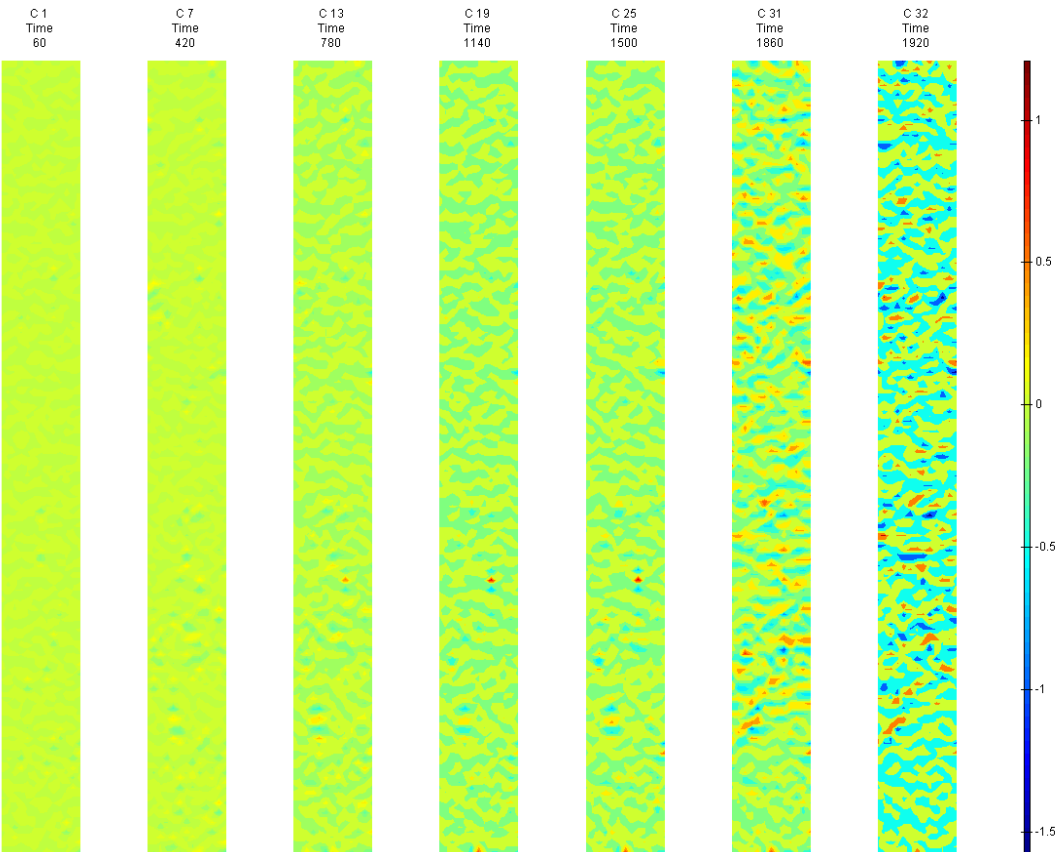
FIGURE 350: Y DIRECTION PIV SEQUENTIAL TRUE STRAIN OVER TIME
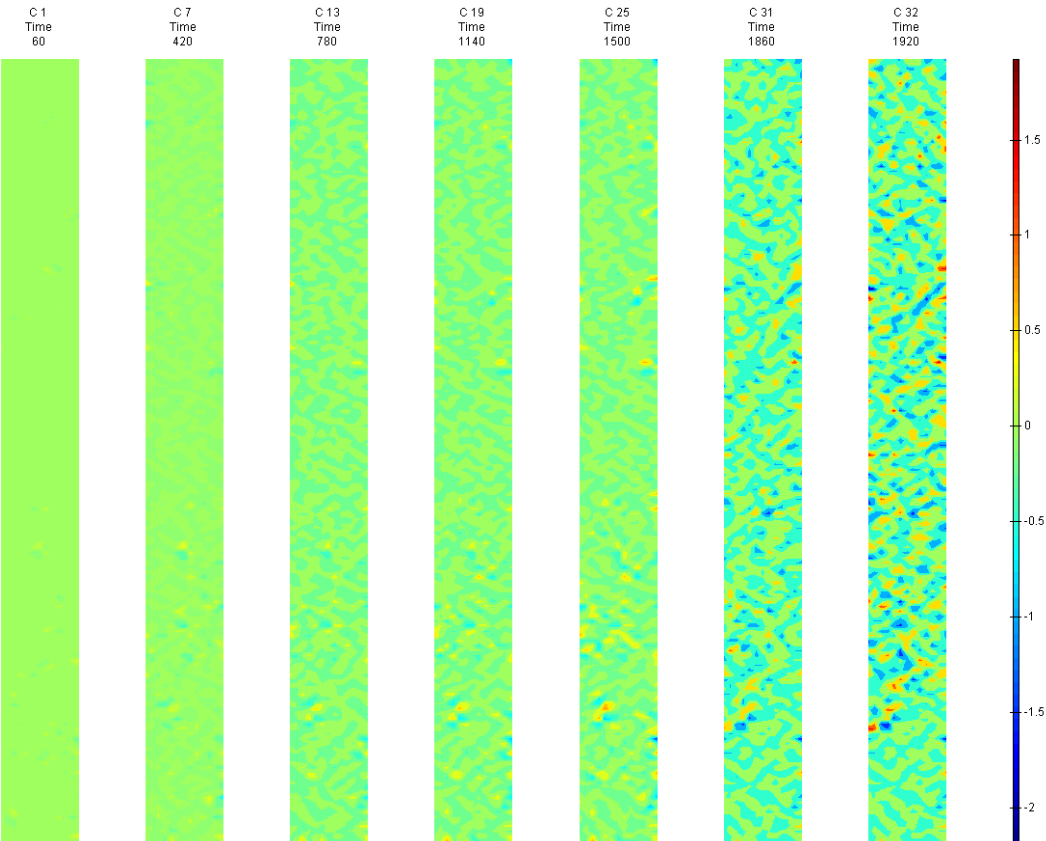
FIGURE 351: XY DIRECTION PIV SEQUENTIAL TRUE SHEAR STRAIN OVER TIME
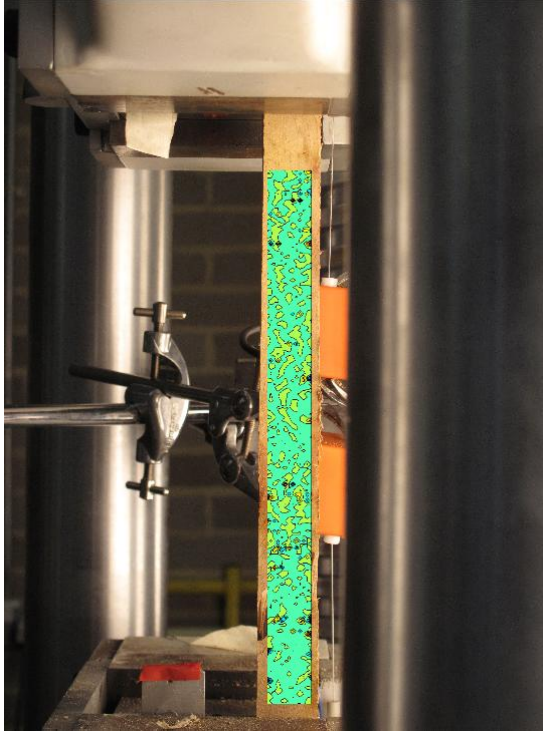
FIGURE 352: X DIRECTION PIV FIRST–LAST DITCH ENGINEERING STRAIN OVER IMAGE
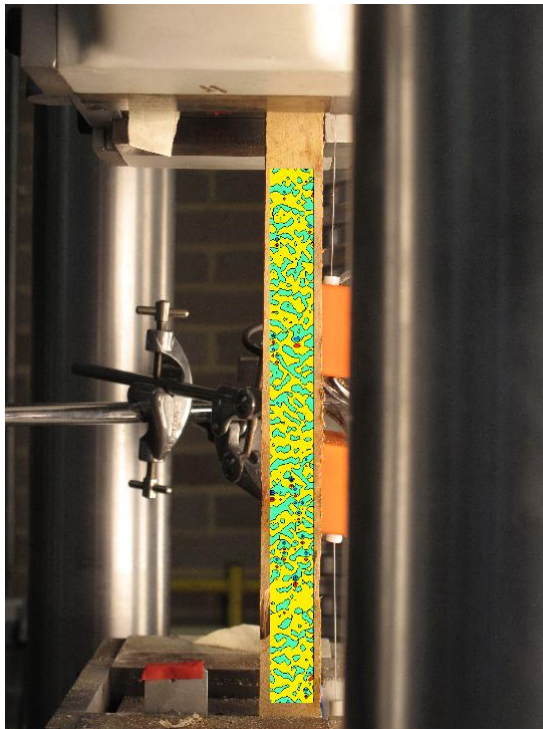
FIGURE 353: Y DIRECTION PIV FIRST–LAST DITCH ENGINEERING STRAIN OVER IMAGE
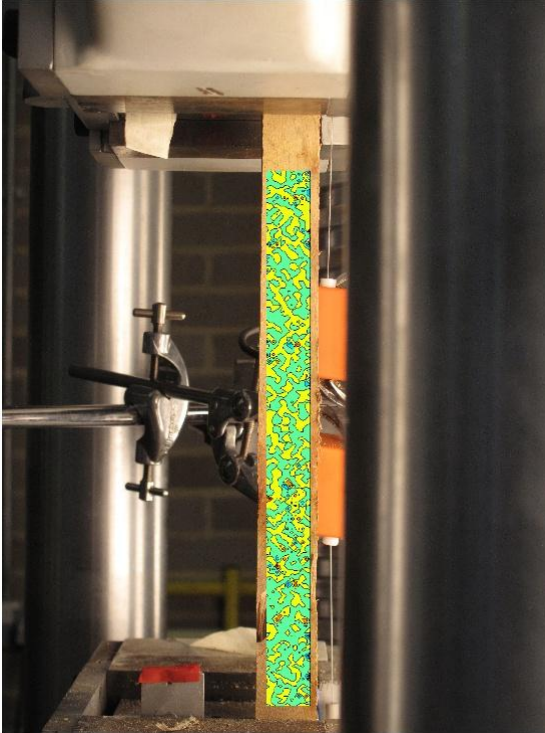
FIGURE 354: XY DIRECTION PIV FIRST–LAST DITCH ENGINEERING SHEAR STRAIN OVER
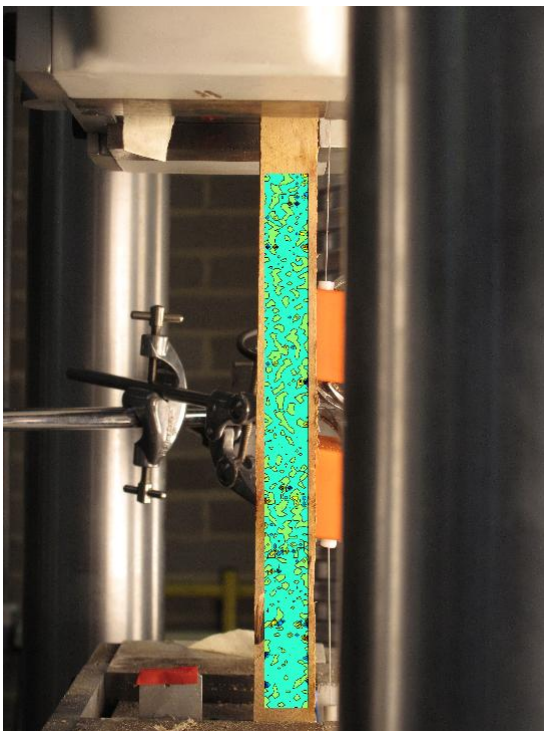
IMAGE

FIGURE 355: X DIRECTION PIV FIRST–LAST DITCH TRUE STRAIN OVER IMAGE

FIGURE 356: Y DIRECTION PIV FIRST–LAST DITCH TRUE STRAIN OVER IMAGE

FIGURE 357: XY DIRECTION PIV FIRST–LAST DITCH TRUE SHEAR STRAIN OVER IMAGE

Appendix 6

FIGURE 358: XY DIRECTION PIV FIRST–SEQUENTIAL ENGINEERING SHEAR STRAIN OVER

IMAGE

FIGURE 359: XY DIRECTION PIV FIRST–SEQUENTIAL ENGINEERING SHEAR STRAIN OVER TIME

G10
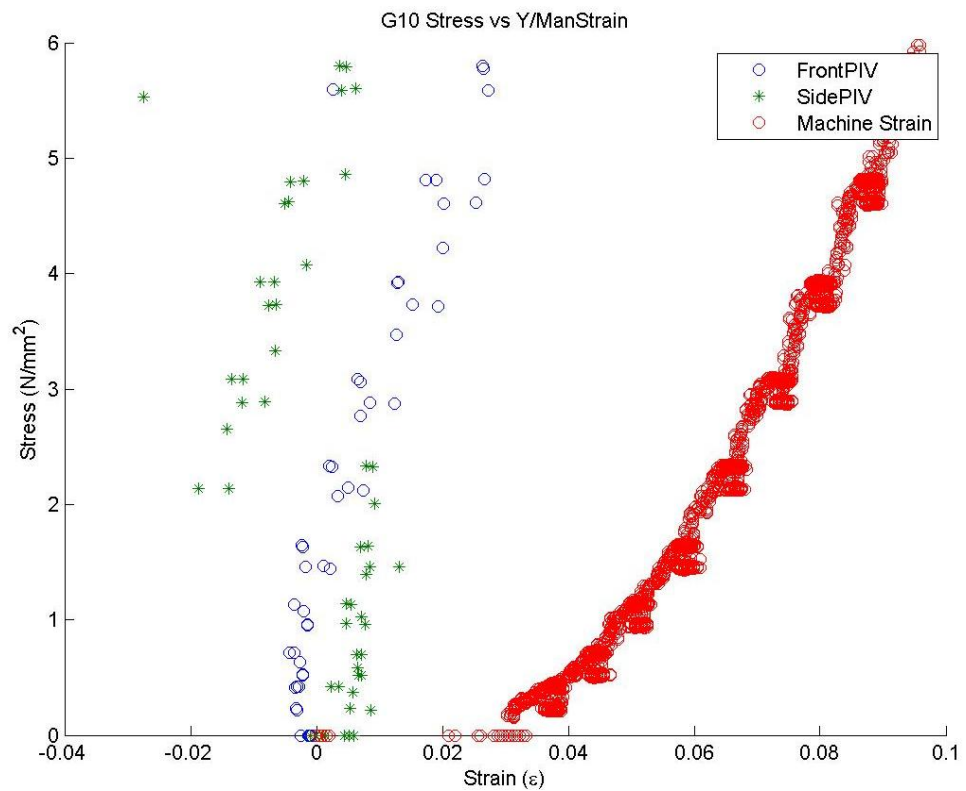
FIGURE 360: G10 TENSILE STRESS VS. MACHINE MEASURED/PIV STRAINS
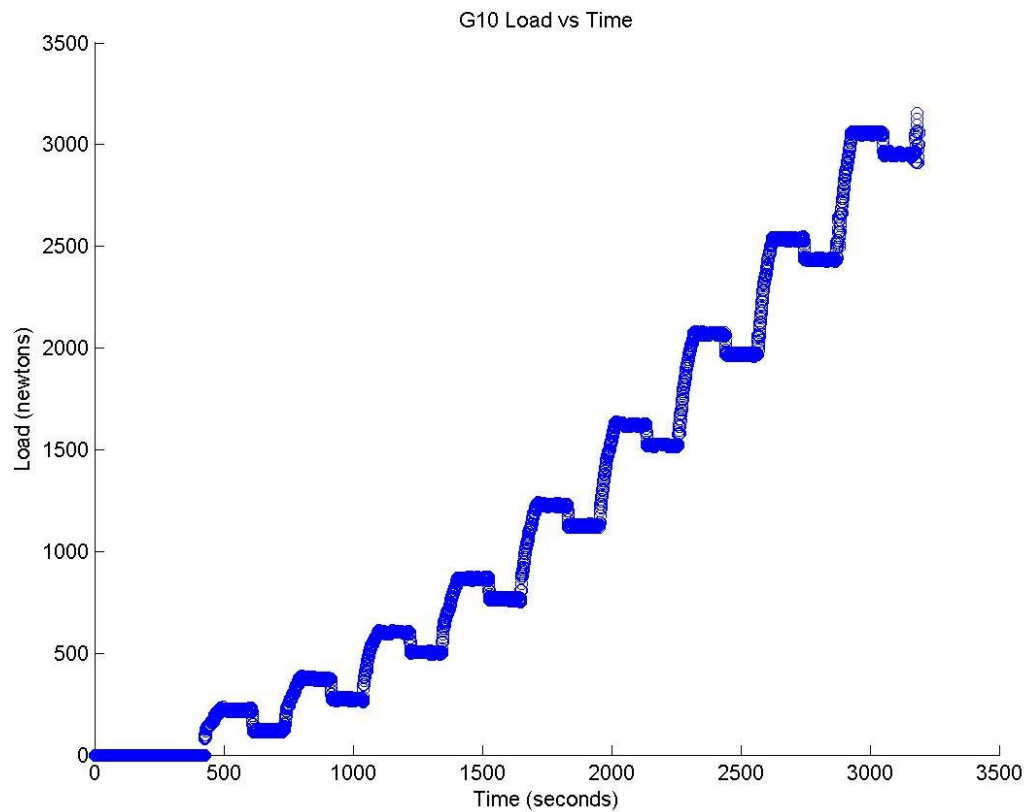
FIGURE 361: G10 TENSILE LOAD VS. TIME

Appendix 6
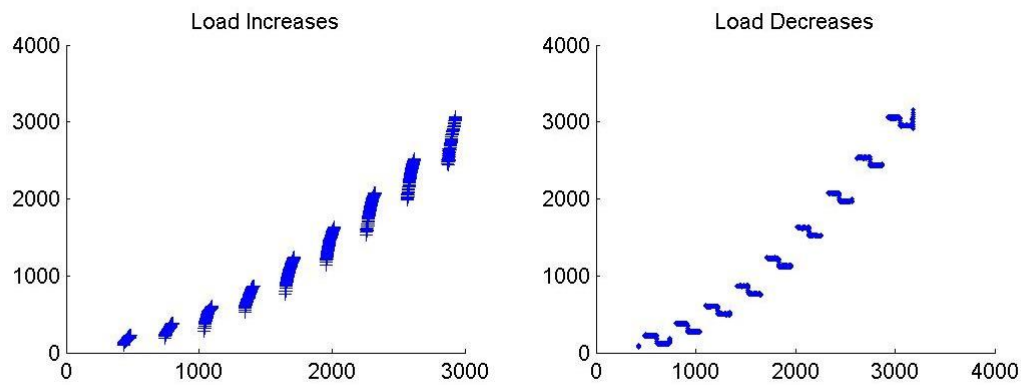
FIGURE 362: G10 CREEP LOADING: INCREMENTS AND RELAXATION
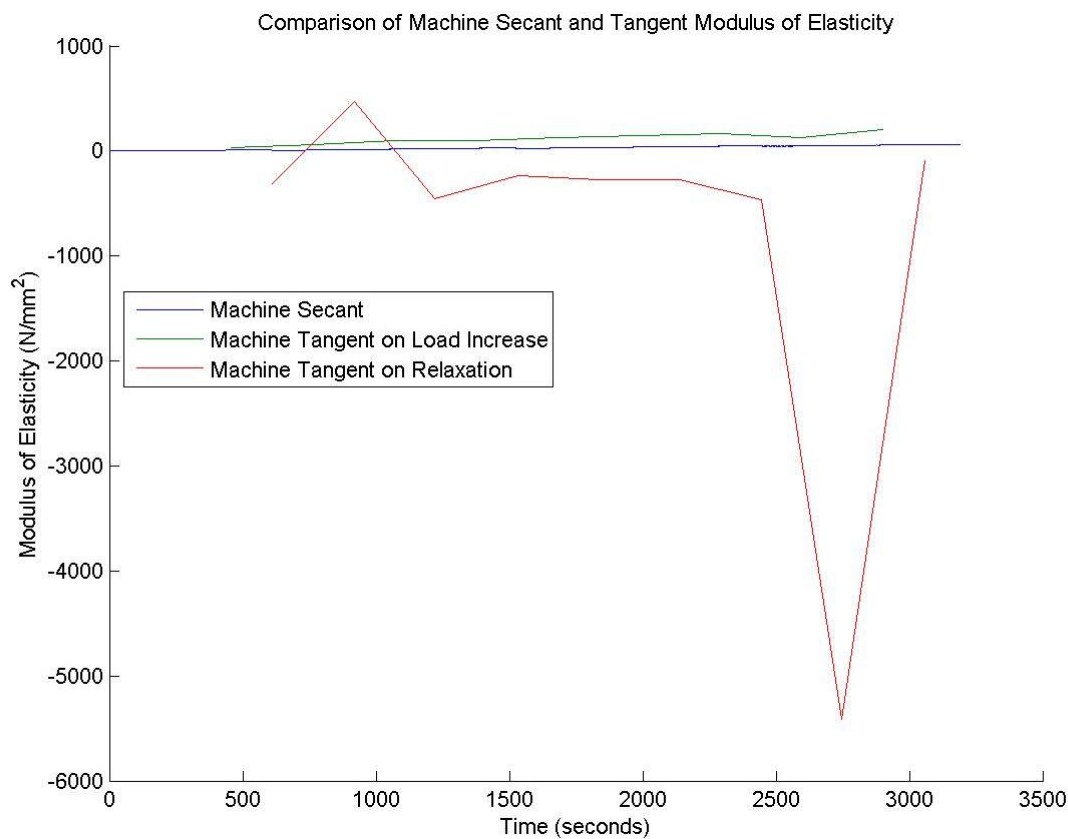
FIGURE 363: G10 MACHINE MEASURED SECANT AND TANGENT MODULUS VS. TIME

FIGURE 364: G10 FRONT VIEW PIV SECANT AND TANGENT MODULUS VS. TIME
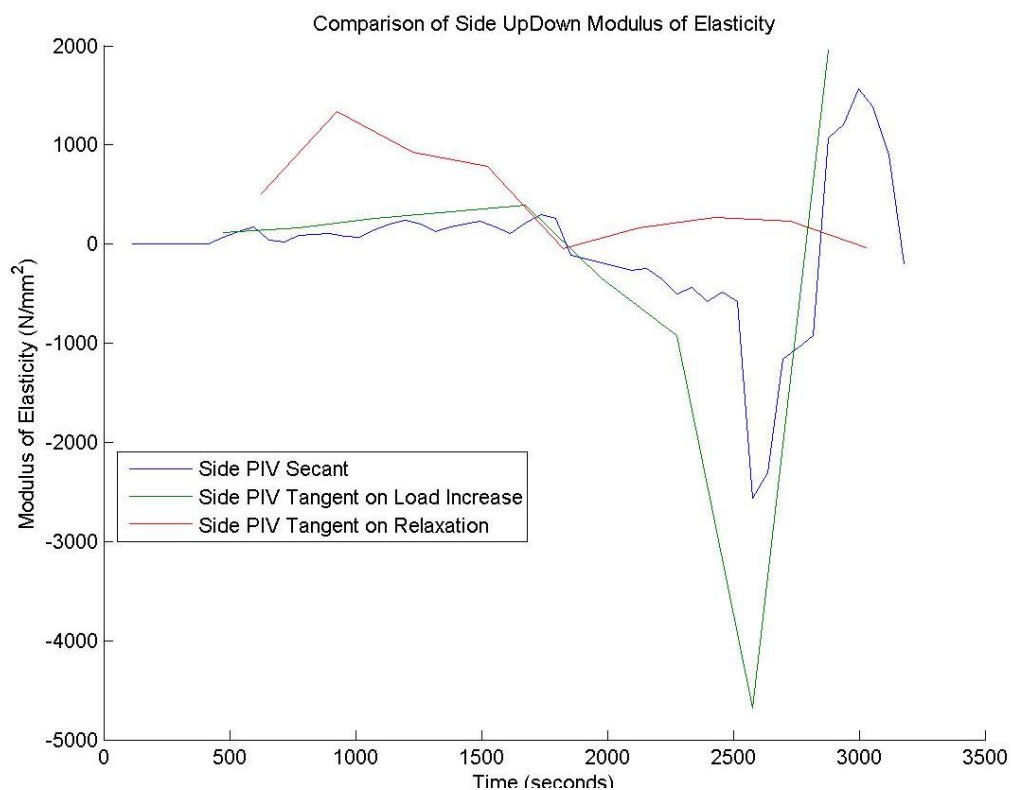
FIGURE 365: G10 SIDE VIEW PIV SECANT AND TANGENT MODULUS VS. TIME

Appendix 6
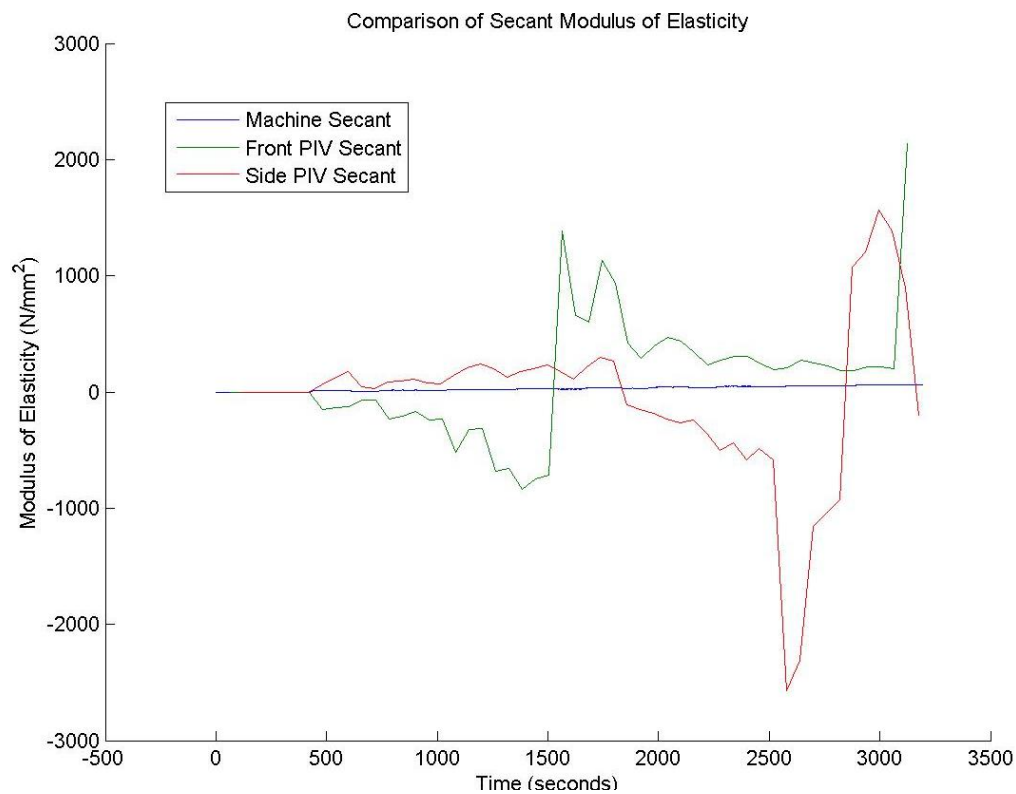
FIGURE 366: G10 COMPARISON OF MACHINE MEASURED AND PIV SECANT MODULUS VS.
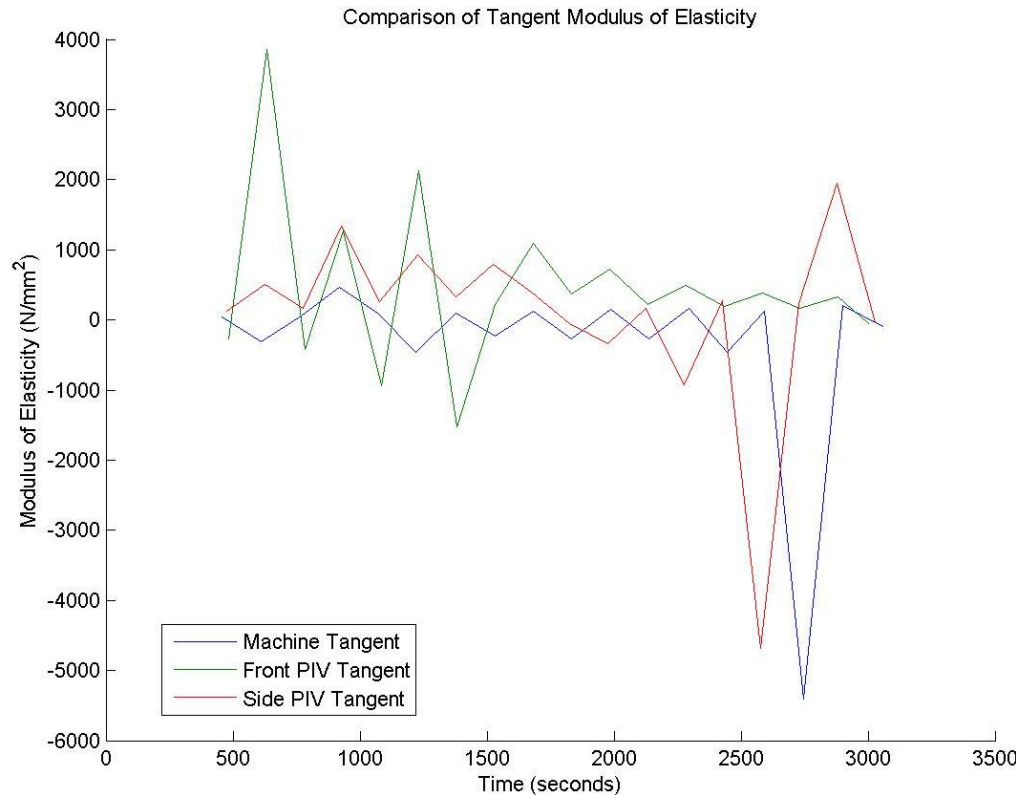
TIME

FIGURE 367: G10 COMPARISON OF MACHINE MEASURED AND PIV TANGENT MODULUS VS.

TIME

G10 Sample
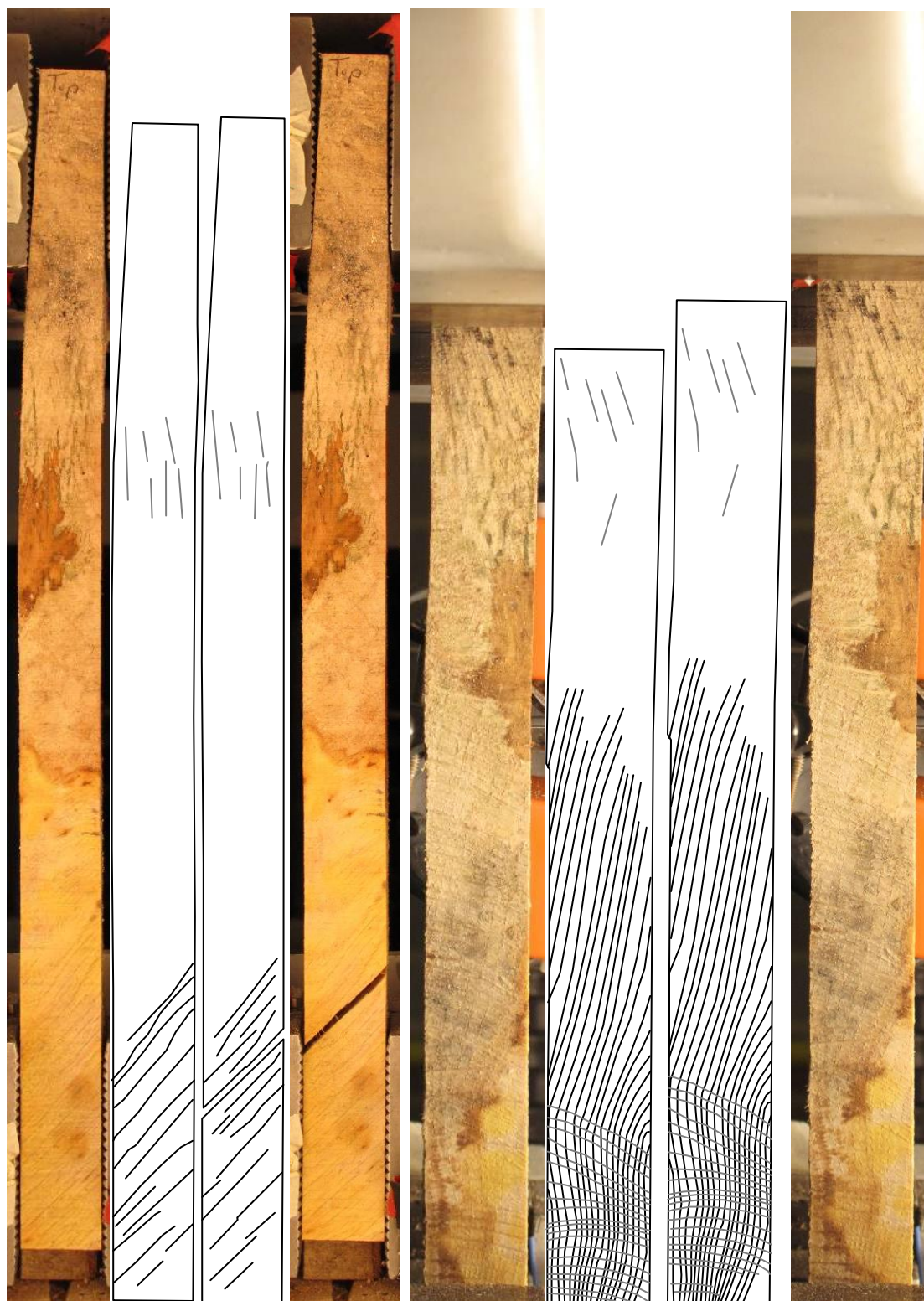
FIGURE 368: SAMPLE GRAIN ORIENTATIONS OF THE FRONT (LEFT 4 IMAGES) AND SIDE (RIGHT 4 IMAGES) VIEW BEFORE (FIRST 2 OF 4 IMAGES) AND AFTER (LAST 2 OF 4 IMAGES) BREAKAGE

Appendix 6

G10 Front View

FIGURE 369: X DIRECTION PIV SEQUENTIAL ENGINEERING STRAIN OVER TIME

FIGURE 370: Y DIRECTION PIV SEQUENTIAL ENGINEERING STRAIN OVER TIME

FIGURE 371: XY DIRECTION PIV SEQUENTIAL ENGINEERING SHEAR STRAIN OVER TIME

FIGURE 372: X DIRECTION PIV SEQUENTIAL TRUE STRAIN OVER TIME

Appendix 6

FIGURE 373: Y DIRECTION PIV SEQUENTIAL TRUE STRAIN OVER TIME

FIGURE 374: XY DIRECTION PIV SEQUENTIAL TRUE SHEAR STRAIN OVER TIME

FIGURE 375: X DIRECTION PIV FIRST–LAST DITCH ENGINEERING STRAIN OVER IMAGE

FIGURE 376: Y DIRECTION PIV FIRST–LAST DITCH ENGINEERING STRAIN OVER IMAGE

FIGURE 377: XY DIRECTION PIV FIRST–LAST DITCH ENGINEERING SHEAR STRAIN OVER

IMAGE

FIGURE 378: X DIRECTION PIV FIRST–LAST DITCH TRUE STRAIN OVER IMAGE

FIGURE 379: Y DIRECTION PIV FIRST–LAST DITCH TRUE STRAIN OVER IMAGE

FIGURE 380: XY DIRECTION PIV FIRST–LAST DITCH TRUE SHEAR STRAIN OVER IMAGE

Appendix 6

FIGURE 381: XY DIRECTION PIV FIRST–SEQUENTIAL ENGINEERING SHEAR STRAIN OVER

IMAGE

FIGURE 382: XY DIRECTION PIV FIRST–SEQUENTIAL ENGINEERING SHEAR STRAIN OVER TIME

G10 Side View

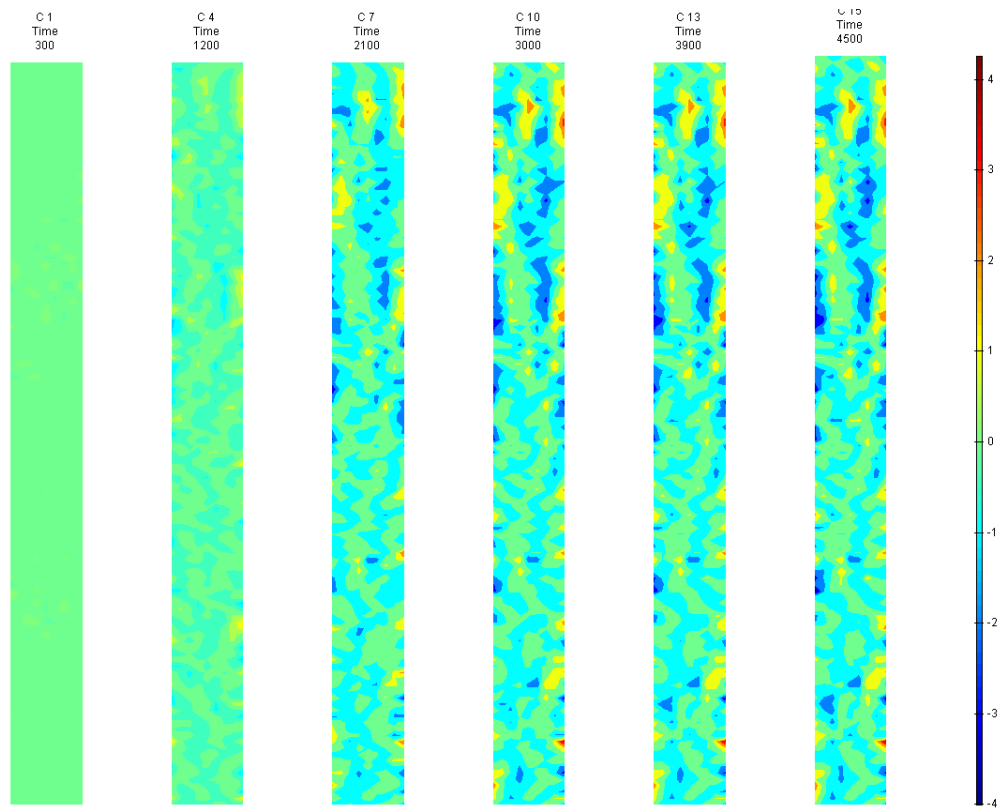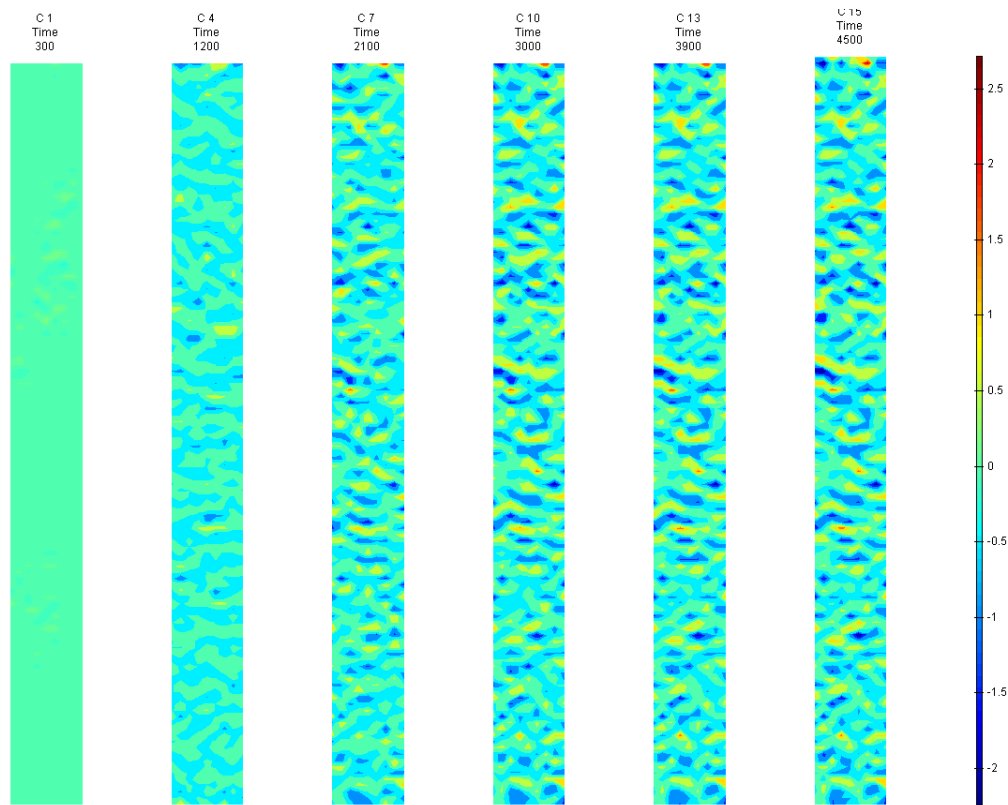FIGURE 383: X DIRECTION PIV SEQUENTIAL ENGINEERING STRAIN OVER TIME

FIGURE 384: Y DIRECTION PIV SEQUENTIAL ENGINEERING STRAIN OVER TIME

Appendix 6
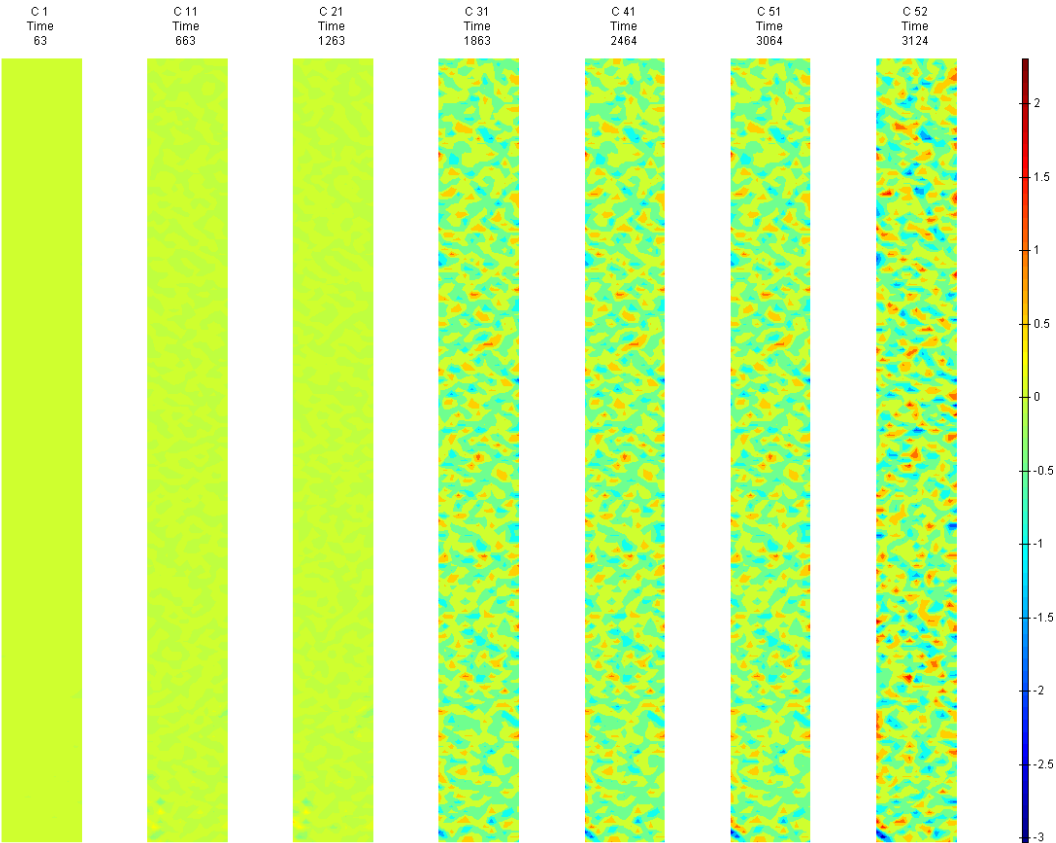
FIGURE 385: XY DIRECTION PIV SEQUENTIAL ENGINEERING SHEAR STRAIN OVER TIME

FIGURE 386: X DIRECTION PIV SEQUENTIAL TRUE STRAIN OVER TIME
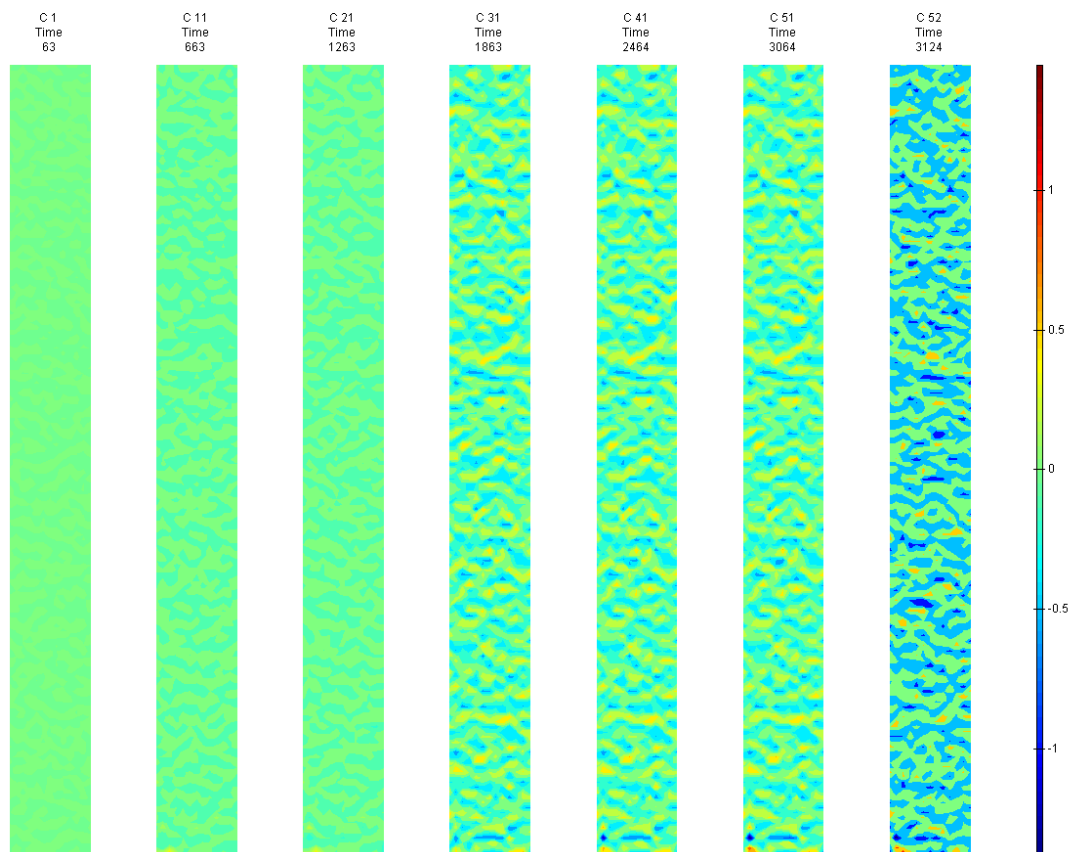
FIGURE 387: Y DIRECTION PIV SEQUENTIAL TRUE STRAIN OVER TIME

FIGURE 388: XY DIRECTION PIV SEQUENTIAL TRUE SHEAR STRAIN OVER TIME

FIGURE 389: X DIRECTION PIV FIRST–LAST DITCH ENGINEERING STRAIN OVER IMAGE

FIGURE 390: Y DIRECTION PIV FIRST–LAST DITCH ENGINEERING STRAIN OVER IMAGE

FIGURE 391: XY DIRECTION PIV FIRST–LAST DITCH ENGINEERING SHEAR STRAIN OVER

IMAGE

FIGURE 392: X DIRECTION PIV FIRST–LAST DITCH TRUE STRAIN OVER IMAGE

Appendix 6

FIGURE 393: Y DIRECTION PIV FIRST–LAST DITCH TRUE STRAIN OVER IMAGE

FIGURE 394: XY DIRECTION PIV FIRST–LAST DITCH TRUE SHEAR STRAIN OVER IMAGE

FIGURE 395: XY DIRECTION PIV FIRST-SEQUENTIAL ENGINEERING SHEAR STRAIN OVER

IMAGE

FIGURE 396: XY DIRECTION PIV FIRST-SEQUENTIAL ENGINEERING SHEAR STRAIN OVER TIME

G11
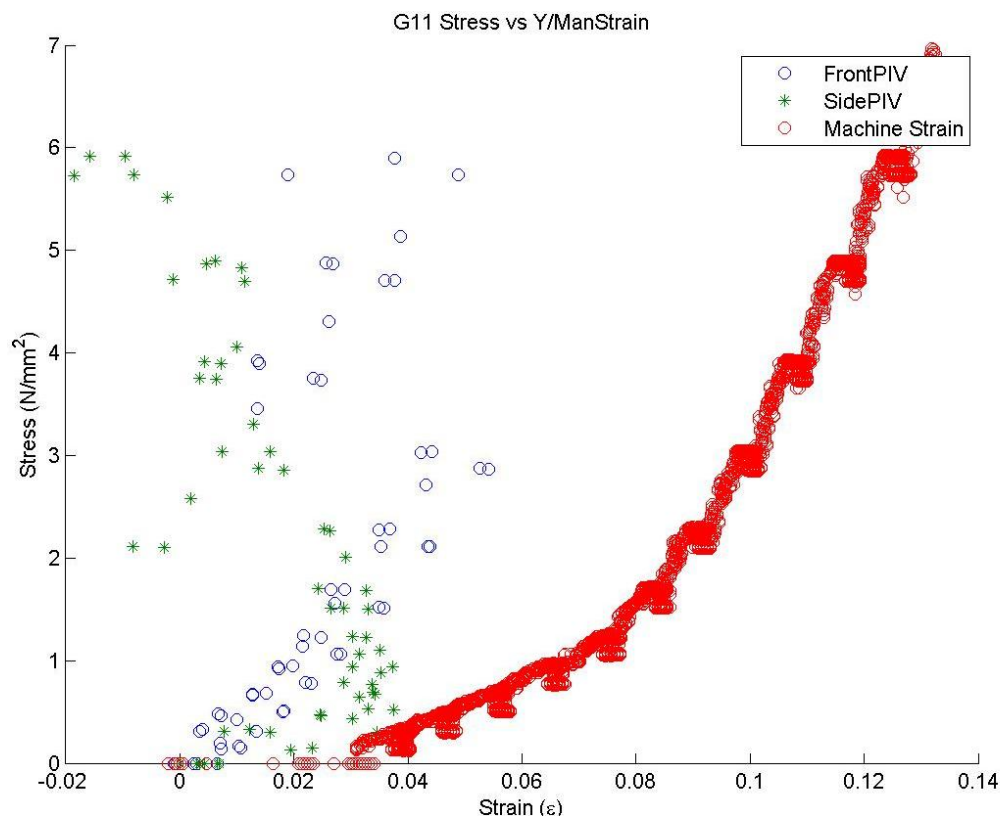
FIGURE 397: G11 TENSILE STRESS VS. MACHINE MEASURED/PIV STRAINS
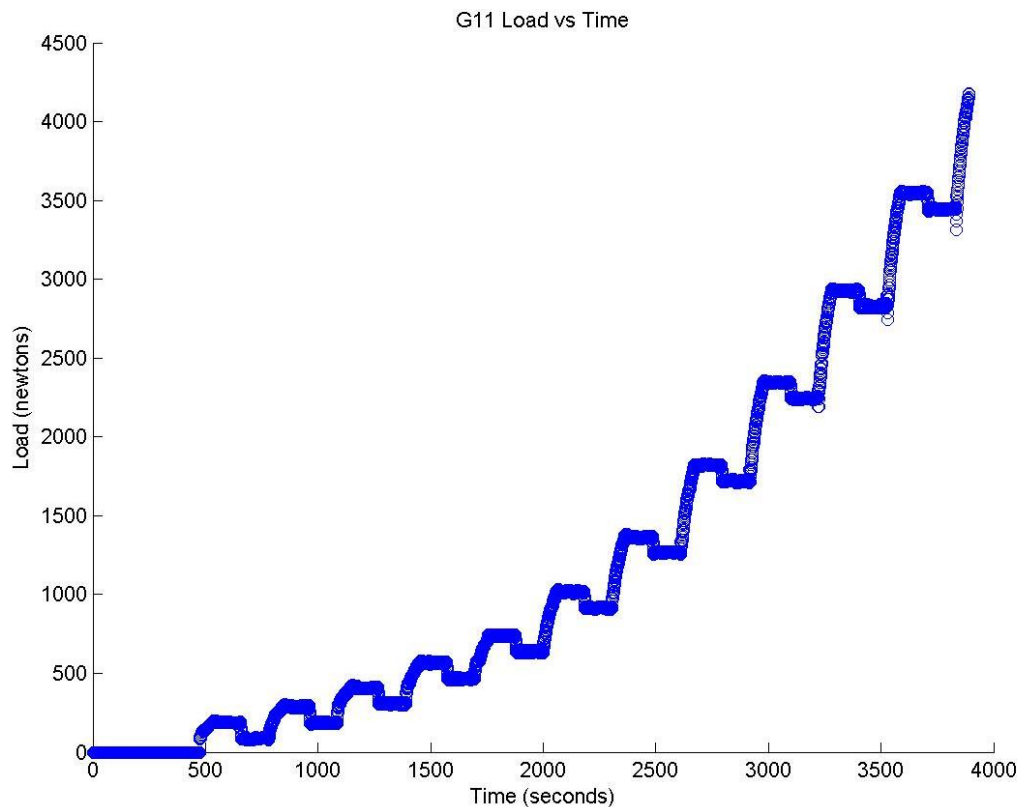
FIGURE 398: G11 TENSILE LOAD VS. TIME

FIGURE 399: G11 CREEP LOADING: INCREMENTS AND RELAXATION

FIGURE 400: G11 MACHINE MEASURED SECANT AND TANGENT MODULUS VS. TIME

Appendix 6

FIGURE 401: G11 FRONT VIEW PIV SECANT AND TANGENT MODULUS VS. TIME

FIGURE 402: G11 SIDE VIEW PIV SECANT AND TANGENT MODULUS VS. TIME

350

FIGURE 403: G11 COMPARISON OF MACHINE MEASURED AND PIV SECANT MODULUS VS.

TIME

FIGURE 404: G11 COMPARISON OF MACHINE MEASURED AND PIV TANGENT MODULUS VS.

TIME

G11 Sample

FIGURE 405: SAMPLE GRAIN ORIENTATIONS OF THE FRONT (LEFT 4 IMAGES) AND SIDE (RIGHT 4 IMAGES) VIEW BEFORE (FIRST 2 OF 4 IMAGES) AND AFTER (LAST 2 OF 4 IMAGES) BREAKAGE

G11 Front View

FIGURE 406: X DIRECTION PIV SEQUENTIAL ENGINEERING STRAIN OVER TIME

FIGURE 407: Y DIRECTION PIV SEQUENTIAL ENGINEERING STRAIN OVER TIME

Appendix 6

FIGURE 408: XY DIRECTION PIV SEQUENTIAL ENGINEERING SHEAR STRAIN OVER TIME

FIGURE 409: X DIRECTION PIV SEQUENTIAL TRUE STRAIN OVER TIME

FIGURE 410: Y DIRECTION PIV SEQUENTIAL TRUE STRAIN OVER TIME

FIGURE 411: XY DIRECTION PIV SEQUENTIAL TRUE SHEAR STRAIN OVER TIME

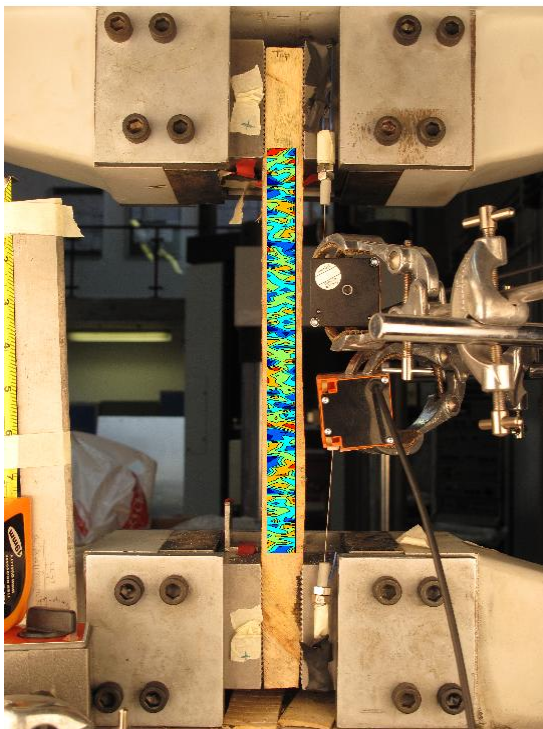FIGURE 412: X DIRECTION PIV FIRST–LAST DITCH ENGINEERING STRAIN OVER IMAGE

FIGURE 413: Y DIRECTION PIV FIRST–LAST DITCH ENGINEERING STRAIN OVER IMAGE

FIGURE 414: XY DIRECTION PIV FIRST–LAST DITCH ENGINEERING SHEAR STRAIN OVER

IMAGE

FIGURE 415: X DIRECTION PIV FIRST–LAST DITCH TRUE STRAIN OVER IMAGE

FIGURE 416: Y DIRECTION PIV FIRST–LAST DITCH TRUE STRAIN OVER IMAGE

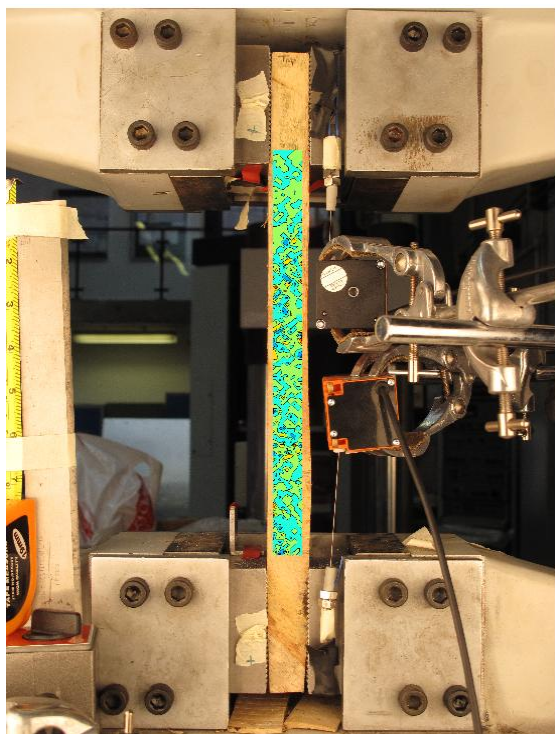FIGURE 417: XY DIRECTION PIV FIRST–LAST DITCH TRUE SHEAR STRAIN OVER IMAGE

FIGURE 418: XY DIRECTION PIV FIRST–SEQUENTIAL ENGINEERING SHEAR STRAIN OVER
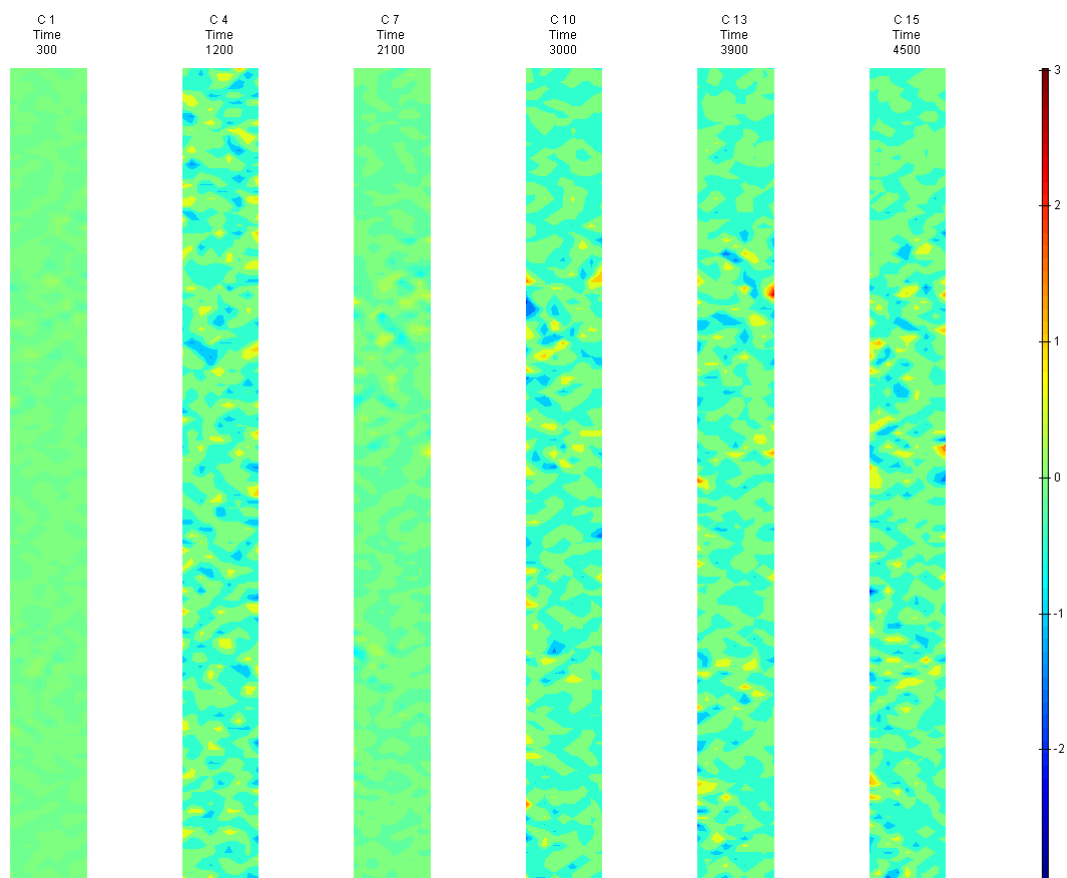
IMAGE

FIGURE 419: XY DIRECTION PIV FIRST–SEQUENTIAL ENGINEERING SHEAR STRAIN OVER TIME

359

Appendix 6

G11 Side View
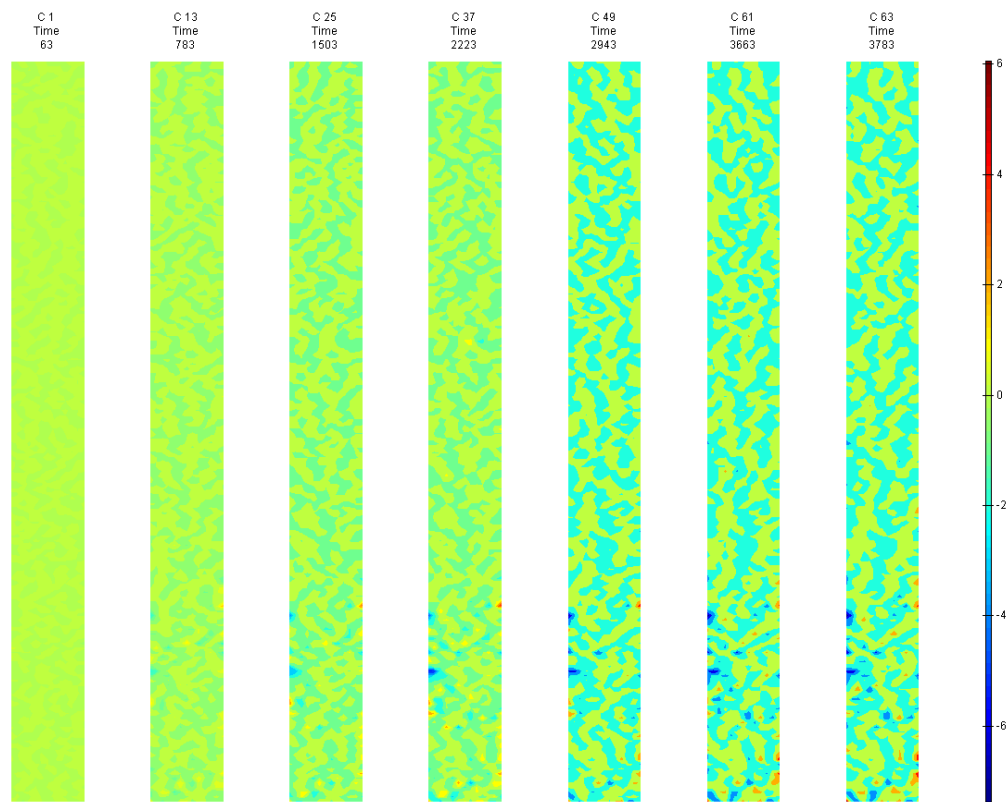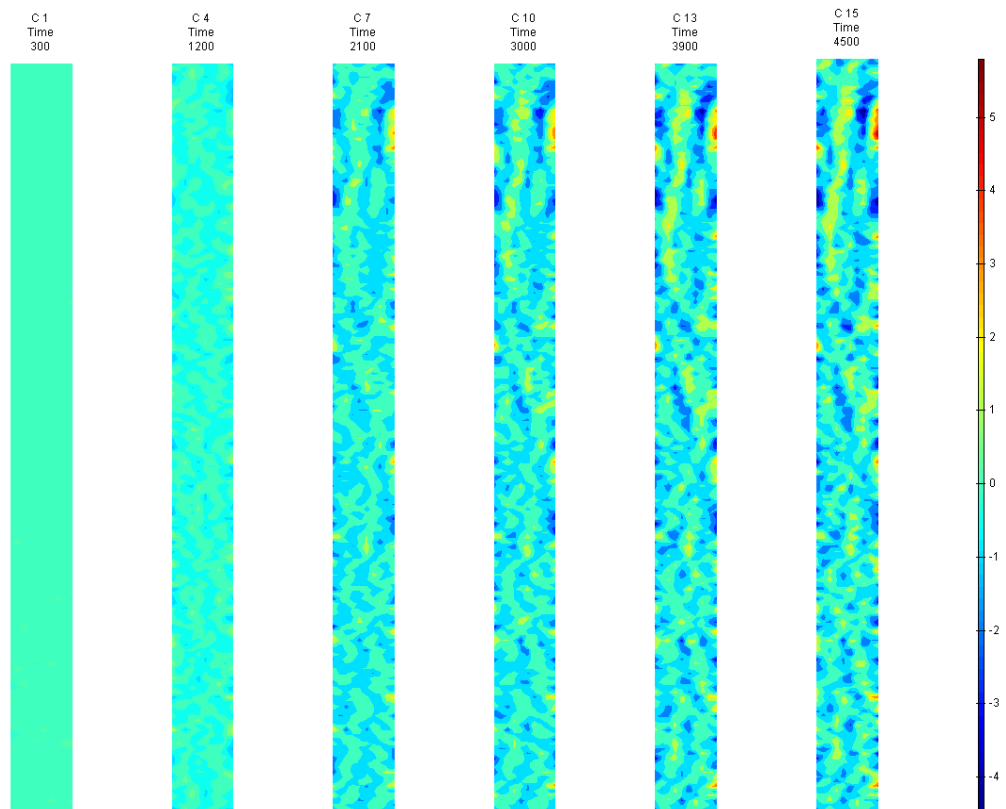

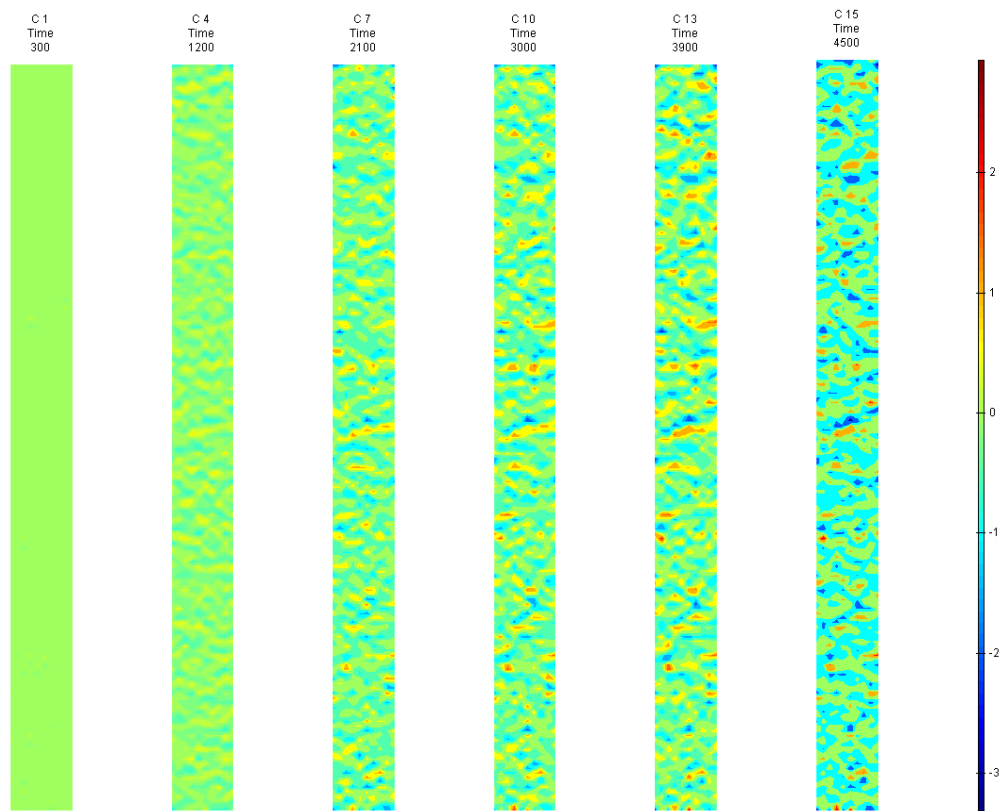FIGURE 420: X DIRECTION PIV SEQUENTIAL ENGINEERING STRAIN OVER TIME
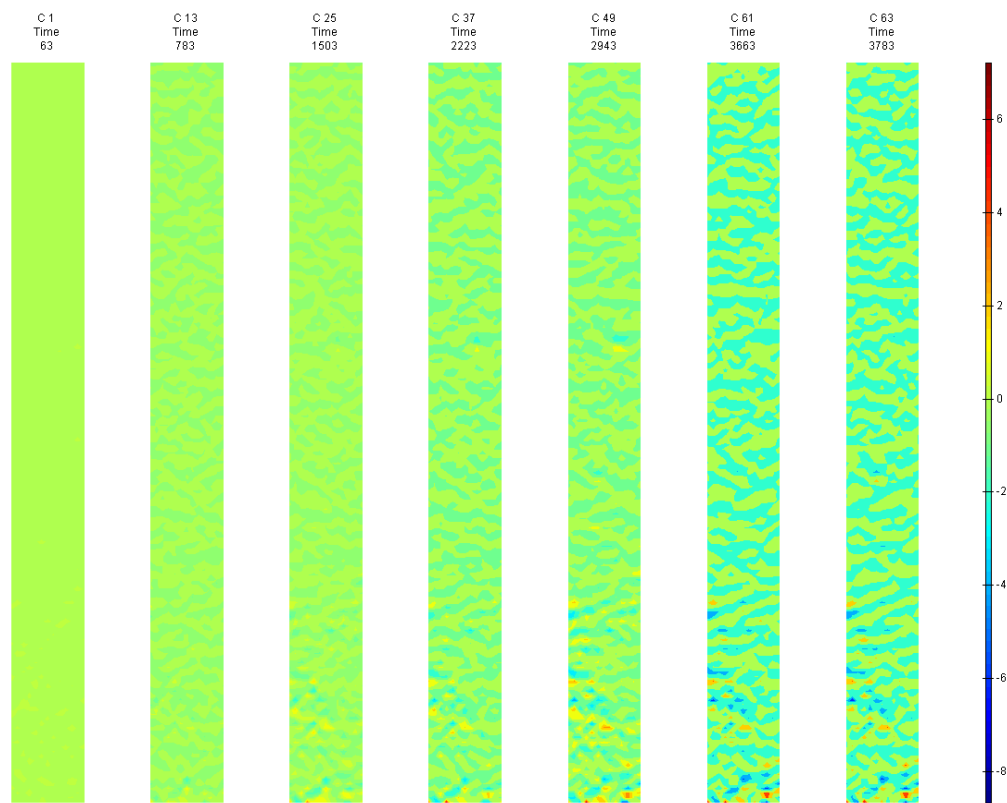
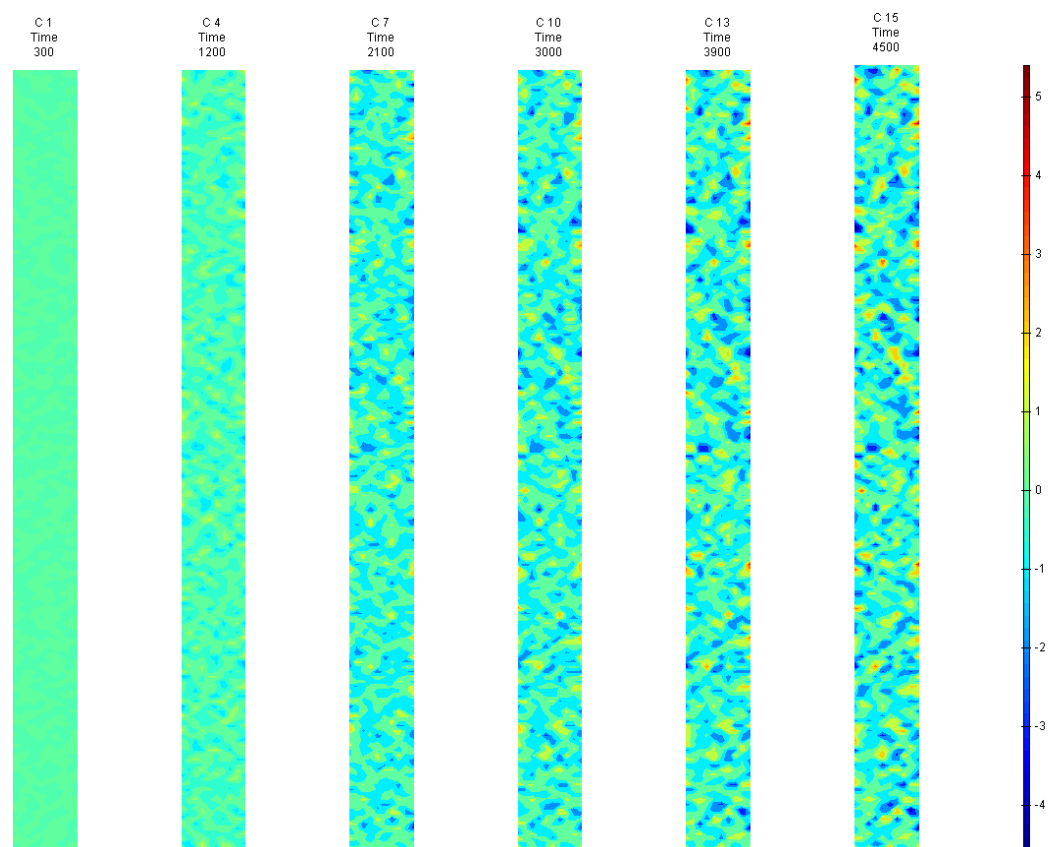FIGURE 421: Y DIRECTION PIV SEQUENTIAL ENGINEERING STRAIN OVER TIME

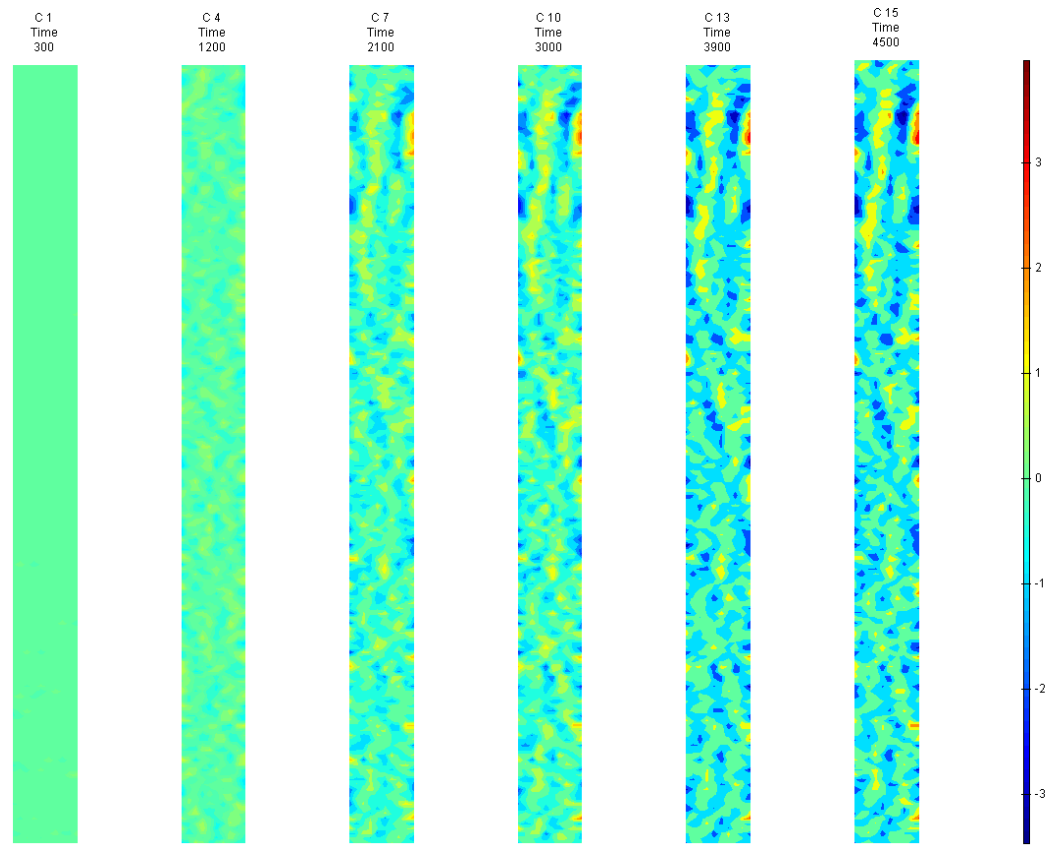FIGURE 422: XY DIRECTION PIV SEQUENTIAL ENGINEERING SHEAR STRAIN OVER TIME

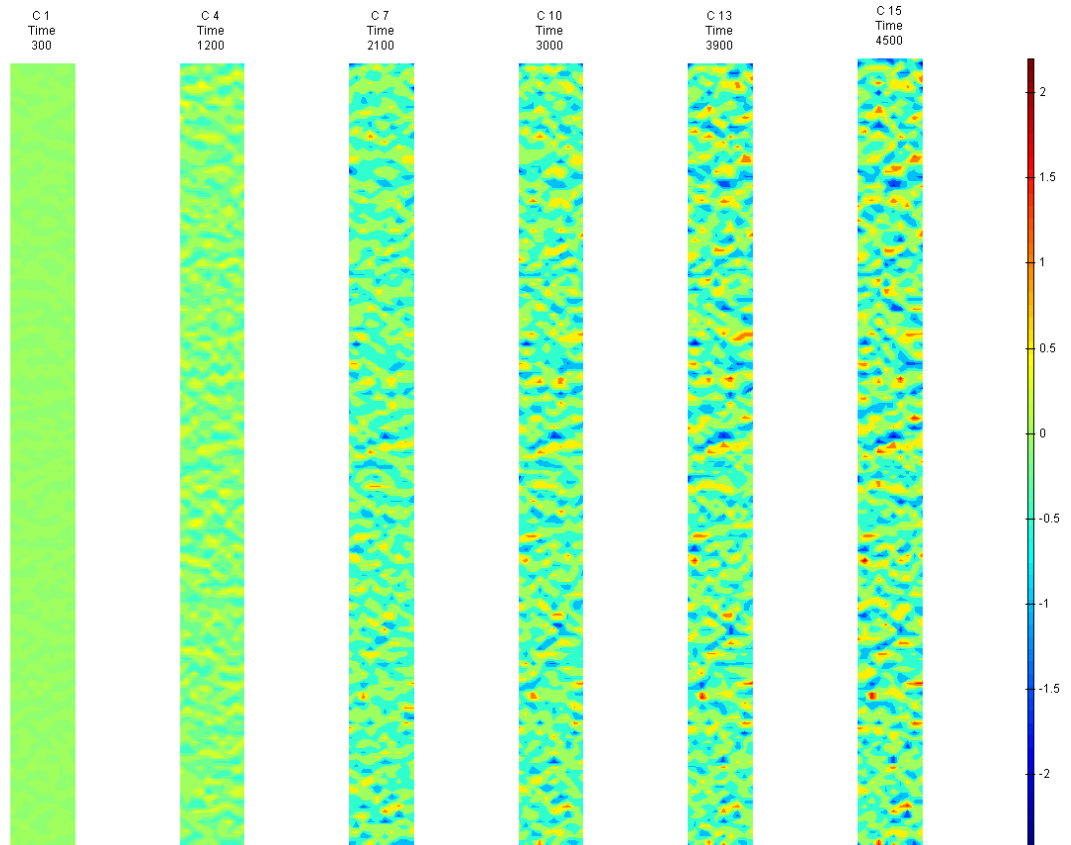FIGURE 423: X DIRECTION PIV SEQUENTIAL TRUE STRAIN OVER TIME

Appendix 6

FIGURE 424: Y DIRECTION PIV SEQUENTIAL TRUE STRAIN OVER TIME
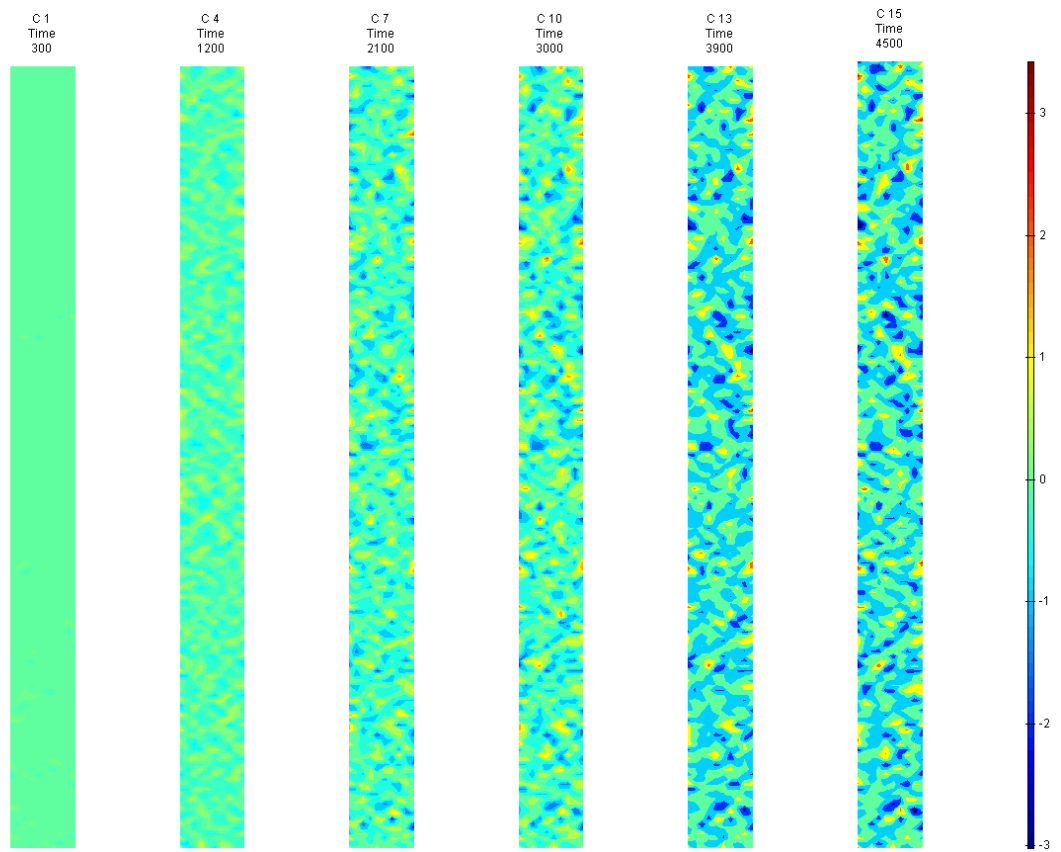

FIGURE 425: XY DIRECTION PIV SEQUENTIAL TRUE SHEAR STRAIN OVER TIME
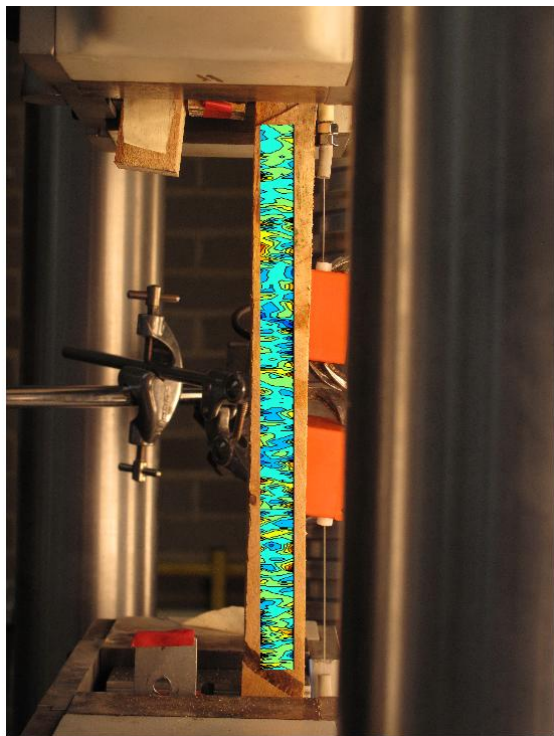
FIGURE 426: X DIRECTION PIV FIRST–LAST DITCH ENGINEERING STRAIN OVER IMAGE
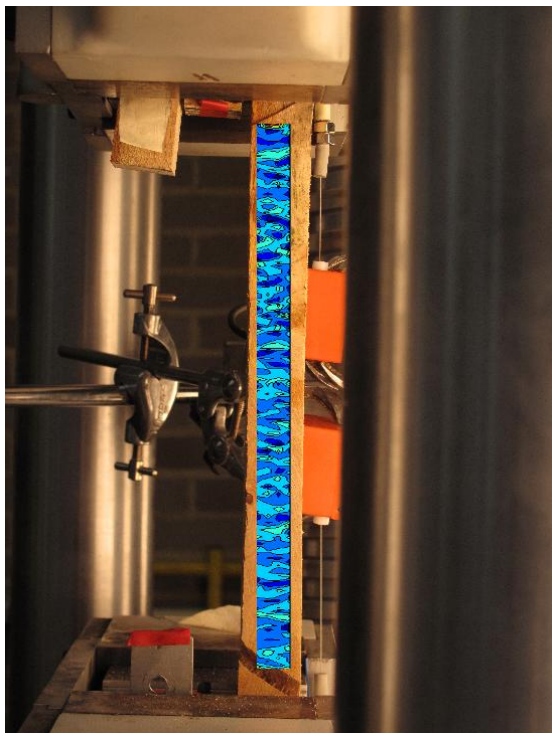

FIGURE 427: Y DIRECTION PIV FIRST–LAST DITCH ENGINEERING STRAIN OVER IMAGE
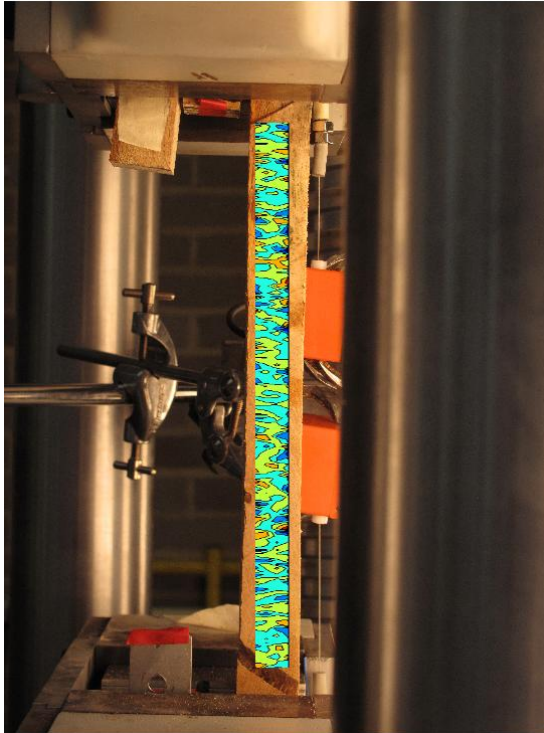
Appendix 6

FIGURE 428: XY DIRECTION PIV FIRST–LAST DITCH ENGINEERING SHEAR STRAIN OVER

IMAGE

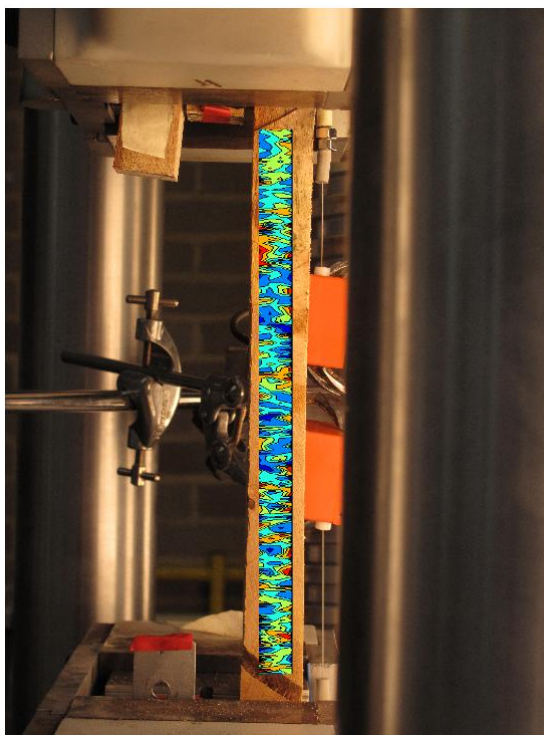
FIGURE 429: X DIRECTION PIV FIRST–LAST DITCH TRUE STRAIN OVER IMAGE

FIGURE 430: Y DIRECTION PIV FIRST–LAST DITCH TRUE STRAIN OVER IMAGE

FIGURE 431: XY DIRECTION PIV FIRST–LAST DITCH TRUE SHEAR STRAIN OVER IMAGE

Appendix 6

FIGURE 432: XY DIRECTION PIV FIRST–SEQUENTIAL ENGINEERING SHEAR STRAIN OVER

IMAGE
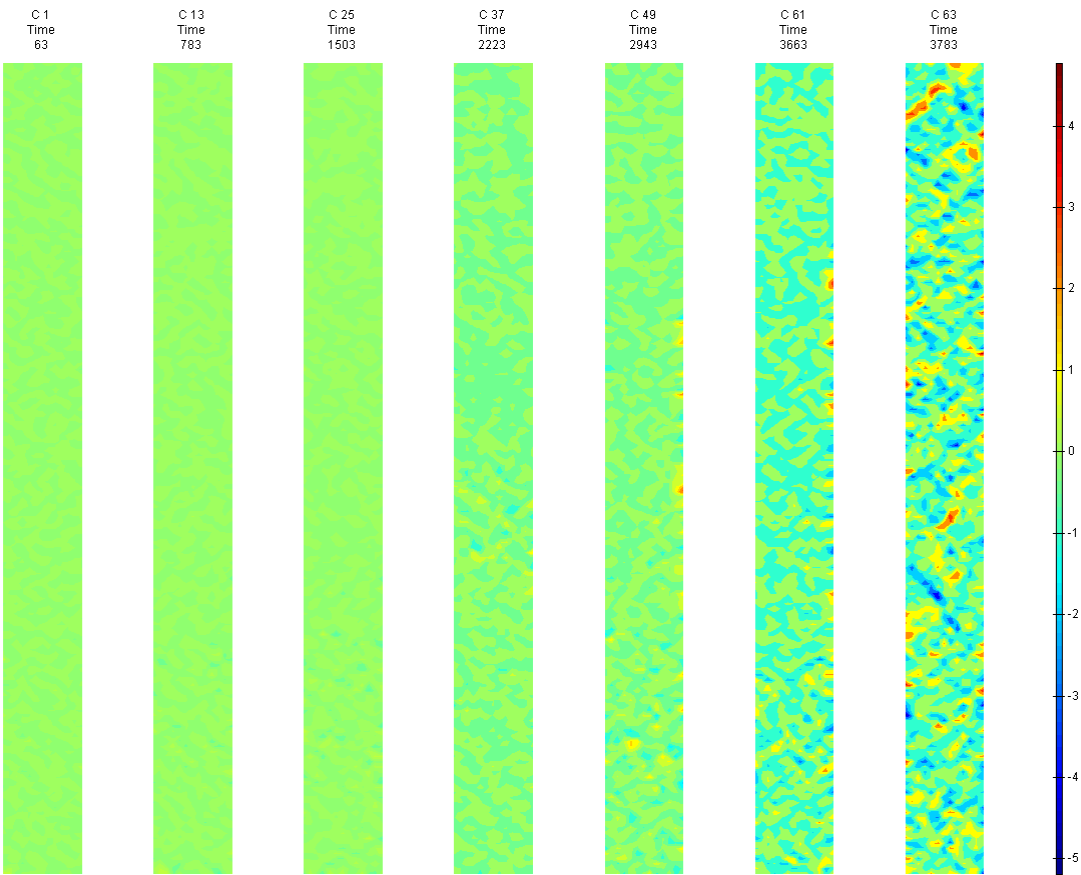
FIGURE 433: XY DIRECTION PIV FIRST–SEQUENTIAL ENGINEERING SHEAR STRAIN OVER TIME

Joint S
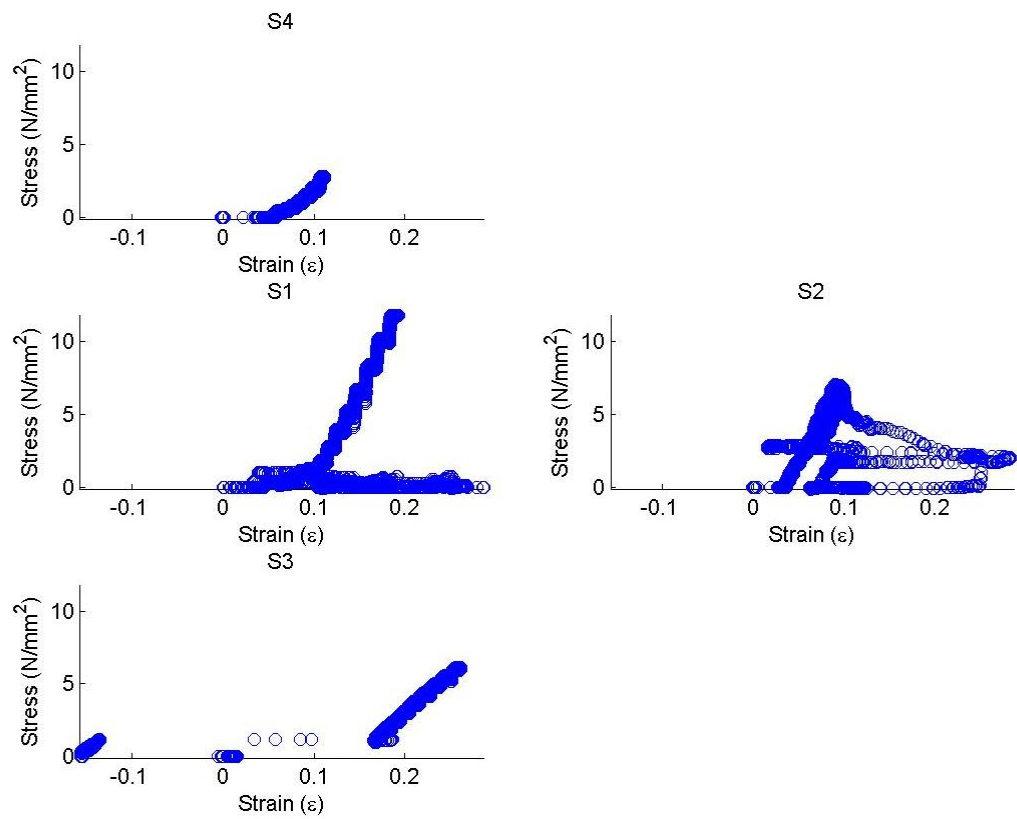
FIGURE 434: S COMPONENTS STRESS VS. MACHINE MEASURED STRAIN AT LOCATION
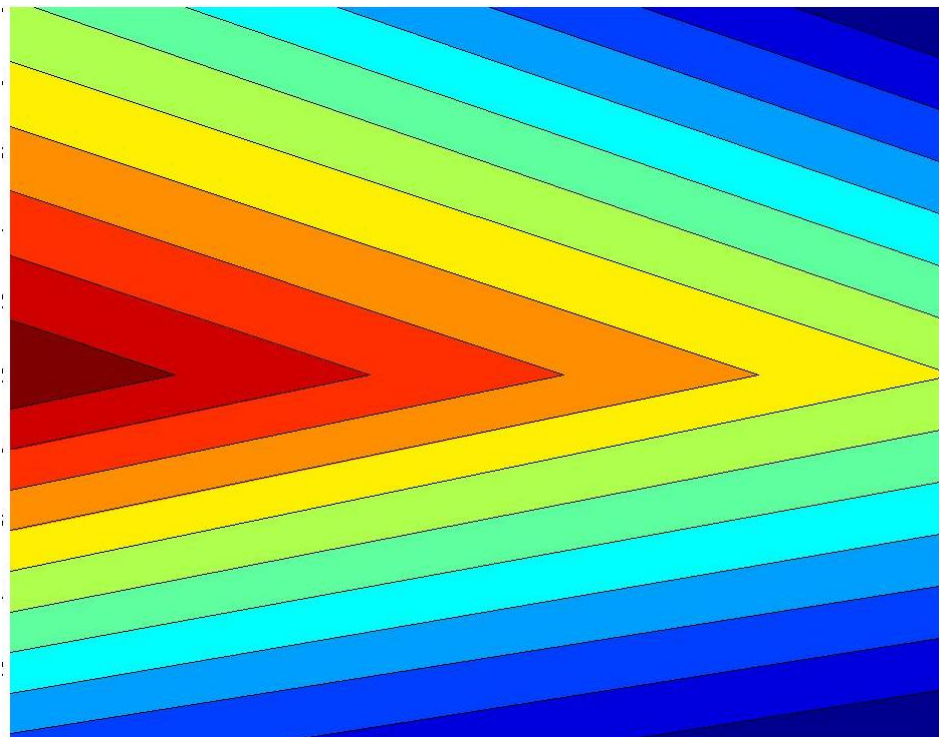
FIGURE 435: S COMPONENTS TENSILE STRESS AT LOCATION AS CONTOUR PLOT
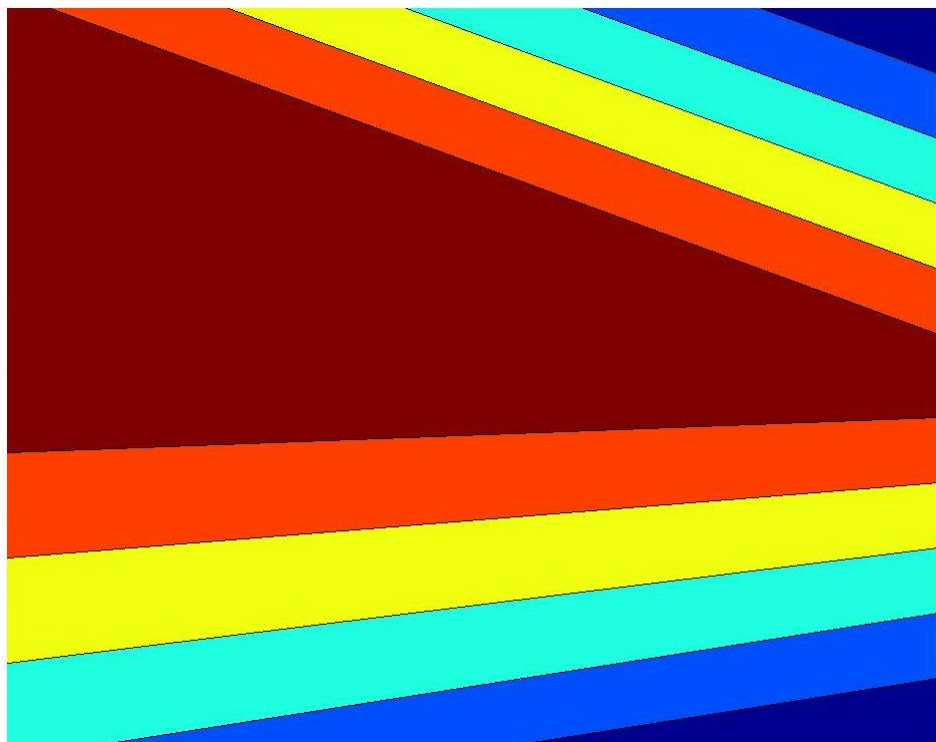
FIGURE 436: S COMPONENTS MACHINE MEASURED STRAIN AT LOCATION AS CONTOUR PLOT
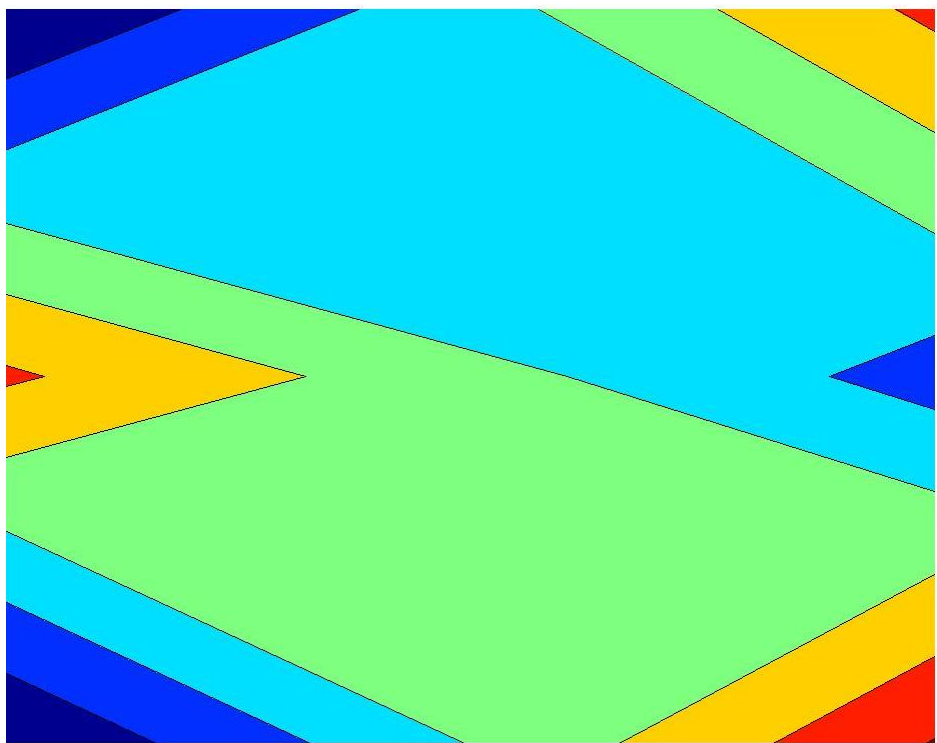
FIGURE 437: S COMPONENTS FRONT SEQUENTIAL STRAIN AT LOCATION AS CONTOUR PLOT
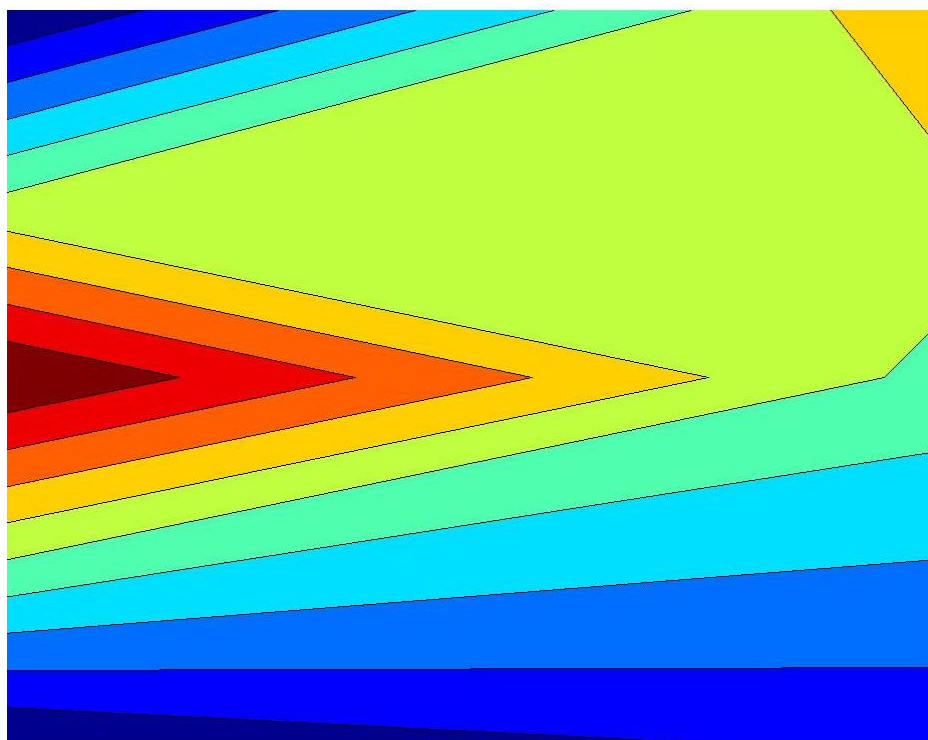
FIGURE 438: S COMPONENTS SIDE SEQUENTIAL STRAIN AT LOCATION AS CONTOUR PLOT
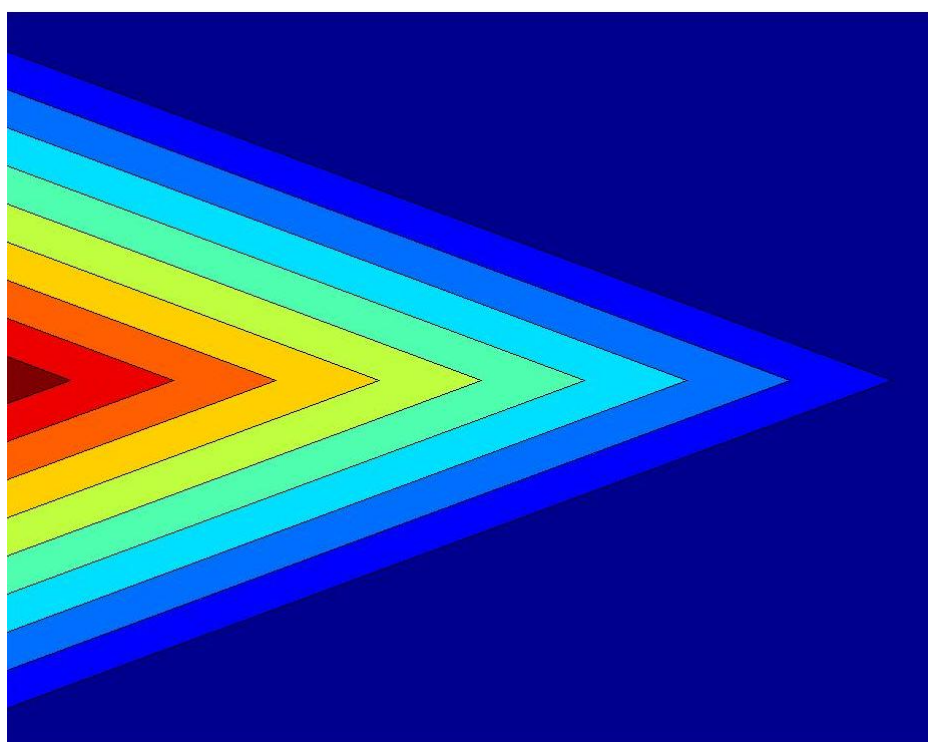
FIGURE 439: S COMPONENTS FRONT FIRST-SEQUENTIAL STRAIN AT LOCATION AS CONTOUR PLOT
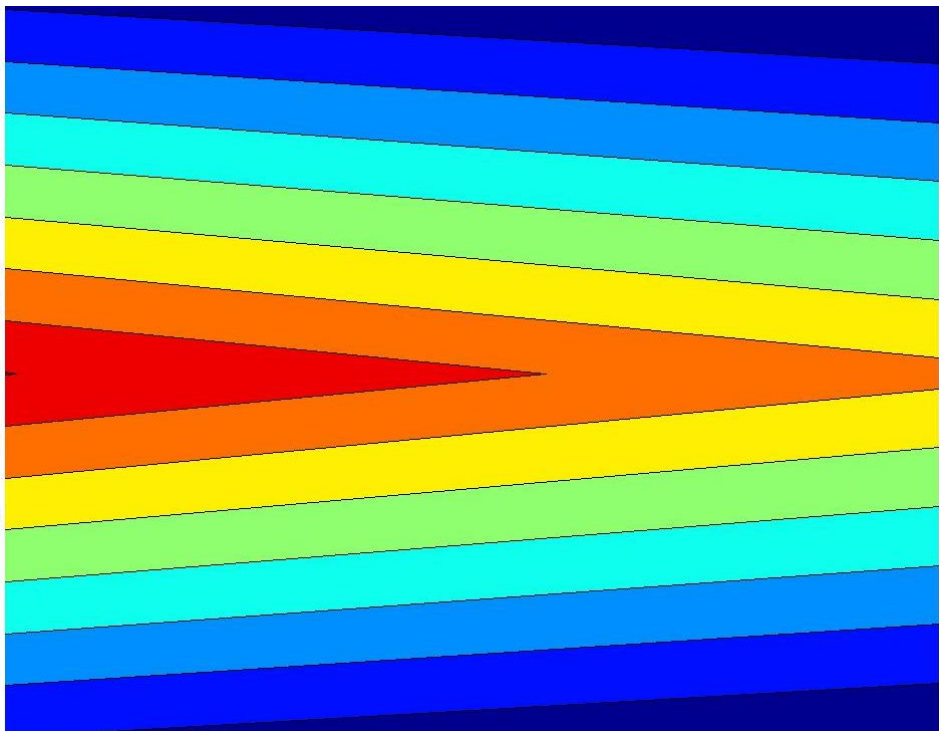
Appendix 6

FIGURE 440: S COMPONENTS SIDE FIRST-SEQUENTIAL STRAIN AT LOCATION AS CONTOUR

PLOT

S1
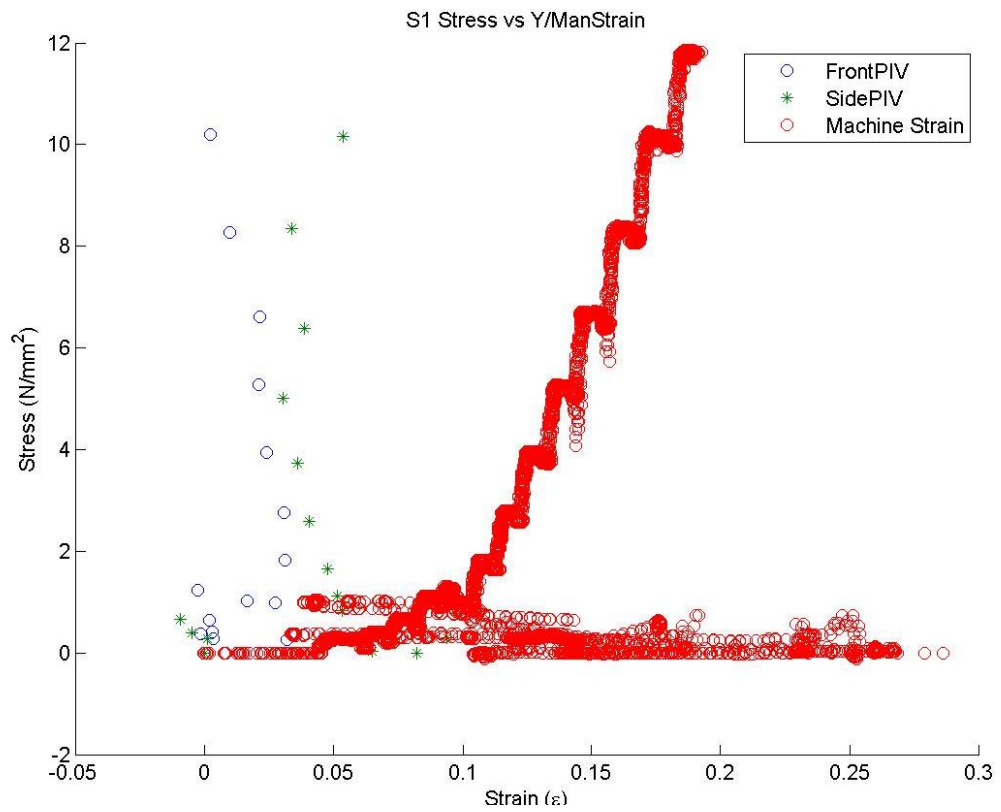
FIGURE 441: S1 TENSILE STRESS VS. MACHINE MEASURED/PIV STRAINS
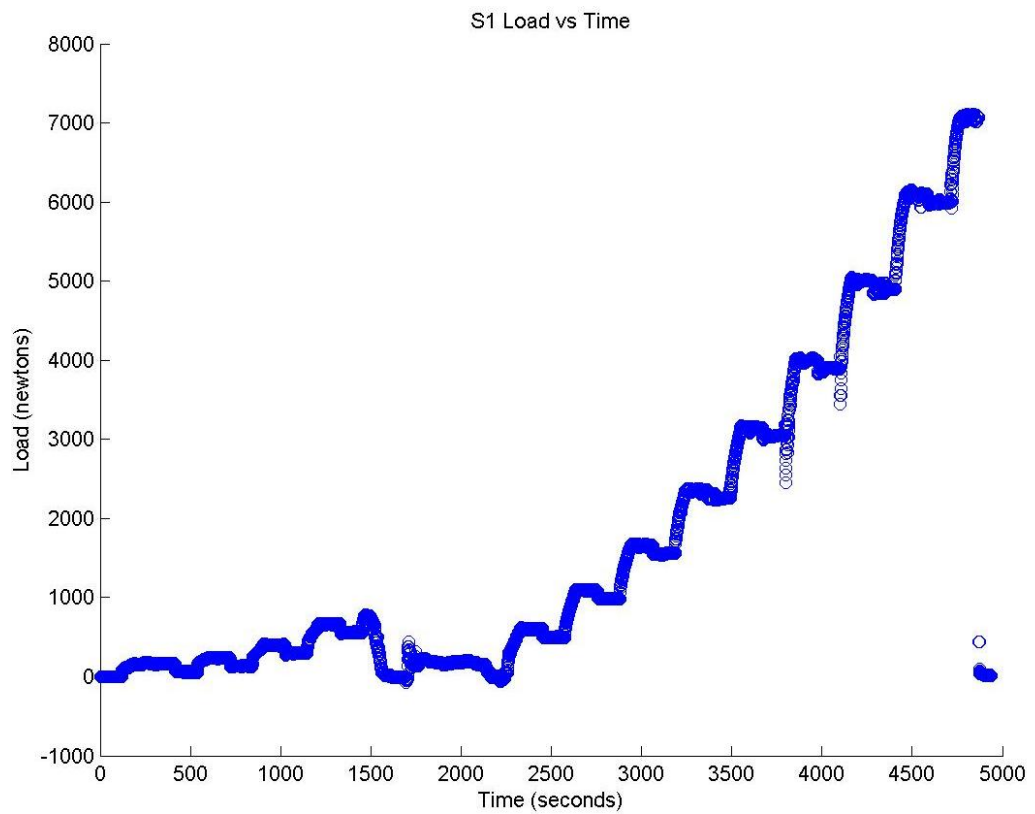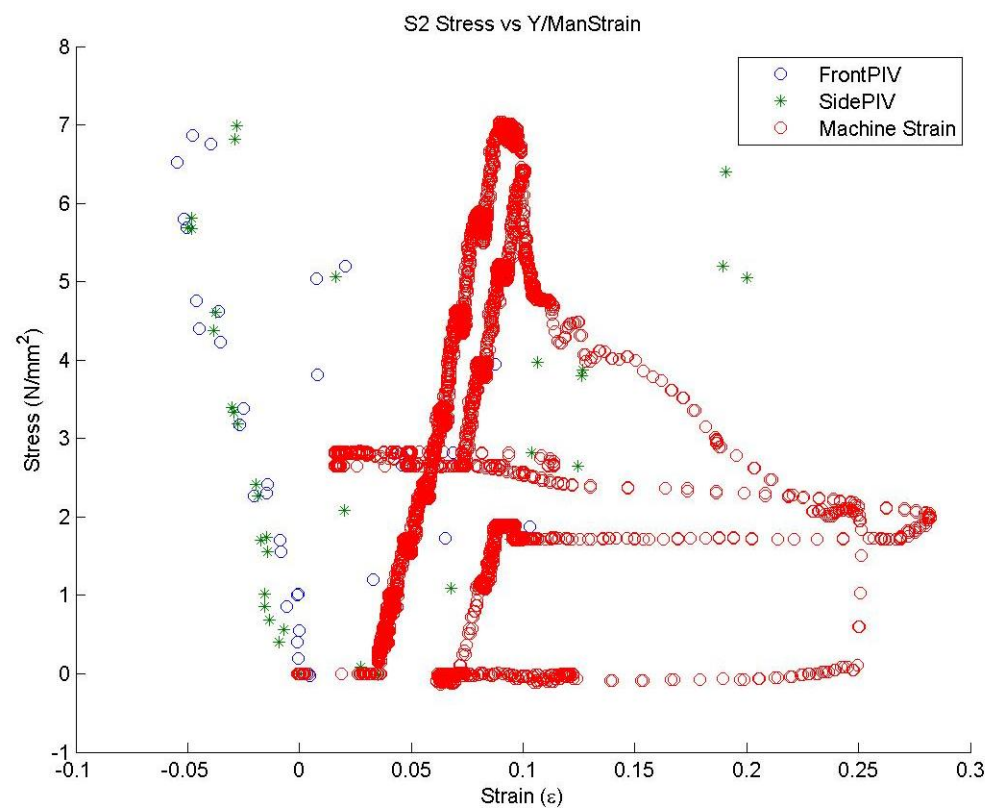

FIGURE 442: S1 TENSILE LOAD VS. TIME
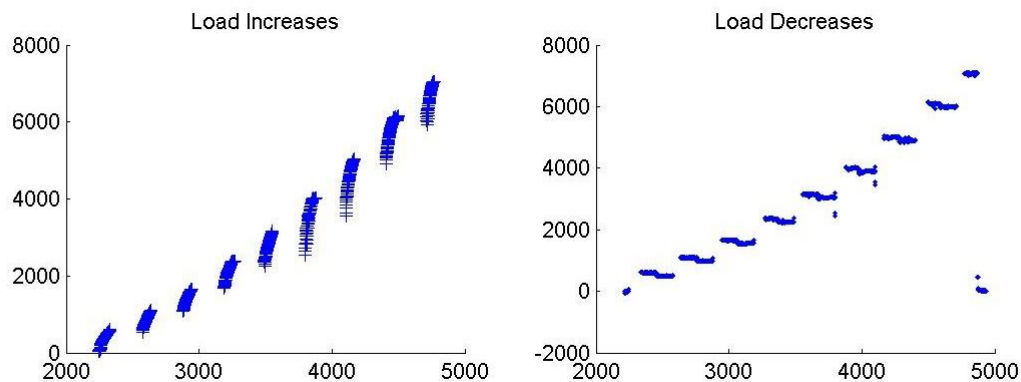
FIGURE 443: S1 CREEP LOADING: INCREMENTS AND RELAXATION
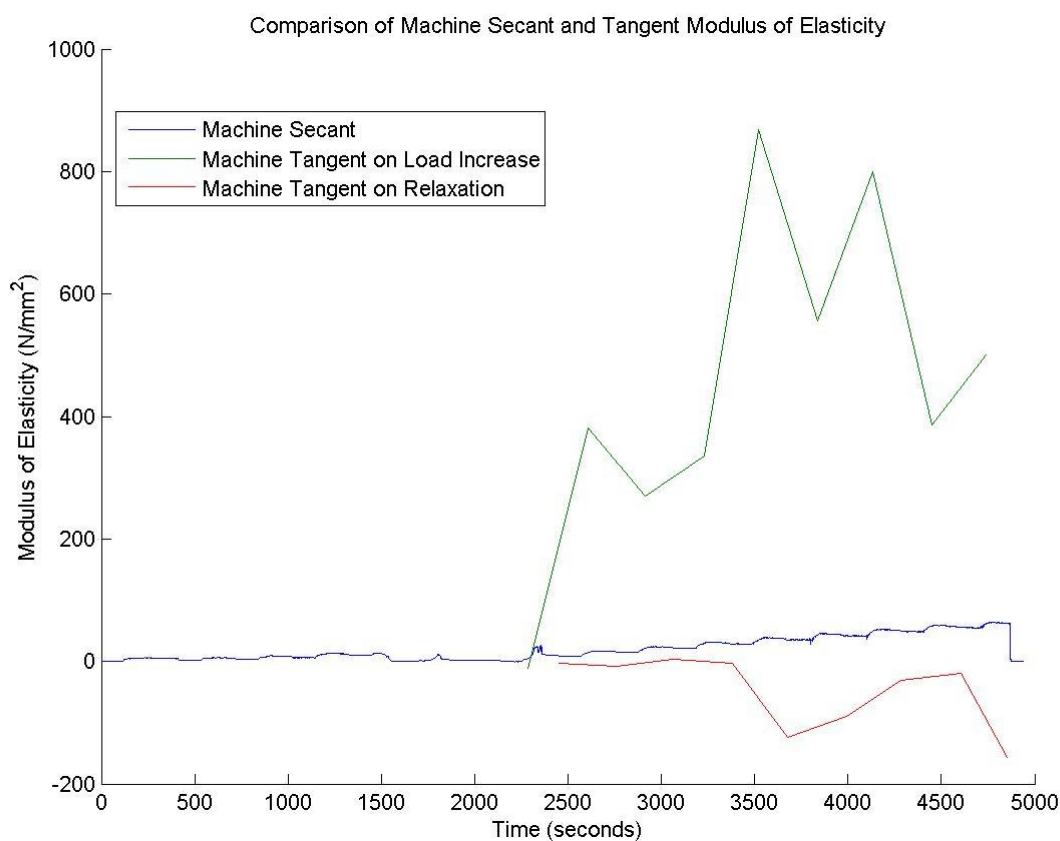
FIGURE 444: S1 MACHINE MEASURED SECANT AND TANGENT MODULUS VS. TIME
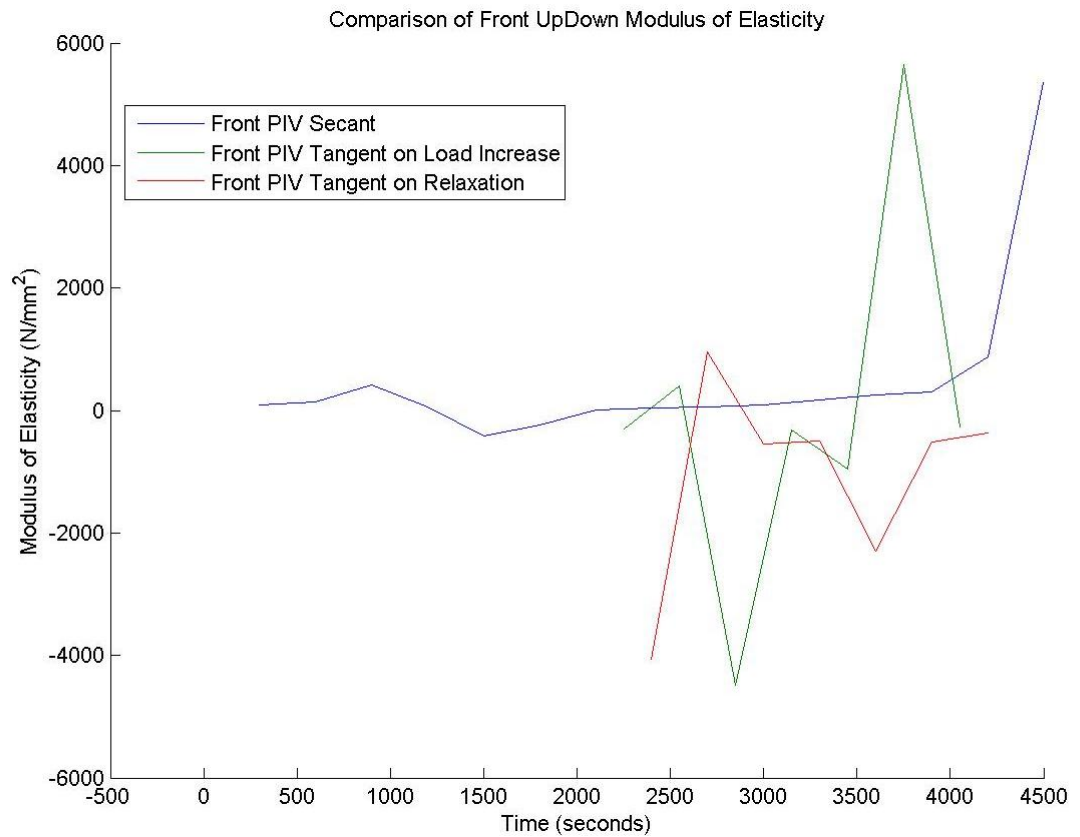
FIGURE 445: S1 FRONT VIEW PIV SECANT AND TANGENT MODULUS VS. TIME
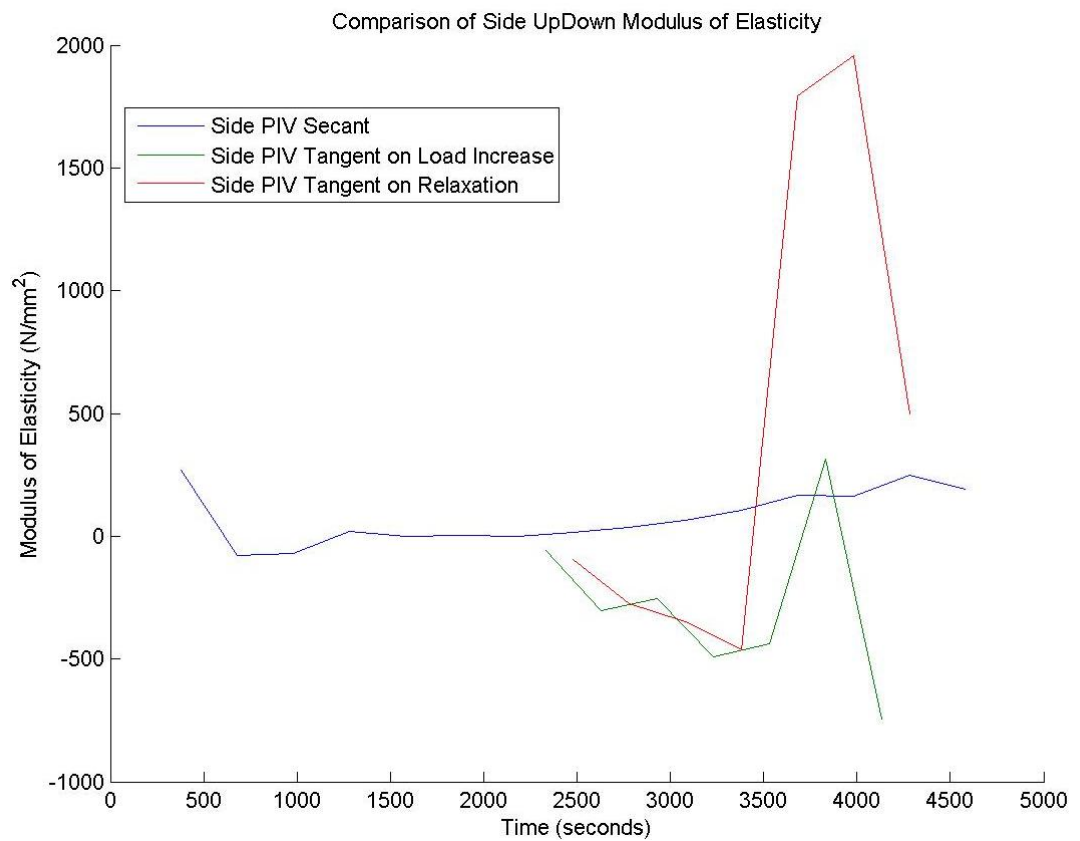
FIGURE 446: S1 SIDE VIEW PIV SECANT AND TANGENT MODULUS VS. TIME

Appendix 6
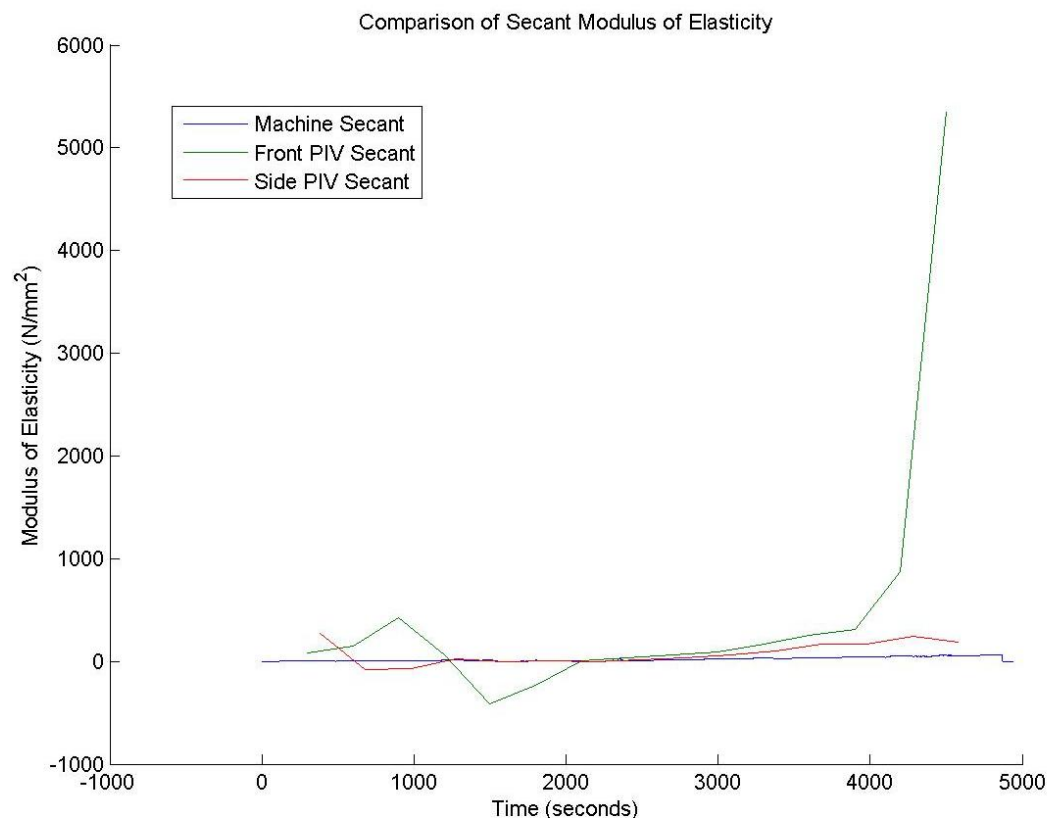
FIGURE 447: S1 COMPARISON OF MACHINE MEASURED AND PIV SECANT MODULUS VS. TIME
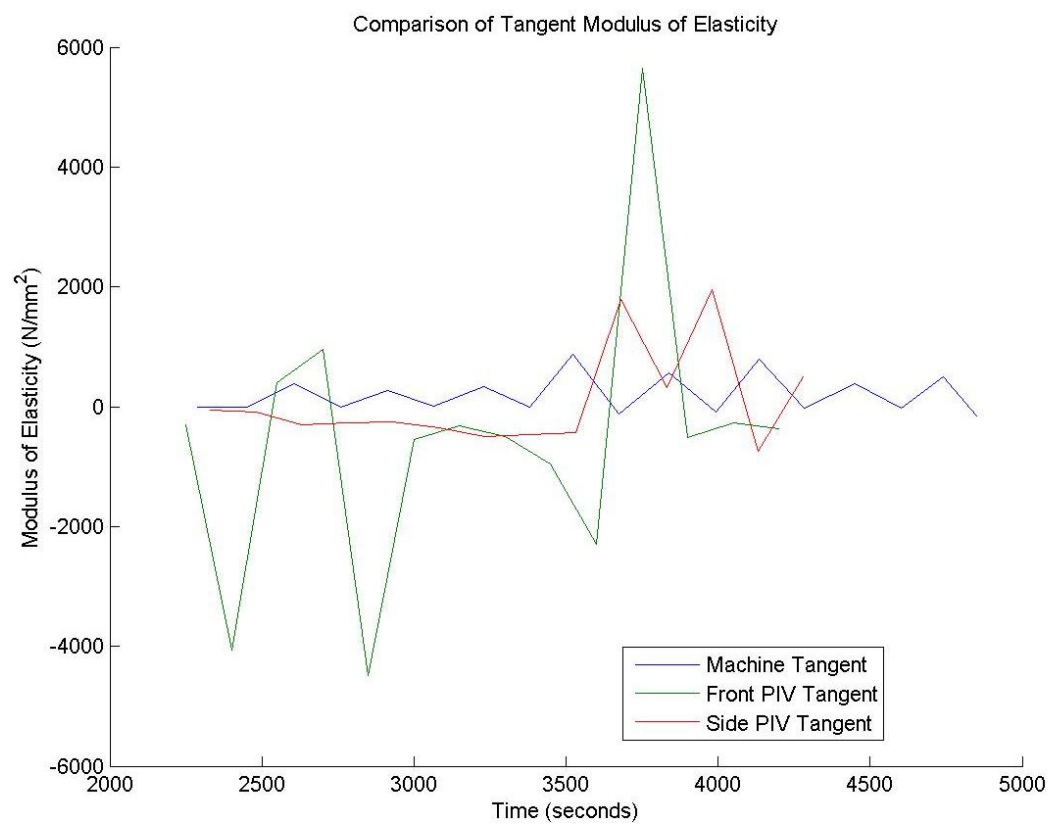
FIGURE 448: S1 COMPARISON OF MACHINE MEASURED AND PIV TANGENT MODULUS VS.

TIME

374

S1 Sample

FIGURE 449: SAMPLE GRAIN ORIENTATIONS OF THE FRONT (LEFT 4 IMAGES) AND SIDE (RIGHT 4 IMAGES) VIEW BEFORE (FIRST 2 OF 4 IMAGES) AND AFTER (LAST 2 OF 4 IMAGES) BREAKAGE

Appendix 6

S1 Front View

FIGURE 450: X DIRECTION PIV SEQUENTIAL ENGINEERING STRAIN OVER TIME

FIGURE 451: Y DIRECTION PIV SEQUENTIAL ENGINEERING STRAIN OVER TIME
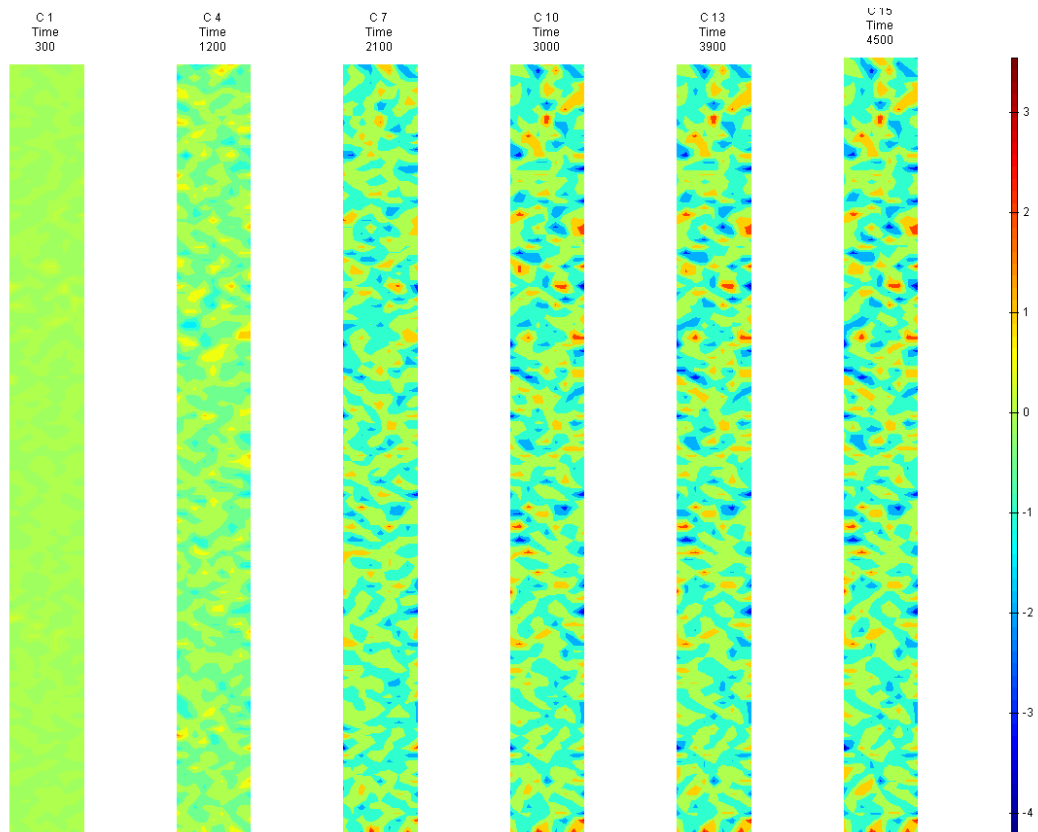
FIGURE 452: XY DIRECTION PIV SEQUENTIAL ENGINEERING SHEAR STRAIN OVER TIME
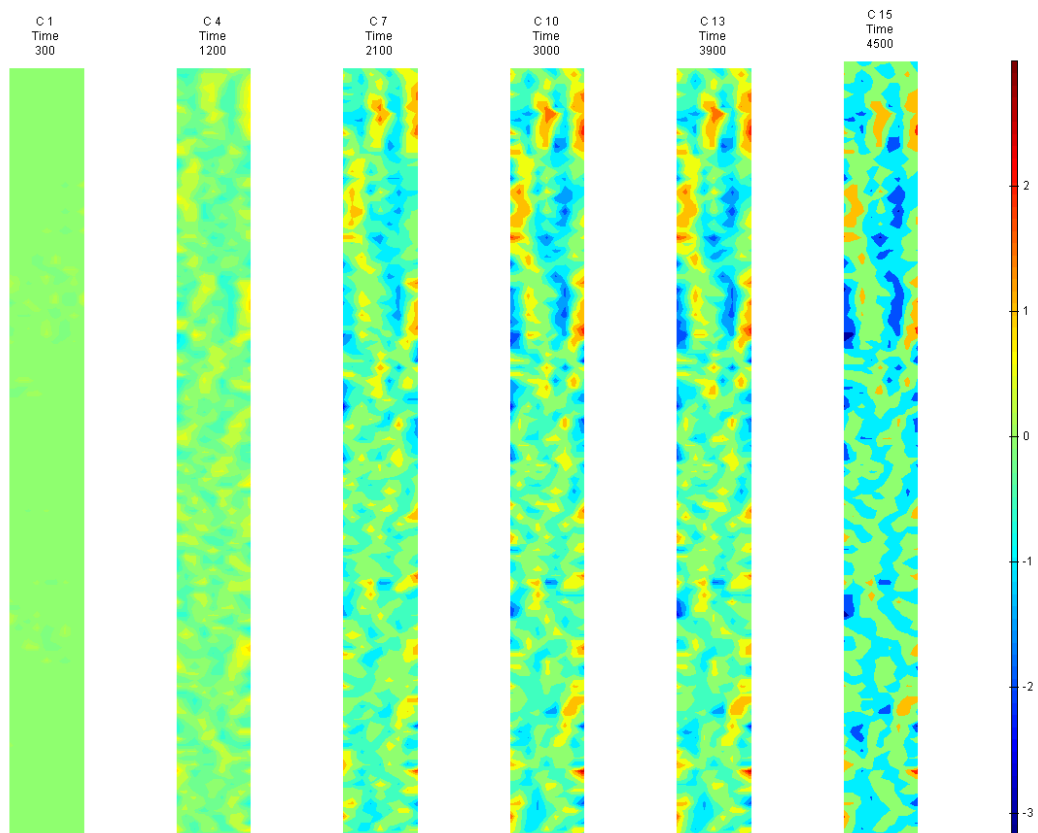
FIGURE 453: X DIRECTION PIV SEQUENTIAL TRUE STRAIN OVER TIME

Appendix 6
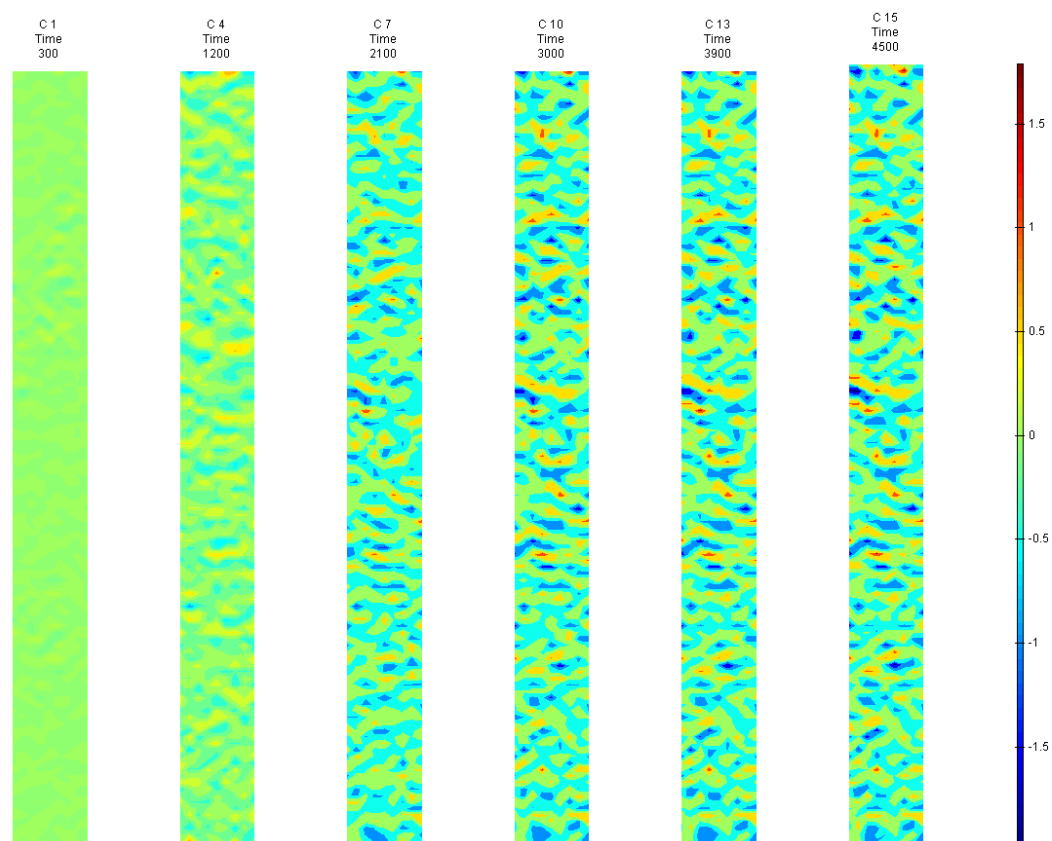
FIGURE 454: Y DIRECTION PIV SEQUENTIAL TRUE STRAIN OVER TIME
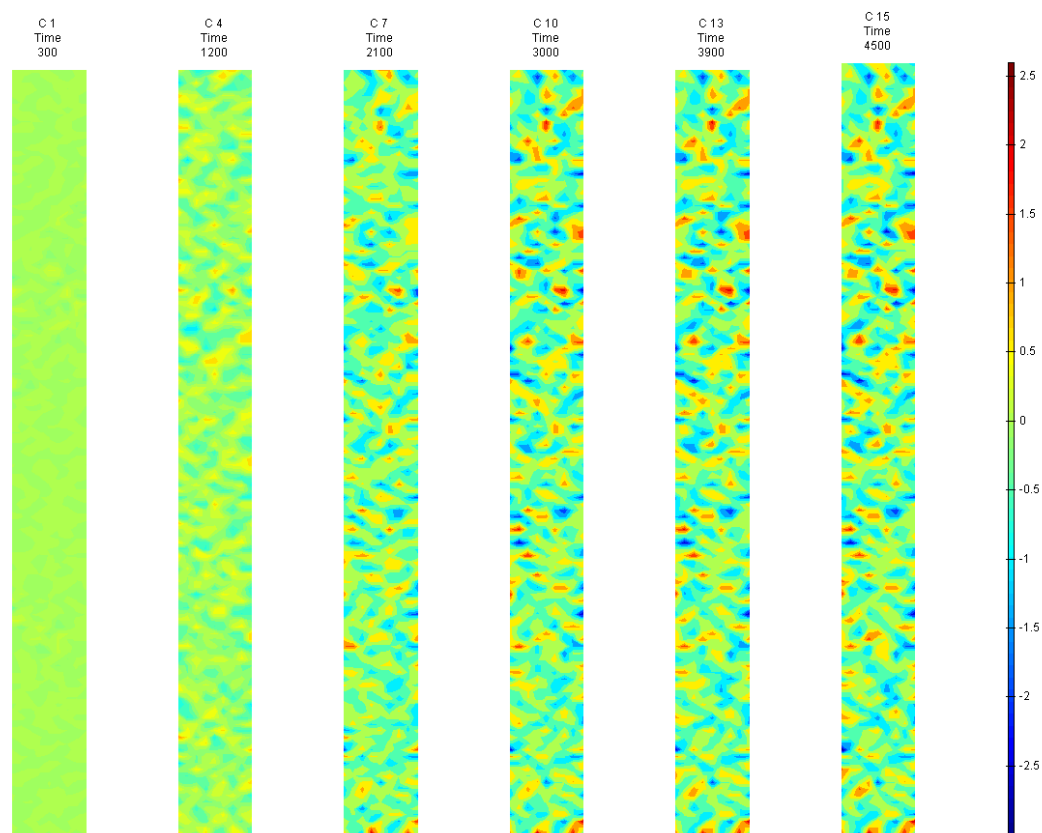
FIGURE 455: XY DIRECTION PIV SEQUENTIAL TRUE SHEAR STRAIN OVER TIME
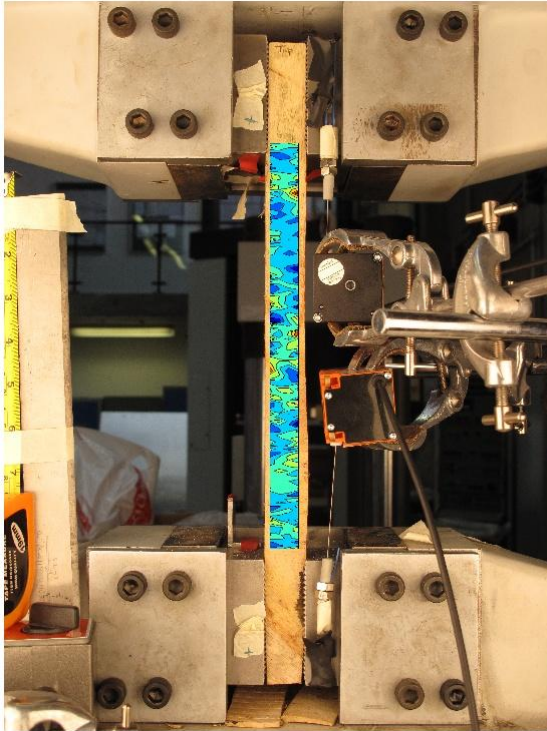
FIGURE 456: X DIRECTION PIV FIRST–LAST DITCH ENGINEERING STRAIN OVER IMAGE

FIGURE 457: Y DIRECTION PIV FIRST–LAST DITCH ENGINEERING STRAIN OVER IMAGE
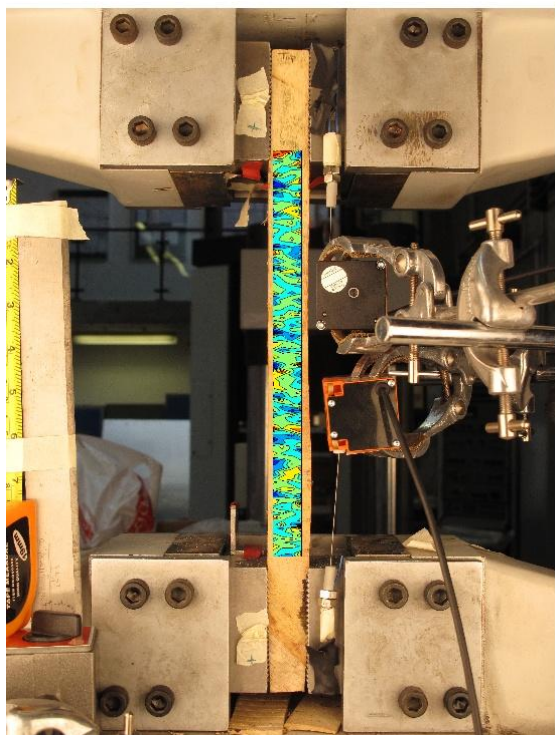
FIGURE 458: XY DIRECTION PIV FIRST–LAST DITCH ENGINEERING SHEAR STRAIN OVER
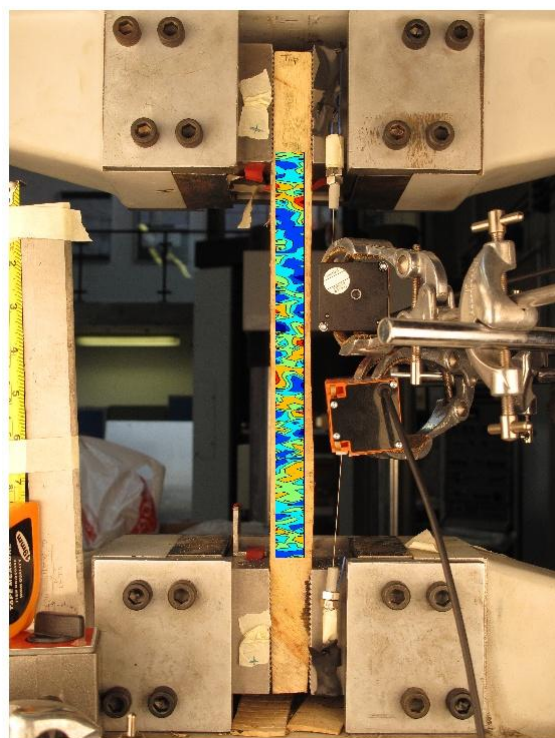
IMAGE

FIGURE 459: X DIRECTION PIV FIRST–LAST DITCH TRUE STRAIN OVER IMAGE

FIGURE 460: Y DIRECTION PIV FIRST–LAST DITCH TRUE STRAIN OVER IMAGE

FIGURE 461: XY DIRECTION PIV FIRST–LAST DITCH TRUE SHEAR STRAIN OVER IMAGE

Appendix 6

FIGURE 462: XY DIRECTION PIV FIRST–SEQUENTIAL ENGINEERING SHEAR STRAIN OVER

IMAGE

FIGURE 463: XY DIRECTION PIV FIRST–SEQUENTIAL ENGINEERING SHEAR STRAIN OVER TIME
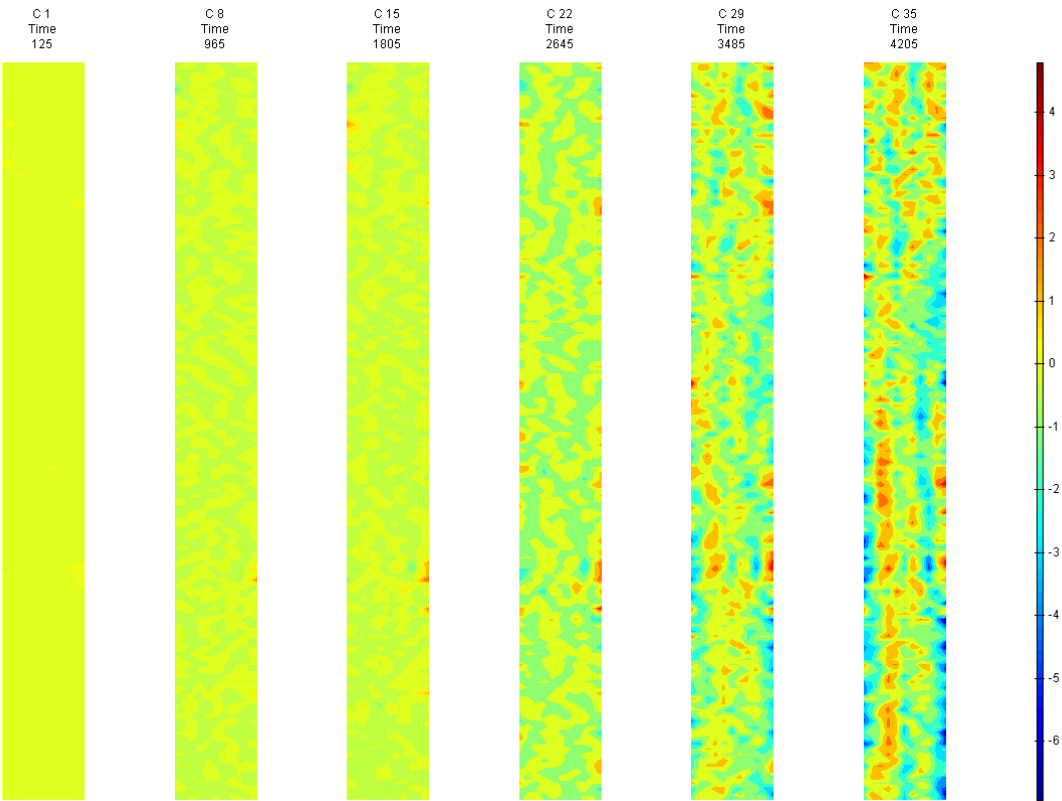
S1 Side View

FIGURE 464: X DIRECTION PIV SEQUENTIAL ENGINEERING STRAIN OVER TIME
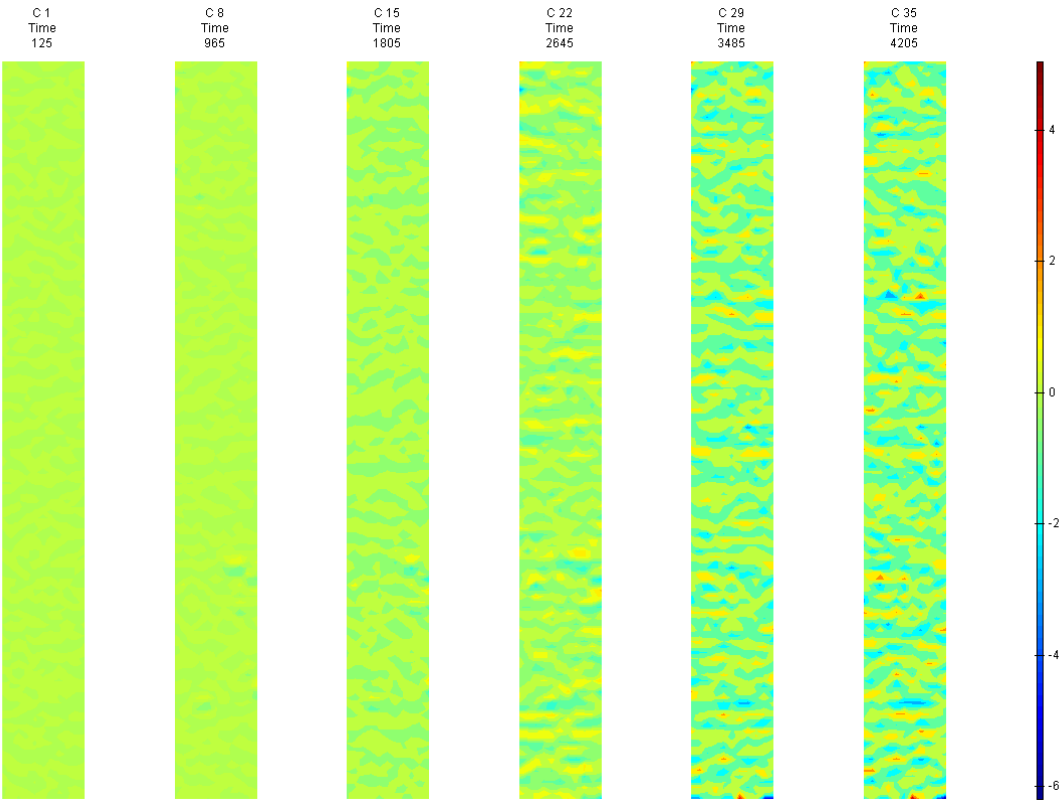

FIGURE 465: Y DIRECTION PIV SEQUENTIAL ENGINEERING STRAIN OVER TIME
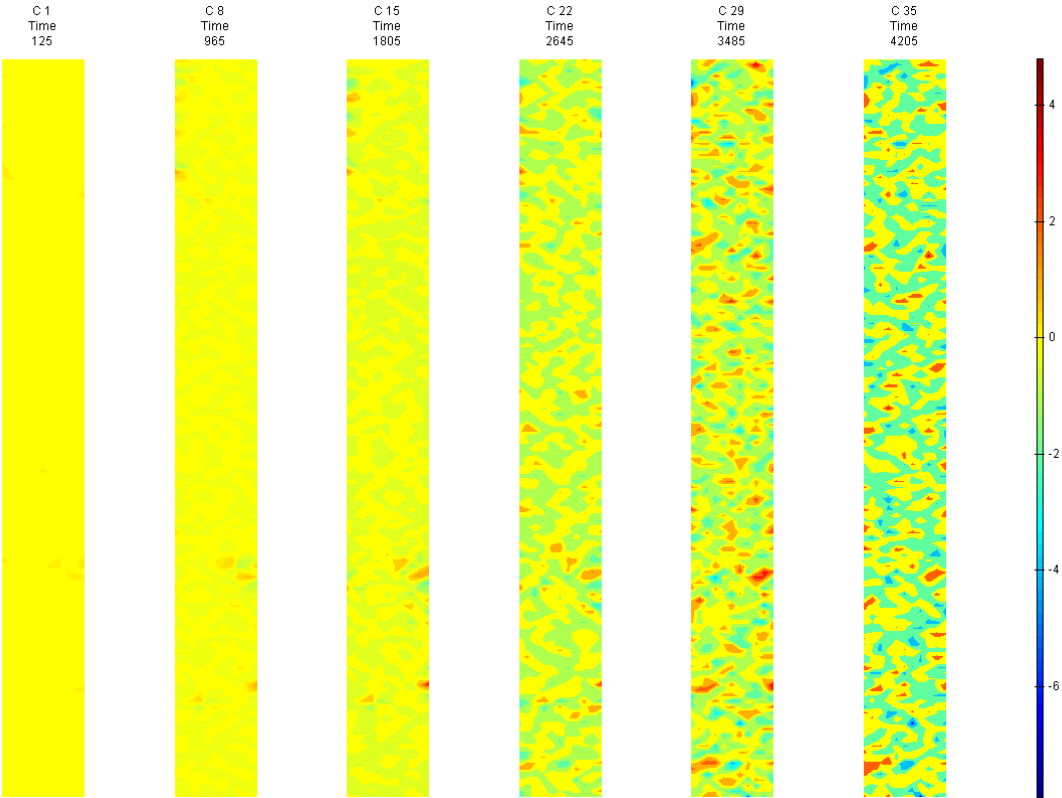
Appendix 6

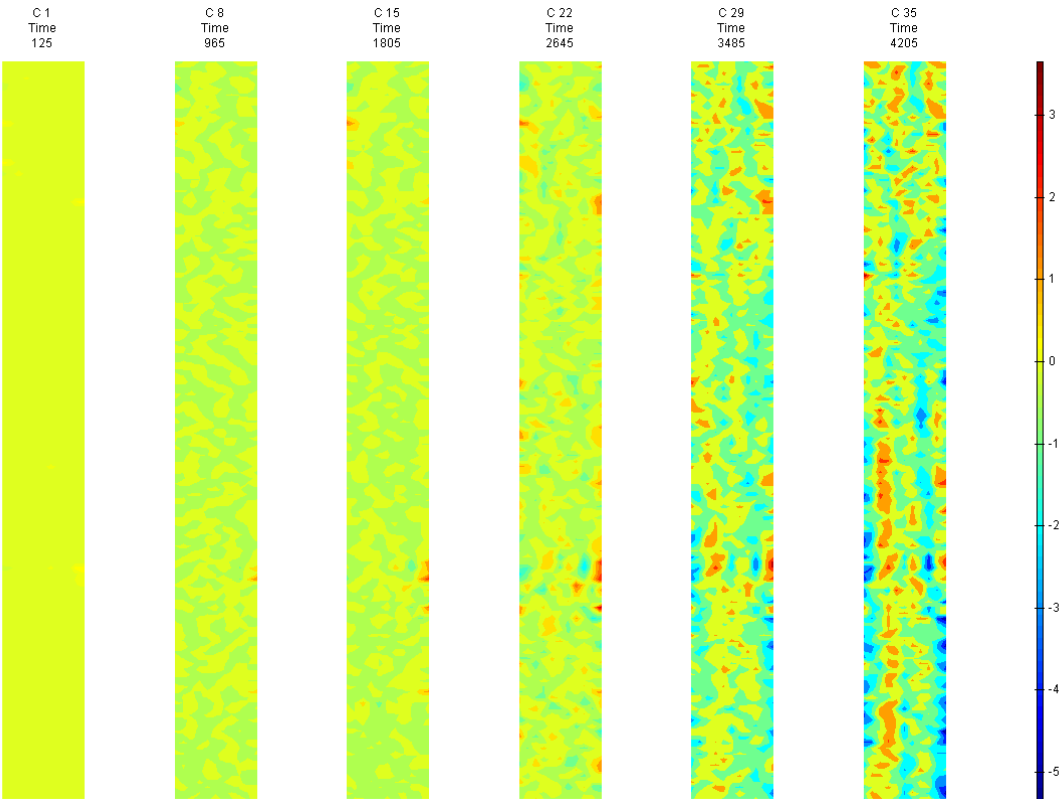FIGURE 466: XY DIRECTION PIV SEQUENTIAL ENGINEERING SHEAR STRAIN OVER TIME

FIGURE 467: X DIRECTION PIV SEQUENTIAL TRUE STRAIN OVER TIME

FIGURE 468: Y DIRECTION PIV SEQUENTIAL TRUE STRAIN OVER TIME

FIGURE 469: XY DIRECTION PIV SEQUENTIAL TRUE SHEAR STRAIN OVER TIME

FIGURE 470: X DIRECTION PIV FIRST–LAST DITCH ENGINEERING STRAIN OVER IMAGE

FIGURE 471: Y DIRECTION PIV FIRST–LAST DITCH ENGINEERING STRAIN OVER IMAGE

FIGURE 472: XY DIRECTION PIV FIRST–LAST DITCH ENGINEERING SHEAR STRAIN OVER

IMAGE

FIGURE 473: X DIRECTION PIV FIRST–LAST DITCH TRUE STRAIN OVER IMAGE

Appendix 6
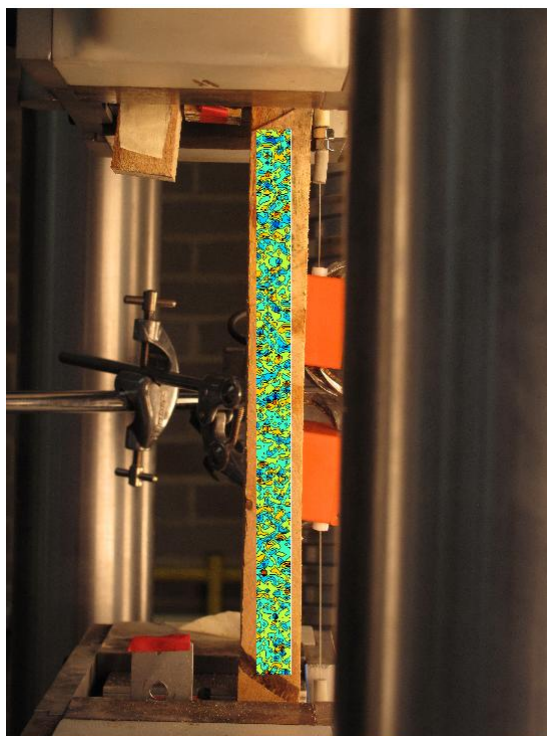
FIGURE 474: Y DIRECTION PIV FIRST-LAST DITCH TRUE STRAIN OVER IMAGE
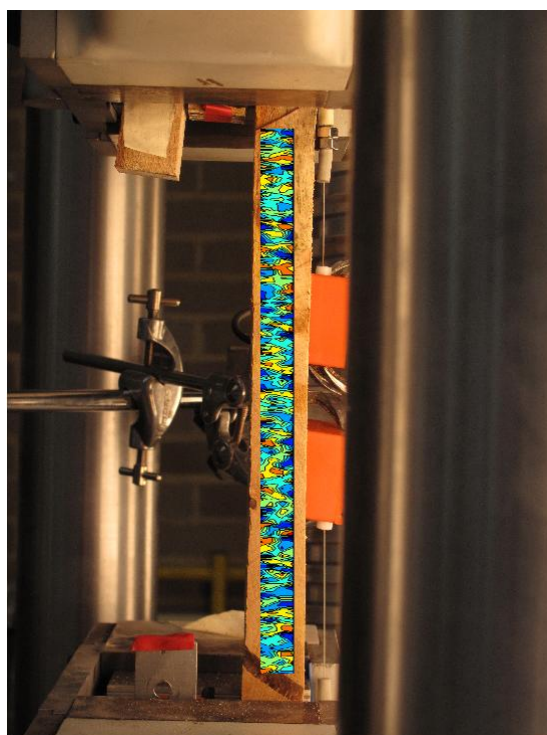
FIGURE 475: XY DIRECTION PIV FIRST-LAST DITCH TRUE SHEAR STRAIN OVER IMAGE
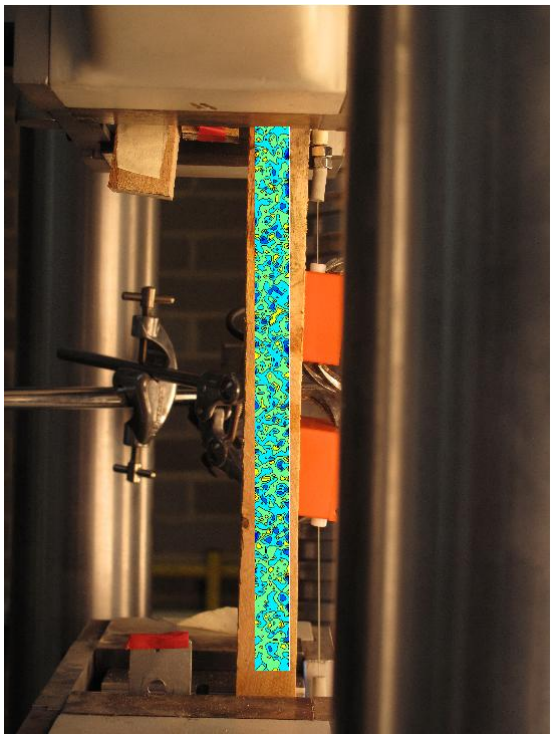
FIGURE 476: XY DIRECTION PIV FIRST–SEQUENTIAL ENGINEERING SHEAR STRAIN OVER

IMAGE
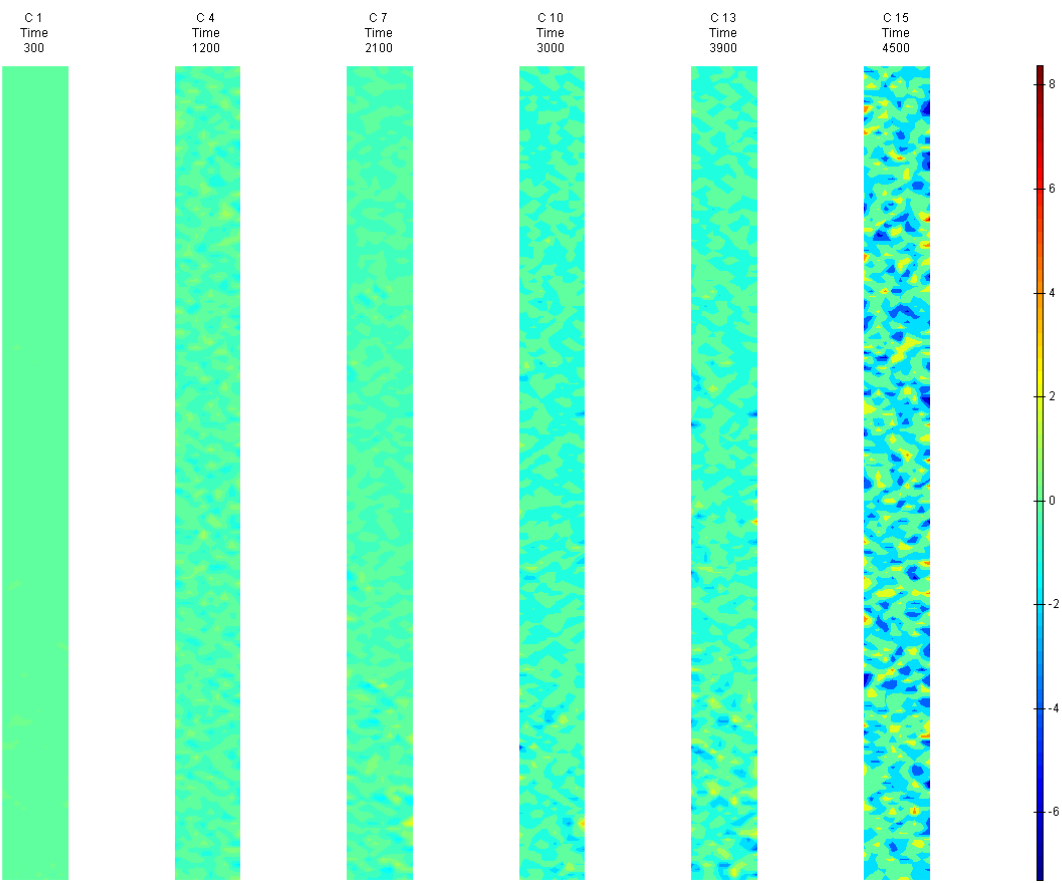

FIGURE 477: XY DIRECTION PIV FIRST–SEQUENTIAL ENGINEERING SHEAR STRAIN OVER TIME

S2

FIGURE 478: S2 TENSILE STRESS VS. MACHINE MEASURED/PIV STRAINS
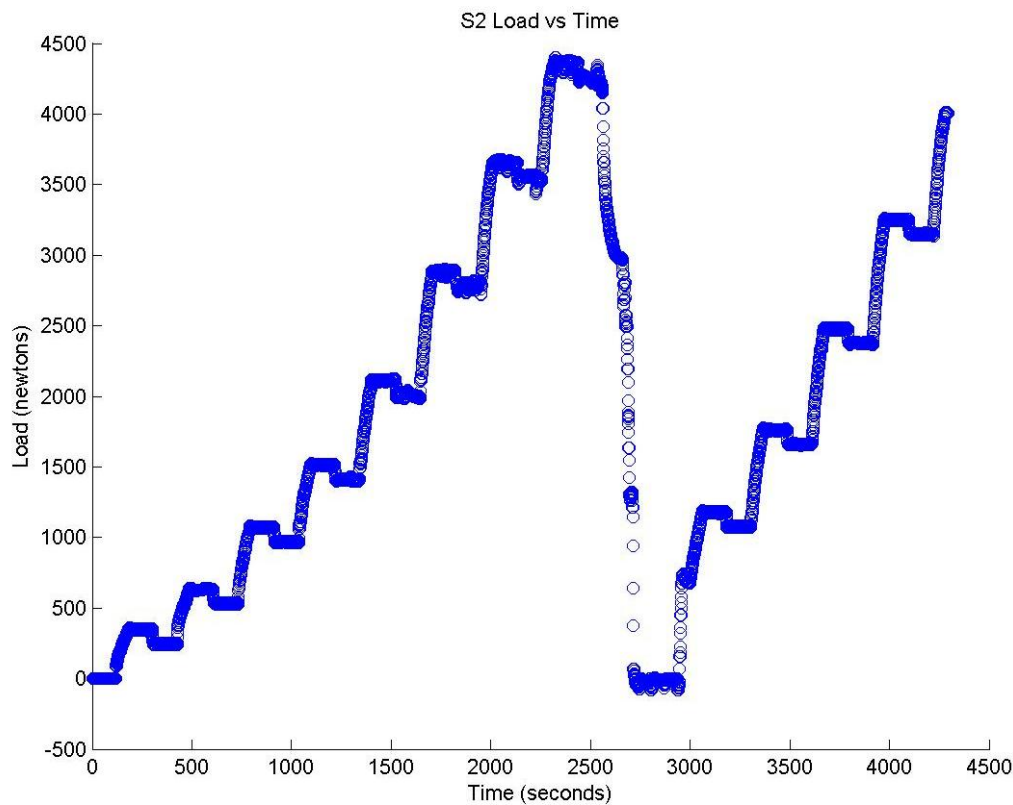
FIGURE 479: S2 TENSILE LOAD VS. TIME
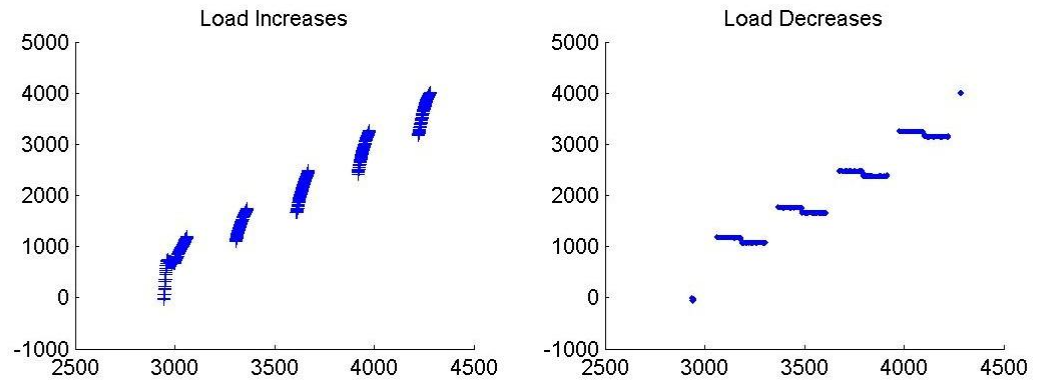
FIGURE 480: S2 CREEP LOADING: INCREMENTS AND RELAXATION
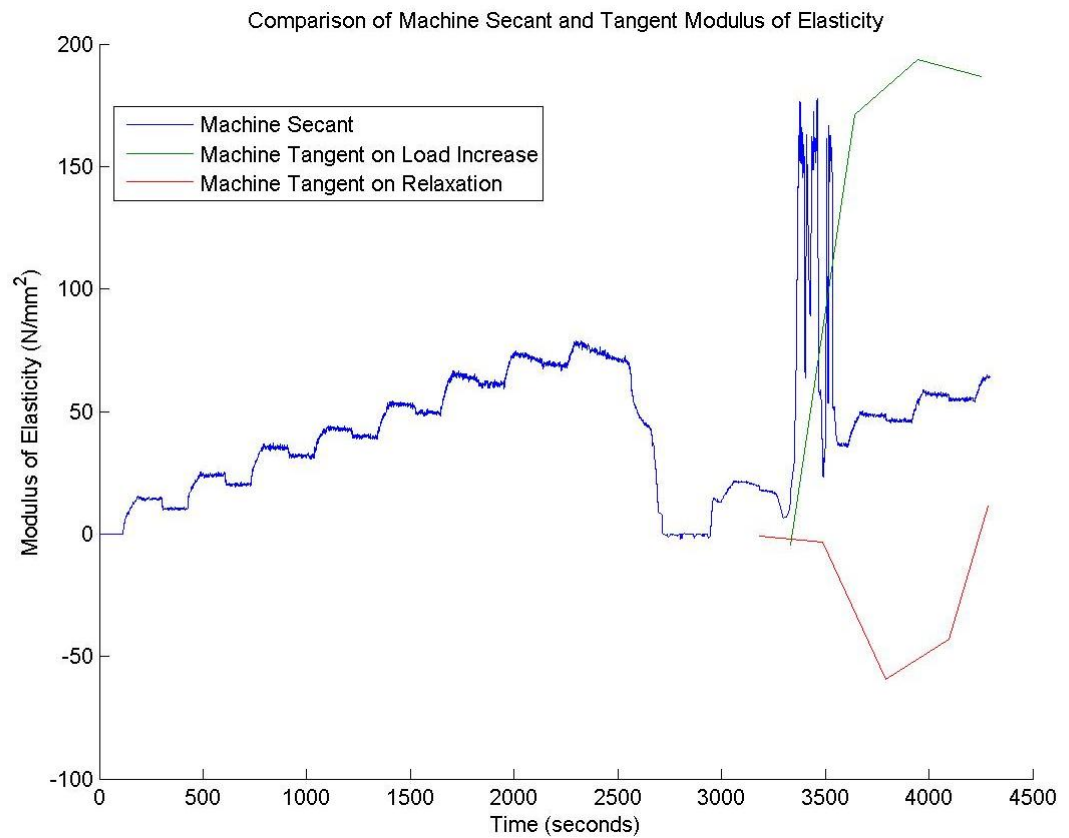
FIGURE 481: S2 MACHINE MEASURED SECANT AND TANGENT MODULUS VS. TIME

Appendix 6
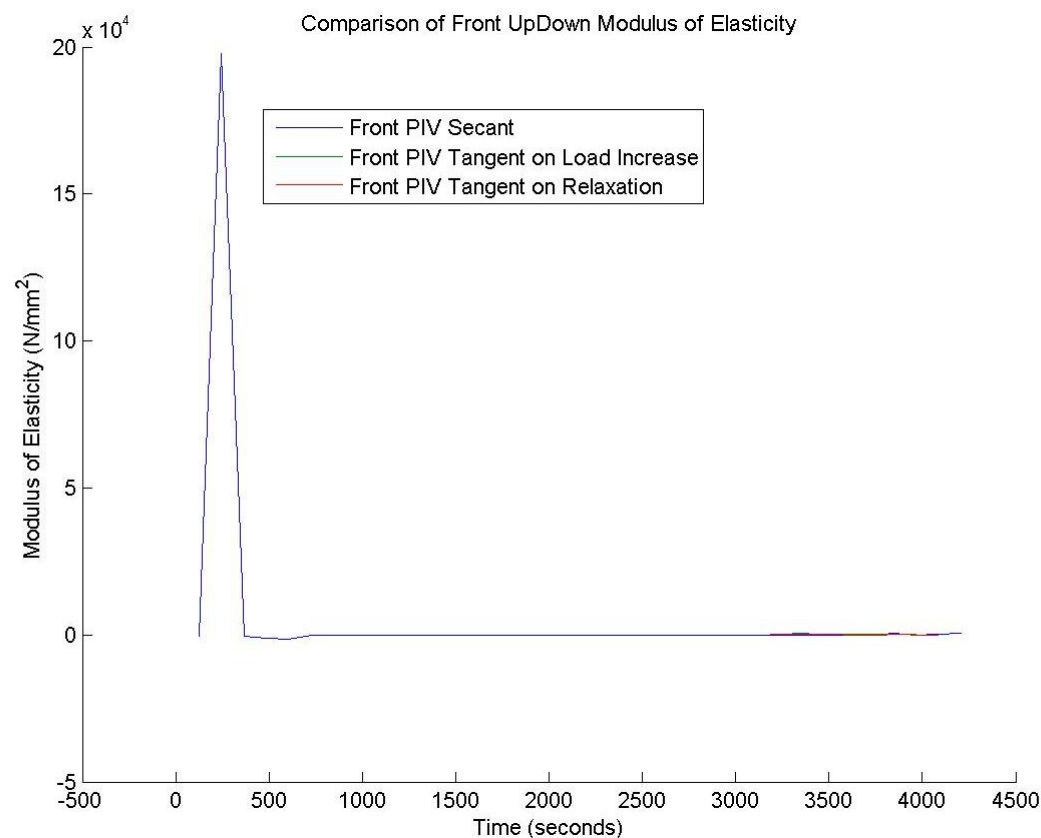
FIGURE 482: S2 FRONT VIEW PIV SECANT AND TANGENT MODULUS VS. TIME
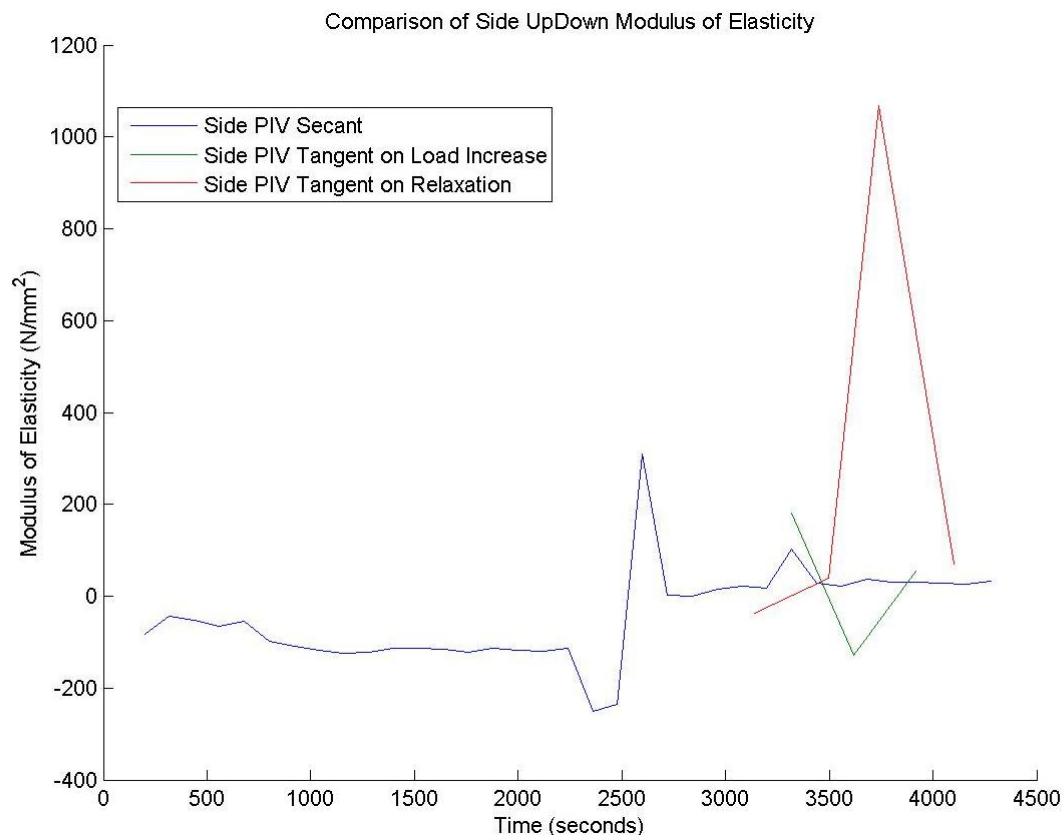
FIGURE 483: S2 SIDE VIEW PIV SECANT AND TANGENT MODULUS VS. TIME

392
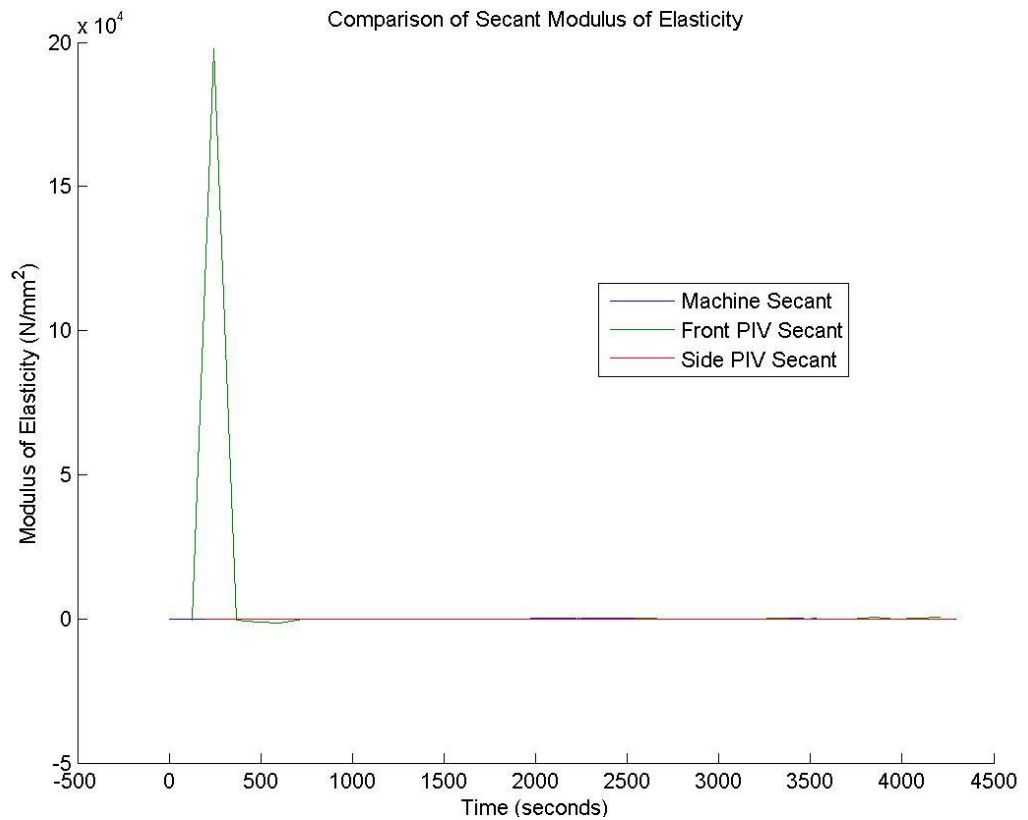
FIGURE 484: S2 COMPARISON OF MACHINE MEASURED AND PIV SECANT MODULUS VS. TIME
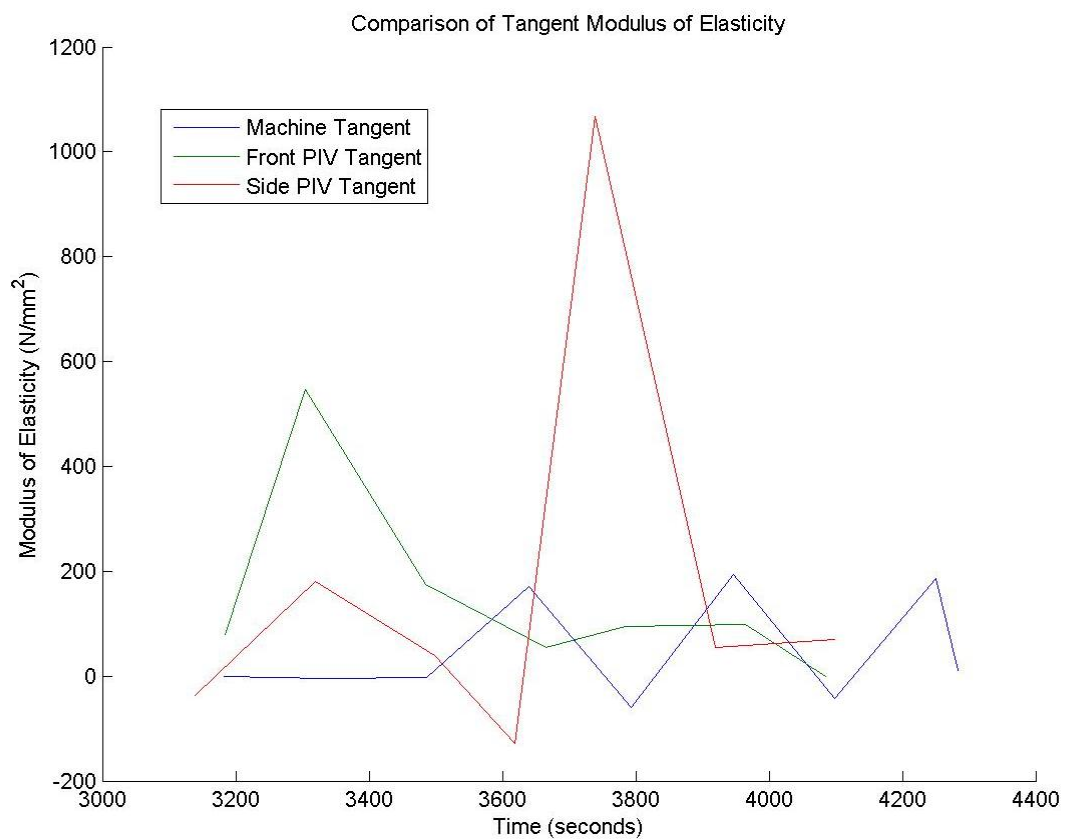
FIGURE 485: S2 COMPARISON OF MACHINE MEASURED AND PIV TANGENT MODULUS VS.

TIME

S2 Sample

FIGURE 486: SAMPLE GRAIN ORIENTATIONS OF THE FRONT (LEFT 4 IMAGES) AND SIDE (RIGHT 4 IMAGES) VIEW BEFORE (FIRST 2 OF 4 IMAGES) AND AFTER (LAST 2 OF 4 IMAGES) BREAKAGE

S2 Front View

FIGURE 487: X DIRECTION PIV SEQUENTIAL ENGINEERING STRAIN OVER TIME

FIGURE 488: Y DIRECTION PIV SEQUENTIAL ENGINEERING STRAIN OVER TIME

Appendix 6

FIGURE 489: XY DIRECTION PIV SEQUENTIAL ENGINEERING SHEAR STRAIN OVER TIME

FIGURE 490: X DIRECTION PIV SEQUENTIAL TRUE STRAIN OVER TIME
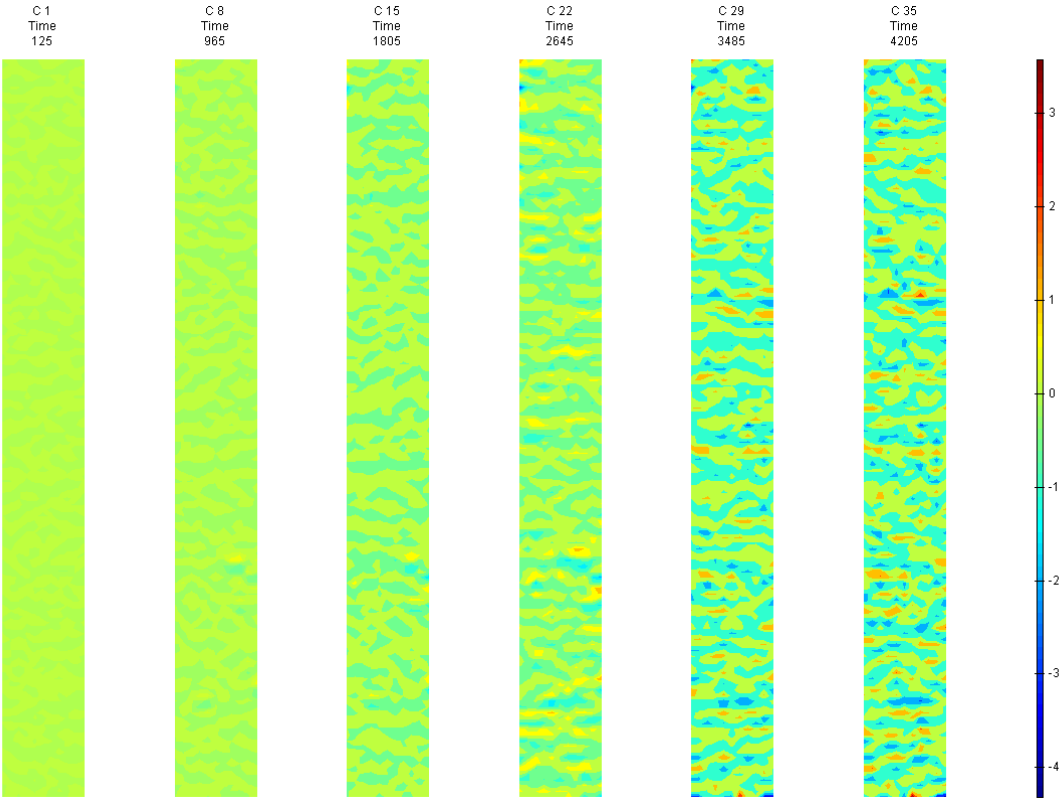
FIGURE 491: Y DIRECTION PIV SEQUENTIAL TRUE STRAIN OVER TIME
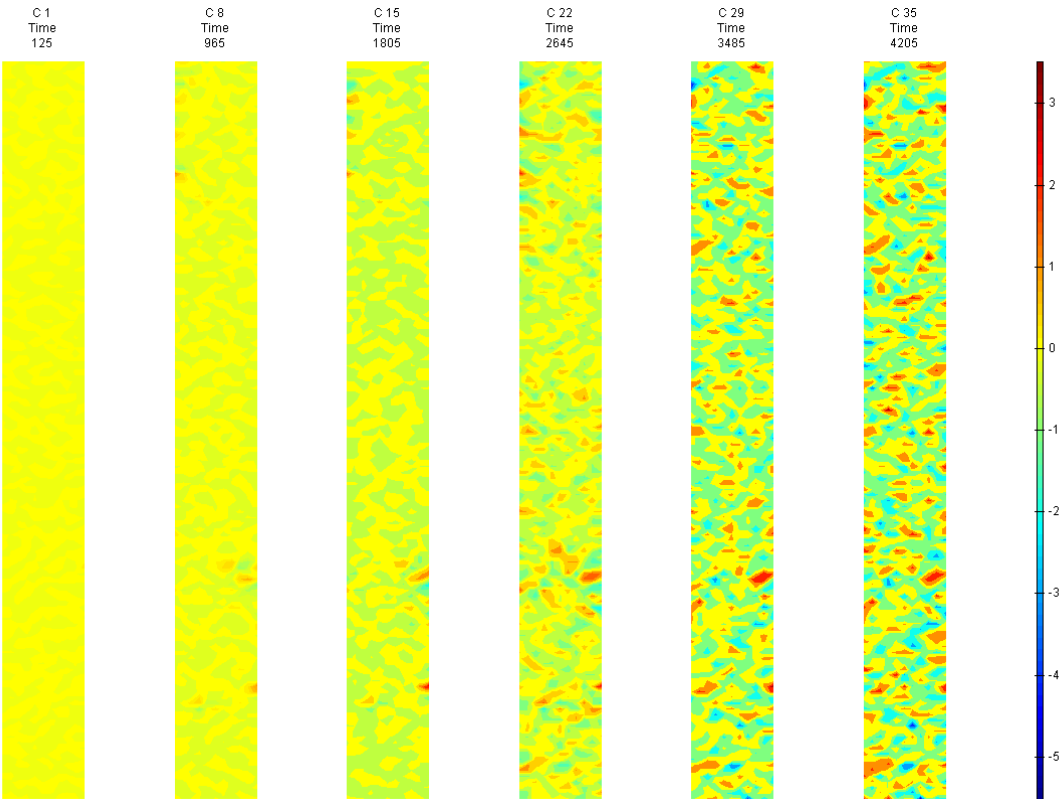
FIGURE 492: XY DIRECTION PIV SEQUENTIAL TRUE SHEAR STRAIN OVER TIME

Appendix 6
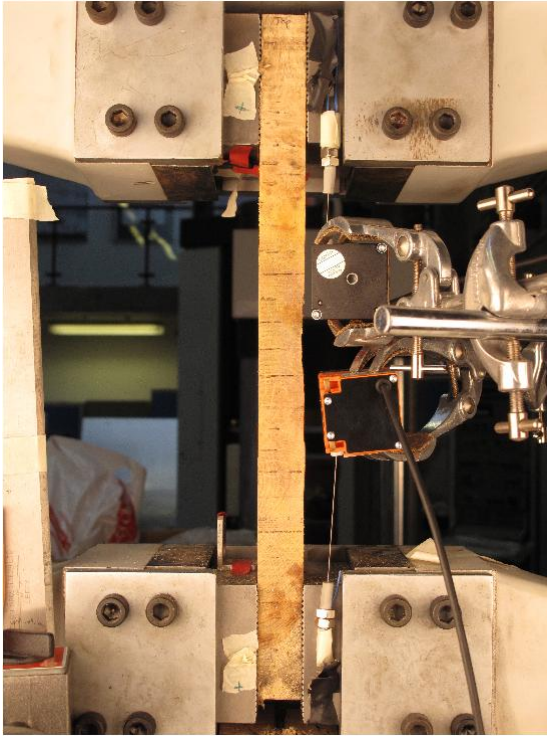
FIGURE 493: X DIRECTION PIV FIRST–LAST DITCH ENGINEERING STRAIN OVER IMAGE
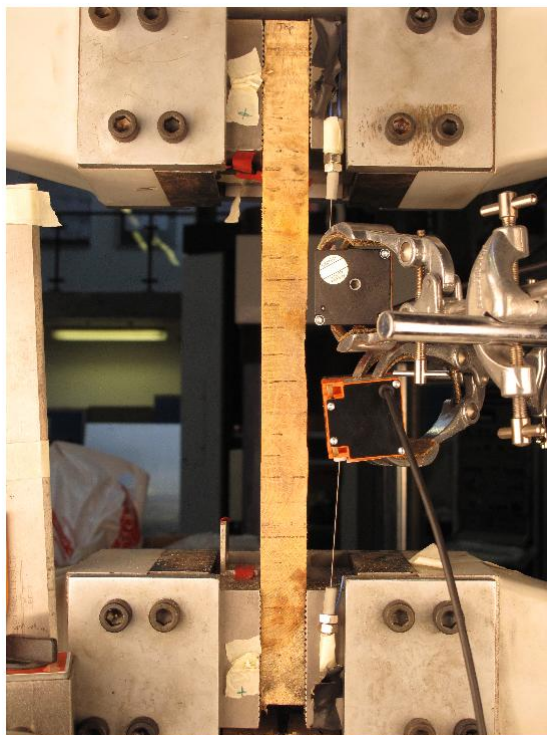
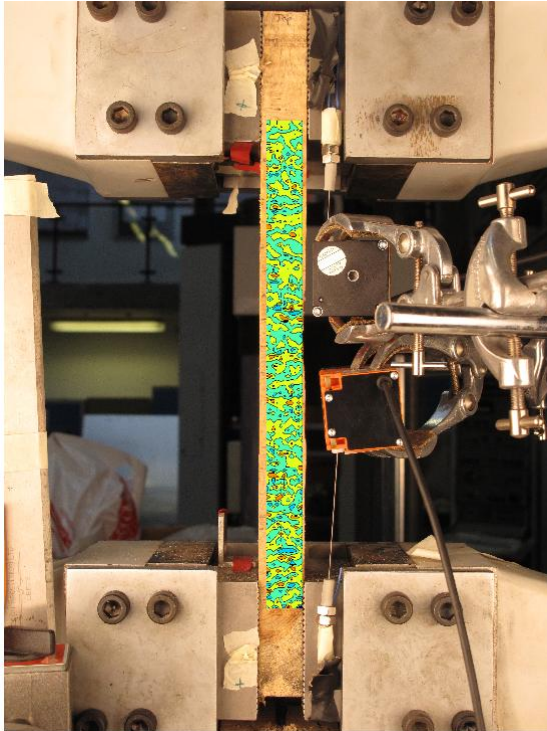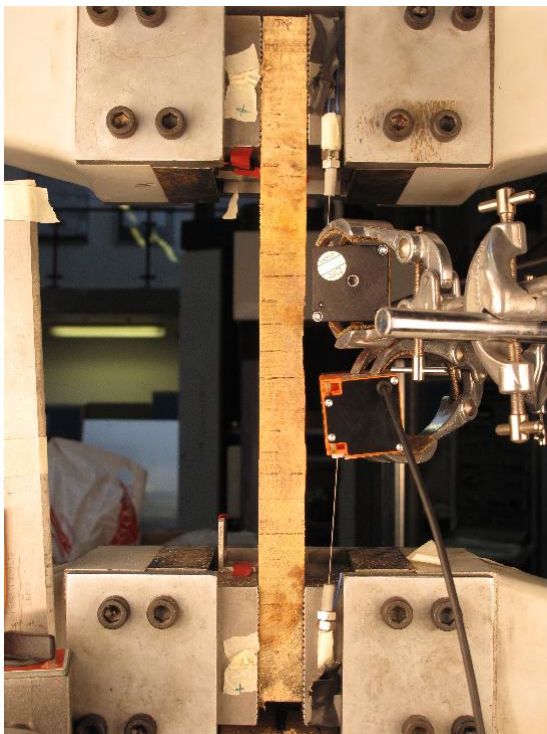FIGURE 494: Y DIRECTION PIV FIRST–LAST DITCH ENGINEERING STRAIN OVER IMAGE
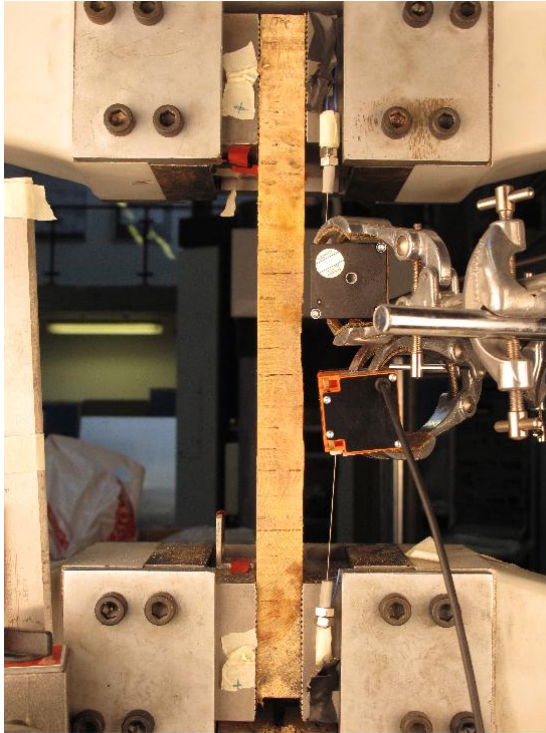
FIGURE 495: XY DIRECTION PIV FIRST–LAST DITCH ENGINEERING SHEAR STRAIN OVER
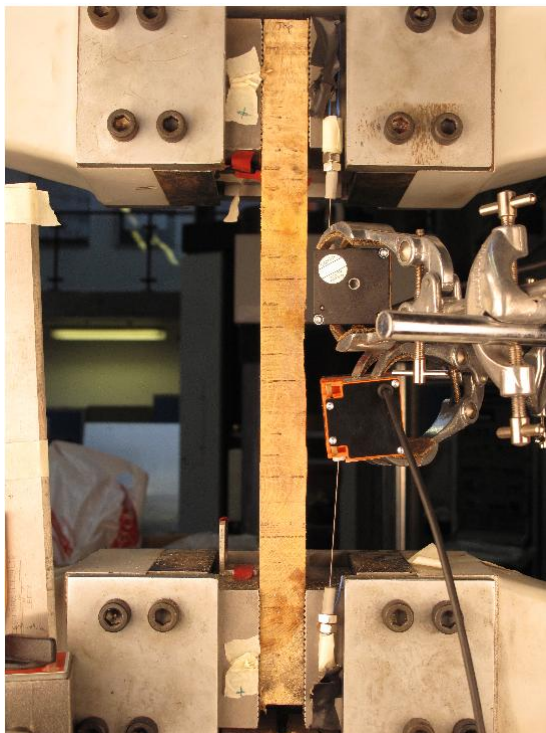
IMAGE

FIGURE 496: X DIRECTION PIV FIRST–LAST DITCH TRUE STRAIN OVER IMAGE

FIGURE 497: Y DIRECTION PIV FIRST–LAST DITCH TRUE STRAIN OVER IMAGE

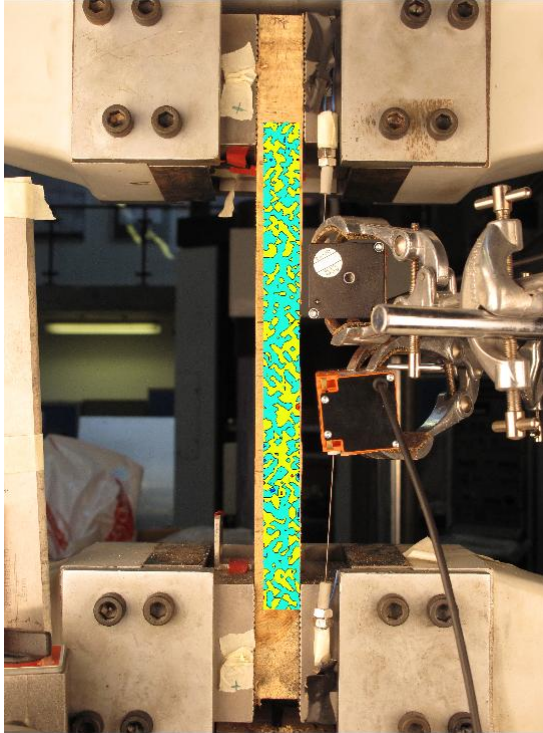FIGURE 498: XY DIRECTION PIV FIRST–LAST DITCH TRUE SHEAR STRAIN OVER IMAGE

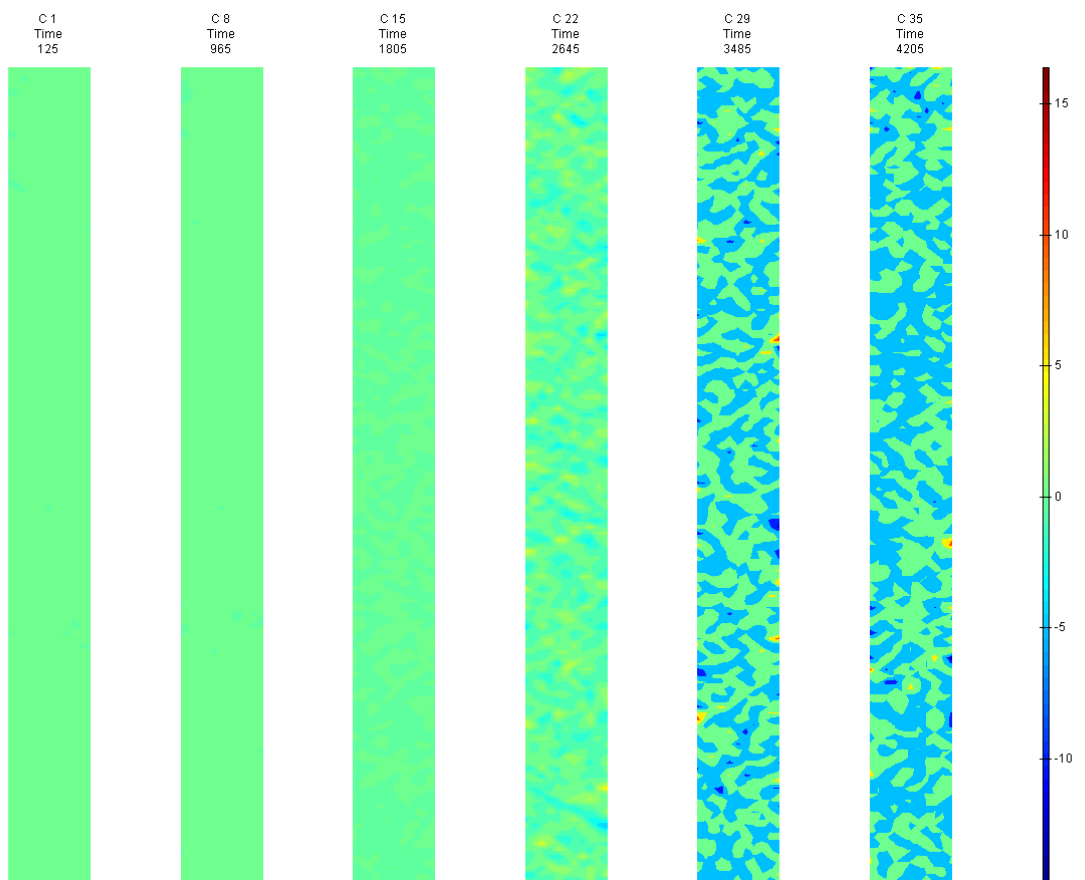FIGURE 499: XY DIRECTION PIV FIRST-SEQUENTIAL ENGINEERING SHEAR STRAIN OVER

IMAGE

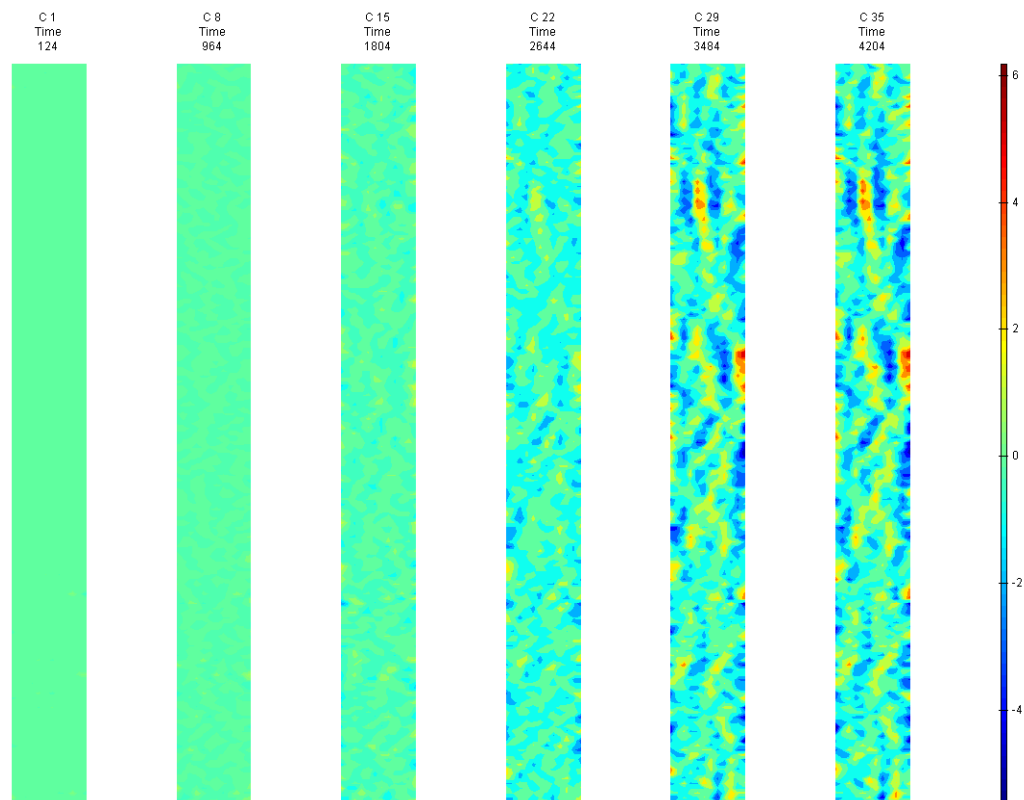FIGURE 500: XY DIRECTION PIV FIRST-SEQUENTIAL ENGINEERING SHEAR STRAIN OVER TIME

Appendix 6

S2 Side View

FIGURE 501: X DIRECTION PIV SEQUENTIAL ENGINEERING STRAIN OVER TIME
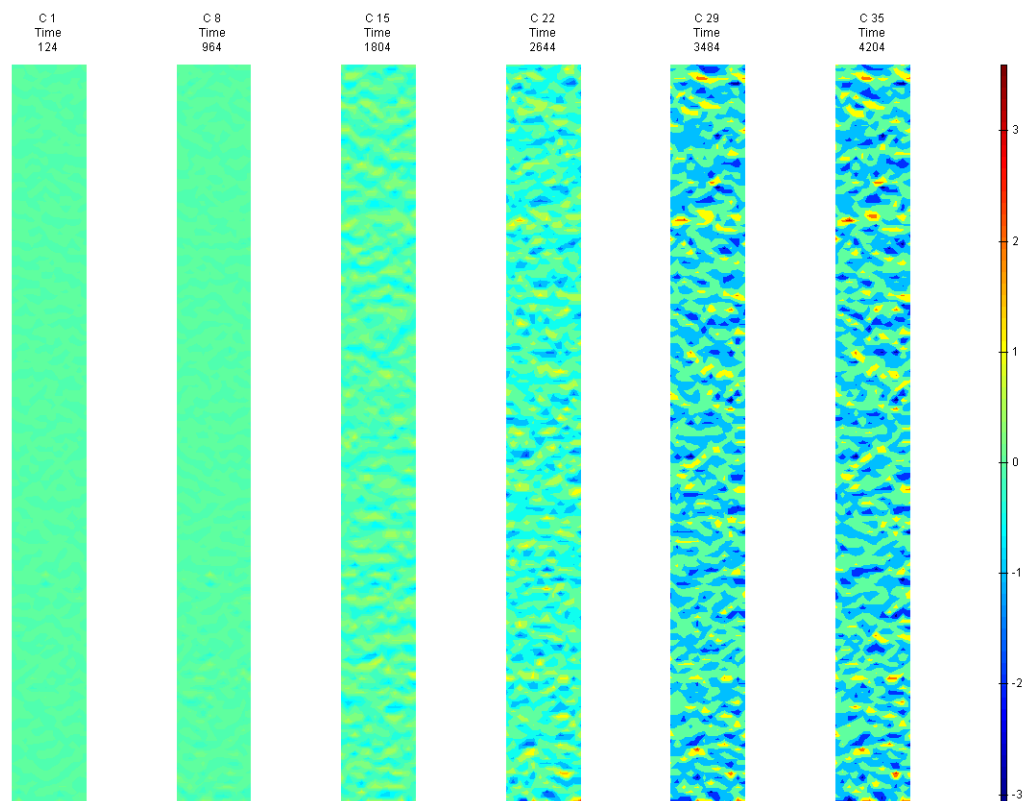

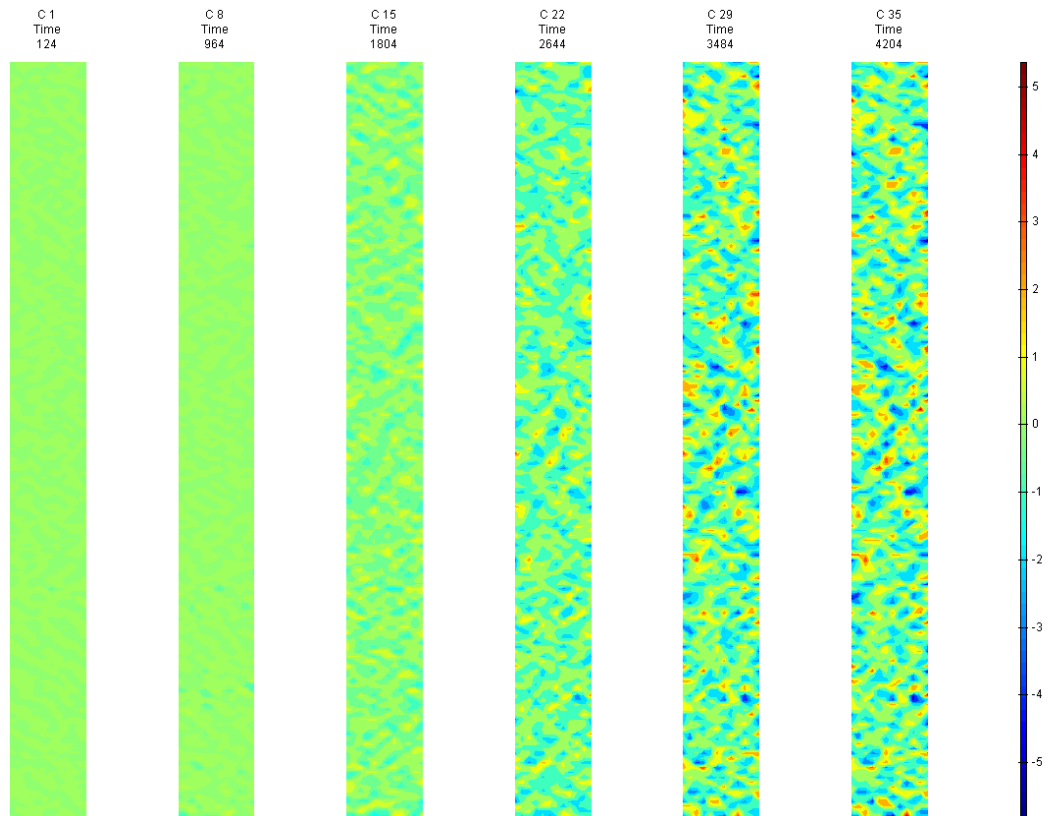FIGURE 502: Y DIRECTION PIV SEQUENTIAL ENGINEERING STRAIN OVER TIME

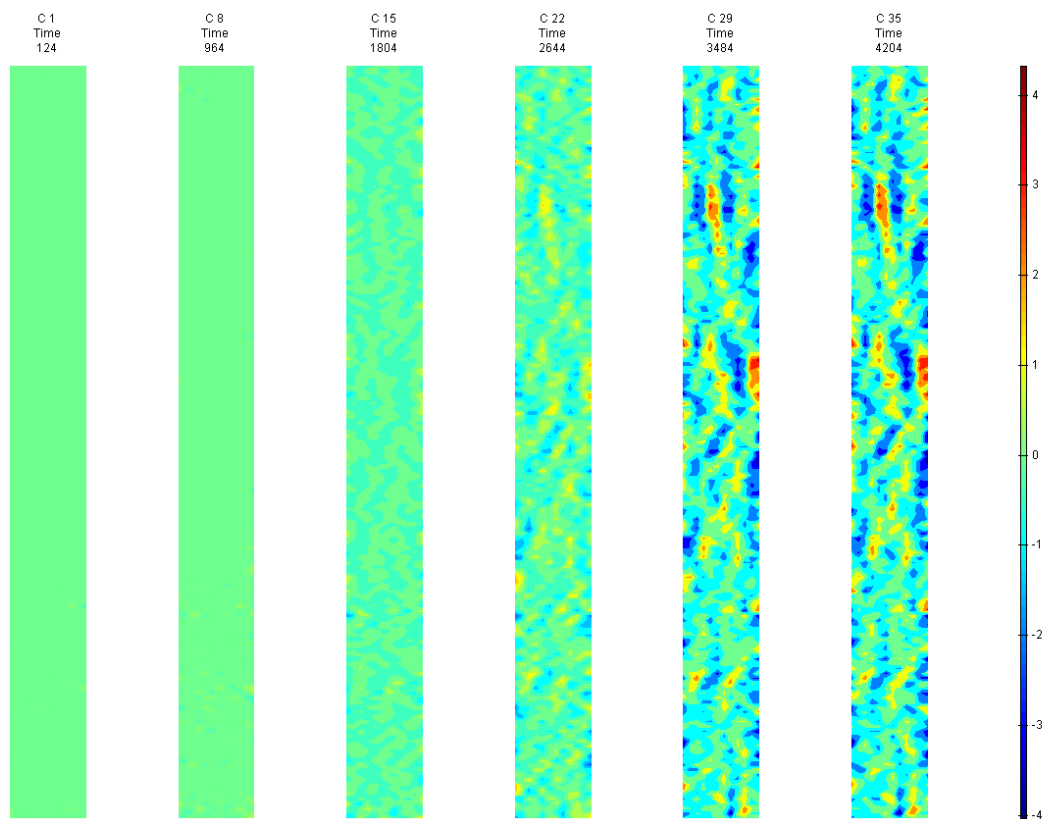FIGURE 503: XY DIRECTION PIV SEQUENTIAL ENGINEERING SHEAR STRAIN OVER TIME

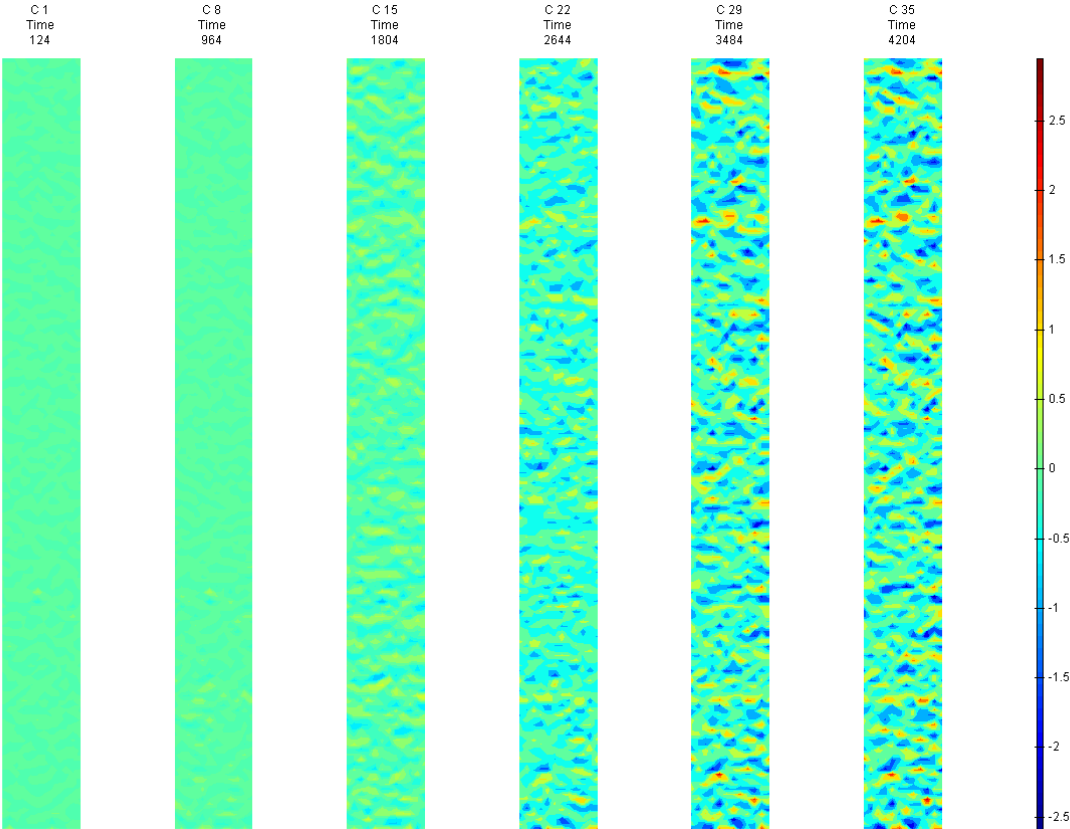FIGURE 504: X DIRECTION PIV SEQUENTIAL TRUE STRAIN OVER TIME

Appendix 6

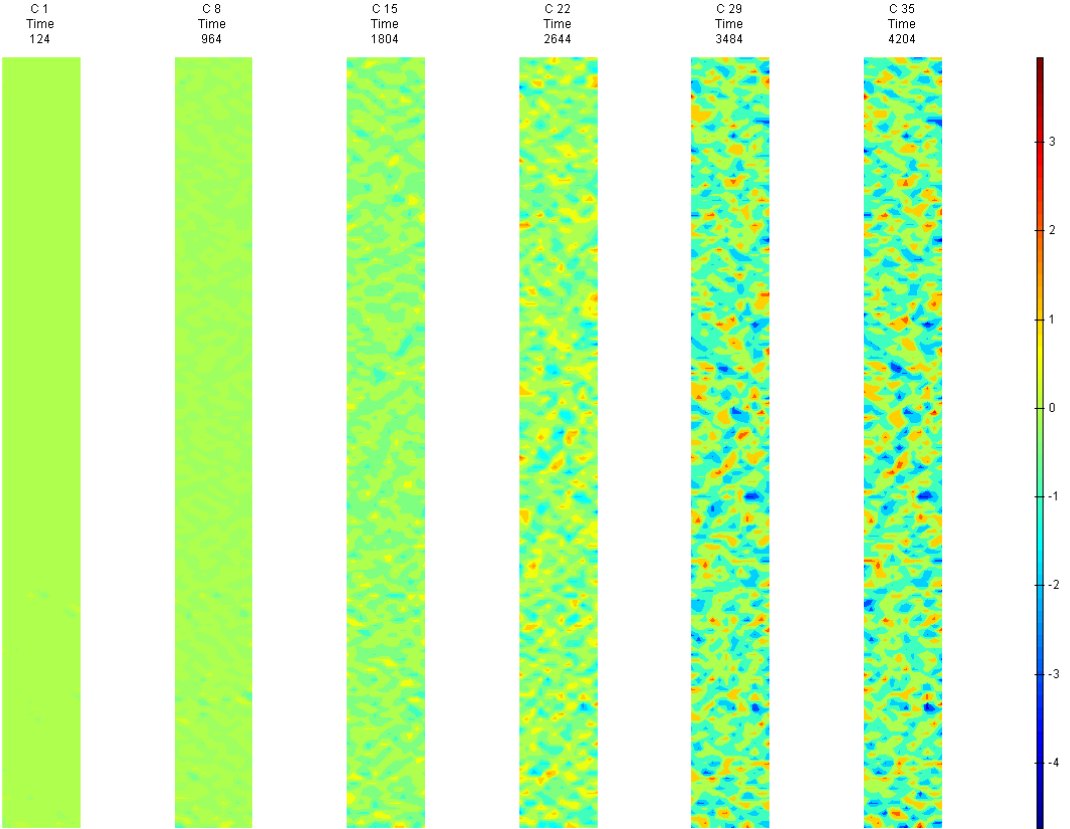FIGURE 505: Y DIRECTION PIV SEQUENTIAL TRUE STRAIN OVER TIME

FIGURE 506: XY DIRECTION PIV SEQUENTIAL TRUE SHEAR STRAIN OVER TIME
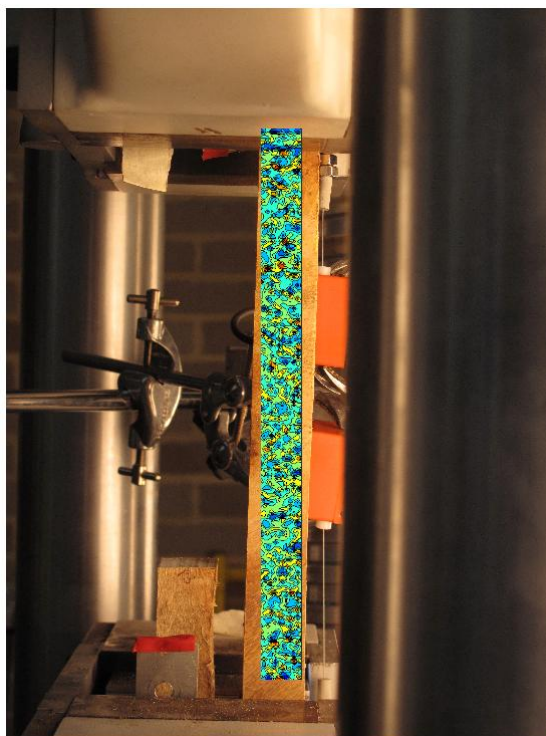
FIGURE 507: Y DIRECTION PIV FIRST–LAST DITCH TRUE STRAIN OVER IMAGE

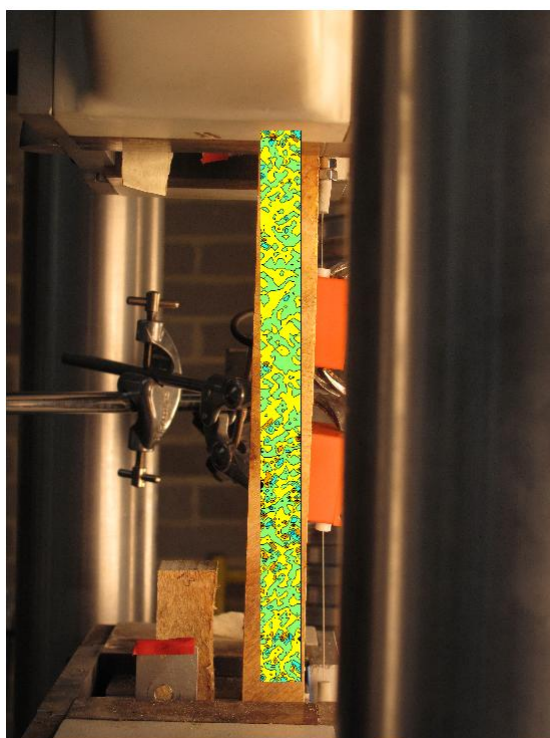
FIGURE 508: XY DIRECTION PIV FIRST–SEQUENTIAL ENGINEERING SHEAR STRAIN OVER
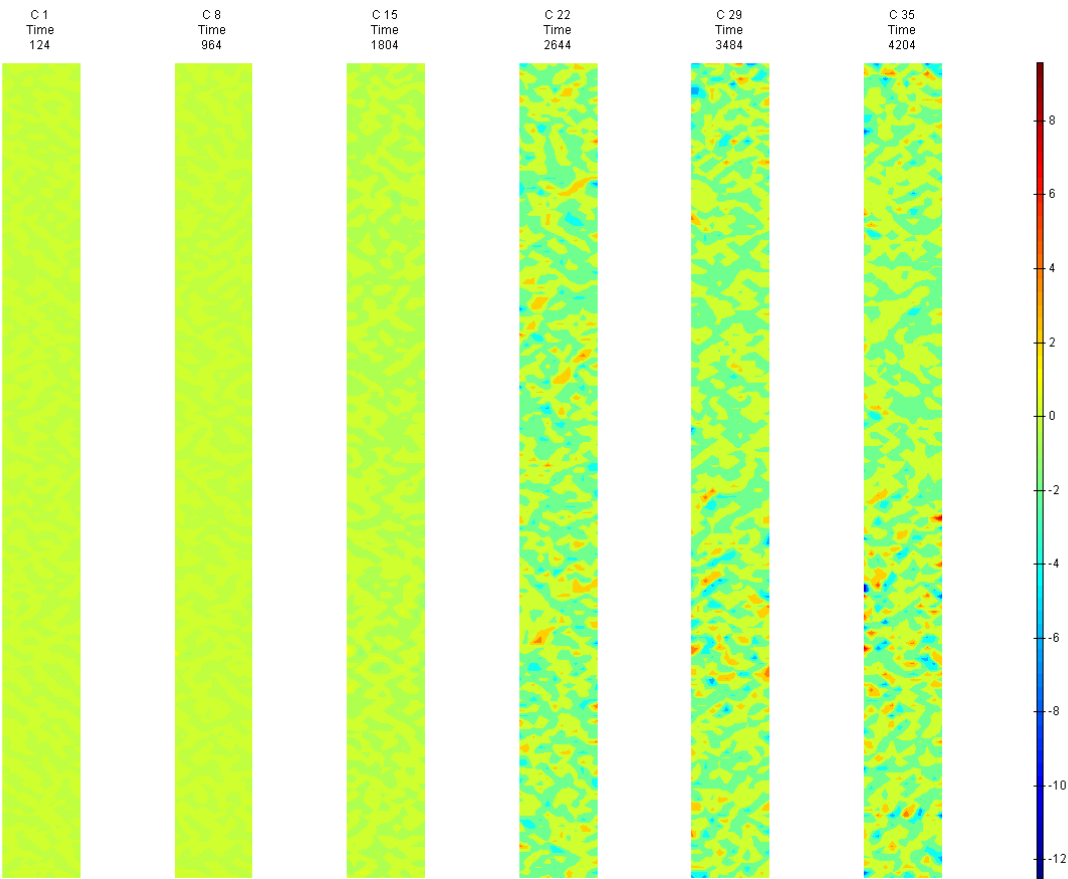
IMAGE

FIGURE 509: XY DIRECTION PIV FIRST–SEQUENTIAL ENGINEERING SHEAR STRAIN OVER TIME
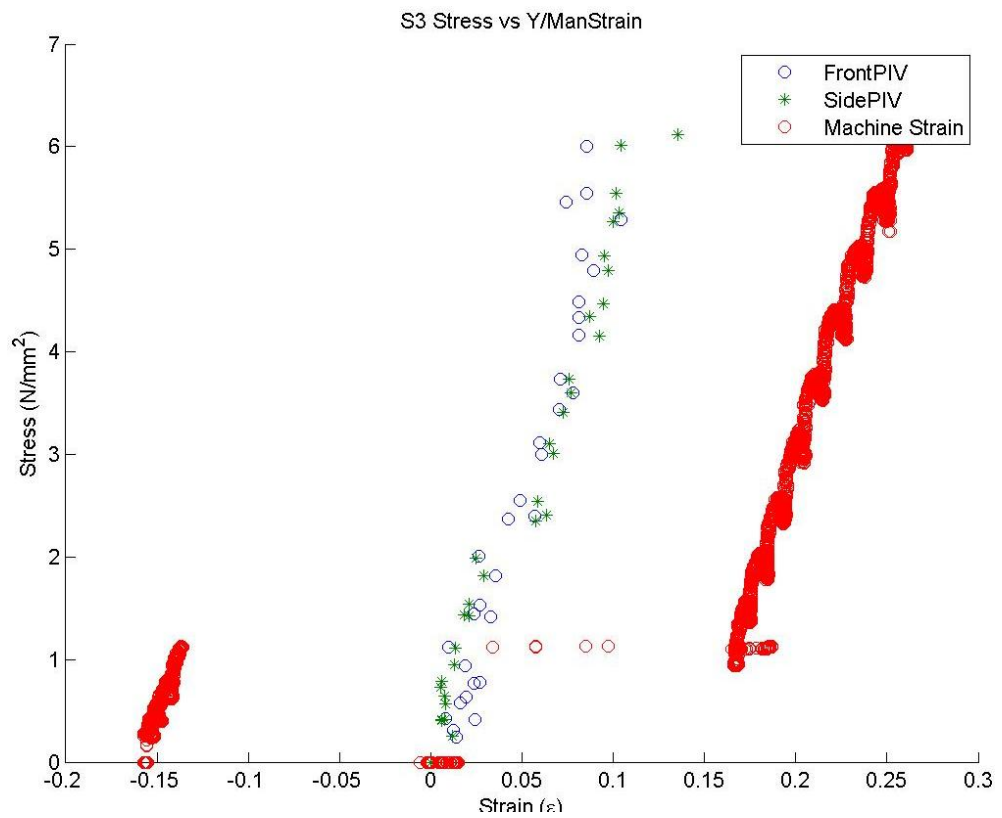
S3

FIGURE 510: S3 TENSILE STRESS VS. MACHINE MEASURED/PIV STRAINS
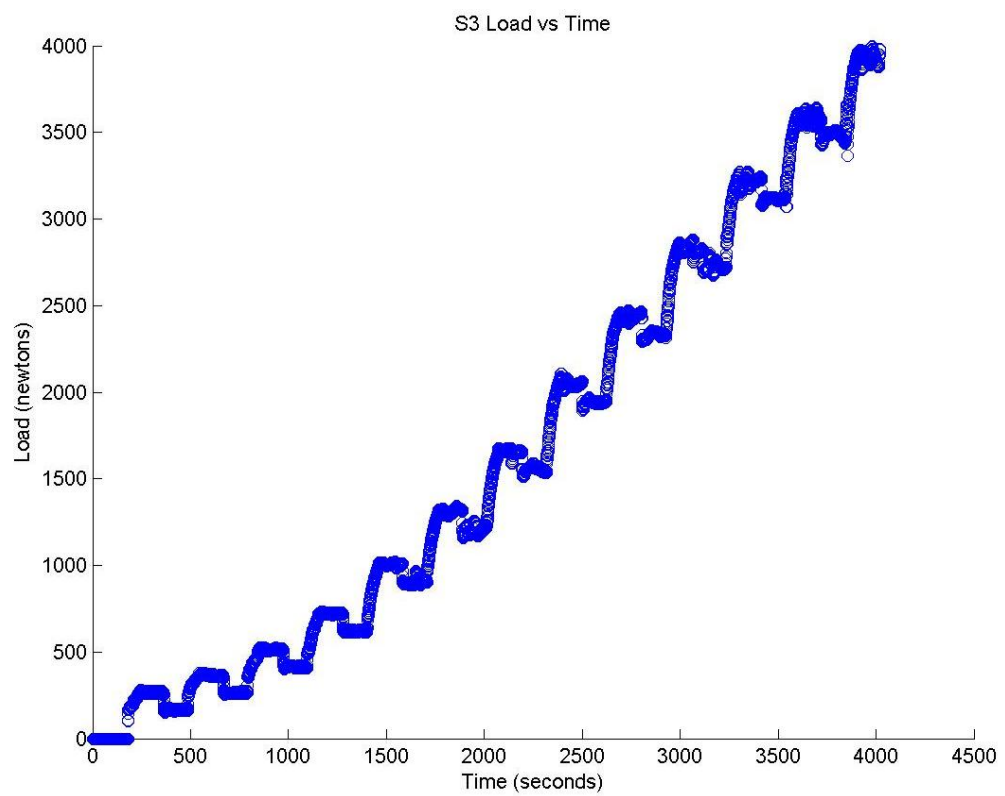
FIGURE 511: S3 TENSILE LOAD VS. TIME

Appendix 6
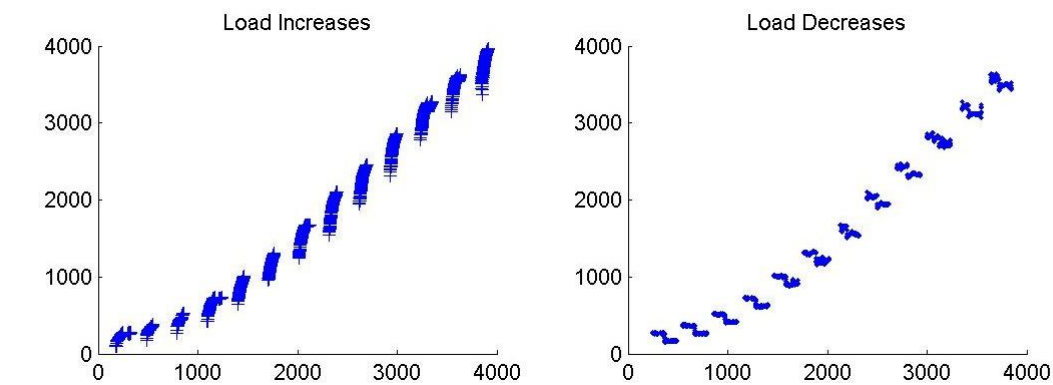
FIGURE 512: S3 CREEP LOADING: INCREMENTS AND RELAXATION
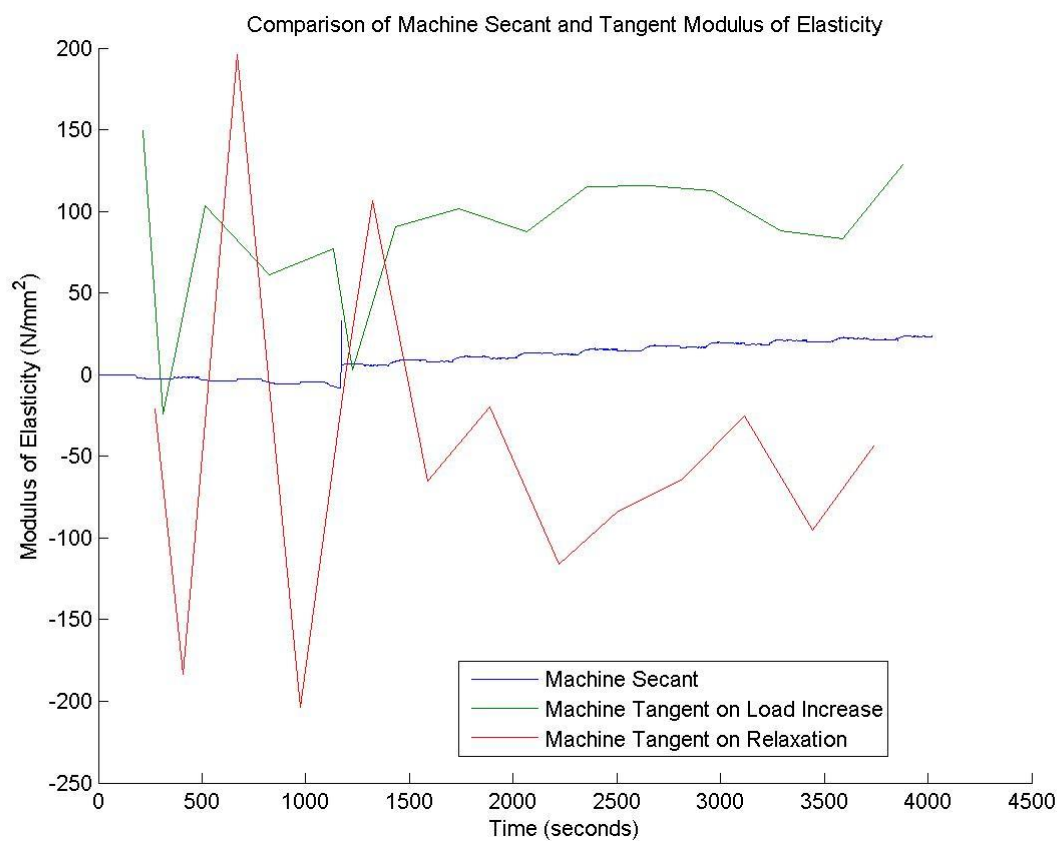
FIGURE 513: S3 MACHINE MEASURED SECANT AND TANGENT MODULUS VS. TIME
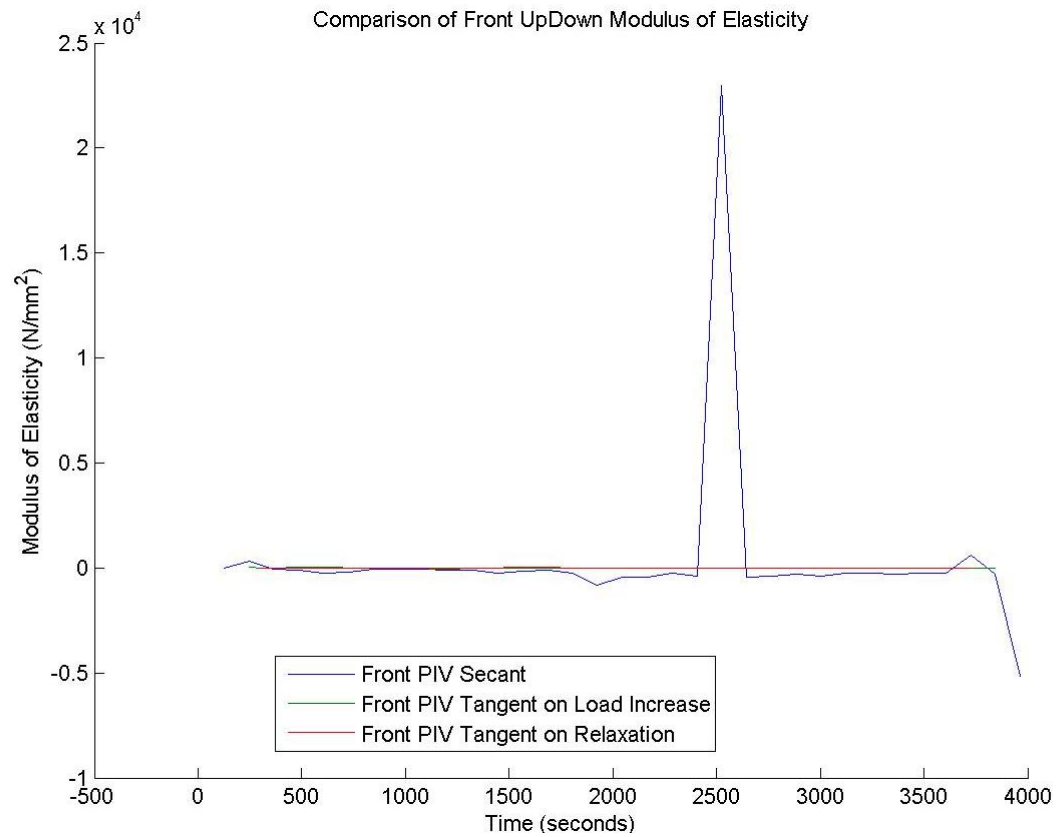
FIGURE 514: S3 FRONT VIEW PIV SECANT AND TANGENT MODULUS VS. TIME
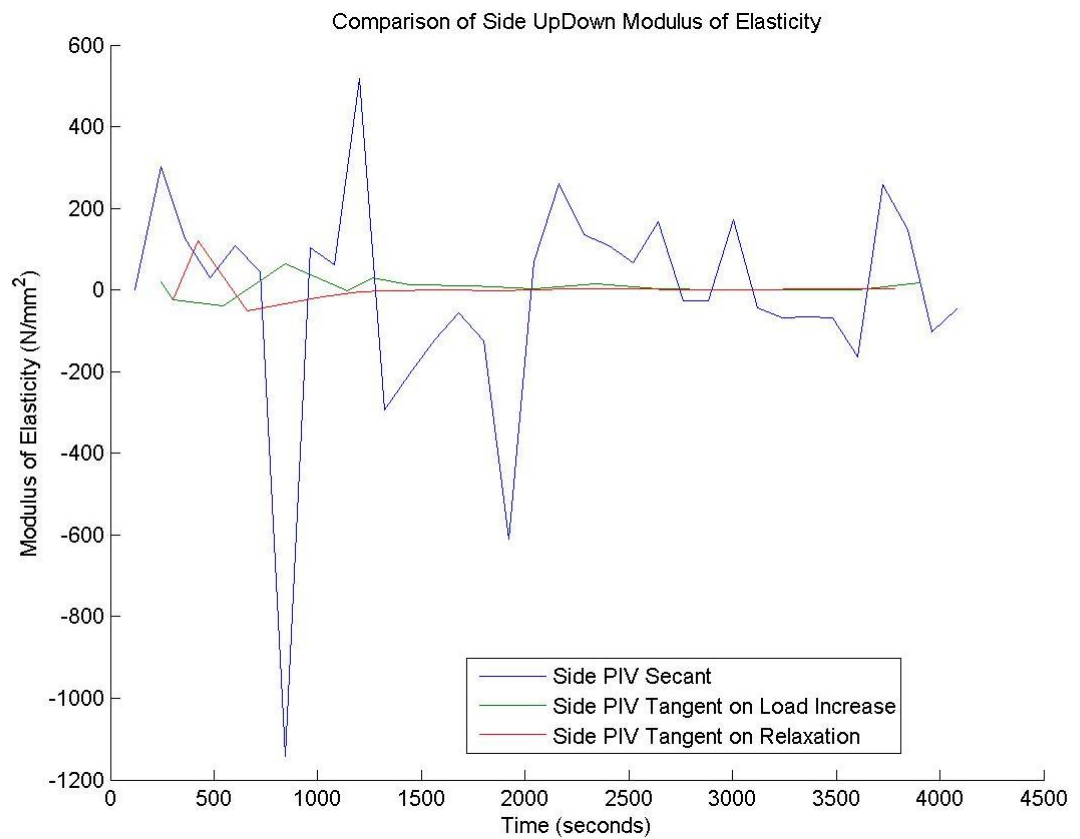
FIGURE 515: S3 SIDE VIEW PIV SECANT AND TANGENT MODULUS VS. TIME

Appendix 6
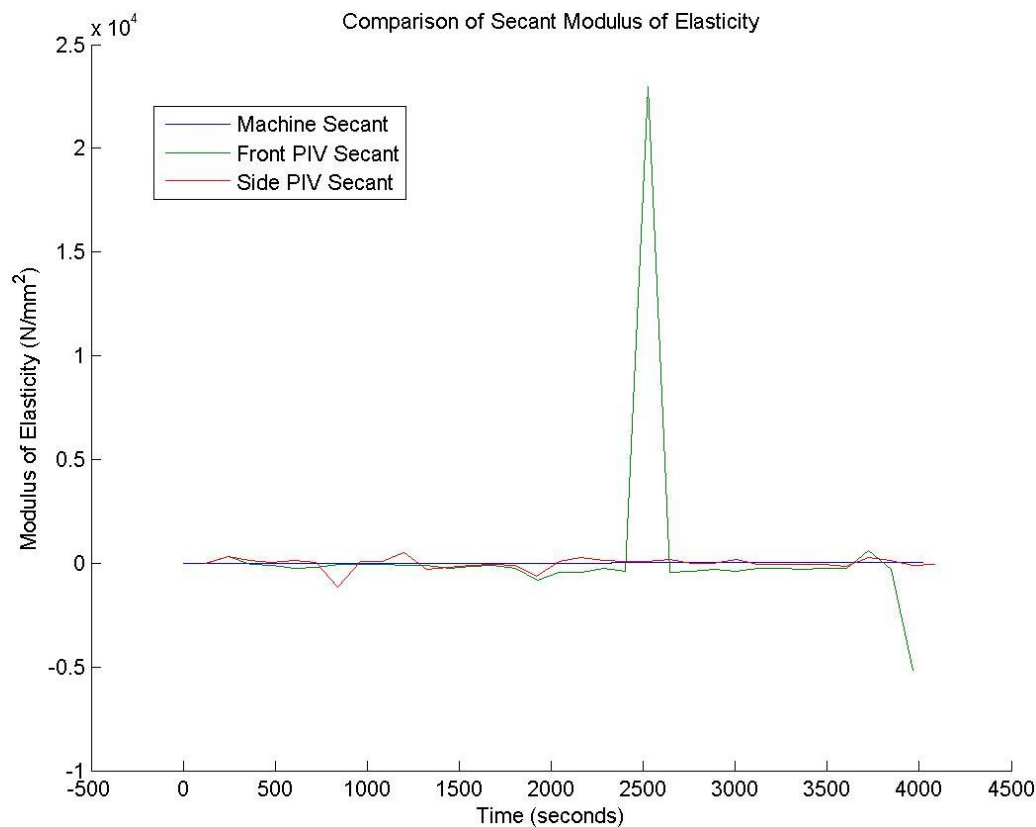
FIGURE 516: S3 COMPARISON OF MACHINE MEASURED AND PIV SECANT MODULUS VS. TIME
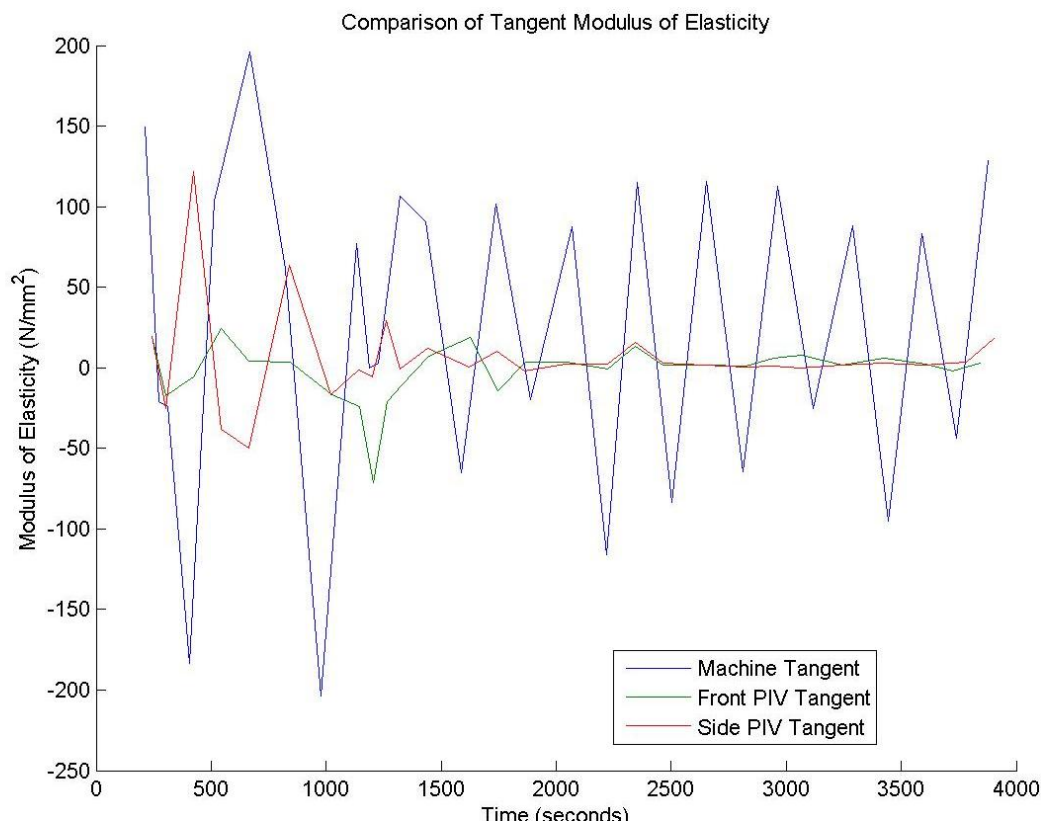
FIGURE 517: S3 COMPARISON OF MACHINE MEASURED AND PIV TANGENT MODULUS VS.

TIME

S3 Sample
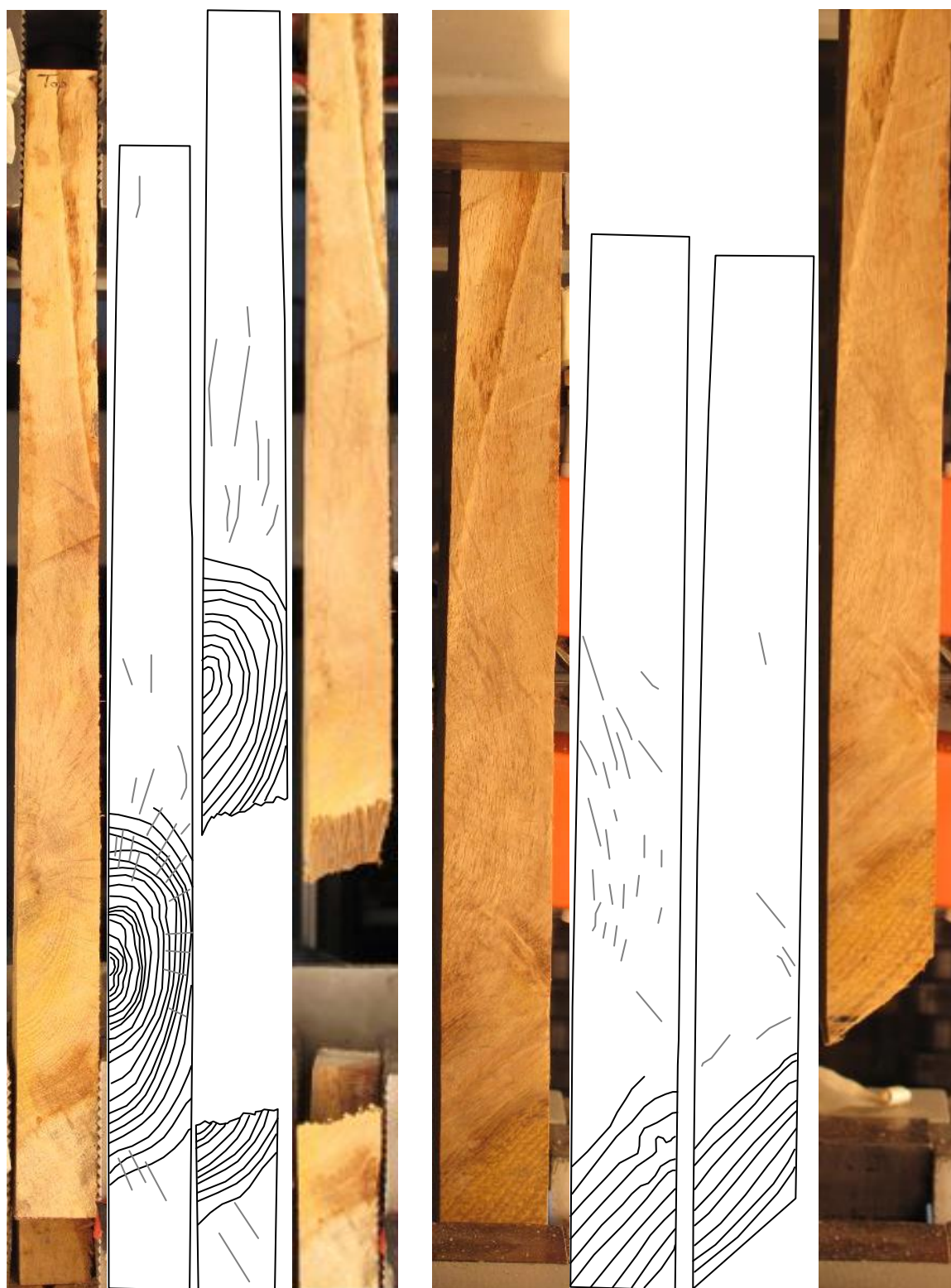
FIGURE 518: SAMPLE GRAIN ORIENTATIONS OF THE FRONT (LEFT 4 IMAGES) AND SIDE (RIGHT 4 IMAGES) VIEW BEFORE (FIRST 2 OF 4 IMAGES) AND AFTER (LAST 2 OF 4 IMAGES) BREAKAGE

Appendix 6

S3 Front View

FIGURE 519: X DIRECTION PIV SEQUENTIAL ENGINEERING STRAIN OVER TIME

FIGURE 520: Y DIRECTION PIV SEQUENTIAL ENGINEERING STRAIN OVER TIME
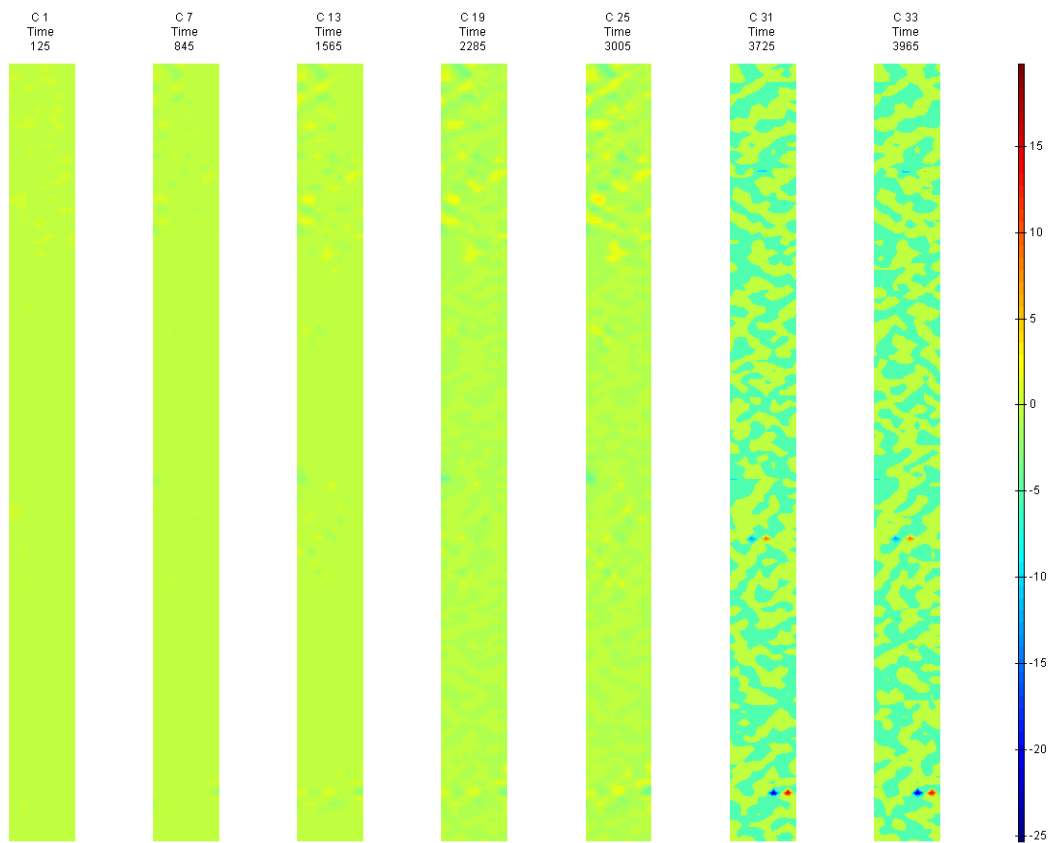
FIGURE 521: XY DIRECTION PIV SEQUENTIAL ENGINEERING SHEAR STRAIN OVER TIME
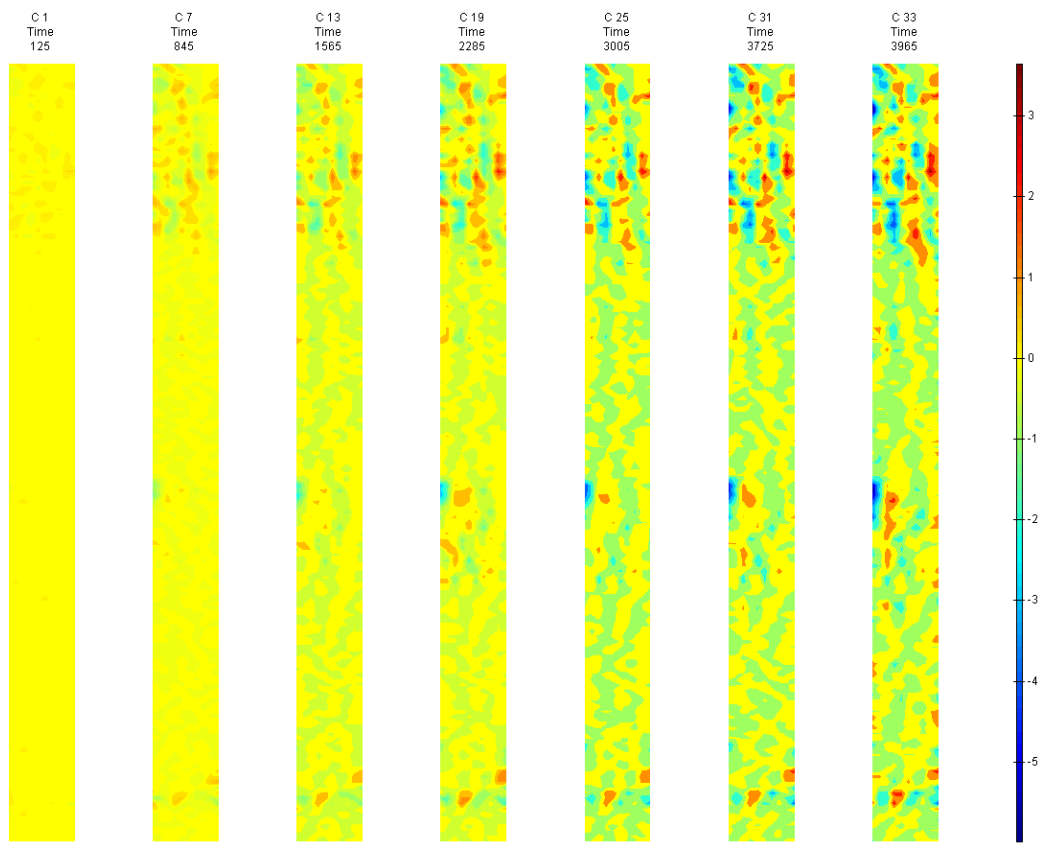
FIGURE 522: X DIRECTION PIV SEQUENTIAL TRUE STRAIN OVER TIME

Appendix 6
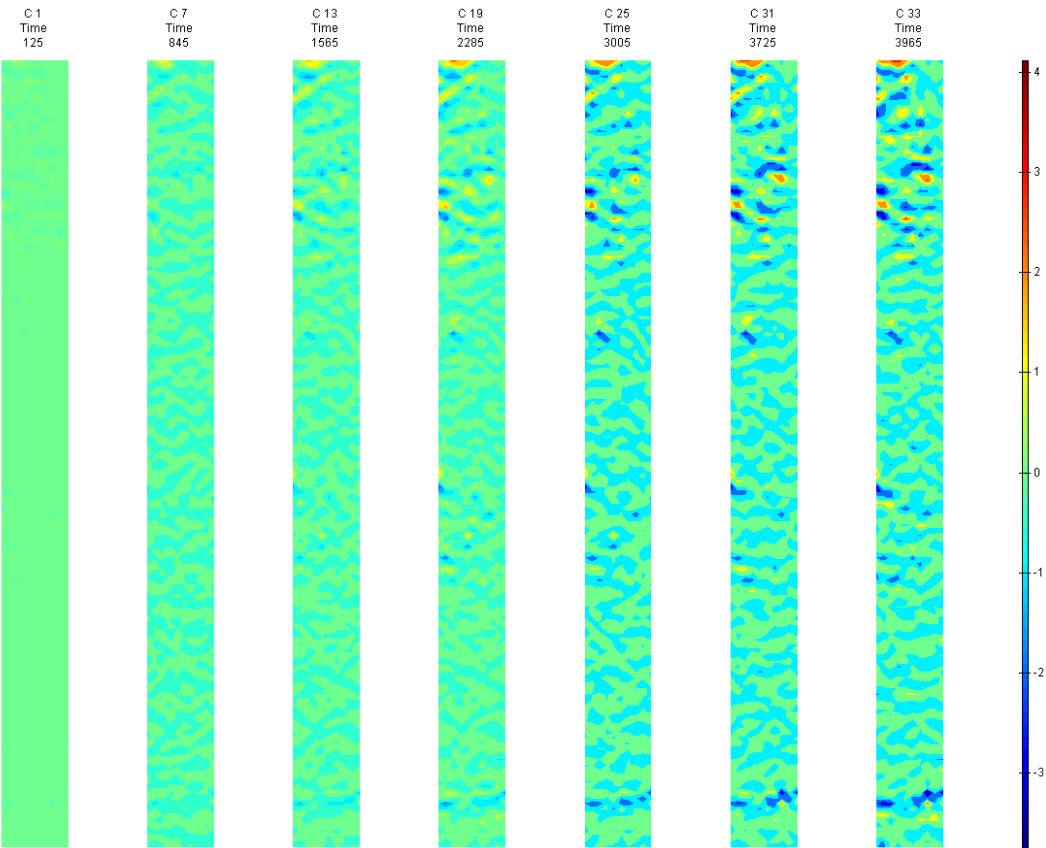
FIGURE 523: Y DIRECTION PIV SEQUENTIAL TRUE STRAIN OVER TIME
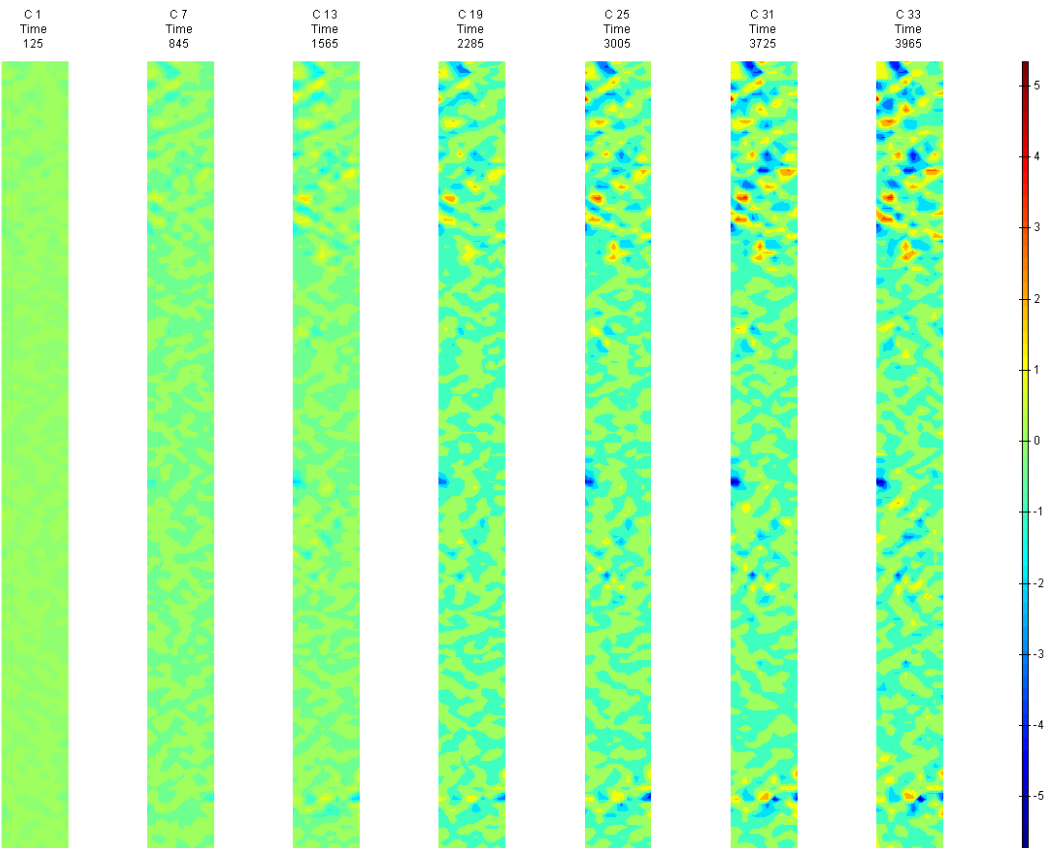
FIGURE 524: XY DIRECTION PIV SEQUENTIAL TRUE SHEAR STRAIN OVER TIME
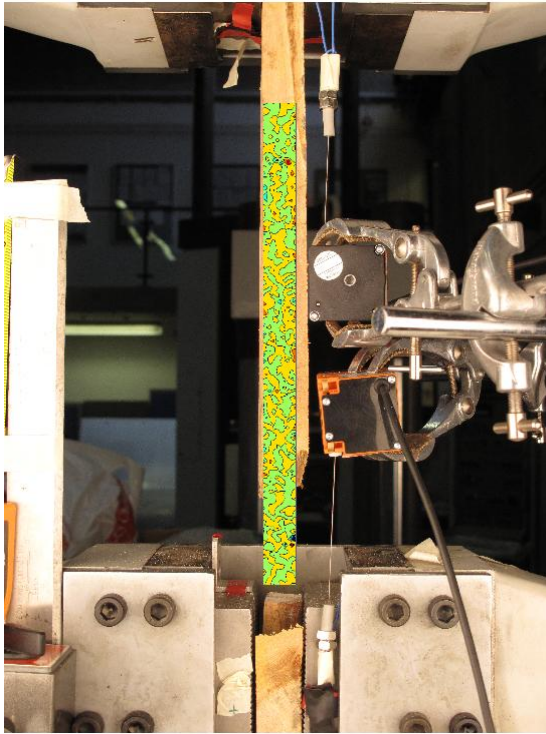
FIGURE 525: X DIRECTION PIV FIRST–LAST DITCH ENGINEERING STRAIN OVER IMAGE
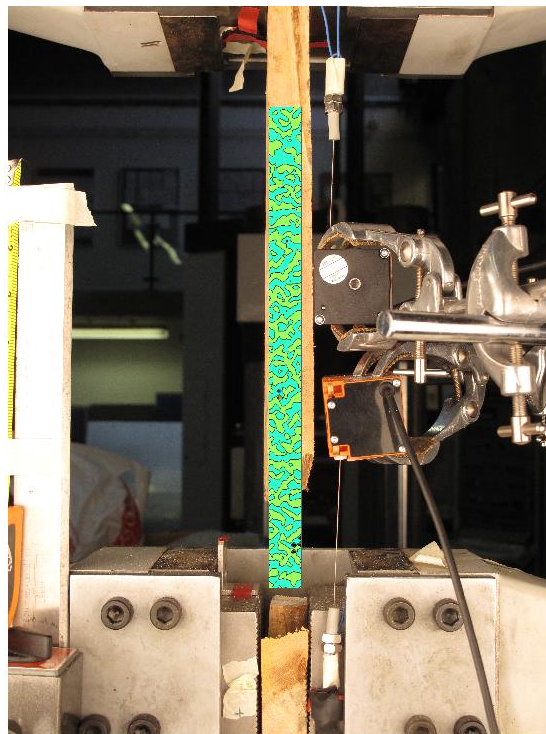
FIGURE 526: Y DIRECTION PIV FIRST–LAST DITCH ENGINEERING STRAIN OVER IMAGE

Appendix 6
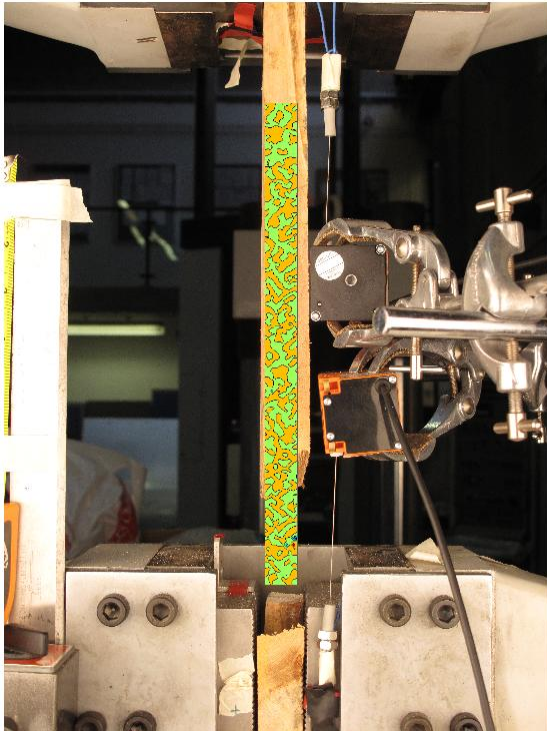
FIGURE 527: XY DIRECTION PIV FIRST–LAST DITCH ENGINEERING SHEAR STRAIN OVER

IMAGE

FIGURE 528: X DIRECTION PIV FIRST–LAST DITCH TRUE STRAIN OVER IMAGE

FIGURE 529: Y DIRECTION PIV FIRST–LAST DITCH TRUE STRAIN OVER IMAGE

FIGURE 530: XY DIRECTION PIV FIRST–LAST DITCH TRUE SHEAR STRAIN OVER IMAGE

Appendix 6

FIGURE 531: XY DIRECTION PIV FIRST–SEQUENTIAL ENGINEERING SHEAR STRAIN OVER

IMAGE

FIGURE 532: XY DIRECTION PIV FIRST–SEQUENTIAL ENGINEERING SHEAR STRAIN OVER TIME

S3 Side View
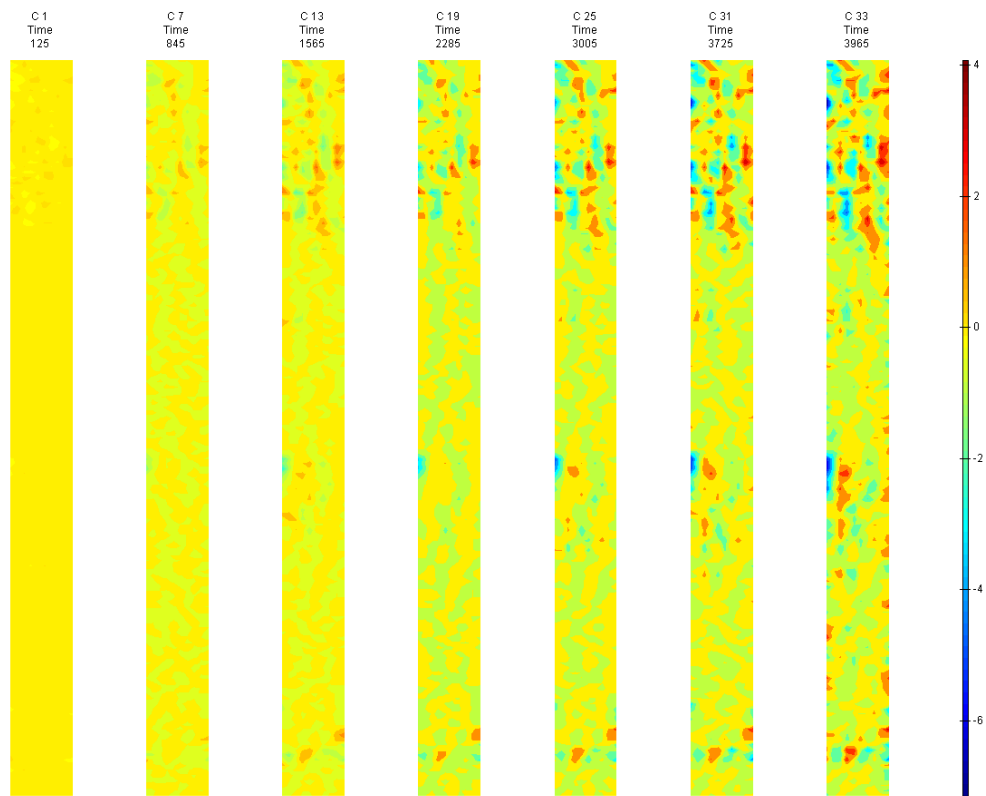

FIGURE 533: X DIRECTION PIV SEQUENTIAL ENGINEERING STRAIN OVER TIME
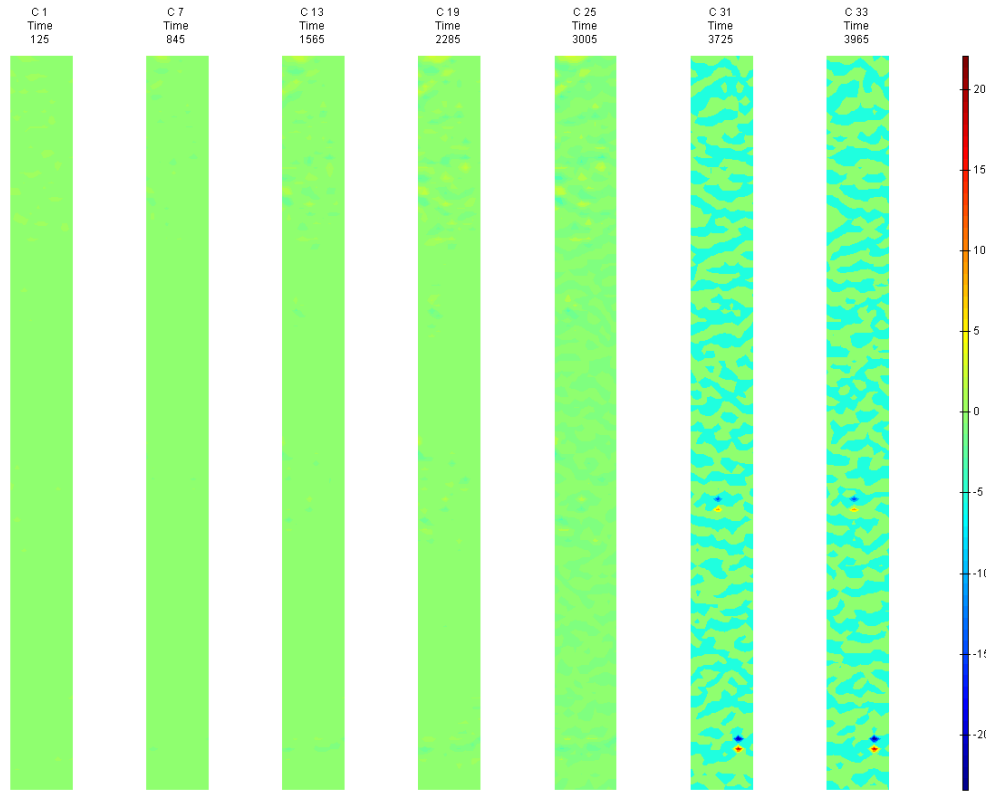

FIGURE 534: Y DIRECTION PIV SEQUENTIAL ENGINEERING STRAIN OVER TIME

FIGURE 535: XY DIRECTION PIV SEQUENTIAL ENGINEERING SHEAR STRAIN OVER TIME

FIGURE 536: X DIRECTION PIV SEQUENTIAL TRUE STRAIN OVER TIME

FIGURE 537: Y DIRECTION PIV SEQUENTIAL TRUE STRAIN OVER TIME

FIGURE 538: XY DIRECTION PIV SEQUENTIAL TRUE SHEAR STRAIN OVER TIME

FIGURE 539: X DIRECTION PIV FIRST–LAST DITCH ENGINEERING STRAIN OVER IMAGE

FIGURE 540: Y DIRECTION PIV FIRST–LAST DITCH ENGINEERING STRAIN OVER IMAGE

FIGURE 541: XY DIRECTION PIV FIRST–LAST DITCH ENGINEERING SHEAR STRAIN OVER
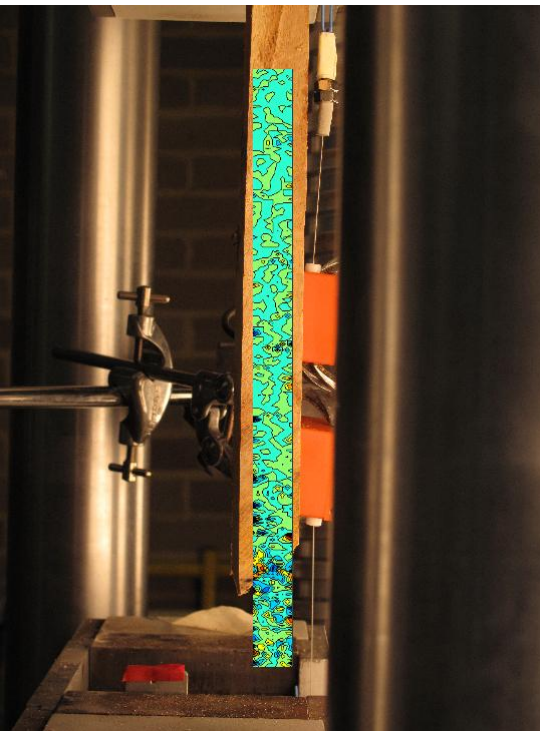
IMAGE

FIGURE 542: X DIRECTION PIV FIRST–LAST DITCH TRUE STRAIN OVER IMAGE
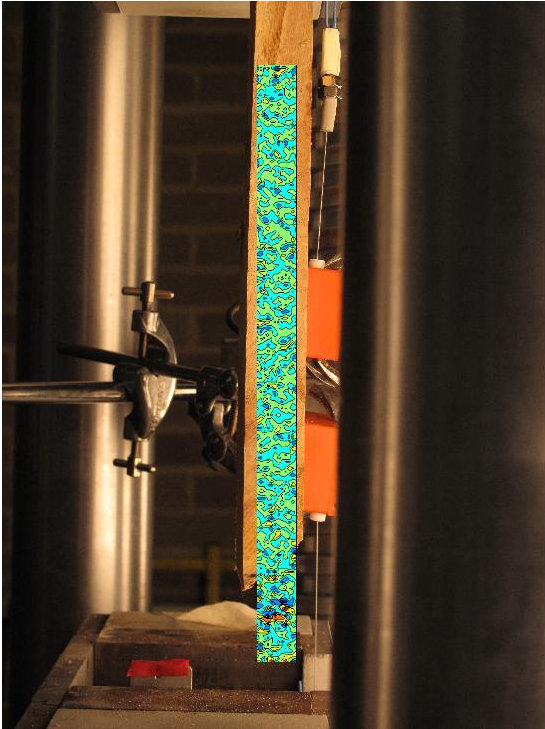
FIGURE 543: Y DIRECTION PIV FIRST–LAST DITCH TRUE STRAIN OVER IMAGE
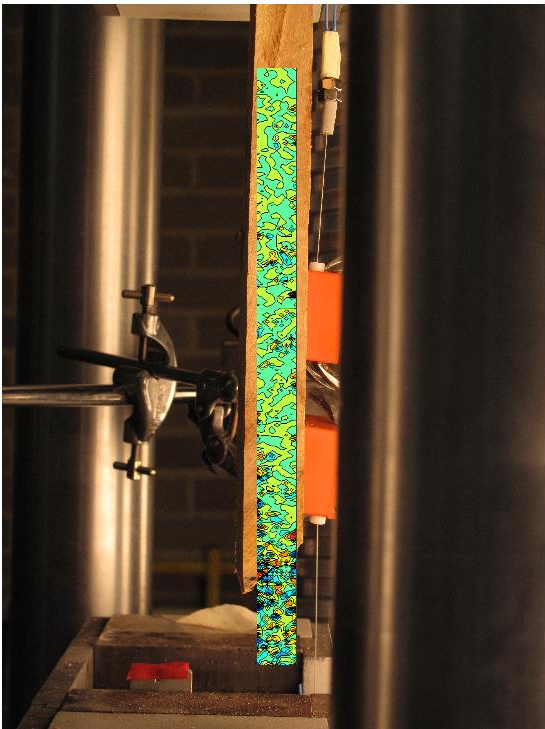
FIGURE 544: XY DIRECTION PIV FIRST–LAST DITCH TRUE SHEAR STRAIN OVER IMAGE
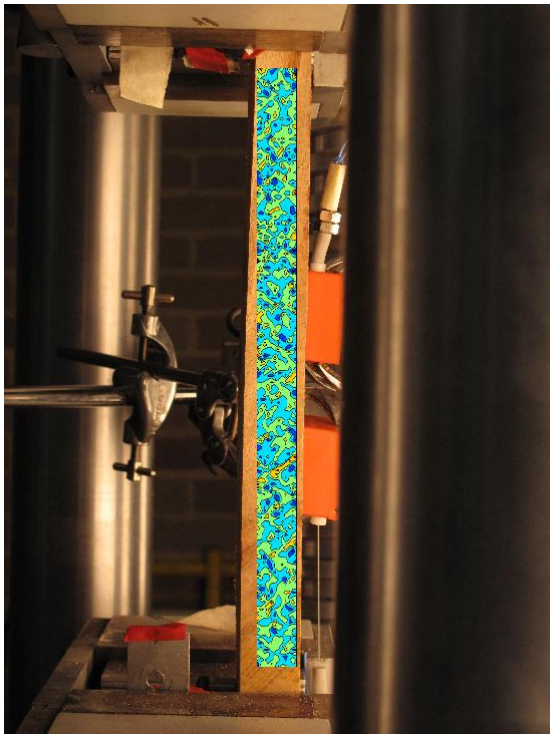
FIGURE 545: XY DIRECTION PIV FIRST–SEQUENTIAL ENGINEERING SHEAR STRAIN OVER

IMAGE
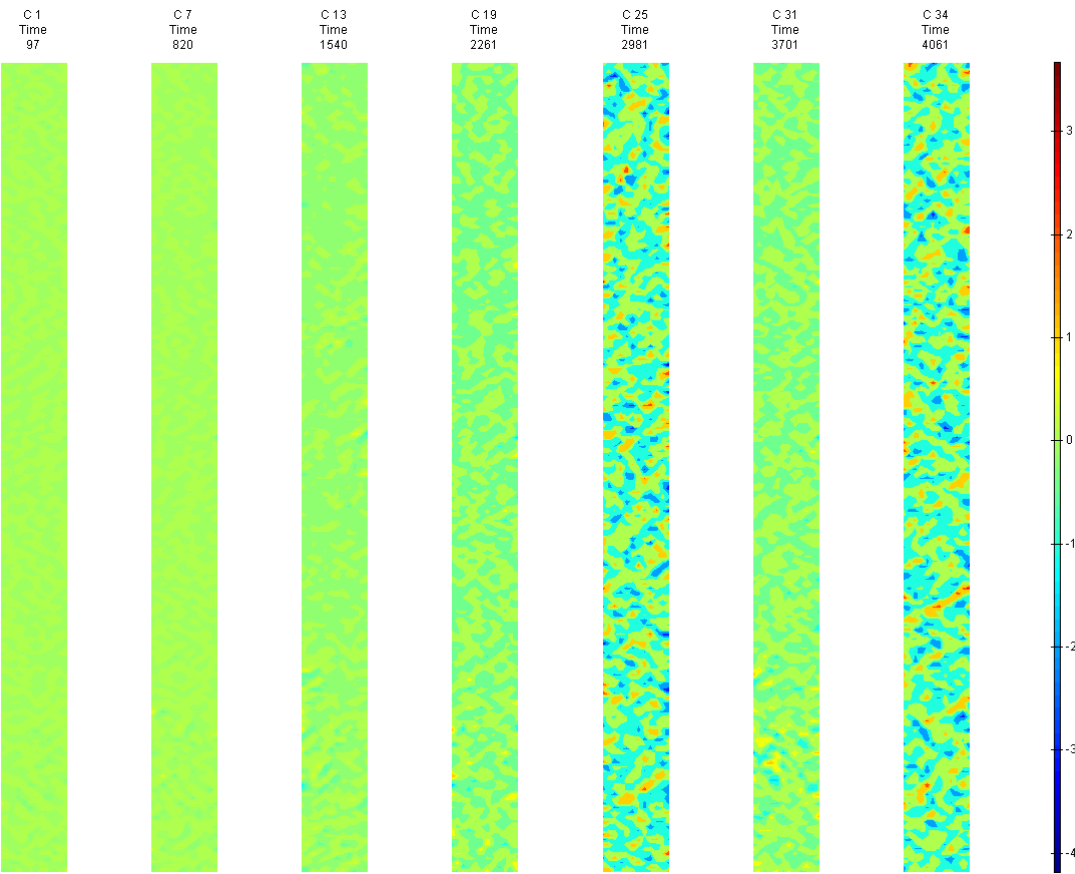
FIGURE 546: XY DIRECTION PIV FIRST–SEQUENTIAL ENGINEERING SHEAR STRAIN OVER TIME

Appendix 6

S4
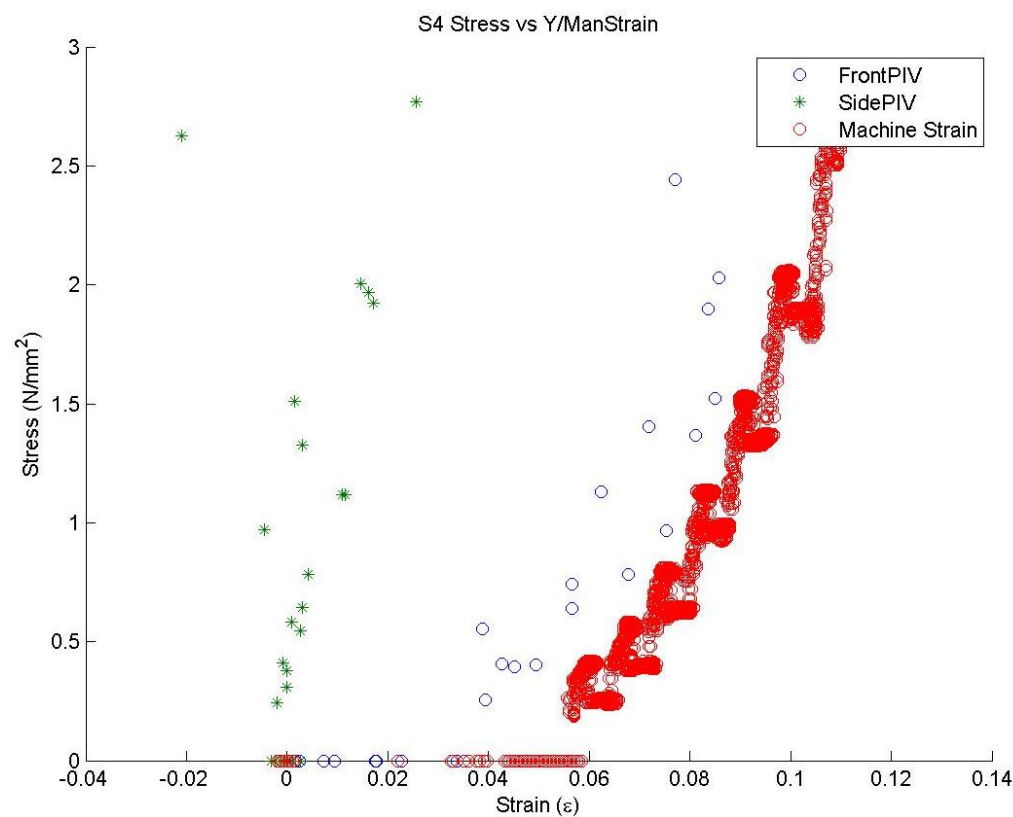
FIGURE 547: S4 TENSILE STRESS VS. MACHINE MEASURED/PIV STRAINS
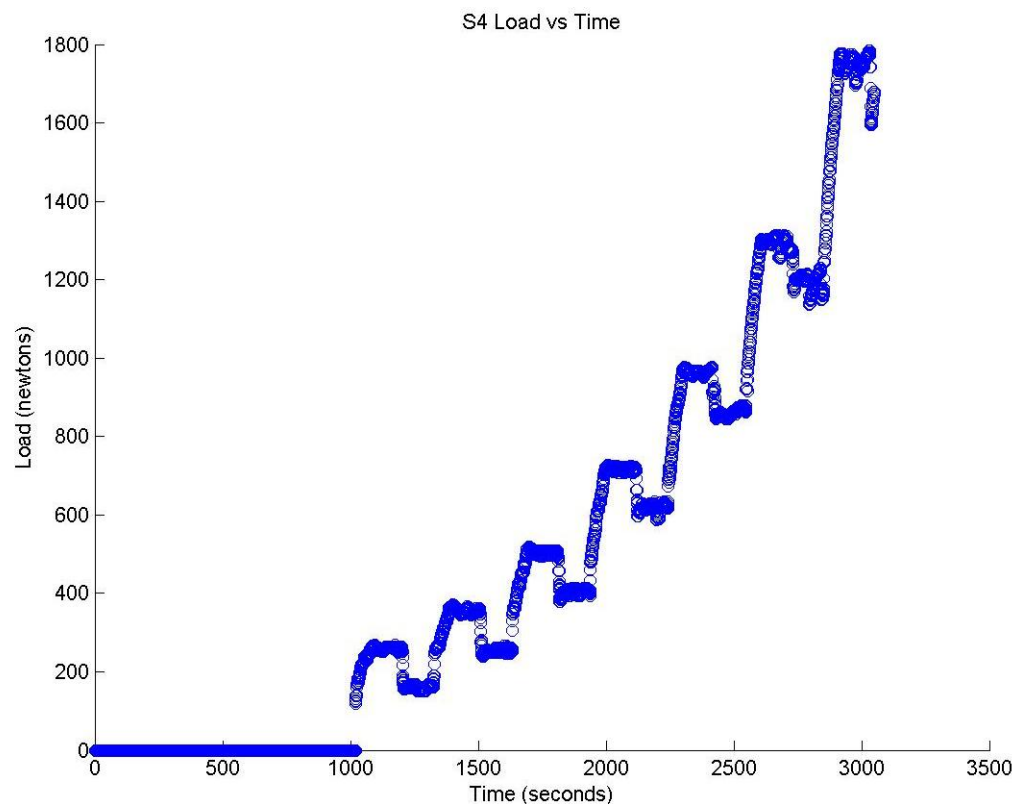
FIGURE 548: S4 TENSILE LOAD VS. TIME
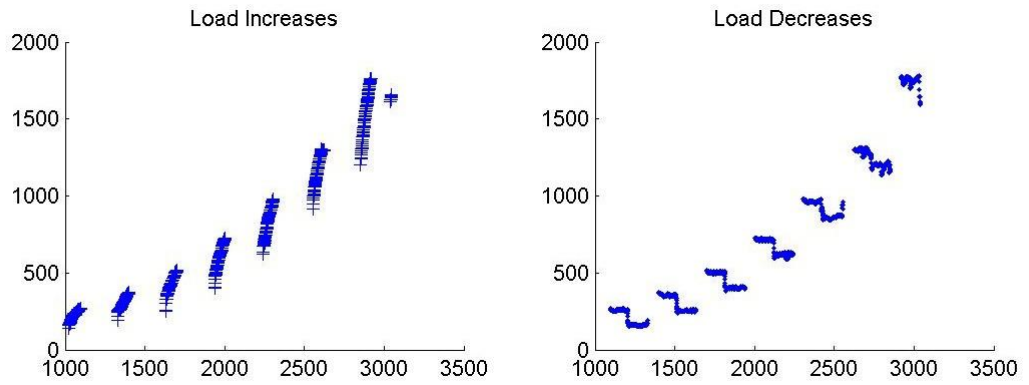
FIGURE 549: S4 CREEP LOADING: INCREMENTS AND RELAXATION
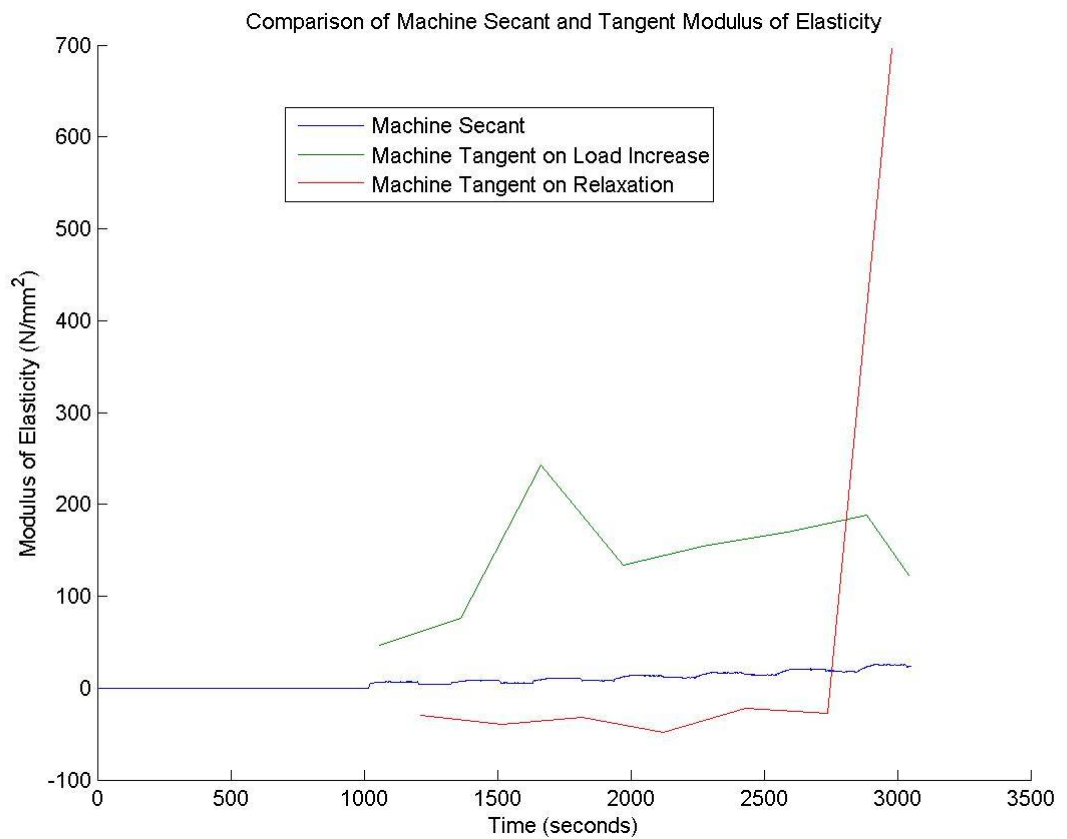
FIGURE 550: S4 MACHINE MEASURED SECANT AND TANGENT MODULUS VS. TIME

Appendix 6
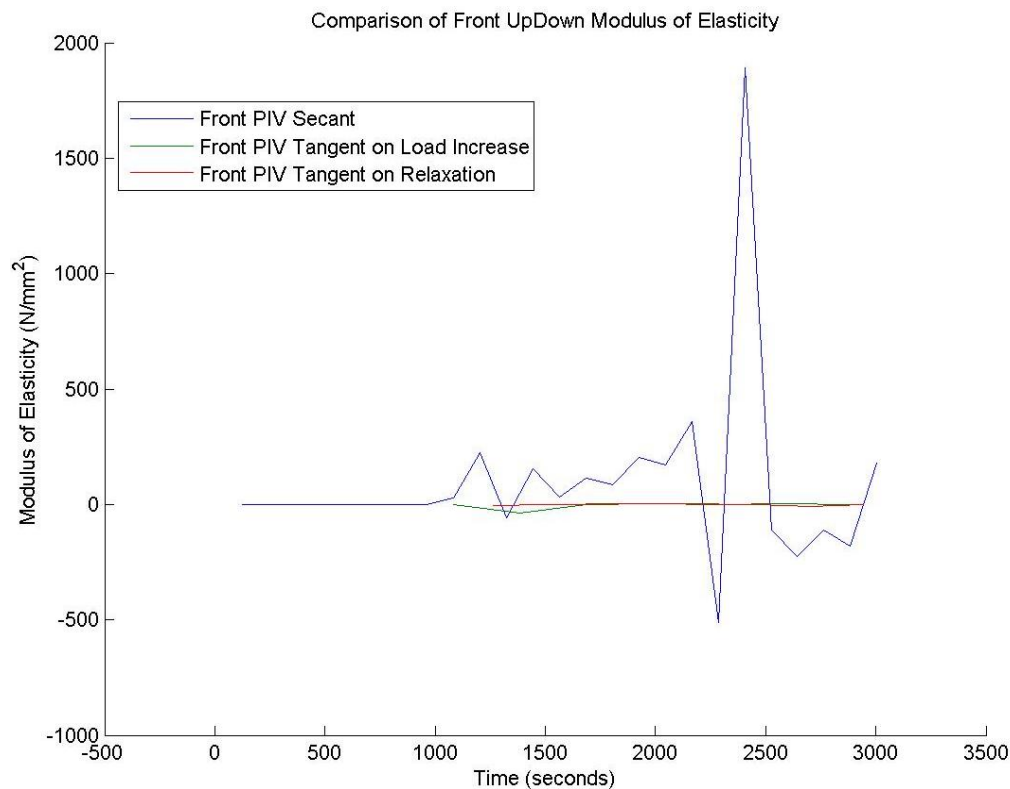
FIGURE 551: S4 FRONT VIEW PIV SECANT AND TANGENT MODULUS VS. TIME
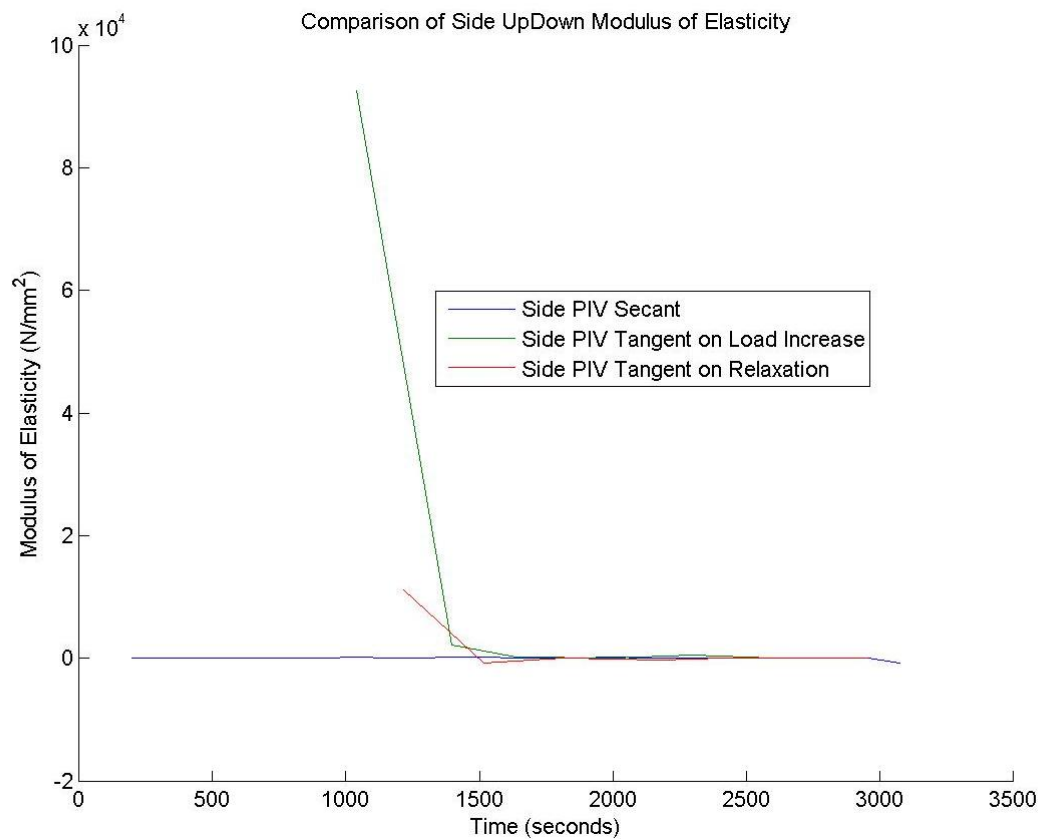
FIGURE 552: S4 SIDE VIEW PIV SECANT AND TANGENT MODULUS VS. TIME
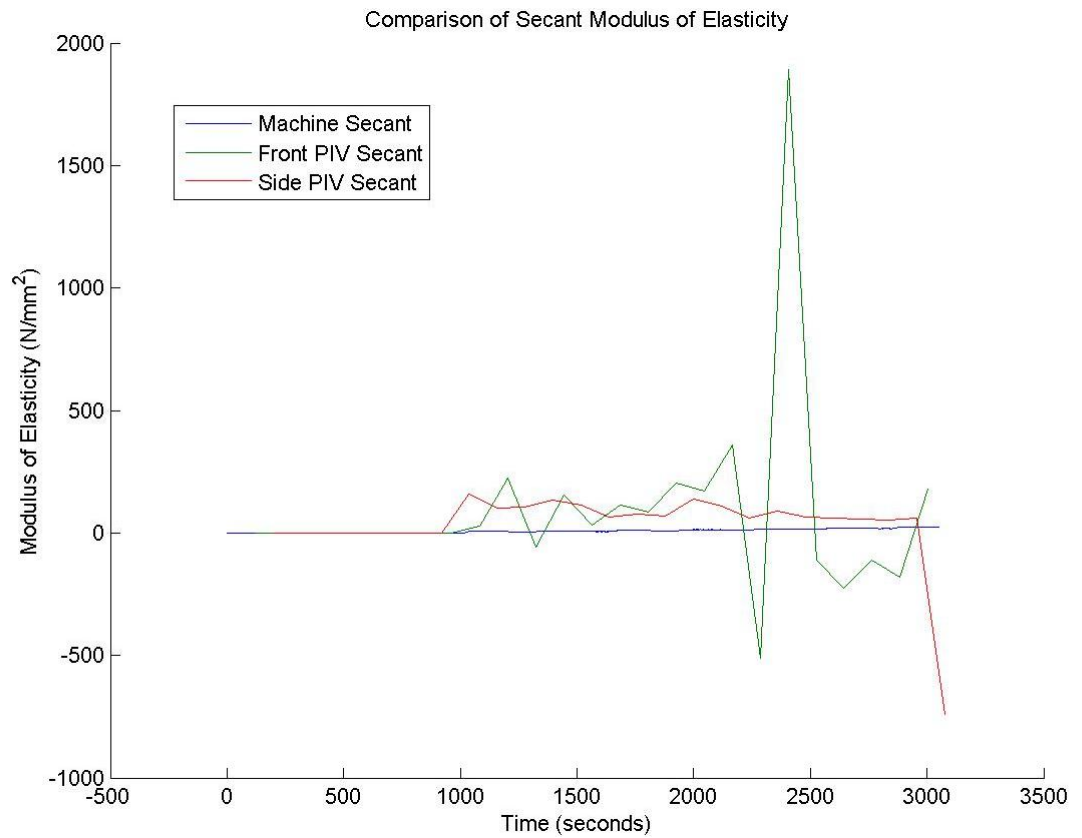
FIGURE 553: S4 COMPARISON OF MACHINE MEASURED AND PIV SECANT MODULUS VS. TIME
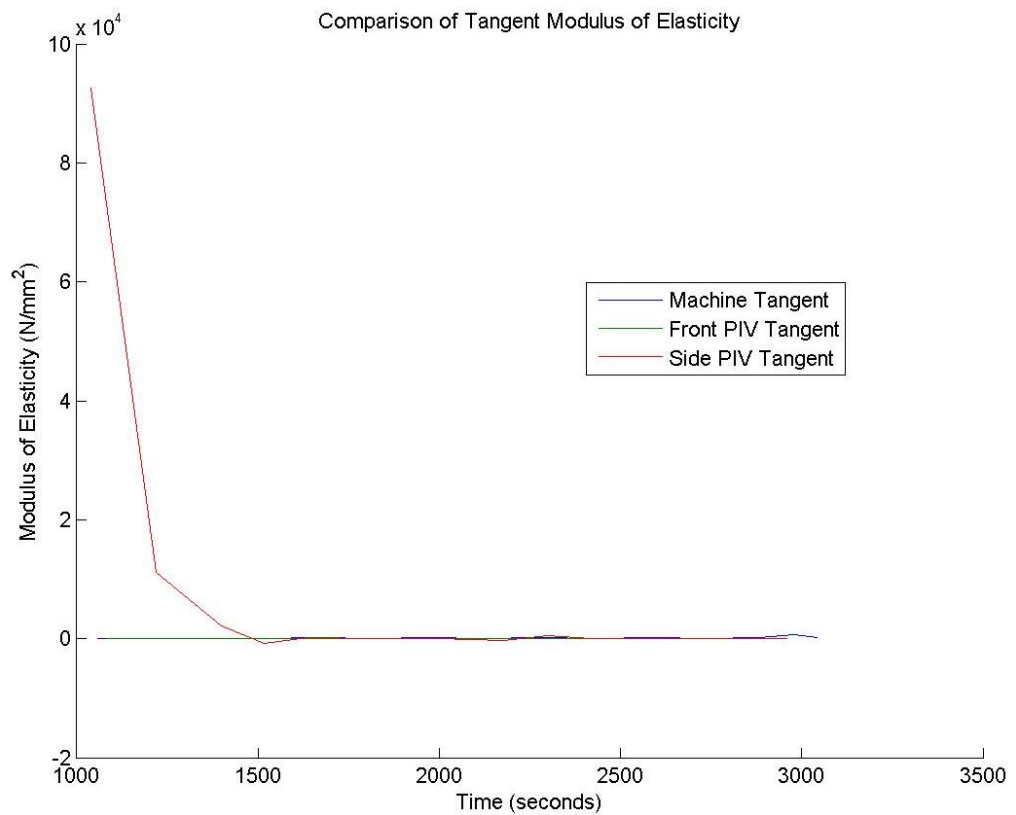
FIGURE 554: S4 COMPARISON OF MACHINE MEASURED AND PIV TANGENT MODULUS VS.

TIME

Appendix 6
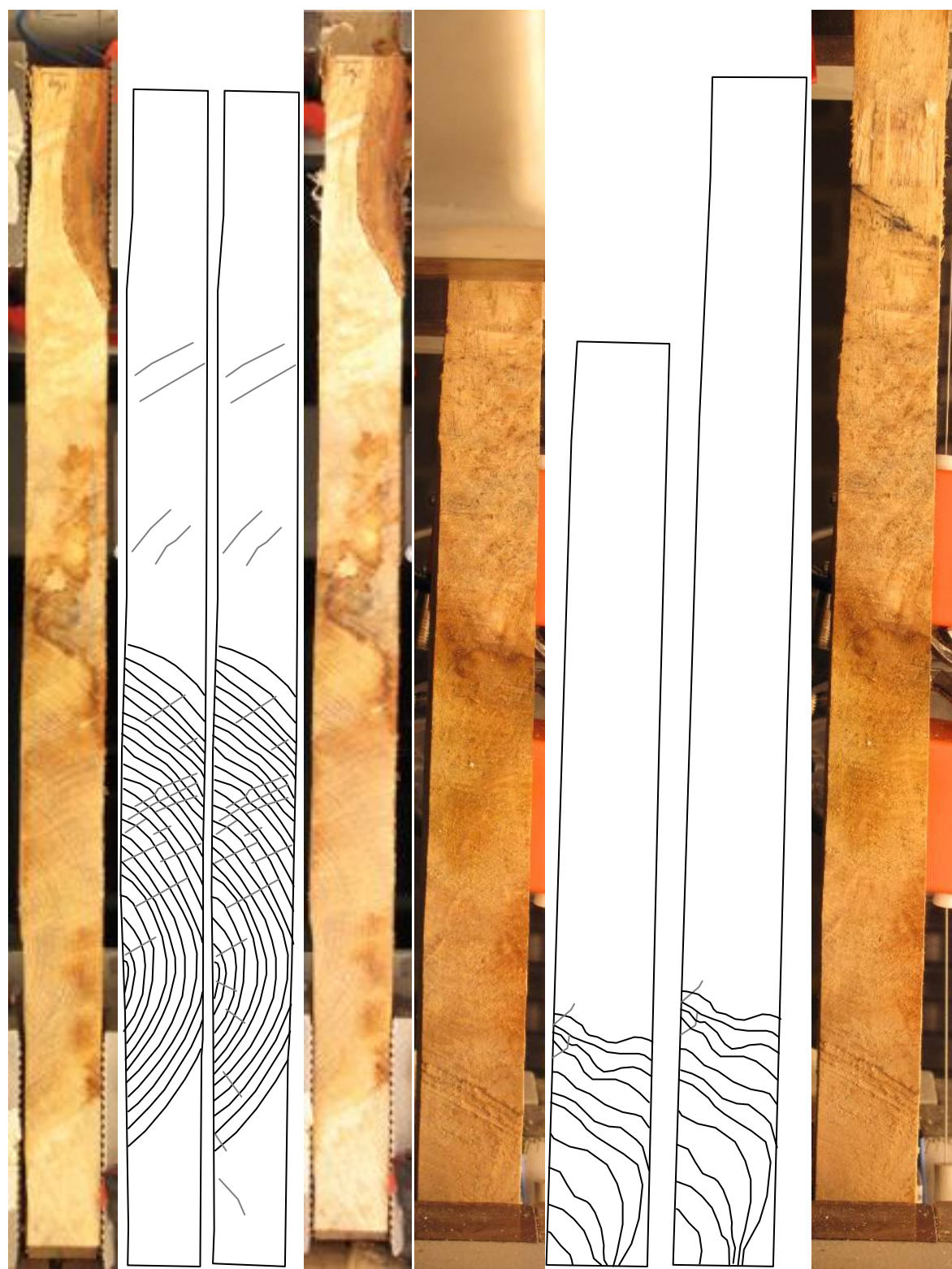
S4 Sample

FIGURE 555: SAMPLE GRAIN ORIENTATIONS OF THE FRONT (LEFT 4 IMAGES) AND SIDE (RIGHT 4 IMAGES) VIEW BEFORE (FIRST 2 OF 4 IMAGES) AND AFTER (LAST 2 OF 4 IMAGES) BREAKAGE

S4 Front View

FIGURE 556: X DIRECTION PIV SEQUENTIAL ENGINEERING STRAIN OVER TIME

FIGURE 557: Y DIRECTION PIV SEQUENTIAL ENGINEERING STRAIN OVER TIME

Appendix 6

FIGURE 558: XY DIRECTION PIV SEQUENTIAL ENGINEERING SHEAR STRAIN OVER TIME
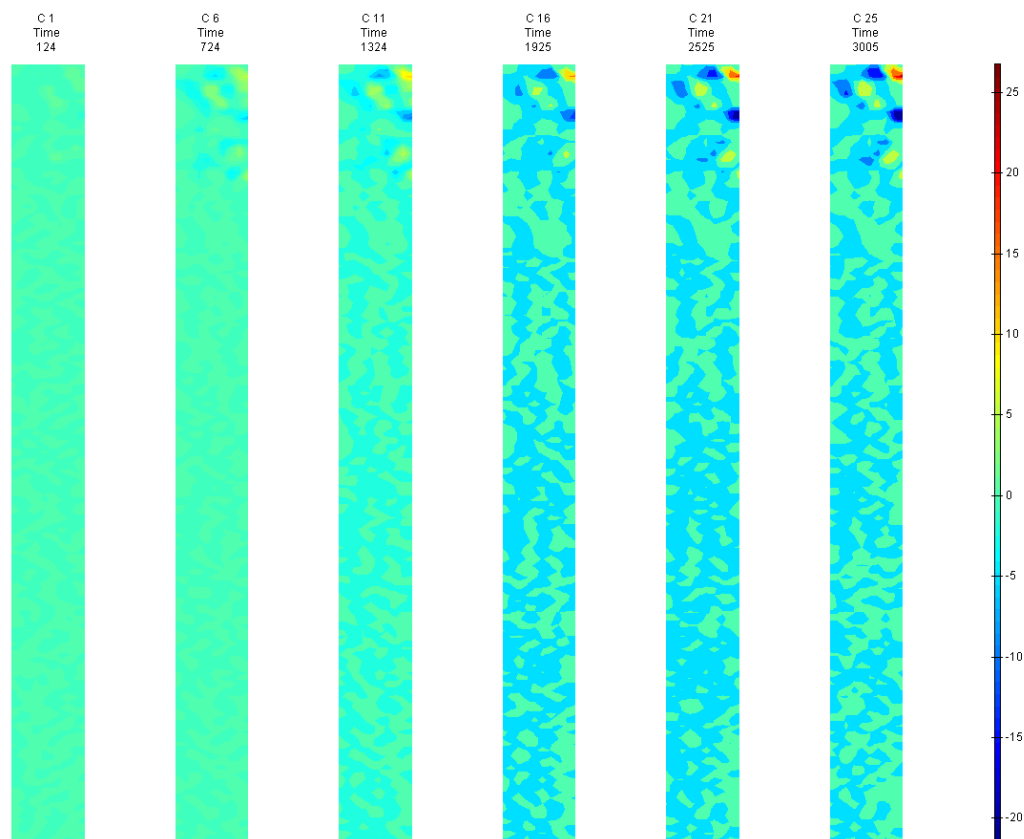
FIGURE 559: X DIRECTION PIV SEQUENTIAL TRUE STRAIN OVER TIME
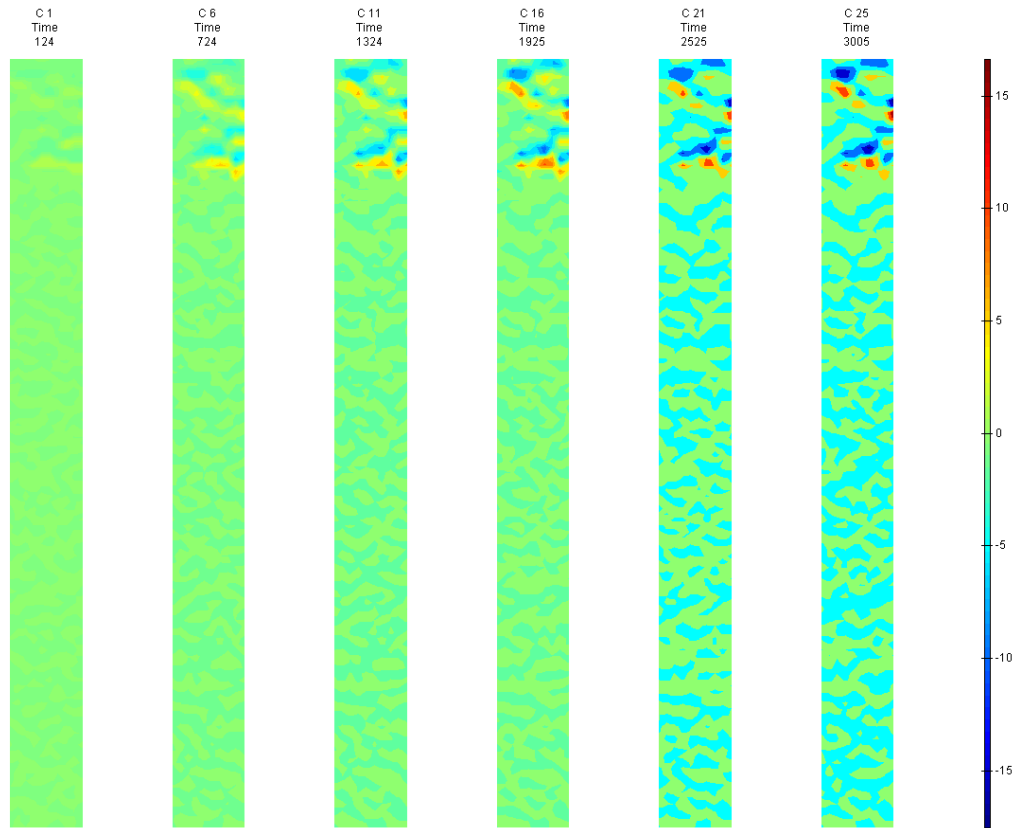
FIGURE 560: Y DIRECTION PIV SEQUENTIAL TRUE STRAIN OVER TIME
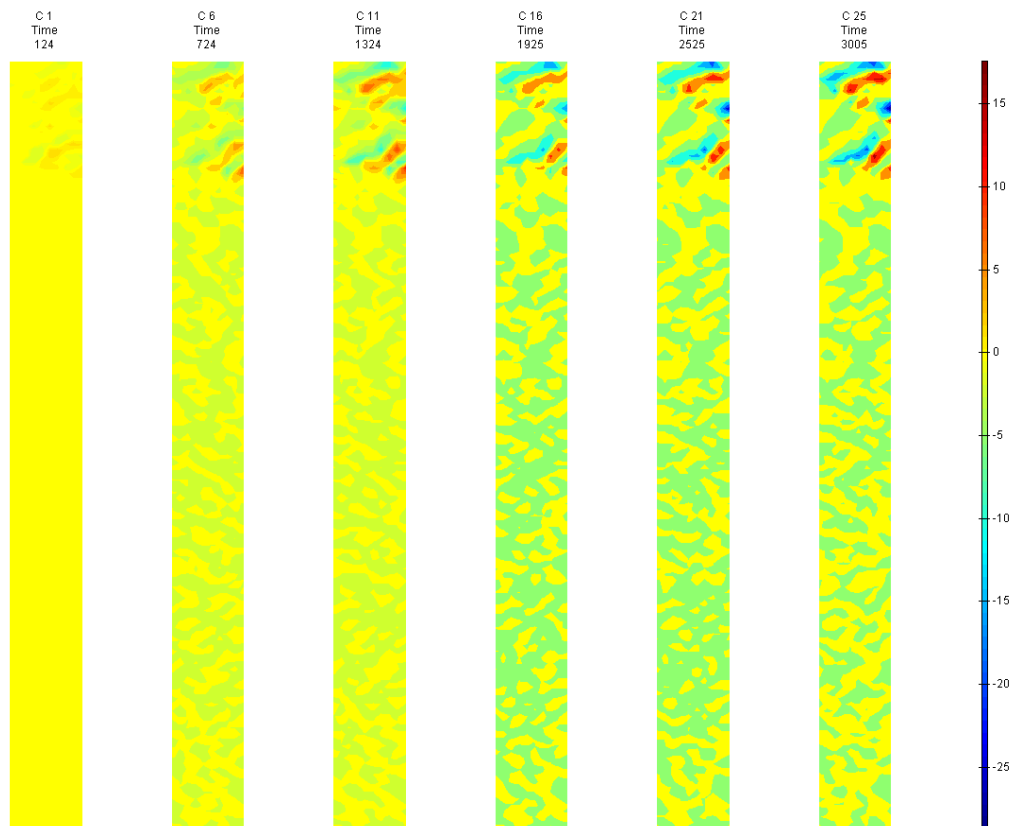
FIGURE 561: XY DIRECTION PIV SEQUENTIAL TRUE SHEAR STRAIN OVER TIME
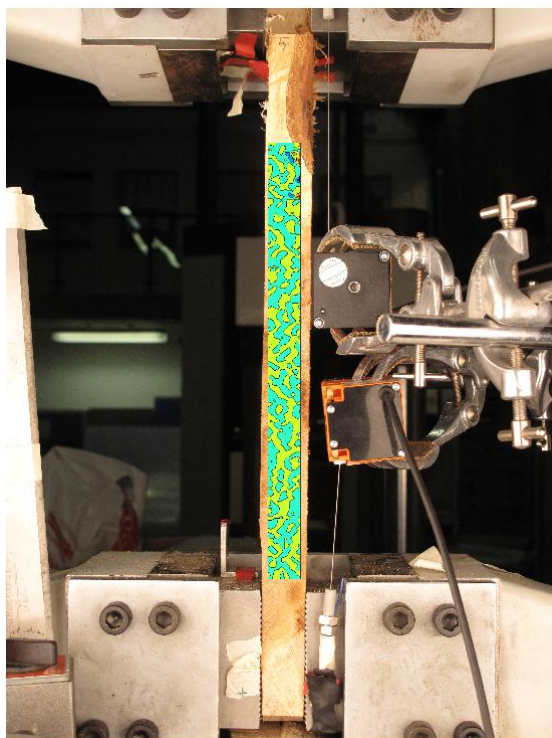
FIGURE 562: X DIRECTION PIV FIRST–LAST DITCH ENGINEERING STRAIN OVER IMAGE
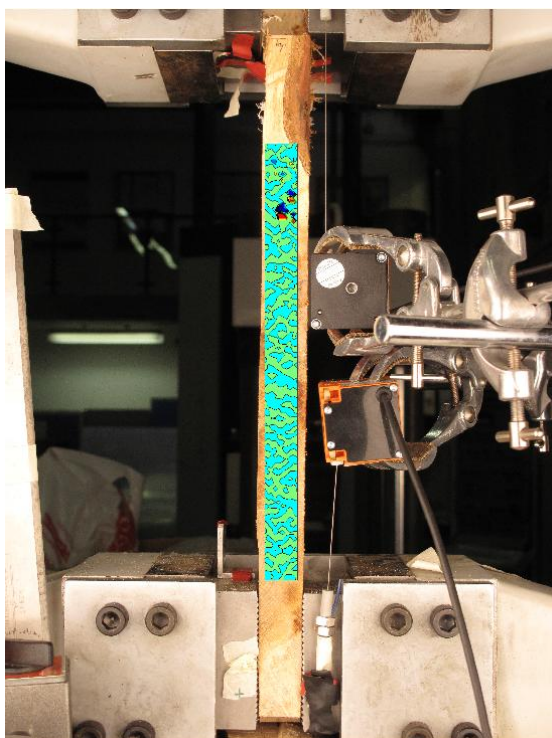
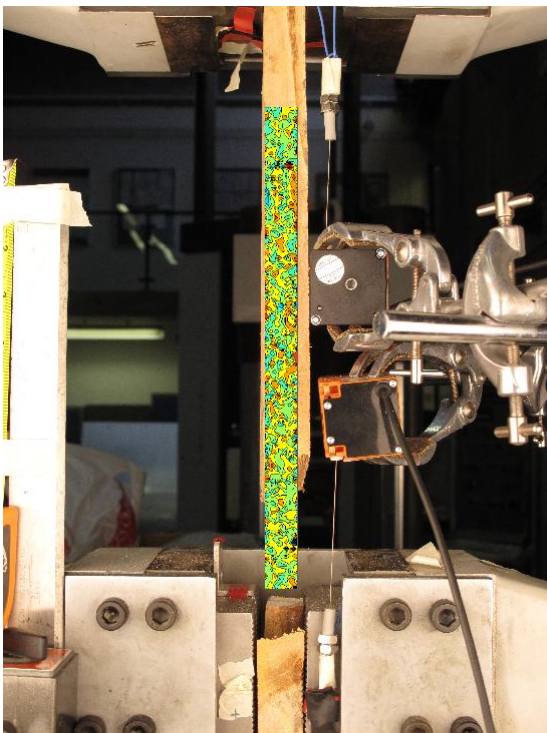FIGURE 563: Y DIRECTION PIV FIRST–LAST DITCH ENGINEERING STRAIN OVER IMAGE
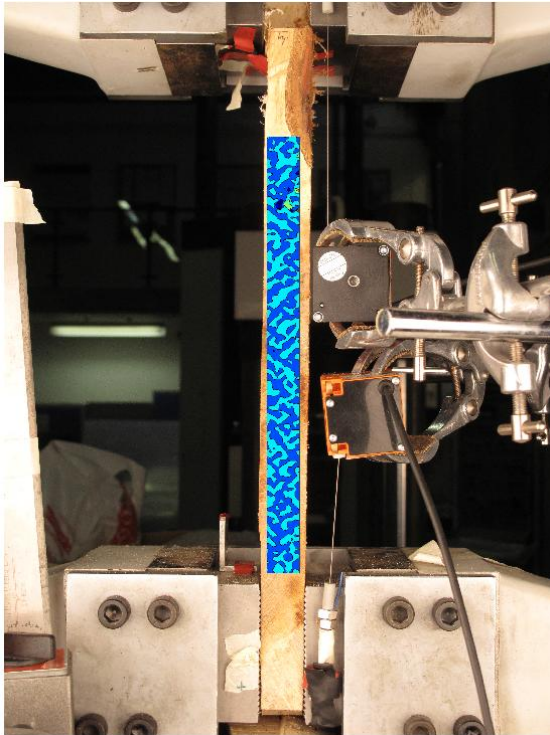
FIGURE 564: XY DIRECTION PIV FIRST–LAST DITCH ENGINEERING SHEAR STRAIN OVER

IMAGE

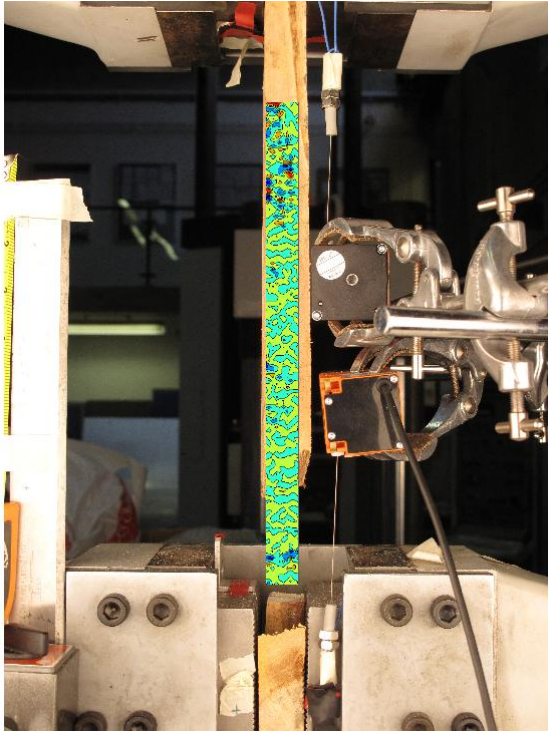FIGURE 565: X DIRECTION PIV FIRST–LAST DITCH TRUE STRAIN OVER IMAGE

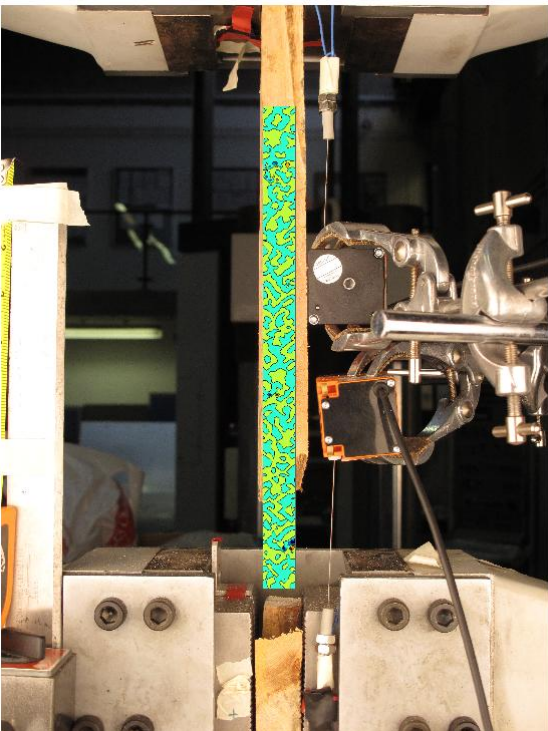FIGURE 566: Y DIRECTION PIV FIRST–LAST DITCH TRUE STRAIN OVER IMAGE

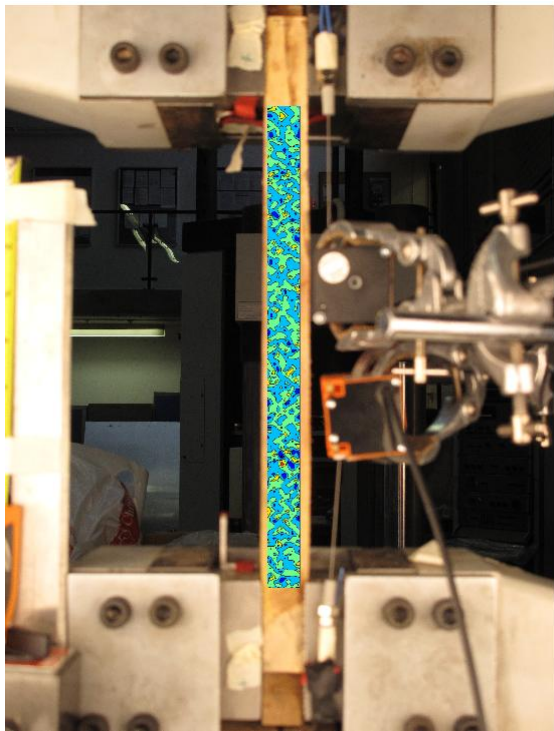FIGURE 567: XY DIRECTION PIV FIRST–LAST DITCH TRUE SHEAR STRAIN OVER IMAGE

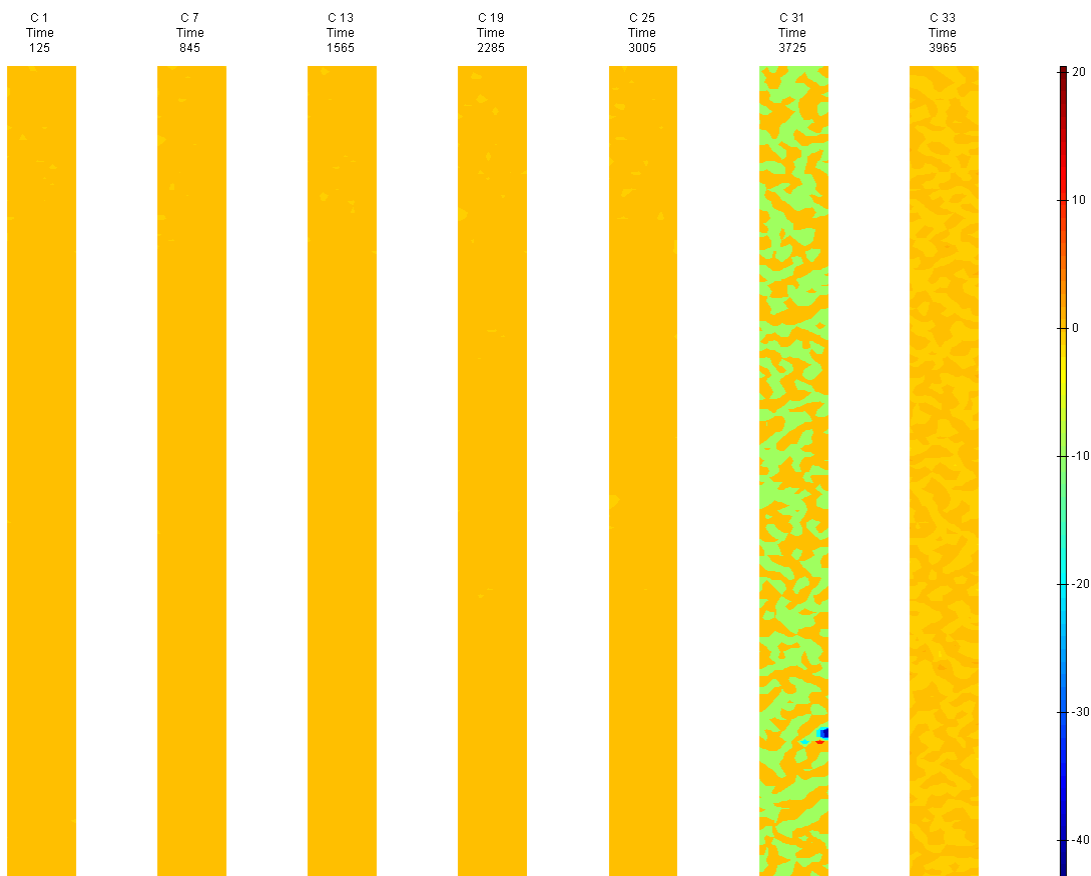FIGURE 568: XY DIRECTION PIV FIRST–SEQUENTIAL ENGINEERING SHEAR STRAIN OVER

IMAGE

FIGURE 569: XY DIRECTION PIV FIRST–SEQUENTIAL ENGINEERING SHEAR STRAIN OVER TIME
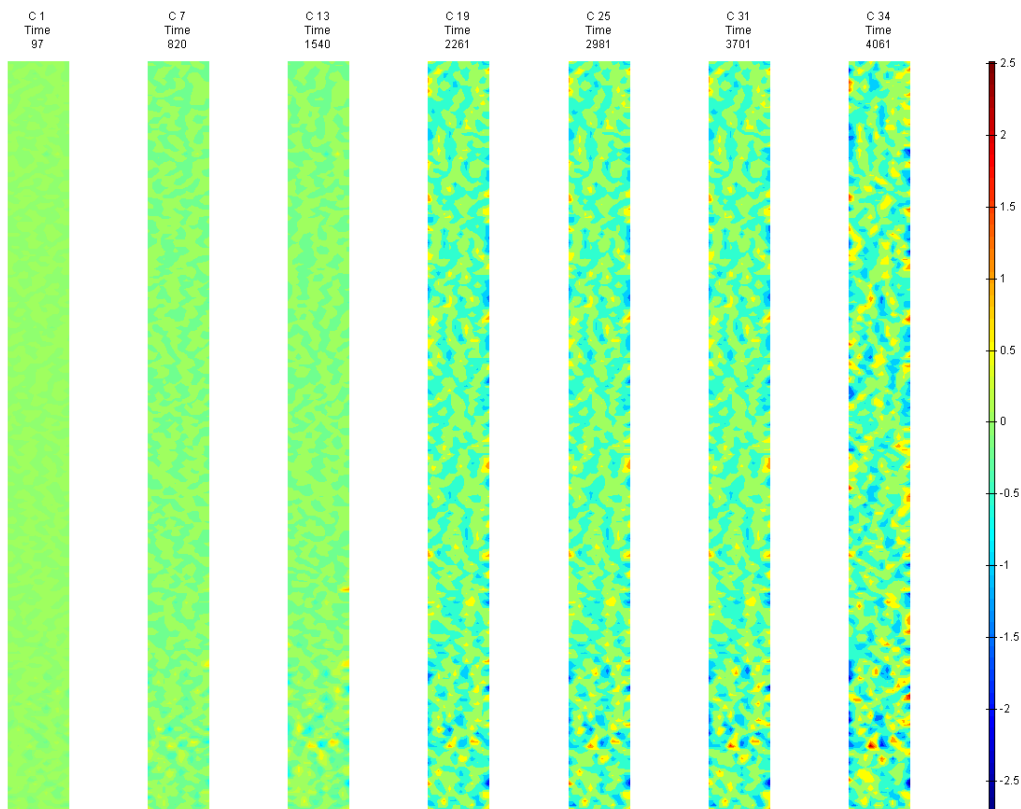
S4 Side View

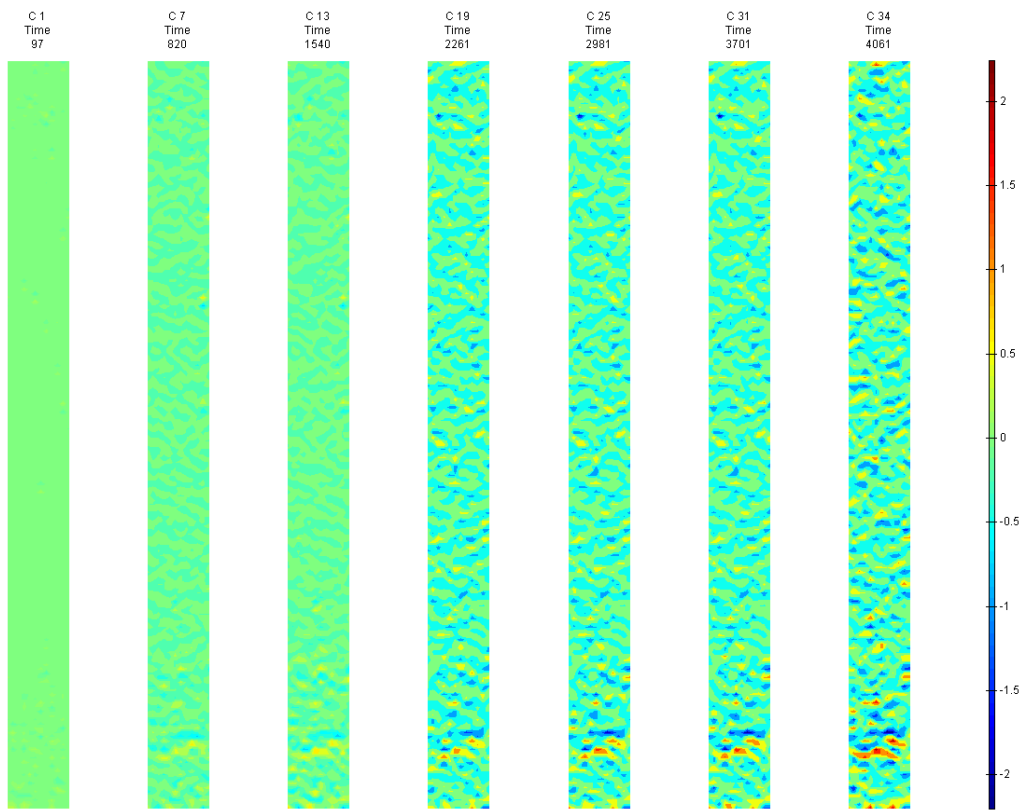FIGURE 570: X DIRECTION PIV SEQUENTIAL ENGINEERING STRAIN OVER TIME

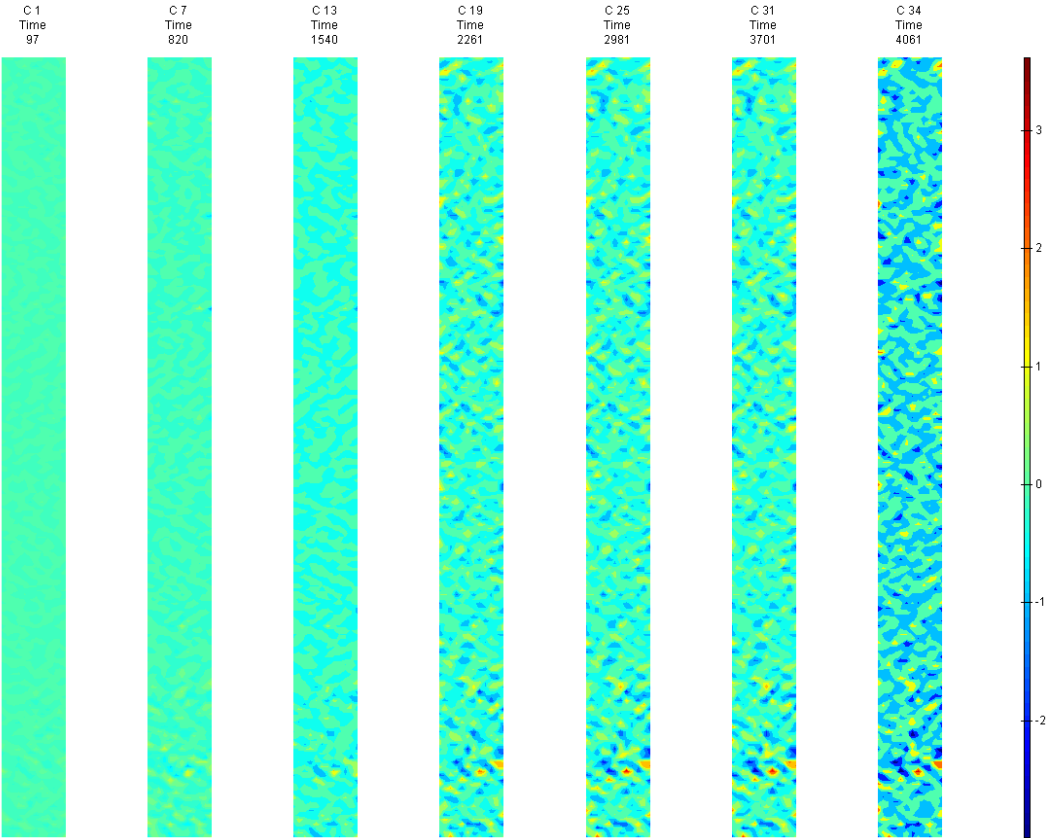FIGURE 571: Y DIRECTION PIV SEQUENTIAL ENGINEERING STRAIN OVER TIME

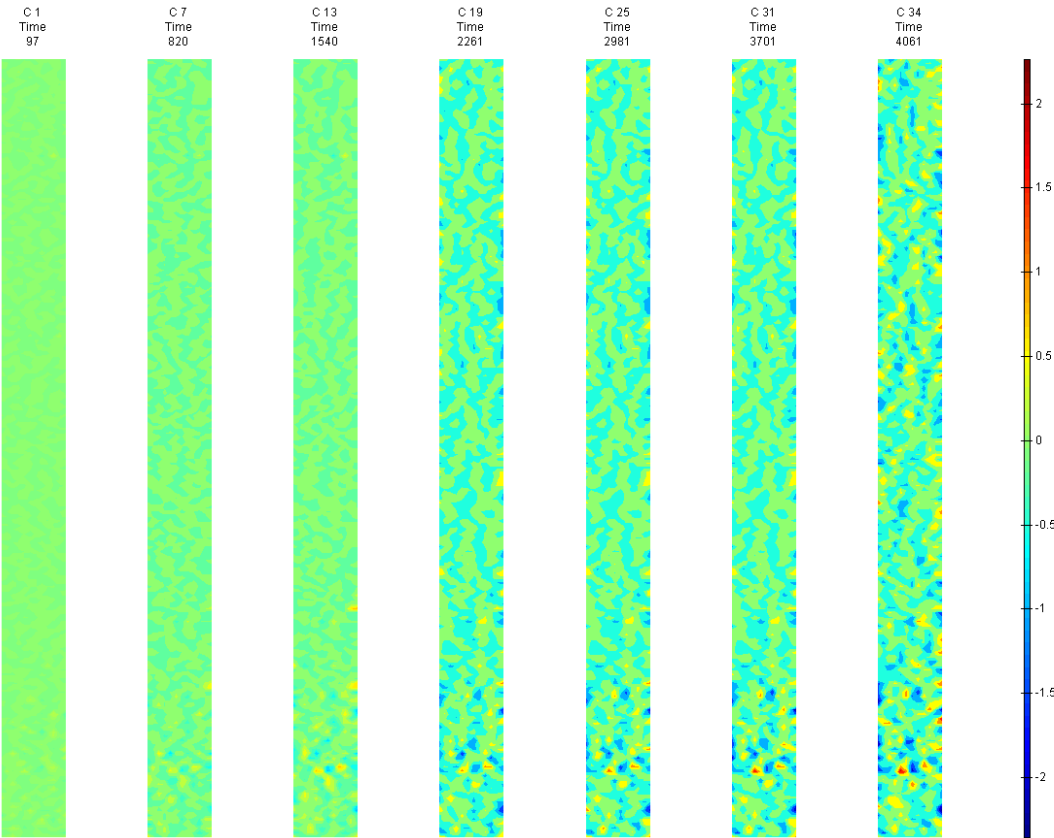FIGURE 572: XY DIRECTION PIV SEQUENTIAL ENGINEERING SHEAR STRAIN OVER TIME

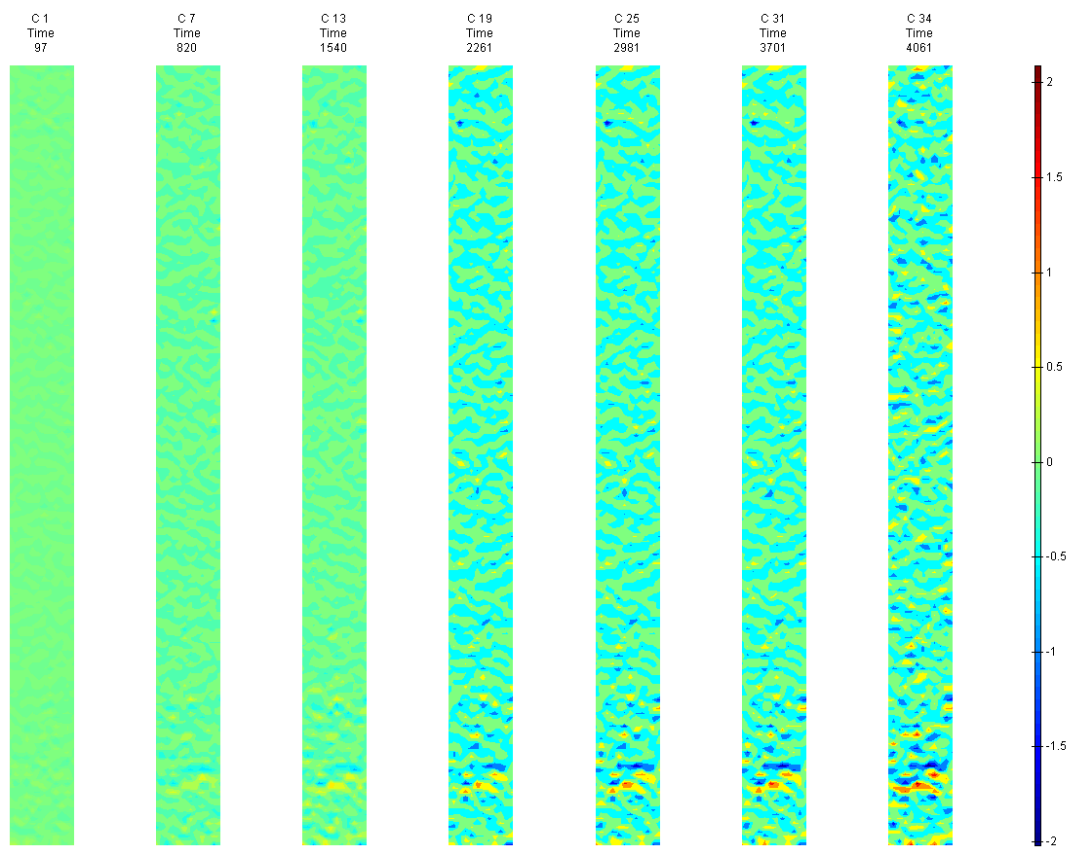FIGURE 573: X DIRECTION PIV SEQUENTIAL TRUE STRAIN OVER TIME

Appendix 6

FIGURE 574: Y DIRECTION PIV SEQUENTIAL TRUE STRAIN OVER TIME
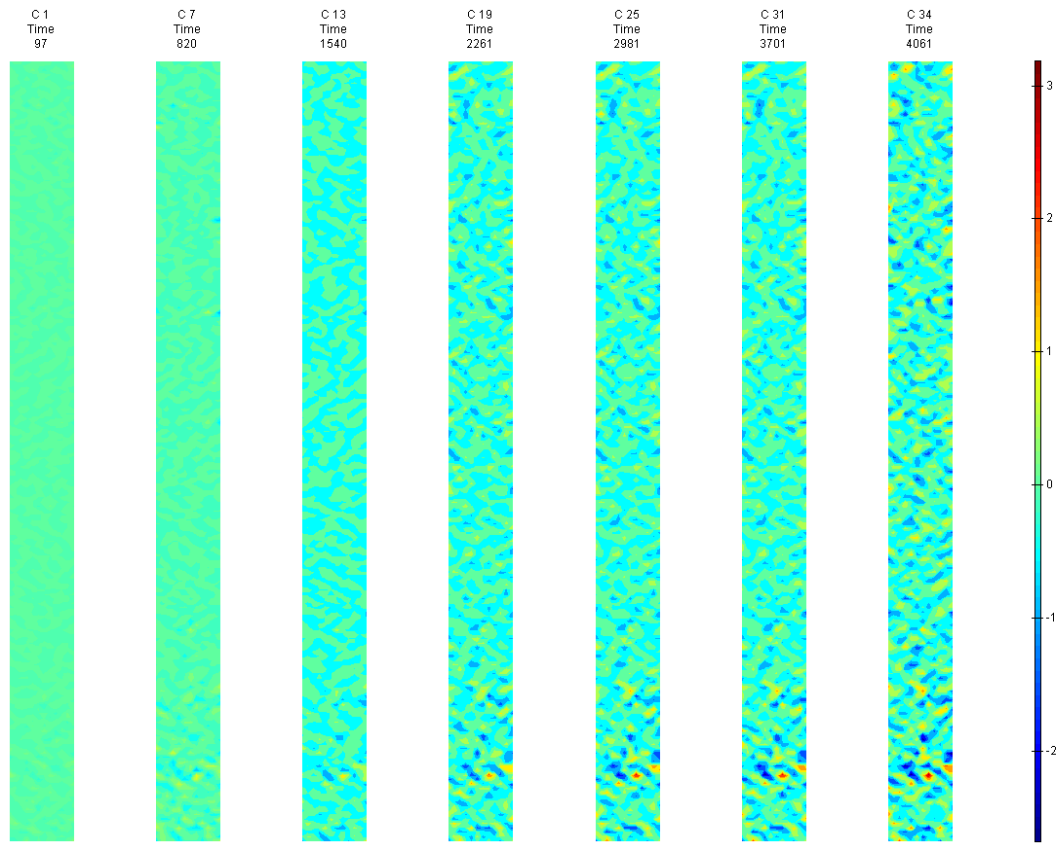

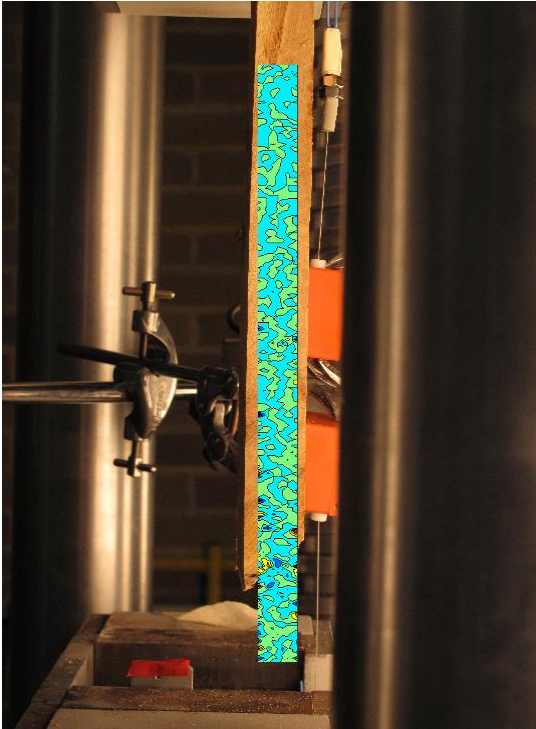FIGURE 575: XY DIRECTION PIV SEQUENTIAL TRUE SHEAR STRAIN OVER TIME

FIGURE 576: X DIRECTION PIV FIRST–LAST DITCH ENGINEERING STRAIN OVER IMAGE
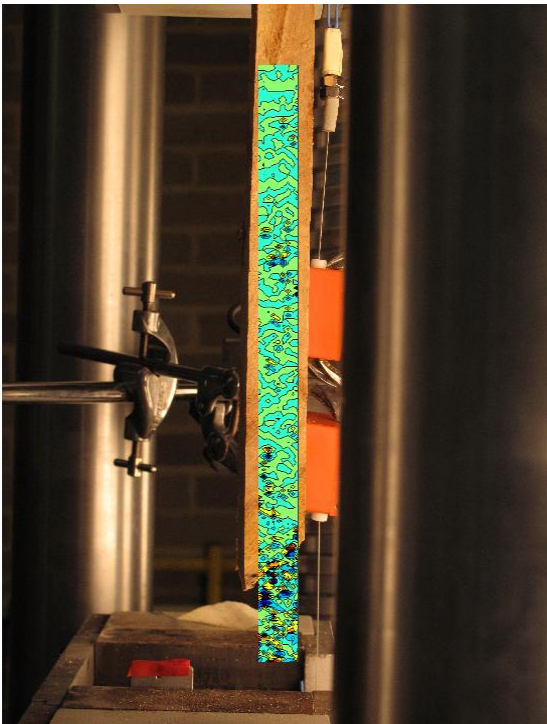

FIGURE 577: Y DIRECTION PIV FIRST–LAST DITCH ENGINEERING STRAIN OVER IMAGE

Appendix 6
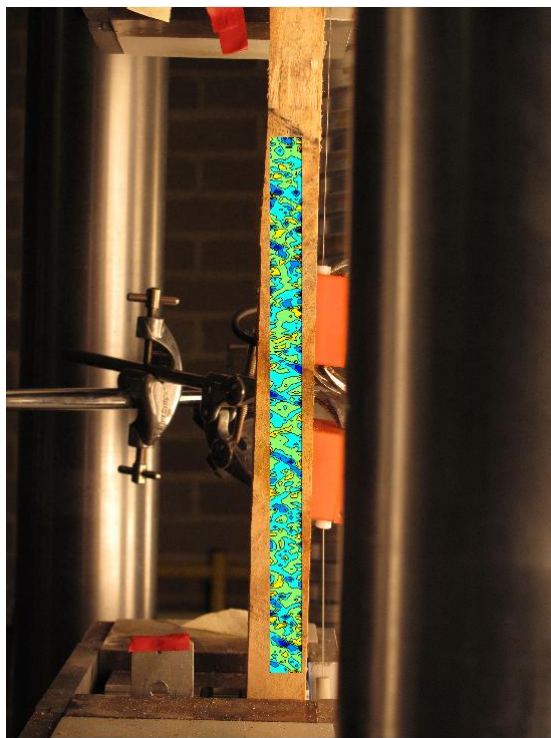
FIGURE 578: XY DIRECTION PIV FIRST–LAST DITCH ENGINEERING SHEAR STRAIN OVER
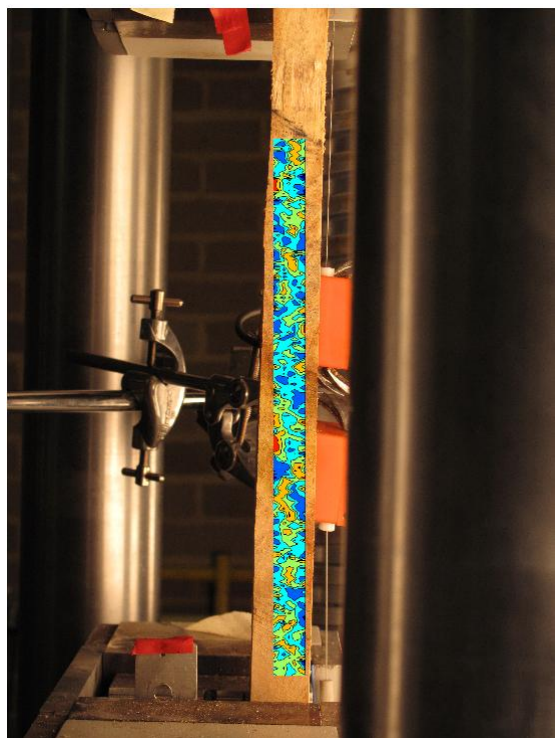
IMAGE

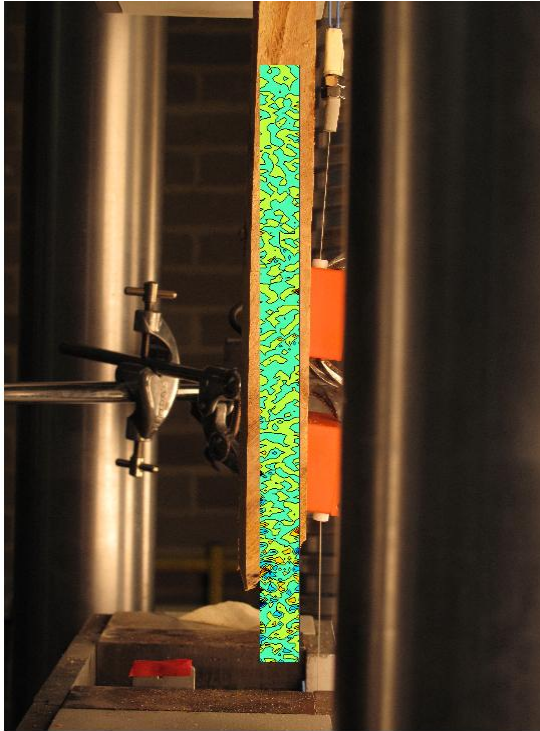
FIGURE 579: X DIRECTION PIV FIRST–LAST DITCH TRUE STRAIN OVER IMAGE
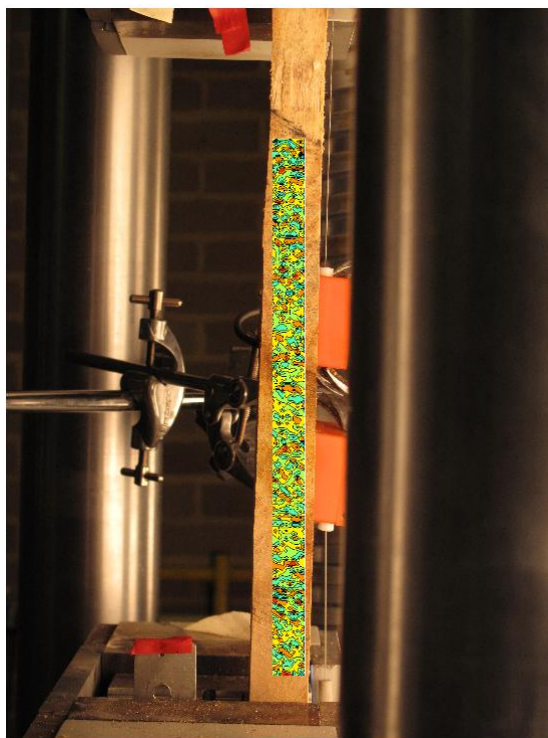
FIGURE 580: Y DIRECTION PIV FIRST–LAST DITCH TRUE STRAIN OVER IMAGE
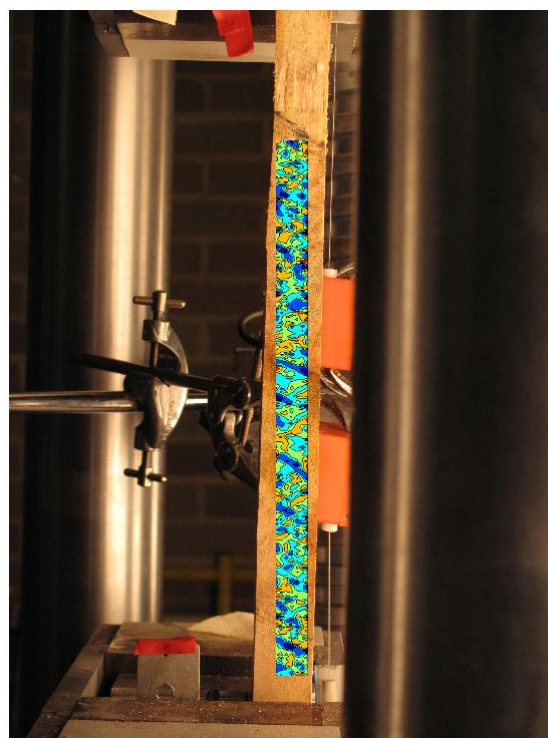
FIGURE 581: XY DIRECTION PIV FIRST–LAST DITCH TRUE SHEAR STRAIN OVER IMAGE

Appendix 6

FIGURE 582: XY DIRECTION PIV FIRST–SEQUENTIAL ENGINEERING SHEAR STRAIN OVER

IMAGE
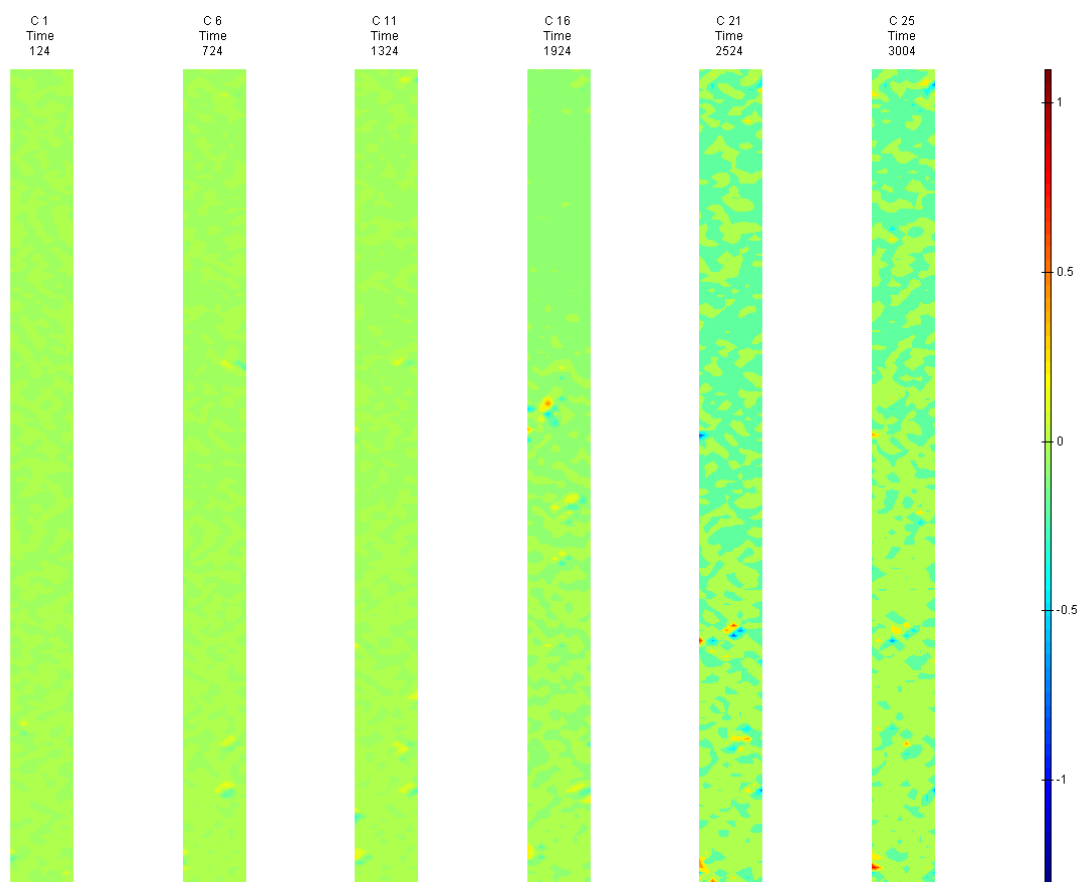
FIGURE 583: XY DIRECTION PIV FIRST–SEQUENTIAL ENGINEERING SHEAR STRAIN OVER TIME

Joint T
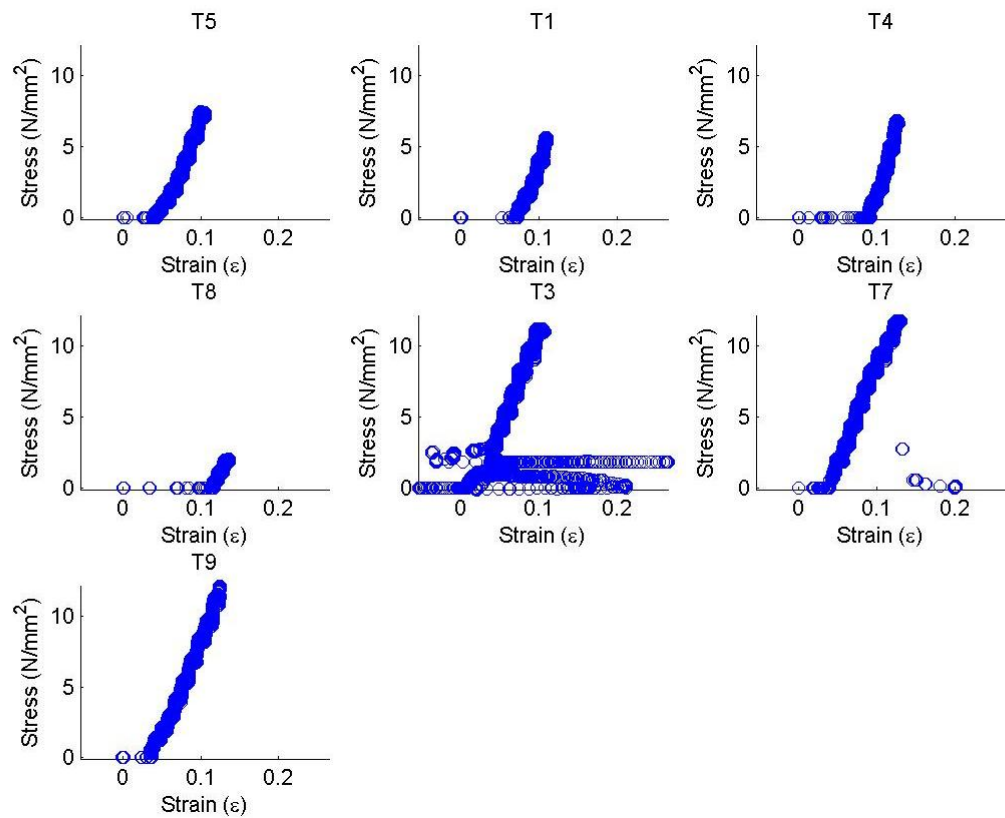
FIGURE 584: T COMPONENTS STRESS VS. MACHINE MEASURED STRAIN AT LOCATION
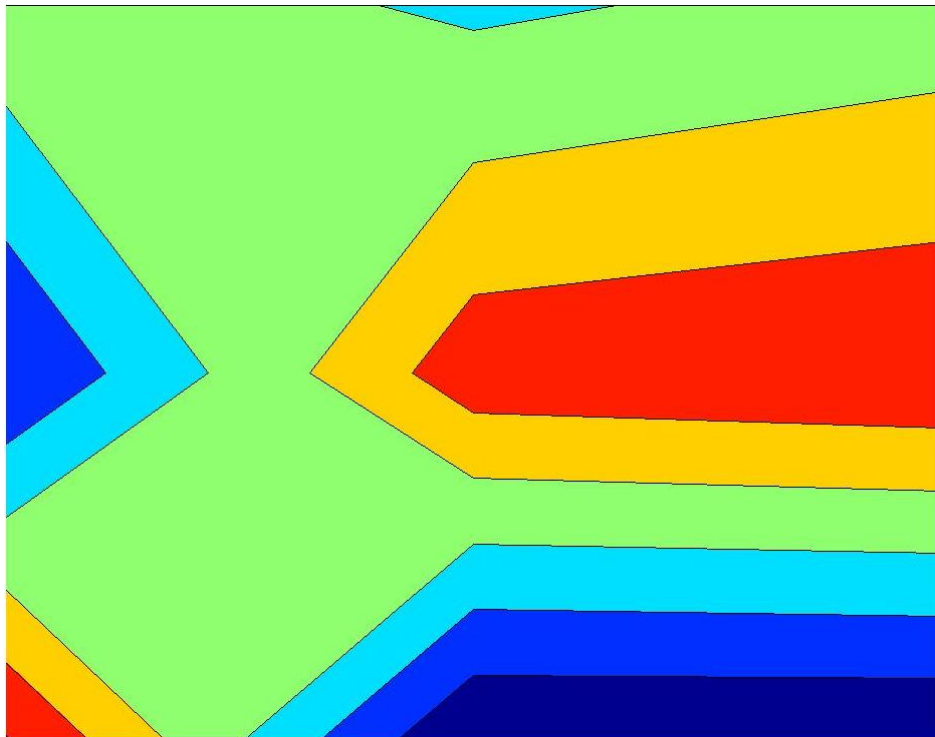
FIGURE 585: T COMPONENTS TENSILE STRESS AT LOCATION AS CONTOUR PLOT

Appendix 6
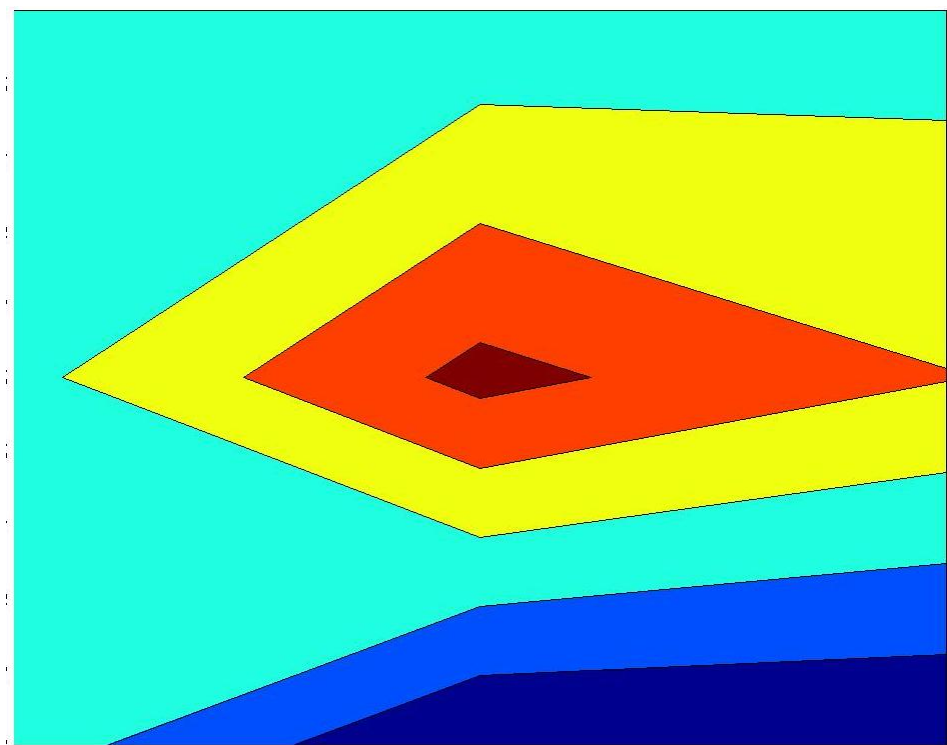
FIGURE 586: T COMPONENTS MACHINE MEASURED STRAIN AT LOCATION AS CONTOUR PLOT
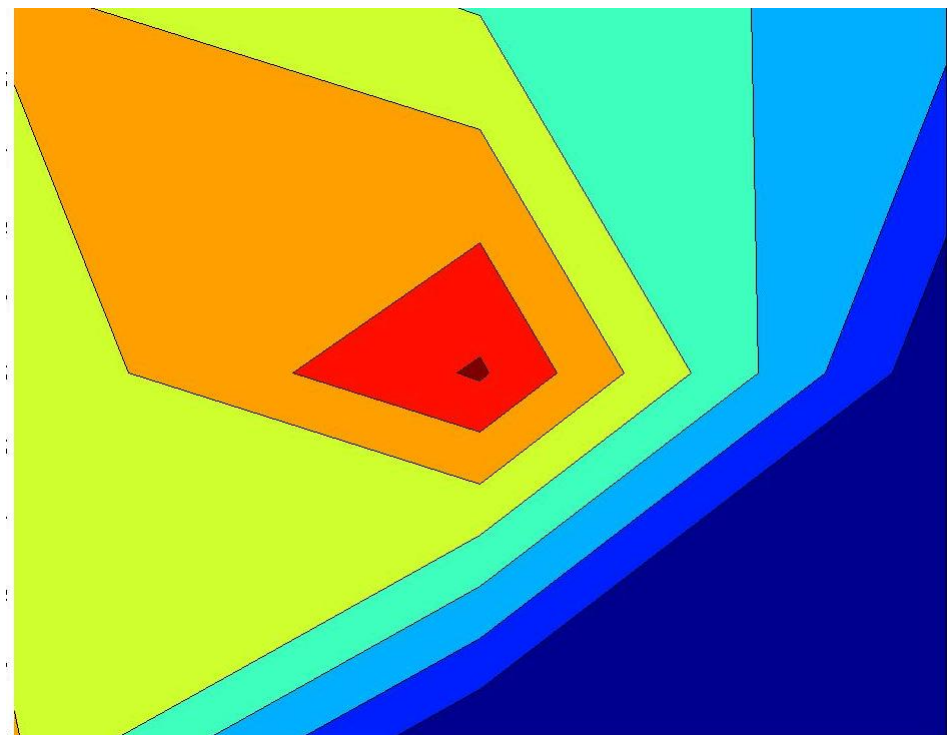
FIGURE 587: T COMPONENTS FRONT SEQUENTIAL STRAIN AT LOCATION AS CONTOUR PLOT
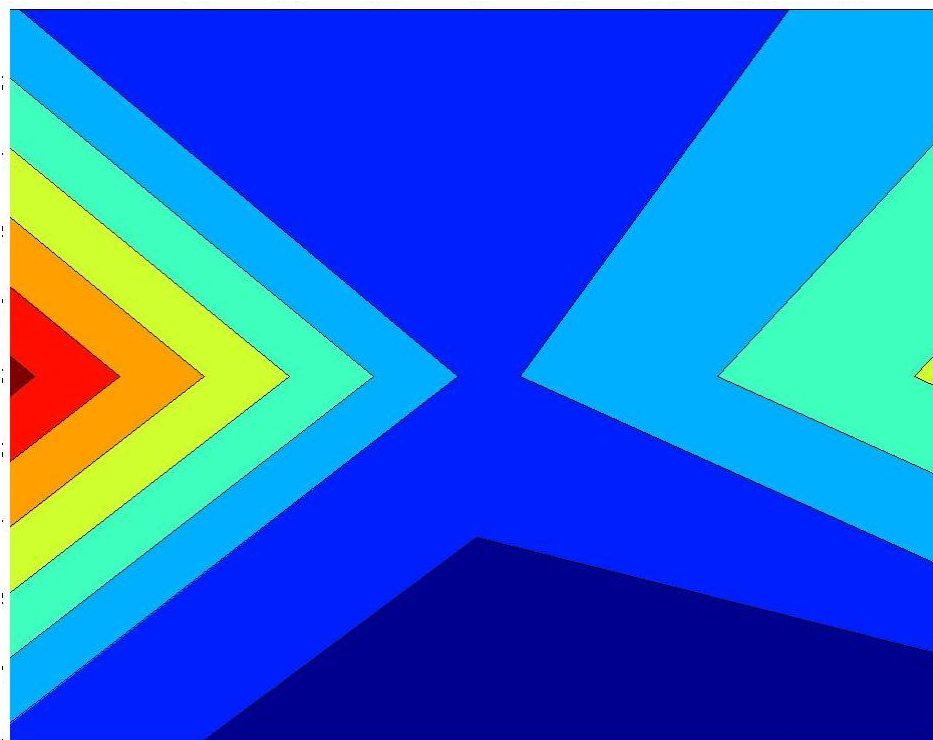
FIGURE 588: T COMPONENTS SIDE SEQUENTIAL STRAIN AT LOCATION AS CONTOUR PLOT
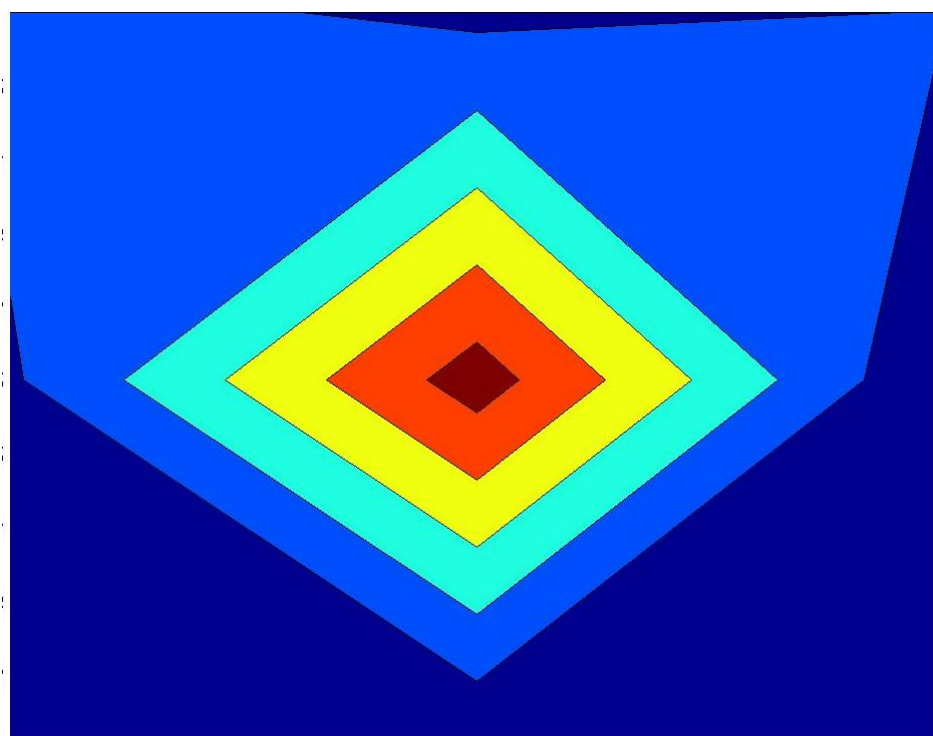
FIGURE 589: T COMPONENTS FRONT FIRST–SEQUENTIAL STRAIN AT LOCATION AS CONTOUR
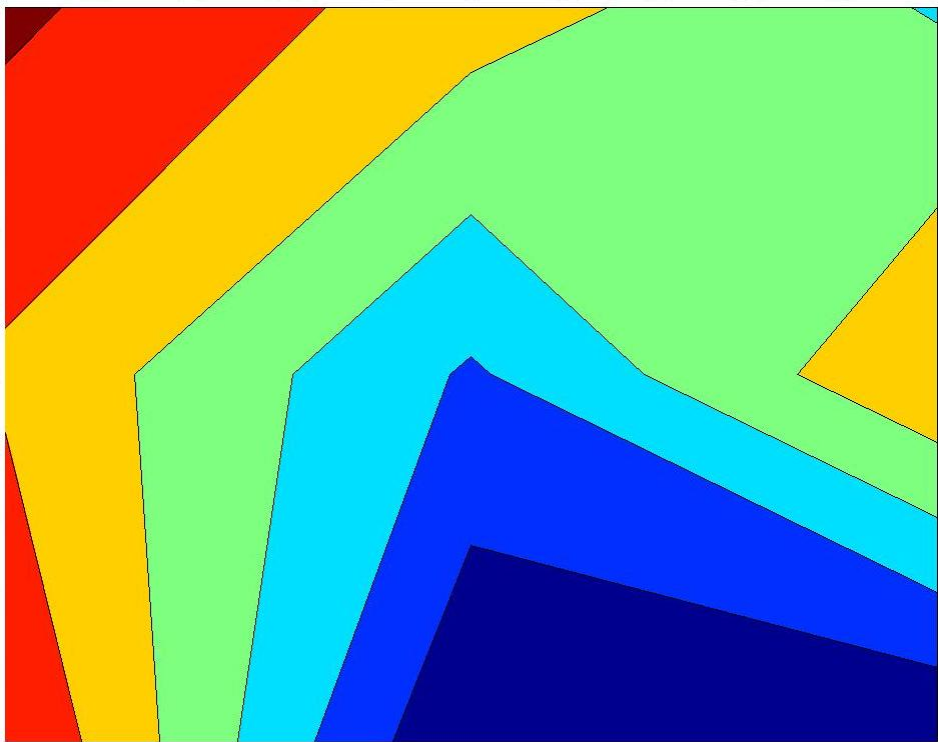
PLOT

Appendix 6

FIGURE 590: T COMPONENTS SIDE FIRST–SEQUENTIAL STRAIN AT LOCATION AS CONTOUR

PLOT

T1
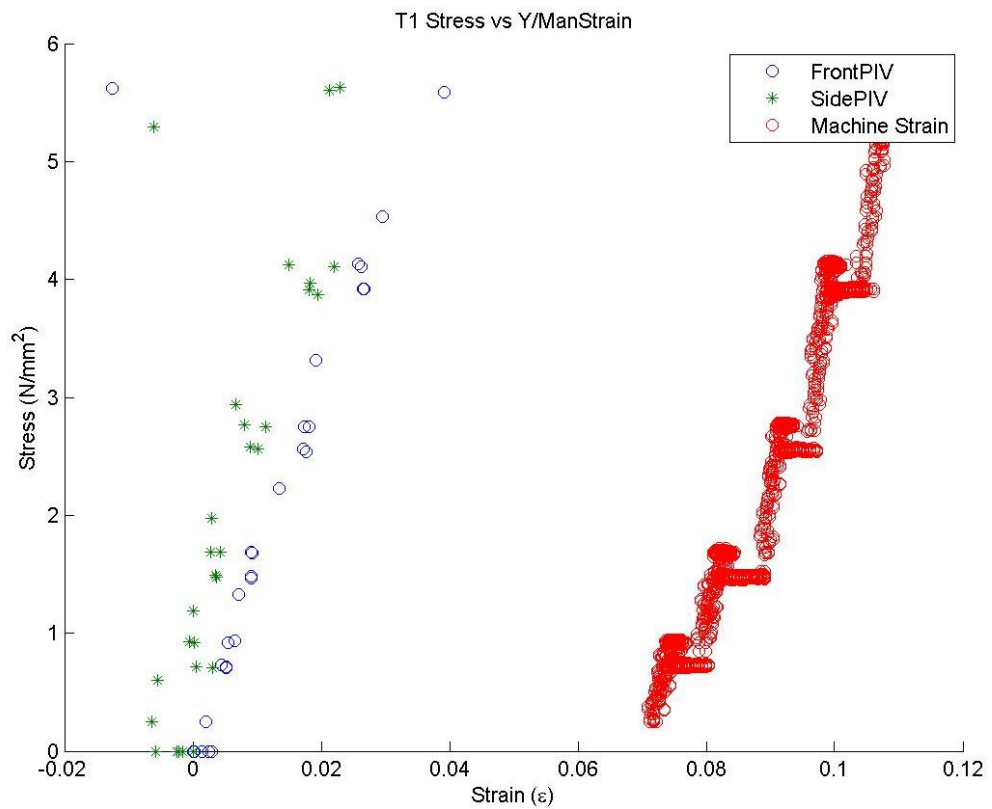
FIGURE 591: T1 TENSILE STRESS VS. MACHINE MEASURED/PIV STRAINS
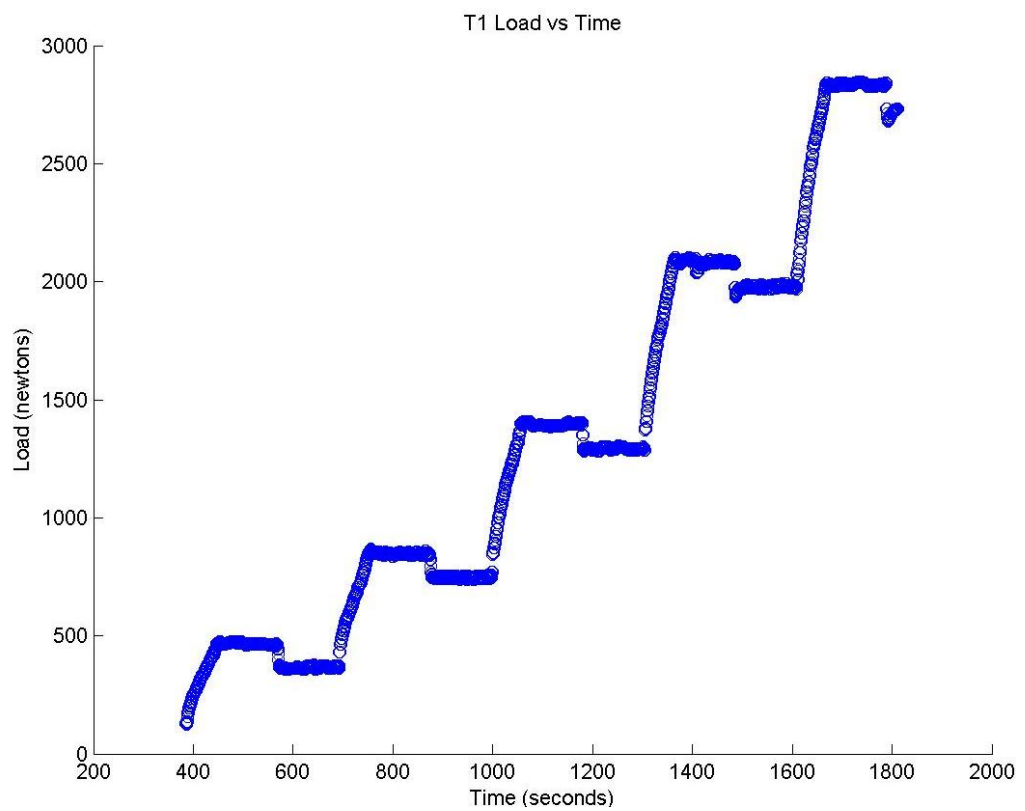
FIGURE 592: T1 TENSILE LOAD VS. TIME

FIGURE 593: T1 CREEP LOADING: INCREMENTS AND RELAXATION

FIGURE 594: T1 MACHINE MEASURED SECANT AND TANGENT MODULUS VS. TIME

FIGURE 595: T1 FRONT VIEW PIV SECANT AND TANGENT MODULUS VS. TIME

FIGURE 596: T1 SIDE VIEW PIV SECANT AND TANGENT MODULUS VS. TIME

Appendix 6

FIGURE 597: T1 COMPARISON OF MACHINE MEASURED AND PIV SECANT MODULUS VS. TIME

FIGURE 598: T1 COMPARISON OF MACHINE MEASURED AND PIV TANGENT MODULUS VS.

TIME

T1 Sample

FIGURE 599: SAMPLE GRAIN ORIENTATIONS OF THE FRONT (LEFT 4 IMAGES) AND SIDE (RIGHT 4 IMAGES) VIEW BEFORE (FIRST 2 OF 4 IMAGES) AND AFTER (LAST 2 OF 4 IMAGES) BREAKAGE

Appendix 6

T1 Front View
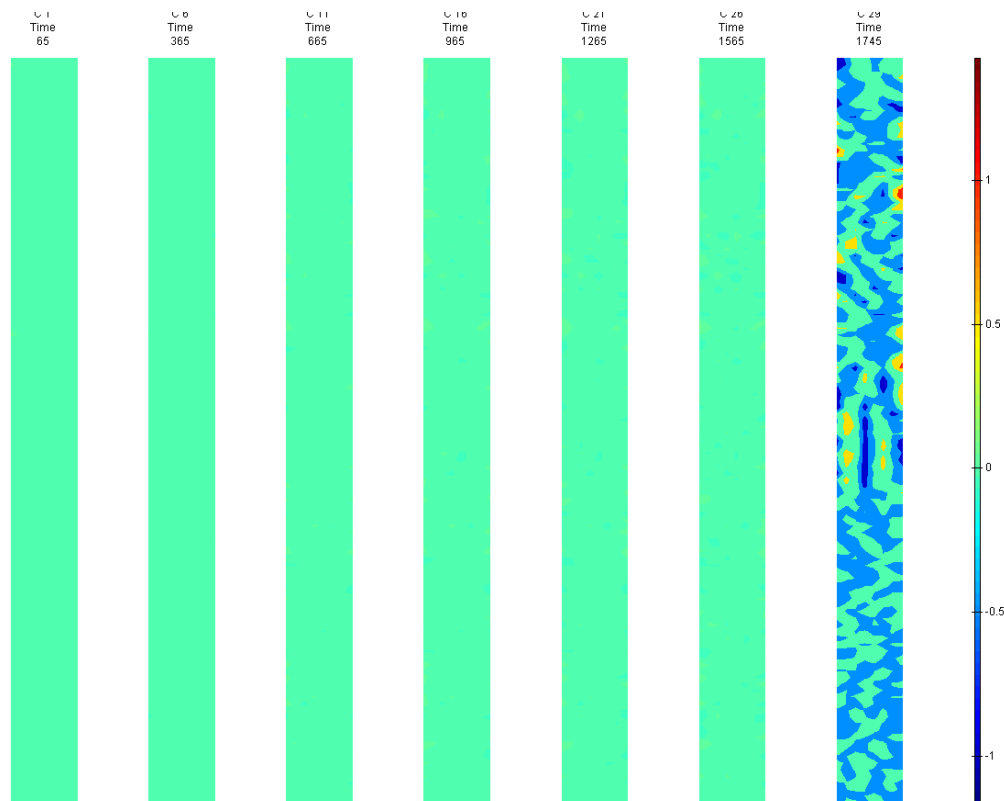
FIGURE 600: X DIRECTION PIV SEQUENTIAL ENGINEERING STRAIN OVER TIME

FIGURE 601: Y DIRECTION PIV SEQUENTIAL ENGINEERING STRAIN OVER TIME
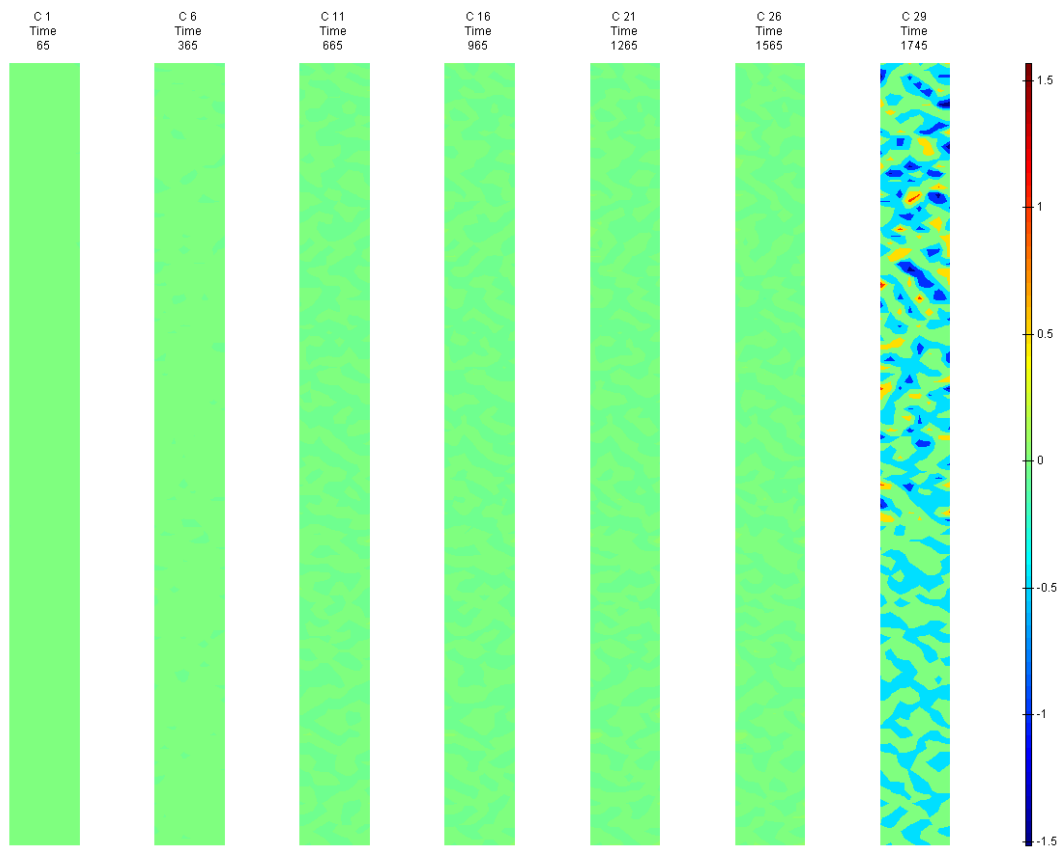
FIGURE 602: XY DIRECTION PIV SEQUENTIAL ENGINEERING SHEAR STRAIN OVER TIME

FIGURE 603: X DIRECTION PIV SEQUENTIAL TRUE STRAIN OVER TIME

FIGURE 604: Y DIRECTION PIV SEQUENTIAL TRUE STRAIN OVER TIME

FIGURE 605: XY DIRECTION PIV SEQUENTIAL TRUE SHEAR STRAIN OVER TIME

FIGURE 606: X DIRECTION PIV FIRST–LAST DITCH ENGINEERING STRAIN OVER IMAGE

FIGURE 607: Y DIRECTION PIV FIRST–LAST DITCH ENGINEERING STRAIN OVER IMAGE

Appendix 6

FIGURE 608: XY DIRECTION PIV FIRST–LAST DITCH ENGINEERING SHEAR STRAIN OVER

IMAGE

FIGURE 609: X DIRECTION PIV FIRST–LAST DITCH TRUE STRAIN OVER IMAGE

FIGURE 610: Y DIRECTION PIV FIRST–LAST DITCH TRUE STRAIN OVER IMAGE

FIGURE 611: XY DIRECTION PIV FIRST–LAST DITCH TRUE SHEAR STRAIN OVER IMAGE

FIGURE 612: XY DIRECTION PIV FIRST-SEQUENTIAL ENGINEERING SHEAR STRAIN OVER

IMAGE
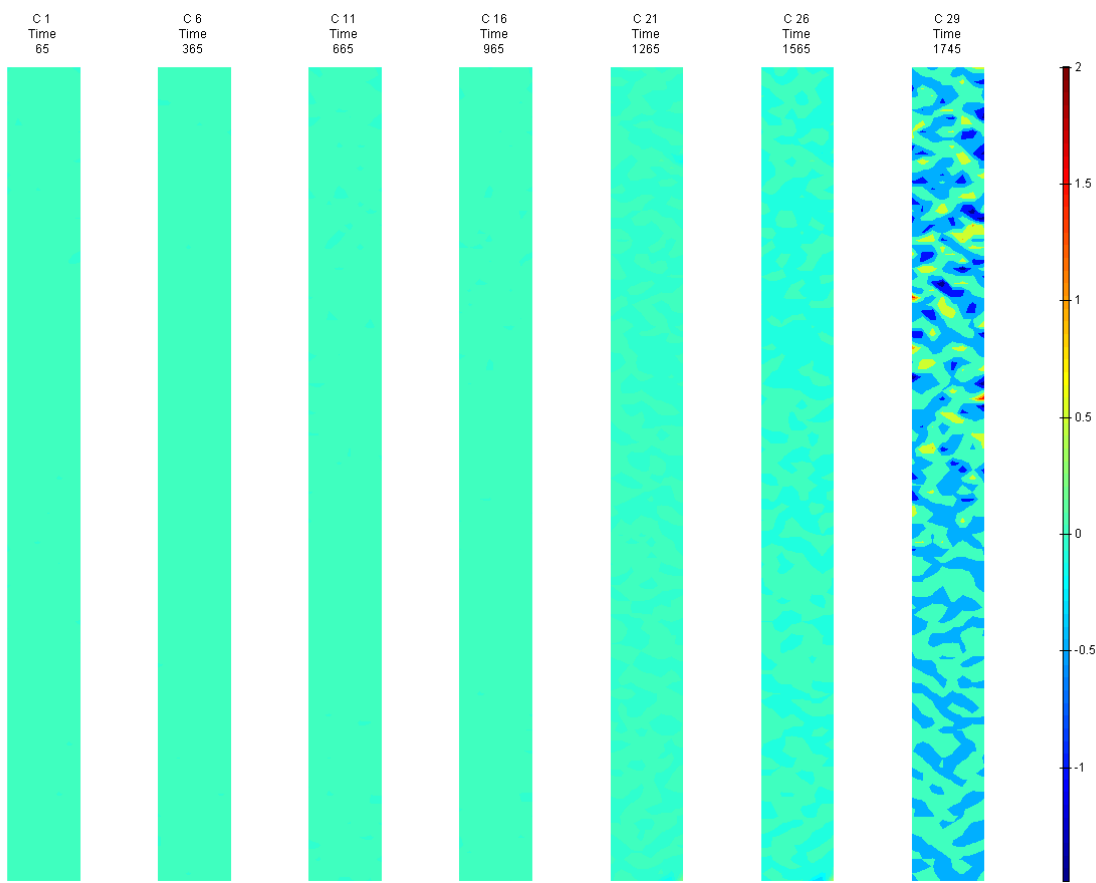
FIGURE 613: XY DIRECTION PIV FIRST-SEQUENTIAL ENGINEERING SHEAR STRAIN OVER TIME

T1 Side View

FIGURE 614: X DIRECTION PIV SEQUENTIAL ENGINEERING STRAIN OVER TIME

FIGURE 615: Y DIRECTION PIV SEQUENTIAL ENGINEERING STRAIN OVER TIME
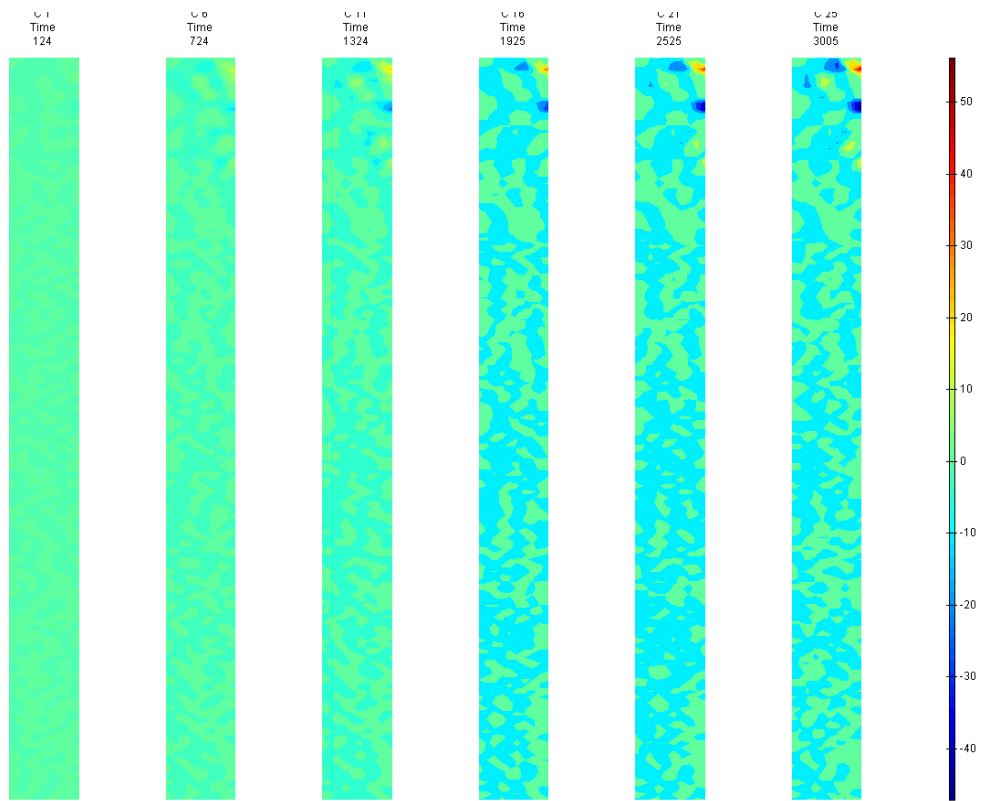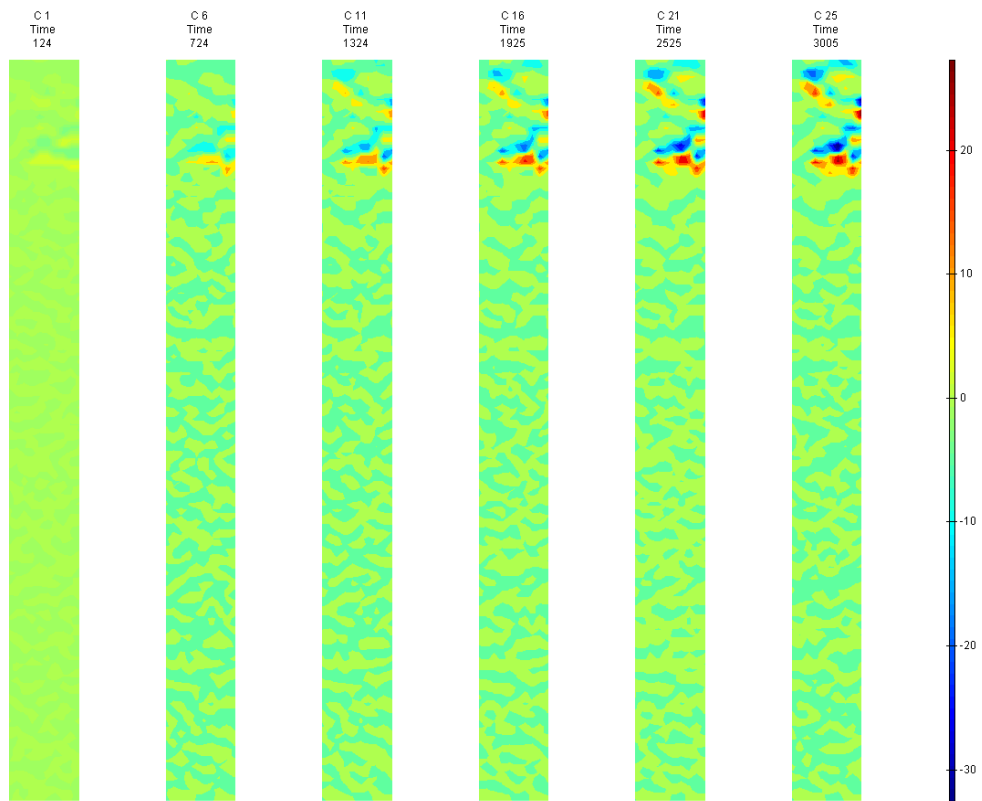
Appendix 6

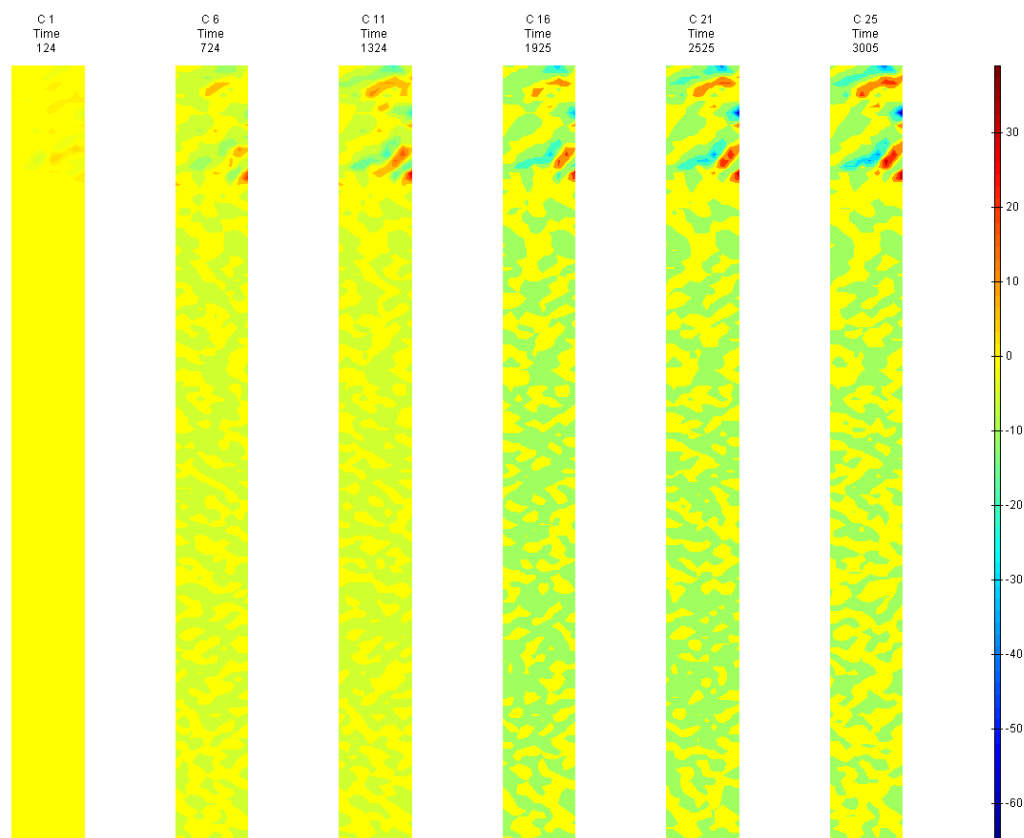FIGURE 616: XY DIRECTION PIV SEQUENTIAL ENGINEERING SHEAR STRAIN OVER TIME

FIGURE 617: X DIRECTION PIV SEQUENTIAL TRUE STRAIN OVER TIME

FIGURE 618: Y DIRECTION PIV SEQUENTIAL TRUE STRAIN OVER TIME

FIGURE 619: XY DIRECTION PIV SEQUENTIAL TRUE SHEAR STRAIN OVER TIME

FIGURE 620: X DIRECTION PIV FIRST–LAST DITCH ENGINEERING STRAIN OVER IMAGE

FIGURE 621: Y DIRECTION PIV FIRST–LAST DITCH ENGINEERING STRAIN OVER IMAGE

FIGURE 622: XY DIRECTION PIV FIRST–LAST DITCH ENGINEERING SHEAR STRAIN OVER

IMAGE

FIGURE 623: X DIRECTION PIV FIRST–LAST DITCH TRUE STRAIN OVER IMAGE

FIGURE 624: Y DIRECTION PIV FIRST−LAST DITCH TRUE STRAIN OVER IMAGE

FIGURE 625: XY DIRECTION PIV FIRST−LAST DITCH TRUE SHEAR STRAIN OVER IMAGE

FIGURE 626: XY DIRECTION PIV FIRST–SEQUENTIAL ENGINEERING SHEAR STRAIN OVER

IMAGE

FIGURE 627: XY DIRECTION PIV FIRST–SEQUENTIAL ENGINEERING SHEAR STRAIN OVER TIME

Appendix 6

T3
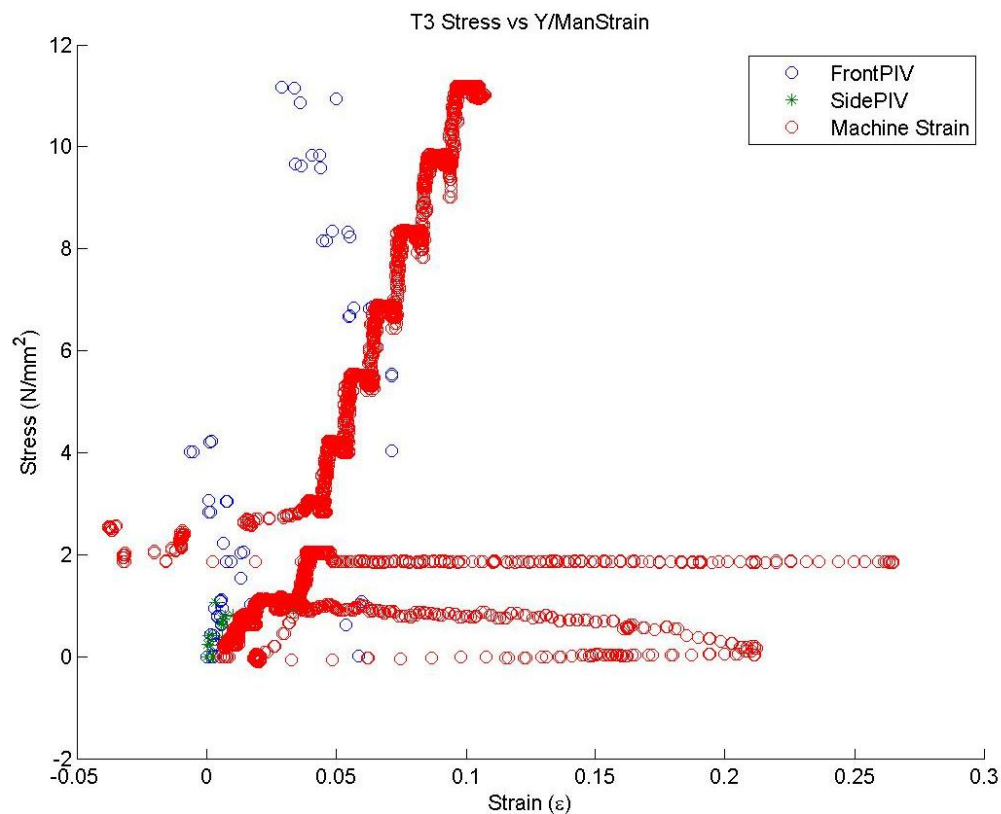
FIGURE 628: T3 TENSILE STRESS VS. MACHINE MEASURED/PIV STRAINS
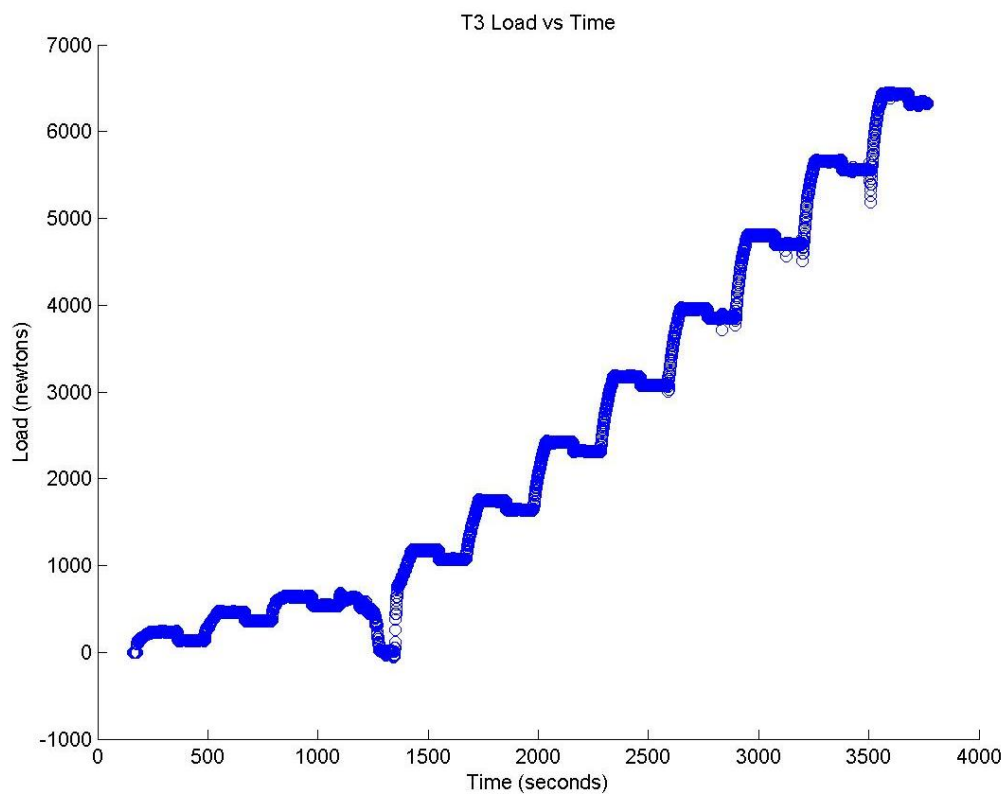
FIGURE 629: T3 TENSILE LOAD VS. TIME

FIGURE 630: T3 CREEP LOADING: INCREMENTS AND RELAXATION

FIGURE 631: T3 MACHINE MEASURED SECANT AND TANGENT MODULUS VS. TIME

Appendix 6
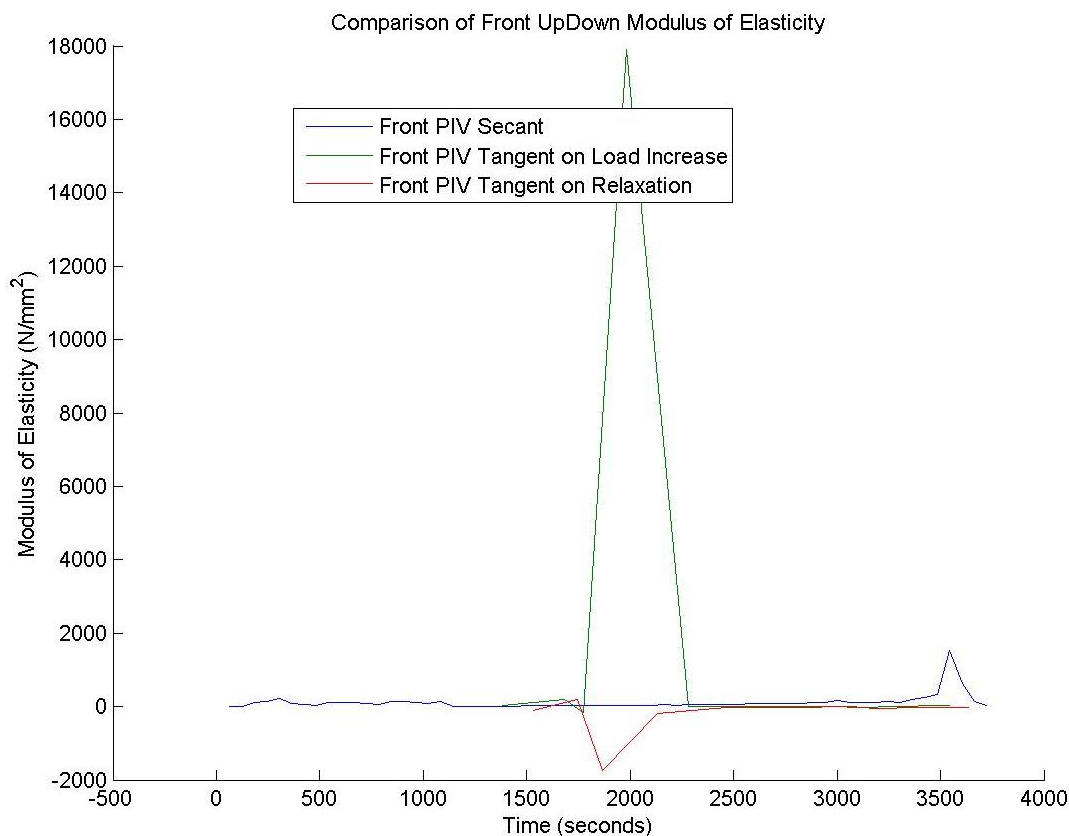
FIGURE 632: T3 FRONT VIEW PIV SECANT AND TANGENT MODULUS VS. TIME
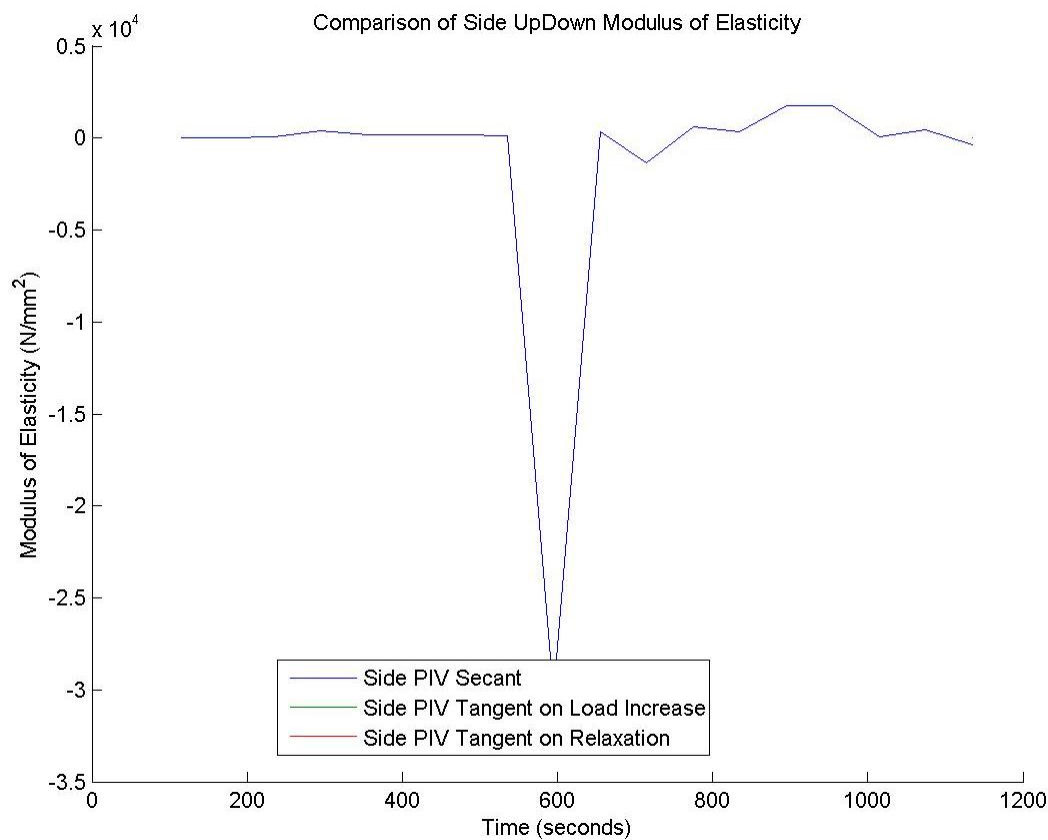
FIGURE 633: T3 SIDE VIEW PIV SECANT AND TANGENT MODULUS VS. TIME
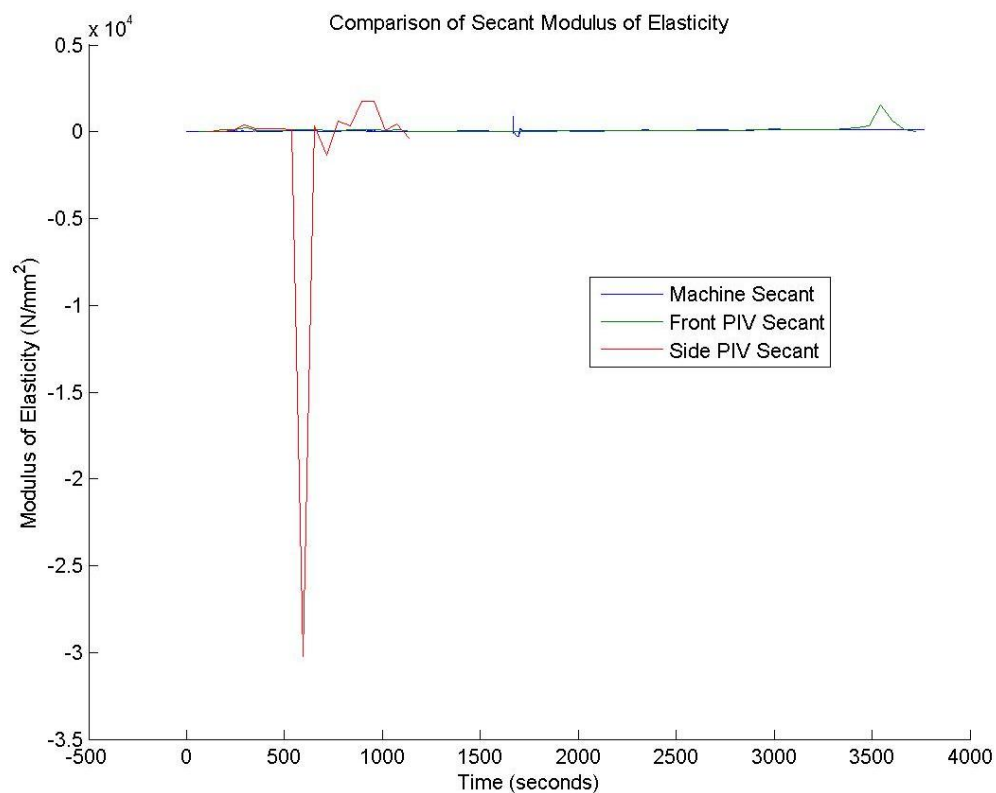
FIGURE 634: T3 COMPARISON OF MACHINE MEASURED AND PIV SECANT MODULUS VS. TIME
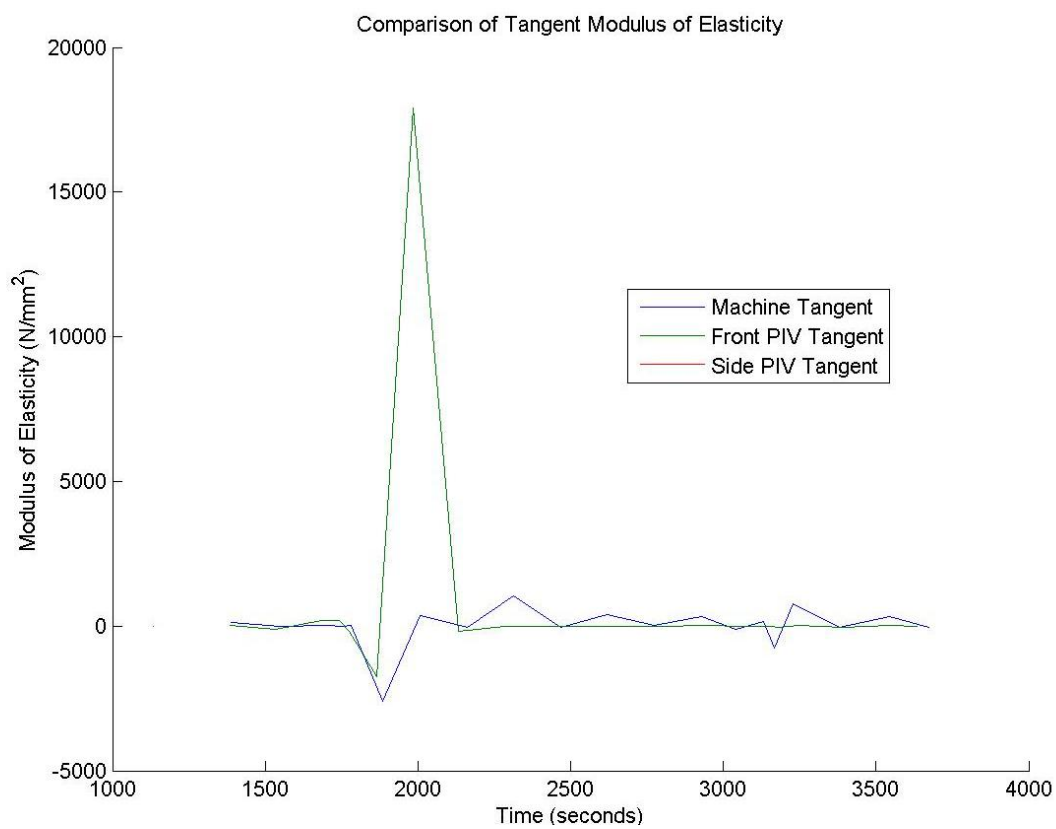
FIGURE 635: T3 COMPARISON OF MACHINE MEASURED AND PIV TANGENT MODULUS VS.

TIME

Appendix 6

T3 Sample

FIGURE 636: SAMPLE GRAIN ORIENTATIONS OF THE FRONT (LEFT 4 IMAGES) AND SIDE (RIGHT 4 IMAGES) VIEW BEFORE (FIRST 2 OF 4 IMAGES) AND AFTER (LAST 2 OF 4 IMAGES) BREAKAGE

T3 Front View

FIGURE 637: X DIRECTION PIV SEQUENTIAL ENGINEERING STRAIN OVER TIME

FIGURE 638: Y DIRECTION PIV SEQUENTIAL ENGINEERING STRAIN OVER TIME

Appendix 6

FIGURE 639: XY DIRECTION PIV SEQUENTIAL ENGINEERING SHEAR STRAIN OVER TIME

FIGURE 640: X DIRECTION PIV SEQUENTIAL TRUE STRAIN OVER TIME

FIGURE 641: Y DIRECTION PIV SEQUENTIAL TRUE STRAIN OVER TIME

FIGURE 642: XY DIRECTION PIV SEQUENTIAL TRUE SHEAR STRAIN OVER TIME

FIGURE 643: X DIRECTION PIV FIRST-LAST DITCH ENGINEERING STRAIN OVER IMAGE

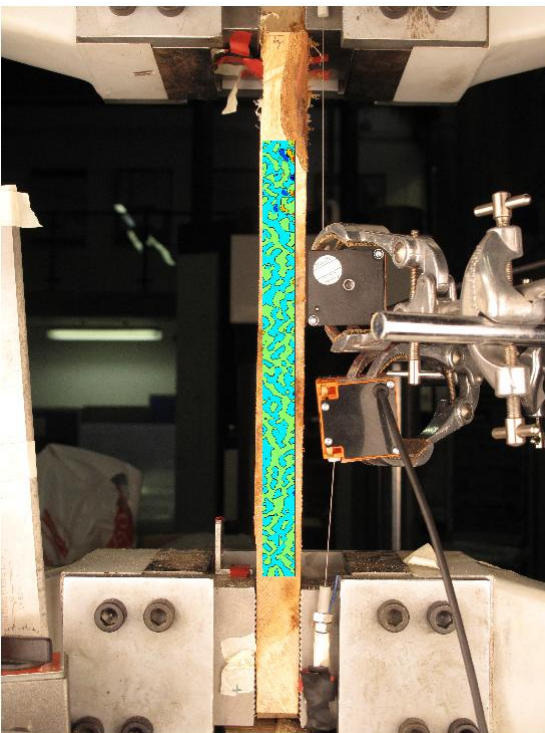FIGURE 644: Y DIRECTION PIV FIRST-LAST DITCH ENGINEERING STRAIN OVER IMAGE
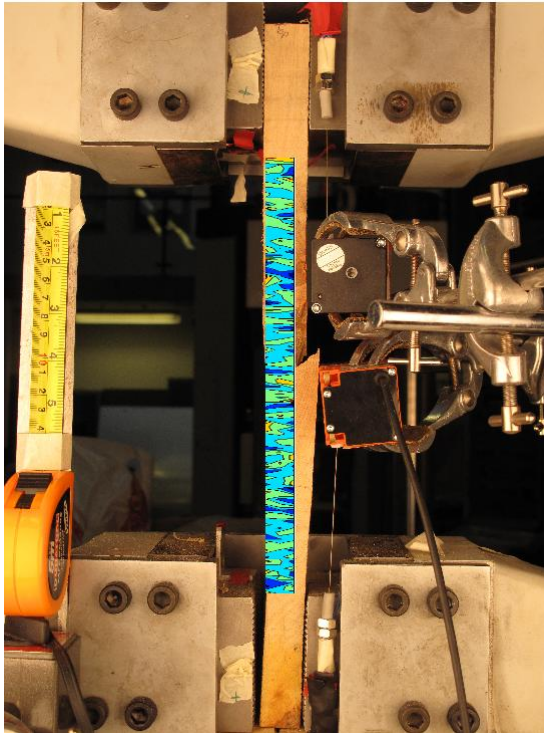
FIGURE 645: XY DIRECTION PIV FIRST–LAST DITCH ENGINEERING SHEAR STRAIN OVER
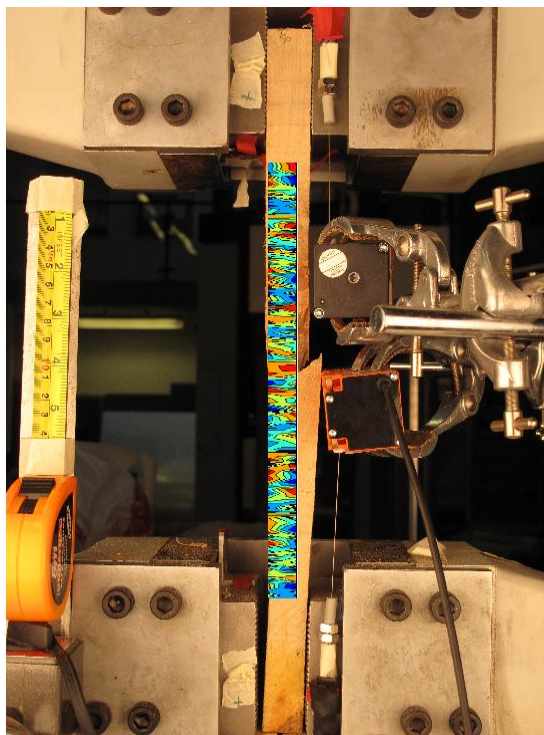
IMAGE

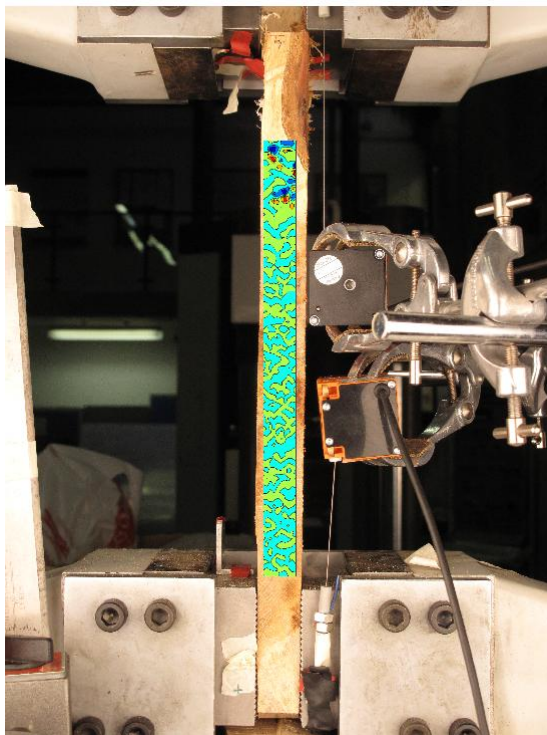FIGURE 646: X DIRECTION PIV FIRST–LAST DITCH TRUE STRAIN OVER IMAGE
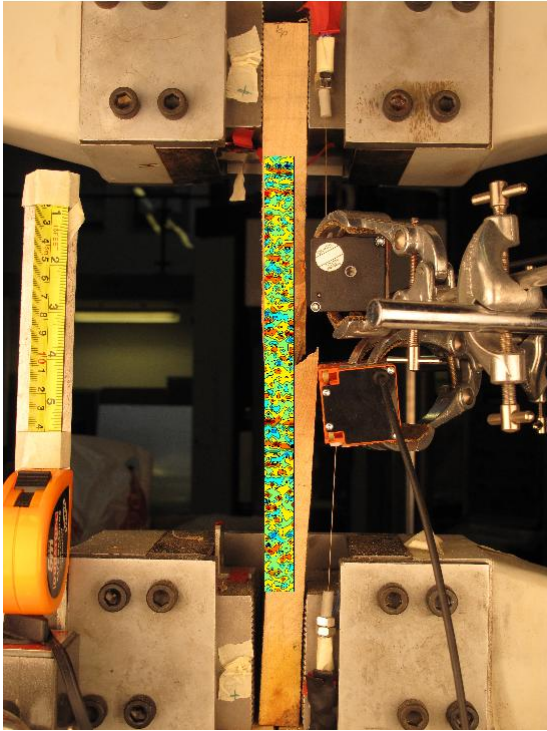
FIGURE 647: Y DIRECTION PIV FIRST–LAST DITCH TRUE STRAIN OVER IMAGE
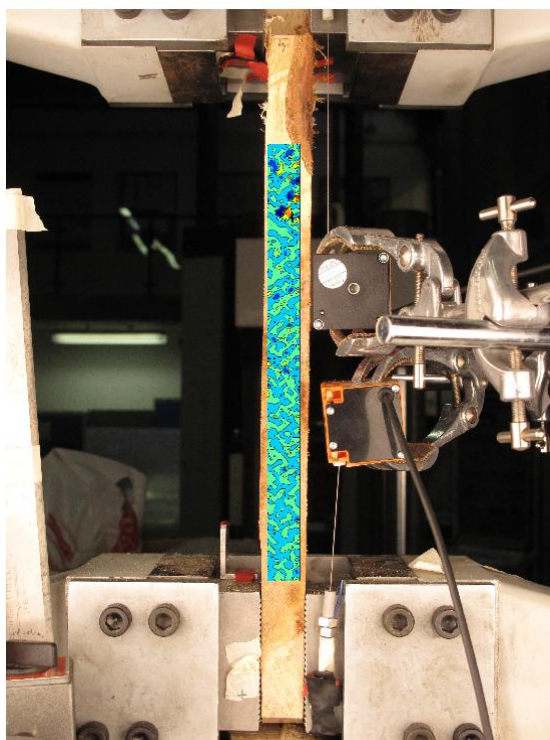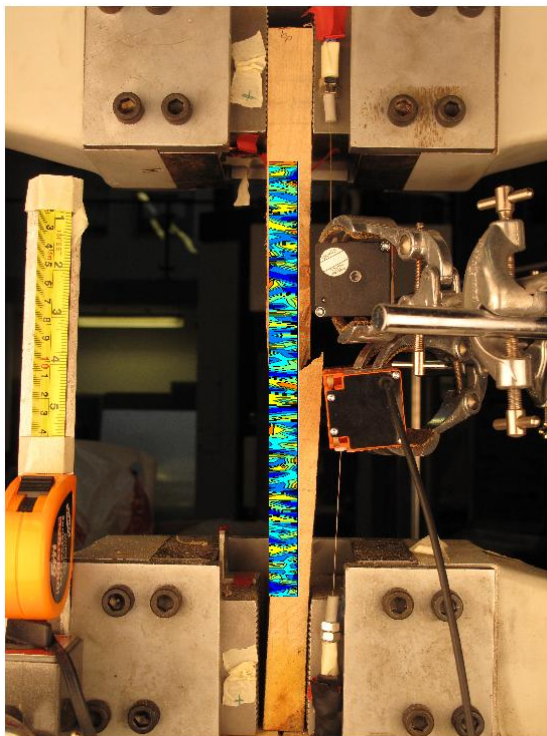

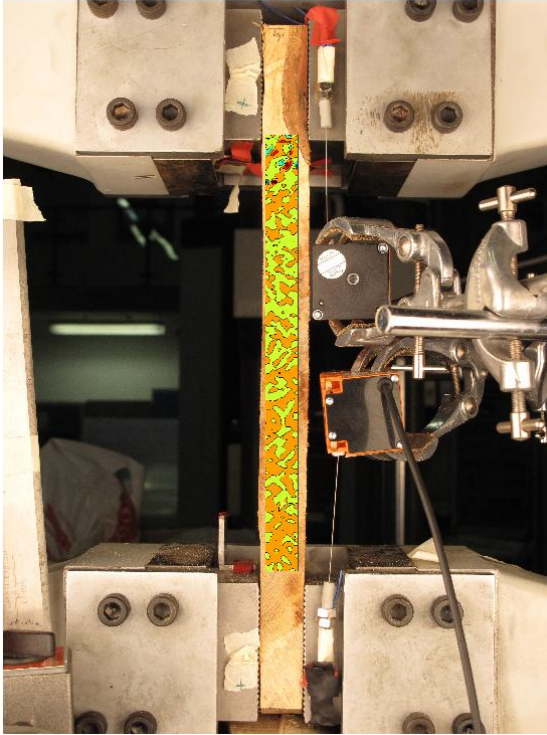FIGURE 648: XY DIRECTION PIV FIRST–LAST DITCH TRUE SHEAR STRAIN OVER IMAGE

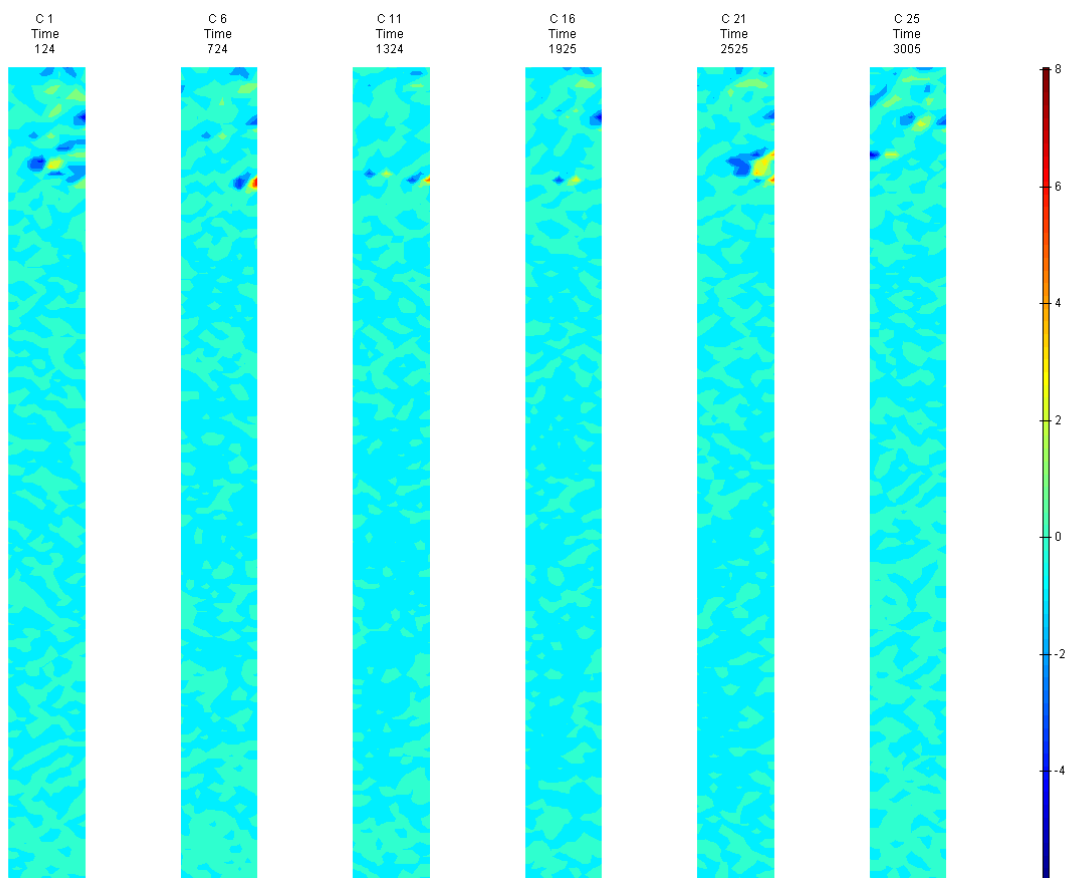FIGURE 649: XY DIRECTION PIV FIRST–SEQUENTIAL ENGINEERING SHEAR STRAIN OVER

IMAGE

FIGURE 650: XY DIRECTION PIV FIRST–SEQUENTIAL ENGINEERING SHEAR STRAIN OVER TIME
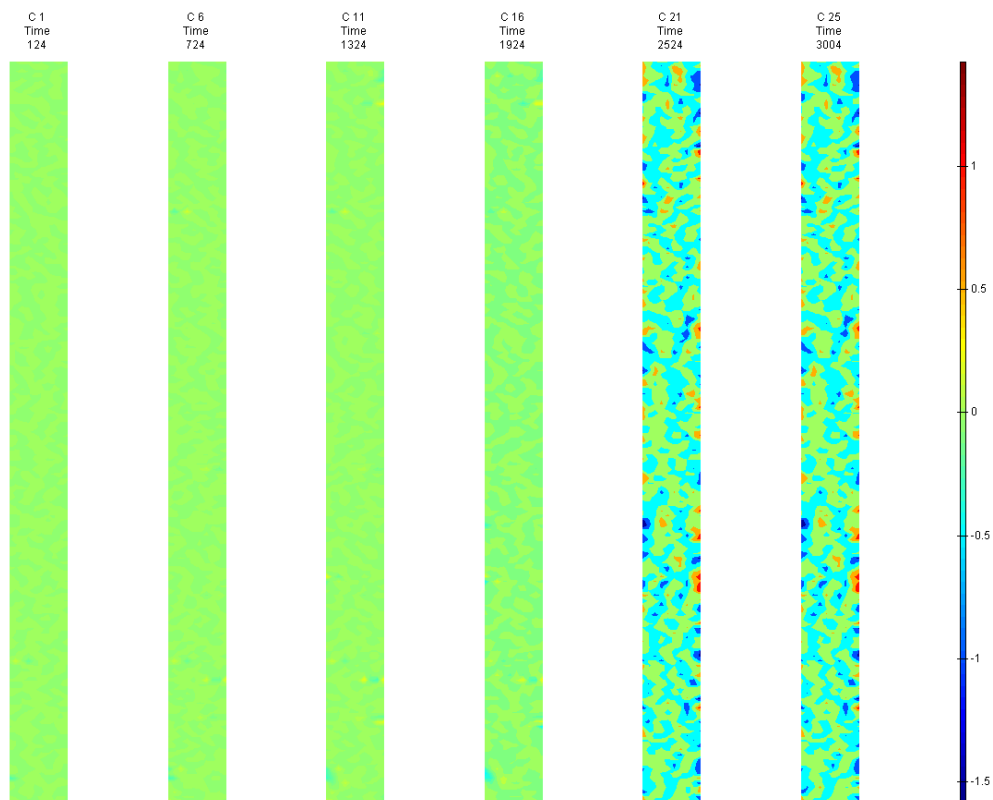
Appendix 6

T3 Side

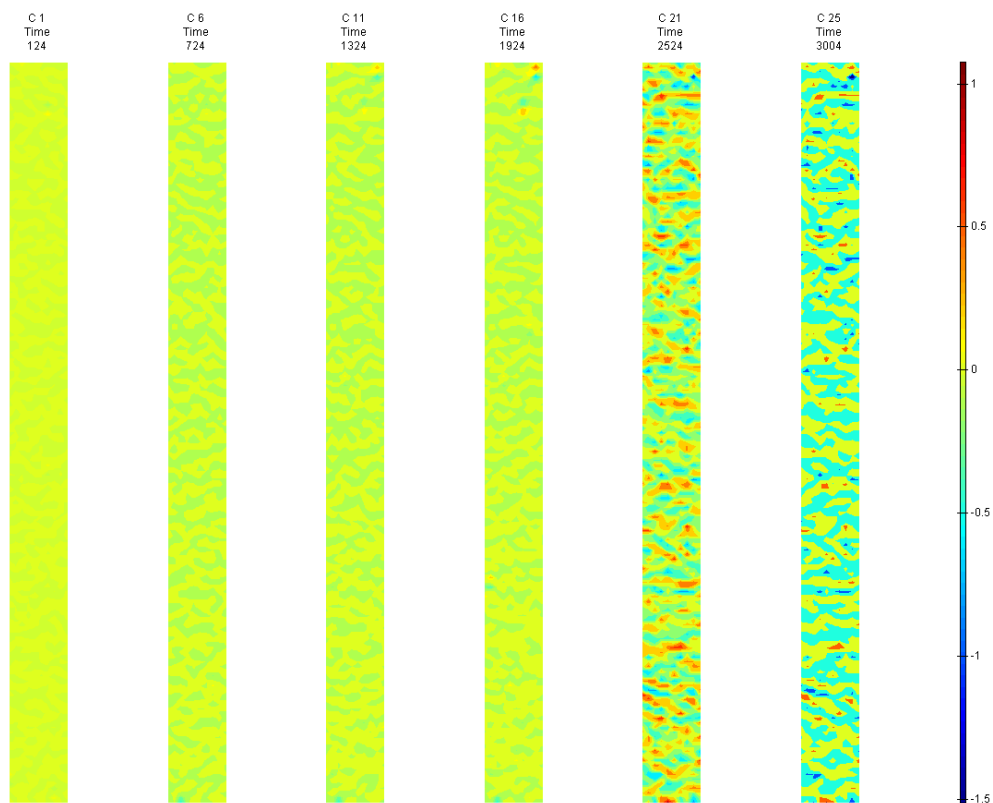FIGURE 651: X DIRECTION PIV SEQUENTIAL ENGINEERING STRAIN OVER TIME

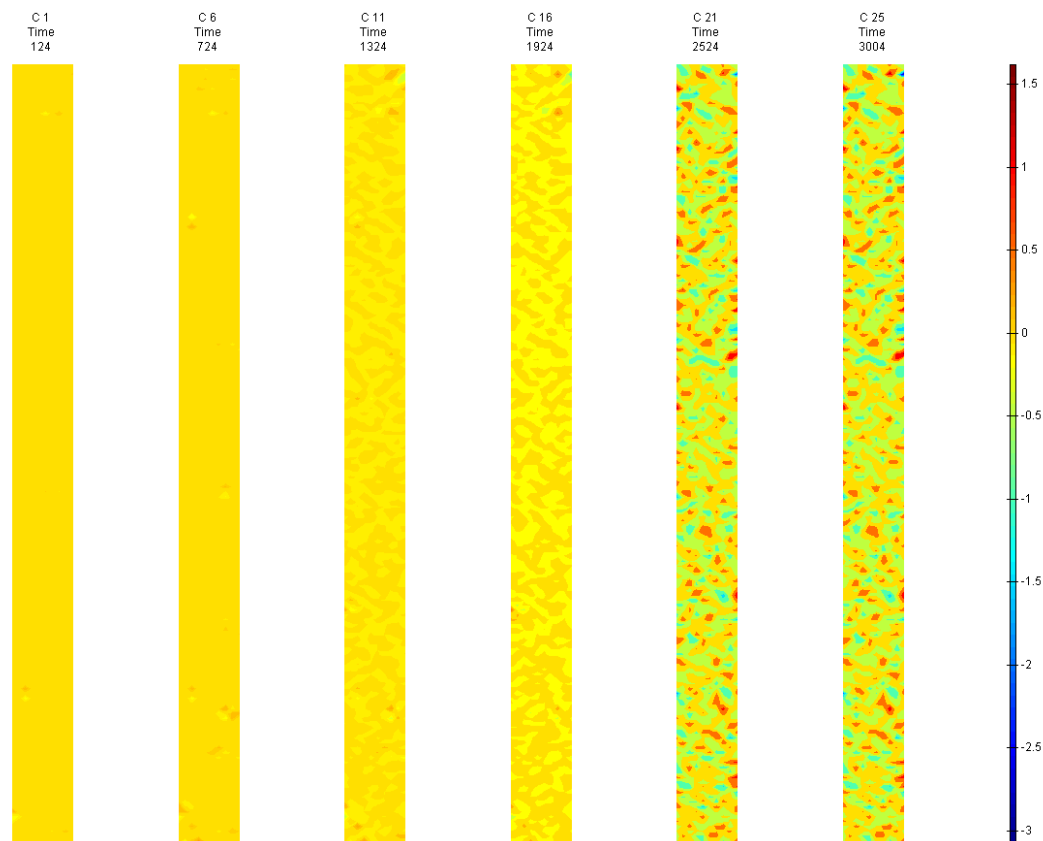FIGURE 652: Y DIRECTION PIV SEQUENTIAL ENGINEERING STRAIN OVER TIME

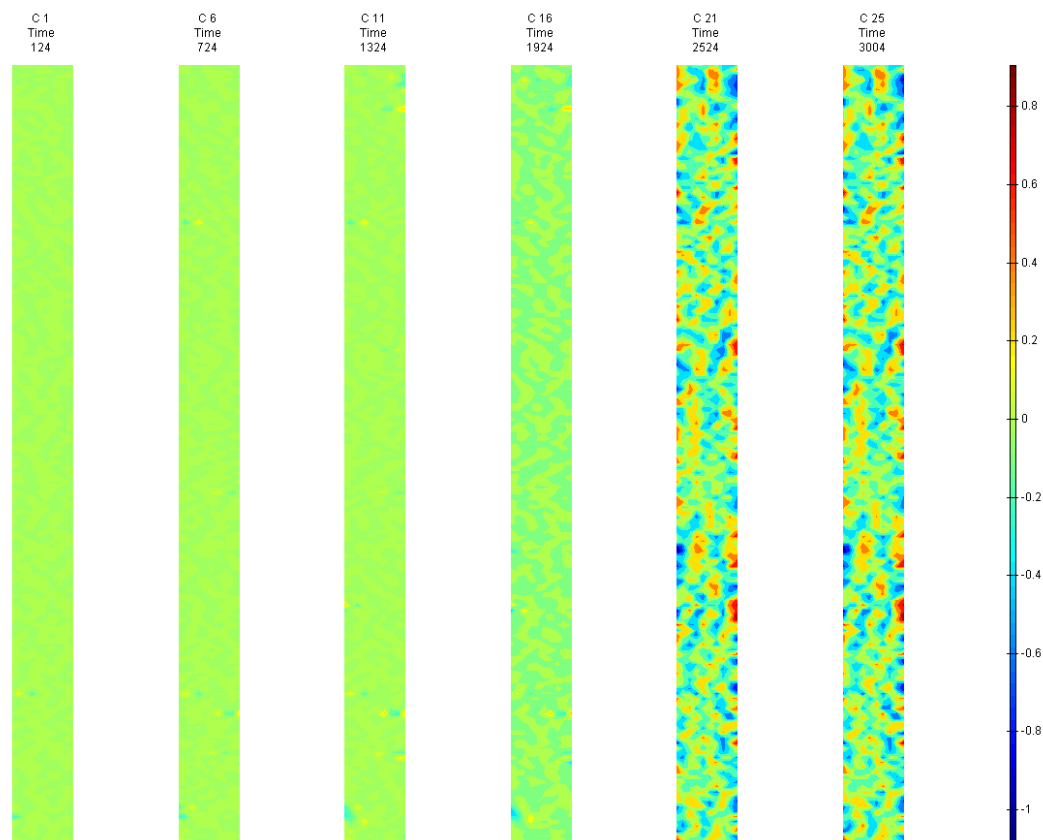FIGURE 653: XY DIRECTION PIV SEQUENTIAL ENGINEERING SHEAR STRAIN OVER TIME

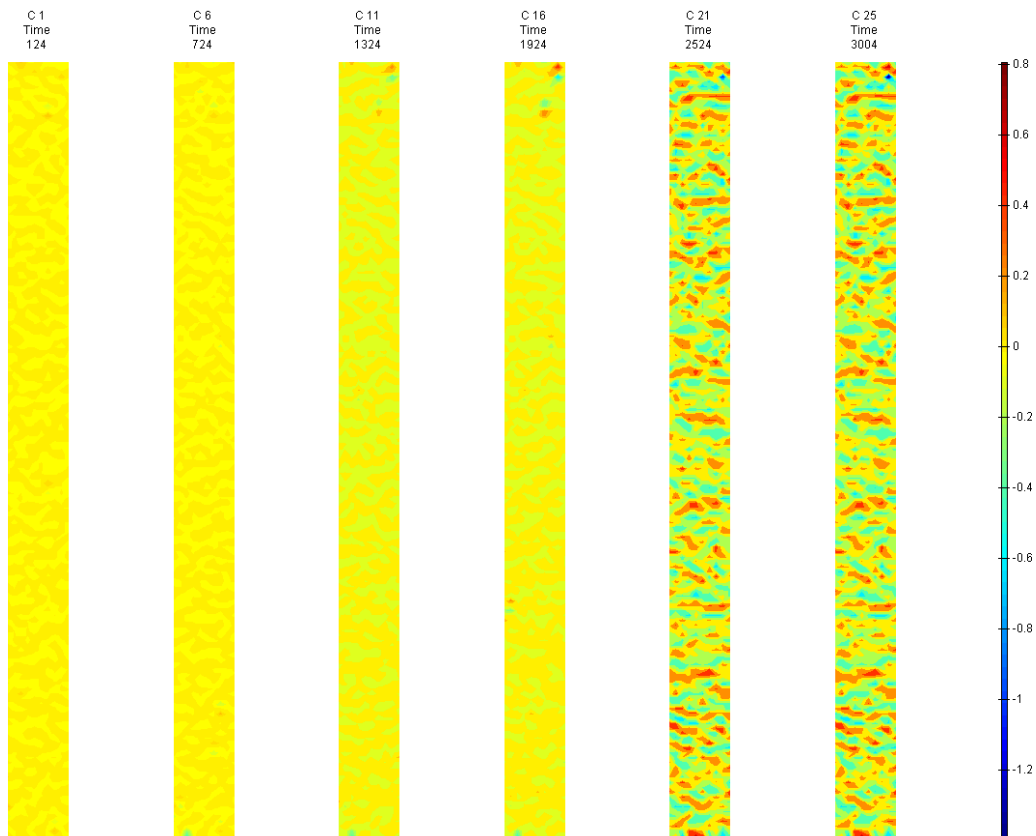FIGURE 654: X DIRECTION PIV SEQUENTIAL TRUE STRAIN OVER TIME

FIGURE 655: Y DIRECTION PIV SEQUENTIAL TRUE STRAIN OVER TIME
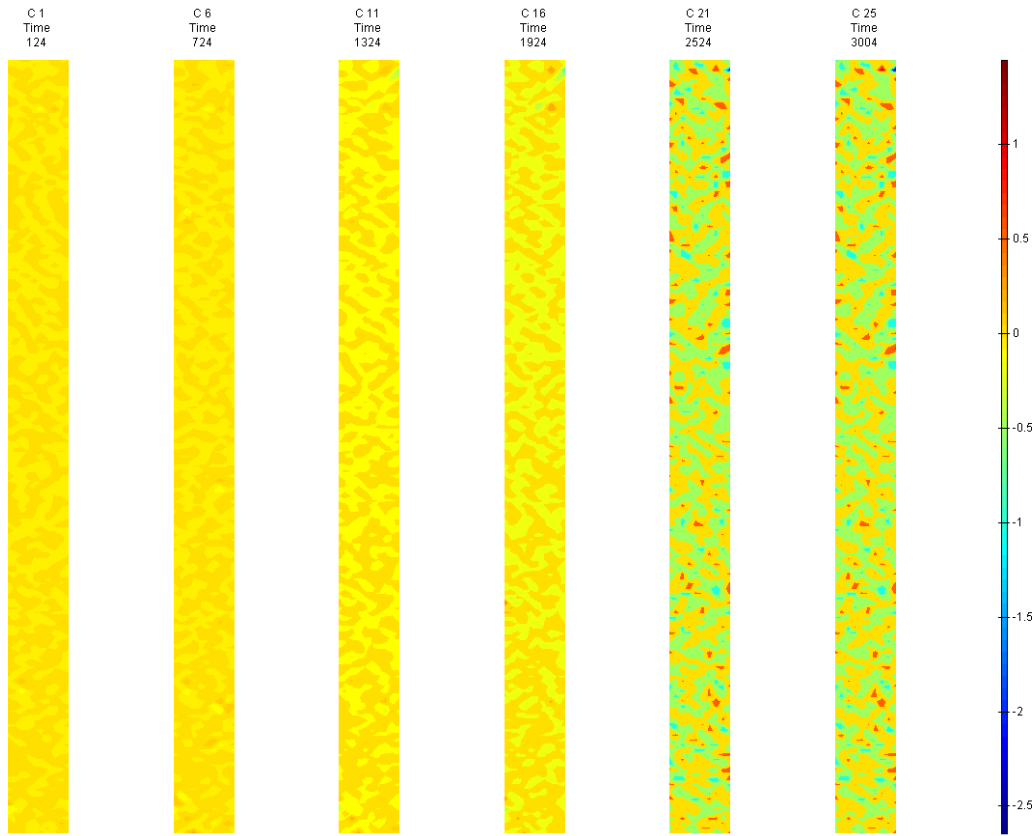

FIGURE 656: XY DIRECTION PIV SEQUENTIAL TRUE SHEAR STRAIN OVER TIME

FIGURE 657: X DIRECTION PIV FIRST–LAST DITCH ENGINEERING STRAIN OVER IMAGE

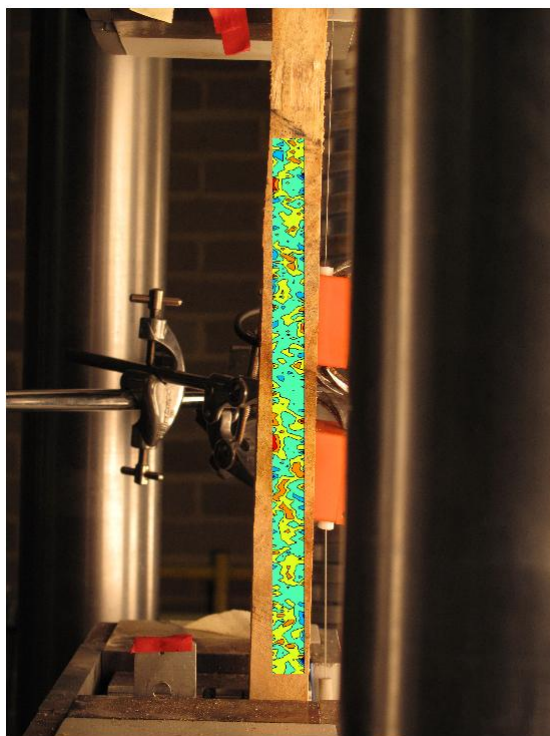FIGURE 658: Y DIRECTION PIV FIRST–LAST DITCH ENGINEERING STRAIN OVER IMAGE

FIGURE 659: XY DIRECTION PIV FIRST–LAST DITCH ENGINEERING SHEAR STRAIN OVER

IMAGE

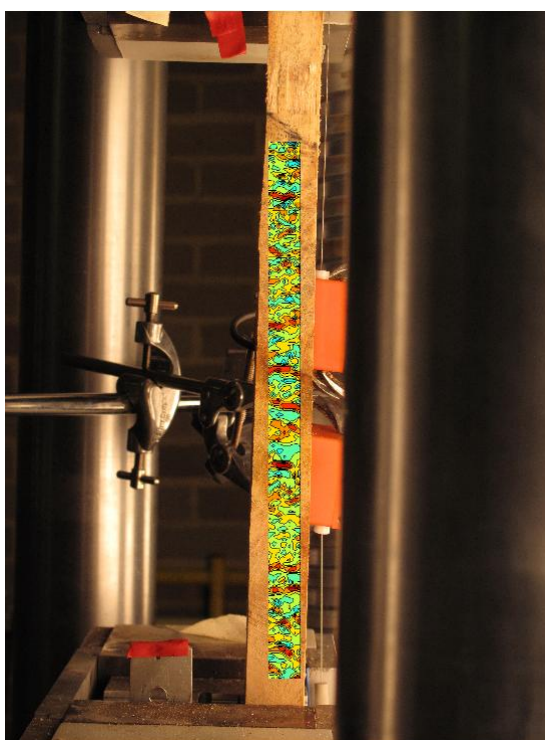FIGURE 660: X DIRECTION PIV FIRST–LAST DITCH TRUE STRAIN OVER IMAGE

FIGURE 661: Y DIRECTION PIV FIRST–LAST DITCH TRUE STRAIN OVER IMAGE

FIGURE 662: XY DIRECTION PIV FIRST–LAST DITCH TRUE SHEAR STRAIN OVER IMAGE

Appendix 6
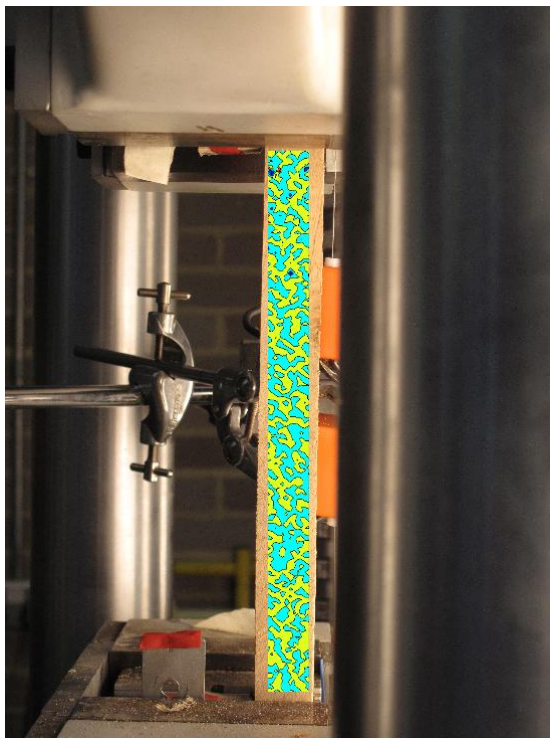
FIGURE 663: XY DIRECTION PIV FIRST–SEQUENTIAL ENGINEERING SHEAR STRAIN OVER

IMAGE
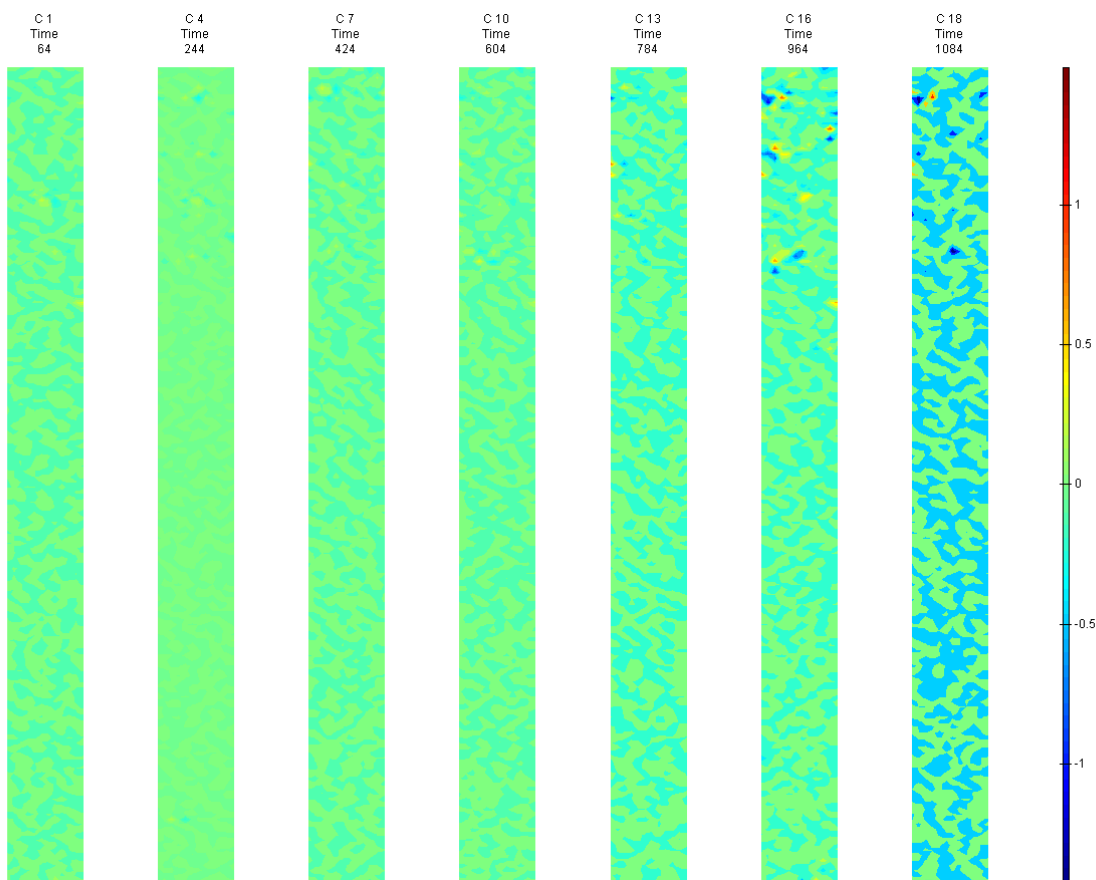
FIGURE 664: XY DIRECTION PIV FIRST–SEQUENTIAL ENGINEERING SHEAR STRAIN OVER TIME

T4
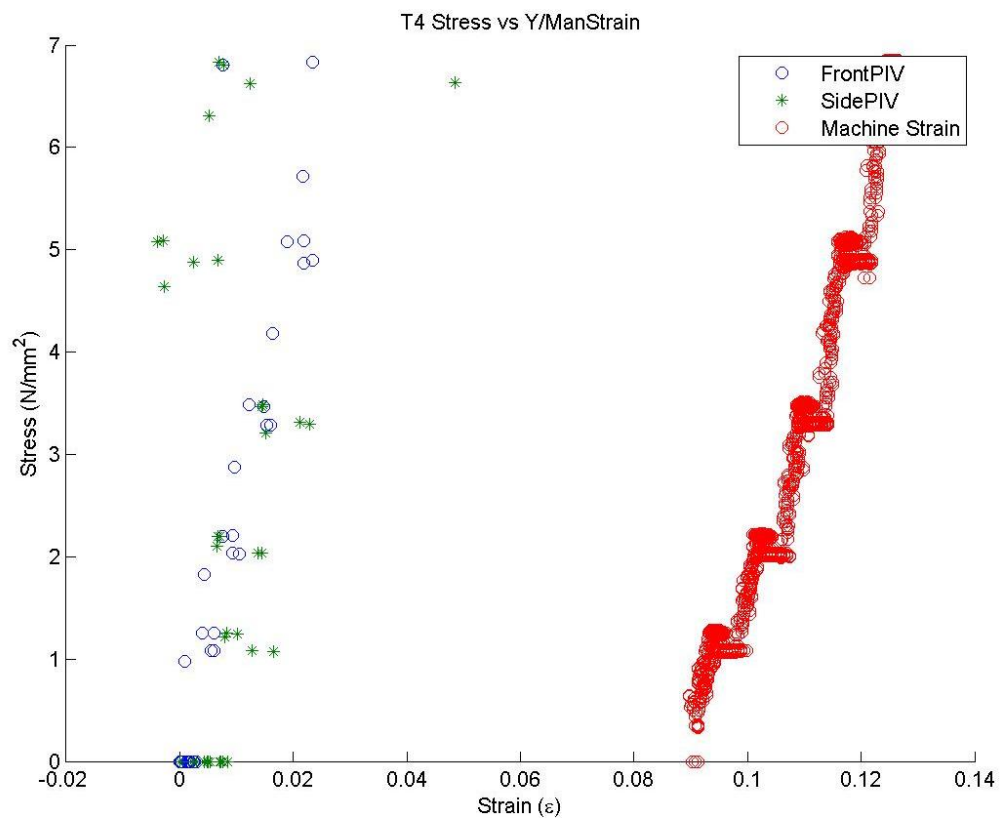
FIGURE 665: T4 TENSILE STRESS VS. MACHINE MEASURED/PIV STRAINS
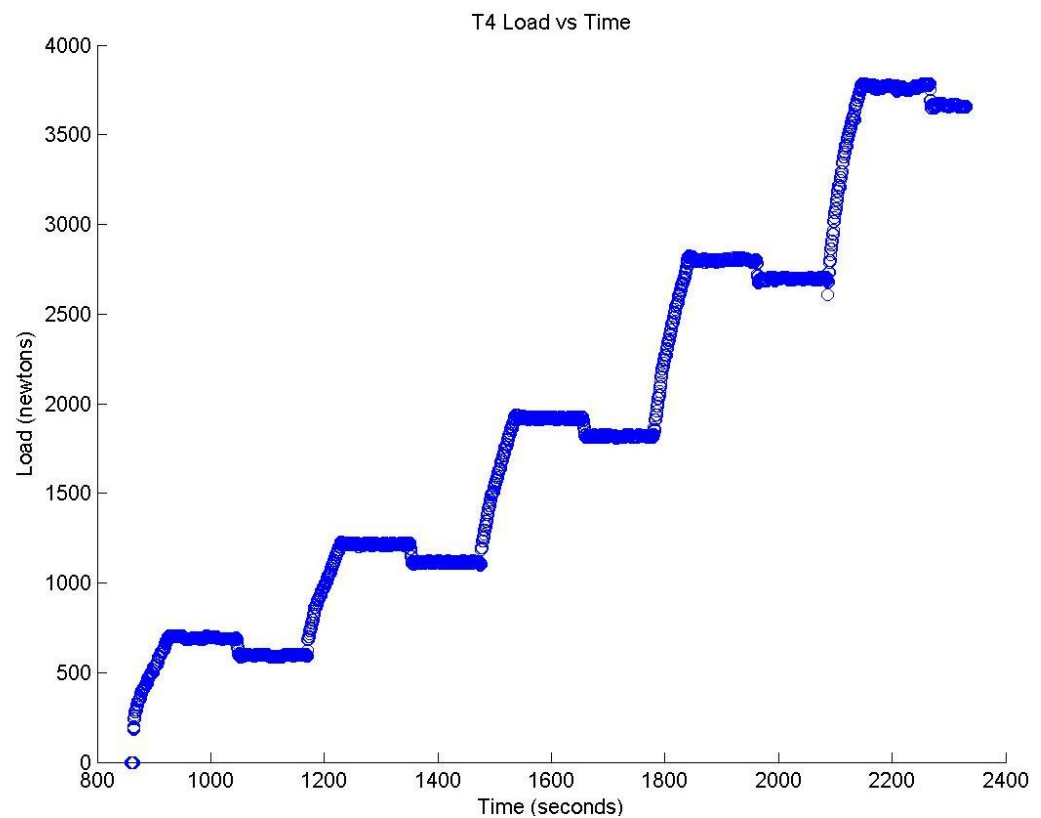
FIGURE 666: T4 TENSILE LOAD VS. TIME
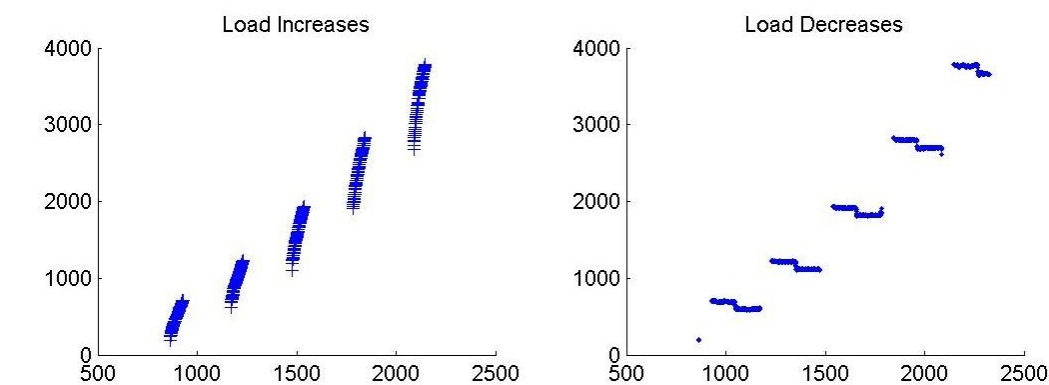
FIGURE 667: T4 CREEP LOADING: INCREMENTS AND RELAXATION
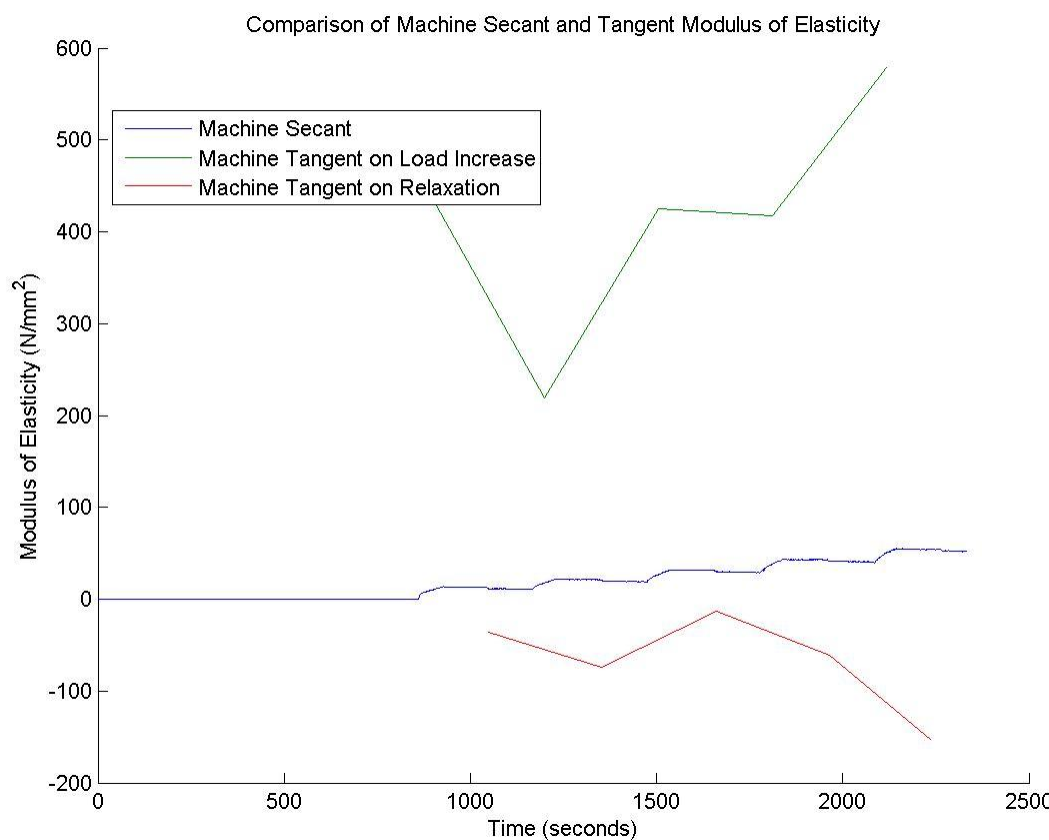
FIGURE 668: T4 MACHINE MEASURED SECANT AND TANGENT MODULUS VS. TIME
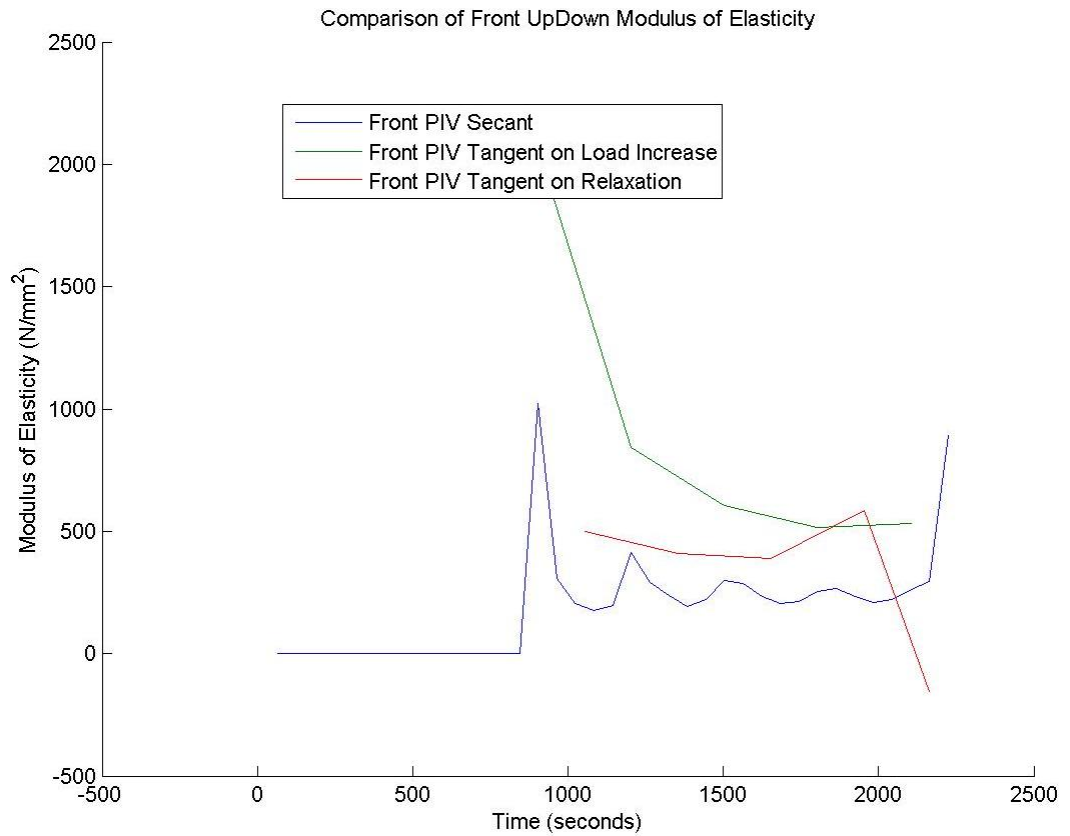
FIGURE 669: T4 FRONT VIEW PIV SECANT AND TANGENT MODULUS VS. TIME
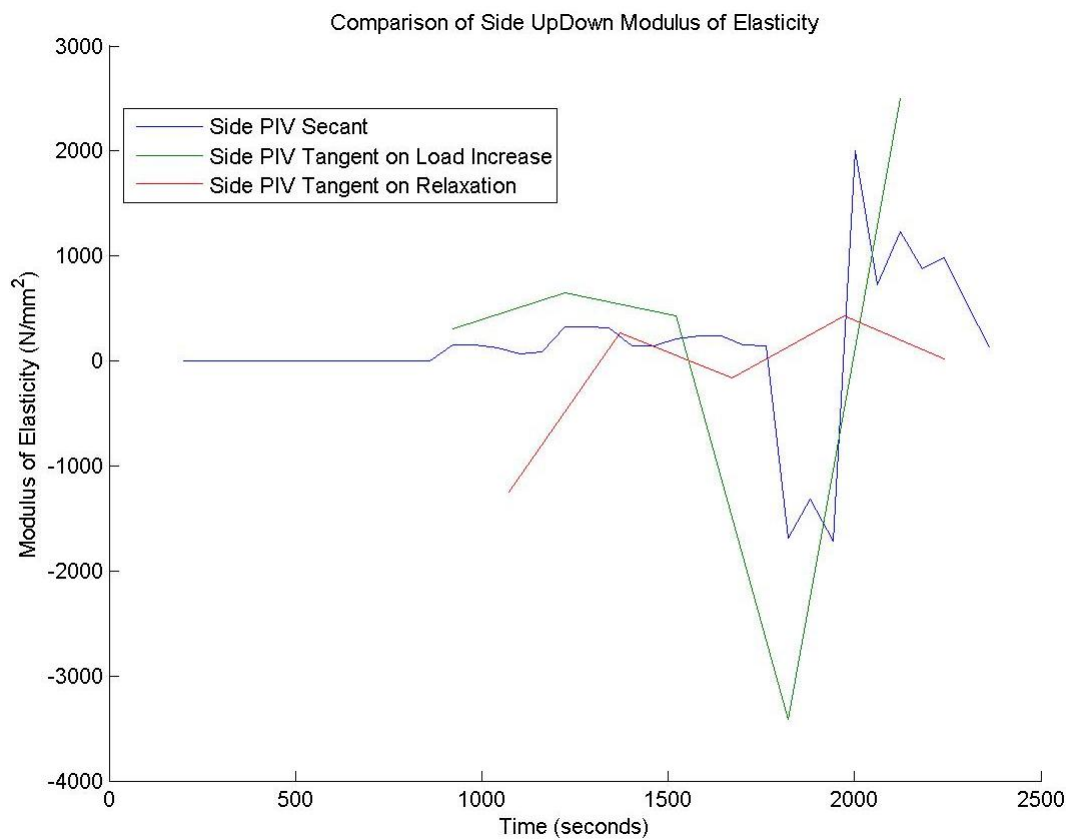
FIGURE 670: T4 SIDE VIEW PIV SECANT AND TANGENT MODULUS VS. TIME

Appendix 6
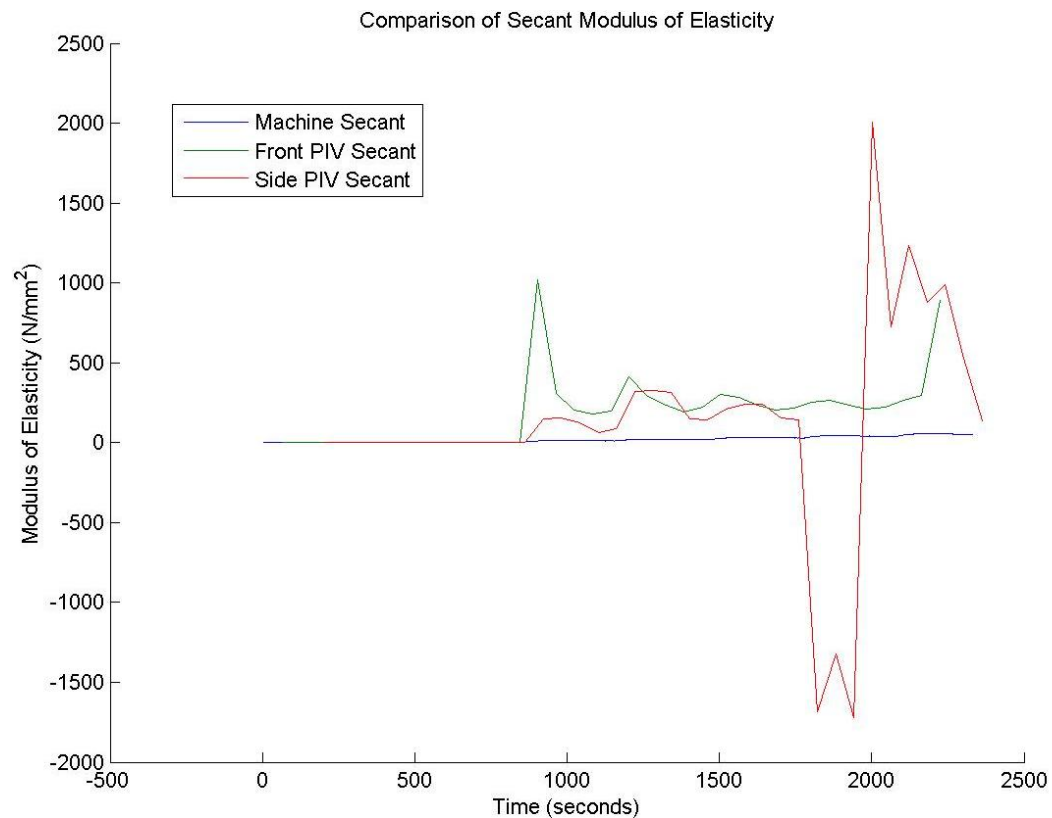
FIGURE 671: T4 COMPARISON OF MACHINE MEASURED AND PIV SECANT MODULUS VS. TIME
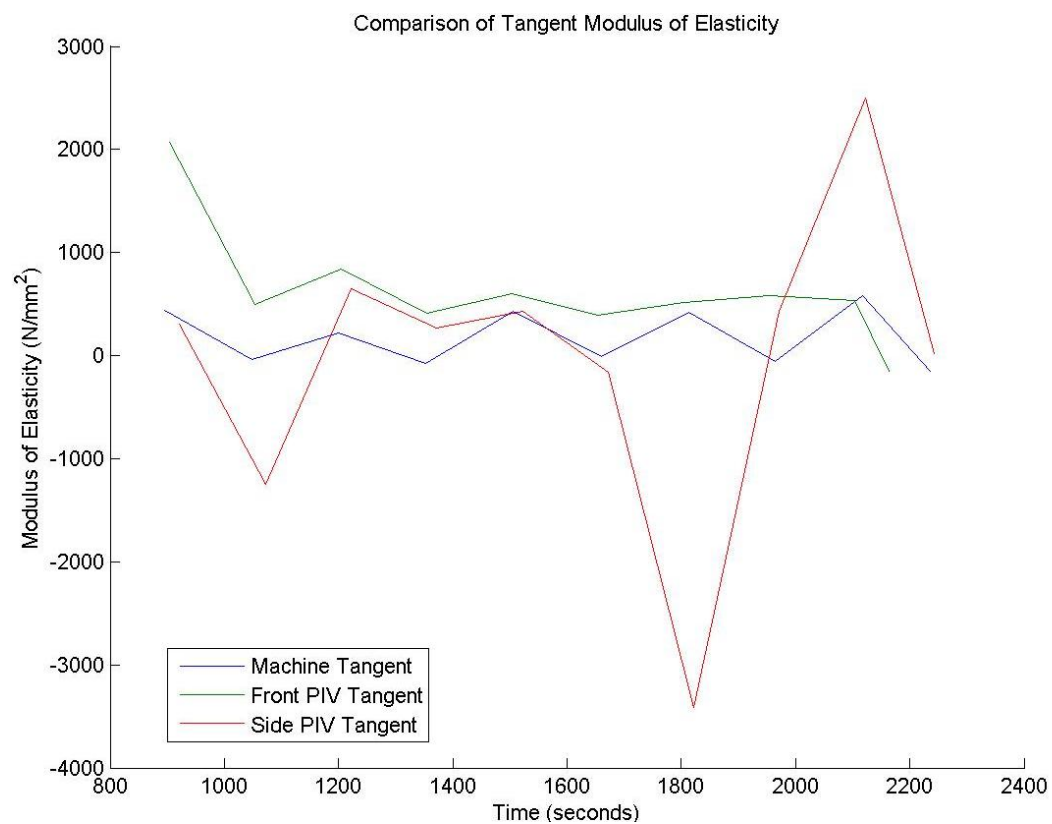
FIGURE 672: T4 COMPARISON OF MACHINE MEASURED AND PIV TANGENT MODULUS VS.

TIME

T4 Sample
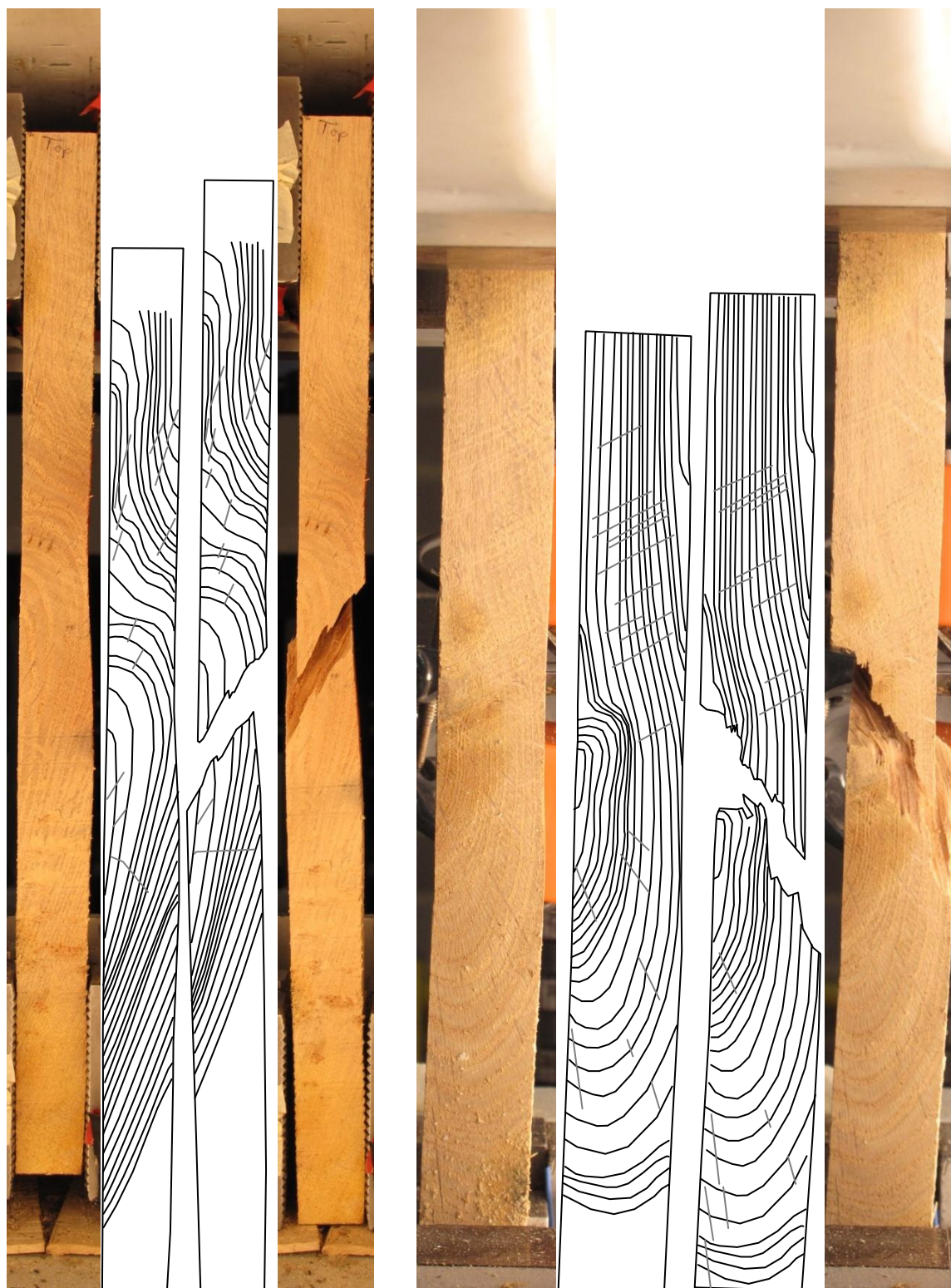
FIGURE 673: SAMPLE GRAIN ORIENTATIONS OF THE FRONT (LEFT 4 IMAGES) AND SIDE (RIGHT 4 IMAGES) VIEW BEFORE (FIRST 2 OF 4 IMAGES) AND AFTER (LAST 2 OF 4 IMAGES) BREAKAGE

T4 Front View
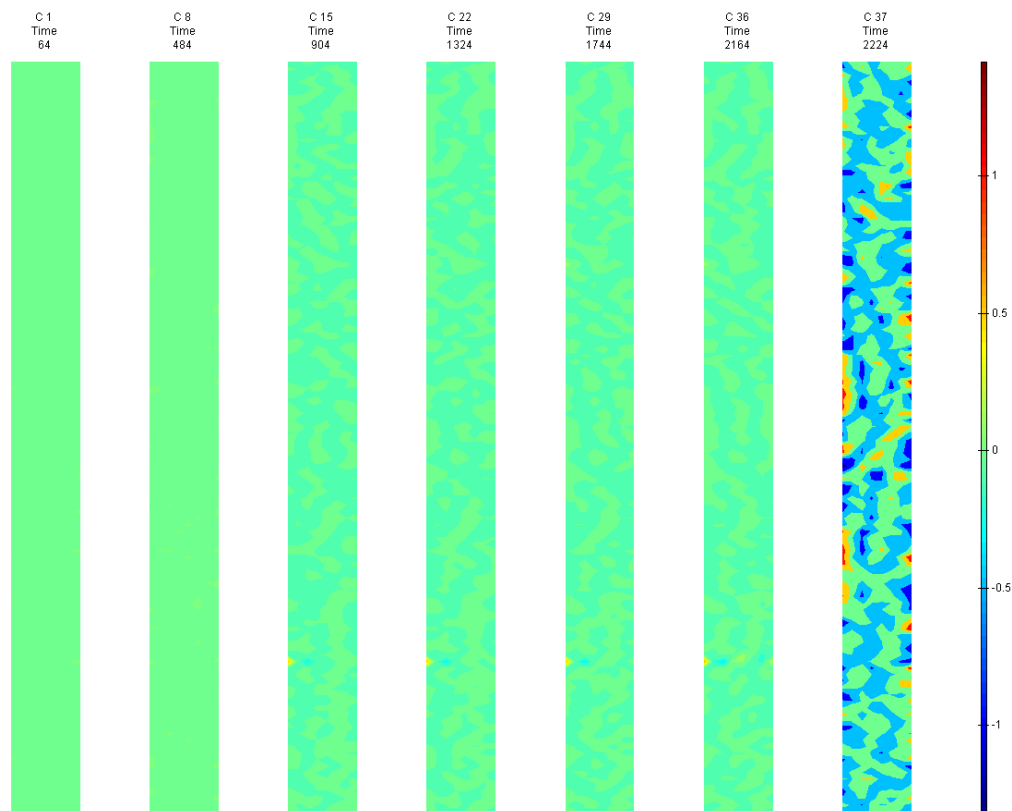
FIGURE 674: X DIRECTION PIV SEQUENTIAL ENGINEERING STRAIN OVER TIME
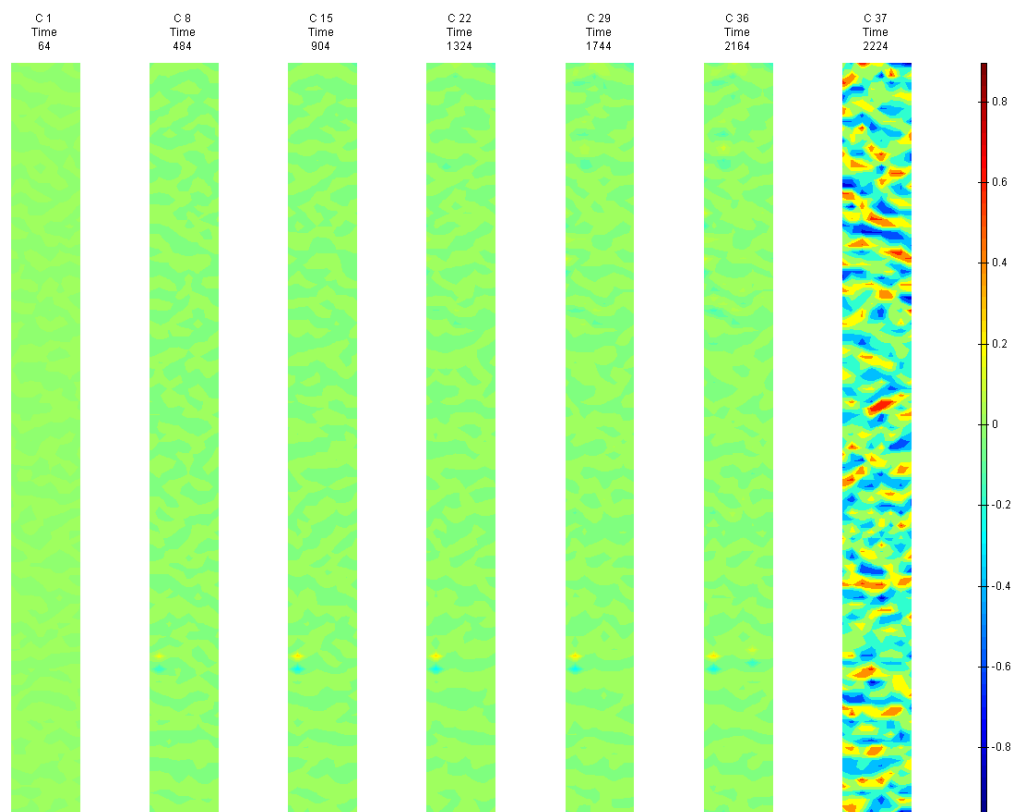
FIGURE 675: Y DIRECTION PIV SEQUENTIAL ENGINEERING STRAIN OVER TIME
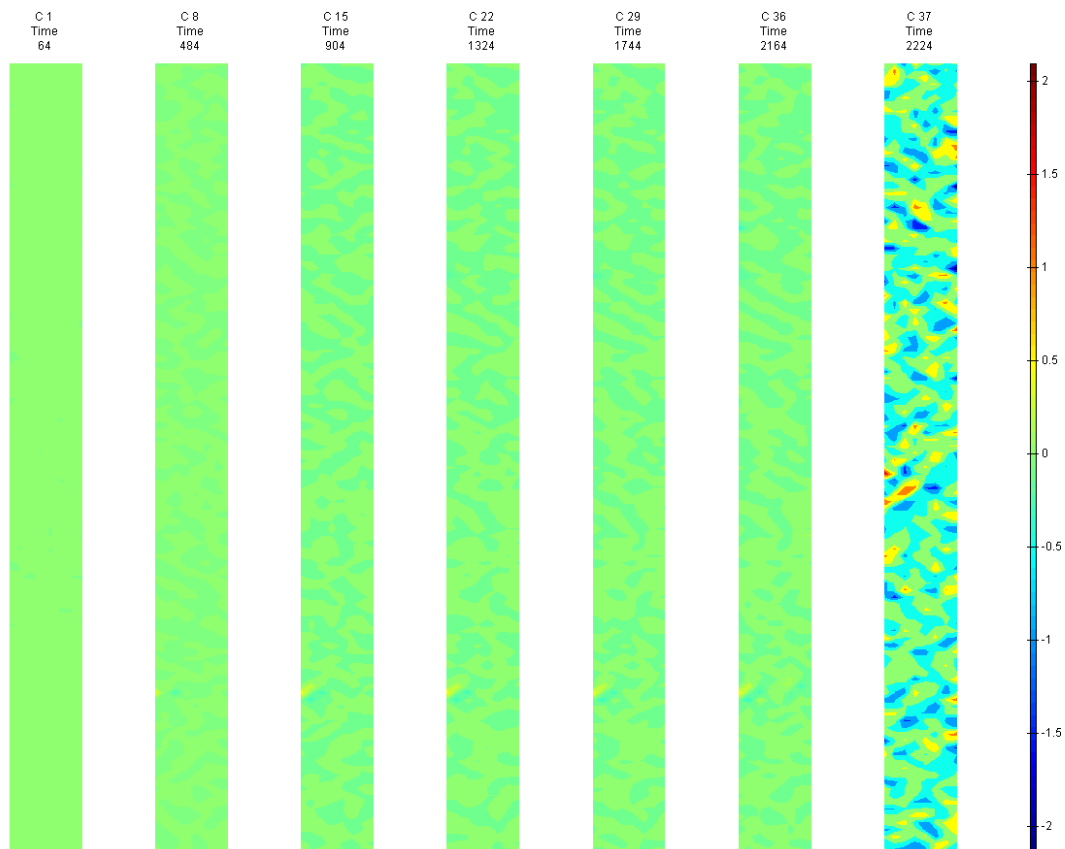
FIGURE 676: XY DIRECTION PIV SEQUENTIAL ENGINEERING SHEAR STRAIN OVER TIME
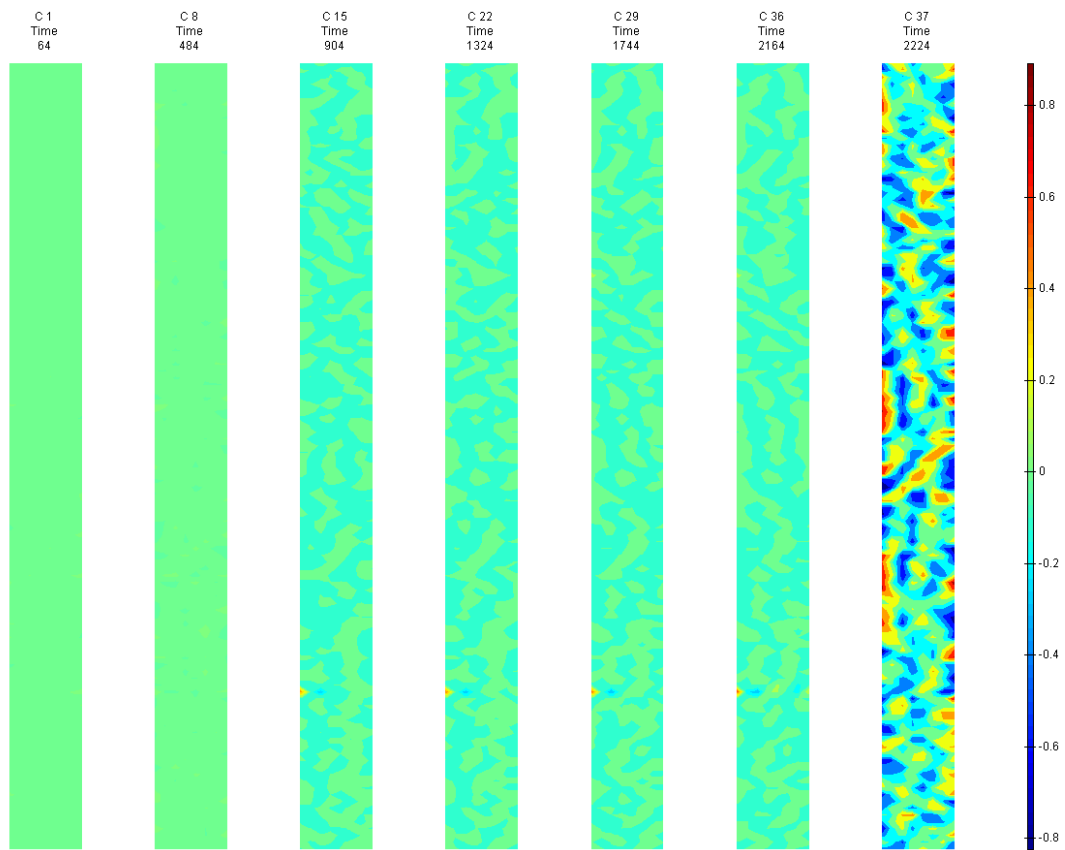
FIGURE 677: X DIRECTION PIV SEQUENTIAL TRUE STRAIN OVER TIME

Appendix 6
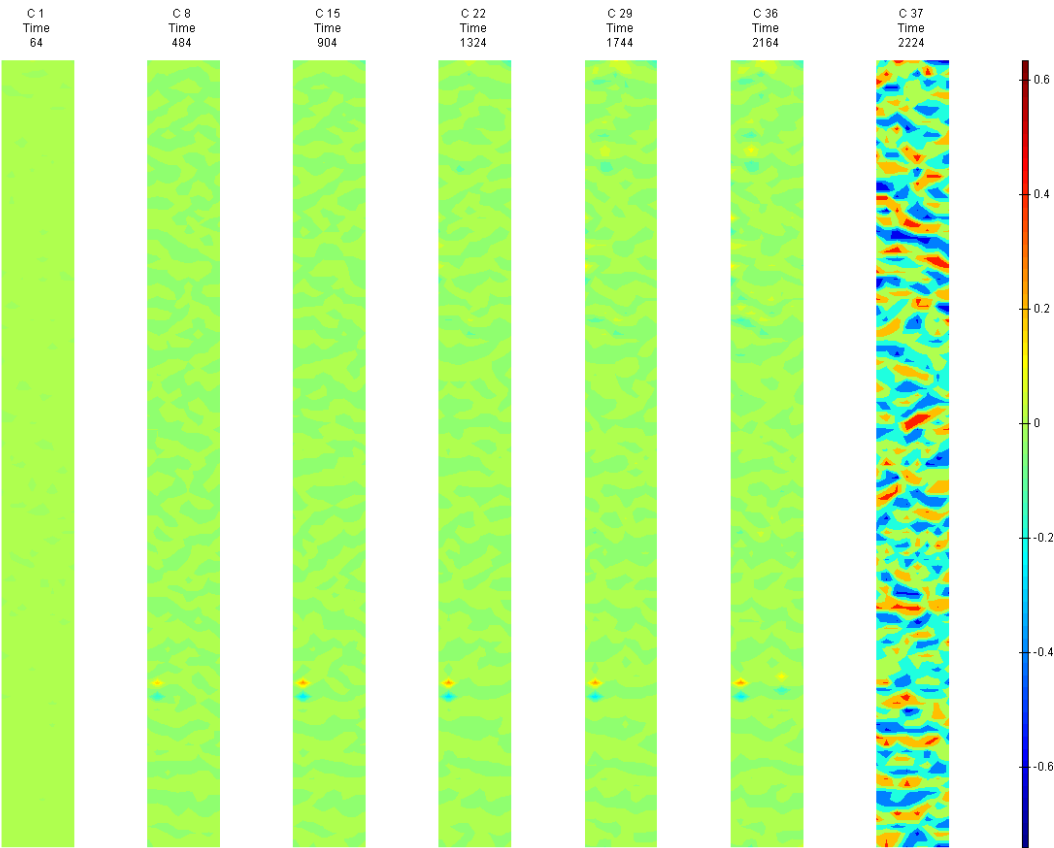
FIGURE 678: Y DIRECTION PIV SEQUENTIAL TRUE STRAIN OVER TIME
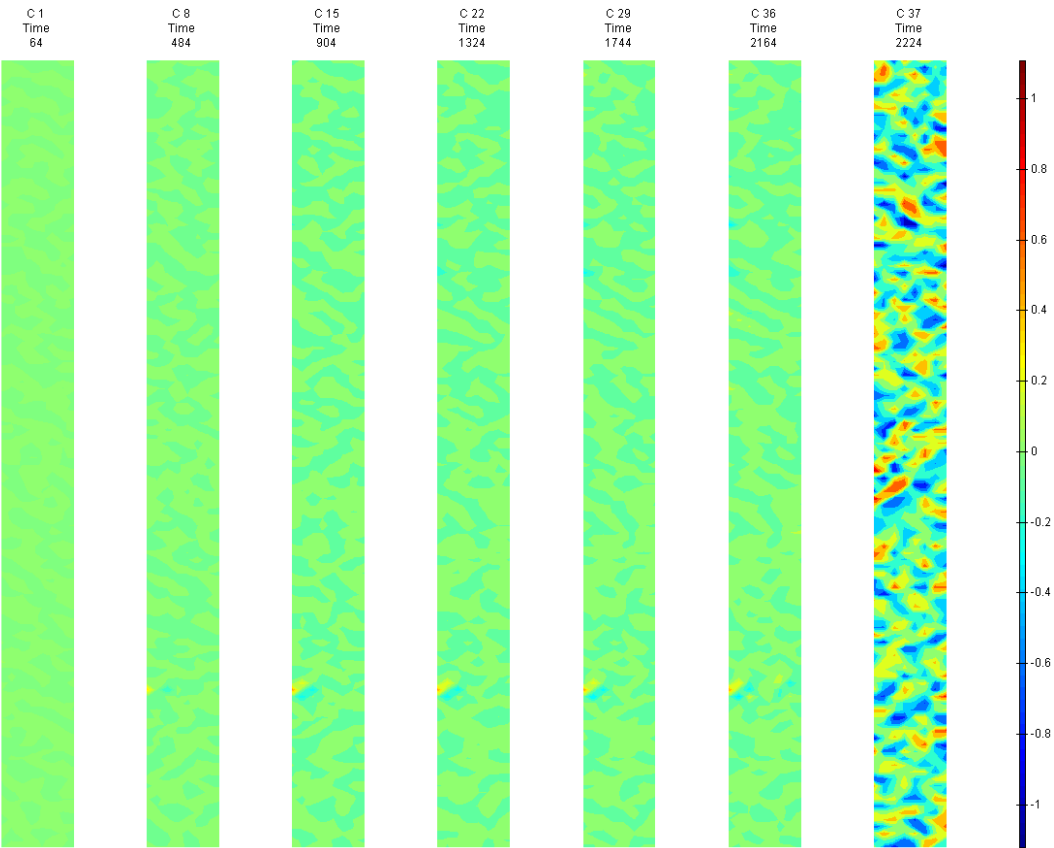
FIGURE 679: XY DIRECTION PIV SEQUENTIAL TRUE SHEAR STRAIN OVER TIME
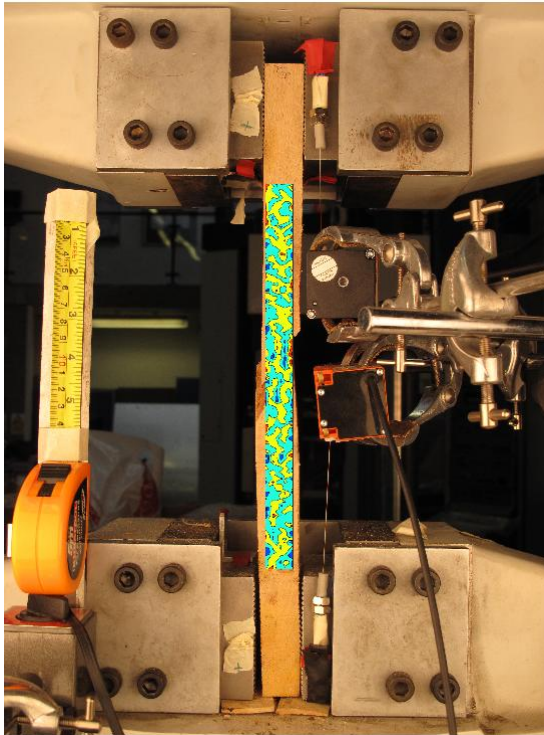
FIGURE 680: X DIRECTION PIV FIRST−LAST DITCH ENGINEERING STRAIN OVER IMAGE
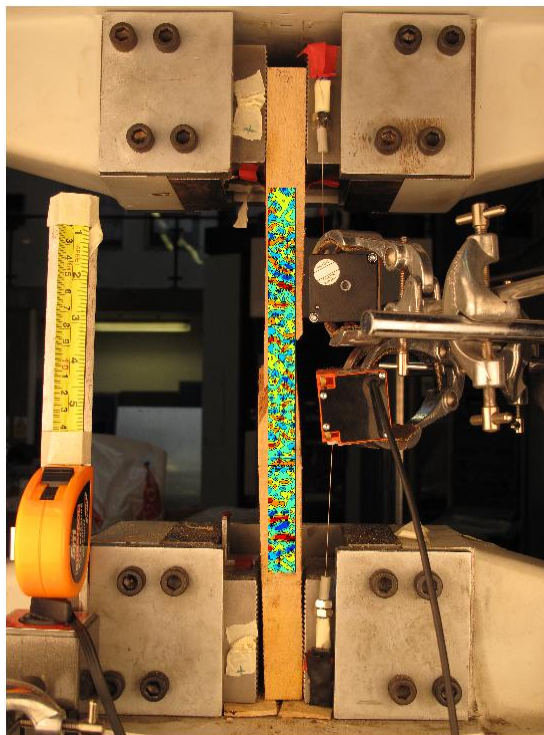
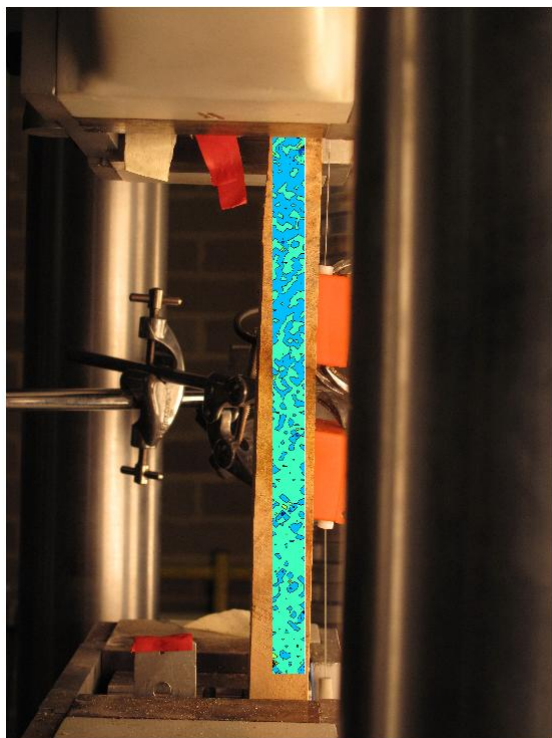

FIGURE 681: Y DIRECTION PIV FIRST−LAST DITCH ENGINEERING STRAIN OVER IMAGE
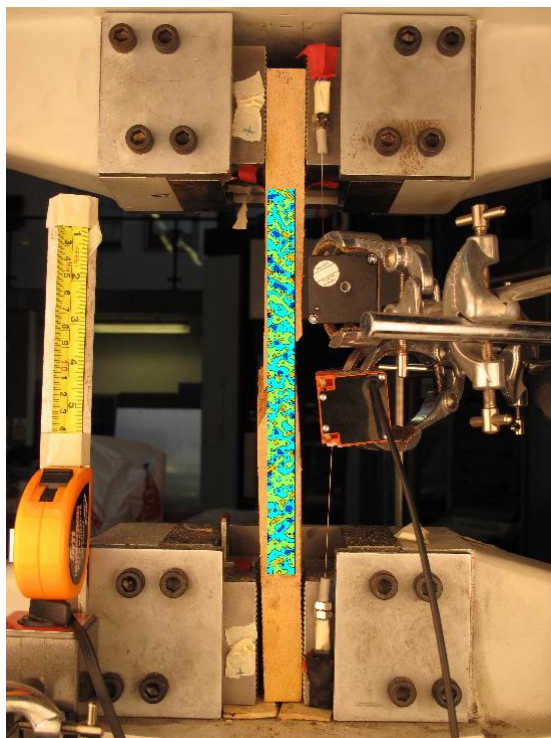
FIGURE 682: XY DIRECTION PIV FIRST-LAST DITCH ENGINEERING SHEAR STRAIN OVER
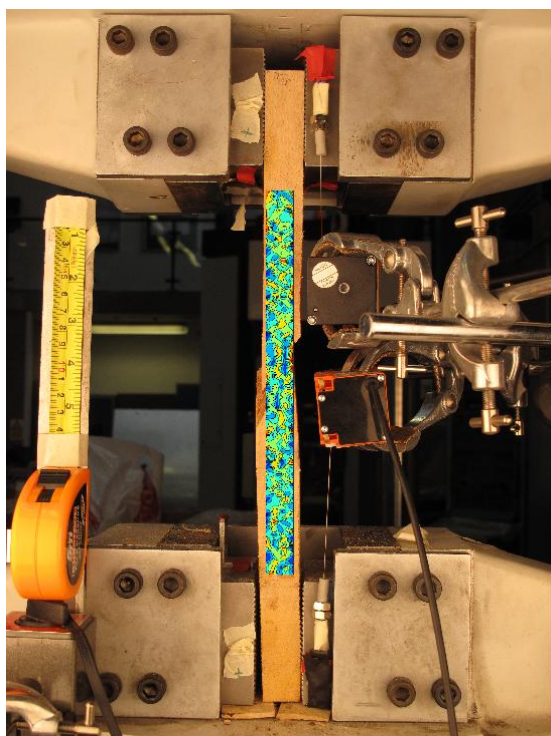
IMAGE

FIGURE 683: X DIRECTION PIV FIRST-LAST DITCH TRUE STRAIN OVER IMAGE
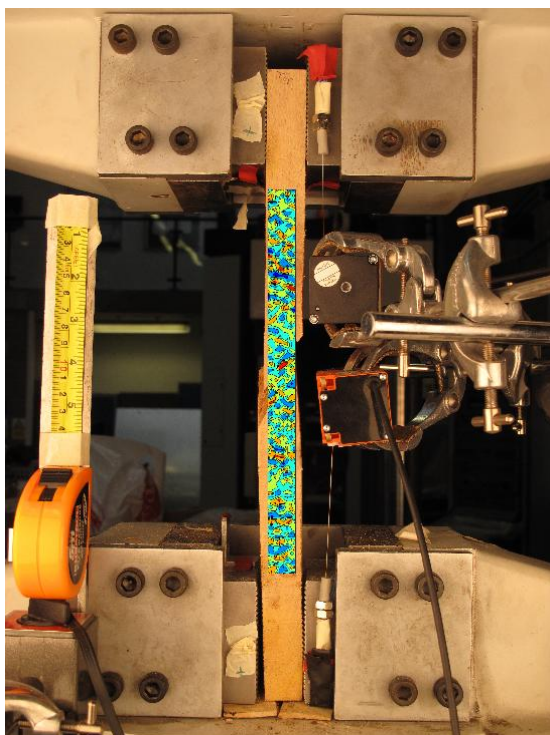
FIGURE 684: Y DIRECTION PIV FIRST–LAST DITCH TRUE STRAIN OVER IMAGE
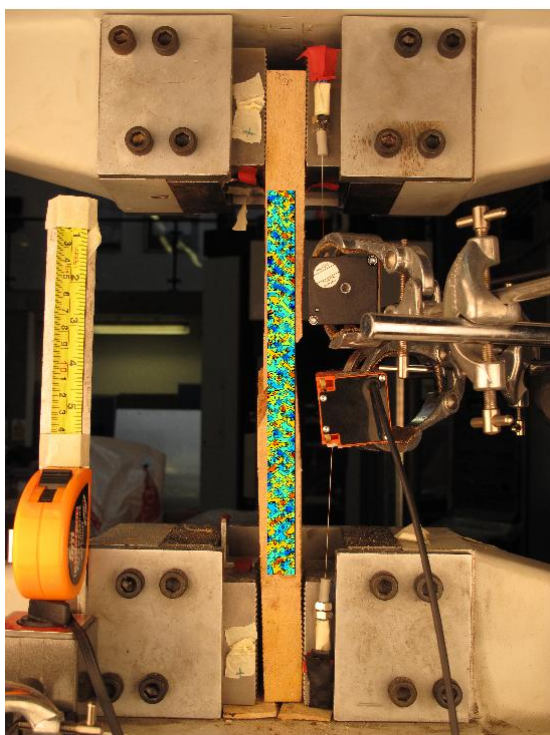
FIGURE 685: XY DIRECTION PIV FIRST–LAST DITCH TRUE SHEAR STRAIN OVER IMAGE

Appendix 6
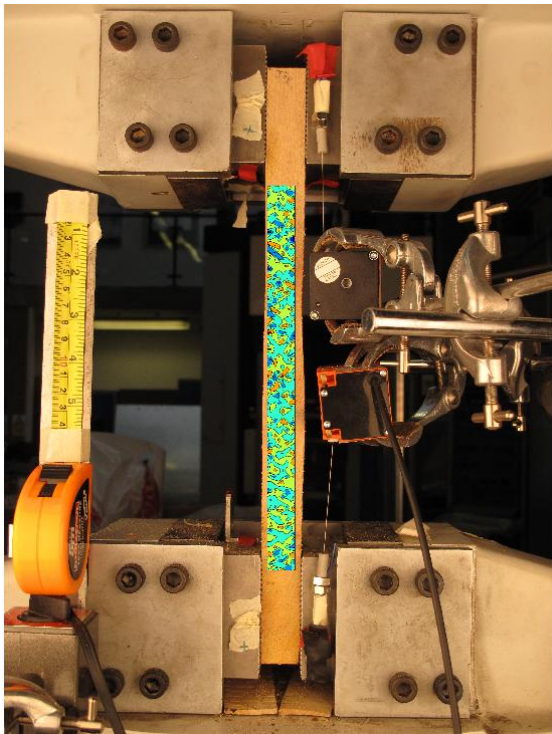
FIGURE 686: XY DIRECTION PIV FIRST–SEQUENTIAL ENGINEERING SHEAR STRAIN OVER

IMAGE
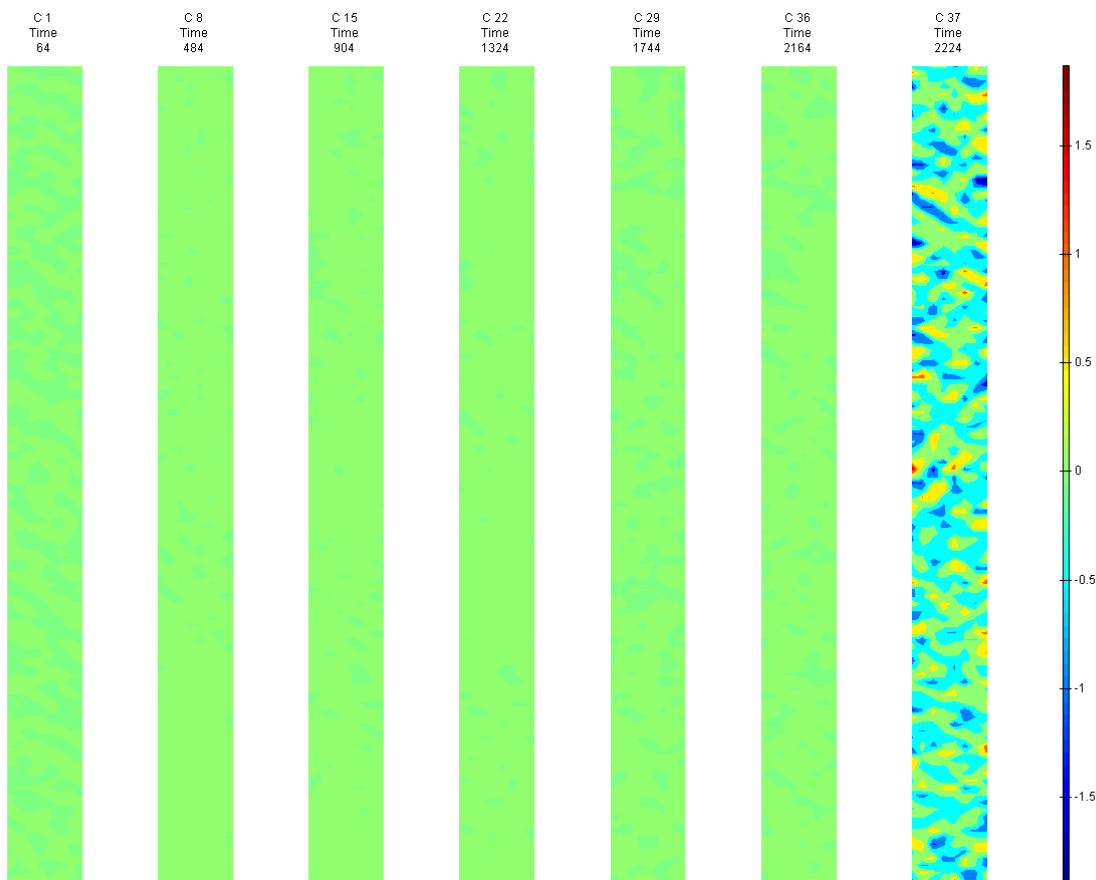
FIGURE 687: XY DIRECTION PIV FIRST–SEQUENTIAL ENGINEERING SHEAR STRAIN OVER TIME

T4 Side View
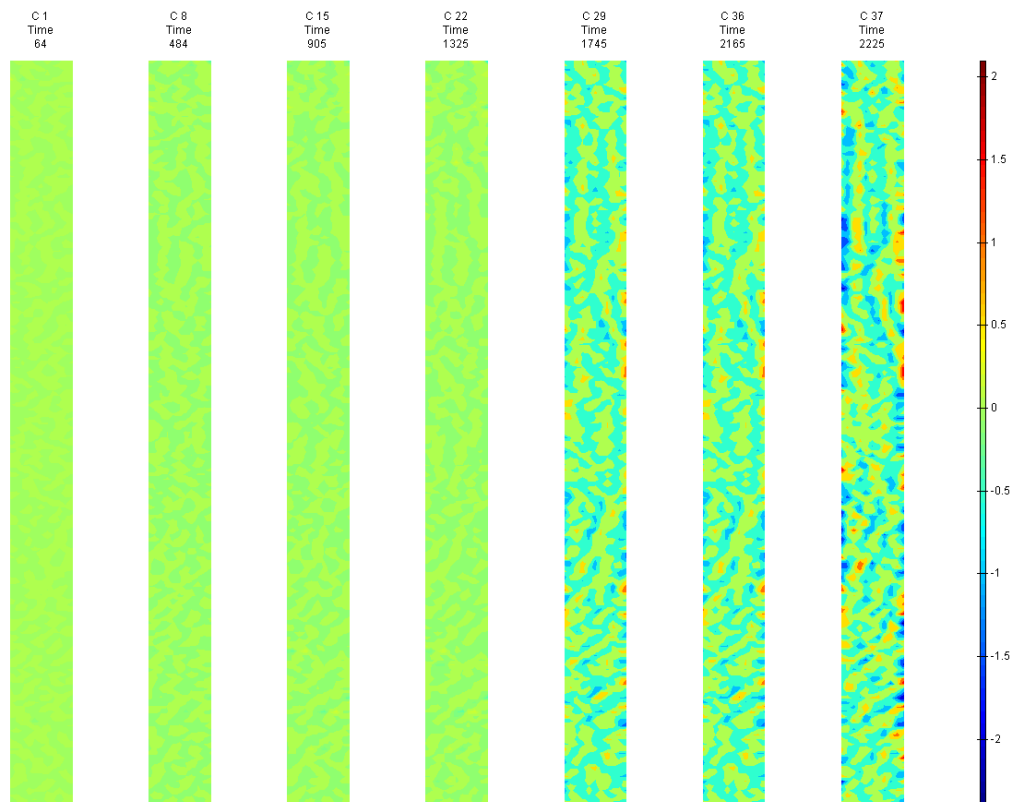
FIGURE 688: X DIRECTION PIV SEQUENTIAL ENGINEERING STRAIN OVER TIME
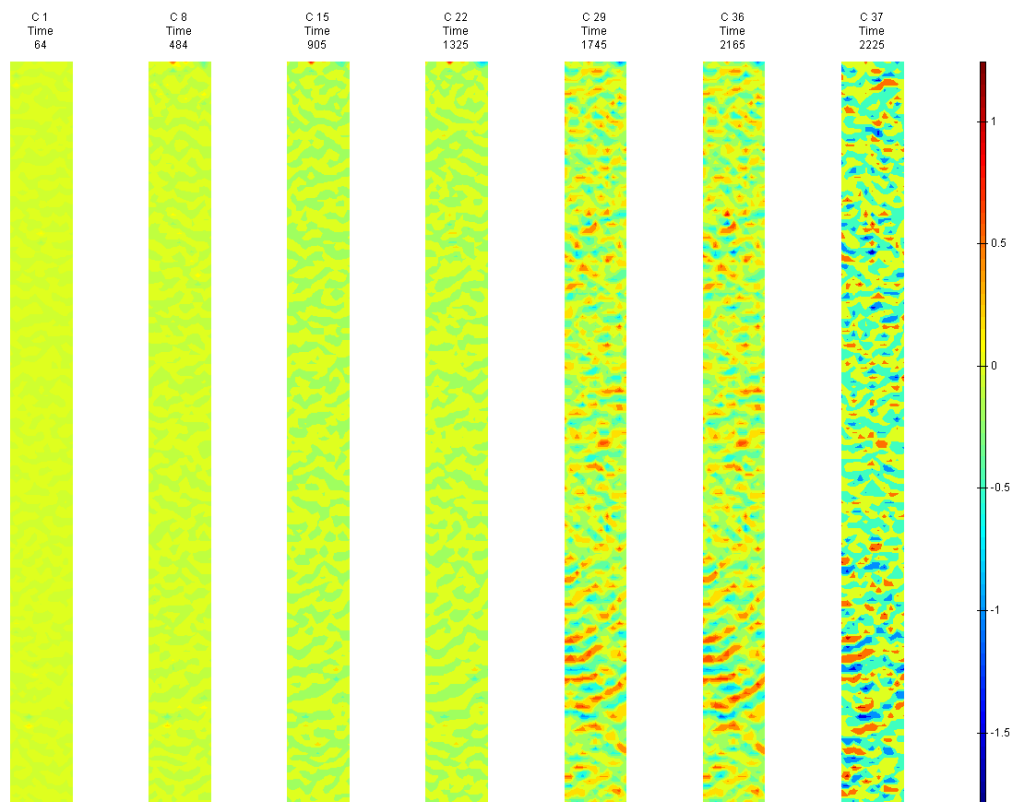
FIGURE 689: Y DIRECTION PIV SEQUENTIAL ENGINEERING STRAIN OVER TIME
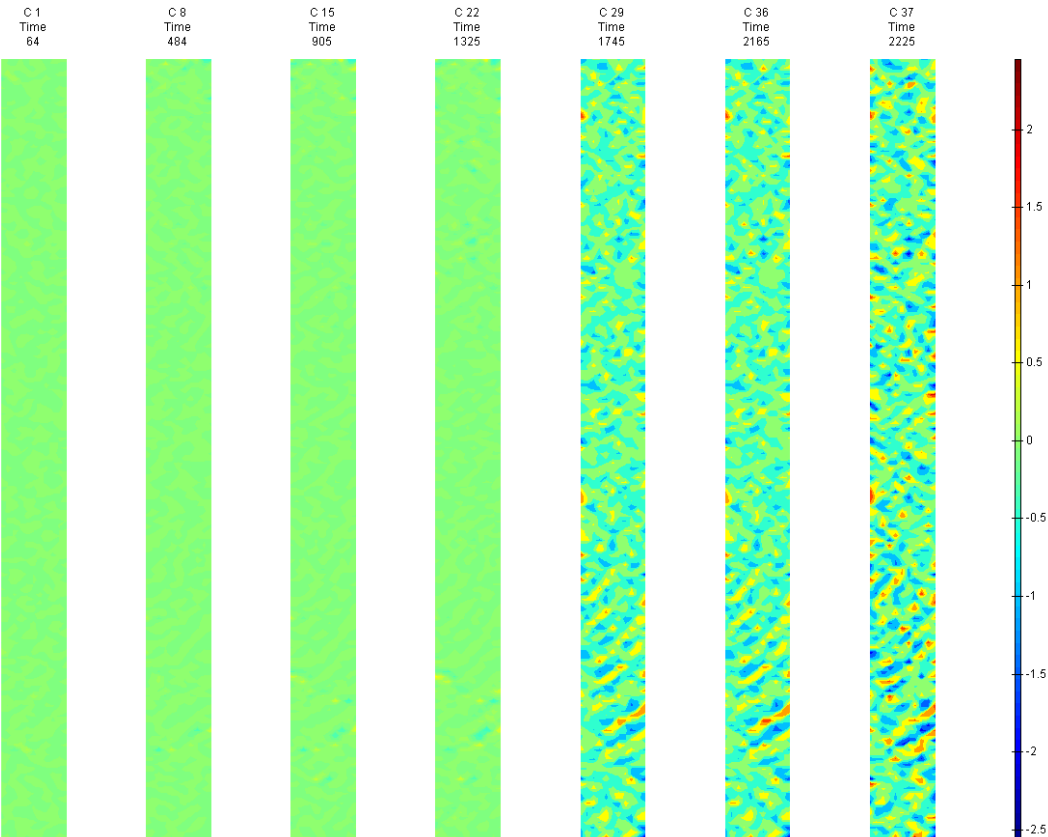
FIGURE 690: XY DIRECTION PIV SEQUENTIAL ENGINEERING SHEAR STRAIN OVER TIME
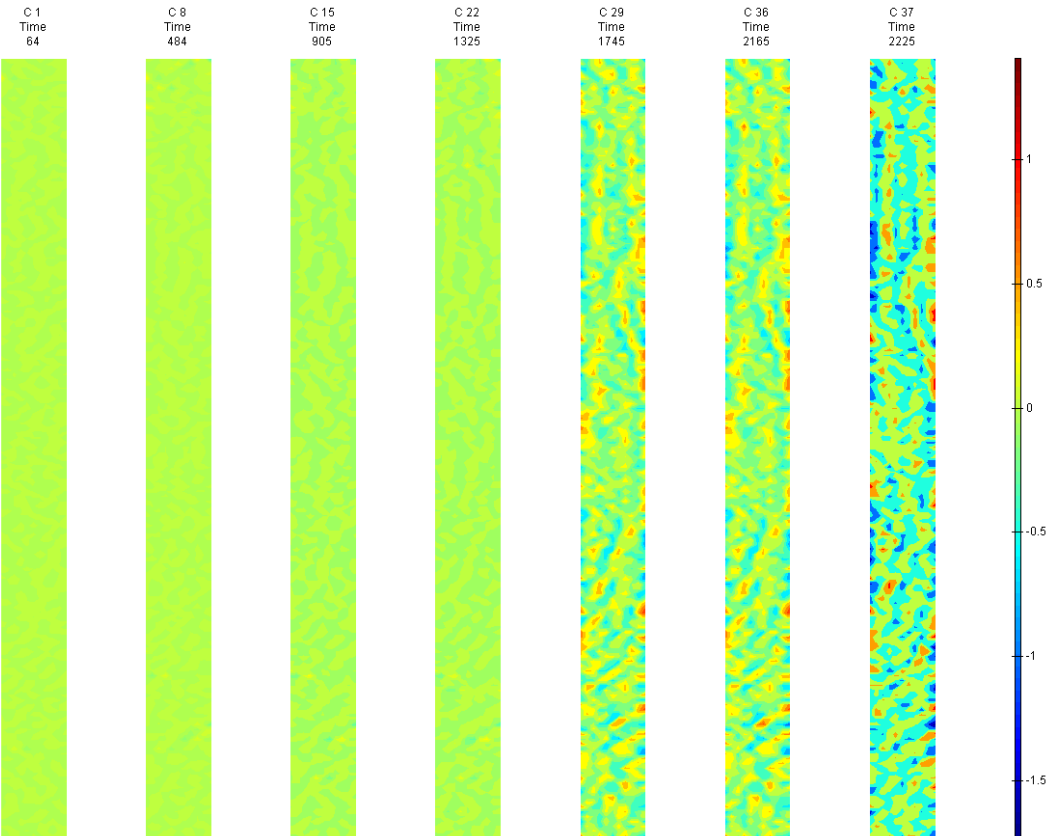
FIGURE 691: X DIRECTION PIV SEQUENTIAL TRUE STRAIN OVER TIME
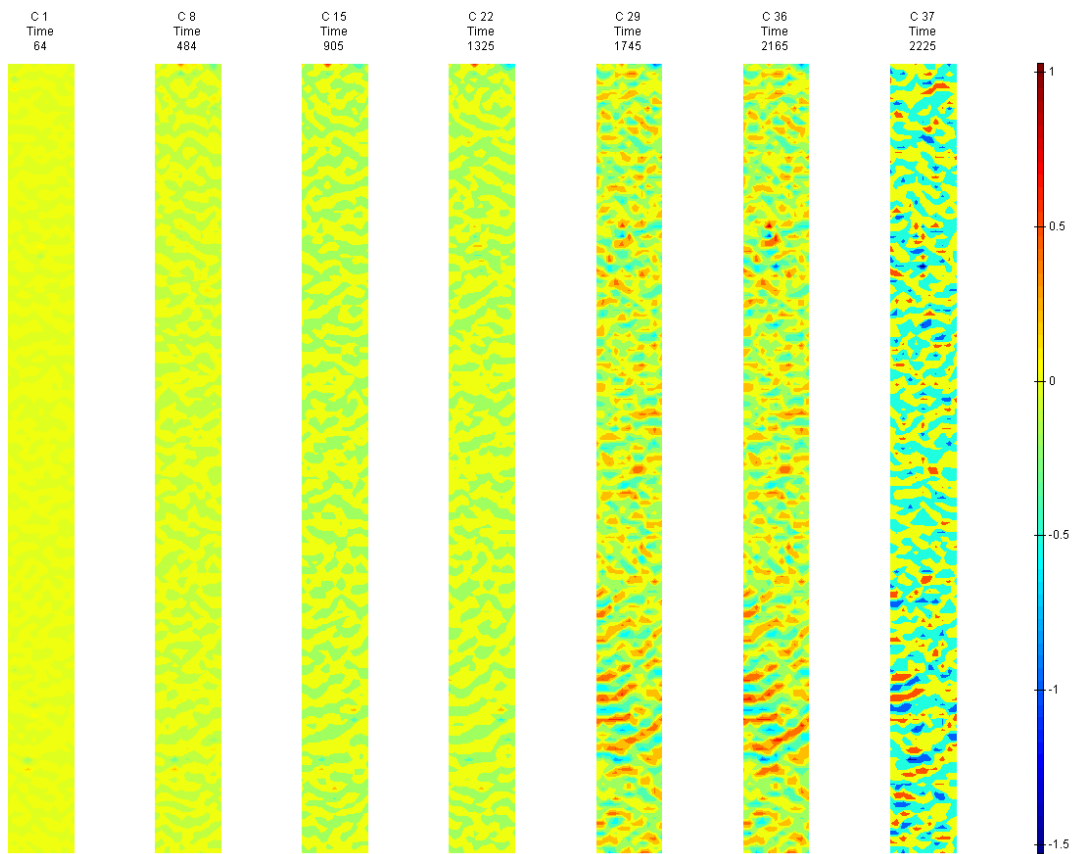
FIGURE 692: Y DIRECTION PIV SEQUENTIAL TRUE STRAIN OVER TIME
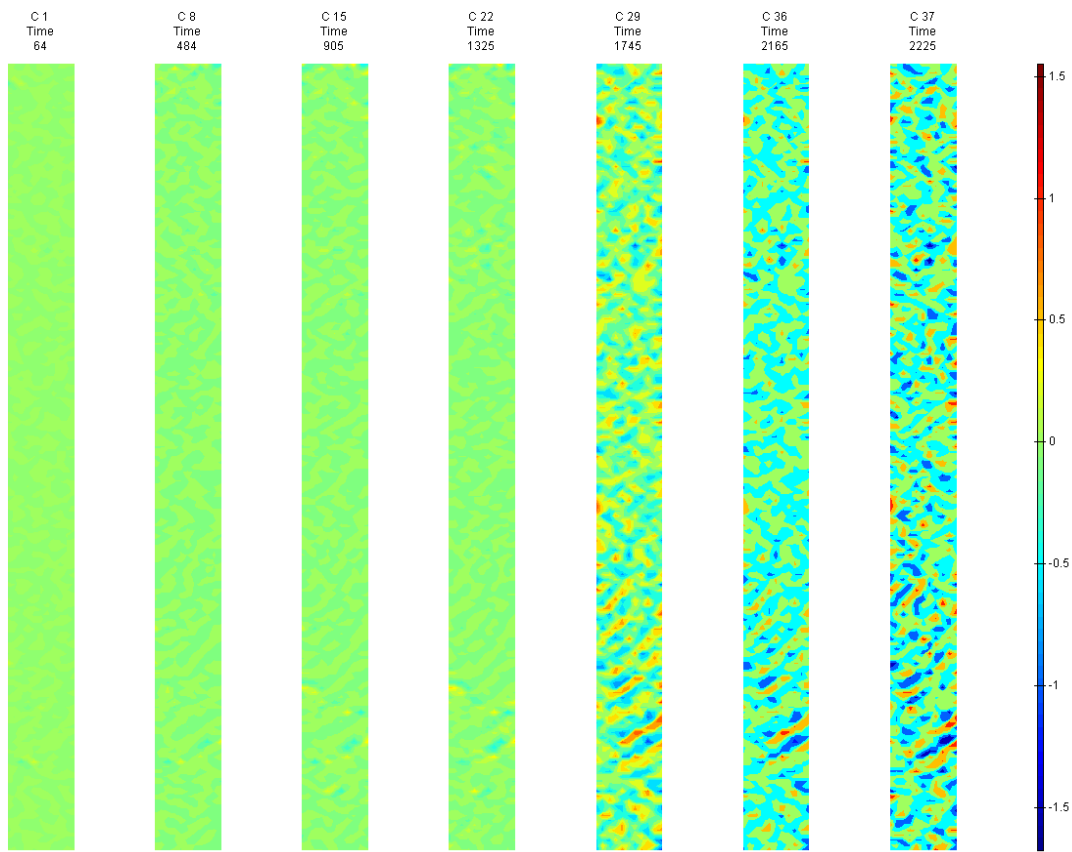
FIGURE 693: XY DIRECTION PIV SEQUENTIAL TRUE SHEAR STRAIN OVER TIME
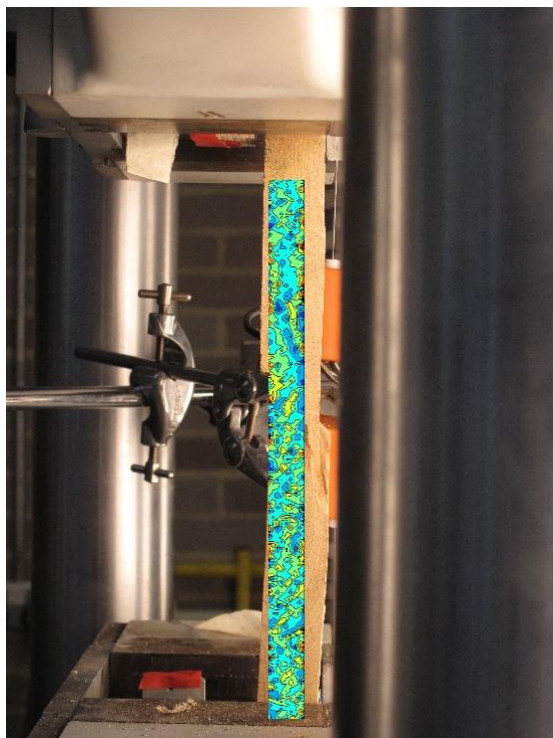
FIGURE 694: X DIRECTION PIV FIRST−LAST DITCH ENGINEERING STRAIN OVER IMAGE
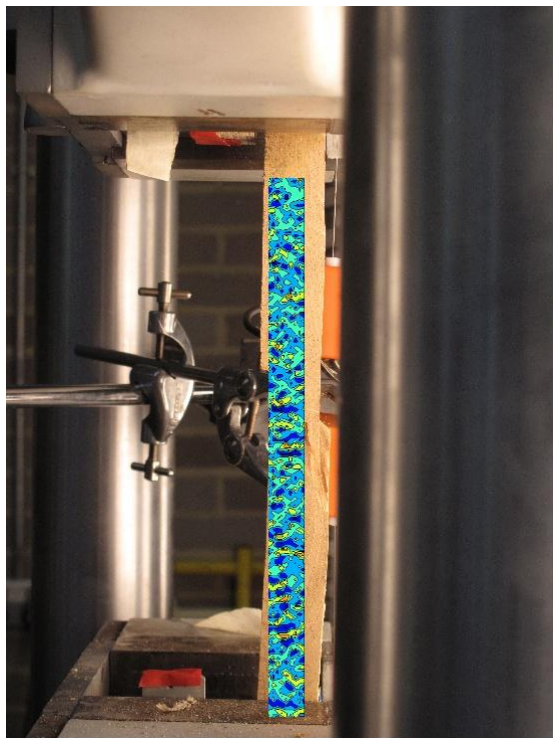
FIGURE 695: Y DIRECTION PIV FIRST−LAST DITCH ENGINEERING STRAIN OVER IMAGE
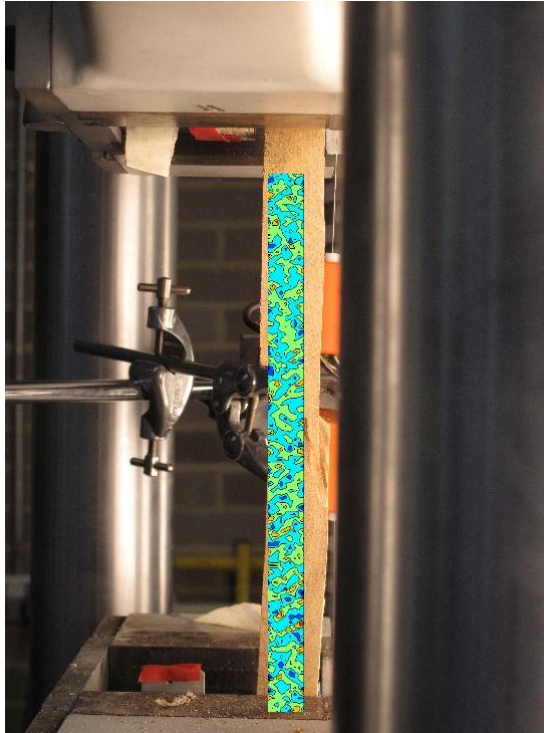
FIGURE 696: XY DIRECTION PIV FIRST–LAST DITCH ENGINEERING SHEAR STRAIN OVER
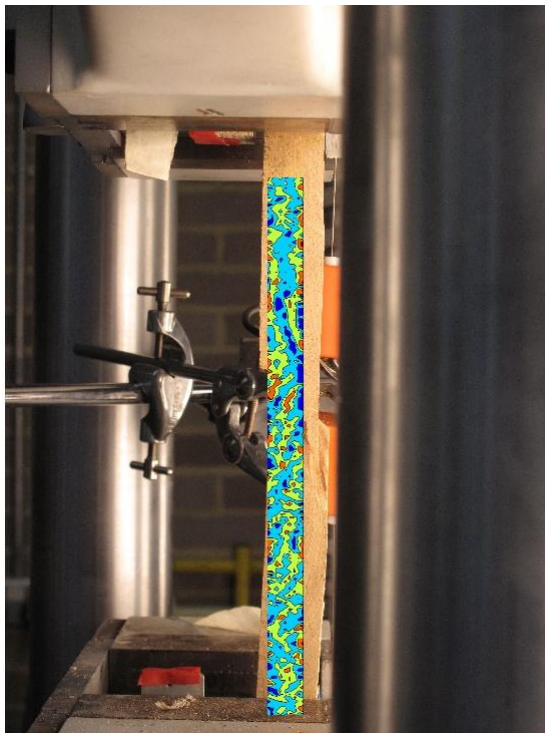
IMAGE

FIGURE 697: X DIRECTION PIV FIRST–LAST DITCH TRUE STRAIN OVER IMAGE

Appendix 6
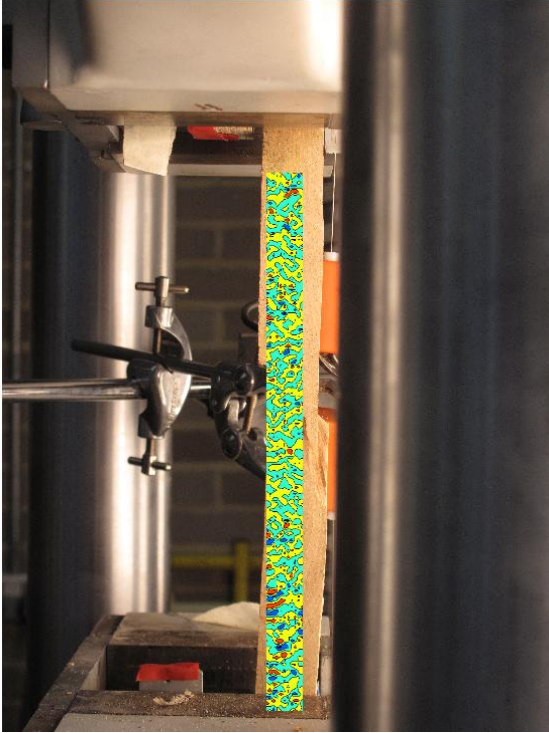
FIGURE 698: Y DIRECTION PIV FIRST–LAST DITCH TRUE STRAIN OVER IMAGE
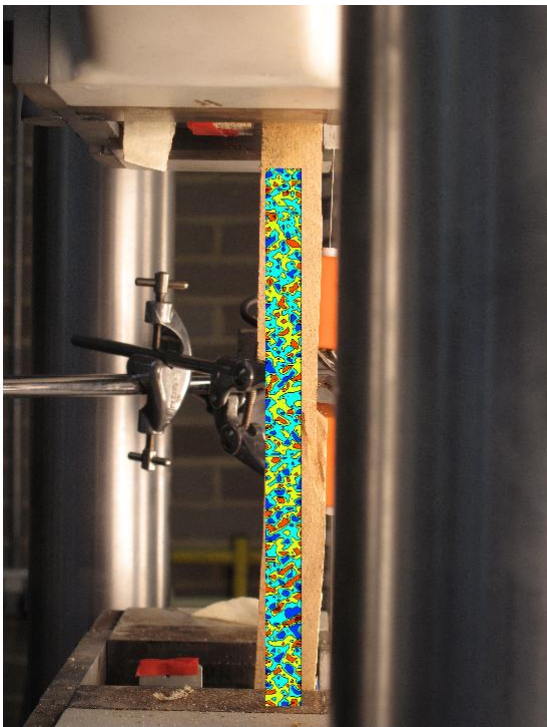
FIGURE 699: XY DIRECTION PIV FIRST–LAST DITCH TRUE SHEAR STRAIN OVER IMAGE
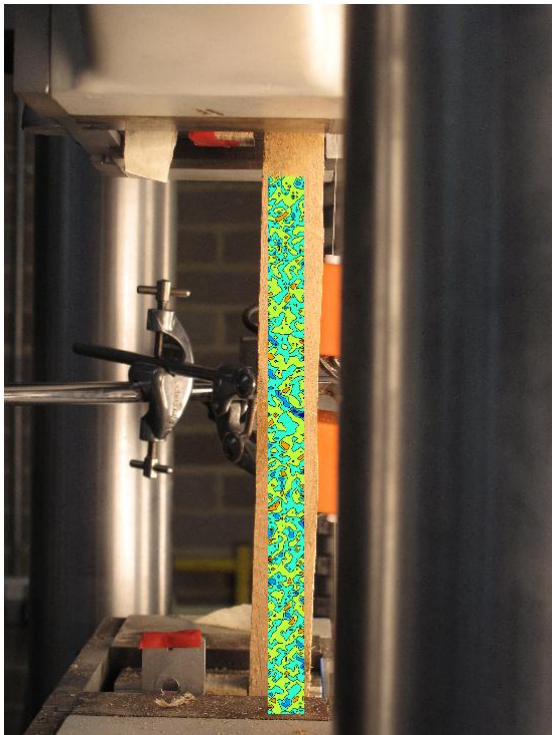
FIGURE 700: XY DIRECTION PIV FIRST-SEQUENTIAL ENGINEERING SHEAR STRAIN OVER

IMAGE
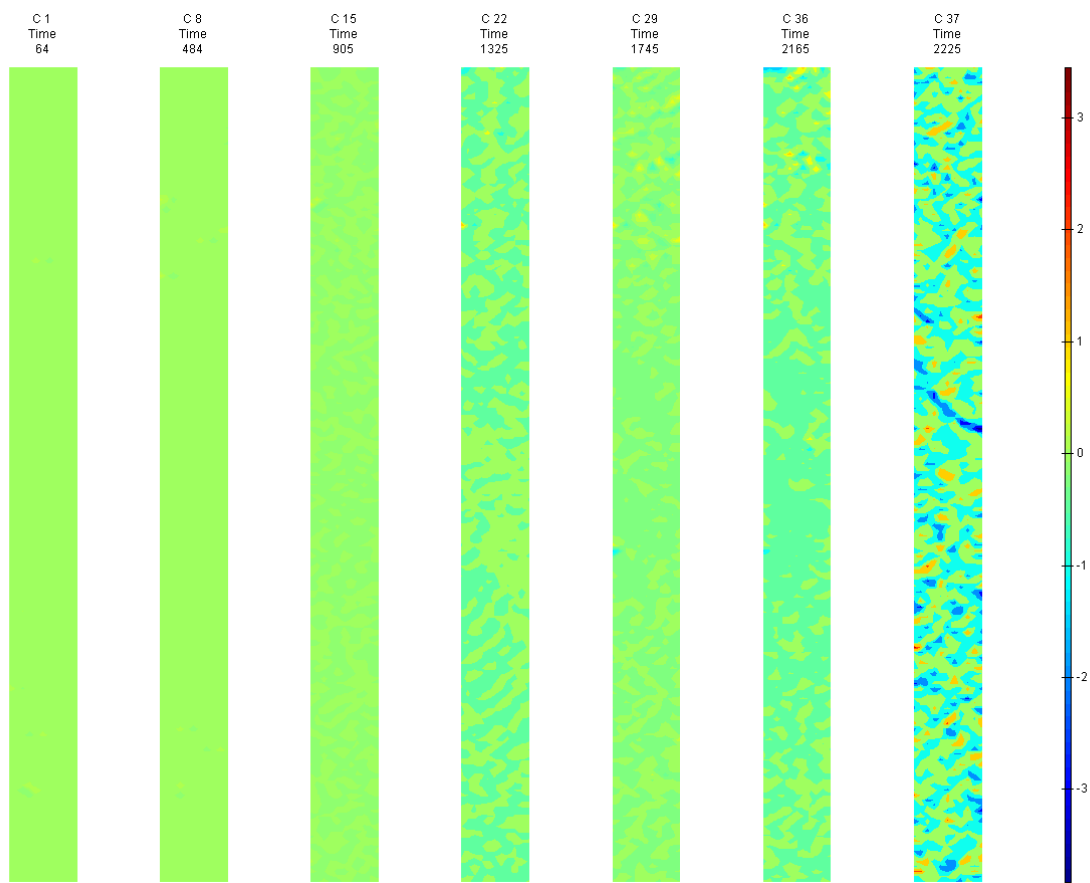
FIGURE 701: XY DIRECTION PIV FIRST-SEQUENTIAL ENGINEERING SHEAR STRAIN OVER TIME

Appendix 6

T5
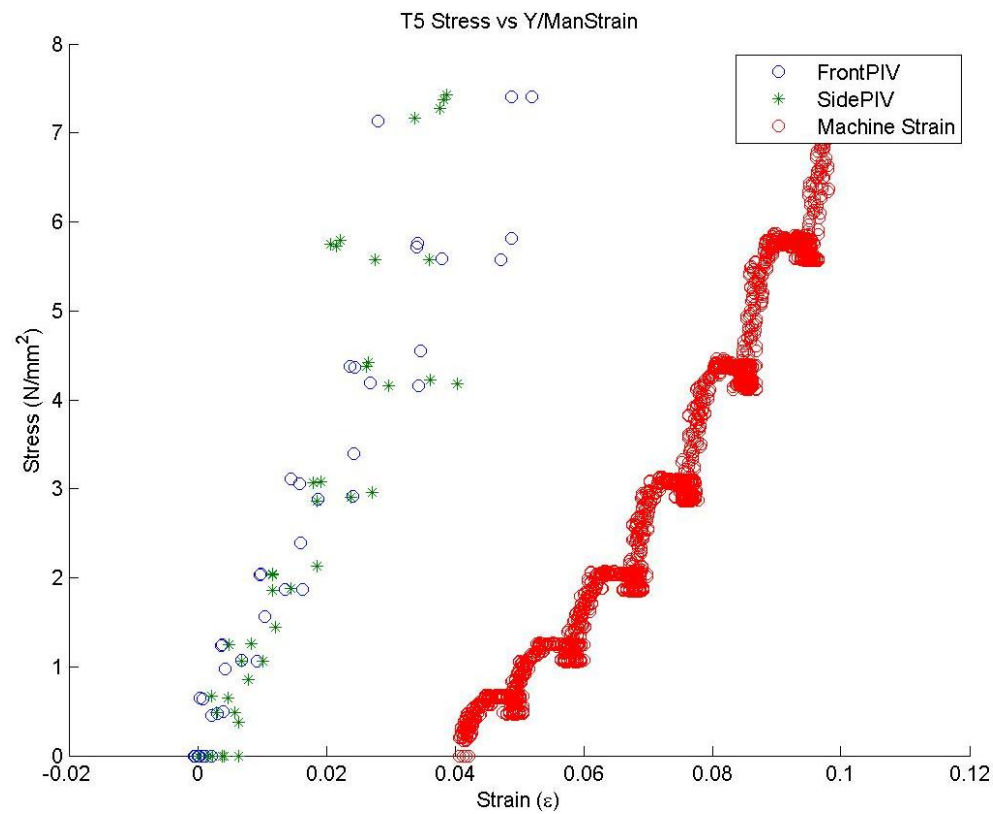
FIGURE 702: T5 TENSILE STRESS VS. MACHINE MEASURED/PIV STRAINS
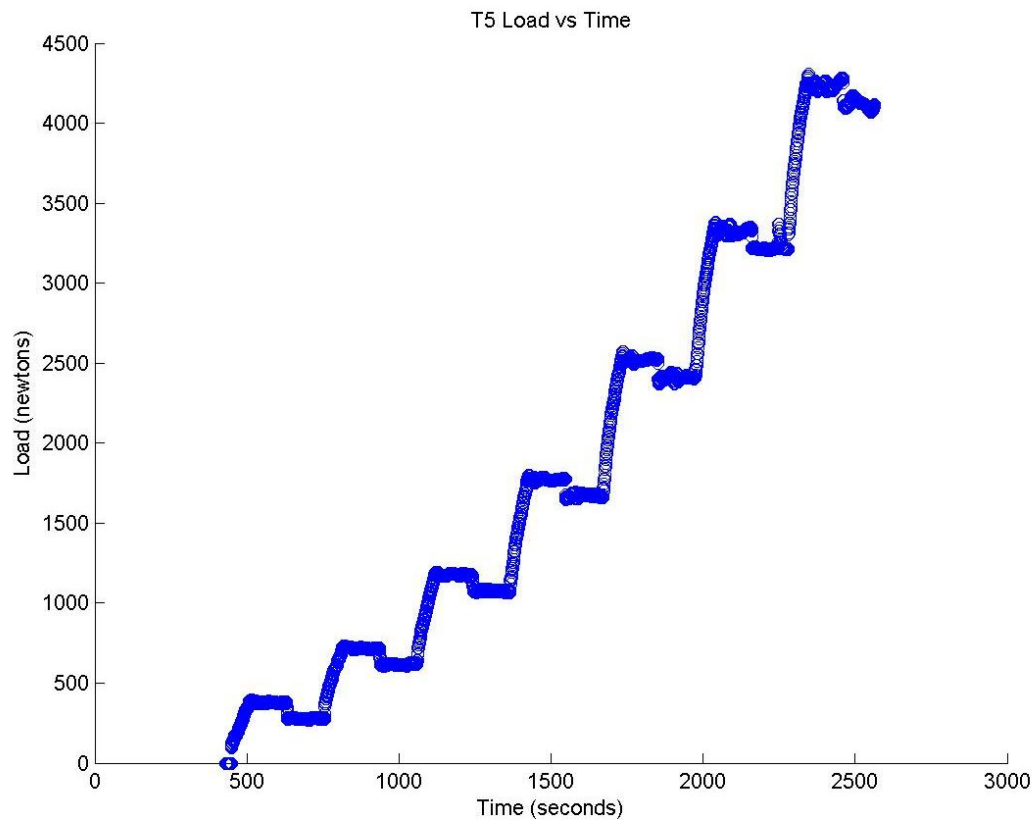
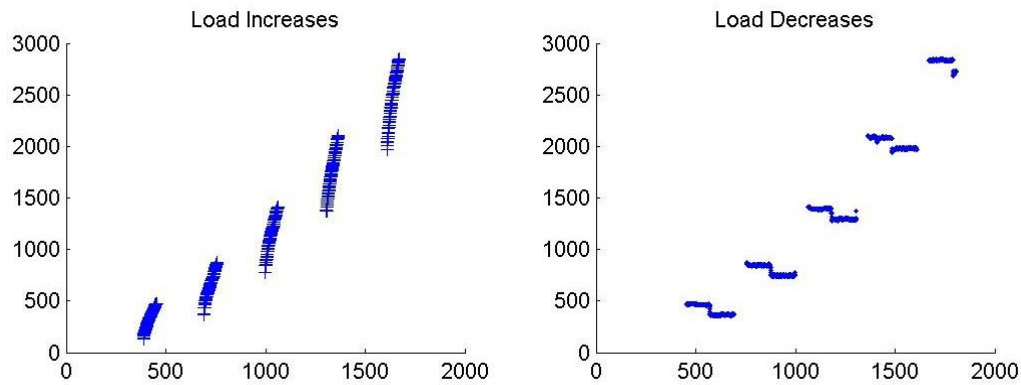FIGURE 703: T5 TENSILE LOAD VS. TIME
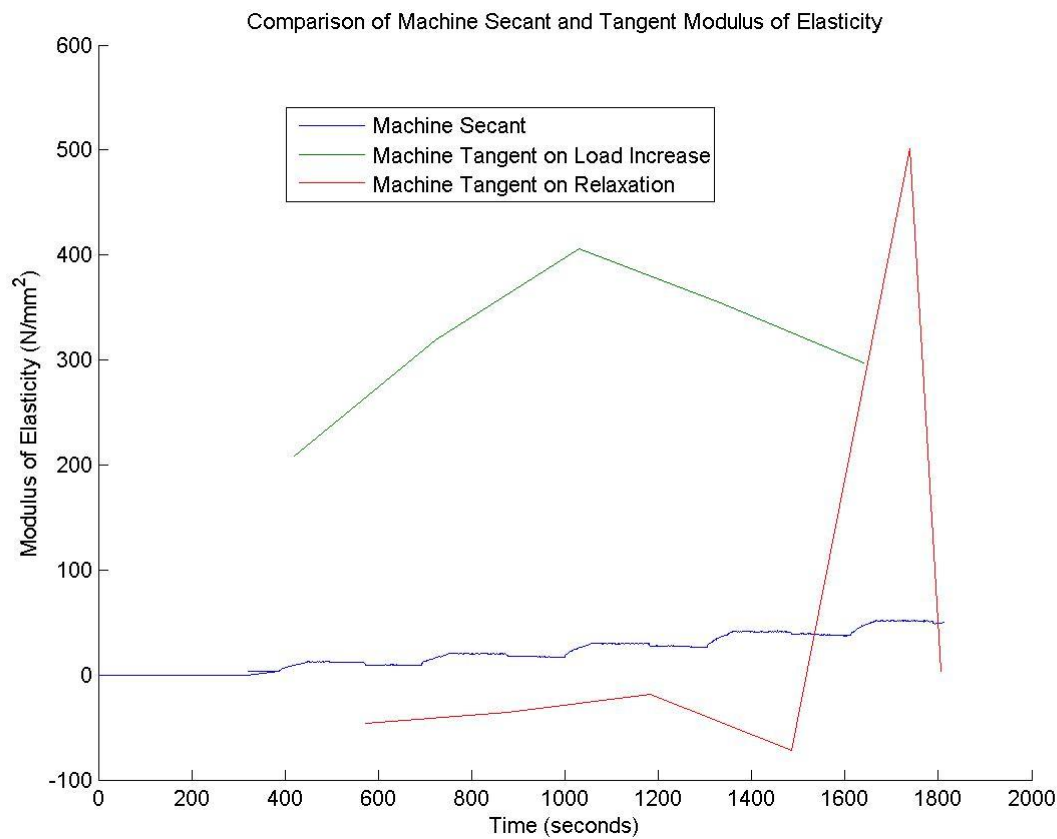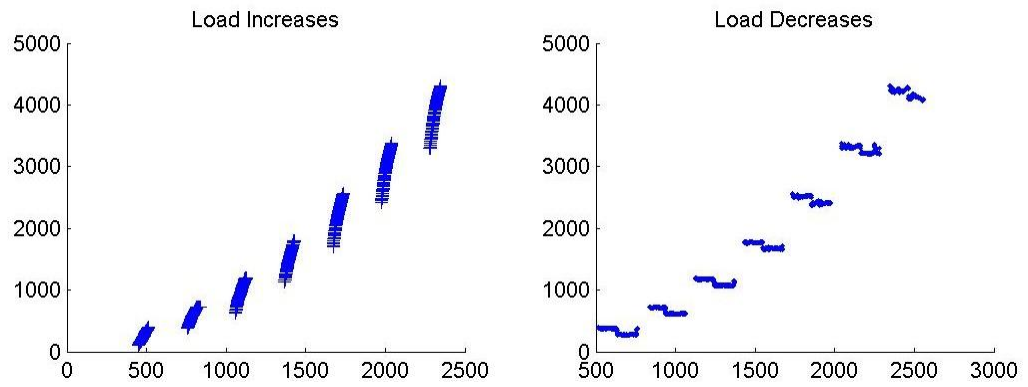
FIGURE 704: T5 CREEP LOADING: INCREMENTS AND RELAXATION
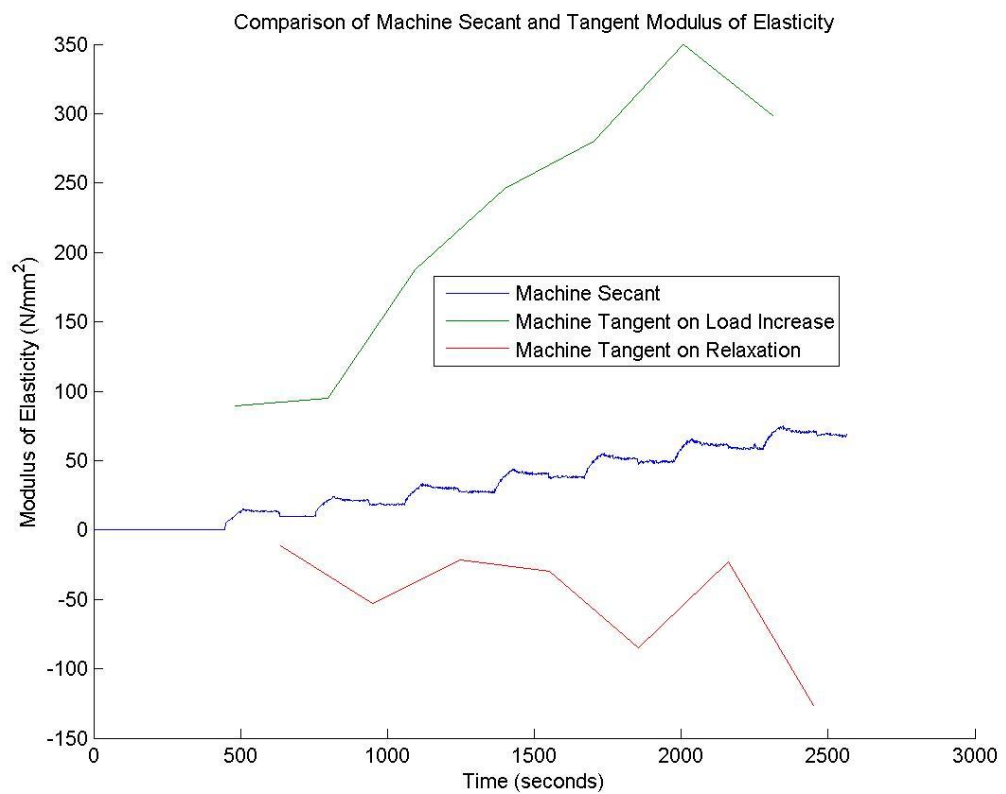
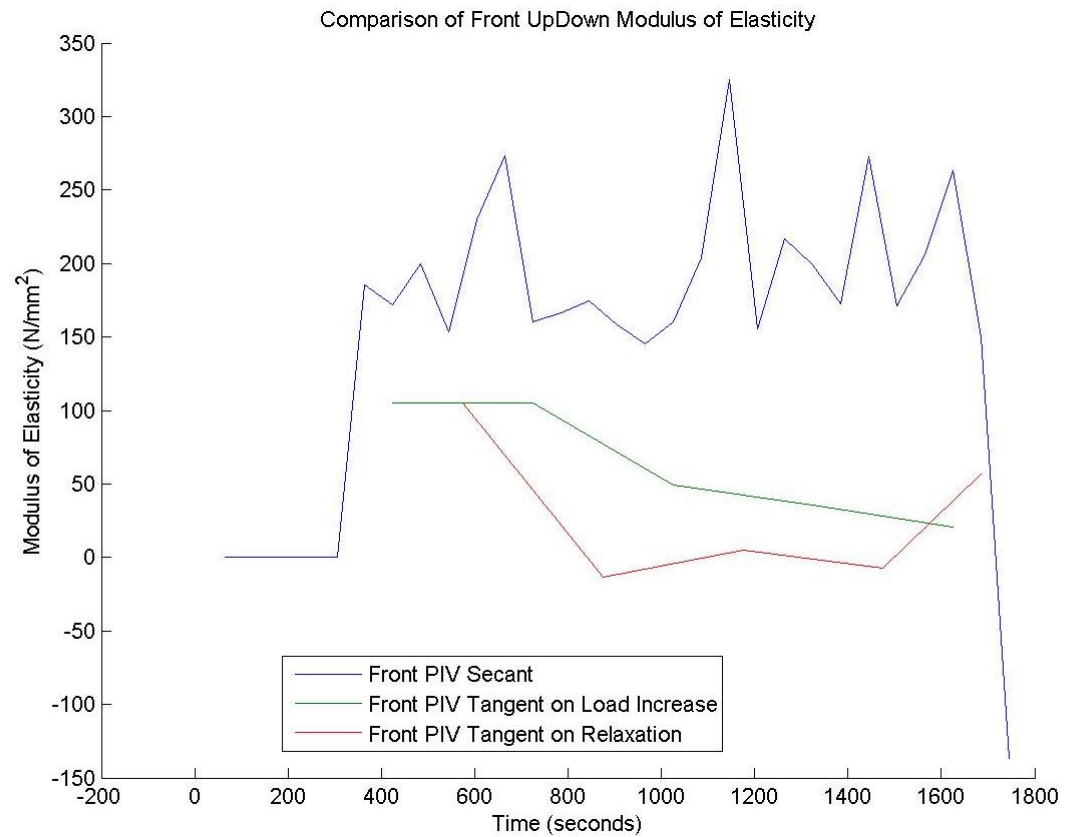FIGURE 705: T5 MACHINE MEASURED SECANT AND TANGENT MODULUS VS. TIME

Appendix 6
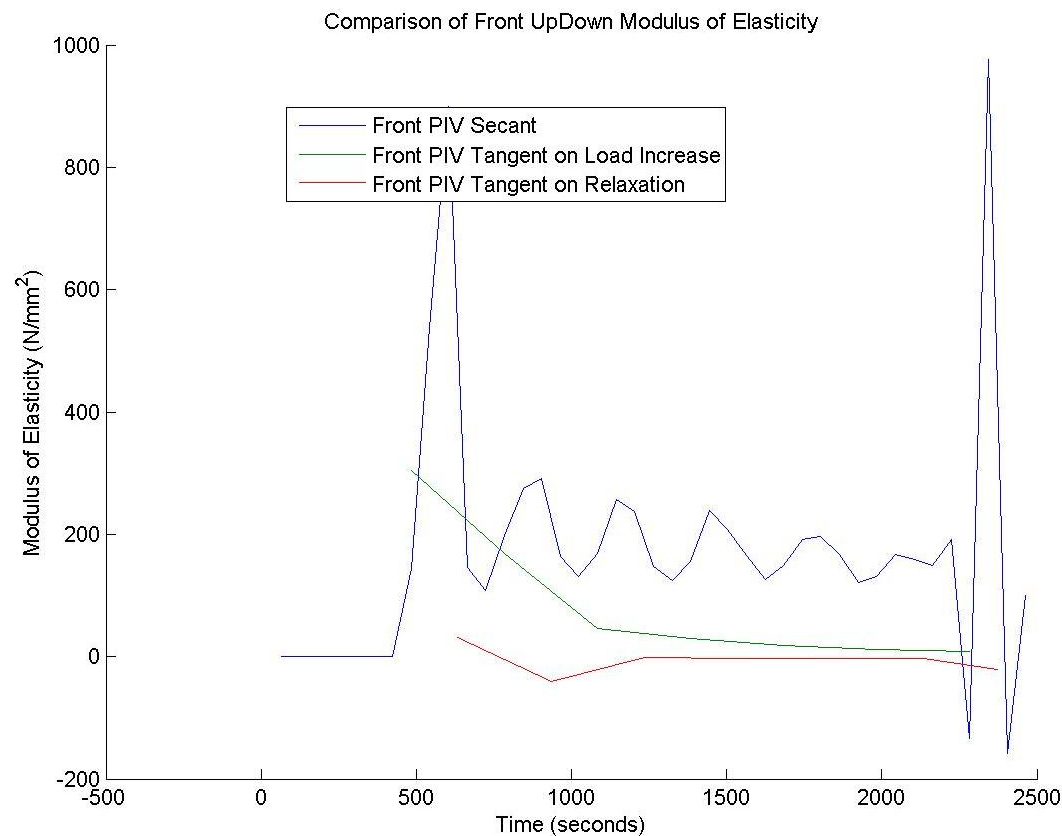
FIGURE 706: T5 FRONT VIEW PIV SECANT AND TANGENT MODULUS VS. TIME
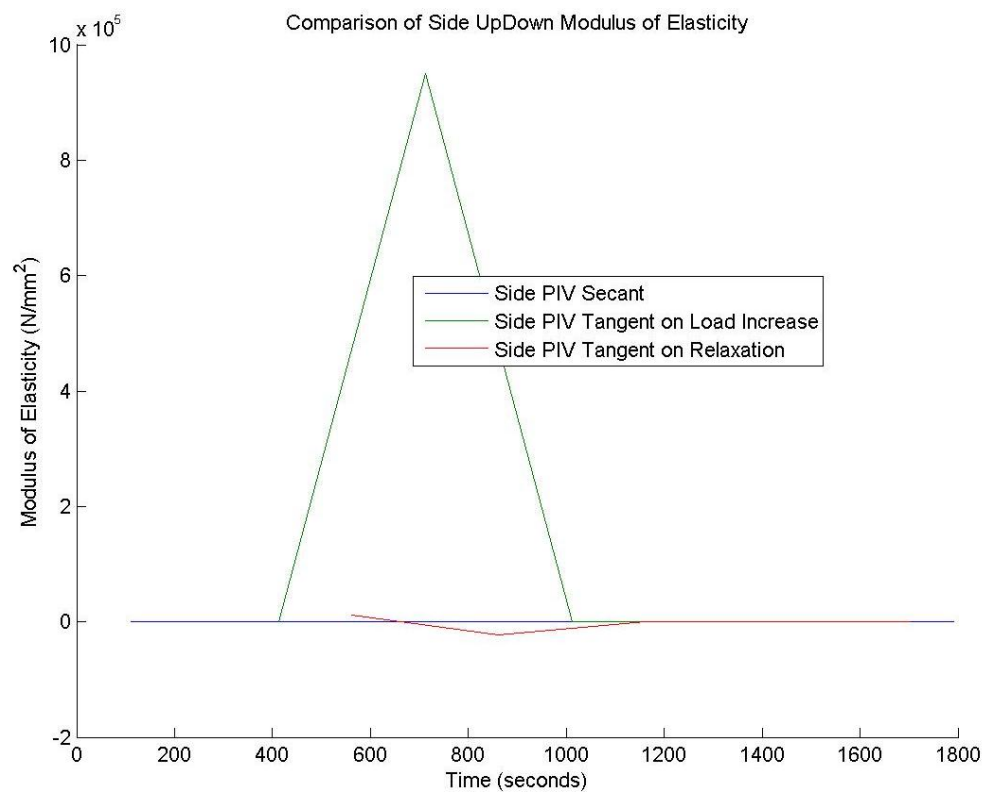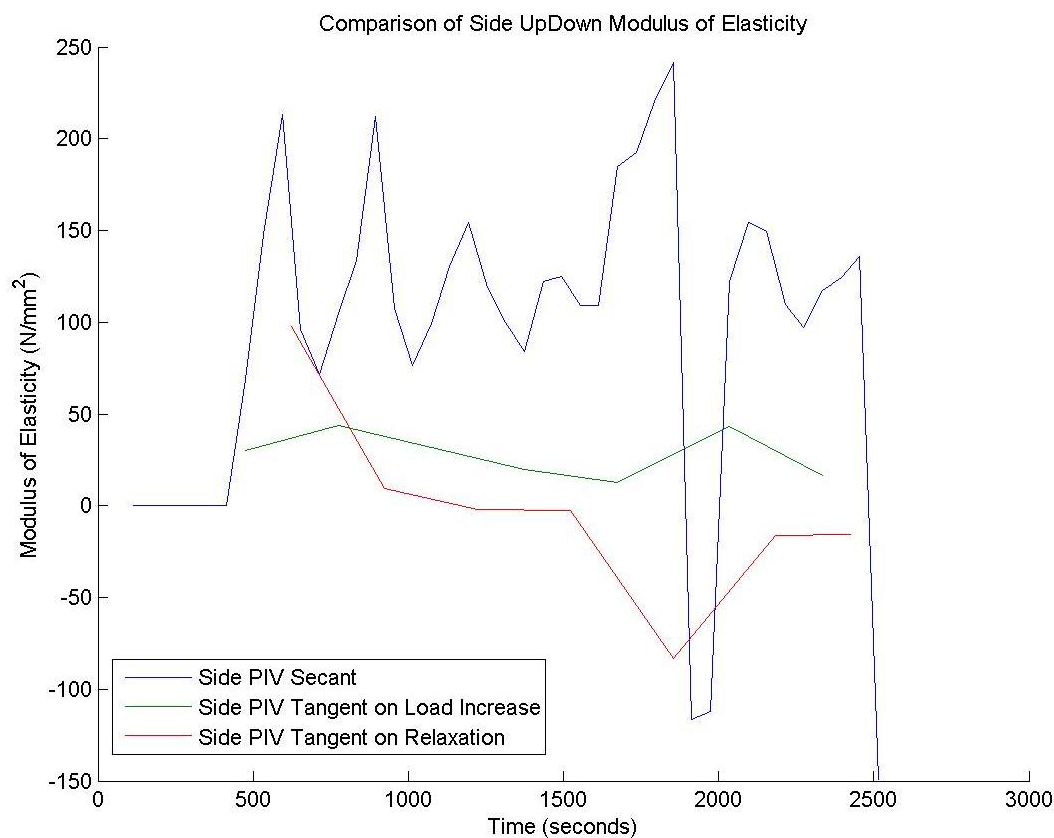

FIGURE 707: T5 SIDE VIEW PIV SECANT AND TANGENT MODULUS VS. TIME
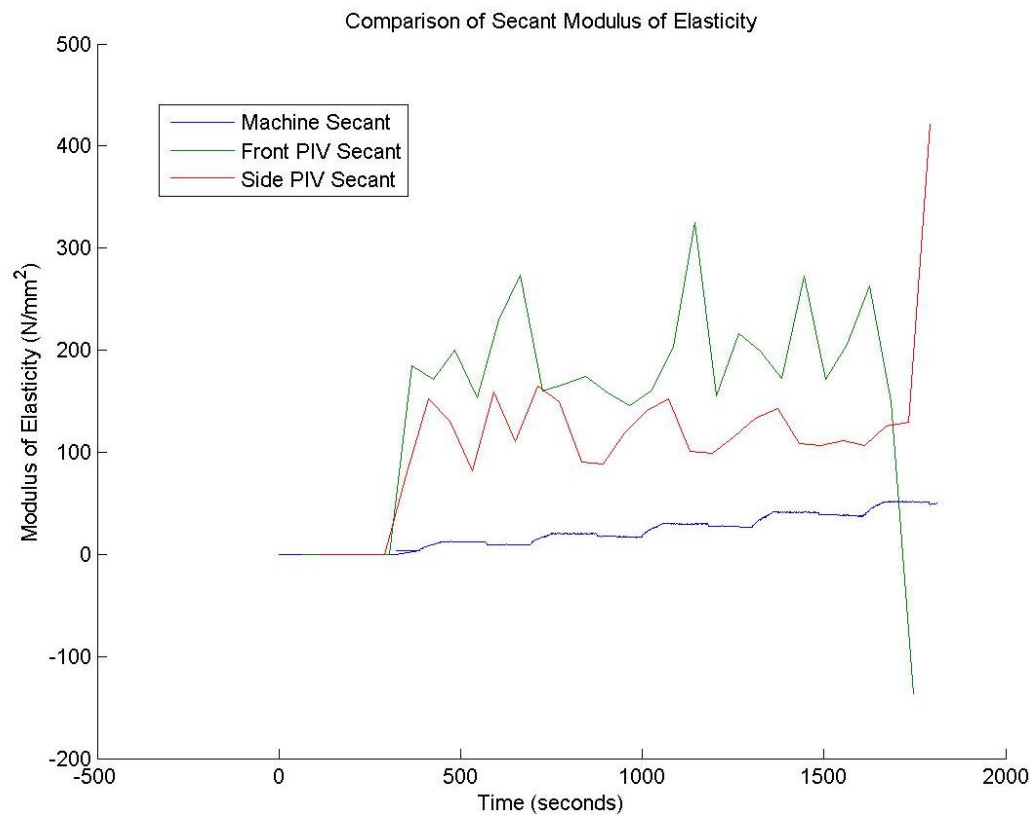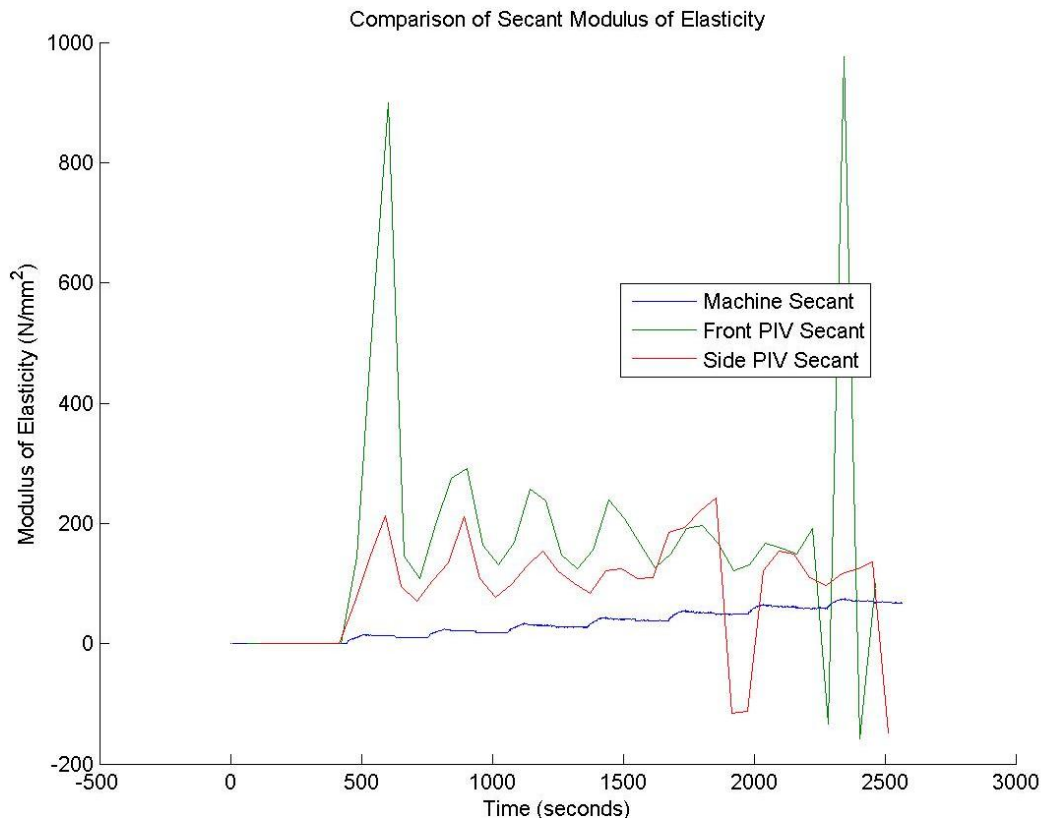
FIGURE 708: T5 COMPARISON OF MACHINE MEASURED AND PIV SECANT MODULUS VS. TIME
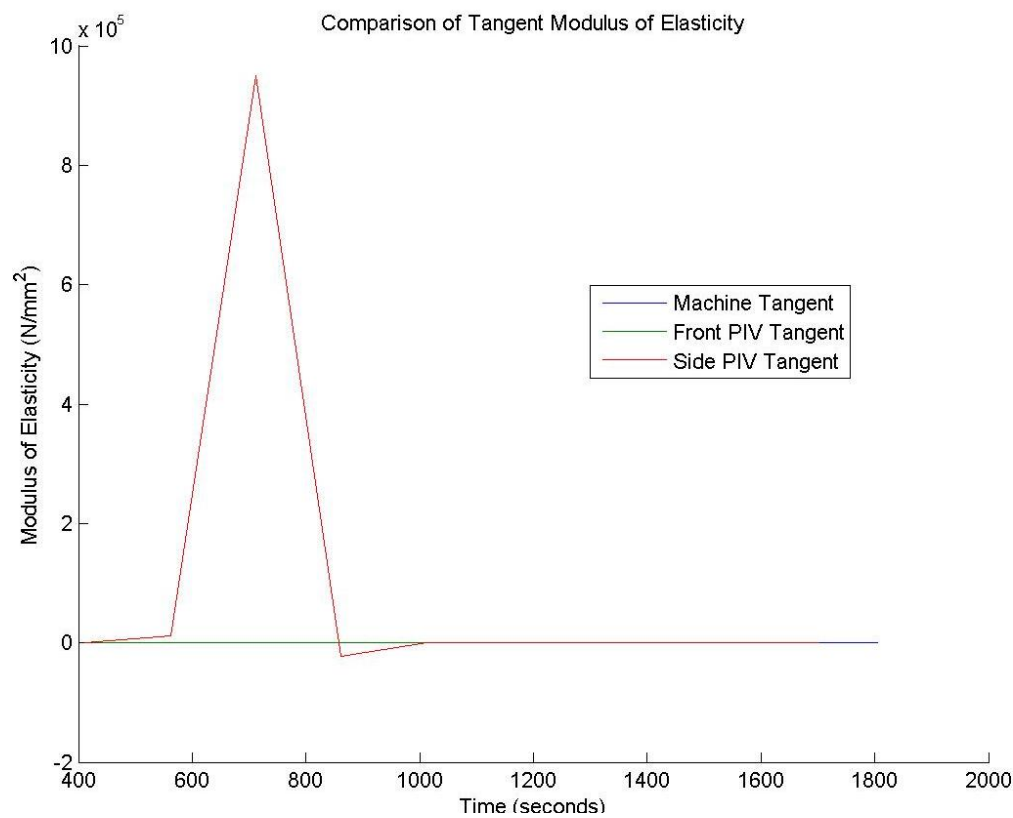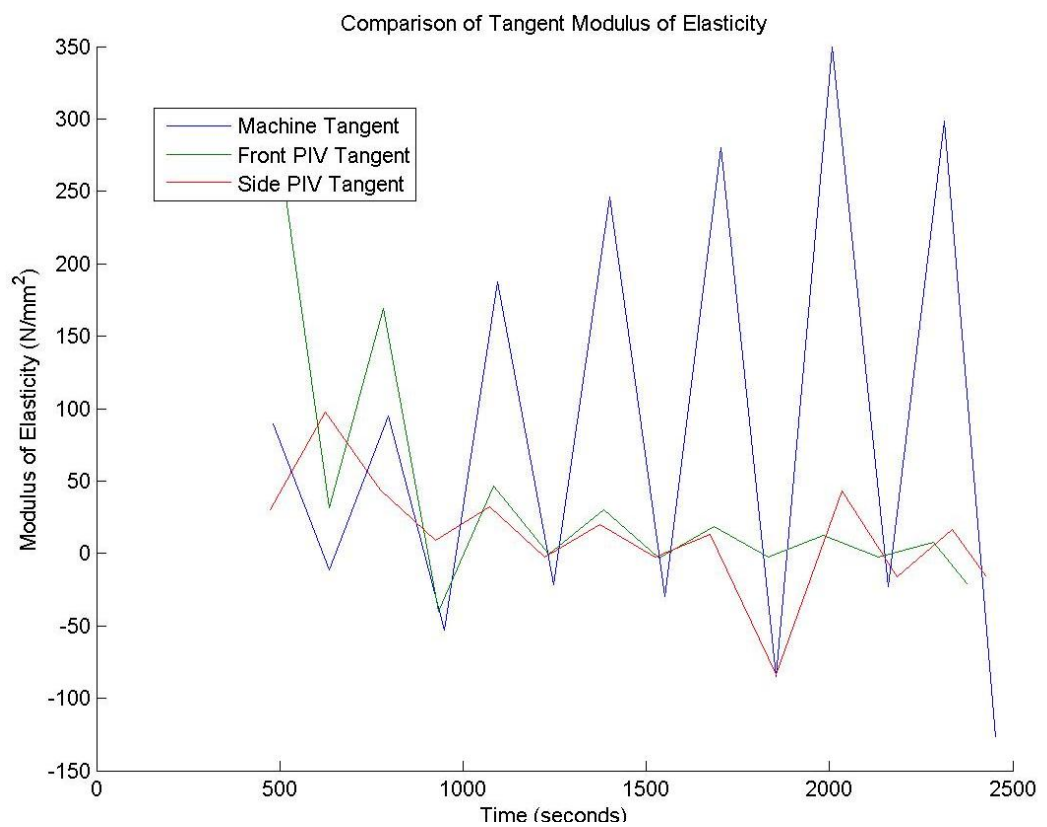

FIGURE 709: T5 COMPARISON OF MACHINE MEASURED AND PIV TANGENT MODULUS VS.

TIME

Appendix 6
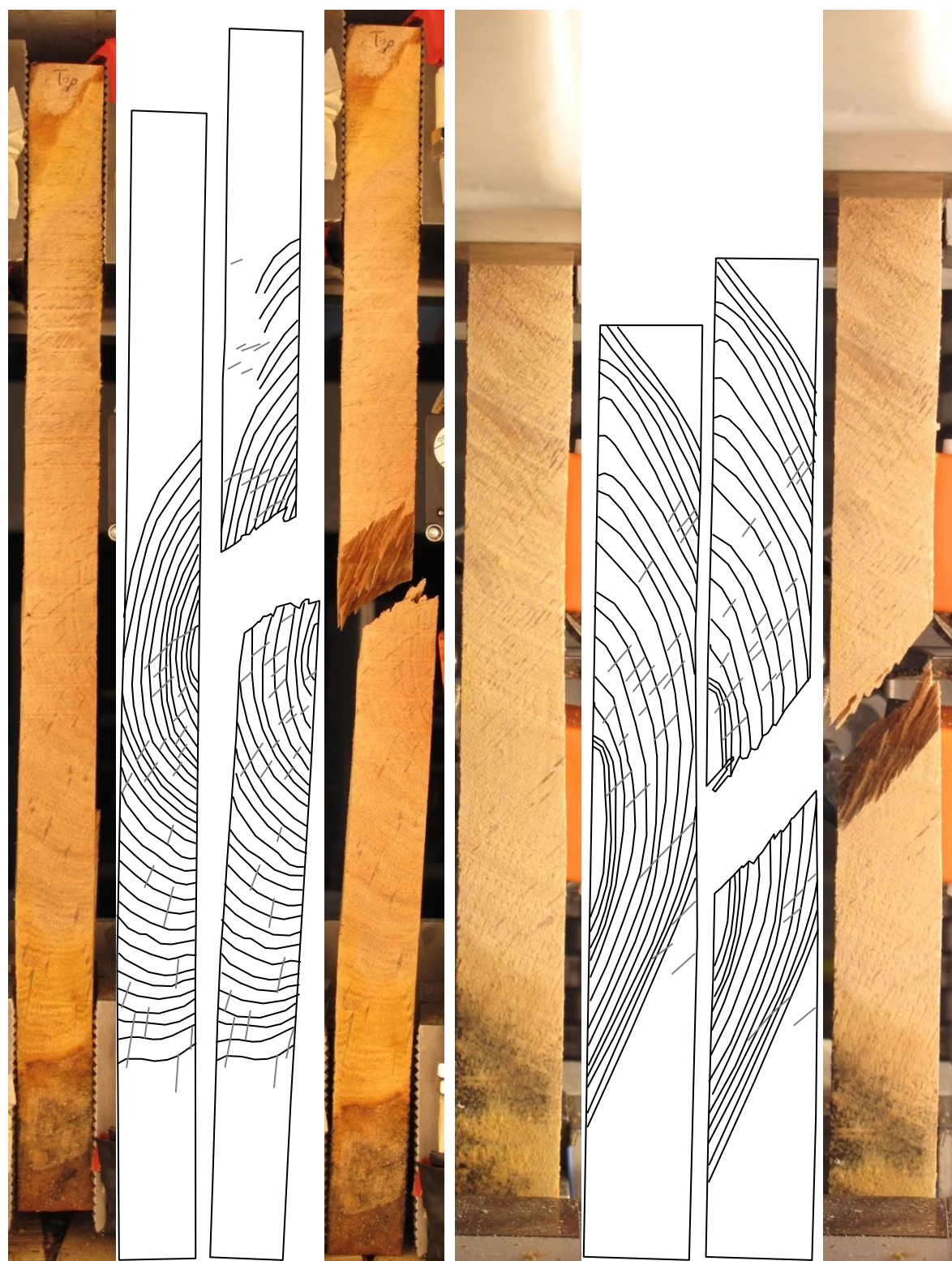
T5 Sample

FIGURE 710: SAMPLE GRAIN ORIENTATIONS OF THE FRONT (LEFT 4 IMAGES) AND SIDE (RIGHT

4 IMAGES) VIEW BEFORE (FIRST 2 OF 4 IMAGES) AND AFTER (LAST 2 OF 4 IMAGES) BREAKAGE

T5 Front View
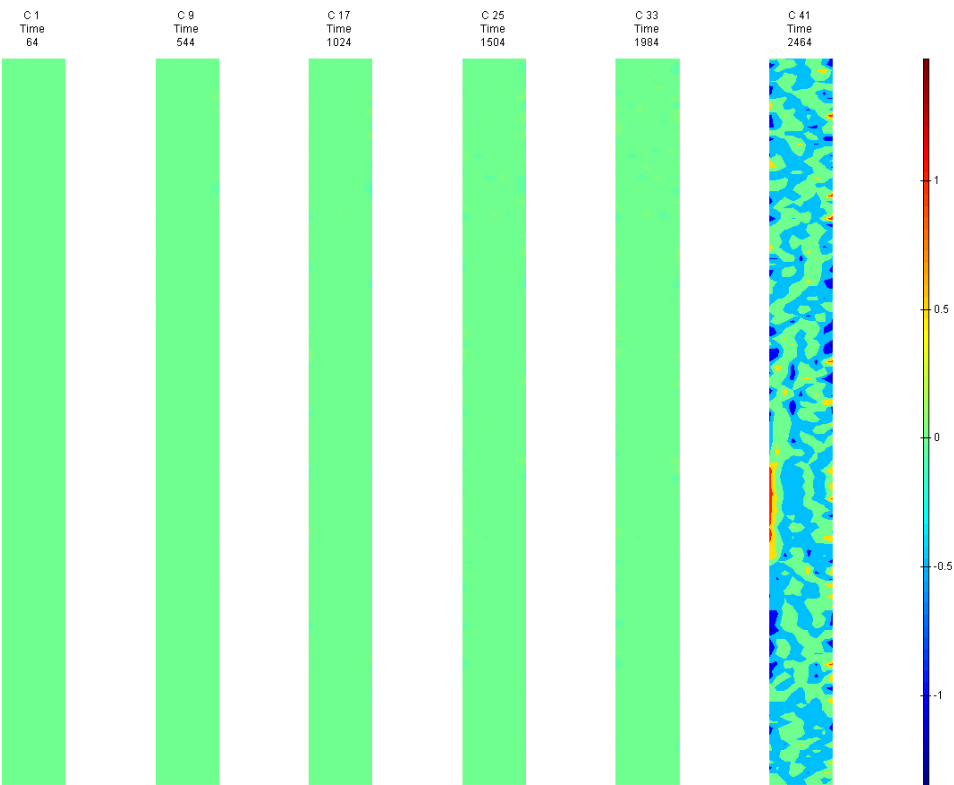
FIGURE 711: X DIRECTION PIV SEQUENTIAL ENGINEERING STRAIN OVER TIME
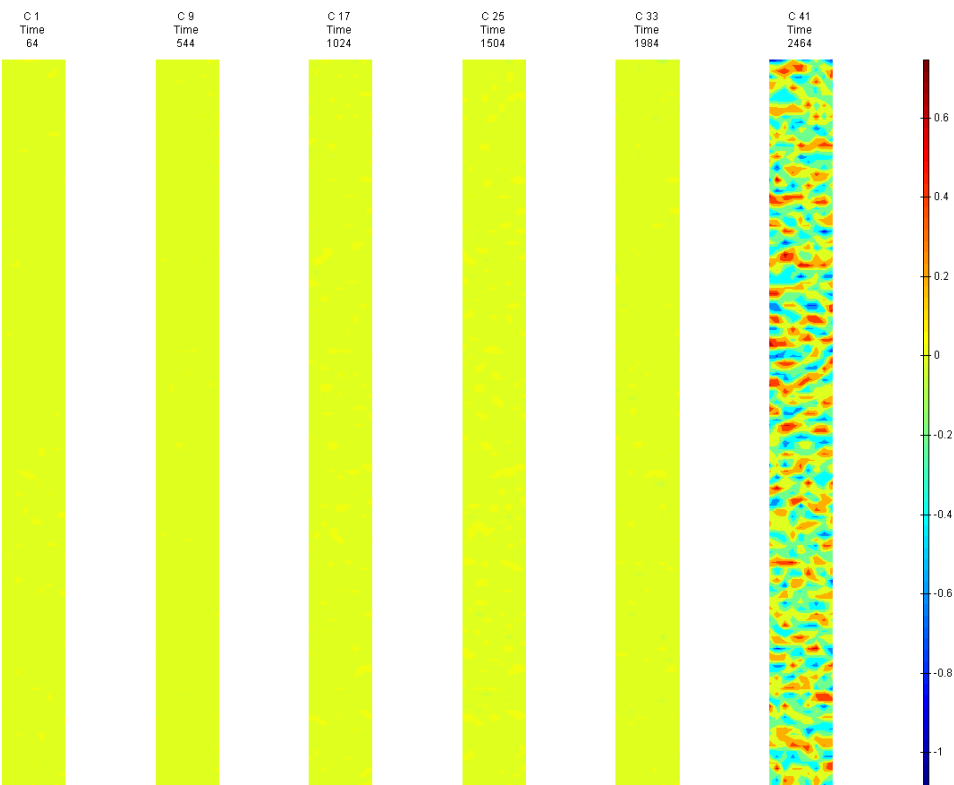
FIGURE 712: Y DIRECTION PIV SEQUENTIAL ENGINEERING STRAIN OVER TIME

Appendix 6
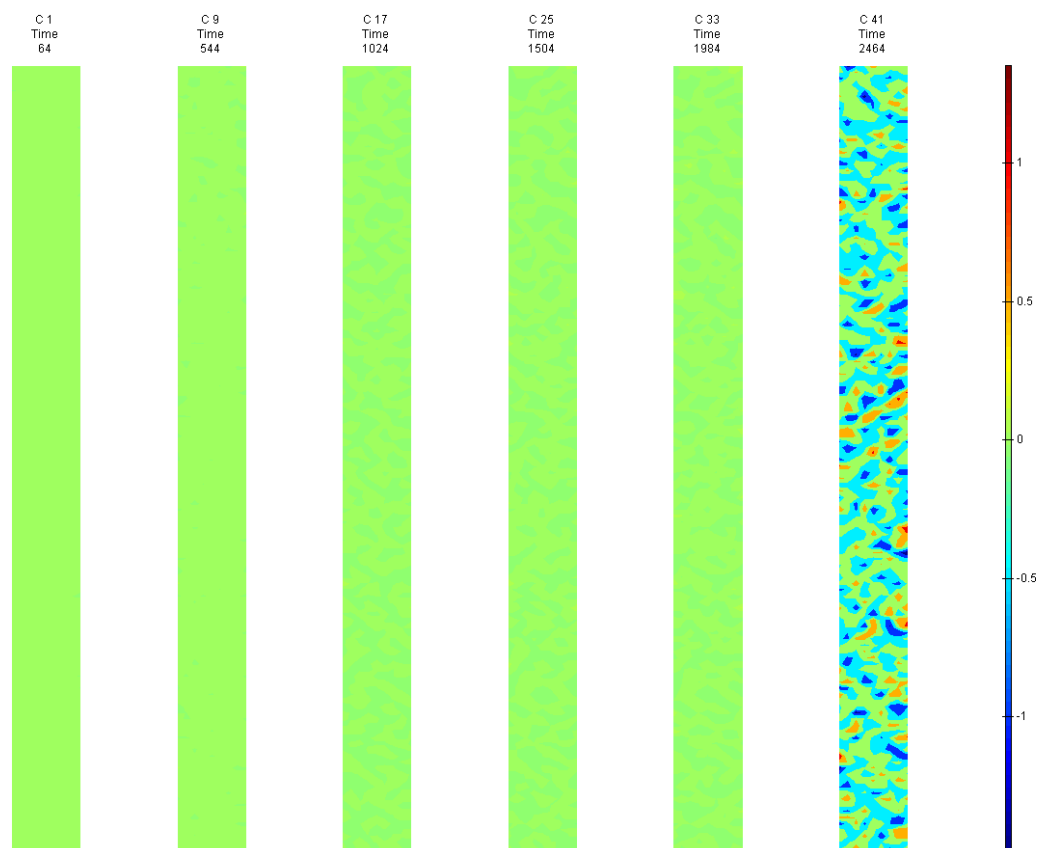
FIGURE 713: XY DIRECTION PIV SEQUENTIAL ENGINEERING SHEAR STRAIN OVER TIME
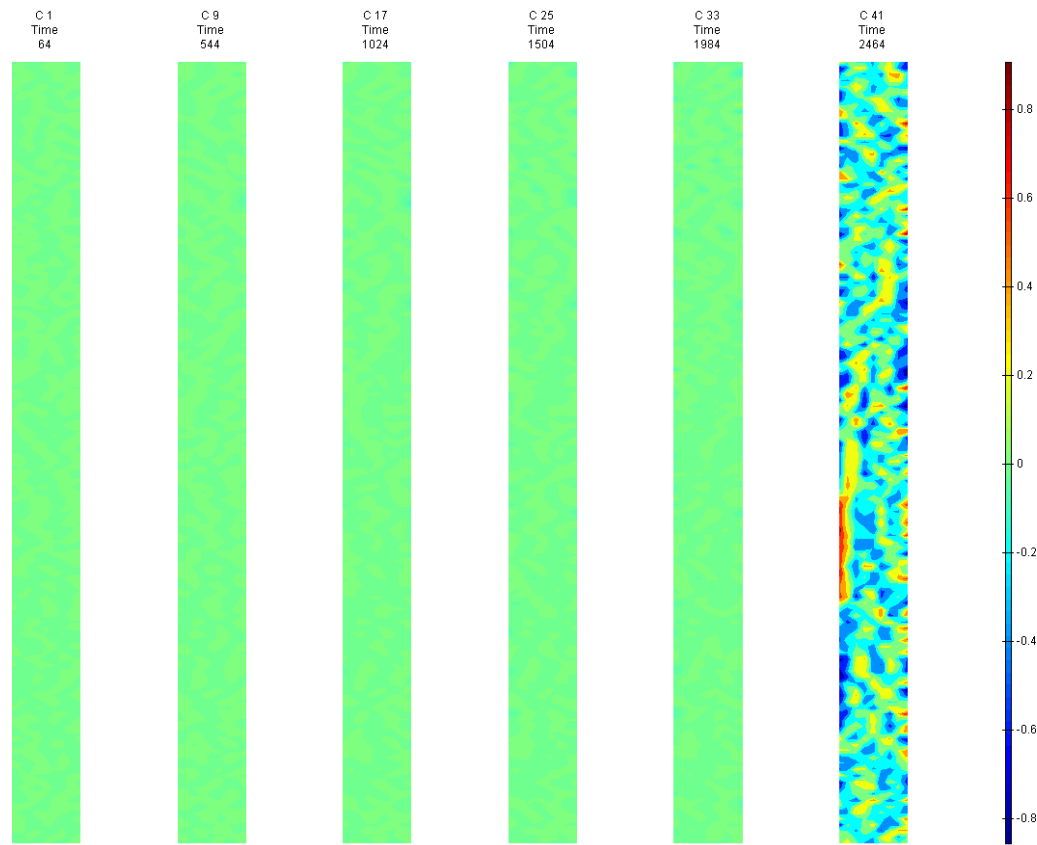
FIGURE 714: X DIRECTION PIV SEQUENTIAL TRUE STRAIN OVER TIME
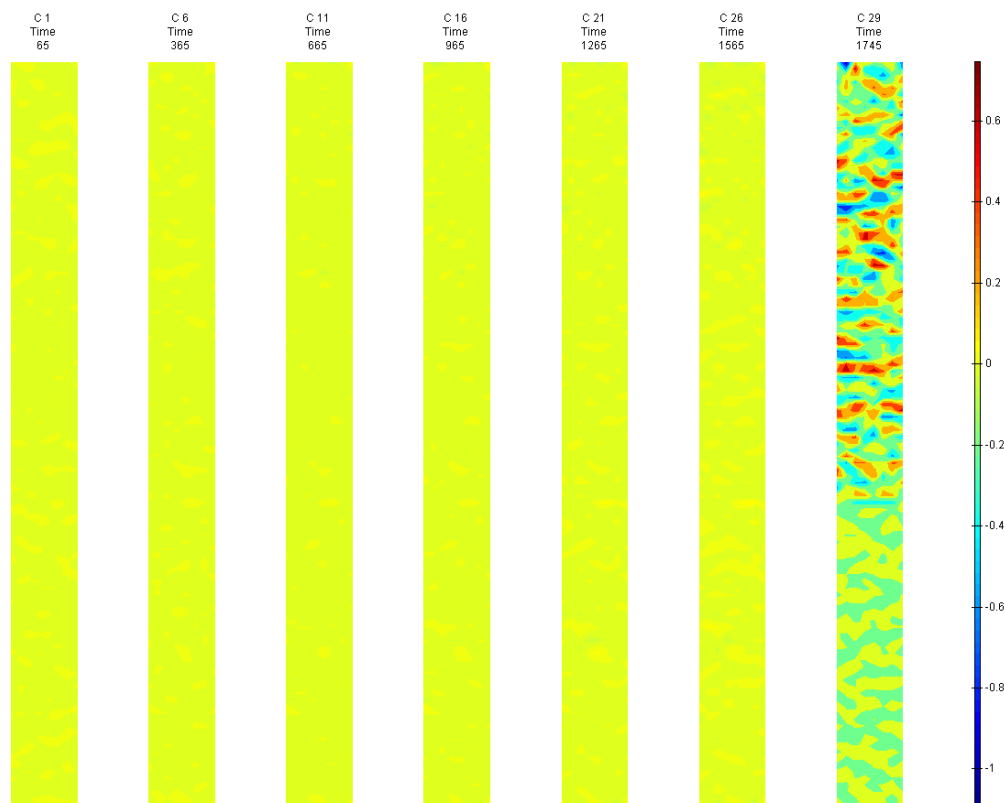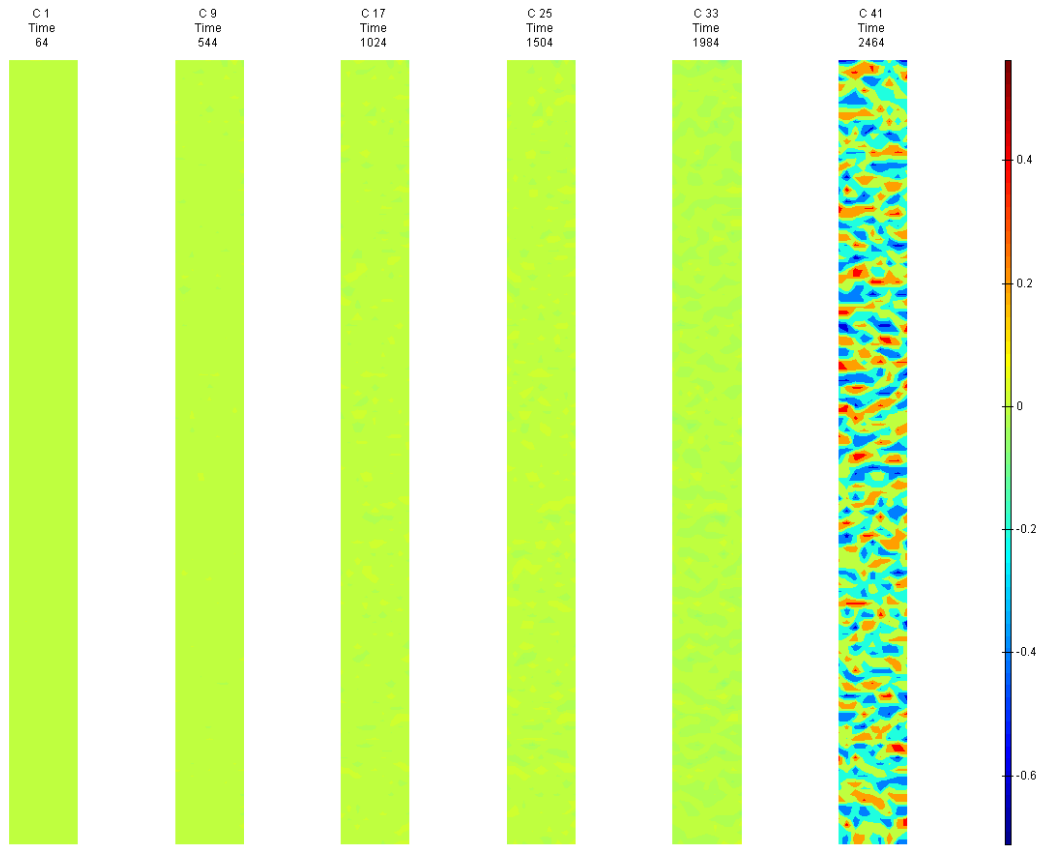
FIGURE 715: Y DIRECTION PIV SEQUENTIAL TRUE STRAIN OVER TIME
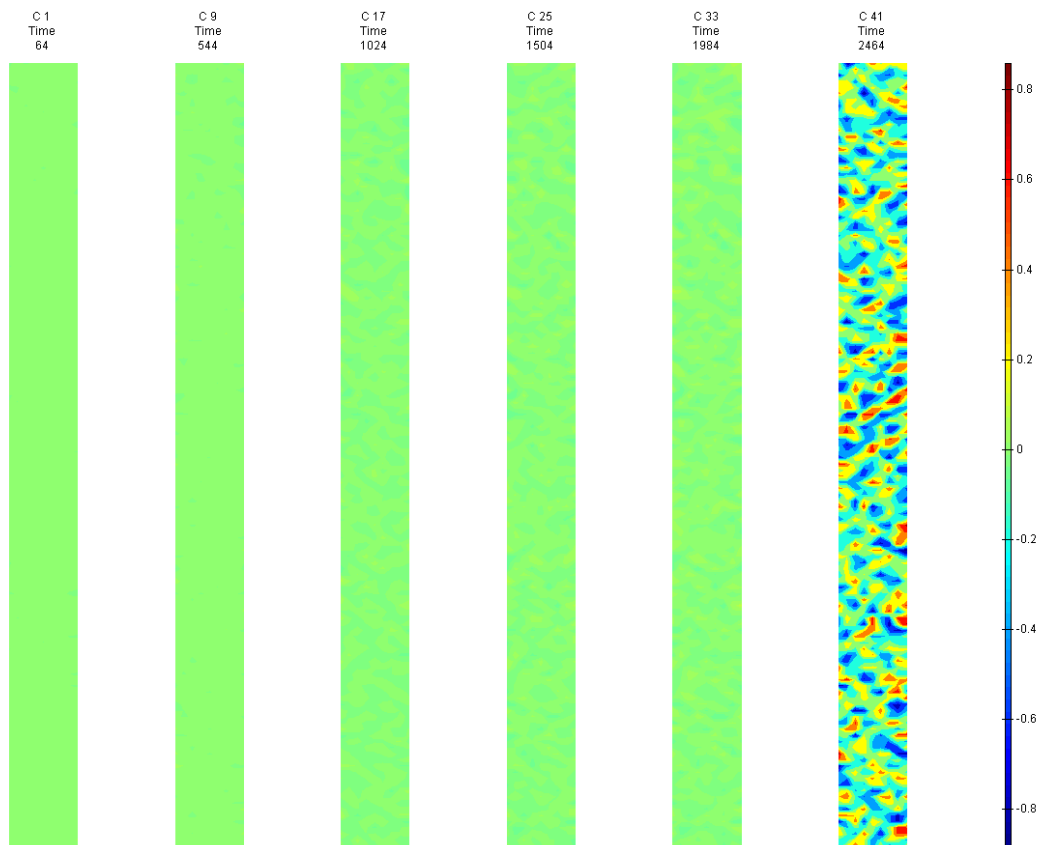
FIGURE 716: XY DIRECTION PIV SEQUENTIAL TRUE SHEAR STRAIN OVER TIME
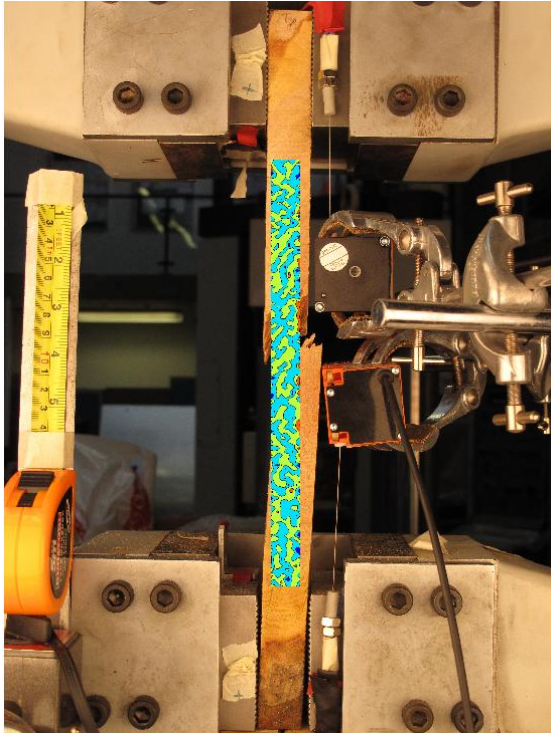
FIGURE 717: X DIRECTION PIV FIRST–LAST DITCH ENGINEERING STRAIN OVER IMAGE
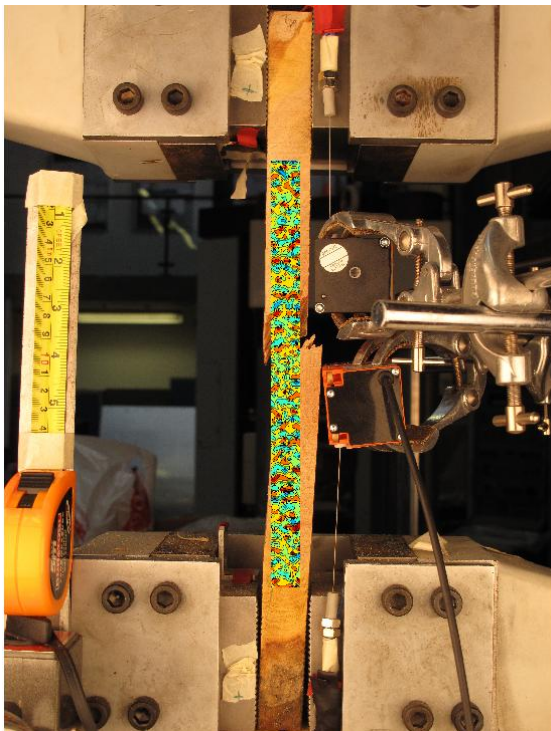
FIGURE 718: Y DIRECTION PIV FIRST–LAST DITCH ENGINEERING STRAIN OVER IMAGE
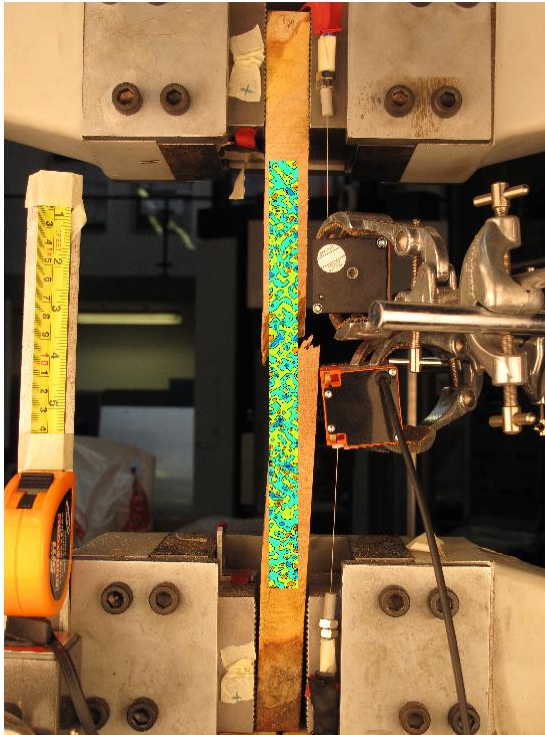
FIGURE 719: XY DIRECTION PIV FIRST–LAST DITCH ENGINEERING SHEAR STRAIN OVER
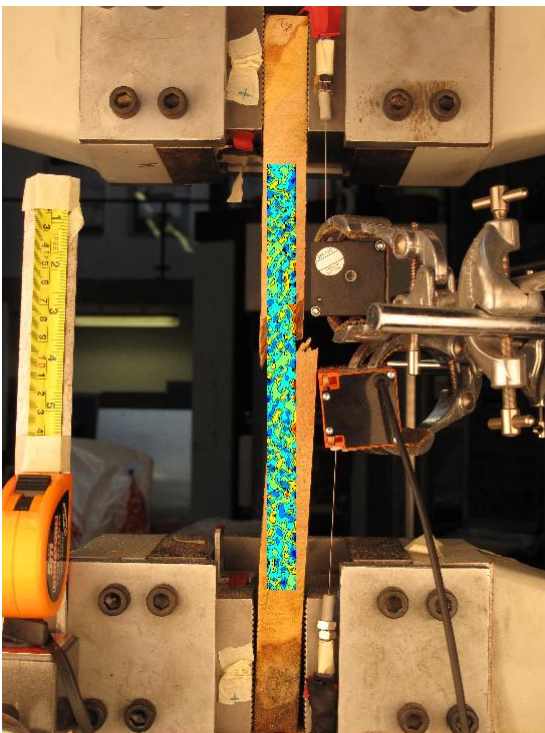
IMAGE

FIGURE 720: X DIRECTION PIV FIRST–LAST DITCH TRUE STRAIN OVER IMAGE
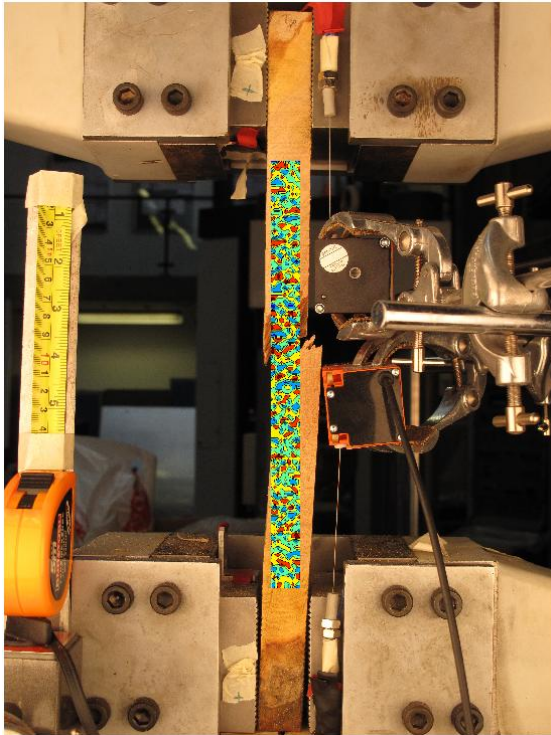
FIGURE 721: Y DIRECTION PIV FIRST–LAST DITCH TRUE STRAIN OVER IMAGE
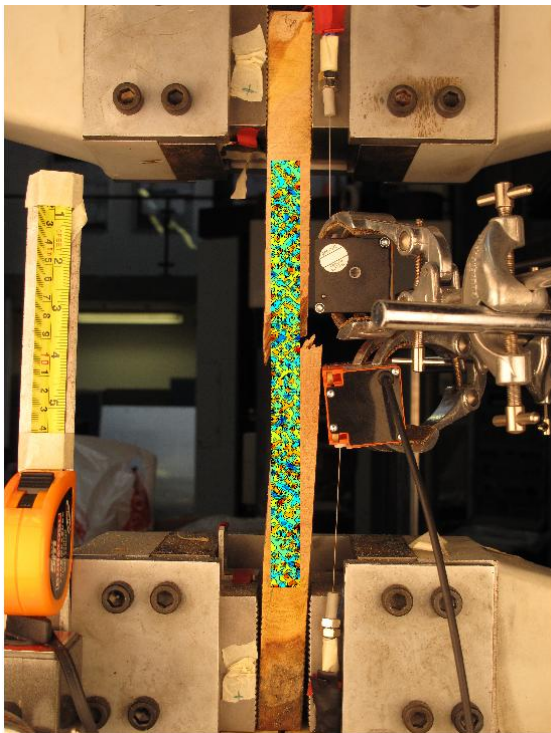
FIGURE 722: XY DIRECTION PIV FIRST–LAST DITCH TRUE SHEAR STRAIN OVER IMAGE
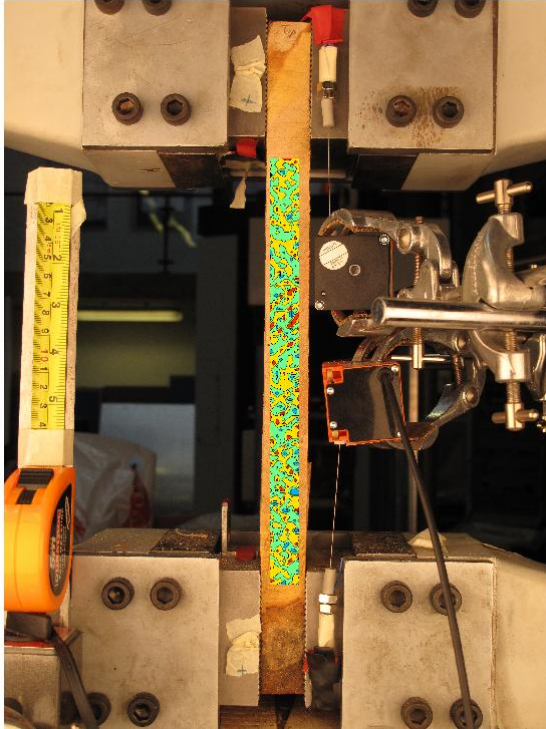
FIGURE 723: XY DIRECTION PIV FIRST–SEQUENTIAL ENGINEERING SHEAR STRAIN OVER

IMAGE
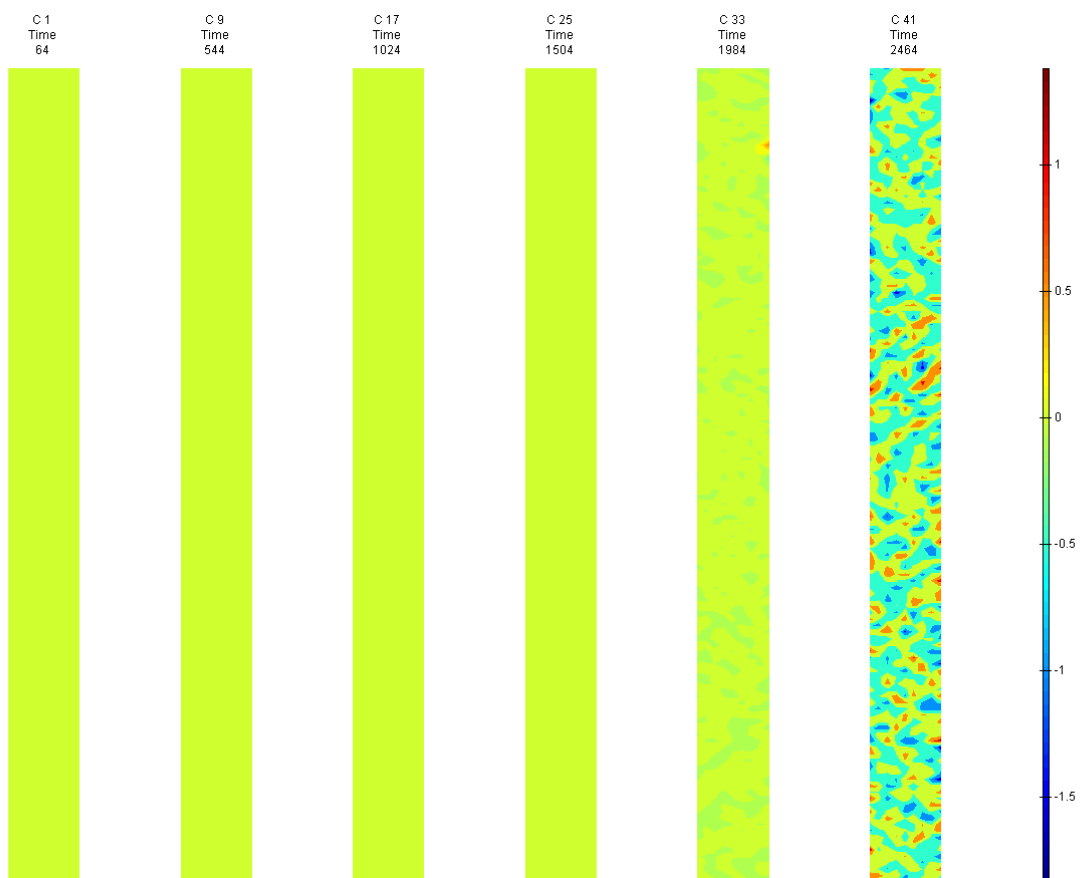
FIGURE 724: XY DIRECTION PIV FIRST–SEQUENTIAL ENGINEERING SHEAR STRAIN OVER TIME

T5 Side View
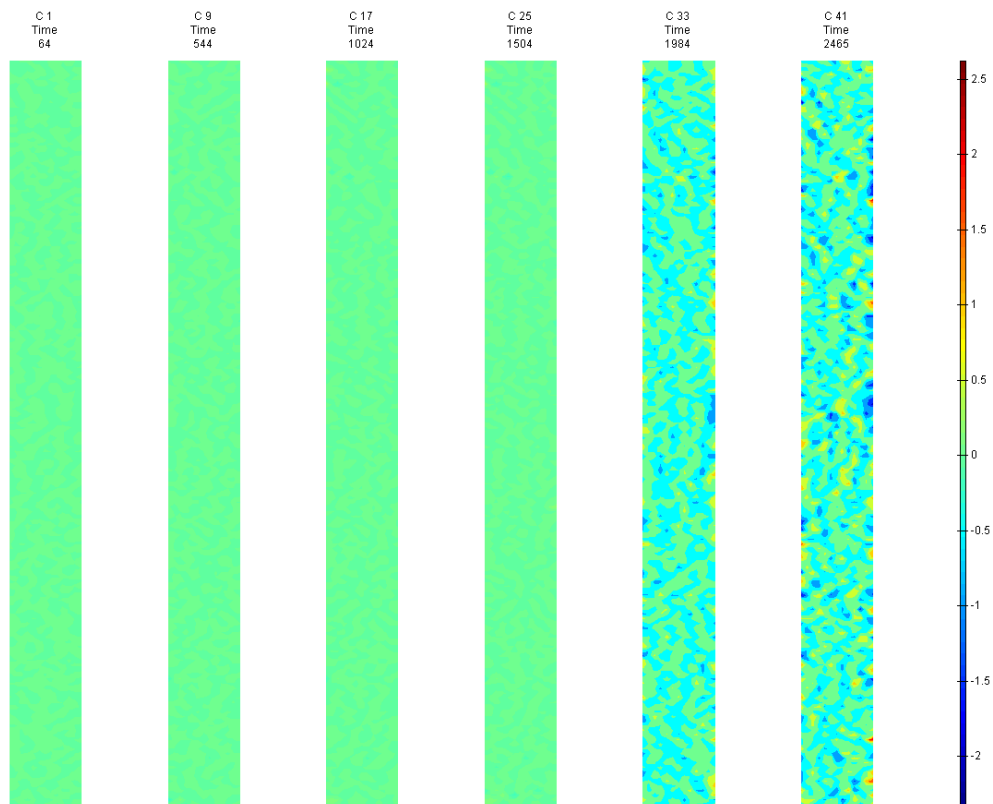
FIGURE 725: X DIRECTION PIV SEQUENTIAL ENGINEERING STRAIN OVER TIME
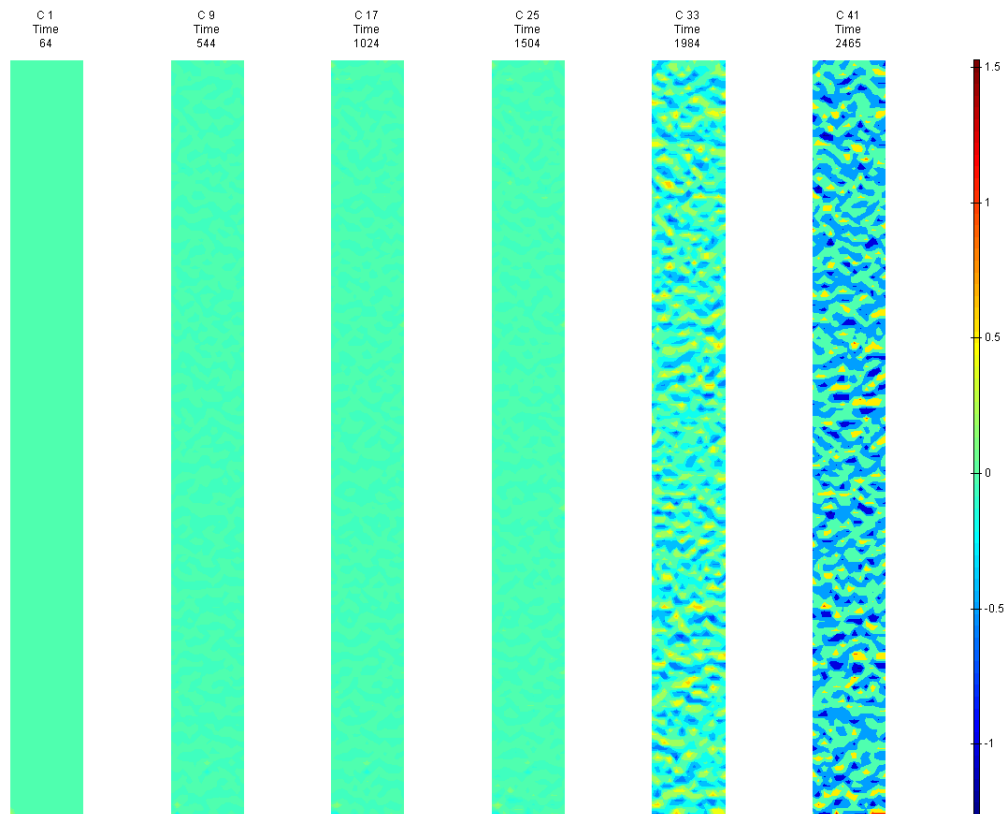
FIGURE 726: Y DIRECTION PIV SEQUENTIAL ENGINEERING STRAIN OVER TIME
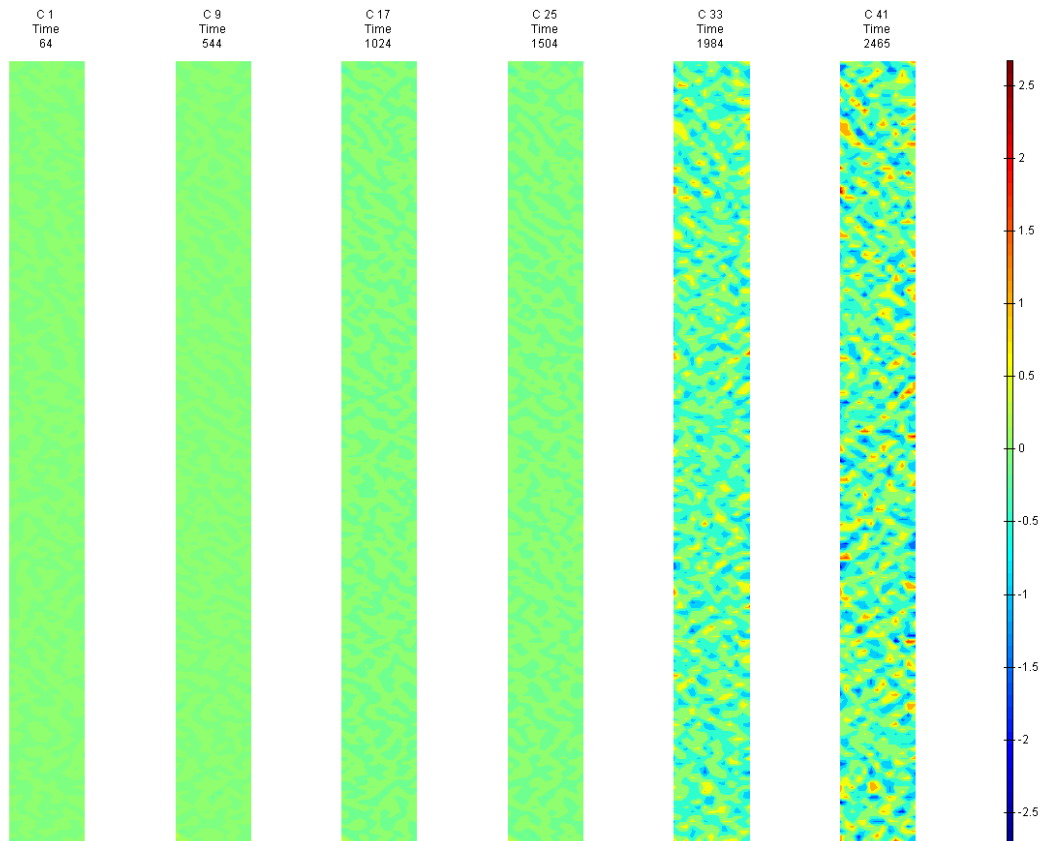
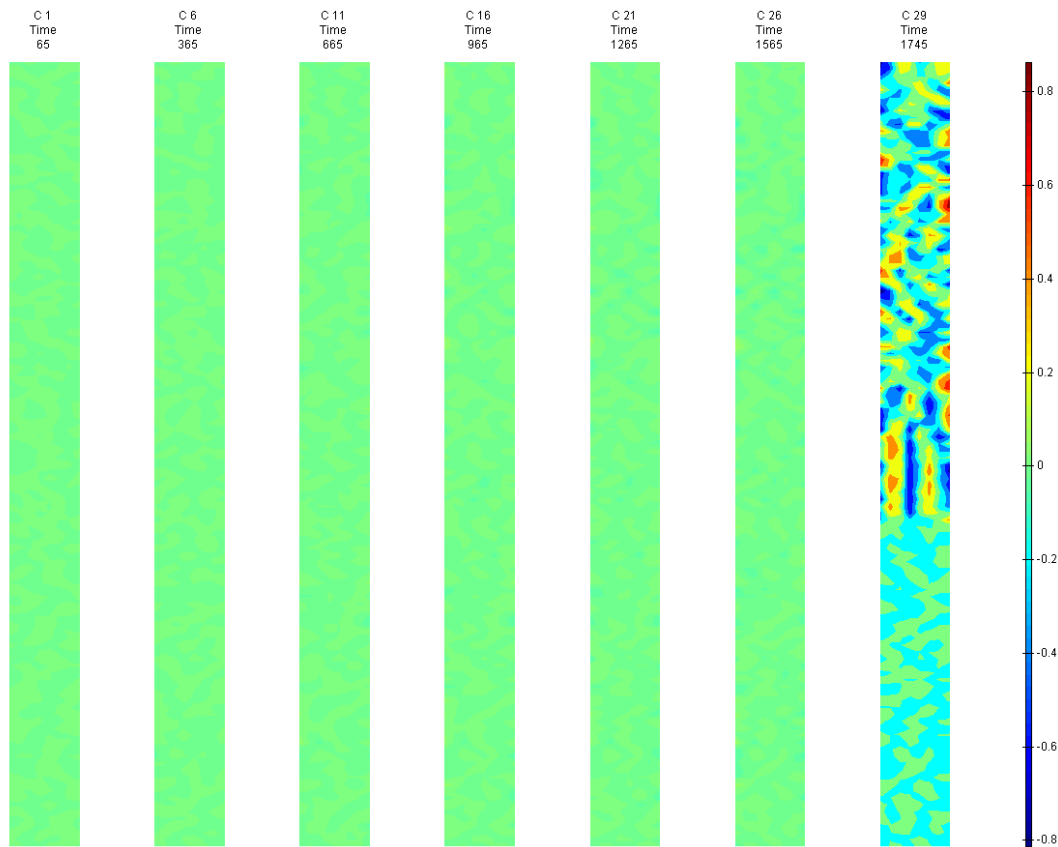FIGURE 727: XY DIRECTION PIV SEQUENTIAL ENGINEERING SHEAR STRAIN OVER TIME
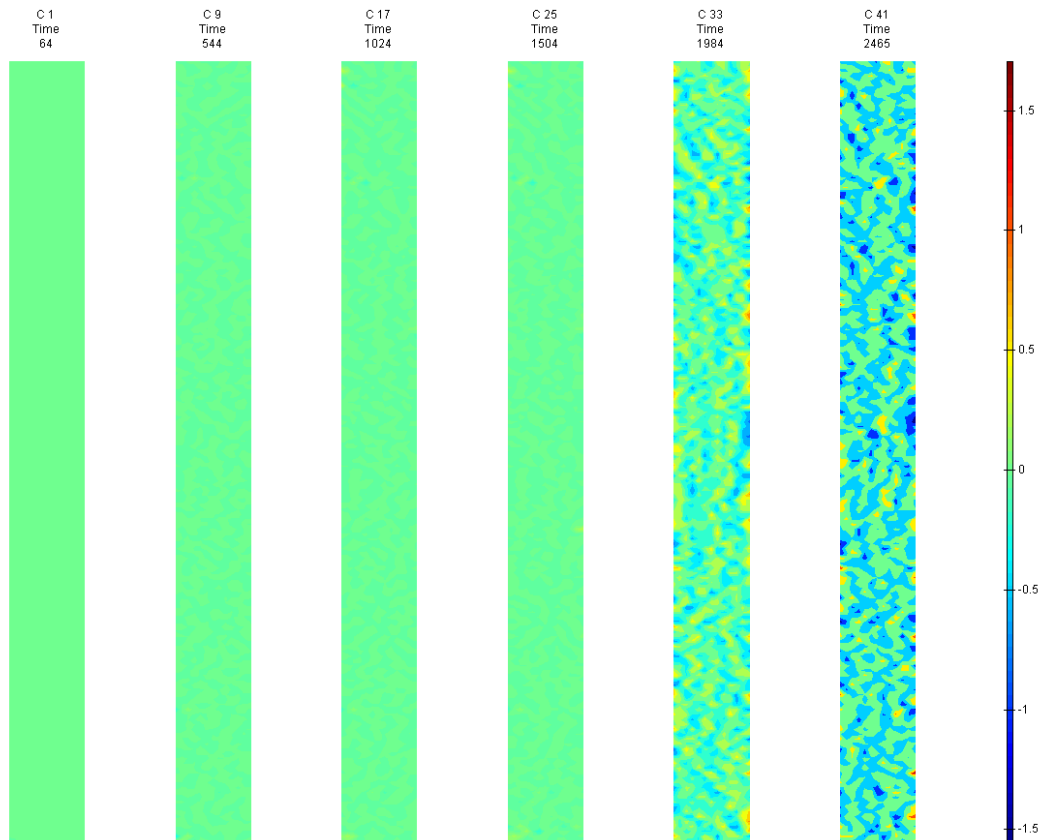
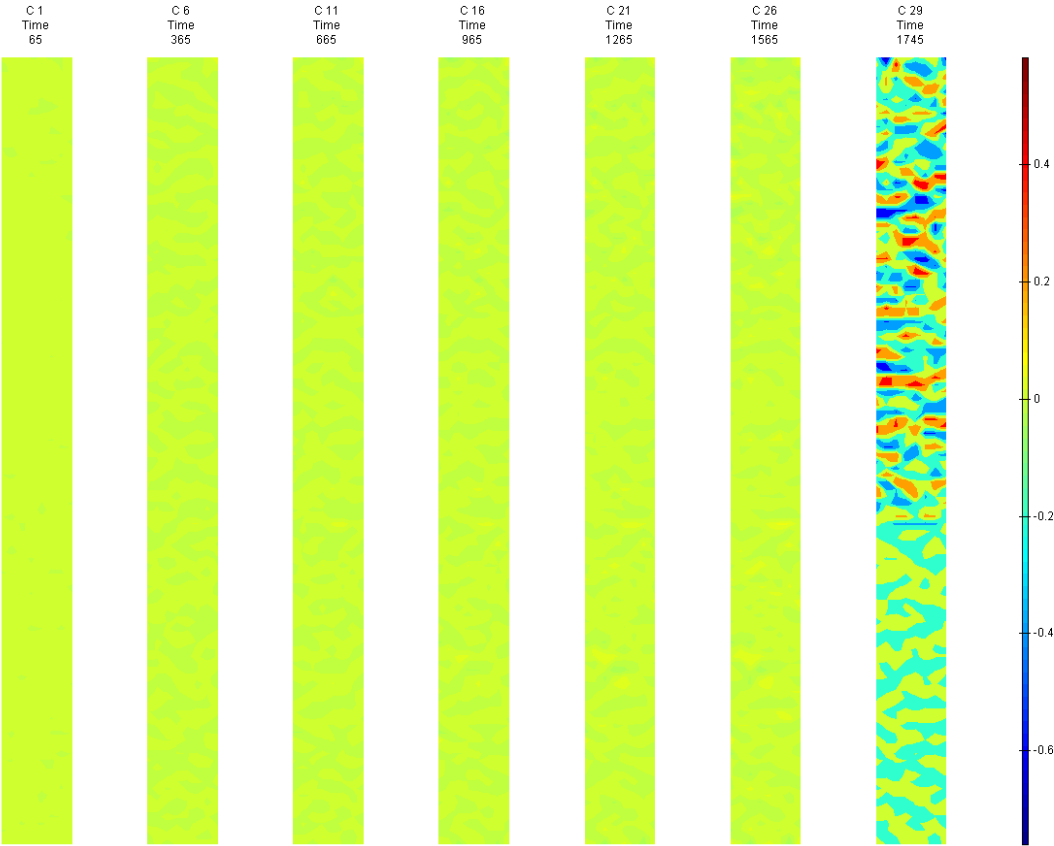FIGURE 728: X DIRECTION PIV SEQUENTIAL TRUE STRAIN OVER TIME

Appendix 6
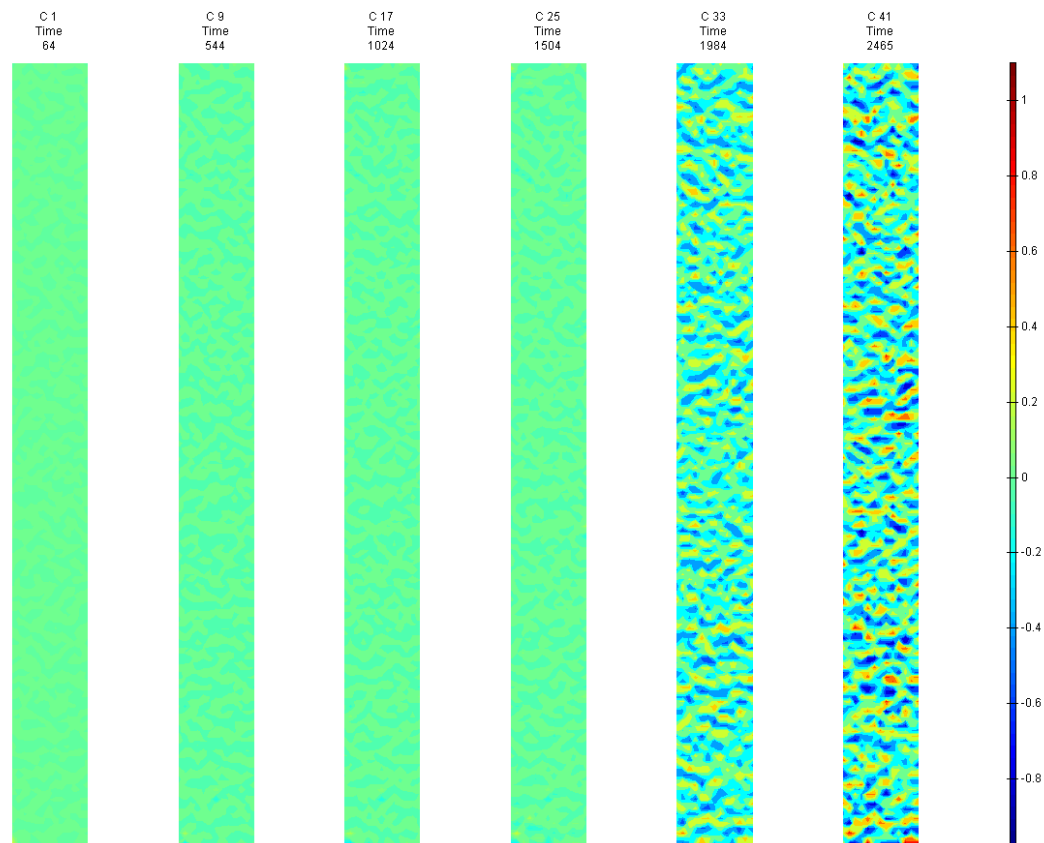
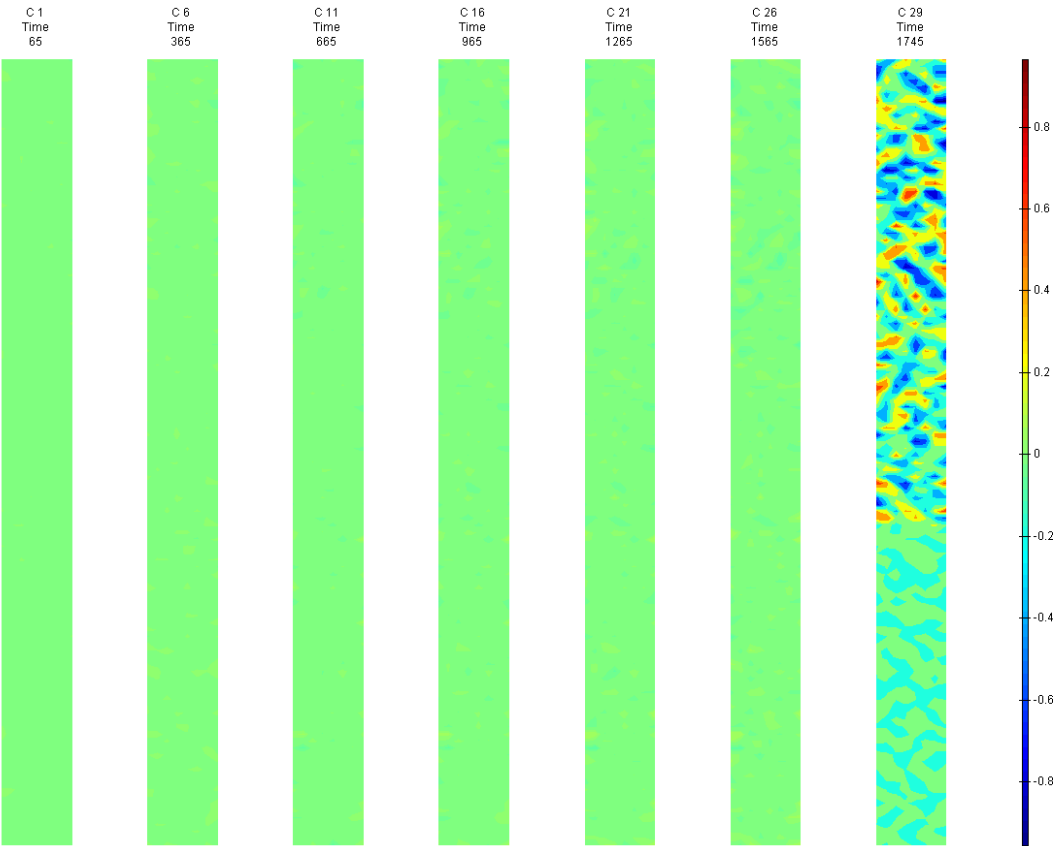FIGURE 729: Y DIRECTION PIV SEQUENTIAL TRUE STRAIN OVER TIME
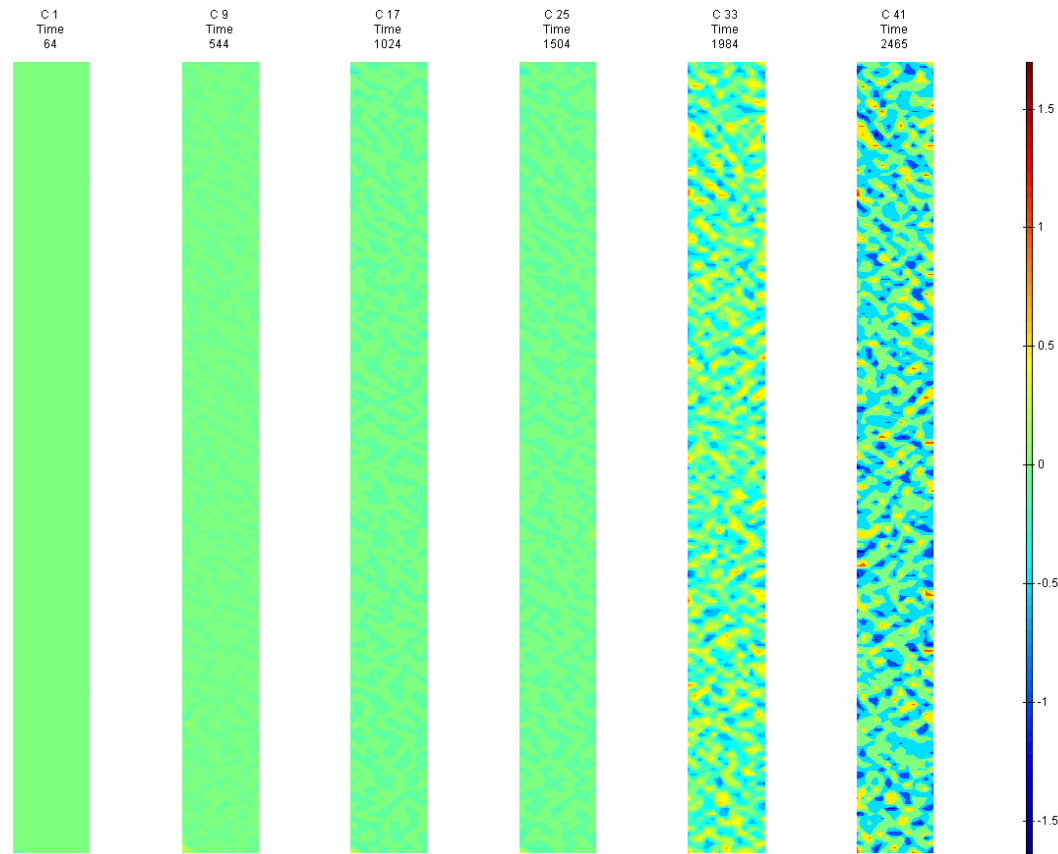
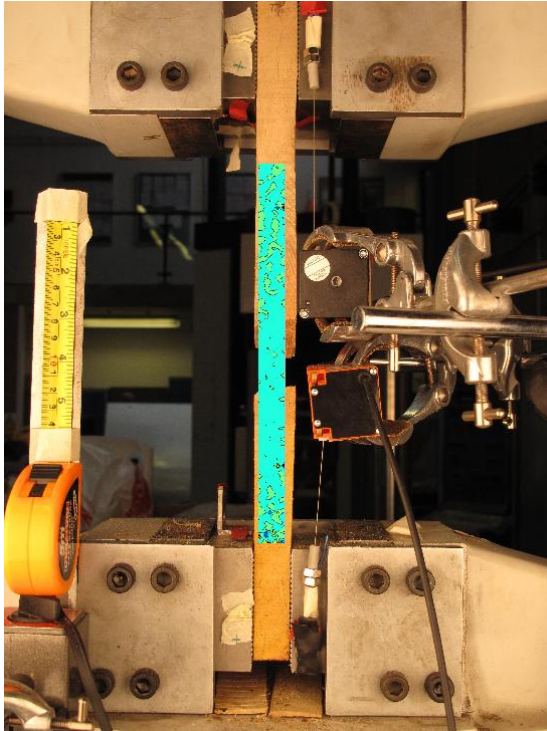FIGURE 730: XY DIRECTION PIV SEQUENTIAL TRUE SHEAR STRAIN OVER TIME
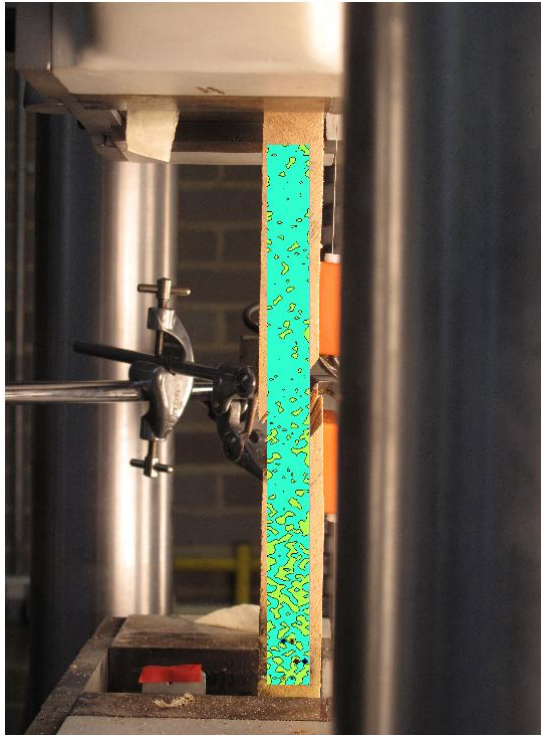
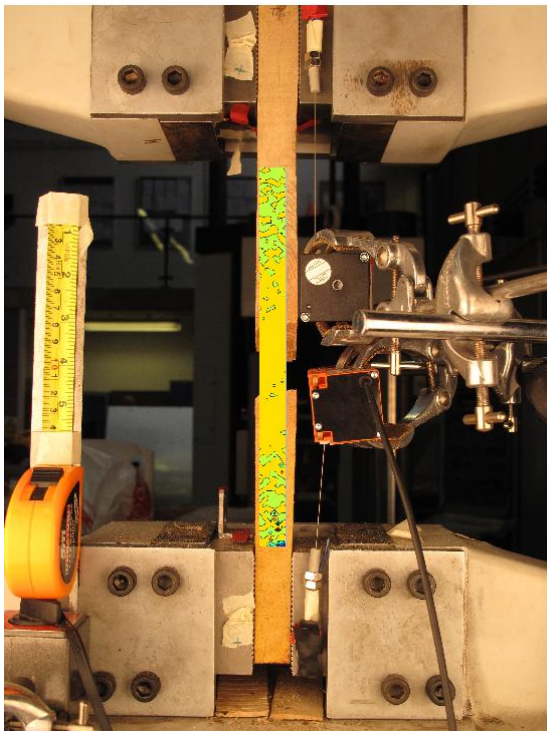FIGURE 731: X DIRECTION PIV FIRST–LAST DITCH ENGINEERING STRAIN OVER IMAGE
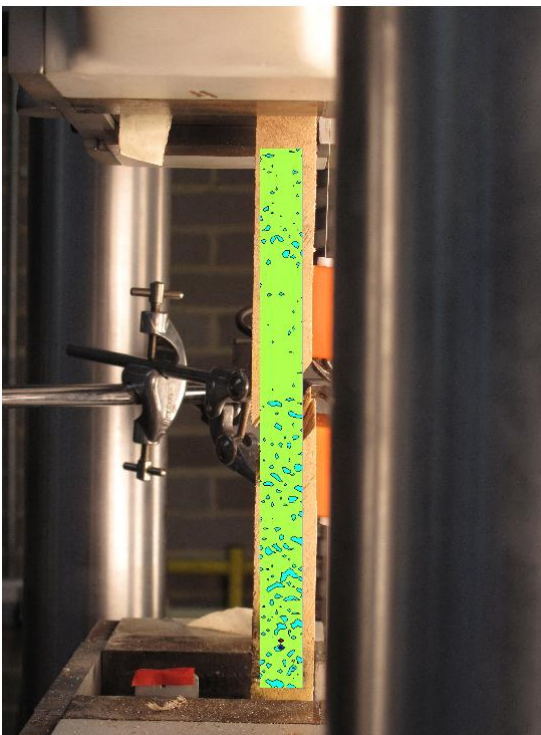
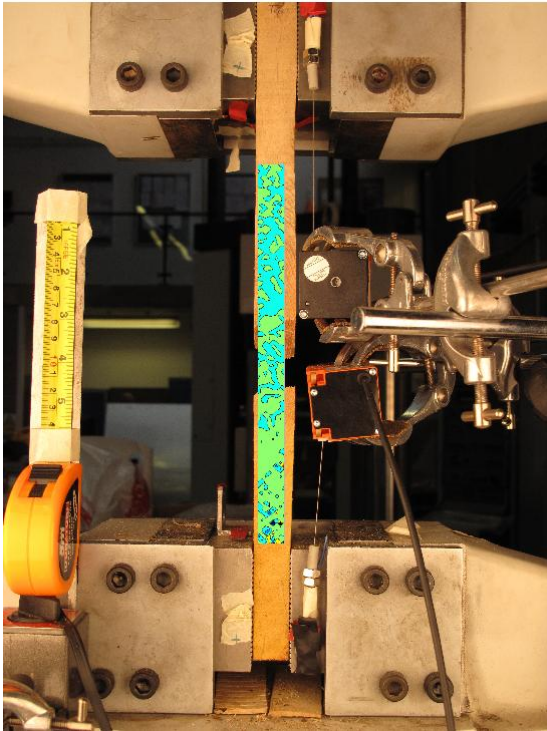FIGURE 732: Y DIRECTION PIV FIRST–LAST DITCH ENGINEERING STRAIN OVER IMAGE

Appendix 6
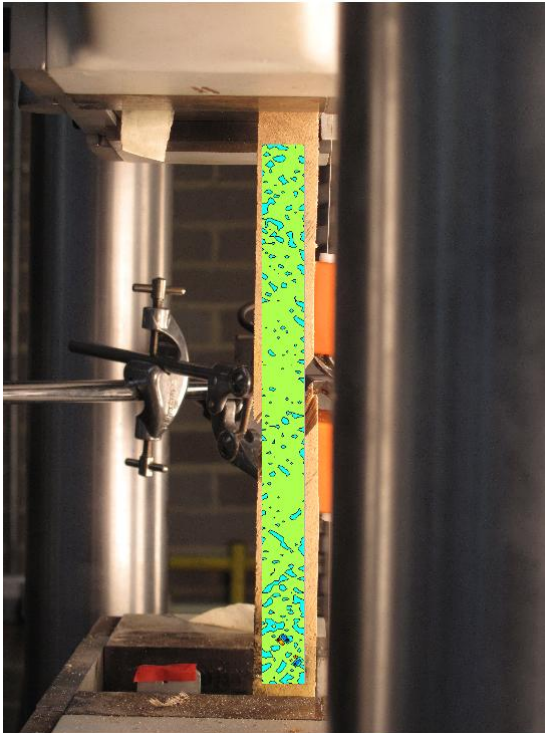
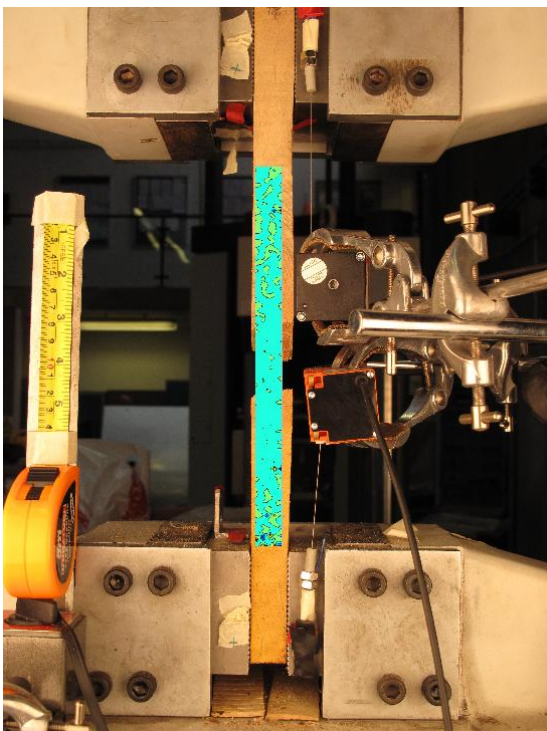FIGURE 733: XY DIRECTION PIV FIRST–LAST DITCH ENGINEERING SHEAR STRAIN OVER
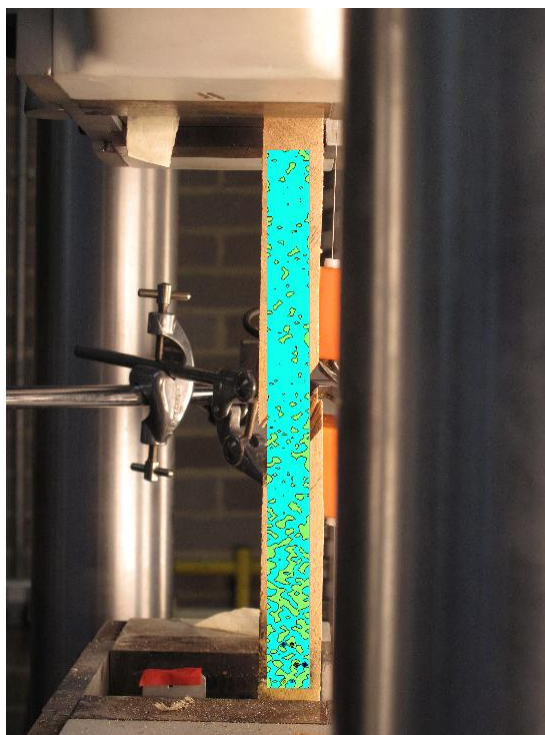
IMAGE

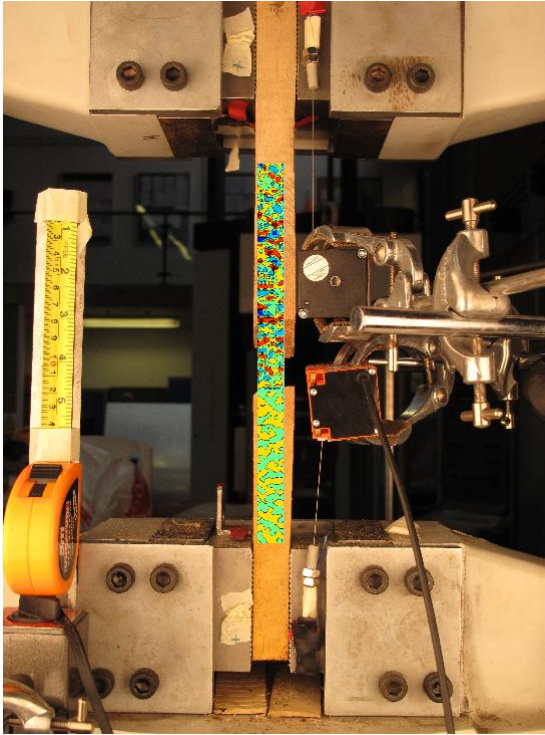FIGURE 734: X DIRECTION PIV FIRST–LAST DITCH TRUE STRAIN OVER IMAGE
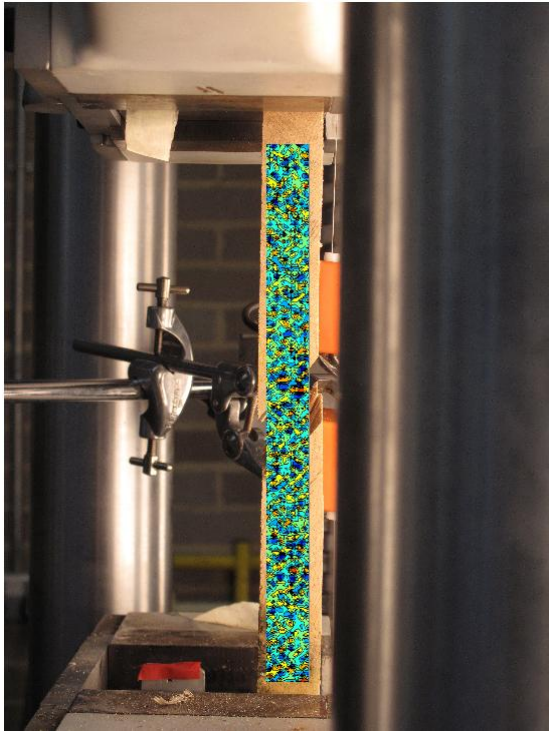
FIGURE 735: Y DIRECTION PIV FIRST–LAST DITCH TRUE STRAIN OVER IMAGE
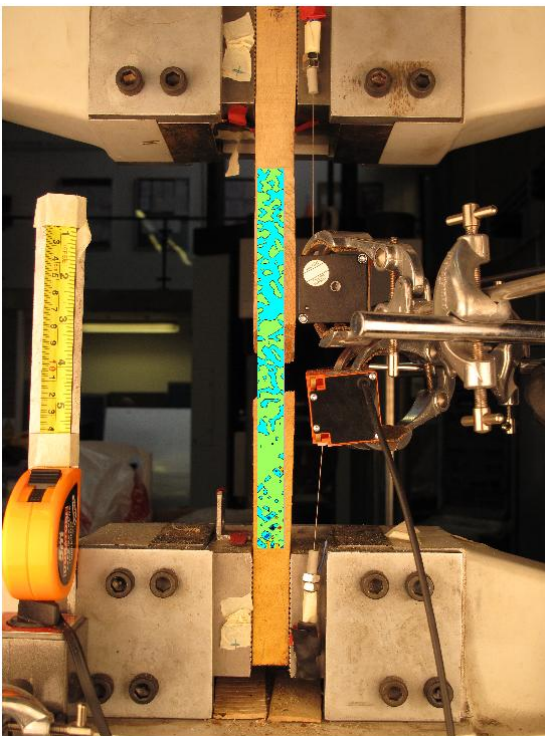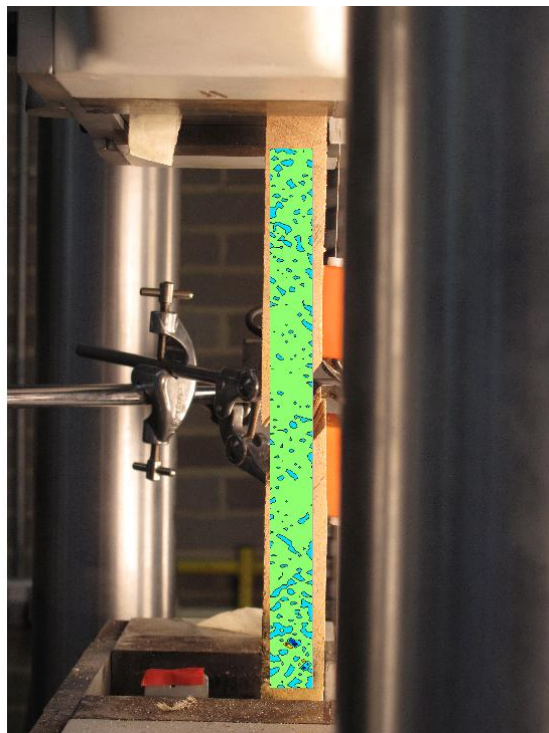

FIGURE 736: XY DIRECTION PIV FIRST–LAST DITCH TRUE SHEAR STRAIN OVER IMAGE

Appendix 6
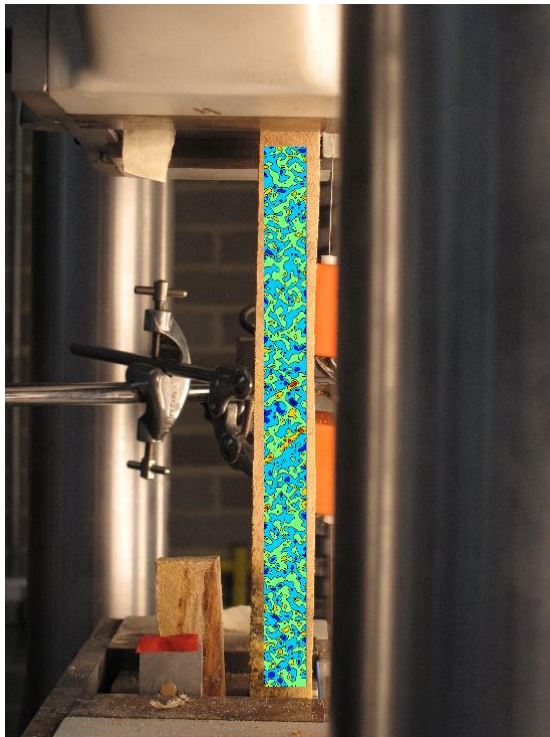
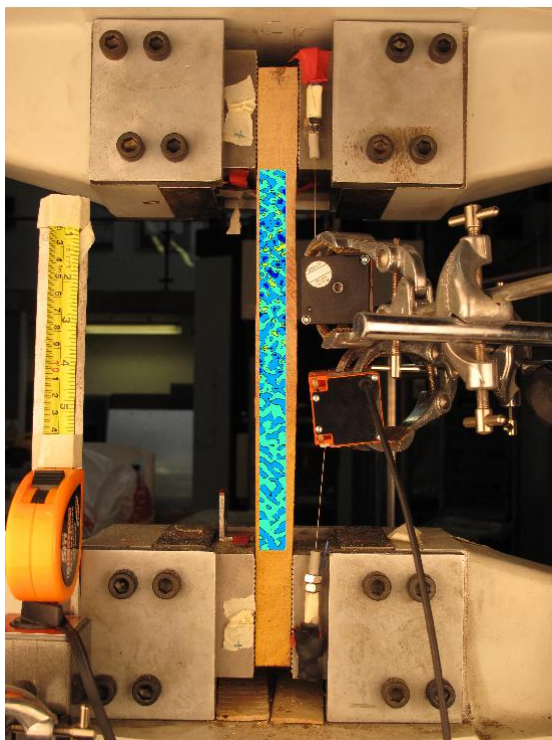FIGURE 737: XY DIRECTION PIV FIRST-SEQUENTIAL ENGINEERING SHEAR STRAIN OVER

IMAGE
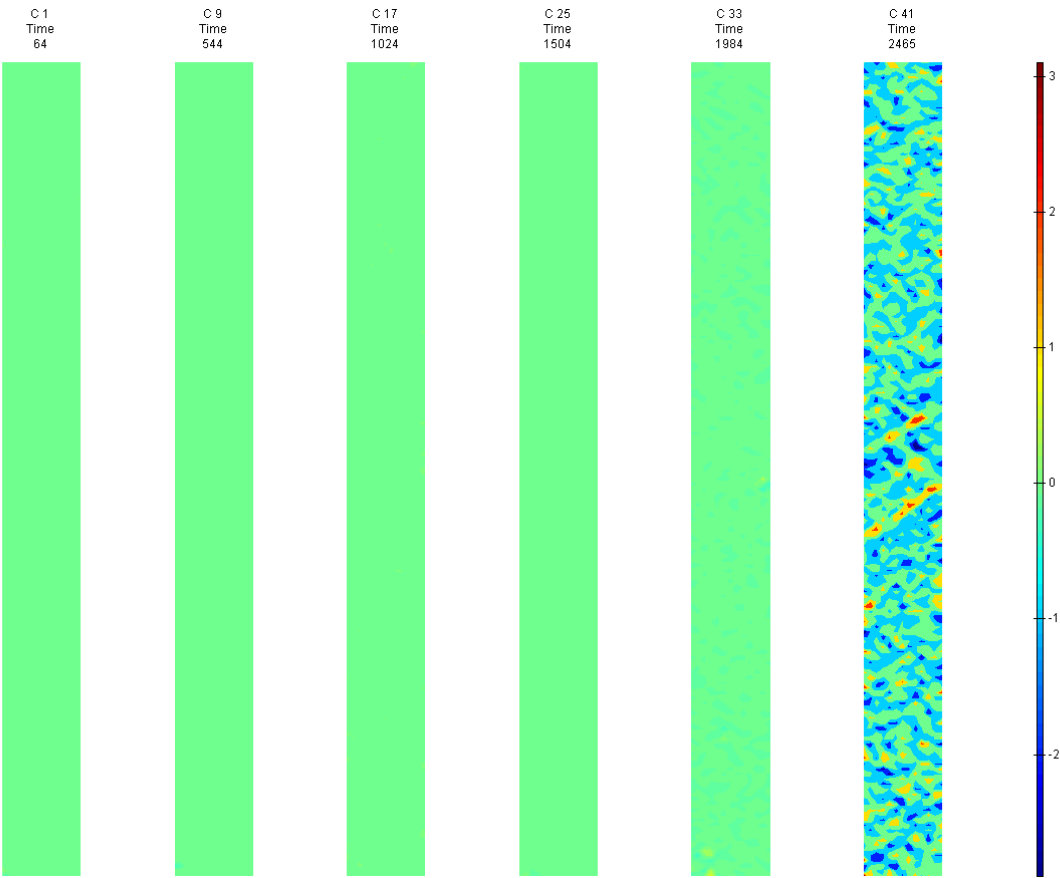
FIGURE 738: XY DIRECTION PIV FIRST-SEQUENTIAL ENGINEERING SHEAR STRAIN OVER TIME

T7
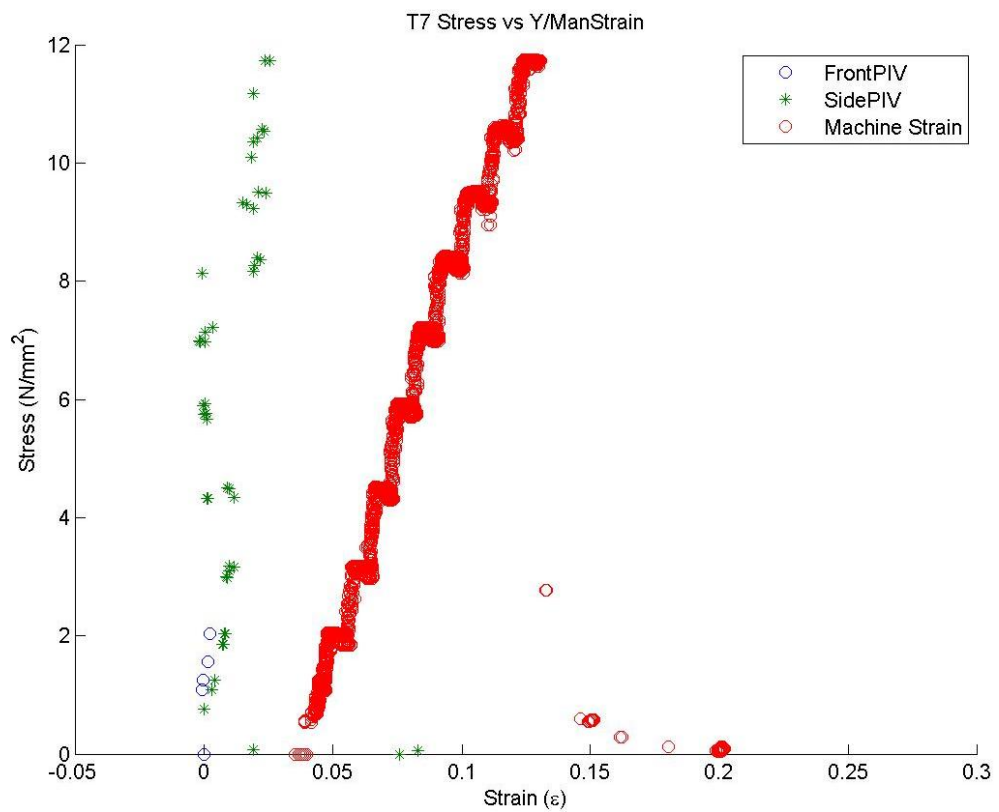
FIGURE 739: T7 TENSILE STRESS VS. MACHINE MEASURED/PIV STRAINS
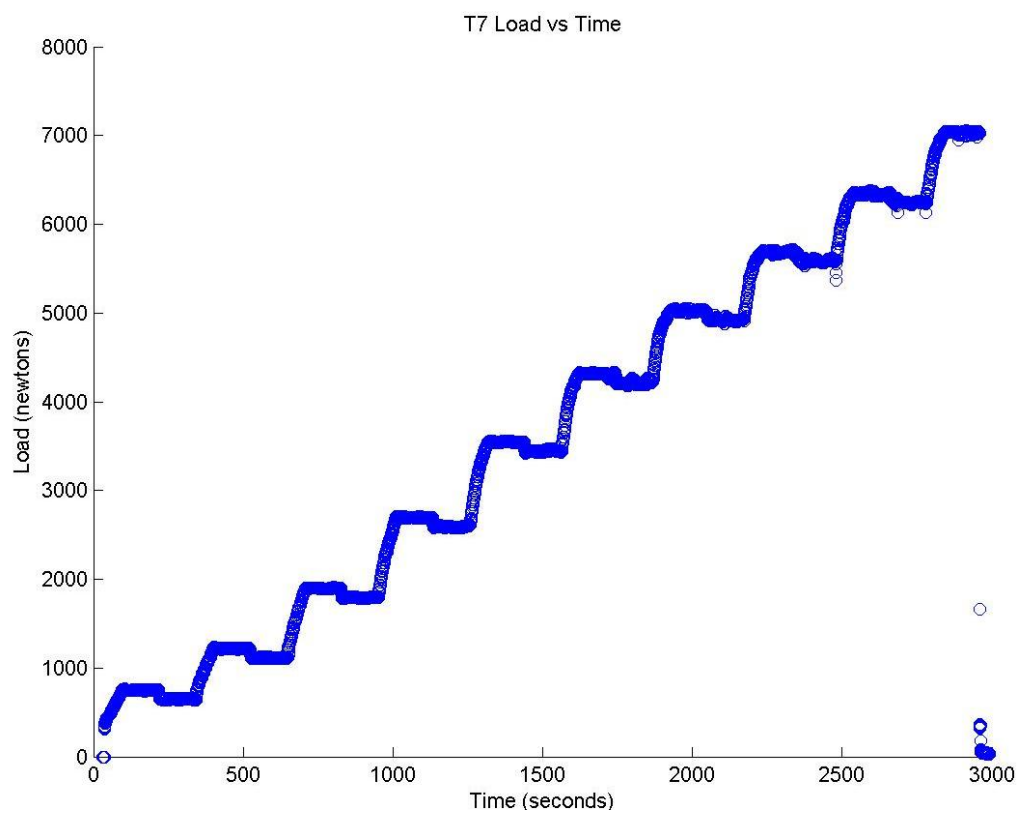
FIGURE 740: T7 TENSILE LOAD VS. TIME
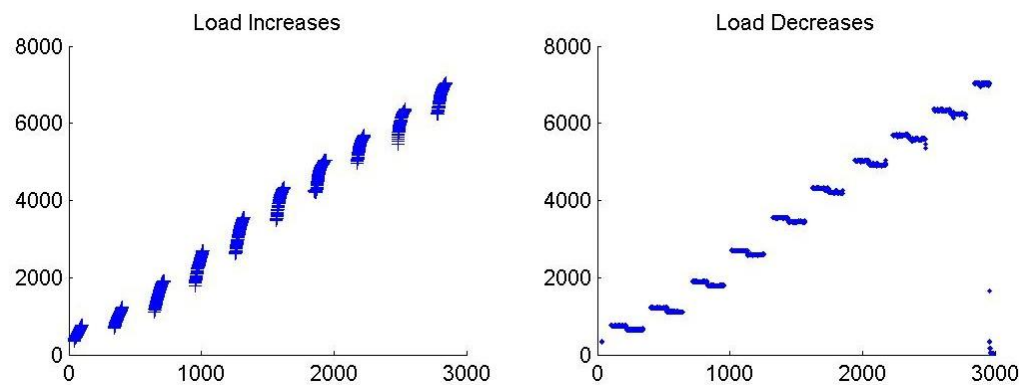
FIGURE 741: T7 CREEP LOADING: INCREMENTS AND RELAXATION
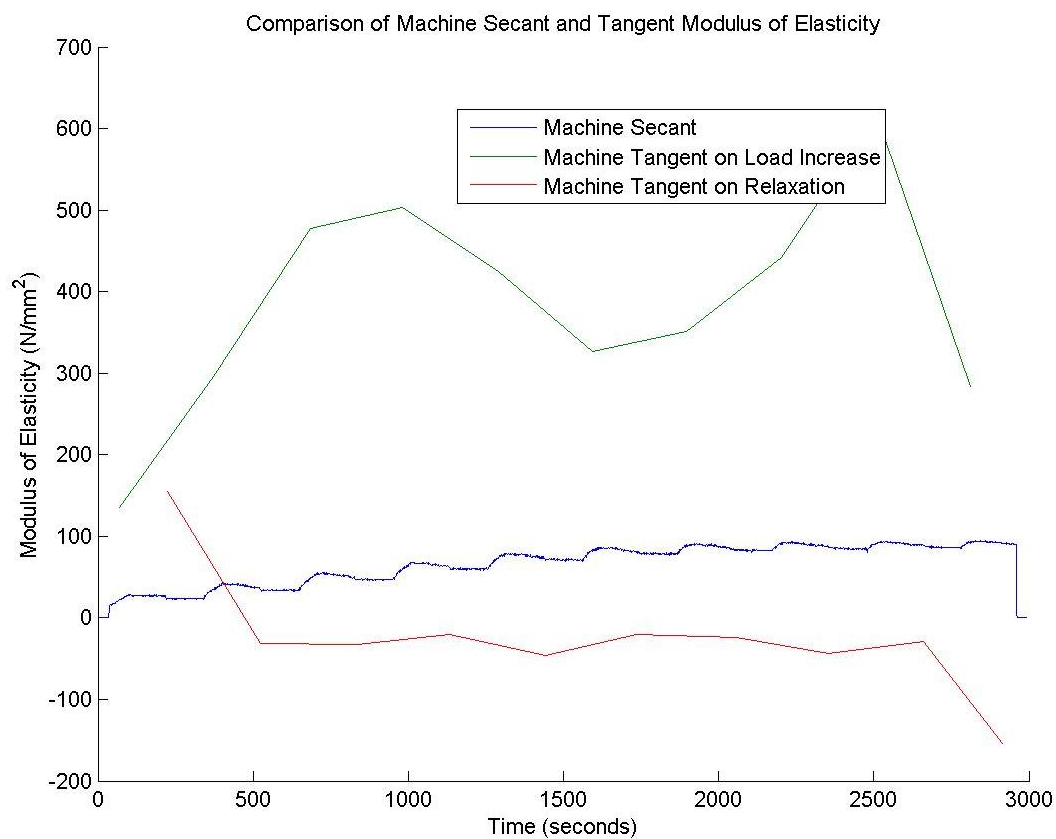
FIGURE 742: T7 MACHINE MEASURED SECANT AND TANGENT MODULUS VS. TIME
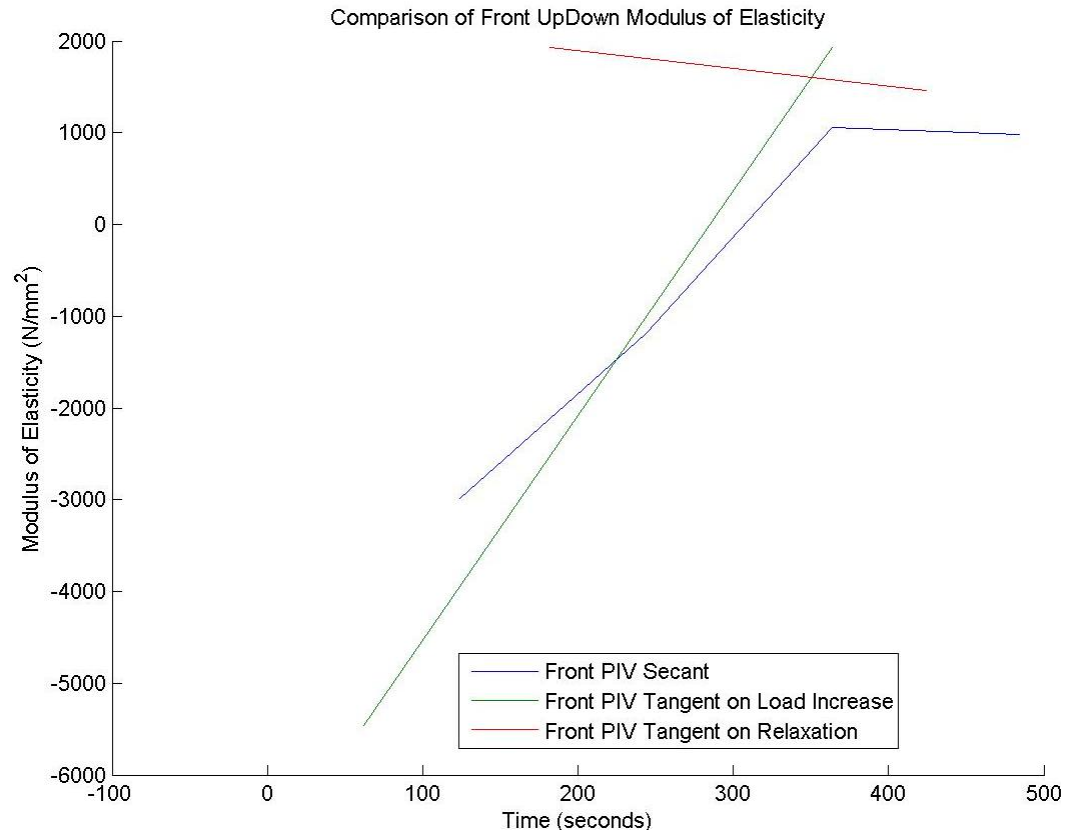
FIGURE 743: T7 FRONT VIEW PIV SECANT AND TANGENT MODULUS VS. TIME
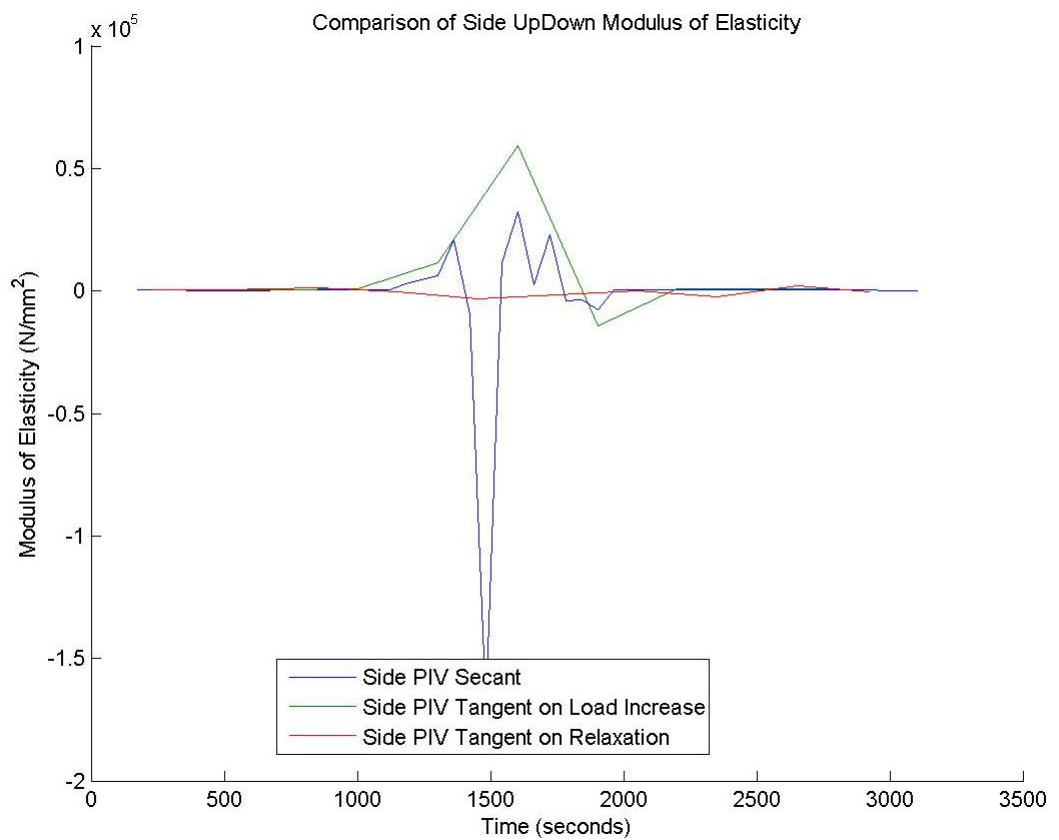
FIGURE 744: T7 SIDE VIEW PIV SECANT AND TANGENT MODULUS VS. TIME

Appendix 6
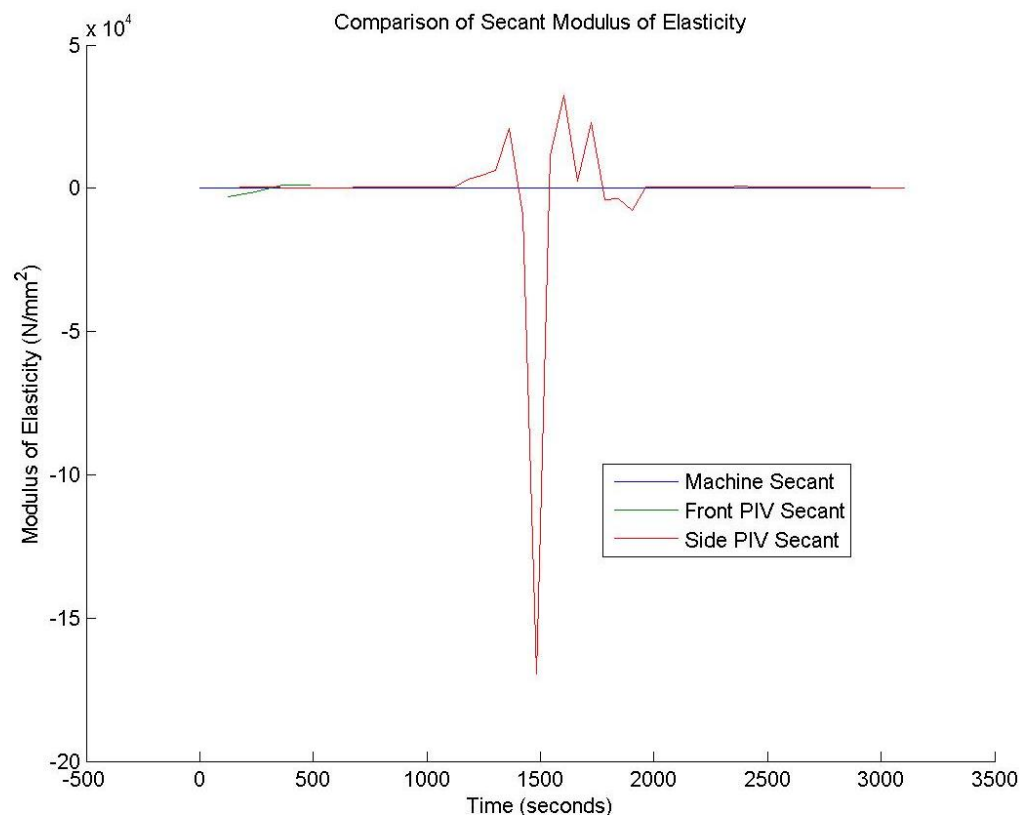
FIGURE 745: T7 COMPARISON OF MACHINE MEASURED AND PIV SECANT MODULUS VS. TIME
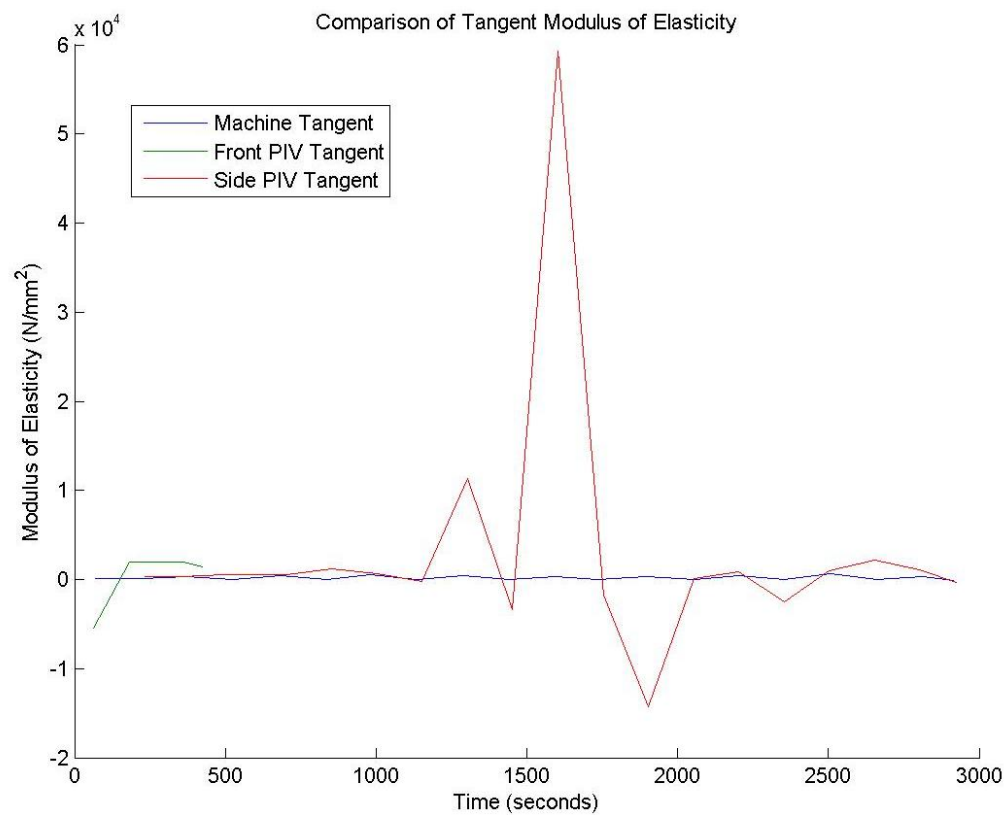
FIGURE 746: T7 COMPARISON OF MACHINE MEASURED AND PIV TANGENT MODULUS VS.

TIME

528

T7 Sample

FIGURE 747: SAMPLE GRAIN ORIENTATIONS OF THE FRONT (LEFT 4 IMAGES) AND SIDE (RIGHT 4 IMAGES) VIEW BEFORE (FIRST 2 OF 4 IMAGES) AND AFTER (LAST 2 OF 4 IMAGES) BREAKAGE

Appendix 6

T7 Front View
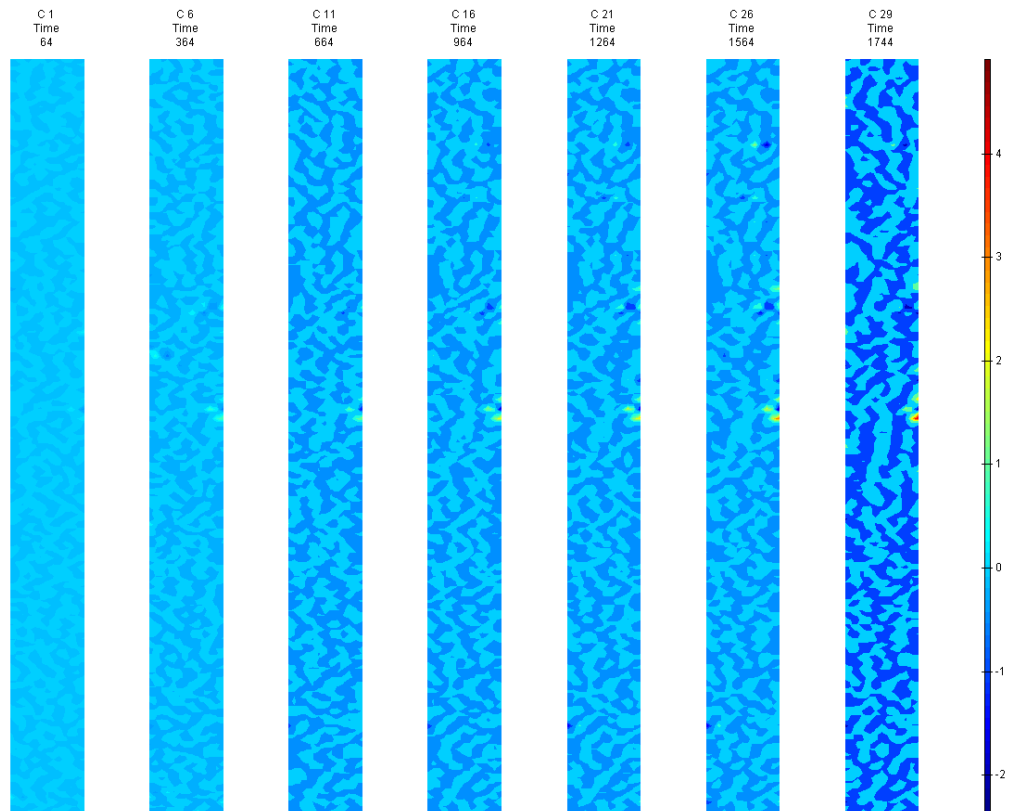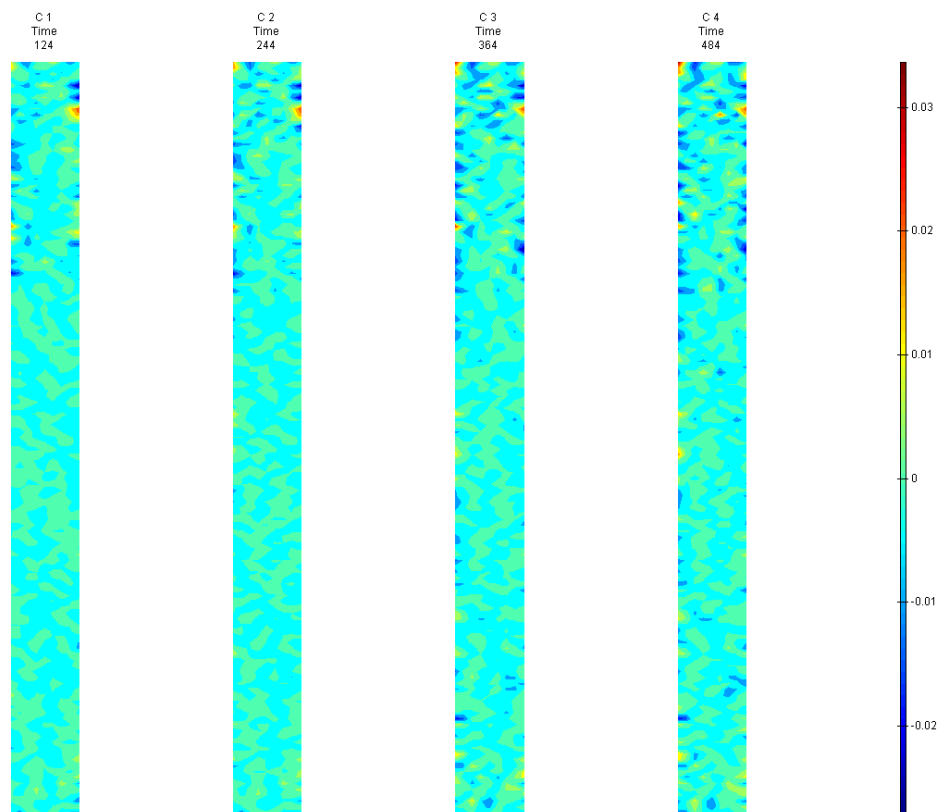

FIGURE 748: X DIRECTION PIV SEQUENTIAL ENGINEERING STRAIN OVER TIME
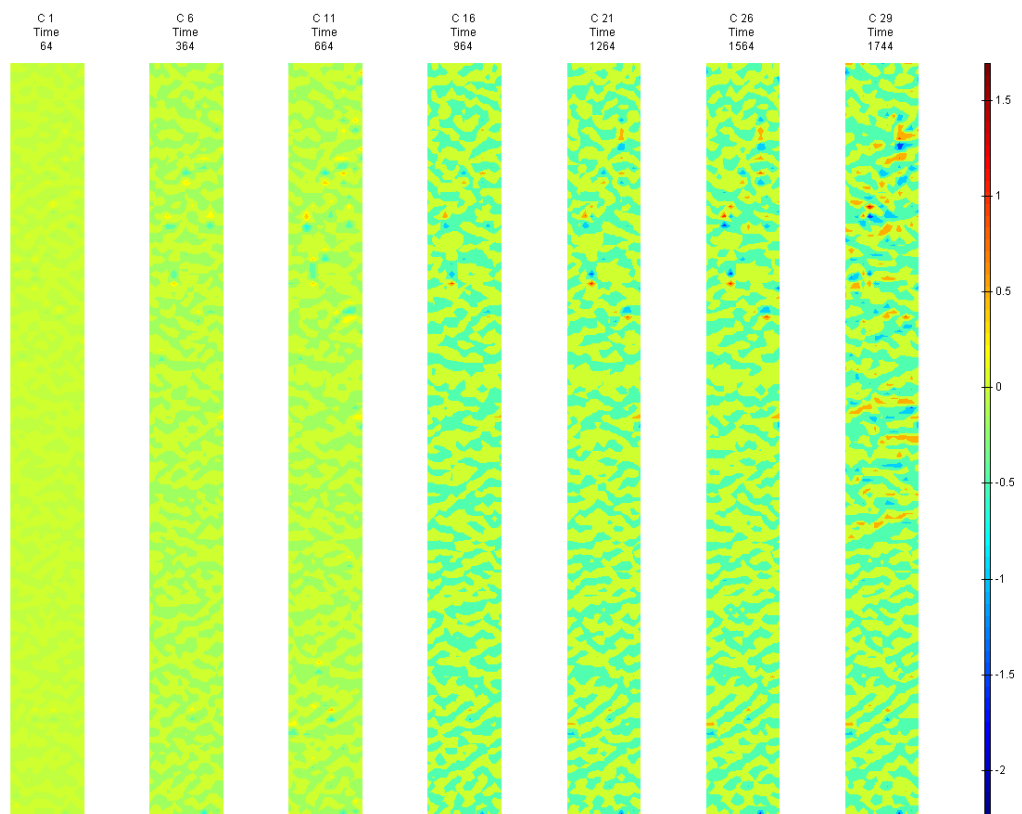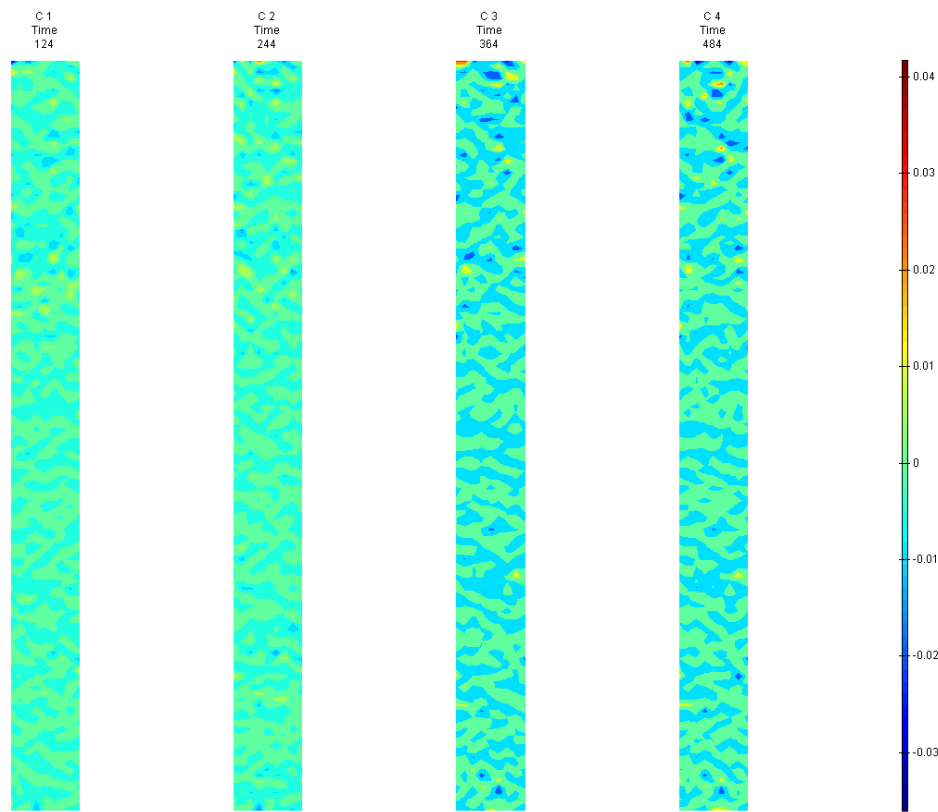

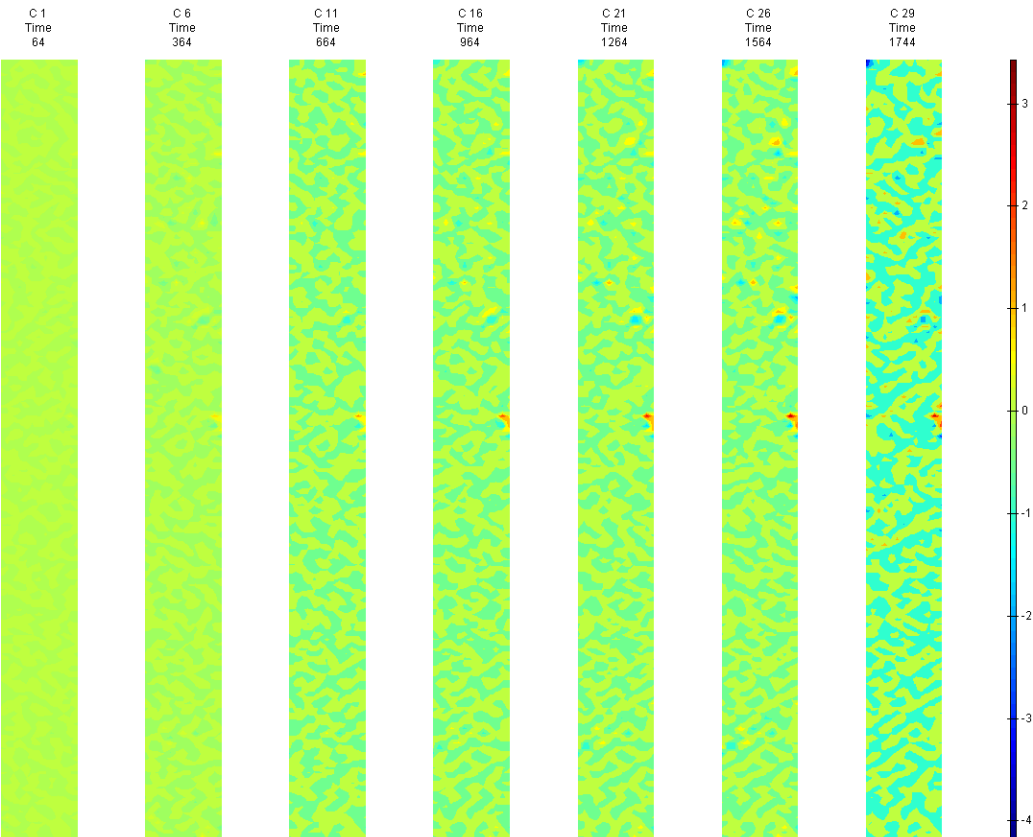FIGURE 749: Y DIRECTION PIV SEQUENTIAL ENGINEERING STRAIN OVER TIME
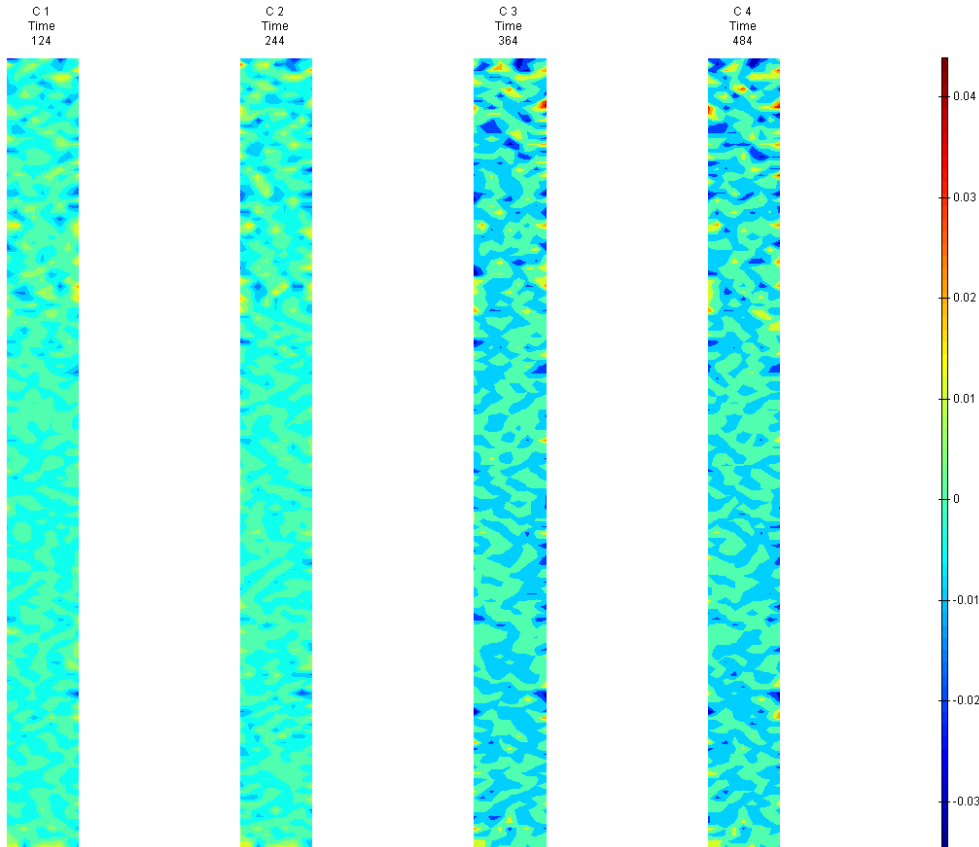
FIGURE 750: XY DIRECTION PIV SEQUENTIAL ENGINEERING SHEAR STRAIN OVER TIME
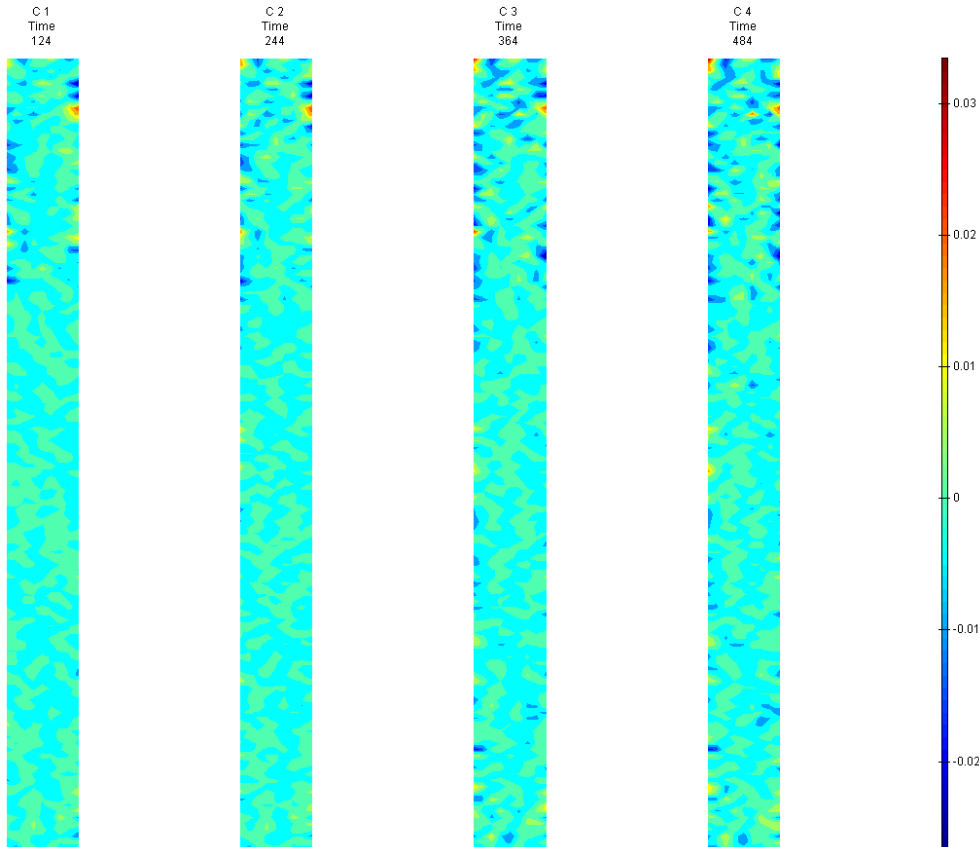
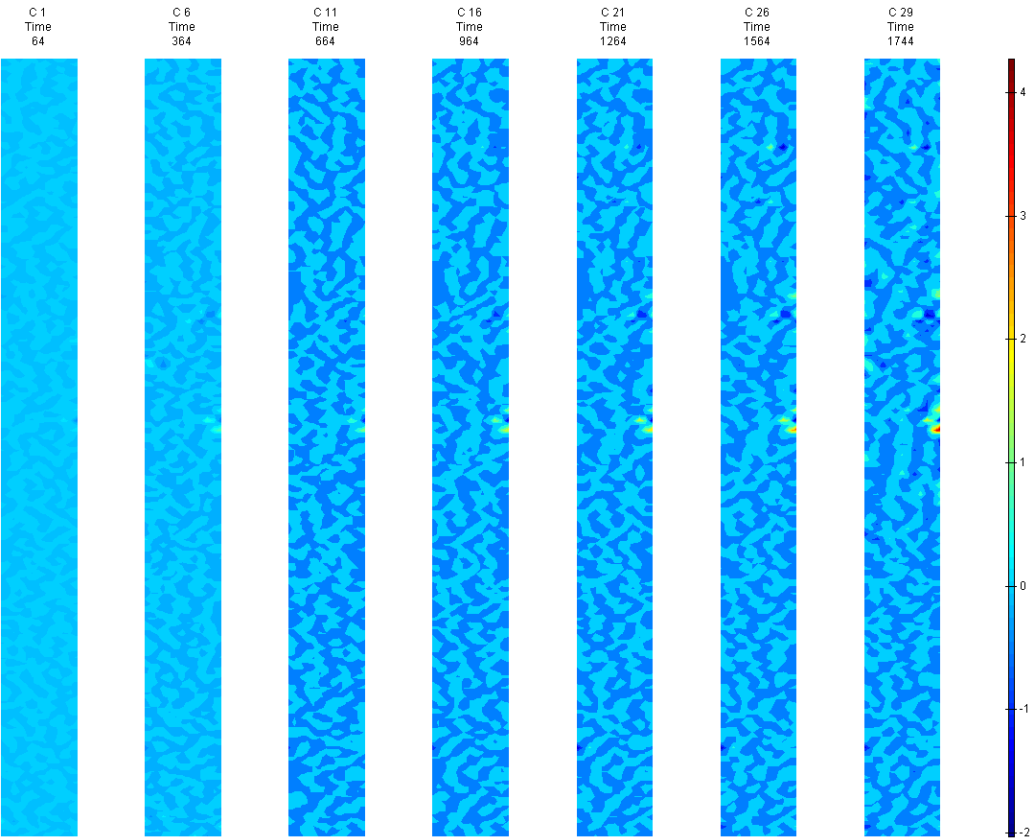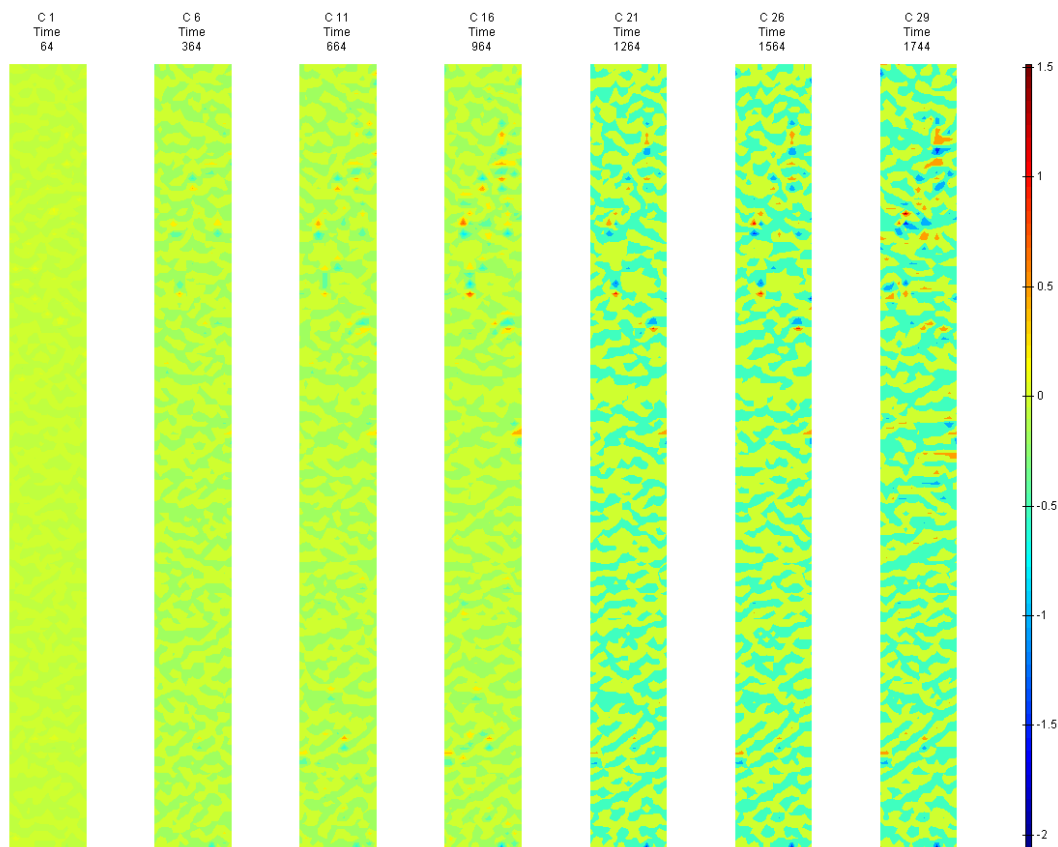FIGURE 751: X DIRECTION PIV SEQUENTIAL TRUE STRAIN OVER TIME

Appendix 6
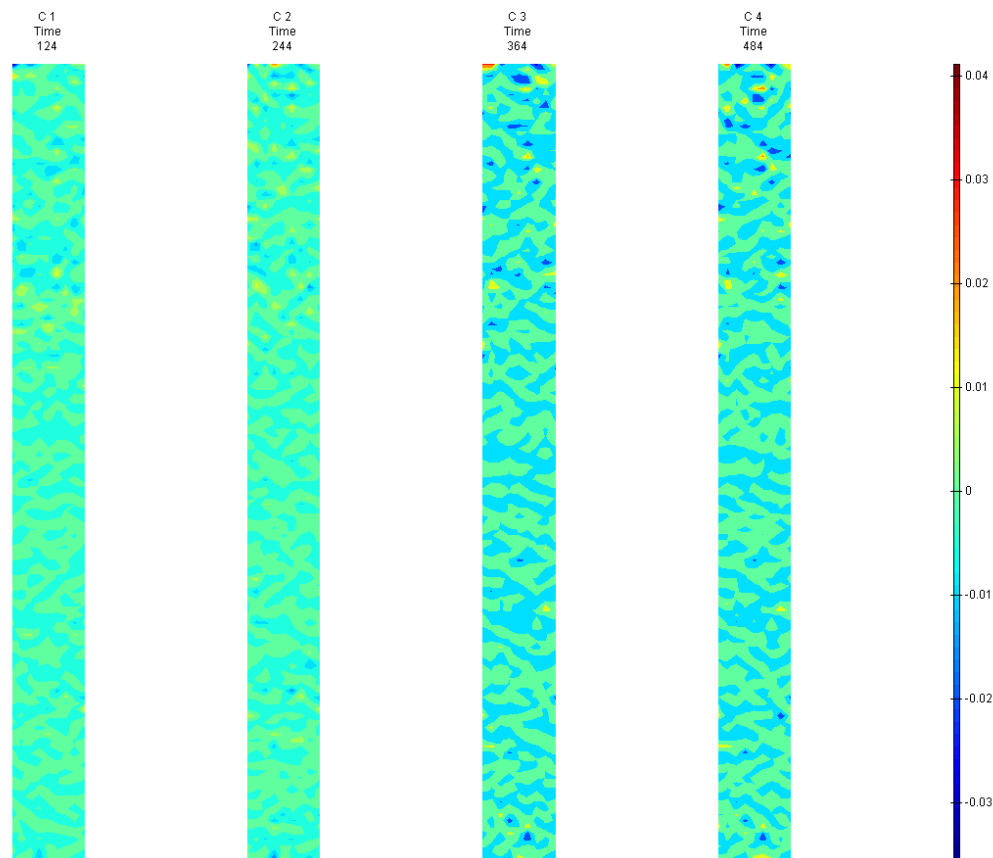
FIGURE 752: Y DIRECTION PIV SEQUENTIAL TRUE STRAIN OVER TIME
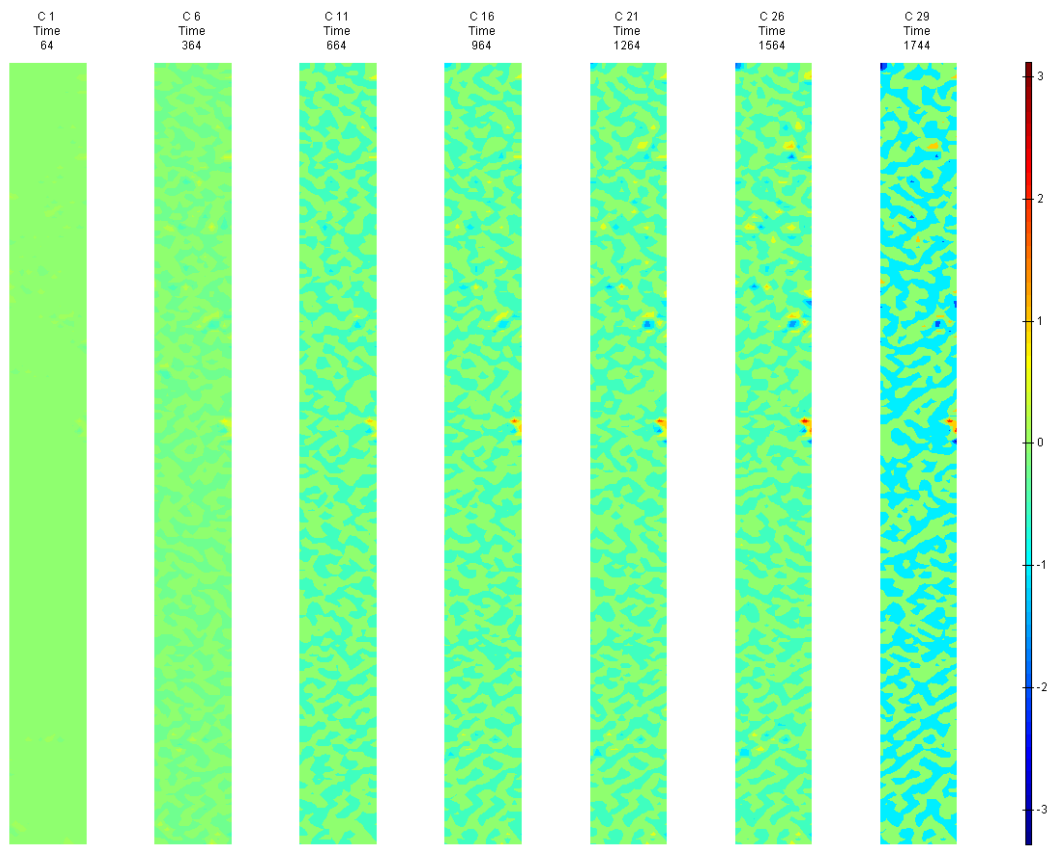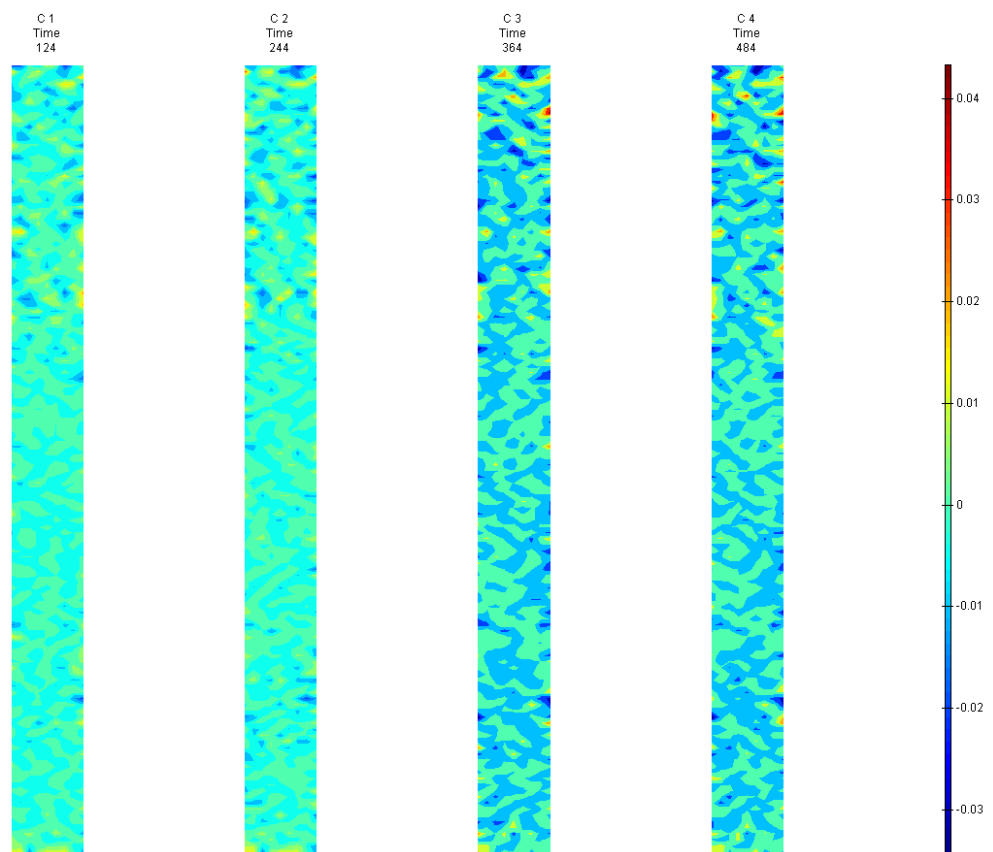

FIGURE 753: XY DIRECTION PIV SEQUENTIAL TRUE SHEAR STRAIN OVER TIME
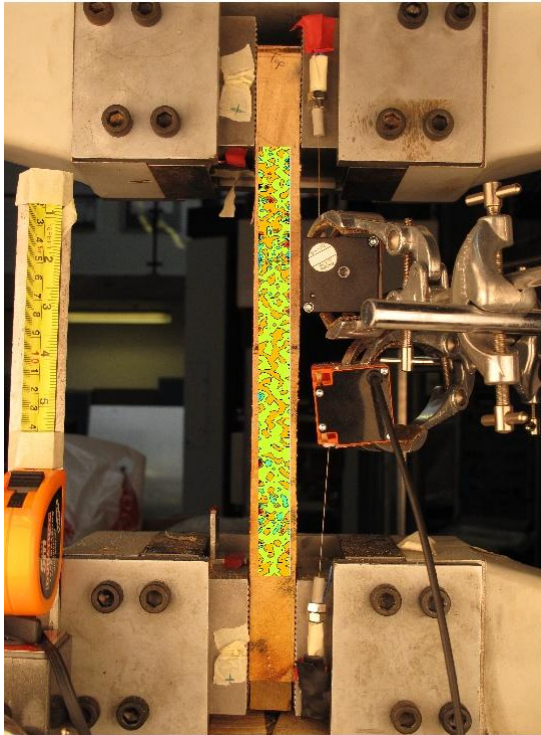
FIGURE 754: X DIRECTION PIV FIRST–LAST DITCH ENGINEERING STRAIN OVER IMAGE
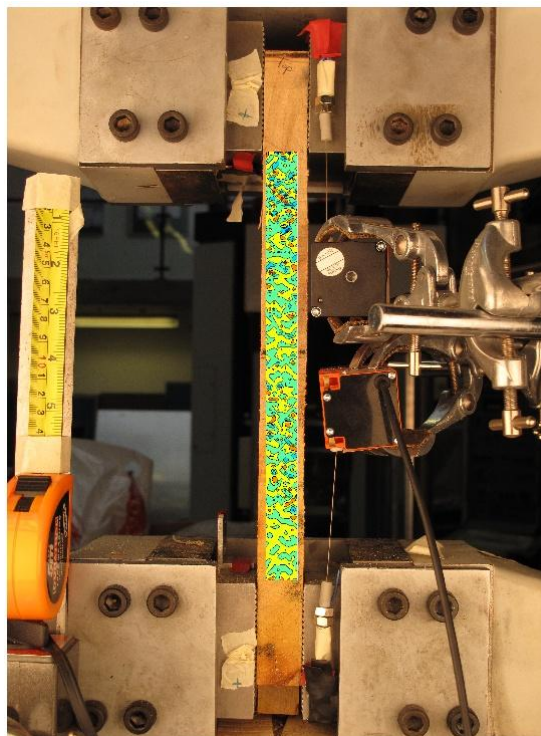
FIGURE 755: Y DIRECTION PIV FIRST–LAST DITCH ENGINEERING STRAIN OVER IMAGE

Appendix 6
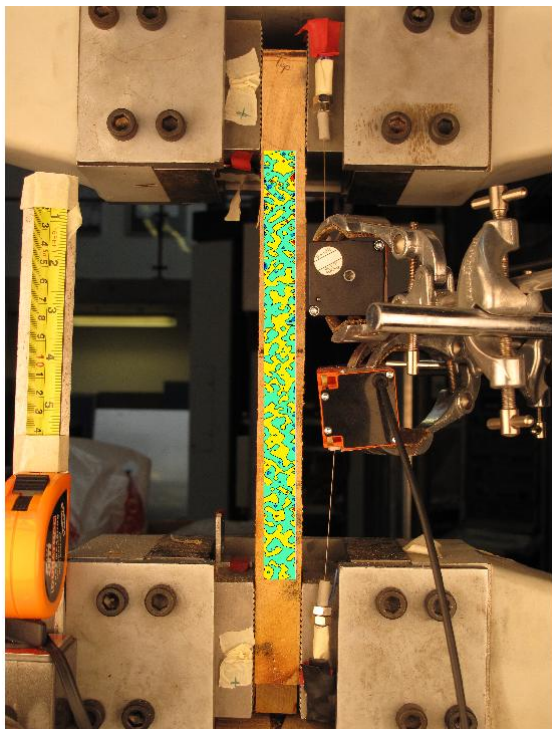
FIGURE 756: XY DIRECTION PIV FIRST–LAST DITCH ENGINEERING SHEAR STRAIN OVER
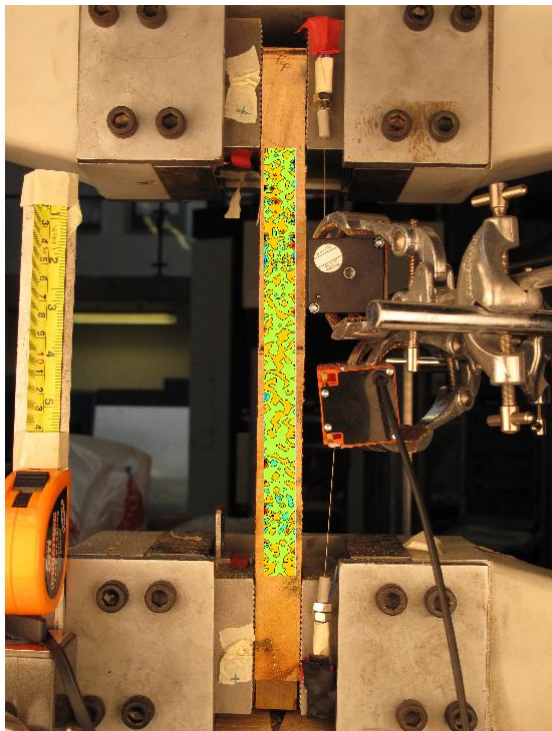
IMAGE

FIGURE 757: X DIRECTION PIV FIRST–LAST DITCH TRUE STRAIN OVER IMAGE
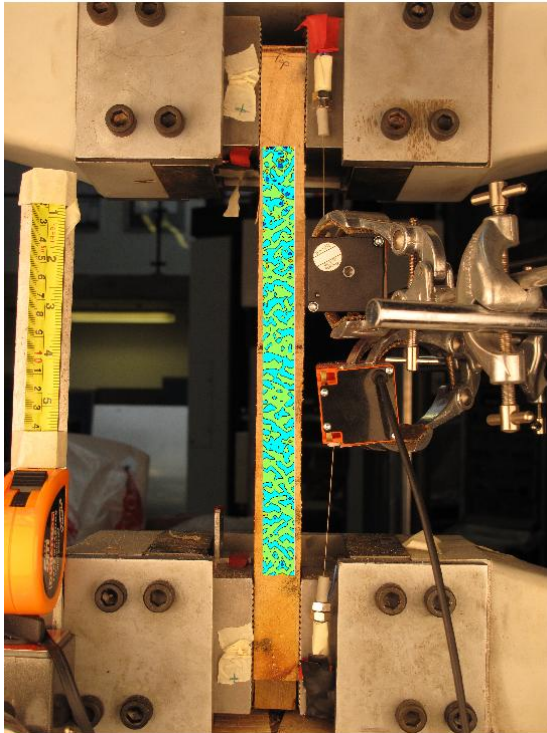
FIGURE 758: Y DIRECTION PIV FIRST–LAST DITCH TRUE STRAIN OVER IMAGE
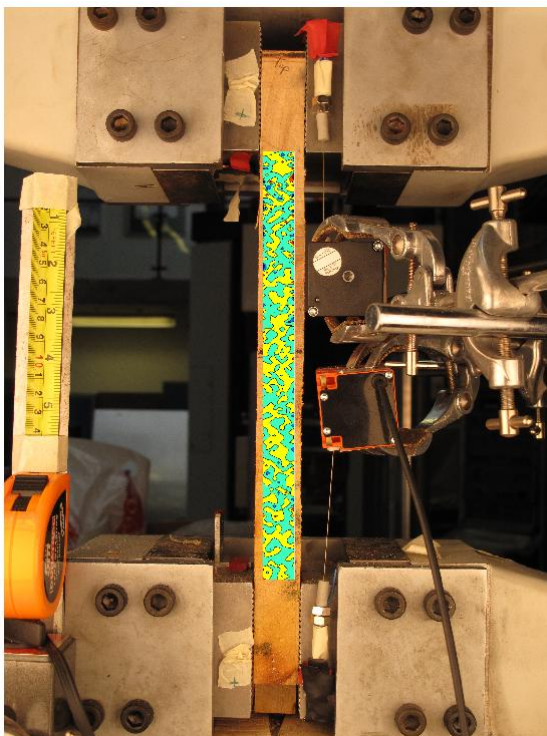
FIGURE 759: XY DIRECTION PIV FIRST–LAST DITCH TRUE SHEAR STRAIN OVER IMAGE

Appendix 6
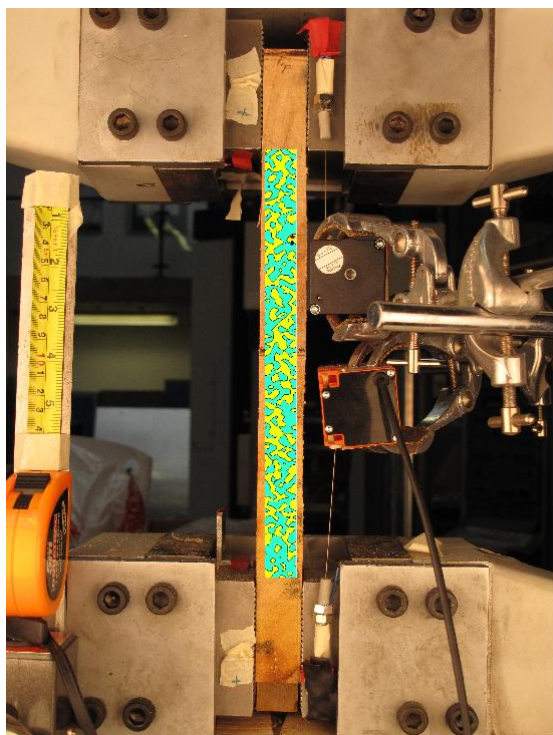
FIGURE 760: XY DIRECTION PIV FIRST–SEQUENTIAL ENGINEERING SHEAR STRAIN OVER

IMAGE
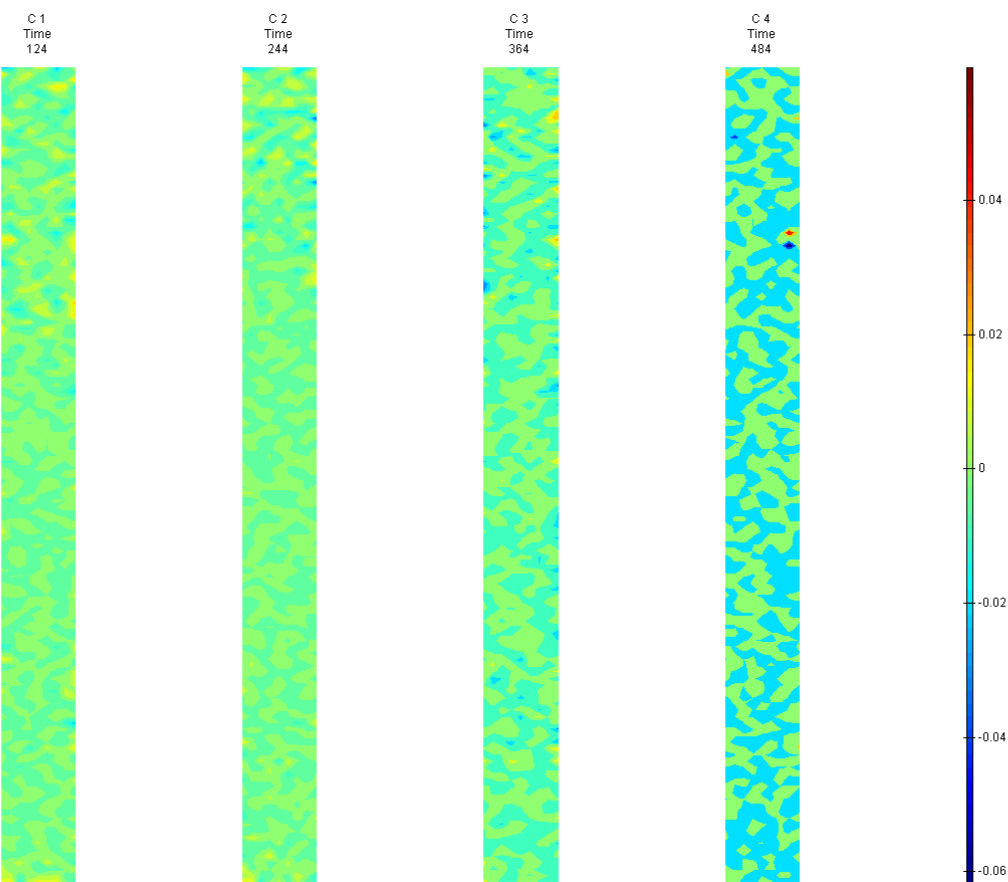
FIGURE 761: XY DIRECTION PIV FIRST–SEQUENTIAL ENGINEERING SHEAR STRAIN OVER TIME

T7 Side View
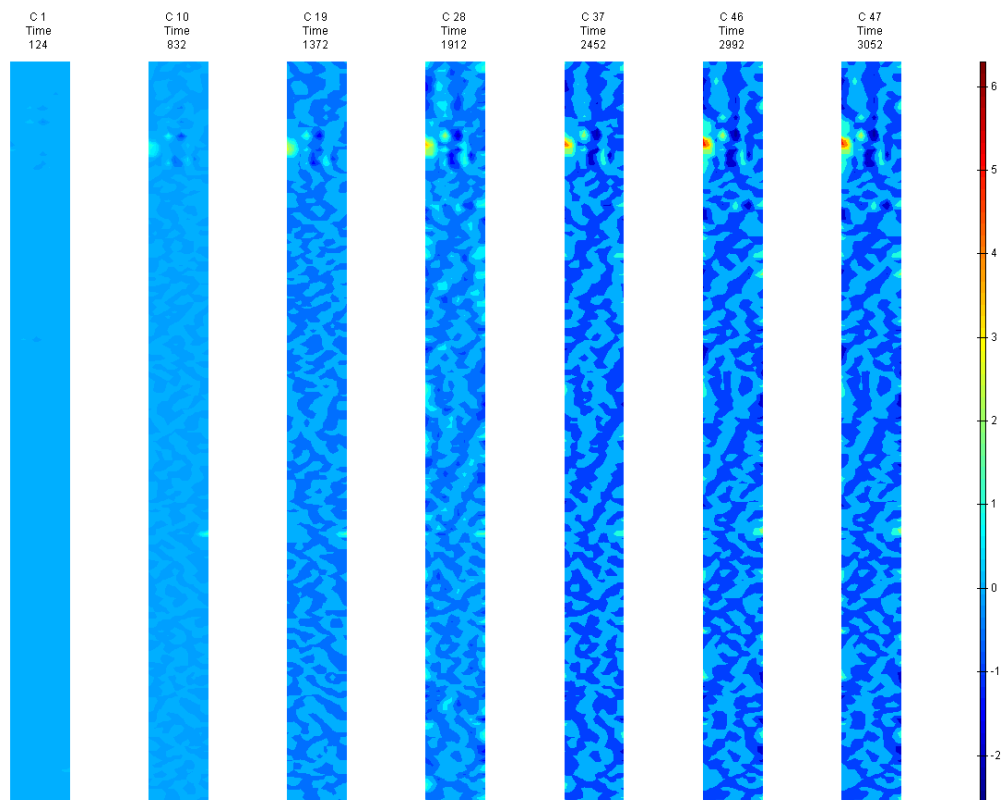
FIGURE 762: X DIRECTION PIV SEQUENTIAL ENGINEERING STRAIN OVER TIME
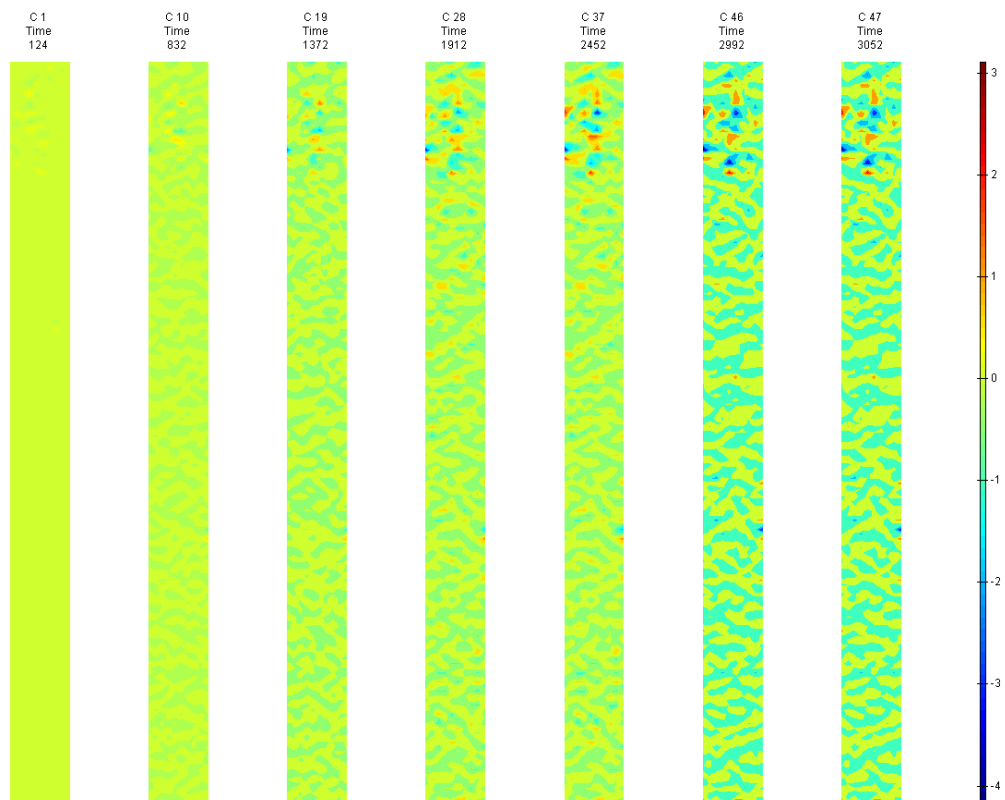
FIGURE 763: Y DIRECTION PIV SEQUENTIAL ENGINEERING STRAIN OVER TIME
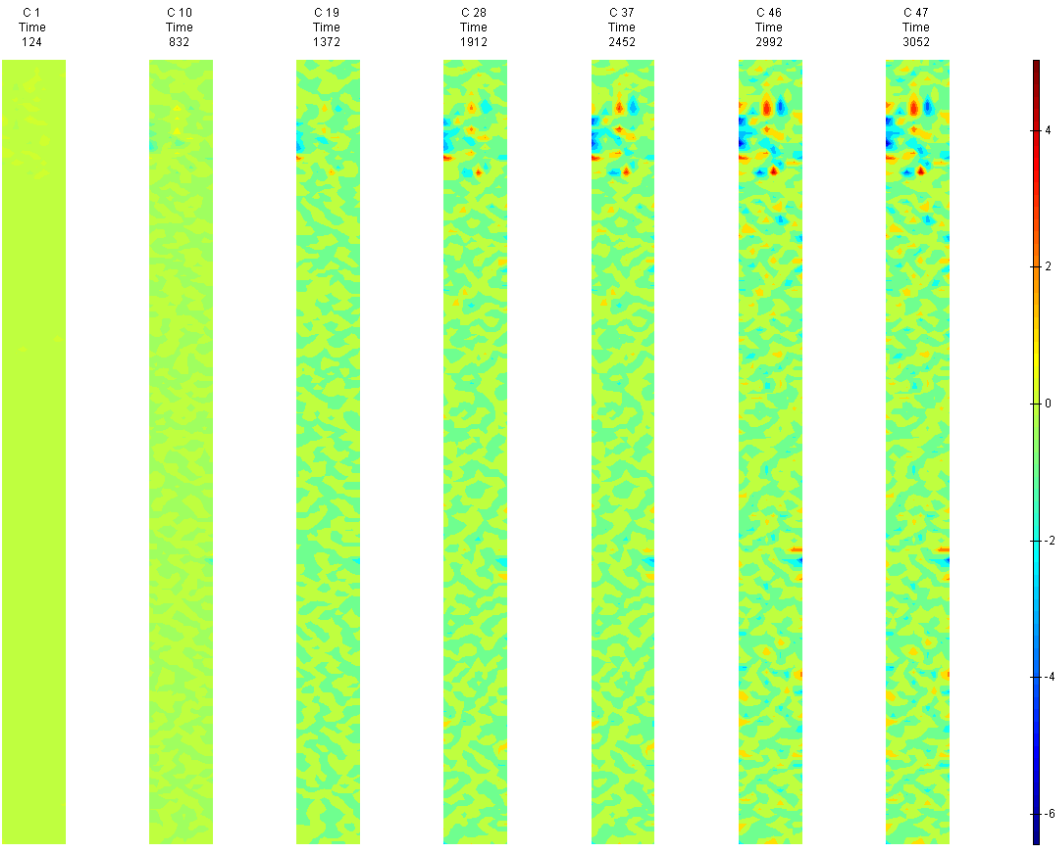
FIGURE 764: XY DIRECTION PIV SEQUENTIAL ENGINEERING SHEAR STRAIN OVER TIME
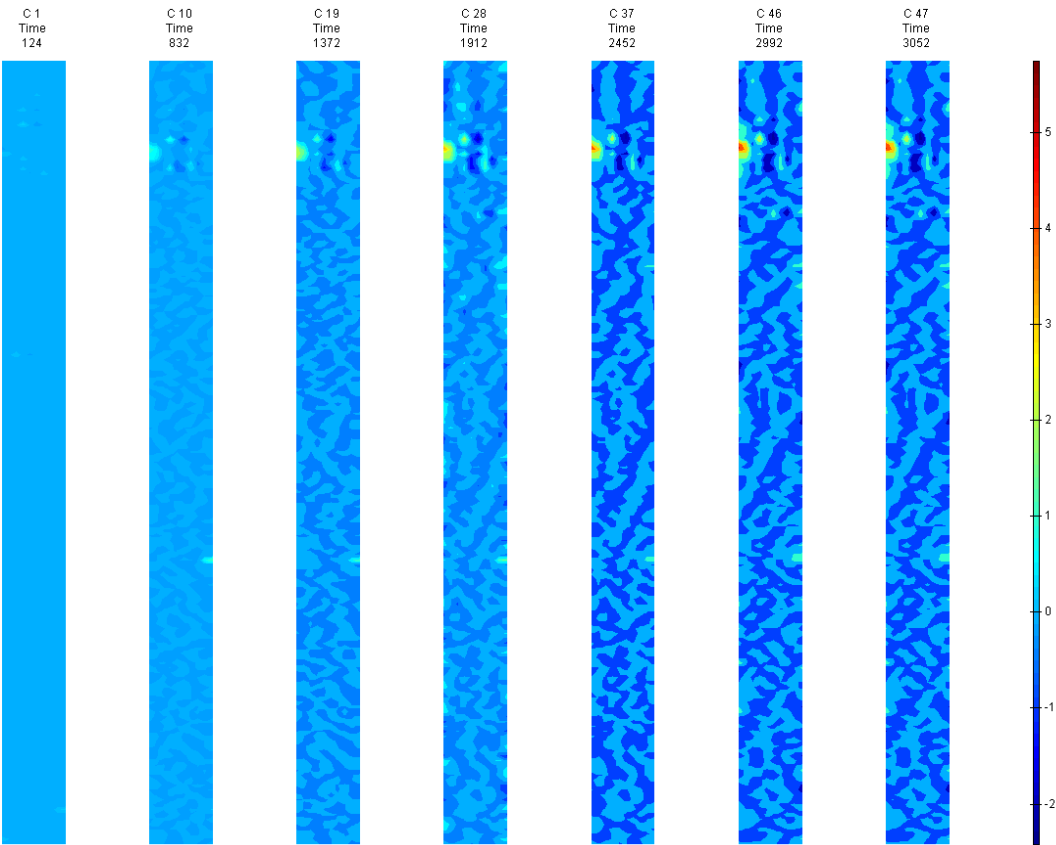
FIGURE 765: X DIRECTION PIV SEQUENTIAL TRUE STRAIN OVER TIME
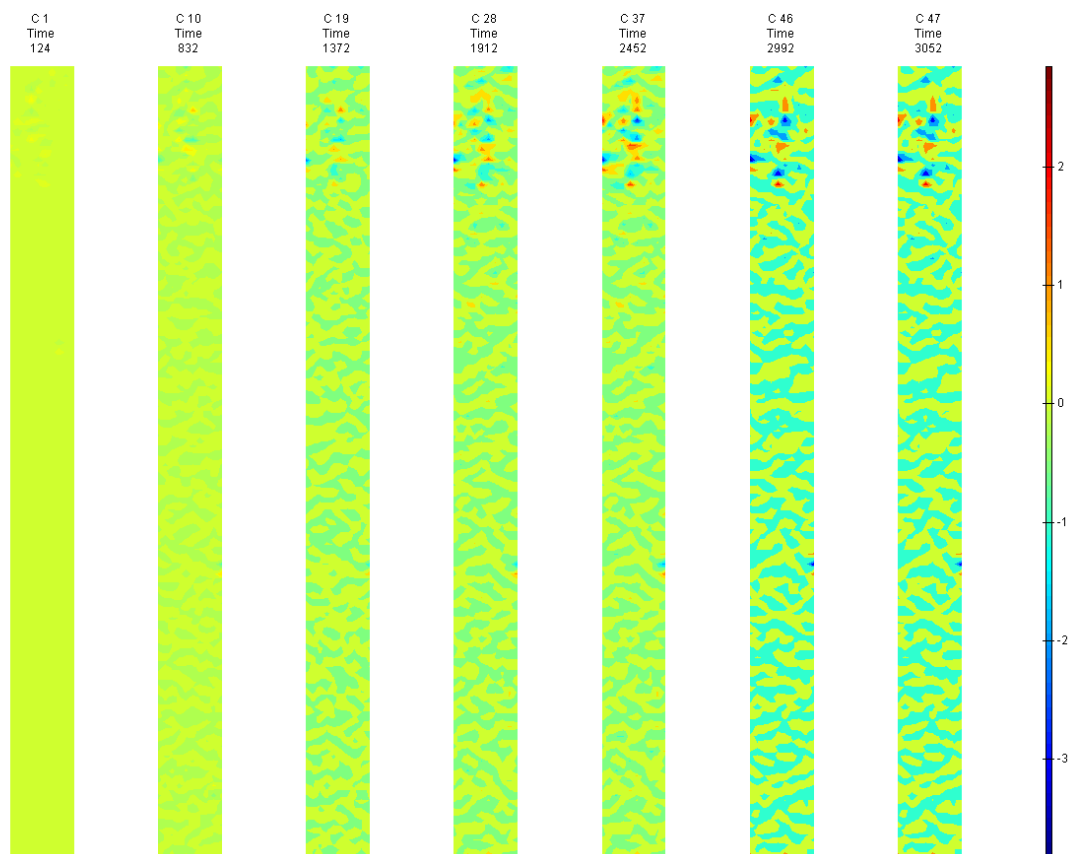
FIGURE 766: Y DIRECTION PIV SEQUENTIAL TRUE STRAIN OVER TIME
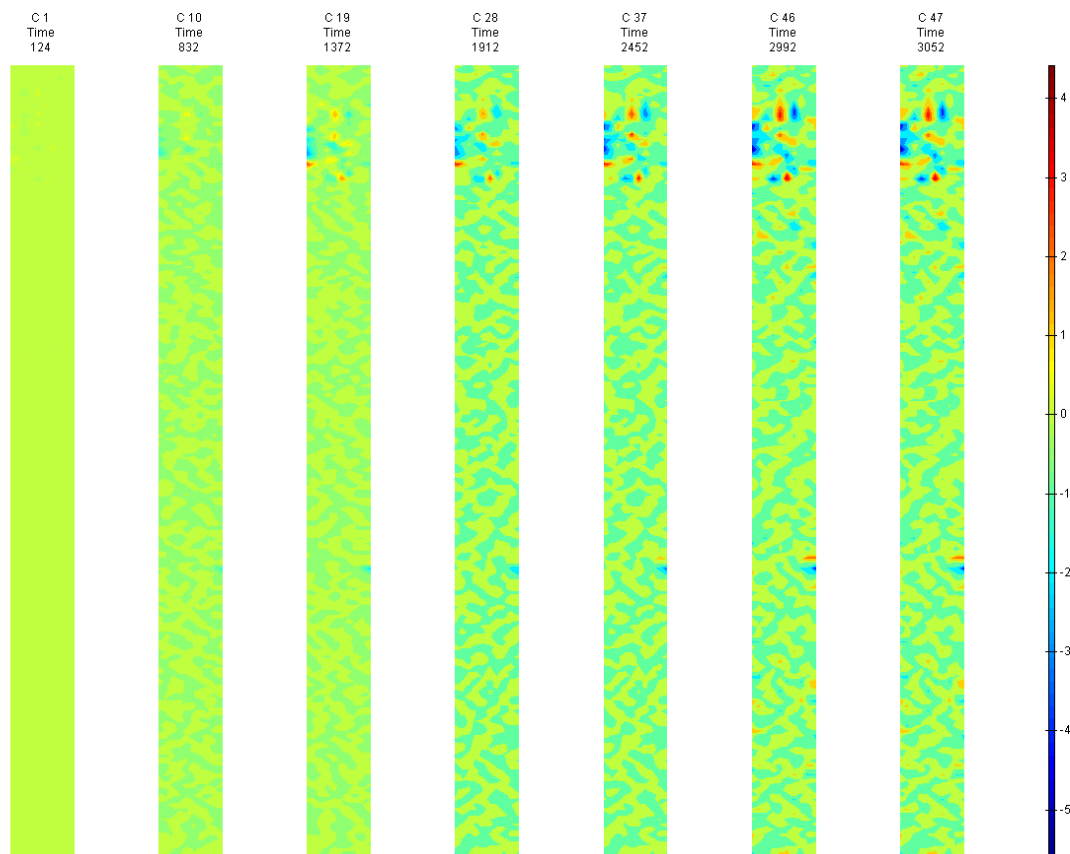
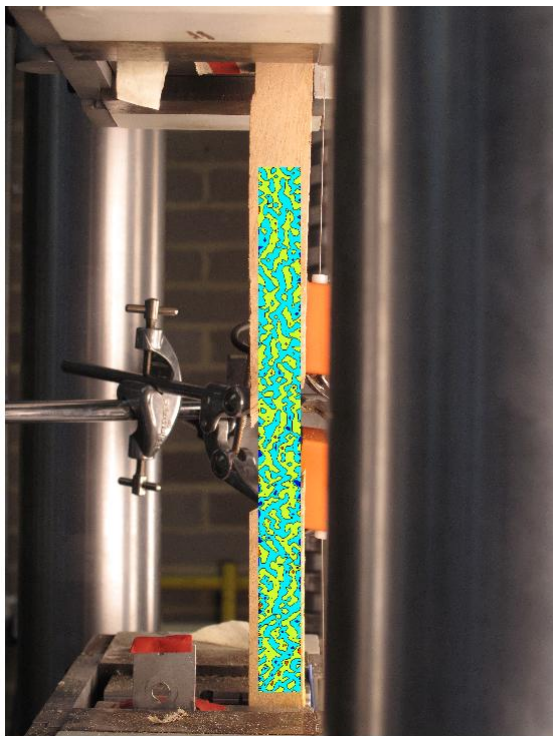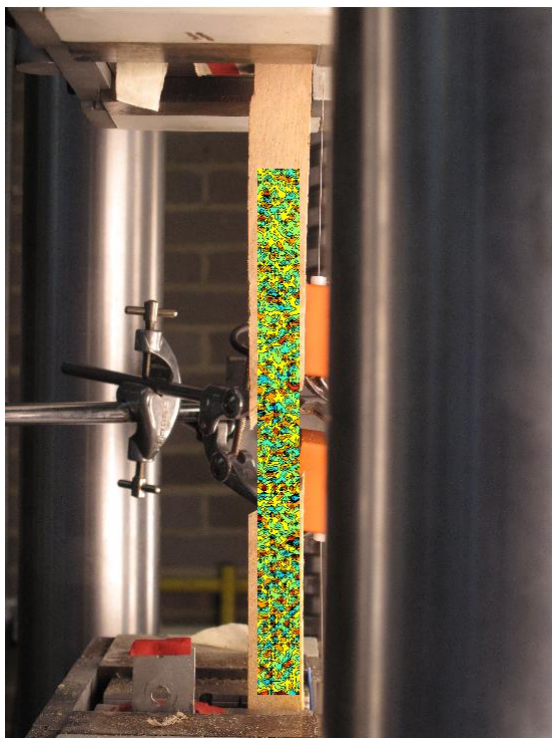FIGURE 767: XY DIRECTION PIV SEQUENTIAL TRUE SHEAR STRAIN OVER TIME

Appendix 6
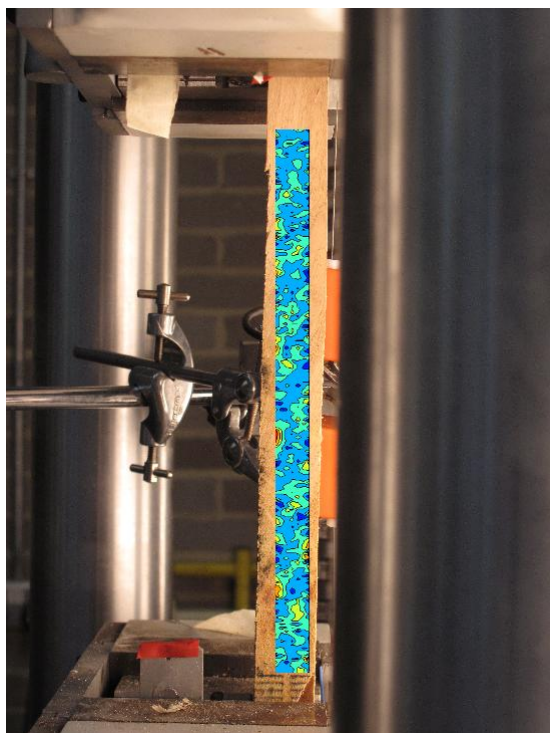
FIGURE 768: X DIRECTION PIV FIRST–LAST DITCH ENGINEERING STRAIN OVER IMAGE
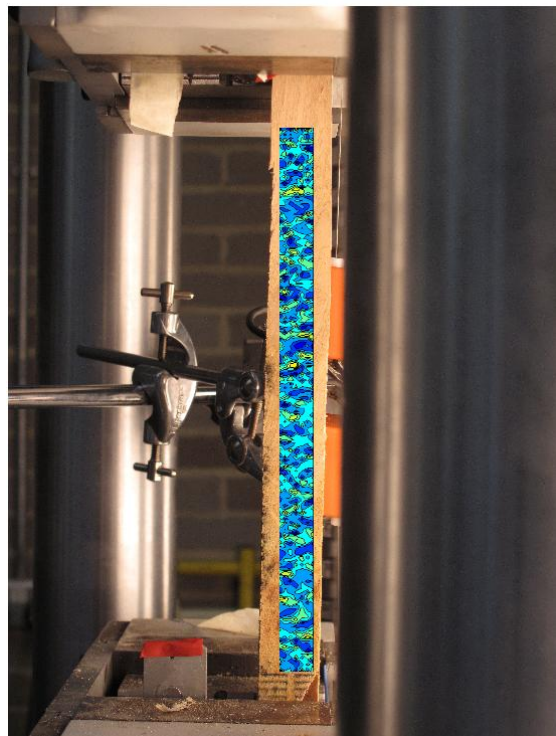
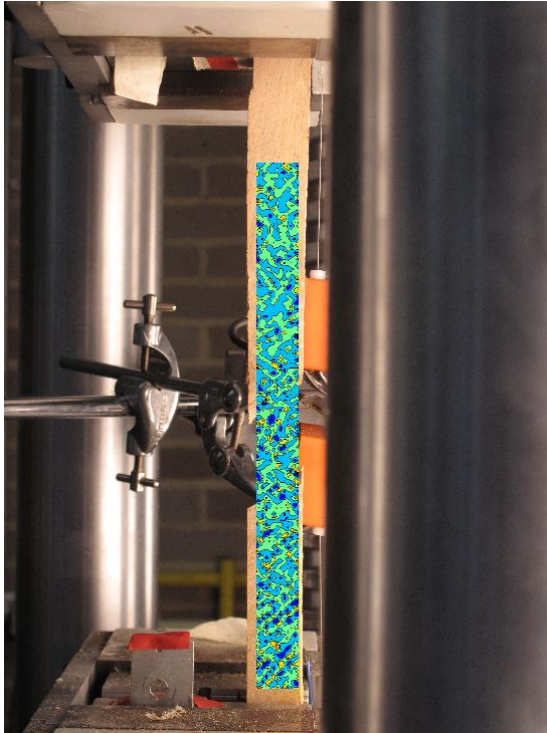FIGURE 769: Y DIRECTION PIV FIRST–LAST DITCH ENGINEERING STRAIN OVER IMAGE
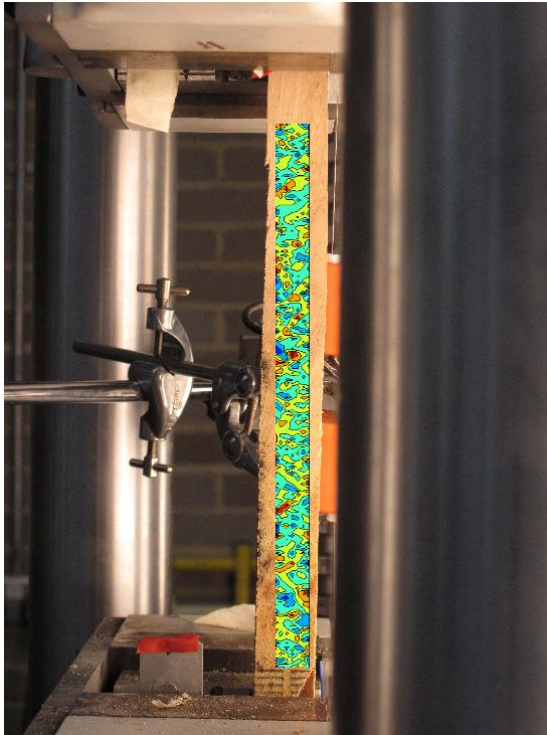
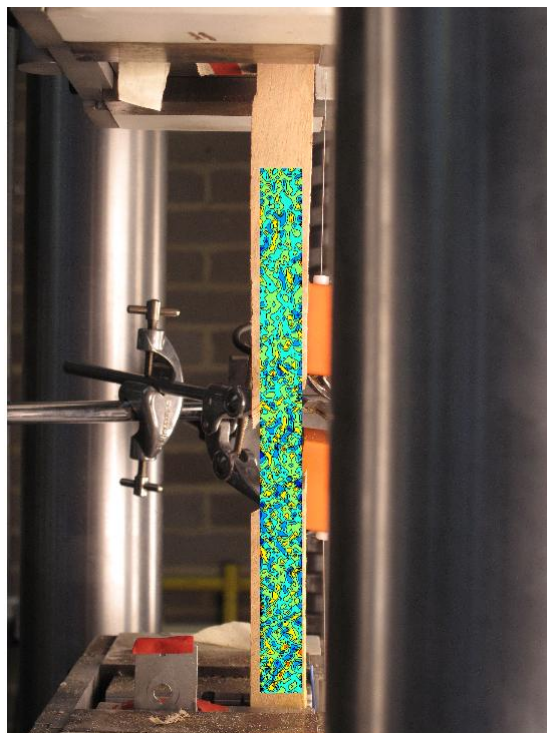FIGURE 770: XY DIRECTION PIV FIRST–LAST DITCH ENGINEERING SHEAR STRAIN OVER
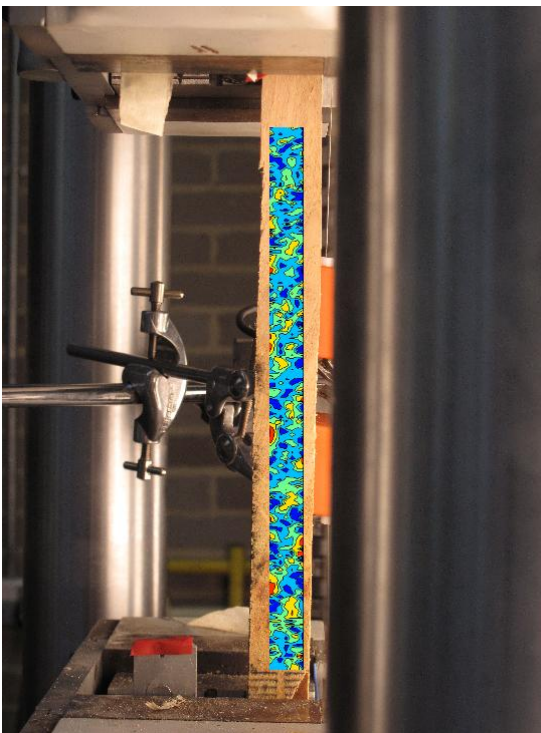
IMAGE

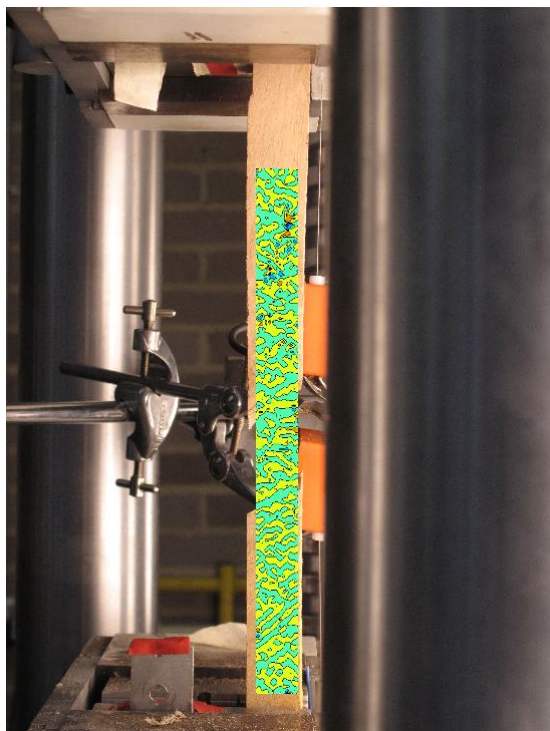FIGURE 771: X DIRECTION PIV FIRST–LAST DITCH TRUE STRAIN OVER IMAGE

Appendix 6
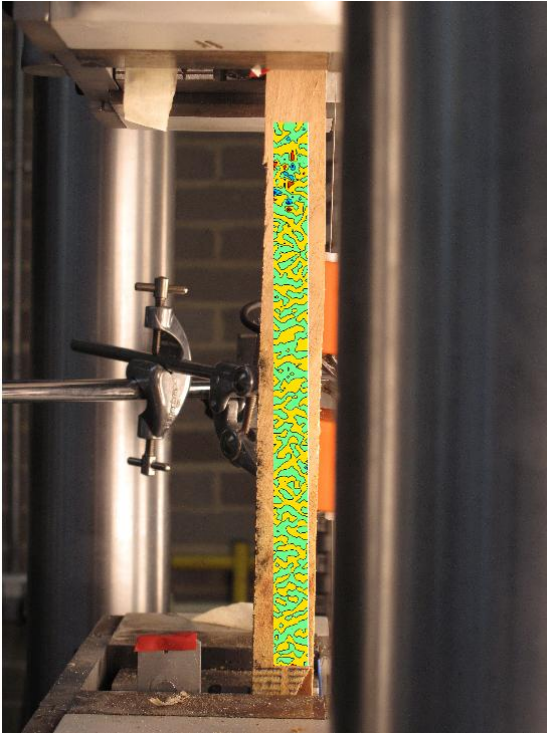
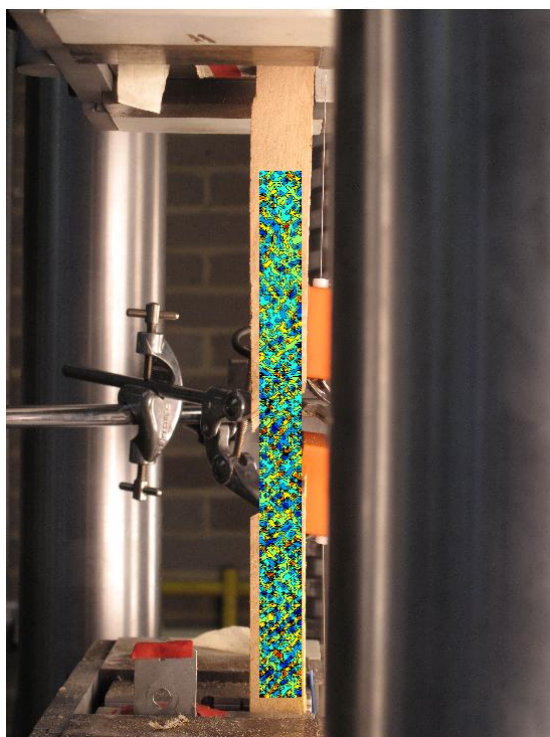FIGURE 772: Y DIRECTION PIV FIRST–LAST DITCH TRUE STRAIN OVER IMAGE
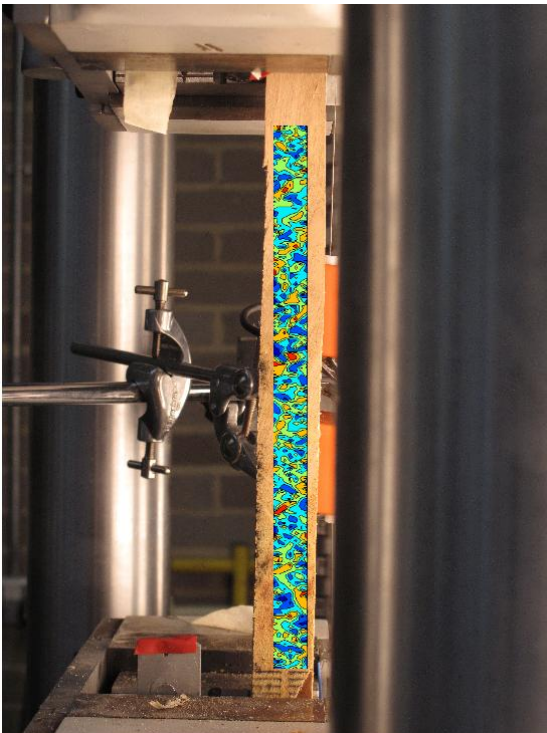
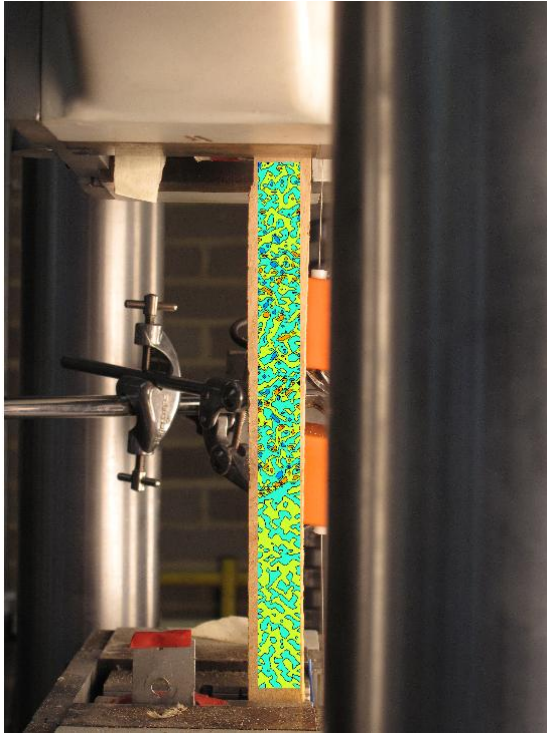FIGURE 773: XY DIRECTION PIV FIRST–LAST DITCH TRUE SHEAR STRAIN OVER IMAGE
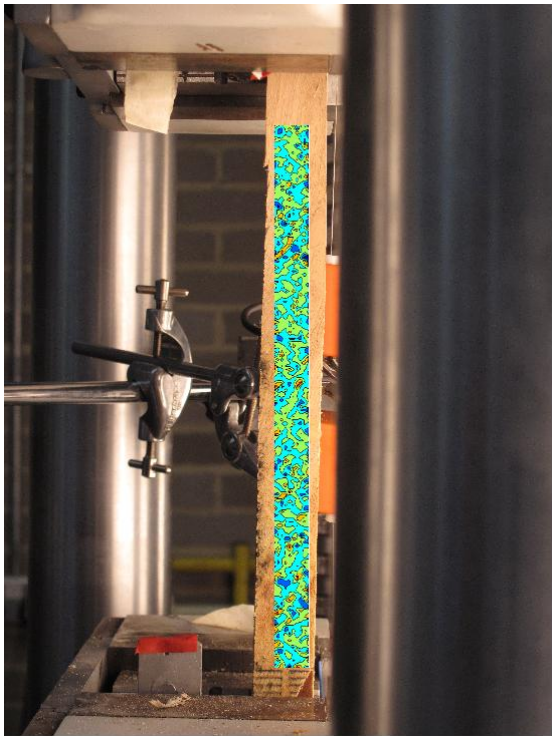
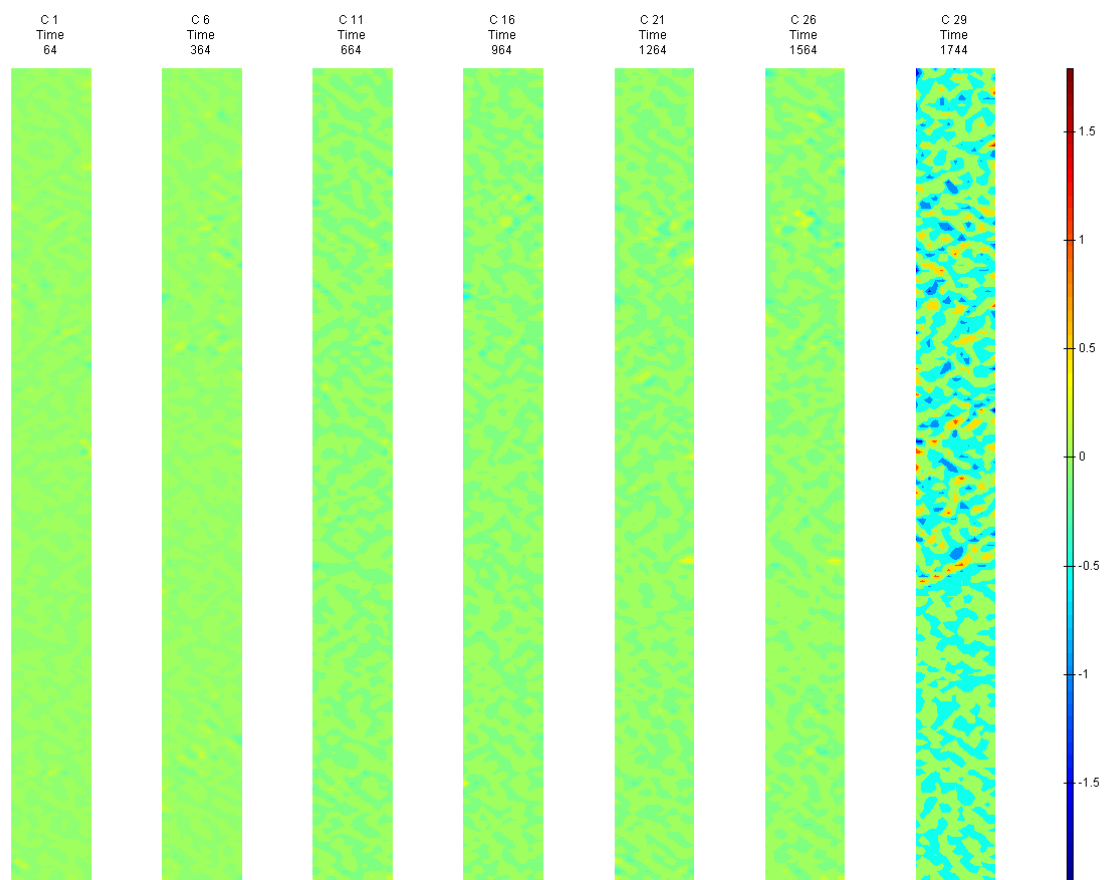FIGURE 774: XY DIRECTION PIV FIRST–SEQUENTIAL ENGINEERING SHEAR STRAIN OVER

IMAGE
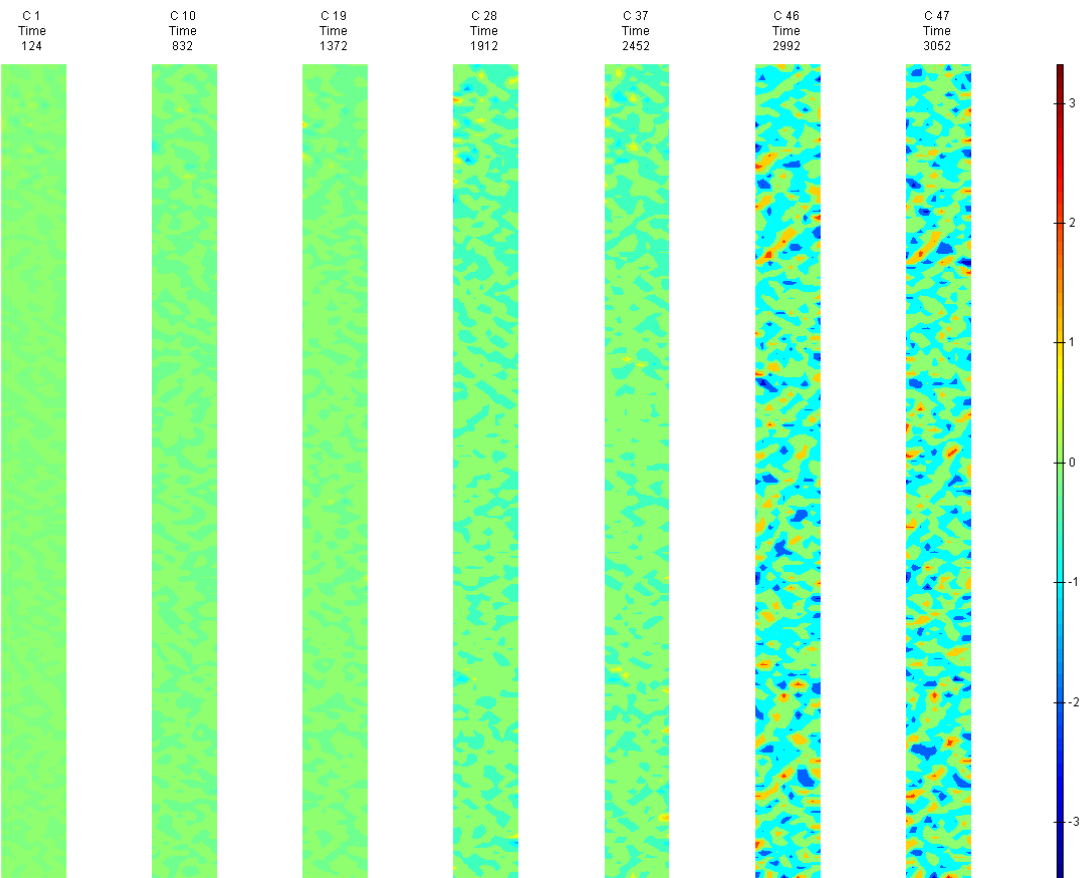
FIGURE 775: XY DIRECTION PIV FIRST–SEQUENTIAL ENGINEERING SHEAR STRAIN OVER TIME

T8
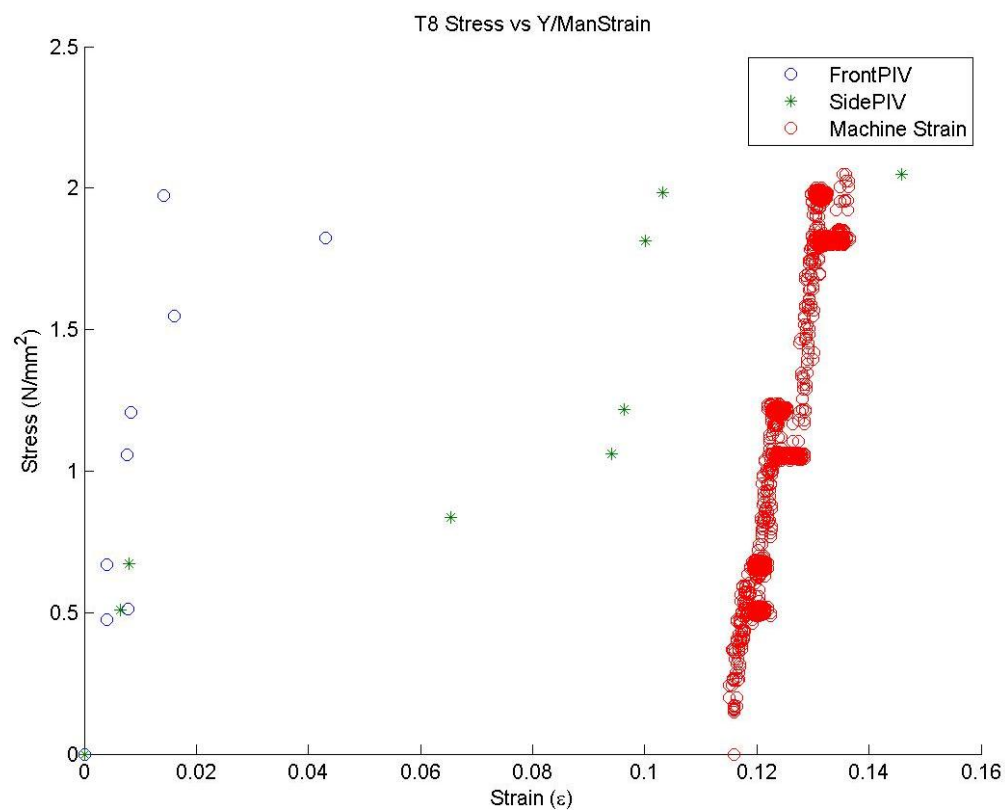
FIGURE 776: T8 TENSILE STRESS VS. MACHINE MEASURED/PIV STRAINS
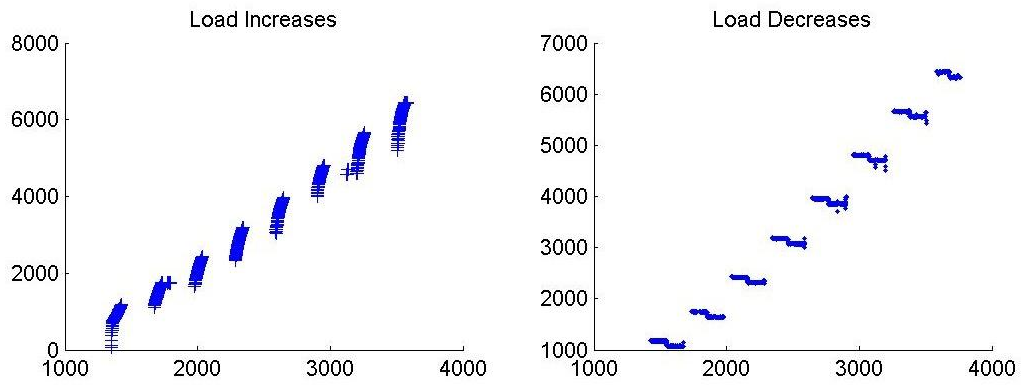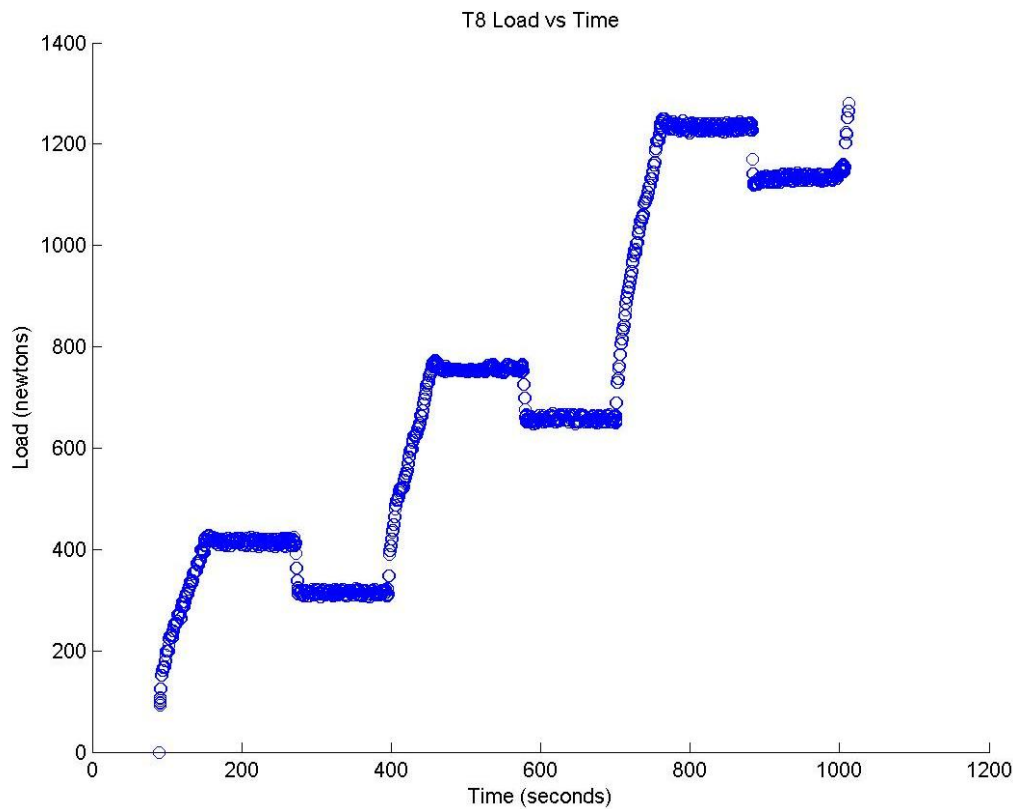

FIGURE 777: T8 TENSILE LOAD VS. TIME
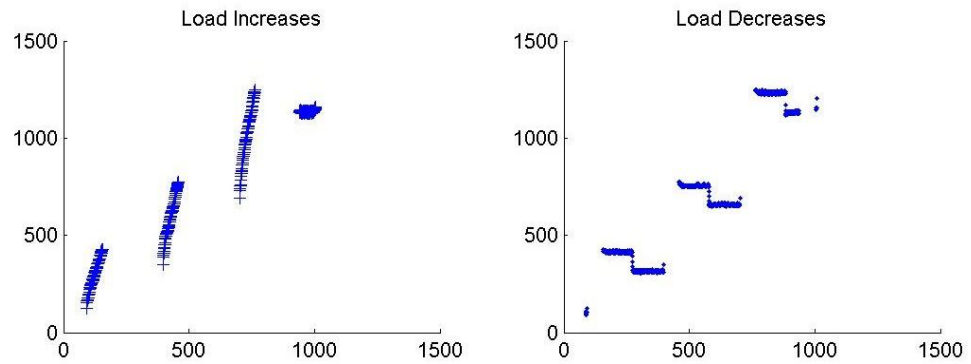
FIGURE 778: T8 CREEP LOADING: INCREMENTS AND RELAXATION
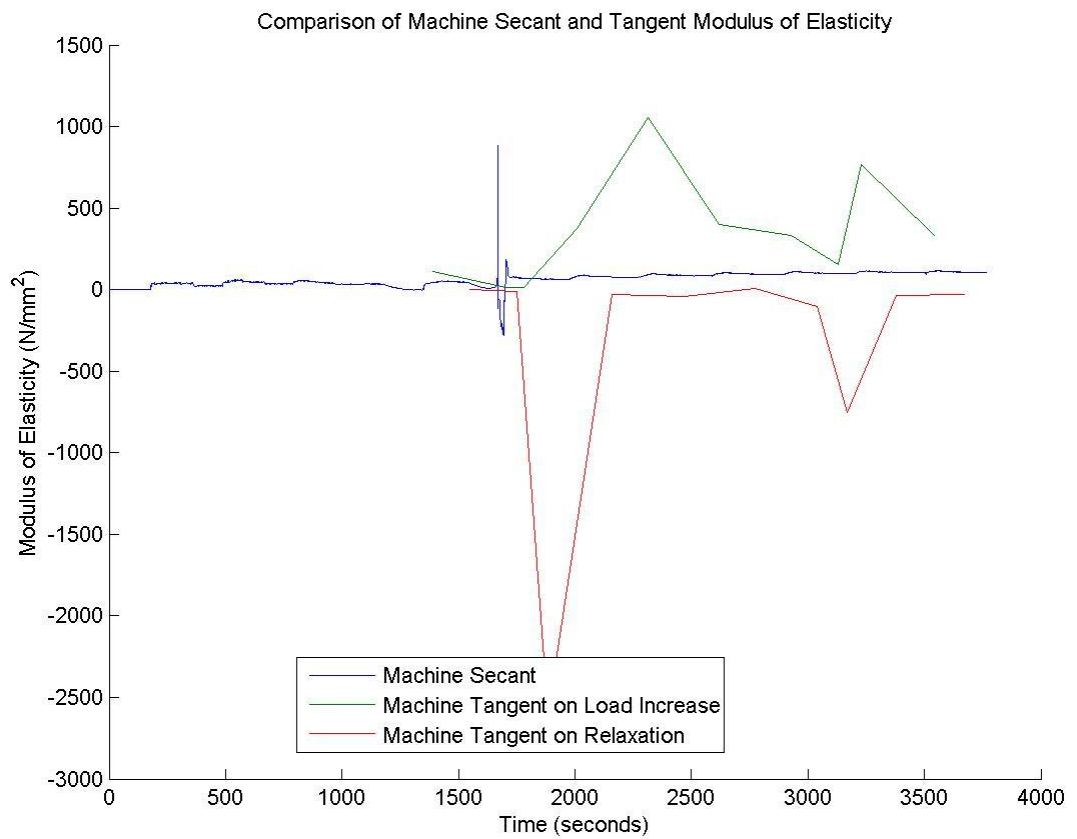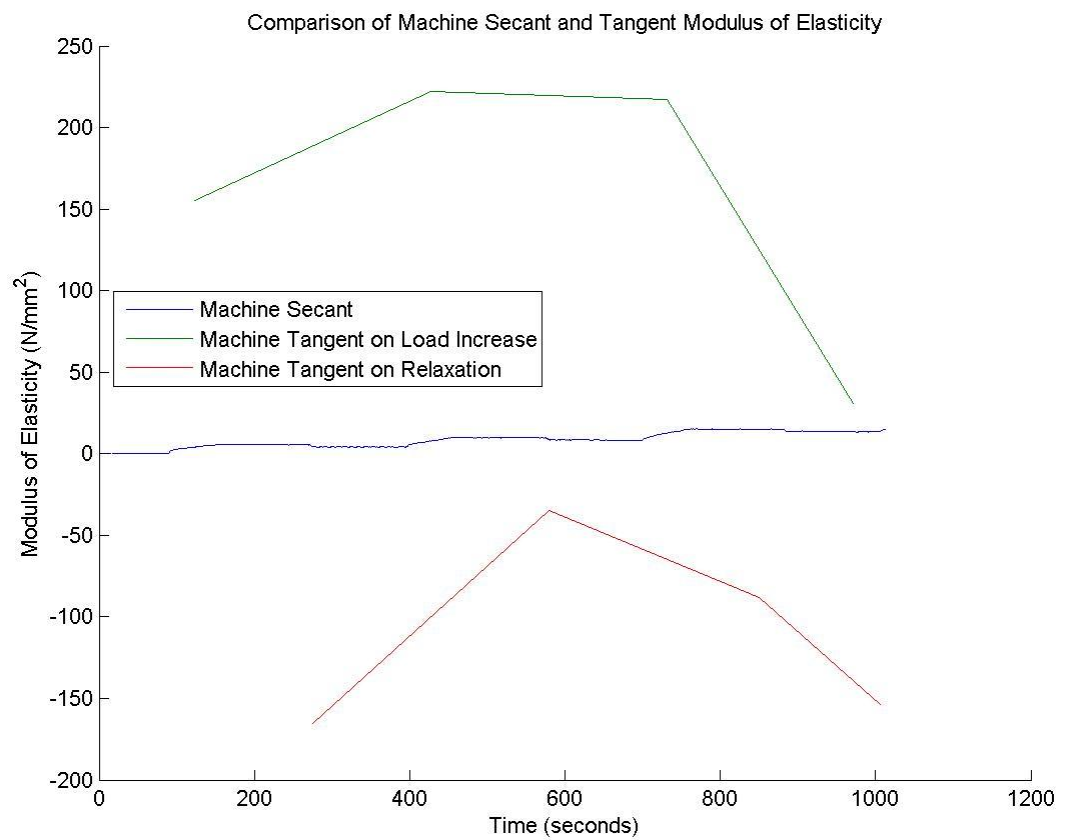

FIGURE 779: T8 MACHINE MEASURED SECANT AND TANGENT MODULUS VS. TIME

Appendix 6
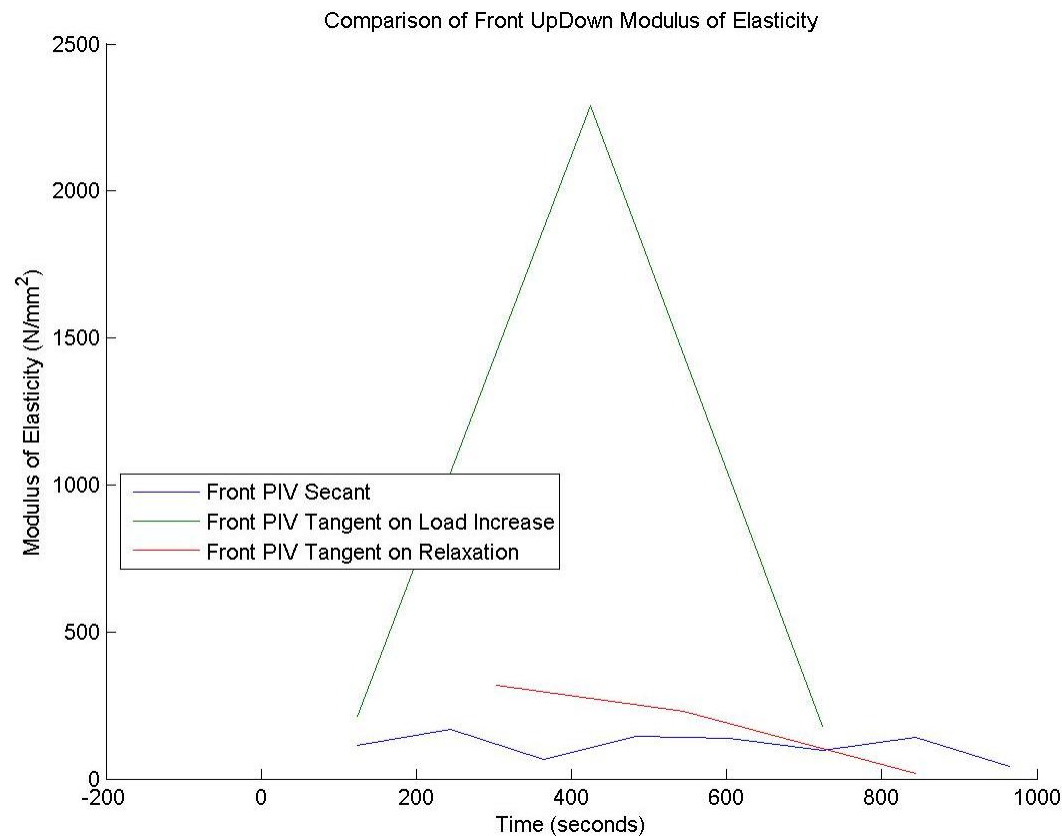
FIGURE 780: T8 FRONT VIEW PIV SECANT AND TANGENT MODULUS VS. TIME
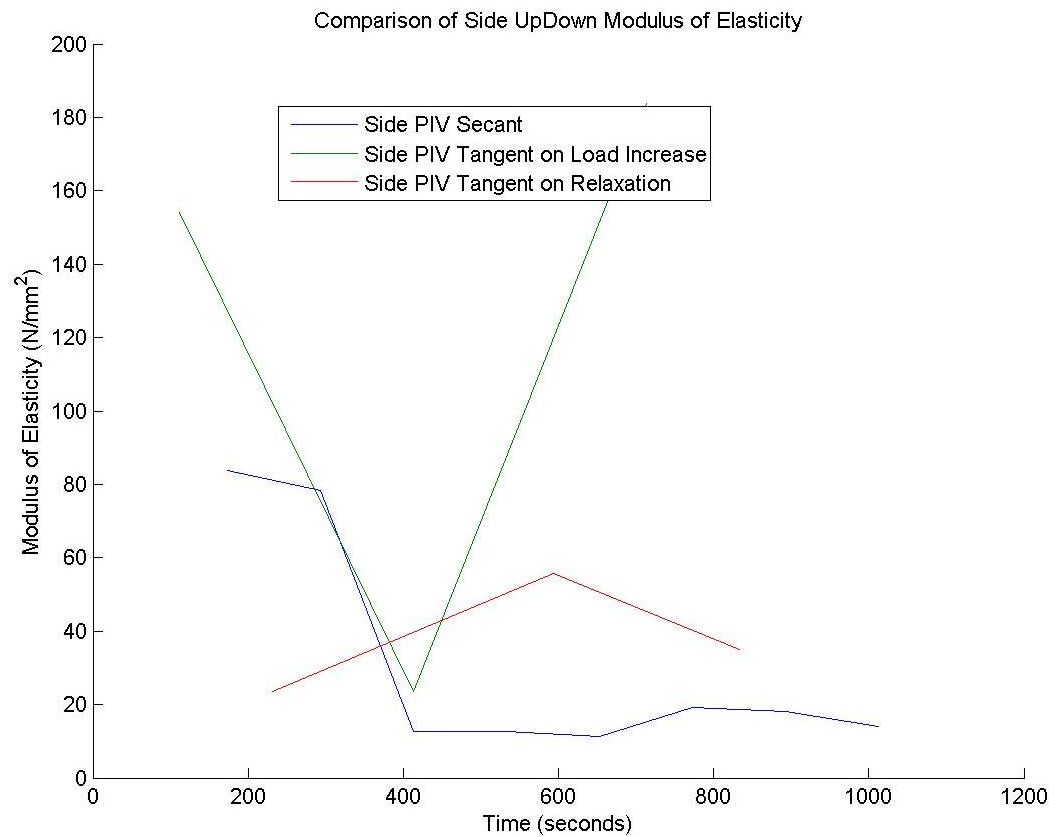
FIGURE 781: T8 SIDE VIEW PIV SECANT AND TANGENT MODULUS VS. TIME
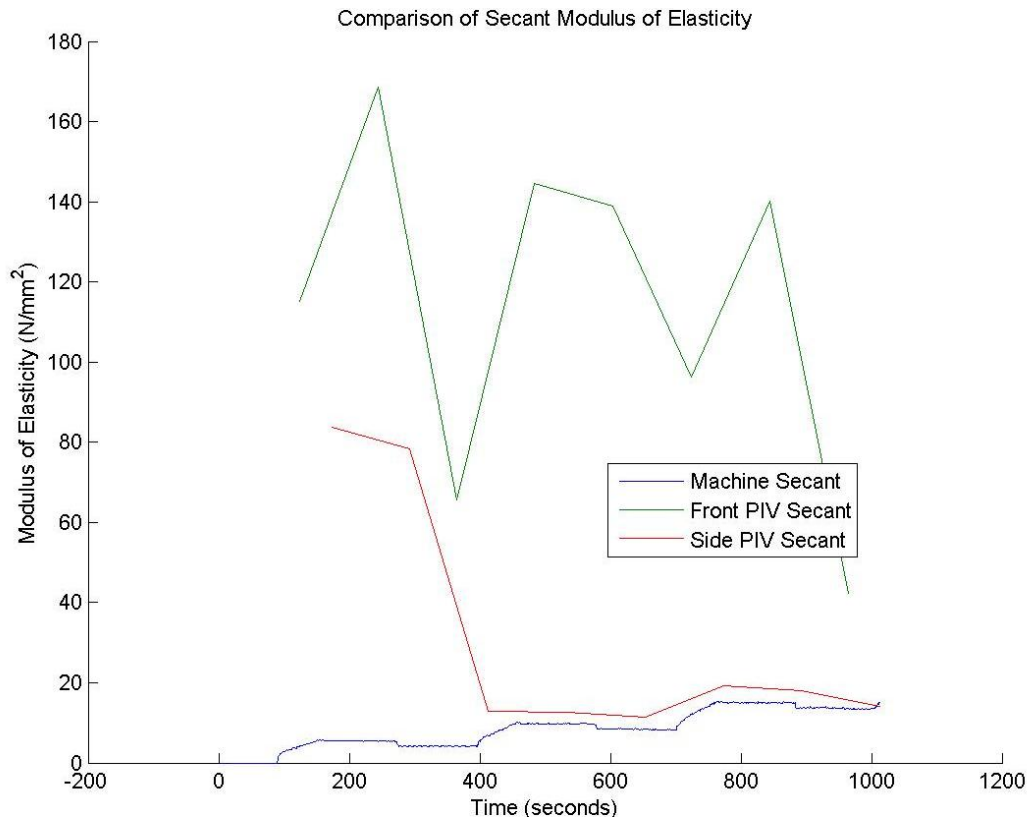
FIGURE 782: T8 COMPARISON OF MACHINE MEASURED AND PIV SECANT MODULUS VS. TIME
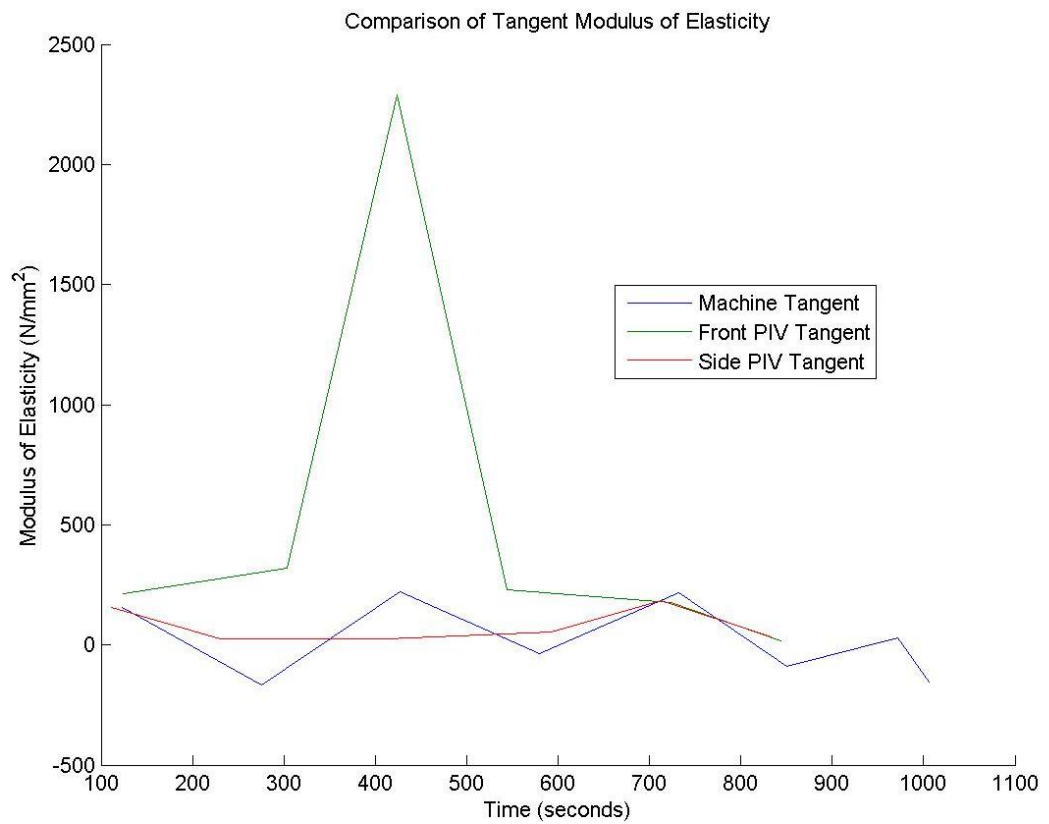
FIGURE 783: T8 COMPARISON OF MACHINE MEASURED AND PIV TANGENT MODULUS VS.

TIME

T8 Sample

FIGURE 784: SAMPLE GRAIN ORIENTATIONS OF THE FRONT (LEFT 4 IMAGES) AND SIDE (RIGHT 4 IMAGES) VIEW BEFORE (FIRST 2 OF 4 IMAGES) AND AFTER (LAST 2 OF 4 IMAGES) BREAKAGE

T8 Front View
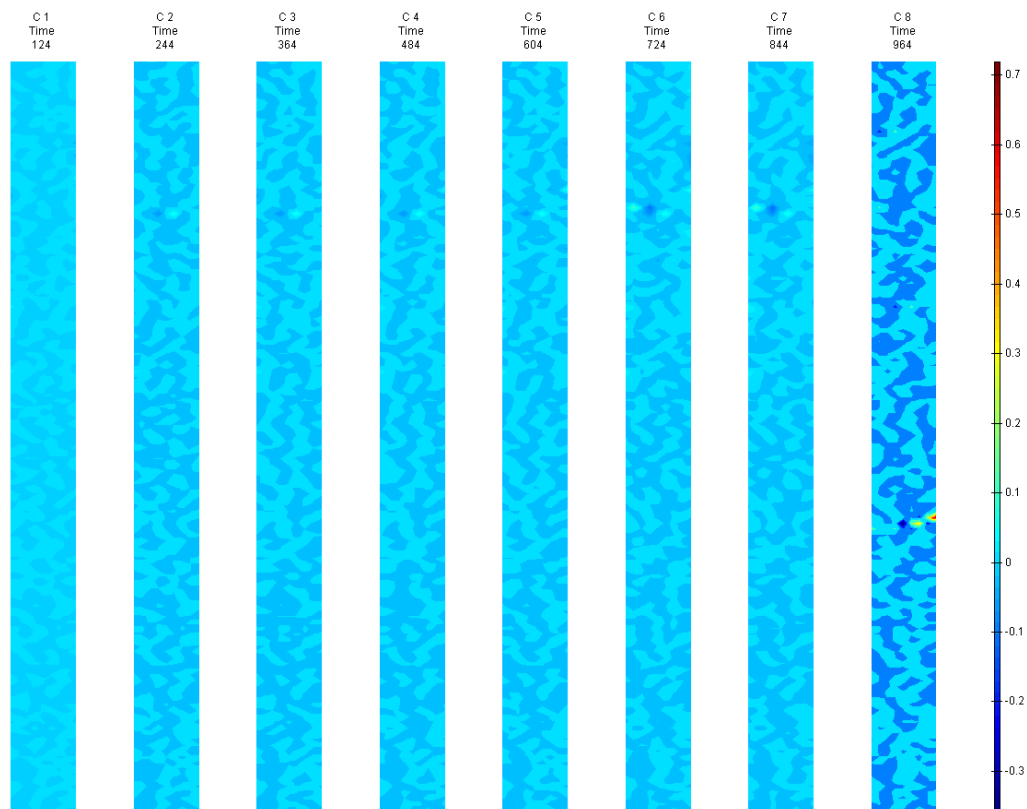
FIGURE 785: X DIRECTION PIV SEQUENTIAL ENGINEERING STRAIN OVER TIME
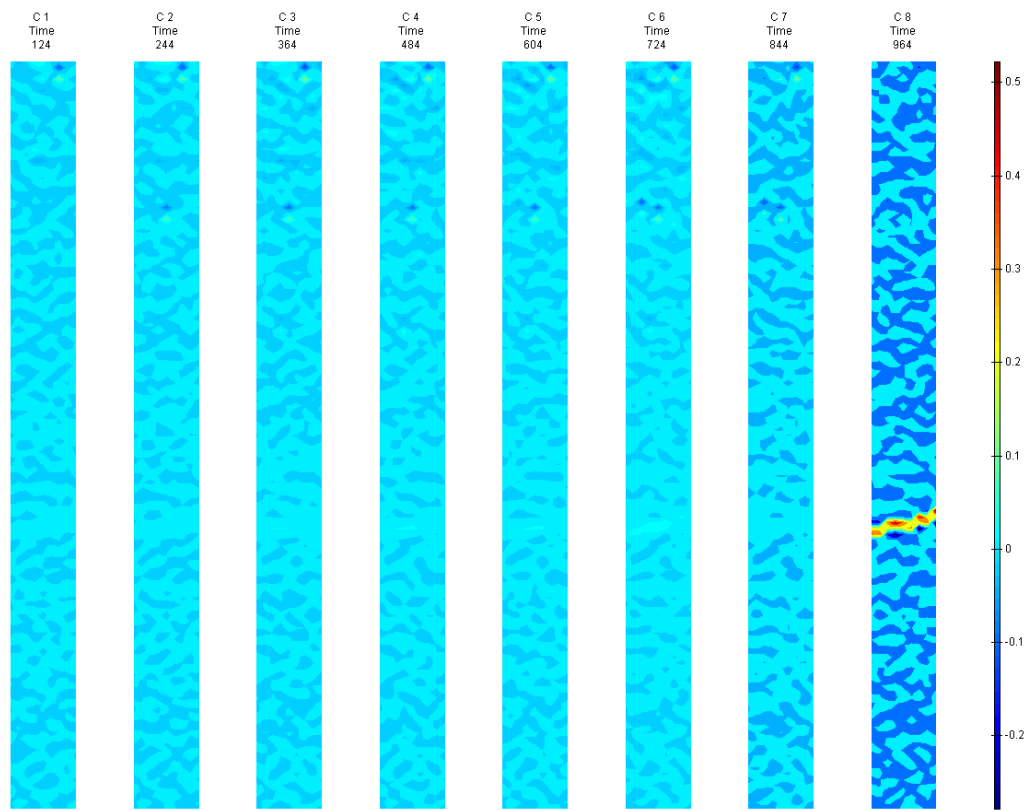
FIGURE 786: Y DIRECTION PIV SEQUENTIAL ENGINEERING STRAIN OVER TIME

Appendix 6
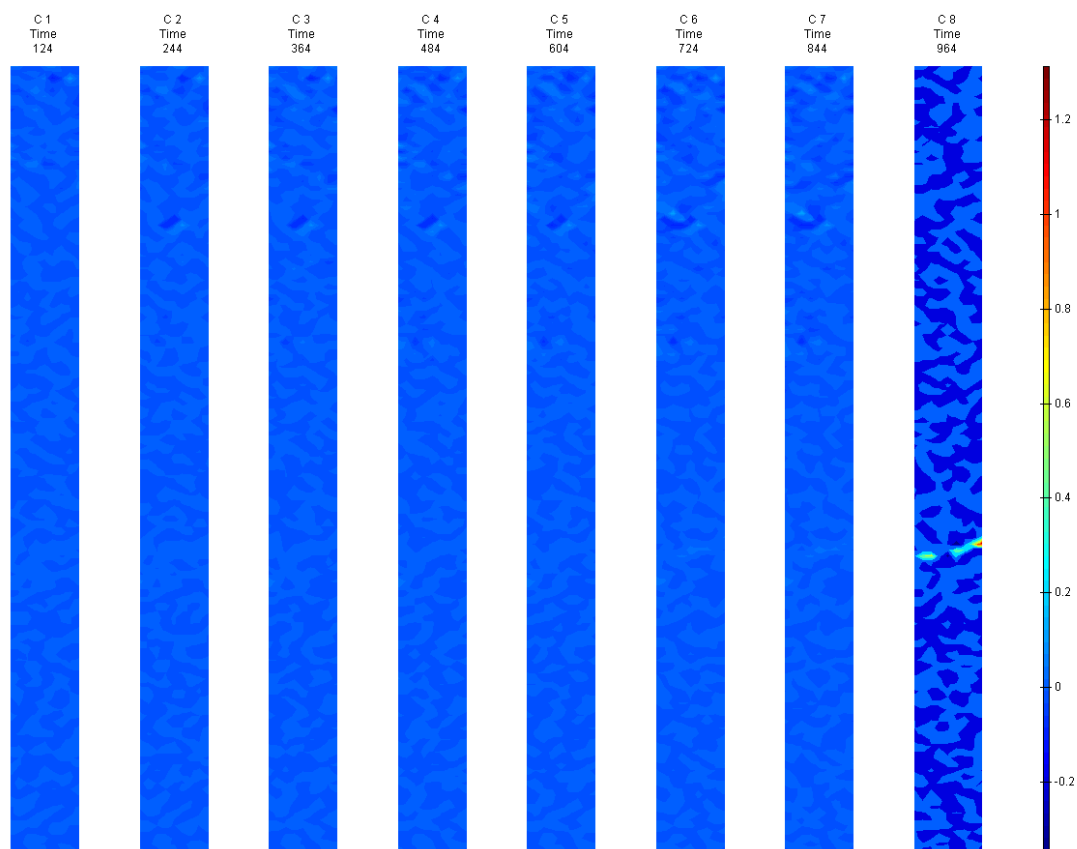
FIGURE 787: XY DIRECTION PIV SEQUENTIAL ENGINEERING SHEAR STRAIN OVER TIME
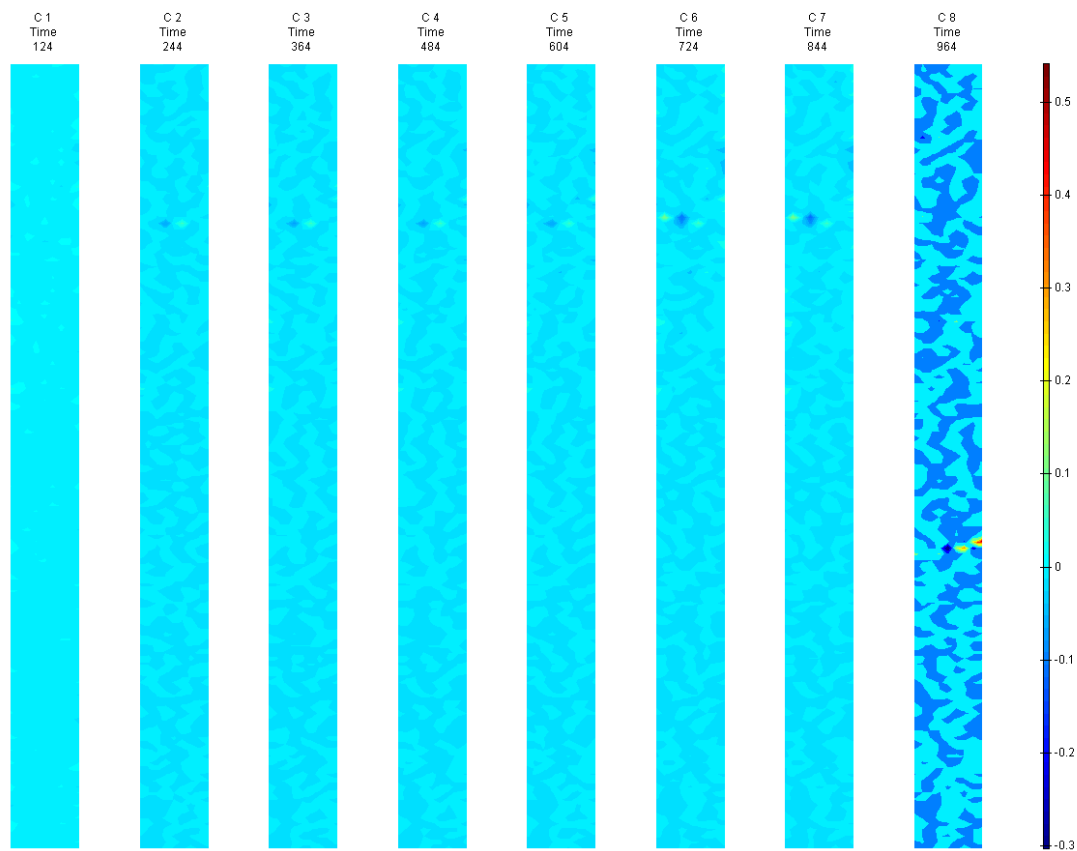
FIGURE 788: X DIRECTION PIV SEQUENTIAL TRUE STRAIN OVER TIME
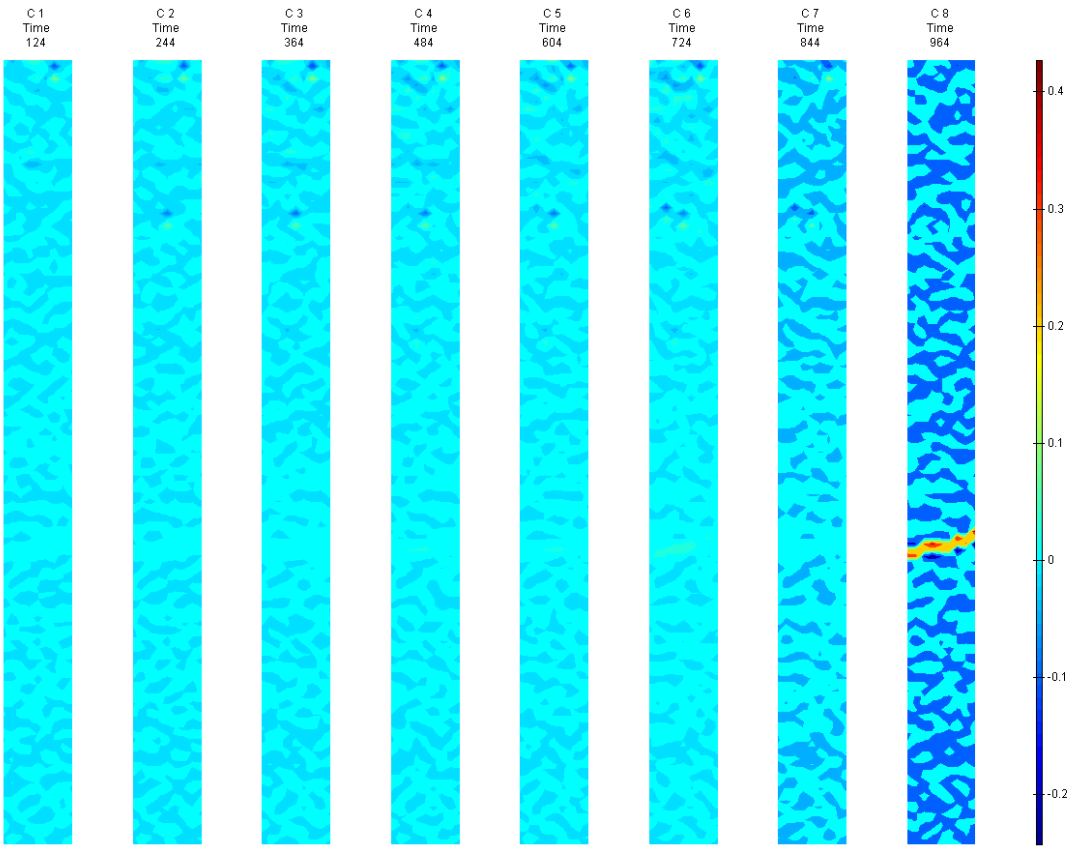
FIGURE 789: Y DIRECTION PIV SEQUENTIAL TRUE STRAIN OVER TIME
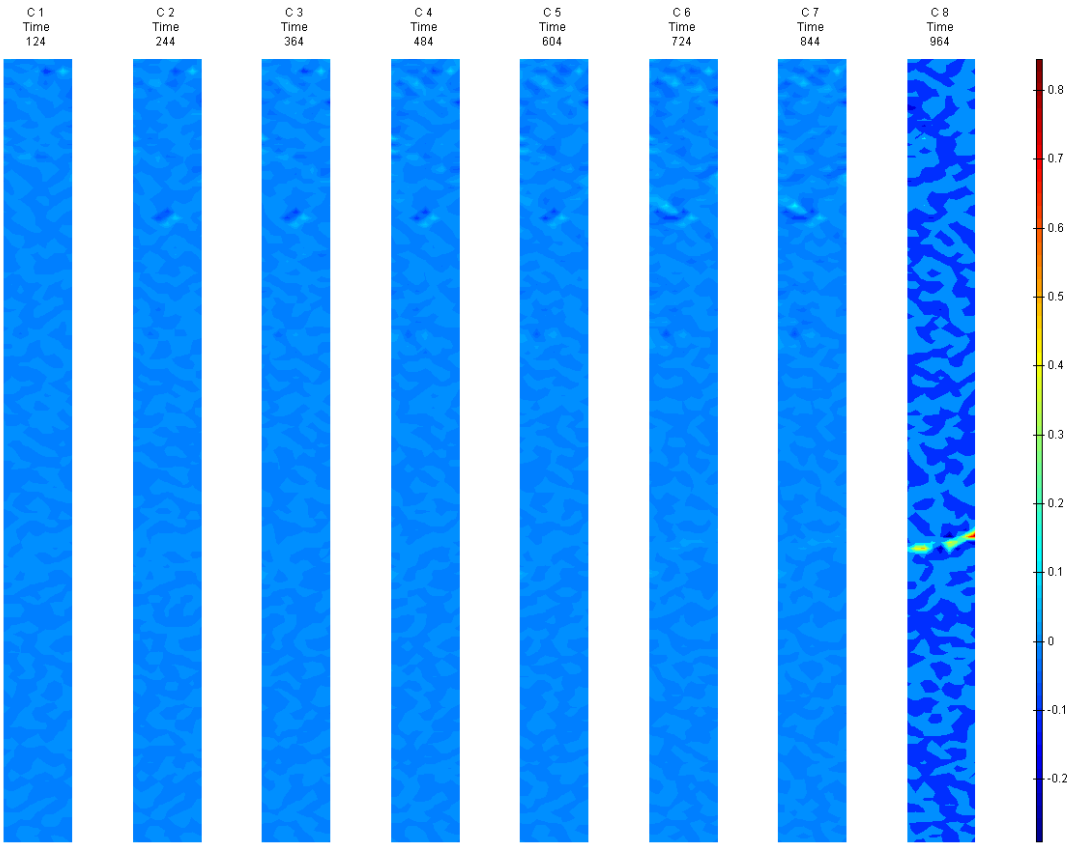
FIGURE 790: XY DIRECTION PIV SEQUENTIAL TRUE SHEAR STRAIN OVER TIME
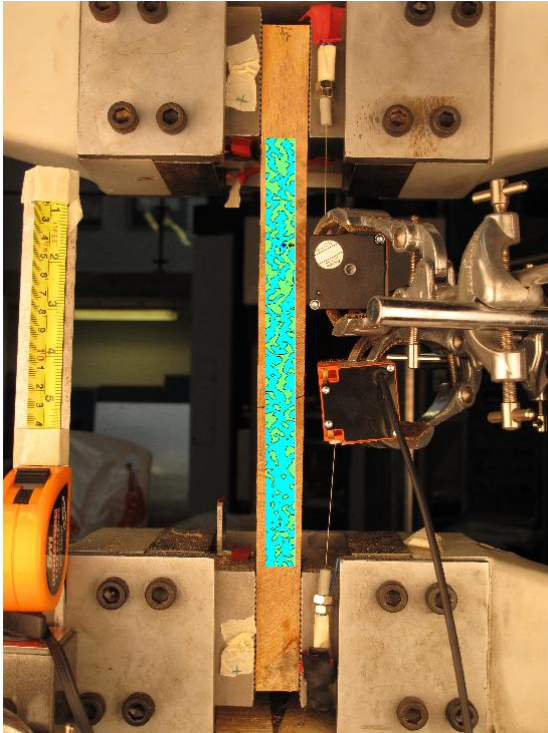
FIGURE 791: X DIRECTION PIV FIRST–LAST DITCH ENGINEERING STRAIN OVER IMAGE
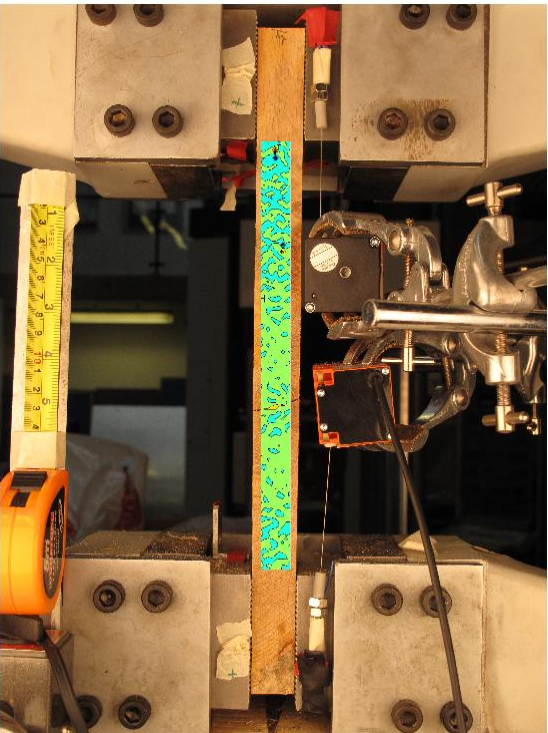
FIGURE 792: Y DIRECTION PIV FIRST–LAST DITCH ENGINEERING STRAIN OVER IMAGE
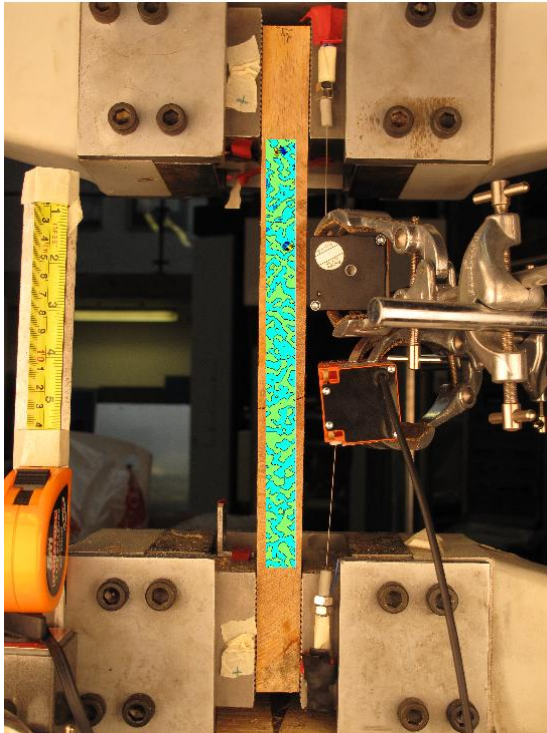
FIGURE 793: XY DIRECTION PIV FIRST–LAST DITCH ENGINEERING SHEAR STRAIN OVER
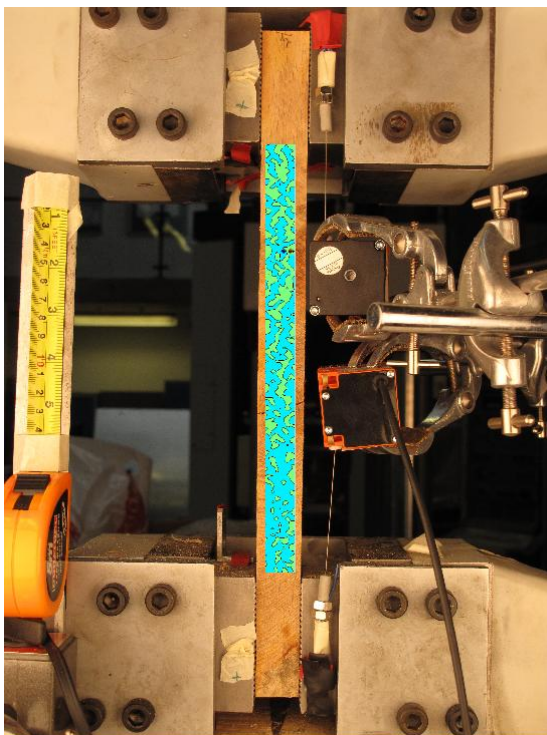
IMAGE

FIGURE 794: X DIRECTION PIV FIRST–LAST DITCH TRUE STRAIN OVER IMAGE

Appendix 6
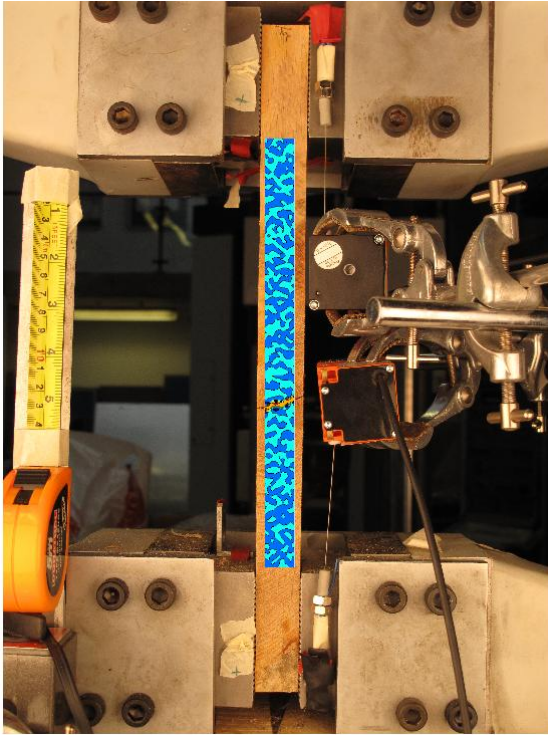
FIGURE 795: Y DIRECTION PIV FIRST–LAST DITCH TRUE STRAIN OVER IMAGE
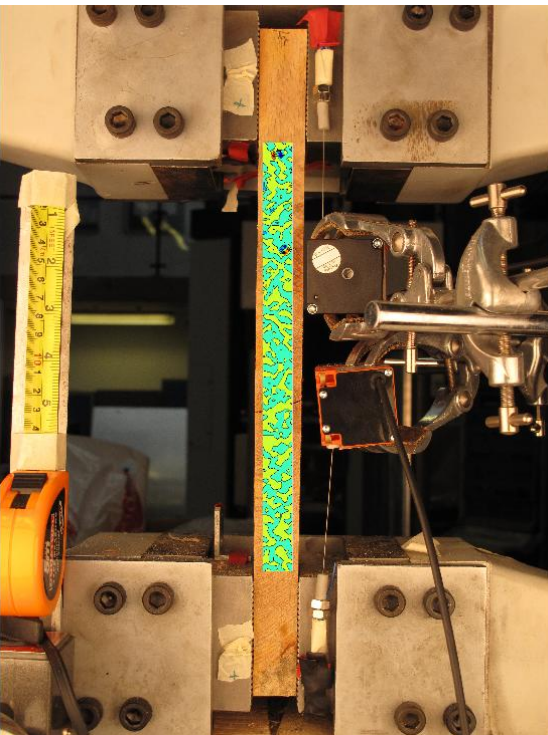
FIGURE 796: XY DIRECTION PIV FIRST–LAST DITCH TRUE SHEAR STRAIN OVER IMAGE
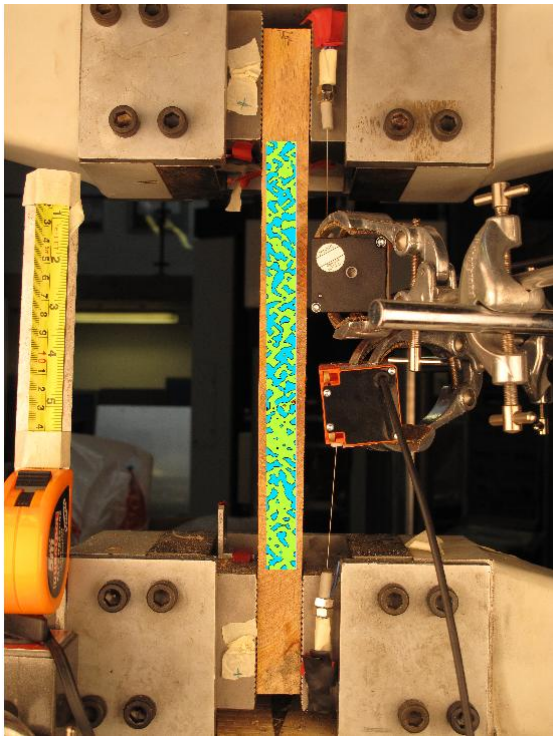
FIGURE 797: XY DIRECTION PIV FIRST–SEQUENTIAL ENGINEERING SHEAR STRAIN OVER

IMAGE
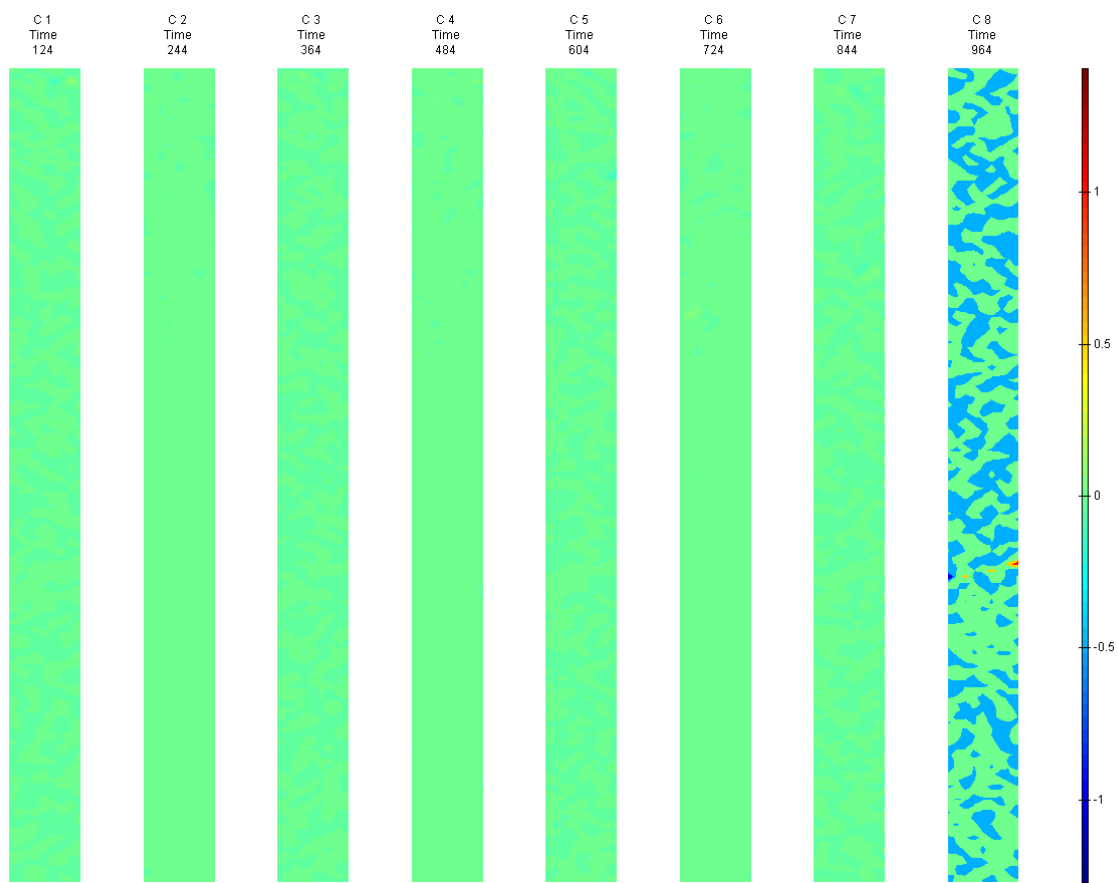
FIGURE 798: XY DIRECTION PIV FIRST–SEQUENTIAL ENGINEERING SHEAR STRAIN OVER TIME

Appendix 6

T8 Side View
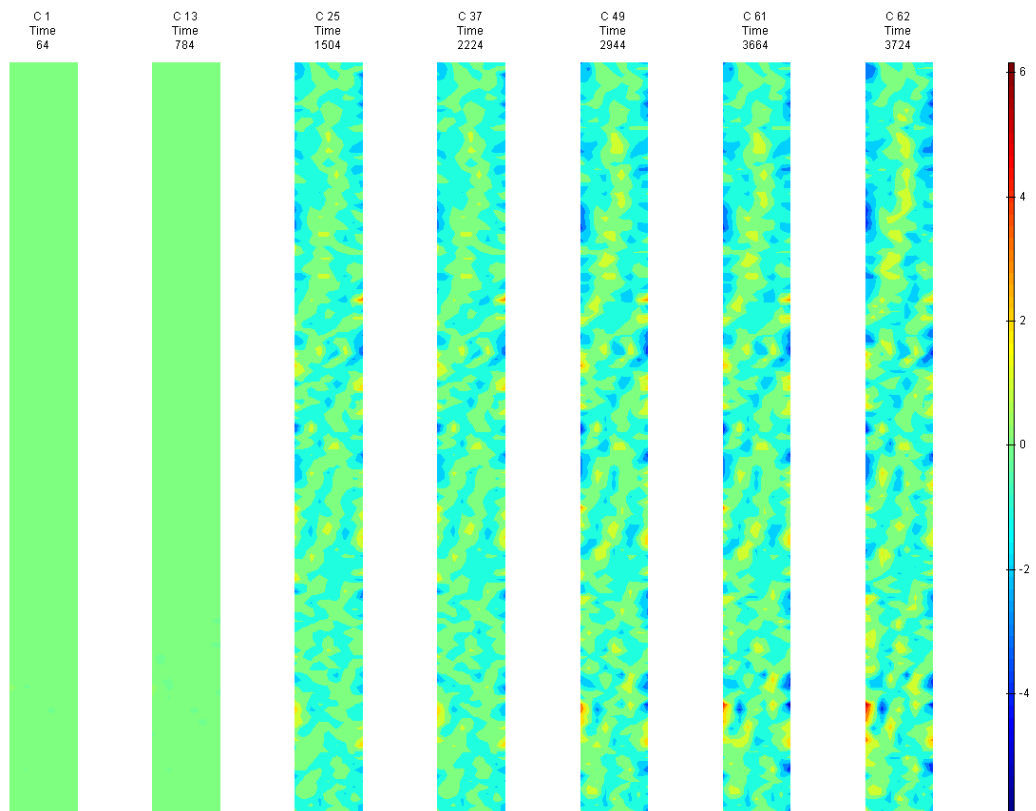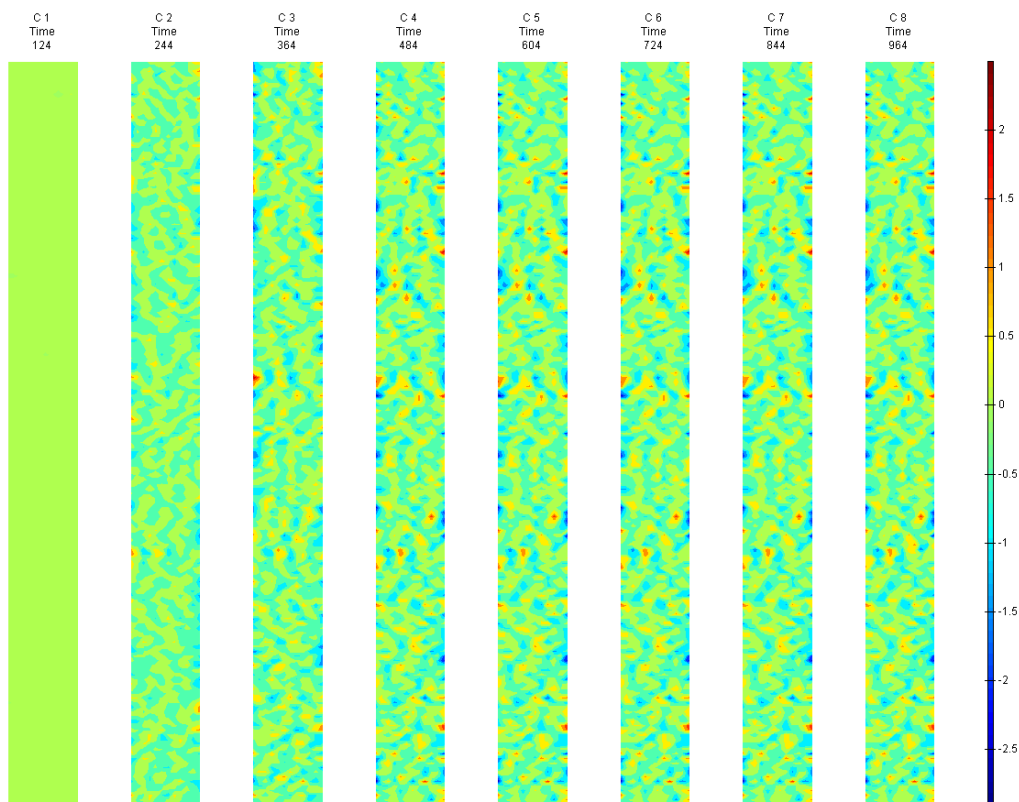

FIGURE 799: X DIRECTION PIV SEQUENTIAL ENGINEERING STRAIN OVER TIME
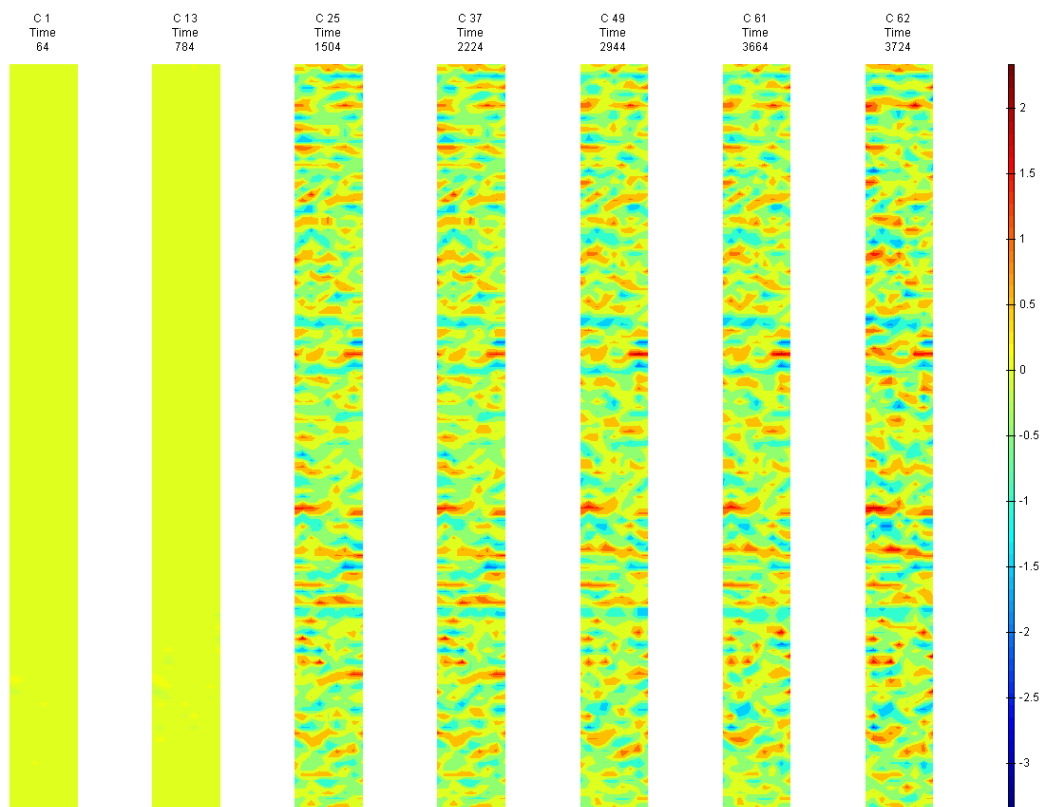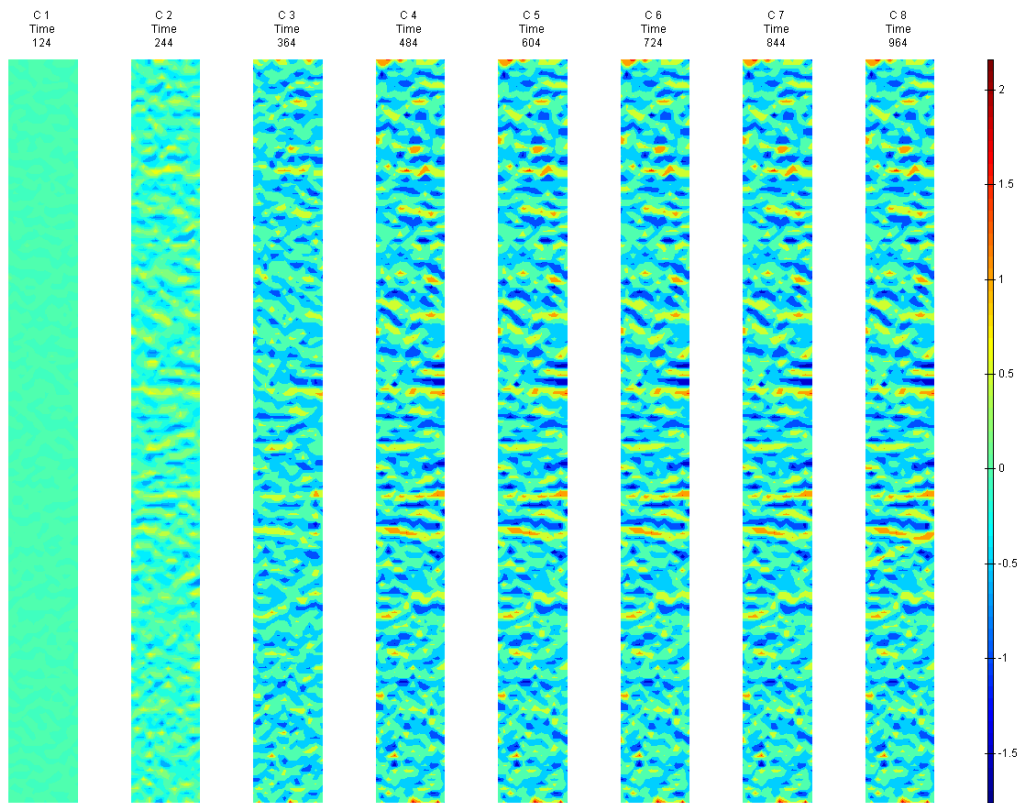

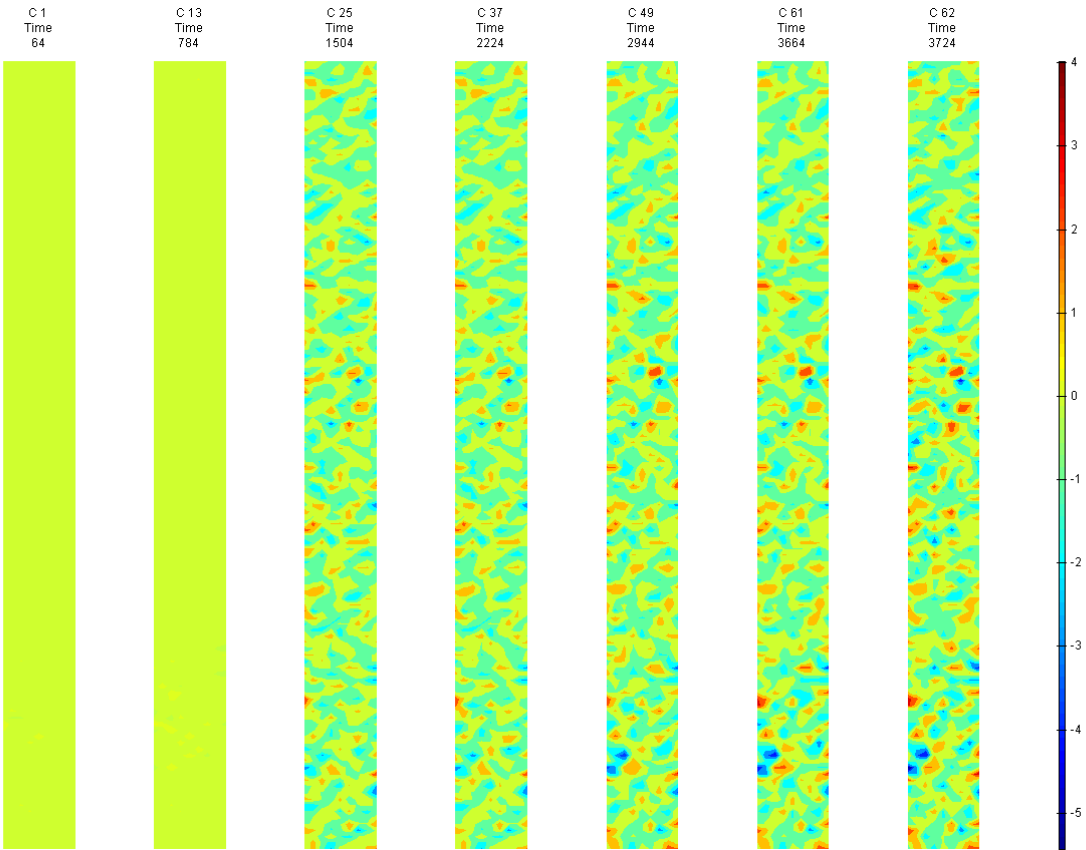FIGURE 800: Y DIRECTION PIV SEQUENTIAL ENGINEERING STRAIN OVER TIME
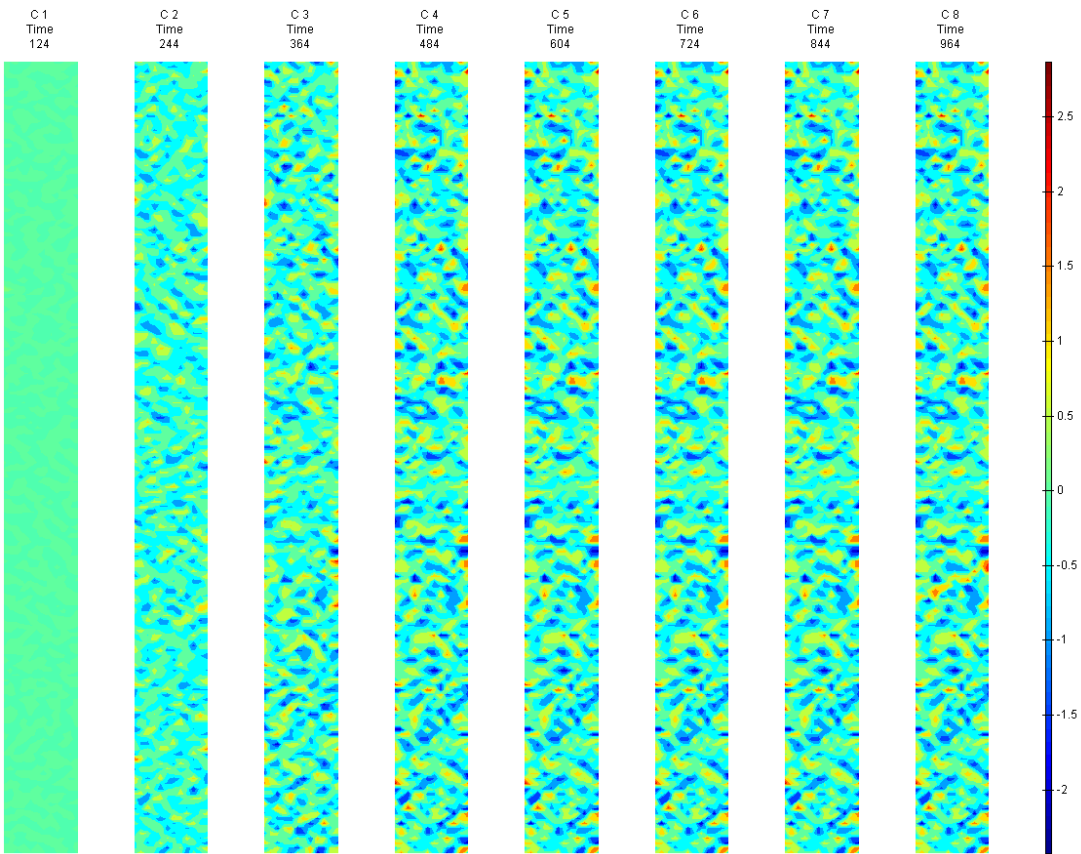
FIGURE 801: XY DIRECTION PIV SEQUENTIAL ENGINEERING SHEAR STRAIN OVER TIME
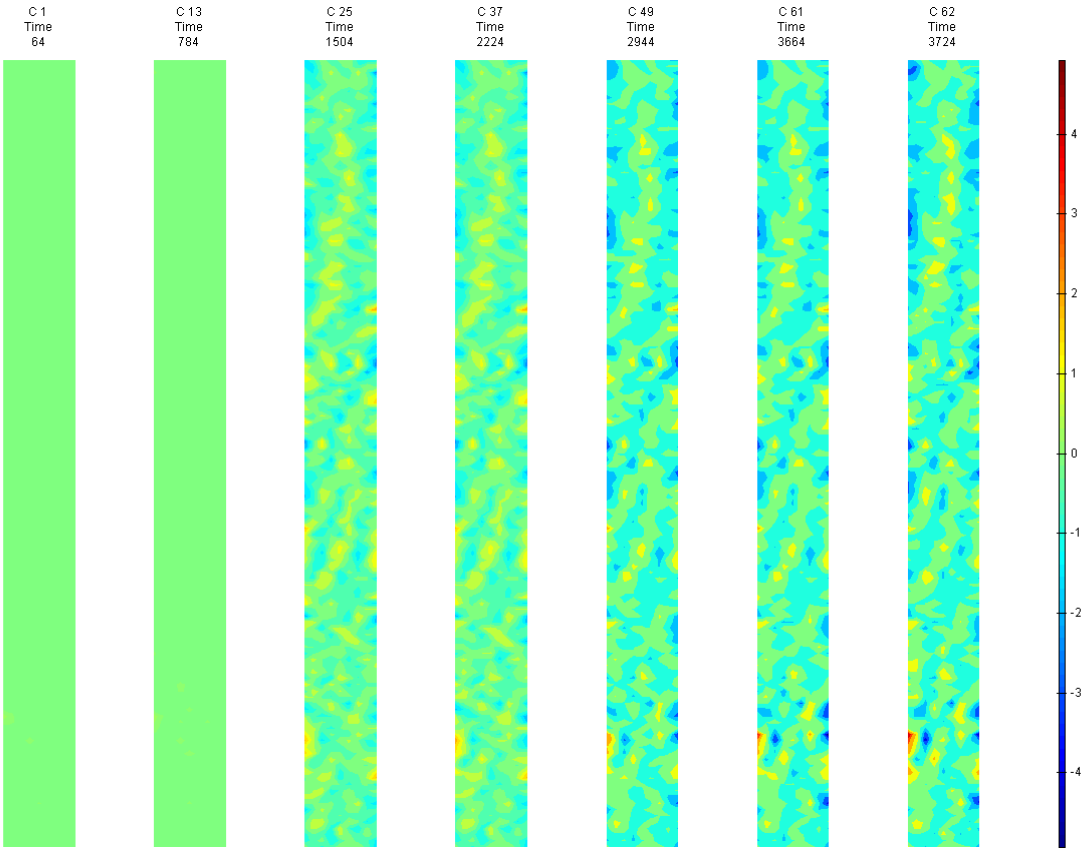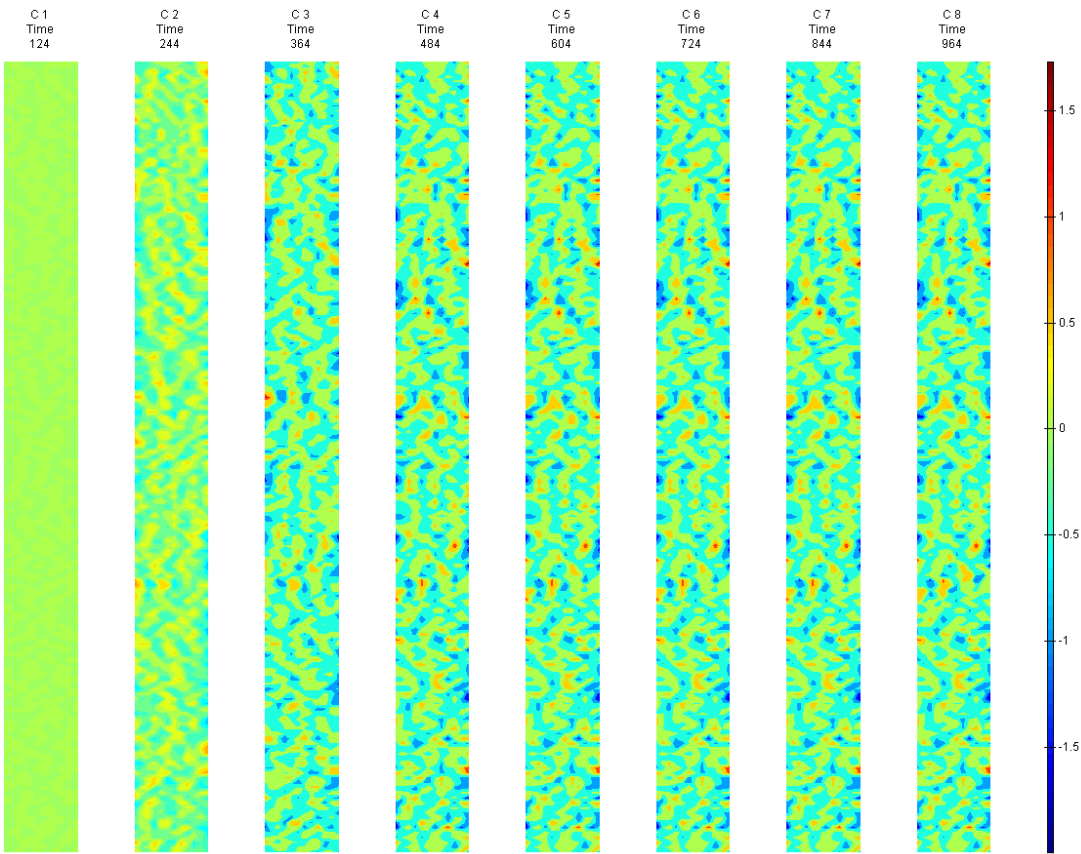

FIGURE 802: X DIRECTION PIV SEQUENTIAL TRUE STRAIN OVER TIME
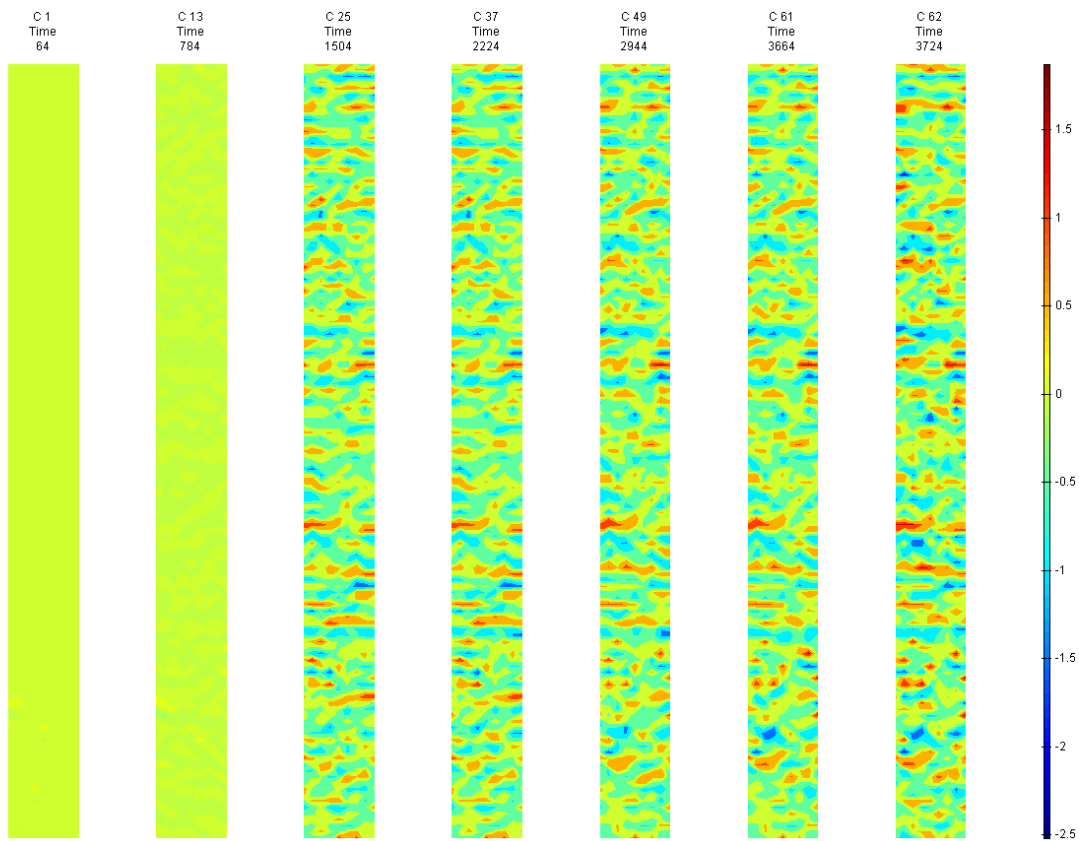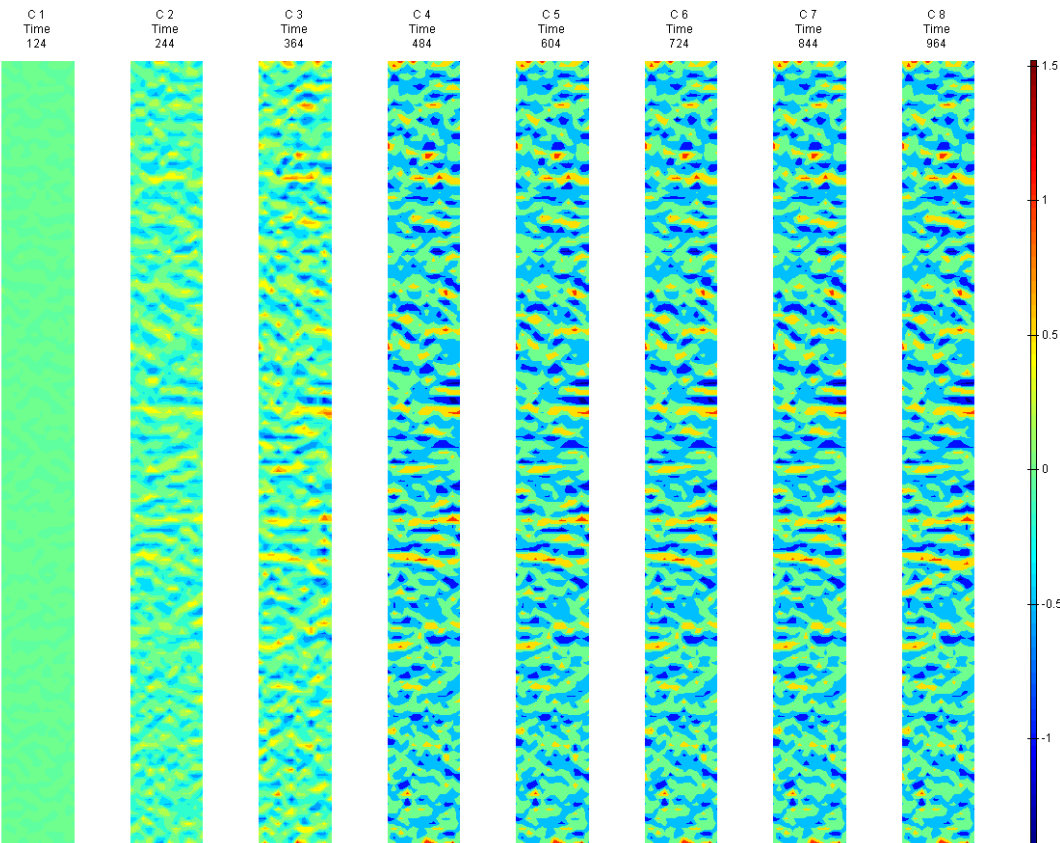
FIGURE 803: Y DIRECTION PIV SEQUENTIAL TRUE STRAIN OVER TIME
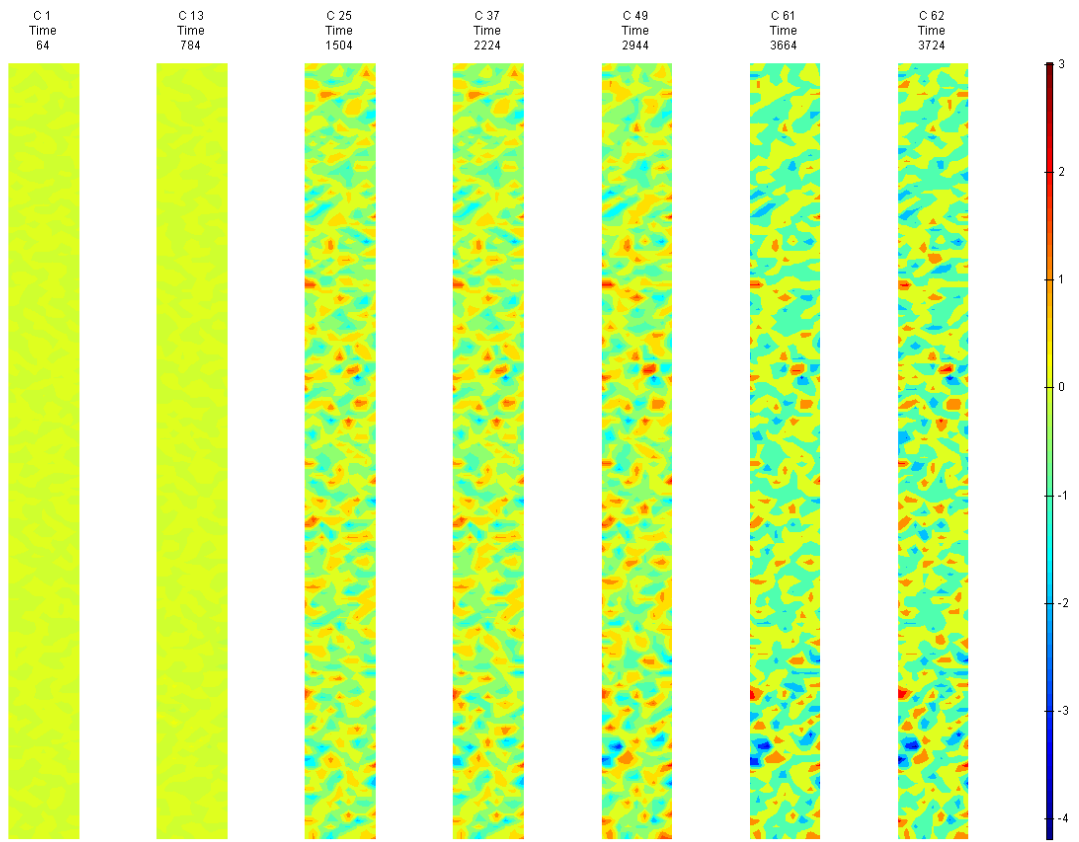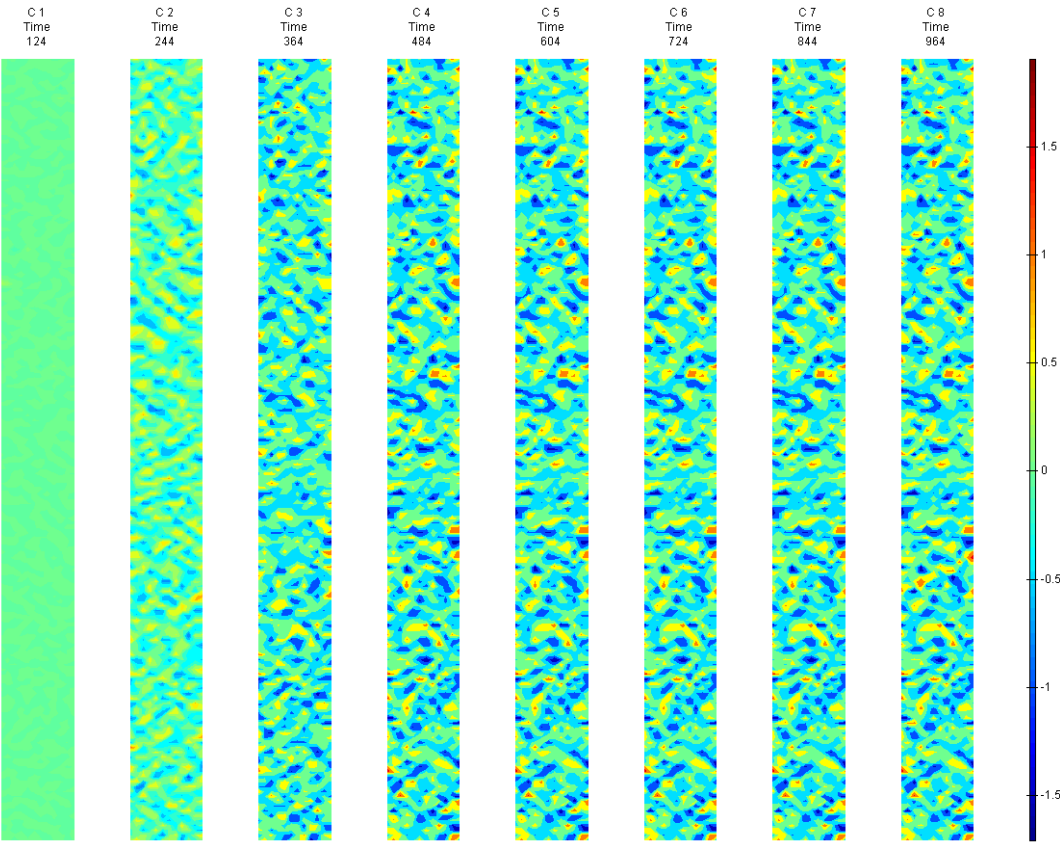

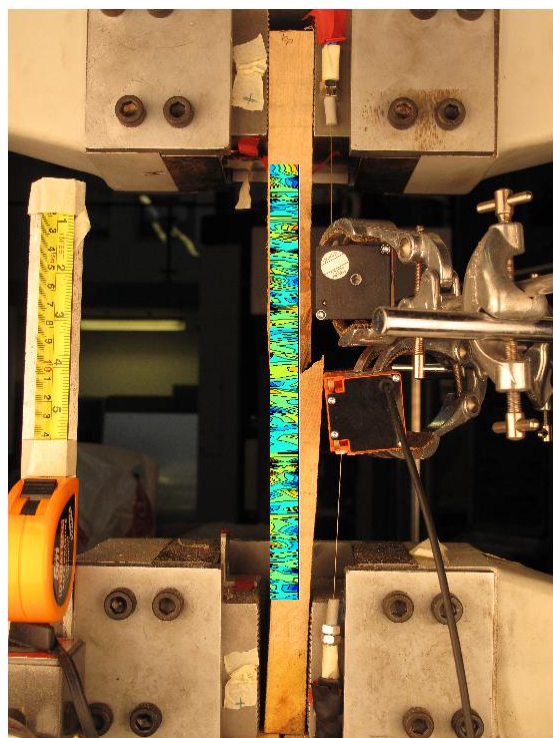FIGURE 804: XY DIRECTION PIV SEQUENTIAL TRUE SHEAR STRAIN OVER TIME
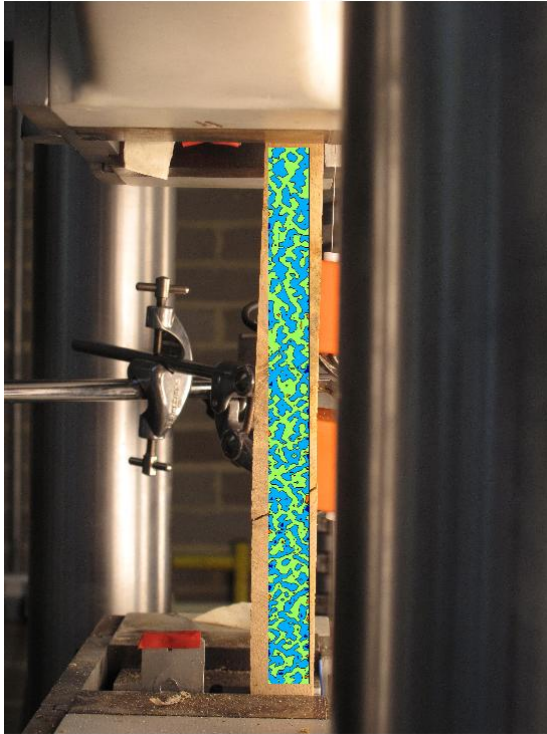
FIGURE 805: X DIRECTION PIV FIRST–LAST DITCH ENGINEERING STRAIN OVER IMAGE
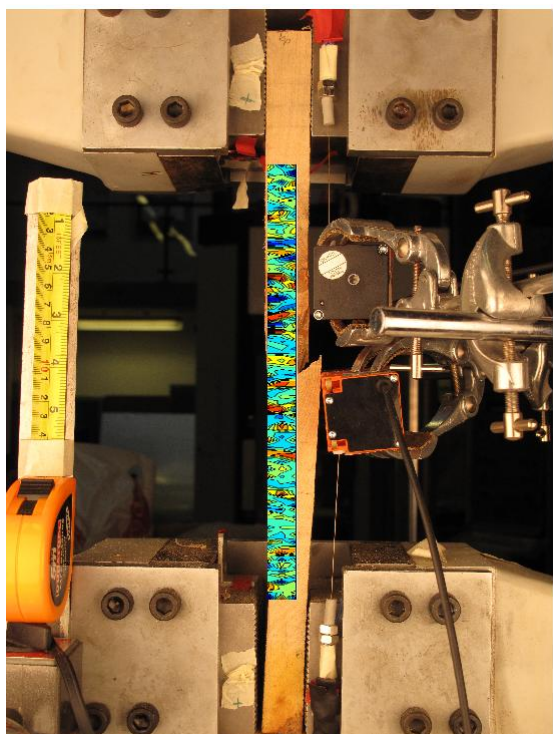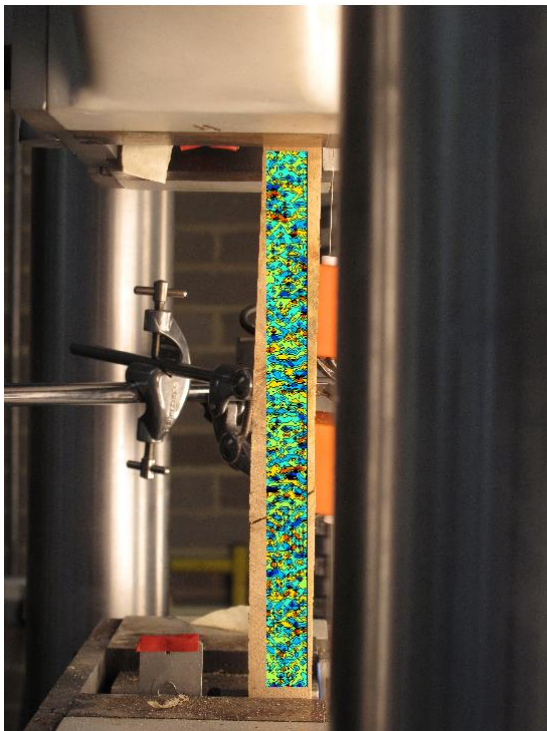

FIGURE 806: Y DIRECTION PIV FIRST–LAST DITCH ENGINEERING STRAIN OVER IMAGE

Appendix 6
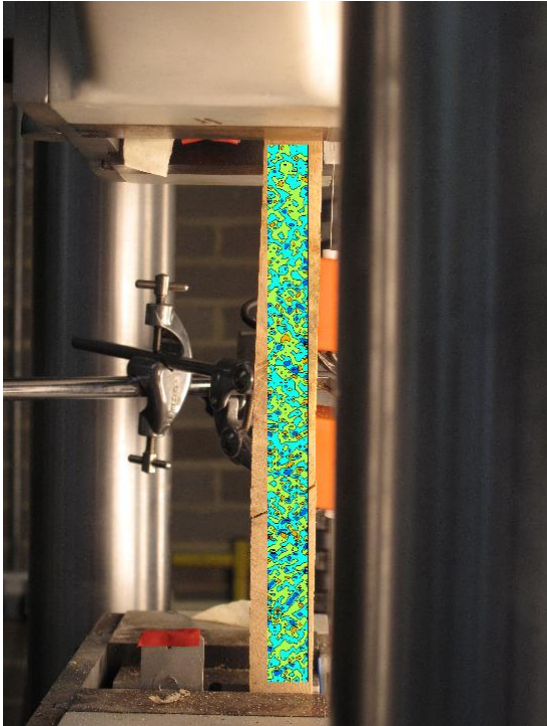
FIGURE 807: XY DIRECTION PIV FIRST–LAST DITCH ENGINEERING SHEAR STRAIN OVER
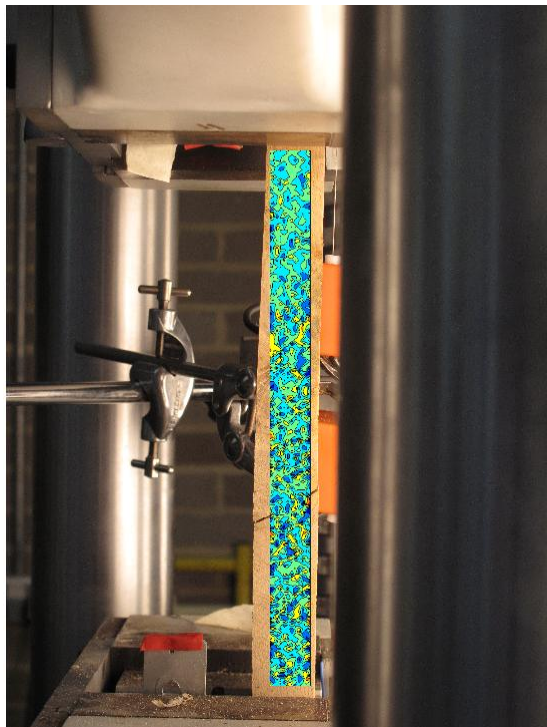
IMAGE

FIGURE 808: X DIRECTION PIV FIRST–LAST DITCH TRUE STRAIN OVER IMAGE
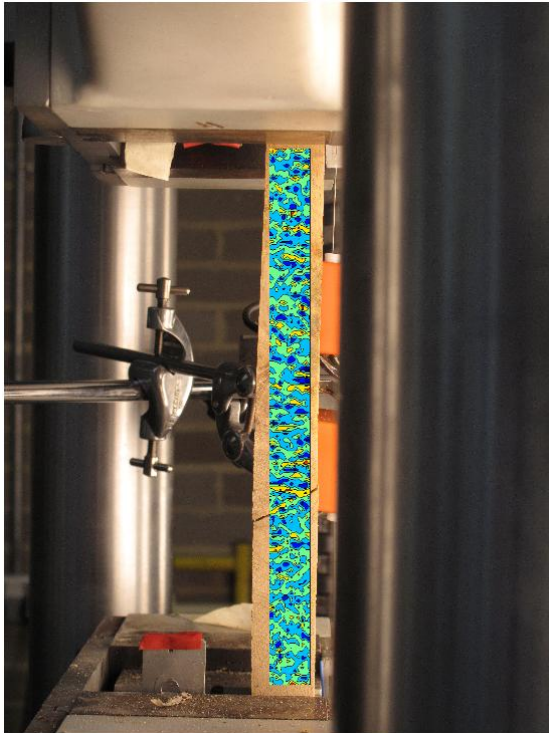
FIGURE 809: Y DIRECTION PIV FIRST–LAST DITCH TRUE STRAIN OVER IMAGE
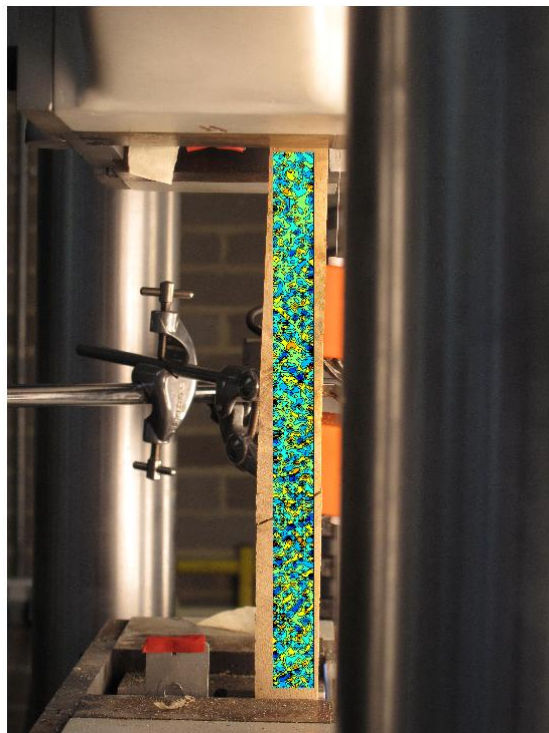
FIGURE 810: XY DIRECTION PIV FIRST–LAST DITCH TRUE SHEAR STRAIN OVER IMAGE
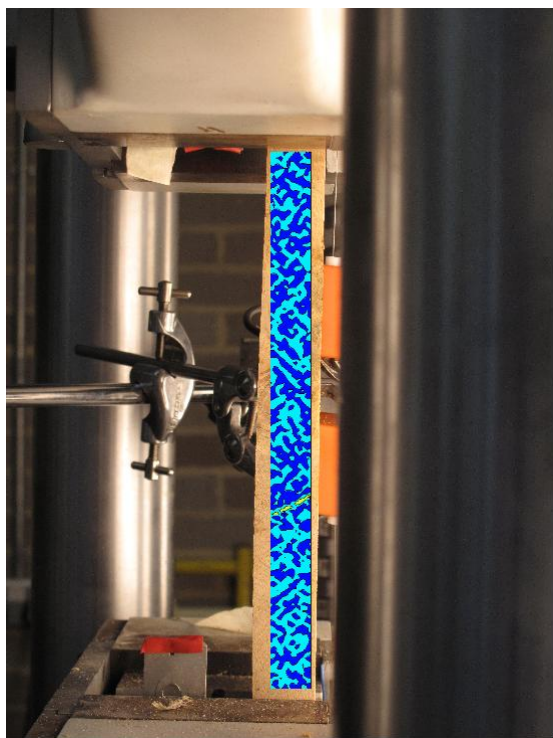
Figure 811: XY Direction PIV First–Sequential Engineering Shear Strain over

Image
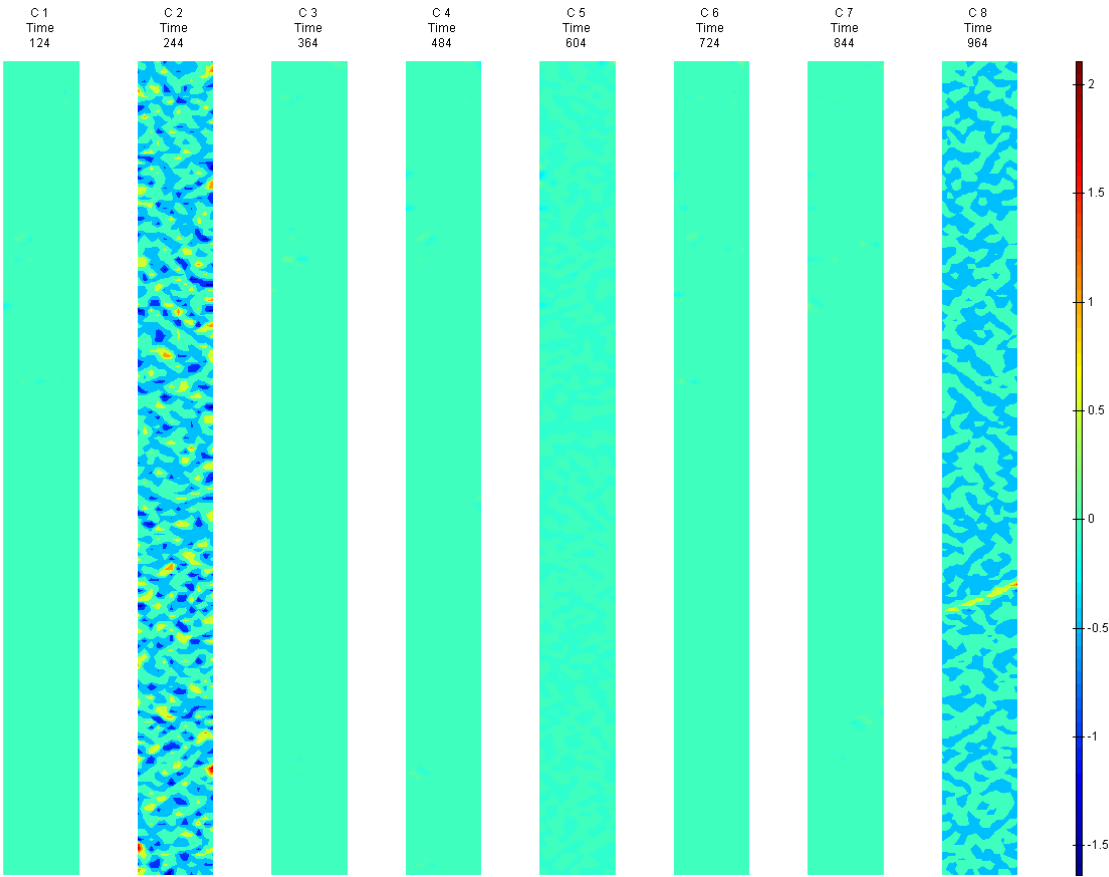
Figure 812: XY Direction PIV First–Sequential Engineering Shear Strain over Time

T9
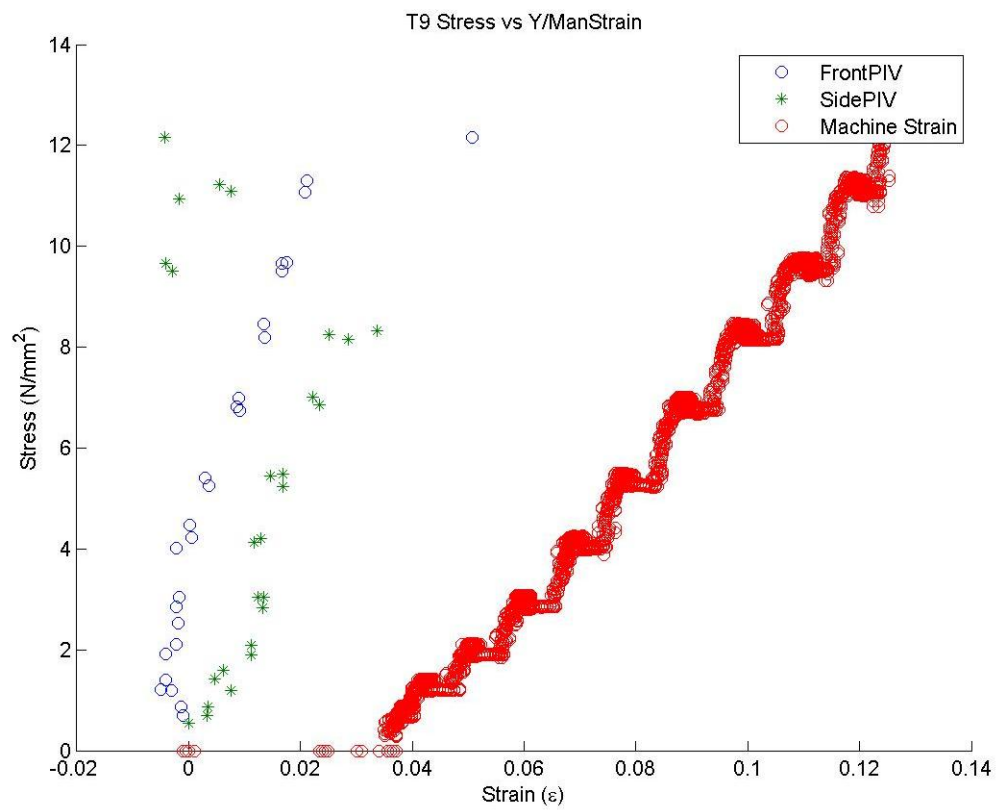
FIGURE 813: T9 TENSILE STRESS VS. MACHINE MEASURED/PIV STRAINS
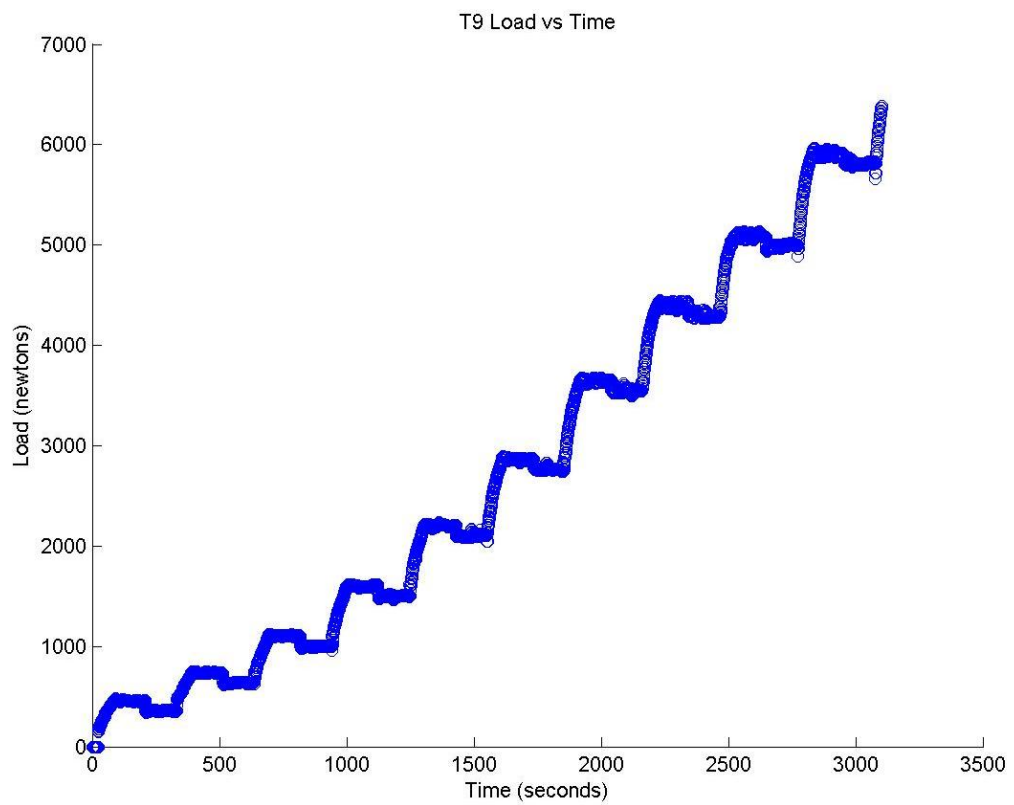
FIGURE 814: T9 TENSILE LOAD VS. TIME
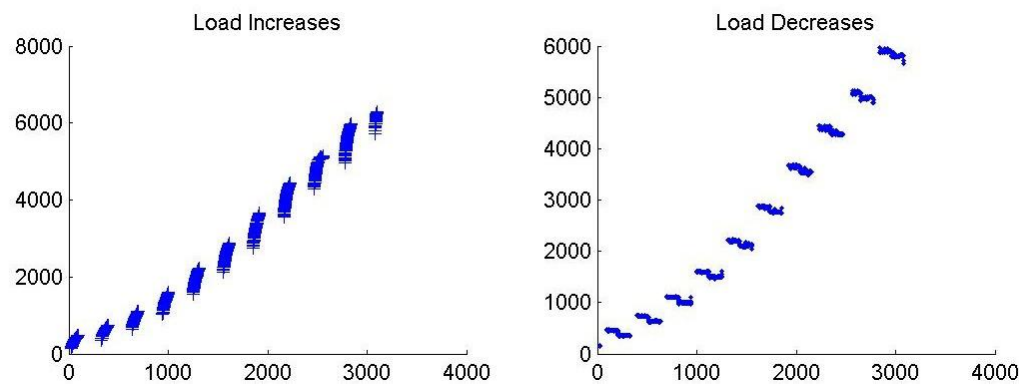
FIGURE 815: T9 CREEP LOADING: INCREMENTS AND RELAXATION
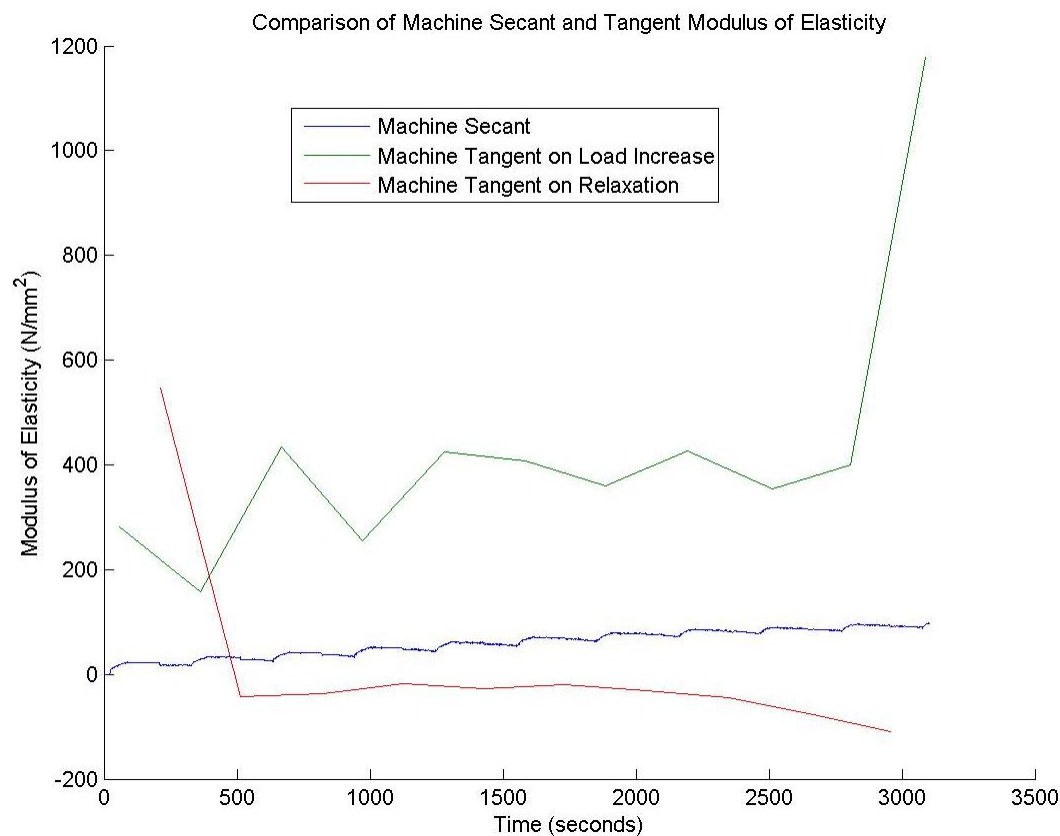
FIGURE 816: T9 MACHINE MEASURED SECANT AND TANGENT MODULUS VS. TIME
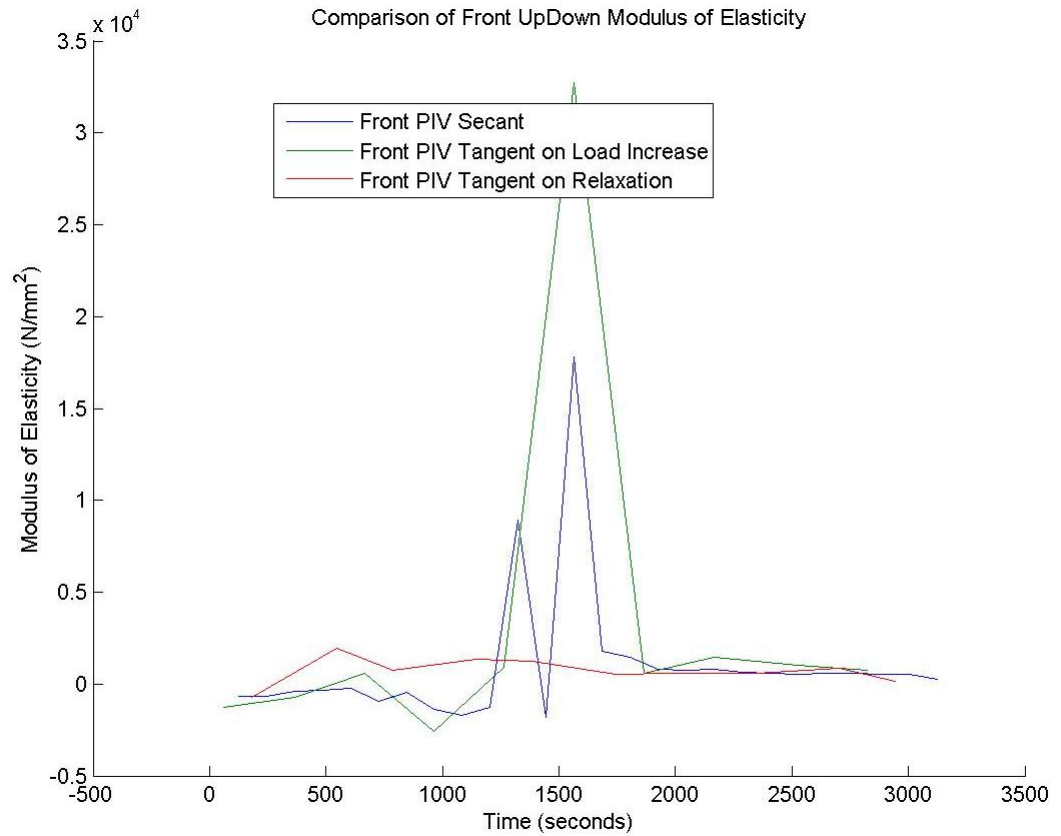
FIGURE 817: T9 FRONT VIEW PIV SECANT AND TANGENT MODULUS VS. TIME
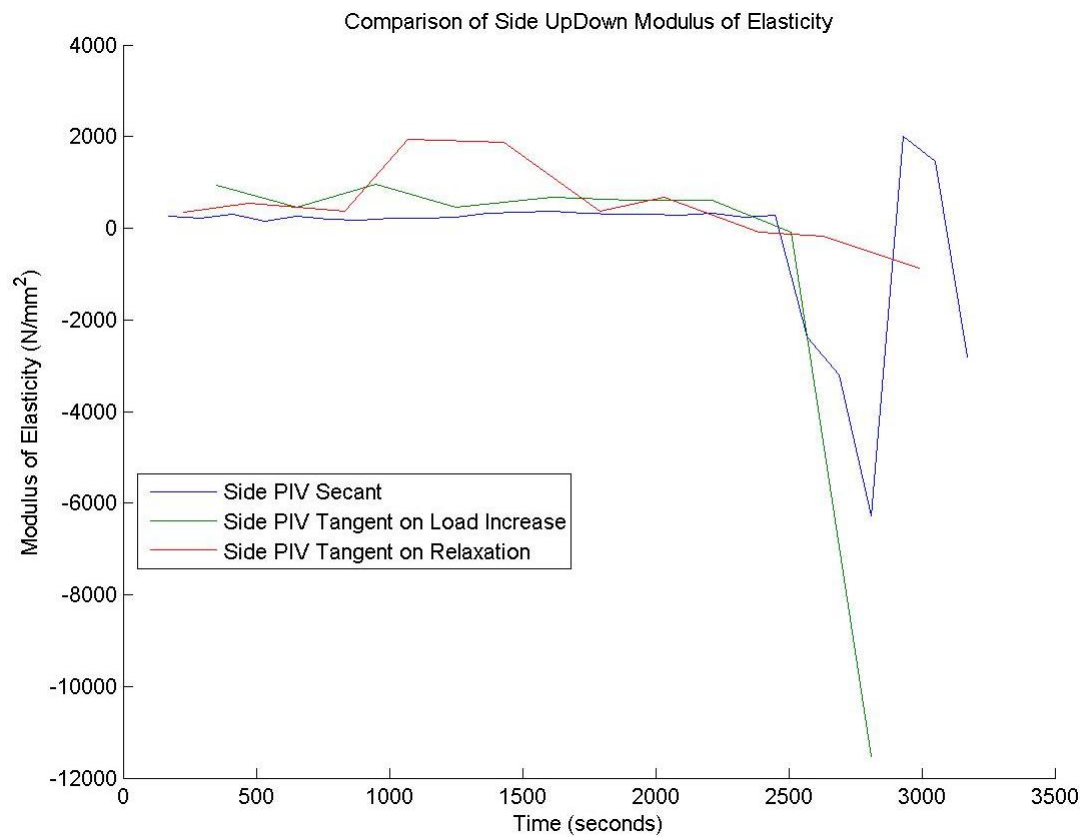
FIGURE 818: T9 SIDE VIEW PIV SECANT AND TANGENT MODULUS VS. TIME

Appendix 6
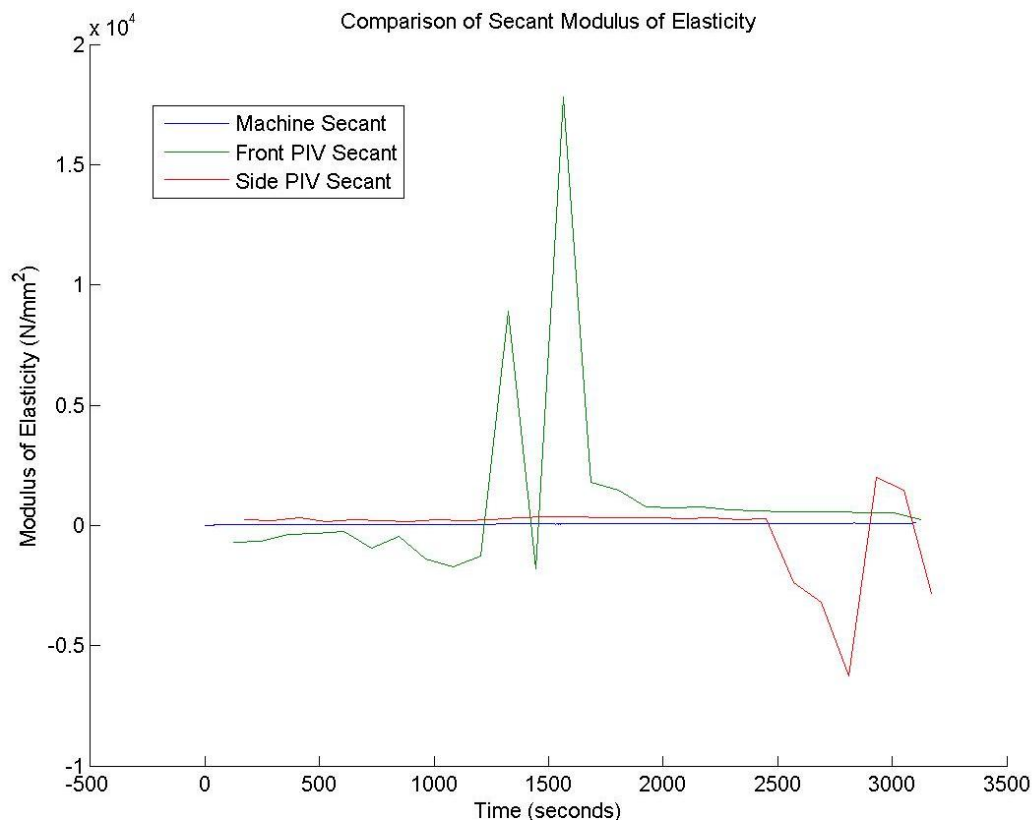
FIGURE 819: T9 COMPARISON OF MACHINE MEASURED AND PIV SECANT MODULUS VS. TIME
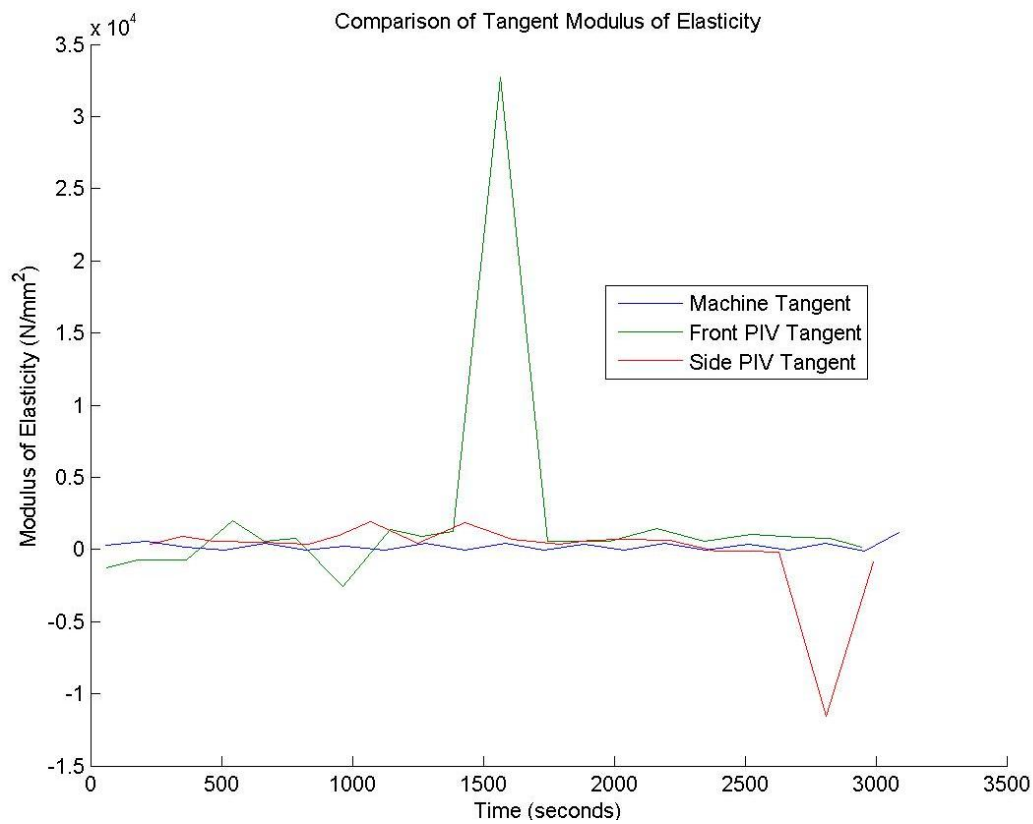
FIGURE 820: T9 COMPARISON OF MACHINE MEASURED AND PIV TANGENT MODULUS VS.

TIME

T9 Sample
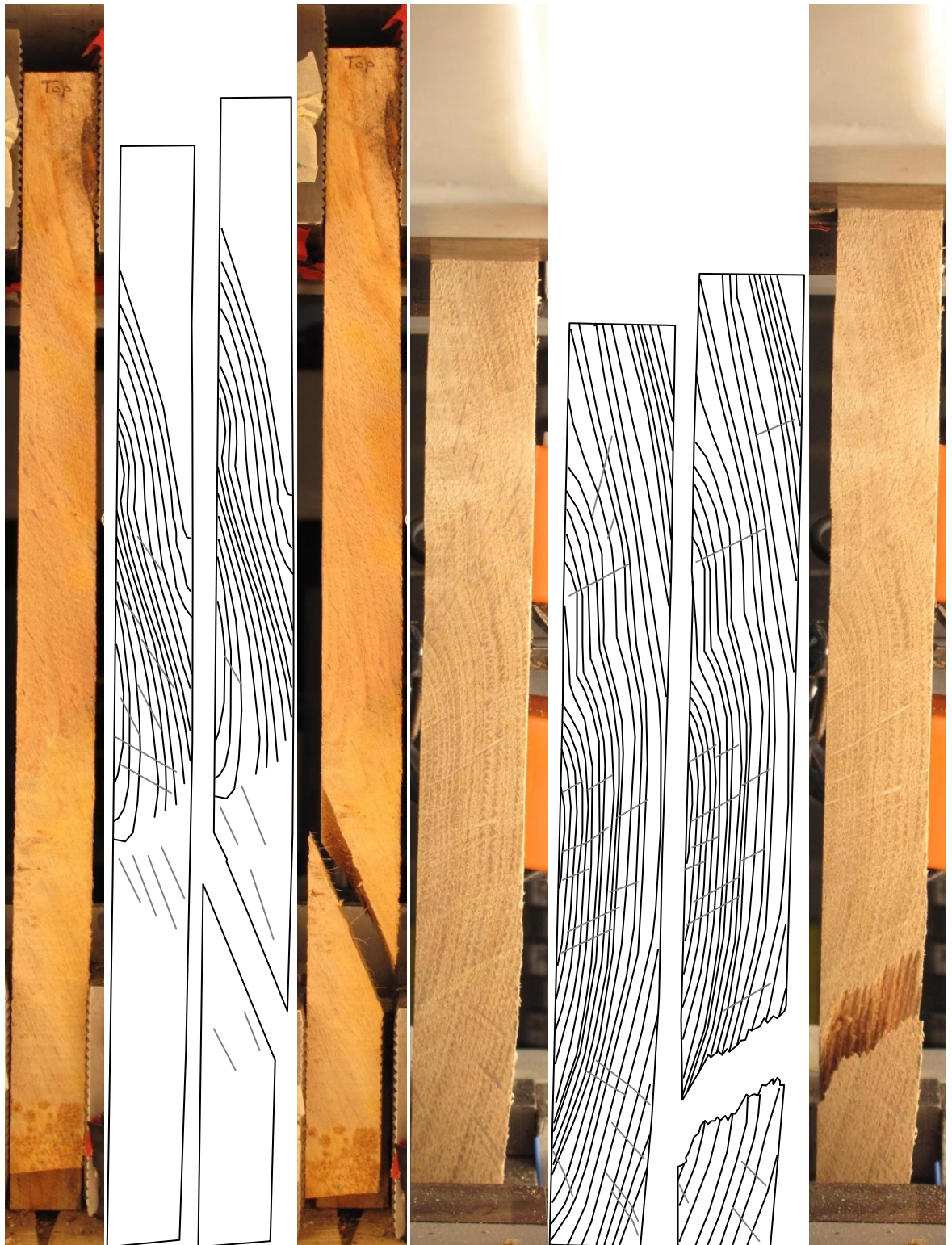
FIGURE 821: SAMPLE GRAIN ORIENTATIONS OF THE FRONT (LEFT 4 IMAGES) AND SIDE (RIGHT 4 IMAGES) VIEW BEFORE (FIRST 2 OF 4 IMAGES) AND AFTER (LAST 2 OF 4 IMAGES) BREAKAGE

Appendix 6

T9 Front View
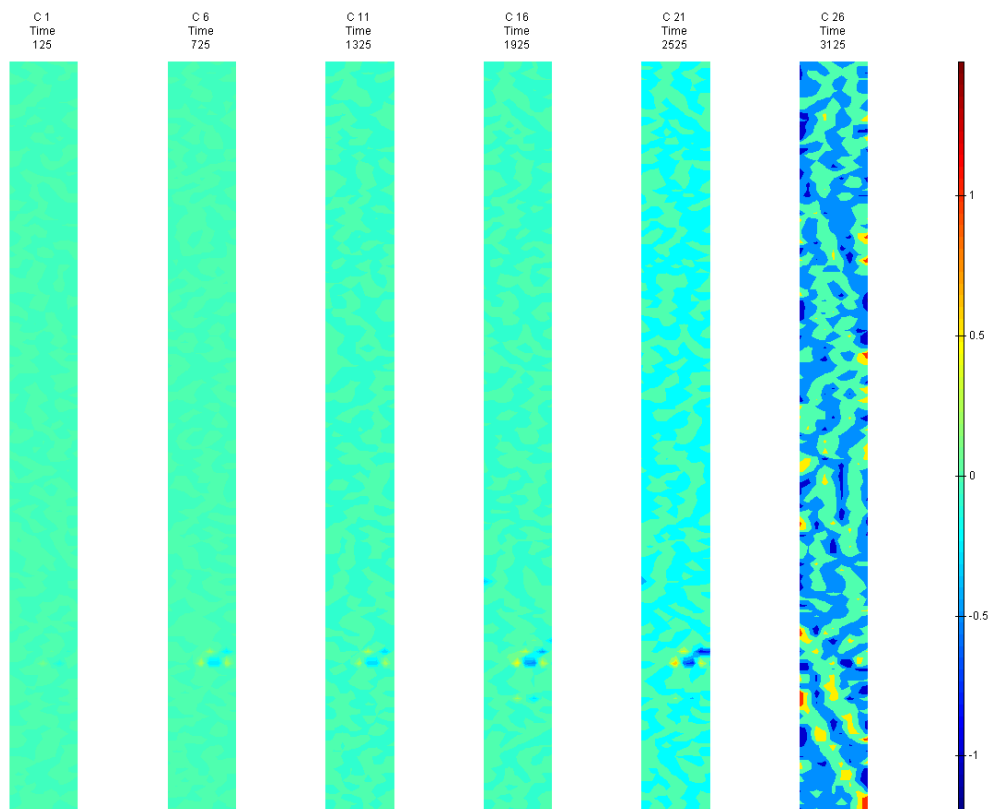
FIGURE 822: X DIRECTION PIV SEQUENTIAL ENGINEERING STRAIN OVER TIME
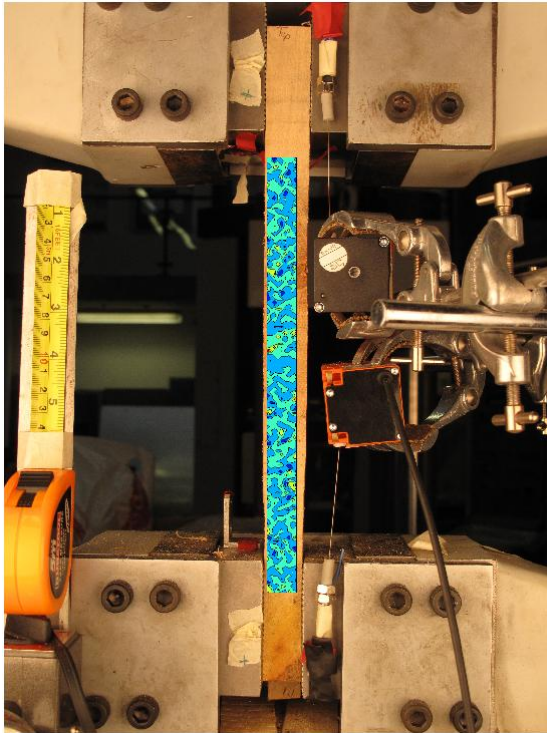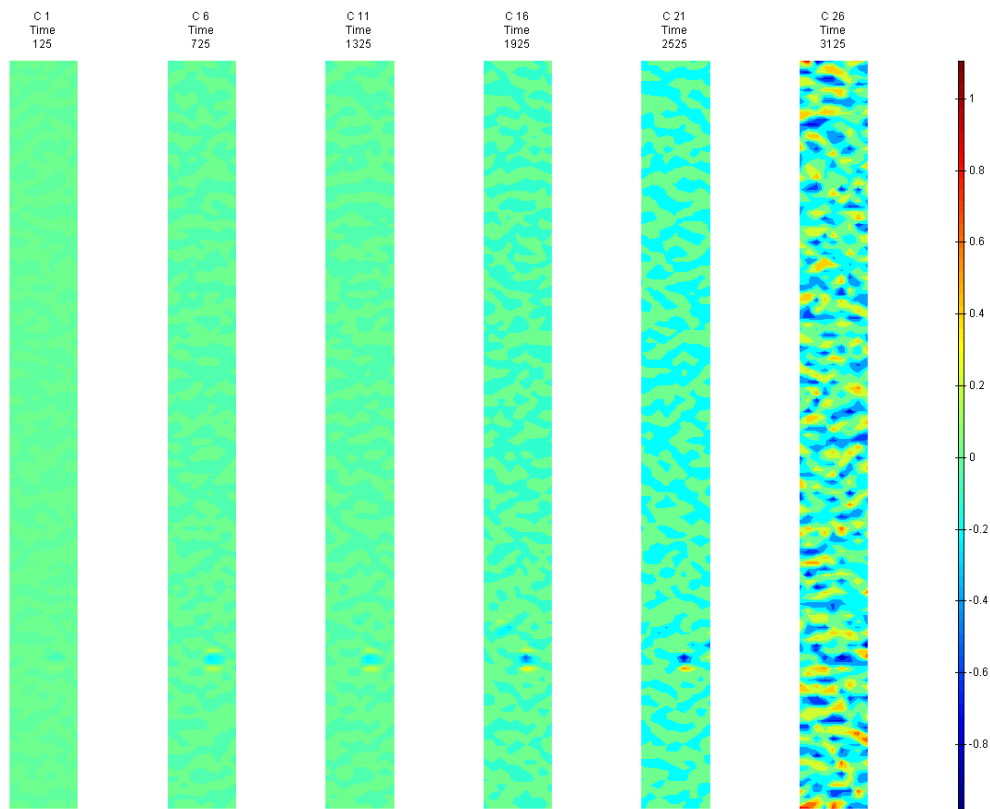

FIGURE 823: Y DIRECTION PIV SEQUENTIAL ENGINEERING STRAIN OVER TIME
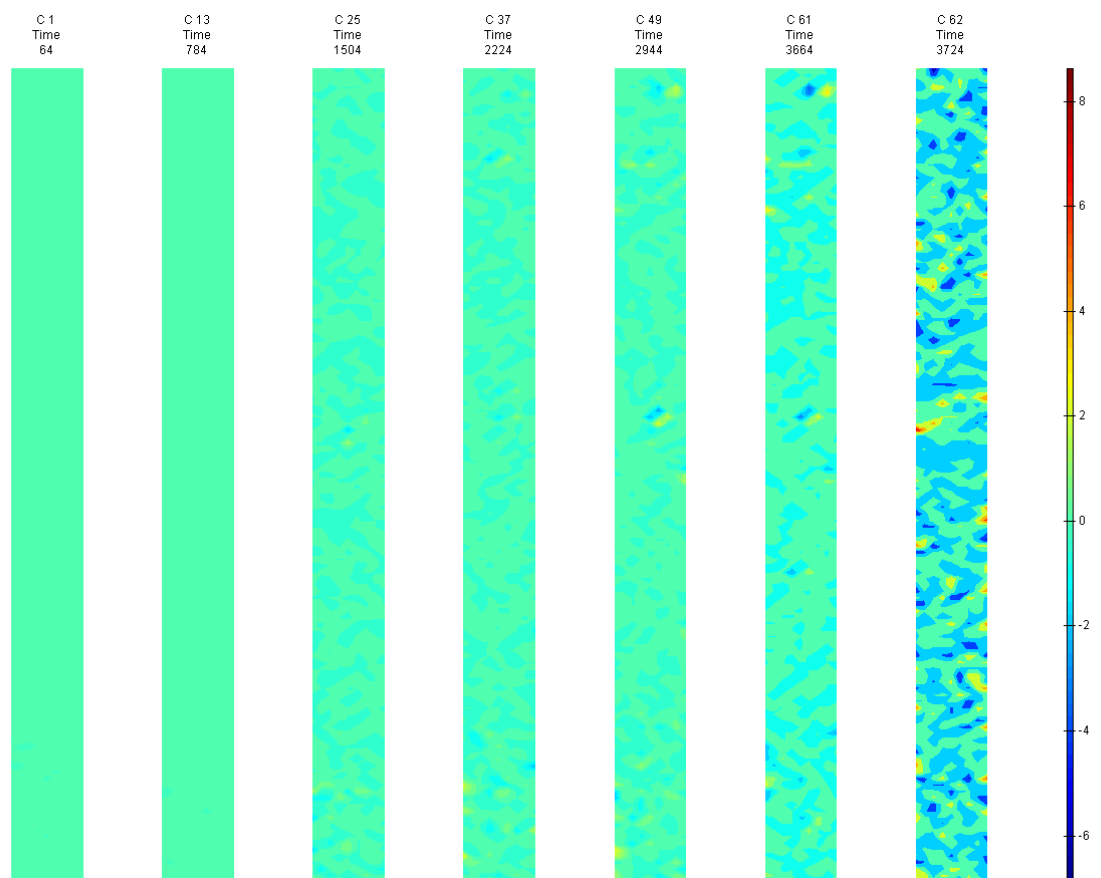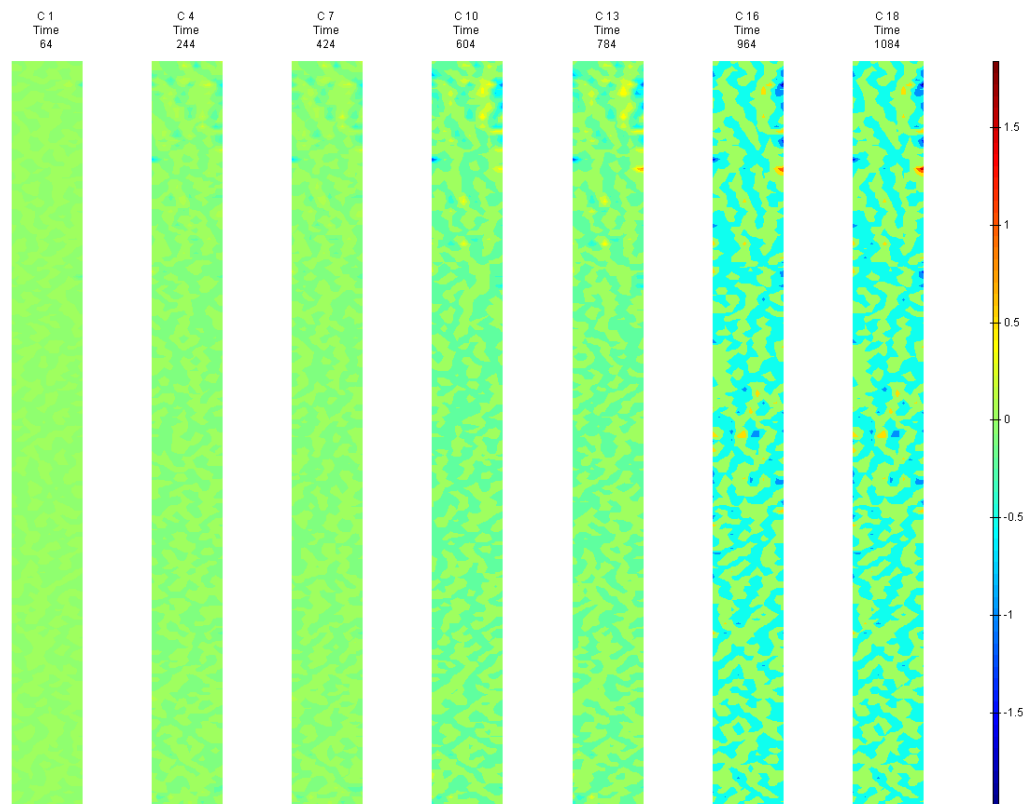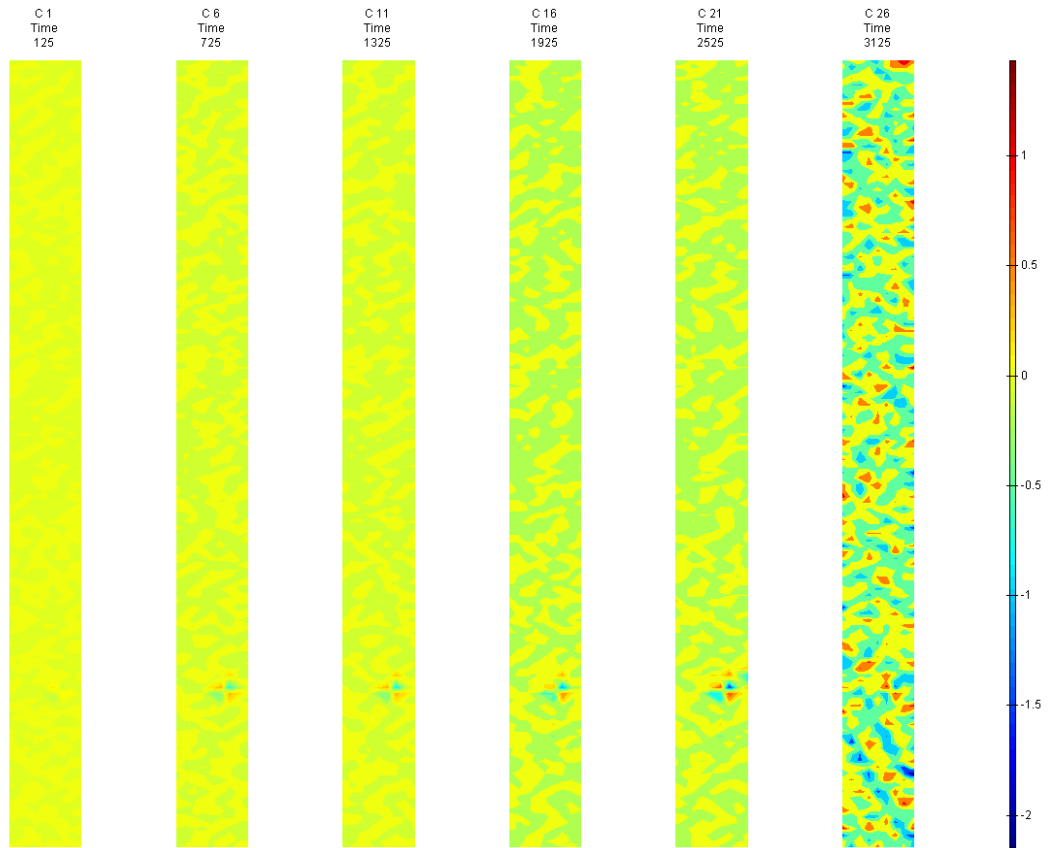
FIGURE 824: XY DIRECTION PIV SEQUENTIAL ENGINEERING SHEAR STRAIN OVER TIME
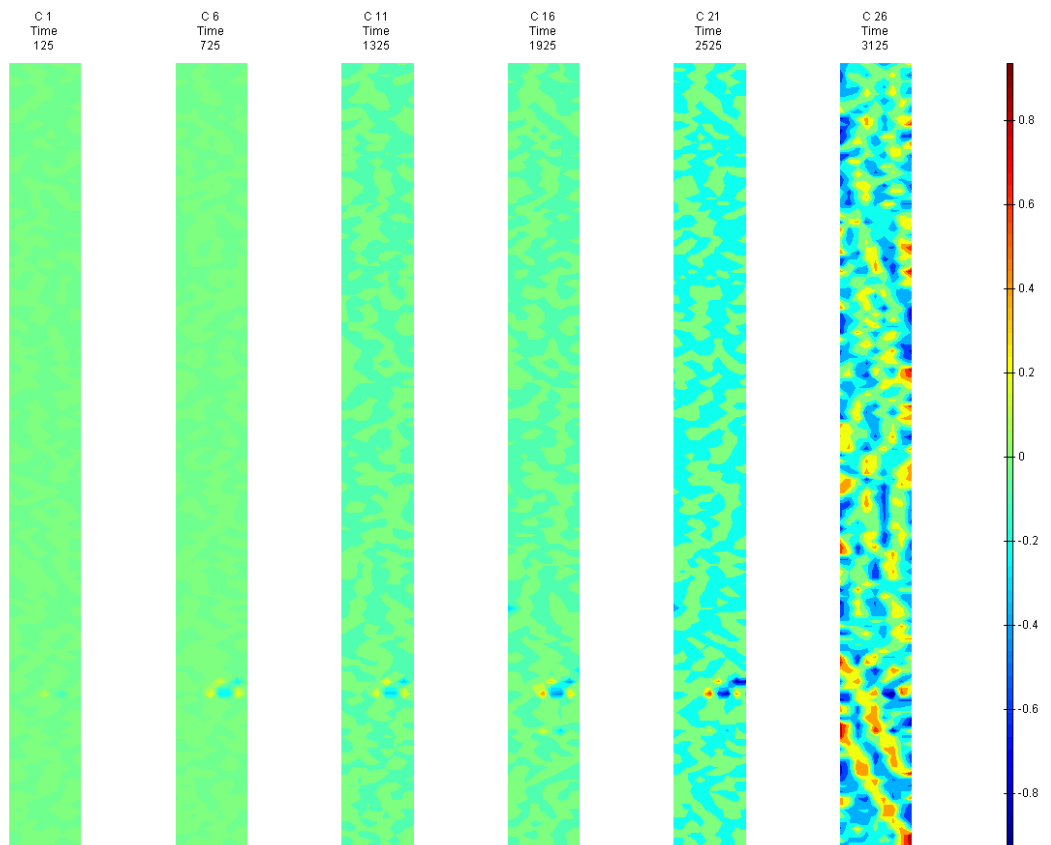
FIGURE 825: X DIRECTION PIV SEQUENTIAL TRUE STRAIN OVER TIME

Appendix 6
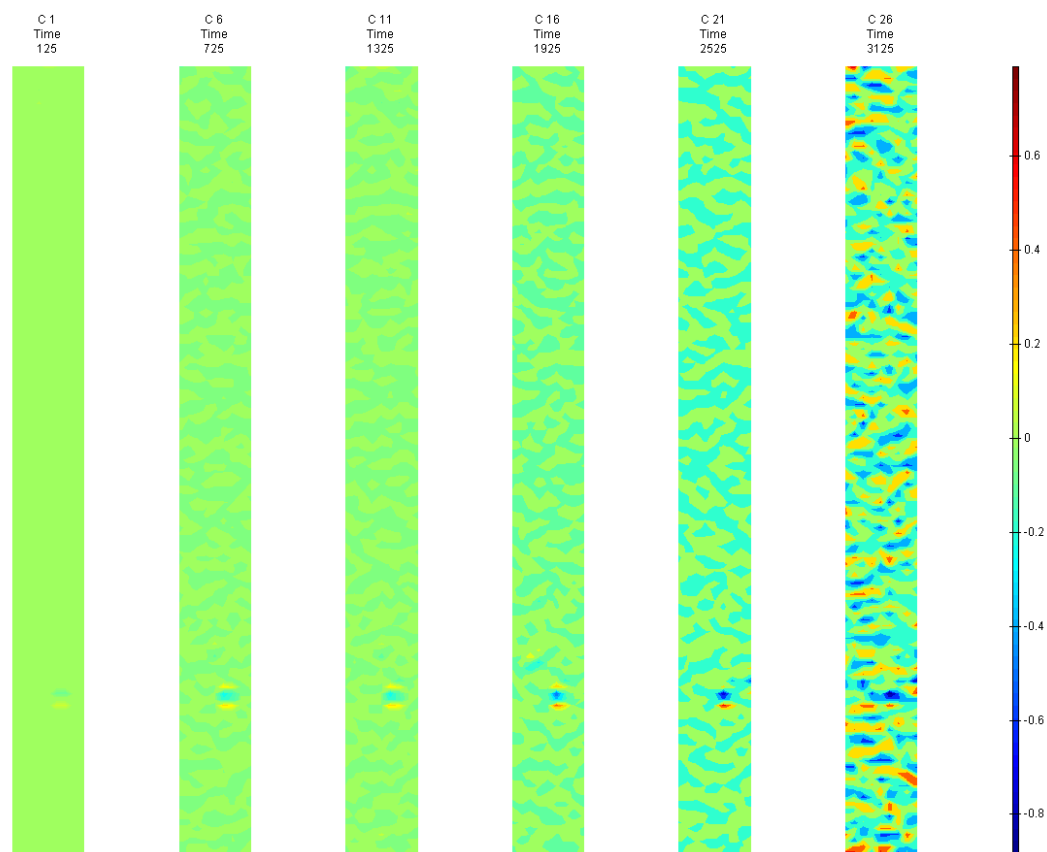
FIGURE 826: Y DIRECTION PIV SEQUENTIAL TRUE STRAIN OVER TIME
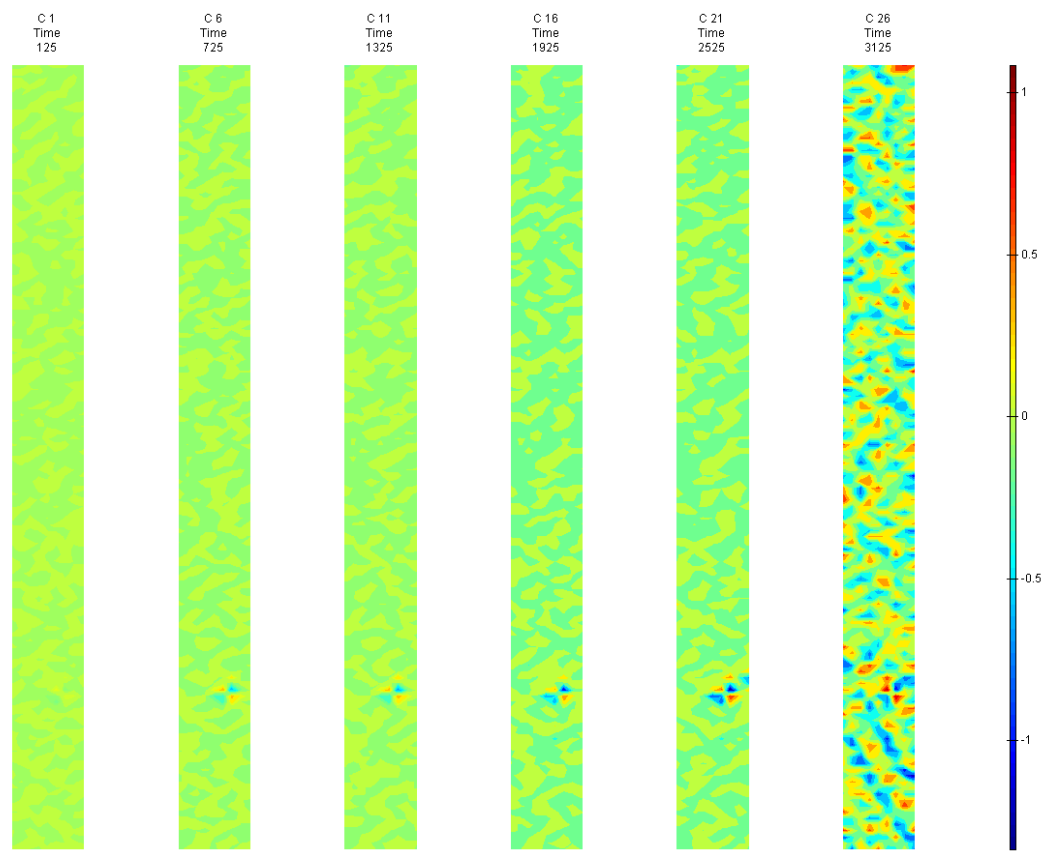
FIGURE 827: XY DIRECTION PIV SEQUENTIAL TRUE SHEAR STRAIN OVER TIME
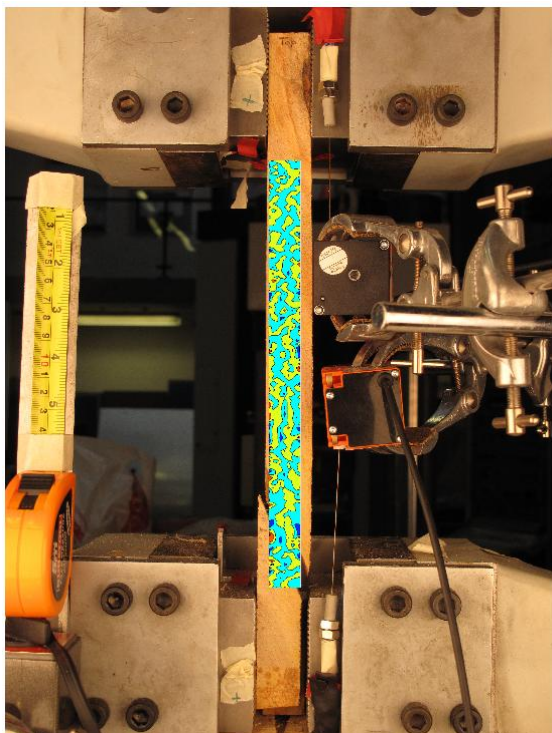
FIGURE 828: X DIRECTION PIV FIRST–LAST DITCH ENGINEERING STRAIN OVER IMAGE
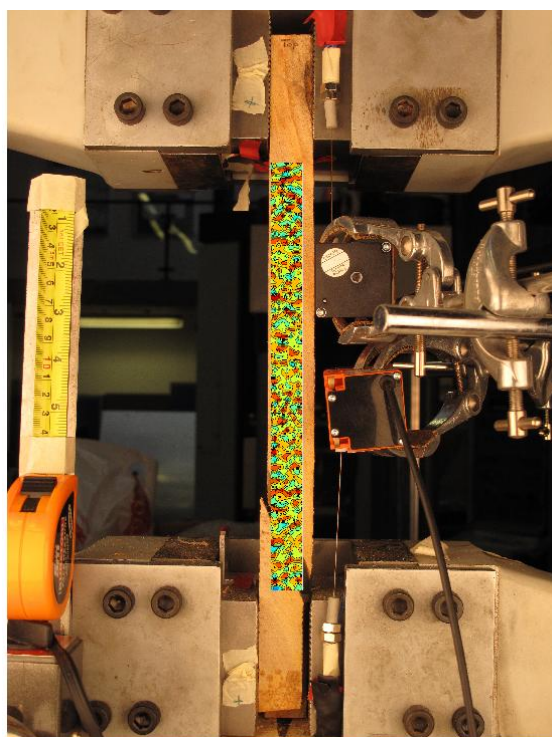
FIGURE 829: Y DIRECTION PIV FIRST–LAST DITCH ENGINEERING STRAIN OVER IMAGE

Appendix 6
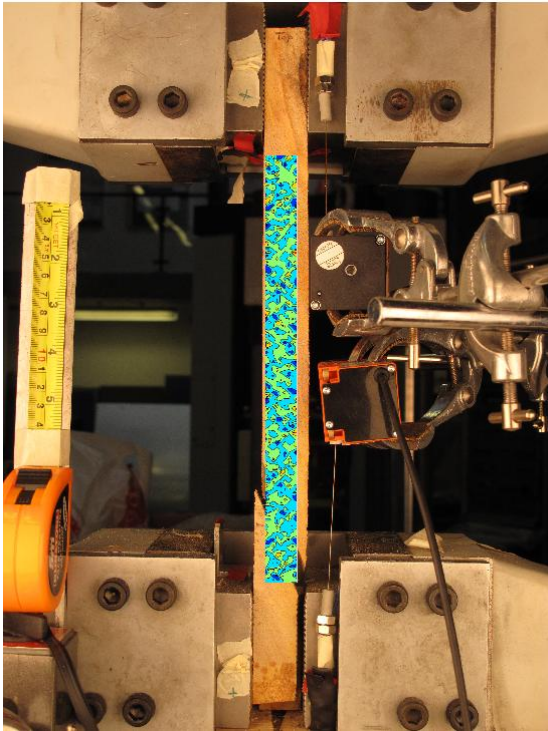
FIGURE 830: XY DIRECTION PIV FIRST–LAST DITCH ENGINEERING SHEAR STRAIN OVER
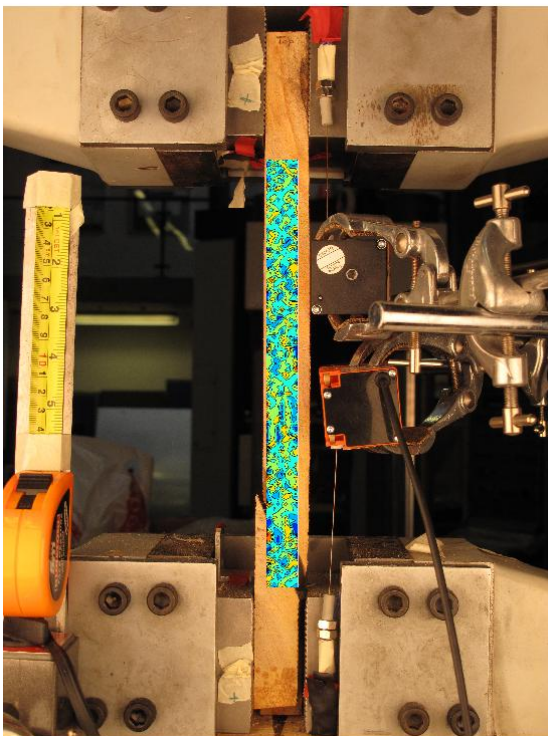
IMAGE

FIGURE 831: X DIRECTION PIV FIRST–LAST DITCH TRUE STRAIN OVER IMAGE
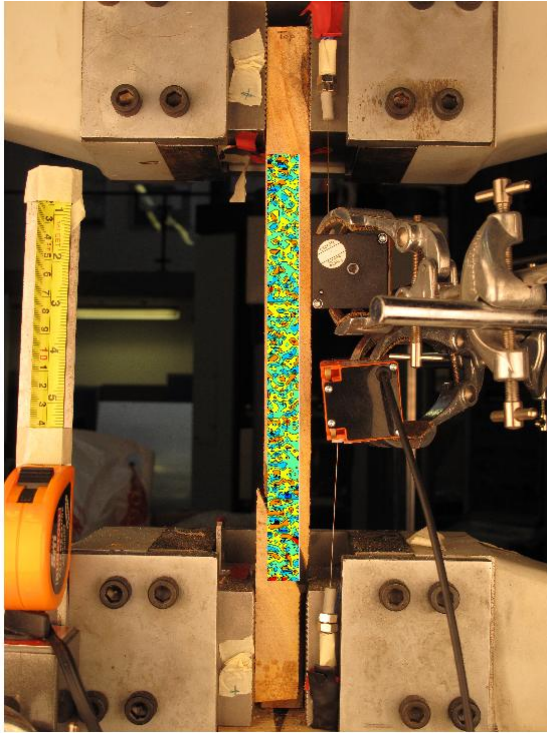
FIGURE 832: Y DIRECTION PIV FIRST–LAST DITCH TRUE STRAIN OVER IMAGE
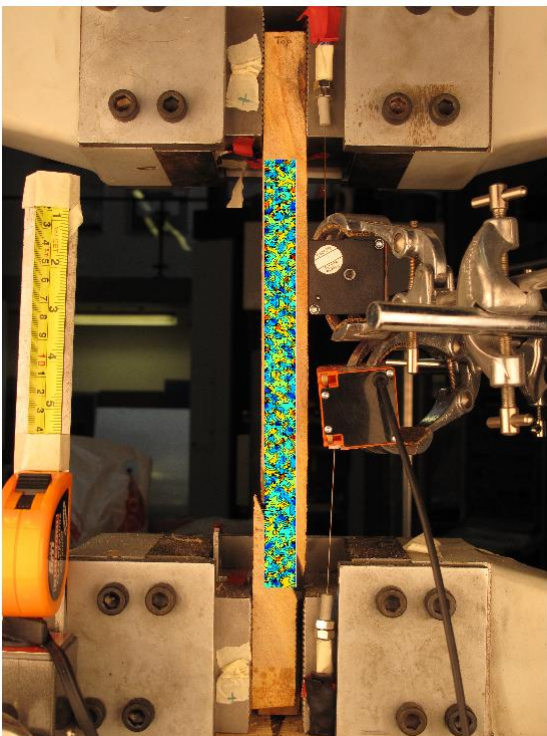
FIGURE 833: XY DIRECTION PIV FIRST–LAST DITCH TRUE SHEAR STRAIN OVER IMAGE

Appendix 6
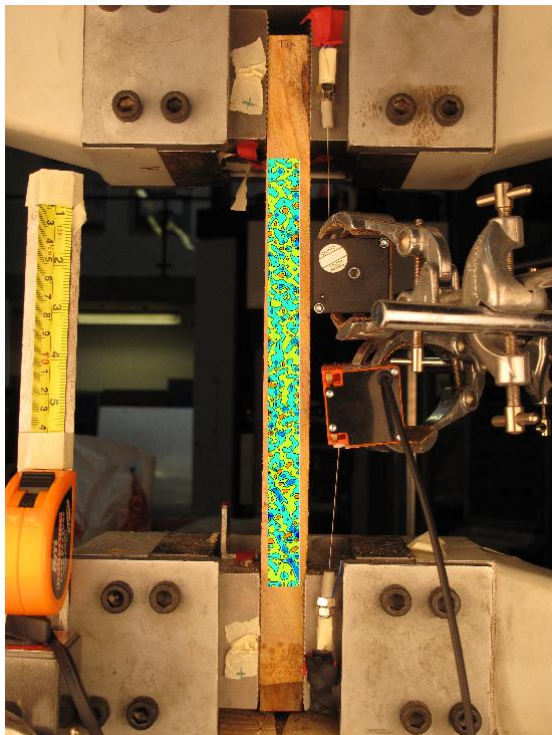
FIGURE 834: XY DIRECTION PIV FIRST–SEQUENTIAL ENGINEERING SHEAR STRAIN OVER

IMAGE
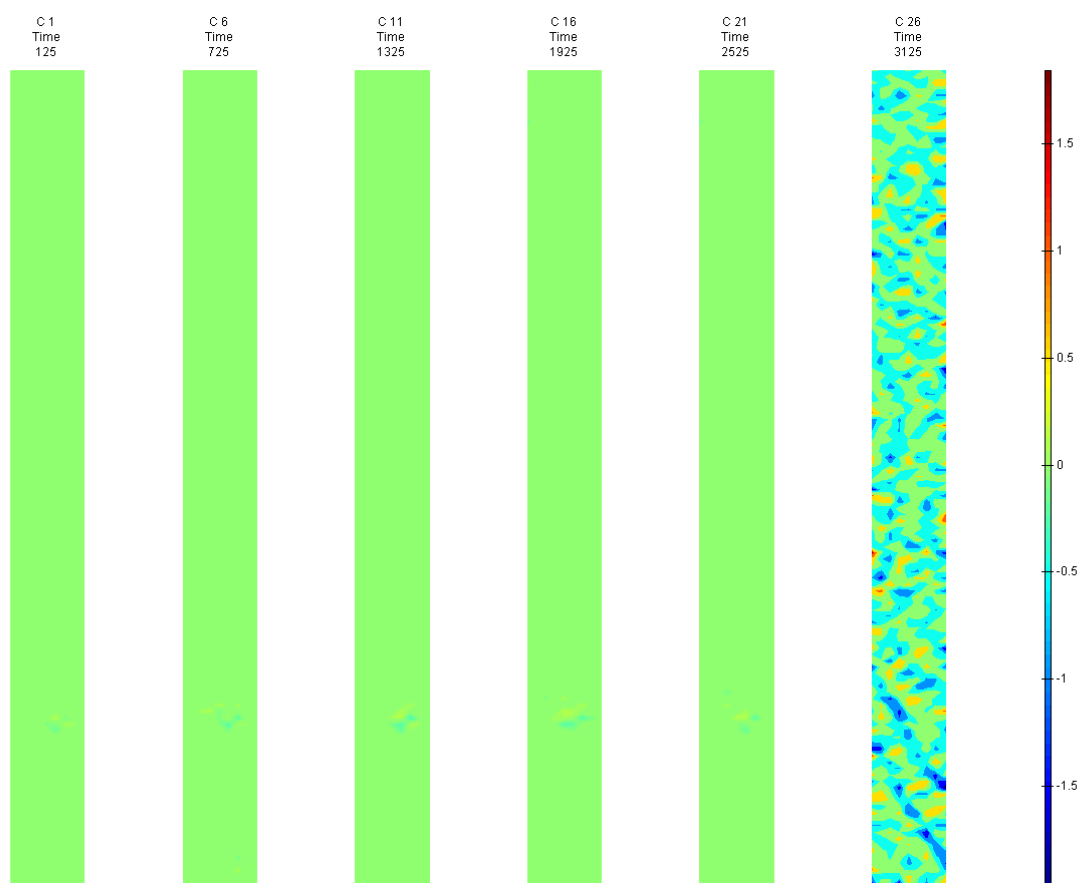
FIGURE 835: XY DIRECTION PIV FIRST–SEQUENTIAL ENGINEERING SHEAR STRAIN OVER TIME

574

T9 Side View
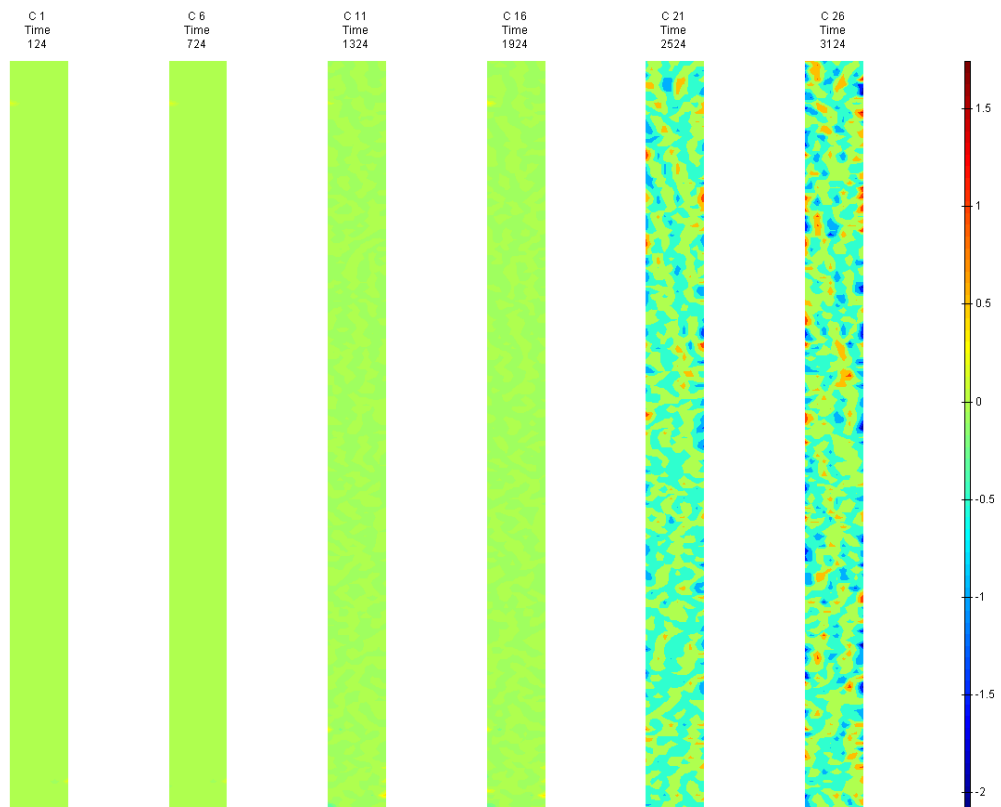
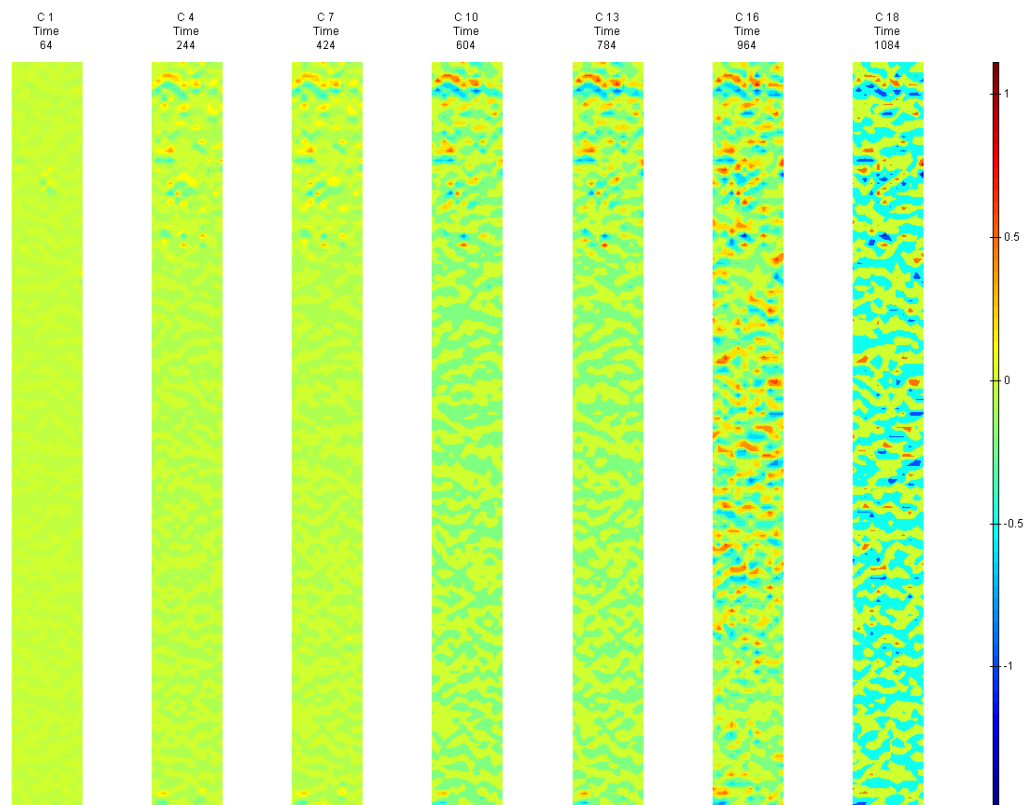FIGURE 836: X DIRECTION PIV SEQUENTIAL ENGINEERING STRAIN OVER TIME
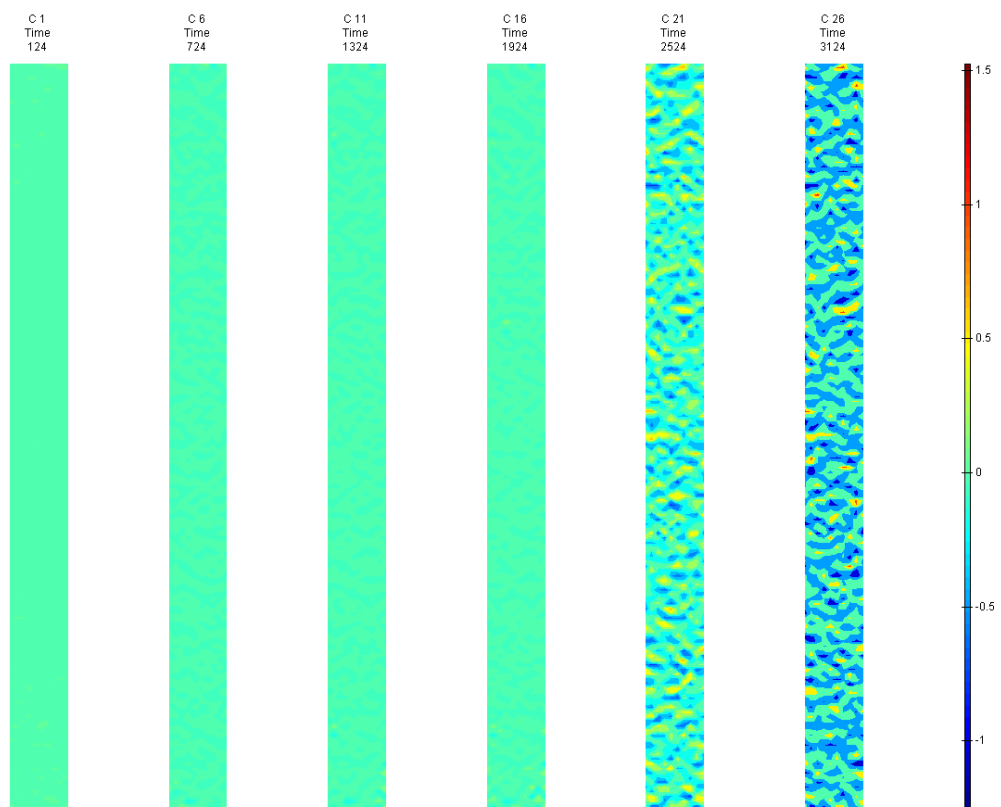
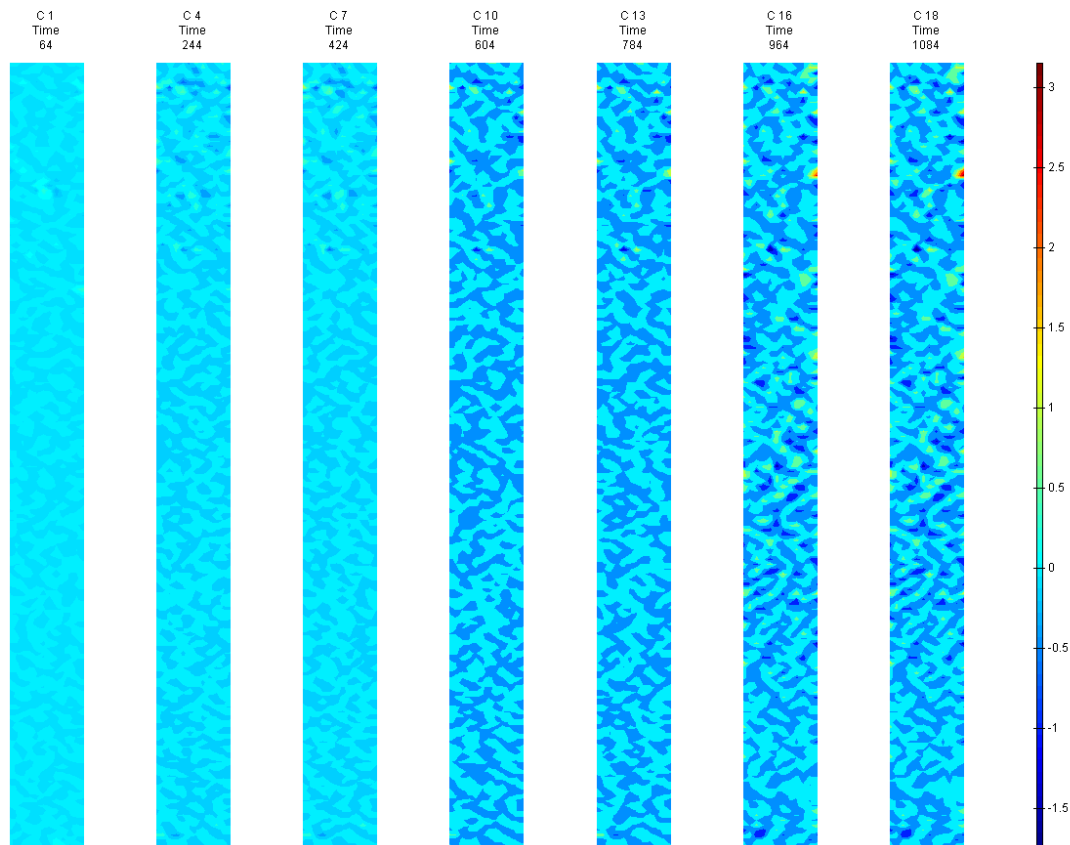FIGURE 837: Y DIRECTION PIV SEQUENTIAL ENGINEERING STRAIN OVER TIME
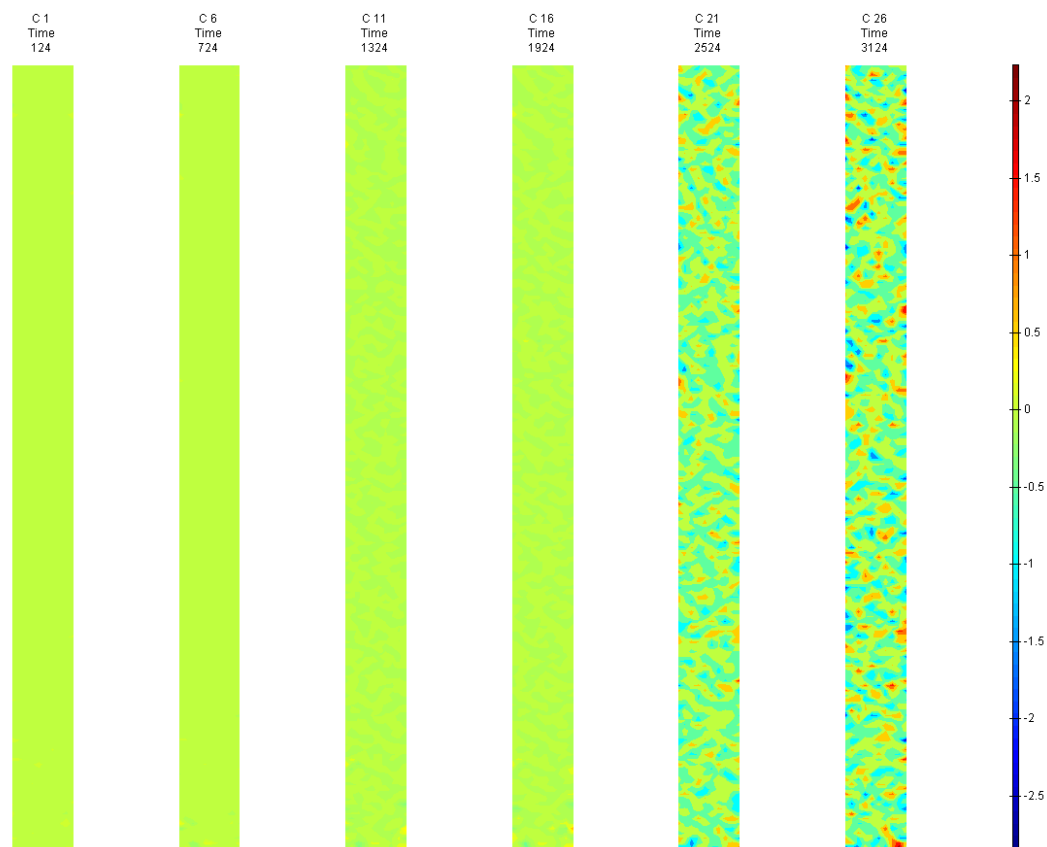
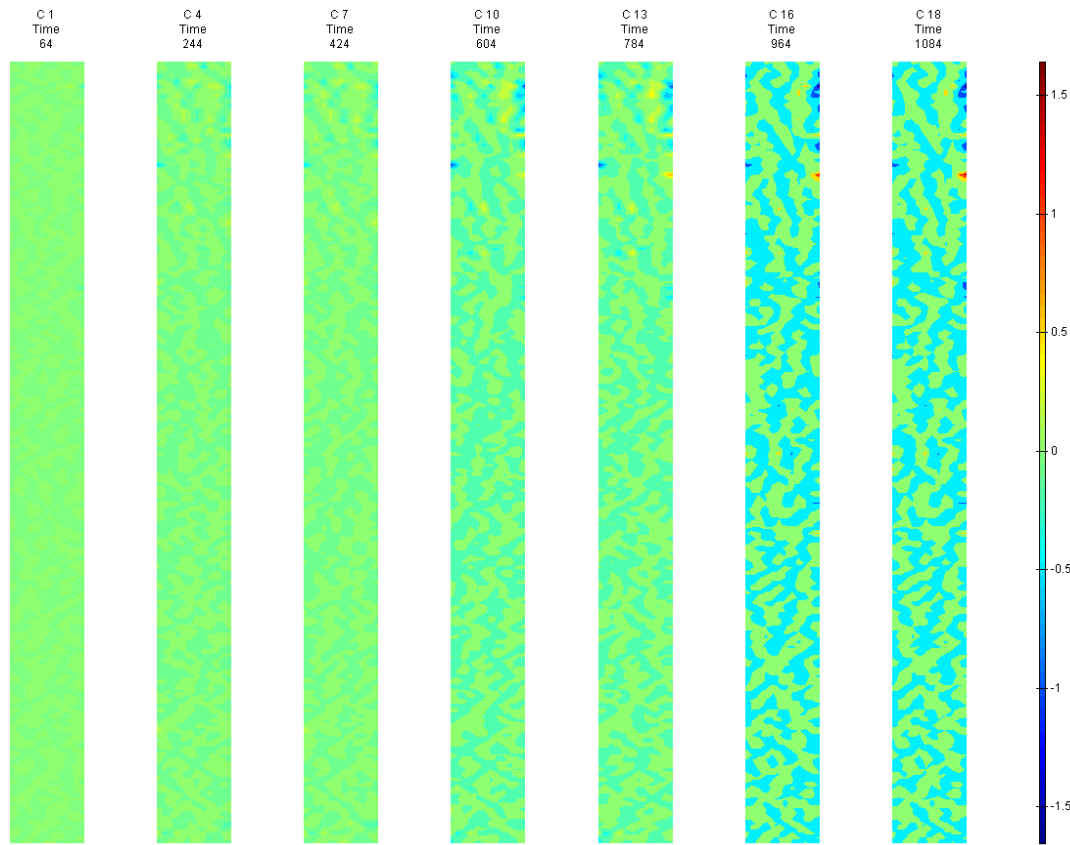FIGURE 838: XY DIRECTION PIV SEQUENTIAL ENGINEERING SHEAR STRAIN OVER TIME
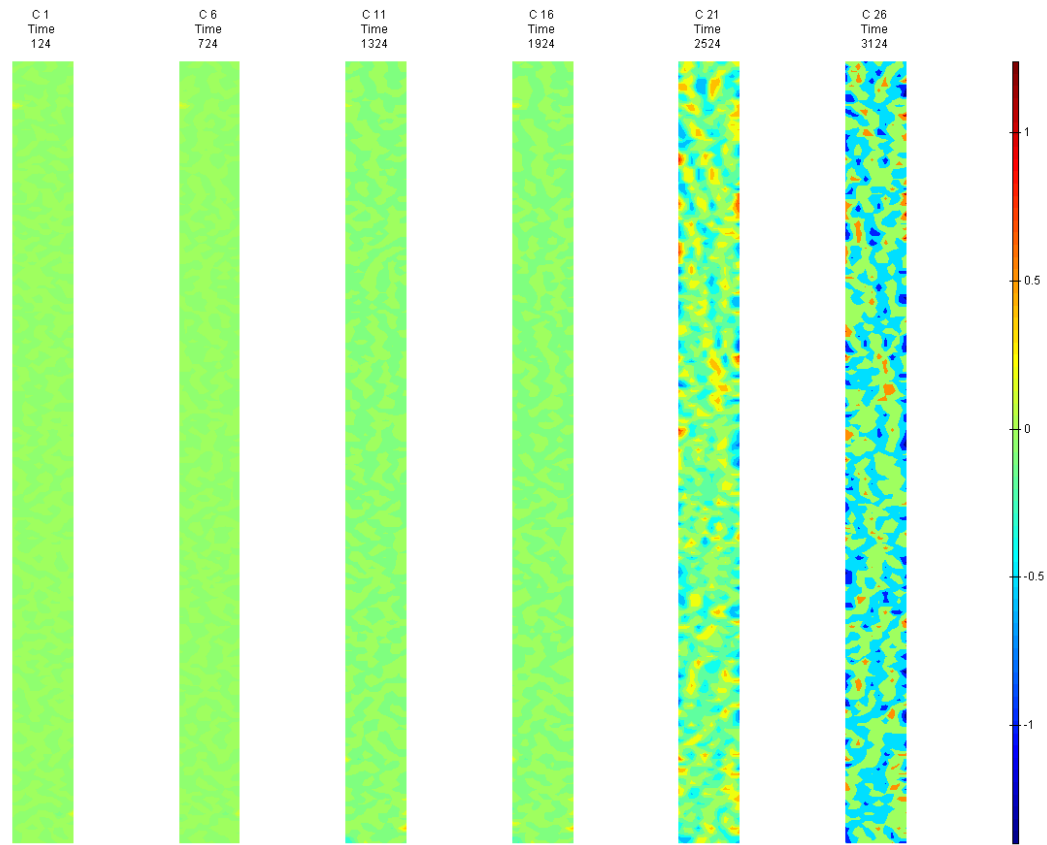
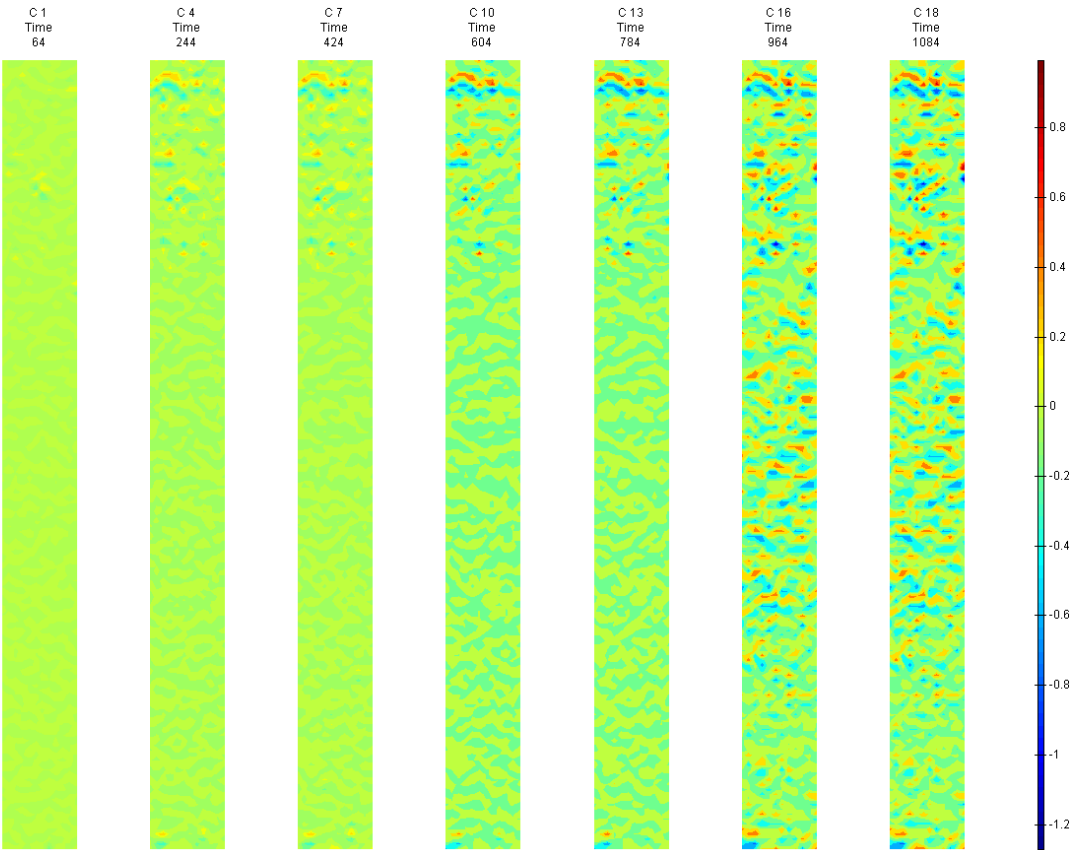FIGURE 839: X DIRECTION PIV SEQUENTIAL TRUE STRAIN OVER TIME
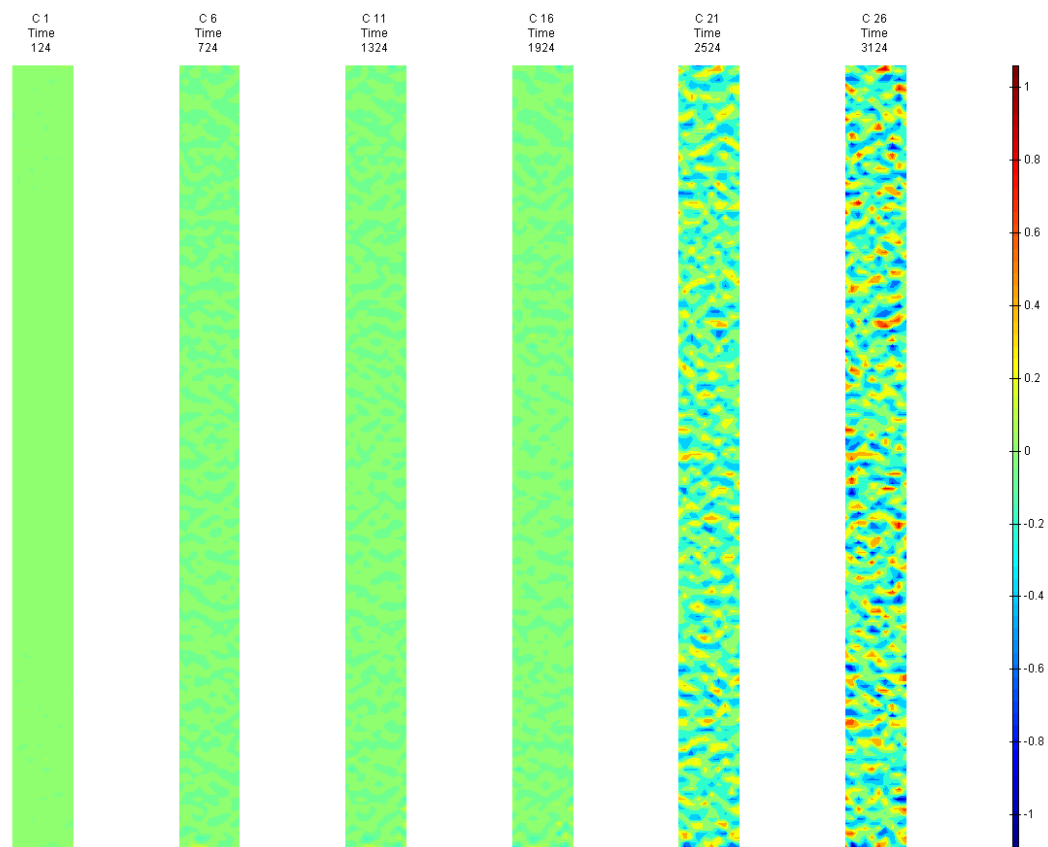
FIGURE 840: Y DIRECTION PIV SEQUENTIAL TRUE STRAIN OVER TIME
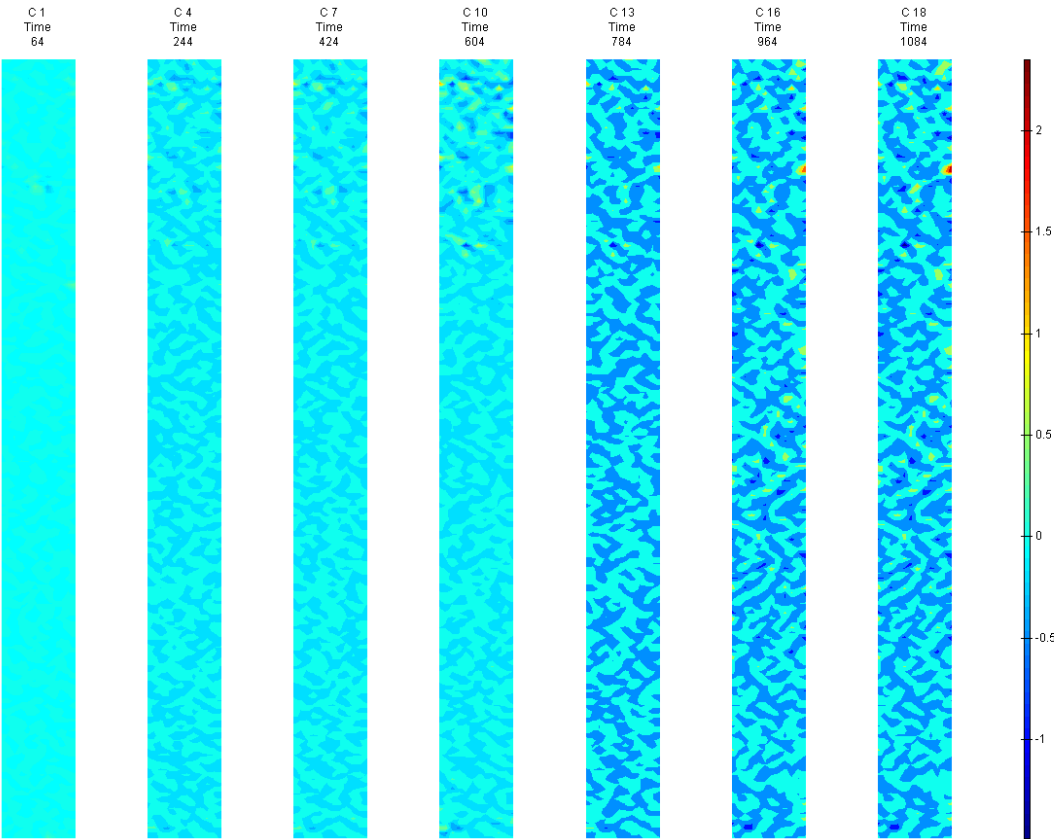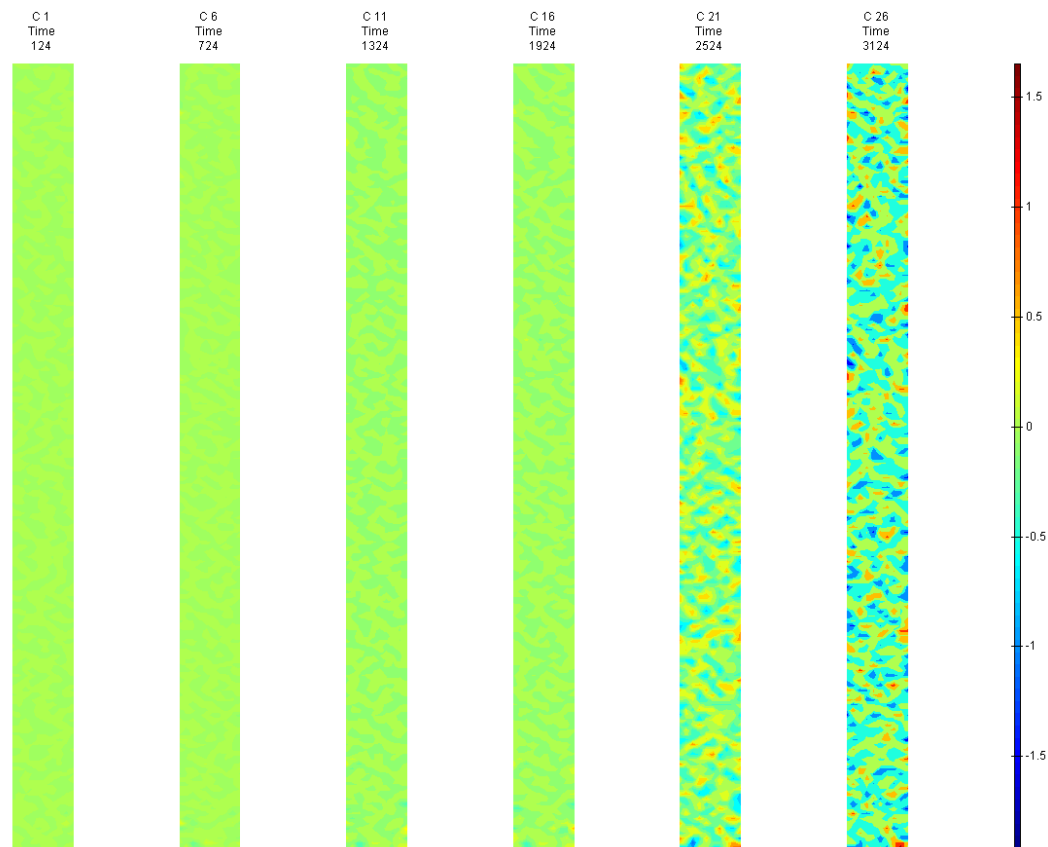

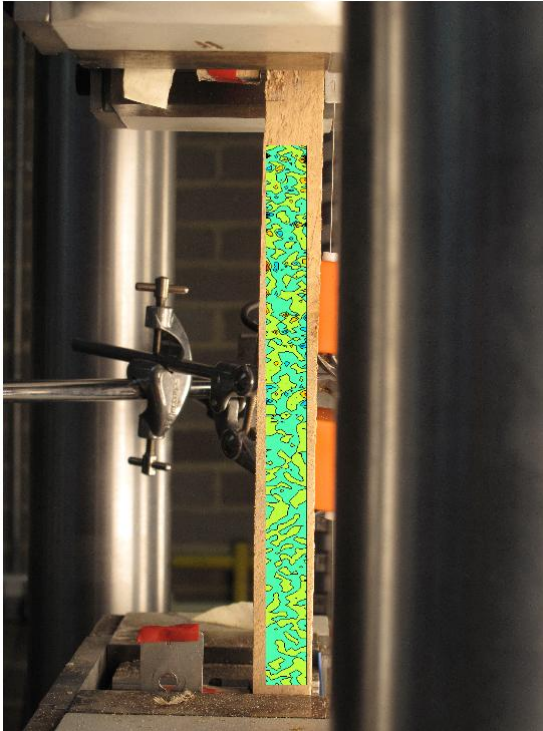FIGURE 841: XY DIRECTION PIV SEQUENTIAL TRUE SHEAR STRAIN OVER TIME
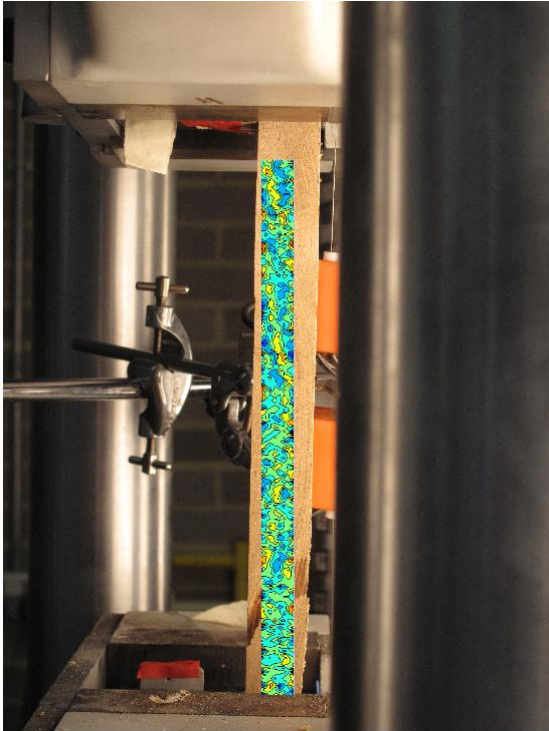
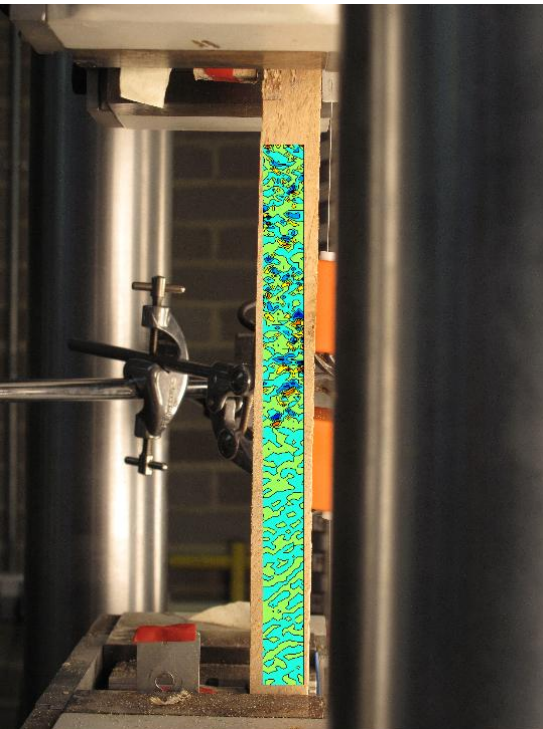FIGURE 842: X DIRECTION PIV FIRST–LAST DITCH ENGINEERING STRAIN OVER IMAGE
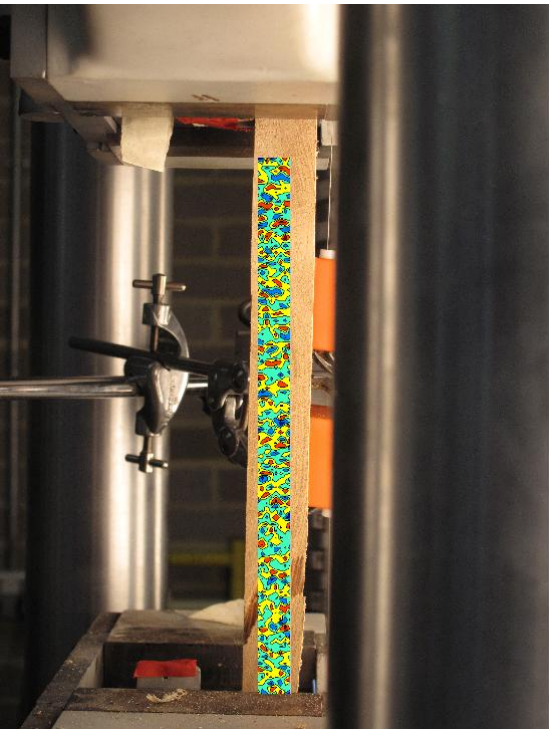
FIGURE 843: Y DIRECTION PIV FIRST–LAST DITCH ENGINEERING STRAIN OVER IMAGE
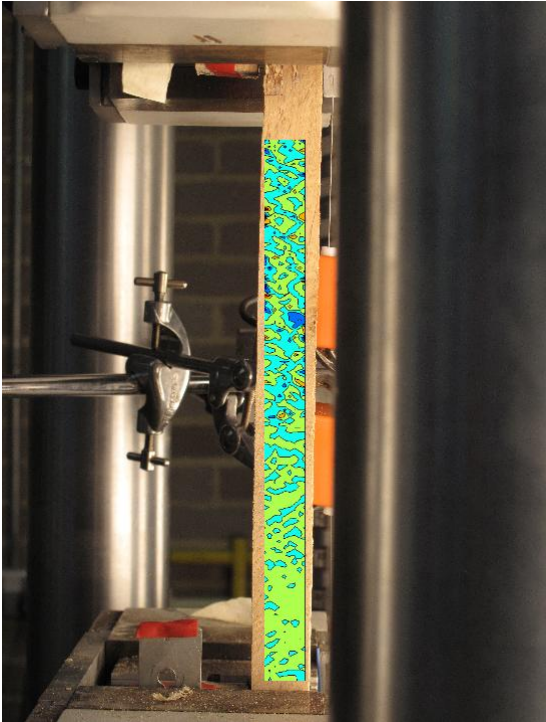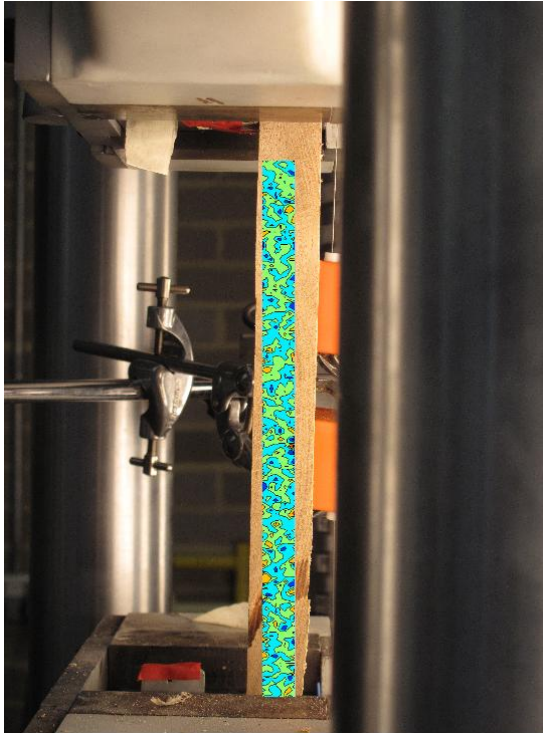
FIGURE 844: XY DIRECTION PIV FIRST–LAST DITCH ENGINEERING SHEAR STRAIN OVER
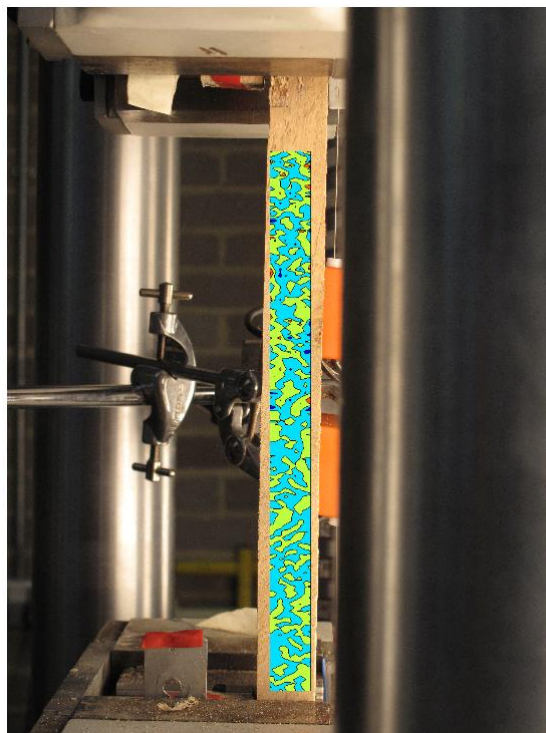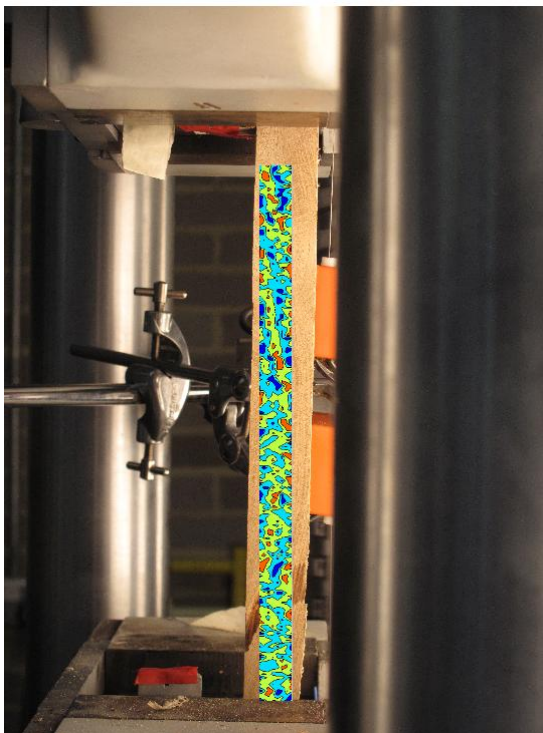
IMAGE

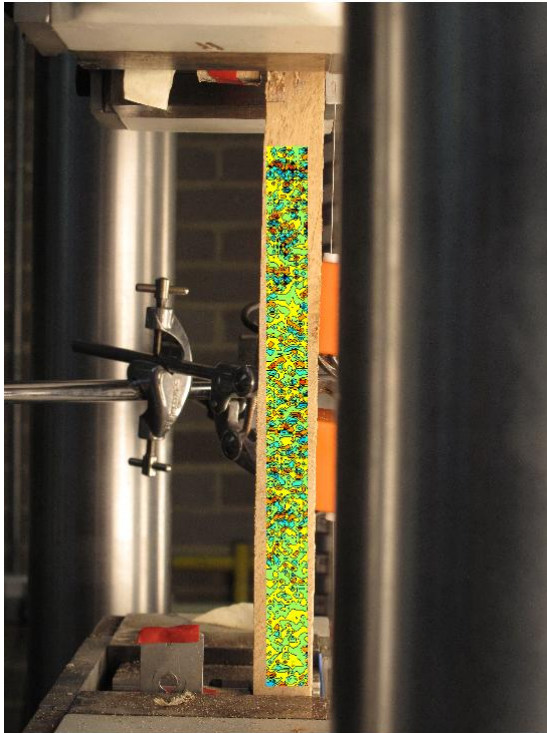FIGURE 845: X DIRECTION PIV FIRST–LAST DITCH TRUE STRAIN OVER IMAGE
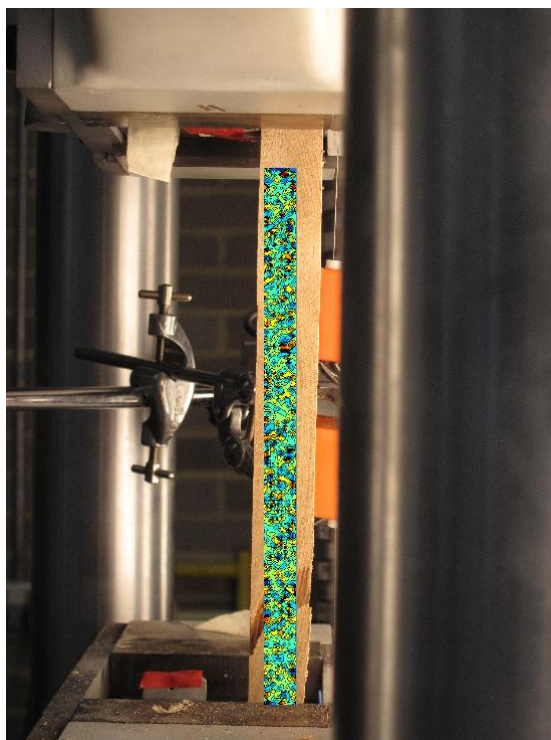
FIGURE 846: Y DIRECTION PIV FIRST–LAST DITCH TRUE STRAIN OVER IMAGE
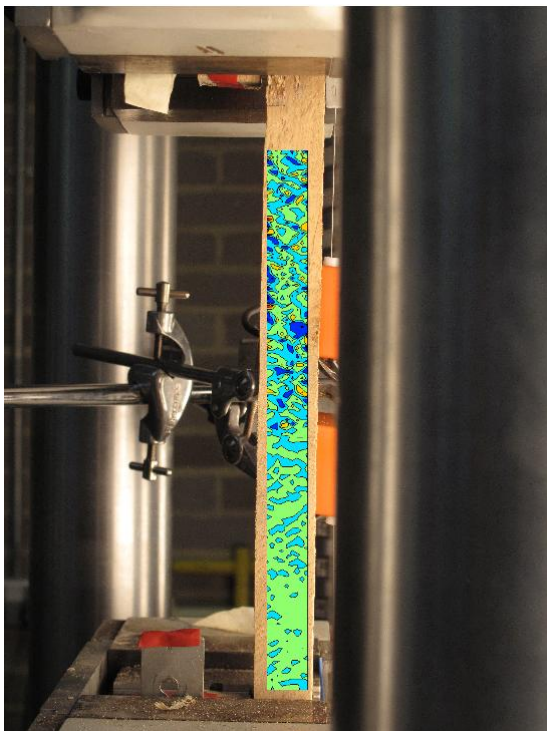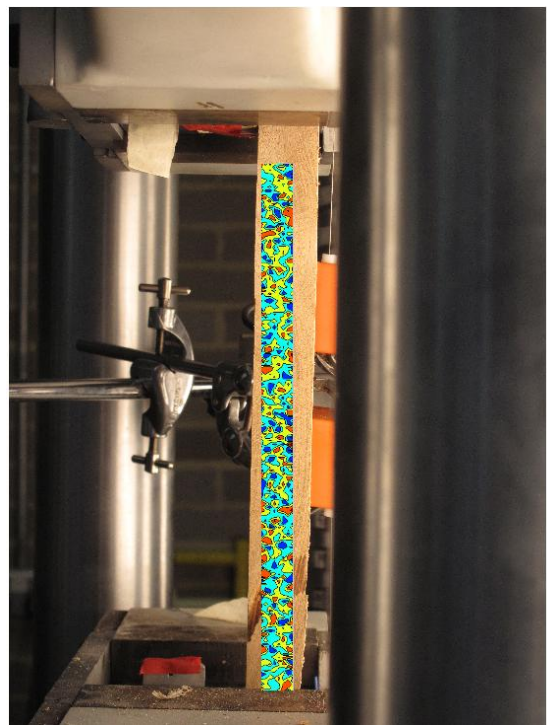

FIGURE 847: XY DIRECTION PIV FIRST–LAST DITCH TRUE SHEAR STRAIN OVER IMAGE
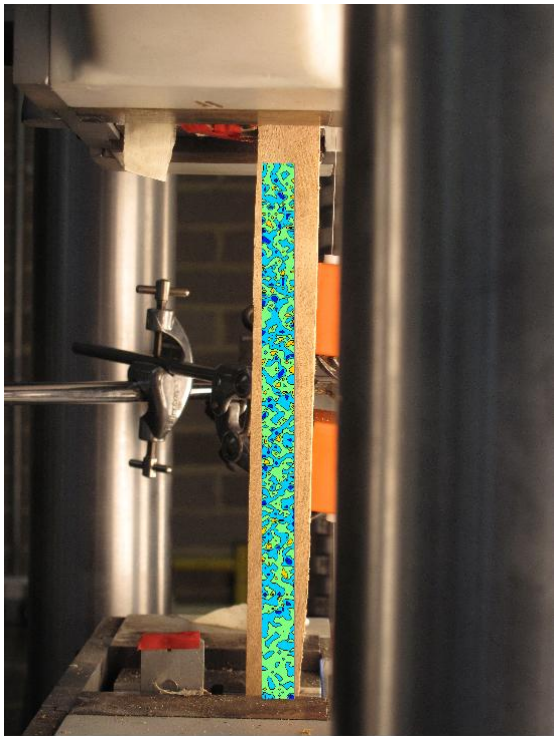
FIGURE 848: XY DIRECTION PIV FIRST–SEQUENTIAL ENGINEERING SHEAR STRAIN OVER

IMAGE
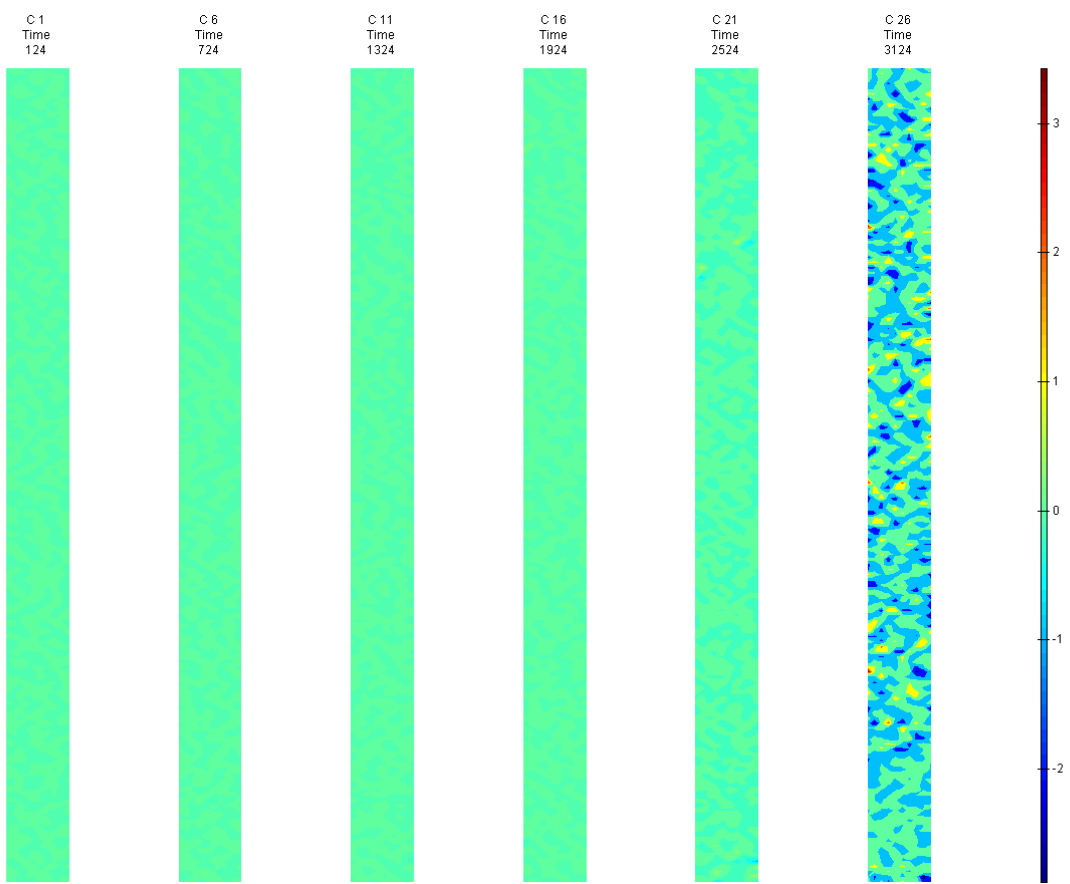
FIGURE 849: XY DIRECTION PIV FIRST–SEQUENTIAL ENGINEERING SHEAR STRAIN OVER TIME

Appendix 7 – Code Map for Results Analysis Modelling

This flowchart shows the coding process of all data results. The bold elements

highlight the main processes in the sequence. The coloured backgrounds

indicate various chapter; yellow –Chapter 5, and orange – Chapter 6.

Appendix 7

PIV Input
Selects original image file location, and records original data such as Active Area and Fixed Points

PIV Analysis and Strain Calculation
Runs through available images in sequence, runs the movement comparison and calculates the strain

Movementcross
facilitates cross matching of images (Based on DJ White Code, but with grid selection calculation

DJ White Code (various files)
Extracts grid element (patch) from image 1, compares with image 2, finds coordinates for best match, and creates movement vector values.

Contour Plot
Creates contour plots of strain to show peaks and dips of strains over time

Contour Overlay
Overlays the contour onto the image for direct comparison

Automated File Locator
Find file locations

Total Strain Calculator and Graph
Calculates the strain totals and correlates data ready for later analysis and graphs

Component Input
Inputs component Data such as sample sizes and results data files

Find Angle
Finds Joint Crotch Angle from image

Component Analyse
Sorts data file and results data ready for calculation and graphical analysis

Component Calculation
Calculates results from test data such as tensile strength and strain etc

Creep Separation
Separates increments and relaxations in the test load data

Component Image Compile
Combines the grain images into joint views

Component Analyse Combine
Allows user corrections on errors in data, and coordinates image and graph analysis

Component PIV Image Compile
Combines contour plots into joint views

Component 2 Joint
Analyses the component results to formulate a rough comparison with the Joint data results.

Line/Scatter Graph Creator
(Various codes) create graphs for results analysis and comparisons)

Joint Compare
Compares all joints tested and combines the component results for comparison

KEY:

Input Data

Process

Output Graph or Image

Direct Flow

Feedback Data

Appendix 8 – Proposal for Live Branch Testing

This chapter shows the proposed methodology and interpretation of live tree branch winch testing to be conducted at a future date.

Introduction

The determination of tree joint strength is still under question. The interconnection of fibres and the tapered cantilever of the tree have previously meant that few predictions outside that of disease risk can determine whether a branch will fall. It is recorded that a healthy branch from a tree can just fall due to 'summer branch drop.' Branches can fall from trees in two ways pull out or shearing, though again this failure mode is not known until the tree branch fails. Many previous investigations have concentrated on the overturning or stem fracture of the tree trunk; these reactions are primarily about soil root interaction rather than about tree strength. Miller (1959) determined by testing apple tree branches whether the Arborists' previous view of the crotch angle affects the joint strength. This found that as the crotch angle decreased, the percentage of branches breaking at the crotch increased, but did not make the joint weaker. However there was a greater correlation between size of branch and stem than the crotch angle, and that narrow crotch angles tend to fail by bark inclusion.

Gilman (2003) highlights previous investigations has shown the force required to break the branch joint decreased as the aspect ratio tend to one. A technique was shown in a further investigation into the strength and aspect ratio of red maple (*Acer Rubrum*). A hundred branches were pulled by unstretchable rope. The trunk was secured horizontally, while the branch was pulled vertically down until the crotch split down the trunk. The branch

diameter was measured beyond any swelling of the collar. The aspect ratio was calculated with branch diameters ranging from 5 to 20mm (expected to have more juvenile wood). The angle was also noted. A stepwise regression model was built to predict ultimate load using angles, and diameters. This found that there was no relationship between angle of branch attachment and strength (secured all the same). Instead the branch strength correlated with diameter ratio and branch diameter.

Basically larger branches require more force to break provided they are small compared to the trunk; however the exception was co-dominant stems that were easier to pull apart. The stress against aspect ratio showed a negative linear correlation, though there appears to be no definitively strong connection.

Lilly and Syndor (1995) simulated static load of branches such as that seen by ice or snow load, to identify factors to predict failure. Their winching test to find bending stress (σ_b) on living tree branches, agreed with Hauer *et al* (1993) that there was no correlations between specific gravity and bending stress and that the crotch angle made no difference either. It may be necessary to think about the real live tree test situation and thus use Lilly equations from live tests, to determine the mechanical properties of the joint:

EQUATION 12: $\sigma_b s_b = \dfrac{4FL_F}{\pi r_b^3}$

where σ_b is bending stress at the crotch, F is the force applied, L_F is the horizontal distance from the crotch to loading point, and r_b is the radius of the branch at the breaking point (see Figure 850).
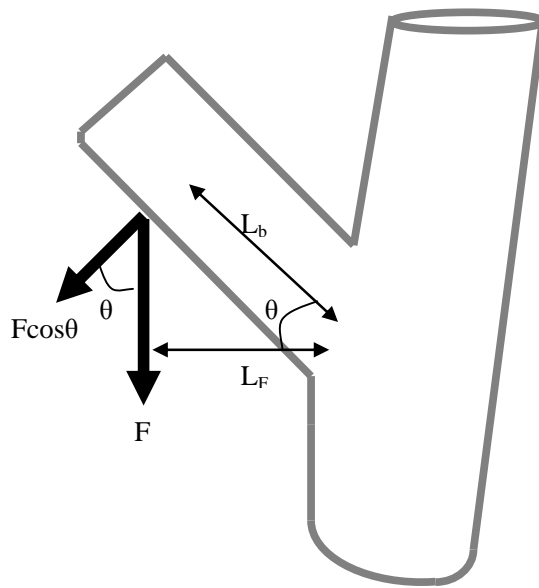
FIGURE 850: LILLY BRANCH MORPHOLOGY FOR CALCULATION DERIVATION

Methods for winching branches have been tried, though these procedures need to be well planned as they may cause a dangerous hazard during testing, as Finch (1997) warns. This leads to some further climbing details by Kane *et al* (2008) given to tree surgeons to ensure the ascent of the tree is safe, this generalises equations for estimating the strength capacity of the tree joint:

EQUATION 13: $\quad v = \frac{1.7P}{d_B^2}$

where v is the shear stress, F is the force, and d_B is the branch diameter

EQUATION 14: $\quad \sigma_b = \frac{10.2PL_B}{d_B^3}$

where σ_b is the bending stress, F is the force, L_B is the branch length to force application and d_B is the branch diameter. These equations follow from a previous investigation by Kane (2007) on Bradford Pear trees which found that aspect ratio of the branch diameter was a better predictor of branch strength, though a more accurate branch cross-section could improve branch strength prediction.

Knowing how a tree branch connection fails can not only help in the hazard investigation of trees within the built environment, but in the biomimicry simulation of composite materials and connection within a structural context. Previous investigation of the branch strength has been done by Cannell and Morgan (1987) but of more relevance to this work is the research done by Shigo (1985), and Müller (2006). These investigations have been limited in their depth and the published work limited. There is a lack of knowledge of the true strength and capabilities of the branch joint/junction. This paper seeks to find a preliminary relationship between the branch dimensions and the load capacity through an original testing technique.

Methodology

1. Find suitable tree with stem and branch connection, measure the test samples height from ground, circumference *etc.* possibly using the LiDAR technology. To reduce the waste of trees pulling branches could be done from top to bottom, or bottom to top on the same tree though balance may affect results.

2. The equipment will need to be set-up. The holding straps on the branch need to be positioned nearer to the stem away from any major kinks or deformations. The holding straps aim to create a uniform load to prevent premature breakage. The branches will be left with all other sub-branches on as unloading prior to test will alter the results.

3. The branch will be pulled in a controlled fashion and monitoring will be done on the movement and load required. The pull direction should be at right angles to the ground, giving a vertical load (Figure 851), or at right-angle transverse (Figure 852) to the trunk on branch pulling. The testing should only be done on a fair day, to prevent the wind creating

extra deformations. A control tree will be scanned to give an idea of data inaccuracy during testing.

4. Once completely broken off (assuming the branch is pulled away from the stem), the stem should be cut to find the depth of break intrusion. The branch should be sawn to find the ring pattern and the off shoots weighed and position of them to the branch measured.

5. If electrical resistance testing is to be done then the needles for the test will be positioned either side of the branch strap point and wires will go into a Wheatstone bridge.
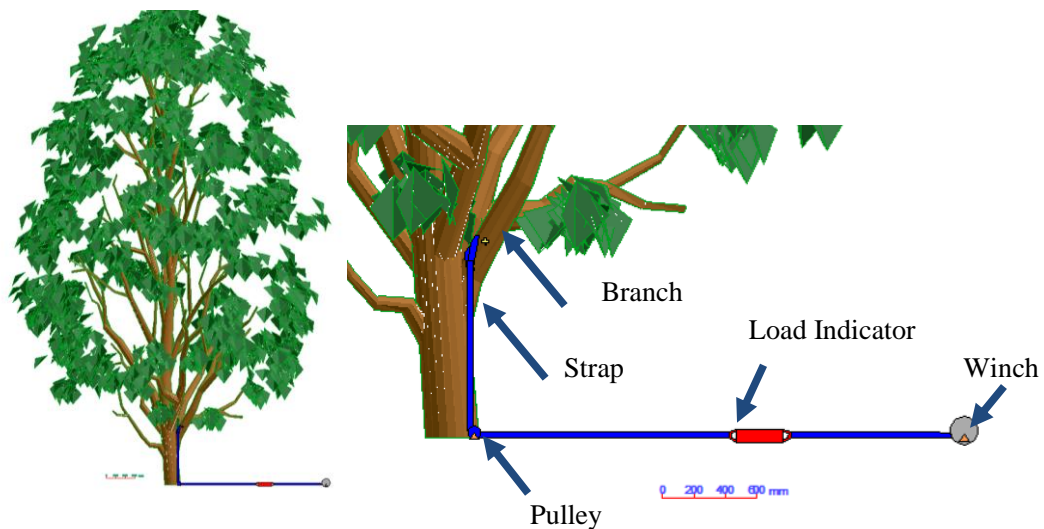
FIGURE 851: VERTICAL LOADING TEST ONSITE
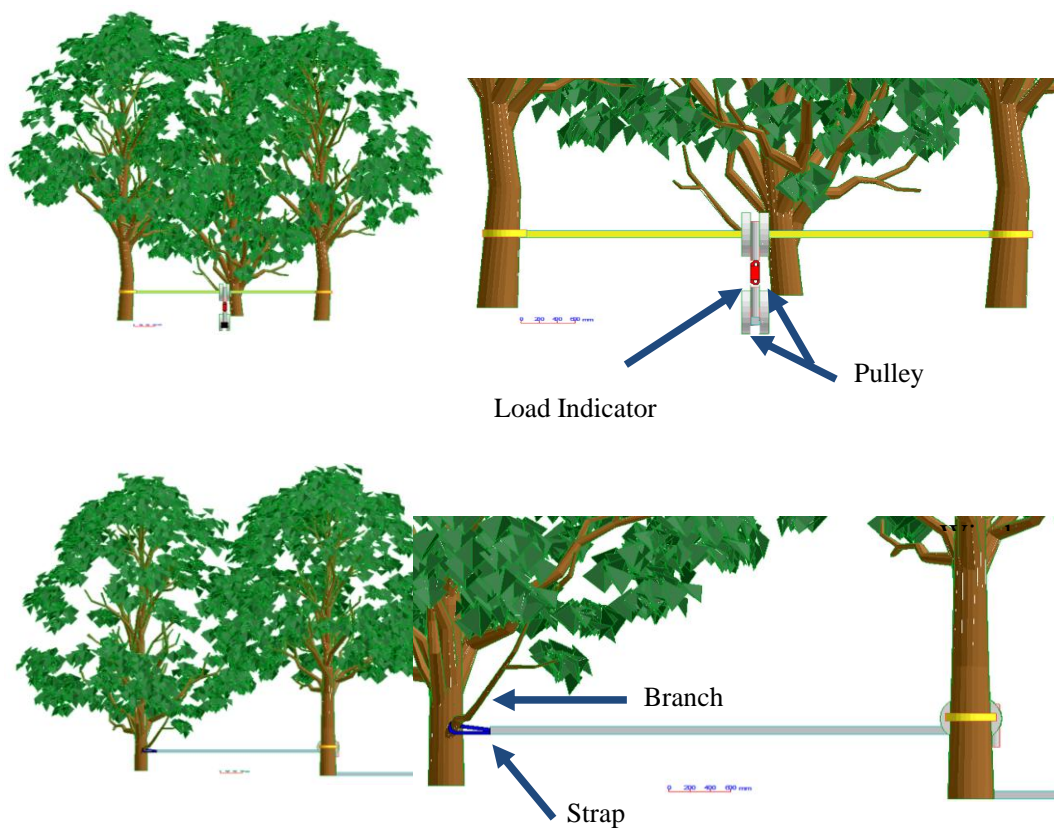
FIGURE 852: TRANSVERSE LOADING TEST ONSITE

Results

The 3D laser scanning will be used to create a point cloud model, this is a relatively new technology and as such using the 3D scanner will be a developing method, and will be used alongside other measurement methods. Using the 3D scanning method the living tree can be measured accurately as it stands and as the loading takes place, it will record the movement of the whole branch and trunk during testing detecting any lever arm movement changes. This technology is also coming into the Forestry Commission (unknown (2010))'s techniques for monitoring forests. The testing should only be done on a fair day, to prevent the wind creating extra deformations. A control tree will be scanned to give an idea of data inaccuracy during testing. The before

and after testing measurement methods will be used to show the displacement of the branch under loading and compared to point cloud data found with the 3D scanner.

The structural properties such as the Young's Modulus *etc.* will be found and compared to similar dimensioned cut joints to find any relationship. Any dimensions and structural property relationships will be investigated, and a finite element analysis done for prediction of strength for further live tests. The failure loads will be compared to estimated storms to see the likelihood of branch breakage due to storm damage. The photographic images used to show the displacement of the branch under loading will be compared to point cloud data found with the 3D scanner. Further the model created in the component test will be verified through the global tests and further used to predict the live tests failure.

Glossary

Active Area – sometimes known as an interrogation window

Allometry – study of the relationship of body size to shape, anatomy, physiology and finally behaviour.

Anisotropic – having different reactions in different directions

Aspect Ratio – the ratio of branch to main stem diameter

Atmospherics – the mood creation through design.

Bark inclusion – where bark comes between touching surfaces of the growing tree and prevents annual wood growing together

Biomechanical– movement of living organisms

Biomimicry – a way of using nature to influence and improve technological solutions

Branch fracture – where the branch splits from the rest of the branch

Branch/Secondary Growth –leads off and supported from primary growth

BS – British Standards

Collar – stem tissue wrapping around the tissue of the branch, enveloping the branch structurally every season to secure it in place

Component– a batten of timber cut from a global joint to be tested

Creep – when a material takes time to deform under continuous loading

Crotch – the join on the leading growth side between the primary and secondary growth (topside of the collar)

Glossary

Crotch Angle – The angle between the primary growth and the secondary growth at the crotch

Dead Load– permanent load of a structure

DIC– Digital Image Correlation compares digital images to find the movement of the subject

Electric Treeing – electrical breakdown phenomena detected through a process of cable manufactured knowledge and partial discharge test results

EPSI – Electronic Speckle Pattern Interferometry

Fork – two primary positive phototropic growths from a main stem that are of similar dimension

Fractometer – A device used to measure the strength of bores of wood

GIGO – 'Garbage In, Garbage Out' Technical computing term for having the wrong information

Global Joint – a section of harvested primary and secondary growth (main stem with branch) from a tree

Green Infrastructure –the importance of the natural environment in land use planning

Greenwood – unseasoned timber with high moisture content, liable to move during drying

GUI –Graphical user interface, the windows and menus used onscreen with computers

Heat Island – The increase in temperature found in cities due to the high density of buildings and population.

Junction/Intersection – meeting of growths within a tree

Live Load– temporary loading on a structure

Main/Primary Growth/Stem –principle structure supporting further growth

Microfibrils– fibre–like strands made of cellulose

MoE– short for Modulus of Elasticity

Morphology– study of forms in a structure

NHS – National Health Service

Notch – the hole created when a branch is formed.

PIV– Particle Image Velocimetry compares digital images to find the movement of the subject

Reaction Wood – wood that grows to reduce the stress found in the tree

Socket tear out – where the branch pulls out from the primary growth

Specific Gravity – ratio of density of a structure compared to water

Stiffness – ability to deform or stretch a material

Strength – ability to withstand stress without failure

Summer branch drop – "sudden limb failure," when an apparently sound and healthy tree limb fails during periods of hot weather.

Sustainability – ability to meet the needs of today without compromising the needs of the future

Glossary

Upper Growth – growth in the phototropism direction

Urban Forest – Trees that line streets, or are in parks and gardens within cities.

Viscoelastic – responds both elastically and viscously in property deformation

List of References

Adam, C. Y. & Milner, H. R. 2012. Wood-Based Prefabricated Composite-Acting Bridge Deck. *Journal of Bridge Engineering,* 17**,** 363-370.

Albrecht, W. A., Bethge, K. A. & Mattheck, C. G. 1995. Is Lateral Strength in Trees Controlled by Lateral Mechanical Stress? *Journal of Arboriculture,* 21**,** 83-87.

Armesto, J., Lubowiecka, I., Ordonez, C. & Rial, F. 2009. Fem Modeling of Structures Based on Close Range Digital Photogrammetry. *Automation in Construction,* 18**,** 559-569.

Ask Nature. unknown. *Crystal Palace in London* [Online]. Ask Nature. Available: http://www.asknature.org/product/a13b2a14313fcc7123e827269a1d8a73#changeTab [Accessed 25 August 2011].

Baker, C. J. 1997. Measurements of the Natural Frequencies of Trees. *Journal of Experimental Botany,* 48**,** 1125-1132.

Bendtsen, B. A. 1978. Properties of Wood from Improved and Intensively Managed Trees. *Forest Products Journal,* 28**,** 61-72.

Biomimicry Institute. *What Is Biomimicry?* [Online]. Available: http://www.biomimicryinstitute.org/about-us/what-is-biomimicry.html [Accessed 2010].

Blackburn, P., Petty, J. A. & Miller, K. F. 1988. An Assessment of the Static and Dynamic Factors Involved in Windthrow. *Forestry,* 61**,** 29-43.

British Standards Institute 1957. Bs373: Methods of Testing Small Clear Specimens of Timber. *BS373.* London: BSI publications.

British Standards Institute 1979. Bs 5820: Methods of Test for Determination of Certain Physical and Mechanical Properties of Timber in Structural Sizes *BS 5820.* London: BSI publications.

British Standards Institute 2002a. Bs5268: Structural Use of Timber. *BS5268.* London: BSI publications.

British Standards Institute 2002b. Bs13183:Moisture Content of a Piece of Sawn Timber *BS13183.* London: BSI publications.

British Standards Institute 2003. Bs En 408: Timber Structures —Structural Timber and Glued Laminated Timber — Determination of Some Physical and Mechanical Properties. *BS EN 408.* London: BSI publications.

Bruechert, F., Becker, G. & Speck, T. 2000. The Mechanics of Norway Spruce (Picea Abies (L.) Karst): Mechanical Properties of Standing Trees from Different Thinning Regimes. *Forest Ecology and Management,* 135**,** 45-62.

List of References

Brundtland Commission (World Commission on Environment and Development) 1987. Our Common Future. Oxford: United Nations

Burgert, I., Bernasconi, A. & Eckstein, D. 1999. Evidence for the Strength Function of Rays in Living Trees. *Holz Als Roh-Und Werkstoff,* 57, 397–399.

Burgert, I. & Eckstein, D. 2001. The Tensile Strength of Isolated Wood Rays of Beech (Fagus Sylvatica L.) and Its Significance for the Biomechanics of Living Trees. *Trees-Structure and Function,* 15, 168–170.

Cannell, M. G. R. & Morgan, J. 1987. Young's Modulus of Sections of Living Branches and Tree Trunks. *Tree Physiology,* 3, 355–364.

Cannell, M. G. R. & Morgan, J. 1989. Branch Breakage under Snow and Ice Loads. *Tree Physiology,* 5, 307–317.

Choi, C., Thorpe, J. L. & Hanna, R. B. 1991. Image Analysis to Measure Strain in Wood and Paper. *Wood Science and Technology,* 25, 251–262.

Dias, A., Ferreira, M., Jorge, L. & Martins, H. 2011. Timber -Concrete Practical Applications – Bridge Case Study. *Proceedings of the Institution of Civil Engineers-Structures and Buildings,* 164, 131–141.

Dwyer, J., Schroeder, H. & Gobster, P. 1994. The Deep Significance of Urban Trees and Forests. *In:* Platt, R., Rowntree, R. & Muick, P. (eds.) *The Ecological City: Preserving and Restoring Urban Biodiversity.* United States of America: The University of Massachusetts Press.

Farnsworth, K. D. & Niklas, K. J. 1995. Theories of Optimization, Form and Function in Branching Architecture in Plants. *Functional Ecology,* 9, 355–363.

Finch, R. 1997a. Caring for Vaterans – the Practicalities. *Quarterly Journal of Forestry,* 91, 231–236.

Finch, R. 1997b. Winching Ancient Trees. *ENACT – Peterborough,* 5, 16–17.

Fons, L. & Pong, W. Y. 1957. Tree Breakage Characteristics under Static Loading Ponderosa Pine. U.S. Department Agricultural Forestry Service.

Franke, S., Franke, B. & Rautenstrauch, K. 2007. Strain Analysis of Wood Components by Close Range Photogrammetry. *Materials and Structures,* 40, 37–46.

Fratzl, P. 2007. Biomimetric Materials Research: What Can We Really Learn from Nature's Structural Materials? *journal of the Royal Society Interface,* 4, 637–642.

Frese, M., Enders-Comberg, M., Blass, H. J. & Glos, P. 2012. Compressive Strength of Spruce Glulam. *European Journal of Wood and Wood Products,* 70, 801–809.

Gilchrist, K. 2011. Promoting Wellbeing through Environment: The Role of Urban Forestry. *Urban Tree Research Conference: Trees, People and the Built Environment.* Birmingham: Institute of Chartered Foresters.

Gilman, E. 2003. Branch-to-Stem Diameter Ratio Effects Strength of Attachment. *Journal of Arboriculture,* 29, 291-293.

Godara, A., Raabe, D., Bergmann, I., Putz, R. & Muller, U. 2009. Influence of Additives on Global Mechanical Behavior and Microscopic Strain Localization in Wood Reinforced Polypropylene Composites During Tensile Deformation Investigated Using Digital Image Correlation. *Composites Science and Tecnology,* 69, 139-146.

Greer, L., Pemberton, S. & Chong Tan, J. 2009. *The Structure and Mechanical Behaviour of Wood* [Online]. Available: http://www.doitpoms.ac.uk/tlplib/wood/printall.php [Accessed 22 October 2009].

Hamza, O., Bengough, A., Bransby, M., Davies, M. & Hallet, P. 2006. Biomechanics of Plant Roots: Estimating Localised Deformation with Particle Image Velocimetry. *Biosystems Engineering,* 94, 119-132.

Harris, R. 1983. Summer Branch Drop. *Journal of Arboriculture,* 9, 111-113.

Hassinen, A., Lemettinen, M., Peltola, H., Kellomaki, D. & Gardiner, B. A. 1998. A Prism-Based System for Monitoring the Swaying of Trees under Wind Loading. *Agricultural & Forest Meteorolog,* 90, 187-194.

I-Tree. 1999. *I-Tree - Tools for Assessing and Managing Community Forests* [Online]. Available: http://www.itreetools.org/ [Accessed 21 August 2011].

James, K., Hallam, C. & Spencer, C. 2013. Measuring Tilt of Tree Structural Root Zones under Static and Wind Loading. *Agricultural and Forest Meteorology,* 168, 160-167.

James, K. R. 2010. *A Dynamic Structural Analysis of Trees Subject to Wind Loading.* Doctor of Philosophy, The University of Melbourne.

Kane, B. 2007. Branch Strength of Bradford Pear (Pyrus Calleryana Var. 'Bradford'). *Arboriculture and Urban Forestry,* 33, 283-291.

Kane, B., Farrell, R., Zedaker, S., Loferski, J. & Smith, D. 2008. Failure Mode and Prediction of Strength of Branch Attachments. *Arboriculture and Urban Forestry,* 34, 308-316.

Koizumi, A. & Hirai, T. 2006. Evaluation of the Section Modulus for Tree-Stem Cross Sections of Irregular Shape. *Journal of Wood Science,* 52, 213-219.

Kramer, E. M. & Borkowski, M. H. 2004. Wood Grain Patterns at Branch Junctions: Modeling and Implications. *Trees-Structure and Function,* 18, 493-500.

List of References

Kubler, H. 1991. Function of Spiral Grain in Trees. *Trees Structure and Function,* 5, 125-135.

Lavers, G. M. 1967. *The Strength Properties of Timber,* Aylesbury, BRE publications.

Lilly, S. & Syndor, T. 1995. Comparison of Branch Failure During Staticloading of Silver and Norway Maples. *journal of Arboriculture,* 21, 302-305.

Lonsdale, D. 1999. *Principles of Tree Hazard Assessment and Management,* London, TSO.

Macdaniels, L. H. 1923. The Apple-Tree Crotch.Bulletin 419. Ithaca, NY: Cornell University Agricultural Experiment Station.

Mattheck, C. 1990. Engineering Components Grow Like Trees. *Materialwissenschaft und Werkstofftech,* 21, 143-168.

Mattheck, C. 1991. *Trees – the Mechanical Design,* Berlin, Springer – Verlag.

Mattheck, C. 1994. *The Body Language of Trees,* London, HMSO Publications Centre.

Mattheck, C. 1998. *Design in Nature: Learning from Trees,* Berlin, Springer-Verlag.

Mattheck, C. 2007. *Secret Design Rules of Nature,* Karlsruhe, Forschungszentrum Karlsruhe GMBH.

Mattheck, C. & Bethge, K. 2000. Simple Mathematical Approaches to

Tree Biomechanics. *Arboricultural Journal,* 24, 307-326.

Mattheck, C., Bethge, K. & Erb, D. 1993. Failure Criteria for Trees. *Arboricultural Journal,* 17, 201-209.

Mattheck, C. & Burkhardt, S. 1990. A New Method of Structural Shape Optimization Based on Biological Growth. *International Journal Fatigue,* 12, 185-190.

Mattheck, C. & Kubler, H. 1997. *Wood-the Internal Optimization of Trees,* Berlin, Springer-Verlag.

Mcmahon, T. A. & Kronauer, R. E. 1976. Trees Structure, Deducing the Principle of Mechanical Design. *Journal of Theoretical Biology,* 59, 443-446.

Mencuccini, M., Grace, J. & Fioravanti, M. 1997. Biomechanical and Hydraulic Determinants of Tree Structure in Scots Pine: Anatomical Characteristics. *Tree Physiology,* 17, 105-113.

Miller, V. Year. Crotch Influence on Strength and Breaking Point of Apple Tree Branches. *In:* Proceedings from the American Society of Horticultural Science, 1959. 27-32.

Moore, J. R. & Maguire, D. A. 2004. Natural Sway Frequencies and Damping Ratios of Trees: Concepts, Review and Synthesis of Previous Studies. *Trees-Structure and Function,* 18, 195-203.

Morgan, J. & Cannell, M. G. R. 1987. Structural Analysis of Tree Trunks and Branches: Tapered Cantilever Beams Subject to Large Deflections under Complex Loading. *Tree Physiology,* 3.

Morgan, J. & Cannell, M. G. R. 1988. Support Costs of Different Branch Designs: Effects of Position, Number, Angle and Deflection of Laterals. *Tree Physiology,* 4.

Muller, U., Gindl, W. & Jeronimidis, G. 2006. Biomechanics of a Branch-Stem Junction in Softwood. *Trees (Berlin),* 20**,** 643-648.

Mundell, C. 2009. *Large Scale Testing of Drystone Retaining Structures.* Doctor of Philosophy, University of Bath.

Nowak, D., Hoehn, R. & Al., E. 2009. Assessing Urban Forest Effects and Values: Chicago's Urban Forest.

O'loinsigh, C., Oudjene, M., Ait-Aider, H., Fanning, P., Pizzi, A., Shotton, E. & Meghlat, E. M. 2012. Experimental Study of Timber-to-Timber Composite Beam Using Welded-through Wood Dowels. *Construction and Building Materials,* 36**,** 245-250.

Padgham, C. A. 1975. *The Perception of Light and Colour,* London, G. Bell and sons.

Papesch, A. J. G., Moore, J. R. & Hawke, A. E. 1997. Mechanical Stability of Pinus Radiata Trees at Eyrewell Forest Investigated Using Static Tests. *New Zealand Journal of Forestry Science,* 27**,** 188-204.

Partnership for Urban South Hampshire (Push). 2010. *Green Infrastructure* [Online]. Available: http://www.push.gov.uk/work/sustainability-and-social-infrastructure/green-infrastructure.htm [Accessed 2011].

Pong, W. Y. 1956. Tree Breakage Characteristics under Static Loading of Several Hardwood Species. U.S. Department Agricultural Forestry Service.

Reames, R. 2005. *Arborsculpture: Solutions for a Small Planet,* Oregon, Arborsmith Studios.

Reiterer, A., Burgert, I., Sinn, G. & Tschegg, S. 2002. The Radial Reinforcement of the Wood Structure and Its Implication on Mechanical and Fracture Mechanical Properties - a Comparison between Two Tree Species. *Journal of Materials Science,* 37**,** 935-940.

Reiterer, A., Lichtenegger, H., Fratzl, P. & Stanzl-Tschegg, S. E. 2001. Deformation and Energy Absorption of Wood Cell Walls with Different Nanostructure under Tensile Loading. *Journal of Materials Science,* 36**,** 4681-4686.

Shigo, A. L. 1985. How Tree Branches Are Attached to Trunks. *Canadian Journal of Botany-Revue Canadienne De Botanique,* 63**,** 1391-1401.

List of References

Skatter, S. & Kucera, B. 1997. Spiral Grain – an Adaptation of Trees to Withstand Stem Breakage Caused by Wind-Induced Torsion. *Holz Als Roh-Und Werkstoff,* 55, 207-213.

Slater, D. 2011. Phd Continuation Report – the Mechanical Properties of Junctions in Trees Manchester: The University of Manchester.

Slater, D. & Harbinson, C. 2010. Towards a New Model of Branch Attachment. *Arboricultural Journal,* 33, 95-105.

Terreform. 2008. *Fab Tree Hab* [Online]. Available: http://www.terreform.org/projects_habitat_fab.html [Accessed November 2008].

Ulrich, R. 1984. View through a Window May Influence Recovery from Surgery. *Science,* 224, 420-421.

Vafai, A. & Farshad, M. 1979. Modulus of Elasticity of Wood in Standing Trees. *Wood Science,* 12, 93-97.

Vukotic, L., Fenner, R. A. & Symons, K. 2010. Assessing Embodied Energy of Building Structural Elements. *Proceedings of the Institution of Civil Engineers-Engineering Sustainability,* 163, 147-158.

White, D. J. & Take, W. A. 2002. Particle Image Velocimetry (Piv) Software for Use in Geotechnical Testing. Cambridge.

White, D. J., Take, W. A. & Bolton, M. D. 2003. Soil Deformation Measurement Using Particle Image Velocimetry (Piv) and Photogrammetry. *Geotechnique,* 53, 619-631.

Bibliography

Abasolo, W., Eder, M., Yamauchi, K., Obel, N., Reinecke, A., Neumetzler, L., Dunlop, J. W. C., Mouille, G., Pauly, M., Hofte, H. & Burgert, I. 2009. Pectin May Hinder the Unfolding of Xyloglucan Chains During Cell Deformation: Implications of the Mechanical Performance of Arabidopsis Hypocotyls with Pectin Alterations. *Molecular Plant,* 2**,** 990–999.

Adam, C. Y. & Milner, H. R. 2012. Wood–Based Prefabricated Composite–Acting Bridge Deck. *Journal of Bridge Engineering,* 17**,** 363–370.

Adams, J. 2007. Dangerous Trees? *Arboricultural Journal,* 30**,** 95–103.

Adrian, R. J. 1991. Particle Imaging Techniques for Experimental Fluid Mechanics. *ANNUAL REVIEW OF FLUID MECHANICS* 23**,** 261–304.

Akagi, Y. & Kitajima, K. 2006. Computer Animation of Swaying Trees Based on Physical Simulation. *Computers & Graphics–Uk,* 30**,** 529–539.

Albrecht, W. A., Bethge, K. A. & Mattheck, C. G. 1995. Is Lateral Strength in Trees Controlled by Lateral Mechanical Stress? *Journal of Arboriculture,* 21**,** 83–87.

Ancelin, P., Courbaud, B. & Fourcaud, T. Y. 2004a. Development of an Individual Tree–Based Mechanical Model to Predict Wind Damage within Forest Stands. *Forest Ecology and Management,* 203**,** 101–121.

Annik, D., Boonstra, C. & John, M. 1996. *Handbook of Sustainable Building: An Enviromental Preference Method for Selection of Materials for Use in Construction and Refurbishment,* London, James & James (Science Publishers) Limited.

Arboricultural Information Exchange. 2010. *Trees and Buildings* [Online]. Available: http://www.aie.org.uk/articles/article_tbuildings.htm [Accessed 2 February 2011 2011].

Armesto, J., Lubowiecka, I., Ordonez, C. & Rial, F. 2009. Fem Modeling of Structures Based on Close Range Digital Photogrammetry. *Automation in Construction,* 18**,** 559–569.

Armstrong, R. 2011. *How Living Technologies Could Reclaim Venice* [Online]. Available: http://www2.warwick.ac.uk/knowledge/themes/virtualfutures/rachelarmstrong/ [Accessed 2013].

Armstrong, R. 2012. *Lawless Sustainability – New Technology and Innovative Solutions for a Sustainable Future* [Online]. Available: http://www.architecturenorway.no/questions/cities-sustainability/armstrong/ [Accessed 2013].

Armstrong, R. & Spiller, N. 2010. Synthetic Biology – Living Quarters. *Nature,* 467**,** 916–918.

Bibliography

Ashori, A., Tabarsa, T. & Amosi, F. 2012. Evaluation of Using Waste Timber Railway Sleepers in Wood-Cement Composite Materials. *Construction and Building Materials,* 27**,** 126-129.

Ask Nature. unknown. *Crystal Palace in London* [Online]. Ask Nature. Available: http://www.asknature.org/product/a13b2a14313fcc7123e827269a1d8a73#changeTab [Accessed 25 August 2011].

Baker, C. J. 1995. The Development of a Theoretical Model for the Wind Throw of Plants. *Journal of Theoretical Biology,* 175**,** 355-372.

Baker, C. J. 1997. Measurements of the Natural Frequencies of Trees. *Journal of Experimental Botany,* 48**,** 1125-1132.

Baumgartner, A., Burkhardt, S. & Mattheck, C. 1992a. The Kill-Option – a Powerful Method to Prepare Engineering Low Weight Design Proposals. *In:* Jono, M. & Inoue, T. (eds.) *Mechanical Behaviour of Materials-Vi, Vols 1-4.*

Baumgartner, A., Harzheim, L. & Mattheck, C. 1992b. Sko (Soft Kill Option) – the Biological Way to Find an Optimum Structure Topology. *International Journal of Fatigue,* 14**,** 387-393.

Beller, M., Mattheck, C. & Schafer, J. 1991. *Shape Optimization on the Basis of Biological Growth with Special Regard to Slanted Joints*.

Bendtsen, B. A. 1978. Properties of Wood from Improved and Intensively Managed Trees. *Forest Products Journal,* 28**,** 61-72.

Bertram, J. E. A. 1989. Size-Dependent Differential Scaling in Branches: The Mechanical Design of Trees Revisited. *Trees,* 4**,** 241-253.

Bethge, K. & Mattheck, C. 1990. Fatigue Testing of a Shape-Optimized Circular Hole in a Plate under Tensile and Bending Loads. *International Journal of Fatigue,* 12**,** 489-492.

Bethge, K. & Mattheck, C. 1995. New Methods for the Assessment of Wood Quality in Standing Trees. *In:* Coutts, M. P. & Grace, J. (eds.) *Wind and Trees.* Cambridge: Cambridge University Press.

Biomimicry Institute. *What Is Biomimicry?* [Online]. Available: http://www.biomimicryinstitute.org/about-us/what-is-biomimicry.html [Accessed 2010].

Blackburn, G. R. A. 1997. *The Growth and Mechanical Response of Trees to Wind Loading.* PhD, University of Manchester.

Blackburn, P., Petty, J. A. & Miller, K. F. 1988. An Assessment of the Static and Dynamic Factors Involved in Windthrow. *Forestry,* 61**,** 29-43.

Blennow, K. & Sallnas, O. 2004. Winda – a System of Models for Assessing the Probability of Wind Damage to Forest Stands within a Landscape. *Ecological Modelling,* 175**,** 87-99.

Bodig, J. & Jayne, B. A. 1982. *Mechanics of Wood and Wood Composites,* New York, Reinhold Company.

Bolton, A. J. & Petty, J. A. 1978. A Model Describing Axial Flow of Liquids through Conifer Wood *Wood Science and Technology,* 12, 37–48.

Booker, R. 1984. Dye-Flow Apparatus to Measure the Variation in Axial Xylem Permeability over a Stem Cross-Section. *Plant, Cell and Environment,* 7, 623–628.

Booker, R. E. 1977. Problems in Measurement of Longitudinal Sapwood Permeability and Hydraulic Conductivity. *New Zealand Journal of Forestry Science,* 7, 297–306.

Borner, M. & Mattheck, C. 1985. A New Profile for the Interlocking Intramedullary Nail with High Fatigue Stability. *Unfallchirurg,* 88, 263–266.

Borner, M., Mattheck, C. & Bernt, J. 1987. An Interlocking Nail with Improved Fatigue-Strength. *Biomedizinische Technik,* 32, 305–308.

Borner, M., Mattheck, C. & Haberer, B. 1985. A Biomechanical Analysis of a Rare Crack in an Interlocking Nail. *Unfallchirurg,* 88, 235–238.

British Standards Institute 1957. Bs373: Methods of Testing Small Clear Specimens of Timber. *BS373.* London: BSI publications.

British Standards Institute 1979. Bs 5820: Methods of Test for Determination of Certain Physical and Mechanical Properties of Timber in Structural Sizes *BS 5820.* London: BSI publications.

British Standards Institute 2002a. Bs5268: Structural Use of Timber. *BS5268.* London: BSI publications.

British Standards Institute 2002b. Bs13183:Moisture Content of a Piece of Sawn Timber *BS13183.* London: BSI publications.

British Standards Institute 2003. Bs En 408: Timber Structures —Structural Timber and Glued Laminated Timber — Determination of Some Physical and Mechanical Properties. *BS EN 408.* London: BSI publications.

Bruchert, F. & Gardiner, B. 2006. The Effect of Wind Exposure on the Tree Aerial Architecture and Biomechanics of Sitka Spruce (Picea Sitchensis, Pinaceae). *American Journal of Botany,* 93, 1512–1521.

Bruder, G. R., Mattheck, C. & Teschner, M. 1997. *Fem Root Growth Simulations*.

Bruechert, F., Becker, G. & Speck, T. 2000. The Mechanics of Norway Spruce (Picea Abies (L.) Karst): Mechanical Properties of Standing Trees from Different Thinning Regimes. *Forest Ecology and Management,* 135, 45–62.

Brundtland Commission (World Commission on Environment and Development) 1987. Our Common Future. Oxford: United Nations

Bibliography

Buck-Sorlin, G. H. & Bell, A. D. 2000. Models of Crown Architecture in Quercus Petraea and Q-Robur: Shoot Lengths and Bud Numbers. *Forestry,* 73, 1- 19.

Burgert, I. 2006. Exploring the Micromechanical Design of Plant Cell Walls. *American Journal of Botany,* 93, 1391-1401.

Burgert, I., Bernasconi, A. & Eckstein, D. 1999. Evidence for the Strength Function of Rays in Living Trees. *Holz Als Roh-Und Werkstoff,* 57, 397- 399.

Burgert, I. & Eckstein, D. 2001. The Tensile Strength of Isolated Wood Rays of Beech (Fagus Sylvatica L.) and Its Significance for the Biomechanics of Living Trees. *Trees-Structure and Function,* 15, 168-170.

Burgert, I., Eckstein, D. & Bernasconi, A. 2000. Elastomechanical Properties of Young Beech Trees (Fagus Sylvatica L.) Grown at Elevated and Ambient Co2 Content. *Holz Als Roh-Und Werkstoff,* 58, 342-343.

Burgert, I., Eder, M., Fruhmann, K., Keckes, J., Fratzl, P. & Stanzl-Tschegg, S. 2005a. Properties of Chemically and Mechanically Isolated Fibres of Spruce (Picea Abies L. Karst.). Part 3: Mechanical Characterisation. *Holzforschung,* 59, 354-357.

Burgert, I., Eder, M., Gierlinger, N. & Fratzl, P. 2007. Tensile and Compressive Stresses in Tracheids Are Induced by Swelling Based on Geometrical Constraints of the Wood Cell. *Planta,* 226, 981-987.

Burgert, I. & Fratzl, P. 2009a. Actuation Systems in Plants as Prototypes for Bioinspired Devices. *Philosophical Transactions of the Royal Society a-Mathematical Physical and Engineering Sciences,* 367, 1541-1557.

Burgert, I. & Fratzl, P. 2009b. The Plant Cell Wall Acts as a Sophisticated Mechanical Device. *Integrative and Comparative Biology,* 49, E23-E23.

Burgert, I. & Fratzl, P. 2009c. Plants Control the Properties and Actuation of Their Organs through the Orientation of Cellulose Fibrils in Their Cell Walls. *Integrative and Comparative Biology,* 49, 69-79.

Burgert, I., Fruhmann, K., Keckes, J., Fratzl, P. & Stanzl-Tschegg, S. 2004. Structure-Function Relationships of Four Compression Wood Types: Micromechanical Properties at the Tissue and Fibre Level. *Trees-Structure and Function,* 18, 480-485.

Burgert, I., Fruhmann, K., Keckes, J., Fratzl, P. & Stanzl-Tschegg, S. 2005b. Properties of Chemically and Mechanically Isolated Fibres of Spruce (Picea Abies L. Karst.). Part 2: Twisting Phenomena. *Holzforschung,* 59, 247-251.

Burgert, I., Fruhmann, K., Keckes, J., Fratzl, P. & Stanzl-Tschegg, S. E. 2003a. Microtensile Testing of Wood Fibers Combined with Video Extensometry for Efficient Strain Detection. *Holzforschung,* 57, 661-664.

Burgert, I., Gierlinger, N. & Zimmermann, T. 2005c. Properties of Chemically and Mechanically Isolated Fibres of Spruce (Picea Abies L. Karst.). Part 1: Structural and Chemical Characterisation. *Holzforschung,* 59, 240–246.

Burgert, I. & Jungnikl, K. 2004. Adaptive Growth of Gymnosperm Branches-Ultrastructural and Micromechanical Examinations. *Journal of Plant Growth Regulation,* 23, 76–82.

Burgert, I., Keckes, J. & Fratzl, P. 2006. *Mechanics of the Wood Cell Wall.*

Burgert, I., Keckes, J., Fruhmann, K., Fratzl, P. & Tschegg, S. E. 2002. A Comparison of Two Techniques for Wood Fibre Isolation Evaluation by Tensile Tests on Single Fibres with Different Microfibril Angle. *Plant Biology,* 4, 9–12.

Burgert, I., Okuyama, T. & Yamamoto, H. 2003b. Generation of Radial Growth Stresses in the Big Rays of Konara Oak Trees. *Journal of Wood Science,* 49, 131–134.

Burgess, S. S. O., Pittermann, J. & Dawson, T. E. 2006. Hydraulic Efficiency and Safety of Branch Xylem Increases with Height in Sequoia Sempervirens (D. Don) Crowns. *Plant Cell and Environment,* 29, 229–239.

Cameron, A. D. & Dunham, R. A. 1999. Strength Properties of Wind- and Snow-Damaged Stems of Picea Sitchensis and Pinus Sylvestris in Comparison with Undamaged Trees. *Canadian Journal of Forest Research-Revue Canadienne De Recherche Forestiere,* 29, 595–599.

Cannell, M. & Coutts, M. 1988. Growing in the Wind. *New Scientist,* 117, 42–46.

Cannell, M. G. R. & Morgan, J. 1987 Young's Modulus of Sections of Living Branches and Tree Trunks. *Tree Physiology,* 3, 355–364.

Cannell, M. G. R. & Morgan, J. 1989. Branch Breakage under Snow and Ice Loads. *Tree Physiology,* 5, 307–317.

Cannell, M. G. R. & Morgan, J. 1990. Theoretical-Study of Variables Affecting the Export of Assimilates from Branches of Picea. *Tree Physiology,* 6, 257–266.

Cannell, M. G. R., Morgan, J. & Murray, M. B. 1988 Diameters and Dry Weights of Tree Shoots – Effects of Youngs Modulus, Taper, Deflection and Angle. *Tree Physiology,* 4, 219–231.

Caspers, M. & Mattheck, C. 1986. Weighted Averaged Stress Intensity Factors of Circular-Fronted Cracks in Cylindrical-Bars. *Fatigue & Fracture of Engineering Materials & Structures,* 9, 329–341.

Cavalier, D. M., Lerouxel, O., Neumetzler, L., Yamauchi, K., Reinecke, A., Freshour, G., Zabotina, O. A., Hahn, M. G., Burgert, I., Pauly, M., Raikhel, N. V. & Keegstra, K. 2008. Disrupting Two Arabidopsis Thaliana

Xylosyltransferase Genes Results in Plants Deficient in Xyloglucan, a Major Primary Cell Wall Component. *Plant Cell,* 20, 1519-1537.

Choi, C., Thorpe, J. L. & Hanna, R. B. 1991. Image Analysis to Measure Strain in Wood and Paper. *Wood Science and Technology,* 25, 251-262.

Clifford, D. R., Gendle, P. & Holgate, M. E. 1987. Gel Formulations for the Treatment of Pruning Wounds .2. Results with Differing Gel and Fungicide Components and Comparison with Sealant Compositions. *Annals of Applied Biology,* 110, 501-514.

Commonwealth Scientific and Industrial Research Organization 1974. Testing Timber for Moisture Content. Melbourne.

Costes, E. & Guedon, Y. 2002. Modelling Branching Patterns on 1-Year-Old Trunks of Six Apple Cultivars. *Annals of Botany,* 89, 513-524.

Costes, E., Smith, C., Renton, M., Guedon, Y., Prusinkiewicz, P. & Godin, C. 2008. Mapplet: Simulation of Apple Tree Development Using Mixed Stochastic and Biomechanical Models. *Functional Plant Biology,* 35, 936-950.

Cournede, P. H., Kang, M. Z., Mathieu, A., Barcz, J. F., Yan, H. P., Hu, B. G. & De Reffye, P. 2006. Structural Factorization of Plants to Compute Their Functional and Architectural Growth. *Simulation-Transactions of the Society for Modeling and Simulation International,* 82, 427-438.

Coutts, M. P. & Grace, J. 1995. *Wind and Trees,* Cambridge, Cambridge University Press.

Cunningham, M. J. 1986. Automatic Datalogging Timber Moisture Contents over the Range 10-Percent-50-Percent W/W. *Isa Transactions,* 25, 73-80.

Czuck, G., Mattheck, C., Munz, D. & Stamm, H. 1985. Crack-Growth under Cyclic Thermal-Shock Loading. *Nuclear Engineering and Design,* 84, 189-199.

Dahle, G. & Grabosky, J. 2009. Review of Literature on the Function and Allometric Relationships of Tree Stems and Branches. *Arboriculture and urban Forestry,* 35, 311-320.

De Langre, E. 2008. Effects of Wind on Plants. *Annual Review of Fluid Mechanics,* 40, 141-168.

Life after People, Year. Broadcast. Directed by De Vries, D. USA.

Deleuze, C., Herve, J. C., Colin, F. & Ribeyrolles, L. 1996. Modelling Crown Shape of Picea Abies: Spacing Effects. *Canadian Journal of Forest Research-Revue Canadienne De Recherche Forestiere,* 26, 1957-1966.

Deshpande, A. S., Burgert, I. & Paris, O. 2006. Hierarchically Structured Ceramics by High-Precision Nanoparticte Casting of Wood. *Small,* 2, 994-998.

Dias, A., Ferreira, M., Jorge, L. & Martins, H. 2011. Timber -Concrete Practical Applications – Bridge Case Study. *Proceedings of the Institution of Civil Engineers-Structures and Buildings,* 164**,** 131-141.

Dietrich, F. & Mattheck, C. 1995. Cracks in Sabre-Shaped Trees and Branches. *Journal of Theoretical Biology,* 173**,** 321-327.

Donaldson, L. 2008. Microfibril Angle: Measurement, Variation and Relationships – a Review. *Iawa Journal,* 29**,** 345-386.

Drakos, N. 2002. *True Stress and True Strain* [Online]. Leeds: University of Leeds. Available: http://dolbow.cee.duke.edu/TENSILE/tutorial/node3.html [Accessed 3 September 2010].

Duncan, J., Dabiri, D., Hove, J. & Gharib, M. 2010. Universal Outlier Detection for Particle Image Velocimetry (Piv) and Particle Tracking Velocimetry (Ptv) Data. *Measurement Science & Technology,* 21**,** 057002 (5 pp.)-057002 (5 pp.).

Dwyer, J., Schroeder, H. & Gobster, P. 1994. The Deep Significance of Urban Trees and Forests. *In:* Platt, R., Rowntree, R. & Muick, P. (eds.) *The Ecological City: Preserving and Restoring Urban Biodiversity.* United States of America: The University of Massachusetts Press.

Dzierzon, H., Sievanen, R., Kurth, W., Perttunen, J. & Sloboda, B. 2003. Enhanced Possibilities for Analyzing Tree Structure as Provided by an Interface between Different Modelling Systems. *Silva Fennica,* 37**,** 31-44.

Eckstein, D., Burgert, I. & Schwab, E. 1998. Is There a Coherence between the Radial and Axial Strength of Living Trees? *Allgemeine Forst Und Jagdzeitung,* 169**,** 101-103.

Edelstein, Z. R. & Ford, E. D. 2003. Branch and Foliage Morphological Plasticity in Old-Growth Thuja Plicata. *Tree Physiology,* 23**,** 649-662.

Eder, M., Jungnikl, K. & Burgert, I. 2009. A Close-up View of Wood Structure and Properties across a Growth Ring of Norway Spruce (Picea Abies L Karst.). *Trees-Structure and Function,* 23**,** 79-84.

Eder, M., Stanzl-Tschegg, S. & Burgert, I. 2008a. The Fracture Behaviour of Single Wood Fibres Is Governed by Geometrical Constraints: In Situ Esem Studies on Three Fibre Types. *Wood Science and Technology,* 42**,** 679-689.

Eder, M., Terziev, N., Daniel, G. & Burgert, I. 2008b. The Effect of (Induced) Dislocations on the Tensile Properties of Individual Norway Spruce Fibres. *Holzforschung,* 62**,** 77-81.

Edwards, W. R. N. & Jarvis, P. G. 1982. Relations between Water Content, Potential and Permeability in Stems of Conifers. *Plant, Cell and Environment,* 5**,** 271-277.

Bibliography

Elbaum, R., Zaltzman, L., Burgert, I. & Fratzl, P. 2007. The Role of Wheat Awns in the Seed Dispersal Unit. *Science,* 316, 884-886.

Elie, J. G. & Ruel, J. C. 2005. Windthrow Hazard Modelling in Boreal Forests of Black Spruce and Jack Pine. *Canadian Journal of Forest Research-Revue Canadienne De Recherche Forestiere,* 35, 2655-2663.

Ellison, M. 2005. Quantified Tree Risk Assessment Used in the Management of Amenity Trees. *Journal of Arboriculture,* 31, 57-65.

Emerson, R. N., Pollock, D. G., Kainz, J. A., Fridley, K. J., Mclean, D. I. & Ross, R. J. 1998. Nondestructive Evaluation Techniques for Timber Bridges. *5th World Conference on Timber Engineering, Vol 1, Proceedings*, 670-677.

Ennos, A. R. 1995. Development of Buttresses in Rainforest Trees: The Influence of Mechanical Stress. *In:* Coutts, M. P. & Grace, J. (eds.) *Wind and Trees.* Cambridge: Cambridge University Press.

Esper, J., Schweingruber, F. H. & Winiger, M. 2002. 1300 Years of Climatic History for Western Central Asia Inferred from Tree-Rings. *Holocene,* 12, 267-277.

Esser, M. H. M. 1946a,b. Tree Trunks and Branches as Optimum Mechanical Supports of the Crown. I. The Trunk.

Tree Trunks and Branches as Optimum Mechanical Supports of the Crown. Ii. The Branches. *Bulletin of Mathematical Biology,* 8, 65-74;95-100.

Fackler, K., Gradinger, C., Schmutzer, M., Tavzes, C., Burgert, I., Schwanninger, M., Hinterstoisser, B., Watanabe, T. & Messner, K. 2007. Biotechnological Wood Modification with Selective White-Rot Fungi and Its Molecular Mechanisms. *Food Technology and Biotechnology,* 45, 269-276.

Farnsworth, K. D. & Niklas, K. J. 1995. Theories of Optimization, Form and Function in Branching Architecture in Plants. *Functional Ecology,* 9, 355-363.

Farquhar, T. & Zhao, Y. 2006. Fracture Mechanics and Its Relevance to Botanical Structures. *American Journal of Botany,* 93, 1449-1454.

Farrell 2003, S. F. R. T. T. C. S., Unpublished Thesis, Faculty of Viginia Polytechnic Institute and State University.

Fernandez, M. P. & Norero, A. 2006. Relation between Length and Diameter of Pinus Radiata Branches. *Scandinavian Journal of Forest Research,* 21, 124-129.

Fett, T. & Mattheck, C. 1989. Stress Intensity Factors of Embedded Elliptical Cracks for Weight Function Applications. *International Journal of Fracture,* 40, R13-R18.

Fett, T., Mattheck, C. & Munz, D. 1987. On the Calculation of Crack Opening Displacement from the Stress Intensity Factor. *Engineering Fracture Mechanics,* 27, 697-715.

Fett, T., Mattheck, C. & Munz, D. 1989a. Approximate Weight Function for 2d and 3d-Problems. *Engineering Analysis with Boundary Elements,* 6, 48–63.

Fett, T., Mattheck, C. & Munz, D. 1989b. On the Accuracy of the Cruse-Besuner Weight Function Approximation for Two-Dimensional Cracks. *International Journal of Fracture,* 40, 307–313.

Fett, T., Mattheck, C. & Munz, D. 1990. Averaged Stress Intensity Factors for Embedded Elliptic Cracks. *Engineering Fracture Mechanics,* 35, 987–996.

Finch, R. 1993. An Alternative Method of Crown Reduction for Ancient Pollards & Dead Trees. *In:* Read, H. (ed.) *Pollard and Veteran Tree Management.* Corporation of London.

Finch, R. 1997a. Caring for Vaterans – the Practicalities. *Quarterly Journal of Forestry,* 91, 231–236.

Finch, R. 1997b. Winching Ancient Trees. *ENACT – Peterborough,* 5, 16–17.

Fons, L. & Pong, W. Y. 1957. Tree Breakage Characteristics under Static Loading Ponderosa Pine. U.S. Department Agricultural Forestry Service.

Forestry Commission. 1999. *Introduction to Lidar* [Online]. Available: http://www.forestry.gov.uk/forestry/infd-6rvc9j [Accessed 2010].

Fournier, C. & Andrieu, B. 1998. A 3d Architectural and Process-Based Model of Maize Development. *Annals of Botany,* 81, 233–250.

Franke, S., Franke, B. & Rautenstrauch, K. 2007. Strain Analysis of Wood Components by Close Range Photogrammetry. *Materials and Structures,* 40, 37–46.

Fratzl, P. 2007. Biomimetric Materials Research: What Can We Really Learn from Nature's Structural Materials? *journal of the Royal Society Interface,* 4, 637–642.

Fratzl, P., Burgert, I. & Gupta, H. S. 2004a. On the Role of Interface Polymers for the Mechanics of Natural Polymeric Composites. *Physical Chemistry Chemical Physics,* 6, 5575–5579.

Fratzl, P., Burgert, I. & Keckes, J. 2004b. Mechanical Model for the Deformation of the Wood Cell Wall. *Zeitschrift Fur Metallkunde,* 95, 579–584.

Fratzl, P., Elbaum, R. & Burgert, I. 2008. Cellulose Fibrils Direct Plant Organ Movements. *Faraday Discussions,* 139, 275–282.

Fratzl, P., Gupta, H. & Burgert, I. 2007. Mechanical Functionality by Hierarchical Structuring Lessons from Biological Materials. *Comparative Biochemistry and Physiology a-Molecular & Integrative Physiology,* 146, 10.

Frese, M., Enders-Comberg, M., Blass, H. J. & Glos, P. 2012. Compressive Strength of Spruce Glulam. *European Journal of Wood and Wood Products,* 70, 801–809.

Bibliography

Fruhmann, K., Burgert, I. & Stanzl-Tschegg, S. E. 2003a. Detection of the Fracture Path under Tensile Loads through in Situ Tests in an Esem Chamber. *Holzforschung,* 57, 326-332.

Fruhmann, K., Burgert, I., Stanzl-Tschegg, S. E. & Tschegg, E. K. 2003b. Mode I Fracture Behaviour on the Growth Ring Scale and Cellular Level of Spruce (Picea Abies L. Karst.) and Beech (Fagus Sylvatica L.) Loaded in the Tr Crack Propagation System. *Holzforschung,* 57, 653-660.

Fux, H. D., Mattheck, C. & Morawietz, P. 1984. New Aspects of Secondary Fracture-Healing in Intramedullary Nailing – a Biomechanical Analysis. *Unfallheilkunde-Traumatology,* 87, 369-373.

Garber, S. M. & Maguire, D. A. 2005. Vertical Trends in Maximum Branch Diameter in Two Mixed-Species Spacing Trials in the Central Oregon Cascades. *Canadian Journal of Forest Research-Revue Canadienne De Recherche Forestiere,* 35, 295-307.

Gardiner, B., Byrne, K., Hale, S., Kamimura, K., Mitchell, S. J., Peltola, H. & Ruel, J. C. 2008. A Review of Mechanistic Modelling of Wind Damage Risk to Forests. *Forestry,* 81, 447-463.

Gardiner, B. A. 1989. *Mechanical Characteristics of Sitka Spruce.*

Gardiner, B. A. 1995. The Interactions of Wind and Tree Movement in Forest Canopies. *In:* Coutts, M. P. & Grace, J. (eds.) *Wind and Trees.* Cambridge: Cambridge University Press.

Gartner, B. L. 1995. Patterns of Xylem Variation within a Tree and Their Hydraulic and Mechanical Consequences. *In:* Gartner, B. L. (ed.) *Physiological Ecology Series; Plant Stems: Physiology and Functional Morphology.*

Gartner, B. L., Robbins, J. M. & Newton, M. 2005. Effects of Pruning on Wood Density and Tracheid Length in Young Douglas-Fir. *Wood and Fiber Science,* 37, 304-313.

Gaspar, F., Lopes, J., Cruz, H., Schwanninger, M. & Rodrigues, J. 2009. Application of near Infrared Spectroscopy and Multivariate Data Analysis for the Evaluation of Glue Lines of Untreated and Copper Azole Treated Laminated Timber before and after Ageing. *Polymer Degradation and Stability,* 94, 1061-1071.

Gierlinger, N., Goswami, L., Schmidt, M., Burgert, I., Coutand, C., Rogge, T. & Schwanninger, M. 2008. In Situ Ft-Ir Microscopic Study on Enzymatic Treatment of Poplar Wood Cross-Sections. *Biomacromolecules,* 9, 2194-2201.

Gierlinger, N., Schwanninger, M., Reinecke, A. & Burgert, I. 2006. Molecular Changes During Tensile Deformation of Single Wood Fibers Followed by Raman Microscopy. *Biomacromolecules,* 7, 2077-2081.

Gilchrist, K. 2011. Promoting Wellbeing through Environment: The Role of Urban Forestry. *Urban Tree Research Conference: Trees, People and the Built Environment.* Birmingham: Institute of Chartered Foresters.

Gilman, E. 2003. Branch-to-Stem Diameter Ratio Effects Strength of Attachment. *Journal of Arboriculture,* 29, 291-293.

Godara, A., Raabe, D., Bergmann, I., Putz, R. & Muller, U. 2009. Influence of Additives on Global Mechanical Behavior and Microscopic Strain Localization in Wood Reinforced Polypropylene Composites During Tensile Deformation Investigated Using Digital Image Correlation. *Composites Science and Tecnology,* 69, 139-146.

Gorner, F., Mattheck, C., Morawietz, P. & Munz, D. 1985. Limitations of the Petroski-Achenbach Crack Opening Displacement Approximation for the Calculation of Weight-Functions. *Engineering Fracture Mechanics,* 22, 269-277.

Goswami, L., Dunlop, J. W. C., Jungnikl, K., Eder, M., Gierlinger, N., Coutand, C., Jeronimidis, G., Fratzl, P. & Burgert, I. 2008a. Stress Generation in the Tension Wood of Poplar Is Based on the Lateral Swelling Power of the G-Layer. *Plant Journal,* 56, 531-538.

Goswami, L., Eder, M., Gierlinger, N. & Burgert, I. 2008b. Inducing Large Deformation in Wood Cell Walls by Enzymatic Modification. *Journal of Materials Science,* 43, 1286-1291.

Goulet, J., Messier, C. & Nikinmaa, E. 2000. Effect of Branch Position and Light Availability on Shoot Growth of Understory Sugar Maple and Yellow Birch Saplings. *Canadian Journal of Botany-Revue Canadienne De Botanique,* 78, 1077-1085.

Grabe, H. 2009. Track Deflection Measurement. *Civil Engineering,* 17, 18-22.

Grebner, H. & Mattheck, C. 1985. Stress Intensity Factors for Complete Circumferential Surface Cracks at the Outer Wall of a Pipe Loaded by Stress Gradients. *Nuclear Engineering and Design,* 88, 327-331.

Greer, L., Pemberton, S. & Chong Tan, J. 2009. *The Structure and Mechanical Behaviour of Wood* [Online]. Available: http://www.doitpoms.ac.uk/tlplib/wood/printall.php [Accessed 22 October 2009].

Grekin, M. & Surini, T. 2008. Shear Strength and Perpendicular-to-Grain Tensile Strength of Defect-Free Scots Pine Wood from Mature Stands in Finland and Sweden. *Wood Science and Technology,* 42, 75-91.

Guggenmoos, S. 2003. Effects of Treemortality on Power Line Security. *journal of Arboriculture,* 29, 181-196.

Bibliography

Guitard, D. G. E. & Castera, P. 1995. Experimental Analysis and Mechanical Modelling of Wind-Induced Tree Sways. *In:* Coutts, M. P. & Grace, J. (eds.) *Wind and Trees.* Cambridge: Cambridge University Press.

Gurevitch, J., Scheiner, S. & Fox, G. 2002. *The Ecology of Plants,* Sunderland, Massachusetts, USA, Sinauer Associates, Inc. Publishers.

Habel, R., Kusternig, A. & Wimmer, M. 2009. Physically Guided Animation of Trees. *Computer Graphics Forum,* 28**,** 523-532.

Hagedorn, M., Platt, I. G., Woodhead, I. M. & Ieee 2009. *Timber Characterisation Using a Non-Invasive Tdr Sensor.*

Hammel, J. W., Vonbodisco, U. & Mattheck, C. 1981. An Elastic-Plastic Finite-Element Analysis of a Ct Fracture Specimen. *Computers & Structures,* 13**,** 757-770.

Hamza, O., Bengough, A., Bransby, M., Davies, M. & Hallet, P. 2006. Biomechanics of Plant Roots: Estimating Localised Deformation with Particle Image Velocimetry. *Biosystems Engineering,* 94**,** 119-132.

Harris, R. 1983. Summer Branch Drop. *Journal of Arboriculture,* 9**,** 111-113.

Hassinen, A., Lemettinen, M., Peltola, H., Kellomaki, D. & Gardiner, B. A. 1998. A Prism-Based System for Monitoring the Swaying of Trees under Wind Loading. *Agricultural & Forest Meteorolog,* 90**,** 187-194.

Haubenre.W, Loser, W., Mattheck, C., Mockel, K. H. & Steinbei.E 1974. Co3o4 as a Model Substance for Thermistor Effect Switching in Coplanar Thin-Film Devices. *Physica Status Solidi a-Applied Research,* 22**,** 427-434.

Hauer, R., Wang, W. & Dawson, J. 1993 Ice Storm Damage to Urban Trees. *Journal of Arboriculture,* 19**,** 187-194.

Head, P. 2008. Entering the Ecological Age: The Engineer's Role. *The Institution of Civil Engineers - The Brunel Lecture 2008.* The Institution of Civil Engineers.

Hearmon, R. F. S. 1948. The Elasticity of Wood. London: Forest Products Research.

Heath and Safety Excutive. 2007. *Lac 23-22: Management of the Risk from Falling Trees* [Online]. Available: http://www.hse.gov.uk/lau/lacs/23-22.htm [Accessed 2 February 2011].

Heilmann, L., Grebner, H., Mattheck, C. & Ludwig, H. 1979. Mathematical, Clinical, and Laboratory Study of Hemodynamic-Changes in the Placental Circulation. *Archives of Gynecology,* 227**,** 303-313.

Heilmann, L., Mattheck, C. & Kurz, E. 1977a. Changes in Blood Rheology and Their Influence on Oxygen Diffusion in Normal and Pathological Pregnancies. *Archiv Fur Gynakologie,* 223**,** 283-298.

Heilmann, L., Mattheck, C., Pruhs, D. & Ludwig, H. 1977b. Reflection on Oxygen Diffusion of Terminal Villus of Human Placenta. *Archiv Fur Gynakologie,* 223**,** 333-344.

Heilmann, L., Mattheck, C. & Wiemer, W. 1977c. Consideration of Hemodynamics in Intervillous Space of Placenta. *Zeitschrift Fur Geburtshilfe Und Perinatologie,* 181**,** 193-198.

Heilmann, L., Mattheck, C., Wiemer, W. & Ludwig, H. 1977d. Mathematical-Model for Description of Oxygen-Diffusion in Intervillous Space of Human Placenta. *Archiv Fur Gynakologie,* 222**,** 353-366.

Hein, S. 2008. Knot Attributes and Occlusion of Naturally Pruned Branches of Fagus Sylvatica. *Forest Ecology and Management,* 256**,** 2046-2057.

Hein, S., Weiskittel, A. R. & Kohnle, U. 2008a. Branch Characteristics of Widely Spaced Douglas-Fir in South-Western Germany: Comparisons of Modelling Approaches and Geographic Regions. *Forest Ecology and Management,* 256**,** 1064-1079.

Hein, S., Weiskittel, A. R. & Kohnle, U. 2008b. Effect of Wide Spacing on Tree Growth, Branch and Sapwood Properties of Young Douglas-Fir Pseudotsuga Menziesii (Mirb.) Franco in South-Western Germany. *European Journal of Forest Research,* 127**,** 481-493.

Heinonen, T., Pukkala, T., Ikonen, V. P., Peltola, H., Venalainen, A. & Dupont, S. 2009. Integrating the Risk of Wind Damage into Forest Planning. *Forest Ecology and Management,* 258**,** 1567-1577.

Heitzer, J. & Mattheck, C. 1989. Fem-Calculation of the Stress Intensity Factors of a Circular Arc Crack under Uniaxial Tension. *Engineering Fracture Mechanics,* 33**,** 91-104.

Helliwell 2004, A. D. O. T. F. O. W. F., Arboricultural Journal, 27, 245-249.

Hempel, D., Kunze, K. H. & Mattheck, C. 1987. Structural-Analysis of the Y-Nail and a Design with Improved Fatigue Resistance. *Chirurg,* 58**,** 755-758.

Heuret, P., Guedon, Y., Guerard, N. & Barthelemy, D. 2003. Analysing Branching Pattern in Plantations of Young Red Oak Trees (Quercus Rubra L., Fagaceae). *Annals of Botany,* 91**,** 479-492.

Honkanen, T. & Haukioja, E. 1994. Why Does a Branch Suffer More after Branch-Wide Than after Tree-Wide Defoliation. *Oikos,* 71**,** 441-450.

Horn, H. 1971. *The Adaptive Geometry of Trees,* New Jersey, USA, Princeton University press.

Hu, S. J., Fujimoto, T. & Chiba, N. 2009. Pseudo-Dynamics Model of a Cantilever Beam for Animating Flexible Leaves and Branches in Wind Field. *Computer Animation and Virtual Worlds,* 20**,** 279-287.

Bibliography

Hu, X. Y., Tao, W. M. & Guo, Y. M. 2008. Using Fem to Predict Tree Motion in a Wind Field. *Journal of Zhejiang University-Science A,* 9**,** 907-915.

Huber, H. & Mattheck, C. 1988. Computer-Simulation of the Knee Kinematics for Different Fixation Types of the Cruciate Ligaments and Their Prosthetical Substitute. *Journal of Biomechanics,* 21**,** 857-857.

Huberbetzer, H., Brown, T. D. & Mattheck, C. 1990. Some Effects of Global Joint Morphology on Local Stress Aberrations near Imprecisely Reduced Intraarticular Fractures. *Journal of Biomechanics,* 23**,** 811-822.

I-Tree. 1999. *I-Tree - Tools for Assessing and Managing Community Forests* [Online]. Available: http://www.itreetools.org/ [Accessed 21 August 2011].

Institue of Chartered Foresters. Year. Trees, People and the Built Environment. *In:* Trees, People and the Built Environment, 2011 Birmingham. Forestry Commission.

Jaffe, M. J. 1973. Thigmomorphogenesis: The Response of Plant Growth and Development to Mechanical Stimulation *Planta,* 114**,** 143-157.

James, K. 2003. Dynamic Loading of Trees. *Journal of Arboriculture,* 29**,** 165-171.

James, K., Hallam, C. & Spencer, C. 2013a. Measuring Tilt of Tree Structural Root Zones under Static and Wind Loading. *Agricultural and Forest Meteorology,* 168**,** 160-167.

James, K., Hallam, C. & Spencer, C. 2013b. Tree Stability in Winds: Measurements of Root Plate Tilt. *Biosystems Engineering,* 115**,** 324-331.

James, K. R. 2010. *A Dynamic Structural Analysis of Trees Subject to Wind Loading.* Doctor of Philosophy, The University of Melbourne.

James, K. R., Haritos, N. & Ades, P. K. 2006. Mechanical Stability of Trees under Dynamic Loads. *American Journal of Botany,* 93**,** 1522-1530.

James, K. R. & Kane, B. 2008. Precision Digital Instruments to Measure Dynamic Wind Loads on Trees During Storms. *Agricultural and Forest Meteorology,* 148**,** 1055-1061.

Jena, A. & Krishna Gupta, K. 2009. Effects of Compressive Stress on Pore Volume of Nonwovens. Ithaca, New York: Porous Materials, Inc.

Jeong, G. Y., Zink-Sharp, A. E. & Hindman, D. P. 2009. Tensile Properties of Earlywood and Latewood from Loblolly Pine (Pinus Taeda) Using Digital Image Correlation. *Wood and Fiber Science,* 41**,** 51-63.

Jungnikl, K., Goebbels, J., Burgert, I. & Fratzl, P. 2009. The Role of Material Properties for the Mechanical Adaptation at Branch Junctions. *Trees-Structure and Function,* 23**,** 605-610.

Jungnikl, K., Koch, G. & Burgert, I. 2008a. A Comprehensive Analysis of the Relation of Cellulose Microfibril Orientation and Lignin Content in the S2 Layer of Different Tissue Types of Spruce Wood (Picea Abies (L.) Karst.). *Holzforschung,* 62**,** 475-480.

Jungnikl, K., Paris, O., Fratzl, P. & Burgert, I. 2008b. The Implication of Chemical Extraction Treatments on the Cell Wall Nanostructure of Softwood. *Cellulose,* 15**,** 407-418.

Kamimura, K. & Shiraishi, N. 2007. A Review of Strategies for Wind Damage Assessment in Japanese Forests. *Journal of Forest Research,* 12**,** 162-176.

Kane, B. 2007. Branch Strength of Bradford Pear (Pyrus Calleryana Var. 'Bradford'). *Arboriculture and Urban Forestry,* 33**,** 283-291.

Kane, B., Dennis, H. & Ryan, P. 2008a. How Strong Is That Branch You've Tied-in To? *Arborist News.* Champaign, IL: International Society of Arboriculture.

Kane, B., Farrell, R., Zedaker, S., Loferski, J. & Smith, D. 2008b. Failure Mode and Prediction of Strength of Branch Attachments. *Arboriculture and Urban Forestry,* 34**,** 308-316.

Kappel, R. & Mattheck, C. 2003. Inspection of Timber Construction by Measuring Drilling Resistance Using Resistograph F300-S. *In:* Brebbia, C. A. (ed.) *Structural Studies, Repairs and Maintenance of Heritage Architecture Viii.*

Kappel, R., Mattheck, C., Bethge, K. & Tesari, I. 2004. Bamboo as a Composite Structure and Its Mechanical Failure Behaviour. *In:* Collins, M. & Brebbia, C. A. (eds.) *Design and Nature Ii: Comparing Design in Nature with Science and Engineering.*

Kato, A. & Nakatani, H. 2000. Deflection and Resistance Performance of Tree Stems Subjected to Snowloads in Sugi Stands *Forest Ecology and Management,* 135**,** 83-96.

Keckes, J., Burgert, I., Fruhmann, K., Muller, M., Kolln, K., Hamilton, M., Burghammer, M., Roth, S. V., Stanzl-Tschegg, S. & Fratzl, P. 2003. Cell-Wall Recovery after Irreversible Deformation of Wood. *Nature Materials,* 2**,** 810-814.

Kellomaki, S., Ikonen, V. P., Peltola, H. & Kolstrom, T. 1999. Modelling the Structural Growth of Scots Pine with Implications for Wood Quality. *Ecological Modelling,* 122**,** 117-134.

Kelly, A. 2011. Who Really Benefits from China's Trade with Latin America? *Guardian*, 16 February 2011.

Bibliography

Kerzenmacher, T. & Gardiner, B. A. 1998. A Mathematical Model to Describe the Dynamic Response of a Spruce Tree to the Wind. *Trees,* 12**,** 385–394.

Keunecke, D., Eder, M., Burgert, I. & Niemz, P. 2008. Micromechanical Properties of Common Yew (Taxus Baccata) and Norway Spruce (Picea Abies) Transition Wood Fibers Subjected to Longitudinal Tension. *Journal of Wood Science,* 54**,** 420–422.

Koizumi, A. & Hirai, T. 2006. Evaluation of the Section Modulus for Tree-Stem Cross Sections of Irregular Shape. *Journal of Wood Science,* 52**,** 213–219.

Kollman, F. F. P. & Côté, W. 1968. *Principles of Wood Science and Technology,* London;Berlin, George Allen &Unwin; Springer.

Kotler, P. 1973. Atmospherics as a Marketing Tool. *Journal of Retailing,* 49**,** 48–64.

Kramer, E. M. 2006. Wood Grain Pattern Formation: A Brief Review. *Journal of Plant Growth Regulation,* 25**,** 290–301.

Kramer, E. M. & Borkowski, M. H. 2004. Wood Grain Patterns at Branch Junctions: Modeling and Implications. *Trees-Structure and Function,* 18**,** 493–500.

Kriechbaum, R., Schafer, J. & Mattheck, C. 1992a. Caio (Computer-Aided Internal Optimization) – a Powerful Method to Optimize Fiber Arrangement in Composite-Materials. *In:* Culshaw, B., Gardiner, P. T. & Mcdonach, A. M. (eds.) *First European Conference on Smart Structures and Materials.*

Kriechbaum, R., Schäfer, J. & Mattheck, C. Year. Caio – Computer Aided Internal Optimization *In:* 1st European Conference on Smart structures and materials, 1992b Glasgow. 281–284.

Kubler, H. 1991. Function of Spiral Grain in Trees. *Trees Structure and Function,* 5**,** 125–135.

Kull, O., Broadmeadow, M., Kruijt, B. & Meir, P. 1999. Light Distribution and Foliage Structure in an Oak Canopy. *Trees-Structure and Function,* 14**,** 55–64.

Kykersnowman, T. D. & Wilson, B. F. 1988. Total Wood, Sapwood, and Heartwood in Branch Bases of 3 Conifers. *Canadian Journal of Forest Research-Revue Canadienne De Recherche Forestiere,* 18**,** 1332–1336.

Lacointe, A., Deleens, E., Ameglio, T., Saint-Joanis, B., Lelarge, C., Vandame, M., Song, G. C. & Daudet, F. A. 2004. Testing the Branch Autonomy Theory: A C-13/C-14 Double-Labelling Experiment on Differentially Shaded Branches. *Plant Cell and Environment,* 27**,** 1159–1168.

Landsberg, J., J,. , Blanchard, T. W. & Warrit, B. 1976. Studies on the Movement of Water through Apple Trees. *Journal of Experitnental Botany,* 11, 579–596.

Lang, R. & Kaliske, M. 2013. Description of Inhomogeneities in Wooden Structures: Modelling of Branches. *Wood Science and Technology,* 47, 1051–1070.

Lanner, R. M. 2002. Why Do Trees Live So Long? *Ageing Research Reviews,* 1, 653–671.

Lavers, G. M. 1967. *The Strength Properties of Timber,* Aylesbury, BRE publications.

Ledermann, M., Tesari, I. & Mattheck, C. 2001. Cao-Shape Optimisation of a Fillet with a Complex, Time Dependent Loading. *In:* Hernandez, S. & Brebbia, C. A. (eds.) *Computer Aided Optimum Design of Structures Vii.*

Leiser, A. T. & Kemper, J. D. 1973. Analysis of Stress Distribution in the Sapling Tree Trunk. *journal of American Society of Horticulture,* 98, 164–170.

Leu, L. J., Huang, C. W. & Chou, J. J. 2003. Topology Optimization of Elastic-Plastic Structures. *Chinese Journal of Mechanics-Series A,* 19, 431–442.

Liang, O. Q. 2007. Performance-Based Optimization: A Review. *Advances in Structural Engineering,* 10, 739–753.

Liang, Q. Q. & Ng, A. W. M. 2008. Performance-Based Optimization of Strut-and-Tie Models in Reinforced Concrete Deep Beams. *In:* Xie, Y. M. & Patnaikuni, I. (eds.) *Innovations in Structural Engineering and Construction, Vols 1 and 2.*

Lilly, S. & Syndor, T. 1995. Comparison of Branch Failure During Staticloading of Silver and Norway Maples. *journal of Arboriculture,* 21, 302–305.

Lin, C. J., Tsai, M. J., Lee, C. J., Wang, S. Y. & Lin, L. D. 2007. Effects of Ring Characteristics on the Compressive Strength and Dynamic Modulus of Elasticity of Seven Softwood Species. *Holzforschung,* 61, 414–418.

Liu, J. Y. & Ross, R. J. 2005. Relationship between Radial Compressive Modulus of Elasticity and Shear Modulus of Wood. *Wood and Fiber Science,* 37, 201–206.

Liu, L. Q., Eder, M., Burgert, I., Tasis, D., Prato, M. & Wagner, H. D. 2007. One-Step Electrospun Nanofiber-Based Composite Ropes. *Applied Physics Letters,* 90.

Ljungdahl, J., Berglund, L. A. & Burman, M. 2006. Transverse Anisotropy of Compressive Failure in European Oak – a Digital Speckle Photography Study. *Holzforschung,* 60, 190–195.

Lobutova, E., Resagk, C. & Putze, T. 2010. Investigation of Large-Scale Circulations in Room Air Flows Using Three-Dimensional Particle Tracking Velocimetry. *Building and Environment,* 45, 1653–1662.

Bibliography

Lonsdale, D. 1999. *Principles of Tree Hazard Assessment and Management,* London, TSO.

Loser, W. & Mattheck, C. 1973. Theory of Thermal Switching Behavior of a Ptc-Resistor Device. *Physica Status Solidi a-Applied Research,* 18, 247-254.

Loser, W., Mattheck, C. & Haubenre.W 1974a. Influence of Intrinsic Thermistor Effect in Vo2 Coplanar Switching Devices. *Physica Status Solidi a-Applied Research,* 21, 487-496.

Loser, W., Mattheck, C. & Haubenre.W 1974b. Thermal Switching Behavior of Co3o4 Thin-Films. *Physica Status Solidi a-Applied Research,* 22, 65-73.

Lundstrom, T., Jonsson, M. J. & Kalberer, M. 2007. The Root-Soil System of Norway Spruce Subjected to Turning Moment: Resistance as a Function of Rotation. *Plant and Soil,* 300, 35-49.

Macdaniels, L. H. 1923. The Apple-Tree Crotch.Bulletin 419. Ithaca, NY: Cornell University Agricultural Experiment Station.

Maguire, D. A. & Hann, D. W. 1987. A Stem Dissection Technique for Dating Branch Mortality and Reconstructing Past Crown Recession. *Forest Science,* 33, 858-871.

Makinen, H. 1996. Effect of Intertree Competition on Branch Characteristics of Pinus Sylvestris Families. *Scandinavian Journal of Forest Research,* 11, 129-136.

Makinen, H. & Colin, F. 1999. Predicting the Number, Death, and Self-Pruning of Branches in Scots Pine. *Canadian Journal of Forest Research-Revue Canadienne De Recherche Forestiere,* 29, 1225-1236.

Marks, C. O. & Lechowicz, M. J. 2006. A Holistic Tree Seedling Model for the Investigation of Functional Trait Diversity. *Ecological Modelling,* 193, 141-181.

Marsal, J., Lopez, G., Mata, M. & Girona, J. 2006. Branch Removal and Defruiting for the Amelioration of Water Stress Effects on Fruit Growth During Stage Iii of Peach Fruit Development. *Scientia Horticulturae,* 108, 55-60.

Mathieu, A., Cournede, P. H., Letort, V., Barthelemy, D. & De Reffye, P. 2009. A Dynamic Model of Plant Growth with Interactions between Development and Functional Mechanisms to Study Plant Structural Plasticity Related to Trophic Competition. *Annals of Botany,* 103, 1173-1186.

Mattheck, C. 1972a. Calculation of a Thermally Produced Current-Voltage Characteristic of N-Type. *Physica Status Solidi a-Applied Research,* 12, K115-&.

Mattheck, C. 1972b. Influence of a High-Conducting Bubble in Vo2 Switching Devices. *Physica Status Solidi a-Applied Research,* 11, K117-&.

Mattheck, C. 1988. The Jointed Bow, a New High-Energy Bow and Arrow. *Zeitschrift Fur Angewandte Mathematik Und Mechanik,* 68, T218-T219.

Mattheck, C. 1990a. Design and Growth Rules for Biological Structures and Their Application to Engineering. *Fatigue & Fracture of Engineering Materials & Structures,* 13, 535-550.

Mattheck, C. 1990b. Engineering Components Grow Like Trees. *Materialwissenschaft und Werkstofftech,* 21, 143-168.

Mattheck, C. 1990c. *A New Method for the 2d-Shape and 3d-Shape Optimization of Engineering Structures.*

Mattheck, C. 1991. *Trees - the Mechanical Design,* Berlin, Springer - Verlag.

Mattheck, C. 1994a. *The Body Language of Trees,* London, HMSO Publications Centre.

Mattheck, C. 1994b. Design in Nature. *Interdisciplinary Science Reviews,* 19, 298-314.

Mattheck, C. 1998. *Design in Nature: Learning from Trees,* Berlin, Springer-Verlag.

Mattheck, C. 2000. Comments on "Wind-Induced Stresses in Cherry Trees: Evidence against the Hypothesis of Constant Stress Levels" by K.J. Niklas, H.-C. Spatz, Trees (2000) 14 : 230-237. *Trees-Structure and Function,* 15, 63-63.

Mattheck, C. 2006. Teacher Tree: The Evolution of Notch Shape Optimization from Complex to Simple. *Engineering Fracture Mechanics,* 73, 1732-1742.

Mattheck, C. 2007. *Secret Design Rules of Nature,* Karlsruhe, Forschungszentrum Karlsruhe GMBH.

Mattheck, C., Albrecht, W., Dietrich, F. & Kriechbaum, R. 1994a. The Biomechanics of Rays in Trees. *Allgemeine Forst Und Jagdzeitung,* 165, 143-147.

Mattheck, C. & Baumgartner, A. 1992. Cao and Sko - Fatigue-Resistant Engineering Design by Simulation of Biological Optimization Mechanisms. *In:* Little, E. G. (ed.) *Experimental Mechanics : Technology Transfer between High Tech Engineering and Biomechanics.*

Mattheck, C., Baumgartner, A., Kriechbaum, R. & Walther, F. 1993a. Computational Methods for the Understanding of Biological Optimization Mechanisms. *Computational Materials Science,* 1, 302-312.

Mattheck, C., Baumgartner, A. & Verein Deut, I. 1992a. Fatigue Prevention by Shape Optimization Based on Biological Growth. *Risk Minimization by Experimental Mechanics : Imeko / Gesa Symposium.*

Bibliography

Mattheck, C., Beller, M. & Schafer, J. 1991a. *2d-Shape-Optimization and 3d-Shape-Optimization Based on Biological Growth*.

Mattheck, C. & Bethge, K. 1990. Wind Breakage of Trees Initiated by Root Delamination. *Trees-Structure and Function,* 4**,** 225-227.

Mattheck, C. & Bethge, K. 1998. The Structural Optimization of Trees. *Naturwissenschaften,* 85**,** 1-10.

Mattheck, C. & Bethge, K. 2000. Simple Mathematical Approaches toTree Biomechanics. *Arboricultural Journal,* 24**,** 307-326.

Mattheck, C. & Bethge, K. 2005. On the Plausibility of the Method of Tensile Triangles (Mtt). *Materialwissenschaft Und Werkstofftechnik,* 36**,** 748-749.

Mattheck, C., Bethge, K. & Albrecht, W. A. 1995. Failure Modes of Trees and Related Failure Criteria. *In:* Coutts, M. P. & Grace, J. (eds.) *Wind and Trees.* Cambridge: Cambridge University Press.

Mattheck, C., Bethge, K. & Erb, D. 1993b. Failure Criteria for Trees. *Arboricultural Journal,* 17**,** 201-209.

Mattheck, C., Bethge, K. & Erb, D. 1993c. Failure Criteria for Trees. *Allgemeine Forst Und Jagdzeitung,* 164**,** 9-12.

Mattheck, C., Bethge, K., Erb, D. & Blomer, W. 1992b. Successful Shape Optimization of a Pedicular Screw. *Medical & Biological Engineering & Computing,* 30**,** 446-448.

Mattheck, C., Bethge, K., Sauer, A., Sorensen, J., Wissner, C. & Kraft, O. 2009. About Cracks, Dunce Caps and a New Way to Stop Cracks. *Fatigue & Fracture of Engineering Materials & Structures,* 32**,** 484-492.

Mattheck, C., Bethge, K. & Schafer, J. 1993d. Safety Factors in Trees. *Journal of Theoretical Biology,* 165**,** 185-189.

Mattheck, C., Bethge, K. & Tesari, I. 2006a. Shear Effects on Failure of Hollow Trees. *Trees-Structure and Function,* 20**,** 329-333.

Mattheck, C., Bethge, K., Tesari, I., Scherrer, M. & Kraft, O. 2004. Is There a Universal Optimum Notch Shape? *Materialwissenschaft Und Werkstofftechnik,* 35**,** 582-586.

Mattheck, C., Bethge, K. & West, P. W. 1994b. Breakage of Hollow Tree Stems. *Trees-Structure and Function,* 9**,** 47-50.

Mattheck, C. & Breloer, H. 1991. Wie Bricht Ein Baum? (How a Tree Breaks?). *Gartenamt,* 40**,** 746-748.

Mattheck, C. & Breloer, H. 1992. Root Cross-Sections Tell the Load History. *Allgemeine Forst Und Jagdzeitung,* 163**,** 142-145.

Mattheck, C., Breloer, H. & Verein Deut, I. 1992c. The Mechanical Failure of Trees. *Risk Minimization by Experimental Mechanics : Imeko / Gesa Symposium.*

622

Mattheck, C. & Burkhardt, S. 1987. Fracture-Mechanics of Cracks Originating from Holes Treated for Notch Stress Relieving. *Zeitschrift Fur Werkstofftechnik-Materials Technology and Testing,* 18, 111-116.

Mattheck, C. & Burkhardt, S. 1990. A New Method of Structural Shape Optimization Based on Biological Growth. *International Journal Fatigue,* 12, 185-190.

Mattheck, C. & Burkhardt, S. 1991. The Hazard Beam - Biomechanics of an Internal Failure Mechanism of Trees. *Allgemeine Forst Und Jagdzeitung,* 162, 170-174.

Mattheck, C., Burkhardt, S. & Erb, D. 1992d. Shape Optimization of Engineering Components by Simulation of Biological Growth. *In:* Jono, M. & Inoue, T. (eds.) *Mechanical Behaviour of Materials-Vi, Vols 1-4.*

Mattheck, C. & Erb, D. 1991. Shape Optimization of a Rubber Bearing. *International Journal of Fatigue,* 13, 206-208.

Mattheck, C., Erb, D., Bethge, K. & Begemann, U. 1992e. 3-Dimensional Shape Optimization of a Bar with a Rectangular Hole. *Fatigue & Fracture of Engineering Materials & Structures,* 15, 347-351.

Mattheck, C., Gerhardt, H. & Breloer, H. 1992f. Vta - Visual Tree Defect Assessment Based on Computer-Simulation of Adaptive Growth. *In:* Little, E. G. (ed.) *Experimental Mechanics : Technology Transfer between High Tech Engineering and Biomechanics.*

Mattheck, C. & Harzheim, L. 1991. Effect of Loading on the Optimized Shape of a Kinked Bar. *Materialwissenschaft Und Werkstofftechnik,* 22, 236-244.

Mattheck, C. & Huberbetzer, H. 1989. The Baud-Curve - a General Design Principle for Biological Load Carriers. *Allgemeine Forst Und Jagdzeitung,* 160, 194-200.

Mattheck, C. & Huberbetzer, H. 1991. *Cao - Computersimulation of Adaptive Growth in Bones and Trees.*

Mattheck, C., Huberbetzer, H. & Borner, M. 1991b. A New Drilling Device and New Anchors for the Fixation of Prosthetic Cruciate Ligaments to the Femur. *Biomedizinische Technik,* 36, 20-23.

Mattheck, C., Huberbetzer, H. & Keilen, K. 1990a. Notch Stresses at Branch Holes as Stimulation of the Wound-Healing of Trees. *Allgemeine Forst Und Jagdzeitung,* 161, 47-53.

Mattheck, C., Kappel, R. & Kraft, O. 2008a. Meaning of the 45 Degrees-Angle in Mechanical Design According to Nature. *In:* Brebbia, C. A. (ed.) *Design and Nature Iv: Comparing Design in Nature with Science and Engineering.*

Mattheck, C. & Kubler, H. 1997. *Wood-the Internal Optimization of Trees,* Berlin, Springer-Verlag.

Bibliography

Mattheck, C. & Moldenhauer, H. 1987. Mode-Extraction from Mixed-Mode Analysis of Cracks by Special Filter-Technique. *International Journal of Fracture,* 34, 209-218.

Mattheck, C. & Moldenhauer, H. 1990. An Intelligent Cad-Method Based on Biological Growth. *Fatigue & Fracture of Engineering Materials & Structures,* 13, 41-51.

Mattheck, C., Morawietz, P. & Munz, D. 1983a. Stress Intensity Factor at the Surface and at the Deepest Point of a Semi-Elliptical Surface Crack in Plates under Stress Gradients. *International Journal of Fracture,* 23, 201-212.

Mattheck, C., Morawietz, P. & Munz, D. 1985a. Calculation of the Stress Intensity Factor of a Circumferential Crack in a Tube Originating from a Hole under Axial Tensile and Bending Loads. *Engineering Fracture Mechanics,* 22, 645-650.

Mattheck, C., Morawietz, P. & Munz, D. 1985b. Stress Intensity Factors of Sickle-Shaped Cracks in Cylindrical-Bars. *International Journal of Fatigue,* 7, 45-47.

Mattheck, C., Morawietz, P., Munz, D. & Stamm, H. 1984a. Comparison of Different Methods for the Determination of Stress Intensity Factors of Cracks in Pipes with Stress Gradients. *Journal of Pressure Vessel Technology-Transactions of the Asme,* 106, 209-213.

Mattheck, C., Morawietz, P., Munz, D. & Wolf, B. 1984b. Ligament Yielding of a Plate with Semi-Elliptical Surface Cracks under Uniform Tension. *International Journal of Pressure Vessels and Piping,* 16, 131-143.

Mattheck, C. & Munz, D. 1982. Bending Failure by Flattening of Circumferentially Cracked Pipes. *Nuclear Engineering and Design,* 67, 165-168.

Mattheck, C., Munz, D. & Stamm, H. 1983b. Stress Intensity Factor for Semi-Elliptical Surface Cracks Loaded by Stress Gradients. *Engineering Fracture Mechanics,* 18, 633-641.

Mattheck, C. & Reuss, S. 1991. The Claw of the Tiger – an Assessment of Its Mechanical Shape Optimization. *Journal of Theoretical Biology,* 150, 323-328.

Mattheck, C., Sauer, A. & Kappel, R. 2006b. Reinforcement Ropes against Shear in Leaves. *In:* Brebbia, C. A. (ed.) *Design and Nature Iii: Comparing Design in Nature with Science and Engineering.*

Mattheck, C., Scherrer, M., Bethge, K. & Tesari, I. 2005. Shape Optimization: An Analytical Approach. *In:* Hernandez, S. & Brebbia, C. A. (eds.) *Computer Aided Optimum Design in Engineering Ix.*

Mattheck, C., Scherrer, M. & Tesari, I. 2003a. Notch Stresses Are Bending Stresses – What Are Good and Bad Notches? *Materialwissenschaft Und Werkstofftechnik,* 34**,** 427–429.

Mattheck, C., Scherrer, M., Tesari, I. & Kraft, O. 2003b. Shape Optimization without the Use of Fem: An Easy Approach for the Reduction of Stress Concentrations. *Materialwissenschaft Und Werkstofftechnik,* 34**,** 514–515.

Mattheck, C. & Schwarze, F. 1994. Xylem Rays as Disguised I-Bars within an Alternative Mechanical Wood Model. *Allgemeine Forst Und Jagdzeitung,* 165**,** 197–201.

Mattheck, C., Sorensen, J. & Bethge, K. 2006c. A Graphic Way for Notch Shape Optimization. *In:* Brebbia, C. A. (ed.) *Design and Nature Iii: Comparing Design in Nature with Science and Engineering.*

Mattheck, C. & Tesari, I. 2000. Design in Nature. *In:* Ibarraberastegi, G., Brebbia, C. A. & Zannetti, P. (eds.) *Development and Application of Computer Techniques to Environmental Studies Viii.*

Mattheck, C. & Tesari, I. 2002. Integrating Biological Optimisation Methods into Engineering Design Process. *In:* Brebbia, C. A., Sucharov, L. J. & Pascolo, P. (eds.) *Design and Nature: Comparing Design in Nature with Science and Engineering.*

Mattheck, C. & Tesari, I. 2003. Shear Bombs in Fibre Composites. *Materialwissenschaft Und Werkstofftechnik,* 34**,** 93–95.

Mattheck, C. & Tesari, I. 2004. The Mechanical Self-Optimisation of Trees. *In:* Collins, M. & Brebbia, C. A. (eds.) *Design and Nature Ii: Comparing Design in Nature with Science and Engineering.*

Mattheck, C. & Tesari, I. 2007. Hidden Design Rules in Nature. *Comparative Biochemistry and Physiology a-Molecular & Integrative Physiology,* 146**,** 11.

Mattheck, C., Tesari, I. & Bethge, K. 2003c. Roots and Buildings. *In:* Brebbia, C. A. (ed.) *Structural Studies, Repairs and Maintenance of Heritage Architecture Viii.*

Mattheck, C., Tesari, I., Sauer, A., Bethge, K. & Kraft, O. 2008b. A Simple Graphic Way to Reduce Stress Concentrations by Growth. *In:* Brebbia, C. A. (ed.) *Design and Nature Iv: Comparing Design in Nature with Science and Engineering.*

Mattheck, C., Teschner, M. & Schafer, J. 1997. Mechanical Control of Root Growth: A Computer Simulation. *Journal of Theoretical Biology,* 184**,** 261–269.

Mattheck, C. & Vorberg, U. 1991. The Biomechanics of Tree Fork Design. *Botanica Acta,* 104**,** 399–404.

Bibliography

Mattheck, C., Vorberg, U. & Kranz, C. 1990b. The Effect of the Hollow-Stem-Prosthesis on the Distribution of Stresses in the Cortical Bone. *Biomedizinische Technik,* 35, 316-319.

Mattheck, C. & Walther, F. 1991. A New Felling Technique to Avoid End Splitting of Logs. *Allgemeine Forst Und Jagdzeitung,* 162, 181-185.

Mattheck, C., Weber, K. & Gotz, K. 2000. How European Beeches Manage the Radial Tensile Forces. *Allgemeine Forst Und Jagdzeitung,* 171, 10-14.

Mattheck, C., Wissner, C., Bethge, K. & Kraft, O. 2008c. Fail Safe Design with Crack Stoppers and Warners. *In:* Brebbia, C. A. (ed.) *Design and Nature Iv: Comparing Design in Nature with Science and Engineering.*

Mcgee, E. J., Gallagher, D., Mitchell, P. I., Baillie, M., Brown, D. & Keogh, S. M. 2004. Recent Chronologies for Tree Rings and Terrestrial Archives Using C-14 Bomb Fallout History. *Geochimica Et Cosmochimica Acta,* 68, 2509-2516.

Mcmahon, T. A. & Kronauer, R. E. 1976. Trees Structure, Deducing the Principle of Mechanical Design. *Journal of Theoretical Biology,* 59, 443-446.

Mencuccini, M., Grace, J. & Fioravanti, M. 1997. Biomechanical and Hydraulic Determinants of Tree Structure in Scots Pine: Anatomical Characteristics. *Tree Physiology,* 17, 105-113.

Metzger, K. 1893. Der Wind Als Massgebender Faktor Fur Das Wachtsum Der Baume. *Mundener Forstiliche Hefte,* 3, 35-86.

Miller, V. Year. Crotch Influence on Strength and Breaking Point of Apple Tree Branches. *In:* Proceedings from the American Society of Horticultural Science, 1959. 27-32.

Milwich, M., Burgert, I., Seidl, R., Speck, T., Speck, O. & Planck, H. 2007. Plant Stems as Role Models for Structurally Optimized Biomimetic Composite Profiles with Gradient Structure. *Comparative Biochemistry and Physiology a-Molecular & Integrative Physiology,* 146, 9.

Mishnaevsky, L. & Qing, H. 2008. Micromechanical Modelling of Mechanical Behaviour and Strength of Wood: State-of-the-Art Review. *Computational Materials Science,* 44, 363-370.

Mittlmeier, T., Mattheck, C. & Dietrich, F. 1994. Effects of Mechanical Loading on the Profile of Human Femoral Diaphyseal Geometry. *Medical Engineering & Physics,* 16, 75-81.

Moldenhauer, H. & Mattheck, C. 1989. Approximate Calculation of Weight-Functions for Cracks under Mixed-Mode Loading. *International Journal of Fatigue,* 11, 193-198.

Moore, J. 2012. Growing Fit-for-Purpose Structural Timber What Is the Target and How Do We Get There? *New Zealand Journal of Forestry,* 57, 17-24.

Moore, J. R. 2000. Differences in Maximum Resistive Bending Moments of Pinus Radiata Trees Grown on a Range of Soil Types. *Forest Ecology and Management*

Moore, J. R., Gardiner, B. A., Blackburn, G. R. A., Brickman, A. & Maguire, D. A. 2005. An Inexpensive Instrument to Measure the Dynamic Response of Standing Trees to Wind Loading. *Agricultural and Forest Meteorology,* 132, 78-83.

Moore, J. R. & Maguire, D. A. 2004. Natural Sway Frequencies and Damping Ratios of Trees: Concepts, Review and Synthesis of Previous Studies. *Trees-Structure and Function,* 18, 195-203.

Moore, J. R. & Maguire, D. A. 2008. Simulating the Dynamic Behavior of Douglas-Fir Trees under Applied Loads by the Finite Element Method. *Tree Physiology,* 28, 75-83.

Moore, J. R., Tombleson, J. D., Turner, J. A. & Van Der Colff, M. 2008. Wind Effects on Juvenile Trees: A Review with Special Reference to Toppling of Radiata Pine Growing in New Zealand. *Forestry,* 81, 377-387.

Morawietz, P., Mattheck, C. & Munz, D. 1984. Application of the Method of Weight-Functions to Crack Problems for the Determination of Stress Intensity Factors Using Fe Calculations. *Zeitschrift Fur Angewandte Mathematik Und Mechanik,* 64, T144-T146.

Morawietz, P., Mattheck, C. & Munz, D. 1985. Calculation of Approximate Weight-Functions in Fracture-Mechanics by Fem. *International Journal for Numerical Methods in Engineering,* 21, 1487-1497.

Morgan, J. & Cannell, M. G. R. 1987. Structural-Analysis of Tree Trunks and Branches - Tapered Cantilever Beams Subject to Large Deflections under Complex Loading. *Tree Physiology,* 3, 365-374.

Morgan, J. & Cannell, M. G. R. 1988. Support Costs of Different Branch Designs - Effects of Position, Number, Angle and Deflection of Laterals. *Tree Physiology,* 4, 303-313.

Morgan, J. & Cannell, M. G. R. 1994. Shape of Tree Stems- a Re-Examination of the Uniform Stress Hypothesis. *Tree Physiology,* 14, 49-62.

Mortensen, L., Rode, C. & Peuhkuri, R. 2008. Investigation of Airflow Patterns in Microclimate by Particle Image Velocimetry (Piv). *Building and Environment,* 43, 1929-1938.

Muller, U., Gindl, W. & Jeronimidis, G. 2006a. Biomechanics of a Branch-Stem Junction in Softwood. *Trees (Berlin),* 20, 643-648.

Muller, U., Gindl, W. & Jeronimidis, G. 2006b. Biomechanics of a Branch-Stem Junction in Softwood. *Trees-Structure and Function,* 20, 643-648.

Bibliography

Muller, U., Joscak, T. & Teischinger, A. 2003. Strength of Dried and Re-Moistened Spruce Wood Compared to Native Wood. *Holz als Roh- und Werkstoff,* 61**,** 439-443.

Muller, U., Sretenovic, A., Gindl, W., Grabner, M., Wimmer, R. & Teischinger, A. 2004. Effects of Macro- and Micro-Structural Variability on the Shear Behavior of Softwood. *Iawa Journal,* 25**,** 231-243.

Mundell, C. 2009. *Large Scale Testing of Drystone Retaining Structures.* Doctor of Philosophy, University of Bath.

Munz, D. & Mattheck, C. 1982. Cross-Sectional Flattening of Pipes Subjected to Bending. *International Journal of Pressure Vessels and Piping,* 10**,** 421-429.

Munzinger, M., Kraft, O. & Mattheck, C. 2006. Computer Aided Adhesive and Assembly Optimization Method: Biomimetic Optimization of Adhesive Joints. *Journal of Materials Research,* 21**,** 2011-2017.

Munzinger, M. & Mattheck, C. 2005. Ca(3)O - a New Method of Adhesive Optimization Modeled on Nature. *Materialwissenschaft Und Werkstofftechnik,* 36**,** 320-324.

Nady, M. & Said, A. 2007. Measurement Methods of Moisture in Building Envelopes – a Literature Review. *International Journal of Architectural Heritage,* 1**,** 293-310.

Nakatani, H., Kato, A., Hasegawa, M., Aiura, H. & Iijima, Y. 1988. Structural Mechanics Study on the Damage of Tree Stems Caused by Accumulating in the Crown Iii. Distribution of Mechanical Properties in Tree Stem,. *Journal Toyama Forestry (Forest Product Research Center),* 1**,** 25-33.

Natural England. 1999. *Natural England – Green Infrastructure* [Online]. Natural England. Available: http://www.naturalengland.org.uk/ourwork/planningtransportlocalgov/greeninfrastructure/default.aspx [Accessed 21 August 2011 2011].

Neely, D. 1991. Water Transport at Stem Branch Junctures in Woody Angiosperms. *journal of arboriculture,* 17 285-290.

Neumetzler, L., Obel, N., Schwarz, T., Burgert, I. & Pauly, M. 2005. Rapid and Sensitive Structural Analysis of Polysaccharide Materials by Oligosaccharide Mass Profiling (Olimp). *Abstracts of Papers of the American Chemical Society,* 229**,** 048-CELL.

Nhs. 1999. *Trust Invests £750,000 in Stockport's Mental Health Facilities* [Online]. Pennine Care NHS Trust. Available: http://www.penninecare.nhs.uk/about/news/news-item/?doc=456 [Accessed 21 August 2011 2011].

Ni, Q., Hird, C. C. & Guymer, I. 2010. Physical Modelling of Pile Penetration in Clay Using Transparent Soil and Particle Image Velocimetry. *Geotechnique,* 60**,** 121–132.

Niklas, K. J. 1992. *Plant Biomechanics an Engineering Approach to Plant Form and Function,* Chicago, The university of Chicago Press.

Niklas, K. J. & Spatz, H. C. 1999. Methods for Calculating Factors of Safety for Plant Stems. *Journal of Experimental Biology,* 202**,** 3273–3280.

Niklas, K. J. & Spatz, H. C. 2006. Allometric Theory and the Mechanical Stability of Large Trees: Proof and Conjecture. *American Journal of Botany,* 93**,** 824–828.

Nowak, D., Hoehn, R. & Al., E. 2009. Assessing Urban Forest Effects and Values: Chicago's Urban Forest.

O'hara, K. L. 2007. Pruning Wounds and Occlusion: A Long-Standing Conundrum in Forestry. *Journal of Forestry,* 105**,** 131–138.

O'loinsigh, C., Oudjene, M., Ait-Aider, H., Fanning, P., Pizzi, A., Shotton, E. & Meghlat, E. M. 2012. Experimental Study of Timber-to-Timber Composite Beam Using Welded-through Wood Dowels. *Construction and Building Materials,* 36**,** 245–250.

Olsson, A. M., Salmen, L., Eder, M. & Burgert, I. 2007. Mechano-Sorptive Creep in Wood Fibres. *Wood Science and Technology,* 41**,** 59–67.

Ong, K. S. 1999. Comparison of Timber Drying Using Solar Energy, Electrical Heating and Dehumidifier. *Drying Technology,* 17**,** 999–1009.

Osgood-Jacobs, L. 2008. Fabrication of Synthetic Trees for the Investigation of Water at Negative Pressures. *Chemistry,* 2008 NNIN REU Research Accomplishments**,** 48–49.

Paatalo, M. L., Peltola, H. & Kellomaki, S. 1999. Modelling the Risk of Snow Damage to Forests under Short-Term Snow Loading. *Forest Ecology and Management,* 116**,** 51–70.

Padgham, C. A. 1975. *The Perception of Light and Colour,* London, G. Bell and sons.

Palaia, L., Monfort, J., Sánchez, R., Gil, L., Álvarez, Á., López, V., Tormo, S., Pérez, C. & Navarro, P. 2008. Assessment of Timber Structures in Service, by Using Combined Methods of Non-Destructive Testing Together with Traditional Ones. *9th International Conference on NDT of Art.* Jerusalem Israel.

Papesch, A. J. G. 1974. A Simplified Theoretical Analysis of the Factors That Influence Windthrow of Trees. *Fifth Australasian conference on hydraulic and fluid mechanics.* University of Canterbury, Christchurch, New Zealand.

Bibliography

Papesch, A. J. G., Moore, J. R. & Hawke, A. E. 1997. Mechanical Stability of Pinus Radiata Trees at Eyrewell Forest Investigated Using Static Tests. *New Zealand Journal of Forestry Science,* 27, 188-204.

Paris, O., Burgert, I. & Fratzl, P. 2010. Biomimetics and Biotemplating of Natural Materials. *Mrs Bulletin,* 35, 219-225.

Partnership for Urban South Hampshire (Push). 2010. *Green Infrastructure* [Online]. Available: http://www.push.gov.uk/work/sustainability-and-social-infrastructure/green-infrastructure.htm [Accessed 2011].

Passo, A., Puntieri, J. G. & Barthelemy, D. 2002. Trunk and Main-Branch Development in Nothofagus Pumilio (Nothofagaceae): A Retrospective Analysis of Tree Growth. *Canadian Journal of Botany-Revue Canadienne De Botanique,* 80, 763-772.

Pedro, A., Carlos, C., Henrique, L. & Julia, A. 2007. 3d Modeling and Section Properties of Ancient Irregular Timber Structures by Means of Digital Photogrammetry. *Computer -Aided Civil and Infrastructure Engineering,* 22, 597-611.

Peltola, H., Kellomaki, S., Hassinen, A. & Granander, M. 2000. Mechanical Stability of Scots Pine, Norway Spruce and Birch: An Analysis of Tree-Pulling Experiments in Finland. *Forest Ecology and Management,* 135, 143-153.

Peltola, H., Kellomaki, S., Vaisanen, H. & Ikonen, V. P. 1999. A Mechanistic Model for Assessing the Risk of Wind and Snow Damage to Single Trees and Stands of Scots Pine, Norway Spruce, and Birch. *Canadian Journal of Forest Research-Revue Canadienne De Recherche Forestiere,* 29, 647-661.

Peltola, H. M. 2006. Mechanical Stability of Trees under Static Loads. *American Journal of Botany,* 93, 1501-1511.

Perttunen, J., Sievanen, R., Nikinmaa, E., Salminen, H., Saarenmaa, H. & Vakeva, J. 1996. Lignum: A Tree Model Based on Simple Structural Units. *Annals of Botany,* 77, 87-98.

Petty, J. A. & Worrell, R. 1981. Stability of Coniferous Tree Stems in Relation to Damage by Snow. *Forestry,* 54, 115-128.

Pong, W. Y. 1956. Tree Breakage Characteristics under Static Loading of Several Hardwood Species. U.S. Department Agricultural Forestry Service.

Praus, L. & Horacek, P. 2005. Assessment of Tree Stability - the Mechanical Behaviour of a Tree. *Wood Research,* 50, 9-18.

Prusinkiewicz, P. 2004. Modeling Plant Growth Development. *Current Opinion in Plant Biology,* 7, 79-83.

Prusinkiewicz, P., Karwowski, R. & Lane, B. 2007. The L+C Plant-Modelling Language. *In:* Vos, J., Marcelis, L. F. M., Devisser, P. H. B., Struik, P. C. &

Evers, J. B. (eds.) *Functional-Structural Plant Modelling in Crop Production.*

Qu, H. C., Zhu, Q. S., Fu, H. G., Zeng, L. Q., Guo, M. W. & Lu, Z. H. 2010. Automatic L-System Discovery for Virtual Plants by Branching Pattern Analysis of Unfoliaged Trees. *Journal of Computational and Theoretical Nanoscience,* 7, 900-910.

Quine, C. P. 1995. Assessing the Risk of Wind Damage to Forests: Practice and Pitfalls. *In:* Coutts, M. P. & Grace, J. (eds.) *Wind and Trees.* Cambridge: Cambridge University Press.

Quine, C. P. & Gardiner, B. A. 2007. Understanding How the Interaction of Wind and Trees Results in Windthrow, Stem Breakage, and Canopy Gap Formation. *In:* Johnson, E. A. & Miyanishi, K. (eds.) *Plant Disturbance Ecology—the Process and the Response*

Raffel, M., Willert, C., Wereley, S. & Kompenhams, J. 2007. *Particle Image Velocimetry - a Practical Guide Second Edition,* Berlin, Springer-Verlag.

Rao, U., Fehn, U., Muramatsu, Y., Mcneil, H., Sharma, P. & Elmore, D. 2002. Tracing the History of Nuclear Releases: Determination of I-129 in Tree Rings. *Environmental Science & Technology,* 36, 1271-1275.

Rautalin, M., Uusitalo, J. & Pukkala, T. 2001. Estimation of Tree Stand Characteristics through Computer Visualisation. *Landscape and Urban Planning,* 53, 85-94.

Reames, R. 2005. *Arborsculpture: Solutions for a Small Planet,* Oregon, Arborsmith Studios.

Reiterer, A., Burgert, I., Sinn, G. & Tschegg, S. 2002. The Radial Reinforcement of the Wood Structure and Its Implication on Mechanical and Fracture Mechanical Properties - a Comparison between Two Tree Species. *Journal of Materials Science,* 37, 935-940.

Reiterer, A., Lichtenegger, H., Fratzl, P. & Stanzl-Tschegg, S. E. 2001. Deformation and Energy Absorption of Wood Cell Walls with Different Nanostructure under Tensile Loading. *Journal of Materials Science,* 36, 4681-4686.

Reuschel, D. & Mattheck, C. 1999a. Optimization of Fiber Arrangement with Caio (Computer Aided Internal Optimization) and Application to Tensile Samples. *In:* Hernandez, S., Kassab, A. J. & Brebbia, C. A. (eds.) *Computer Aided Optimum Design of Structures Vi.*

Reuschel, D. & Mattheck, C. 1999b. Three-Dimensional Fibre Optimisation with Computer Aided Internal Optimisation. *Aeronautical Journal,* 103, 415-420.

Bibliography

Reuschel, D., Mattheck, C. & Althaus, C. 1998a. The Mechanical Effect of Climbing Plants Upon the Host Tree. *Allgemeine Forst Und Jagdzeitung,* 169**,** 87-91.

Reuschel, D., Mattheck, C. & Royal Aeronaut Soc, R. a. S. 1998b. *Three Dimensional Fibre Optimisation with Computer Aided Internal Optimisation (Caio)*.

Reuschel, D., Mattheck, C. & Teschner, M. 1997. *Determination of Optimal Fibre Arrangement of Complex Two or Three Dimensional Geometries*.

Right Trees. 1999. *Right Trees for a Changing Climate* [Online]. Available: www.right-trees.org.uk [Accessed 21 August 2011 2011].

Rodgers, M., Casey, A. & Hendrick, E. 1991. Deformation of Soils and Displacements of Structures : X Ecsmfe, Vol 2: Effects of Experimental Dynamic Loading on Coniferous Trees. *10TH EUROPEAN CONF OF SOIL MECHANICS AND FOUNDATION ENGINEERING* Florence, Italy.

Rodgers, M., Casey, A., Mcmenamin, C. & Hendrick, E. 1995. An Experimental Investigation of the Effects of Dynamic Loading on Coniferous Trees Planted on Wet Mineral Soils. *In:* Coutts, M. P. & Grace, J. (eds.) *Wind and Trees.* Cambridge: Cambridge University Press.

Rodriguez-Abad, I., Martinez-Sala, R., Capuz Lladro, R., Diez Barra, R. & Garcia-Garcia, F. 2011. Assessment of the Variation of the Moisture Content in the Pinus Pinaster Ait Using the Non Destructive Gpr Technique. *Materiales De Construccion,* 61**,** 143-156.

Rosenthal, M., Wagenfuhr, A., Burgert, I. & Speck, T. 2007. Design and Development of a Bio-Inspired, Three-Dimensional Deformable Veneer. *Comparative Biochemistry and Physiology a-Molecular & Integrative Physiology,* 146**,** 36.

Royal Forestry Society. 2009. *How Trees Work* [Online]. Available: http://www.rfs.org.uk/learning/how-trees-work [Accessed 22 October 2009].

Rudnicki, M., Silins, U., Lieffers, V. J. & Josi, G. 2001. Measure of Simultaneous Tree Sways and Estimation of Crown Interactions among a Group of Trees. *Trees-Structure and Function,* 15**,** 83-90.

Rueggeberg, M., Speck, T. & Burgert, I. 2007. Fibre-Matrix Interfaces in Plants as Model Systems for Technical Composites. *Comparative Biochemistry and Physiology a-Molecular & Integrative Physiology,* 146**,** 12.

Ruggeberg, M., Burgert, I. & Speck, T. 2010. Structural and Mechanical Design of Tissue Interfaces in the Giant Reed Arundo Donax. *Journal of the Royal Society Interface,* 7**,** 499-506.

Ruggeberg, M., Speck, T. & Burgert, I. 2009. Structure-Function Relationships of Different Vascular Bundle Types in the Stem of the Mexican Fanpalm (Washingtonia Robusta). *New Phytologist,* 182, 443-450.

Ruggeberg, M., Speck, T., Paris, O., Lapierre, C., Pollet, B., Koch, G. & Burgert, I. 2008. Stiffness Gradients in Vascular Bundles of the Palm Washingtonia Robusta. *Proceedings of the Royal Society B-Biological Sciences,* 275, 2221-2229.

Sachs, T. & Hassidim, M. 1996. Mutual Support and Selection between Branches of Damaged Plants. *Vegetatio,* 127, 25-30.

Salmen, L. & Burgert, I. 2009. Cell Wall Features with Regard to Mechanical Performance. A Review Cost Action E35 2004-2008: Wood Machining – Micromechanics and Fracture. *Holzforschung,* 63, 121-129.

Samson, M., Bindzi, I. & Kamoso, L. M. 1996. Mathematical Representation of Knots in Tree Trunks. *Canadian Journal of Forest Research-Revue Canadienne De Recherche Forestiere,* 26, 159-165.

Savidge, R. A. 2001. Intrinsic Regulation of Cambial Growth. *Journal of Plant Growth Regulation,* 20, 52-77.

Schadel, C., Blochl, A., Richter, A. & Hoch, G. 2009. Short-Term Dynamics of Nonstructural Carbohydrates and Hemicelluloses in Young Branches of Temperate Forest Trees During Bud Break. *Tree Physiology,* 29, 901-911.

Schamp, B. S., Schurer, M. & Aarssen, L. W. 2007. Testing Hypotheses for Stem Bending in Tree Saplings. *International Journal of Plant Sciences,* 168, 547-553.

Schelhaas, M. J., Kramer, K., Peltola, H., Van Der Werf, D. C. & Wijdeven, S. M. J. 2007. Introducing Tree Interactions in Wind Damage Simulation. *Ecological Modelling,* 207, 197-209.

Schindler, D. 2008. Responses of Scots Pine Trees to Dynamic Wind Loading. *Agricultural and Forest Meteorology,* 148, 1733-1742.

Schindler, D., Grebhan, K., Albrecht, A. & Schonborn, J. 2009. Modelling the Wind Damage Probability in Forests in Southwestern Germany for the 1999 Winter Storm 'Lothar'. *International Journal of Biometeorology,* 53, 543-554.

Schreiber, N., Gierlinger, N., Putz, N., Fratzl, P., Neinhuis, C. & Burgert, I. 2010. G-Fibres in Storage Roots of Trifolium Pratense (Fabaceae): Tensile Stress Generators for Contraction. *Plant Journal,* 61, 854-861.

Schwarze, F., Lonsdale, D. & Mattheck, C. 1995. Detectability of Wood Decay Caused by Ustulina Deusta in Comparison with Other Tree-Decay Fungi. *European Journal of Forest Pathology,* 25, 327-341.

Bibliography

Sebastian, W., Bishop, R. & Evans, R. 2010. Timber-Limecrete Composite Floors Using Timber Connectors Sloped toward or against Slip. *Journal of Structural Engineering-Asce,* 136, 1585-1595.

Sellier, D. & Fourcaud, T. 2009. Crown Structure and Wood Properties: Influence on Tree Sway and Response to High Winds. *American Journal of Botany,* 96, 885-896.

Shigo, A. 1986. *The New Tree Biology,* Durham, Shigo and Trees, Associates.

Shigo, A. L. 1985. How Tree Branches Are Attached to Trunks. *Canadian Journal of Botany-Revue Canadienne De Botanique,* 63, 1391-1401.

Sievanen, R., Nikinmaa, E., Nygren, P., Ozier-Lafontaine, H., Perttunen, J. & Hakula, H. 2000. Components of Functional-Structural Tree Models. *Annals of Forest Science,* 57, 399-412.

Sigmund, O. 2001. A 99 Line Topology Optimization Code Written in Matlab. *Structural and Multidisciplinary Optimization,* 21, 120-127.

Silva, G., Ruel, J. C., Samson, M. & Pin, D. 1998. Influence of Some External Defects on the Resistance of Trees to the Mechanical Simulation of Wind. *Canadian Journal of Forest Research-Revue Canadienne De Recherche Forestiere,* 28, 123-131.

Sinoquet, H. & Rivet, P. 1997. Measurement and Visualization of the Architecture of an Adult Tree Based on a Three-Dimensional Digitising Device. *Trees-Structure and Function,* 11, 265-270.

Skatter, S. & Kucera, B. 1997. Spiral Grain - an Adaptation of Trees to Withstand Stem Breakage Caused by Wind-Induced Torsion. *Holz Als Roh-Und Werkstoff,* 55, 207-213.

Slater, D. 2011. Phd Continuation Report - the Mechanical Properties of Junctions in Trees Manchester: The University of Manchester.

Slater, D. & Harbinson, C. 2010. Towards a New Model of Branch Attachment. *Arboricultural Journal,* 33, 95-105.

Sone, K., Suzuki, A., Miyazawa, S. I., Noguchi, K. & Terashima, I. 2009. Maintenance Mechanisms of the Pipe Model Relationship and Leonardo Da Vinci's Rule in the Branching Architecture of Acer Rufinerve Trees. *Journal of Plant Research,* 122, 41-52.

Spatz, H. C. & Bruechert, F. 2000. Basic Biomechanics of Self-Supporting Plants: Wind Loads and Gravitational Loads on a Norway Spruce Tree. *Forest Ecology and Management,* 135, 33-44.

Speck, T., Milwich, M., Busch, S., Speck, O., Burgert, I. & Ruggeberg, M. 2009. Arborescent Monocots as Role Models for Biomimetic Fibre-Reinforced Composites with Gradient Structure. *Comparative Biochemistry and Physiology a-Molecular & Integrative Physiology,* 153A, S116-S116.

Spickenheuer, A., Schulz, M., Gliesche, K. & Heinrich, G. 2008. Using Tailored Fibre Placement Technology for Stress Adapted Design of Composite Structures. *Plastics Rubber and Composites,* 37**,** 227-232.

Sprugel, D. G., Hinckley, T. M. & Schaap, W. 1991. The Theory and Practice of Branch Autonomy. *Annual Review of Ecology and Systematics,* 22**,** 309-334.

Stahle, D. 1996. Tree Rings and Ancient Forest History. *Eastern Old-Growth Forests: Prospects for Rediscovery and Recovery.*

Stanislas, M., Kompenhans, J. & Westerweel, J. 2000. *Partcile Image Velocimetry - Progress Towards Industrial Application,* Netherlands, Kluwer Academic Publishers.

Stansfield, K. 1999. St James's Park - a Redevelopment Challenge. *The Structural Engineer.* Institute of Structural Engineers.

Stanzl-Tschegg, S. E. 2006. Microstructure and Fracture Mechanical Response of Wood. *International Journal of Fracture,* 139**,** 495-508.

Stanzl-Tschegg, S. E. 2009. Fracture Properties of Wood and Wood Composites. *Advanced Engineering Materials,* 11**,** 600-606.

Sterck, F. J. & Schieving, F. 2007. 3-D Growth Patterns of Trees: Effects of Carbon Economy, Meristem Activity, and Selection. *Ecological Monographs,* 77**,** 405-420.

Sterck, F. J., Schieving, F., Lemmens, A. & Pons, T. L. 2005. Performance of Trees in Forest Canopies: Explorations with a Bottom-up Functional-Structural Plant Growth Model. *New Phytologist,* 166**,** 827-843.

Steudle, E. unknown. *Xylem Transport* [Online]. Institute of Plant Ecology. Available: http://www.homepage.steudle.uni-bayreuth.de/xylem.htm [Accessed 25 November 2009].

Stokes, A. & Mattheck, C. 1996. Variation of Wood Strength in Tree Roots. *Journal of Experimental Botany,* 47**,** 693-699.

Stokes, A., Salin, F., Kokutse, A. D., Berthier, S., Jeannin, H., Mochan, S., Dorren, L., Kokutse, N., Abd Ghani, M. & Fourcaud, T. 2005. Mechanical Resistance of Different Tree Species to Rockfall in the French Alps. *Plant and Soil,* 278**,** 107-117.

Suzuki, A. A. & Suzuki, M. 2009. Why Do Lower Order Branches Show Greater Shoot Growth Than Higher Order Branches? Considering Space Availability as a Factor Affecting Shoot Growth. *Trees-Structure and Function,* 23**,** 69-77.

Suzuki, M. & Hiura, T. 2000. Allometric Differences between Current-Year Shoots and Large Branches of Deciduous Broad-Leaved Tree Species. *Tree Physiology,* 20**,** 203-209.

Bibliography

Takenaka, A. 1997. Structural Variation in Current-Year Shoots of Broad-Leaved Evergreen Tree Saplings under Forest Canopies in Warm Temperate Japan. *Tree Physiology,* 17**,** 205-210.

Takeshita, K., Jeong, Y., Kim, S., Watahiki, K., Nakao, H. & Hardwinarto, S. 1994. Mechanical Analysis of Lateral Transmission of Failure Resistant Force by Root Block of Forest Trees on Slope Stability. *Bulletin of the Institute of Tropical Agriculture Kyushu University,* 17**,** 1-32.

Tannenberg, K. & Tannenberg, G. 2011. Wood Moisture Content Measurements Using Capacitance Based Moisture Meters. *Pomiary Automatyka Kontrola,* 57**,** 161-4.

Tanskanen, P. 2002. The Evolutionary Structural Optimization Method: Theoretical Aspects. *Computer Methods in Applied Mechanics and Engineering,* 191**,** 5485-5498.

Tardif, J. & Bergeron, Y. 1997. Ice-Flood History Reconstructed with Tree-Rings from the Southern Boreal Forest Limit, Western Quebec. *Holocene,* 7**,** 291-300.

Tatarinov, F. & Cermak, J. 1999. Daily and Seasonal Variation of Stem Radius in Oak. *Annals of Forest Science,* 56**,** 579-590.

Telewski, F. W. 1995. Wind-Induced Physiological and Developmental Responses in Trees. *In:* Coutts, M. P. & Grace, J. (eds.) *Wind and Trees.* Cambridge: Cambridge University Press.

Terreform. 2008. *Fab Tree Hab* [Online]. Available: http://www.terreform.org/projects_habitat_fab.html [Accessed November 2008].

Tesari, I. & Mattheck, C. 1999. The Adaptation of the Compression Strength of Hardwood Branches to the Loading Caused by Gravity. *Allgemeine Forst Und Jagdzeitung,* 170**,** 128-132.

Teschner, M. & Mattheck, C. 1993. *Optimization of Soil Anchorage.*

Thunell, B. 1951. Über Die Drehwüchsigkeit (over the Spiral?). *Holz als Roh- und Werkstoff,* 9**,** 293-297.

Thygesen, L. G., Eder, M. & Burgert, I. 2007. Dislocations in Single Hemp Fibres-Investigations into the Relationship of Structural Distortions and Tensile Properties at the Cell Wall Level. *Journal of Materials Science,* 42**,** 558-564.

Tomlinson, P. B., Fisher, J. B., Halle, F. & Villalobos, R. 2005. Development of Woody Branch Attachments in Schefflera (Araliaceae or Apiaceae). *American Journal of Botany,* 92**,** 1765-1773.

Trada Technology Ltd 2006. Moisture in Timber. *In:* Trada (ed.).

Turner, N. 1988. Measurement of Plant Water Status by the Pressure Chamber Technique *Irrigation Science,* 9**,** 289-308.

Tyree, M. T. & Ewers, F. W. 1991. Tansley Review No. 34 the Hydraulic Architecture of Trees and Other Woody Plants. *New Phytologist,* 119**,** 345-360.

Ulrich, R. 1984. View through a Window May Influence Recovery from Surgery. *Science,* 224**,** 420-421.

Umeki, K. 1997. Effect of Crown Asymmetry on Size-Structure Dynamics of Plant Populations. *Annals of Botany,* 79**,** 631-641.

United Nations Framework Convention on Climate Change. 2006. *Mechanisms under the Kyoto Protocol* [Online]. United Nations Framework Convention on Climate Change. Available: http://unfccc.int/kyoto_protocol/mechanisms/items/1673.php [Accessed 2 January 2011].

Unknown. 2005. *Transport of Water and Minerals in Plants* [Online]. Available: http://users.rcn.com/jkimball.ma.ultranet/BiologyPages/X/Xylem.html [Accessed 30 November 2009].

Unknown 2006. London's Urban Heat Island: A Summary for Decision Makers. London: Greater London Authority.

Unknown. 2010a. *Introduction to Lidar* [Online]. Forestry Commission UK. Available: http://www.forestry.gov.uk/forestry/INFD-6RVC9J [Accessed 20 August 2010 2010].

Unknown. 2010b. *Multi-Storey Marvel* [Online]. Available: http://www.timber-building.com/news/fullstory.php/aid/624/Multi-storey_marvel.html [Accessed 24 July 2011].

Unknown. 2010c. *World's Tallest Wooden Building* [Online]. Available: http://www.norway.org/News_and_events/Culture/Architecture--Design/Worlds-Tallest-Wooden-Building/ [Accessed 24 July 2011].

Unknown 2011a. Approved Judgement Bowen V National Trust *In:* Justice, R. C. O. (ed.).

Unknown. 2011b. *Sutyagin House* [Online]. Wikipedia. Available: http://en.wikipedia.org/wiki/Sutyagin_House [Accessed 24 July 2011].

Unknown. unknown. *Horyu-Ji Temple* [Online]. House of Japan. Available: http://www.houseofjapan.com/architecture/horyu-ji-temple [Accessed 24 July 2011].

Vafai, A. & Farshad, M. 1979. Modulus of Elasticity of Wood in Standing Trees. *Wood Science,* 12**,** 93-97.

Valentine, H. T. & Makela, A. 2005. Bridging Process-Based and Empirical Approaches to Modeling Tree Growth. *Tree Physiology,* 25**,** 769-779.

Van Der Beek, J., Tiitta, M., Tomppo, L. & Lappalainen, R. 2011. Moisture Content Determination of Thermally Modified Timber by Electrical and Ultrasound Methods. *International Wood Products Journal,* 2**,** 60-6.

Vangardingen, P. & Grace, J. 1991. Plants and Wind. *Advances in Botanical Research Incorporating Advances in Plant Pathology,* 18**,** 189-253.

Vos, J. & Heuvelink, E. 2007. *Concepts to Model Growth and Development of Plants.*

Vukotic, L., Fenner, R. A. & Symons, K. 2010. Assessing Embodied Energy of Building Structural Elements. *Proceedings of the Institution of Civil Engineers-Engineering Sustainability,* 163**,** 147-158.

Walkden, E. 2011a. Inspiration through Tree Design (Unpublished). Southampton: Institution of Civil Engineers – Papers Competition 2011.

Walkden, E. 2011b. Structures and Natural Sustainability Influence *Engineers without Borders – Our Global Future.* The Royal Academy of Engineering, London: Engineers without Borders.

Walther, F., Baumgartner, A. & Mattheck, C. 1993. *Finding New Designs for Pressure Tools Using Optimization Methods Which Are Based on the Simulation of Biological, Growth.*

Walther, F. & Mattheck, C. 1993a. *Local Stiffening of Shell Structures by Sko and Cao – a Method to Find Fatigue Resistant and Lightweight Designs in Engineering.*

Walther, F. & Mattheck, C. 1993b. *Reduction of Thermal-Stresses in Ceramics by Shape Optimization with Cao.*

The Secret Design Life of Buildings, Year. Directed by Wardle, L. UK: Renegade Pictures (UK) Ltd.

Watson, A. J. 1995. Measurement of Wind-Induced Tree-Root Stresses in New Zealand. *In:* Coutts, M. P. & Grace, J. (eds.) *Wind and Trees.* Cambridge: Cambridge University Press.

Weber, K. & Mattheck, C. 2005. The Double Nature of the Root Plate. *Allgemeine Forst Und Jagdzeitung,* 176**,** 77-85.

Weber, K. & Mattheck, C. 2006. The Effects of Excessive Drilling Diagnosis on Decay Propagation in Trees. *Trees-Structure and Function,* 20**,** 224-228.

Weber, R. 1988. The Detection of Rot in Standing Timber. *Schweizerische Technische Zeitschrift,* 85**,** 17-19.

Wei, C., Steudle, E., Tyree, M. T. & Lintilhac, P. M. 2001. The Essentials of Direct Xylem Pressure Measurement. *Plant, Cell and Environment,* 24**,** 549-555.

Wei, C., Tyree, M. T. & Bennink, J. P. 2009. The Transmisson of Gas Pressure to the Xylem Fluid Pressure When Plants Are inside a Pressure Bomb. *Journal of Experimental Botany,* 51**,** 309-316.

Weiskittel, A. R., Maguire, D. A. & Monserud, R. A. 2007. Response of Branch Growth and Mortality to Silvicultural Treatments in Coastal Douglas-Fir

Plantations: Implications for Predicting Tree Growth. *Forest Ecology and Management,* 251**,** 182-194.

Weiskittel, A. R., Seymour, R. S., Hofmeyer, P. V. & Kershaw, J. A. 2010. Modelling Primary Branch Frequency and Size for Five Conifer Species in Maine, USA. *Forest Ecology and Management,* 259**,** 1912-1921.

White, D. J. & Take, W. A. 2002. Particle Image Velocimetry (Piv) Software for Use in Geotechnical Testing. Cambridge.

White, D. J., Take, W. A. & Bolton, M. D. 2003. Soil Deformation Measurement Using Particle Image Velocimetry (Piv) and Photogrammetry. *Geotechnique,* 53**,** 619-631.

Wieser, G., Tegischer, K., Tausz, M., Haberle, K. H., Grams, T. E. E. & Matyssek, R. 2002. Age Effects on Norway Spruce (Picea Abies) Susceptibility to Ozone Uptake: A Novel Approach Relating Stress Avoidance to Defense. *Tree Physiology,* 22**,** 583-590.

Willfor, S. M., Sundberg, A. C., Rehn, P. W., Saranpaa, P. T. & Holmbom, B. R. 2005. Distribution of Lignans in Knots and Adjacent Stemwood of Picea Abies. *Holz Als Roh-Und Werkstoff,* 63**,** 353-357.

Wilson, B. F. 1998. Branches Versus Stems in Woody Plants: Control of Branch Diameter Growth and Angle. *Canadian Journal of Botany-Revue Canadienne De Botanique,* 76**,** 1852-1856.

Wilson, B. F. 2000. Apical Control of Branch Growth and Angle in Woody Plants. *American Journal of Botany,* 87**,** 601-607.

Wilson, F. 1988. *The Growing Tree,* Amherst, University of Massachusetts Press.

Wood, C. J. 1995. Understanding Wind Forces on Trees. *In:* Coutts, M. P. & Grace, J. (eds.) *Wind and Trees.* Cambridge: Cambridge University Press.

Wu, Z. X. 2005. An Efficient Approach for Shape Optimization of Components. *International Journal of Mechanical Sciences,* 47**,** 1595-1610.

Xavier, J., Avril, S., Pierron, F. & Morais, J. 2009. Variation of Transverse and Shear Stiffness Properties of Wood in a Tree. *Composites Part a-Applied Science and Manufacturing,* 40**,** 1953-1960.

Yang, Z. J. & Midmore, D. J. 2009. Self-Organisation at the Whole-Plant Level: A Modelling Study. *Functional Plant Biology,* 36**,** 56-65.

Zhang, H., Mohamed, A. & Xiao, Z. Year. Evaluation of the Shear Constant of a Timber Beam Using a Photogrammetric Approach. *In:* 13th International Conference on civil, Structural and Environmental Engineering Computing, 2011. Civil-Comp Press.

Zhu, J.-J., Liu, Z.-G., Li, X.-F., Matsuzaki, T. & Gonda, Y. 2004. Review: Effects of Wind on Trees. *Journal of Forestry Research (Harbin),* 15**,** 153-160.

Bibliography

Zimmermann, M. & Brown, C. 1980. *Trees – Structure and Function,* Berlin, Springer

Zimmermann, U., Haase, A., Langbein, D. & Meinzer, F. 1993. Mechanism of Long-Distance Water Transport in Plants: A Reexamination of Some Paradigms in the Light of New Evidence. *Philosophical Transactions of the Royal Society of London B,* 341, 19-31.

Zimmermann, U., Meinzer, F. & Bentrup, F. W. 1995. How Does Water Ascend in Tall Trees and Other Vascular Plants? *Annals of Botany,* 76, 545-551.

Zipse, A., Albrecht, W. & Mattheck, C. 1997a. How the Wood of Hollow and Leaning Trees Resists Failure. *Allgemeine Forst Und Jagdzeitung,* 168, 59-62.

Zipse, A., Mattheck, C. & Bethge, K. 1995. The Relationship of Strength Properties in Trees. *Allgemeine Forst Und Jagdzeitung,* 166, 215-222.

Zipse, A., Teschner, M., Mattheck, C. & Grabe, D. 1997b. *Optimum Wall Thickness Distribution for Shell Structures*.